Atlas of Ultrasonography in Urology, Andrology, and Nephrology

Pasquale Martino
Andrea B. Galosi
Editors

EXTRAS ONLINE

Springer

Atlas of Ultrasonography in Urology, Andrology, and Nephrology

Pasquale Martino • Andrea B. Galosi
Editors

Atlas of Ultrasonography in Urology, Andrology, and Nephrology

Springer

Editors
Pasquale Martino
Department of Emergency and
Organ Transplantation Urology
Andrology and Kidney
Transplantation Unit
University of Bari
Bari
Italy

Andrea B. Galosi
Division of Urology
Polytechnic University of Marche
Ancona
Italy

This title has been previously published in Italian by Scripta Manent Edizioni 2016.
ISBN 978-3-319-40780-7 ISBN 978-3-319-40782-1 (eBook)
DOI 10.1007/978-3-319-40782-1

Library of Congress Control Number: 2017934335

Printed on acid-free paper

This Springer imprint is published by Springer Nature
The registered company is Springer International Publishing AG
The registered company address is: Gewerbestrasse 11, 6330 Cham, Switzerland

To my wife Teresa
and to my son Lucio
P.M.,

To my wife Barbara
and to my sons Matilde
and Alessandro Ernesto
A.B.G.

Foreword

The role of ultrasound in urology is expanding at a rapid pace. Whereas in Europe it is almost an extension of a physical exam, in the USA the urologists are rapidly learning to incorporate this in the practice. The American Urological Association through its office of education has made available the course to enable the urologist to learn this important tool.

Atlas of Ultrasonography in Urology, Andrology, and Nephrology (Martino-Galosi Editors) is a welcome addition, as this provides a compendium of comprehensive use of ultrasound in all aspects of urological care. It not only covers the basics but provides advanced techniques for application in both males and females. It fulfills the need for universally recognized, standardized parameters for the correct performance of ultrasound investigations, as well as a scheme for reporting clinical findings that may be relevant in clinical practice.

The table of contents is exhaustive and conveniently organized in organ-specific format starting with renal, to the urethra. Almost one thousand ultrasound images; hundreds of graphs, tables, and figures; photographs of anatomical, histological, and contrast-enhanced details; and many videos are very helpful to the reader – from a novice to an experienced practitioner.

The applications of ultrasound in emergency, functional ultrasound, and 3D ultrasound are particularly interesting topics in this emerging field. Authors include not only urologists, andrologists, and nephrologists but also general surgeons and specialist radiologists, all offering practical tips in diagnostic imaging techniques.

I am pleased to recommend this publication to you.

Gopal H. Badlani
Wake Forest University
Winston Salem, NC, USA

Preface

Ultrasound scanning is a widespread and essential diagnostic tool in all specialist branches of medicine. This is particularly true in the study of diseases of the urinary and genital apparatuses, and the method has largely replaced the classic investigations involving the use of contrast medium.

The technique is an essential part of the cultural armamentarium of urologists, andrologists, and nephrologists, and for this reason, nowadays the need for universally recognized, standardized parameters for the correct performance of US investigations, as well as a scheme for reporting clinical findings that may be relevant in clinical practice, is widely perceived.

This volume is addressed both to those taking their first steps in the field of US scanning and to expert scholars and ultrasound specialists, who wish to make in-depth studies of particular aspects of the urinary and genital apparatuses.

This Atlas includes almost one thousand ultrasound images; hundreds of graphs, tables, figures; photographs of anatomical, histological, and contrast-enhanced details; and many videos that accompany the reader during the consultation of the work and help to make it easy to follow.

This text provides a close examination of benign and malignant diseases, malformations, and trauma of the urogenital system. Particular attention has been paid to the ultrasound scanning methods for investigating these, as well as to mini-invasive US-guided surgical techniques.

The most accredited guidelines and practical recommendations for performing ultrasound scanning in the urological, andrological, and nephrological fields have been taken into account and are frequently referred to. They are quoted in detail at the end of this Atlas.

Continuous research is still ongoing in the ultrasound field (elastosonography, 3D US, the use of contrast medium, histoscanning, etc.), associated with the design and construction of ever more sophisticated dedicated devices and probes (intraoperative, laparoscopic, endocavitary probes, etc.). Thanks to this close interest, the use of ultrasound scanning is being applied in an increasingly vast field: not only diagnostic but also interventional and intraoperative ultrasound scanning.

Contributors to this work include not only urologists, andrologists, and nephrologists but also specialist radiologists and general surgeons, all experts in diagnostic imaging techniques. We would like to thank them all, for without their expertise this work could never have been completed.

We are very grateful to Dr. Gopal H. Badlani, MD, Professor and Vice Chairman of the Department of Urology at Wake Forest University, North Carolina, for having kindly agreed to present this work. He was former Secretary of the AUA and is currently Scientific Program Director and Member BOD of SIU and Secretary-elect of the American Association of Genitourinary Surgeons.

We also gratefully acknowledge the support of Ms. Saanthi Shankhararaman, Project Coordinator for Springer, in preparing this volume and Mary V.C. Pragnell, B.A., for language assistance.

We hope that the commitment and efforts devoted to writing this work will be rewarded by an appreciative reception of the work by all those who deal in the various different ways with diagnostic and interventional ultrasound scanning of the urinary and genital apparatuses.

Bari, Italy — Pasquale Martino

Ancona, Italy — Andrea Benedetto Galosi

Contents

List of Videos

Electronic supplementary material is available in the online version of the related chapter on SpringerLink: http://link.springer.com/

Part I

The Kidney

Kidney: Ultrasound Anatomy and Scanning Methods

1

Giulio Argalia, Serena Campa, Fatjon Cela, Nicola Carboni, Fabio Salvatori, and Gian Marco Giuseppetti

1.1 Sonographic Scanning Technique

US examination of the native kidney is performed with multifrequency convex probe with transmission frequency between 2 and 5 MHz according to the patient's body structure, using longitudinal, coronal, transversal, oblique scans and an anterior or abdominal, posterior or dorsal, and lateral or lumbar approach.

In anterior abdominal approach, in lateral or supine decubitus, the kidney is imaged with longitudinal or oblique subcostal scans, during inspiratory apnea. This approach avoids obstruction due to gas bowel, using the liver as an acoustic window. In anterior longitudinal scans, the kidney assumes an ellipsoidal shape and parenchymal ring appears uninterrupted. The ultrasound bipolar diameter does not exactly coincide with the anatomical larger diameter, because of the organ spatial arrangement. For this reason, the bipolar kidney diameter, determined in the longitudinal scan, tends to be overestimated or underestimated depending on the case. Subcostal scans represent the hilum with anterior and posterior lip, the renal vessels, and just below the pelvis. On the left, gas in the stomach and splenic flexure often represents an insurmountable impediment to view the kidney in anterior scans. However, upward subcostal scan in deep inspiration is required for the definition of topographic relations of a possible left adrenal mass.

The dorsal approach, with the patient in the prone position, finds its main indication in performing ultrasound-guided minimally invasive procedures such as renal biopsy and percutaneous pyelostomy. It's also useful for viewing the lower pole and the middle part of the kidney in the presence of intense bloating and colic stasis.

The lumbar approach through middle and posterior axillary line, with the patient in supine or lateral position, allows a good assessment of the left and right kidney, in coronal and transversal scans.

Coronal scan is the most suitable to measure correctly the repeatable bipolar diameter and cortical thickness. Parenchymal thickness must be determined close to chalices of the lower or upper lobe.

In the coronal scan, the probe is located in posterior-anterior and cranio-caudal direction with the purpose of following ideally anatomical arrangement of the kidney in the lumbar loggia. Remember that the largest axis of the kidney is oblique from top to bottom in the frontal plane, because of the forward rotation of the renal sinus, and is anterior posterior oblique in the sagittal plane because of lumbar lordosis.

G. Argalia (✉) • S. Campa • F. Cela • N. Carboni
F. Salvatori • G.M. Giuseppetti
University Politecnica delle Marche,
Az. Ospedali Riuniti, Ancona, Italy
e-mail: giulio.argalia@gmail.com

P. Martino, A.B. Galosi (eds.), *Atlas of Ultrasonography in Urology, Andrology, and Nephrology*,
DOI 10.1007/978-3-319-40782-1_1

In the transversal scan, the kidney appears as an incomplete ring, open anterior medially on the renal hilum.

Lumbar approach allows evaluation of the pyelo-vascular central zone, pyelo-ureteral junction, third proximal ureter, calyceal and pyelic structures, and the renal hilum.

1.2 Normal Sonographic Appearance

Normal kidney longitudinal diameter is between 10.9 and 12 cm (median 10 cm), and transverse extent is on average 5–6 cm, despite individual differences related to age and size. In the age group between 30 and 60, differences are minimal; in patients over 70 years, kidneys have a smaller size, due to the reduction of the parenchyma. The length of the organ correlates with the height, and, in the same way, the renal volume appears conditioned by age and individual body mass (Fig. 1.1).

In axial scans, acquired at the renal hilum, the transverse diameter measures between 5 and 6.5 cm (median 5.7 cm) (Fig. 1.2).

Three different areas in the context of the renal parenchyma may be distinguishable, according to their echogenic characteristics: the cortex, medulla (constituted by the pyramids), and renal pelvis.

The cortex is located between the base of the pyramids and the surface of the organ, but it goes even deeper between the pyramids themselves, separating them from each other and forming the kidney Bertin columns.

Parenchymal thickness (calculated as the total of cortical and medullary thickness), measured from the outer edge to the border of the renal sinus, varies in normal subjects between 16 and 20 mm (Fig. 1.3). Parenchymal thickness <13 mm is an absolute contraindication to renal biopsy.

Cortical thickness (or corticomedullary) is measured between the outer contour of the kidney and the base of the pyramid, considered normal between 8 and 11.5 mm.

Determining cortical echogenicity is also important; it is measured in relation to renal and extrarenal structures, as it can allow to make evaluations about eventual kidney damage.

The cortex, as already mentioned, is the outermost portion of the renal parenchyma and proves to be hyperechoic compared to the medulla and hypoechoic compared to the pelvis.

A useful tool is represented by the attempt to quantify the alteration in terms of grades or numbers expressing the relative cortical echogenicity, using the scale of Hrikak et al.

This scale, constituted by four grades, compares the normal liver and/or renal sinus echogenicity, considered as the two opposed terms of comparison:

0 – *normal* hypoechoic compared to the liver (Fig. 1.4)
1 – *isoechoic* compared to the liver
2 – *moderately hyperechogenic* compared to the liver but less than the renal sinus
3 – *hyperechogenic* compared to the liver but equivalent to that of the renal sinus

The renal capsule is not easily distinguishable from the perirenal band and from the perirenal fat, but normal kidney outline shows a regular trend. In coronal scans, the regularity of the profile of the upper pole can be broken by a hyperechoic triangular formation, called hyperechoic renal triangle.

The hyperechoic renal triangle is formed by an incomplete fusion of two adjacent lobules in the metanephric kidney, with penetration of the renal sinus fat tissue into the external capsule fat.

The continuity between the triangle and the renal sinus should be carefully researched as a distinctive sign, which can be distinguished by a scar or a parenchymal angiomyolipoma.

The *renal pyramids* (the medulla) are hypoechoic; they may not be well delineated and also in normal conditions, their display can be modest or absent (except in children and thin patients) in relation to the hydration; in some ultrasound scans, they can be easily confused with microcysts or chaliceal diverticula. Corticomedullary differentiation can be well defined when pyramidal margins are net. In conditions where there is interstitial edema (acute tubular necrosis, tubulointerstitial nephropathy), the upper boundary of the pyramidal base can be nuanced, making it difficult to distinguish between the two areas.

The *renal sinus* is the oval hyperechoic area between the inner profile of the parenchyma and the renal hilum; the echogenicity is high for the presence of numerous interfaces and components with different acoustic impedance (collector, vessels, nerves, lymphatics, fibrous tissue, fat).

A variable amount of fibroadipose tissue surrounds the renal pelvis, the chalices, and their infundibula. In cases where the sinus fibroadipose tissue is exuberant, the renal pelvis is compressed, and infundibula are elongated and ironed. This condition is known as "renal sinus sclerolipomatosis," a benign alteration of physiological echostructure due to a fat proliferation in relation to old age, obesity, and corticosteroids. The proliferation of fat causes a mass effect that compresses the intrarenal collecting system without causing chaliceal obstruction. Obesity in the elderly is the main cause of sinus sclerolipomatosis.

Sometimes in young the sinus fibroadipose tissue can have medium-low echogenicity and simulates a pelvis urothelioma, a hydronephrosis, or a cluster of peripelvic cysts.

Sometimes, even the scars of a chronic infection, especially if this is associated with lithiases, can simulate an asymmetric lipomatosis.

On the other side, a venous sinus ectasia or a peripelvic cyst cluster can simulate an expansion of the pelvis.

The use of color Doppler allows the differential diagnosis in the first case, while the absence of communications between the single cysts is diriment in the second one. An extrarenal pelvis can simulate a dilation and/or a ureteropelvic junction anomaly (Fig. 1.5).

In elderly patients with diffuse atherosclerotic disease, the arcuate arteries, located at the corticomedullary junction, may present as thin hyperechoic interfaces and be confused with microcalculi or medullary fibrotic calcifications. Occasionally, small hyperechoic foci, picturesquely called "unidentified bright objects" (UBOs), can be found in the context of the parenchyma. These "spots" are frequently associated with reverberation artifacts, while the acoustic rear cone is usually absent. The possible causes of the "UBOs" may actually be represented by small lithiases foci at the apex of the papilla (Randall bodies), but also by microcysts, small chaliceal diverticula with calcified wall or intraluminal calcium milk, small calcified angiomyolipomas, or arteriole fibro-calcifications.

The pelvis and major and minor chalices are usually virtual and not detectable by B-mode

ultrasound. Their profile can stand out clearly, into the hyperechoic sinus; in relation to physiological causes such as hyperhydration, a hyperrepletion of the bladder, pregnancy, antispasmodic abuse, and elastic hypotonia; or for an intersection with abnormal vessels. In these cases, the intrarenal excretory system appears, and the hypo-anechoic cavity running through the renal sinus, and corresponding to the urinary tract, has a very thin wall. The presence of complex chalices arising from the fusion of several smaller chalices is a frequent anomaly of the polar areas (particularly of the upper pole) and can simulate a pseudo-mass [1–3].

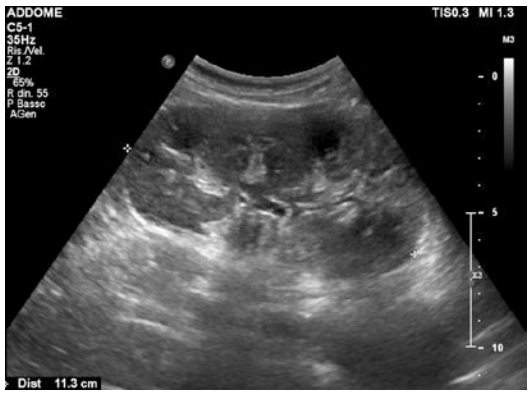

Fig. 1.1 B-mode shows longitudinal section of a left kidney, with normal volume and echostructure and bipolar diameter of 11.3 cm

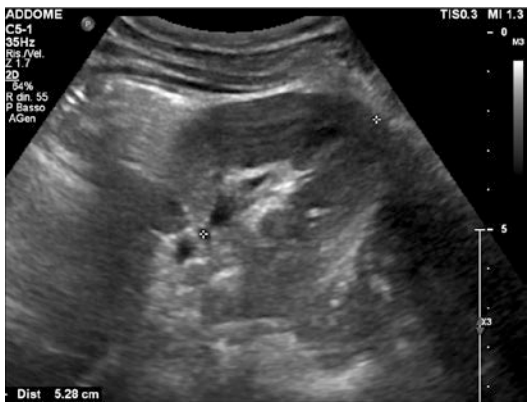

Fig. 1.2 B-mode shows axial section of a left kidney, with normal volume and echostructure and transverse diameter of 5.28 cm

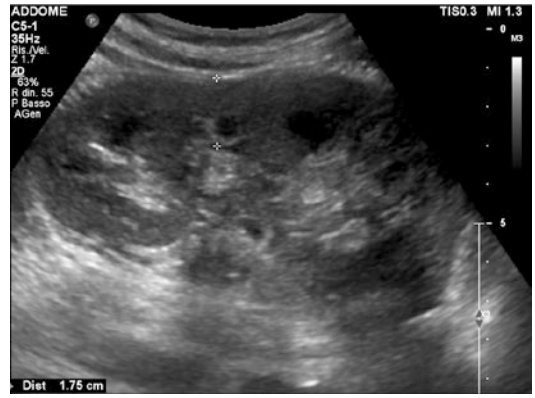

Fig. 1.3 B-mode shows longitudinal section of a left kidney, with normal volume and echostructure and with cortical thickness of 1.75 cm

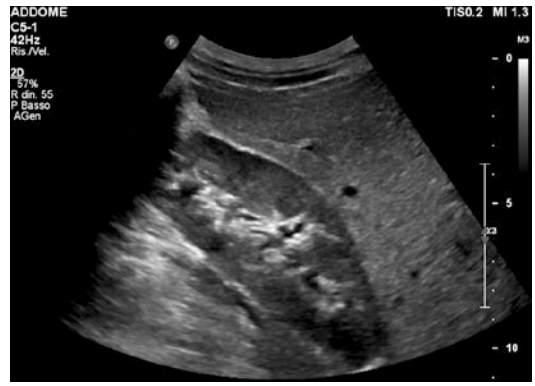

Fig. 1.4 B-mode image of the right kidney with hypoechoic echostructure compared to the liver parenchyma (Hrikak scale 0)

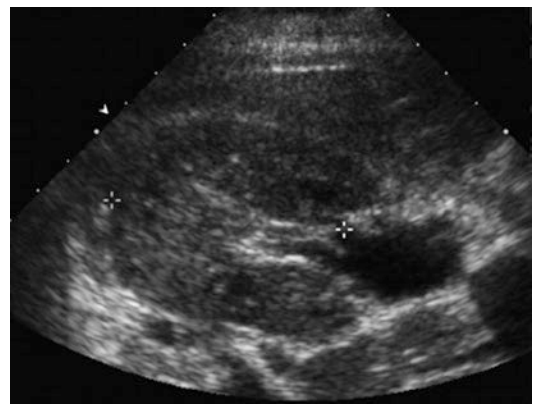

Fig. 1.5 B-mode image of extrarenal pelvis without evidence of hydronephrosis

1.3 Anatomic Variations

The knowledge of anatomic variants that come into differential diagnosis with various pathological conditions is very important; the morphological variants of renal ultrasonography are more commonly found in:

- Lobulations and fetal incisures, the hyperechoic line, and triangle
- Dromedary humps
- Hypertrophy of the tubercles and renal rims
- Mesorenal column hypertrophy or mesorenal septa

1.3.1 Lobulations and Fetal Incisures

Normally the renal outer profile is smooth, while the inner one is jagged, for the presence of columns and pyramids which protrude in the renal sinus. It may happen, however, that also the outer profile is irregular for the presence of prominent areas, bounded by incisions and expression, respectively, of the *lobulations* and the *fetal incisures* (Fig. 1.6). The fetal lobulations coincide with a lobar unit (consisting of the cortical mantle with his pyramid): fetal sulci split two contiguous lobar units that correspond to the cortical columns. They must be differentiated from the segmental pyelonephritis scars that are located in correspondence of the renal chalices and not of the Bertin columns; another sign of benignity, which facilitates the differential diagnosis, is the presence of homogeneous parenchyma below the capsular incision and the absence of distorted and dilated chalices [4–7].

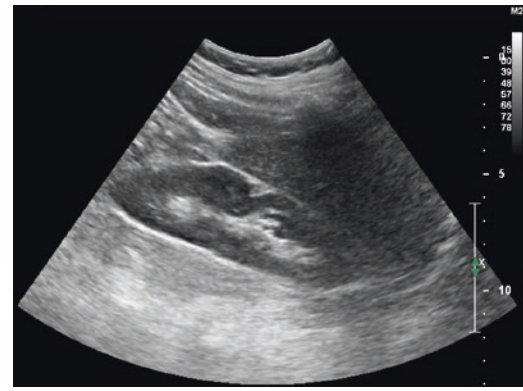

Fig. 1.6 US: compatible image of fetal incisure

1.3.2 Dromedary Hump Kidney

The close proximity to other abdominal organs during fetal life can modulate the growth of the renal parenchyma; the most typical example is the dromedary hump kidney, more frequent to the left, as a result of pressure on the splenic upper pole. In the "hump," the parenchymal structure is homogeneous and the intrarenal circulation is regular [4–7].

1.3.3 Hypertrophy of the Tubercles and Renal Rims

Tubercle and rim hypertrophy is manifested by the increase in volume of these structures that determine swellings, often difficult to distinguish from expansive processes [4–7].

1.3.4 Mesorenal Column Hypertrophy

In normal conditions it may be observed, in the mesorenal zone, a columnar hypertrophy with echogenicity similar to that of the remaining parenchyma that goes deep into the renal sinus (Fig. 1.7), sometimes dividing it completely into two halves, of which the lower one is prevalent (this condition is associated typically with a double excretory system). The homogeneity of the mesorenal column compared to the adjacent areas of parenchyma, the lack of alteration in the capsular profile, and the radially, regular, and centrifugal disposition of arteries and veins are all useful for the differential diagnosis.

The *segmental compensatory hypertrophy*, usually resulting in a chronic multifocal pyelonephritis, is also worth mentioning. It is characterized by the alternation of coarse scars with pseudonodular areas of compensatory regeneration [4–7].

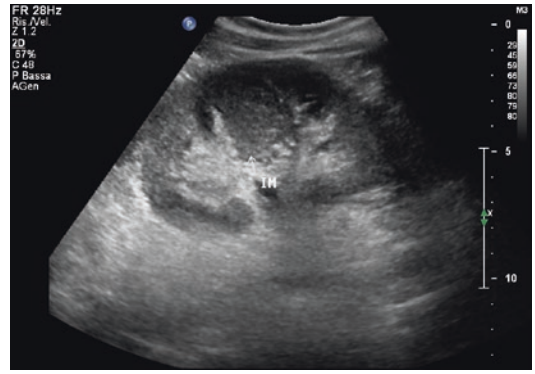

Fig. 1.7 US: incomplete hypertrophy of the column of Bertin

1.3.4.1 Vascularization

The arterial renal circulation is a type of a terminal circulation (Fig. 1.8). The renal arteries originate from the anterolateral wall of the aorta, about 1.5–2 cm from superior mesenteric artery. The right renal artery runs out and then rear, describing an anterior convexity curve, and reaches the renal hilum after crossing posteriorly the inferior vena cava. The left renal artery originates from the lateral profile of the aorta, extends back to the ipsilateral vein, and sinks obliquely toward the lumbar fossa. At the hilum, the renal arteries are divided into a front branch and a rear one (Fig. 1.9). The first gives rise to four segmental branches destined for the upper pole, the anterior superior segment, the segment lower front, and the lower pole. The posterior branch irrigates the posterior region of the kidney.

Renal arteries give rise to few side branches: the lower adrenal arteries, upper ureteral arteries, and some capsular branches. In the case of stenosis of the main branch, these arteries can vascularize renal parenchyma with a retrograde vicar flow. Among the many and frequent anatomical arterial variants, they have to remember the supernumerary arteries originating from the main branch or the aorta. At autopsy, they found two more renal arteries in 20 % of cases and three or more arteries in 4 % of cases; they are unilateral in 32 % of cases, while it shows the bilateral in 12 % of cases. Among the supernumerary arteries include polar arteries and additional arteries. Polar arteries reach directly the right renal parenchyma, through a path that bypasses the hilum. These are further classified into superior polar arteries (which show the origin by the same renal artery in 12 % of cases and from the aorta in 7 % of cases) and lower polar artery (originating from the aorta in 5.5 % of cases and from the renal artery in 1.4 % of cases). Additional arteries enter into the kidney through the renal hilum and may start out from the aorta, the iliac arteries, the superior and inferior mesenteric arteries, and also the lumbar and sacral contralateral kidney. These generally supply for the perfusion of the lower pole (72 % of cases) more often than the upper one.

In some cases, the division of the renal artery in its branches takes place in the section between the origin of the aorta and the renal hilum (extrahilar branching), constituting another variant that can complicate the sonographic exploration of the renal artery along its course. These variants are of complex ultrasound demonstration, but their presence is always assumed where there is difficulty in following the renal arteries themselves or their framework flowmeter does not result in agreement with clinical expectations. They are also increasingly demonstrated in investigations characterized by greater panoramic views, such as CT angiography and MR angiography. The curve speed/time recorded in the main renal artery is a "low resistance" curve. The front of the systolic rise is rapid and is followed by a mild and progressive deceleration, marked by rapid modulations and relevant end-diastolic flow (diastolic velocity 30–40 cm/s). The high continuous component of the flow corresponds to a low resistance index (RI) and pulsatility index (PI) and a high renal blood flow (about 600–650 mL/min for the kidney). The segmental arteries, interlobar and arcuate, show RI <0.60 in normal subjects and a path as smooth and toned and with a peak systolic more prolonged and less pronounced compared to the main artery (Fig. 1.10). The systolic velocity peak in the renal artery varies from 60 to 120 cm/s. However, there are physiological conditions (young subjects), paraphysiological (kinking) or pathologic (hyperdynamic circulation), which increase the PSV even in the absence of significant stenosis of the renal artery. For this reason, a PSV 100 ± 40 cm/s in the main renal artery is considered normal.

The renal venous system differs substantially from the arterial one, in the presence of free intrarenal anastomoses. At the level of the cortical, peritubular capillary blood is drained from the veins that are converged to interlobular veins. These veins drain successively to arched and main interlobar veins (upper, lower, and hilarious) following the general design of the arterial circulation. Interlobar veins, flowing hilum, form the renal vein.

The right renal vein occasionally competes with a branch to form the azygos vein and pours into the inferior vena cava after a short course of 2–2.5 cm at the level of L2. The left renal vein,

longer (6–10 cm), opens into the vena cava at a slightly higher level, after a complex course engaging into aorto-mesenteric clamp. The left renal vein receives the adrenal and gonadal vein and is in connection with the hemiazygos system and ascending lumbar (renal-arch-azygos-lumbar). On the right adrenal and gonadal veins directly flow into the vena cava.

Contrary to what happens in other parts of the body, abnormal renal veins (multiple renal veins, retroaortic left renal vein, circumaortic left renal vein, persistence of the left cardinal vein communicating with the renal vein) are much rarer than the arterial ones.

Overall, the renal venous circle constitutes efficient outflow route for the presence of numerous anastomoses intra- and extrarenal. Therefore, the main vein obstruction rarely causes renal infarction.

At the spectral sampling, renal veins show a modulated and multiphasic and very similar to that of inferior vena cava (auricular and respiratory modular) path. These modulations are less obvious in the left renal vein due to incarceration in the aorto-mesenteric compass. Changing the decubitus, the vein is more simple to explore and commonly used to display the normal modulations [1, 8–12].

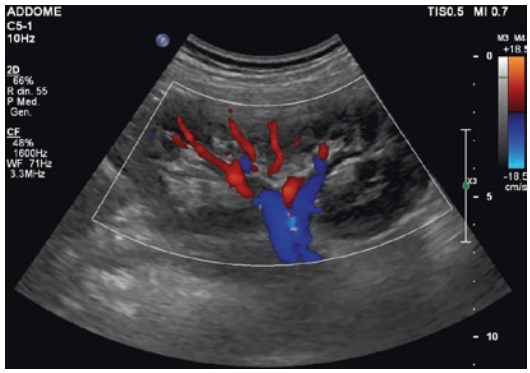

Fig. 1.8 Color Doppler image of native kidney with normal intraparenchymal vascularization

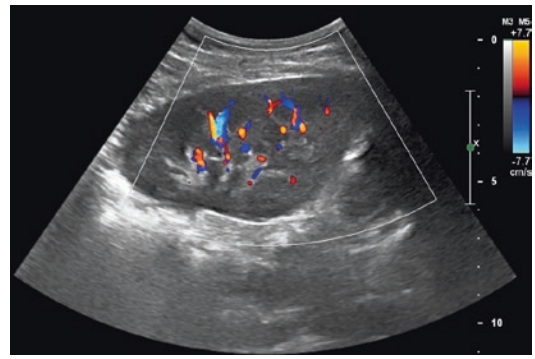

Fig. 1.9 CD: regular intraparenchymal vascularization

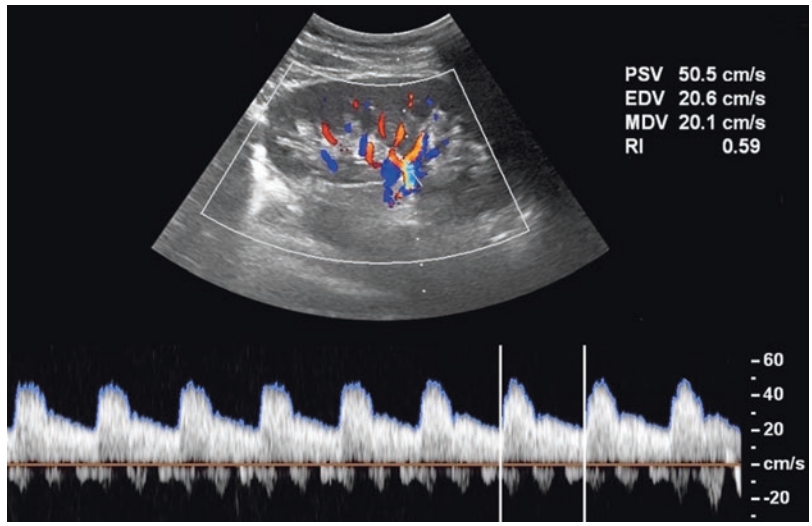

Fig. 1.10 Color and spectral wave Doppler of the main renal artery at the hilum (RI 0.59)

1.3.4.2 Technical Examination

Patient's preparation is very important for a correct evaluation of renal arteries. Prolonged fasting (>8 h) associated with a diet low in fiber reduces the use of antigas drugs. In some cases, like those in cardiorespiratory failure or pathologically obese, the assessment of renal arteries is unsatisfactory. The difficulty of US color Doppler comes also from the frequency of vascular abnormalities (20–25 % cases) and the necessity to explore the whole path of the artery. The hemodynamic alteration induced by the stenosis ends at 1–2 cm so it becomes necessary to sample the ostial/preostial part to document an arteriosclerotic stenosis and the medium-distal part for a fibrodisplastic stenosis.

The renal artery can be sampled with various angular approaches:

1. Axial scans in the peduncle origination, in epigastric or mesogastric area
2. Subcostal scans in lateral decubitus
3. Coronal scans of the aorta in lateral left decubitus
4. Coronal scans on the kidney and the kidney hilum

Axial scan allows to find the peduncle origin of both renal arteries, the anatomical relationship with the homolateral vein, and the accessory arteries if present. In this scan, the transducer is held oblique to the peduncle, so the insonation angle of the ostial part of the right renal artery is unfavorable (angle 60°–70°), while the left one is ideal (<30°–45°) (Fig. 1.11).

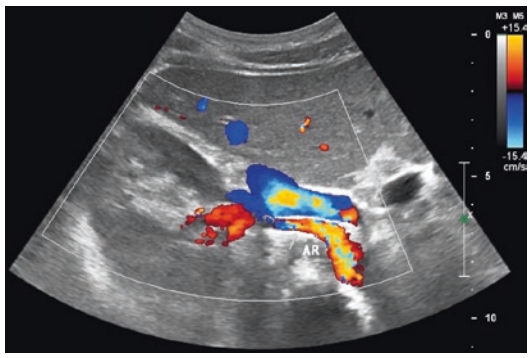

Fig. 1.11 CD: axial scan of the renal artery

In the subcostal scans, left lateral decubitus, the right renal artery is easier to evaluate in all of its length with a sampling angle <20°–30°. On the left the angle is less favorable (>40°).

The coronal scan of the aorta in left lateral decubitus allows to find the ostium of both arteries and define, if present, additional branches. It also gives a good view of the relationship between the medial diaphragmatic pillars and renal arteries. The advantage of this scan is that both arteries' ostia can be sampled with a low insonation angle (20°–25°). Low-frequency transducers (2.5 MHz) are used in obese patients, reducing the image quality.

The coronal scan of the kidney in the mid axillary/posterior line offers a panoramic view of the kidney, of the artery and vein, and of the segmental vessels and intraparenchymal ones that radiate from the renal hilum to the periphery. In this scan the arteries are colored in red (centrifugal flux), while the veins are colored in blue because the flux is going away from the transducer. Interlobar arteries can easily be sampled and their resistive indexes can be calculated.

A good scan for a patient can be bad for another; it is up to the operator and his experience to choose the one that fits best.

An experienced ecographist completes the exam in 15–20 min. Concentration and patience tend to be lower in difficult, badly prepared, and not properly fasting patients.

The scans described here require the use of B-mode of color Doppler/power Doppler and a spectral analysis in duplex (B-mode image + spectra analysis) or triplex (B-mode image, color Doppler/power Doppler in real-time and spectral analysis).

It is very important to have a proper setting of the machine: PRF (1.5–3 KHz), color box, gain and depth of field, and filter. If the settings are correct, the color Doppler image will be clean and will show a colorimetric and uniform red/blue map, without oversaturation. It will be easier in the next step to record an adequate velocity/time curve.

If the colorimetric map is homogeneous and uniform and the V/t curve marks a VPS <100 cm/s, only a comparative calculation of intraparenchy-

mal IR is needed (to exclude lateralization of the vascular resistance) to consider the exam concluded.

The V/t curve will have to be recorded multiple times, at insonation angles between 30 and 60 for a reliable value of the velocities.

An early bifurcation or course abnormalities such as kinking can cause false acceleration and be the source of error.

The presence of color aliasing in the color Doppler sampling indicates the necessity to do multiple samplings in various angles of insonation to find the stenosis.

The appearance of aliasing in the spectral curve is an artifact that can indicate an erroneous setting of PRF or an increase of blood flow speed.

If put above the renal parenchyma, color box shows a rich vascularization arranged radially. Arteries and veins radiate from the hilum to the parenchyma giving birth to the arcuate vessels and interlobar arteries. The cortical blushing, particularly evident in the power Doppler, is highlighted with a thin and pulsing appearance of the vessels that reproduce the systolic/diastolic expansion of cortical vessels.

The intraparenchymal RI and PI should be evaluated preferably in an interlobar vessel, close to the mesorenal column.

In adults the mean RI is to be considered normal if <0.70, while in children in the first 4 years, RI is considered normal even if >0.70.

RI tends to increase in arterial hypertension, in elderly, in diabetes, and in interstitial nephropathies. Cutoff values are near 0.70 in the interstitial nephropathy and >0.80 in the vascular nephropathy, nephroangiosclerosis, and atheroembolism.

In synthesis, the colorimetric map of the flux gives an immediate and qualitative information (course, vessel patency, flux direction), while the toning of the fundamental colors and the oversaturation will indicate the presence of acceleration and turbulence, typical findings of a hemodynamically significative stenosis.

The spectral analysis with the VPS calculation will conclude the examination of the main branch, while the evaluation of intraparenchymal resistive indexes and the velocimetric ratio between the renal artery and the aorta (renal-aortic ratio, RAR) will conclude the exam.

Bibliography

1. Meola M et al (2012) L'ecografia e il color Doppler in nefrologia. Il rene normale: anatomia ecografica, vascolarizzazione e anomalie congenite. G Ital Nefrol 29(3):333–347
2. Emamian SA et al (1993) Kidney dimensions at sonography: correlation with age, sex, and habitus in 665 adults volunteers. AJR 160:83–86
3. Subramanyam BR et al (1983) Replacement lipomatosis of the kidney: diagnosis by computed tomography and sonography. Idelson - Gnocchi. Radiology 148(3):791–792
4. Dyer RB, Chen MY, Zagoria RJ (2004) Classic signs in uroradiology. Radiographics 24(Suppl 1):S247–S280
5. Felson B, Moskowitz M (1969) Renal pseudotumors: the regenerated nodule and other lumps, bumps and dromedary humps. Am J Roentgenol Radium Ther Nucl Med 107:720–729
6. Thornbury JR, McCormick TL, Silver TM (1980) Anatomic/radiologic classification of renal cortical nodules. AJR Am J Roentgenol 134:1–7
7. Hodson CJ, Mariani S (1982) Large cloisons. AJR Am J Roentgenol 139:327–332
8. Busilacchi, Rapaccini (2006) Ecografia clinica. Idelson - Gnocchi
9. Klatte T et al (2015) A literature review of renal surgical anatomy and surgical strategies for partial nephrectomy. Eur Urol 68(6):980–992, pii: S0302-2838(15)00312-7
10. Platt J, Ellis J, Rubin J (1991) Examination of native kidneys with duplex Doppler ultrasound. Semin Ultrasound CT MR 12:308–318
11. Mitchell E et al (2003) The resistive index in renal doppler sonography: where do we stand? Am J Roentgenol 180(4):885–892
12. Olivetti L, Grazioli L (2008) Diagnostica per immagini dell'apparato urogenitale. Springer, Milan

Acute and Chronic Nephropathy

2

Antonio Granata, Dario Galeano,
and Fulvio Fiorini

2.1 Introduction

Imaging techniques, especially ultrasonography, can give an effective assistance in the differential diagnosis of renal diseases, in both acute and chronic setting. As stated by American College of Radiology, renal Doppler ultrasonography (DUS) is the most appropriate imaging first-line test in the evaluation of patients with acute kidney injury (AKI). It allows the assessment of intrinsic causes of AKI, distinguishing acute from chronic kidney disease (CKD) and detecting acute obstruction of the urinary tract [1].

A. Granata (✉) • D. Galeano • F. Fiorini
Nephrology and Dialysis Unit,
"S. Giovanni di Dio" Hospital,
Agrigento, Italy

Nephrology and Dialysis Unit,
"S. Maria della Misericordia" Hospital,
Rovigo, Italy
e-mail: antonio.granata4@tin.it

2.2 Kidney's General Evaluation

Differential diagnosis of renal diseases by DUS is based on the proper interpretation of specific parameters such as kidney size, echogenicity, and resistive index, besides appropriate clinical symptoms (Fig. 2.1).

Kidney's length is the most clinically useful measurement of kidney size because it is simple to obtain and shows only minimal intra- and inter-observer variations. Normal kidneys are approximately 10–12 cm in length, with the left kidney slightly longer than the right. Size also varies with sex and age: women and elderly, respectively, have kidneys smaller than men and young.

Length is especially important in differential diagnosis between AKI and CKD: small kidneys suggest the diagnosis of CKD, although in early diabetic nephropathy, kidney size is normal or increased. Indeed increased kidney size is often a feature of AKI: large kidney may result from infiltrative diseases (amyloidosis, multiple myeloma, lymphoma), edema and inflammation (acute glomerulonephritis, acute interstitial nephritis), and vascular injury (renal vein thrombosis) [2].

Echogenicity is a main criterion to evaluate kidney diseases. Normal parenchyma, including the cortex and medulla, is isoechoic or slightly hypoechoic compared with the liver or spleen. But in the case of bright liver due to steatosis, the evaluation of renal echogenicity may result more

P. Martino, A.B. Galosi (eds.), *Atlas of Ultrasonography in Urology, Andrology, and Nephrology*,
DOI 10.1007/978-3-319-40782-1_2

difficult and is based principally on operator's experience (Fig. 2.2).

Increased parenchymal echogenicity in CKD is a consequence of fibrous tissue that reflects sound waves back. Hyperechogenicity may occur in AKI by acute interstitial nephritis and glomerulonephritis because of inflammatory infiltrates. Proteinaceous casts are thought to cause increased echogenicity that occurs in ATN. Hypoechogenic renal cortex may be the ultrasonographic feature of cortical necrosis, a rare cause of AKI, and consequence of severe ischemia due to hemolytic–uremic syndrome, eclampsia, or sepsis, which results in necrosis of tubular cells of the cortex and increase in interstitial fluid.

The measure of renal resistive index (RI) is one of the most sensitive parameters in the study of disease-derived alterations of renal plasma flow, providing quantitative hemodynamic information about the intrarenal and extrarenal vasculature [3]. A standardized protocol is required to perform a correct measurement of RI, with color Doppler focused on interlobar arteries and low pulse repetition frequency (PRF) of 1–1.5 kHz. When pulsed wave Doppler module is activated, the sample volume should be placed in the lumen of interlobar arteries with a size of 1–2 mm in order to avoid artifacts. Renal RI is the arithmetic average obtained from at least three different samplings in different areas of the kidney (Fig. 2.3).

In adult a value <0.70 is considered normal, but many confounding factors, such as severe hypotension, heart rhythm disorders, renal compressions for perirenal or subcapsular fluid collections, and extrarenal causes of impaired vascular elasticity, should be always kept in account.

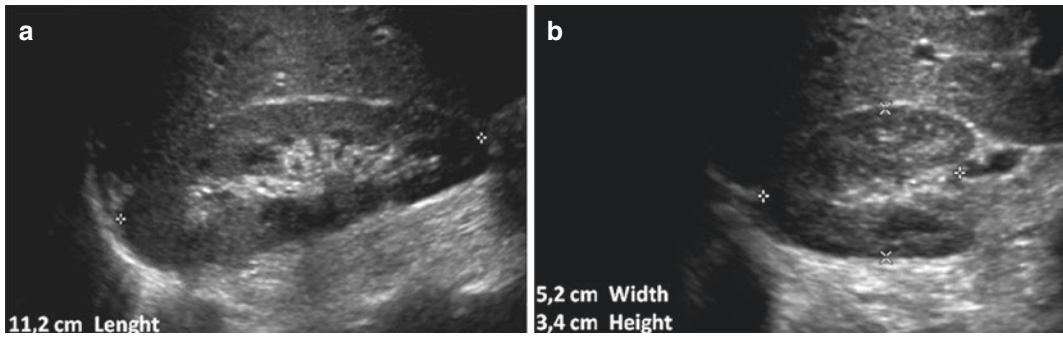

Fig. 2.1 Grayscale image of normal kidney size and echogenicity. Elementary information given by B-mode includes kidney size, parenchymal thickness, cortical echogenicity, corticomedullary differentiation, and renal profiles. (**a**) Coronal section is considered the most accurate scan to estimate kidney's longitudinal length. (**b**) Oblique cross section allows measurement of renal width and thickness for renal volume estimation through the ellipsoid formula

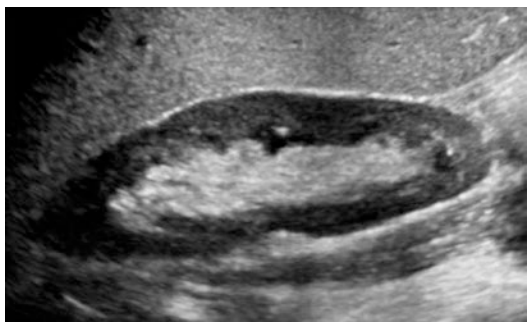

Fig. 2.2 Grayscale ultrasonographic image demonstrating normal kidney compared to a bright liver

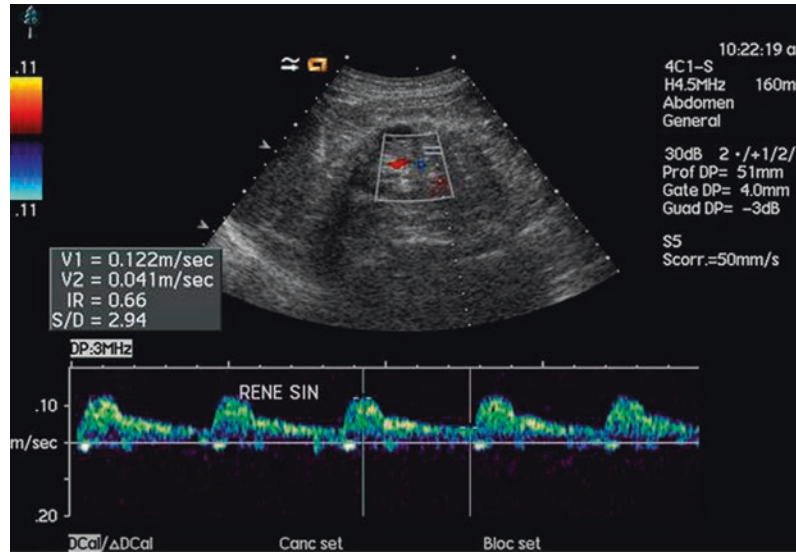

Fig. 2.3 Duplex ultrasound with normal RI finding. The renal RI is calculated through the measure of peak systolic velocity (*PSV*) and the telediastolic velocity (*TDV*) according to the formula RI = (PSV – TDV)/PSV

2.3 Acute Kidney Injury (AKI)

Acute kidney injury is a clinical syndrome including all renal physiopathology. AKI may be determined by renal hypoperfusion (prerenal), renal parenchymal diseases (renal), or acute obstruction of the urinary tract (postrenal). Differential diagnosis between prerenal, renal, and postrenal AKI is necessary, because the therapy is different [4].

2.3.1 Prerenal AKI

Prerenal AKI (30–60%) is essentially the functional and reversible syndrome that results from kidney hypoperfusion due to hypovolemia, low cardiac output, systemic vasodilatation, or intrarenal vasoconstriction. Classic urinary biomarkers, including urinary sodium (Na) and fractional excretion of sodium (FENa), cannot be used in anuric patients and are unreliable after diuretics or hemodialysis administration. New proposed biomarkers, as NGAL and KIM-1, have still limited clinical value because of low specificity and high costs. In this setting DUS with calculation of intrarenal RI can play a crucial role in the differential diagnosis between two most common types of AKI: functional (prerenal) and organic (renal) AKI. The former is characterized by a reduction in renal perfusion and is rapidly reversible if promptly treated, whereas the latter is caused by a direct damage of the renal parenchyma or by the evolution of a prerenal form in ATN and tends to be persistent (Fig. 2.4).

While B-mode echogenicity and parenchymal thickness are nonspecific, a RI value > 0.75 is reported as optimal in attempting differential diagnosis between prerenal AKI and ATN. An RI > 0.80 is even a more reliable indicator of persistent AKI than the common urinary markers and could be a promising tool to predict the reversibility of AKI in critically ill patients [5].

Appraisal of the inferior vena cava collapsibility index (IVC-CI), lung B-lines, and pleural or peritoneal fluid effusions can give an idea of the patient's global hydration status, supporting or confuting the diagnosis of prerenal AKI and eventually directing effective therapy (Fig. 2.5) [6–8].

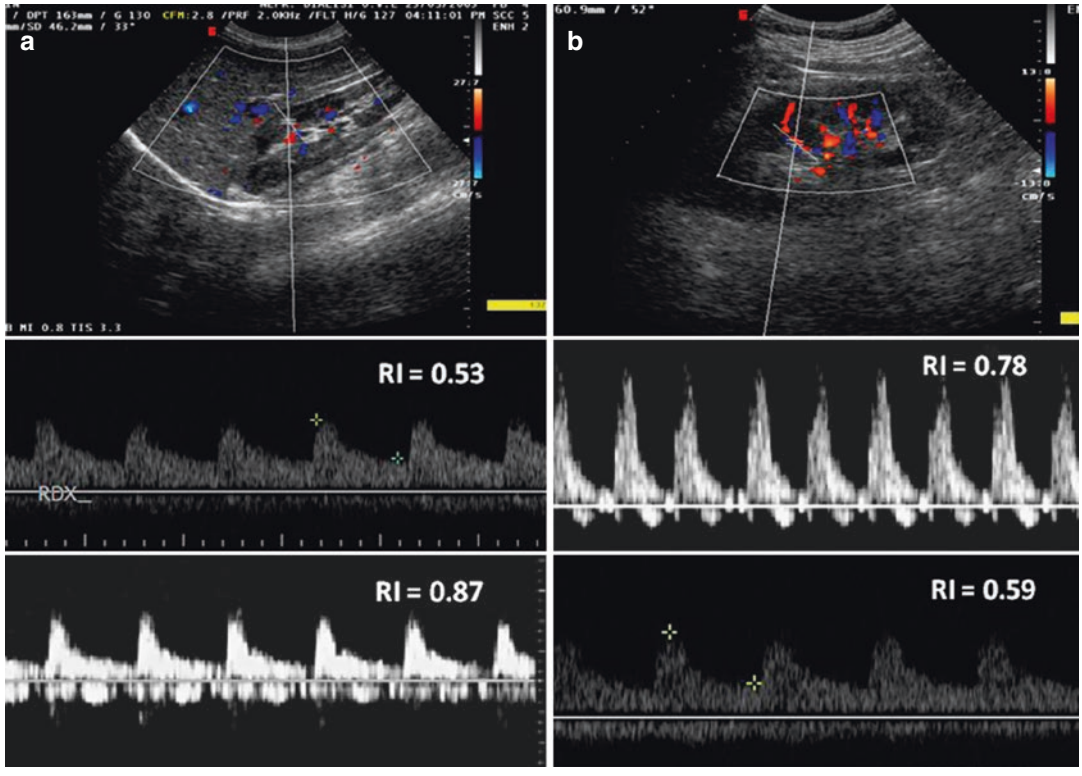

Fig. 2.4 Two cases of AKI followed through RI variation. (**a**) On the left side of the image, a patient treated for transient AKI showed a clinical worsening to persistent AKI despite medical therapy with progressive elevation of RI from 0.53 to 0.87. (**b**) On the right side of the image, an oliguric patient with a remarkable urea and resistive index increase (RI = 0.78) responsive to medical therapy with significative intrarenal hemodynamic improvement (final RI = 0.59)

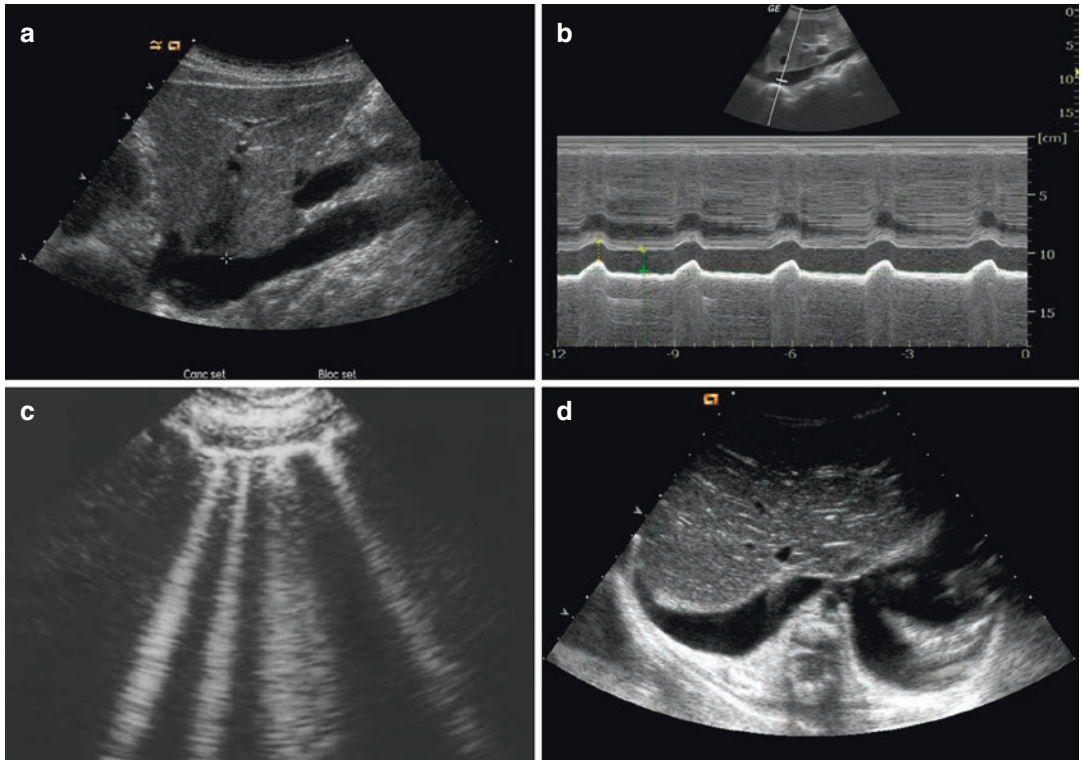

Fig. 2.5 Hydration assessment is important to establish the correct diagnosis and the right therapy for patient with renal injury: (**a**) echo B-mode with longitudinal scan of IVC may give a gross idea of patient hydration status; (**b**) better estimation comes from the measurement of the IVC collapsibility index in M-mode with the following formula: $(D_{max}–D_{min})/(D_{max})$. The patient should always be checked for (**c**) lung ring-down artifacts and (**d**) pleural and peritoneal effusions to complete the clinical picture and administrate the right fluid therapy

2.3.2 Renal AKI

Renal AKI (20–50 %) is caused mostly by ATN, acute interstitial nephritis due to ischemia or nephrotoxic agents (i.e., radiologic contrast agents), glomerulonephritis, and vasculitis.

In acute primitive or secondary glomerulonephritis, kidneys are usually symmetrically involved, sometimes showing a globular appearance with renal sinus compression (Fig. 2.6a). More often they are near normal in size and morphology, with hyperechogenic parenchyma and marked differentiation between the cortex and medulla (Fig. 2.6b) [9].

Color Doppler signals may reveal parenchymal hypervascularization, while RI value is usually normal. In tubulointerstitial diseases instead, parenchymal perfusion is reduced and RI increased. In hemolytic–uremic syndrome, the renal cortex is hyperechogenic with increased corticomedullary differentiation, and DUS shows RI >0.80 with low diastolic flux [10]. In acute lupus nephritis, kidneys may present reduced or increased dimensions and an increased cortical echogenicity with reduced corticomedullary differentiation.

Anyway echo-guided renal biopsy is imperative to diagnose AKI derived by acute glomerular diseases or vasculitis, such as Wegener's granulomatosis or polyarteritis nodosa.

Acute pyelonephritis and renal infarction can both lead to AKI [11]. In the right clinical context, renal ultrasound implemented with microbubble contrast enhancement ultrasound (CEUS) may help in the diagnosis of both, depicting one or more hypovascularized areas into the renal parenchyma, whereas echo B-mode and ECD alone show less sensibility and specificity (Fig. 2.7) [12].

ECD has a central role in the diagnosis of AKI of vascular origin. DUS is essential to diagnose renal artery stenosis (RAS) demonstrating the well-known direct and indirect criteria (Fig. 2.8) [13].

In renal artery thrombosis, ECD provides evidence for flux absence in the main artery and the lack of parenchymal signal or the *tardus–parvus phenomenon* (Fig. 2.8d). Power Doppler may be even more sensitive to a lobular ischemia.

In acute renal vein thrombosis, a rare condition that may lead to renal transplant failure, ECD shows the dilated, uncompressible vein without signal on spectral analysis. Intraparenchymal RI appears increased with the typical diastolic phase inversion [14].

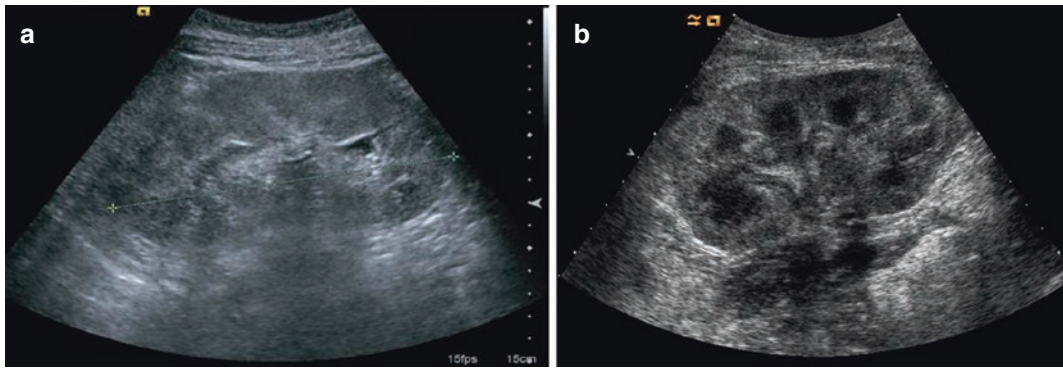

Fig. 2.6 AKI arising from acute glomerulonephritis or systemic vasculitis involving the kidneys. Renal morphology on ultrasound sometimes shows (**a**) a specific globular pattern with central sinus compression and increased volume with width/length ratio >0.5; more often (**b**) kidney's appearance is near normal with hypoechogenic pyramids and marked differentiation between the cortex and medulla

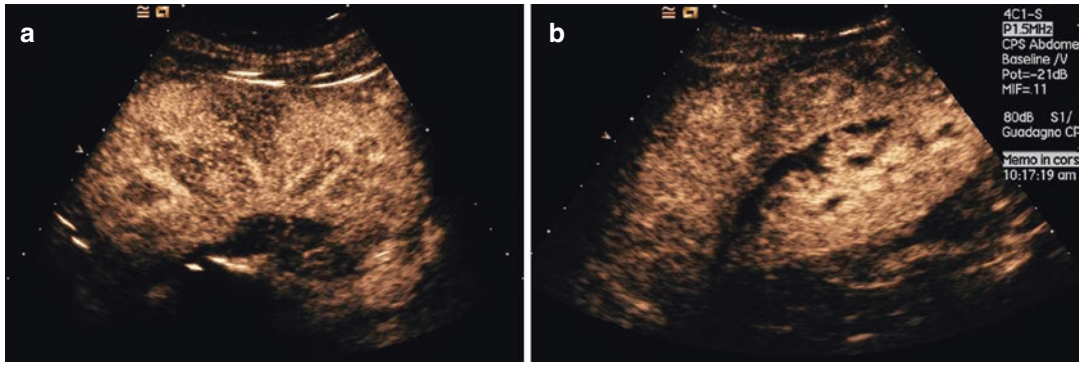

Fig. 2.7 Effectiveness of CEUS as diagnostic tool. (**a**) In acute pyelonephritis microbubbles indentify hypoenhanced areas due to inflammation, edema, and pus collection with performances comparable to CT. (**b**) Renal infarcts appear as triangular or wedge-shaped areas without contrast uptake. Although a high grade of clinical suspicion is necessary, in both renal diseases, CEUS represents an effective diagnostic tool

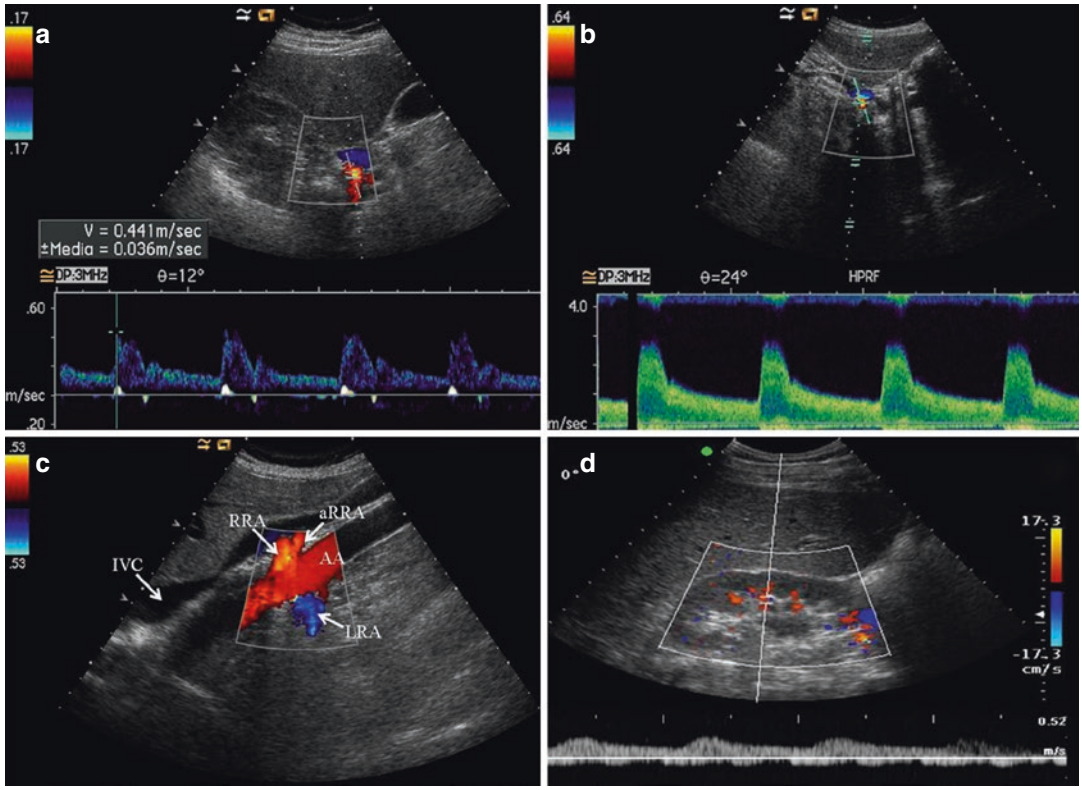

Fig. 2.8 Renal artery stenosis (*RAS*): direct and indirect evaluation through DUS. (**a**) Renal artery (*RA*) normal finding on spectral analysis. (**b**) Increased peak systolic velocity (PSV 288 cm/s) and diastolic velocity (DV 99 cm/s) with marked dispersion of signal on spectral analysis represent main criteria to diagnose RAS. (**c**) Banana peel view showing all together the inferior vena cava (*IVC*), abdominal aorta (*AA*), right renal artery (*RRA*), left renal artery (*LRA*), and accessory right renal artery (*aRRA*). In banana peel view technique, Doppler beam angle is optimal to perform the renal–aortic ratio (*RAR*). (**d**) *Tardus–parvus* phenomenon sampling the interlobar renal arteries, together with marked lateralization of RI, represents a reliable indirect criterion of RAS

2.3.3 Postrenal AKI

Postrenal AKI (1–10 %) is caused by the obstruction of the urinary tract (extrarenal, retroperitoneal tumors or retroperitoneal fibrosis; intrarenal, stones, tumors, tubular obstruction). The obstruction can be monolateral in a mononephrous or in a chronic renal failure patient and is classified in four grades (Fig. 2.9).

Differentiation between a real obstruction and a nonobstructive dilatation can be found through RIs, which are higher in the case of real obstruction because of the increase in pelvic pressure leading to increase in vascular resistances. RI>0.70 in obstructed kidneys can be used to distinguish dilated obstructed from dilated unobstructed kidneys. The diagnostic accuracy of Doppler ultrasonography in assessing renal obstruction may improve after administration of loop diuretics. Post furosemide RI increases in the affected kidney >0.08–0.10 (Fig. 2.10). The ureteral jet phenomenon absence or a marked asymmetry between the two sides can be a further sign of obstruction to keep in mind [15].

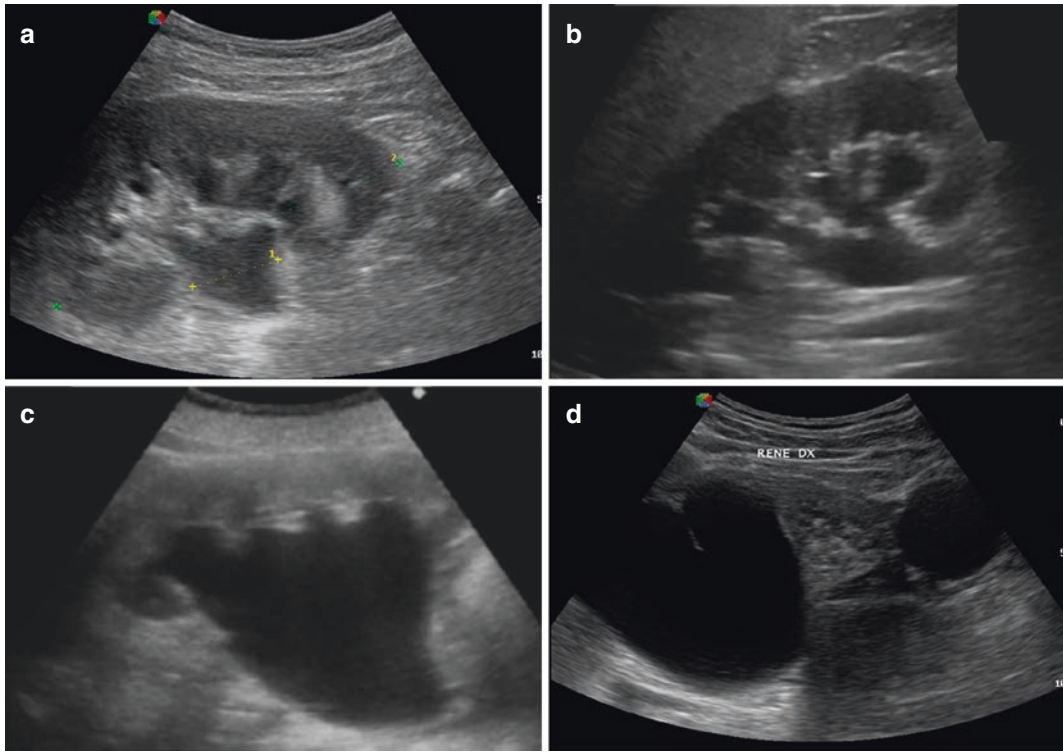

Fig. 2.9 Hydronephrosis classification: (**a**) dilatation of renal pelvis without calyces is classified as grade I; (**b**) the dilatation of the renal pelvis and calyces with attenuated sinus reflex but without parenchymal atrophy is classified as grade II; (**c**) marginal sinus reflex and minor signs of parenchymal atrophy depict grade III; and (**d**) massive dilatations of renal pelvis and calyces with missing borders between renal pelvis and calyces and thin parenchyma are signs of grade IV hydronephrosis

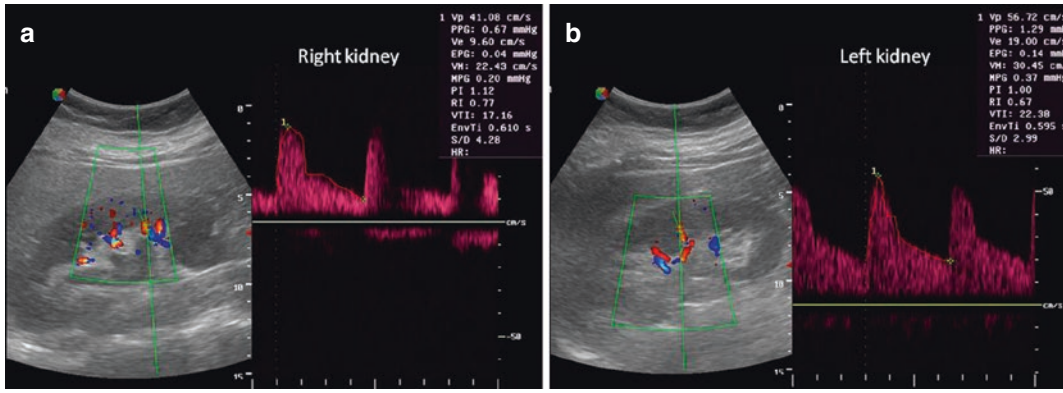

Fig. 2.10 Usefulness of RI in obstructive uropathy. (**a**) Renal RI >0.70 identifies an obstructive dilatation distinguishing it from other nonobstructive causes of renal pelvis dilatation. Indeed about 5 % of obstructive uropathies present without hydronephrosis: in this setting a difference >0.08–0.10 in RI between the two kidneys can help to detect the pathological and the healthy organ. (**b**) Same subject: the left kidney with normal RI (0.67)

2.4 Chronic Kidney Disease (CKD)

According to KDIGO's guideline definition, chronic kidney disease is the clinical syndrome characterized by abnormalities of kidney structure or function, present for >3 months. Markers of kidney damage are albuminuria, electrolyte and acid–base imbalance, urine sediment abnormalities, and structural and ultrastructural abnormalities, respectively, detected by imaging and histology.

Decreased GFR estimated by serum creatinine-based equations is the main criterion to classify CKD; albuminuria is the second one. The best progression predictors of disease are the cause of CKD, age, sex, GFR level at the first diagnosis, level of albuminuria, blood pressure, hyperglycemia, smoking, obesity, dyslipidemia, cardiovascular diseases, and nephrotoxin exposition.

Ultrasound imaging, including both echo B-mode and echo color Doppler (ECD), is the first-line imaging to assess renal structural abnormalities in CKD.

Advanced CKD acts as the common final way in any renal disease and can be easily identified with US. Its typical features are small kidneys, <9 cm in longitudinal diameter and <125 cm^2 in total volume for adult, with the parenchyma thinner than 1 cm (Fig. 2.11a). Anyway diabetic nephropathy, one of the most frequent causes of CKD, prior to terminal failure is most always associated with normal or enlarged kidneys (Fig. 2.11b).

Hyperechogenicity is another nonspecific but important finding in CKD evaluation. When the ultrasonography machine operates in B-mode, it produces a grayscale image in which returning echoes from underling tissues are represented as bright dots. The strength of reflected echoes is processed by the software and displayed as brightness intensity. Renal parenchymal echogenicity is usually classified in 4° (from 0 to 3) in comparison with adjacent liver parenchymal echogenicity. Diseased kidneys in general show increased echogenicity that is correlated to global sclerosis and tubular atrophy. Indeed this parameter is somehow subjective because also normal aging is related to increase in cortical echogenicity. Normal children and young adults usually show evident hypoechoic renal pyramids, while elders typically lose the corticomedullary differentiation.

Furthermore when renal medulla (inner portion of the kidney) appears brighter than normal, this can be the marker of a metabolic, endocrine, or storage disorder bringing about to chronic kidney disease independently of age. Lysosomal storage disorders, such as Gaucher's disease, gout nephropathy, or nephrocalcinosis by different causes (primary hyperparathyroidism, renal tubular acidosis), are some of the most common origin of this appearance (Fig. 2.12).

Renal outline is a major feature to depict kidney's ultrasound appearance. Chronic pyelonephritis with impaired renal function is frequently associated with reduced renal volume and renal scars that traverse the parenchyma near to a calyceal ectasia (Fig. 2.13) [16]. Instead in chronic ischemic kidney, reduced renal volume is associated with the presence of typical hyperechoic wedge-shaped scars.

A further criterion separating normal from abnormal kidneys is renal perfusion. The renal resistive index (RI = peak systolic velocity – telediastolic velocity/peak systolic velocity) is widely used sampling the interlobar arteries to assess parenchymal perfusion. The RI is increased in hypertensive nephropathy and correlates to the histological severity of nephrosclerosis and to CKD in hypertensive patients. The impaired microcirculation due to atherosclerosis, hypertension, and many other risk factors leads to increased difference between PSV and TDV, estimating an increase in vascular impedance [17]. Furthermore, RI >0.80 in the case of renal artery stenosis has a negative prognostic value for revascularization. Glomerular hyperfiltration represents the first reversible stage of diabetic nephropathy leading to chronic kidney disease. RI <0.55 and total renal volume >400 ml are both regarded as possible marker of hyperfiltration in diabetic patients. On the other hand, in diabetic patients with serum creatinine as high as 1.4 mg/dl and proteinuria, RI shows a positive correlation to creatinine clearance and proteinuria.

Although there is no ultrasonographic sign for glomerulonephritic disease, a renal

segmental artery RI value >0.80 acts as a major prognostic sign for progression. In lupus nephritis, a RI >0.70 correlates to interstitial fibrosis and glomerulosclerosis, but not to disease activity [18].

Color signals by using the right pulse repetition frequency scale can give an idea of kidney perfusion: nephrosclerotic kidney usually shows less signals than normal with a pulsatory pattern related to high vascular impedance (Fig. 2.14).

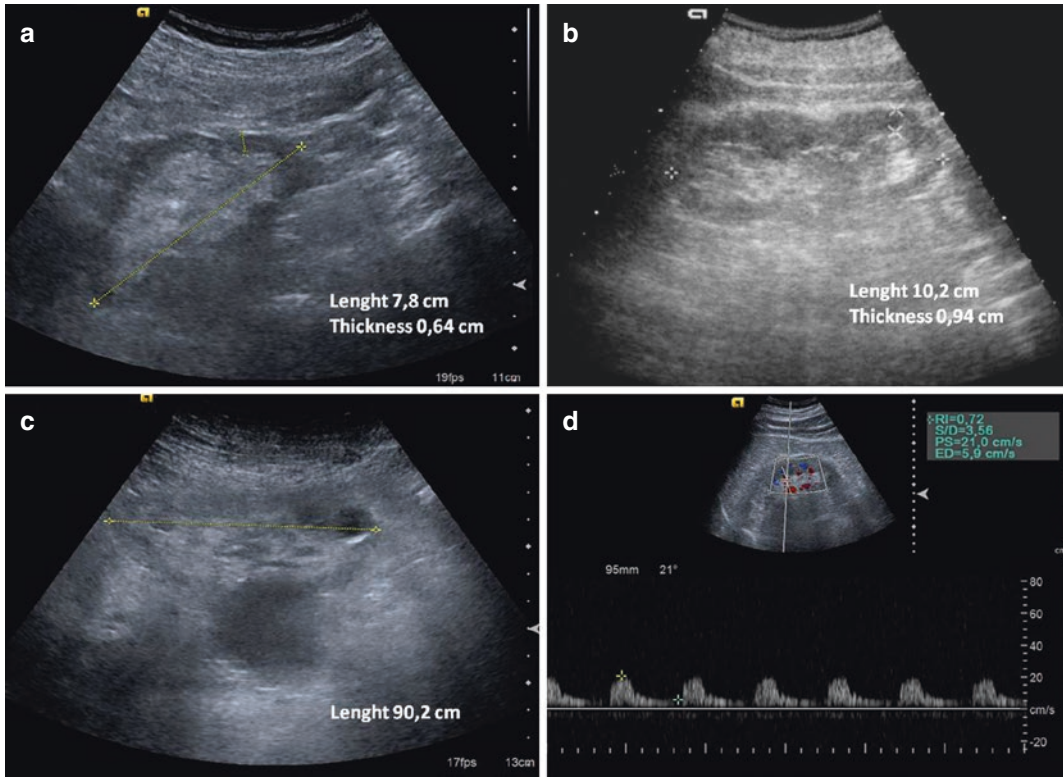

Fig. 2.11 CKD sonographic features. (**a**) Longitudinal length <9 cm and parenchymal thickness <1 cm easily identify the final pattern of CKD, together with loss of corticomedullary differentiation and renal sinus lipomatosis. (**b**) In diabetic nephropathy, before ESRD, kidneys appear near normal or enlarged with quite good corticomedullary differentiation; some vascular scar may alter the renal outline. (**c**) Chronic kidneys often show acquired cysts, especially in dialysis-treated people. (**d**) RI >0.70 is a common finding in CKD, reflecting the impaired renal microcirculation due to atherosclerosis, hypertension, and other risk factors

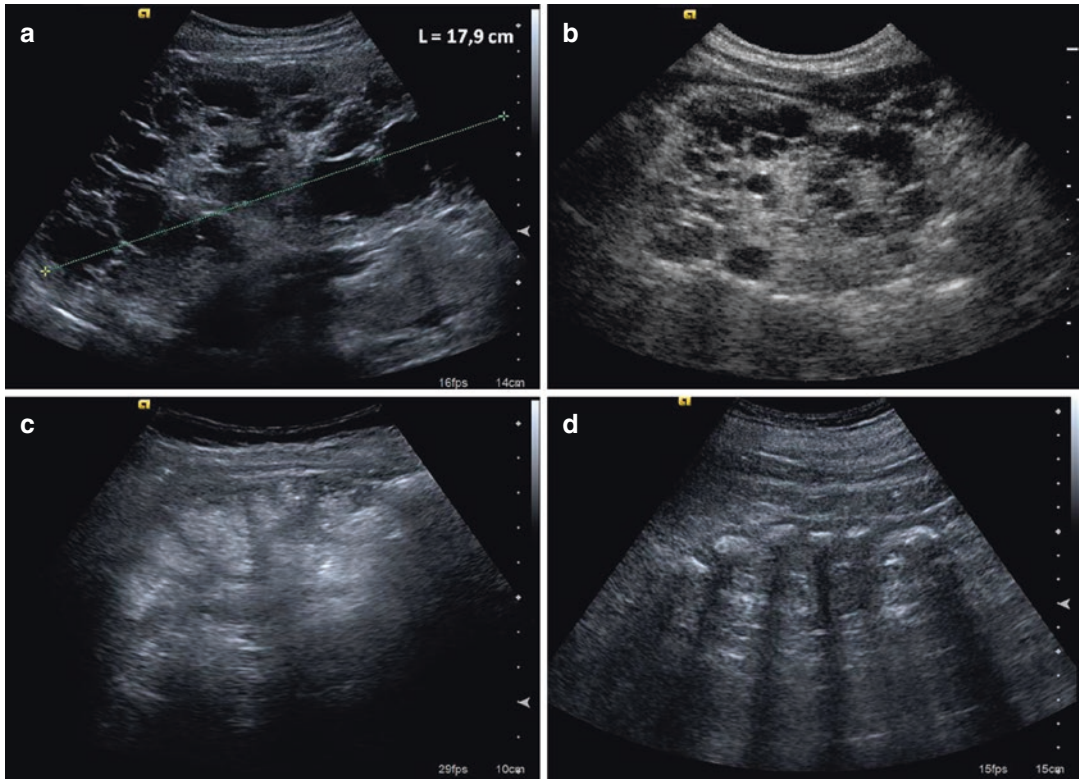

Fig. 2.12 Structural abnormalities as markers of chronic kidney damage. (**a**) Adult polycystic kidney disease (*ADPKD*) is an autosomal dominant progressive disorder characterized by cyst formation and enlargement in the kidney, diagnosed by ultrasound as multiple anechoic cysts impairing adult renal parenchyma. (**b**) In multicystic dysplastic kidney (*MDK*), congenital cysts derive by abnormal metanephric differentiation, and the affected kidney is nonfunctional. (**c**) Medullary sponge kidney (*MSK*) is characterized by calcium deposits within kidney parenchyma and inverted corticomedullary US pattern. (**d**) Frank nephrocalcinosis derived from distal renal tubular acidosis

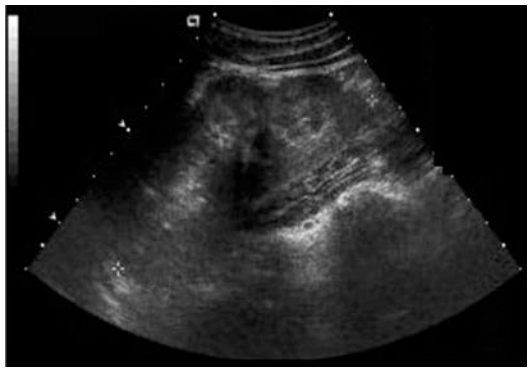

Fig. 2.13 CKD secondary to chronic pyelonephritis. Vesicoureteral reflux is frequently an origin of a CKD due to infection relapse. Renal outline is characterized by one or more scars over blunted calyces

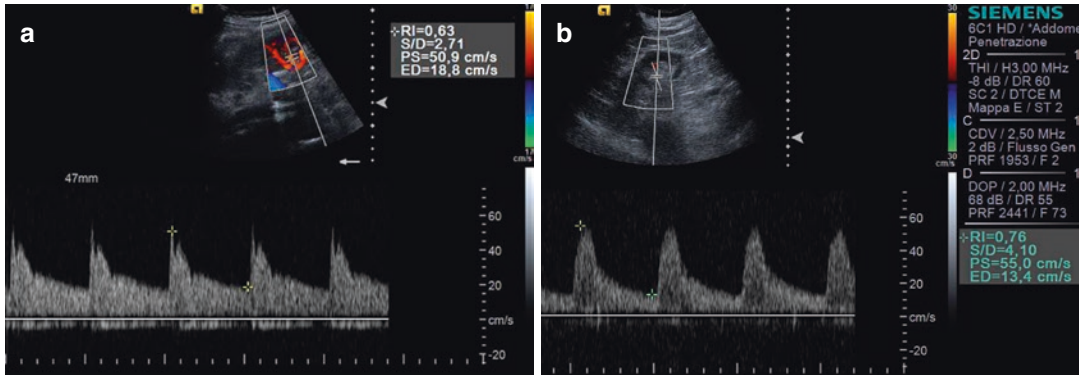

Fig. 2.14 Renal resistive index in a normal kidney and in chronic hypertensive nephropathy. (**a**) RI shows usually a well-represented diastolic phase, an expression of the low-resistance pattern into normal kidney. (**b**) Impaired microcirculation due to hypertension, atherosclerosis, and other risk factors increases resistances and dramatically reduces intraparenchymal flow in diastolic phase

Bibliography

1. Faubel S, Patel NU, Lockhart ME, Cadnapaphornchai MA (2014) Renal relevant radiology: use of ultrasonography in patients with AKI. Clin J Am Soc Nephrol 9(2):382–394
2. Ozmen CA, Akin D, Bilek SU, Bayrak AH, Senturk S, Nazaroglu H (2010) Ultrasound as a diagnostic tool to differentiate acute from chronic renal failure. Clin Nephrol 74:46–52
3. Granata A, Zanoli L, Clementi S, Fatuzzo P, Di Nicolò P, Fiorini F (2014) Resistive intrarenal index: myth or reality? Br J Radiol 87(1038):20140004. doi:10.1259/bjr.20140004, Epub 2014 Apr 15
4. Nori G, Granata A, Leonardi G, Sicurezza E, Spata C (2004) The US color Doppler in acute renal failure. Minerva Urol Nefrol 56(4):343–352
5. Platt JF, Rubin JM, Ellis JH (1991) Acute renal failure: possible role of duplex Doppler US in distinction between acute prerenal failure and acute tubular necrosis. Radiology 179(2):419–423
6. Di Lullo L, Floccari F, Granata A, D'Amelio A, Rivera R, Fiorini F, Malaguti M, Timio M (2012) Ultrasonography: Ariadne's thread in the diagnosis of the cardiorenal syndrome. Cardiorenal Med 2(1):11–17
7. Fiorini F, Zanforlin A, D'Amelio A, Battaglia Y, Zamboli P, Granata A (2014) Chest ultrasound in nephrology. G Ital Nefrol 31(3):1–11. pii: gin/31.3.4
8. Prencipe M, D'Amelio A, Aucella F, Granata A, Fiorini F (2012) Ultrasonography in the hyperhydrated patient. G Ital Nefrol 29(Suppl 57):S58–S64
9. Quaia E, Bertolotto M (2002) Renal parenchymal diseases: is characterization feasible with ultrasound? Eur Radiol 12(8):2006–2020
10. Scholbach TM (2001) Changes of renal flow volume in the hemolytic-uremic syndrome – color Doppler sonographic investigations. Pediatr Nephrol 16(8):644–647
11. Granata A, Andrulli S, Fiorini F, Basile A, Logias F, Figuera M, Sicurezza E, Gallieni M, Fiore CE (2011) Diagnosis of acute pyelonephritis by contrast-enhanced ultrasonography in kidney transplant patients. Nephrol Dial Transplant 26(2):715–720
12. Granata A, Zanoli L, Insalaco M, Valentino M, Pavlica P, Di Nicolò PP, Scuderi M, Fiorini F, Fatuzzo P, Bertolotto M (2015) Contrast-enhanced ultrasound (CEUS) in nephrology: has the time come for its widespread use? Clin Exp Nephrol 19(4):606–615
13. Radermacher J, Chavan A, Bleck J, Vitzthum A, Stoess B, Gebel MJ, Galanski M, Koch KM, Haller H (2001) Use of Doppler ultrasonography to predict the outcome of therapy for renal-artery stenosis. N Engl J Med 344(6):410–417
14. Granata A, Clementi S, Londrino F, Romano G, Veroux M, Fiorini F, Fatuzzo P (2014) Renal transplant vascular complications: the role of Doppler ultrasound. J Ultrasound 18(2):101–107
15. Granata A, Andrulli S, Bigi MQ, Pozzoni P, Fiorini F, Logias F, Figuera M, Basile A, Fiore CE (2009) Predictive role of duplex Doppler ultrasonography in the diagnosis of acute renal obstruction in patients with unilateral renal colic. Clin Nephrol 71(6):680–686
16. Granata A, Floccari F, Insalaco M, Clementi A, Di Lullo L, D'Amelio A, Zamboli P, Logias F, Romano M, Fiorini F (2012) Ultrasound assessment in renal infections. G Ital Nefrol 29(Suppl 57):S47–S57
17. Radermacher J, Ellis S, Haller H (2002) Renal resistance index and progression of renal disease. Hypertension 39(2 Pt 2):699–703
18. Conti F, Ceccarelli F, Gigante A, Barbano B, Perricone C, Massaro L, Martinelli F, Spinelli FR, Giannakakis K, Valesini G, Cianci R (2014) Ultrasonographic evaluation of renal resistive index in patients with lupus nephritis: correlation with histologic findings. Ultrasound Med Biol 40(11):2573–2580

Ischemic Nephropathy

3

Antonio Granata, Elnaz Rahbari, Dario Galeano, and Pasquale Fatuzzo

3.1 Introduction

Ischemic nephropathy or renal ischemic disease is a clinical condition characterized by insufficient renal blood supply, followed by anatomical, functional, and hormonal changes that make progressive reduction in glomerular filtration until complete loss of renal function. The main cause of renal blood reduction is a one or both renal artery stenoses, resulting from atherosclerotic renal artery stenosis or fibromuscular dysplasia (FMD).

The most common etiology of renal artery stenosis (RAS) is an atherosclerotic renal artery stenosis (ARAS) that typically involves the ostium or proximal one-third of the renal artery [1].

Chronic kidney disease is a result of artery narrowing that can be reversible or evitable if diagnosed in early stage. In the last 10 years, many authors found in the atherosclerotic renal artery stenosis (ARAS) a significant cause of terminal uremic, with variable incidence between 5 and 22 %.

Less common renal artery stenosis (RAS) is caused by FMD, a rare vascular pathology that predominantly affects middle-aged women (from the third to fourth decade of life). FMD commonly involves the media layer of the arterial wall and medial tract of the artery, with classic aspect, the "string of bead." The sign is caused by areas of relative stenosis alternating with small aneurysm.

The basic characteristic of ischemic nephropathy is the absence of significant symptoms. The average of prevalence is around 5 % in general population, although a higher prevalence due to unrecognized pathology is conceivable, especially in some groups of patients such as severe hypertensive or diabetic hypertensive. Often, RAS comes out in autopsy finding of the patients whose exitus was provoked by stroke or acute myocardial infarction, with a percentage higher than 75 % of the cases and prevalence between 10 and 34 %.

It is important to establish diagnostic criteria that allow us to identify patients with ischemic nephropathy by research of risk factors and pathognomonic signs.

Main clinical findings are reported in Tables 3.1 and 3.2, which presence makes suspect of ischemic nephropathy. There are no available reliable predictable data for each sign and symptom; therefore in the case of clinical

A. Granata (✉) • D. Galeano
Nephrology and Dialysis Unit,
"S. Giovanni di Dio" Hospital,
Agrigento, Italy
e-mail: antonio.granata4@tin.it

E. Rahbari • P. Fatuzzo
School of Nephrology, University of Catania,
A.O.U. "Policlinico- Vittorio Emanuele",
Catania, Italy

P. Martino, A.B. Galosi (eds.), *Atlas of Ultrasonography in Urology, Andrology, and Nephrology*,
DOI 10.1007/978-3-319-40782-1_3

suspicion, the choice of diagnostic methods depends on the appropriated interpretation of detected symptoms.

The ideal imaging method for diagnosing of ischemic nephropathy should allow identifying the main renal artery as well as the accessory branches, to localize the stenosis site, to identify significant hemodynamic lesion, to suggest the type of the treatment (medical therapy or angioplasty), to identify the associated pathology (renal mass or abdominal aorta aneurysm), and to distinguish chronic ischemic damage induced by nephroangiosclerosis or thromboembolism [2, 3].

The method should be able to prove or exclude the diagnosis of RAS or eventually to evaluate if ischemic nephropathy is due to an involvement of atherosclerosis without renal artery stenosis [4, 5].

Angiography, which in the past was the gold standard test for arterial diagnosis, is an invasive method, expensive with some severe complications such as adverse reaction to iodinated contrast, dissection, and atheroembolism.

For all these reasons, angiography is not more used like screening method, but like therapeutic instrument. In the last years, many less invasive imaging methods were introduced, such as renal scintigraphy with captopril test, Doppler ultrasound, computed tomography (CT), or magnetic resonance angiography (MRA). In many centers, Doppler ultrasound was accepted as the main screening instrument for identifying RAS [6].

Table 3.1 The main risk factors linked to suspect of ischemic nephropathy

Age >55 years (considering that ischemic nephropathy predominantly interests to age >55/60 years old)
Positive family history for coronary disease (mainly in the male patients in the age >50 years old)
Smoking
Hypercholesterolemia
Obesity
Diabetes mellitus (DM)
Atherosclerotic vasculopathy

Table 3.2 Indicative sign of renal ischemic pathology

Renal asymmetry
Severe hypertension state after 55 years old
Rapid worsening of arterial hypertension previously well controlled
Sudden appearance of severe hypertensive state that may be treatment resistant to medical therapy, defined as an inability to reach a good control of pressure in a patient who is under full-dose antihypertensive therapy with at least three drugs
Malignant hypertension or hypertension with evidence of acute renal damage or acute renal insufficiency
Recurrent episodes of pulmonary edema without anomaly or heart dysfunction
Hypertensive retinopathy III or IV
Continuous abdominal systolic-diastolic bruit (can be inaudible in the case of subtotal stenosis), it is a sign that presents a positive predictive value and especially is related to renovascular hypertension
A rise in serum creatinine following the administration of ACEI or ARBs
The presence of the pathology related to atherosclerosis or peripheral vasculopathy disease (e.g., femoral iliac stenosis, intermittent claudication, etc.)

3.2 Technical Study of the Renal Artery

Depth of the arteries, respiration movement, and intestinal meteorism are the factors that can complicate the exam. To decrease the intestinal meteorism, it is important to perform examination in the early morning time, after 12 h of fasting. In clinical practice, the duration of exam is about 15–20 min and depends on the experience of the operator, the number of performed exams, and the ultrasound platform performance.

If the exam would be lasting for more than 20–30 min, it should be repeated with adequate intestinal preparation; otherwise the operator's performance tends rapidly to decrease.

The procedure starts with the patient in supine position and the head upward of 30° in order to relax the abdominal wall with the use of multifrequency convex probe (2.5─6.0 MHz). Numerous scans let us study the abdominal aorta (AA) and renal artery (RA). Both of the RA arise off the anterolateral side of the AA (Fig. 3.1). Generally in correspondence of the superior border of the second lumbar vertebra, immediately 12 cm below the superior mesenteric artery, this artery is divided to form the segmental arteries that irrigate different segments of the kidney. Segmental arteries divide within the renal sinus to form the interlobar arteries which originate the arcuate arteries located between the cortex and medulla. Arcuate arteries give off interlobular or cortical radial artery branches.

Two principal scans to study the RA are sagittal and coronal scan through anterior and lateral abdominal wall. Scan choice depends on the anatomical location of renal vascular system to be investigated.

In the most cases, anterior scan is used to evaluate proximal portion of the RA, while lateral scan with the patient in lateral decubitus can be used to evaluate intrarenal vascularization and main branches of the RA (Fig. 3.2). Each scan has limits that depend on the patient's habits and other many parameters such as ability to breath hold.

The right RA originates from lateral antrum of the AA and passes behind the inferior vena cava (IVC) and the right renal vein to reach the renal hilum. Indeed in transversal scan, proximal portion of the right RA is deep and perpendicular to ultrasound's wave and difficult to intonate with an angle lesser than 60°. In this condition, the best approach is subcostal view with the patient in left lateral decubitus position. In fact, blood flow of the RA in this scan runs parallel over the ultrasound's wave [7] (Fig. 3.3).

Additional aid in locating the RA is given by the "banana peel" view, which consists of imaging the IVC and AA with a longitudinal scan and moving anterior to posterior direction until the RA arising from the AA is identified (Fig. 3.4). This approach is particularly useful to insonate ostial areas, where most stenosis occur in elderly patients. The patient is in lateral decubitus position opposite from the vessel being examined, and the transducer is oriented longitudinally [7, 8]. When the AA and RA are detected together, it can be the appearance of half-peeled banana with skin curved alongside. This scan lets to detect the RA with optimal angle (<60°) and to notice the presence of accessory RA branches, approximately in 20–30 % of the patients (Fig. 3.5) [7, 9].

The left RA tends to originate from the posterolateral of the aorta and courses posteriorly and obliquely to the lumbar region; an aid to locating the left RA is to first identify the left renal vein, which is usually large and easy to find. Once the vein is identified, the artery will often be apparent as a smaller vessel directly behind it, coursing in the opposite direction. The inferior mesenteric artery (IMA) origin should not be mixed up for left RA origin; in fact the IMA tends to have a high-resistance pattern, which is quite different from the low-resistance pattern of the left RA [7]. The IMA also originates much lower than the left renal artery, unless arises from an atypical location.

Another approach to image the left RA is placing the patient in right lateral decubitus and locate the RA between the kidney and AA with a very close angle. The lateral decubitus position is essential, because the kidney acts as its own window [8].

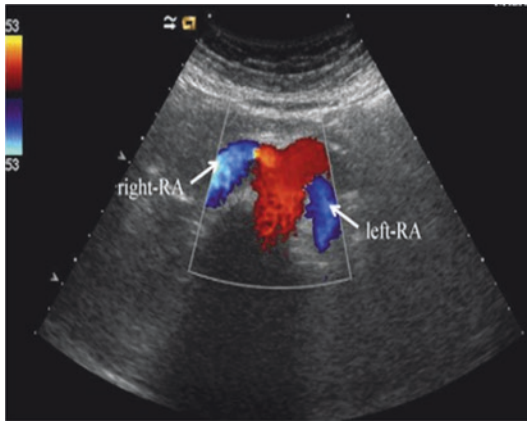

Fig. 3.1 Renal arteries via transverse anterior abdominal approach. Both renal arteries rise off the anterolateral side of the aorta. The *right RA* passes behind the inferior vena cava (*IVC*) and the right renal vein to reach the renal hilum. The *left RA* tends to originate from the posterolateral side of the aorta and courses posteriorly and obliquely to lumbar region reaching the renal hilum

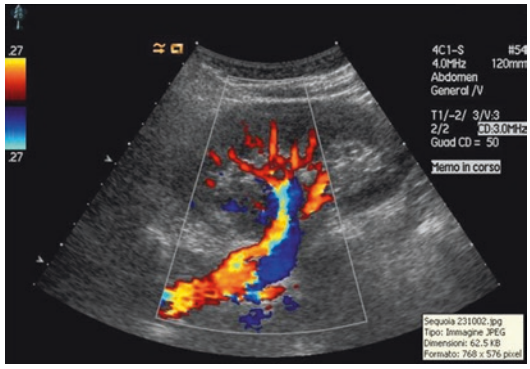

Fig. 3.2 Kidney's lateral scan identifying intrarenal vascularization, main branches, and the renal artery. The lateral decubitus position is essential, because the kidney itself acts as a sonographic window making visible intrarenal vascularization, main branches of the renal artery, and the renal artery. Doppler angle is optimal and US beam is pointed in the line of arterial flow

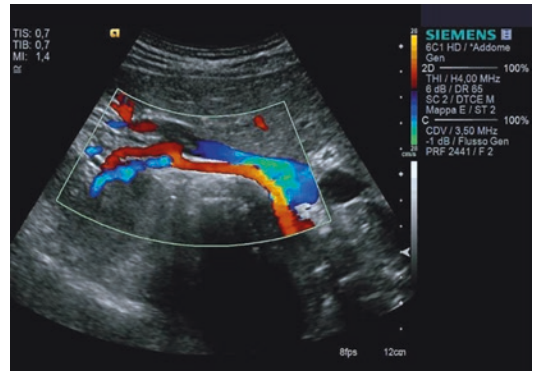

Fig. 3.3 The right renal artery in subcostal view. A transverse anterior abdominal approach with the patient in lateral decubitus can help in recognizing of the renal artery behind the corresponding vein. RA flow is in the parallel direction to the Doppler beam

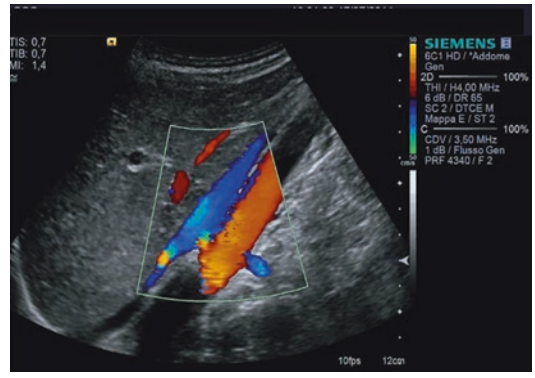

Fig. 3.4 "Banana peel" view. The patient is turned to the opposite decubitus position from the vessel we want to examine, and transducer is oriented longitudinally. The operator locates the aorta first and then moves the transducer in anterior to posterior direction until renal arteries are identified. The right RA moving toward the probe in *red* and the left RA moving away in *blue* color confer to this image the half-peeled banana aspect. Doppler beam angle is close to zero and gives optimal vision of ostial region. Moreover, this maneuver allows precise calculation of RAR and clear identification of accessory renal arteries

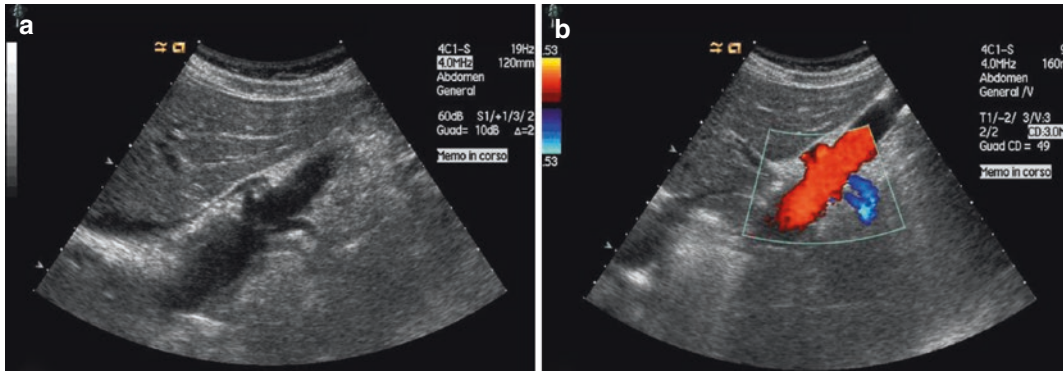

Fig. 3.5 Accessory renal artery. (**a**) B-mode imaging of double left RA: when the main renal artery diameter is less than 4.5 mm, the presence of the accessory RA is extremely possible. Accessory arteries are seen approximately in 25–30 % of the cases, but their stenosis occur in less than 1 % of cases. (**b**) Color Doppler enhances the vision of double right (in *red color*) and left (in *blue color*) renal arteries

3.3 Color Doppler Study

The current platform ultrasound lets to find the RA in more than 90 % of patients, with overcoming problems caused by the obesity or intestinal meteorism. Direct visualization of both main RAs is possible in 84 % of the cases, while visualization of the right RA or left RA is possible in 91 % and in 85 % of the cases. In 5 % of cases, lack of diagnosis is related to the total occlusion of the RA without intrarenal Doppler signals.

The origin of the RA especially appears in B-mode station with successive modification in box color: with correct adjustment of Doppler function such as pulse repetition frequency (PRF), wall filters, and gain, colorimetric map should be uniform and without artifacts.

The flow of the first segment of the right RA is directed toward the transducer depicted in red, while immediately after, the color changing to blue shows the reverse direction of the blood flow that directed posteriorly, away from the probe.

If the origin of the RA is imaged in the longitudinal section, the right RA passes directly toward the transducer so the color is red, whereas the left RA is directed away from the transducer and the color is blue.

The normal waveform of the main renal artery demonstrates a low-resistance pattern similar to that found in all parenchyma (Fig. 3.6). Although the main RA may be imaged from an anterior approach, the deep location in the abdomen often limits the resolution of the transducer that may be applied.

Lower-frequency transducers will have better sonographic penetration, but there is a trade-off of decreased spatial resolution. The highest-frequency transducer that allows good demonstration of arterial waveforms is preferable. Doppler gain should be optimized to detect flow by increasing the gain to a level just below color artifact visualization in adjacent structures.

Pulse repetition frequency (PRF) should be carefully adjusted to avoid to fall in frequency ambiguity if the PRF is very low (overturning of the superior portion of the V/t curve) or space ambiguity if the PRF is very high (the presence of the "ghost vessels").

Volume sample dimension should be set including the entire artery lumen and angled with the direction of the flow. The angle of insonation should be maintained at 60° or less [7, 8, 10]. The PRF depends on the angle between the vessel and the ultrasound (US) beam and even depends on the frequency of transducer used. If the course of the main RA is well recognized, velocity angle corrected can be calculated.

The peak systolic velocity (PSV) in the main RA and its branches should be less than 100 ± 20 cm/s [15] and decreases slowly in the intrarenal arteries as they branch into the kidney.

The resistive index (RI) that measures the degree of intrarenal arterial impedance is calculated by this formula [PSV – telediastolic velocity]/PSV. RI values in healthy subjects show significant dependence to age and area of the sampling. It is suggested to determine RI in interlobar artery level because it lets to get the optimal color signal and because it is easily reproducible. The normal RI values in the main RA are higher in the hilar region (0.65 ± 0.17) than in the more distal small arteries, and they are lowest in the interlobar arteries (0.54 ± 0.20). Some renal pathology such as nephroangiosclerosis, hypertension, tubular interstitial disease, diabetes mellitus, and severe bradycardia can cause an increase of RI, even in the presence of serum creatinine in the normal range [11]. In clinical practice 0.7 is the cutoff distinguishing between normal and pathologic state.

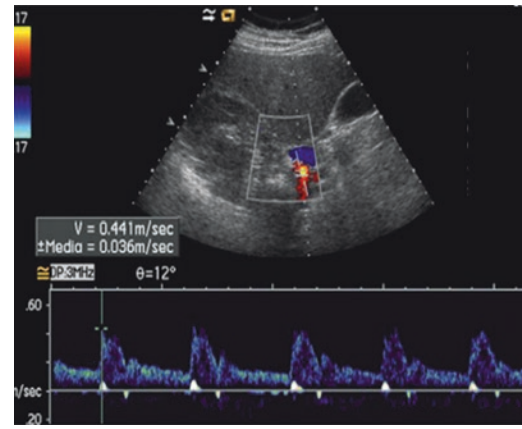

Fig. 3.6 Normal features of the renal artery. Duplex ultrasound image of the right renal artery in a normal subject. At the end of systolic spike is a recognizable small spike called early systolic peak (ESP)

3.4 Doppler Criteria for Diagnosis of RAS (Renal Artery Stenosis)

Doppler US criteria of RAS can be divided into two groups:

(a) Direct criteria or extrarenal (Doppler changes in the site of stenosis)
(b) Indirect criteria or intrarenal (flow changes distal to the site of stenosis)

3.5 Direct Criteria or Extrarenal (Direct Evaluation of the Stenosis)

RAS is defined by the presence of stenosis greater than 60 % of vessel diameter. Stenosis causes a significant reduction in renal blood flow.

Four direct criteria allow Doppler ultrasound diagnosis of RAS at the site of stenosis:

1. Peak systolic velocity (PSV) increase: velocity higher than 180 cm/s suggests the presence of a significant (>60 %) stenosis (Fig. 3.7). Telediastolic velocity (TDV) higher than 150 cm/s suggests the presence of stenosis >80 %.

   Cutoff value of 180 cm/s and more than 50 % reduction in RA diameter give a sensitivity of 96.7 % and a specificity of 98 % [12], while cutoff value of 200 cm/s and more than 60 % reduction in diameter give a sensitivity of 91 % and a specificity of 75 % [12, 13].

   PSV >180 cm/s has been suggested as the optimal threshold to diagnose a 60 % reduction of the RA diameter [14]. Positive predictive value (PPV), negative predictive value (NPV), and accuracy are, respectively, 60 %, 95 %, and 79 %, while PSV >200 cm/s gives a sensitivity of 97 %, specificity of 72 %, PPV of 81 %, and NPV of 95 % [13, 14]. In recent meta-analysis PSV was the best predictor of RAS, with a sensitivity of 85 % and a specificity of 92 % [7].
2. Renal/aortic ratio (RAR): the ratio between PSV values in the site of the stenosis and PSV values in abdominal aorta prerenal tract is predictive of RAS when greater than 3.5. The use of RAR instead of the absolute PSV is preferable since hypertension itself can cause an increase in PSV that can cause a reduction of global diagnostic accuracy [8]. Normal value of RAR is less than 3.5, but RAR should not be used for the large numbers of false positive if PSV obtained in the prerenal abdominal aorta is abnormally low (less than 40 cm/s). A RAR ≥3.5 identifies hemodynamically significant lesion with sensitivity and specificity, respectively, of 91–92 % and 75–95 % [15, 16].

In another study [17], a diagnosis of severe RAS based on RAR more than 3 gives a sensitivity of 77 %, specificity of 90 %, PPV of 90 %, and NPV of 76 %. With the use of RAR >3.5, sensitivity rises to 91 % [18]. Technical failure is reported because of severe obesity, older platform use, marked abdominal gas, and low blood flow in the RA secondary to chronic renal failure.

The renal-segmental ratio (RSR), a ratio of PSV measured in the renal artery and PSV measured in the segmental artery, is the best reported parameter to identify RAS ≥50 %, showing a sensitivity of 93.33 % and specificity of 89.47 %. [19]. Another parameter characterized by high sensitivity and specificity (88 %) [13] is the relation between PSV in the stenosis site and PSV in the interlobar artery.

3. The renal-renal ratio (RRR) is the rate between PSV in RA proximal or mid-segment and PSV in RA distal segment. The PSV increases at the stenosis site, and the PSV decrease in distal segment is proportional to the degree of the stenosis. Intra-examination variability was good (correlation 0.86, coefficient 8.95), while the best cutoff value for the RRR was 2.7 [12]. The RRR values in the comparison with other method parameters (PSV >200 cm/s and RAR >3) demonstrated a sensitivity of 97 % and specificity of 96 %. One of the limitations of this study was that evaluation "in the static analysis" of only the main RA because these vessels have a more important role in renovascular disease and are treatable by endovascular therapy, while the results obtained with other parameters (PSV and RAR) included accessory RA detected in the arteriography in other studies [7, 15, 20].

To obtain the high-accuracy diagnosis of the RAS >50 % should be determined with three hemodynamic parameters (PSV, RAR, RIR, or RSR). In fact, the single determination of the PSV in the AA and RA can decrease the accuracy of RAR, because they can be affected by many other factors.

The PSV stenosis/post-stenosis is little affected by PSV in abdominal aorta or by the proportional change in PSV in the RA trunk and intrarenal branches so the use of that ratio overcomes the limitation of RAR. Accessory RA is common, seen approximately in 25–30 % of the cases. Even that they are not always evaluable in the color Doppler [17].

Angiography study showed that the RA caliber of the single RA originated from the AA in adults is variable from 5 to 10 mm, with the inferior values in the women. If the diameter of the RA estimated with B-mode US is 4.65 mm or less, the presence of the accessory RA is possible, with a sensitivity and specificity of 80 % and 80.5 %. In practice if the diameter of the RA is 4.5 mm, the presence of the accessory RA is extremely possible with a specificity of 98.8 %, while if the diameter is more than 5.5 mm, none verify accessory RA with the specificity of 100 % [18].

Detection of the RA without Doppler signal suggests complete renal occlusion, while the visualization of the color artifacts such as aliasing at the site of the stenosis or the turbulence of the Doppler evaluation indicates the presence of the significant stenosis upstream. Usually, these two patterns are the first immediate sign [13].

Criteria for the classification of RAS are listed in Table 3.3, while Table 3.4 summarizes the principal parameters used in RA stenosis diagnosis.

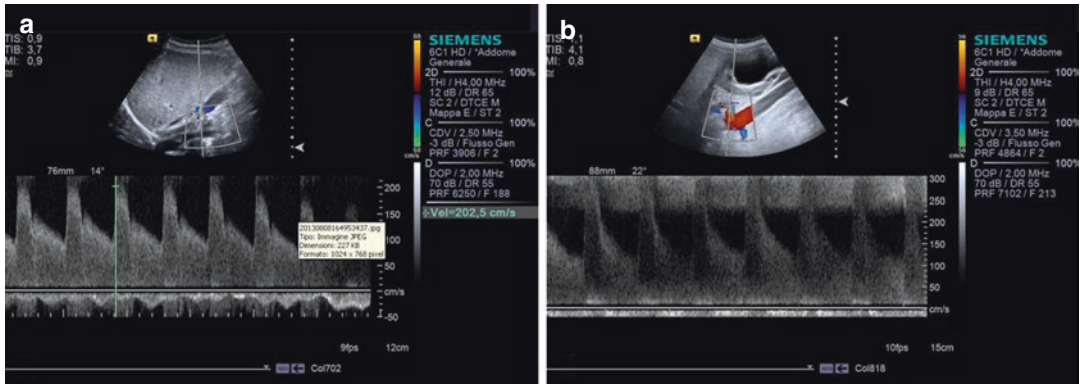

Fig. 3.7 Renal artery stenosis (*RAS*): color Doppler features. (**a**) Spectral analysis highlights the marked PSV (>180 cm/s) and TDV (>120 cm/s) increases with spectral broadening. (**b**) In addition to PSV and TDV, increase is possible to measure RAR (>3.5)

Table 3.3 Criteria for the classification of RA stenosis with color Doppler by Zieler and Strandness (*Am J Hypertens*, 1996)

Renal artery diameter reduction	Renal artery PSV	RAR
Normal[a]	<180 cm/s	<3.5
<60 %	>180 cm/s	<3.5
≥60 %	>180 cm/s	≥3.5
Occlusion	No signal indeterminable	

[a]PSV = 100 ± 20

Table 3.4 Principal parameters used in the diagnosis of the RA stenosis

Direct or extrarenal Peak systolic velocity (PSV)
Renal/aortic ratio (RAR)
Renal-renal ratio (RRR) Renal-intralobar ratio (RIR)
Renal-segmental ratio (RSR)
Indirect or intrarenal Systolic acceleration index (AI)
Systolic acceleration time (AT)
Resistive index = v.n. <0.06–0.08
Maximal acceleration index (AI_{max}, s-1)

3.6 Intrarenal or Distal Criteria (Indirect Evaluation of Stenosis)

The difficulties related to the direct evaluation of the stenosis (the main examination time was 69 min for full examination and 14 min for distal evaluation) let several investigators to identify the alternation of the V/t curve distal to the stenosis in arterial segments more accessible with Doppler, like hilar and interlobar artery [21]. Many distal quantitative criteria have been proposed in literature [7, 22]: loss of early systolic peak (ESP), acceleration index (AI) less than 3 m/s^2, acceleration time (AT<0.07), more than 5 % difference between kidneys' RI, or pulsatility index >0.12.

Correlative studies using angiography are confusing because of the variability in employed criteria and reported a high interobserver and intraobserver variability [22].

Downstream to a significant hemodynamic stenosis, blood flow becomes damped and demonstrates a slow systolic peak [13]: this phenomenon has been called *tardus-parvus* (*tardus* means slow and late, while *parvus* means little and small). Waveform systolic acceleration is slow with increase in time required to reach the peak that is low in height (Fig. 3.8). Even if the presence of this finding is useful for the RAS diagnosis, its absence does not exclude it. In a patient with atherosclerosis, vessel compliance may be reduced, making the tardus-parvus waveform less visible [23]. Numerous studies [1, 9, 11–13] show optimal results using this indirect diagnostic method. A slow systolic upstroke or AI (acceleration index), increase of the AT (time between the onset of the systolic acceleration wave and the systolic peak), and loss of early systolic peak (ESP) seem to be the most useful parameters [22, 24]. Anyway many factors influence the systolic acceleration, making this test less specific: valvular disease, left ventricular dysfunction, some cardiac drugs, age, hypertension, and diabetes affect the vascular compliance [1].

The indirect criterion use is advised only when there is particular evidence, when it is important to quantify the stenosis as severe >75 %, or when the direct exam of renal districts is not well analyzed (e.g., in the suspect of renal segmental artery or accessory artery stenosis) [21]. Anyway, a combination of intra- and extrarenal parameters is recommended, because together they have the sensitivity and specificity of 89 % and 92 % [13].

Recently some authors introduced new intrarenal velocimetric index for RAS diagnosis, the maximal acceleration index ($AI_{MAX}s^{-1}$), defined as the maximal slope of the systolic acceleration corrected for the relative district flow. The AI_{MAX} sensitivity and specificity at the best cut of value (9.0 s^{-1}) were founded to be 88 % and 89 % for stenosis >50 %, 93 % and 84 % for stenosis >60 %, and 92 % and 82 % for stenosis >70 %. The main limit of the study design is that it did not compare intrarenal to extrarenal index, so it is not possible to choose the best approach. Accuracy has not been evaluated in the other study.

A great difference of the RI, between two kidneys, is another diagnostic criterion for diagnosis of the RA.

The post-stenotic flow in the RA beyond the region of the stenosis will often have low-resistance waveform; however this criterion is not commonly used. Unlike the acute hydronephrosis where RI has a determinant clinical role, many nephropathies show the reduction and asymmetric values of the RI without the stenosis.

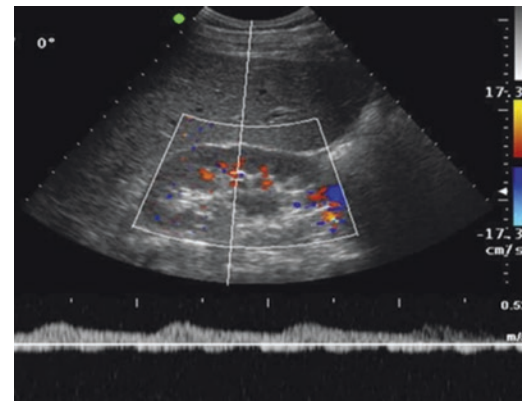

Fig. 3.8 Tardus-parvus phenomenon: an indirect criterion for diagnosis of renal artery stenosis. In the presence of renal artery stenosis, intrarenal Doppler analysis may reveal a slow and late (*tardus*), little and small (*parvus*) peak systolic velocity (*PSV*) which is useful for RAS diagnosis. Slowing acceleration index, increase in acceleration time, and loss of early systolic peak (ESP) waveform enable RAS identification with 95 % sensitivity and 97 % specificity. Moreover, the *tardus-parvus* phenomenon predicts a successful revascularization intervention

3.7 Pre- and Post-revascularization Evaluation

RAS is virtually reversible and treatable; therefore RAS early diagnosis is the clinical target. Meanwhile early treatment can preserve the renal function. RAS is treatable through vessel revascularization with percutaneous angioplasty if the stenosis is in the ostial part and through percutaneous angioplasty with stenting if the stenosis is in the medial or distal tract.

Revascularization treatment is indicated only if the decrease in the vessels' lumen diameter is more than 75 %, and the intervention can improve renal function.

In respect to other imaging methods, US lets to evaluate if the patient can benefit from the intervention or not: the renal function index should not improve if the IR despite the intervention remains >0.80 [17].

Other authors [21] notice that the 29 % of the patients with renal insufficiency and IR 0.80 will improve renal function after the revascularization, and 50 % have better pressure control.

Several studies [25] demonstrated that the RAS can relapse (restenosis) with variable index of 2–36 % in the 6–12 months of the follow-up. The evaluation of the restenosis is important for the treatment of the patient and even to determine long-term advantages. MRA and CTA are less suitable to assess the restenosis because of the artifacts caused by the stent material. Doppler US follow-up to assess the stenosis is advised after stent placement for RAS, even without clinical sign of stenosis (Figs. 3.9 and 3.10). Girndt et al. [25] reported a sensitivity and specificity of 100 % and 74 % and used the published threshold value of in-stent PSV 180 cm/s. If published threshold value of in-stent RAR >3.5 was used, the sensitivity and specificity reported were 50 % and 89 %. In another study, Bakker et al., using the optimal threshold value of 226 cm/s instead of 180 cm/s in-stent PSV and the optimal threshold value for the RAR of 2.7 instead of 3.5, reported a sensitivity of 100 % for both parameters and a specificity of 90 % for in-stent PSV and 84 % for RAR.

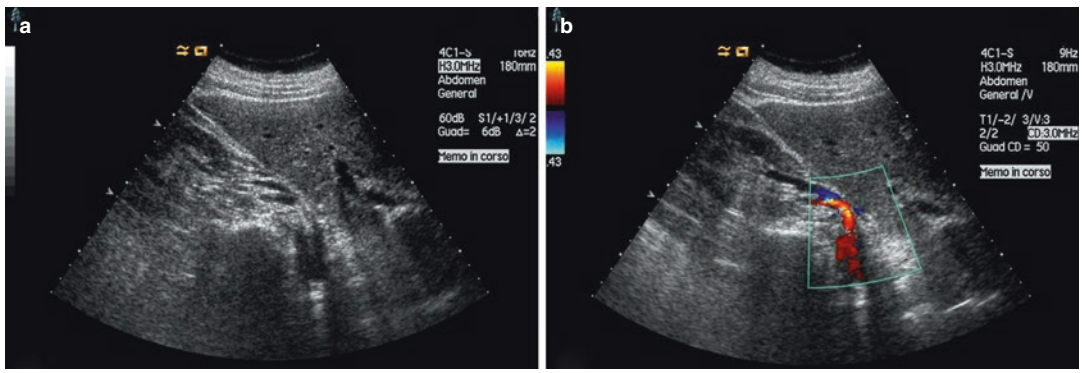

Fig. 3.9 Renal artery stenosis treated with stent. Renal artery stenosis may be treated by revascularization, mainly using percutaneous angioplasty, with or without stenting. Although excellent primary patency rates, long-term results are less satisfactory, especially in patients with arteriosclerotic disease. Restenotic evaluation through DUS should always be guaranteed to ensure long-term patency of treated vessel

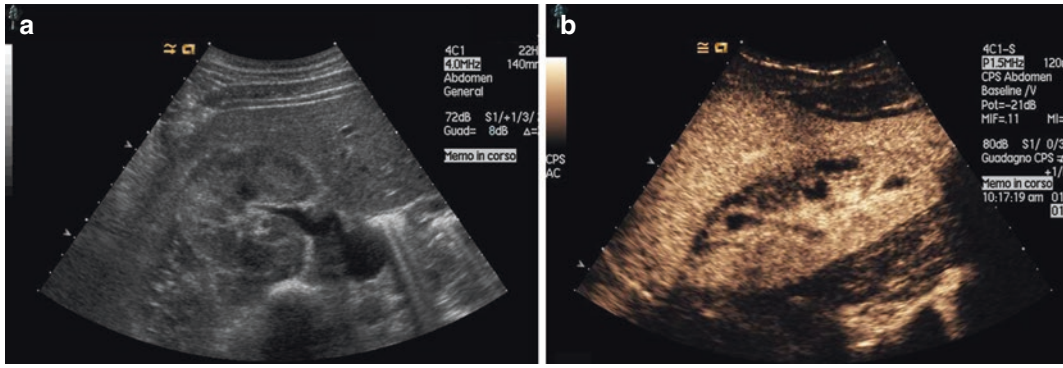

Fig. 3.10 Renal infarction diagnosis by ultrasound. (**a**) B-mode transversal scan: the right kidney appears slightly enlarged with hypoechoic areas and poor intraparenchymal arterial signal on color Doppler (*not showed*). (**b**) CEUS points out to parenchymal areas of hypoenhancement

3.8 Contrast-Enhanced Ultrasound and Renal Artery Stenosis

Renal contrast-enhanced ultrasound (CEUS) increases the diagnostic ability of color Doppler US in RAS detection, as it improves main renal artery and accessory vessels' visualization and reduces the equivocal examinations. CEUS increases the intensity of Doppler's signals having a more rapid and complete visualization of RA stenosis. The main indication of CEUS includes cases where Doppler V/t curve is difficult to obtain because of the overlying tissue, obesity, and wall calcification.

CEUS increases exam accuracy and decreases time wasting, improving sensibility and specificity to 94% and 88%, while DUS without contrast enhancement shows lower sensibility and specificity, respectively, of 85% and 79%. Anyway, the sensibility and specificity of the exam do not seem to increase significantly with CEUS. In fact, despite reduction in procedure duration and increase in specificity, CEUS does not seem to improve the accuracy of RAS diagnosis [2].

Preliminary studies [26] showed variation in the time-intensity curve of the kidney with artery stenosis, compared to the contralateral one. The distribution/reperfusion technique helps to detect the reduction of the cortical mean velocity blood flow in the renal artery with stenosis and reduction of the blood volume fraction.

Renal perfusion study, thanks to the alteration of parenchymal flow, allows easier detection of the stenosis than color Doppler exam.

CEUS feasibility depends on the equipment's quality: contrast injection does not give substantial advantage if the ultrasound platform does not provide the highest performance. Otherwise diagnosis of RAS with contrast ultrasound does not seem adding the relevant diagnostic elements. In the future, the application of parametric software will let to better define renal flow, probably adding relevant elements for RAS diagnosis and eventually PTA response evaluation. Further studies are necessary to define better the role of the contrast ultrasound in the light of the new and further coming technologies (Fig. 3.11).

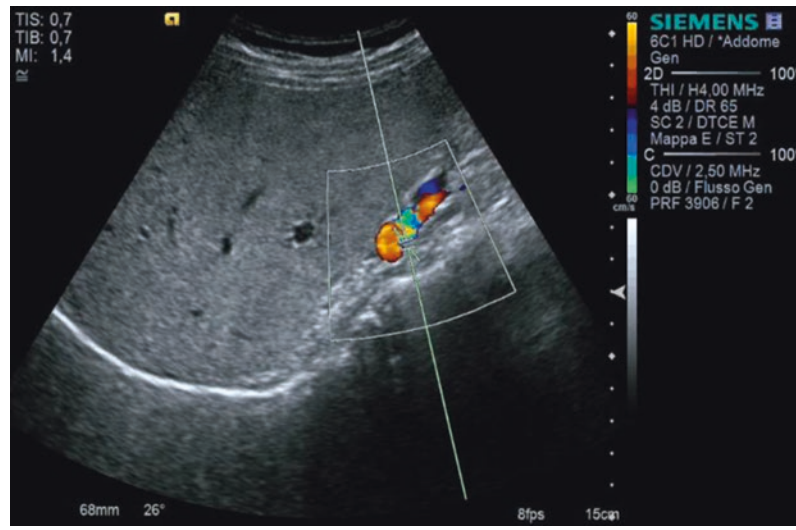

Fig. 3.11 Renal artery aneurysm detection with duplex ultrasound. Renal artery aneurysm is a segment of dilated renal artery that can cause renal infarction. It occurs with equal frequency in men and women, but rupture is more common in women in reproductive age

Bibliographies

1. Granata A, Fiorini F, Andrulli S, Logias F, Gallieni M, Romano G, Sicurezza E, Fiore CE (2009) Doppler ultrasound and renal artery stenosis: an overview. J Ultrasound 12(4):133–143. doi:10.1016/j.jus.2009.09.006, Epub 2009 Oct 12
2. Granata A, Zanoli L, Insalaco M, Valentino M, Pavlica P, Di Nicolò PP, Scuderi M, Fiorini F, Fatuzzo P, Bertolotto M (2015) Contrast-enhanced ultrasound (CEUS) in nephrology: has the time come for its widespread use? Clin Exp Nephrol 19(4):606–615. doi:10.1007/s10157-014-1040-8, Epub 2014 Oct 29. Review
3. Granata A, Andrulli S, Bigi MC et al (2009) Predictive role of Duplex Doppler ultrasonography in the diagnosis of acute renal obstruction in patients with unilateral renal colic. Clin Nephrol 71:680–686
4. Ritchie J, Green D, Chrysochou C et al (2014) High-risk clinical presentations in atherosclerotic renovascular disease: prognosis and response to renal artery revascularization. Am J Kidney Dis 63(2):186–197
5. Textor SC (2004) Ischemic nephropathy: where are we now? J Am Soc Nephrol 15:1974–1982
6. Safian RD, Textor SC (2001) Renal-artery stenosis. N Engl J Med 344:431–442
7. AbuRahma AF, Srivastava M, Mousa AY et al (2012) Critical analysis of renal duplex ultrasound parameters in detecting significant renal artery stenosis. J Vasc Surg 56(4):1052–1060
8. Krumme B (2006) Renal Doppler sonography-update in clinical nephrology. Nephron Clin Pract 103:c24–c28
9. Williams GJ, Macaskill P, Chan SF et al (2007) Comparative accuracy of renal duplex sonographic parameters in the diagnosis of renal artery stenosis: paired and unpaired analysis. Am J Roentgenol 188:798–811
10. Bude RO, Forauer AR, Caoili EM, Nghiem HV (2003) Is it necessary to study accessory arteries when screening the renal arteries for renovascular hypertension? Radiology 226:411–416
11. Labropoulos N, Ayuste B, Leon LR Jr (2007) Renovascular disease among patients referred for renal duplex ultrasonography. J Vasc Surg 46:731–737
12. Aytac SK, Yigit H, Sancak T et al (2003) Correlation between the diameter of the main renal artery and the presence of an accessory renal artery. Sonographic and angiographic evaluation. J Ultrasound Med 22:433–439
13. Zachrisson K, Herlitz H, Lönn L, Falkenberg M, Eklöf H (2016) Duplex ultrasound for identifying renal artery stenosis: direct criteria re-evaluated. Acta Radiol pii: 0284185116641345. [Epub ahead of print]
14. Li JC, Jiang YX, Zhang SY et al (2008) Evaluation of renal artery stenosis with hemodynamic parameters of Doppler sonography. J Vasc Surg 48:323–328
15. Staub D, Canevascini R, Huegli RW et al (2007) Best duplex-sonographic criteria for the assessment of renal artery stenosis-correlation with intra- arterial pressure gradient. Ultraschall Med 28:45–51
16. Hirsch AT, Haskal ZJ, Hertzer NR, American Association for Vascular Surgery/Society for Vascular Surgery, Society for Cardiovascular Angiography and Interventions, Society for Vascular Medicine and Biology, Society for Vascular Medicine and Biology, Society of Interventional Radiology, ACC/AHA Task Force on Practice Guidelines et al (2006) ACC/AHA Guidelines for the Management of Patients with Peripheral Arterial Disease (lower extremity, renal, mesenteric, and abdominal aortic): a collaborative report from the American Associations for Vascular Surgery/Society for Vascular Surgery, Society for Cardiovascular Angiography and Interventions, Society for Vascular Medicine and Biology, Society of Interventional Radiology, and the ACC/AHA Task Force on Practice Guidelines (writing committee to develop guidelines for the management of patients with peripheral arterial disease)—summary of recommendations. J Vasc Interv Radiol 17(9):1383–97
17. Crutchley TA, Pearce JD, Craven TE et al (2009) Clinical utility of the resistive index in atherosclerotic renovascular disease. J Vasc Surg 49:148–155
18. Lockhart ME, Robbin ML (2007) Renal vascular imaging. Ultrasound and other modalities. Ultrasound Q 23:279–292
19. Lewis S, Kanadian-Dodov D, Bansal A, Lookstein RA (2016) Multimodality imaging of fibromuscolar dysplasia. Abdom Radiol (NY) 41(10):2048–60. doi:10.1007/s00261-016-0778-8. Review
20. Schäberle W, Leyerer L, Schierling W, Pfister K (2016) Ultrasound diagnostics of renal artery stenosis: Stenosis criteria, CEUS and recurrent in-stent stenosis. Gefasschirurgie 21:4–13, Epub 2015 Aug 28
21. Mousa AY, Gill G (2013) Renal fibromuscular dysplasia. Semin Vasc Surg 26(4):213–218. doi:10.1053/j.semvascsurg.2014.06.006, Epub 2014 Jun 13
22. AbuRahma AF, Yacoub M (2013) Renal imaging: duplex ultrasound, computed tomography angiography, magnetic resonance angiography, and angiography. Semin Vasc Surg 26(4):134–143. doi:10.1053/j.semvascsurg.2014.06.001, Epub 2014 Jun 12
23. Yoshida K, Kitauchi T, Yoneda T, Kimura S, Takao M, Ishibashi M, Hirao Y, Kikkawa K (2004) Metal stent placement for two patients with post-transplantation renal artery stenosis, using intravascular ultrasound imaging. Clin Exp Nephrol 8(2):155–159
24. Sidhu R, Lockhart ME (2009) Imaging of renovascular disease. Semin Ultrasound CT MR 30(4):271–288
25. Girndt M, Kaul H, Maute C, Kramann B, Köhler H, Uder M (2007) Enhanced flow velocity after stenting of renal arteries is associated with decreased renal function. Nephron Clin Pract 105(2):c84–9, Epub 2006 Dec 11
26. Ciccone MM, Cortese F, Fiorella A, Scicchitano P, Cito F, Quistelli G, Pertosa G, D'Agostino R, Guida P, Favale S (2011) The clinical role of contrast-enhanced ultrasound in the evaluation of renal artery stenosis and diagnostic superiority as compared to traditional echo-color-Doppler flow imaging. Int Angiol 30(2):135–9

Cystic Diseases of the Kidney

4

Marco Misericordia, Eleonora Tosti, Marco Macchini, Andrea B. Galosi, and Gian Marco Giuseppetti

Renal cysts constitute the most commonly found benign lesions in adults during the diagnostic imaging: a renal cyst is detected in 10 % up to 50 % at abdominal ultrasound [1]. Also the prevalence of renal cysts is more than 50 % in adults 50 years old or older detected in autopsy studies [2].

Cyst classification and cystic disease of the kidney are summarized in Tables 4.1 and 4.2, respectively. Cysts are classified as "simple" or "complex," on the basis of the morphology, dimensions, wall characteristics, and features of content. Cyst may be acquired or associated with hereditary or non-hereditary diseases; therefore identification and classification of renal cysts have a clear clinical relevance.

Ultrasound examination is the first imaging test, often with immediate and reliable diagnosis. Diagnostic accuracy depends on the operator experience, ultrasound device available, and ability to find valid acoustic windows due to patient's habitus that are the same as those for the US examination of other abdominal organs. In selected cases, further imaging examinations by CT or MRI are preferred to obtain a better definition of cystic content and parietal aspects.

The diagnosis is almost always occasional, during US or CT examinations carried out in search of other pathologies. Rarely even large renal cysts cause symptoms or complications secondary to infection, bleeding, or urinary tract compression. The compression on the parenchyma only occurs for voluminous cystic formations that sometimes can stretch out on the renal pelvis, compressing it, with partial obstruction of the excretory duct.

Anatomical location of renal cysts is in the cortical, subcapsular, or renal hilum.

The role of the contrast-enhanced ultrasound (CEUS) in the identification and characterization of the complex renal cystic lesions is widely debated [3, 4].

M. Misericordia, MD (✉)
Azienda Ospedaliera Ospedali Riuniti, Ancona, Italy
e-mail: marco.misericordia@gmail.com; marco.misericordia@tele2.it

E. Tosti, MD • M. Macchini, MD • G.M. Giuseppetti, MD
Polytechnic University of Marche, Ancona, Italy

A.B. Galosi, MD, PhD
Institute of Urology, Polytechnic University of Marche, Ancona, Italy

P. Martino, A.B. Galosi (eds.), *Atlas of Ultrasonography in Urology, Andrology, and Nephrology*,
DOI 10.1007/978-3-319-40782-1_4

Table 4.1 Ultrasound classification of renal cysts

US renal cyst classification
1. Simple
2. Complex or atypical
Calcification
Septa
Intracystic lesion and wall thickness
3. Cysts of the renal sinus
Parapelvic
Peripelvic

Table 4.2 Cystic kidney diseases [1]

Cystic kidney diseases
1. *Renal cystic dysplasia – multilocular renal cysts (cystic nephroma)*
2. *Medullary cystic disease*
(a) Medullary sponge kidney
(b) Uremic medullary cystic disease and nephronophthisis
3. *Renal polycystic disease*
(a) *Autosomal-dominant polycystic kidney disease*
Classic ADPKD
Early-onset ADPKD in children
(b) *Autosomal-recessive polycystic kidney disease*
Classic ARPKD in neonates and infants
Medullary duct ectasia in older children with hepatic fibrosis
4. *Acquired renal cystic disease* (associated with dialysis)
5. *Renal cysts in hereditary malformative syndromes* (tuberous sclerosis)

4.1 Simple Renal Cyst

The vast majority of these are usually unilateral and solitary, sometimes multiple or bilateral (Fig. 4.1). It is believed that the development is due to a progressive dilation of the Bowman's capsule or the contorted proximal tubule, so they have a cortical origin.

They can spread everywhere throughout the renal tissue. The causes of the onset are not certain, although it is possible to assume damages to the basement membrane of the distal tubules. Other causes can be medullary interstitial fibrosis and ischemic renal parenchymal damages. They are more frequent in males than in females, particularly in middle-aged people; the frequency increases in the elderly population, particularly in males [5, 6]. On the contrary, they are much less frequent in the pediatric population.

The classic simple renal cyst demonstrates well-defined features. They have a completely anechoic content, round/oval shape, and sharp, thin posterior walls (Fig. 4.2a); an imperceptibly thin wall with no enhancement, delimited by a thin layer of fibrous tissue covered by epithelium single layer, is undetectable when the cyst is parenchymal.

It is important not to confuse the cysts with cortical medullary pyramids, taking hypoechoic appearance especially in the young (Fig. 4.2b).

The cysts generate the formation of artifacts due to the interaction of the ultrasound beam with the substrate analyzed; the ultrasonic beam crossing the cyst is neither attenuated nor absorbed and nor reflected, contrary to the surrounding tissues. The tissues located deeper than the fluid-filled structure emit signals that are reinforced, in comparison with the surrounding tissues. It follows the artifact of the increased through transmission (Fig. 4.3a). For this reason the back wall of the cyst appears thicker than how it really is. Another artifact is the lateral edge or acoustic shadows: thin acoustic shadow that appears behind edges of cystic structures (Fig. 4.3b). The speed of the ultrasounds in the fluid is faster than the propagation speed of the parenchymal tissues around the cystic formation. The matching between ultrasounds and the

lateral profile of the cyst causes a refraction that makes the cystic lesion behave like an acoustic lens. This causes the formation of lateral acoustic shadows: the phenomenon of the refraction along the sidewalls. Anechoic renal cysts may show some artifact internal low-level echoes [7]. This may be improved by using harmonic imaging techniques.

Complications are rare with a reported range of 2–4 %. The most common complications are hemorrhage, infections, or rupture. Generally, the increase of the inner content echogenicity relates with hemorrhagic complication (Fig. 4.4).

A sudden intracystic hemorrhage can clinically occur with pain, and sometimes it is possible to document a fluid-fluid level of the content, with layers of echoes because of the concentration of the protein components deriving from intracystic bleeding.

Hemorrhage generally affects only one cyst, but frequently it is possible to notice multiple cysts with hemorrhagic content in the same kidney. Those with a diameter less than 3 cm, if homogeneous and without calcifications, can be regarded as lacking in particular clinical implications. Sometimes they develop residual calcification in a central pattern or within the cystic wall that becomes thickened and develops septa and the cyst becoming multilocular or multilobular, acquiring the features of a complex cyst (Fig. 4.5) [1, 8].

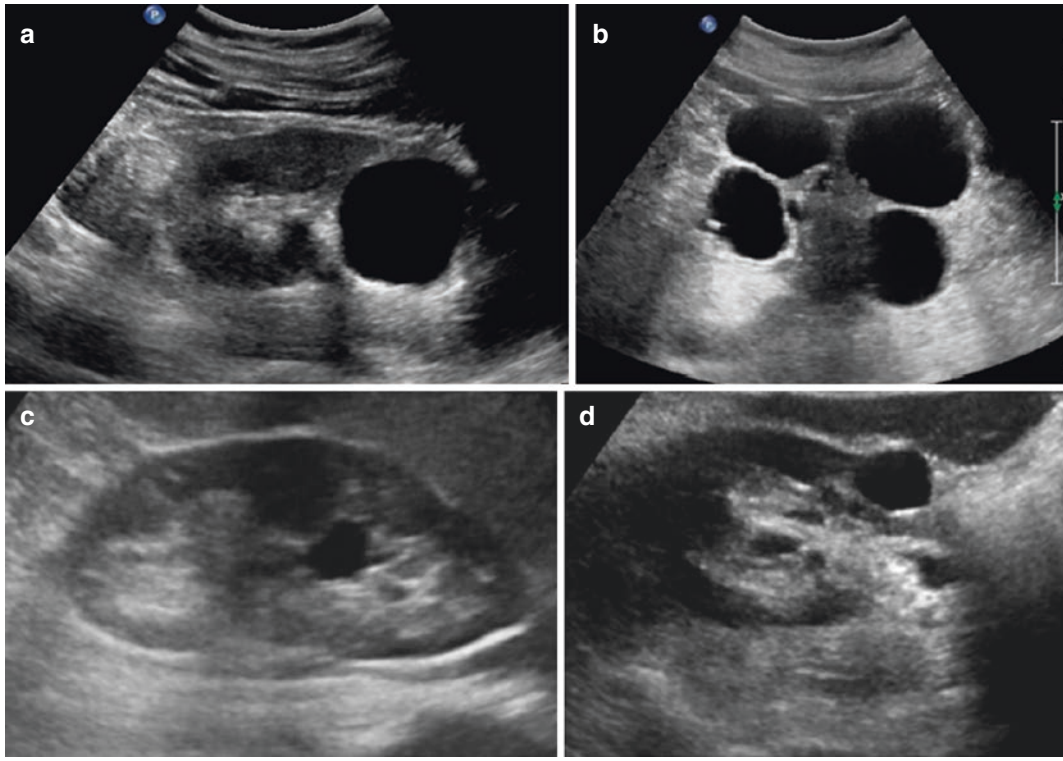

Fig. 4.1 (**a**) Simple renal cyst with completely anechoic content. (**b**) Multiple simple renal cysts. (**c**) Intrarenal cystic lesion. (**d**) Exophytic cystic lesion

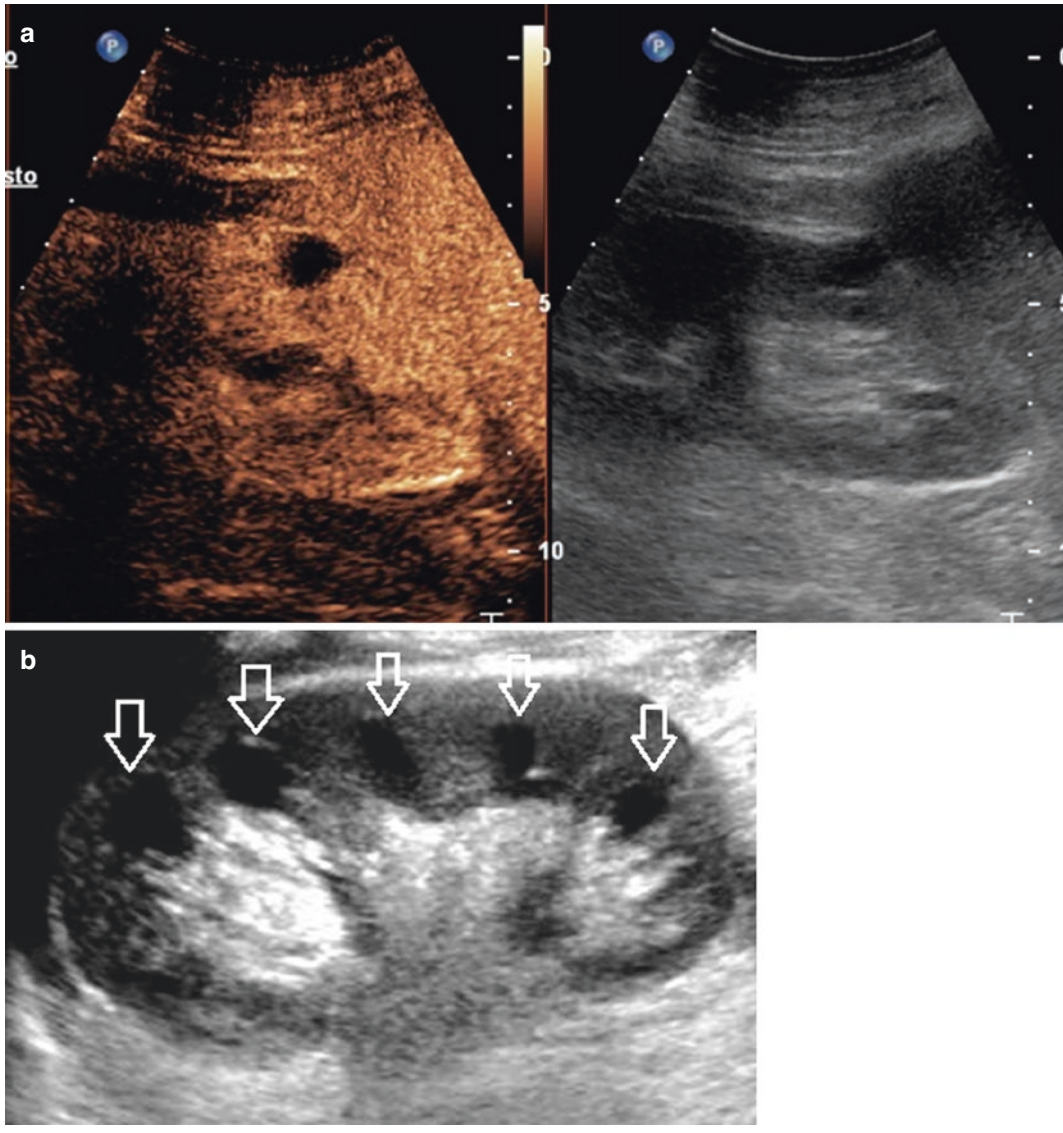

Fig. 4.2 (**a**) Renal cyst without enhancement after infusion of contrast medium. (**b**) Roundish hypo-anechoic images in the renal cortex at the cortico-medullary passage: renal pyramids. Not to be confused with cortical cysts

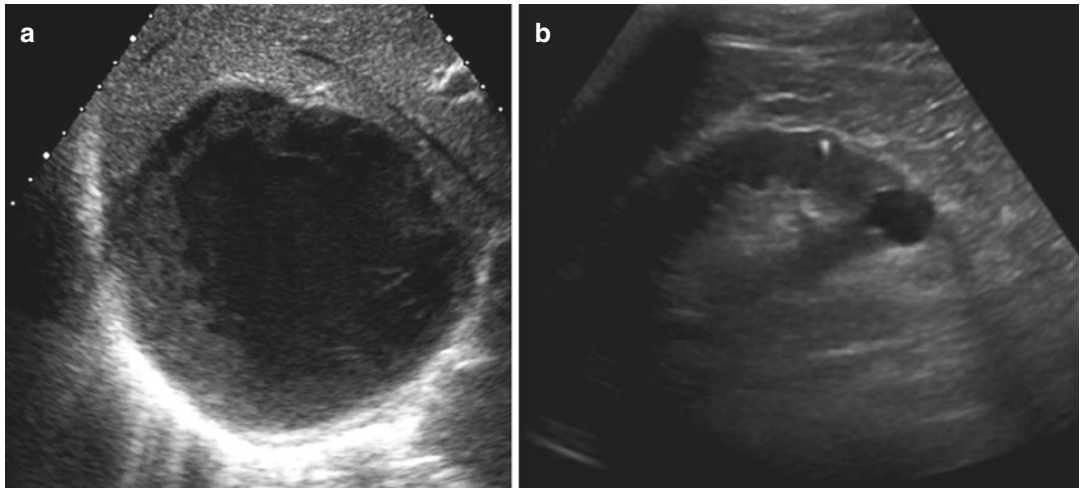

Fig. 4.3 (**a**) A large cyst with inhomogeneous intracystic material located in the peripheral parts and strong posterior increased through transmission. (**b**) Simple renal cyst with the artifact of lateral acoustic shadows

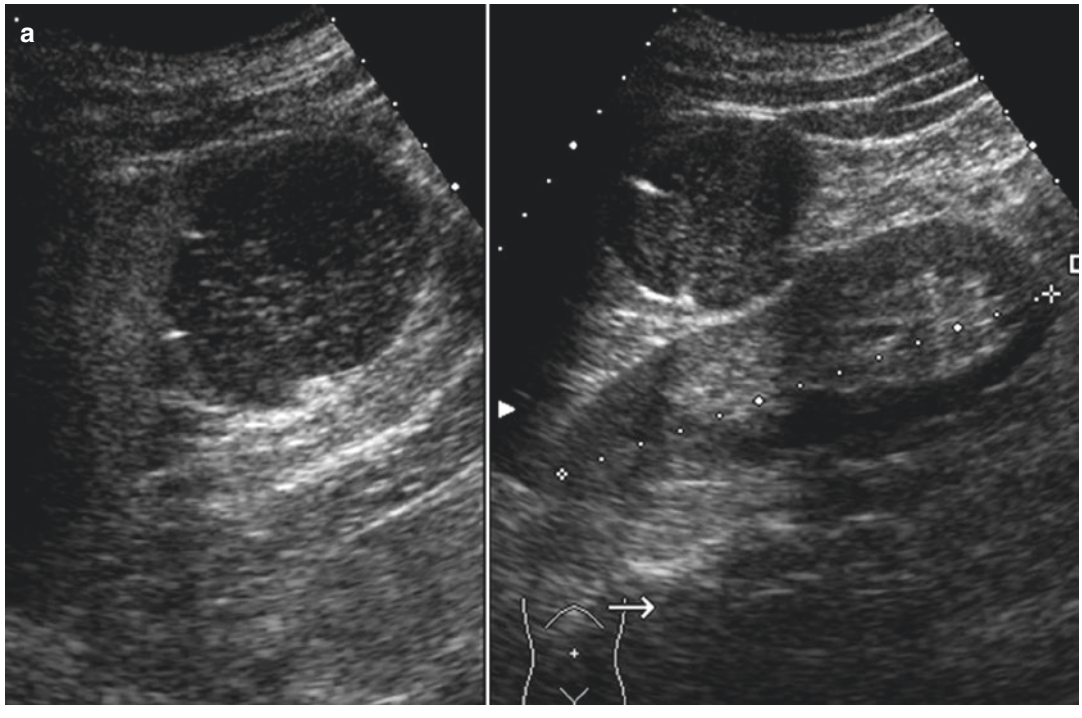

Fig. 4.4 (**a**) Exophytic cyst with inhomogeneous and corpuscular content in a patient with fever and shaking chills: infected cyst. (**b**) Partly exophytic cystic formation with endocystic iso-anechoic level: intracystic bleeding with declive layers of echoes. (**c**) Cyst containing blood. US (multiple low-level echoes) and CT axial view (hyperdense oval lesion without intravenous administration of iodinated contrast medium)

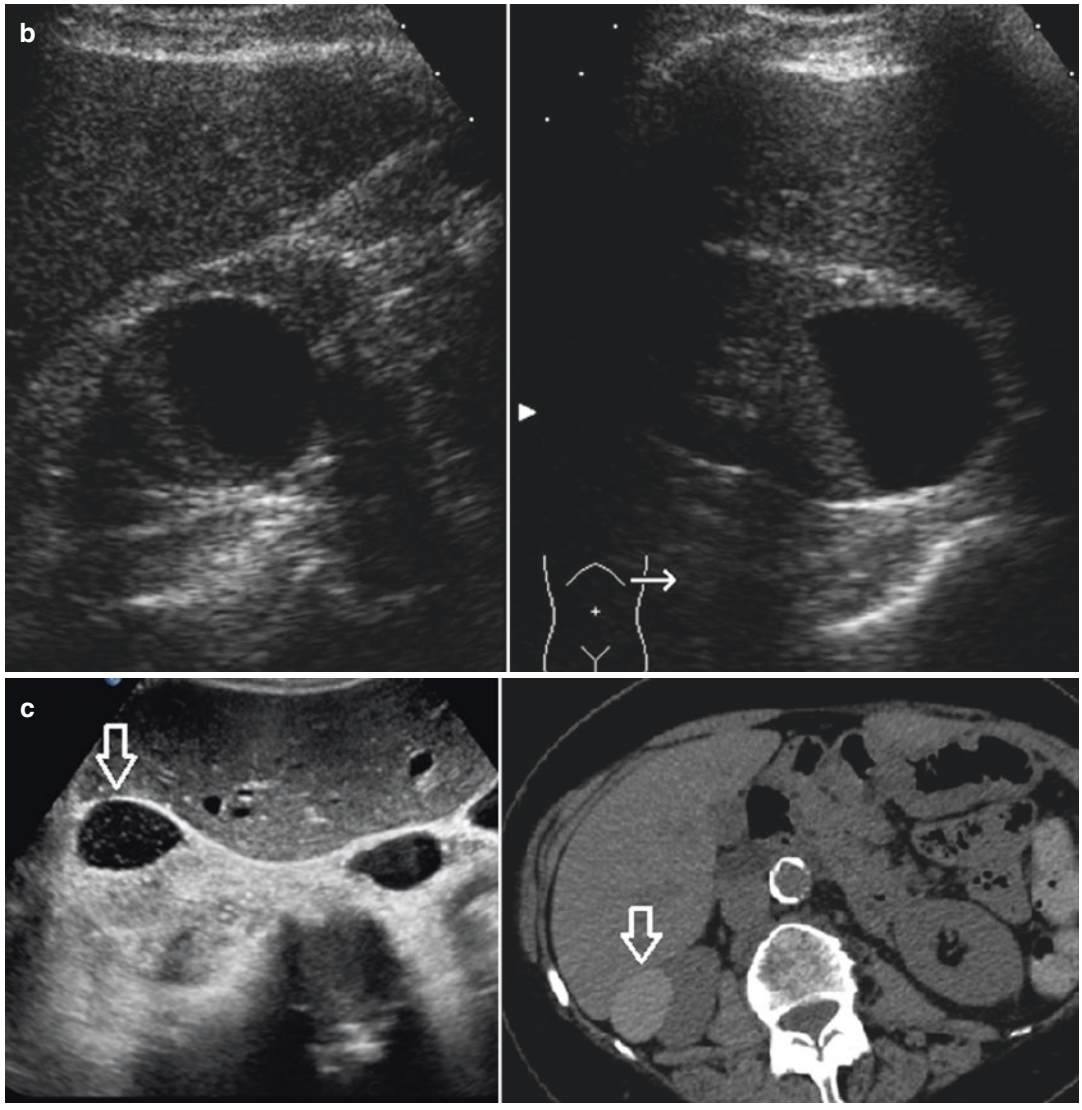

Fig. 4.4 (continued)

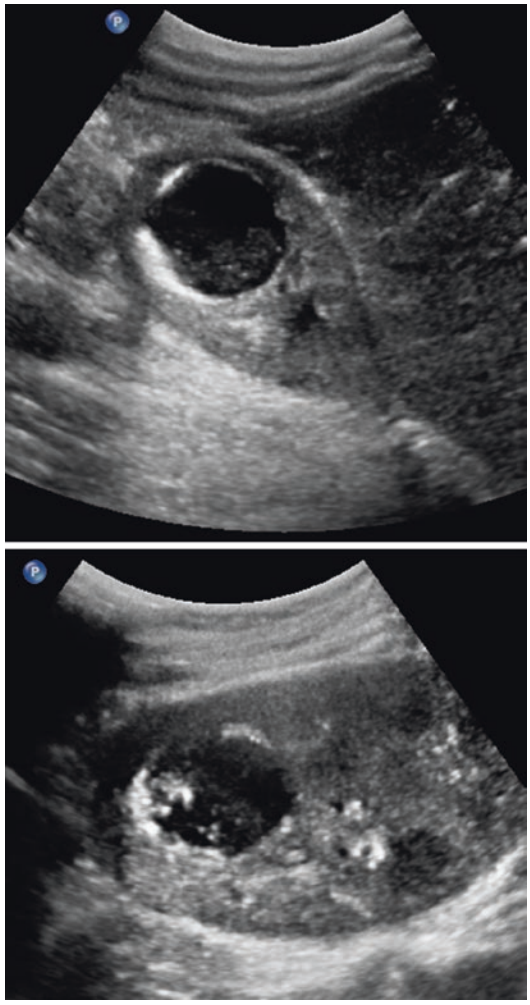

Fig. 4.5 Cyst with a fluid-fluid level due to an intracystic bleeding with parietal calcifications

4.2 Complex or Atypical Cysts

Complex or atypical cysts differ in shape and content from simple cysts. Sonographically, the criteria for a simple cyst are (1) an anechoic lesion, (2) sharply defined walls, and (3) acoustic enhancement behind the lesion. Complex or atypical cyst is defined as any deviations from at least one of these standards. A complex cyst includes irregular walls or non-anechoic content or calcifications or diffuse or focal low-level echoes [3, 9].

Oval, polygonal, or elongated shape is suspicious for a complex cyst (Fig. 4.6). As hemorrhagic cysts resolve, they develop residual calcification in a central pattern or within the cystic wall that becomes thickened and develops septa (Fig. 4.7) with the cyst becoming multilocular or multilobular; also the wall of infected cysts is often thickened markedly and calcified occasionally and has parietal irregularities such as endocystic vegetations [1–10] (Fig. 4.8). They have intrinsic echo content and sometimes clots that are indicative of bleeding.

The definition of complex cyst is made by the presence of one or more atypical aspects. Furthermore, the septum vascularization on color Doppler is suspicious for cancer. Also CEUS may be useful to show vascularity of septa or nodular protuberances in a renal cyst and can help differentiate a benign cyst from an indeterminate cyst or a malignant-appearing cyst [11]. During US examination, underlining this kind of aspects can raise suspicion of the presence of a malignant lesion. Therefore, a correct evaluation of the cystic lesion is essential in order to recommend an in-depth diagnosis by means of CT or MRI exams.

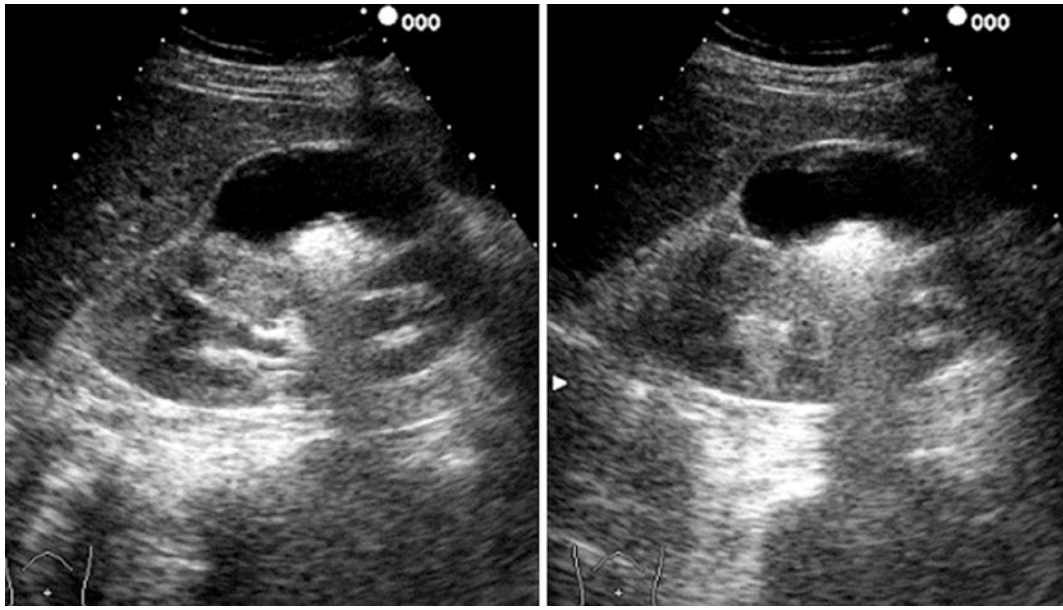

Fig. 4.6 Elongated cystic lesion

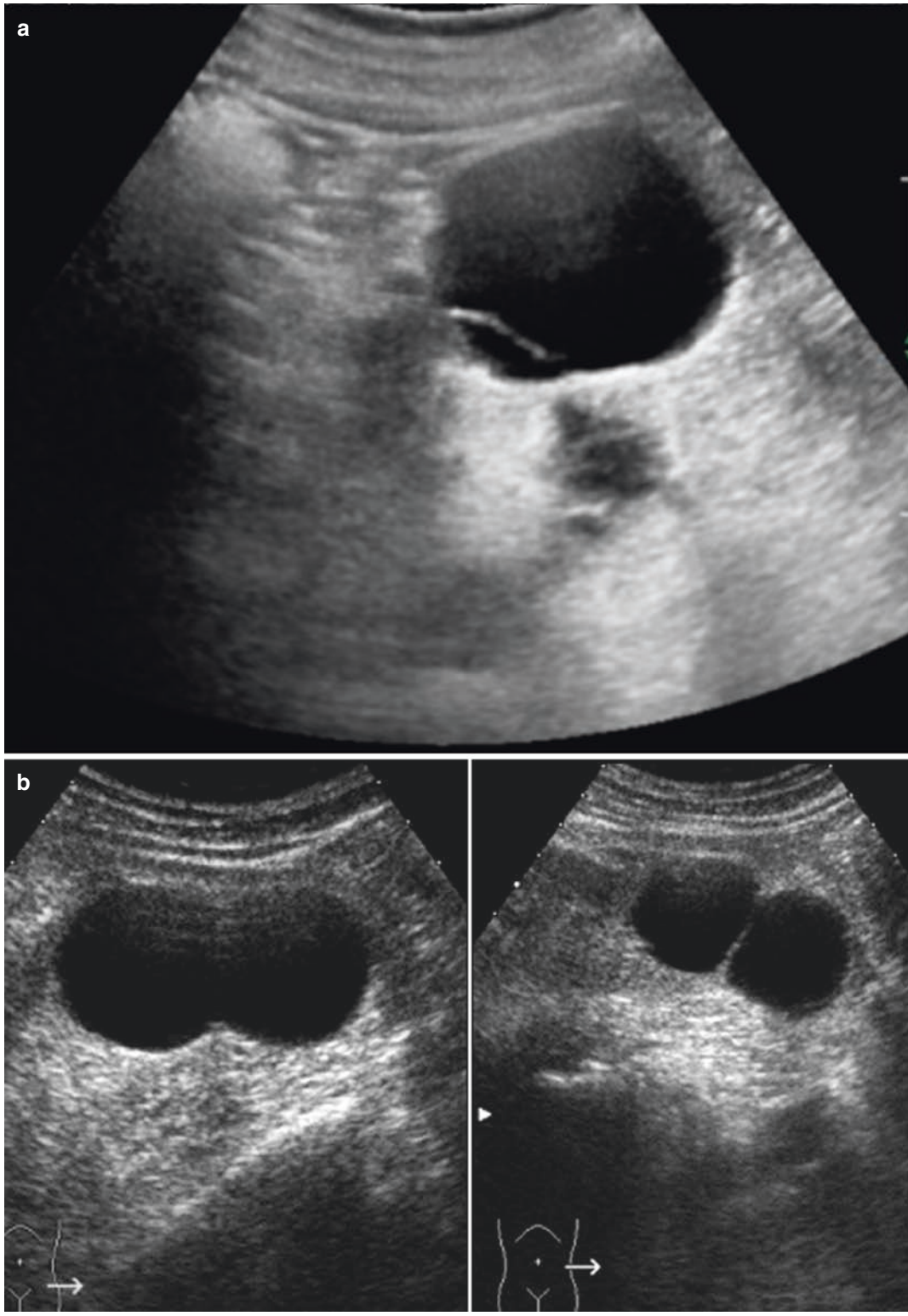

Fig. 4.7 (**a**) Cyst with a thin internal septum. (**b**) Two adjacent cystic lesions: the walls of the cysts come into contact appearing as just only one cyst, not to be confused with an intracystic septum

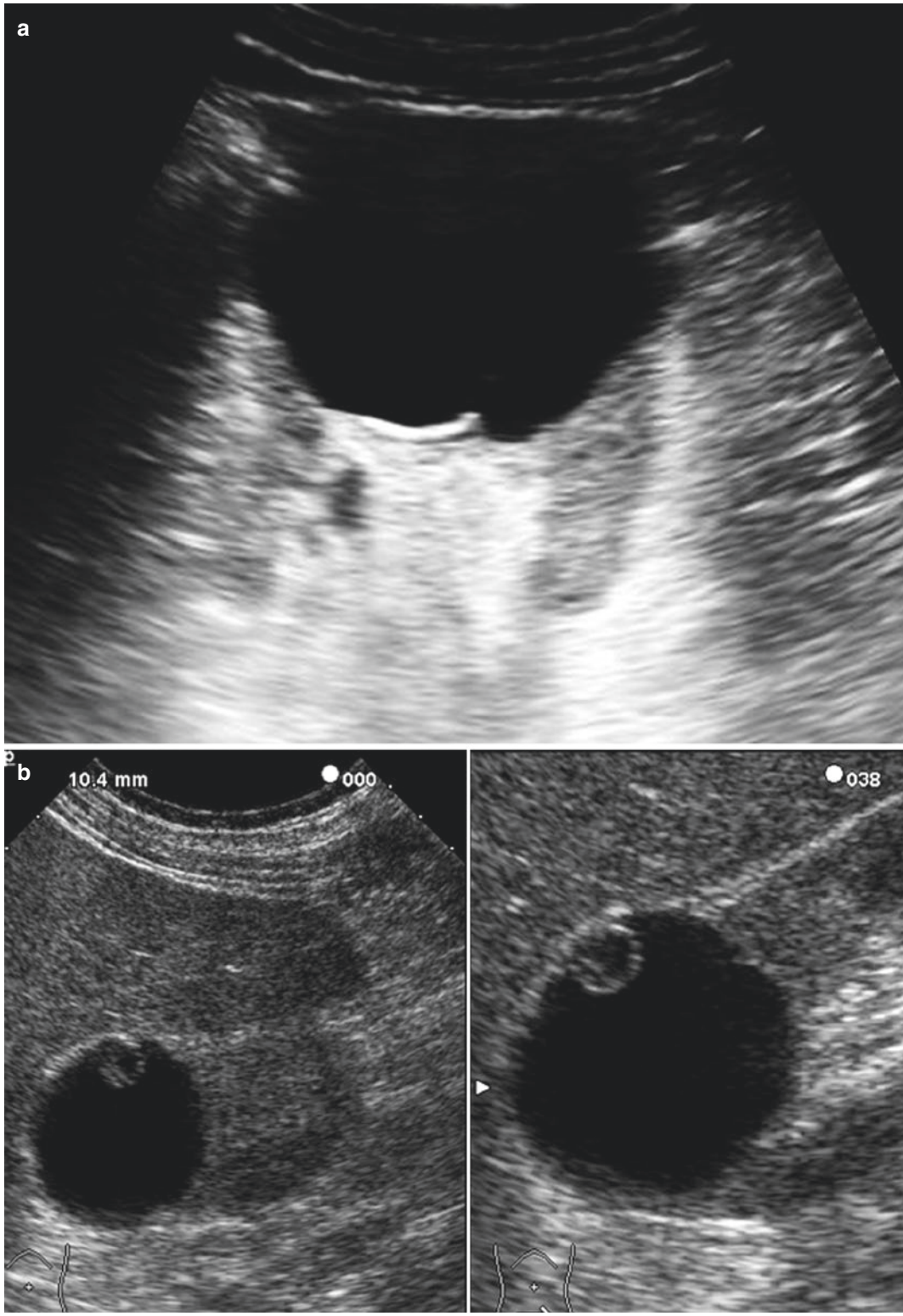

Fig. 4.8 (**a**) Cyst with a thin focal parietal thickening in the posterior wall. (**b**) Cyst with a little endocystic vegetation emerging from the anterior wall. (**c**) Cystic formation with internal low-level echoes: hemorrhagic cyst

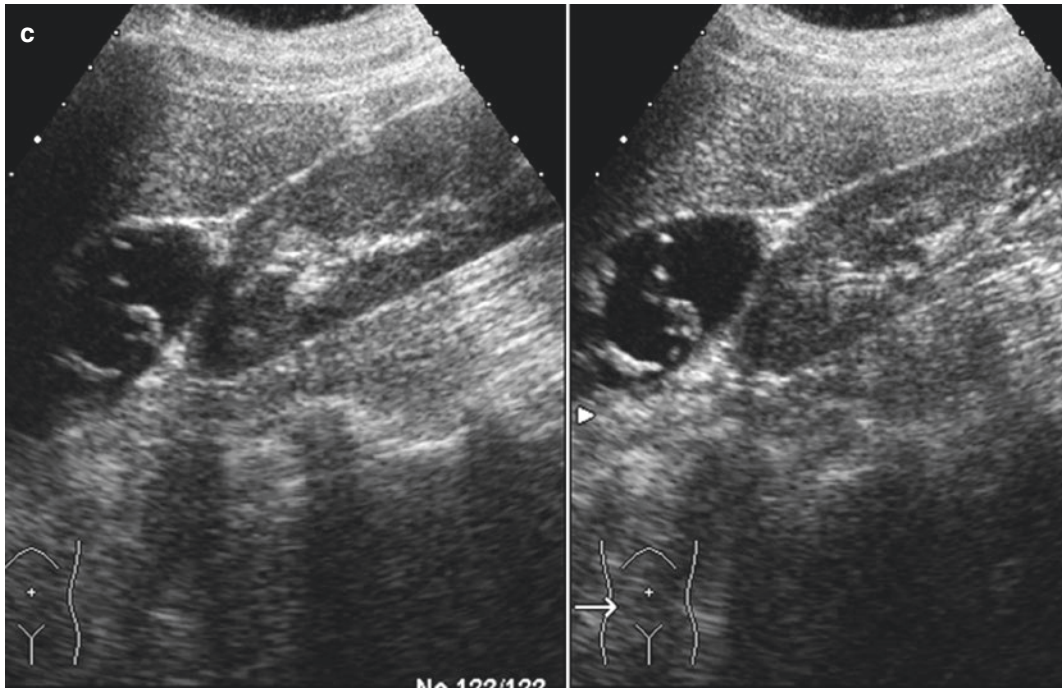

Fig. 4.8 (continued)

4.2.1 Cyst with Calcifications

Calcification can occur in the wall or the septa of benign as well as malignant lesions. The presence of calcification may influence the decision to surgically explore or follow up a lesion [12, 13]. CT allows higher spatial resolution than US in the evaluation of cystic parietal and endoluminal calcifications. The posterior acoustic shadowing and the reverberation effect of the echoes in the presence of cystic calcifications during US examination can constitute a limit on the detection of the other components of the cyst itself. There are three categories of calcifications:

1. Small and regular calcification: it is a small quantity of calcium which linearly settles on the wall (Fig. 4.9a, b) or on a septum or, appearing like "milk of calcium," on the declive part of the cystic lumen.
2. Multiple and irregular calcification: it is a calcification associated with parietal thickening of the cyst, with nodules or with aspects of cystic vascularization.
3. Single or few isolated calcifications with thickness (Fig. 4.9c) or nodular appearance (Fig. 4.9d, e), without signs of vascularization and without parietal nodules, worthy of follow-up in time.

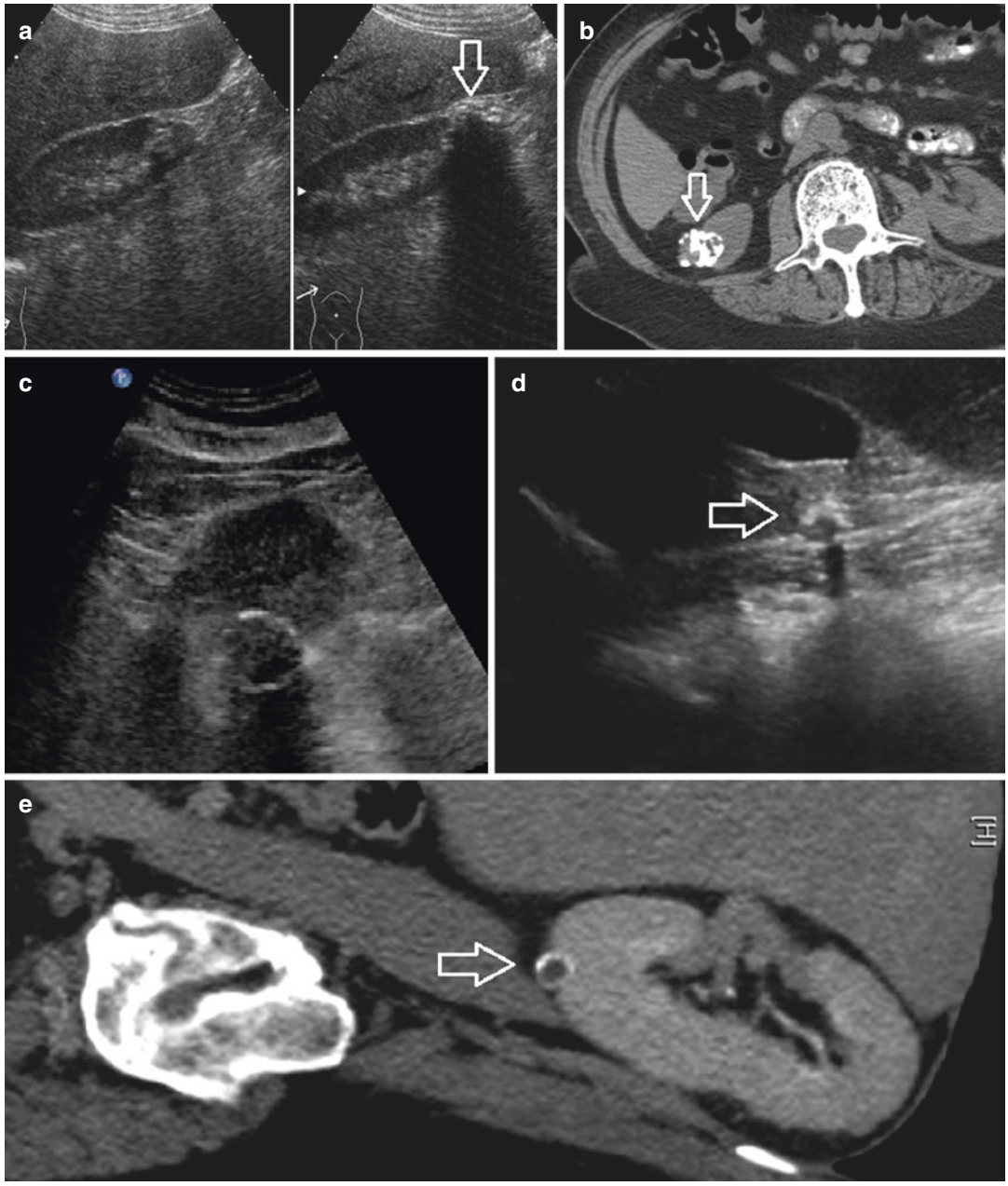

Fig. 4.9 (**a**) A cystic lesion with parietal and inner calcifications. This determines the formation of a wide posterior acoustic shadowing. (**b**) CT axial view. (**c**) Echoic annular image with posterior positive through transmission due to a cyst with parietal lamellar calcifications. (**d**) Echoic image with a posterior positive through transmission. (**e**) CT sagittal view

4.2.2 Cyst with Septa

The renal cysts sometimes reveal thin septations (Fig. 4.10) that divide them into single compartments. Such septations need a diagnostic evaluation by ultrasound, since they have to be distinguished from those present in the renal cell cystic carcinoma. In this case it can be a useful diagnostic completion by means of CEUS. Vascularization of neoplastic septa suggests a malignant aspect. The septa, not all of a malignant nature, can be partial or complete and can develop as results of healing or previous infection or intracystic bleeding. Ultrasound performs better than CT, thanks to the increased contrast echogenicity between the anechoic content of the cyst and vascularized lesion or septum. The number of the septa discovered in the cystic lesion is of fundamental importance in order to recommend the surgical removal of the lesion (Fig. 4.11a). Cysts with three or more septa (Fig. 4.11b) are defined as multilocular cyst. The finding of a thickened septum or multiple and vascularized thickened septa (Fig. 4.11c) put a strong suspicion in favor of neoplastic lesion. There has been a controversy in the literature regarding the ability of CT and sonography to define internal septations. Some reports have shown that ultrasound is superior to CT in this regard [14]:

US parameters	Benign septa	Malignant septa
Thickness	1 mm or less	>1 mm
Shape	Linear (without nodules)	Irregular
Nodules	Absent	Present (in particular at the insertion point with the renal wall)
Calcification	Small and thin	Large and irregular
Number	Few	Multiple
Recommendation	Follow-up with ultrasound (optional)	Must be characterized by CT/MRI and strictly followed or treated

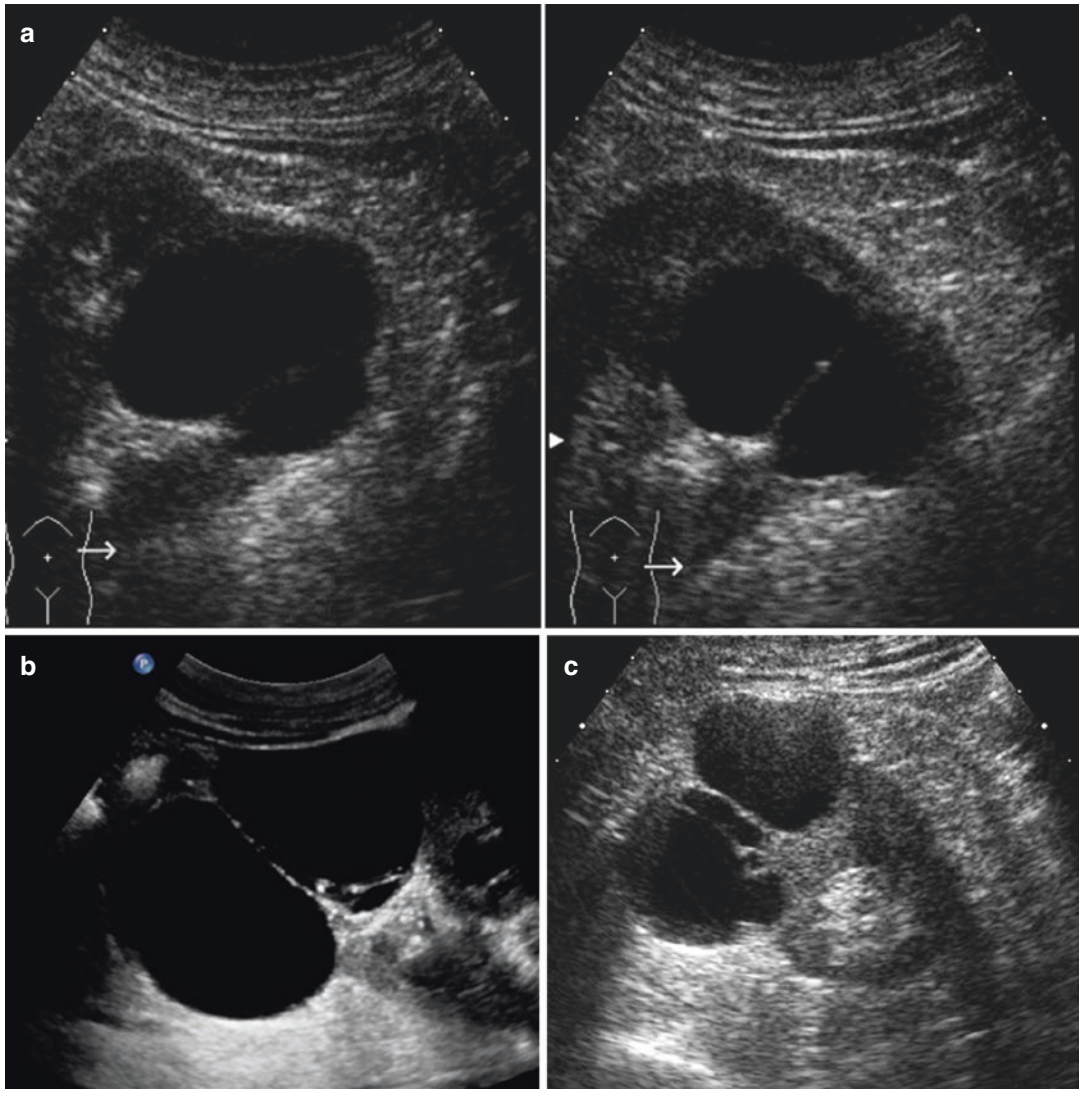

Fig. 4.10 (**a**) Cyst with only one thin endoluminal septum with regular profile less than 1 mm thick. (**b**) Two voluminous paired cysts with multiple and thin intracystic septa inside one of the two. (**c**) A thin intracystic septum. (**d**) Multiple and thick intracystic septa

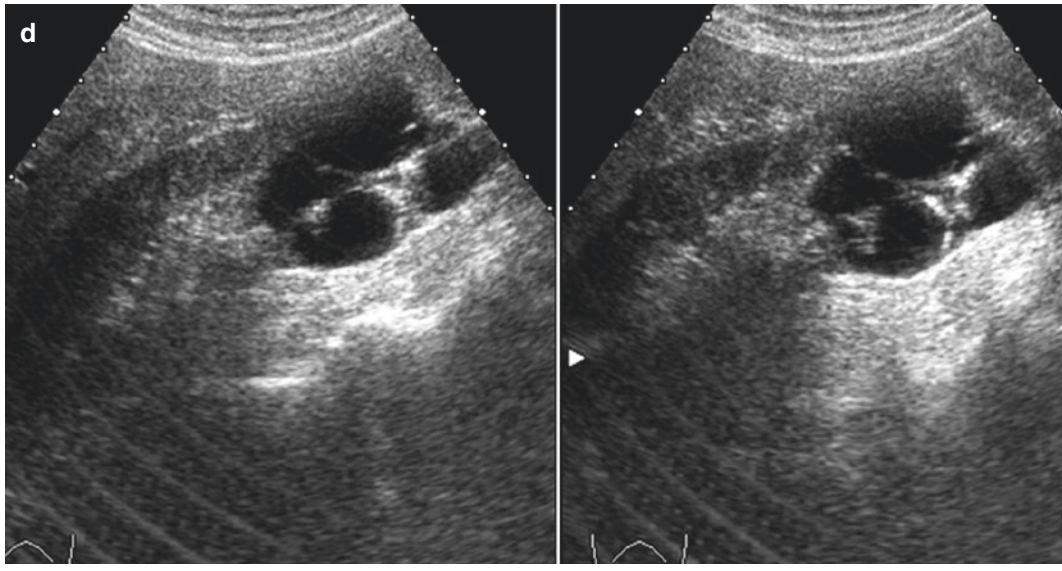

Fig. 4.10 (continued)

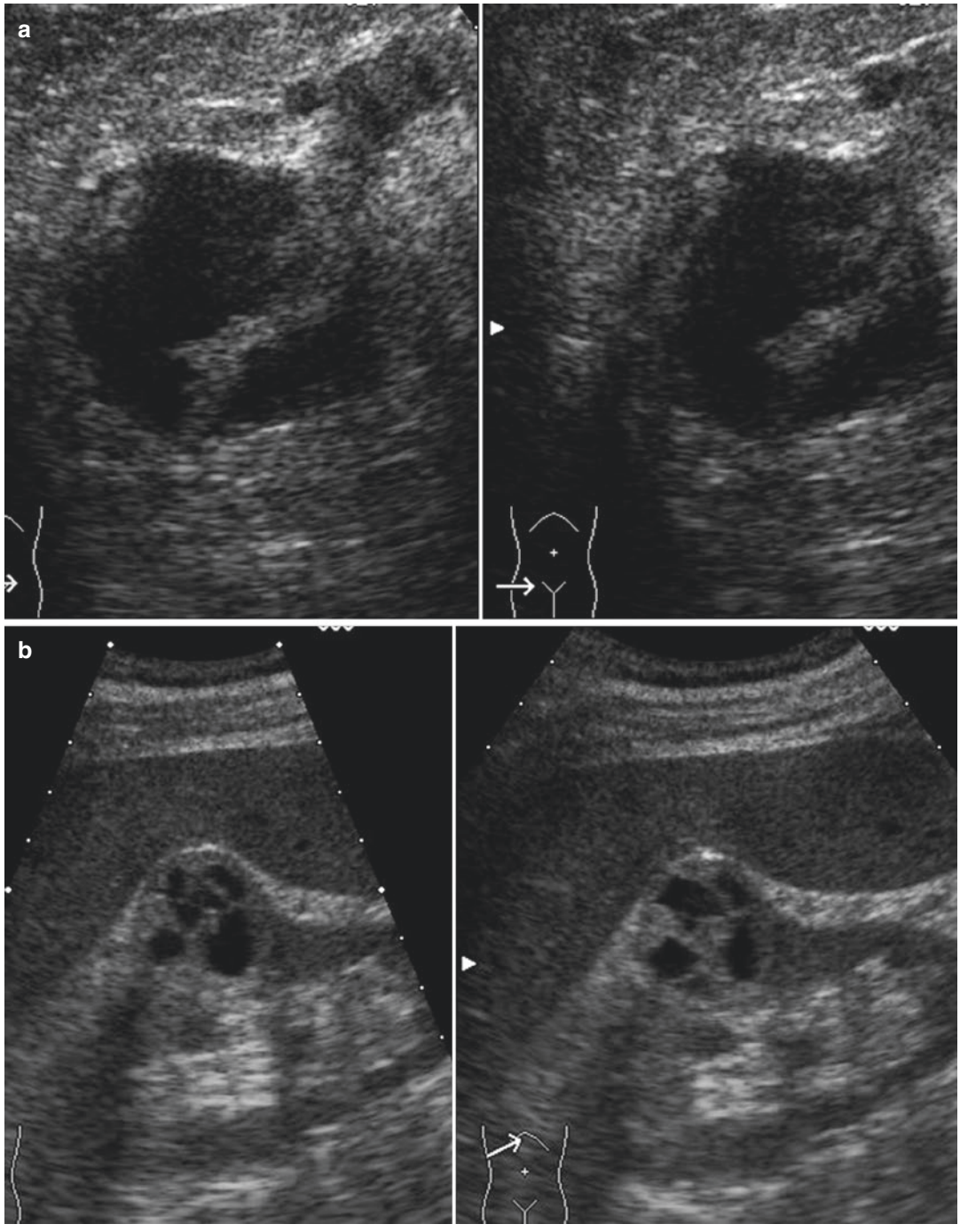

Fig. 4.11 (**a**) Cyst with thick walls with nodular septa. (**b**) Cyst with thick walls and nodular and diffused septa. (**c**) Abundant vascularization of the walls and the septa at Doppler US. Cystic renal cell carcinoma

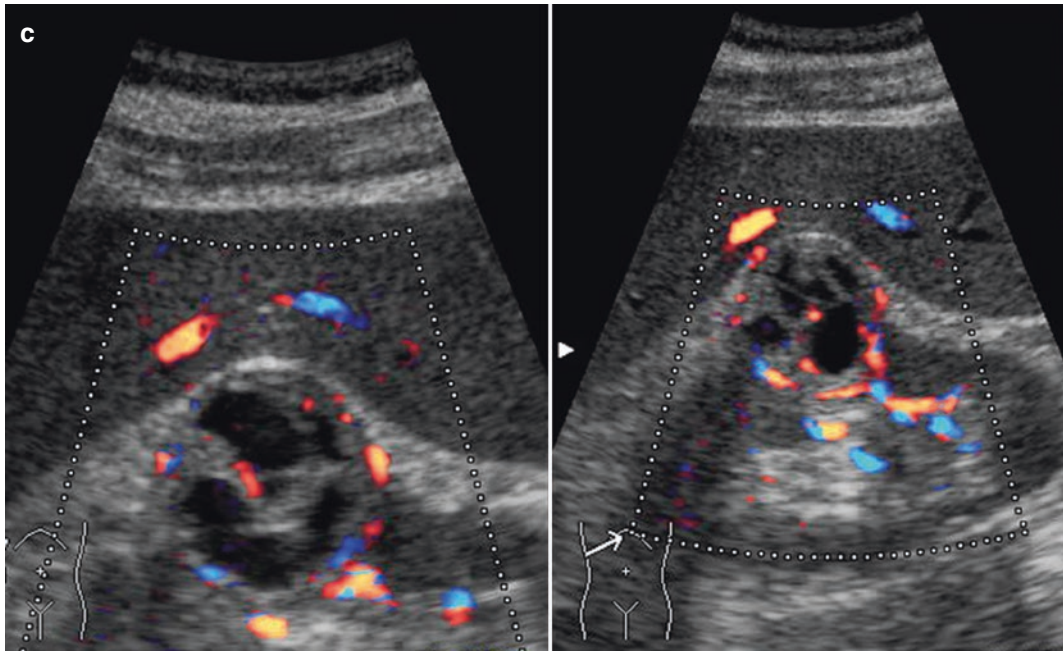

Fig. 4.11 (continued)

4.2.3 Nodularity or Cystic Wall Thickening

US allows to evaluate intracystic nodules of very small dimensions, adherent to the wall or to cystic septations, that do not move to various patient positions (Fig. 4.12a). They have to be distinguished from intracystic sediment, often detectable as a little carpet of echoes crammed in the declive place or suspended in the cystic lumen. The evaluation of cystic parietal thickening is possible when at least a quarter of the wall is exophytic. To find a thickened cystic wall (more than 1 mm) refers for surgical excision (Fig. 4.12b). CEUS is helpful for the diagnosis of nodule vascularization and refers surgical resection. On the other hand, follow-up is proposed for the small intracystic nodularities without a perceptible contrast enhancement. However in the presence of parietal enhancement, after ultrasound contrast medium administration, the possibility of excising the cyst should be assessed (Fig. 4.12c–e). Another potential advantage of US is its capacity of defining the cystic or solid nature of the lesion. In some situations, the characterization of hypovascular lesions may be difficult on CT too. The papillary renal cell carcinoma is an example of such tumors.

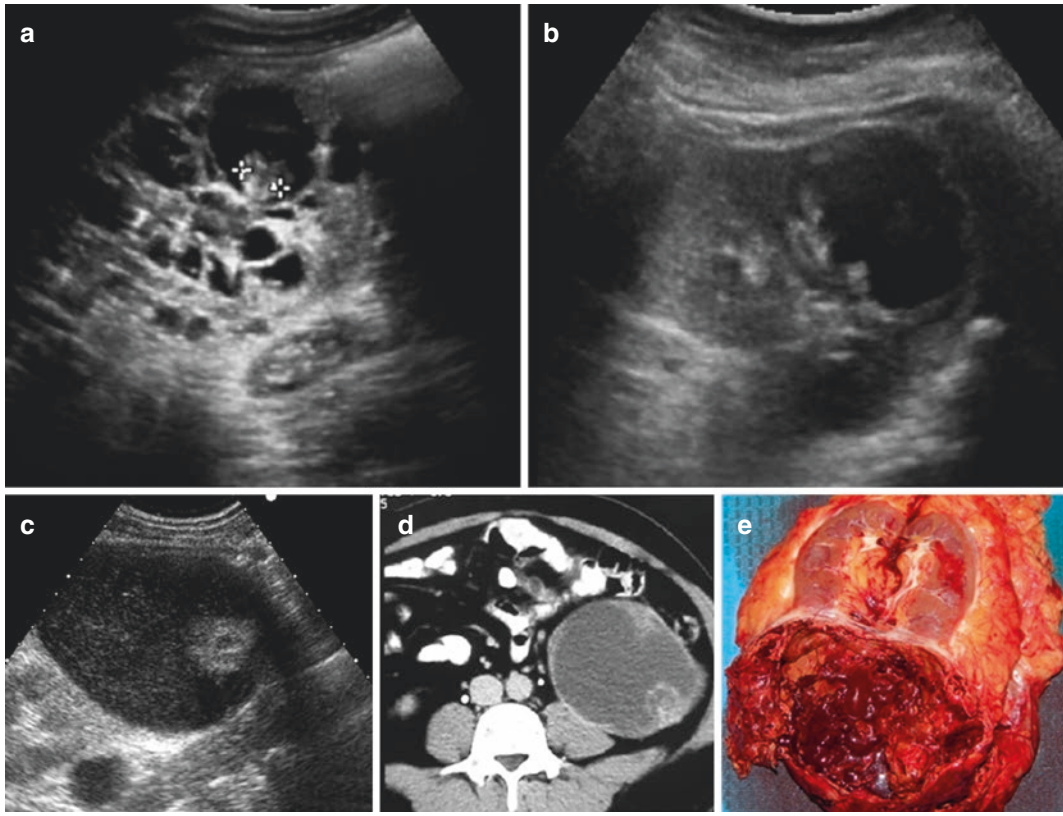

Fig. 4.12 (**a**) Scattered renal cystic lesions (polycystosis) with a nodule in the lumen of the largest one. (**b**) Complex cystic lesion: multiple parietal thickenings protruding into the cystic lumen. (**c**) US: cystic formation with multiple echoic intracystic echoes and coarse parietal vegetation. (**d**) CT scan with contrast medium. (**e**) Surgical findings

4.2.4 Bosniak Classification of Complex Cyst

The Bosniak classification, based on contrast CT, is the most useful and widely employed method for characterizing renal cystic lesions and assessing the likelihood of the presence of a concomitant malignancy within the cyst. Based on contrast CT, the renal cysts are classified into five categories so as to allow a proper evaluation of the risk of malignancy. The fundamental part of the classification is the detection of neovascularization by contrast enhancement of solid components, septa, or walls. Bosniak classification, proposed in 1986 and then revised in 2005, uses diagnostic criteria that refer to the semiotics of the lesions in CT and MRI. The use of ultrasound in the Bosniak classification has never been unquestionably accepted. Ultrasound is not used to classify renal cystic lesions according to the Bosniak criteria; however, US can accurately indicate features of complexity: calcification, septa, nodules, intracystic pattern, and vascularization by power Doppler and CEUS [15, 16]. A potential advantage of US is its capacity of defining the cystic or solid nature of the lesion. In some situations such as the papillary renal cell carcinoma, characterization of remarkably hypovascular lesions may be difficult on CT, and US correlation may have a potential role.

However, it is known that US may demonstrate internal septa better than CT and even MRI. Accordingly, it has been suggested that simple (Bosniak type I) and minimally complex (Bosniak type II) cysts may be followed up with US only [17].

Nevertheless, the improvement of the ultrasound technique, supported by the use of specific contrast media, allows to use it also during ultrasound evaluations and to provide extremely important diagnostic criteria all the same, associated with indications of follow-up of the cystic lesions. In each of the five categories, there are useful elements to characterize the cystic lesions in order to suggest the procedures for clinical and therapeutic management [18].

Bosniak Type I In this category the simple cysts are classified: cysts without contrast enhancement and septa or parietal thickening, with homogeneous urinous content and a visible interface as compared to the adjacent renal parenchyma. Lesions of this type do not need follow-up.

Bosniak Type II In this category the minimally complex cysts are classified: cysts with one or two thin septa, less than 1 mm thick, and with thin calcifications at the level of the wall, the septa, and the hyperdense benign cysts at the baseline evaluation through CT (>20 HU 40–90) with all the other features of type I. The diameter must not exceed 3 cm without parietal enhancement after intravenous contrast medium. Lesions of this type do not need follow-up.

Bosniak Type II F (Follow-Up) In this category the cysts belonging to type II are classified: cysts with many and thick (>3 mm) septa and minimally thickened wall, irregular parietal calcifications without measurable contrast enhancement, and the cysts with diameter exceeding 3 cm, mainly intrarenal. Lesions of this type need follow-up (6–12 months for 5 years) to confirm the benign nature and show malignancy percentage of about 5 %. Ultrasound and CEUS have an important role in the follow-up of patients with chronic renal failure or CT contrast media allergy.

Bosniak Type III In this category the indeterminate cysts are classified with one or more than the following features: measurable enhancement, parietal nodules, thick peripheral calcifications, thickened walls, hyperattenuating lesions, hypervascular septa, and multilocularity (Fig. 4.13a). These cysts need surgical excision or ablation since the incidence of malignancy is 33 %.

Bosniak Type IV This category includes cysts with irregular or smooth walls (Fig. 4.13b), with measurable enhancement, sometimes associated with intralesional necrosis (Fig. 4.13c). They are cysts with malignancy percentage close to 92–100 % and call for surgical treatment.

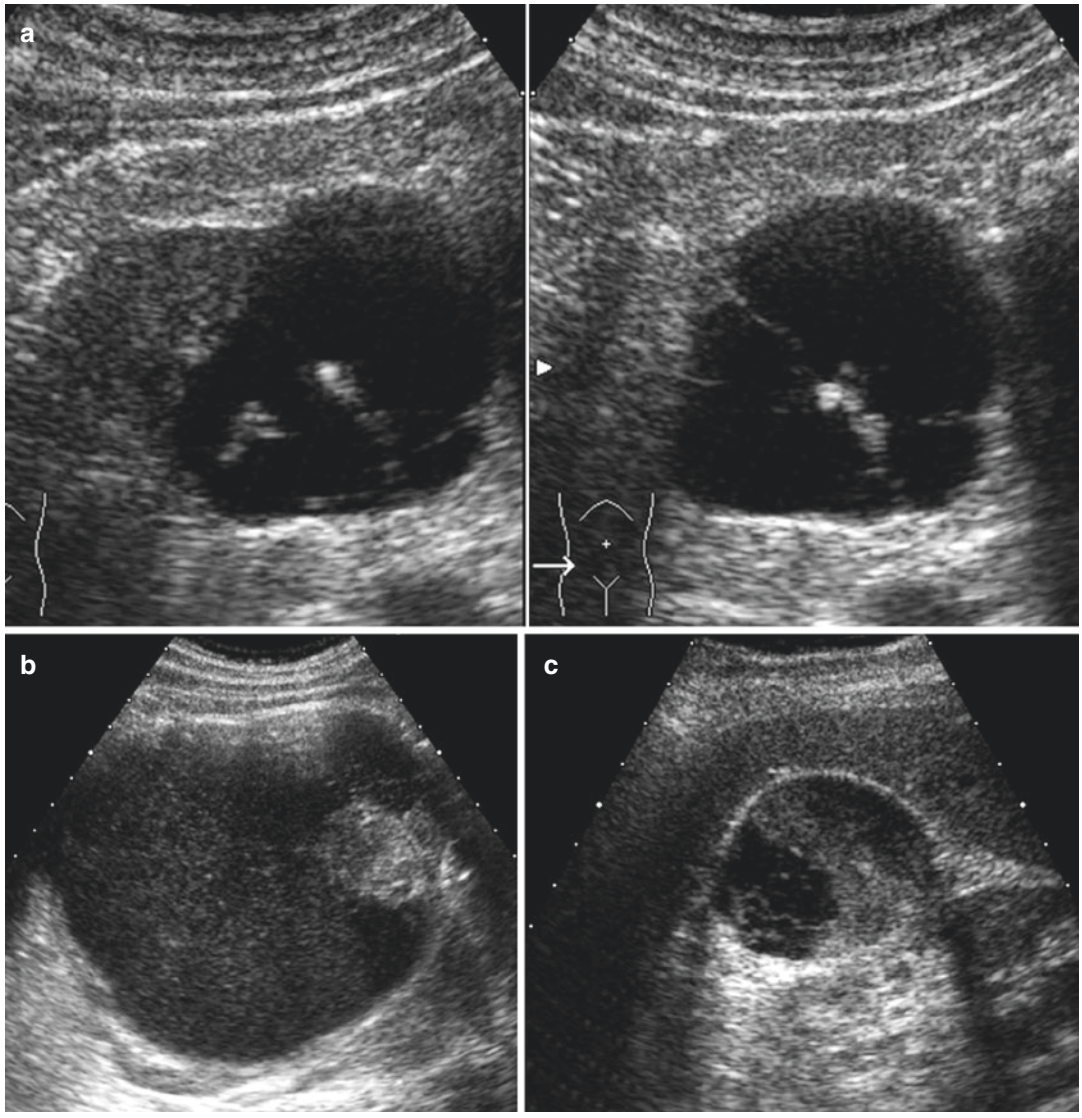

Fig. 4.13 (**a**) The presence of multiple thickened and nodular septa. (**b**) Large cystic lesion with corpuscular content and solid nodule protruding into the cystic lumen. Clear-cell carcinoma. (**c**) Exophytic expansive formation with unhomogeneous content due to the coexistence of liquid and solid component

4.3 Cysts of the Renal Sinus

Peripelvic cysts have lymphatic origin and coated with the epithelium and are the most frequent extra-parenchymal cysts of the kidney. These lesions generally are multiple, avascular, egg shaped, and tending to flattening. They can be bilateral, with radial aspect in correspondence of the renal hilum with peripheral echoicity due to the tissue included in the renal sinus, strained and compressed by the cysts themselves (Fig. 4.14a–e).

Parapelvic cysts plunge into the renal sinus from the adjacent renal parenchyma (Fig. 4.14f). They are usually single and are similar to simple renal cortical cyst. Seldom, cyst may cause compression of the pelvicalyceal system resulting into hydronephrosis. Therefore, in the absence of precise pathologic-radiologic correlative data, the term renal sinus cyst is recommended as a generic description of any fluid-filled cyst found in the renal sinus.

Differential diagnosis is pyelocalyceal, perinephric pseudocyst, calyceal diverticulum, lymphocele, hydronephrosis or uretero-pielic junction (UPJ) obstruction in duplicated collecting system urinary, and parapelvic lymphangiectasia.

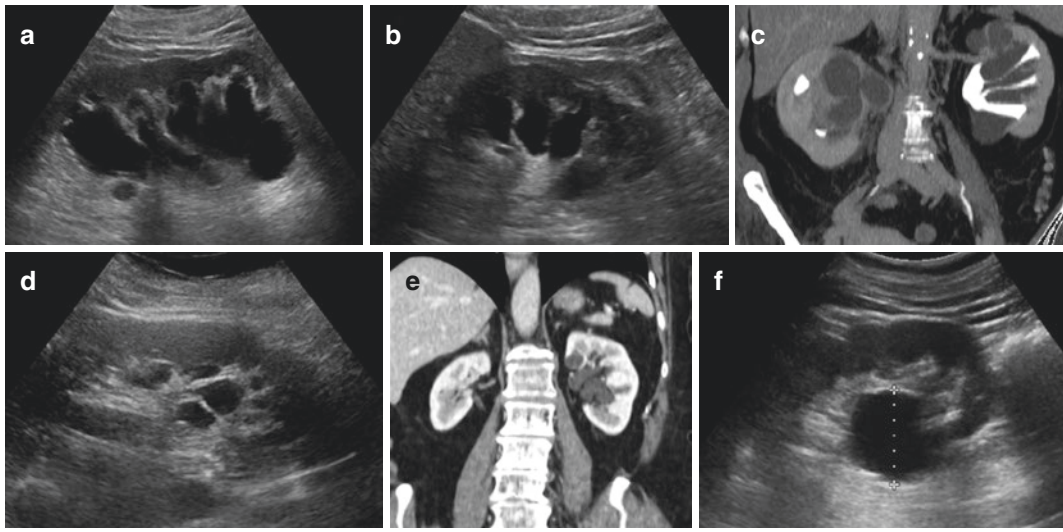

Fig. 4.14 (**a**, **b**) Peripelvic cysts (elongated cystic formations in the medullary). (**c**) Straining of the calyceal structures due to the resting of the cysts. (**d**, **e**) Multiple peripelvic cysts in US and CT coronal view. (**f**) Single parapelvic cyst

4.3.1 Renal Cystic Dysplasia: Multilocular Renal Cysts (Cystic Nephroma)

Renal cystic dysplasia (multicystic kidney)
Rare disease
Anomaly in metanephric differentiation
Coexistence of anomalous structures made of dysplastic collector ducts, fibrosis, and cartilage
Disorder of the architecture of renal lobations
Sometimes associated with excretory urinary tract disorders (agenesis or obstructive)
Generally prenatal diagnosis
Multiple cortical and medullary cystic lesions and complete disarrangement of the kidney (Fig. 4.15a–c)

Multilocular cystic nephroma
Benign tumor made of the epithelium and stroma
Unknown cause
All ages
More frequent in the women
Generally asymptomatic
Unilateral
Generally solitary lesion

US findings
Variable dimensions (5–15 cm)
Cysts separated by fibrous septa
Capsulated with calcifications
Well defined by the surrounding parenchyma
Certain diagnosis is exclusively histological

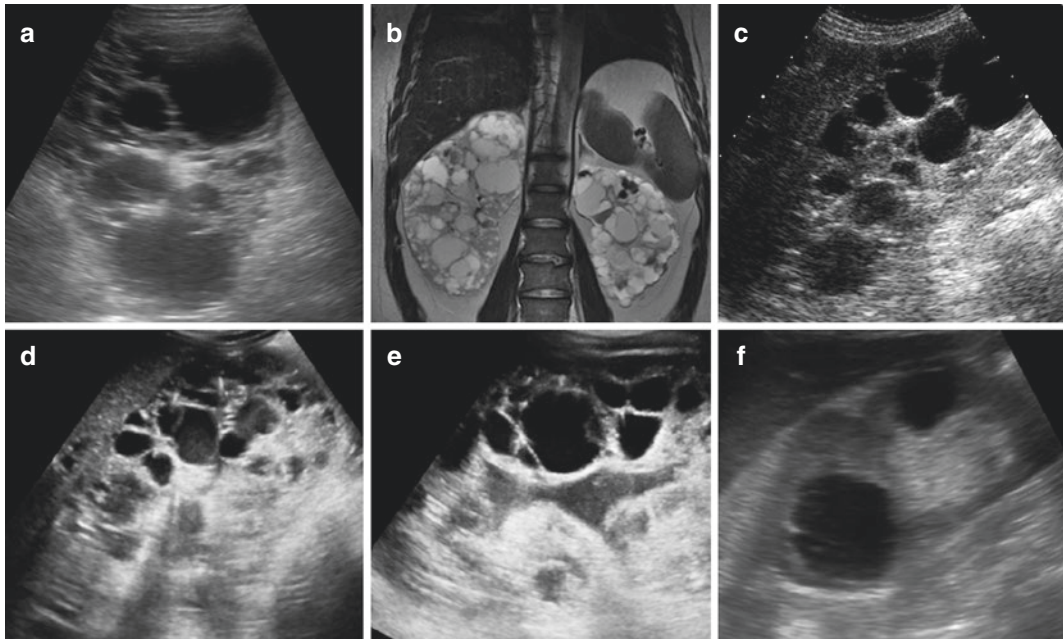

Fig. 4.15 (**a**) Cystic dysplasia. Marked enlargement of the kidneys with multiple cortical, medullary cystic lesions of various dimensions and loss of the renal cortex. (**b**) MRI. T2-weighted images in coronal plane. (**c**) Cystic dysplasia. The right kidney with multiple simple cystic lesions and loss of cortico-medullary differentiation. (**d**) Renal polycystosis. (**e**) The same patient with mild ectasia of the renal pelvis. (**f**) Acquired dialysis-induced cysts

4.3.2 Medullary Cystic Disease

Renal medullary cystic disease
Medullary sponge kidney (*Cacchi-Lenarduzzi-Ricci disease*)
Unknown pathogenesis
Multiple cystic dilatations of the collector ducts in the medullary
Precipitation of calcium salts along with the formation of small parenchymal stones
Nephronophthisis complex – uremic medullary cystic disease
Infancy
Cystic formations in the medullary
Interstitial fibrosis and cortical tubular atrophy
Renal failure

US findings
Kidneys reduced in volume
Small medullary cystic lesions, mainly against cortico-medullary junction
Not properly valuable at US

4.3.3 Renal Polycystic Disease

Autosomal-dominant polycystic kidney disease (Potter type III)
Multisystemic hereditary disease, 100 % of penetrance, and variable expressivity
Genetic mutation of chromosome 16
Polycystic malformation of the distal convoluted tubules, epithelium, and tubular walls, renal failure, and hypertension, commonly between the sixth and the seventh decade
Multiple expansive cysts with disarrangement of the renal parenchyma, always bilateral
Over 60 % of patients have hepatic cysts
5–10 % associated with small cerebral aneurysms of the anterior circulation
Sometimes associated with aortic aneurysms, aortic dissections, and cardiac valvulopathies

US findings
Enlarged kidneys, with irregular margins
Simple cysts, dimensions range from few millimeters to several centimeters (Fig. 4.15d, e)
Often echoic due to intracystic bleeding
Frequent calcifications of the cystic walls

Autosomal-recessive polycystic kidney disease (infantile)
Congenital periportal hepatic fibrosis and ectasia of the bile ducts
In childhood or in young age, before the second decade of life
US detectable

US findings
Bilateral disease
Volumetric increase of the kidneys
Numerous and small cortical medullary cysts

4.3.4 Acquired Renal Cystic Disease (Associated with Dialysis)

Acquired renal cystic disease
Common to all the end-stage renal pathologies
Development in previously non-cystic kidneys
In patients who have undergone a long treatment with hemodialysis or peritoneal dialysis (Fig. 4.15f)
Possible causes: fibrosis, ischemia, and production of unknown metabolites
Us findings
Various dimension cysts, with possibility of malignant degeneration
Early stages: small and intrarenal cysts
Late stages: larger with intraluminal bleeding and calcifications

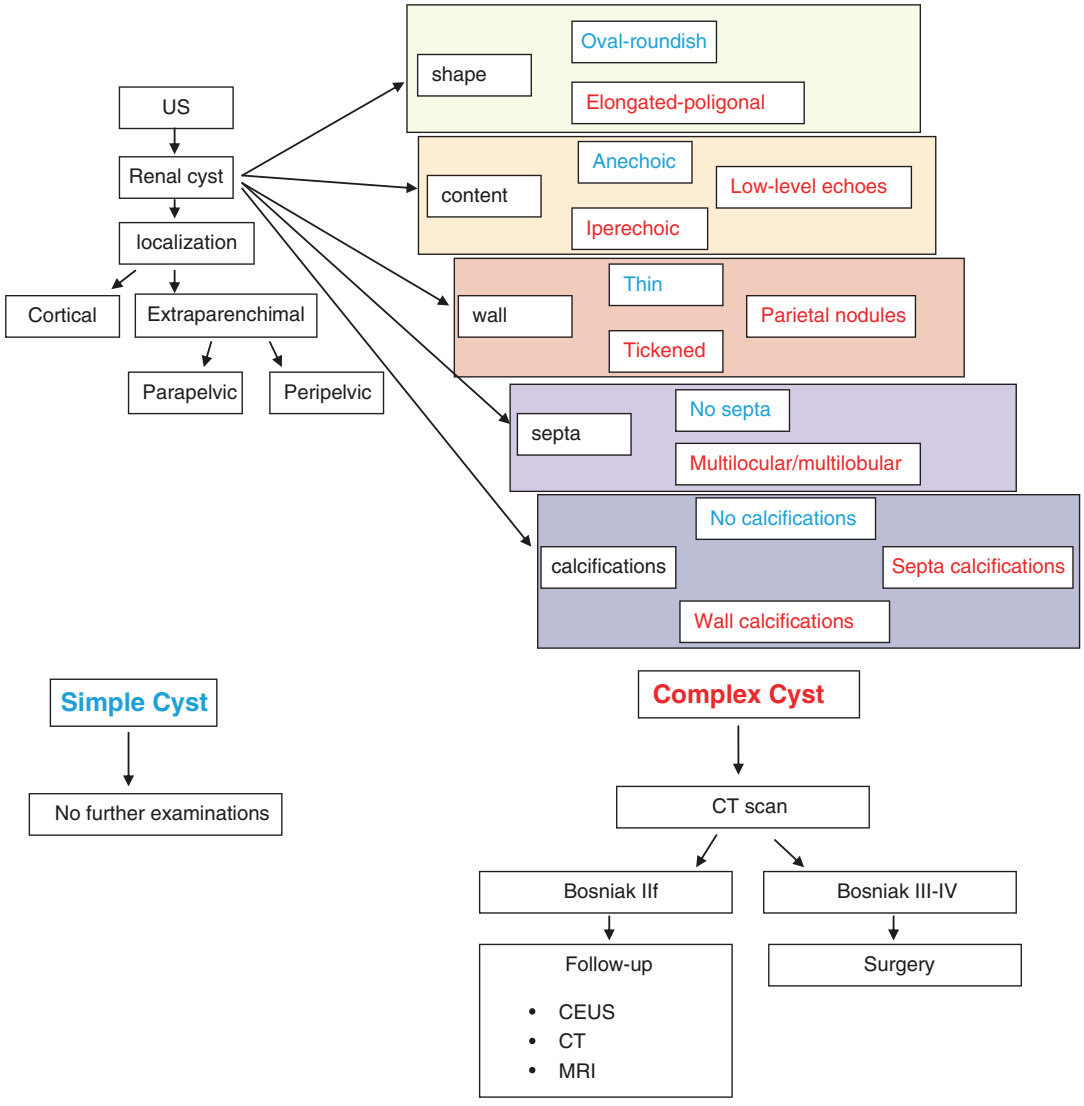
US
Renal cyst
localization
Cortical
Extraparenchimal
Parapelvic
Peripelvic
shape
Oval-roundish
Elongated-poligonal
content
Anechoic
Low-level echoes
Iperechoic
wall
Thin
Parietal nodules
Tickened
septa
No septa
Multilocular/multilobular
calcifications
No calcifications
Septa calcifications
Wall calcifications
Simple Cyst
No further examinations
Complex Cyst
CT scan
Bosniak IIf
Bosniak III-IV
Follow-up
CEUS
CT
MRI
Surgery

Bibliography

1. Bisceglia M, Galliani CA, Senger C et al (2006) Renal cystic disease: a review. Adv Anat Pathol 13(1): 26–56
2. Al-Said J, Brumback MA, Moghazi S et al (2004) Reduced renal function in patients with simple renal cysts. Kidney Int 65(6):2303–2308
3. Terada N, Arai Y, Kinukawa N, Terai A (2002) The 10-year natural history of simple renal cysts. J Urol 167(1):21–23
4. Hartman DS, Choyke PL, Hartman MS (2004) A practical approach to the cystic renal mass. Radiographics 24:S101–S115
5. Ravine D, Gibson RN, Donlan J, Sheffield LJ (1993) An ultrasound renal cyst prevalence survey: Specificity data for inherited renal cystic disease. Am J Kidney Dis 22(6):803–807
6. Clayman RV, Surya V, Miller RP et al (1984) Pursuit of the renal mass. Is ultrasound enough? Am J Med 77(2):218–223
7. Feldman MK, Katyal S, Blackwood MS (2009) US Artifacts. RadioGraphics 29:1179–1189
8. Battaglia M, Ditonno P, Mancini V et al (2002) Long-term follow-up of peripelvic renal multicystic lymphangiectasia. Arch Ital Urol Androl 74:200–205
9. Amis ES Jr (2000) Cysts of the renal sinus. In: Pollack HM, McClennan BL (eds) Clinical urography, 2nd edn. Saunders, Philadelphia, pp 1404–1412
10. Eknoyan G (2009) A clinical view of simple and complex renal cysts. J Am Soc Nephrol 20(9):1874–1876
11. Malhi H, Grant EG, Duddalwar V (2014) Contrast-Enhanced Ultrasound of the Liver and Kidney. Radiol Clin North Am 52(6):1177–1190
12. Kim WS, Goldman SM, Gatewood OM et al (1981) Computed tomography in calcified renal masses. J Comput Assist Tomogr 5(6):855–860
13. Weyman PJ, McClennan BL, Lee JK, Stanley RJ (1982) CT of calcified renal masses. AJR Am J Roentgenol 138:1095–1099
14. Rosenberg ER, Korobkin M, Foster W et al (1985) The significance of septations in a renal cyst. AJR Am J Roentgenol 144(3):593–595
15. Ascenti G, Mazziotti S, Zimbaro G et al (2007) Complex cystic renal masses: characterization with contrast-enhanced US. Radiology 243:158–165
16. Park BK, Kim B, Kim SH et al (2007) Assessment of cystic renal masses based on Bosniak classification: comparison of CT and contrastenhanced US. Eur J Radiol 61:310–314
17. McGuire BB, Fitzpatrick JM (2010) The diagnosis and management of complex renal cysts. Curr Opin Urol 20:349–354
18. Bosniak MA (1994) How does one deal with a renal cyst that appears to be Bosniak class II on a CT scan but has sonographic features suggestive of malignancy (e.g. nodularity of wall or a nodular or irregular septum)? AJR Am J Roentgenol 163(1):216

Kidney Stones

5

Libero Barozzi, Diana Capannelli,
Massimo Valentino, and Michele Bertolotto

5.1 Introduction

Urolithiasis is a frequent complaint at emergency department. The classic presentation is an abrupt, unilateral severe pain in the flank that radiates inferiorly and anteriorly to the groin. The typical pain is described as crampiform ("waxing and waning") and the acute phases may last 20–60 min. The pain occurs with the passage of the stone within the ureter with consequent obstruction of excretory system, while patients with small, non-obstructing stones may be asymptomatic or experience moderate symptoms. Patients may also refer intense nausea with or without vomiting and hematuria. When the stone approaches the ureterovesical junction, lower-quadrant pain, urinary frequency, dysuria, or stranguria may occur.

The peak incidence is between 20 and 50 years. Predisposing factors for stone-forming disease include sex (male vs female 4:1), age, inherited and individual predisposing factors (obesity), diet, and fluid intake.

Several theories have been proposed for pathogenesis of kidney stones. There are different types of calculi associated with different etiopathogenesis. Urinary supersaturation is necessary for calcific stone formation. Several substances found in urine (pyrophosphate, Tamm-Horsfall proteins, and magnesium) help in precipitating crystal formation. The crystals are trapped in the papillary collecting duct and result in stone formation. Underlying chronic urinary infections (*Proteus mirabilis*, *Escherichia coli*, *Candida albicans*) are responsible of struvite, matrix, or xanthine calculi. Also cysteine and acid uric calculi may occur, often associated to systemic diseases (cystinuria and hyperuricosuria).

5.2 Role of Imaging

The aim of imaging is the detection and characterization of kidney stones (site, number, size) and complications of urinary obstruction and

L. Barozzi (✉)
Radiology Unit, Casa di Cura Madre Fortunata Toniolo, Via Toscana 34, Bologna 40141, Italy
e-mail: libero.barozzi@alice.it

D. Capannelli
Radiology Unit, Cardio Thoracic Vascular Department, University of Bologna, Policlinico Sant'Orsola-Malpighi, Via Massarenti 9, Bologna 40138, Italy
e-mail: diana.capannelli@yahoo.it

M. Valentino
Radiology Department, Tolmezzo Hospital, Via Morgagni 18, Tolmezzo (UD) 33028, Italy
e-mail: mvm.valentino@gmail.com

M. Bertolotto
Radiology Department, University of Trieste, Ospedale di Cattinara, Strada di Fiume 447, Trieste 34149, Italy
e-mail: bertolot@units.it

P. Martino, A.B. Galosi (eds.), *Atlas of Ultrasonography in Urology, Andrology, and Nephrology*,
DOI 10.1007/978-3-319-40782-1_5

differential diagnosis of other causes of acute intense back pain.

Principal imaging techniques employed to diagnose renal colic include plain abdominal radiography, ultrasonography (US), intravenous urography (IVU), and computed tomography (CT).

5.2.1 Plain Abdominal Radiography

Plain abdominal radiography is useful to detect calcific stones, especially in ureteral segments not easily visualized with US. Typical sites are the anatomical key points of narrowing such as the ureteropelvic junction, the ureterovesical junction, and the crossing of ureter over the iliac vessels.

Calcium stones as small as 1–2 mm can be seen. Cystine stones as small as 3–4 mm may be depicted, but uric acid stones are usually not seen unless they have become calcified.

The main limitations include the presence of bowel gas and fecal material within the large bowel, which can obscure small calculi, or the overlapping of extraurinary calcifications including vascular calcifications, calcified lymph nodes, focal zones of compact bone, and phleboliths.

Renal calculi are usually single and polymorphic and with homogeneous opacity, while phleboliths typically appear as multiple round or oval opacities with a central lucency and are usually located lower than and lateral to the ureter, projecting over the lateral inferior portion of the sacrum.

5.2.2 Intravenous Urography

Intravenous urography (IVU) is a traditional invasive imaging technique, widely abandoned in emergency department. It consists of a baseline plain abdominal radiography, followed by intravenous administration of low-osmolality nonionic contrast medium and a series of delayed films evaluating the excretion of contrast through the urinary system.

The presence of kidney stone is visualized as a filling defect. Even if direct abdominal plain film can detect only calcific stones, the collection of contrast into the renal system is able to visualize filling defects both from radiopaque and radiolucent stones. On the other hand, IVU is not able to differentiate a stone from a blood clot: in these cases, only unenhanced CT helps in the differential diagnosis.

IVU is useful for confirming the exact location of a stone within the urinary tract, but also provides both structural and functional information, such as the degree of obstruction, the blunting of the calyceal fornices (hydronephrosis), and also the delayed excretion of contrast in the affected kidney (delayed or absent nephrogram and pyelogram).

Immediately after the passage of a stone, a residual mild obstruction or edema can be detected at the ureteropelvic junction. In these cases, the abdominal compression (prone patients) or films acquired in erect position may allow the passage of small amounts of contrast.

Extravasation of contrasted urine is a possible complication, easily detected by IVU. It is often first indicated by blurring of the calyceal fornices, but in case of greater extravasation, the contrast may collect in the perinephric space (urinoma).

IVU can also depict anatomic abnormalities that may predispose patients to stone formation or alter therapy, such as calyceal diverticula, duplication, ureteropelvic junction obstruction, or dysplasia.

The main disadvantages include high radiation exposure (multiple delayed films are often required), possible adverse reaction to intravenous contrast media, and risk of nephrotoxicity. In particular, this examination is contraindicated in patients with renal impairment (serum creatinine over 150 mmol/L), and it is not suggested in case of acute frank ureteral obstruction due to contrast-induced diuresis.

The risk of these complications above makes this examination largely been superseded by unenhanced CT.

5.2.3 Computed Tomography

Computed tomography (CT) is the most sensitive radiologic examination for the detection, localization, and characterization of urinary stones

(sensitivity of 96–98 %, specificity near 100 %), but also helps in identifying other causes of abdominal pain.

As for the detection of stones, helical CT frequently depicts small and non-obstructing stones that can be missed on IVU. CT is also able to differentiate between nonopaque stones and blood clots or tumors (compared with IVU, which may depict only a filling defect).

Even if a stone cannot be directly visualized, CT may depict secondary signs of obstruction or stone passage, such as hydronephrosis, ureteral dilatation, enlarged kidneys, perinephric fluid (reactive), perirenal urinoma (suggesting calyceal rupture), or soft-tissue rim sign (due to circumferential edema of the ureteral wall). If contrast material is administered, a delayed or hyperattenuating nephrogram may also be visible if the ureter has an obstruction.

Unenhanced CT is usually preferred, because stones in the collecting system may be obscured by contrast material. Sometimes intravenous injection of contrast material is required for further evaluation, such as in the differential diagnosis between phleboliths and urinary stones.

The main limit of CT is the exposure of patients to ionizing radiation, and, in particular, most of patients with urinary stones are young. Low-dose CT protocols are largely adopted, allowing to reduce the exposure from 5.5 to 18 mSv of helical CT to 0.7–2 mSv. Special concern should be regarded to pregnant women and children: in these cases, US should be the study of choice.

Another recent advance in CT imaging is the dual-energy computed tomography (DECT). It uses both a high-energy and a low-energy source to define stone composition, by assessing stone attenuation at two different kVp levels. However, DECT has the important disadvantage of high radiation exposure.

5.2.4 Ultrasound

Ultrasonography (US) is the procedure of choice for pregnant women and children because of the risks associated with radiation exposure.

US has several limitations in the direct visualization of stones, especially stones smaller than 2 mm, stones at the ureteropelvic junction, or stones in the mid ureter (25–45 %) [1]. Otherwise, US shows a higher sensitivity for the identification of indirect signs, such as hydronephrosis (approximately 85–90 %) [2].

Compared with nonenhanced CT, US is more dependent on the body habitus of the patient and the skill level of the operator, but the combination of US and abdominal plain radiography provides comparable results with noncontrast CT [3].

Stones appear on US as bright echogenic foci with posterior acoustic shadowing (Figs. 5.1 and 5.2). Other US criteria for the diagnosis of a kidney stone include twinkle and comet-tail artifacts on color Doppler examination. These artifacts are the result of intrinsic machine noise in the presence of small highly reflective objects. Comet-tail artifact occurs immediately deep to the object as a tail linear aliased band of color that extends away from the probe. Twinkle artifact (Fig. 5.3) appears as a focus of alternating colors behind the stone with the appearance of turbulent blood flow. Twinkle artifact is more sensitive than posterior acoustic shadowing in case of small stones.

Stones can be easily visualized if they are in the kidneys and the distal ureter at or near the ureterovesical junction, especially if dilatation is present (Fig. 5.4), while small stones (<5 mm) or stones within the ureter cannot be detected with US. Sometimes the ureterovesical junction is not easy to be visualized: in these cases, a urine-filled bladder is mandatory and provides an excellent acoustic window for US. Even if US remains less accurate than IVU or CT in the assessment of this region, color Doppler examination can provide useful additional information as the presence or absence of ureteral jet. The pumping effects of calyceal peristalsis and the renal diuresis that lead to protrusion of urine into the bladder. On color Doppler it appears as a colored jet near the ureterovesical junction. In normal conditions,

deep breath and Valsalva maneuver lead to a bilateral ureteral jet (Fig. 5.5). The unilateral absence of ureteral jet on the symptomatic side in a well-hydrated patient is pathognomonic of complete obstruction, while asymmetry of ureteral jets is suggestive of incomplete obstruction [4].

Diagnostic criteria of obstructive urolithiasis include direct visualization of the stone and dilatation of ureter more than 6 mm in diameter.

The dilatation of renal collecting system is scored from grade 1 to 3, which means a minimal, moderate, or severe calyceal dilatation with thinning of the renal cortex (Fig. 5.6).

However, false negative is significant because some patients with acute obstruction show little or no dilatation, probably due to intermittent or incomplete obstruction. On the other hand, also false positives can occur: sometimes differential diagnosis between ureteropelvic junction obstruction and an extrarenal pelvis is not possible with US alone, and a large extrarenal pelvis can easily be misread for hydronephrosis. Especially in slim habitus patients and more within the left kidney (probably due to the compression of the left renal vein between the abdominal aorta and mesenteric vessels), prominent vessels in the renal sinus may mimic grade 1 hydronephrosis: in these cases, color Doppler can show a vessel signal and exclude urinary obstruction [5]. Other causes of obstructive dilatation include inflammatory or neoplastic stenosis of the ureter (often unilateral), retroperitoneal fibrosis, and pregnancy. Also some causes of nonobstructive dilatation can mimic obstructive urolithiasis: vesicoureteral reflux (frequently unilateral) and full bladder (bilateral).

Doppler might be useful to evaluate cases with documented acute ureteral obstruction that do not demonstrate any significant hydroureteronephrosis (up to perhaps 35 % of patients) [6–8], by assessing an increase of intrarenal resistive index (RI). Under normal conditions, renal vascular resistance is relatively low and renal blood flow is continued, with a reasonable flow continuing even during diastole. In acute ureteric obstruction, a decrease in renal blood flow during diastole occurs, and it is proportionately greater than that during systole with a consecutive increase of RI (calculated as peak systolic velocity minus end-diastolic velocity divided by peak systolic velocity). The criteria to quantify a significant change of RI include elevation of the RI above 0.7 and an interrenal difference in RI between normal (contralateral) and pathological (obstructed) kidney of 0.04 or more. However, the main limit of intrarenal RI evaluation is that it does not identify partial or intermittent obstructions (not severe enough to induce renal vasoconstriction) and cannot differentiate between intrinsic and extrinsic urinary obstructions.

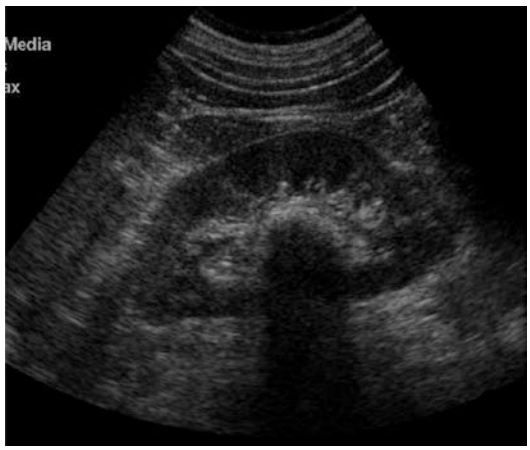

Fig. 5.1 Longitudinal US scanning of the kidney shows a calcific stone, which appears as bright echogenic foci with posterior acoustic shadowing. No dilatation of collecting system is present

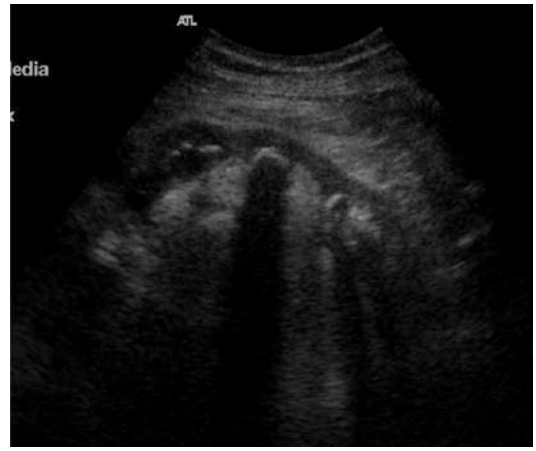

Fig. 5.2 Staghorn stone: renal pelvic stones may grow to large size by occupying completely the pelvic space and forming a cast of the renal pelvis and calices. They are usually associated with chronic urinary tract infections. Staghorn stone usually appears as a densely calcified mass, producing marked posterior acoustic shadowing

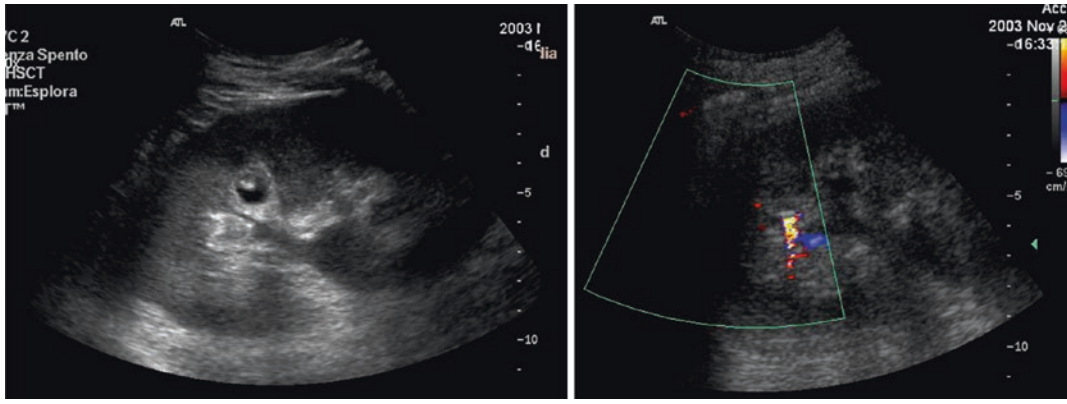

Fig. 5.3 Twinkle artifact appears as a tail linear band of alternating colors behind the stone

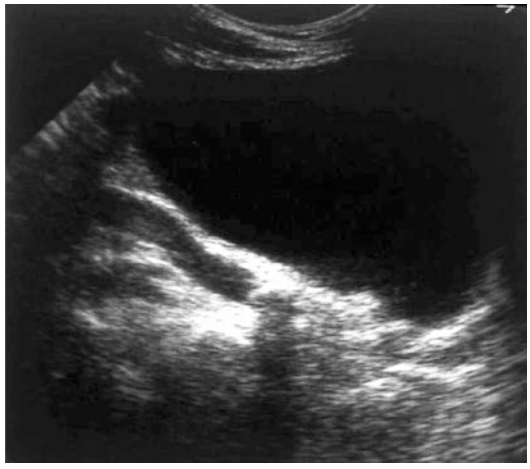

Fig. 5.4 Obstructive calculus within the distal ureter, near the ureterovesical junction. The stone provides complete obstruction and dilatation of the distal tract of the ureter

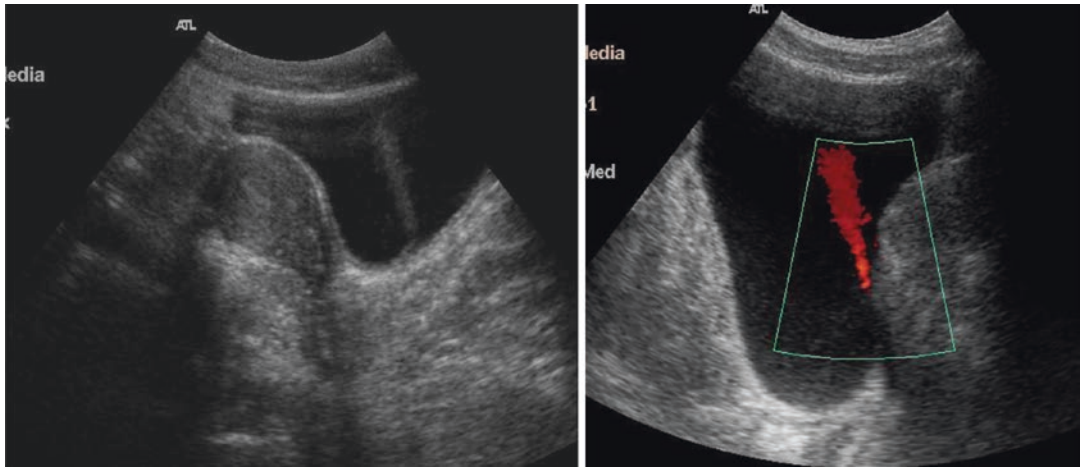

Fig. 5.5 Normal ureteral jet. The arrival of urine into the bladder appears as a turbulence of the flow near the ureterovesical junction. Color Doppler confirms the presence of a high-velocity flow

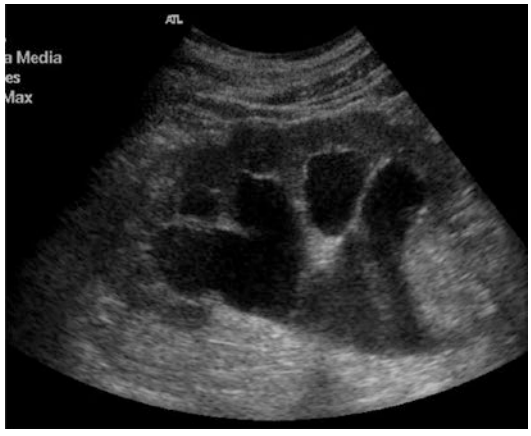

Fig. 5.6 Grade 3 hydronephrosis. Longitudinal US scan shows a severe dilatation of the pelvis and calices with thinning of the renal cortex

References

1. Fowler KA, Locken JA, Duchesne JH, Williamson MR (2002) US for detecting renal calculi with nonenhanced CT as a reference standard. Radiology 222:109
2. Graham A, Luber S, Wolfson AB (2011) Urolithiasis in the emergency department. Emerg Med Clin North Am 29:519
3. Patlas M, Farkas A, Fisher D, Zaghal I, Hadas-Halpern I (2001) Ultrasound vs CT for the detection of ureteric stones in patients with renal colic. Br J Radiol 74:901
4. Burge HJ, Middleton WD, McClennan BL, Hildebot CF (1991) Ureteral jets in healthy subjects and in patients with unilateral calculi: comparison with color Doppler ultrasound. Radiology 180:437
5. Scola FH, Cronan JJ, Schepps B (1989) Grade 1 hydronephrosis: pulsed Doppler US evaluation. Radiology 171:519
6. Mostbeck GH, Zontsich T, Turetschek K (2001) Ultrasound of the kidney: obstruction and medical diseases. Eur Radiol 11:1878
7. Mallek M, Bankier AA, Etele-Heinz A, Kletter K, Mostbeck GH (1996) Distinction between obstructive and nonobstructive hydronephrosis: value of diuresis duplex Doppler sonography. AJR Am J Roentgenol 166:113
8. Fung LC, Steckler RE, Khoury AE, McLorie GA, Chait PG, Churchill BM (1994) Intrarenal resistive index correlates with renal pelvis pressure. J Urol 152:607

Renal Masses

6

Libero Barozzi, Diana Capannelli,
Massimo Valentino, and Michele Bertolotto

6.1 Introduction

CT is the gold standard in detecting and characterizing renal masses and staging renal cell carcinomas (RCCs). Although US plays a key role in the early detection of solid renal masses, US is also a useful tool to guide percutaneous biopsies with more advantages than CT-guided biopsy: it provides a real-time imaging of the procedure and allows a follow-up of post-procedure complications (subcapsular hematomas or arteriovenous fistulas).

6.2 Benign Masses

Benign tumors are a frequent incidental finding in asymptomatic adult patients: autopsy studies demonstrated that almost 40 % of patients older than 70 years have adenomas. Differential diagnosis from RCC is difficult because imaging findings of many benign renal tumors are not characteristic and overlapped with those of malignant ones.

The most common benign solid renal tumors are angiomyolipomas and oncocytomas.

L. Barozzi (✉)
Radiology Unit, Casa di Cura Madre Fortunata Toniolo,
Via Toscana 34, Bologna 40141, Italy
e-mail: libero.barozzi@alice.it

D. Capannelli
Radiology Unit, Cardio Thoracic Vascular Department,
University of Bologna, Policlinico Sant'Orsola-Malpighi,
Via Massarenti 9, Bologna 40138, Italy
e-mail: diana.capannelli@yahoo.it

M. Valentino
Radiology Department, Tolmezzo Hospital,
Via Morgagni 18, Tolmezzo (UD) 33028, Italy
e-mail: mvm.valentino@gmail.com

M. Bertolotto
Radiology Department, University of Trieste,
Ospedale di Cattinara, Strada di Fiume 447,
Trieste 34149, Italy
e-mail: bertolot@units.it

P. Martino, A.B. Galosi (eds.), *Atlas of Ultrasonography in Urology, Andrology, and Nephrology*,
DOI 10.1007/978-3-319-40782-1_6

6.2.1 Angiomyolipoma

Angiomyolipoma is the most frequent mesenchymal benign neoplasm of the kidney, and it contains smooth muscle, vascular, lipomatous, and myeloid components in different proportions, giving it a heterogeneous appearance on imaging.

It occurs more frequently in women and in a solitary form (80%). Angiomyolipomas are rare in children but occur in up to 80% of children with tuberous sclerosis: in these cases angiomyolipomas are bilateral, small, and multifocal, whereas in sporadic forms, they are more commonly solitary, large, and symptomatic lesions. Also in lymphangioleiomyomatosis (a rare progressive disease that affects both the lungs and kidney of young women), multiple renal angiomyolipomas can be found.

US characteristics change on the basis of the size of the lesion.

Small angiomyolipomas (<3 cm) appear as subcapsular, hyperechoic, sharply marginated, and homogeneous lesions on B-mode. After microbubble contrast agent injection at contrast-enhanced US (CEUS), they usually appear persistently hypovascular in comparison to the adjacent renal parenchyma [1] (Figs. 6.1 and 6.2).

Large angiomyolipomas (>3 cm) typically have a heterogeneous bright appearance at US due to solid, adipose, and hemorrhagic components and frequently present an exophytic development with a wedge-shaped connection with the renal parenchyma.

Sometimes large angiomyolipomas may be complicated by hemorrhage (spontaneous or associated with relatively minor or incidental trauma). The risk of bleeding is associated with the size of the lesion (>4 cm) and the amount of angiogenic component, usually constituted of irregular and dysplastic blood vessels with abnormal thick wall and therefore predisposed to aneurysmal dilatation and hemorrhage. US findings include intralesional hemorrhage (poorly defined hyperechogenicity), subcapsular hematoma, or retroperitoneal bleeding. Management options include conservative management, embolization, and nephrectomy depending on hemodynamic considerations. Therefore, trans-arterial embolization of lesions >4 cm (or with intratumoral aneurysm size larger than 5 mm) is highly recommended [2].

Renal angiomyolipomas are benign, but they can be locally invasive, extending into the perirenal fat or into the renal vein and even the inferior vena cava with a tumorous thrombus. Further CT assessment should be performed to help in differential diagnosis.

Differentiating angiomyolipomas from RCC is the key point of the diagnostic algorithm because while asymptomatic angiomyolipoma does not need surgical resection, RCC should be completely removed. Marked echogenicity in a renal mass is not pathognomonic of angiomyolipomas. Also small RCC may be hyperechoic, even if angiomyolipoma tends to be much more echogenic than RCC. Conversely, intratumoral cysts and hypoechoic rim are suggestive of RCC, because these findings are absent in angiomyolipomas. A false-negative diagnosis may also occur in cases involving a hemorrhagic tumor. If clinical suspect is present (hematuria), also echogenic lesions should be further investigated with CT scans, and the fat content of the tumor should be assessed.

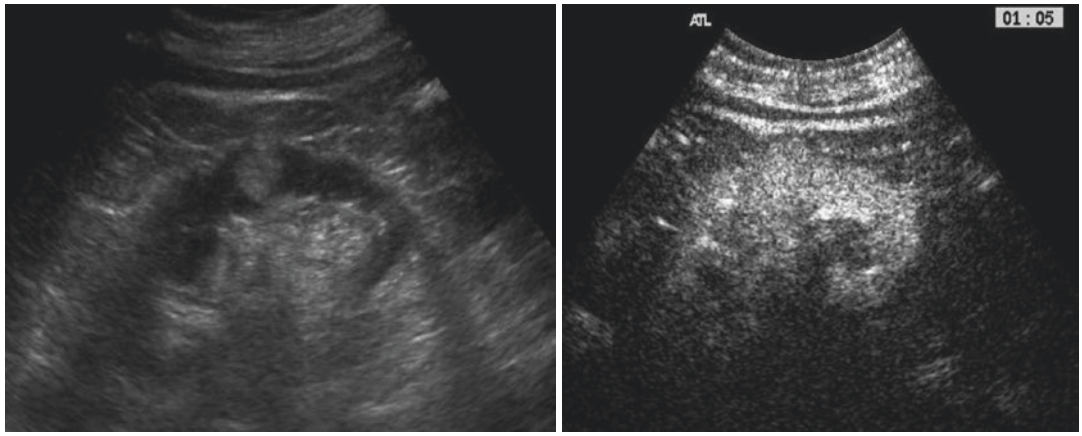

Fig. 6.1 B-mode examination shows a subcapsular, hyperechoic, sharply marginated, and homogeneous lesion. After microbubble contrast agent injection, it appears as iso-hypovascular in comparison to the adjacent cortex

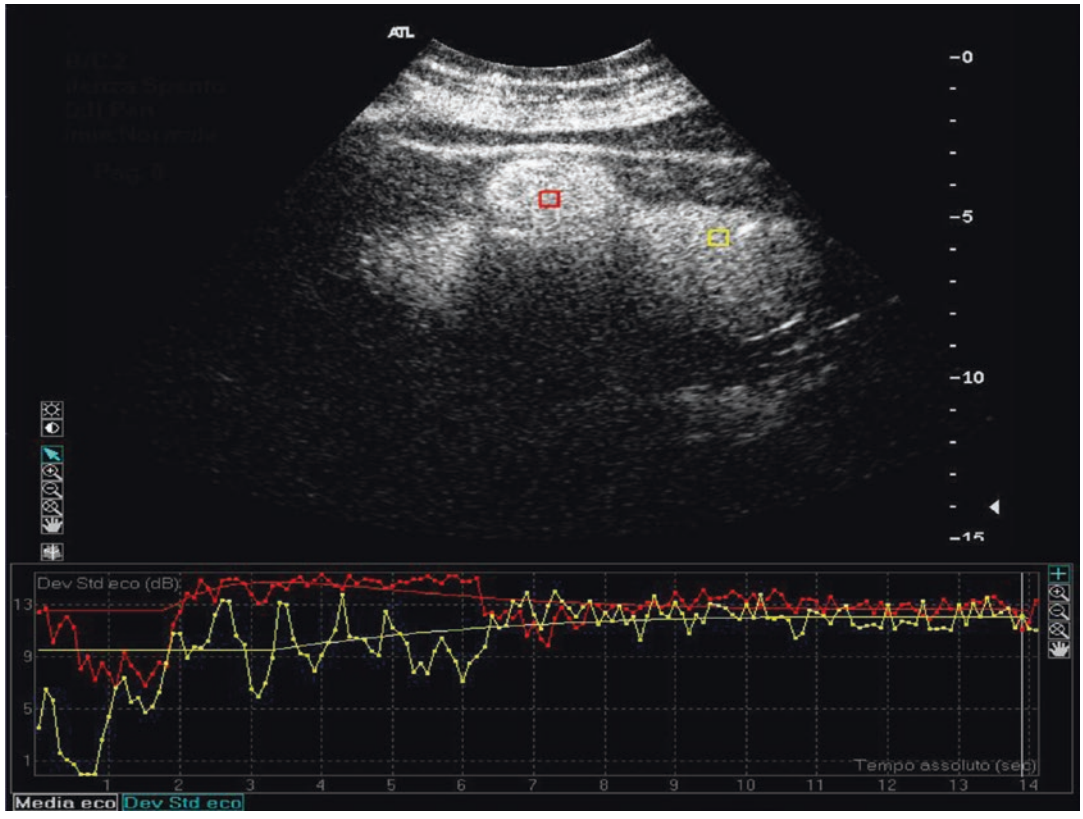

Fig. 6.2 Time-intensity curves display a typical pattern of angiomyolipoma contrast enhancement. The red ROI was drawn in a hyperechoic lesion on B-mode, whereas the yellow ROI was drawn in an area representing the normal renal cortex. The red time-intensity curve shows a higher fast filling hyperenhancement with reference to the normal renal parenchyma, suggestive of angiomyolipoma

6.2.2 Oncocytoma

Oncocytoma is a benign tumor arising from proximal tubular epithelial cells. In literature cases of coexistent oncocytoma and RCC (10 %); multicentric, bilateral, or metachronous oncocytomas (4–6 %) [3]; and recurrence or even metastases following surgical resection are reported, suggesting that these neoplasms can become malignant. No reliable pattern on US has been reported to differentiate oncocytomas from RCC. Tumor homogenicity has been considered as suggestive of small oncocytomas, but it is not useful in differential diagnosis because of the considerable overlap among small renal tumors including RCC. Percutaneous biopsy may help in differentiating diagnosis; in difficult cases partial nephrectomy or minimally invasive approaches are also performed.

6.3 Cystic Lesions

Renal cysts are a common finding, but any cyst that does not show the typical features of a benign cyst is by definition "complicated" and requires further assessment. US findings that suggest a cystic or pseudocystic renal neoplasm include thick irregular wall, multiple septa, solid mural nodule, heterogeneous echoic content, and the demonstration of signal flow on color Doppler evaluation within the solid components.

In 1986, Morton Bosniak proposed a simple classification that classifies renal cysts into five categories based on their CT imaging appearance criteria, including morphological and enhancement characteristics [4–6]:

- I: Simple cyst with thin wall and no septa, calcification, or solid components. Fluid density (10–20 uH) and no enhancement after contrast medium infusion. Benign.
- II: Cyst that may contain a few thin septa or fine calcifications in the wall or septa. Uniformly high-attenuation lesions (<3 cm) because of the presence of hemorrhagic/proteinaceous content, with sharp margins but without enhancement. Benign.
- IIF: Cysts with more hairline-thin septa or minimal thickening of the septa/wall: a minimal enhancement of a hairline-thin septum or wall can be seen. The cysts may contain calcifications (nodular and thick) but without contrast enhancement. No enhancing soft-tissue elements. This category also includes intrarenal, well-marginated, non-enhancing, high-attenuation renal lesions >3 cm in size. This category was introduced in 2003 by Israeli and Bosniak [7] to stratify the malignancy risk of these lesions, malignant in a small proportion. Serial closed follow-up is required (6 months) to assess the lesion stability.
- III: Indeterminate cystic masses with thickened irregular walls or septa, with or without contrast enhancement. Surgery or close follow-up is recommended because over 50 % of these lesions are malignant.
- IV: Clearly malignant cystic lesions with enhancing soft-tissue components. Surgical therapy is required (cystic or necrotic RCC).

Even if the Bosniak classification system was developed on the basis of contrast enhancement findings of cystic renal masses on CE-MDCT [5, 6], CEUS can provide useful information to predict the risk of malignancy and, therefore, for the management of these lesions: surgical treatment or observation.

The problematic aspect is the differential diagnosis between lesions classified in category IIF, which require serial imaging follow-up [8] and category III lesions that require prompt surgery because of potential malignancy. In particular, CEUS is acquiring an increasing role in the assessment of indeterminate cystic lesions (Bosniak IIF and III) by detecting the presence and the enhancement of solid components. Recent comparative studies [9] between CEUS and CT revealed that CEUS imaging was superior to CT in terms of detecting additional septa, thickness of the wall or septa, and solid components. Microbubble contrast agents circulate in the microvessels of septa and walls, and CEUS provides the evaluation of internal structures of cystic renal masses with a higher resolution than CT. In particular, the demonstration of solid components is the key factor in differential with categories III and IV that are considered malignant and must be surgically removed (Fig. 6.3). A recent study [10] also introduced an independent diagnostic classification system for CEUS that was based on the enhancement patterns involving or not involving the peripheral wall, the intracystic septa, and the mural or septal nodule. This approach reveals a high correspondence between CEUS and CT, particularly for lesions of category III undetermined on CT, by proposing CEUS as an alternative to CT in the follow-up of complex renal cysts and in case of contraindications to iodinate contrast.

In conclusion, hyperattenuating lesion at CT with no significant contrast enhancement should be considered as possible hypovascularized tumor (RCC): in these cases, prompt US examination should be performed because hyperdense cysts are typically anechoic in 30–50 % of cases.

Sometimes necrotic RCC may mimic a cystic lesion on CT because of a necrotic content similar to fluid cysts in attenuating values: in these cases, US examination is able to show a heterogeneous echoic content consistent with necrosis, associated to irregular thickening of peripheral walls (Bosniak IV).

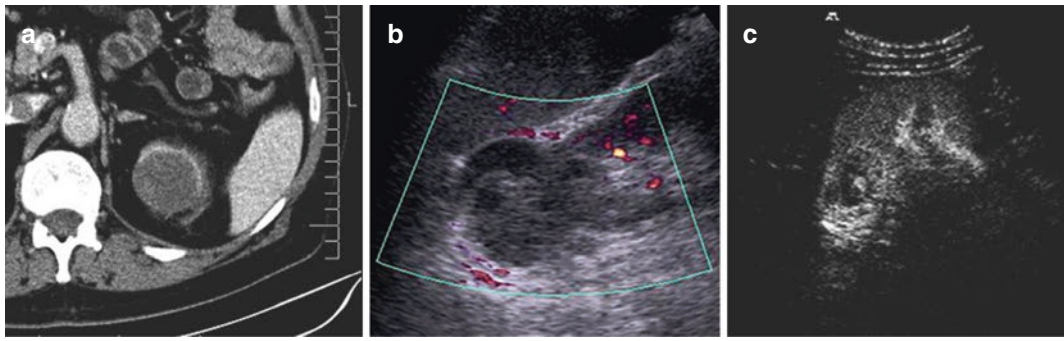

Fig. 6.3 Contrast enhancement CT scan shows a complicated cystic lesion with diffuse and smooth contrast enhancement (**a**). Color Doppler examination demonstrates a heterogeneous mass with hypoechoic and fluid component without significant vascular application (**b**). CEUS reveals an internal enhancing soft-tissue component, suggestive of Bosniak IV category (**c**)

6.4 Solid Masses

The majority of primary renal tumors are renal cell carcinomas (RCCs), whereas angiomyolipomas and oncocytomas represent a small part of renal solid lesions.

Most RCCs are first detected by US, while CT is the gold standard imaging modality for staging and surgical planning. CT can also provide information for the differentiation of RCC subtypes, which is important in planning treatment and closely related with prognosis. Magnetic resonance imaging (MRI) is used as a problem-solving modality and for staging. In doubt cases, percutaneous renal biopsy is a safe and accurate method of sampling the lesion and reaching a final histopathological diagnosis, which is closely related with prognosis.

The 2004 World Health Organization (WHO) classification recognizes several distinct histologic subtypes of RCC: clear cell RCC, papillary RCC, chromophobe RCC, multilocular cystic RCC, collecting duct carcinoma, medullary carcinoma, mucinous tubular and spindle cell carcinoma, hereditary cancer syndromes (von Hippel-Lindau disease, Birt-Hogg-Dubé syndrome, tuberous sclerosis, and other genetic conditions), and unclassified lesions.

- Clear cell RCC is also known as conventional RCC since it accounts for nearly 70 % of all RCCs. It originates from the renal cortex and typically exhibits an expansive growth pattern. It usually appears as a heterogeneous mass due to the presence of hemorrhage, necrosis, and cysts. Clear cell RCCs typically show hypervascularity on contrast-enhanced CT. Calcification may be seen in 10–15 %.
- Papillary RCC is the second most common subtype (10–15 %). It is often bilateral and multifocal, especially with hereditary syndromes. It usually has a good prognosis, and more than 80 % of tumors are confined to the cortex and within the renal capsule at the time of nephrectomy. It usually shows a lower contrast enhancement than a typical RCC. Reduced or absent tumor vascularity also correlates with intratumoral hemorrhage and necrosis (66 % of cases).
- Chromophobe RCC can mimic an oncocytoma: it is typically well circumscribed and solitary and shows uniform hyperechogenicity both in small and large masses. It appears hypovascular/avascular on early and delayed phase on CT. Sometimes biopsy is not able to differentiate it from oncocytoma because of the presence of chromophobe cells in both lesions.
- Multilocular cystic RCC consists of multiple variable-sized cysts with irregular, thick, and fibrous septa, surrounded by a fibrous capsule and with heterogeneous content. Most of RCC can present microcysts, but in multilocular cystic RCC, cysts are the predominant component. Differentiation between complicated cyst and cystic RCC may be problematic. As for Bosniak classification, any lesion that does not respect class II criteria but does not need surgical exploration is categorized into IIF and may underwent close follow-up (6 months) to detect any change.
- Collecting duct carcinoma is a highly aggressive subtype of RCC, associated with poor prognosis: metastasis is present in about 30 % of cases at presentation, with low 2-year survival rate after diagnosis (less than 30 %). It originates from the medulla and invades both the cortex, by distorting calyces and pelvis, and the adjacent renal parenchyma with a desmoplastic response with necrosis and hemorrhage. It metastasizes at the regional lymph nodes (80 %), lungs and adrenal glands (25 %), and liver (20 %). It can appear as a heterogeneous hyperechoic mass at US due to the presence of necrosis and hemorrhage.
- Medullary carcinoma is a rare highly aggressive subtype of RCC with a dismal prognosis:

it early metastasizes to the regional lymph nodes, liver, and lung. As collecting duct carcinoma, it originates from the medulla and early infiltrates the renal sinus (caliectasis) and cortex. At US it appears as a heterogeneous mass due to tumor necrosis. While the mass may enlarge the kidney, the renal shape is maintained because of infiltrative growth.

- Sarcomatoid RCC is no longer considered as a distinct histologic subtype of RCC, because any type of RCC can undergo a sarcomatoid dedifferentiation with poor prognosis. Imaging features are not typical because it can appear both as a confined mass and (more commonly) as an ill-defined mass, infiltrating the renal sinus and cortex, heterogeneous on US examination and after contrast injection because of necrosis and hemorrhage. The renal shape is maintained because of infiltrative growth.

At US examination, RCC characteristics depend on the size and proportions of the components. Larger tumors are usually hypoechoic or isoechoic to the renal parenchyma, sometimes with a heterogeneous aspect because of central necrosis, whereas small RCCs are typically hyperechoic. Major differential diagnosis of small RCC is small angiomyolipoma that usually shows higher echogenicity than RCC with strong sonic attenuation. Small RCCs also differ from angiomyolipoma because of the presence of intratumoral cysts and thin hypoechoic rim.

Grayscale US is sensitive but not specific enough for the characterization of small renal masses, and a solid mass in the kidneys may be considered as possible RCC unless strong evidence suggests another diagnosis.

Color and power Doppler examinations can provide useful additional information: Spectral Doppler US performed in the mass can show a low-resistant pattern of vascular flow (because of the increase of vascularization in hypervascular lesions) in contrast with the spectrum obtained in the adjacent parenchyma (resistance index in range in normal conditions or high in end-stage renal disease). Otherwise, spectral analysis does not provide definitive diagnostic criteria for RCC because also angiomyolipomas may exhibit a high-velocity pattern of intralesional vessels [11]. The analysis of vascular distribution with color or power Doppler has not increased the diagnostic accuracy for small solid renal tumors, while contrast-enhanced US (CEUS) can increase the detection of intratumoral vascularity. Renal malignancies have a rich blood supply (except for hypovascular lesions), and CEUS can show an increased and heterogeneous enhancement, fast filling, and rapid washout. However, the kidney itself has abundant blood supply, and sometimes the lesion may appear isoechoic to the surrounding renal cortex [12, 13]. CEUS is not currently used for differentiating benign lesions from malignant solid tumors. Even if several studies propose new methods for qualitative and quantitative assessment of contrast enhancement, solid malignancies do not show a specific perfusion pattern [12, 14].

Even if CT is the gold standard method for tumoral staging in RCC, US is useful to assess the involvement of the inferior vena cava by demonstrating the extent of venous thrombosis: on CT the inhomogeneous contrast filling of the inferior vena cava on cortico-medullar and delayed phase does not allow an accurate evaluation of thrombus. At US, the tumor thrombus appears as a solid echoic mass lying within the venous lumen, associated with enlargement of the vessel or surrounded by color flow. Power Doppler and CEUS may show color signal or contrast enhancement inside the thrombus due to tumor neovascularity. In US examination is very important to detect the cranial extension of the thrombus with respect to the hepatic veins and right atrium [15, 16]. Otherwise, US is not adequate to detect lymph node metastasis, while CT is highly accurate.

6.4.1 Other Differential Diagnoses

Another important role of US is to differentiate normal anatomical variants or pseudotumors from solid malignancies. Cortical defects or fetal lobations may mimic, respectively, hyperechoic or hypoechoic subcapsular tumors. Color Doppler and CEUS can add some useful information in differential diagnosis. For example, in renal column hypertrophy (a congenital renal dysplasia that mimics a solid lesion of the cortex), color Doppler and CEUS are able to demonstrate normal courses of renal vessels without an occupying lesion and a dynamic pattern of contrast enhancement identical to the surrounding parenchyma (Fig. 6.4).

Other differential diagnoses include lymphoma, metastasis, and inflammatory disease.

Lymphoma can have a variable appearance and may mimic RCC. It usually appears as bilateral solid renal masses, homogeneously hypoechoic. Primary renal lymphoma is very rare, and it is one of the most common extranodal sites of metastatic lymphoma (commonly a non-Hodgkin's lymphoma).

Characteristically, renal lymphoma shows an infiltrating growth into the renal sinus or a retroperitoneal extension. In most of the cases, it appears as multiple homogeneous parenchymal masses (50–60 %), variable in size (1–4.5 cm in diameter). In 25–30 % of cases, it can also appear as a gross retroperitoneal mass that invades directly the renal sinus or a perirenal mass that surrounds the kidneys. On rare occasion, lymphoma may appear as a solitary parenchymal mass (10–25 %) or a gross enlargement of the kidney (which usually maintains a reniform shape) due to diffuse infiltration [17]. Adenopathies are typically associated.

Also metastatic disease to the kidney typically manifests as multiple bilateral renal masses, often secondary to breast and lung cancers and associated with metastatic involvement of other organs.

In the case of lymphoma or previous history of solid cancer, the finding of a solitary renal mass needs further assessment, and percutaneous renal biopsy is required for a definitive diagnosis.

Inflammatory renal masses, such as pyelonephritis and renal abscess, may also mimic the appearance of a renal neoplasm. In the presence of a previous history of fever, leukocytosis, or urinary tract infection, inflammatory nature of the lesion may be suspected, and, in doubt cases, a needle aspiration should be performed to confirm the diagnosis [18].

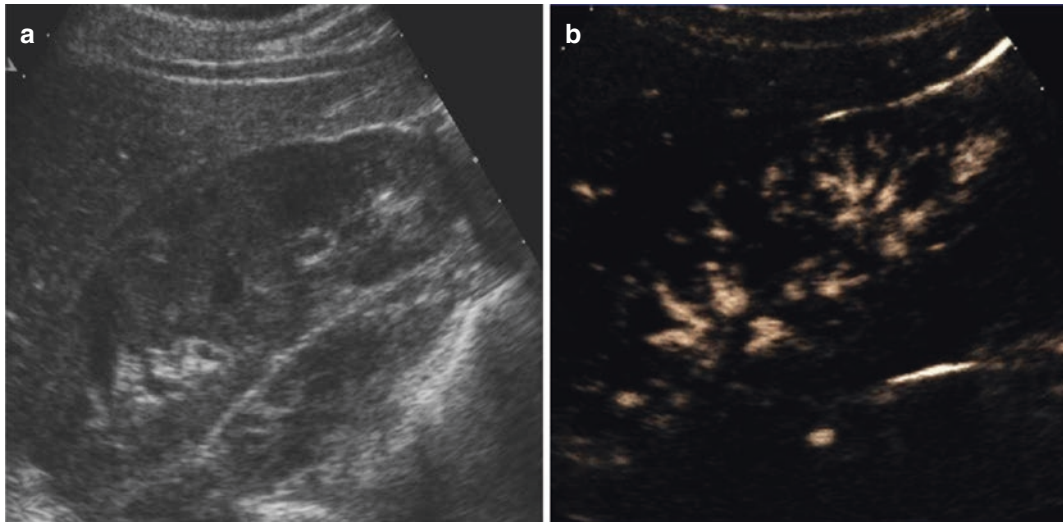

Fig. 6.4 Baseline US examination (**a**) shows an isoechoic mass that develops in the renal sinus and that simulates a solid occupying lesion. CEUS reveals a normal intravascular flow within this region, with homogeneous vascular enhancement without vessel distortion, suggestive of renal column dysplasia (**b**)

6.5 Pediatric Masses

Renal masses are the most common abdominal masses in childhood and include developmental anomalies with hydronephrosis, cystic renal diseases, and primary renal neoplasms.

Neoplastic renal masses in pediatric populations include Wilms tumor, nephroblastomatosis, RCC, mesoblastic nephroma, multilocular cystic renal tumor, clear cell sarcoma, angiomyolipoma, renal medullary carcinoma, ossifying renal tumor of infancy, metanephric adenoma, and lymphoma.

Wilms tumor is by far the most common renal neoplasm in childhood and accounts for 87 % of pediatric renal masses. Its peak incidence is at 3–4 years of age and in 80 % of patients presents before 5 years of age. Wilms tumor is bilateral in 4–13 % of children (more commonly synchronous, but also metachronous, tumors). Bilateral tumors are correlated with a higher incidence of nephroblastomatosis (present in up to 90 % of cases of bilateral Wilms) and may be associated with congenital genitourinary congenital anomalies (cryptorchidism, hypospadias, and horseshoe kidneys) or other genetic syndromes (hemihypertrophy). In these risk patients, US screening is recommended until 7 years of age with close controls (3–6 months) because a prompt diagnosis allows decrease in morbidity and permits curative nephron-sparing surgery. After the age of 7 years, the risk of developing Wilms tumor decreases significantly [19].

Wilms tumor appears a solid intrarenal mass, heterogeneously echoic (hemorrhage, fat, necrosis, or calcification). It shows a massive growth with distortion of the adjacent renal parenchyma (pseudocapsule) and the collecting system. It also spreads into perirenal adipose tissue by contiguous extension and displaces adjacent structures. Vascular invasion is frequent, and Wilms typically involves renal vein by direct spread with successive propagation of tumor thrombus into the inferior vena cava and right atrium (up to 20 % of cases of inferior vena cava involvement). Wilms does not typically encase the aorta: such encasement is a distinguishing characteristic of neuroblastoma. Metastases are most commonly found in the lungs (85 % of cases), liver, and regional lymph nodes.

CT preoperative examination is important to detect nodal or hepatic metastases, vascular extension of tumor thrombus, contralateral synchronous tumor, and associated nephrogenic rests, at risk of future malignant transformation into Wilms tumor.

Wilms tumor includes several histological subtypes and the prognosis depends on histologic findings, although Wilms tumor is associated with a good prognosis with an overall survival of 90 %. Unilateral Wilms tumor is generally treated with nephrectomy followed by adjuvant chemotherapy. Bilateral tumors are staged separately, and preoperative chemotherapy is useful to reduce the masses and allows at least unilateral nephron-sparing surgery.

Nephroblastomatosis consists of the presence of diffuse or multifocal nephrogenic rests in the renal cortex. Nephrogenic rests are foci of metanephric blastema that persist beyond 36 weeks of gestation and have high potential for malignant transformation into Wilms tumor. They usually appear as multiple bilateral subcapsular homogeneous nodules at US, CT, or MR imaging, whereas Wilms tumors are generally heterogeneous.

Nephroblastomatosis is associated with genetic syndromes, such as hemihypertrophy, sporadic aniridia, and Denys-Drash and Beckwith-Wiedemann or Perlman syndrome, which all are also associated with Wilms tumors.

Mesoblastic nephroma is the most common renal neoplasm in the first year of life.

Other less common renal masses include multilocular cystic renal tumor, renal cell carcinoma, angiomyolipoma, and lymphoma, which present the same characteristics than in the adult population.

References

1. Li R, Zhang X, Hua X, Cai P, Zhong H, Guo Y, Ding S, Yan XC (2010) Real-time contrast-enhanced ultrasonography of resected and immunohistochemically proven hepatic angiomyolipomas. Abdom Imaging 35:676

2. Yamakado K, Tanaka N, Nakagawa T et al (2002) Renal angiomyolipoma: relationships between tumor size, aneurysm formation, and rupture. Radiology 225:78
3. Dechet CB, Bostwick DG, Blute ML et al (1999) Renal oncocytoma: multifocality, bilateralism, metachronous tumor development and coexistent renal cell carcinoma. J Urol 162:40
4. European Association of Urology (EAU) Guidelines. 2014 edition
5. Bosniak MA (1997) Diagnosis and management of patients with complicated cystic lesions of the kidney. AJR Am J Roentgenol 169:819
6. Bosniak MA (1997) The use of the Bosniak classification system for renal cysts and cystic tumors. J Urol 157:1852
7. Israel GM, Bosniak MA (2003) Follow-up CT "of moderately complex cystic lesions of the kidney (Bosniak category IIF)". AJR Am J Roentgenol 181:627
8. Bosniak MA (1993) Problems in the radiologic diagnosis of renal parenchymal tumors. Urol Clin North Am 20:217
9. Park BK, Kim B, Kim SH, Ko K, Lee HM, Choi HY (2007) Assessment of cystic renal masses based on Bosniak classification: comparison of CT and contrast-enhanced US. Eur J Radiol 61:310
10. Quaia E, Bertolotto M, Cioffi V, Rossi A, Baratella E, Pizzolato R, Cova MA (2008) Comparison of contrast-enhanced sonography with unenhanced sonography and contrast-enhanced CT in the diagnosis of malignancy in complex cystic renal masses. AJR Am J Roentgenol 191:1239
11. Hélénon O, Correas JM, Balleyguiter C, Ghouadni M, Cornud F (2001) Ultrasound of renal tumors. Eur Radiol 11:1890
12. Cokkinos DD, Antypa EG, Skilakaki M, Kriketou D, Tavernaraki E, Piperopoulos PN (2013) Contrast enhanced ultrasound of the kidneys: what is it capable of? Biomed Res Int 595:873
13. Ignee A, Straub B, Schuessler G, Dietrich CF (2010) Contrast enhanced ultrasound of renal masses. World J Radiol 2:15
14. Wang XH, Wang YJ, Lei CG (2011) Evaluating the perfusion of occupying lesions of kidney and bladder with contrast-enhanced ultrasound. Clin Imaging 35:447
15. Hélénon O, Correas JM, Chabriais J et al (1998) Renal vascular Doppler imaging: clinical benefits of the power mode. Radiographics 18:1441
16. Bos SD, Mensik HJ (1998) Can duplex Doppler ultrasound replace computerized tomography in staging patients with renal cell carcinoma? Scand J Urol Nephrol 32:87
17. Urban BA, Fishman EK (2000) Renal lymphoma: CT patterns with emphasis on helical CT. Radiographics 20:197
18. Israel GM, Bosniak MA (2005) How I do it: evaluating renal masses. Radiology 236:441–450
19. Beckwith JB (1998) Children at increased risk for Wilms tumor: monitoring issues. J Pediatr 132: 377–379

Renal Trauma

7

Libero Barozzi, Diana Capannelli,
Massimo Valentino, and Michele Bertolotto

7.1 Introduction

Injury to the kidney is seen in approximately 8–10% of patients with blunt or penetrating abdominal injuries [1]. The vast majority (80–90%) of cases involve blunt rather than penetrating injury. Renal trauma is usually associated with the involvement of other organs, such as spleen and liver.

Trauma is classified into major or minor trauma depending on the severity of the injury, the location of damage, or a combination of both.

Major trauma occurs in injuries with complex dynamics (road accidents, falls from height), and usually multi-organ involvement occurs, while minor trauma is caused by localized forces that act with a small kinetic force and cause only confined damage.

Renal involvement in abdominal trauma is usually suspected on the base of the presence of hematuria, location of impact, wounds, or multiple fractures of the lower ribs. Hematuria is present in almost 80% of cases with renal injury; however, hematuria may be absent in patients with main renal artery thrombosis and devascularization [2].

The protocol for the management of patients with suspected renal injury divides patients into three groups:

1. Hemodynamically instable patients: surgical exploration; patients stabilized after initial poor scores: CT scan or repeat FAST
2. Hemodynamically stable patients with hematuria: CT scan
3. Hemodynamically stable patients with no hematuria and negative FAST: follow-up with clinical observation of at least 6 h duration [2]

L. Barozzi (✉)
Radiology Unit, Casa di Cura Madre Fortunata Toniolo, Via Toscana 34, Bologna 40141, Italy
e-mail: libero.barozzi@alice.it

D. Capannelli
Radiology Unit, Cardio Thoracic Vascular Department, University of Bologna, Policlinico Sant'Orsola-Malpighi, Via Massarenti 9, Bologna 40138, Italy
e-mail: diana.capannelli@yahoo.it

M. Valentino
Radiology Department, Tolmezzo Hospital, Via Morgagni 18, Tolmezzo (UD) 33028, Italy
e-mail: mvm.valentino@gmail.com

M. Bertolotto
Radiology Department, University of Trieste, Ospedale di Cattinara, Strada di Fiume 447, Trieste 34149, Italy
e-mail: bertolot@units.it

P. Martino, A.B. Galosi (eds.), *Atlas of Ultrasonography in Urology, Andrology, and Nephrology*,
DOI 10.1007/978-3-319-40782-1_7

7.2 Diagnostic Imaging

In major trauma, hemodynamically unstable patients on admission are most likely going to surgery immediately. In other cases, radiological imaging plays an important role in the detection of organ damage.

Contrast-enhanced multi-detector computed tomography (CE-MDCT) is the gold standard in the evaluation of patients with high-energy abdominal trauma, because of high spatial resolution, very fast execution, and higher sensibility. CE-MDCT also allows excluding active bleeding, multitraumatic involvement of deep organs (pancreatic trauma), and gut perforations.

In the acute management of trauma, ultrasonography (US) plays a role only as second-step evaluation in the emergency room after the primary survey of the advanced trauma life support (ATLS) protocol as focused assessment with sonography in trauma US (FAST-US) [3]. FAST-US is the ideal imaging modality of choice because it can be performed simultaneously with other resuscitative cares and has the primary goal to detect hemoperitoneum. Recently, FAST exam has been extended to the assessment of pleuropericardial compartments with the detection of pneumo- and hemothorax or cardiac hematic tamponade (extended FAST, EFAST) [4]. The examination includes six locations for the existence of free fluid: the right upper quadrant with the hepatorenal recess, the left upper quadrant with the splenorenal recess, both paracolic gutters, the pelvis and its various peritoneal cavity recesses, and the pericardial space. If the examination demonstrates the presence of fluid, surgeons will generally perform an exploratory laparotomy. FAST-US has low sensitivity in detection of parenchymal traumatic lesions, which may be isoechoic and can be missed [5, 6], so CE-MDCT remains the imaging modality of choice for parenchymal evaluation.

US is useful during the follow-up of traumatic lesions, and the introduction in the clinical practice of intravenous contrast materials specific for US finds an indication in the surveillance of these patients.

Contrast-enhanced US (CEUS) with second-generation contrast agents shows a high sensitivity both in lesion detection and grading, but CEUS should be reserved for the assessment of stable, low-energy isolated trauma patients with unilateral pain. These patients have low risk for multi-organ and severe traumatic involvement, are hemodynamically stable, and can be conservatively treated and evaluated during the follow-up [5, 6].

Contrast-enhanced US (CEUS) demonstrated an accuracy similar to CE-MDCT in detecting and grading renal traumatic lesions. Parenchymal lacerations appear as nonenhancing areas after contrast injection (Fig. 7.1).

In addition, CEUS exceeded the limits of the B-mode US and the US color and power Doppler and expanded the applications of the method especially in abdominal trauma in children.

The main limit of CEUS in kidney traumatic lesions is the impossibility to visualize pelvicalyceal and ureter injuries, since contrast agents are not concentrated in the collecting system. In these cases, CE-MDCT should be always performed in CEUS-positive patients to exclude active bleeding and urinomas.

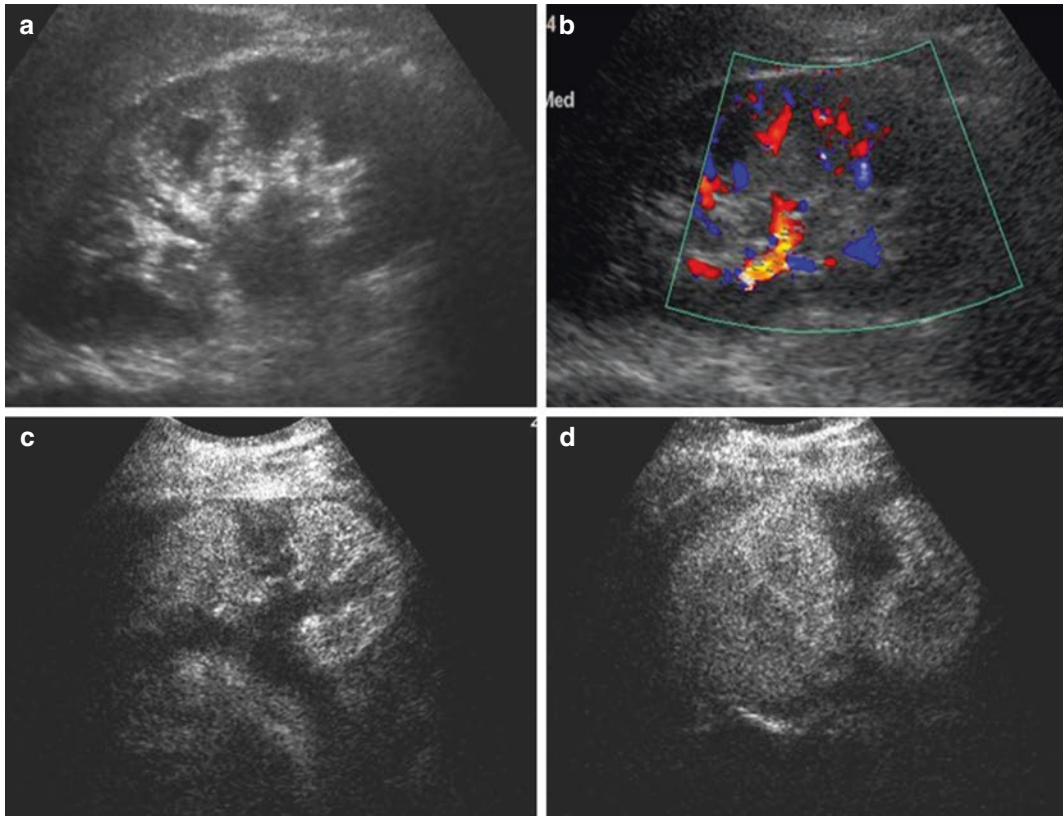

Fig. 7.1 Baseline US examination (**a**) is inadequate to detect renal laceration because it is slightly hypo-isoechoic to the surrounding parenchyma. Color Doppler (**b**) shows a relative homogeneous perfusion. After contrast injection, CEUS demonstrates a large filling defect due to deep parenchymal laceration (**c**, **d**)

7.3 Classification

Several classifications have been defined for the assessment of the type of renal injury, but the classification proposed by the Committee on Organ Injury Scaling of the American Association for the Surgery of Trauma (AAST) is now widely accepted as the grading scale, which also ensures a common consensus between surgeons and radiologists for proper management of renal injuries. The current AAST grading system is based on surgical findings, which can be diagnosed by MDCT [7]:

- I – Renal contusion or subcapsular hematoma with intact capsule
- II – Superficial cortex laceration (<1 cm) that does not extend to deep medulla or collecting system or nonexpanding hematoma
- III – Deep laceration(s) (>1 cm) without urine extravasation
- IV – Laceration(s) extending into collecting system with contained urine leak, main renal artery or vein injury with contained hemorrhage, segmental parenchymal infarction
- V – Shattered renal parenchyma, renal vascular pedicle avulsion, or devitalized kidney

7.3.1 Grade 1

Intrarenal hematomas (or contusions) are not easily detectable on B-mode evaluation. Contusions usually appear as ill-defined, round, or ovoid hyperechoic areas within the renal parenchyma. They constitute 75–85 % of all renal injuries [8]. The treatment is conservative and the lesion tends to resolve within 1 or 2 weeks.

Subcapsular hematomas appear as round or elliptic inhomogeneous hyper- and hypoechoic fluid collection along the renal contour, under the renal capsule. If the hematoma is large in size, it may cause flattening or depression of the underlying renal surface and compress the parenchyma (Fig. 7.2).

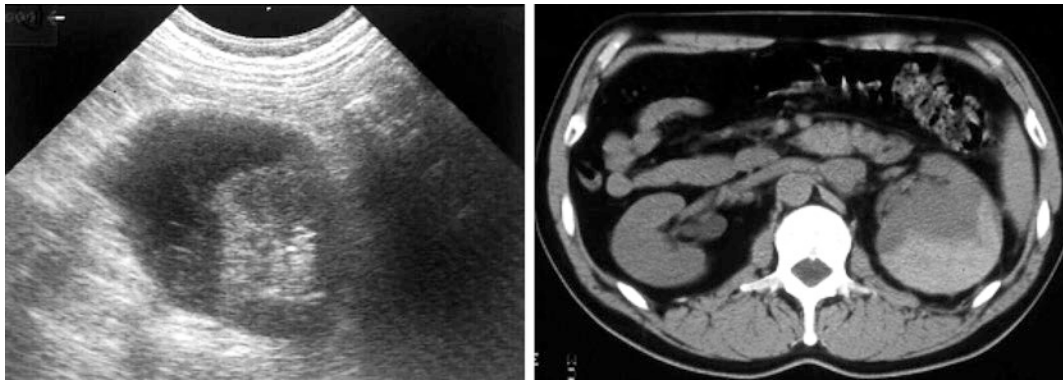

Fig. 7.2 Grade 1: subcapsular hematoma. Conventional US shows an elliptic inhomogeneous hypoechoic collection along the renal contour, which flattens the renal surface. CT confirms the presence of large subcapsular hyperdense hematoma, confined under the renal capsule. The attenuation values are between 45 and 90 HU

7.3.2 Grade 2

Subsegmental infarcts or minor lacerations (<1 cm) may appear as defects in the periphery of the renal parenchyma without involvement of the collecting system. CEUS has a limited sensitivity in the detection of these lesions, while CE-MDCT can demonstrate small, sharply demarcated, wedge-shaped areas of decreased contrast enhancement, due to stretching and thrombotic occlusion of small accessory renal artery, capsular artery, or intrarenal subsegmental branch. The treatment is conservative and subsegmental infarction results in cortical small incisure.

Perinephric hematomas appear as semilunar inhomogeneous hyper- and hypoechoic fluid collection near the kidney (Fig. 7.3). These are differentiated from subcapsular hematomas because perinephric hematomas are confined between the renal parenchyma and Gerota's fascia, outlining the renal contour extending over a wider area without producing flattening or depression of renal margins, and occur following a laceration of the renal capsule.

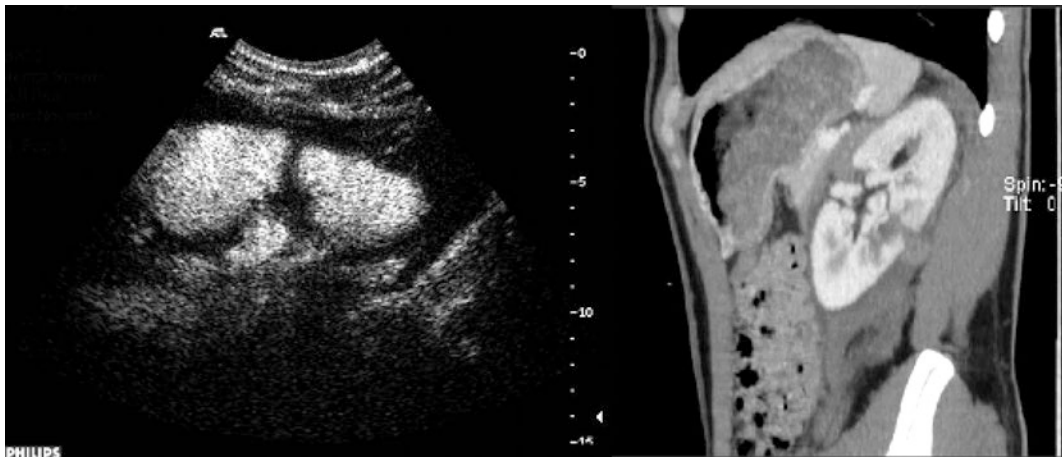

Fig. 7.3 Grade 4: major laceration (>1 cm) involving the collecting system. Both CEUS and CE-MDCT show deep wedge-shaped areas of decreased contrast enhancement. The deepest laceration also involves the pelvis with extensive anechoic fluid perinephric collection, confined into the Gerota's fascia

7.3.3 Grades 3–4

Major lacerations (>1 cm) may appear as deep defects of the renal parenchyma that involve the collecting system with urine extravasation. Both CEUS and CE-MDCT show multiple deep wedge-shaped areas of decreased contrast enhancement (Fig. 7.3). Severe lacerations are usually associated with one or more devitalized fragments, deep lacerations of the renal pelvis, and collecting system. Extensive hemorrhage appears as inhomogeneous echoic fluid collection near the kidney and can be refilled by an active arterial bleeding, easily demonstrated by CE-MDCT. Urine extravasation conversely appears as anechoic fluid collection in the subcapsular or more often the perinephric space: CE-MDCT can demonstrate bleeding of contrasted urine from the pelvis (Fig. 7.4). The management of these severe lesions generally requires surgical exploration and often nephrectomy. Intra-arterial embolization may prevent nephrectomy.

Category 4 also includes vascular injuries involving the renal pedicle. The most significant vascular injury is thrombosis of the main renal artery due to the stretching and tearing of the intima (less elastic than the media and adventitia) caused by deceleration [8]. The consequent intimal flap with clot formation may lead to complete renal artery thrombosis, typically starting in the proximal one-third of the vessel. CEUS demonstrates extensive decrease of vascularization, and CE-MDCT typically reveals amputation of the renal artery. Thrombosis of the renal vein may also occur.

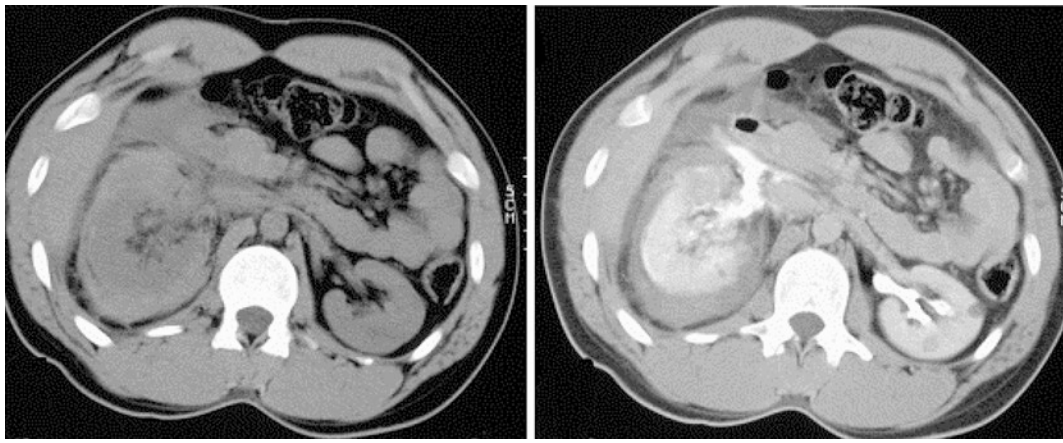

Fig. 7.4 Grade 4: major laceration (>1 cm) with urine bleeding. MDCT without CE shows large perinephric hematoma (attenuation values between 45 and 90 HU) and extensive hypodense fluid collection into the peritoneal space. 10 min after intravenous administration of CE (urographic phase), CE-MDCT demonstrates extensive and active bleeding of contrasted urine from the pelvis

7.3.4 Grade 5

The term "shattered kidney" refers to gross renal parenchymal disruption by multiple lacerations, frequently associated with multiple areas of renal infarction.

Avulsion of the vascular hilum and of the ureteropelvic junction may occur, by resulting in massive active arterial bleeding or large urinoma. Devascularization of the entire kidney constitutes the most severe form of renal injury. Nephrectomy is the only treatment.

7.4 Complication Assessment

7.4.1 Color Doppler

Even if the role of US is limited in the first phases of trauma management, color Doppler largely employed in the follow-up of traumatic patients.

Color Doppler duplex sonography is a widely available, noninvasive, and accurate technique that plays an important role in the detection and differential diagnosis of late vascular complications, such as pseudoaneurysms and arteriovenous fistulas.

A pseudoaneurysm is a pulsatile hematoma that communicates through a channel (neck) with the injured artery. It follows total disruption in the arterial wall and continuous extravascular flow, contained by the surrounding tissues. B-mode usually demonstrates a large inhomogeneous cavity, with a fluid-fluid level inside in large pseudoaneurysms due to hematocrit layering. Color Doppler duplex sonography is the diagnostic imaging modality of choice: it can demonstrate the degree of clotting, the communication with the artery, and the blood flow pattern. The lumen has bidirectional, swirling, or "yin-yang" color flow and turbulent or pulsatile flow on a spectral display. The neck typically has a "to-and-fro" waveform due to flow entering during systole and exiting during diastole [9].

Arteriovenous fistula instead is an abnormal communication between arterial and venous flow. On B-mode, it appears as an anechoic area, while color and spectral Doppler sonography may show an intense and turbulent high-velocity flow with low resistance in the renal parenchyma [10].

References

1. McAninch JW (1996) Renal injuries. In: Gillenwater JY, Grayhack JT, Howards SS, Duckett JW (eds) Adult and pediatric urology, 3rd edn. Mosby, St Louis, pp 539–553
2. Dayal M, Gamanagatti S, Kumar A (2013) Imaging in renal trauma. World J Radiol 5:275
3. Williams SR, Perera P, Gharahbaghian L (2014) The FAST and E-FAST in 2013: trauma ultrasonography: overview, practical techniques, controversies, and new frontiers. Crit Care Clin 30:119
4. Kirkpatrick AW, Sirois M, Laupland KB, Liu D, Rowan K, Ball CG, Hameed SM, Brown R, Simons R, Dulchavsky SA, Hamiilton DR, Nicolaou S (2004) Hand-held thoracic sonography for detecting post-traumatic pneumothoraces: the Extended Focused Assessment with Sonography for Trauma (EFAST). J Trauma 57:288
5. Valentino M, De Luca C, Galloni SS, Branchini M, Modolon C, Pavlica P, Barozzi L (2010) Contrast-enhanced US evaluation in patients with blunt abdominal trauma. J Ultrasound 13:22
6. Cokkinos DD, Antypa E, Kalogeropoulos I, Tomais D, Ismailos E, Matsiras I, Benakis S, Piperopoulos PN (2013) Contrast-enhanced ultrasound performed under urgent conditions. Indications, review of the technique, clinical examples and limitations. Insights Imaging 4:185
7. Moore EE, Shackford SR, Pachter HL, McAninch JW, Browner BD, Champion HR, Flint LM, Gennarelli TA, Malangoni MA, Ramenofsky ML (1989) Organ injury scaling: spleen, liver, and kidney. J Trauma 29:1664
8. Kawashima A, Sandler CM, Corl FM, West OC, Tamm EP, Fishman EK, Goldman SM (2001) Imaging of renal trauma: a comprehensive review. Radiographics 21:557
9. Barozzi L, Pavlica P, Santoro A (1999) Ecografia e color doppler in nefrologia. Poletto Editore
10. Lusenti T, Fiorini F, Barozzi L (2011) Renal arteriovenous fistula simulating hydronephrosis: A case report. J Ultrasound 14:233

The Transplanted Kidney

8

Giulio Argalia, Nicola Carboni, Daniela Dabbene, Giuliano Peta, Paola Piccinni, Anna Clara Renzi, and Gian Marco Giuseppetti

Ultrasound evaluation of the transplanted kidney is fairly simple because the graft is commonly placed in the retroperitoneal space of the right iliac fossa in a superficial position. The vessels are in the medial side of the organ and are connected with the recipient's common or external iliac vessels. After identifying the transplanted kidney, images are acquired in the transverse and sagittal planes, and the renal size is recorded. The adjacent soft tissues are scanned to identify any perirenal fluid collections. After that, color or power Doppler is applied to evaluate the parenchymal flow and to identify the renal hilum and the anastomoses. Flow quantification can be measured by the resistivity index (RI), pulsatility index (PI), and systolic/diastolic ratio.

The study is normally performed with a convex transducer with variable frequency between 3.5 and 5 MHz (Fig. 8.1). The healthy graft has comparable ultrasound features to the healthy native kidney; however, a more detailed two-dimensional image is obtained as the transplant is usually located more superficially. Graft sizes are similar to native kidneys; however, gradual increase of its dimensions can be seen over the first few weeks by up to 32% of the initial length by the first month. The size of the vessels can depend on whether the donor is living or not which, in the first case, are smaller.

The Doppler ultrasound is performed by positioning the color box in the area of study (Fig. 8.2). The pulse repetition frequency (PRF) is set to 1–1.5 KHz and wall filter to 100 Hz, and the gain is set in order to optimize the image without having aliasing or color bleed. The spectral analysis is executed with the sample volume positioned in the vessel lumen of the interlobar artery.

The RI is used as a measure of the resistances to the blood flow of the arteries of the transplanted kidney. An RI between 0.70 and 0.80 is considered normal. A value higher than 0.80 is an expression of graft dysfunction (Fig. 8.3).

The US Doppler plays an important role in the differential diagnosis of vascular, urological, and surgical complications. It has less important impact in the parenchymal complications because of the lack of specific signs. Various elements can affect the RI such as age, heart rate, arterial pressure, and pharmacological therapy, so it has low diagnostic value in the parenchymal complications, especially if not repeated.

The diagnostic impact increases if the measurements are repeated over time and correlated with laboratory parameters like creatinine and azotemia [1–3].

G. Argalia (✉) • N. Carboni • D. Dabbene • G. Peta
P. Piccinni • A.C. Renzi • G.M. Giuseppetti
University Politecnica delle Marche,
Az. Ospedali Riuniti, Ancona, Italy
e-mail: giulio.argalia@gmail.com

P. Martino, A.B. Galosi (eds.), *Atlas of Ultrasonography in Urology, Andrology, and Nephrology*,
DOI 10.1007/978-3-319-40782-1_8

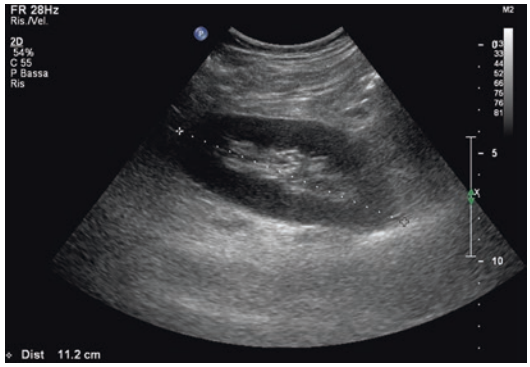

Fig. 8.1 US: B-mode shows regular transplanted kidney with bipolar diameter of 11.2 cm

Fig. 8.2 CDUS: normal Doppler spectra (RI 0.73) of transplanted kidney with regular morphology

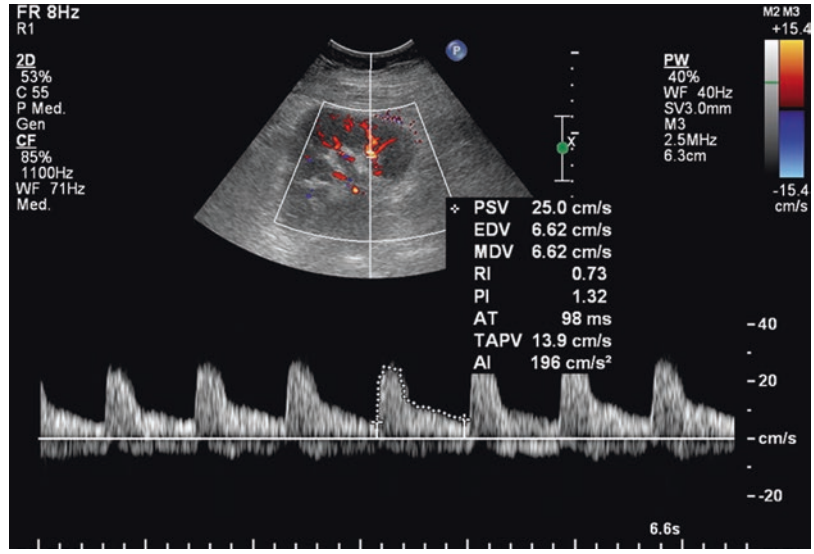

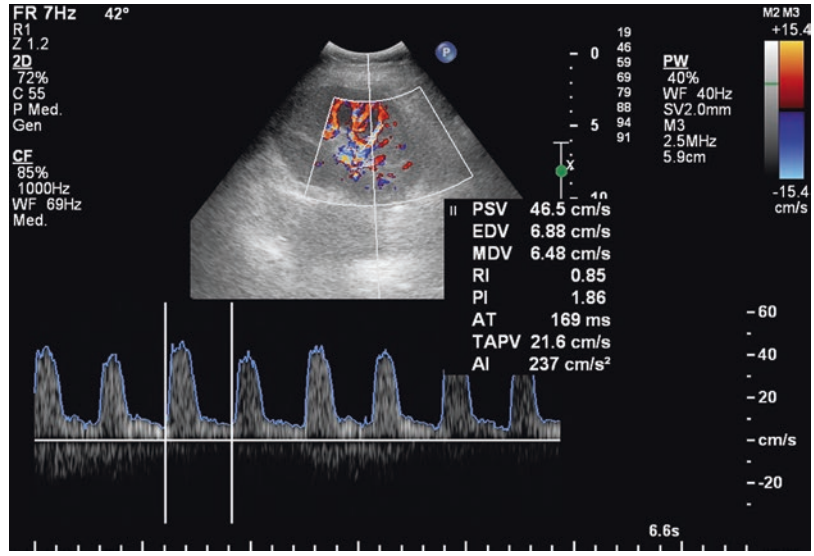

Fig. 8.3 CDUS: transplanted kidney with regular morphology and Doppler spectra increased (RI 0.85)

8.1 Complications

The ultrasound is the first, easy to apply and to repeat and easily accessible in posttransplant surgery evaluation and its complications.

The complications can be divided into immediate (within the first week), early (between the first and twelfth week), and late (after the twelfth week of transplant) [4–6].

Aside from this division, it can be classified depending on the anatomical district:

- Parenchymal: acute tubular necrosis, hyperacute/acute transplant rejection, chronic rejection, pharmacological toxicity, and infections
- Vascular: renal artery stenosis, renal infarct, renal vein thrombosis, arteriovenous fistulas, and pseudoaneurysms
- Urinary collector system: urinomas, urinary obstruction, and kidney stones
- Liquid collections: hematomas, lymphoceles, and abscesses
- Neoplasms and recurrent renal diseases

8.1.1 Parenchymal Complications

8.1.1.1 Rejection

It can be hyperacute, acute, or chronic.

Hyperacute rejection is a rare eventuality that occurs in the immediate posttransplant period (from a few minutes to a few hours after transplant surgery), and it is caused by the presence of preformed antibodies in the receiver's serum. In a few minutes, the graft undergoes necrosis. The US features are nonspecific and similar with those of the acute rejection or the acute tubular necrosis.

Acute rejection is more common (10–37 %) and occurs in the first 3 weeks after transplantation (20–30 % of nonliving donors). An episode of rejection in high-dose immunosuppressive therapy is an adverse long-term prognostic indicator. Clinically, the patient could be asymptomatic or can have flu-like symptoms. The US and Doppler features appear to be nonspecific:

- Kidney enlargement with globular aspect due to edema.
- Hypoechoic and enlarged pyramids.
- The cortical can be both hypoechoic and thinned or hyperechoic and thickened.
- Enlargement of the collector system with obliteration and hyperechoic appearance.
- Perinephric fluid collections due to necrosis/hemorrhage.
- IR > 0.8. The diastolic arterial flow is lowered in all arterial branches. An inversion of diastolic flow can be seen in the main renal artery.

These findings are similar to those of the acute tubular necrosis; the main difference is the time when they occur since the acute rejection doesn't usually happen in the first 48 h after transplant surgery.

Chronic rejection is the common cause of late transplant failure. To be classified as chronic, it has to take place at least 12 weeks after transplant surgery (Fig. 8.4). Various factors can contribute to the chronic rejection such as acute tubular necrosis, drug toxicity, and donor age. A progressive renal deterioration is seen. Hyperechoic parenchymal appearance, cortical thinning, reduced number of intrarenal vessels, and mild hydronephrosis could be detected on US examination [5, 7, 8].

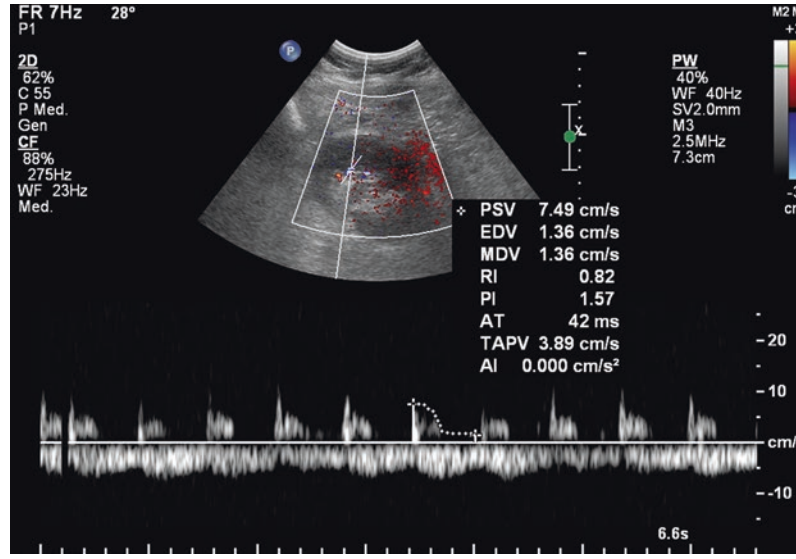

Fig. 8.4 CDUS: sampling of interlobar artery of transplanted kidney with abnormal Doppler spectrum, RI mildly increased (0.82). Chronic rejection

8.1.1.2 Acute Tubular Necrosis

Acute tubular necrosis is a more common condition in cadaveric donors than in living donors, due to ischemia and a reperfusion injury. Other causes could be donor hypotension, the hot (>30 min) and cold (>24 h) ischemic period, and age and weight of the donor and receiver. It usually resolves in 2 weeks.

US reveals nonspecific signs such as renal enlargement, reduced echogenicity of parenchyma and pyramids, and low cortical-medullary differentiation. Other authors have reported a thickening of the cortex and increase of its echogenicity with pyramidal prominence (present also in acute rejection).

Renal sinus can be compressed or obliterated from the edema, while the intraparenchymal RI can be increased (>0.8). Doppler evaluation of severe cases can be characterized by the absence of flow during all the diastolic phase [9, 10].

8.1.1.3 Drug Toxicity

The immunosuppressive therapy used in the post-transplant, such as cyclosporine and tacrolimus, is nephrotoxic. It can cause the afferent artery vasoconstriction and interstitial fibrosis. Recently, it has been suggested that the polyomavirus is reactivated by immunosuppression and causes a nephropathy indistinguishable from acute tubular necrosis. From the point of view of US-ECD, you can notice an increase of the indices of resistance that should be correlated with the serum values of the drugs [11].

8.1.1.4 Infections

More than 80 % of transplant patients can present an infectious episode in the first 6 months. Opportunistic infections are facilitated by immunosuppressive drugs, catheters, and urine. Patients present with fever and pain or may be completely asymptomatic.

Ultrasound examination will show focal or diffuse areas of alteration and thickening of the cortical echogenicity. A dilatation in renal chalices and pelvis system associated with an increase of echogenicity may indicate a pyonephrosis (Figs. 8.5, 8.6, and 8.7), while a rounded focal area with a slight shadow cone is typical of fungal infections (fungus balls).

In acute pyelonephritis, transplanted kidney can appear with an increased volume for acute inflammation, with focal areas of increased or decreased echogenicity in its interior, while the renal sinus appears reduced in volume. The power Doppler, for the ability to detect slow flows in the arteries, is more sensitive, than the simple ultrasound B-mode.

Even the enhanced US has a key role in the diagnosis of acute pyelonephritis posttransplant.

In emphysematous pyelonephritis, the presence of gas content in the parenchyma is due to reverberation artifacts.

Abscesses may look nonspecific, sometimes complex, like cystic, with mixed echogenicity and are usually treated by drainage [12, 13].

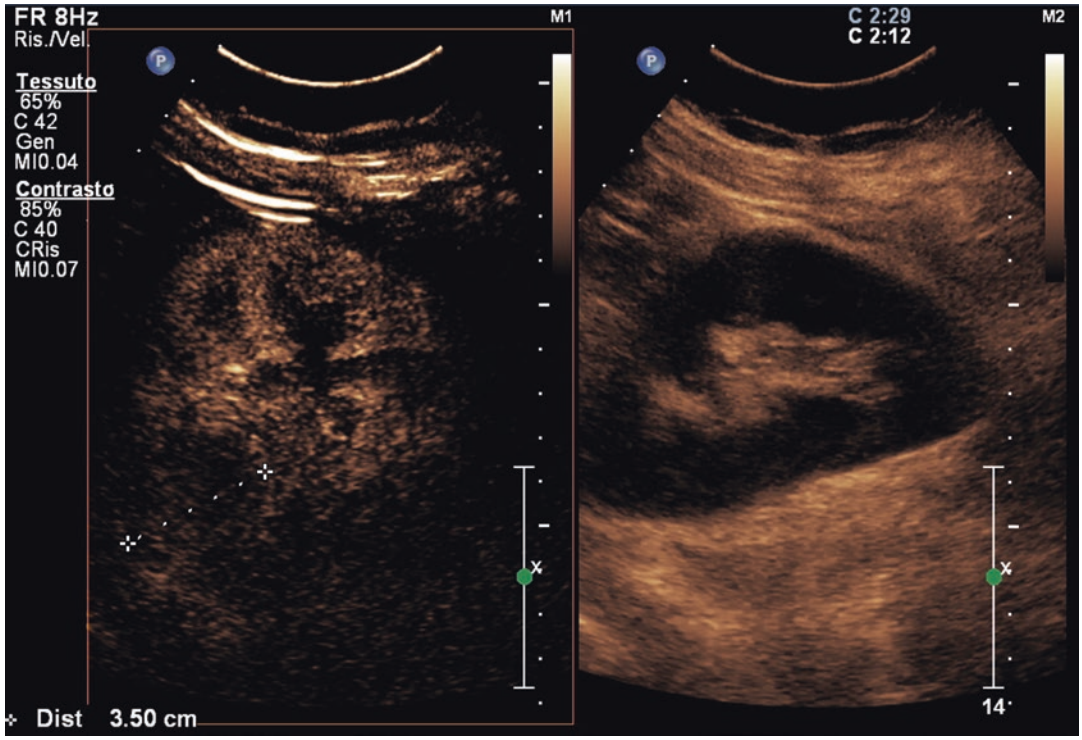

Fig. 8.5 CEUS of transplanted kidney: renal abscess with a size of 3.5 cm in the lower pole

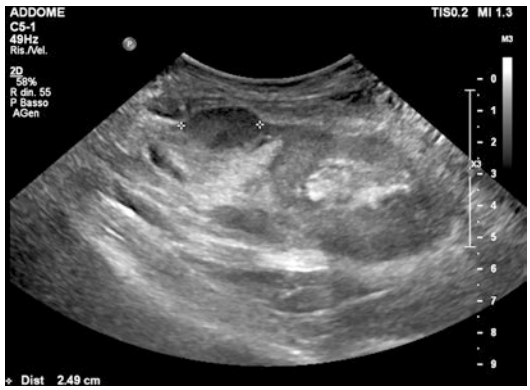

Fig. 8.6 US B-mode of transplanted kidney: hypoanechoic lesion in the lower pole with a size of 2.49 cm abscess

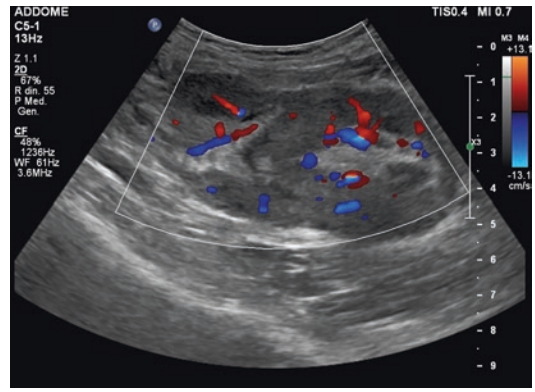

Fig. 8.7 Renal abscess studied with CDUS

8.1.2 Vascular Complications

Vascular complications occur in less than 10 % of patients, but are a major cause of graft dysfunction and are associated with high morbidity and mortality. Once identified, vascular lesions can be easily treated by interventional radiology.

Despite that angiographic MRI is the gold standard for diagnosis of vascular complications, the color Doppler is an excellent noninvasive technique for the investigation of vascular lesions [3, 11].

8.1.2.1 Renal Artery Stenosis

Stenosis of renal arteries is the most common vascular complication. It usually occurs in the first 3 months after transplantation. The segments most affected are the iliac artery proximal to the anastomotic site (atherosclerosis of the donor, by clamping surgical lesion), the anastomosis itself (due to the surgical technique), or proximal to the renal artery (intimal ischemia). The type of anastomosis that most frequently undergoes this type of complication is the T-T anastomosis because they have a possibility of stenosis greater than in those T-L.

ECD examination shows aliasing color due to the increase in flow velocity. The Doppler criteria for significant stenosis are speed higher than 200 cm/s; velocity gradient; between the stenotic segment and prestenotic, higher than 2:1; and accentuated turbulence distally (spread spectrum). Resistance indices are normally increased [14, 15].

8.1.2.2 Infarction

The main renal artery thrombosis is a rare complication (<1 % of cases), but severe and generally leads to the loss of the organ. It occurs mainly in the first postoperative and pathogenetic mechanisms which may include rejection, severe stenosis of the anastomosis, kinking, or intimal arterial dissection.

Clinically, it is manifested by anuria and swelling of soft consistency at the site of transplantation.

The sonographic appearance may vary depending on diffuse infarct (from the main renal artery thrombosis) or segmental infarct (accessory renal artery thrombosis or intraparenchymal branches) (Fig. 8.8).

In the first case, the kidney will occur globally increased in volume and diffusely hypoechoic, with suppression of the signal flow distal to the thrombus and intraparenchymal level. Since it is not a pathognomonic sign of renal infarction, as also seen in the case of severe rejection, a more detailed diagnosis by angiography or MRA may be nullifying.

In the case of segmental infarction, we observe a focal area, most typically triangular hypoechoic with hypoperfusion signal to color Doppler and after infusion of contrast agents. Also in this case, the signs are not specific and could be the expression of pyelonephritis severe, focal, or breakage organ.

The most frequent outcome of infarction is widespread nephrectomy, although there are some positive experiences regarding locoregional treatment with percutaneous thrombolysis. Early diagnosis resulting in timely treatment is key factors for the safety of the transplanted organ [4].

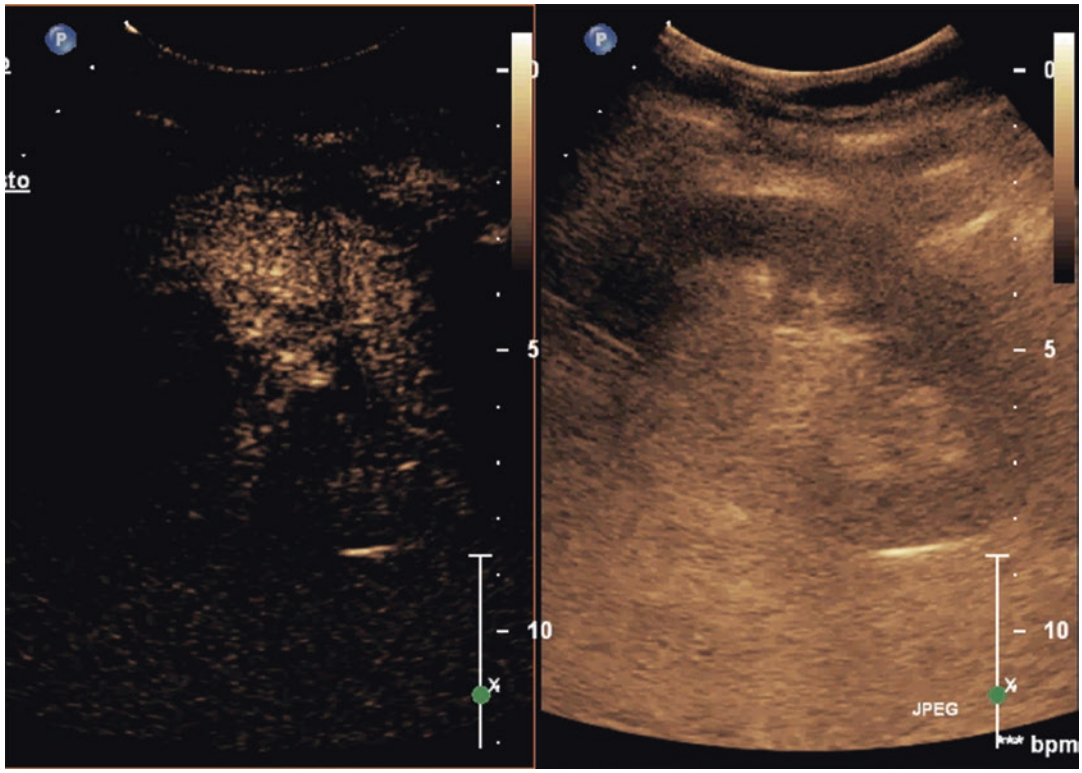

Fig. 8.8 CEUS of transplanted kidney: hypoperfusion of the lower lobe, compatible with ischemic area

8.1.2.3 Renal Vein Thrombosis

Renal vein thrombosis is a frequent complication of renal transplantation (<5 % of cases) and usually occurs within a week after surgery, mostly on the left in relation to the different anatomical course of the common iliac vein, which is compressed between sacrum posteriorly and common iliac artery anteriorly (silent iliac artery compression syndrome).

Clinical findings are comparable to the arterial infarction; it can occur as a result of difficulties in the packaging of the anastomosis, in hypovolemia, in ab-extrinsic compression by perirenal collection or in deceleration flow secondary to rejection.

We can find a swollen and hypoechoic kidney at ultrasound with loss of cortical-medullary differentiation and possible evidence of echogenic material in the lumen of the renal vein.

The color Doppler shows a reduced or absent venous flow associated with an increase in arterial resistance indices ending with an inversion in diastolic flow in the renal artery or its intraparenchymal branches.

Focal increments of the speed of venous flow can be observed also in case of partial thrombosis, kinking, or ab-extrinsic compression, as well as the reversal of diastolic flow may also be present in case of acute tubular necrosis or acute rejection; the association of these signs with the absence of venous hilum flow is however diagnostic for renal vein thrombosis, and early recognition of this condition is crucial to carry out a rapid treatment and save the organ [16].

8.1.2.4 Pseudoaneurysm and Arteriovenous Fistulas

An extrarenal pseudoaneurysm is very rare and generally occurs in correspondence of the anastomosis due to the surgery or infections. The breakage has a high mortality rate.

Ultrasound appears as a cyst-like formation with a systolic-diastolic flow turbulent ECD, associated with characteristic spectrum “to-and-fro” at the neck.

The arteriovenous fistulas are a common complication of biopsies and occur when the needle biopsy pass through artery and vein (Fig. 8.9).

ECD examination shows turbulent flow and the presence of aliasing with very high flow rates, low rates of resistance artery, and arterialized vein flow (Fig. 8.10) and usually resolves spontaneously and has no consequences from the hemodynamic point of view but sometimes may bleed and leads to ischemia of the organ because of the phenomenon of “theft”; in this case, an embolization by interventional radiologists is necessary [17].

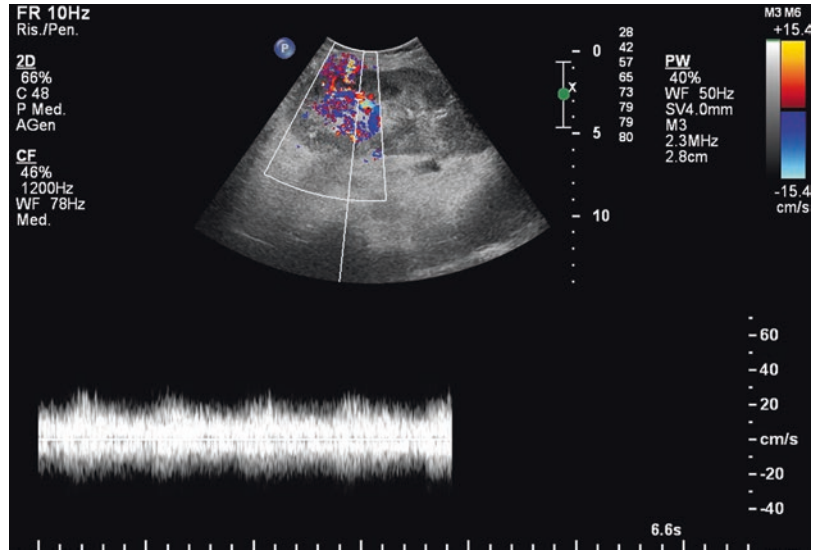

Fig. 8.9 CDUS: arteriovenous fistula with normal Doppler spectrum in the lower pole of the transplanted kidney

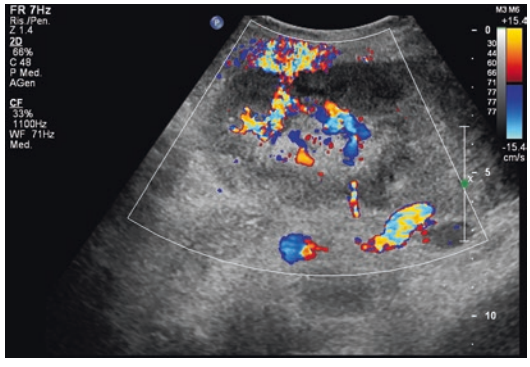

Fig. 8.10 CDUS: arteriovenous fistula in the lower pole of the transplanted kidney

8.1.3 Urological Complications

Nearly 2/3 of early urological complications (mainly urinary leaks and obstructions) occur within the first 30 days after transplantation. New surgical techniques drastically reduced the incidence of these complications (1–8 %) and the associated mortality [4, 12, 18–20].

8.1.3.1 Urinary Leaks and Urinomas

Urine extravasation can affect every point along the whole urinary tract, from the renal pelvis to the uretero-cysto-anastomosis, due to the surgical technique or ureteral ischemia and necrosis.

Urinomas widely vary in size and generally occur within the first 2 weeks after transplantation between the graft and the bladder.

Patients affected with urine leakage may present local pain and tenderness at the transplant site, oliguria, surgical wound discharge, scrotal/labial edema, or even ipsilateral leg swelling, often needing US-guided drainage to reduce compression and urinary ascites.

The fluid/serum creatinine ratio can be employed to differentiate a urine leak from a seroma or a lymphocele.

The US appearance of these lesions is that of an anechoic, fluid, and well-delimited collection, with no intralesional septa.

Urinomas can undergo superinfection and generate abscesses.

More specific instrumental evaluation is needed to localize the site of leak and to plan the appropriate intervention. Small urine leaks may be treated with percutaneous nephrostomy and stent placement [4, 12].

8.1.3.2 Urinary Obstruction

Urinary obstruction is a rare complication of renal transplant (2 % of cases).

More than 90 % of ureteral stenosis occurs within the distal third of the ureter, usually at the ureterovesical junction, because of its poor vascular compensation.

Strictures are mainly due to ischemia, rejection, surgical technique, or kinking. Uncommon etiologies are ureteral compression by peritransplant fluid collections, pelvic fibrosis, calculi, papillary necrosis, fungus balls, and clots.

Patients are typically asymptomatic, because kidney and ureter denervation prevent renal colic manifestations. Diagnosis is based on elevated serum creatinine levels and US demonstration of hydronephrosis, which are both also chronic rejection manifestations.

Differential diagnosis is aided by temporal criteria (<30 days vs. > 3 months after transplantation).

Evaluation of collecting system status requires empty bladder, as a distended bladder should explain the presence of dilatation.

Evidence of echoes in the collecting system may be suggestive for pyonephrosis, fungal infections, clots, or tumor.

Percutaneous nephrostomy, ureteral stenting, and balloon ureteroplasty are usually the early treatments employed to relieve obstruction, whereas US-guided drainage of fluid collections is the choice to solve extrinsic compression on the collecting system.

Surgical reconstruction may be required for long or recurrent strictures [18, 19].

8.1.3.3 Lithiasis

Compared with the general population, patients who undergo renal transplantation show an increased risk for development of urinary stones, even for clinical relevant lithiasis (1–2 %).

Persisting secondary hyperparathyroidism and hypercalcemia are frequent in graft recipients, representing a risk factor for renal stone formation.

Because of kidney and ureter denervation, patients will be asymptomatic; thus, a renal lithiasis should be suspected in the presence of an acute deterioration in renal graft function.

The US findings are the same of a native kidney lithiasis: a hyper-reflective focus producing acoustic shadowing and collecting system dilatation.

Most of renal stones can be removed through endoscopic intervention, whereas percutaneous nephrostomy can be useful to relieve pyelocaliceal compression and stabilize renal function [6, 20].

8.1.4 Perirenal Fluid Collections

Perirenal fluid collections are observed in about half of patients and include hematomas, lymphocele, urinomas, and abscesses. The clinical impact is given by their size, location, and the possibility to increase in size.

The small hematomas, seromas, and the urinomas usually occur in the immediate postoperative period. The lymphocele occurs between 4 and 8 weeks after surgery [4, 6, 11, 12].

8.1.4.1 Hematomas and Lymphoceles

Hematomas are fairly common in the immediate postoperative period, but can also occur after trauma. They usually are located in the subcutaneous tissue or around the graft.

Much of hematomas tend to resolve spontaneously; only large hematomas can dislocate the transplanted organ causing hydronephrosis or compromising the blood supply.

Sonographically hematomas have a complex and mixed echogenicity, over time tend to become more defined and form septa fibrin with debris clots within them.

The size of the hematoma should always be measured as an increase could put an indication for surgery.

The lymphocele is the most frequent fluid collection during peritransplant and occurs in approximately 20% of patients. They appear in the first 2 months after transplantation and are due to the lesion of the iliac lymph vessels during surgery.

At the ultrasound examination, they have an anechoic echostructure, but in some cases may contain septa (Figs. 8.11 and 8.12). They are usually located between the bladder and the medial side of the graft.

The lymphocele is discovered accidentally and requires monitoring over time because, if large, it may have a mass effect and cause hydronephrosis or ischemia of the graft. They can also compress iliac vessels causing edema of the lower extremity, abdominal wall, scrotum, or labia. These eventualities pose an indication to surgical drainage [4, 12].

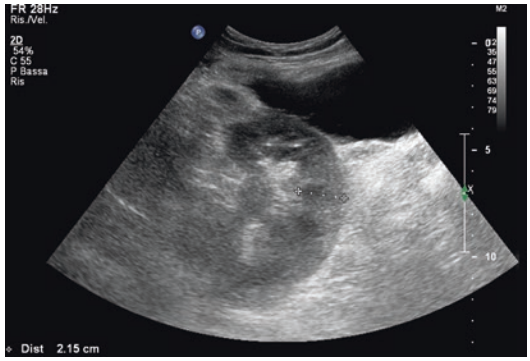

Fig. 8.11 B-mode image of transplanted kidney with regular echostructure with pararenal front lymphocele

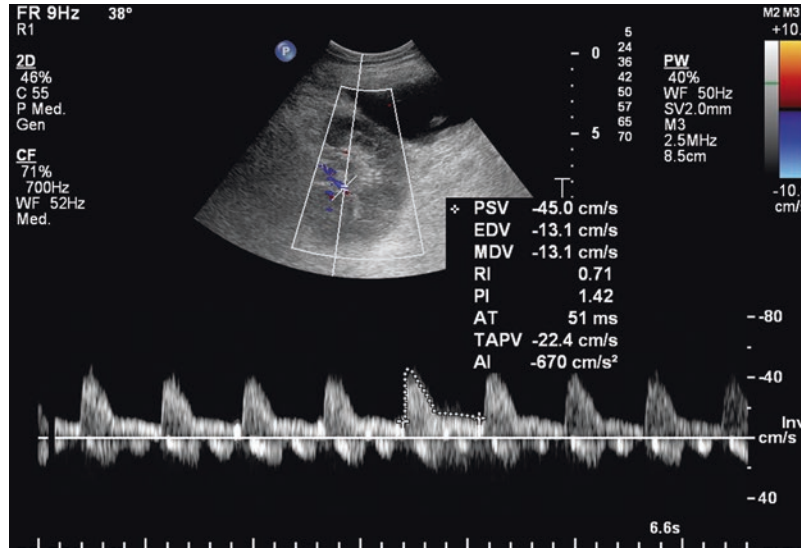

Fig. 8.12 Color Doppler normal spectra of interlobar artery and vein

8.1.4.2 Perirenal Abscesses

Perirenal abscesses are not very frequent and usually develop in the first weeks after surgery. Each perirenal fluid collection can become infected, and it is difficult to distinguish from the hematoma; also the clinical manifestations of the abscess may be absent because of immunosuppression.

The sonographic features of the abscess include low-level echoes and a thick and uneven wall. Even the presence of a gaseous component in a fluid collection lays for an abscess.

At the ECD examination, you may notice an increase in vascularity of the wall and of the tissues surrounding the abscess. The use of the contrast medium could help the diagnosis [6, 11].

8.1.5 Neoplasms

The condition of immunosuppression, due to drug therapy, poses transplanted patients at a higher risk for the development of neoplasms, almost 100 times higher than the normal population. The most frequent tumors are skin cancers and lymphomas.

The neoplasms tend to develop more frequently in native kidneys, which evolve toward acquired polycystic disease. Instead, neoplasms of transplanted kidneys have a less aggressive behavior compared to those of native kidneys.

Ultrasound is also useful in identifying solid masses or complex cysts [4] (Fig. 8.13).

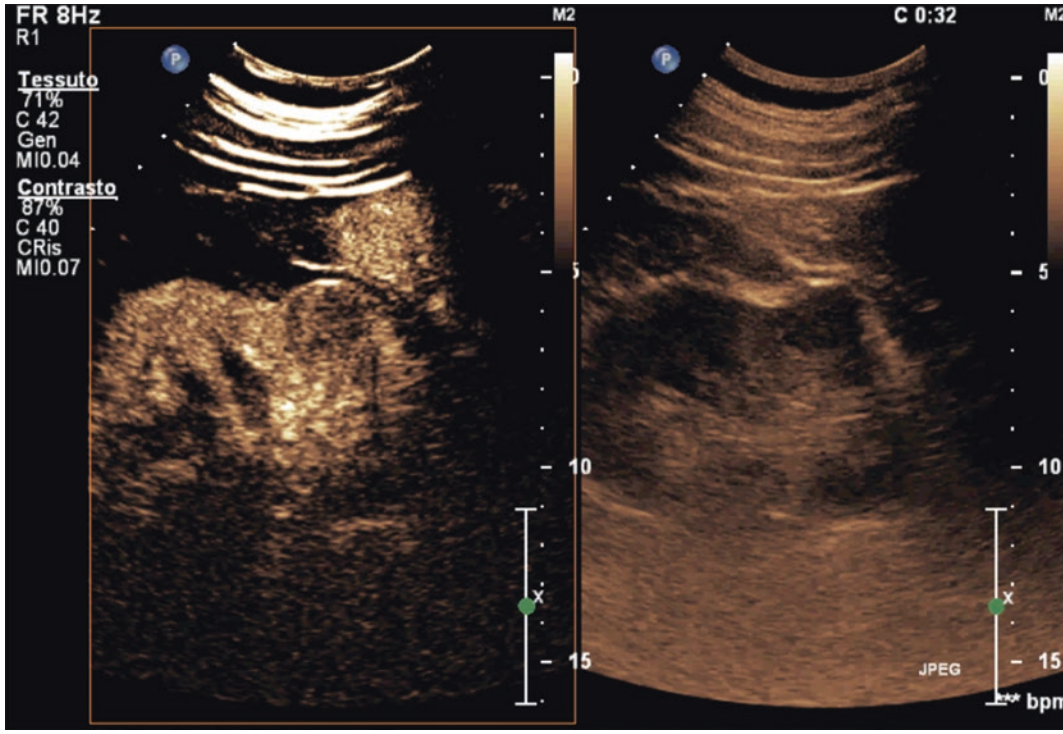

Fig. 8.13 CEUS of transplanted kidney: superior Middle of the kidney exophytic hypoechoic nodule, with inhomogeneous contrast enhancement and fast washout. Suspicion of renal cancer

8.1.6 Contrast-Enhanced Ultrasound

The ultrasound contrast agent is ideal for the study of transplanted kidney because of its superficial and fixed position that is not affected by breathing.

Moreover, the ultrasound contrast agent is not nephrotoxic and allows the assessment of focal areas of reduced blood flow, thereby facilitating the detection of ischemic areas. In the early postoperative period, the CEUS allows the assessment of a hypothetical rejection since it allows to identify a delay of parenchymal perfusion or perfusion defects in general.

Another indication for CEUS is the assessment of perirenal hematoma, as it allows a better view of the extension [21, 22].

8.2 Limitations

The two main limitations of ultrasound are its dependence on the operator and the patient's constitution, as in obese patients it is more difficult to assess the organ and its perfusion.

There are also other factors that may influence, some of which are not related to the disease, for example, the evaluation site of the resistance index, the increase in intra-abdominal pressure during inspiration, the heart rate, and cyclosporine. Although the ultrasound is an excellent method of evaluation of the transplanted kidney, at present the gold standard for assessment of rejection remains the renal biopsy [6, 23, 24].

References

1. Rajiah P, Lim YY, Taylor P (2006) Renal transplant imaging and complications. Abdom Imaging 31(6): 735–746
2. Elsayes KM, Menias CO, Willatt J et al (2011) Imaging of renal transplant: utility and spectrum of diagnostic findings. Curr Probl Diagn Radiol 40(3): 127–139
3. Tublin ME, Bude RO, Platt JF (2003) The resistive index in renal Doppler sonography: where do we stand? Am J Roentgenol 180(4):885–892
4. Akbar SA, Jafri SZH, Amendola MA, Madrazo BL et al (2005) Complications of renal transplantation. Radiographics 25(5):1335–1356
5. Brown ED, Chen MY, Wolfman NT, Ott DJ, Watson NE Jr (2000) Complications of renal transplantation: evaluation with US and radionuclide imaging. Radiographics 20(3):607–622
6. Kolofousi C, Stefanidis K, Cokkinos DD et al (2013) Ultrasonographic features of kidney transplants and their complications: an imaging review. ISRN radiology 2013:1–12
7. Vella J, Koch MJ, Brennan DC. Acute renal allograft rejection. Diagnosis UpToDate 1/7/2006
8. Tittelbach-Helmrich D, Bausch D, Drognitz O, et al (2014) Hyperacute rejection of a living unrelated kidney graft. Case Reports in Medicine 2014:613641
9. Rigg KM (1995) Renal transplantation: current status, complications, and prevention. J Antimicrob Chemother 36(suppl B):51–57
10. Isoniemi HMN, Krogerus L, von Willebrand E et al (1992) Histopathological findings in well-functioning, long-term renal allografts. Kidney Int 41:155–160
11. Parthipun A, Pilcher J (2010) Renal transplant assessment: sonographic imaging. Ultrasound Clin 5(3): 379–399
12. Pozniak MA, Dodd GD III, Kelcz F (1992) Ultrasonographic evaluation of renal transplantation. Radiol Clin North Am 30:1053–1066
13. Kamath NS, John GT, Neelakantan N, Kirubakaran MG et al (2006) Acute graft pyelonephritis following renal transplantation. Transpl Infect Dis 8(3):140–147
14. Platt J, Rubin J, Ellis J (1991) Acute renal failure: possible role of duplex Doppler US in distinction between acute prerenal failure and acute tubular necrosis. Radiology 179:419–423
15. JordanML CGT, Cardella CJ (1982) Ten years of experience with vascular complications in renal transplantation. J Urol 128:689–692
16. Dodd GD, Tublin ME, Shah A et al (1991) Imaging of vascular complications associated with renal transplantation. Am J Roentgenol 157(3):449–459
17. Irshad A, Ackerman S, Sosnouski D et al (2008) A review of sonographic evaluation of renal transplant complications. Curr Probl Diagn Radiol 37(2):67–79
18. Tublin ME, Dodd GD III (1995) Sonography of renal transplantation. Radiol Clin North Am 33:447–459
19. Bennett LN, Voegeli DR, Crummy AB (1986) Urologic complications following renal transplantation: role of interventional radiologic procedures. Radiology 160(2):531–536
20. Surlan M, Popovic P (2003) The role of interventional radiology in management of patients with end-stage renal disease. Eur J Radiol 46:96–114
21. McArthur C, Baxter GM (2012) Current and potential renal applications of contrast-enhanced ultrasound. Clin Radiol 67:909–922
22. Fischer T, Filimonow S, Dieckhöfer J et al (2006) Improved diagnosis of early kidney allograft dysfunction by ultrasound with echo enhancer—a new method for the diagnosis of renal perfusion. Nephrol Dial Transplant 21(10):2921–2929
23. Radermacher J, Mengel M, Ellis S et al (2003) The renal arterial resistance index and renal allograft survival. N Engl J Med 349(2):115–124
24. Takano R, Ando Y, Taniguchi N et al (2001) Power Doppler sonography of the kidney: effect of Valsalva's maneuver. J Clin Ultrasound 29(7):384–388

Children's Kidney and Urinary Tract Congenital Anomalies

9

Maria Ludovica Degl'Innocenti
and Giorgio Piaggio

Urinary tract malformations can often be demonstrated already in prenatal age. They are usually represented by urinary tract dilatations, the most frequently detected alteration at obstetric ultrasound examination, with an incidence up to about 4.5 % of pregnancies (possible causes are shown in Table 9.1).

Most authors use anteroposterior diameter (APD) of the renal pelvis for diagnostic classification purposes [1, 2]. In obstetric ultrasound (US), pelvis APD is normally considered pathologic when >4 mm on axial scan during the second trimester and/or >7 mm during the third trimester (in agreement with the results of Corteville et al. reported in the early 1990s and subsequently confirmed) [3].

Dilatation can be further classified according to Grignon et al. [4] into V degrees, associating pyelectasis and calycectasis or, as summarized in the meta-analysis by Lee et al., into mild to moderate to severe (Table 9.2) [5].

Congenital uropathies, in which the etiopathological role of genetic factors is today generally recognized, cause 10–20 % of cases of chronic renal failure in pediatric age [6].

Many of these anomalies are included in the acronym *CAKUT* (congenital anomalies of the kidney and urinary tract) (Table 9.3) [7].

Warning Terms such as calycectasis, pyelectasis, hydronephrosis, and megaureter should be dropped since they have a functional connotation of obstruction which US morphology scan is not able to show. According to ESPR uroradiology task force 2014, the term "dilatation" of calyces and/or pelvis and/or ureter should be used, with indication of diameters and related calibers.

CAKUT visualized on US images as urinary tract dilatation are the following: ureteropelvic junction stenosis (UPJS), ureterovesical junction stenosis (UVJS), vesicoureteral reflux (VUR), duplicate collecting system, horseshoe kidney associated with dilatation, and urethral anomalies.

Electronic supplementary material The online version of this chapter (doi:10.1007/978-3-319-40782-1_9) contains supplementary material, which is available to authorized users.

M.L. Degl'Innocenti, MD (✉) • G. Piaggio, MD
Pediatric Nephrology Department, Giannina Gaslini Institute, Genoa, Italy
e-mail: mludovicadegl'innocenti@gaslini.org; giorgiopiaggio@gaslini.org

P. Martino, A.B. Galosi (eds.), *Atlas of Ultrasonography in Urology, Andrology, and Nephrology*,
DOI 10.1007/978-3-319-40782-1_9

Table 9.1 Causes of prenatal hydronephrosis

Cause
Transient hydronephrosis
Physiologic hydronephrosis
UPJS
VUR
Megaureter (obstructed and nonobstructed)
MCDK
Ureterocele
Renal cysts
Ectopic ureter
Prune belly syndrome
Urethral atresia
Urachus cysts
Extrarenal causes
Ovarian cyst
Hydrocolpos
Sacrococcygeal teratoma
Gut duplication
Duodenal atresia
Meningocele

UPJS ureteropelvic junction stenosis, *VUR* vesicoureteral reflux, *MCDK* multicystic dysplastic kidney

Table 9.3 Nephrourologic diseases that can be classified as CAKUT (congenital anomalies of the kidney and urinary tract)

Aplasia, hypoplasia, and multicystic dysplastic kidney
Ureteropelvic junction stenosis
Ureterovesical junction stenosis
Vesicoureteral reflux
Duplicate collecting system
Ureteral ectopia
Vesicourethral anomalies
Horseshoe kidney

Table 9.2 Classification of dilatation of renal excretory system according to Grignon et al. and according to Lee et al.

Grignon et al.	APD (mm)	Lee et al.		
Grade I	<10	Hydronephrosis	APD (mm)	
Grade II	10–15		Second trimester	Third trimester
Grade III	>15 mild calycectasis	Mild	≤7	≤9
Grade IV	>15 moderate calycectasis	Moderate	7–10	9–15
Grade V	>15 severe calycectasis	Severe	≥10	≥15

9.1 Ureteropelvic Junction Stenosis (UPJS)

Dilatation of the pelvis and/or renal calyces due to anatomic obstruction of ureteropelvic junction, either congenital or due to extrinsic compression (adhesion bands, abnormal vessels) or to functional compression (e.g., ureteral kinking in renal ptosis/ectopia or horseshoe kidney)

UPJS is often bilateral, usually asymmetric, and more frequent on the left side.

9.1.1 US Findings

Dilatation of renal pelvis of different degrees, with rattail appearance at ureteropelvic junction, without evidence of the ureter under the junction

Color Doppler US imaging is important to identify possible abnormal inferior pole vessels that can cross the ureteropelvic junction. In patients with UPJS, this examination must always be associated with classical bidimensional US.

In our hospital, about 21 % of UPJS treated with surgery between 2006 and 2014 were due to vascular compression suspected at US examination and confirmed by MRI.

9.2 Ureterovesical Junction Stenosis (UVJS)

UVJS is defined as *primary* when characterized by distal ureteral dilatation due to functional obstruction caused by aperistalsis of the terminal ureter and *secondary* when due to vesical anomalies or urethral obstructions (neurogenic bladder, low-compliance bladder, ureterocele, abnormal ureteral implantation, posterior urethral valves).

9.2.1 US Findings

Dilatation of the whole ureter, sometimes also of pelvis and calyxes, with caudo-cranial decrease.

The lumbar ureter, when markedly dilated, presents typically convoluted, mainly in the newborn and nursling, due to "immaturity." The pelvic ureter is easily studied using the vesical window both with transverse, longitudinal, and oblique scans. Generally, it is possible to identify the pre- and/or intramural stenotic tract.

9.3 Vesicoureteral Reflux (VUR)

VUR is due to a congenital anomaly of the ureterovesical junction determined by an altered ratio of length to diameter of intramural ureter.

VUR is classified into five grades, from the less severe to the most severe, according to the importance of urinary tract dilatation.

Depending on VUR grade and on the possible presence of parenchymal scars, US findings can range from fully normal kidneys to kidneys with different degrees of urinary tract dilatation and with parenchymal dysmorphisms (thinned poles, stretched and "corticalized" calyces, reduced renal size).

Vesico-ureteral reflux grading by the international classification (degrees I to V from left to right). Fowler JE Jr: Urinary tract infection and inflammation. Chicago, Year Book Medical Editor,

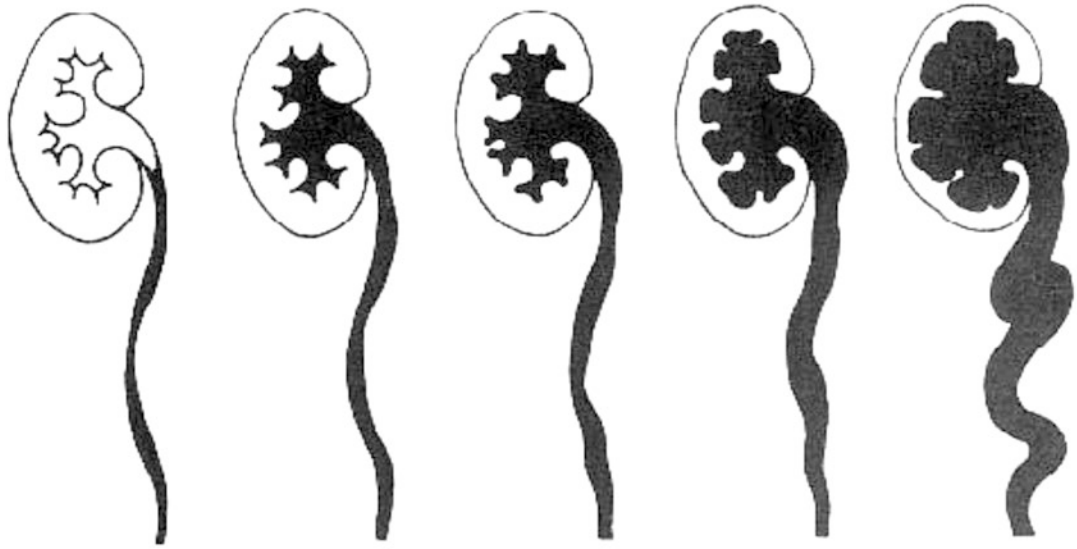

9.3.1 Cystosonography

Investigation of VUR is indicated in case of renal pelvis dilatation associated with ureteral dilatations and/or of recurrent UTI symptoms.

The use of second-generation US contrast media allows the US diagnosis of VUR. In children, the introduction of contrast medium into the bladder for US examination has been proposed for the identification of VUR for radiation protection purposes, even though this use in children is off-label [8–11].

Second-generation US contrast media, characterized by signal intensity no longer related to rupture of microbullae but rather to their excitation, allow the execution of cystosonography with more intense and long-lasting signal and therefore with an improved diagnostic efficacy and anatomic definition.

Cystosonography combines morphological information provided by US examination and functional data obtained with real-time study of UVJ continence. It is not an irradiating procedure, it has high sensitivity and specificity, and it allows VUR grading.

Cystosonography can be used at first diagnosis in females and, even in males, in the follow-up of VUR, treated either conservatively or endoscopically.

Even though in the child it is difficult to obtain micturition during the examination, it is possible to visualize US contrast medium passing through the urethra with transverse perineal scans. Therefore, cystosonography makes it possible to demonstrate anomalies of the urethral caliber, mainly posterior urethral valves, which could previously be demonstrated only by voiding cystourethrography (VCUG) (Videos 9.1, 9.2, and 9.3) [12].

A gold standard technique for VUR diagnosis seems to be lacking, even though radiological cystography was historically considered to have this role. This is mainly due to the fact that VUR is very often intermittent, i.e., occurring only in certain cases of bladder filling, sometimes in the passive phase, i.e., during bladder filling and in other cases only during the active phase, i.e., during active bladder voiding.

9.4 Duplicate Collecting System

Defect of primitive ureteral bud with evidence of double pelvis and/or double ureter per each kidney. Ureteropelvic duplication can be unilateral or bilateral.

It's usual an ectopic end (vesical neck or urethra) of the upper pole ureter with frequent associated ureterocele. Usually there is an orthotopic site of the lower pole ureter, often refluent.

9.4.1 US Findings

- Possible bread-stick appearance of the kidney
- Increased longitudinal axis compared to the contralateral kidney
- Midrenal parenchymal septum dividing the two moieties
- Often asymmetric dilatation of the two poles

9.5 Ureterocele

Cystic dilatation of the intravesical ureter, presenting in most cases a stenotic and/or ectopic meatus

In single excretory system (not very frequent, about 10%), it is generally intravesical and stenotic.

In duplicate collecting system (90% of cases), 6/10 ureters have an ectopic orifice, low vesical neck or urethra.

9.5.1 US Findings

Typical double contour parietal alteration with interposed anechogenic area (intravesical ureterocele)

Ectopic ureterocele can cause dilatation of the ureters and of the calico-pyelic systems.

9.6 Horseshoe Kidneys

- Morphologic anomaly consisting of defective ascent of renal buds associated with their fusion
- Generally ptotic, malrotated kidneys with inferior poles connected by a fibrous, or, more often, parenchymatous isthmus, positioned in front of the aorta, lower vena cava, and rachis
- Quite frequently associated with VUR or ureteropelvic junction stenosis

When should inferior pole fusion of the two kidneys be suspected?

- Distance between the posterior pillar of the diaphragm and upper pole of the kidney ≥3 cm
- Difficult visualization of kidney inferior poles on usual sagittal/coronal scans for inferior kidney intrarotation
- Renal long axes directed downward and from outside to inside on posterior longitudinal scan

9.7 Vesicourethral Anomalies

Vesicourethral anomalies can be primary (vesical exstrophy, prune-belly syndrome, overactive bladder, etc.) or secondary (neurological bladder, intravesical ureteroceles, obstructions due to urethral caliber defect as posterior urethral valves, syringoceles, urethral meatus stenosis).

In the latter case, especially in anomalies secondary to subvesical obstruction, the US findings are the following:

- Thickening of bladder walls[1]
- Irregular bladder contours
- Pseudodiverticula

[1]Normal values for bladder wall thickness are ≤0.3 cm for distended bladder and ≤0.5 cm for empty bladder

9.8 Photos

UPJS: "Mickey Mouse pattern"

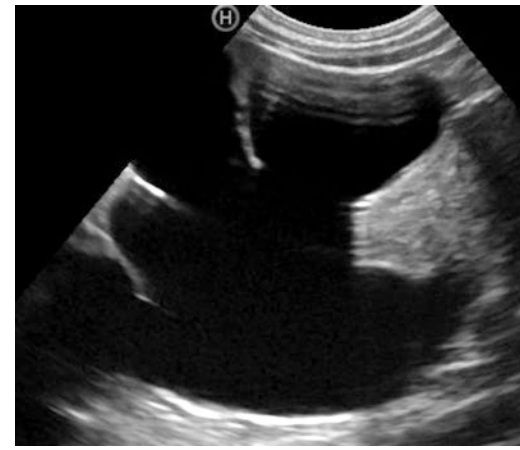

UPJS: "rattail" appearance of the stenotic ureteropelvic junction (no evidence of ureteral dilatation)

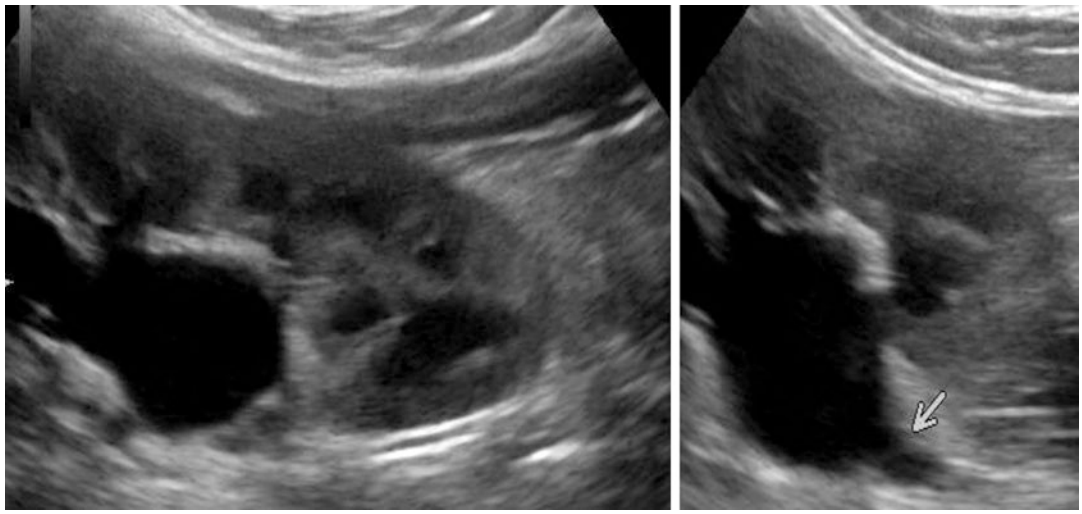

UPJS: different degrees of calyxes and renal pelvis dilatation

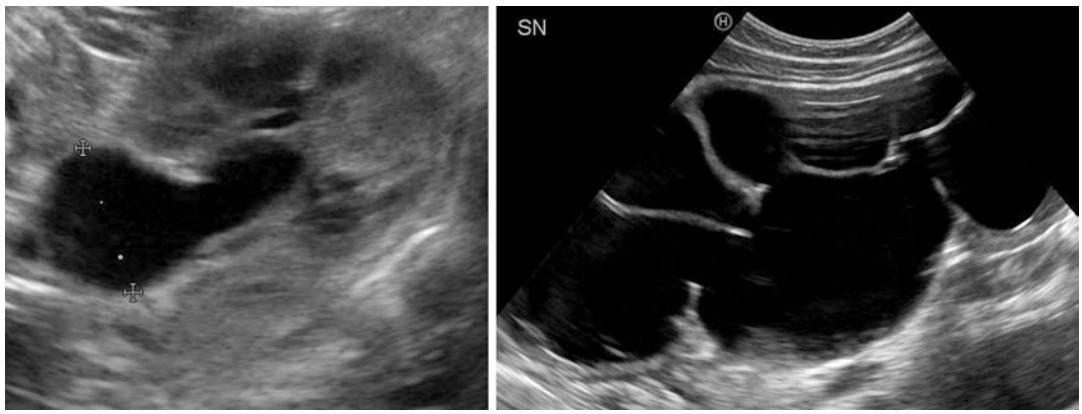

Extrinsic compression (supernumerary lower renal artery) of ureteropelvic junction (on the right MR confirmation)

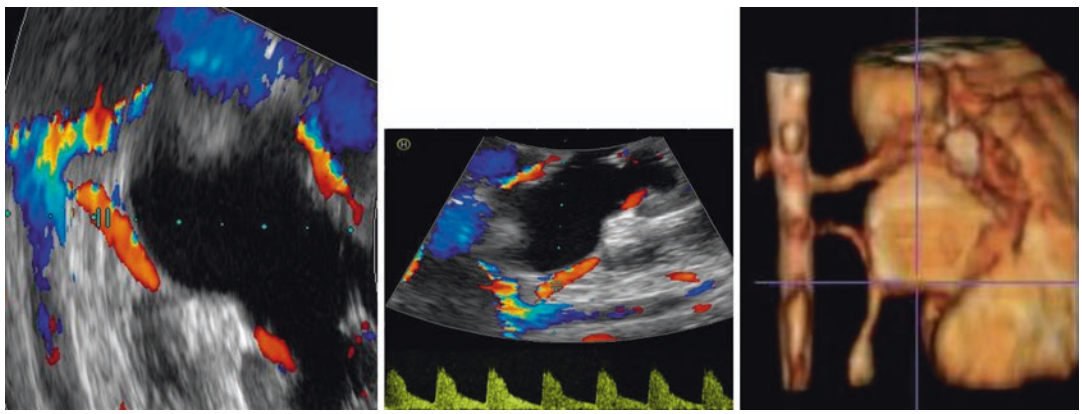

Extrinsic compression (lower main renal artery branch) of renal pelvis

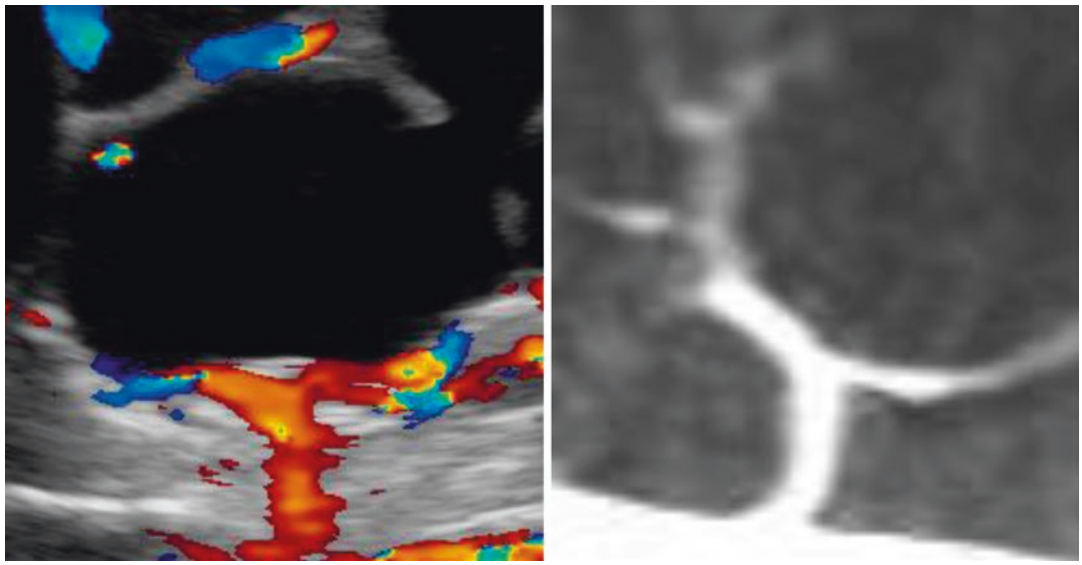

UVJS: bilateral thickening of the ureteral walls

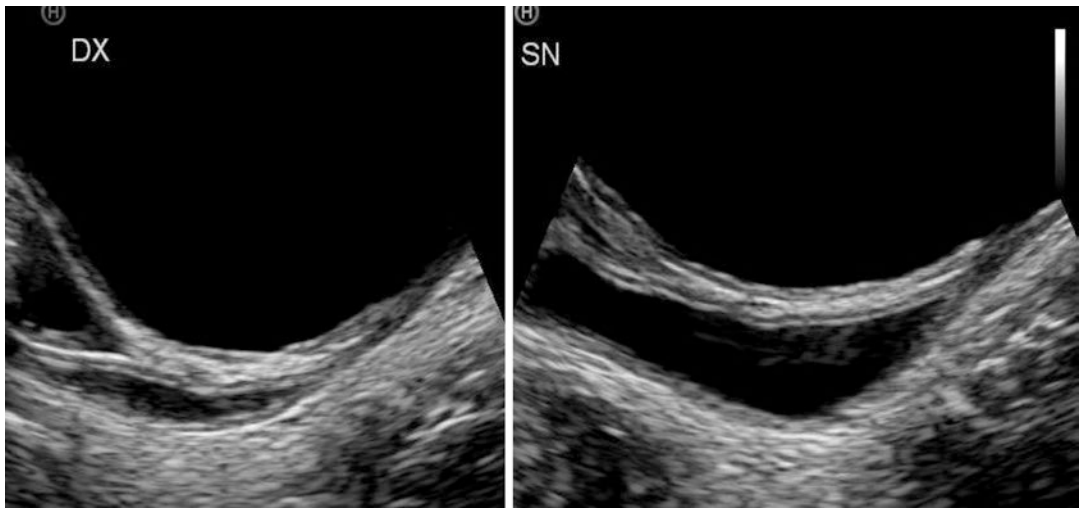

UVJS: severe ureteronephrosis due to distal ureteral stenosis

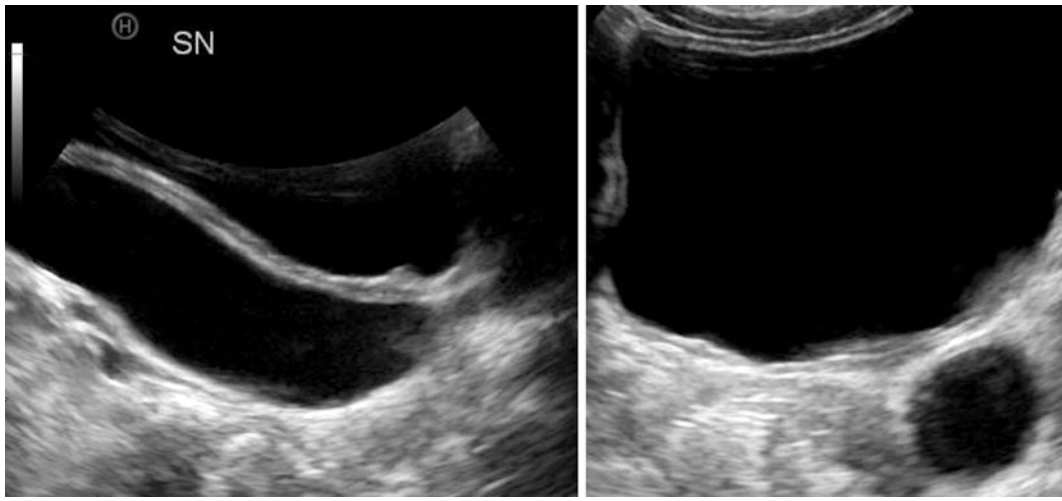

UVJS: ureteral "jet flow"

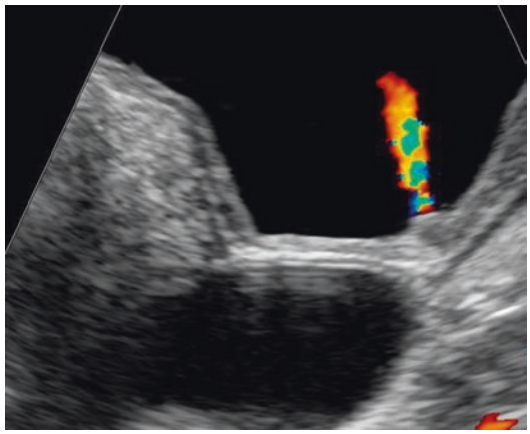

Voiding cystourethrography vs cystosonography:

Grade II VUR

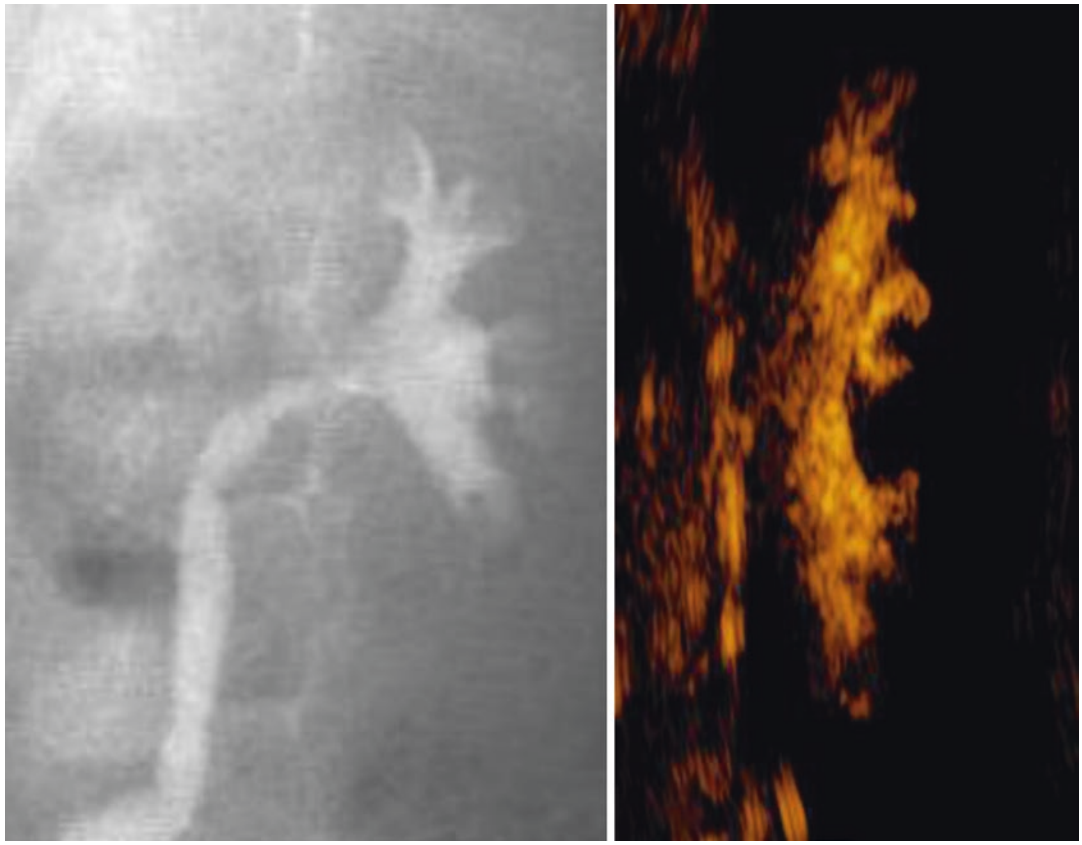

Grade III VUR

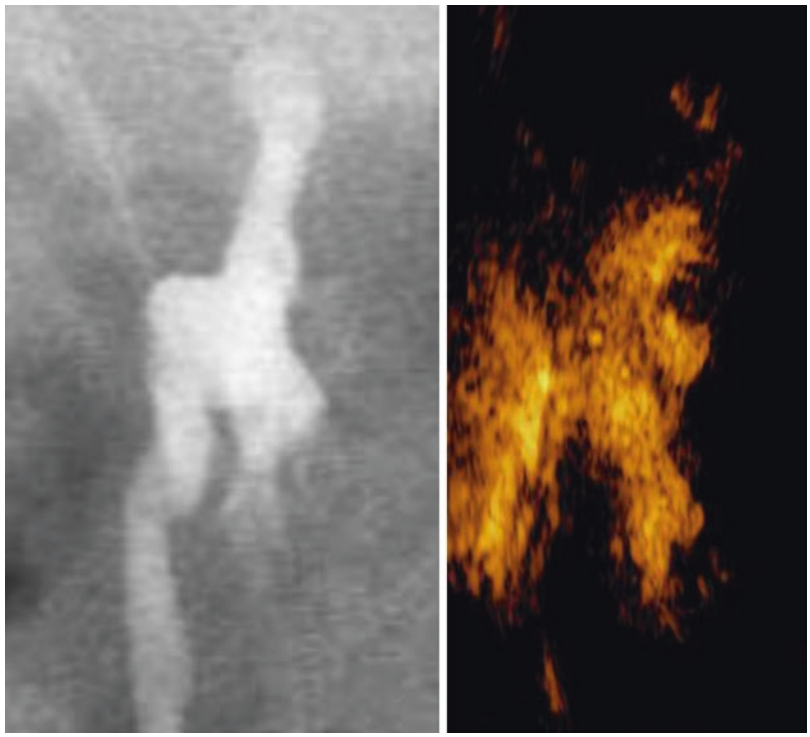

Grade IV VUR

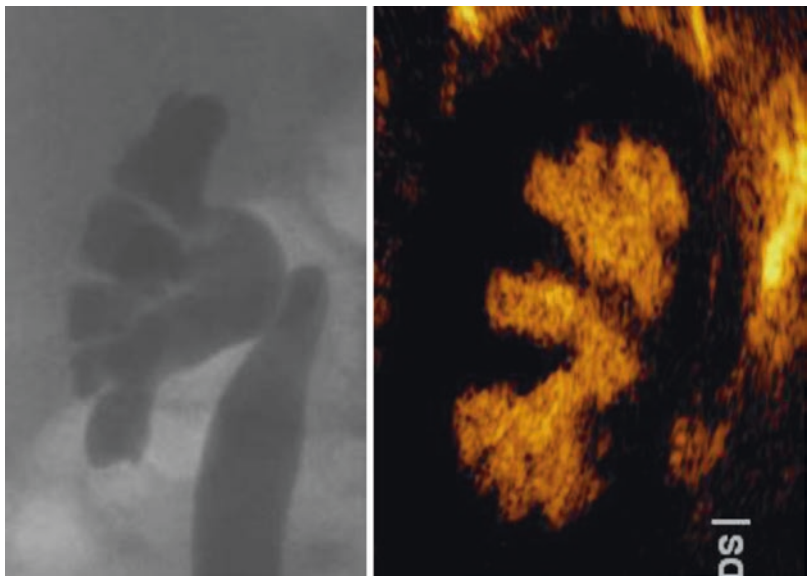

Intrarenal VUR

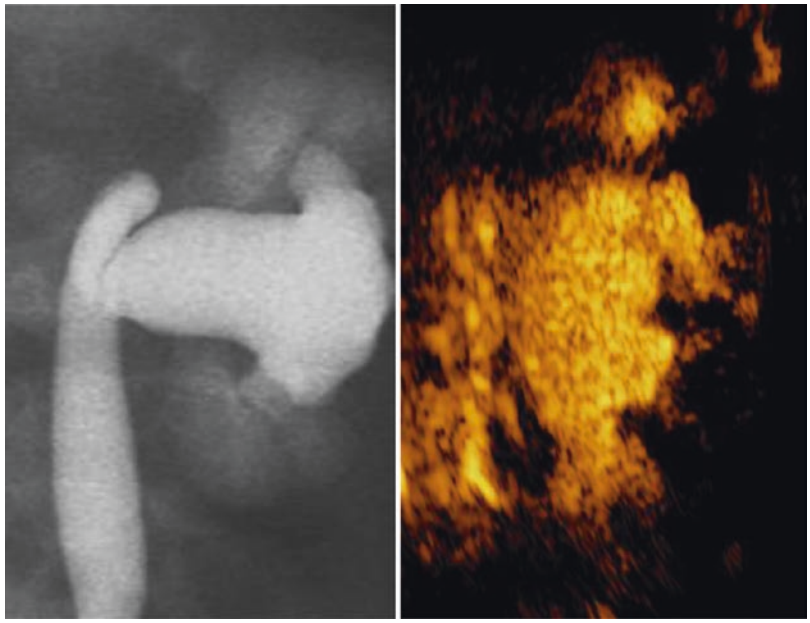

Lower pole contour incisure in a kidney with "reflux nephropathy"

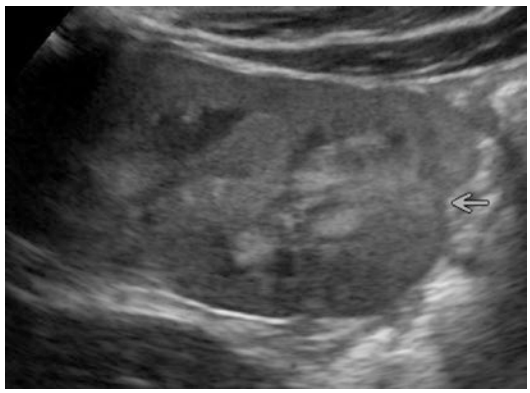

A lower pole scar withirregular contour and corticalized calyces in "reflux nephropathy"

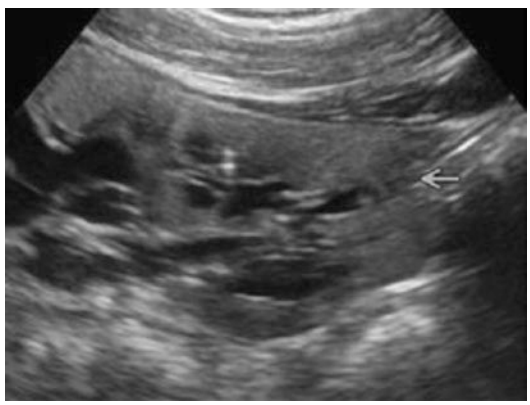

Incomplete midrenal parenchymal septum

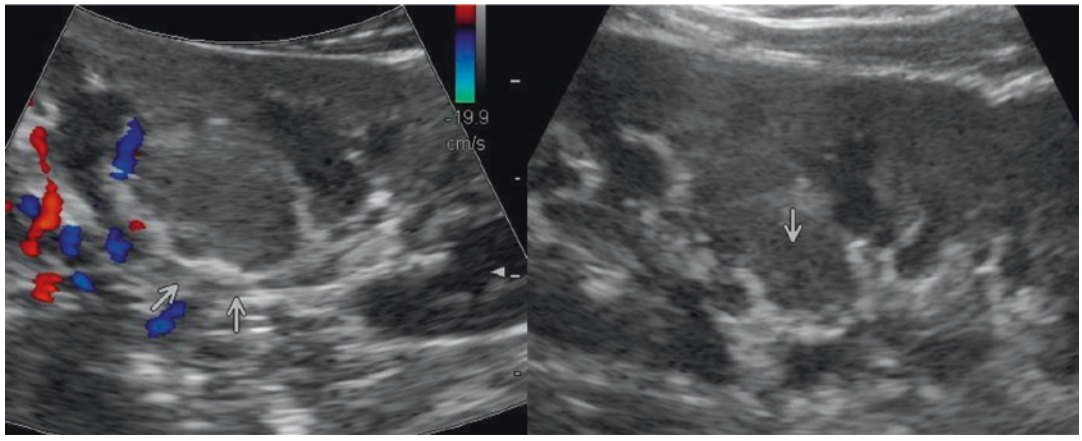

Complete midrenal parenchymal septum

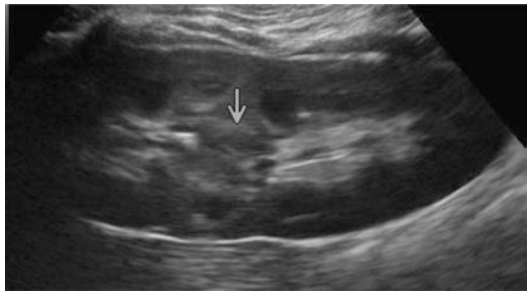

Complicated duplicate collecting system with dilatation of lower urinary tract

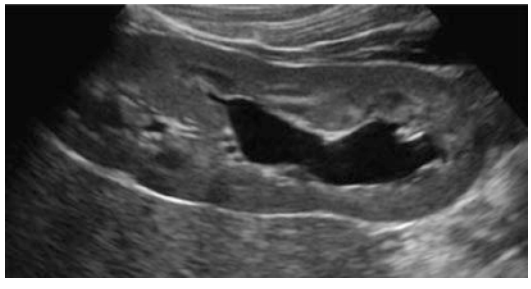

Complicated duplicate collecting system with severe upper renal pelvis dilatation

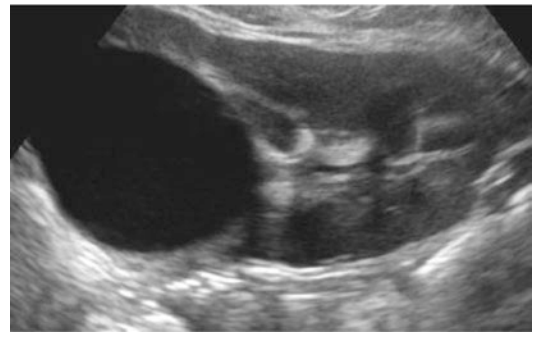

Two bladder separate ureteral orifices in complete ureteropelvic duplication

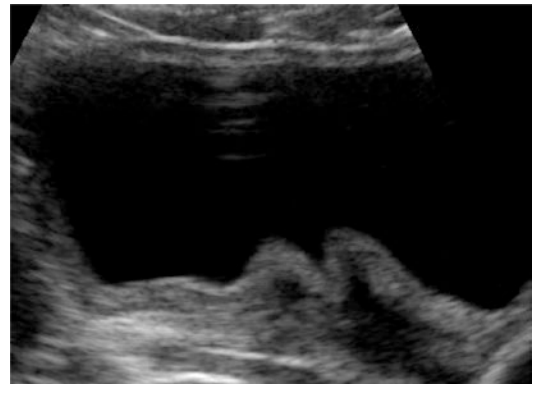

Two separate ureters of a duplicate collecting system joining to become a single ureter in their intermediate tract

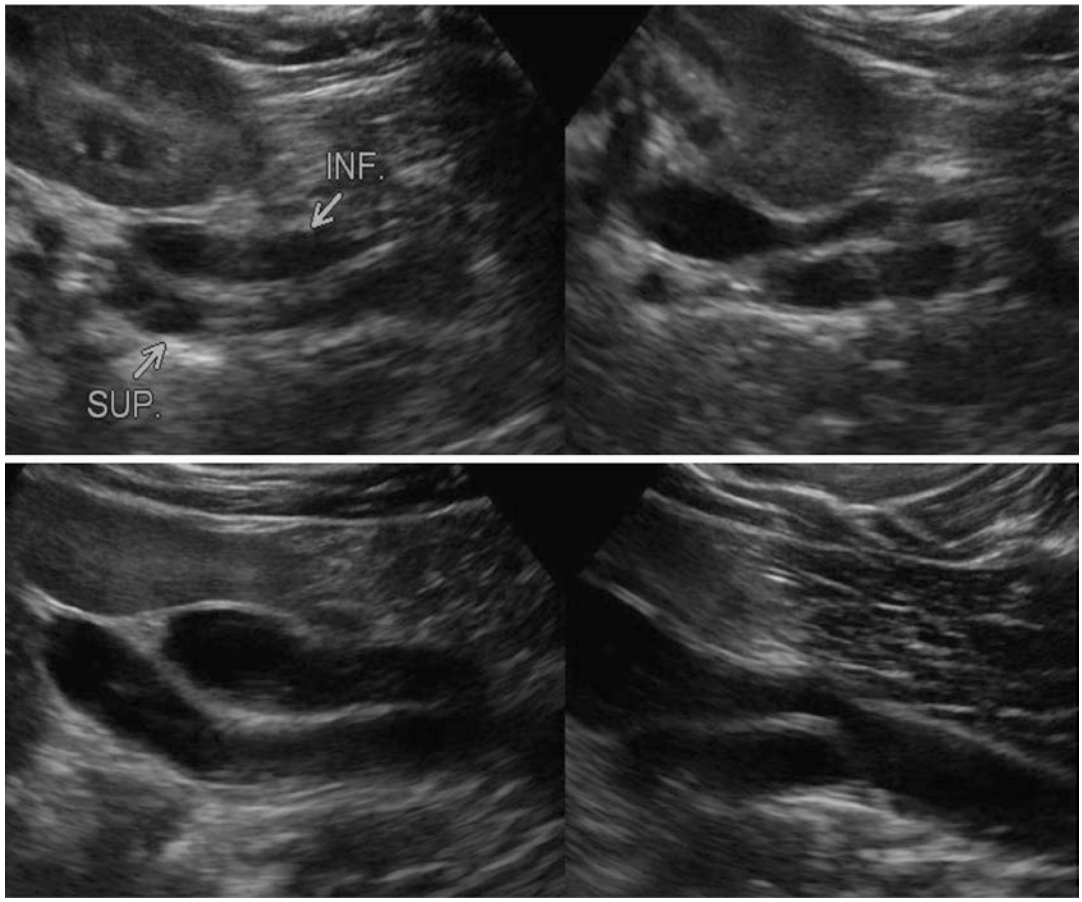

Low-size ureterocele

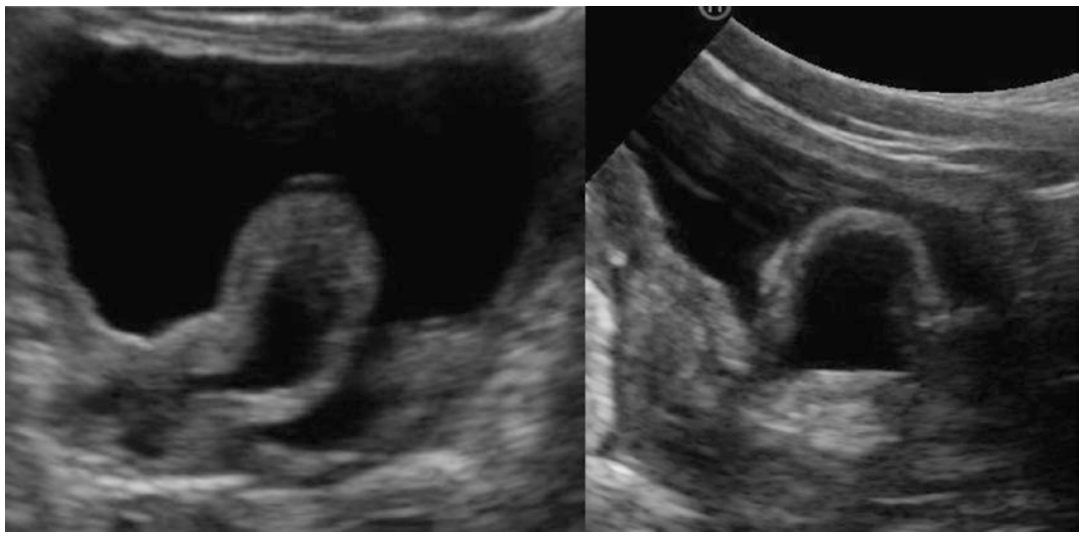

Severe ureterocele

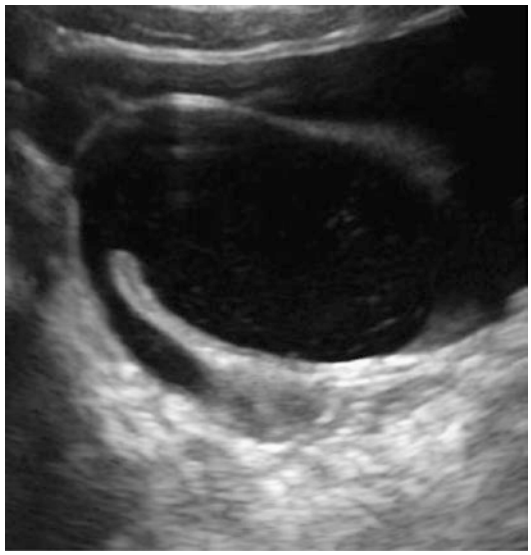

Stenotic megaureter emptying into an intravesical ureterocele

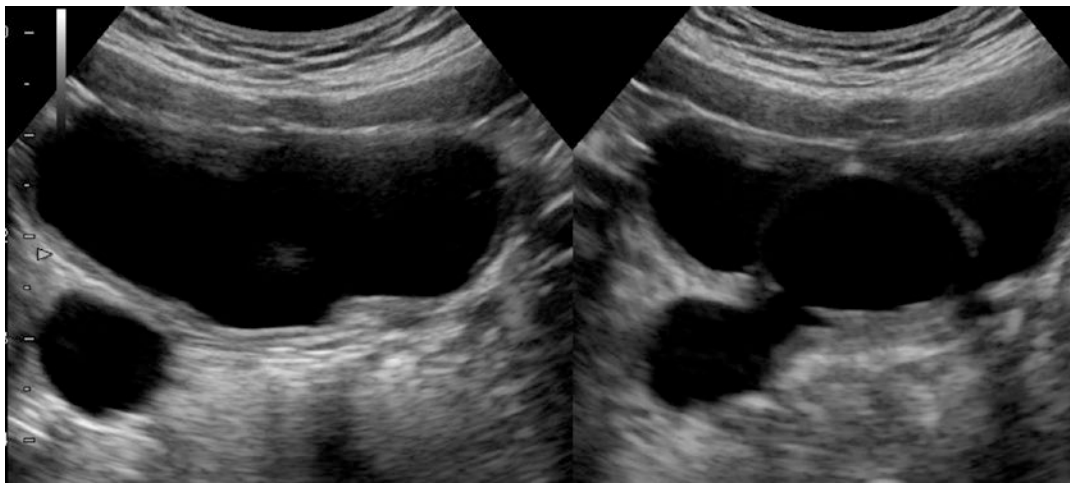

Ureterocele prolapsing into the urethra

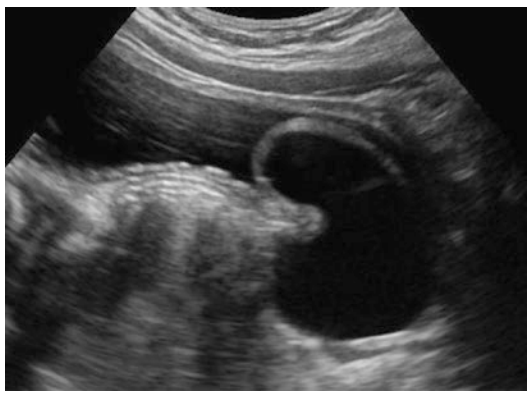

Thickened bladder walls (neurogenic bladder)

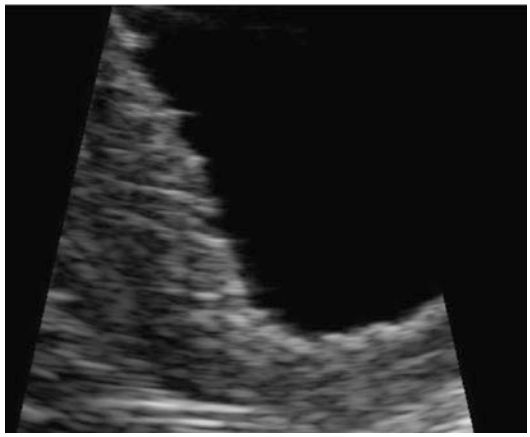

Bladder pseudodiverticula (posterior urethral valves)

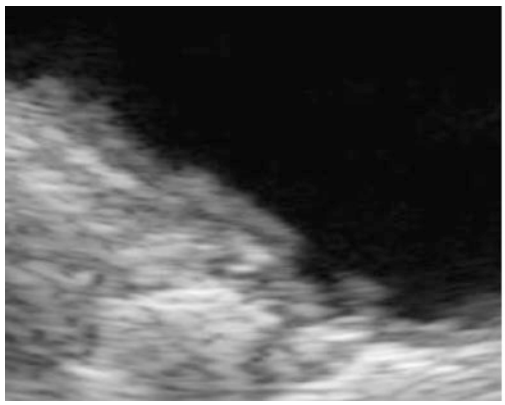

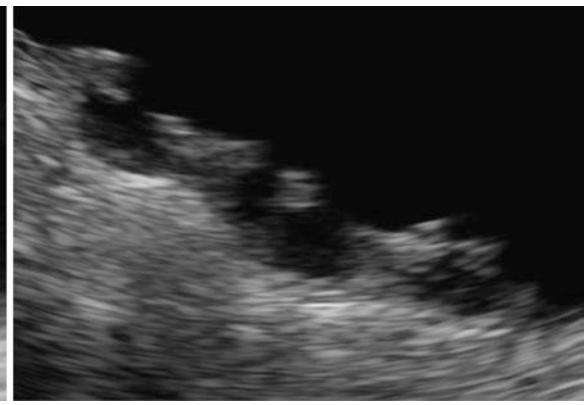

Dilatation of proximal urethra in a patient with posterior urethral valves

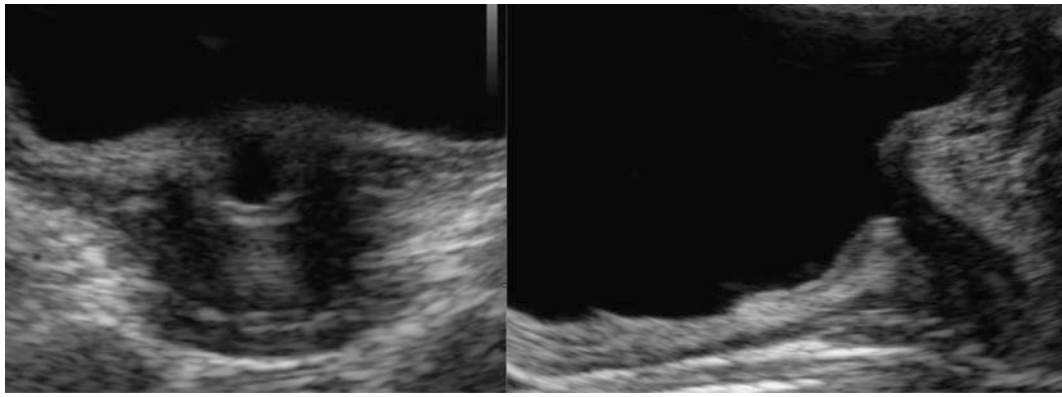

Posterior urethral valves shown by urethrosonography

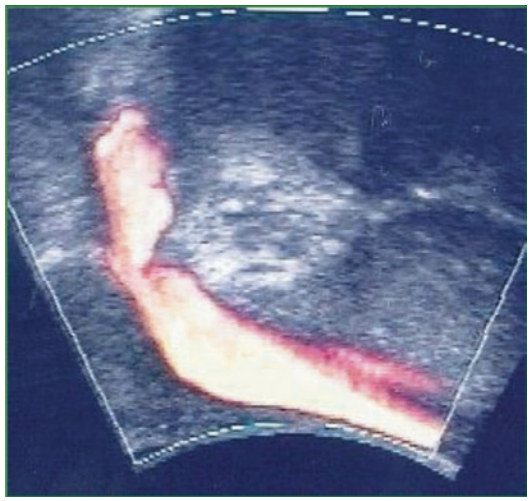

Comparison of US and cystourethrographic images in a 1-month-old male with posterior urethral valves determining gross dilatation of the upper urethral tract and bladder wall thickening

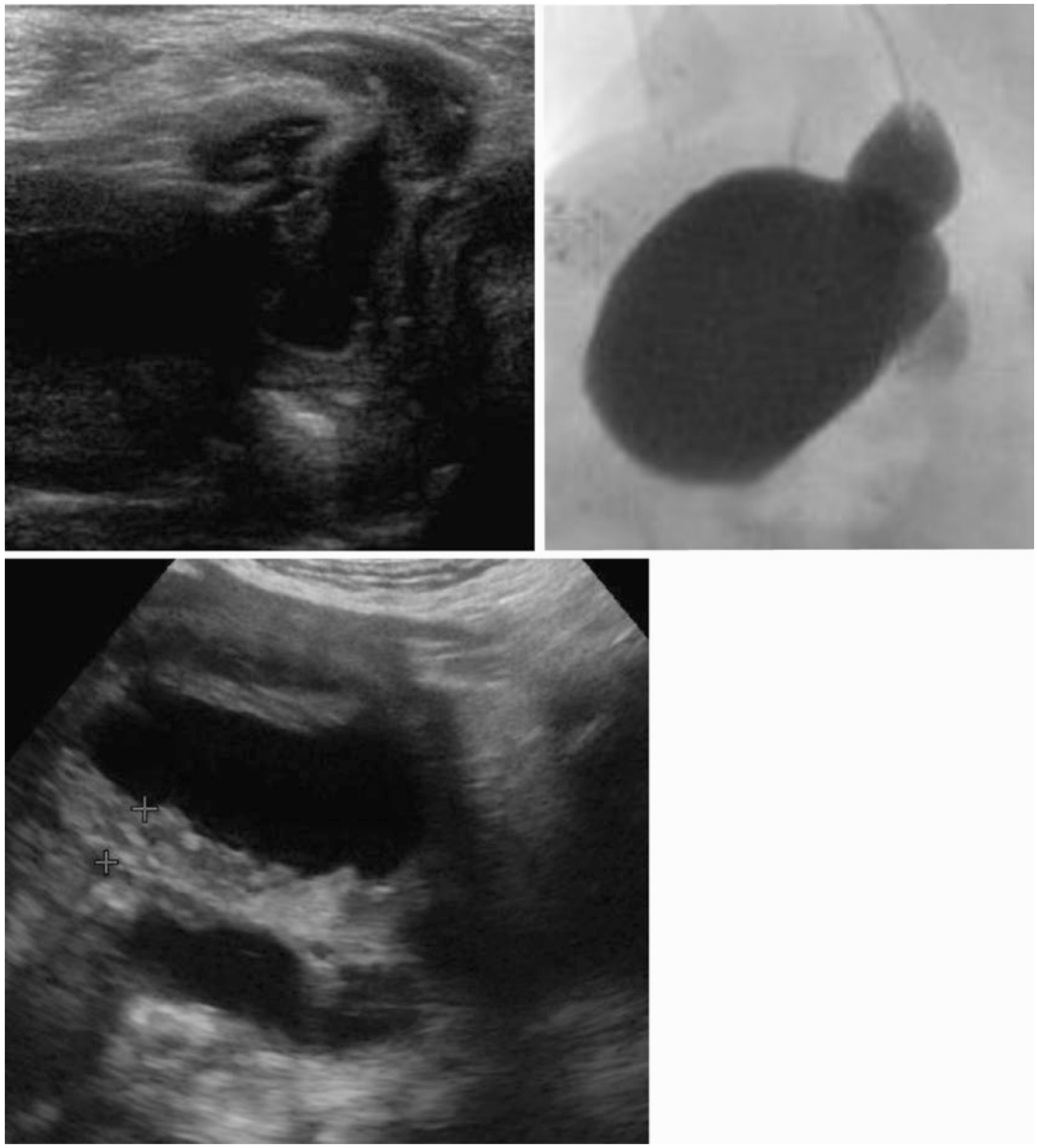

Urethral polyp with a large implantation base (pre- and post-resection images)

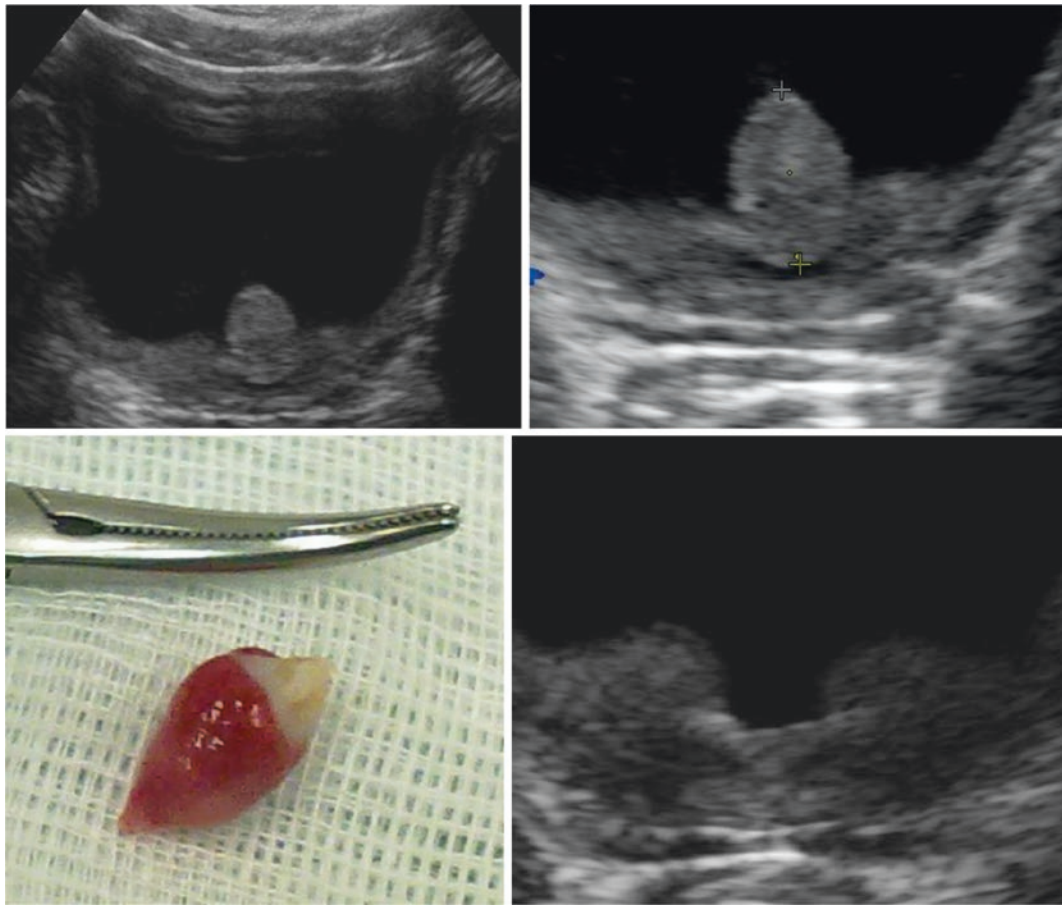

Bladder neurofibromatosis with severe thickening of bladder walls, determining compression and dilatation of the ureter and of the renal pelvis

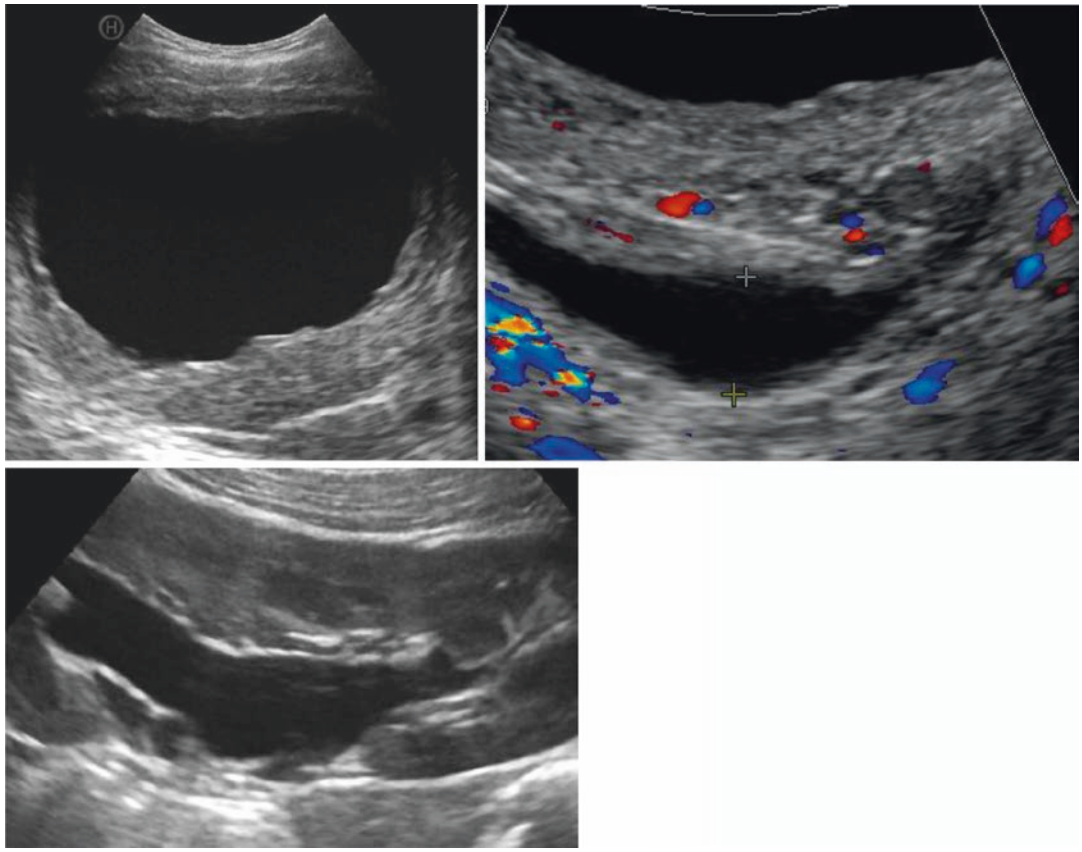

References

1. Richter-Rodier M, Lange AE, Hinken B, Hofmann M, Stenger RD, Hoffmann W, Fusch C, Haas JP (2012) Ultrasound screening strategies for the diagnosis of congenital anomalies of the kidney and urinary tract. Ultraschall Med 33(7):E333–E338
2. Tsuchiya M, Hayashida M, Yanagihara T, Yoshida J, Takeda S, Tatsuma N, Tsugu H, Hino Y, Munakata E, Murakami M (2003) Ultrasound screening for renal and urinary tract anomalies in healthy infants. Pediatr Int 45(5):617–623
3. Corteville JE, Gray DL, Crane JP (1991) Congenital hydronephrosis: correlation of fetal ultrasonographic findings with infant outcome. Ultrasonographic standards for measuring renal collecting system dilation. Am J Obstet Gynecol 165(2):384–8
4. Grignon A, Filion R, Filiatrault D, Robitaille P, Homsy Y, Boutin H, Leblond R (1986) Urinary tract dilatation in utero: classification and clinical applications. Radiology 160(3):645–7
5. Kim SY, Kim MJ, Yoon CS, Lee MS, Han KH, Lee MJ (2013) Comparison of the reliability of two hydronephrosis grading systems: the Society for Foetal Urology grading system vs. the Onen grading system. Clin Radiol 68(9):e484–90
6. Sanna-Cherchi S, Ravani P, Corbani V, Parodi S, Haupt R, Piaggio G, Innocenti ML, Somenzi D, Trivelli A, Caridi G, Izzi C, Scolari F, Mattioli G, Allegri L, Ghiggeri GM (2009) Renal outcome in patients with congenital anomalies of the kidney and urinary tract. Kidney Int 76(5):528–533. doi:10.1038/ki.2009.220, Epub 2009 Jun 17
7. Toka HR, Toka O, Hariri A, Nguyen HT (2010) Congenital anomalies of kidney and urinary tract. Semin Nephrol 30(4):374–386. doi:10.1016/j.semnephrol.2010.06.004
8. Riccabona M, Avni FE, Damasio MB, Ording-Müller LS, Blickman JG, Darge K, Lobo ML, Papadopoulou F, Vivier PH, Willi U (2012) ESPR Uroradiology Task Force and ESUR Paediatric Working Group – Imaging recommendations in paediatric uroradiology, part V: childhood cystic kidney disease, childhood renal transplantation and contrast-enhanced ultrasonography in children. Pediatr Radiol 42(10):1275–1283. doi:10.1007/s00247-012-2436-9, Epub 2012 Sep 22
9. Faizah M, Kanaheswari Y, Thambidorai C, Zulfiqar M (2011) Echocontrast cystosonography versus mic-

turating cystourethrography in the detection of vesicoureteric reflux. Biomed Imaging Interv J 7(1):e7. doi:10.2349/biij.7.1.e7, Epub 2011 Jan 1
10. Piaggio G, Degl' Innocenti ML, Tomà P, Calevo MG, Perfumo F (2003) Cystosonography and voiding cystourethrography in the diagnosis of vesicoureteral reflux. Pediatr Nephrol 18(1):18–22, Epub 2002 Nov 14
11. Riccabona M, Mache CJ, Lindbichler F (2003) Echo-enhanced color Doppler cystosonography of vesicoureteral reflux in children. Improvement by stimulated acoustic emission. Acta Radiol 44(1):18–23
12. Bosio M, Manzoni GA (2002) Detection of posterior urethral valves with voiding cystourethrosonography with echo contrast. J Urol 168(4 Pt 2):1711–1715

Normal and Pathological Adrenal Glands

10

Pasquale Martino, Silvano Palazzo, Francesco Paolo Selvaggi, Carlos Miacola, and Michele Battaglia

10.1 Introduction

The adrenals are endocrine glands located cranially to the kidneys, deep in the abdomen, sheathed inside the opening of Gerota's fascia. Since the introduction, in relatively recent times, of high-resolution probes and devices, it has been possible to perform ultrasound (US) studies of the adrenal glands. In 1980, Sample was the first to describe the ultrasound approaches best suited to studying the normal adrenal gland [1]. Although other imaging techniques (MRI, CT, scintigraphy) are considered primary techniques in the study of adrenal diseases, US can offer an important contribution both in pediatric patients and in adults, when disease induces an increase in the volume of these glands. The adrenals are studied together with the kidneys using convex 3.5 MHz probes or, preferably, multifrequency 5–2 MHz probes. Higher frequencies can be used to study the adrenal glands in children, in whom the glands are relatively larger and better defined. When available, tissue harmonics is routinely employed to reduce reverberation artifacts and obtain more detailed images.

In the study of the adrenal glands, ultrasound shows good sensitivity but poor specificity; it can distinguish solid or fluid lesions, but in the context of solid lesions, it is difficult to resolve doubts as to the histological nature of the lesion [2]. In any case, its good sensitivity justifies the use of US as the first-choice imaging technique in cases of suspected adrenal masses, especially in the newborn. In addition, US plays an important role in the follow-up of neonatal adrenal hemorrhage and adult adrenal hematoma, as well as in localizing nonoperated secondary neoplastic lesions, and it provides a valid support of targeted adrenal biopsies.

In view of the considerable percentage of adrenal masses discovered incidentally, it is always advisable to scan the adrenal loggia when performing other US studies of the abdomen [3].

P. Martino (✉) • S. Palazzo • F.P. Selvaggi
C. Miacola • M. Battaglia
Department of Emergency and Organ Transplantation – Urology, Andrology and Kidney Transplantation Unit, University of Bari, Bari, Italy
e-mail: pasqualeluciomartino@libero.it

P. Martino, A.B. Galosi (eds.), *Atlas of Ultrasonography in Urology, Andrology, and Nephrology*,
DOI 10.1007/978-3-319-40782-1_10

10.2 Preparation

No preparation is necessary because it has not been demonstrated that fasting can improve the visibility of the adrenal glands nor has the administration of gas-absorbent substances been shown to improve the images.

10.3 Performance of the Examination

To carry out US study of the adrenal glands, the patient is positioned in lateral decubitus, with the side of the gland to be studied upward. Longitudinal, oblique, intercostal scans are done, at the level of the ninth to tenth intercostal space of the posterior or medial axillary line on the left and subcostal anterior space on the right, because the topographic anatomical situation of the adrenal glands is not symmetrical. The probes used are sector or convex 3.5 and 5 Mhz [4, 5, 6]. The normal adrenal gland is isoechogenic as compared to the renal parenchyma and hypoechogenic as compared to the surrounding perirenal fat. This fat offers a natural contrast that highlights the hypoechogenicity of the adrenal glands. The cortical portion is slightly hyperechogenic as compared to the medullary portion, a characteristic due to the architectural arrangement of the cortical cells [7]. The medullary portion is visible as a thin, central, linear isoechogenic structure [8] as compared to the renal parenchyma. Each gland has a body (anteromedial region) and two wings (medial and lateral) [5]. Owing to its complex shape, it is extremely difficult to visualize the whole gland in a single scan [9]. The difficulties in recognizing whether the adrenal glands are normal depend on their deep position in the retroperitoneal space, their small size, the hypoechogenic echostructure that is quite similar to that of the diaphragmatic pillar, the fact that they are surrounded by retroperitoneal adipose tissue that often poses a barrier to the passage of the ultrasound waves, the biotype being examined (obesity but also extreme underweight), the operator's experience, a previous splenectomy (when the acoustic window for the left adrenal gland is lost), a concomitant renal or hepatic polycystosis, and, lastly, the anchorage of the gland to Gerota's fascia that does not allow the gland to follow the kidney during the rise and fall of breathing movements.

In the past, the percentage of visualizations of normal adrenal glands in the adult was decidedly low (78 % on the right and 44 % on the left), but nowadays they range between 90 and 100 % on

the right and 70 and 90 % on the left. Generally, in the adult, the adrenal loggia can be visualized in 85–95 % of cases [4, 10, 11].

The variations in the size of the glands depend on their trophism, but they are generally 40–60 mm long, 25–35 mm wide, and 3–9 mm thick. Some comparative studies of imaging (CT and US) versus autopsy [1] have demonstrated that comparable measurements are obtained.

The shape of the adrenal glands varies remarkably: they can be sickle shaped, upside-down Y shaped, triangular, upside-down V shaped, and star shaped (Fig. 10.1). The most common form on the right is a linear shape. The adrenal margins are nearly always rectilinear or concave.

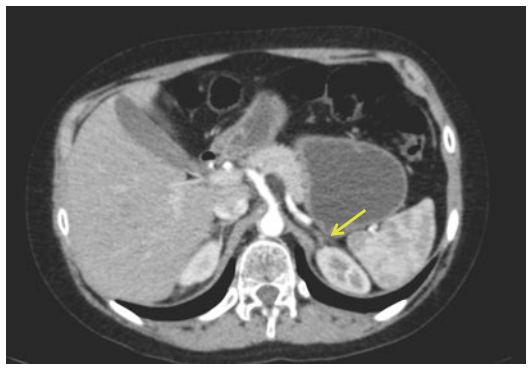

Fig. 10.1 Triangle-shaped normal left adrenal gland (*arrow*)

10.4 The Right Adrenal Gland

The patient is placed in left lateral decubitus and asked to breathe in deeply to improve the acoustic window offered by the liver. The right adrenal is better identifiable by sonography than the left, thanks to the presence of anatomical landmarks like the vena cava, diaphragm pillar, and liver, as well as the better scanning options. In fact, on the right, as well as intercostal scans, it is possible to perform anterior subcostal scans, whereas these are more difficult to achieve on the left.

The right adrenal gland is posterior to the left gland, located at the level of the 12th dorsal vertebra and retrocavally. Medially, the reference point is the diaphragm pillar and laterally the eighth liver segment. The lower part of the right adrenal gland is anteromedial to the right kidney, and the upper part extends upward toward the bare liver area (a liver portion that is devoid of the peritoneum covering, this portion lies between the two layers of coronary ligaments), separated from it by a thin layer of areolar fat. On intercostal scans, it appears as a hypoechogenic linear structure between the bare liver area and the diaphragm. On transverse scans it is visible at about the level of the liver hilum. On subcostal transverse scans, it appears as a hypoechogenic linear structure between the bare liver area and the diaphragm (it can sometimes be masked by the liver hilum structures).

10.5 The Left Adrenal Gland

The left adrenal is located more anteriorly than the right gland, extends anteriorly to the superior pole of the homolateral kidney, and lies vertically between the bodies of T12 and L1, being about 4 cm long. It can be examined with the patient in lateral right decubitus, making longitudinal scans along the medial or posterior axillary line, exploiting the acoustic window offered by the spleen. Visualization of the left adrenal gland may be unsuccessful due to colonic and/or gastric meteorism, but it is typically located between the lateral margin of the aorta and anteriorly to the superior pole of the left kidney. Medially, the point of reference is the diaphragm pillar, while laterally it is visible in contact with the inferior-medial face of the spleen; anteriorly it borders the tail of the pancreas and the splenic vein. The gland can be seen posteriorly to the splenic vein as a hypoechogenic linear structure, but it is frequently masked by the stomach shadow. In thin patients, compression can improve the acoustic window, by shifting the stomach. In left lateral decubitus, the left hepatic lobe can improve the acoustic window.

10.6 Ultrasound Characteristics of Adrenal Lesions

The indication for US study of adrenal gland disorders is to assess all those diseases that cause an increased volume of the organ: adenoma, carcinoma, trauma, hemorrhage, thrombosis, infections, TBC, metastases, histoplasmosis, and medullary tumors such as pheochromocytoma and pheochromoblastoma. Adrenal lesions are frequently diagnosed as "incidentalomas" that account for 13% of all US examinations of the abdomen: 2/3 of incidentalomas are cortical adenomas and metastases [12].

10.6.1 Hyperplasia of the Glands and Adenomas

In adrenal hyperplasia, the gland is larger and presents clear-cut margins with an isoechogenic structure as compared to the renal parenchyma. Adenomas are generally rounded neoformations, mostly small and hypoechogenic (Fig. 10.2). A left adrenal adenoma can be confused with an accessory spleen. It has recently been reported that the use of contrast medium while performing the sonography can enable a differential diagnosis between adenomas and nonadenomatous lesions, with a comparable sensitivity to that of CT and MRI [13].

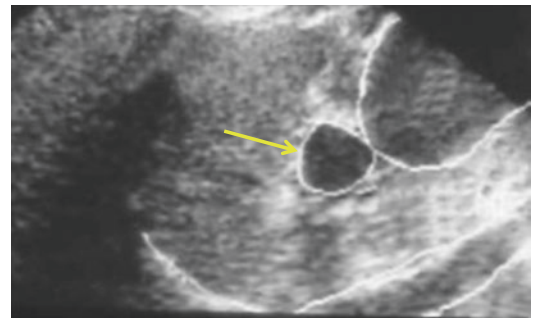

Fig. 10.2 Adrenal adenoma: hypoechogenic rounded mass (*arrow*)

10.6.2 Myelolipomas

Adrenal myelolipomas are rare, nonfunctioning tumors consisting of variable proportions of myeloid elements and fat, deriving from the cortical fascicular area. The age incidence of this tumor is between the 50s and 60s, with no difference between males and females. Because they are benign and nonsecreting, they are typically diagnosed incidentally. The usual size is between 2 and 10 cm (more rarely, 10–20 cm). For myelolipoma, US can have a specificity value: in general, it presents as a rounded mass with clear-cut margins and a hyperechogenic structure (Fig. 10.3), although this may not be true if the myeloid component exceeds the adipose portion. In this case it may present as hypoechogenic and difficult to differentiate from hyperplasia. If the tumor is large (>4 cm) and has a high-fat content, it is reasonable to expect artifacts due to variations in the propagation of the ultrasound wave through the fat that can provoke an apparent deformity of the diaphragm [14]. Differential diagnosis must be made with hemorrhagic cysts (generally well defined and circular, with a heterogeneous aspect if seen at onset, but hypoechogenic if long standing), pheochromocytoma (highly vascularized with hemorrhagic areas and necrosis), adjacent tumors (exophytic renal clear cell carcinoma, renal angiomyolipoma, exophytic liver hemangioma, or hepatocellular carcinoma), liposarcoma (primary retroperitoneal sarcoma involving the perirenal space, simulating an adipose tumor), and adrenal adenoma.

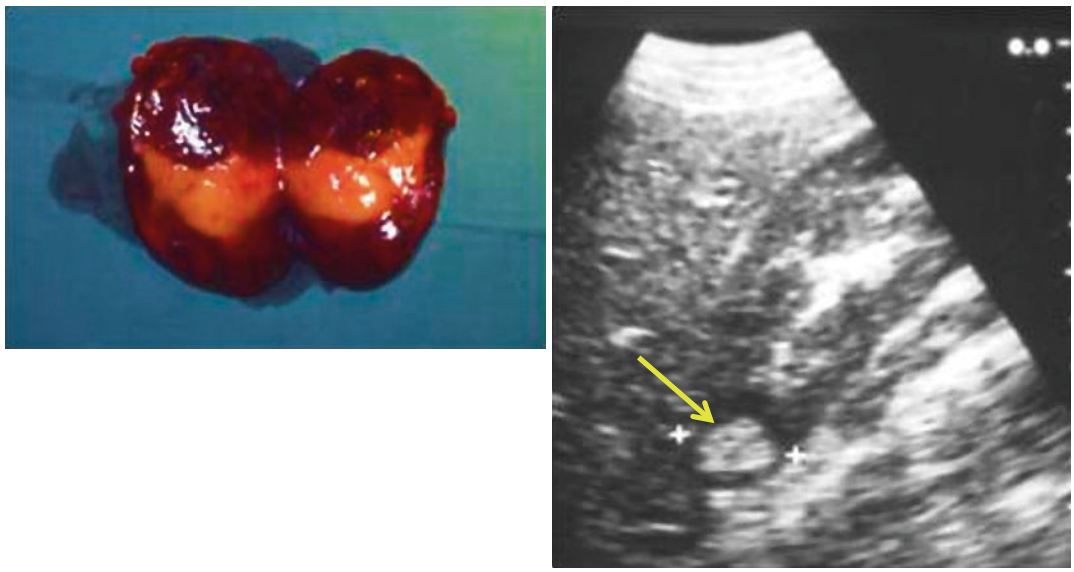

Fig. 10.3 Adrenal myelolipoma: hyperechogenic mass (*arrow*)

10.6.3 Pheochromocytomas

Pheochromocytomas typically derive from the neuroectodermic tissue of the adrenal medulla. They are associated with many neuroectodermic diseases (tuberous sclerosis, neurofibromatosis, von Hippel-Lindau disease, MEN IIa and IIb). These tumors affect patients aged between 40 and 60, and the right/left gland ratio is 2:1. Most pheochromocytomas are poorly defined at US and sometimes appear isoechogenic, sometimes heterogeneous, depending on the presence of necrosis or internal hemorrhagic spots (Fig. 10.4). Because of their rich vascularization, in some cases, they may look like cystic lesions with a hemorrhagic content and necrotic fragments accounting for the heterogeneous ultrasound appearance. Calcifications are rare. A differential diagnosis needs to be made between pheochromocytoma and adenoma or hyperplasia if it is small, while it may be confused with a carcinoma if it is larger.

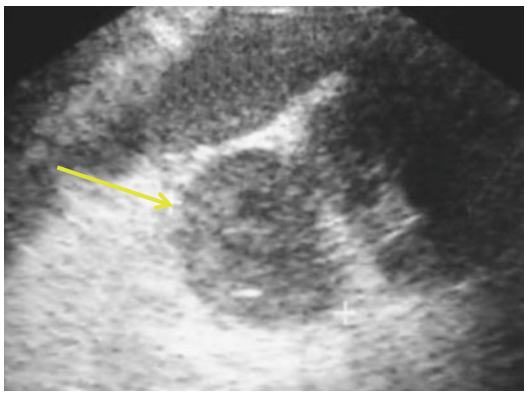

Fig. 10.4 Pheochromocytoma: mass with mixed echostructure (*arrow*)

10.6.4 Carcinoma

Carcinomas of the cortex are rare. At ultrasonography they have a variable aspect according to their size. They generally present as solid dyshomogeneous masses with irregular or transonic margins, illustrating necrotic, hemorrhagic, calcified areas. Smaller lesions are homogeneous and can be difficult to differentiate from adenomas. Some authors have described the presence of a thin pseudocapsule sometimes seen as an echogenic border [15], probably correlated to the atypical peripheral vascularization. Instead, large masses with internal necrosis and hemorrhagic areas can mimic pheochromocytomas. If it is greater than 10 cm, it may be impossible to make a differential diagnosis between an adrenal mass and other large tumors of a nonadrenal origin (liver, kidney) (Fig. 10.5). In general, it can be said that an adrenal mass that infiltrates the surrounding structures will appear fixed, limiting the movements of the infiltrated structures to follow the breathing rise and fall movements [16]. In about 50% of cases, carcinomas are hyperfunctioning and so symptomatic. In cases diagnosed late, very large masses can cause compression of the vena cava that may wrongly appear infiltrated.

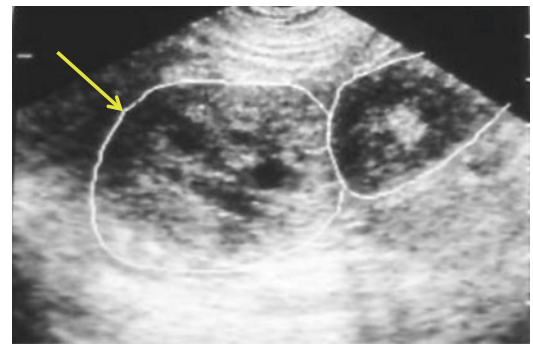

Fig. 10.5 Adrenal carcinoma (*arrow*): the hypoanechogenic areas are attributable to necrotic-hemorrhagic masses

10.6.5 Lymphomas

A primary localization of a lymphoma in an adrenal gland is a very rare observation; in general, there is secondary involvement, often bilaterally. A non-Hodgkin lymphoma is the most common form. At US, the echogenicity will depend on the tumor cell component. A lymphoma will mostly appear as a hypoechogenic mass, but it is no rare occurrence for it to have a hyperechogenic or anechogenic appearance, as if mimicking a cyst [8, 17].

10.6.6 Metastases

The adrenal gland is the fourth most common localization of metastases in the human body, after the lung, stomach, and bones, and if the percentage of metastasization is considered in respect to its size, then it becomes the first site of metastases [18]. Evidently in the adrenal gland, metastatic cells find a favorable environment, with a rich content of growth factors and ample blood flow. In the explanation of the high incidence of metastasization, the action of cortisol is also implicated, in that it reduces the immune response of the adrenal tissue to neoplastic aggression. The metastases are usually hypoechogenic with clear-cut margins; this is particularly true if the lesion is <3 cm, which will make it indistinguishable from an adenoma. The main element for differential diagnosis is that adrenal metastases are more frequently bilateral, unlike adenomas. Large lesions can be sonographically heterogeneous due to central necrosis or hemorrhage [8, 19].

10.6.7 Adrenal Cysts

Cysts account for 0.6 % of all adrenal diseases and even these are generally hemorrhagic pseudocysts. They stem from adrenal hemorrhages in patients with neoplastic diseases or affected by Waterhouse-Friderichsen syndrome. Some cysts can be parasitic or an involution of an adenoma (Fig. 10.6). True cysts are transonic areas like those in other apparatuses and organs; they may be uni- or multiloculated.

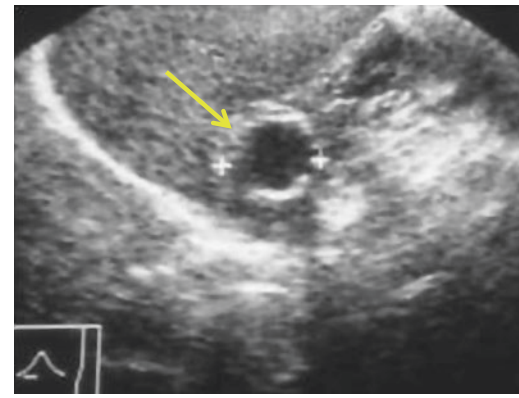

Fig. 10.6 Adrenal cysts of parasitic origin (*arrow*)

10.6.8 Adrenal Hemorrhage

Spontaneous adrenal hemorrhage is very rare in the adult but can be associated with physical stress events like septic shock, severe hypotension, and diffuse burns. By contrast, in the perinatal period, it is relatively frequent. Trauma is often the cause of adrenal bleeding (about 2 % of patients suffering from trauma undergoing CT scanning have adrenal bleeding, most frequently involving the right gland) [20]. Partial hepatectomy can be implicated as the cause of right adrenal hemorrhage [21]. Typically, adrenal hemorrhage appears as oval or rounded echogenic areas at the center of the gland, with a lengthened or interrupted cortex and consequent periadrenal hemorrhage. A differential diagnosis must be made with various lesions such as pheochromocytoma, myelolipoma, and adjacent tumors (renal angiomyolipoma, clear cell carcinoma, exophytic liver tumor, atypical liver hemangioma, and hepatocellular carcinoma).

References

1. Diagnostic ultrasound (1980) In: Frederick Sample W, Sarti DA. Renal, adrenal, retroperitoneal, and scrotal ultrasonography: Martinus Niyhoff Pubblischer The Hague, Boston, london, pp 268–411
2. Martino P (1993) Ruolo dell'ecografia nella diagnosi delle masse surrenaliche. Arch It Urol LXV:337–340
3. Martino P, Selvaggi FP (1998) Diagnostica delle malattie del surrene. In: Porena M, Guercini F (eds) Diagnostica Urologica ed Andrologica per immagini, vol 11. CIC Ed. Inter, Roma, pp 61–65
4. Zappasoldi F, Derchi L, Rizzato G (1986) Ultrasonography of the normal adrenal glands; a study using linear-array real time equipment. Br J Radiol 59:759–764
5. Kim KW, Kim JK, Choi HJ, Kim MH, Lee J, Cho KS (2012) Sonography of the adrenal glands in the adult. J Clin Ultrasound 40(6):357–363
6. Little AF (2000) Adrenal gland and renal sonography. World J Surg 24(2):171–182, Review
7. Wilms G, Marchal G, Baert A, Adisoejoso B, Mangkuwerdojo S (1987) CT and ultrasound features of post-traumatic adrenal hemorrhage. J Comput Assist Tomogr 11(1):112–115
8. Thurston W, Wilson SR (2005) The adrenal gland. In: Rumack CM, Wilson SR, Charboneau JW (eds) Diagnostic ultrasound. Mosby, St. Louis, p 425
9. Marchal G, Gelin J, Verbeken E et al (1986) High-resolution real-time sonography of the adrenal glands: a routine examination? J Ultrasound Med 5:65
10. Martino P, Carrieri V, Palasciano G, Selvaggi FP (1980) Ecotomografia del surrene: possibilità e limiti. Atti del 53° Congr Soc Ital Urol 859–865
11. Vespasiani G, Rosi P, Giurioli A, Virgili V (1992) L'ecotomografia nella diagnosi delle malattie del surrene. Acta Urol Ital Supp 3:95–107
12. Fontana D, Porpiglia F, Destefanis P, Fiori C, Ali A, Terzolo M, Osella G, Angele A (1999) What is the role of ultrasonography in the follow-up of incidentalomas? Gurppo Piemontese Incidentalomi Surrenalici. Urology 54(4):612–616
13. Friedrich-Rust M, Schneider G, Bohle RM et al (2008) Contrast-enhanced sonography of adrenal masses: differentiation of adenomas and nonadenomatous lesions. AJR Am J Roentgenol 191:1852
14. Musante F, Derchi LE, Zappasodi F et al (1988) Myelolipoma of the adrenal gland: sonographic and CT features. AJR Am J Roentgenol 151:961
15. Hamper UM, Fishman EK, Hartman DS et al (1987) Primary adrenocortical carcinoma: sonographic evaluation with clinical and pathologic correlation in 26 patients. AJR Am J Roentgenol 148:915
16. Lim JH, Ko YT, Lee DH (1990) Sonographic sliding sign in localization of right upper quadrant mass. J Ultrasound Med 9(8):455–459
17. Antoniou A, Spetseropoulos J, Vlahos L et al (1983) The sonographic appearance of adrenal involvement in non-Hodgkin's lymphoma. J Ultrasound Med 2:235
18. Korobkin M, Brodeur FJ, Francis IR, Quint LE, Dunnick NR, Goodsitt M (1996) Delayed enhanced CT for differentiation of benign from malignant adrenal masses. Radiology 200(3):737–742
19. Dunnick NR (1990) Hanson lecture. Adrenal imaging: current status. AJR Am J Roentgenol 154:927
20. Rana AI, Kenney PJ, Lockhart ME et al (2004) Adrenal gland hematomas in trauma patients. Radiology 230:669
21. Gouliamos AD, Metafa A, Ispanopoulou SG et al (2000) Right adrenal hematoma following hepatectomy. Eur Radiol 10:583

Intraoperative Ultrasound in Renal Surgery

11

Nicola Pavan, Tommaso Silvestri, Calogero Cicero, Antonio Celia, and Emanuele Belgrano

11.1 Introduction

Management of renal cell carcinoma (RCC) has evolved over the last decade because of improved surgical techniques and more accurate preoperative staging by diagnostic imaging, like computed tomography (CT), magnetic resonance imaging (MRI) and contrast-enhanced ultrasound (CEUS). Surgery remains the definitive therapy and the means of a cure.

Partial nephrectomy (PN) as a nephron-sparing technique to optimize resection with minimal loss of normal tissue, either open or laparoscopic or robot assisted, has increasingly replaced radical nephrectomy and is reported to result in lower morbidity, better recovery of renal function and favourable patient survival rates compared with radical nephrectomy over the long term [1–5]. Preoperatively, thin-section CT and MRI, both being the standard of care for staging RCC, have limitations in detecting small additional multifocal lesions and resolving indeterminate lesions because of volume averaging and image noise. In addition, both modalities provide only an estimate to the surgeon of the extent of surgical resection required for a PN, with no real-time guidance during surgery.

In this context, in recent years, we have seen an increasing use of intraoperative ultrasound (IOUS) probes in step with technological breakthroughs. The use of ultrasound in the intraoperative renal surgery with the high spatial resolution of IOUS transducers is crucial not only for the traditional surgery but also for the laparoscopic and robot-assisted technique. The ultrasound is able to provide indications regarding the parenchyma and vascularization of the kidney, which currently no intraoperative radiological method is able to give.

The first use of IOUS occurred in 1958, where for the first time the ultrasound was used during an operation for the identification of a stone in the urinary tract [6].

The imaging is important and sometimes essential especially when the intraoperative palpation cannot be performed. For this reason, the use of ultrasound in the intraoperative kidney surgery has undergone strong growth in recent years, in addition to laparoscopic and robot-assisted techniques, that still does not offer the possibility to the surgeon, to have a tactile feedback during surgical steps [7].

N. Pavan (✉) • T. Silvestri • E. Belgrano
Clinica Urologica, Università degli Studi di Trieste, Azienda Ospedaliero-Universitaria Ospedali Riuniti, Strada per Fiume 447, Trieste 34149, Italy
e-mail: nicpavan@gmail.com

C. Cicero
S.C. di Radiologia, Ospedale San Bassiano, Via dei Lotti 40, Bassano del Grappa (VI) 36061, Italy

A. Celia
S.C. di Urologia, Ospedale San Bassiano, Via dei Lotti 40, Bassano del Grappa (VI) 36061, Italy

P. Martino, A.B. Galosi (eds.), *Atlas of Ultrasonography in Urology, Andrology, and Nephrology*,
DOI 10.1007/978-3-319-40782-1_11

The high spatial resolution of IOUS transducers, placed directly on the capsular surface of the kidney during surgery, aids in detecting small additional lesions, as well as in characterizing the anatomic relationship of the primary tumour to adjacent renal sinus, pelvi-calyceal system and major blood vessels, and helps determine the site of parenchymal transection and surgical resection [8, 9]. IOUS has the potential to achieve the clinical objectives of obtaining an optimal tumour-free surgical margin [10], decreasing the rate of recurrence [11] and improving survival [12]. Recent literature indicates that a 1–5-mm tumour-free surgical margin, rather than the traditionally required 1-cm margin, may be considered adequate [12–14].

IOUS may help determine more precisely the surgical margin while maximizing nephron sparing [13]. PN is particularly challenging for central tumours, which may involve renal sinus fat, blood vessels or renal pelvis, and visualizing anatomic relationships is made considerably easier with IOUS [8, 9]. It provides intraoperative guidance to the surgeon in deciding the extent of the PN, the need for resecting additional lesions or the conversion of a PN to a radical nephrectomy (RN) (Figs. 11.1 and 11.2).

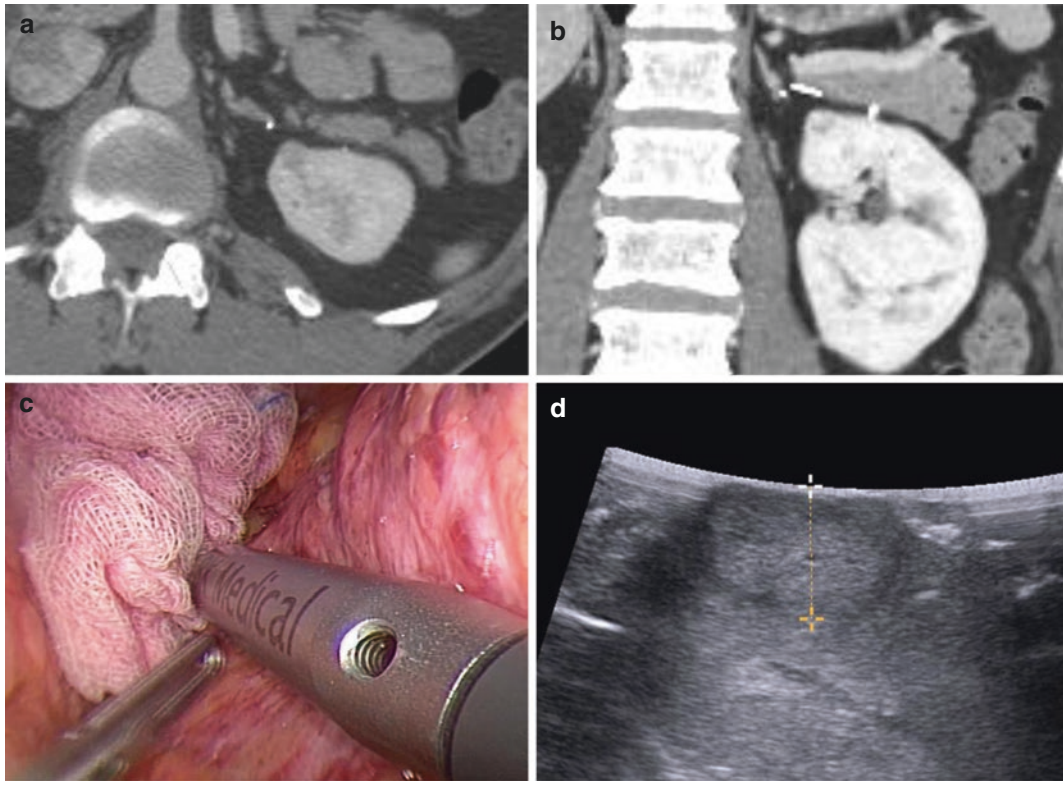

Fig. 11.1 (**a**–**d**) Male patient 50 years old with small renal cell carcinoma recurrence of clear cell that is 1 cm at the upper pole of the left kidney. Axial (**a**) and coronal (**b**) CT investigation with evidence of solid hypovascularization lesion adjacent to the metal clips of previous surgery. During the laparoscopic enucleoresection (**c**), intraoperative ultrasound (**d**) was performed for the identification of the lesion with a clear visualization of the solid oval intracortical lesion with net profiles

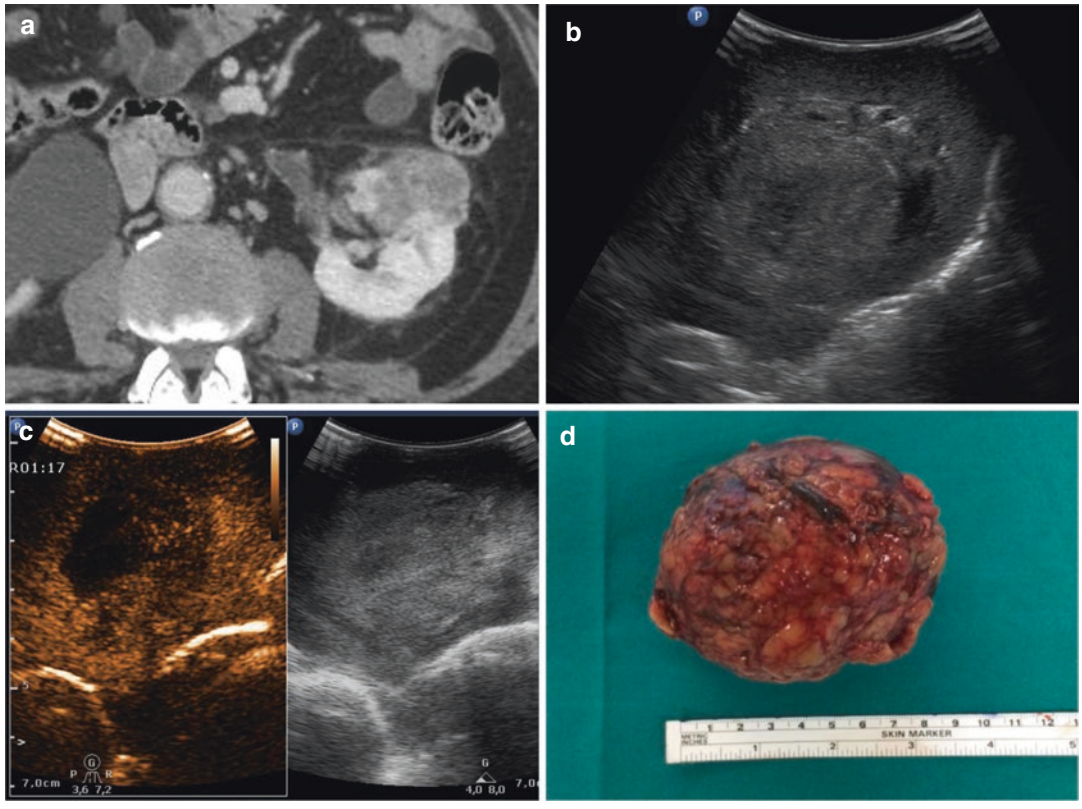

Fig. 11.2 (**a**–**d**) A 68-year-old male patient with massive primitive endophytic lesion (8 cm in diameter) at the middle third of the left kidney. Axial CT investigation (**a**) with evidence of a solid endophytic lesion with heterogeneously hypo-vascularization that comes to affect pyelic region without apparent infiltration on vascular structures. During the laparoscopic surgery, intraoperative ultrasound (**b**) was performed with subsequent administration of contrast (**c**) to better delineate the lesion from surrounding structures. Surgical specimen (**d**) with a definite diagnosis of renal clear cell carcinoma (nuclear grade 4 sec. Fuhrman)

11.2 Instrumentation and Technical Characteristics

The use of ultrasound in the clinical practice involves the use of frequencies between 1 and 30 MHz [15].

The transducer transmits ultrasonic waves and receives reflected echoes. Image resolution and penetration into the tissue depend on the frequency. If the frequency is lower, then also the resolution becomes lower, but the penetration of the waves is definitely increased.

The frequency normally used for laparoscopy with ultrasound guidance is between 7.5 and 10 MHz. A probe with a frequency of 7.5 MHz can surely provide excellent images by distances ranging from 1 to 4 cm. In this context ultrasound is able to detect tumours up to 3 mm in diameter, cysts of 2 mm and stones below 1 mm [16].

The probe may be linear, with multiple transducers positioned longitudinally or convex. The first is particularly effective for scanning organs with large flat surfaces such as the liver, while the second for tissue with curved surfaces such as the kidney. The saline irrigation is often able to eliminate the possible presence of air on the contact surface, to make the best image resolution [17].

In most surgical procedures performed in laparoscopic or robot-assisted technique, the assistant rather than the surgeon controls the laparoscopic ultrasound probe, which might limit surgeon autonomy and precision. Additionally, the laparoscopic probe might require adjustment of probe positioning with also a robotic instrument to reduce probe slippage from tumour surface [18, 19].

Recently there have been the introduction and use of ultrasound probes, which are directly related to the robotic arm and then directly controlled by the surgeon. The robotic ultrasound probe (e.g. *Hitachi Aloka*, Tokyo, Japan) has a grooved ridge on its ventral aspect that fits the robotic grasping instrument. The probe has a flexible cable that allows the passage through the assistant port and allows for full articulation of the robotic instruments. Ultrasound images were shown as a picture-on-picture image on the console screen using the *TilePro* feature of the *da Vinci Surgical System* (Intuitive Surgical, Sunnyvale, CA, USA) [18].

Finally, in different series of laparoscopic or robot-assisted partial nephrectomy (LPN or RPN) with laparoscopic ultrasonography, they have been described with more difficulties in finding the near and far tumour border, because when the laparoscopic probe is turned at a right angle, the transducer is not exactly perpendicular to the surface of the kidney. The robotic ultrasound probe can be manoeuvred independently by the surgeon, achieving difficult angles while maintaining perpendicular contact of the probe with the kidney surface [19].

11.3 Laparoscopic or Robot-Assisted Partial Nephrectomy and Intraoperative Ultrasonography

The goal of surgery in renal cancers localized to the kidney is to obtain an adequate tumour-free margin to prevent recurrence with a complete resection of the lesions, while preserving nephrons and therefore renal function [20]. The technique described by the school of Cleveland has become the most widely used for the execution of the LPN [21]. According to the American and European Urological Association guidelines [22], PN should be offered to all patients who have T1 tumours (i.e. tumours <7 cm), and it has been found to have comparable, possibly better, survival than RN [23]. Although the RENAL or PADUA nephrometry scoring system [24, 25], which is based on cross-sectional imaging, could help the surgeon's decision between PN and RN, IOUS provides more detailed real-time guidance in the operating room for selected T1 lesions. CT and MRI clearly showed the proximity of a lesion to the renal sinus fat or involvement of the renal vessels, but on the other hand, IOUS helps determine whether the distance between a main or segmental blood vessel and the tumour is greater than 3–5 mm [11, 12], thus making PN feasible. Kletscher et al. reported that 6% of patients undergoing RN had unsuspected multifocal tumours that were not seen on cross-sectional imaging and suggested that this true unknown may correspond to the recurrence rate if a PN is performed [26].

Therefore, there is a perceived need for IOUS, especially if the tumour is intraparenchymal and complex according to the nephrometry score (Figs. 11.3 and 11.4).

The intraoperative ultrasound with laparoscopic probe has revolutionized our diagnostic possibilities for small indeterminate renal masses and for tumour identification to facilitate complete tumour removal [8, 10, 27]. It is able to assist the surgeon in locating the mass to be removed remarking with precision the margin of a tumour. *Gilbert* et al. reported the use of intraoperative ultrasonography to help identify renal cell carcinoma in patients with poorly visualized and non-palpable disease [28]. IOUS does not require the removal of perirenal fat tissue, and it is particularly useful in cases where there is a particularly dense perirenal adipose tissue with predominant fibrous component potentially reducing the surgical time. Such a technique allows the targeted removal and minimizes the removal of normal parenchyma, again minimizing the loss of nephrons. It could also get a good view of the organ to have further confirmation that there are no further injuries, possibly not identified preoperative imaging. *Assimos* et al. reported using intraoperative ultrasonography for tumour identification to achieve negative surgical margins during partial nephrectomy and recommended its use to facilitate precise identification of adequate resection margins [10].

Marshall et al. reported their experience with intraoperative ultrasonography in 41 kidney surgeries and found intraoperative ultrasonography to be most beneficial for the identification of extrarenal venous extension and multifocality and the identification of associated renal cysts [27]. In a subsequent analysis of 100 cases, *Marshall* et al. reported that the use of intraoperative ultrasonography influenced the choice of surgical approach in 13% of cases [8].

Gill et al. described laparoscopic ultrasonography for laparoscopic kidney surgery [29] and the use of this technique as a routine step for deciding on the line of parenchymal incision during LPN [30].

In some cases, the use of colour Doppler is able to facilitate the surgeon in the search and isolation of the renal artery for the execution of the selective clamping, in anticipation of a resection with ischemia [31].

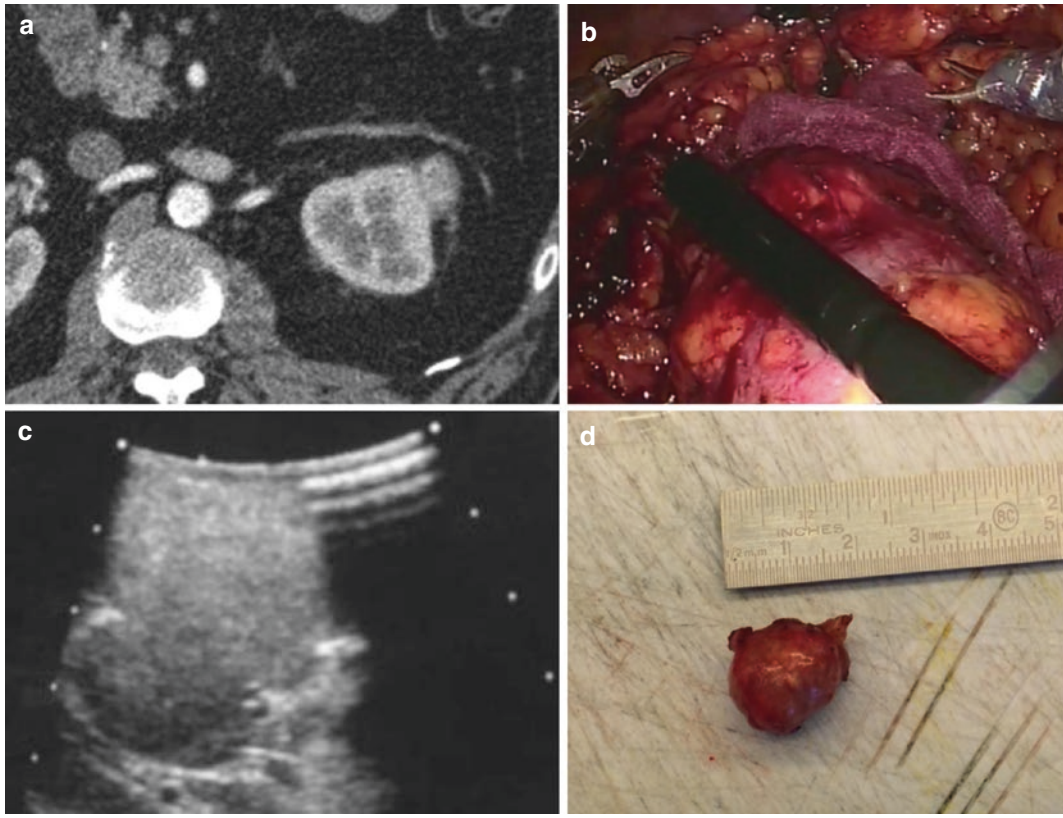

Fig. 11.3 (**a**–**d**) Female patient 45 years old with solid lesion measuring 2 cm in correspondence of the middle third of the left kidney. Survey axial CT (**a**) demonstrates heterogeneously hypervascular lesion predominantly exophytic. During robotic enucleoresection (**b**) intraoperative ultrasound (**c**) was performed for the study of the margins of resection with a clear visualization of the solid oval lesion with sharp profiles. Surgical specimen (**d**) with papillary carcinoma definitive diagnosis of type 1 kidney (nuclear grade 2 s. Fuhrman)

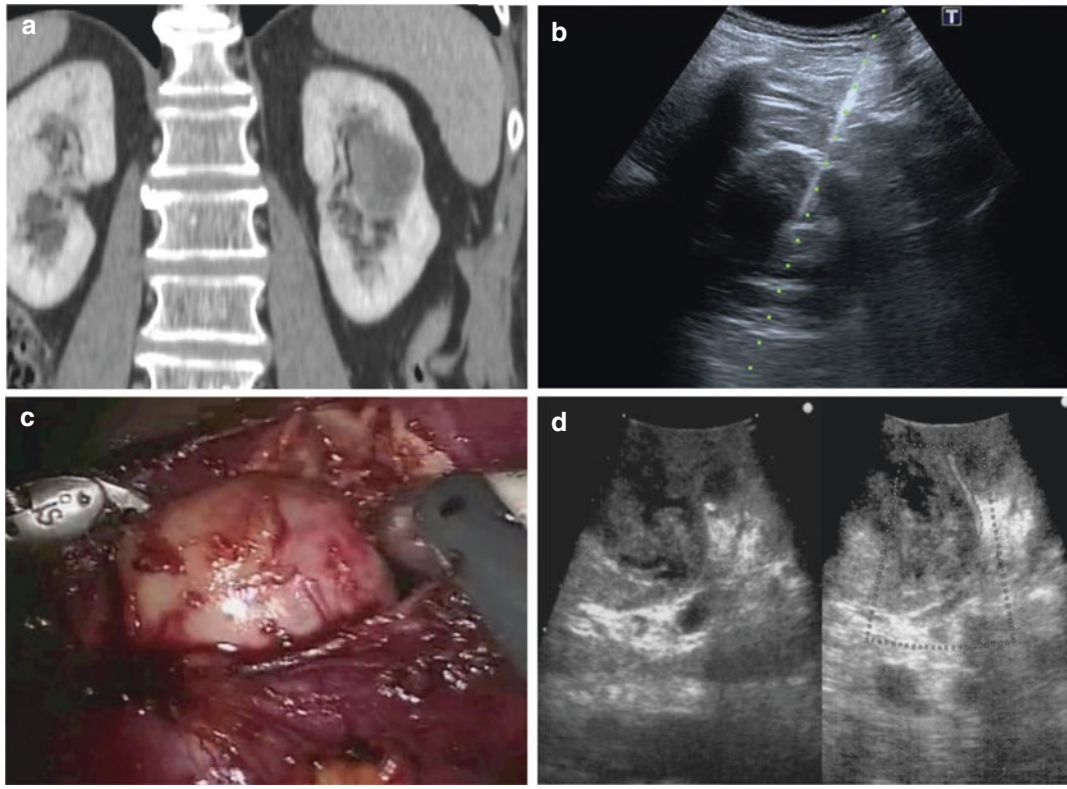

Fig. 11.4 (**a**–**d**) A 65-year-old male patient with massive endophytic lesion at the upper middle third of the left kidney. Coronal CT (**a**) shows predominantly endophytic hypodense lesion as wide avascular component that comes to affect pyelic region without apparent infiltration on the vascular structures. Intraoperative ultrasonography is performed in the diagnostic doubt between complex cyst and solid-cystic lesion, and then ultrasound-guided biopsy (**b**) is performed which confirmed the diagnosis later confirmed by histological examination on the final surgical specimen of type 2 papillary renal cell carcinoma of cystic appearance (nuclear grade G2 sec. Fuhrman). During surgery (**d**) intraoperative ultrasound (**c**) was performed both with B-mode and colour Doppler imaging for the identification of the tumour, the possible margins of resection and the relationships with the main vascular structures

11.4 Intraoperative Ultrasonography with Contrast Administration (CEUS)

CEUS is a well-established technique for imaging the kidney study [32] and plays a key role in the characterization of malignant renal lesions [33].

This new technique in recent years can also be used with the laparoscopic probes and allows both a better characterization of the lesions and a possible reduction of the operating time. The partial nephrectomy may be carried out with the clamping of the hilar vessels to allow an adequate margin of resection and reduce bleeding and to prevent ischemia of the whole kidney in conservative surgery which is an emerging concept because the time of ischemia during surgery, if prolonged, can be detrimental to the function of the kidney recovery. Several techniques have been described to perform partial ischemia which runs the selective clamping of an artery or ligation of vessels feeding the tumour [34]. A preliminary survey of five patients showed that CEUS has the potential for real-time monitoring the effectiveness of selective clamping intraoperative during a robot-assisted partial nephrectomy [35].

11.5 Other Uses of Ultrasound in Renal Surgery

The intraoperative ultrasound can be used for the surgery of renal neoplasms, associated with the presence of venous thrombus. In case not being able to detect and/or palpate the extension of the thrombus in the venous level, the use of ultrasound may be essential to identify the distal portion of the thrombus itself [36, 37] (Fig. 11.5).

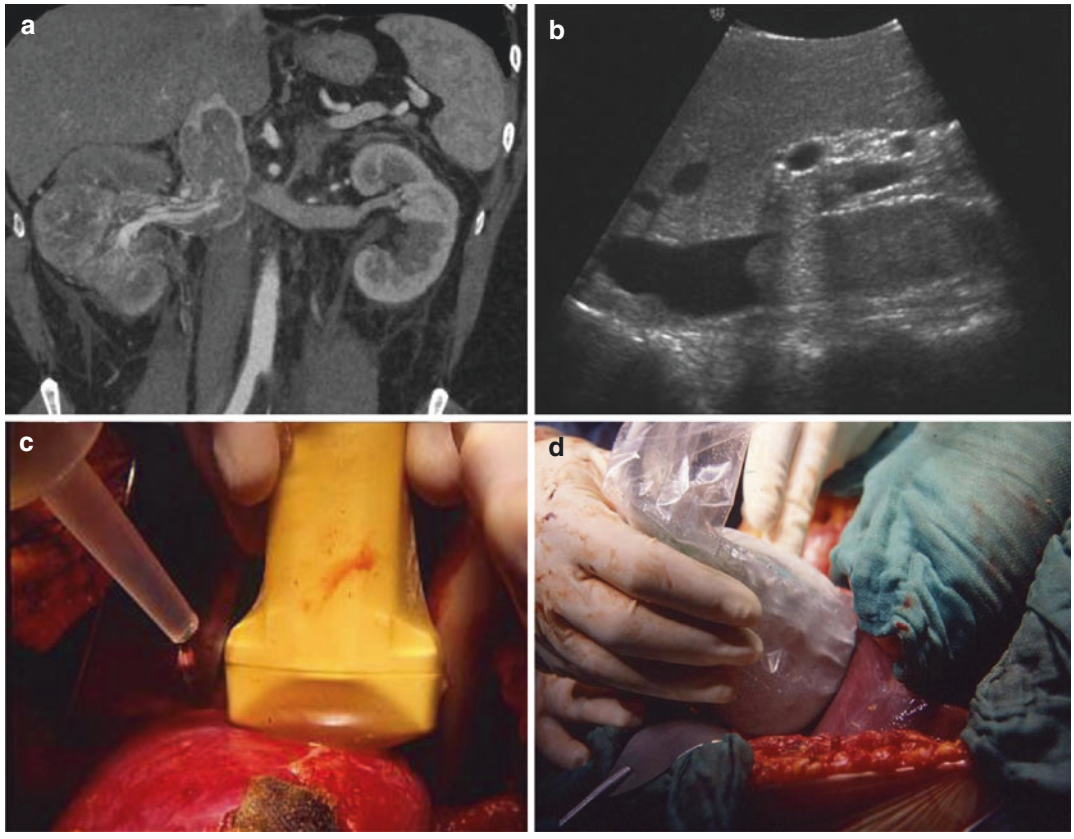

Fig. 11.5 (**a**–**d**) A 43-year-old male patient with massive lesion of the right kidney. Coronal CT (**a**) shows the massive bone lesion of the right kidney with the presence of tumour thrombus in the vena cava. Intraoperative ultrasound (**b**) is performed with B-mode study that allowed us to confirm the cranial extension of the tumour thrombus in the vena cava. Some surgery moments of intraoperative ultrasonography (**c**, **d**): the organ irrigation with saline solution at 37 °C allows to obtain a better quality of intraoperative images (**c**). The transhepatic ultrasound (**d**) allows the identification of the under-hepatic tract of the vena cava and the identification of a possible extension of the thrombus beyond the hepatic veins, which would result in a change in the surgical technique

References

1. Kim JM, Song PH, Kim HT, Park TC (2010) Comparison of partial and radical nephrectomy for pT1b renal cell carcinoma. Korean J Urol 51:596–600
2. Novick AC (2002) Nephron-sparing surgery for renal cell carcinoma. Annu Rev Med 53:393–407
3. Becker F, Siemer S, Hack M, Humke U, Ziegler M, Stockle M (2006) Excellent long-term cancer control with elective nephron-sparing surgery for selected renal cell carcinomas measuring more than 4 cm. Eur Urol 49:1058–1063; discussion, 1063–1064
4. Crispen PL, Boorjian SA, Lohse CM et al (2008) Outcomes following partial nephrectomy by tumor size. J Urol 180:1912–1917
5. Margulis V, Tamboli P, Jacobsohn KM, Swanson DA, Wood CG (2007) Oncological efficacy and safety of nephron-sparing surgery for selected patients with locally advanced renal cell carcinoma. BJU Int 100:1235–1239
6. Makuuchi M, Torzilli G, Machi J (1998) History of intraoperative ultrasound. Ultrasound Med Biol 24(9):1229–1242
7. Fazio LM, Downey D, Nguan CY et al (2006) Intraoperative laparoscopic renal ultrasonography: use in advanced laparoscopic renal surgery. Urology 68:723–727
8. Polascik TJ, Meng MV, Epstein JI, Marshall FF (1995) Intraoperative sonography for the evaluation and management of renal tumors: experience with 100 patients. J Urol 154:1676–1680
9. Kolla SB, Ercole C, Spiess PE, Pow-Sang JM, Sexton WJ (2010) Nephron-sparing surgery for pathological stage T3b renal cell carcinoma confined to the renal vein. BJU Int 106:1494–1498

10. Assimos DG, Boyce H, Woodruff RD, Harrison LH, McCullough DL, Kroovand RL (1991) Intraoperative renal ultrasonography: a useful adjunct to partial nephrectomy. J Urol 146:1218–1220
11. Sutherland SE, Resnick MI, Maclennan GT, Goldman HB (2002) Does the size of the surgical margin in partial nephrectomy for renal cell cancer really matter? J Urol 167:61–64
12. Li QL, Guan HW, Wang FP, Jiang T, Wu HC, Song XS (2008) Significance of margin in nephron sparing surgery for renal cell carcinoma of 4 cm or less. Chin Med J (Engl) 121:1662–1665
13. Lam JS, Bergman J, Breda A, Schulam PG (2008) Importance of surgical margins in the management of renal cell carcinoma. Nat Clin Pract Urol 5:308–317
14. Rozanec JJ, Ameri C, Holst P et al (2010) Nephron-sparing surgery: our experience in open and laparoscopic approach in 254 cases. Arch Esp Urol 63:62–69
15. McIntyre RC Jr, Stiegmann GV, Pearlman NW (1994) Update on laparoscopic ultrasonography. Endosc Surg Allied Technol 2(2):149–152
16. Polascik TJMF (1997) Intraoperative sonographic evaluation of the kidney. AUA Update Ser 16(18):137
17. Lirici MM, Caratozzolo M, Urbano V, Angelini L (1994) Laparoscopic ultrasonography: limits and potential of present technologies. Endosc Surg Allied Technol 2(2):127–133
18. Rogers CG, Laungani R, Bhandari A et al (2009) Maximizing console surgeon independence during robot-assisted renal surgery by using the Fourth Arm and TilePro. J Endourol 23:115–121
19. Kaczmarek BF, Sukumar S et al (2013) Robotic ultrasound probe for tumor identification in robotic partial nephrectomy: initial series and outcomes. Int J Urol 20:172–176
20. Li QL, Guan HW, Zhang QP, Zhang LZ, Wang FP, Liu YJ (2003) Optimal margin in nephron-sparing surgery for renal cell carcinoma 4 cm or less. Eur Urol 44:448–451
21. Haber GP (2006) Gill IS "Laparoscopic partial nephrectomy contemporary technique and outcomes". Eur Urol 49(4):660–665
22. Campbell SC, Novick AC, Belldegrun A et al (2009) Guideline for management of the clinical T1 renal mass. J Urol 182:1271–1279
23. Leibovich BC, Blute ML, Cheville JC, Lohse CM, Weaver AL, Zincke H (2004) Nephron sparing surgery for appropriately selected renal cell carcinoma between 4 and 7 cm results in outcome similar to radical nephrectomy. J Urol 171:1066–1070
24. Kutikov A, Uzzo RG (2009) The R.E.N.A.L. nephrometry score: a comprehensive standardized system for quantitating renal tumor size, location and depth. J Urol 182(3):844–853
25. Ficarra V, Novara G, Secco S, Macchi V, Porzionato A, De Caro R, Artibani W (2009) Preoperative aspects and dimensions used for an anatomical (PADUA) classification of renal tumours in patients who are candidates for nephron-sparing surgery. Eur Urol 56(5):786–793
26. Kletscher BA, Qian J, Bostwick DG, Andrews PE, Zincke H (1995) Prospective analysis of multifocality in renal cell carcinoma: influence of histological pattern, grade, number, size, volume and deoxyribonucleic acid ploidy. J Urol 153:904–906
27. Marshall FF, Holdford SS, Hamper UM (1992) Intraoperative sonography of renal tumors. J Urol 148:1393–1396
28. Gilbert BR, Russo P, Zirinsky K, Kazam E, Fair WR, Vaughan ED Jr (1988) Intraoperative sonography: application in renal cell carcinoma. J Urol 139:582–584
29. Matin SF, Gill IS (2001) Laparoscopic ultrasonography. J Endourol 15:87–92
30. Gill IS, Desai MM, Kaouk JH et al (2002) Laparoscopic partial nephrectomy for renal tumor: duplicating open surgical techniques. J Urol 167:469–470; discussion 75–76
31. Hyams ES, Perlmutter M, Stifelman MD (2011) A prospective evaluation of the utility of laparoscopic Doppler technology during minimally invasive partial nephrectomy. Urology 77(3):617–620
32. Piscaglia F, Nolsøe C, Dietrich CF et al (2012) The EFSUMB Guidelines and Recommendations on the Clinical Practice of Contrast Enhanced Ultrasound (CEUS): update 2011 on non-hepatic applications. Ultraschall Med 33(1):33–59
33. Bertolotto M, Derchi LE, Cicero C, Iannelli M (2013) Renal masses as characterized by ultrasound contrast. Ultrasound Clin 8(4):581–592
34. Gill IS, Eisenberg MS, Aron M et al (2011) "Zero ischemia" partial nephrectomy: novel laparoscopic and robotic technique. Eur Urol 59:128–134
35. Rao AR, Gray R, Mayer E et al (2013) Occlusion angiography using intraoperative contrast-enhanced ultrasound scan (CEUS): a novel technique demonstrating segmental renal blood supply to assist zero-ischaemia robot-assisted partial nephrectomy. Eur Urol 63(5):913–919
36. Hsu TH, Jeffrey RB Jr, Chon C, Presti JC Jr (2003) Laparoscopic radical nephrectomy incorporating intraoperative ultrasonography for renal cell carcinoma with renal vein tumor thrombus. Urology 61(6):1246–1248
37. Hoang AN, Vaporcyian AA, Matin SF (2010) Laparoscopy-assisted radical nephrectomy with inferior vena caval thrombectomy for level II to III tumor thrombus: a single-institution experience and review of the literature. J Endourol 24(6):1005–1012

Interventional Ultrasound: Renal Biopsy

12

Carlo Manno, Anna Maria Di Palma, Elisabetta Manno, Michele Rossini, and Loreto Gesualdo

12.1 Essential History of Renal Biopsy

In the first half of the twentieth century (about 65 years ago), 90 % of nephropathies were unknown to nephrologists and pathologists, and they would have remained so without the use of the renal biopsy. Indeed, the history of the renal biopsy is tightly bound to the birth and development of nephrology, a relatively recent specialty to which it has provided an undeniable impulse. The first article that had by subject the practice of a percutaneous renal biopsy was written in 1950 by a Cuban doctor, Antonino Pérez-Ara, who worked at the military hospital in Havana, and published in a local journal with little diffusion [1]. Only in 1951 the potential importance of renal pathology was underlined by two Danish investigators in a study where the renal biopsy had allowed determination of the cause of the acute renal failure in the majority of patients dialyzed [2]. In this study, the patient was placed in sitting position, and intravenous pyelography was made to visualize the lower right pole to avoid large vessels and the spleen. The needle used was comparable to that used for liver biopsies and was connected to a syringe that was taking off a core piece of the kidney by vacuum section approximately 10–20 mm in length. Unfortunately, the success of their technique was limited, with adequate tissue obtained in only 53 % of biopsies. In 1954, Kark and Muehrcke in Chicago modified the procedure by positioning the patient in the prone position with a pillow placed under the abdomen to lift up the right kidney. They used the Franklin-modified Vim-Silverman needle, a precursor of the needle currently used today, which trapped the tissue in the needle and then sheared it off in "blind approach" to procure renal tissue, reporting a success rate of 96 % and no major complications [3]. Furthermore, a magnifying glass was used to observe glomeruli and to increase the efficiency of the technique (in 96 % of procedures, a renal cortex useful for diagnosis was obtained). This technique would remain prevalent for more than 40 years.

From 1961 to 1975, the study of specimen by using the technique of immunofluorescence and of electron microscopy ameliorated the diagnostic accuracy and the prognostic value of light microscopy and disseminated widely the renal biopsy in clinical practice. Furthermore, the use

Electronic supplementary material The online version of this chapter (doi:10.1007/978-3-319-40782-1_12) contains supplementary material, which is available to authorized users.

C. Manno • A.M. Di Palma • E. Manno • M. Rossini
L. Gesualdo (✉)
Nephrology, Dialysis and Transplantation Unit, Department of Emergency and Organ Transplantation, University of Bari, Bari, Italy
e-mail: loreto.gesualdo@uniba.it

P. Martino, A.B. Galosi (eds.), *Atlas of Ultrasonography in Urology, Andrology, and Nephrology*,
DOI 10.1007/978-3-319-40782-1_12

of various imaging modalities, such as intravenous pyelography, fluoroscopy, renal scintigraphy, and ultrasound, was also used to localize the kidneys. Of these, ultrasound was found the best to localize the lower pole with the lowest-risk approach and highest yield for glomeruli and was also not affected by renal failure. Despite the lack of well-designed clinical trials with supporting evidence, these techniques have proliferated and become the de facto standard for kidney biopsies in the worldwide.

The values of renal biopsy are represented by the fact that it condition sine 9ua non is for a correct diagnosis of acute and chronic renal diseases. The histological diagnosis alters clinical diagnosis in 25–50 % of cases, guides treatment by determining reversibility and activity of lesion, and may change the therapy in 30–40 % of patient. Furthermore, the renal biopsy predicts prognosis by assessing specific pathologic features and extent of changes and validates outcome when used as endpoint in clinical trials. Finally, it reveals pathogenesis by studying the molecular and cellular mechanisms of renal diseases and opens new horizons and novel therapies.

12.2 Indications and Contraindications for Renal Biopsy

The most important indications for renal biopsy in clinical practice are numerous. The presence of elevated serum creatinine with decreased glomerular filtration rate may indicate the need to perform renal biopsy, especially in undiagnosed acute kidney injury or in acute tubular necrosis not resolving after 3–4 weeks, while in advanced chronic kidney disease and ultrasound imaging of reduced kidney volume, the renal biopsy is generally contraindicated. The presence of hematuria, asymptomatic or symptomatic (gross hematuria), isolated, or associated with subnephrotic proteinuria, is an indication to perform a renal biopsy, especially when the hematuria is combined with acute renal failure (nephritic syndrome). The nephrotic syndrome, proteinuria >3.5 g/d, hypoalbuminemia, edema, and hyperlipidemia, is a mandatory indication to biopsy in adults and in children with atypical features. Finally, the renal biopsy should be performed in systemic diseases with renal dysfunction.

The absolute contraindication to perform a renal biopsy is generally represented by uncontrolled bleeding diathesis, uncontrolled severe arterial hypertension, solitary kidney, multiple renal cysts, renal mass or renal neoplasm, acute pyelonephritis and perinephric abscess, end-stage or near end-stage kidney disease with small kidneys, patients unable to cooperate, obese patients, or patients with respiratory difficulties. However, in 1998, the American College of Physicians in a paper position on the Clinical Privileges Subcommittee on nephrology and clinical competence in percutaneous renal biopsy stated that the list of contraindication would be modified by clinical judgment in the single patient and by future advance in clinical practice. A consensus approach to the management of high-risk patients needs to know medical and technic approaches and the difference between absolute and relative contraindications.

12.3 Preparation of the Patient

Although kidney biopsy may provide important diagnostic information and guide therapeutic decisions, the important benefits must be weighed against the potential harms of biopsy. The clinicians should not neglect the risks of bleeding complications, and therefore a rigorous procedure to describe clinical processes in a quality assurance system may increase the ratio benefit/harm. The benefits are determined by meticulous preparation of the patient, adequacy of study techniques of renal specimen, consensus approach on clinical indications, and technical aspects of biopsy procedure. The reduction of harms may be obtained by the

performance of procedure by an expert nephrologist in renal biopsy and ultrasound guidance, informed consent, and clinical, laboratory, and instrumental monitoring post procedure. A first question in clinical practice is the choice to perform the renal biopsy on inpatient or outpatient. A mounting pressure by managed care to not only switch to outpatient management but to decrease period of observation to 6–8 h may reduce the safety of procedure. However, a study on the timing of bleeding complications showed that the complications were identified in 89 % of patients at 24 h. Therefore, after biopsy, an observation up to 24 h remains optimal, but since 11 % of major complications occur after 24 h, some patients may require a longer period of stay in hospital [4].

The prerequisites of procedure are focusing on relevant history and examination of the patient; ultrasound bilateral kidney evaluation of form, size, and cortical thickness; and coagulation parameters such as hemoglobin, platelets, prothrombin time and partial thromboplastin time and bleeding time, blood group, and sometimes dosage of von Willebrand factor and lupus anticoagulant. The available literature has not established that a specific test can select patients with a major risk of post-biopsy bleeding and the impact of bleeding time on the complication rate is controversial [5]. In the future, evaluating some measure of platelet function, such as with a platelet function analyzer (PFA-100), may have a role in predicting risk [6].

The alterations of coagulation parameters should be corrected prior to the renal biopsy by means of erythrocyte transfusion if anemia is present or infusion of coagulation factors (e.g., factor VIII if the levels are reduced) or if bleeding time is prolonged by administration of desmopressin acetate (DDAVP) 0.4 μg/kg/intravenous or 0.3 μg/kg/subcutaneous. The antiplatelet or anticoagulant drugs should be withdrawn; ticlopidine, aspirin, and clopidogrel should be withdrawn from 5 to 10 days before the biopsy; it may be necessary to substitute these drugs by a short-acting drug such as indobufen which should be withdrawn 2 days before the biopsy. The warfarin and dicoumarol drugs should be withdrawn 5 days before the biopsy, while 1–2 days are enough for novel oral anticoagulant drugs such as apixaban, rivaroxaban, and dabigatran; during the withdrawal period, sodic heparin or low molecular weight heparins should be administrated and withdrawn 12 h before the renal biopsy. However, in cases which present an elevated thrombotic risk, for example, patients on therapy by two drugs (aspirin plus clopidogrel) for recent (<6–12 months) angioplasty and coronary stents, clopidogrel should be withdrawn 5 days before the biopsy maintaining the administration of aspirin; 3 days before the biopsy, tirofiban, an antiplatelet characterized by short plasmatic half-life, should be introduced to be withdrawn 8 h before the biopsy. This procedure presents an intermediate hemorrhagic risk but an elevated thrombotic risk, and thus the patient should be monitored for 24 h after the renal biopsy in intensive cardiologic unit. The informed consent specific for cardiologic risk should be obtained [7].

As regards this crucial point within the risk management, an explicit informed consent, personally signed by a conscious patient and specific for the procedure of renal biopsy, should be obtained. The informed consent occurs in various steps; first, the physician that prescribed renal biopsy should inform the patient about its health status and advantages which derive from a certain diagnosis and specific treatments. In the second step, the physician that performs the renal biopsy should describe the phases of procedure and the possible complications and the procedures to prevent and treat each complication. Finally, the patient should confirm the consent or the refusal to procedure; for underage patient or the patient unable to understand, the physician should follow the law of its country.

12.4 Procedure

The technique has significantly improved over the past two decades because of the introduction of ultrasonography and automated-gun biopsy devices. Ultrasound assistance enables skin surface marking of the lower pole, and real-time ultrasound guidance allows visualization of the biopsy needle and its path during the procedure. Retrospective and uncontrolled studies have shown that real-time ultrasound-guided percutaneous renal biopsy performs better than freehand renal biopsy. Likewise, automated-gun biopsy devices are easy to use and less risky than conventional manual puncture methods (Figs. 12.1 and 12.2).

In the classic procedure of percutaneous renal biopsy, the patient is in prone position with a pillow below the abdomen (Video 12.1). After a light sedation, local anesthesia with 2 % lidocaine was made from the subcutaneous stratus down to the capsule. Sometimes a skin incision can be performed to facilitate the entry of the needle. Subsequently, the gun is advanced to reach the capsule, the patient should stop the deep breath, and finally the gun is fired to the lower pole of the left kidney (or sometimes the right kidney) (Fig. 12.3). Generally, two or three cores should be taken and evaluated by dissecting microscope to check the presence of the cortical tissue and an adequate sampling of glomeruli (Fig. 12.4). Finally, a compression on the wound for 5–10 min should be made, and an ultrasonography after 60 min can reveal an early complication [8]. In the post-procedure period, the patient is recommended to bed rest in supine position for at least 24 h, and blood pressure and arterial pulse are monitored; if necessary, hemoglobin and hematocrit are monitored every 4–6 h. The voided urine sample should be examined for macroscopic hematuria.

The experience gained over the last decades has shown this technique to be safe and effective in most but not all patients. For example, the obese patients, whose proportion is rapidly growing in developed countries, are at highest risk for bleeding complications and technical failures caused by poorer ultrasound visualization of the kidney as well as severe respiratory difficulties. To overcome these drawbacks, a number of technical refinements have been proposed over the years, including computerized tomography guidance, laparoscopic renal biopsy, and transjugular biopsy.

The possibility to maintain an easy procedure such as percutaneous ultrasound-guided renal biopsy also to patients obese or with respiratory problems has been reached by the supine anterolateral position (SALP) [9]. The SALP is obtained by placing towels under the ipsilateral shoulder and gluteus to elevate the flank by an angle of 30° (Video 12.2). The ipsilateral arm is placed over the thorax, while the contralateral is abducted and used for intravenous perfusion. The ipsilateral leg is slightly flexed over a pillow, whereas the contralateral is flexed and abducted so that its lateral aspect is lying on the table. This position provides full exposure of Petit's triangle (latissimus dorsi muscle – 12th rib – iliac bone), thus providing enough space to perform ultrasound scanning and to easily orientate the ultrasound-guided puncture toward the inferior renal pole. In this position, the posterior face of the kidney is expected to be almost parallel to the operating table, while the ipsilateral colon is expected to fall anteromedially, sufficiently far from the puncture paths. After shaving and draping the flank, the kidney is ultrasound scanned to determine the ideal puncture path. The identification of the lower kidney pole by ultrasound scanning is easy, and the quality of image resolution is similar to the prone position. The entire path is then anesthetized with 10 ml of 2 % lidocaine solution. An automatic needle is ultrasound guided to the capsule in the lower pole of the kidney and fired into the renal parenchyma.

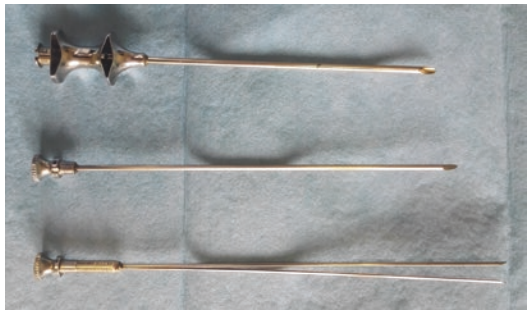

Fig. 12.1 Manual-gun biopsy device; the three parts of the Franklin-modified Vim-Silverman needle: the outer sheath, the obturator, and the cutting prongs

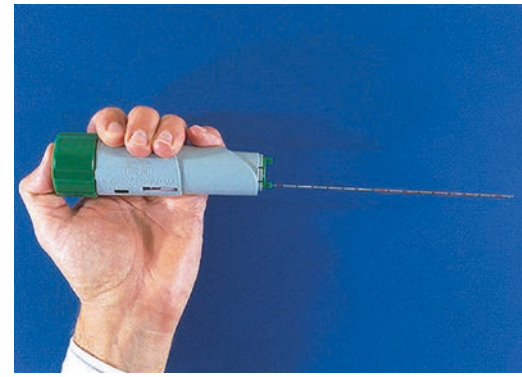

Fig. 12.2 Automated-gun biopsy device

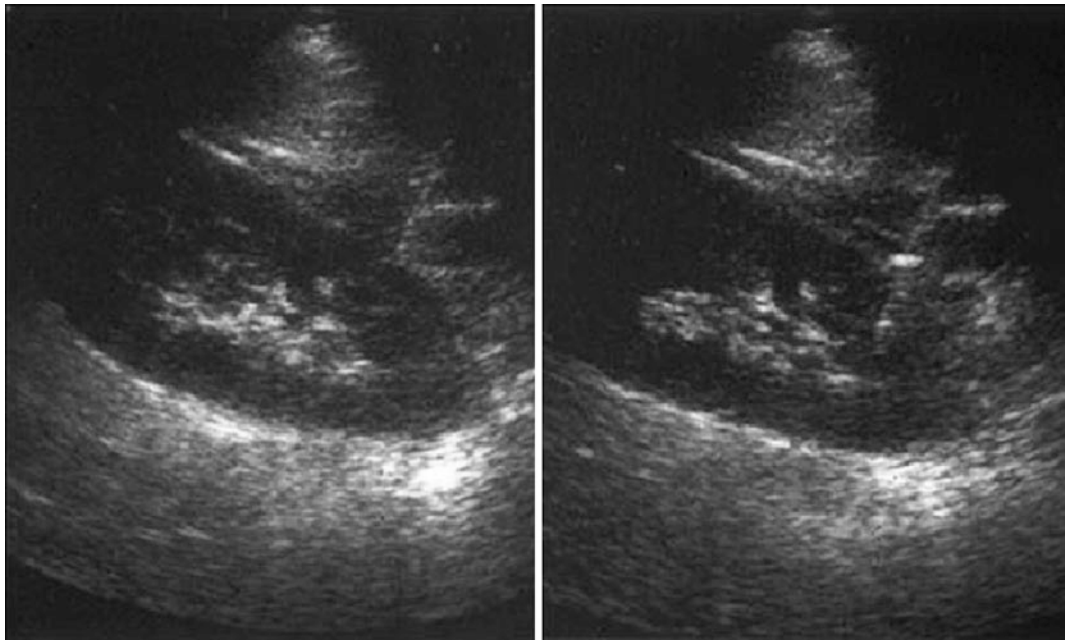

Fig. 12.3 The gun is advanced to the capsule and fired to the lower pole of the left kidney

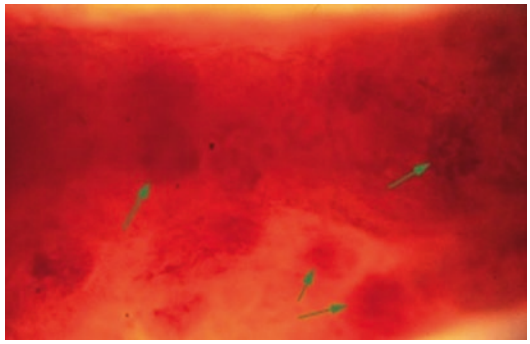

Fig. 12.4 Evaluation by dissecting microscope

12.5 Complications

Few systematic data exist to estimate the complication rate of kidney biopsy. The current standard procedure for kidney biopsy involves the use of real-time ultrasound guidance and an automated spring-loaded biopsy device that may be associated with lower rates of procedural complications [10]. The bleeding complications include silent hematomas detected only by post-biopsy imaging (Fig. 12.5), macroscopic hematuria (Fig. 12.6), large hematomas and blood loss requiring erythrocyte transfusion (Fig. 12.7), arteriovenous fistula (Fig. 12.8), and, rarely, the need for emergent angiographic intervention (Fig. 12.9) or nephrectomy. The incidence of the complications associated with kidney biopsy and possible predictors fluctuates across studies, due to different definitions and patient selection, procedural technique, and monitoring protocol. A rare complication is the page kidney, caused by the accumulation of blood in the perinephric or subcapsular space resulting in extrinsic compression of the involved kidney, renal ischemia, activation of the renin-angiotensin-aldosterone system, and systemic hypertension [11].

In a recent systematic review and meta-analysis, the authors aimed to evaluate the incidence of hemorrhagic complication in terms of rates of macroscopic hematuria and the need for erythrocyte transfusion after native kidney biopsy performed with real-time ultrasound guidance and automated spring-loaded biopsy device and to identify potential risk factors [12]. The rate of macroscopic hematuria was 3.5 % and erythrocyte transfusion was 0.9 %. Significantly higher rates of transfusion were seen with the following covariates: 14-gauge compared with smaller needles (2.1 % vs 0.5 %), serum creatinine level greater than 2.0 mg/dl, female gender, acute kidney injury, mean age of 40 years or older, and mean systolic blood pressure greater than 130 mmHg. Although macroscopic hematuria and the need for erythrocyte transfusion are important complications of kidney biopsy because they may necessitate hospital admission and therefore increased health-care expenditure and patient morbidity, the most frequent bleeding complication of kidney biopsy, i.e., the perinephric hematoma, was not considered among principal outcomes of this study, since the presence of hematoma was reported inconsistently in source studies, with rates varying by whether ultrasonography was performed routinely or for symptoms. The rate of this complication increases remarkably when screened using computed tomography. Even though the majority of these hematomas are clinically asymptomatic, the presence of perinephric hematoma increases the discomfort for the patient and the costs due to further laboratory and instrumental examinations with longer hospitalization. In a minority of cases, the hematoma is a clinically relevant complication, which needs an even longer stay at the hospital for diagnostic and therapeutic procedures (artery embolization).

In conclusion the risk of hemorrhagic complications is relatively low with real-time ultrasound guidance and automated biopsy needles. However, to improve patient safety, the use of large-gauge needles (14 gauge) should be discouraged. Since the prognostic value of potential risk factors is debatable, further studies are necessary to find more sensitive tests to assess coagulation disorders and to better identify patient and procedural characteristics required to improve biopsy technique and patient selection in an effort to improve the safety profile of kidney biopsy. Finally, the use of DDAVP should be considered among modifiable procedure, since the only randomized controlled trial included in this review demonstrates the risk reduction of bleeding complication in treated group compared to controls [13]. A caution in the use of this drug should be considered in patients at thromboembolic risk.

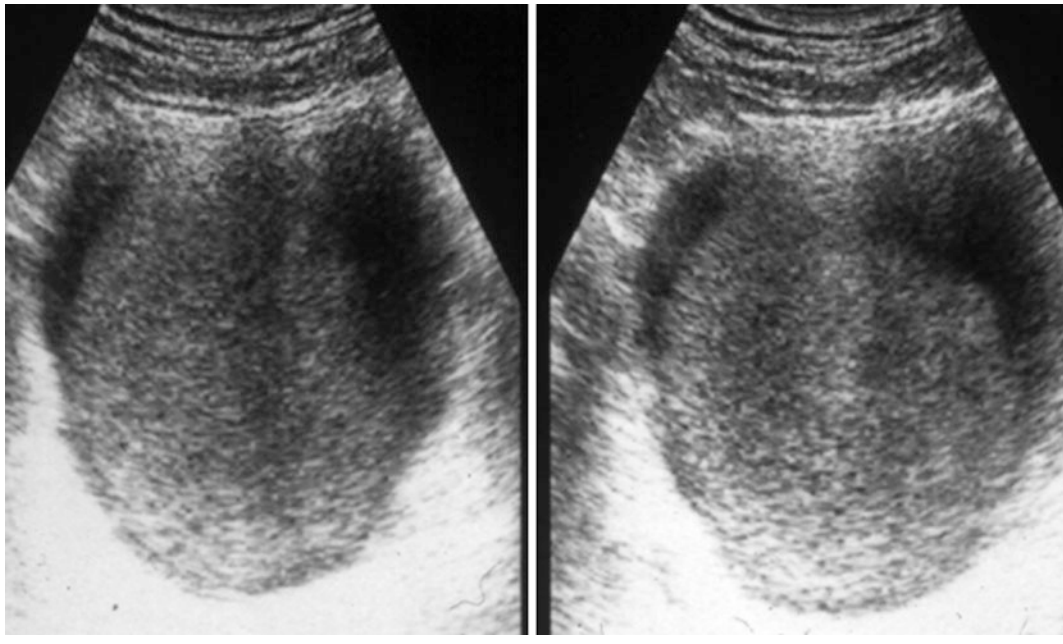

Fig. 12.5 Macroscopic hematuria and vesical coagulum

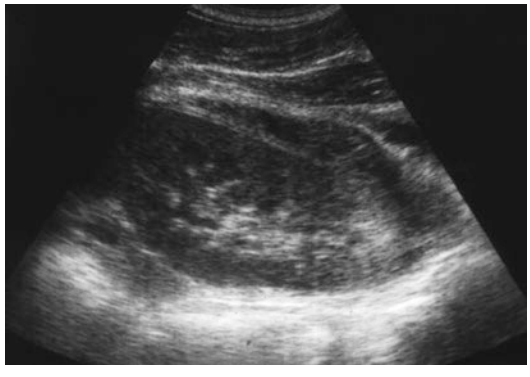

Fig. 12.6 Silent perinephric hematoma

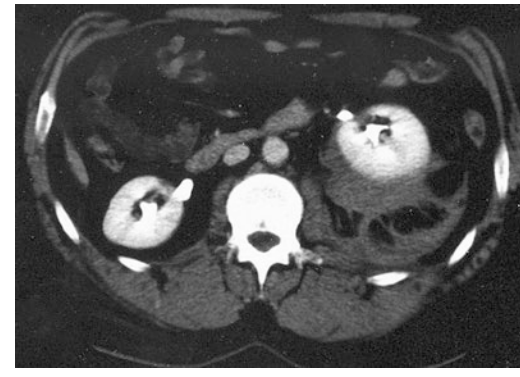

Fig. 12.7 Large hematoma requiring erythrocyte transfusion and artery embolization

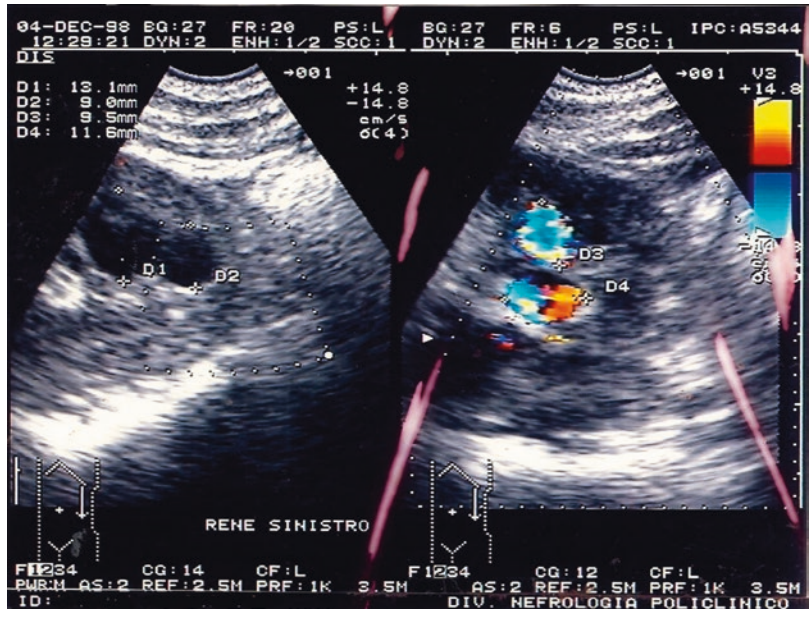

Fig. 12.8 Arteriovenous fistula by ultrasound imaging

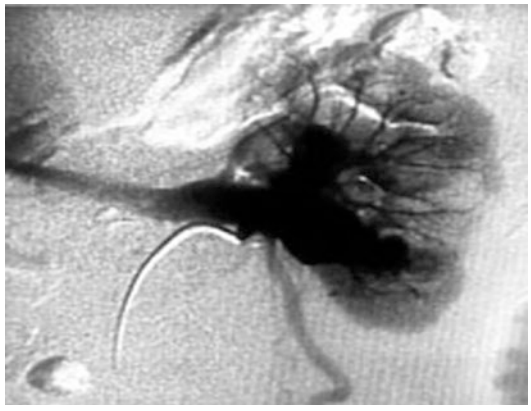

Fig. 12.9 Arteriovenous fistula by angiographic imaging

12.6 Specimen Processing

Since the 1960s, renal pathologists, besides light microscopy, introduced and utilized new techniques such as electron microscopy and immunohistochemistry-immunofluorescence microscopy. After a core of tissue is obtained, it should be analyzed under a dissecting microscope to check adequacy (kidney tissue is easily recognized and distinguished from the fat, muscle, other tissues, kidney cortex from the medulla) and to help in sectioning the tissue to allocate for the different techniques. How much renal tissue is necessary for pathologic diagnosis is a complex question, but it depends on the indication for biopsy. At least two biopsy cylinders with a minimal length of 10 mm and a diameter of at least 1.2 mm characterize the adequacy of the sample. Also we need 10–15 glomeruli for optimal sampling (e.g., in systemic lupus erythematosus), but very often 6–10 glomeruli are sufficient to make diagnosis. For diseases in which lesions are focally distributed in glomeruli (such as focal segmental glomerulosclerosis), more glomeruli are needed to rule out a "missed diagnosis" [14]. In other diseases, such as amyloidosis or membranous glomerulonephritis, even a single glomerulus may be sufficient for diagnosis.

For light microscopy morphology, formalin-fixed paraffin-embedded tissue is cut into 2–3 μm histologic sections that are routinely stained with hematoxylin and eosin, methenamine silver-periodic acid (Jones stain), Masson trichrome, and periodic acid-Schiff (PAS). Additional stainings are used under certain circumstances (i.e., Congo red staining for amyloid, von Kossa to point out calcifications, elastic vezheeth Van-Gieson for normal or pathologic elastic fibers).

The immunofluorescence is performed on unfixed, frozen section prepared from fresh tissues (on saline-soaked gauze) or in Michel's fixative and immediately frozen in laboratory. The sample is then cut with a cryostat and sections with a thickness of 2–4 μm are obtained. The antigens that should be routinely stained include immunoglobulins (primarily IgG, IgM, and IgA), complement components (especially C3, C4, and C1q), fibrin, λ and k light chains, collagen IV α chains (Alport's disease), IgG subclasses, viral antigens, and lymphocyte subclasses. In allograft biopsies it is necessary to stain for C4d to detect antibody-mediated rejection and sometimes phenotype lymphocytic infiltrates when a posttransplant lymphoproliferative disorder is suspected. The method should report if the reaction is positive or not, describe the pattern of staining (mesangial or capillary), differentiate a linear or granular staining, and, finally, describe the position of the deposits (i.e., subendothelial, intramembranous, or subepithelial).

The electron microscopy is performed on sample fixed into a mixture of 2–3 % glutaraldehyde or 1–4 % paraformaldehyde, then cleared with a transitional fluid (1,2-epoxypropane), and, finally, embedded in epon. A thick section of 1 μm stained with toluidine blue is used as an initial guide. The sample is then cut in ultrathin sections of 50–70 nm stained with uranyl acetate, lead citrate, and gold. The method allows to assess the presence and degree of cell proliferation (mesangial or endothelial proliferation) and to evaluate the changes of glomerular basement membrane (such as thickening, thinning, splicing, or irregularities) or cell structure (i.e., podocyte foot process effacement or podocyte vacuolization) and the necrosis or apoptosis of cells. Furthermore, the electron microscopy shows also the localization of immune complex deposits and may demonstrate specific ultrastructural organization of the deposits that may be diagnostic of specific disease (amyloid, fibrillary glomerulonephritis, immunotactoid, cryoglobulin).

12.7 Elementary Lesions

The renal biopsy can show different lesions in the three parts of the kidney: glomerulus, tubulointerstitium, and vessels.

The glomerular lesions are thickening of glomerular basement membrane, proliferation (mesangial, endo-/extra-capillary), sclerosis, and crescents. Glomerular basement membrane thickened is seen in membranous glomerulonephritis, in diabetic nephropathy, and in the latest Alport's syndrome. Other nephropathies in which it is possible

to find thickened glomerular basement membrane are chronic thrombotic microangiopathy, membranoproliferative glomerulonephritis, and fibrillary glomerulonephritis. The mesangial proliferation, including matrix and/or cell proliferation, can be organized in nodules (diabetic nephropathy, amyloidosis, light-chain deposition disease) or not (IgA nephropathy, lupus nephritis class II, and post-infectious glomerulonephritis). Endocapillary proliferation, an active and severe lesion, can be found in proliferative lupus nephritis and membranoproliferative and cryoglobulinemic glomerulonephritis. Crescents are the expression of a proliferation of the parietal epithelium of Bowman's capsule in response to pro-inflammatory stimuli and growth factors released into Bowman's space by inflammatory cells from the circulation following a lesion of the capillary walls. Fibrinoid necrosis is a histological lesion characterized by the presence of fibrin at the level of the glomerular capillaries (often associated with breaks in the basement membrane) and in the arterial vessels, associated with karyorrhexis; it is the expression of an inflammatory process, particularly active, as found in the course of vasculitis, lupus nephritis, etc.

The tubular active lesions are represented by those that are found commonly in the course of acute tubular necrosis: loss of brush border, detachment of epithelial cells from the tubular basement membrane with stripping of the membrane, and pseudo-dilatation of the tubules. Also there may be inflammatory cells that infiltrate the tubular epithelium (tubulitis) and the interstitium during acute interstitial nephritis. It is also important to recognize certain cell types within the infiltrate, because the presence of eosinophils suggests an immune-allergic pathogenesis (drug). In infectious form, such as pyelonephritis, there are neutrophils in clusters in the tubular lumen and within the infiltrate. Tubulitis and interstitial infiltrate in the transplant kidney are the basis of the diagnosis of acute T-cell-mediated rejection.

In vessels the most frequent active lesion is fibrinoid necrosis of the wall, similar to those described in the glomerulus, and it is pathognomonic of vasculitides. When this lesion is present in a kidney graft, it is diagnostic of acute vascular rejection. Inflammation of vessels can be wider, and it is called "transmural artearitis," which often is associated with fibrinoid necrosis. Another important vascular lesion is the lumen's obliteration of glomerular capillary or small arterioles by thrombi (thrombotic microangiopathy) or emboli (i.e., cholesterol emboli).

Chronic lesions of the parenchyma are glomerulosclerosis (segmental or global), tubular atrophy, interstitial fibrosis, medium-intimal fibrosis of arteries, and hyalinosis. The grade of chronic damage can be assessed by considering the number of sclerotic glomeruli of total glomeruli examined and percentage of tubular atrophy and interstitial fibrosis.

12.8 Kidney Biopsy Report

Kidney biopsy reporting put together crucial clinical data and features examined on light, immunofluorescence, and electron microscopy to come up with a diagnosis. In each report, a brief summary of clinical data should be noticed, and few words on gross material description should be spent. In light microscopy, each compartment of renal parenchyma should be analyzed and detailed (glomeruli, tubulointerstitium, vessels) in every feature. Elements such as number of total glomeruli sampled, percent of totally or segmentaley sclerosed glomeruli, number of crescents, the presence of fibrinoid necrosis and endocapillary proliferation, active (interstitial infiltrates, edema, tubulitis) or chronic (interstitial fibrosis, tubular atrophy) tubulointerstitial changes, and their semiquantitative scoring are important data regardless of the final diagnosis. For immunofluorescence, again, total number of glomeruli and number of totally sclerosed glomeruli should be noticed. Then for each antibody intensity of staining (semiquantitative on a 0–3+ or 0–4+ scale), location and pattern should be expressed. For electron microscopy, the ultrastructural appearance of glomeruli should include podocyte foot process analysis (effacement, microvillous transformation, actin cytoskeleton condensation, etc.), the presence and exact location of electron-dense deposits, thickness and abnormalities of basal membrane (i.e., double contour, splitting of lamina densa, "basket weav-

ing" lesions, etc.), and additional pathologic findings (i.e., deposits with substructures, fibrillary deposits, tubule-reticular inclusions, etc.). Tubulointerstitial areas should also be examined along with peritubular capillary and pathologic findings stated (particularly in a transplanted kidney). Finally and of particular importance, the comment in which clinicopathological correlation is made in that particular clinical setting, eventual limitation of the biopsy results may be pointed out, and further studies may be suggested [15].

Conclusion

Although renal biopsy is the gold standard for the diagnosis and evaluation for treatment of glomerular diseases, it is invasive and rarely may have several serious complications. The presentation, clinical course, and outcome of glomerular diseases are highly variable, and in many cases, histopathology is neither diagnostic nor prognostic and fails to predict response to therapy, because heterogeneous pathogenic mechanisms are involved. For these reasons, clinical biomarkers of specific pathogenic processes may improve subclassification and facilitate therapeutic choices. Fortunately, a number of new promising diagnostic tests are being evaluated in patients with a variety of primary glomerulopathies including minimal change nephropathy, focal segmental glomerulosclerosis, membranous nephropathy, and IgA nephropathy [16].

It is expected that the measurement of serum and/or urinary biomarkers will improve our diagnostic and therapeutic strategy in patients with glomerulonephritis in general and nephrotic syndrome in particular. However, there are some caveats, since promising results so far are based on small, mostly retrospective studies. The accuracy of the test to identify primary glomerulonephritis and to exclude secondary causes awaits well-designed prospective studies. In our opinion it is too early to discard a renal biopsy in patients with suspicion of glomerulonephritis, especially if nephrotic syndrome is present in adults.

The main finding of the literature is that a percutaneous renal biopsy should be regarded as a safe procedure and successful procedure both in adults and children, and the overall rate of major complications is very low if general contraindications are respected [17]. To minimize biopsy risk, meticulous control of clinical routines is mandatory, especially in patients with reduced renal function. A wake-up call for the nephrology community is that smaller biopsy needles are being used and biopsies are increasingly being performed by radiologists rather than nephrologists. The declining trend in the performance of percutaneous renal biopsy by practicing nephrologists should be alarming, while the importance of performing renal biopsies should be emphasized because the information provided by this procedure directly affects the care of nephropathic patients.

References

1. García Nieto V, Luis Yanes MI, Ruiz Pons M (2009) Celebrating fifty years of percutaneous renal biopsies in Spain. Nefrologia 29:71–76
2. Iversen P, Brun C (1951) Aspiration biopsy of the kidney. Am J Med 11:324–330
3. Kark RM, Muehrcke RC (1954) Biopsy of kidney in prone position. Lancet 266:1047–1049
4. Whittier WL, Korbet SM (2004) Timing of complications in percutaneous renal biopsy. J Am Soc Nephrol 15:142–147
5. Manno C, Strippoli GFM, Arnesano L et al (2004) Predictors of bleeding complications in percutaneous ultrasound-guided renal biopsy. Kidney Int 66: 1570–1577
6. Islam N, Fulop T, Zsom L et al (2010) Do platelet function analyzer-100 testing results correlate with bleeding events after percutaneous renal biopsy? Clin Nephrol 73:229–237
7. Culkin DJ, Exaire EJ, Green D et al (2014) Anticoagulation and antiplatelet therapy in urological practice: ICUD/AUA review paper. J Urol 192:1–9
8. Waldo B, Korbet SM, Freimanis MG, Lewis EJ (2009) The value of post-biopsy ultrasound in predicting complications after percutaneous renal biopsy of native kidneys. Nephrol Dial Transplant 24:2433–2439
9. Gesualdo L, Cormio L, Stallone G et al (2008) Percutaneous ultrasound-guided renal biopsy in supine antero-lateral position. Nephrol Dial Transplant 23:971–976
10. Ishikawa E, Nomura S, Hamaguchi T et al (2009) Ultrasonography as a predictor of overt bleeding after renal biopsy. Clin Exp Nephrol 13:325–331

11. Dopson SJ, Jayakumar S, Velez JC (2009) Page kidney as a rare cause of hypertension: case report and review of the literature. Am J Kidney Dis 54:334–339
12. Corapi KM, Chen JL, Balk EM, Gordon CE (2012) Bleeding complications of native kidney biopsy: a systematic review and meta-analysis. Am J Kidney Dis 60:62–73
13. Manno C, Bonifati C, Torres DD, Campobasso N, Schena FP (2011) Desmopressin acetate in percutaneous ultrasound-guided kidney biopsy. A randomized controlled trial. Am J Kidney Dis 57:850–855
14. Corvin HL, Schwartz MM, Lewis EJ (1988) The importance of sample size in the interpretation of the renal biopsy. Am J Nephrol 8:85–89
15. Sethi S, Haas M, Markowitz GS et al (2015) Mayo clinic/renal pathology society consensus report on pathologic classification, diagnosis, and reporting of GN. J Am Soc Nephrol 27:1278–1287.
16. Segarra-Medrano A, Carnicer-Cáceres C, Arbós-Via MA et al (2012) Biological markers of nephrotic syndrome: a few steps forward in the long way. Nefrologia 32:558–572
17. Tøndel C, Vikse BE, Bostad L, Svarstad E (2012) Safety and complications of percutaneous kidney biopsies in 715 children and 8573 adults in Norway 1988–2010. Clin J Am Soc Nephrol 7:1591–1597

Interventional Ultrasound: Biopsy of Renal Masses

13

Alessandro Volpe and Luisa Zegna

13.1 Introduction

Percutaneous biopsy of renal tumors has been historically used with limited indications: (1) differential diagnosis of lymphoma and renal abscesses, (2) diagnosis of metastatic renal disease in the presence of known extrarenal malignancy, and (3) diagnosis of a renal primary tumor in the presence of disseminated metastases or surgically unresectable retroperitoneal tumors.

Beyond these indications, biopsies of renal tumors have been rarely used for a number of uncertainties in terms of (1) safety, for the potential risk of tumor seeding along the needle track and hemorrhagic complications, (2) diagnostic rate and accuracy, and (3) effectiveness in terms of impact on clinical decisions, due to the perception that all solid renal masses have malignant potential and should be removed surgically up front.

Many of these uncertainties have now been overcome due to the growing experience of urologists and interventional radiologists in performing biopsies, to the growing experience of pathologists in interpreting biopsy specimens, and to the growing confidence of urologists in using biopsy information to support the clinical decisions.

The increasing incidence of small renal masses (SRMs), the development of alternative treatments for these lesions in selected patients, and the development of effective biological therapies for metastatic disease have increased the awareness that pretreatment histological information are necessary to choose the best-suited treatment for each individual patient [1].

13.2 Rationale of Percutaneous Renal Tumor Biopsy

Percutaneous biopsy can today provide important information for clinical management of renal tumors, with major impact on clinical practice.

13.2.1 Decrease of Surgical Indications for Benign Tumors

SRMs are benign tumors in a non-negligible proportion of cases, with a probability that significantly increases with decreasing tumor size [2–4].

Conventional radiology (CT, MRI, CEUS) does not allow an accurate diagnosis of oncocytoma. In fact, the typical appearance of the oncocytoma as a homogeneous hypervascular mass

A. Volpe, MD (✉) • L. Zegna
Division of Urology, Department of Translational Medicine, Maggiore della Carità Hospital, University of Eastern Piedmont, Corso Mazzini, 18 – 28100, Novara, Italy
e-mail: alessandro.volpe@med.uniupo.it

P. Martino, A.B. Galosi (eds.), *Atlas of Ultrasonography in Urology, Andrology, and Nephrology*,
DOI 10.1007/978-3-319-40782-1_13

with a central starry scar is observed only in few cases. No other radiological feature is sufficiently reliable for the diagnosis of this benign tumor [5, 6].

Moreover, although most angiomyolipomas are easily recognizable at CT scan for the characteristic fatty content, fat-free angiomyolipomas (leiomyoma-like and epithelioid variants) cannot be properly diagnosed at imaging [7]. Overall, Remzi et al. observed that only 17 % of benign tumors are correctly characterized at preoperative CT [8].

Performing a percutaneous biopsy before treatment decision can therefore decrease the number of unnecessary surgery for benign tumors, especially in elderly and comorbid patients.

13.2.2 Support of Treatment Decision-Making for Localized Renal Tumors

A significant proportion of SRMs are benign tumors or low-grade RCC with a relatively indolent biological and clinical behavior [9, 10]. Furthermore, most SRMs are incidentally detected in older patients, in whom comorbidities are more frequent and the risk of competitive mortality is higher [11].

Surgical resection is the gold standard treatment for SRMs, but focal ablative therapies and active surveillance are alternative options in patients with advanced age, reduced life expectancy, or high surgical risk [12]. Renal tumor biopsy can be useful to select patients who are good candidates for a conservative management. In fact, active surveillance is more suitable for low-grade tumors, with limited risk of progression. A biopsy may also help to decide the intensity of follow-up for patients in active surveillance. In fact, benign tumors can be followed with a less rigid scheme, reducing the risks of radiation exposure and the costs for the health-care system.

Percutaneous biopsy can also be performed for larger localized renal lesions (T1b–T2). Although the decision to perform a radical or partial nephrectomy depends essentially on patient's characteristics and tumor's radiological features, the histological characterization of the renal mass may favor a radical surgical treatment in case of aggressive disease and a conservative treatment even in highly complex cases in case of benign or indolent histology.

13.2.3 Support to Define the Oncological Outcomes of Focal Ablative Therapies

Although the outcomes of cryoablation and radiofrequency ablation are encouraging, the persistence of viable tumor cells after these ablative procedures is not infrequent [13]. The guidelines of the American Urological Association recommend a percutaneous biopsy of renal tumors after ablation if recurrence or persistent disease is suspected at follow-up imaging. Routine biopsies after treatment can allow the histological confirmation of the success of minimally invasive therapies and check for local recurrences [14].

13.2.4 Support of Treatment Decision-Making for Metastatic Renal Tumors

Percutaneous biopsies of renal tumors can be useful for treatment decision-making in the setting of metastatic disease. The presence of sarcomatoid differentiation predicts a poor prognosis, with limited response to systemic therapy and less benefit of cytoreductive nephrectomy, which should not be performed to avoid unnecessary morbidity [15, 16].

In addition, molecular targeted drugs have different response rates according to RCC histology. Studies have shown that mTOR inhibitors have better activity in the treatment of chromophobe RCC than tyrosine kinase inhibitors. Similarly, foretinib demonstrated good responses in the treatment of papillary RCC, particularly in cases with MET germline mutations [17, 18].

Currently, biopsy is required to characterize primary renal tumors before starting systemic therapy for metastatic disease. In particular, percutaneous biopsy is recommended when cytore-

ductive nephrectomy is not indicated or when a neoadjuvant systemic therapy is planned [12].

13.3 Current Indications of Percutaneous Renal Tumor Biopsy

Percutaneous biopsy of renal tumors can be useful in several clinical settings and is currently recommended for the histological characterization of:

- Indeterminate renal masses at abdominal imaging (including Bosniak IV cystic lesions)
- Small incidental renal masses in patients who are candidates for active surveillance or minimally invasive ablative therapy
- Radiological suspicion of local recurrence after ablative therapy
- Renal masses which are suspicious for metastatic disease in the presence of a known extrarenal tumor
- Retroperitoneal tumors involving the kidney when surgery is not feasible or indicated
- Metastatic primary renal tumors in patients who are not candidates for cytoreductive nephrectomy or when a neoadjuvant systemic therapy is planned [12]

13.4 Technique of Percutaneous Renal Tumor Biopsy

13.4.1 Preparation

Before biopsy of a renal mass, a screening for the presence of coagulative disorders (assessment of PTT, INR, and platelet count) should be performed. Antiplatelet drugs should be stopped 5–7 days before biopsy, and anticoagulants should be discontinued in time to achieve acceptable INR values. Anticoagulants are generally replaced with low molecular weight heparin which are then continued for a few days after biopsy.

13.4.2 Anesthesia

Percutaneous renal biopsy can be performed in an outpatient or day hospital setting and is generally well tolerated under local anesthesia with lidocaine 2%. Local anesthesia should be ideally performed on the selected needle track (Fig. 13.1). Sedation is indicated only in selected patients who are particularly anxious. In fact, patient's consciousness is generally useful to perform biopsies of upper pole masses under deep inspiration.

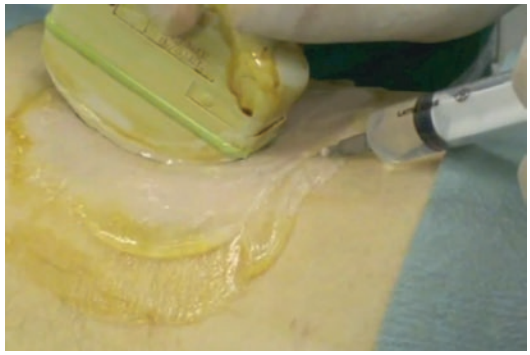

Fig. 13.1 Local anesthesia

13.4.3 Radiological Guidance

Biopsies can be performed under ultrasound, CT, or MRI guidance. The choice of the imaging guidance depends on the operator's experience and habits, on tumor size and location, and on patient's habitus. MRI is rarely used for the high costs and the need of ferromagnetic needles. Ultrasound guidance is used in most cases, since it allows a real-time puncture, avoids radiation exposure, and is associated with lower costs (Fig. 13.2). However, in some obese patients, CT guidance should be preferred, since the presence of significant subcutaneous and perivisceral fat can hinder a clear ultrasound visualization of the renal mass, which is essential to perform an accurate biopsy. Renal masses located at the upper pole or on the anterior face of the kidney and smaller than 15 mm in size are also more likely to be sampled under CT guidance (Fig. 13.3). A major limitation of CT guidance is that it does not allow biopsies in real time. This can be overcome with the use of modern techniques such as CT fluoroscopy.

At present there is no solid evidence of the superiority of the ultrasound or CT guidance. In a large series of biopsies of SRMs performed at the University of Toronto, no significant difference was observed between the detection rates of biopsies performed with the two approaches [19, 20].

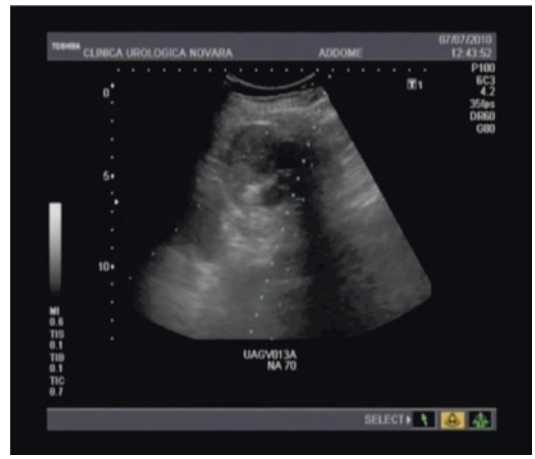

Fig. 13.2 Biopsy of a renal mass under ultrasound guidance

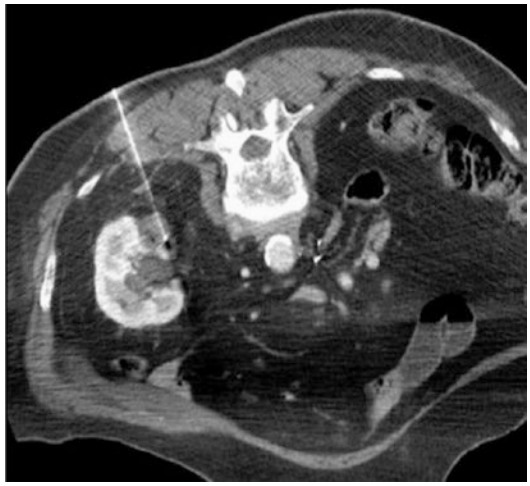

Fig. 13.3 Biopsy of a small renal mass under CT guidance

13.4.4 Biopsy Needles

Biopsies are usually performed with a Tru-Cut 18-gauge needle loaded on an automatic biopsy gun, which achieves the best compromise between safety and detection rate (Fig. 13.4a). The biopsy is generally performed coaxially to a 17-gauge cannula which is previously placed near or just inside the renal mass (Fig. 13.4b). The use of full-core needles seems to allow better results both in terms of diagnostic rate and accuracy.

Fine-needle aspiration (FNA) for cytology is performed instead with smaller (≤21 G) needles.

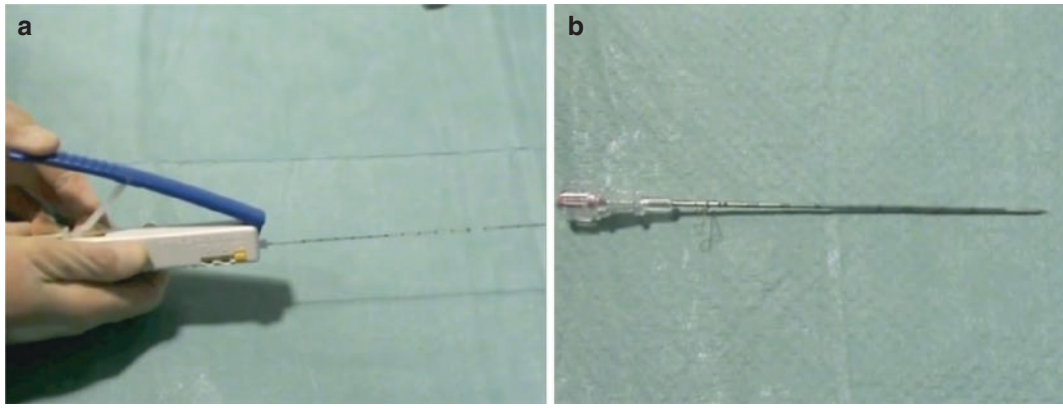

Fig. 13.4 (**a**) Full-core 18-gauge needle loaded on an automatic biopsy gun; (**b**) 17-gauge cannula through which the biopsy needle is introduced

13.4.5 Biopsy Technique

The patient is generally placed in a lateral decubitus, but a prone or semiprone position can be also used based on the characteristics of the renal lesion and on the selected imaging guidance. After performing local anesthesia, the most appropriate biopsy track is chosen, and a guided cannula is inserted percutaneously to approach the lesion (Fig. 13.5).

The puncture can be performed "freehand" or with the use of an ultrasound guide that directs the needle in a predetermined angle within the plane of view of the transducer (Fig. 13.6). The freehand technique requires more experience, but has the advantage of greater flexibility by allowing subtle adjustments that can compensate for improper needle trajectory and patient movement.

Once the lesion is reached, the stylet is removed, and the needle core biopsy or FNA is performed through the guiding cannula (Fig. 13.7). The biopsy can be performed after removal of the ultrasound guide or under real-time ultrasound guidance based on operator's preference. Multiple biopsies can be obtained through the guiding cannula which is finely repositioned within the lesion to allow sampling of different areas of the tumor. This technique is called "coaxial" and is useful to reduce the risk of tumor seeding along the needle track, since it minimizes the potential risk of contact of the needle with the healthy tissues interposed between the skin surface and the renal mass.

When a FNA is planned together with a core biopsy, it should be performed first to limit the risk of hemorrhagic contamination of the sample, which makes the cytological diagnosis more challenging. The quality of the FNA sample should be checked by a cytologist during the procedure (Fig. 13.8). This increases the diagnostic yield and confirms the proper placement of the cannula through which the core biopsies will be then performed.

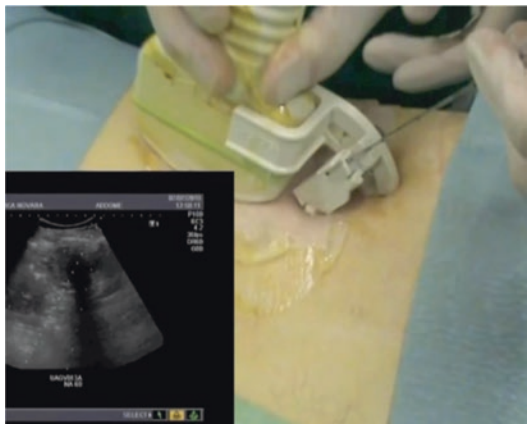

Fig. 13.5 Skin puncture and advancement of the guiding cannula to reach the tumor capsule under ultrasound guidance

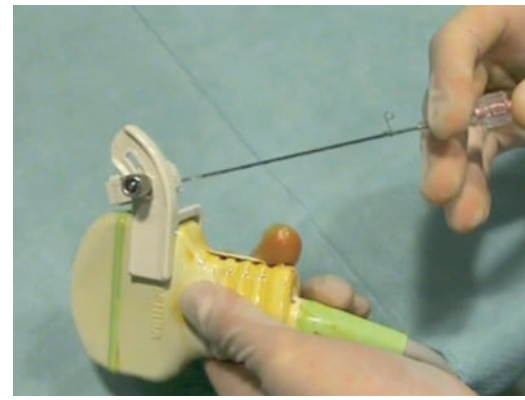

Fig. 13.6 Ultrasound guide for percutaneous biopsy

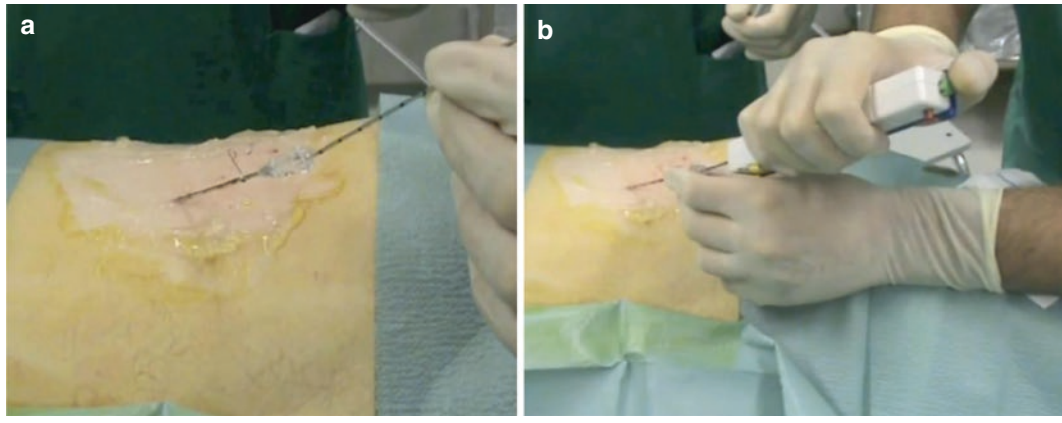

Fig. 13.7 (**a**) Coaxial introduction of the 18G needle in the guiding cannula to perform the biopsy of a renal mass. (**b**) The sampling is performed with the automatic biopsy gun

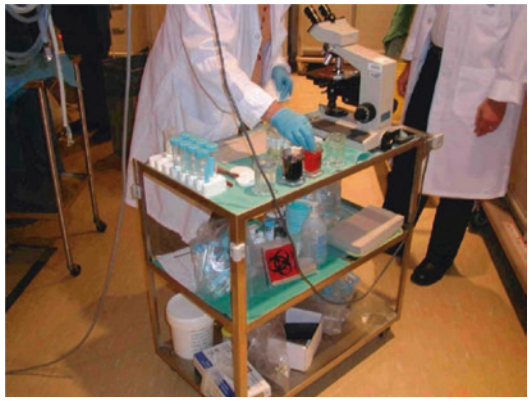

Fig. 13.8 Check of the quality of the cytologic specimen during the procedure

13.4.6 Biopsy Pattern

At present, the ideal biopsy pattern to sample renal masses of different sizes is not standardized. However, at least two good quality samples should be always obtained from different areas of the tumor, avoiding areas of necrosis. A good quality core is at least 1 cm long and not fragmented. Wunderlich et al. observed a poorer diagnostic accuracy for central biopsies in tumors >4 cm, likely due to the higher likelihood of necrosis in the central portion of larger tumors [21]. Based on these results, it is currently generally recommended to obtain at least a central and a peripheral core in <4 cm tumors and two peripheral cores in larger tumors.

13.4.7 Biopsy Processing

To favor an optimal histological assessment, every biopsy should be placed between two sponges in a single histological cassette (Fig. 13.9).

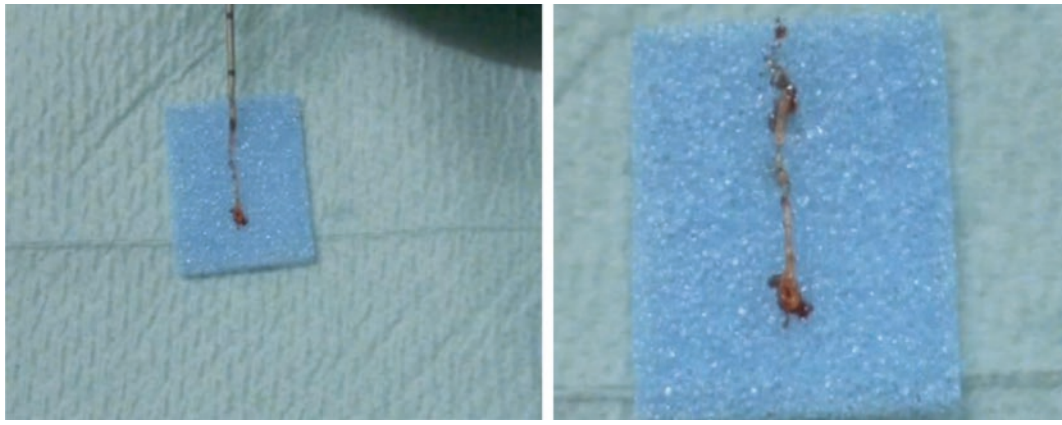

Fig. 13.9 Release of the core biopsy on a dedicated sponge for the following histological processing

13.4.8 Patient Management

Patients should be monitored for at least 4 h after the biopsy. The vital parameters and a cell blood count should be assessed. Post-procedural ultrasound and CT scans are generally not required in the absence of clinical or laboratory signs of active bleeding.

13.5 Safety

Complications after renal tumor biopsy are infrequent with the use of proper biopsy techniques and are mainly represented by immediate or delayed bleeding, since renal tumors are generally hypervascularized. However, significant bleedings requiring hospitalization and/or blood transfusion are rare in experienced centers (<1 %) [1].

The risk of tumor seeding along the needle track is anecdotal. Only seven cases of seeding of renal parenchymal tumors have been reported to date in the literature. Most of these cases were observed before 2001 when the biopsy was performed with different instruments and techniques [22]. The use of the coaxial technique is particularly important to avoid tumor seeding. In fact, the only case of seeding that has been recently described was not carried out with a coaxial technique [23].

Other possible rare complications of biopsy are pneumothorax in case of biopsies of upper polar lesions with a posterior approach and infections [24].

13.6 Diagnostic Rate and Accuracy of Renal Tumor Biopsies

Renal tumor biopsy has been shown to have a good diagnostic rate (78–97 %) and a high specificity (98–100 %) and sensitivity (86–100 %) for the diagnosis of histological malignancy in several large series from experienced centers [1].

A recent systematic review and meta-analysis of the literature observed that the overall median diagnostic rate of renal tumor biopsy is 92 %. The sensitivity and specificity of diagnostic core biopsies and FNAs were 99.1 % and 99.7 % and 93.2 % and 89.8 %, respectively [25].

The risk of a nondiagnostic biopsy remains a concern for clinicians. When a biopsy is not diagnostic in the presence of suspicious radiological findings for malignancy, a repeat biopsy or surgical exploration should always be recommended [12].

The accuracy of the biopsy for the diagnosis of histological subtype is high (86–100 %) [1, 25]. The evaluation of the tumor grading on biopsy is challenging for pathologists. The accuracy for the assessment of Fuhrman grade (I–IV) is only fair (43–75 %), but can be increased using a simplified grading system (high grade vs. low grade) [1, 25].

Percutaneous biopsies have a lower detection rate for cystic renal masses and should not be recommended for characterization of these lesions, except for Bosniak IV lesions which have a visible and targetable solid area in their context [12]. The combination of needle core biopsy and FNA can obtain complementary results especially for the characterization of complex cystic masses [26, 27].

13.7 Limitations and Future Perspectives of Renal Tumor Biopsies

Prospective studies with larger series are needed to confirm the good results of percutaneous biopsy of renal masses, to establish the role of the repeat biopsy in nondiagnostic cases, criteria for quality control of biopsy samples, and guidelines for the standardization of pathological results.

The accuracy of renal tumor biopsies is limited by factors that are intrinsic to the procedure (risk of insufficient sampling), by factors related to histology of renal tumors (difficult differential diagnosis between different histological subtypes such as oncocytoma and chromophobe RCC, difficult assessment of tumor grade, the presence of intratumoral heterogeneity), and by factors relating to the interpretation of biopsy specimens (intra- and interobserver variability).

Intratumoral heterogeneity in terms of histological type is not frequently found, but 18 % of oncocytomas can show patterns of chromophobe RCC. Recent studies indicate that the oncological outcomes of surgery for these hybrid tumors are similar to those obtained for pure oncocytomas [28]. The differential diagnosis between oncocytoma, eosinophilic variant of chromophobe RCC, oncocytic papillary RCC, and clear-cell RCC with granular cytoplasm remains the most difficult challenge for pathologists in the interpretation of biopsy. In a recent study, Kummerlin et al. observed a good intraobserver and interobserver agreement in the histologic assessment of renal tumor biopsies performed on the bench after surgery. However, the diagnosis was less reproducible for chromophobe RCC when only the classical hematoxylin-eosin staining was used [29].

The challenging definition of tumor grade on biopsy samples represents a limitation when grading is used for treatment decision-making. The assessment of grading is also limited by the potential presence of intratumoral heterogeneity, which is reported in 5–25 % of renal tumors [1].

The detection rate and accuracy of biopsies of renal masses could be optimized by the definition of standardized biopsy protocols. Further studies are therefore needed to define the optimal number of cores and the ideal location where the samples should be taken according to tumor size.

Finally, the use of cytogenetic and molecular markers on biopsy samples has the potential to provide more diagnostic and prognostic information, thereby further increasing the utility of percutaneous biopsy in the management of renal neoplasms.

References

1. Volpe A, Finelli A, Gill IS, Jewett MA, Martignoni G, Polascik TJ et al (2012) Rationale for percutaneous biopsy and histologic characterisation of renal tumours. Eur Urol 62:491–504
2. Sahni VA, Ly A, Silverman SG (2011) Usefulness of percutaneous biopsy in diagnosing benign renal masses that mimic malignancy. Abdom Imaging 36:91–101
3. Tsivian M, Mouraviev V, Albala DM, Caso JR, Robertson CN, Madden JF et al (2011) Clinical predictors of renal mass pathological features. BJU Int 107:735–740
4. Frank I, Blute ML, Cheville JC, Lohse CM, Weaver AL, Zincke H (2003) Solid renal tumors: an analysis of pathological features related to tumor size. J Urol 170:2217–2220
5. Choudhary S, Rajesh A, Mayer NJ, Mulcahy KA, Haroon A (2009) Renal oncocytoma: CT features cannot reliably distinguish oncocytoma from other renal neoplasms. Clin Radiol 64:517–522
6. Rosenkrantz AB, Hindman N, Fitzgerald EF, Niver BE, Melamed J, Babb JS (2010) MRI features of renal oncocytoma and chromophobe renal cell carcinoma. AJR Am J Roentgenol 195:W421–W427
7. Kim JK, Park SY, Shon JH, Cho KS (2004) Angiomyolipoma with minimal fat: differentiation from renal cell carcinoma at biphasic helical CT. Radiology 230:677–684
8. Remzi M, Katzenbeisser D, Waldert M, Klingler HC, Susani M, Memarsadeghi M et al (2007) Renal tumour size measured radiologically before surgery is an unreliable variable for predicting histopathological features: benign tumours are not necessarily small. BJU Int 99:1002–1006
9. Jewett MA, Mattar K, Basiuk J, Morash CG, Pautler SE, Siemens DR et al (2011) Active surveillance of small renal masses: progression patterns of early stage kidney cancer. Eur Urol 60:39–44
10. Smaldone MC, Kutikov A, Egleston BL, Canter DJ, Viterbo R, Chen DY et al (2012) Small renal masses progressing to metastases under active surveillance: a systematic review and pooled analysis. Cancer 118: 997–1006
11. Hollingsworth JM, Miller DC, Daignault S, Hollenbeck BK (2007) Five-year survival after surgical treatment for kidney cancer: a population-based competing risk analysis. Cancer 109: 1763–1768
12. Ljungberg B, Bensalah K, Canfield S, Dabestani S, Hofmann F, Hora M et al (2015) EAU guidelines on renal cell carcinoma: 2014 update. Eur Urol 67(5): 913–924
13. Klingler HC, Marberger M, Mauermann J, Remzi M, Susani M (2007) 'Skipping' is still a problem with radiofrequency ablation of small renal tumours. BJU Int 99:998–1001
14. Donat SM, Diaz M, Bishoff JT, Coleman JA, Dahm P, Derweesh IH et al (2013) Follow-up for clinically localized renal neoplasms: AUA guideline. J Urol 190:407–416
15. Shuch B, Said J, La Rochelle JC, Zhou Y, Li G, Klatte T et al (2009) Cytoreductive nephrectomy for kidney cancer with sarcomatoid histology – is up-front resection indicated, and if not, is it avoidable? J Urol 182:2164–2171
16. Abel EJ, Culp SH, Matin SF, Tamboli P, Wallace MJ, Jonasch E et al (2010) Percutaneous biopsy of primary tumor in metastatic renal cell carcinoma to predict high risk pathological features: comparison with nephrectomy assessment. J Urol 184:1877–1881

17. Choueiri TK, Vaishampayan U, Rosenberg JE, Logan TF, Harzstark AL, Bukowski RM et al (2013) Phase II and biomarker study of the dual MET/VEGFR2 inhibitor foretinib in patients with papillary renal cell carcinoma. J Clin Oncol 31:181–186
18. Koh Y, Lim HY, Ahn JH, Lee JL, Rha SY, Kim YJ et al (2013) Phase II trial of everolimus for the treatment of nonclear-cell renal cell carcinoma. Ann Oncol 24:1026–1031
19. Volpe A, Mattar K, Finelli A, Kachura JR, Evans AJ, Geddie WR et al (2008) Contemporary results of percutaneous biopsy of 100 small renal masses: a single center experience. J Urol 180:2333–2337
20. Leveridge MJ, Finelli A, Kachura JR, Evans A, Chung H, Shiff DA et al (2011) Outcomes of small renal mass needle core biopsy, nondiagnostic percutaneous biopsy, and the role of repeat biopsy. Eur Urol 60:578–584
21. Wunderlich H, Hindermann W, Al Mustafa AM, Reichelt O, Junker K, Schubert J (2005) The accuracy of 250 fine needle biopsies of renal tumors. J Urol 174:44–46
22. Volpe A, Jewett MA (2009) Current role, techniques and outcomes of percutaneous biopsy of renal tumors. Expert Rev Anticancer Ther 9:773–783
23. Mullins JK, Rodriguez R (2013) Renal cell carcinoma seeding of a percutaneous biopsy tract. Can Urol Assoc J 7:E176–E179
24. Hopper KD, Yakes WF (1990) The posterior intercostal approach for percutaneous renal procedures: risk of puncturing the lung, spleen, and liver as determined by CT. AJR Am J Roentgenol 154:115–117
25. Marconi L, Dabestani S, Lam TB, Hofmann F, Stewart F, Norrie J, Bex A, Bensalah K, Canfield SE, Hora M, Kuczyk MA, Merseburger AS, Mulders PF, Powles T, Staehler M, Ljungberg B, Volpe A (2016) Systematic review and meta-analysis of diagnostic accuracy of percutaneous renal tumour biopsy. Eur Urol 69(4):660–673. doi:10.1016/j.eururo.2015.07.072
26. Parks GE, Perkins LA, Zagoria RJ, Garvin AJ, Sirintrapun SJ, Geisinger KR (2011) Benefits of a combined approach to sampling of renal neoplasms as demonstrated in a series of 351 cases. Am J Surg Pathol 35:827–835
27. Wood BJ, Khan MA, McGovern F, Harisinghani M, Hahn PF, Mueller PR (1999) Imaging guided biopsy of renal masses: indications, accuracy and impact on clinical management. J Urol 161:1470–1474
28. Waldert M, Klatte T, Haitel A, Ozsoy M, Schmidbauer J, Marberger M et al (2010) Hybrid renal cell carcinomas containing histopathologic features of chromophobe renal cell carcinomas and oncocytomas have excellent oncologic outcomes. Eur Urol 57:661–665
29. Kummerlin I, ten Kate F, Smedts F, Horn T, Algaba F, Trias I et al (2008) Core biopsies of renal tumors: a study on diagnostic accuracy, interobserver, and intraobserver variability. Eur Urol 53:1219–1225

Interventional Ultrasound: Positioning Nephrostomy

14

Pasquale Martino, Carlos Miacola,
Michele Barbera, and Silvano Palazzo

14.1 Indications

The indications for positioning a percutaneous nephrostomy are both diagnostic (e.g., descending pyelography) and therapeutic, when an immediate decompression of the upper urinary tract is needed and the transureteral approach is impossible, not indicated, or likely to fail [1, 2].

Indications of an urgent nature include postrenal obstruction with urosepsis (and/or uremia) and postoperative (or traumatic) urinoma. The approach is particularly useful in the course of pyonephrosis, when antibiotic treatment alone may not be efficacious due to obstruction of the collector ducts. In such cases, a rapid decompression of the obstructed system is obtained, thereby reducing the risk of urosepsis.

Nonurgent (or elective) indications include:

- Temporary drainage after urological treatment or during radiotherapy (or radiochemotherapy) for neoplastic-type obstructions
- Palliative drainage in patients with cancers causing ab-extrinsic compression of the ureters (e.g., invasive prostate cancer, bladder sarcoma, squamous carcinoma, cancer of the uterus and ovaries, retroperitoneal fibrosis)
- Temporary drainage in the treatment of urinary fistulas [3, 4]

The procedure may also be useful when instilling chemotherapeutic drugs, even if this is a rare indication.

Percutaneous nephrostomy may be the important first step in surgical procedures like the extraction of urinary stones, percutaneous lithotripsy, the removal of foreign bodies, excision of urothelial cancers, and the treatment of renal cysts and calyceal diverticuli, in antegrade positioning of double J stents, in the access for endoscopic correction of stenosis of the pyeloureteral junction.

Electronic supplementary material The online version of this chapter (doi:10.1007/978-3-319-40782-1_14) contains supplementary material, which is available to authorized users.

P. Martino (✉) • C. Miacola • S. Palazzo
Department of Emergency and Organ Transplantation – Urology, Andrology and Kidney Transplantation Unit, University of Bari, Bari, Italy
e-mail: pasqualeluciomartino@libero.it; luciomartino@tin.it; pasquale.martino@uniba.it

M. Barbera
U.O. Urologia – Presidio Ospedaliero di Sciacca – Asp Agrigento, Agrigento, Italy

P. Martino, A.B. Galosi (eds.), *Atlas of Ultrasonography in Urology, Andrology, and Nephrology*,
DOI 10.1007/978-3-319-40782-1_14

14.2 Preparation

Positioning a percutaneous nephrostomy is numbered among surgical maneuvers, and as such, it is important to observe some precautions. It is necessary to verify blood count and clotting and to monitor arterial pressure and heart rate. It is advisable to administer antibiotic prophylaxis and to be able to rely on a venous access (so as to be able to administer catecholamines and/or anticholinergics if necessary).

The nephrostomic access will be posterior or posterolateral, owing to the relationships of the kidney with the adjacent organs. The liver and spleen lie laterally and sometimes quite posteriorly to the cranial third of the homologous kidney. The ascending and descending colon are anterior but sometimes lateral to the lower third of the kidneys.

For posterior access, the patient is placed in prone position, and a thickness is put underneath the abdomen to arch the spine and so superficialize the kidney. The anatomical reference points for access are the iliac crest, the spine, and the ribs. In general, the access is created under the 12th rib, 10 cm to the side of the spinal apophysis.

Instead, for posterolateral access, the patient should be in oblique prone position, angled at 30–40° to the horizontal plane. The puncture is made on the medial axillary line. Unfortunately, if the patient is allowed to take up a more comfortable position, there is a higher risk of perforation of the peritoneum or of a bowel loop.

An important point to remember is the vascular anatomy of the kidney. The renal artery divides into an anterior branch that then further divides into three or four secondary branches and a posterior branch that is generally only a single branch; from these, the interlobar arteries run along the medullary substance, between the calyces, and follow on as arcuate arteries into the corticomedullary junction. The calyces are arranged in two rows, anterior and posterior. The anterior branches supply both the calyces in the anterior row and the anterior face of the posterior row calyces, so they extend their territory beyond the median frontal plane of the kidney. The posterior arterial branches serve the posterior face of the posterior row of calyces. Owing to this anatomical arrangement, a zone named Brodel's avascular plane can be observed (Fig. 14.1), where the terminal branches of the posterior and anterior branches meet, delimiting a poorly vascularized area. This is the safest place through which to pass the catheter that is generally fixed at the level of the inferior calyx.

Before positioning the patient and individuating the point of access, it is important to check that the operative trolley contains all the instruments needed to complete the procedure. It must contain a support for the needle guide, to be attached to the ultrasound probe, skin disinfectant, a drape/drapes to outline the operative field, sterile gel, local anesthetic, a scalpel with a pointed blade, a bowl of physiological solution, a metal guidewire, fascia dilators, nephrostomic stents of a suitable caliber, drainage tubes, silk sutures, and sterile gauzes for dressings (Fig. 14.2).

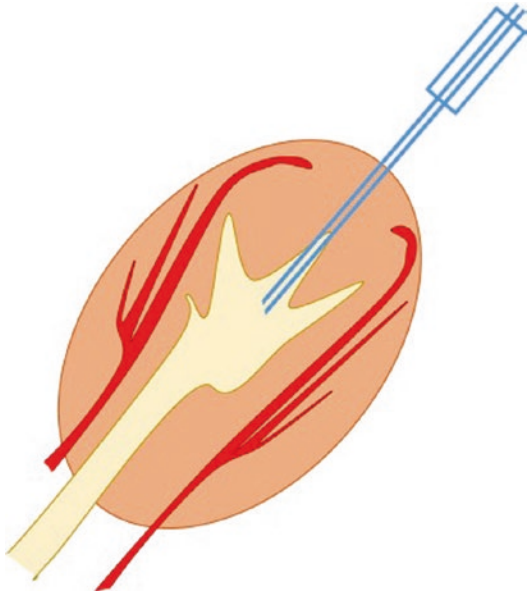

Fig. 14.1 Brodel's avascular plane

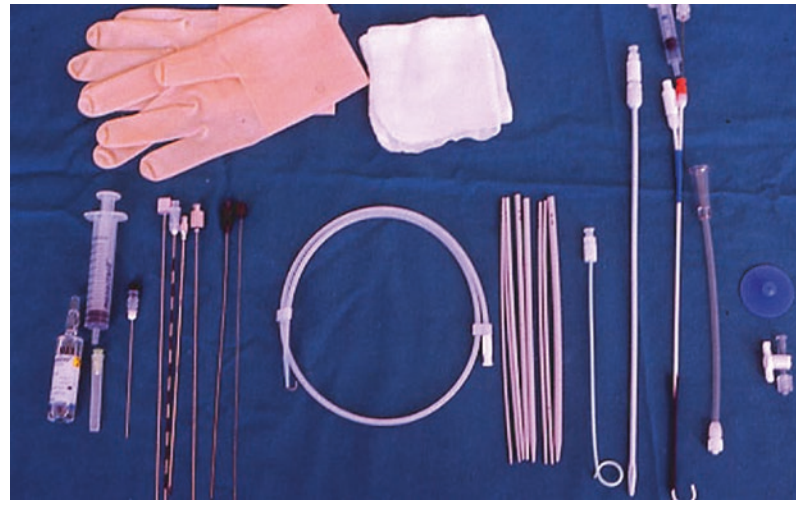

Fig. 14.2 Surgical kit

14.3 Description of the Technique

The control system when positioning a nephrostomic catheter relies largely on ultrasound guidance, using 3.5 or 5 MHz probes. The advantages of the ultrasound guidance system are the ease of localization of the renal cavities and of determining the depth of the kidneys; the possibility of using this system even in pregnant women and in subjects who are allergic to contrast medium, or with a reduced renal function; and the fact that it can be used in a dedicated outpatients clinic. When possible, it is better to associate the US guidance with radiological control: this association guarantees a success rate exceeding 98 %.

The possible access techniques include Seldinger's angiographic approach (Video 14.1), the one step or the combined technique, with the catheter equipped with a metal cannula and pointed obturator so as to insert it in the renal cavity.

The method most commonly employed is Seldinger's technique that involves explorative puncture of the renal cavity and then positioning of the nephrostomy. After copious disinfection of the skin, the operative field is outlined with sterile drapes, and local anesthesia of the superficial and deep planes is given with 2 % Xylocaine or Carbocaine (Fig. 14.3). Sterile gel can be used for the contact between the skin and US probe that has previously been immersed, with its needle guide in sterile solution. The needle (generally 18 ch) is passed through the collimator, and then the procedure can commence.

In Seldinger's technique, the needle with the obturator is followed (thanks to the reflecting echo), under ultrasound guidance the whole way (Video). When the needle arrives at the renal capsule, a deformity will be noted, caused by the pressure of the needle on the parenchyma about to be penetrated. Once the excretory tract is reached, generally the inferior calyx, the obturator is withdrawn, and urine can be seen running down. The skin is incised up to the fascia with the pointed scalpel. The metal guidewire is inserted through the needle sheath that is then withdrawn, and the dilator or progressive dilators are inserted, up to a caliber of one size greater than the caliber of the nephrostomic catheter to be used. After the last dilator has been withdrawn, the nephrostomy is inserted and the metal guidewire removed. Then the nephrostomic stent is fixed to the skin plane, normally with silk sutures (Fig. 14.4). Lastly, the wound is dressed, covering the nephrostomy with sterile gauze and taking care to avoid bending it or provoking stricture.

The critical point of the method is when the catheter is pushed down along the guidewire, at the level of the passage through the perirenal fat, because its J shape tends to push the point away from the initial, correct course. The reason for this is that the perirenal fat offers little resistance that would help to maintain the right course. This difficulty can be overcome by using a rigid Lunderquist guidewire, on which, after the dilation maneuvers, the nephrostomic catheter equipped with a metal cannula is passed (combined technique).

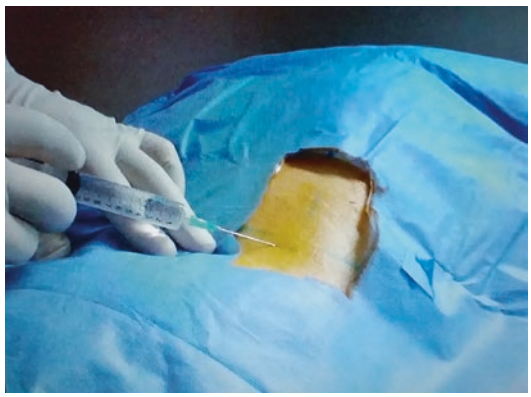

Fig. 14.3 Local anesthetic injection

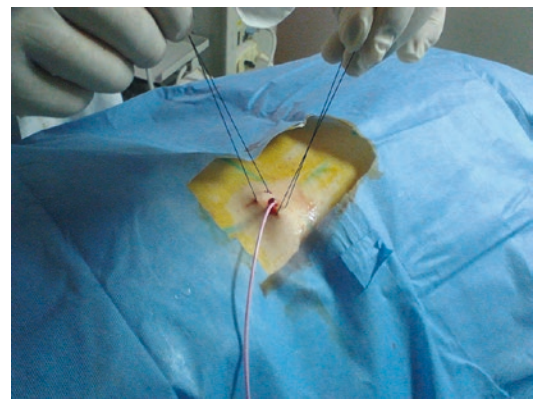

Fig. 14.4 Set for percutaneous nephrostomy

14.4 Characteristics of the Necessary Devices

The *metal guidewire* is extremely important when adopting this method. It may have a variable rigidity, will be hydrophilic (thanks to its contact with urine or physiological solution, it will be extremely slippery and run easily), and can be obturated so as to facilitate movement of the point. The length too will be variable and the point generally soft to avoid inducing trauma; it may be straight or J shaped that makes it more easily visualized at ultrasound.

The *fascia dilators* are of a progressively higher-scaled caliber and may be single or coaxial. They are not usually echoreflectant, and their correct positioning is visualized indirectly by ultrasound because they cover the guidewire echoes (Fig. 14.5).

The nephrostomic *catheter* may be made of different materials, with a variable caliber and point. The ideal catheter must run easily and have a good flexibility and softness and a strong resistance to encrustation. Each of the possible materials has its own peculiar characteristics: polyurethane runs more easily, is soft, and has a greater resistance to encrustation and kinking than silicone. The latter is softer and so ideal for long indwelling purposes, but owing to these characteristics, it is much thicker than all the other types. As a result, for the same internal caliber, the feature that serves its drainage function, the external caliber will be much larger than that of the polyurethane catheter.

Polyurethanes are the most ductile material employed for nephrostomic catheters. These materials can have different degrees of softness and other characteristics, depending on what treatment is made during production: there are softened, hydrogel, silver-coated polyurethane, polyvinyl chloride (PVC), silicone, latex.

The catheter can be anchored according to various systems. In clinical practice, silk sutures are always used to fix it to the patient's skin. Autostatic nephrostomies can be of balloon (Fig. 14.6), malecot (Fig. 14.7), or cope loop type. The first of these relies on a balloon that is inflated once the catheter has reached the correct position. The cope loop type is held in place by a thread that passes from the point through it out to the skin, where it is pulled to form a loop; malecot catheters are used when ample drainage is necessary (uro-pyonephrosis), using the wings at the point to hold it in place.

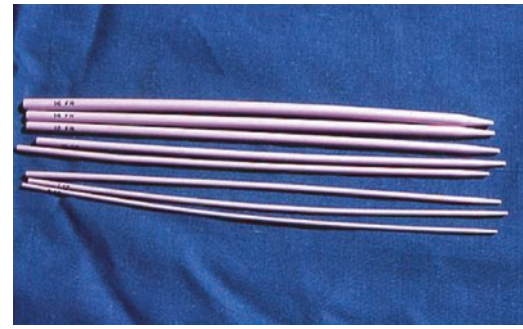

Fig. 14.5 Fascia dilators

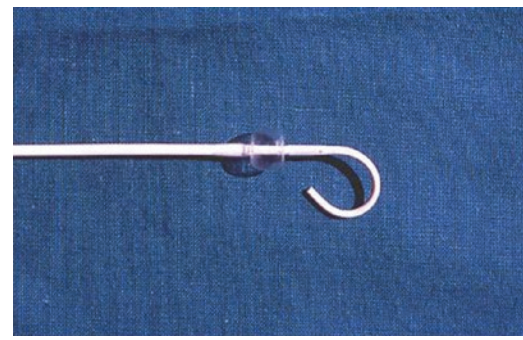

Fig. 14.6 Balloon nephrostomy

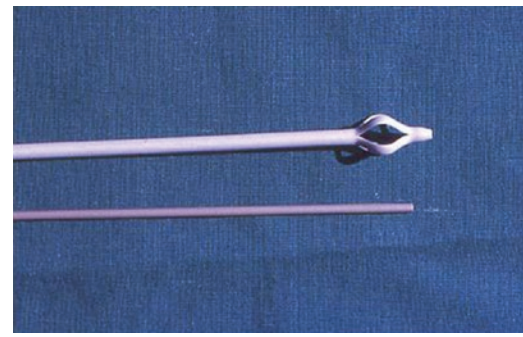

Fig. 14.7 Malecot nephrostomy

14.5 Complications

The mortality rate from percutaneous nephrostomy is low, being approximately 0.2 %, while complications (mostly bleeding and infection) occur in about 4 % of cases [3, 4]. Possible complications include early events: hemorrhage, retroperitoneal hematoma, arteriovenous fistula, pseudoaneurysm, urinoma, infections, septicemia, shock, hydrothorax, pneumothorax, hemothorax, and lesions of adjacent organs. Late complications include stenosis of the pyeloureteral junction and the ureter, retroperitoneal fibrosis, loss or accidental rupture of the catheter that may jeopardize the success of the whole procedure, decubitus wheals, kinking, fissurization, and encrustation of the nephrotomy (Fig. 14.8).

Fig. 14.8 Encrustation of nephrostomy loop

References

1. Goodwin WE, Casey WC (1956) Percutaneous antegrade pyelography and translumbar needle nephrostomy in hydronephrosis. AMA Arch Surg 72(2):357–365
2. Goodwin WE, Casey WC, Woolf W (1955) Percutaneous trocar (needle) nephrostomy in hydronephrosis. J Am Med Assoc 157(11):891–894
3. Brix D, Ignee A, Dietrich CF (2011) Urologische interventionen. In: Dietrich CF, Nuernberg D (eds) Interventioneller ultraschall. Thieme, Stuttgart: in press
4. Dyer RB, Assimos DG, Regan JD (1997) Update on interventional uroradiology. Urol Clin North Am 24(3):623–652

15 Interventional Ultrasound: Puncture and Sclerotherapy of Renal Cysts

Pasquale Martino, Silvano Palazzo, and Giuseppe Carrieri

15.1 Introduction

The treatment of simple renal cysts is generally confined to symptomatic lesions. In particular, the main indications for the treatment of simple cysts are pain due to the mass compression effect, obstruction of the excretory tract, arterial hypertension, and patient anxiety [1, 2]. In general, there is an indication to treat all renal cysts with a longitudinal diameter of 9 cm or more to avoid dangerous intracystic bleeding in cases of trauma. The principal contraindications to the treatment are hemorrhagic diathesis, severe respiratory failure, gross obesity, and malformations. The therapeutic options for the treatment of renal cysts include open surgery, laparoscopic surgery, and percutaneous procedures. The latter approach is preferred nowadays to avoid the costs and morbidity of surgery [3]. Therefore surgery, both open and laparoscopic, is reserved to those cases in which percutaneous treatment is unsuccessful [3].

Electronic supplementary material The online version of this chapter (doi:10.1007/978-3-319-40782-1_15) contains supplementary material, which is available to authorized users.

P. Martino (✉) • S. Palazzo
Department of Emergency and Organ Transplantation – Urology, Andrology and Kidney Transplantation Unit, University of Bari, Bari, Italy
e-mail: pasqualeluciomartino@libero.it; luciomartino@tin.it; pasquale.martino@uniba.it

G. Carrieri
Department of Urology, Policlinico Ospedali Riuniti, University Hospital, Foggia 71100, Italy

P. Martino, A.B. Galosi (eds.), *Atlas of Ultrasonography in Urology, Andrology, and Nephrology*,
DOI 10.1007/978-3-319-40782-1_15

15.2 Technique

In the percutaneous approach, an ultrasound probe is used as a "guide" to localize and treat the cyst. Three different types of percutaneous approach can be distinguished: simple, involving drainage, and then normally simple sclerosing [4]. In the simple percutaneous approach (see Video 15.1), the renal cyst is punctured and the content aspirated, under US guidance, for assessment. In fact, in view of the high recurrence rate of renal cysts (30–80 %), this method is generally employed purely for diagnostic purposes to differentiate between cysts containing blood and those with an ample corpuscular component. The second percutaneous method consists of completely emptying the cyst and then positioning a nephrostomic drainage in the cyst cavity for 24 h, to prolong the collapse of the cyst walls. This method, too, is burdened by a high recurrence rate (65–80 %), so a third method has been devised, which consists of introducing a sclerosing solution into the cyst cavity through the drainage, after completely emptying it of its content under US guidance. This treatment aims to sclerose the cyst walls in order to reduce the risk of recurrence. This method can be repeated (for large cysts) after 24 and 48 h [5]. In literature, many different sclerosing substances have been described, but ethanol is surely the one most commonly employed. The exposure time to the sclerosing substance varies, largely according to its composition, ranging from 10 min to 4 h. In the case of ethanol, it has been demonstrated that contact of the cyst wall cells with this substance (at 95–99 % concentration), for a period of between 1 and 3 min, is enough to determine their immobilization and death [6]. Instead, it takes 4–12 h for penetration of the capsule to occur.

The main complications associated with the treatment of renal cysts include acute hemorrhage (<5 %) (Fig. 15.1), sclerosing of the excretory tract (<0.1 %), late hemorrhage (<0.5 %), septicemia (<1 %), incorrect access (<5 %), and intestinal perforation and splenic lesions (<1 %). A rare complication ensuing after the use of ethanol is intoxication, due to accidental passage of the sclerosing substance into the bloodstream. In any case, the symptoms of alcoholic intoxication tend to regress within 24 h after the procedure.

As regards the technique used to treat simple renal cysts, the method most commonly adopted is the Seldinger that involves first of all puncture of the cyst with an 18-gauge needle under US guidance, after administering local anesthetic with or without an associated systemic painkiller. Subsequently, a guidewire is placed, and dilators of increasing caliber are inserted until the passage is sufficiently wide to position a nephrostomic catheter. Patient preparation for this procedure includes associated antibiotic prophylaxis. Percutaneous puncture of the cyst can be done via posterior or posterolateral access depending on its anatomical position. After the drainage catheter has been positioned inside the cyst cavity and secured in place with silk stitches, the cyst content is aspirated [7]. After aspiration, we believe it is important for safety reasons to fill the cyst cavity firstly with 60 ml of physiological solution that is completely re-aspirated after a few minutes, to confirm the integrity of the cyst wall. Then ethanol is instilled at a quantity equal to 30 % of the previously drained liquid (generally never more than 60 ml). The patient is asked to change the decubitus position frequently, and then, after 40 min, the alcohol is completely re-aspirated and the transcutaneous catheter is removed [8]. In rare cases (of very voluminous cysts), this procedure can be repeated after an interval of 24 h (leaving the nephrostomic catheter in situ) [5].

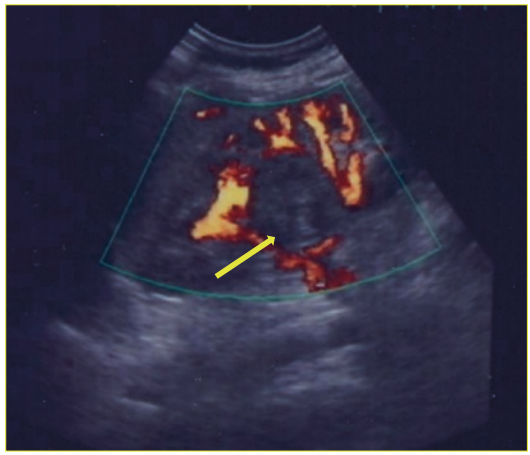

Fig. 15.1 Acute hemorrhage after ultrasound-guided puncture of simple renal cysts (power Doppler)

15.3 Outcome and Complications

In literature, a number of reports have been published claiming that the procedure needs to be performed two or three times in order to achieve a complete remission of the clinical picture. Nevertheless, the results, expressed in terms of lack of recurrence, are heterogeneous, and in many experiences, a single treatment guaranteed a comparable outcome to repeated sclerosing (Table 15.1). The success of the treatment seems to depend on how long the ethanol remains in contact with the cyst walls. The authors who performed more than one treatment preferred not to exceed 20 min contact, while in more recent experiences, a single sclerosing session prolonged for 40/60 min yielded a satisfactory outcome with a comparable rate of complications [9].

It is useful to perform US follow-up of sclerosed cysts at 6 months and 1 year after the procedure.

Table 15.1 Sclerosing treatment of renal cysts

Author	Year	Patients	Treatment	Success (complete-partial)	Volume reduction	Symptoms resolution
Porpiglia	1996	49	Repeated sclerosing	96 %–···/	/	/
Fontana	1999	69	Repeated sclerosing	98 %–···/	/	55 %
Paananen	2001	32	Repeated sclerosing	22 %–···/	79 %	75 %
Delakas	2001	68	Repeated sclerosing	83–11 %	/	/
Akinci	2005	97	Single sclerosing	18 %–···/	93 %	83 %
Martino	2010	204	Single sclerosing	68–32 %	100 %	/

References

1. Laucks SP Jr, McLachlan MSF (1981) Aging and simple renal cysts of the kidney. Br J Rad 54:12–14
2. Rockson SG, Stone RA, Gunnells JC Jr (1974) Solitary renal cyst with segmental ischemia and hypertension. J Urol 112:550–552
3. Holmberg G, Hietala SO (1989) Treatment of simple renal cysts by percutaneous puncture and instillation of bismuthphosphate. Scand J Urol Nephrol 23:207–212
4. Hubner W, Pfaf R, Porpaczy P (1990) Renal cysts: percutaneous resection with standard urologic instruments. J Endourol 4:61–64
5. Hanna RM, Dahniya MH (1996) Aspiration and sclerotherapy of symptomatic simple renal cysts: value of two injections of a sclerosing agent. AJR Am J Roentgenol 167:781–783
6. Porpiglia F, Morra I, Rocca A et al (1996) Percutaneous alcoholization of simple serous cysts of the kidney. Arch Ital Urol Anrol 65(suppl 5):197–199
7. Amar AD, Das S (1984) Surgical management of benign renal cysts causing obstruction of the renal pelvis. Urology 14:429–433
8. Ilkka P et al (2001) Treatment of renal cysts with single session percutaneous drainage and ethanol sclerotherapy: long term outcome. Urology 57(1):30–33
9. Martino P, Palazzo S, Crudele V, Benedetto G, Tedeschi M, Bettocchi C, Ditonno P, Lucarelli G, Selvaggi FP (2010) Echoguided treatment of simple renal cysts: our experience from 1995 to 2010. Arch Ital Urol Androl 82(4):284–286

Part II

The Male Pelvis, Ureters and Urethra

Ultrasound Study of the Ureters and Intrarenal Excretory Tract

16

Paolo Rosi, Giovanni Rosi, Paolo Guiggi, and Michele Del Zingaro

Ultrasound was long considered inadequate to assess the ureter. More recently, advances in ultrasound devices, together with the increased interest of operators in this method, have partly modified this view. However, some elements that can make the examination difficult still need to be taken into account, such as the ureter's deep position in the peritoneum and the interference of the bowel loops and contents.

Visualization of a normal, non-ectatic ureter is possible in some conditions (thin subject, little bowel gas) but by no means certain. If it is only slightly ectatic (diameter greater than 4 mm), the proximal tract below the junction is easy to visualize in most cases. The iliolumbar tract is always difficult to view because of the presence of intestinal gas. The terminal vesicoureteral tract is normally easy to see even without dilation. The ectatic ureter appears as a transonic tube-like structure delimited by a thin parietal hyperintense echogenic stripe. In some conditions, periodical variations of its caliber may be evident due to peristalsis that can sometimes be particularly strong (obstacle peristalsis). In any case, because it is noninvasive, ultrasound plays a very important role in the assessment of diseases of the ureter.

Ultrasound was long considered inadequate to assess the ureter. More recently, advances in ultrasound devices, together with the increased interest of operators in this method, have partly modified this view. However, some elements that can make the examination difficult still need to be taken into account.

The ureter's deep position in the peritoneum and the interference of the bowel loops and contents can make the examination difficult. In normal, non-ectatic conditions, imaging of the ureter by ultrasound can be inconstant, apart from the tract immediately below the junction and the terminal vesicoureteral tract. For ultrasound examination of the ureter to be possible, a certain degree of ectasia of the upper excretory tract is therefore necessary that can be defined as a diameter exceeding 4 mm. Naturally, failure to visualize the ureter at ultrasound may not be indicative of the absence of disease. In addition, ultrasound being a morphological investigation, it does not provide information on renal function (functionally excluded kidneys). So even

P. Rosi (✉)
Private Practice, Perugia, Italy
e-mail: giovannirosi1@hotmail.it

G. Rosi
Division of Radiology 2, Department of Surgical and Biomedical Sciences, Perugia University, Santa Maria della Misericordia Hospital, Perugia, Italy

P. Guiggi • M. Del Zingaro
Urological and Andrological Clinic, University of Perugia, Dir: Prof. M. Porena, Square Menghini 1, Perugia 16100, Italy
e-mail: micheledelzingaro@tin.it

P. Martino, A.B. Galosi (eds.), *Atlas of Ultrasonography in Urology, Andrology, and Nephrology*,
DOI 10.1007/978-3-319-40782-1_16

nowadays it is essential to perform diagnostic imaging techniques with contrast medium (CT, MRI) and endoscopy (ureteropyeloscopy) to study the upper urinary tract.

For ultrasound studies of the ureter, the classic probes for abdominal use are employed (convex and, in particular conditions, linear) with an optimal frequency of 3.5 mHz. To study the urinary tract in kidney transplant patients, a 5 mHz probe may be used. Because the organ is located deep inside the peritoneum, as pointed out above, patient preparation may be justified, consisting of a fiber-free diet and the administration of bowel absorbents for the 3 days prior to the investigation, as well as fasting for 5–6 h before. However, thanks to the high level of definition of the ultrasound tools now available, this preparation is nearly always superfluous. A sufficient bladder distension is always necessary. As regards the ultrasound technique, it will vary according to the ureteral segment to be assessed. To examine the proximal subjunctional ureter, the patient is placed in supine decubitus or inclined contralaterally with the hip slightly raised. The scans made in this case are the anterior longitudinal, lateral longitudinal, or oblique posterior longitudinal. The iliolumbar ureter can be studied in supine decubitus or at a contralateral angle of about 30–40°, pressing the probe into the flank or the lateral portion of the mesogastrium and making anterior longitudinal or oblique anterior scans. Very useful reference points in this case are the common iliac vessels; the latter should be firstly viewed in longitudinal scanning and then transverse or oblique. This makes it possible to view even a ureter with minor ectasia at the point where it crosses the iliac vessels and passes anteriorly to them. The ureteral tract running from about 2 cm below the iliac vessels down to 3–4 cm from the ureteral ostium is certainly the segment that is most difficult to visualize because of its deep position and of the interference of bowel contents even if there is a sufficient degree of ectasia. For the vesicoureteral and intramural ureter, the technique is the same as for the study of the bladder. The patient is placed in supine decubitus, and a preliminary transverse scan is made at the bladder base, so as to visualize the ureteral ostia that appear as two small symmetrical raised areas on each side of the trigone. Then the investigation proceeds from axial to oblique scanning bilaterally so as to view the terminal ureters, shown as transonic tubular structures that cross the bladder wall. To sum up, imaging of the normal non-ectatic ureter is to be considered inconstant but possible in certain conditions (thin subject, minor bowel gas). If even moderately ectatic (with a diameter exceeding 4 mm), it can more easily be seen in most cases, at least as far as the subjunctional tract is concerned. The iliolumbar tract is always very difficult to visualize due to the presence of bowel gas. The terminal, vesicoureteral tract is easy to see in most subjects even if there is no dilation [1].

The ectatic ureter presents as a transonic tube-like structure delimited by a thin hyperintense echogenic parietal stripe. In some conditions, periodical variations of its caliber may be evident due to peristalsis that can sometimes be particularly strong (obstacle peristalsis).

The forms of ureteral disease that can be assessed by ultrasound are essentially the following:

- Stones
- Malformations
- Extrinsic compression
- Secondary neoplasia
- Primary neoplasia
- Specific or aspecific inflammation

Ureteral stones are undoubtedly the most common indication for ultrasound study of the ureter. The investigation allows assessment of the conditions of the urinary tract during the course of colic and can localize the presence and position of a stone in a high percentage of cases. It offers precise indications for any further imaging techniques to be carried out, as well as for the most suitable therapeutic solutions (extracorporeal lithotripsy, endoscopic, percutaneous, surgical procedures). It also makes it possible to monitor variations in volume and position of the stone after extracorporeal lithotripsy. The ultrasound images of ureteral stones are always typical and diagnostic, showing an ectatic ureteral

tract that abruptly thins at one or more points, with endoluminal echo-reflecting formations (Fig. 16.1). If the ureteral ectasia continues beyond the stone that has a smaller caliber than the ureter at the point in question, it is reasonable to suppose that the stone is a secondary or in any case non-obstructive symptom. By extending the ultrasound exploration distally, it will then be possible to reveal the true cause of the obstruction (another wedged stone, inflammatory stenosis, or a tumor) (Fig. 16.2). By changing the patient's position, the mobility of the stone inside the lumen of the ectatic tract can be seen (Fig. 16.3). Using color and power Doppler, the so-called twinkle artifact is very useful for diagnostic purposes; this is an artifact shaped like a comet's tail, dyshomogeneous in color, that starts from the stone and outlines its acoustic shadow. The artifact may be attributable to the whirlpool motion of the urine around the stone (Fig. 16.4).

Ureteral malformations that can be seen with ultrasound scanning include:

- Megaureter
- Ureterocele
- Duplication of the upper urinary tract (a duplex renal district)
- Retrocaval ureter

In megaureter the ultrasound picture is generally aspecific, consisting of ureteral ectasia, associated or not with dilation of the pelvis and calyces. An ectatic ureter that suddenly narrows about 2–3 cm before the ureteral ostium is indicative of megaureter (Fig. 16.5).

By contrast, the ultrasound picture of ureterocele is surely diagnostic, showing a rounded transonic mass outlined by a thin echogenic wall, at the level of the ureteral ostium and protruding into the bladder lumen. In an ultrasound study of ureterocele, it is helpful to assess the bladder with only moderate-minor filling because if it is too distended, it could mask the ureter itself. Variations in the voIume of the ureterocele will be evident during ureteral peristalsis. There may be a concomitant ectasia of the entire upper urinary tract. Ureterocele may frequently be associated with a duplex upper urinary tract (ectopic ureterocele) often affecting the upper and less frequently the lower hemidistrict (Fig. 16.6).

As regards the presence of a duplex upper urinary tract, ultrasound has poor sensitivity unless there is ectasia. Elements that may raise the suspicion of a duplex district are an enlarged kidney, with a complete parenchymal septum at the level of the median third or at the limit between the median and the superior third. Often there is a marginal groove at the level of the septum, and color Doppler will sometimes show a duplicated vascular pedicle. If the system is ectatic, a transonic mass can be seen at the upper pole of the kidney, due to ectasia of the upper district, from which the dilated ureter can be seen to emerge, often with an ectopic ostium (bladder neck, proximal urethra) (Fig. 16.7).

In the case of a retrocaval ureter, a rare congenital malformation, ultrasound has reduced specificity and cannot be considered diagnostic. Suspicious signs include an ectatic ureter that tends to have a horizontal course at the subjunctional or lumbar level, crossing the inferior vena cava posteriorly. In any case, a definitive diagnosis must be made with CT or MRI (Fig. 16.8).

For primary ureteral tumors, too, the ultrasound picture is generally aspecific and rarely allows an immediate diagnosis to be made. Generally, some degree of ureteral ectasia is shown, above a markedly stenotic tract. In some cases it may be possible to see a vegetative mass protruding into the ureteral lumen and sometimes infiltrating the periureteral tissues.

The ureter may be a secondary location of a tumor arising in the surrounding organs or structures. Tumors that most frequently involve the ureter include:

- Bladder tumors
- Prostate tumors
- Gynecological tumors
- Bowel tumors
- Retroperitoneal tumors

The most common case is surely a bladder or prostate tumor that, in an advanced stage, infiltrates the ureteral ostia. It is usually easy to visualize the mass infiltrating the bladder wall at the

level of the ostium, because it will cause some degree of ectasia of the overlying ureter. The ureter can also be involved in various neoplastic diseases of the retroperitoneum (lymphadenomegalies of various origins, retroperitoneal sarcomas). On the basis of ultrasound findings alone, it may be difficult to establish the ureteral tract involved or possibly just compressed (Figs. 16.9 and 16.10).

Also in the case of ureteral inflammatory diseases, ultrasound yields only an aspecific picture of stenosis or wall irregularities, but does not generally help to identify the nature of the problem. In most cases of inflammation of the ureteral wall, there will be thickening of up to 2–3 mm, showing a triple layer: hyperintense, intermediately hypointense, and then again hyperintense. An uncommon form of ureteral inflammation is cystic parietal dysplasia of the upper urinary tract (cystic pyeloureteritis), whose etiology is not yet entirely understood but is thought to be autoimmune. This is characterized by the presence of countless millimetric cystic formations on the pelvic wall and ureters, even bilaterally. The ultrasound picture features wall thickening, often very pronounced, sometimes extending along the entire tract, from the bladder to the calyces. Owing to the hematuria that this disease provokes that may also be massive, there may be endoluminal clots. In initial forms, differential diagnosis with urothelial tumors may be difficult.

Iatrogenic lesions of the ureter can occur during maneuvers of endoscopic (both diagnostic and therapeutic) or endourological type, during ureteral, prostate-vesical, obstetric, and gynecological surgery. Stenosis is the iatrogenic injury most frequently observed at ultrasound that can sometimes be secondary to a ureteral stone.

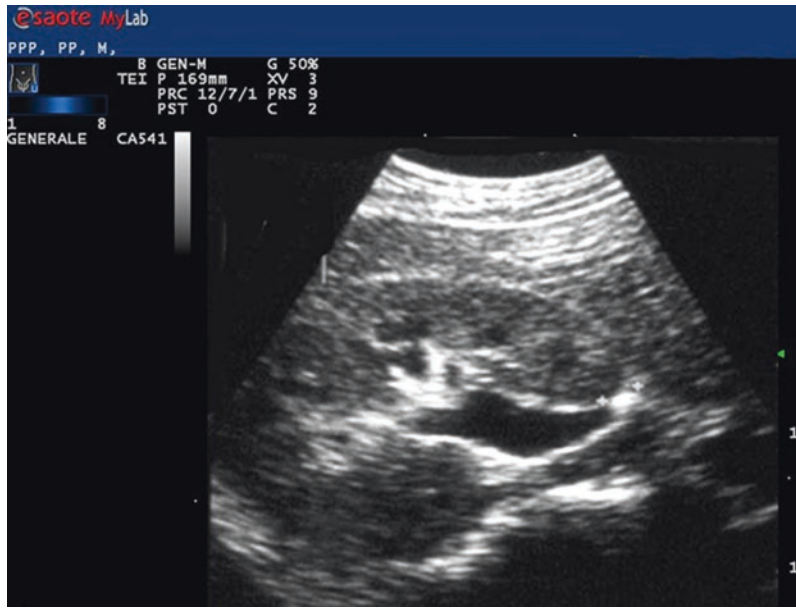

Fig. 16.1 A stone in the subjunctional tract of the right ureter

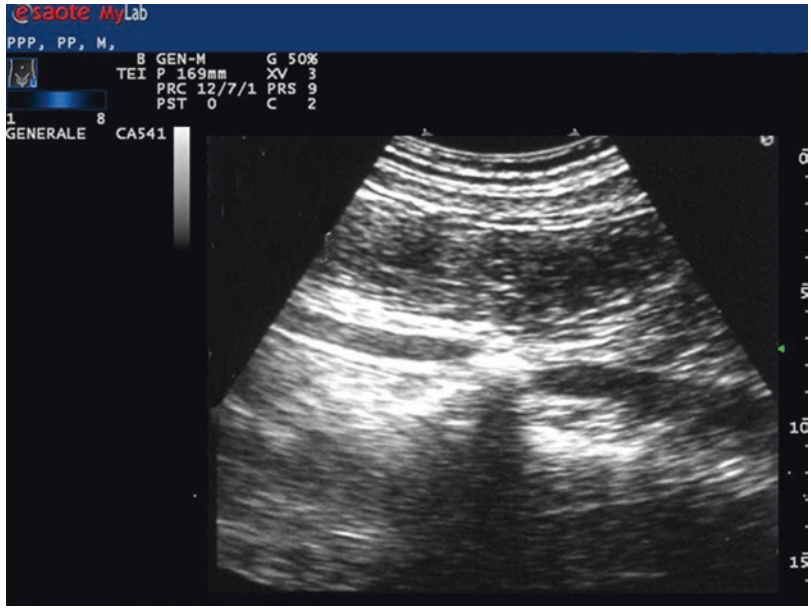

Fig. 16.2 A stone in the lumbar tract of the left ureter. The ureteral ectasia continues beyond the stone (possible distal obstruction)

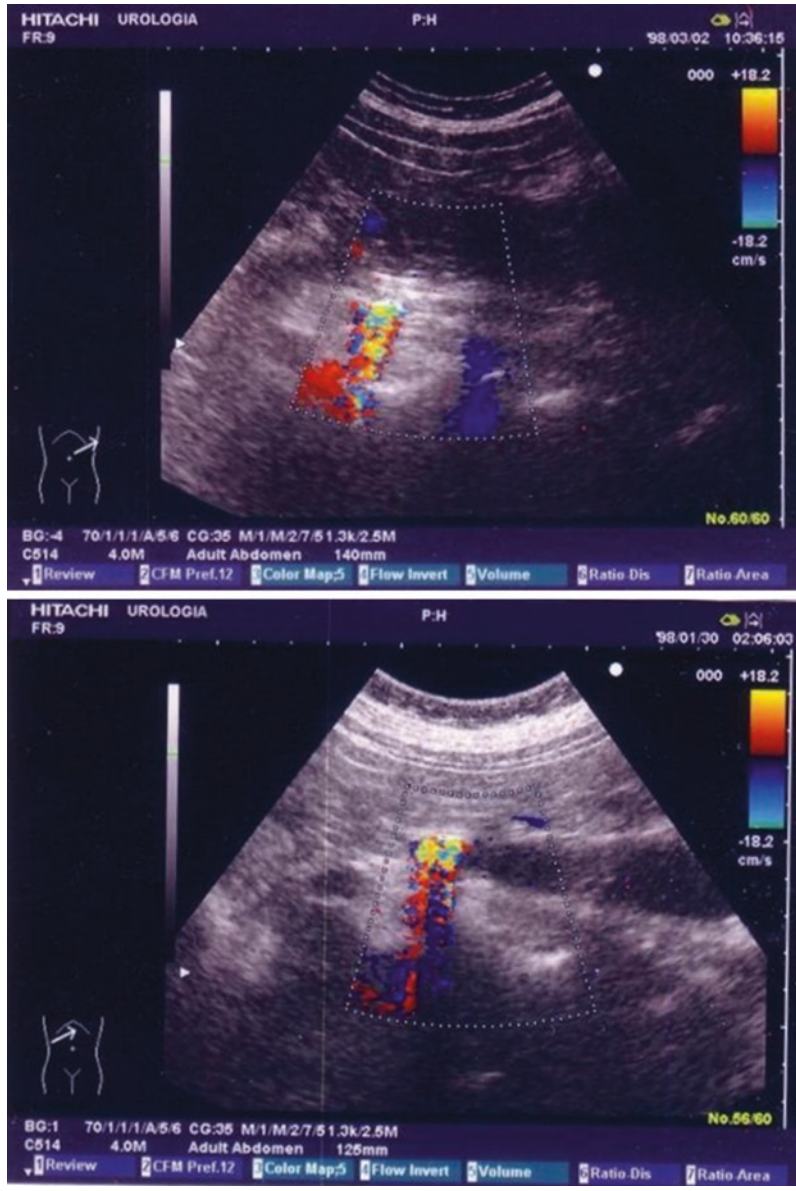

Fig. 16.3 Ultrasound study with diuretic test of the right ureter, secondary to a ureteral stone that is mobile inside the lumen. The patient underwent right ureterocystoneostomy with reimplantation of the ureter on the bladder dome and stenosis of the anastomosis

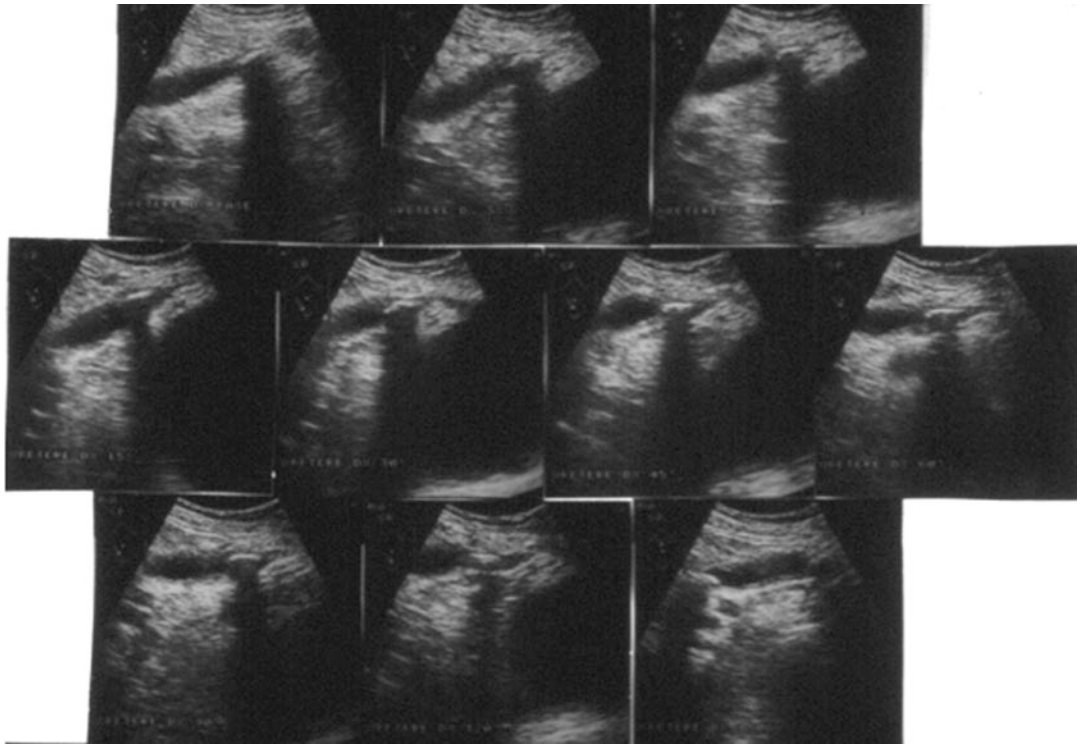

Fig. 16.4 Twinkle artifact, a stone in the left lumbar ureter

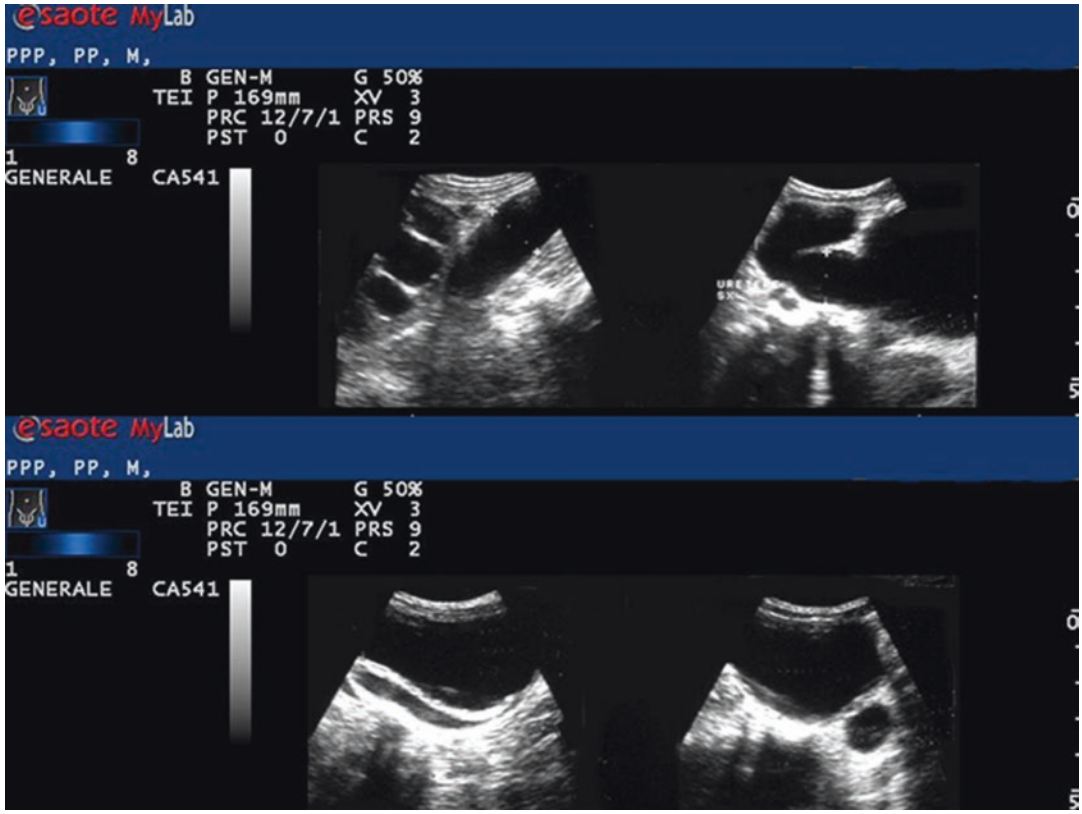

Fig. 16.5 Picture of a megaureter in a pediatric patient, showing marked ureterohydronephrosis with narrowing of the terminal ureter about 3 cm from the ostium

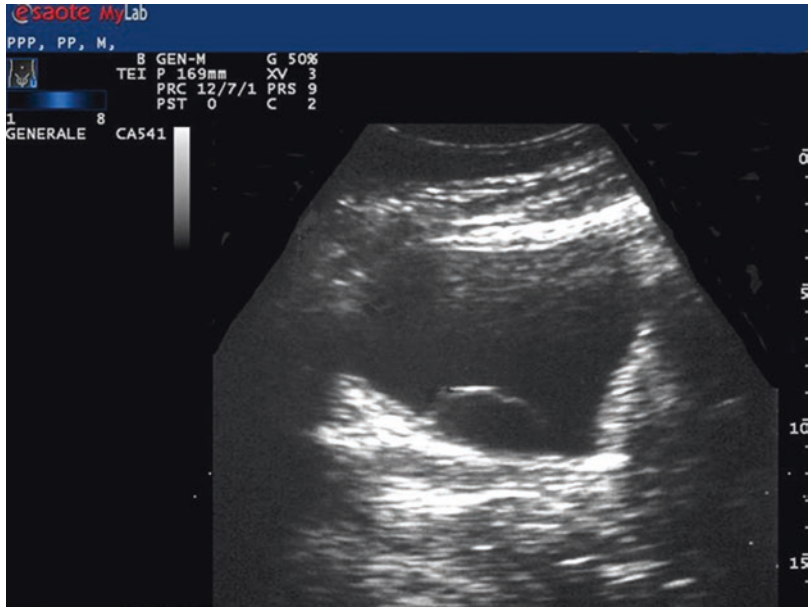

Fig. 16.6 Right ureterocele

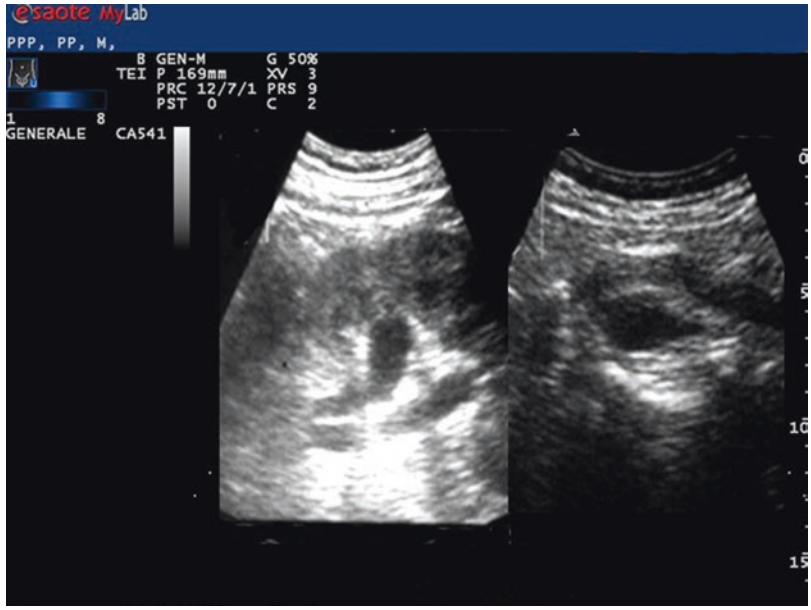

Fig. 16.7 Incomplete dual left upper urinary tract; the ureters are seen to be ectatic up to the point of confluence, immediately above the crossing of the iliac vessels. The system is visible owing to the presence of a stone wedged in the distal ureter at the confluence point, below the crossing of the iliac vessels

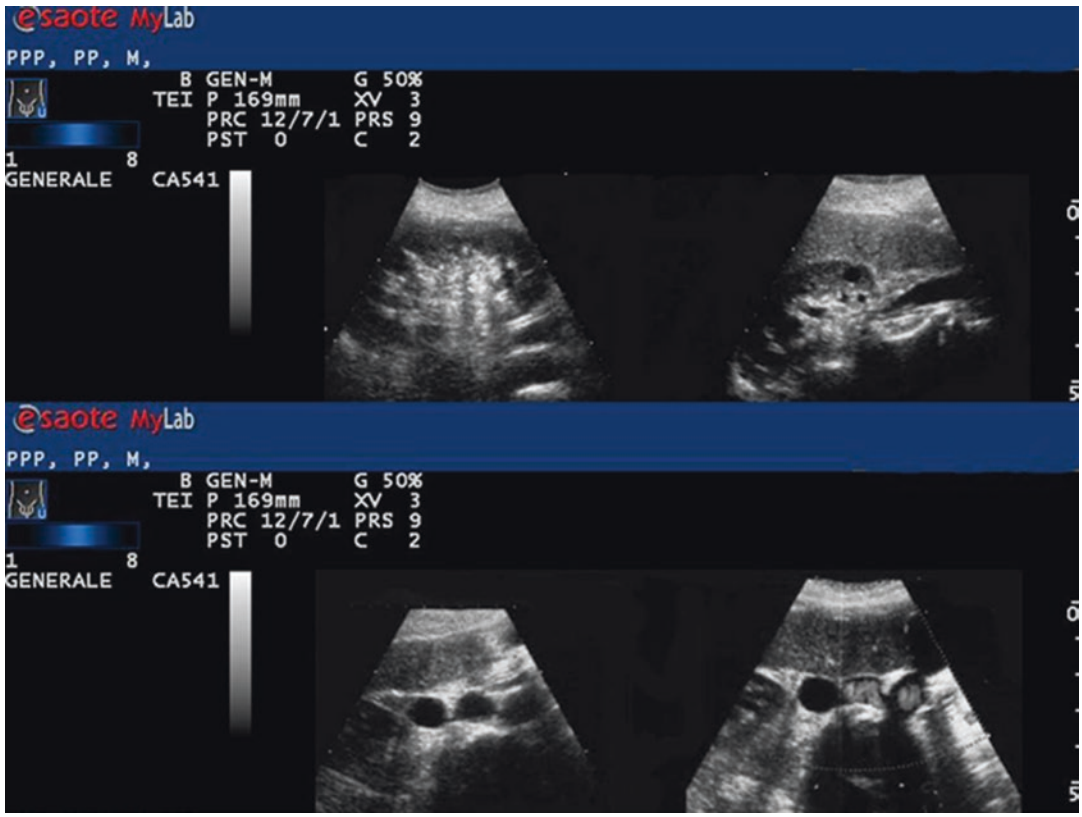

Fig. 16.8 Retrocaval ureter

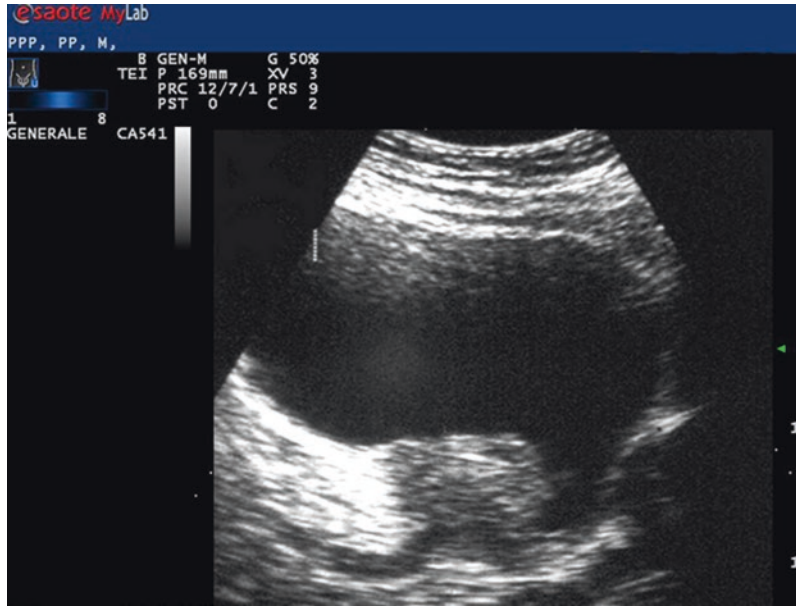

Fig. 16.9 Bladder tumor with full-thickness infiltration of the bladder wall up to the pericystic adipose tissue and the right ureteral ostium

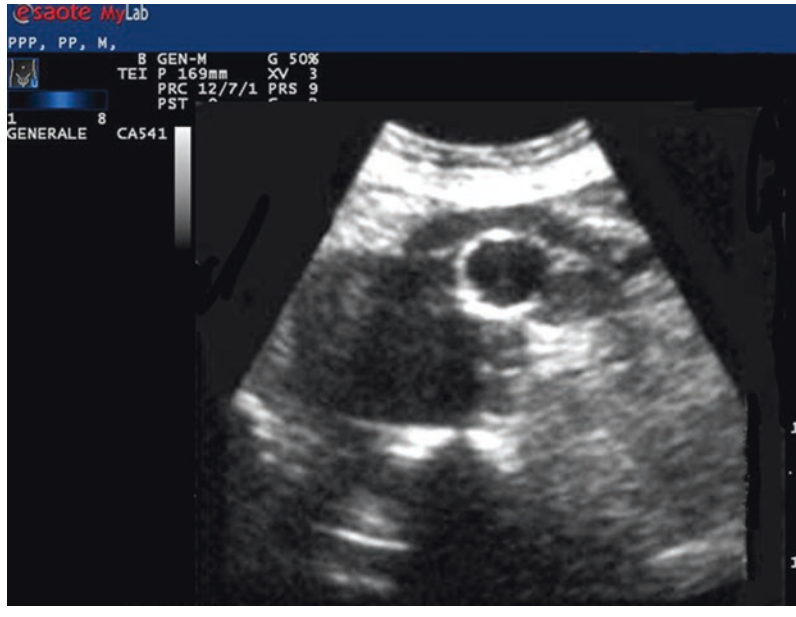

Fig. 16.10 Left ureterohydronephrosis due to compression of the sub-iliac ureter by a voluminous lymphadenomegaly

16.1 Ectasia of the Upper Urinary Tract During Pregnancy

A significant incidence of ectasia of the upper urinary tract has been demonstrated during pregnancy (in about 60 % of subjects in the third trimester). A series of concomitant factors, both mechanical (compression by the uterus) and hormonal (progesterone reduces the smooth muscle tone of the urinary tract), underlie this finding. It is prevalent on the right side, mainly because of the transverse crossing of the ureter and the right common iliac artery, so that the ureter compresses itself at this level. A less likely possibility is compression by the ectatic tributary veins of the right ovarian vein.

As regards the role of ultrasound in the diagnosis of vesicoureteral reflux, it is not currently considered a first-line investigation, although it is still complementary to traditional radiology and scintigraphy. The main indication can be contrast medium-enhanced cystosonography in pediatric patients [2].

In conclusion, ultrasound cannot be considered an alternative to radiological methods with contrast medium and endoscopic techniques for the study of the ureter. Nevertheless, it does have a role as first-line investigation in patients with a suspected ureteral stone, since it can show calculi in a high percentage of cases. It is useful for patients' selection for subsequent imaging or endoscopic techniques (URO-CT, URO-MRI), providing precise indications for the performance of these. In some cases it can integrate the information provided by these other investigations, if they do not yield significant findings. Moreover, it is useful in all cases requiring frequent controls at close intervals (extracorporeal lithotripsy or surgical-endoscopic treatments for ureteral diseases) [3].

References

1. Rosi P (1992) Uretere normale e patologico. In Campani R, Gortenuti G, Micali M, Talia B (eds) Ecografia dell'apparato urogenitale, Minerva medica, Italy, pp 139–145
2. Adibi A et al (2013) Value of sonography in the diagnosis of mild, moderate and severe vesicoureteral reflux in children. Saudi J Kidney Dis Transpl 24(2): 297–302
3. Komiakov BK, Strokova LA (2011) Classification of hydroureteronephrosis by ultrasonography findings [Russian]. Urologia (2):13–19

Functional Ultrasound Study of the Upper Excretory Tract

17

Paolo Rosi, Giovanni Rosi, Paolo Guiggi, and Michele Del Zingaro

Dynamic US study with diuretic challenge test is easy to perform but consists of various phases. Firstly, a bilateral renal examination is made, along various scanning planes after setting a scanning base bilaterally that is usually the oblique posterior longitudinal plane. This allows optimal visualization of the intrarenal excretory tract and renal pelvis, similar to the classic urographic images. Then a diuretic challenge test is performed after infusing 40 mg furosemide, and scanning is done at precise times to assess the dilation of the excretory tract and any modifications. With this method it is possible to assess any presence and the true degree of obstruction of the upper urinary tract [1].

Today, ultrasound (US) is still considered one of the most valid methods for diagnostic and preoperative assessment of ectasia of the upper urinary tract. It has extremely high sensitivity (nearly 100 %) in the assessment of hydronephrosis, associated with a very low number of false positives that are in most cases lipomatosis of the pyelic sinus and parapyelic cysts, and an equally low incidence of false negatives, in cases of so-called intermittent hydronephrosis.

An important limit of US when evaluating obstruction of the upper urinary tract is the difficulty in making a functional assessment. Over the years, many investigations have been adopted to define the presence, and within limits also the degree, of upper urinary tract obstructions. We briefly list below some of the methods employed, many of which are no longer in use in clinical practice but that still have a historical interest.

Radiological methods

- Urography with diuretic challenge
- Urography in the acute phase
- Dynamic urographic studies (spot camera roentgen cinematography)
- Spiral CT

P. Rosi (✉)
Private Practice, Perugia, Italy
e-mail: giovannirosi1@hotmail.it

G. Rosi
Division of Radiology 2, Department of Surgical and Biomedical Sciences, Perugia University, Santa Maria della Misericordia Hospital, Perugia, Italy

P. Guiggi • M. Del Zingaro
Urological and Andrological Clinic, University of Perugia, Dir: Prof. M. Porena, Square Menghini 1, Perugia 16100, Italy
e-mail: micheledelzingaro@tin.it

P. Martino, A.B. Galosi (eds.), *Atlas of Ultrasonography in Urology, Andrology, and Nephrology*,
DOI 10.1007/978-3-319-40782-1_17

Radioisotopic methods
- Sequential renal scintigraphy
- Radionephrogram with diuretic challenge
- Measurement of parenchymal transit time

Urodynamic methods
- Vela Navarrete test
- Pyelomanometry with Whitaker test

Combined methods
- Pyelomanometric study with radiological monitoring
- Pyelomanometric study with radioisotopes

Despite this large number of diagnostic tests made to assess obstructive urinary tract disease, a sufficient diagnostic reliability has not yet been achieved. As long ago as 1982, Gillenwater had declared "in my opinion, there is no single best test to define whether upper dilatations represent significant obstruction."

Limiting the assessment only to the three methods most commonly used (radiological study with contrast medium and diuretic challenge test, radionephrogram with diuretic challenge test, and pyelomanometry), an overall accuracy of about 90–95 % is obtained, but only when associating two of these three methods. Error most frequently arises in cases of intermittent hydronephrosis, in cases of a high-compliance renal pelvis and of atypical decline curves. In particular, if peripyelic fibrosis is present, it can affect the reliability of radiological examinations with the use of contrast medium and a diuretic challenge test. Chronic and acute renal failure and renal vascular diseases induce error when employing both radiological methods and scintigraphic and radionephrographic methods. The latter investigations are also affected by concomitant infection, vesicoureteral reflux, and atypical decline curves. Situations of partial obstruction and intermittent hydronephrosis affect the results of almost all the previously cited methods (radiology, radionephrography, pyelomanometry). Already by the end of the 1980s, dynamic ultrasound studies with a diuretic challenge test had been introduced in order to obtain as reliable as possible an assessment of any obstruction of the upper urinary tract and, within limits, of the degree of the obstruction. The first studies were conducted by Rosenfield in 1980 and Bono and colleagues in 1987. The method of performance of the examination is simple but consists of various phases. Firstly, a bilateral renal examination is made, along various scanning planes after setting a scanning base bilaterally that is usually the oblique posterior longitudinal plane. This allows optimal visualization of the intrarenal excretory tract and renal pelvis, similar to the classic urographic images [2].

Then a rapid (about 20 min) intravenous infusion of 250 ml of physiological solution added with 40 mg of furosemide (dose valid for an adult weighing about 70 kg) is administered. Bilateral renal ultrasound scanning is then done, carefully maintaining the original scans, at 5, 10, and 15 min after the start of the infusion. At the end of the infusion, the patient is asked to urinate and then walk for a few minutes. Further ultrasound scans are then done at 30, 45, 60, 90, 120, and 150 min. To avoid retrostatic phenomena, the bladder must be kept as empty as possible (by frequent urination) throughout the examination. In subjects with nephroptosis, the US scans are done in both clinostatic and orthostatic position. In pediatric patients, the physiological solution will be proportional to the patient's weight, and the furosemide dosage must be 0.5 mg/kg. We can summarize the indications for dynamic ultrasound scanning of the upper urinary tract as:

Indication 1
- As a second-line investigation after previous diagnostic imaging (uro-CT, uro-MRI) showing ectasia of the upper urinary tract (a suspected obstruction located at any level from the calyces to the vesicoureteral junction)
- For suspected intermittent hydronephrosis (pain with clinical signs of a urological complaint but no kidney dilation at previous diagnostic imaging)

Indication 2
- As an alternative investigation to contrast-enhanced imaging if the latter is not possible (allergy to contrast medium, renal failure), in cases of ultrasound findings of pyeloureteral ectasia

- In the case of US findings of hypoechogenic or anechogenic areas of the renal sinus (DD between lipomatosis and peri- and parapyelic cysts versus ectasia of the intrarenal excretory tract) with no modifications of cystic formations under diuretic challenge and some degree of increase of the pyelocalyceal diameters in hydronephrosis
- Clinical situations in which ionizing radiation or contrast medium need to be limited or excluded (pregnancy, pediatric patients, follow-up after surgical, or endourological procedures on the upper urinary tract)

In short, the role of ultrasound with diuretic challenge (USDC) is to identify the presence and degree of any obstruction of the upper urinary tract. After analyzing the data obtained with this method, four types of observations have been identified and classified, ranging from a normal picture to a severe obstruction. In detail:

Normal pictures
- No modification of the intrarenal excretory tract after USDC (Fig. 17.1)
- Increased pyelocalyceal diameters with a return to basal conditions within 60' from the start of the examination (Fig. 17.2)

Pictures of non-obstructive urine stagnation (pyeloureteral hypotone)
- Return to basal conditions of various degrees of pyelocalyceal dilation between 60' and 90' (Fig. 17.3)

Pictures of a moderate degree of obstruction
- Return to basal conditions of various degrees of pyelocalyceal dilation between 90' and 150' (Figs. 17.4 and 17.5)

Pictures of severe obstruction
- None or mild pyelocalycectasia at baseline, increased pyelocalyceal diameters after USDC, and failure to return to basal conditions within 150' (Fig. 17.6)
- Hydronephrosis at baseline, increased pyelocalyceal diameters after USDC, and failure to return to basal conditions within 150' (Fig. 17.7)

To illustrate the reliability of the method, we report a case series of 150 patients (nine with a single kidney), assessing a total of 291 upper urinary tracts. Mean patients' age was 38.5 years; there were 52 male and 98 female patients. Any presence and the degree of obstruction of the upper urinary tract were defined on the results of multiple examinations and diagnostic findings (radiological and contrast-enhanced examinations with diuretic challenge test, pyelomanometry with Whitaker test, ureteral catheterization, intraoperative findings). The overall results of these investigations were compared to the results of ultrasound with the diuretic challenge test.

Patients' group with US findings of a return to basal conditions within 60' (indicative of a normal upper urinary tract)

- 156 cases
- Correct diagnosis in 147 cases (94.2 %)
- Incorrect diagnosis (false negatives) in nine cases of mild obstruction (5.7 %)

Patients' group with US findings of a return to basal conditions between 60' and 90' (indicative of non-obstructive stasis-pyeloureteral hypotone)

- 41 cases
- Correct diagnosis: 38 cases (92.6 %)
- Incorrect diagnosis: 3 cases (7.3 %)

One false negative (mild obstruction): 2.4 %
Two false positives (normal): 4.8 %

Patients' group with US findings of a return to basal conditions between 90' and 150' (indicative of moderate obstruction)

- 42 cases
- Correct diagnosis: 38 cases (90.4 %)
- Incorrect diagnosis: 4 cases (9.5 %)

Two false negatives (high-grade obstruction): 4.7 %
Two false positives (non-obstructive stasis): 4.7 %

Patients' group with no return to basal conditions within 150' (indicative of high-grade obstruction)

- 49 cases
- Correct diagnosis: 45 cases (91.8 %)
- Incorrect diagnosis (false positives)

Four cases, 8.1 %: three cases of mild obstruction and one case of non-obstructive stasis

Intermittent hydronephrosis: three cases correctly diagnosed (Fig. 17.8)

In our experience, USDC showed the following diagnostic reliability:

- Sensitivity: 91.24 %
- Specificity: 94.83 %
- Positive predictive value: 93.98 %
- Negative predictive value: 92.45 %
- Total diagnostic capacity: 93.15 %

As regards USDC in pediatric patients

(23 upper urinary tracts assessed in pediatric patients)

The diagnostic reliability was:

- Sensitivity: 91.66 %
- Specificity: 90.90 %
- Positive predictive value: 91.56 %
- Negative predictive value: 90.90 %
- Total diagnostic capacity: 91.30 %

In conclusion, ultrasound of the upper urinary tract with a diuretic challenge test showed a good reliability and diagnostic accuracy. Importantly, it is a noninvasive examination, with no contraindications, as well as being simple to perform and having good repeatability. It can be used as first-line assessment method in suspected obstructions of the upper urinary tract, reserving further investigations to doubtful cases [3].

Among the drawbacks we must include: the duration of the examination (about 2 h 30' overall), the cost (equivalent to that of ten kidney US examinations), the slight "operator dependency," and the poor reliability in cases with a reduced renal function. Moreover, it is difficult to interpret the findings in cases of mild obstruction (return to basal conditions between 90' and 150'), and in our hands it yielded 9.7 % of incorrect diagnoses [4].

As regards the use of this technique in pediatric patients, USDC is highly indicated for the study of the upper urinary tract due to its noninvasive nature. However, the technical performance may be difficult (problems in maintaining constant reference scans due to poor patient collaboration). For this reason, the reliability and diagnostic accuracy were slightly lower in our pediatric case series than in the adults.

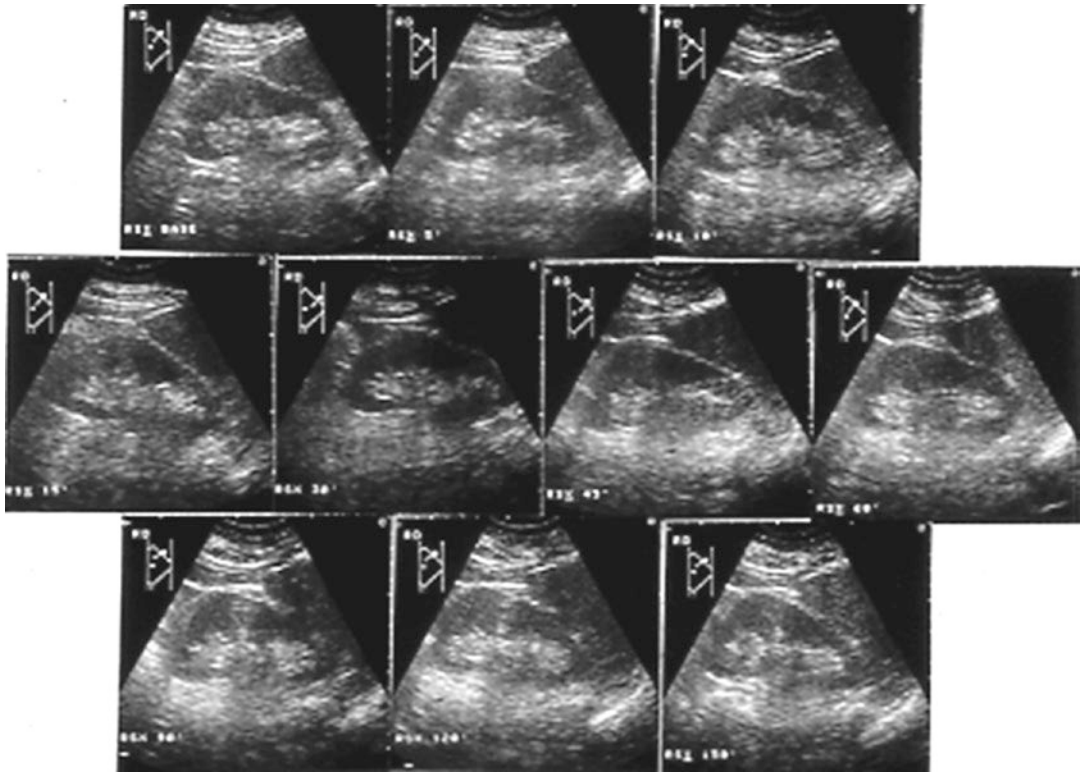

Fig. 17.1 Normal conditions; no evident modifications of the intrarenal excretory tract after the administration of a diuretic challenge test

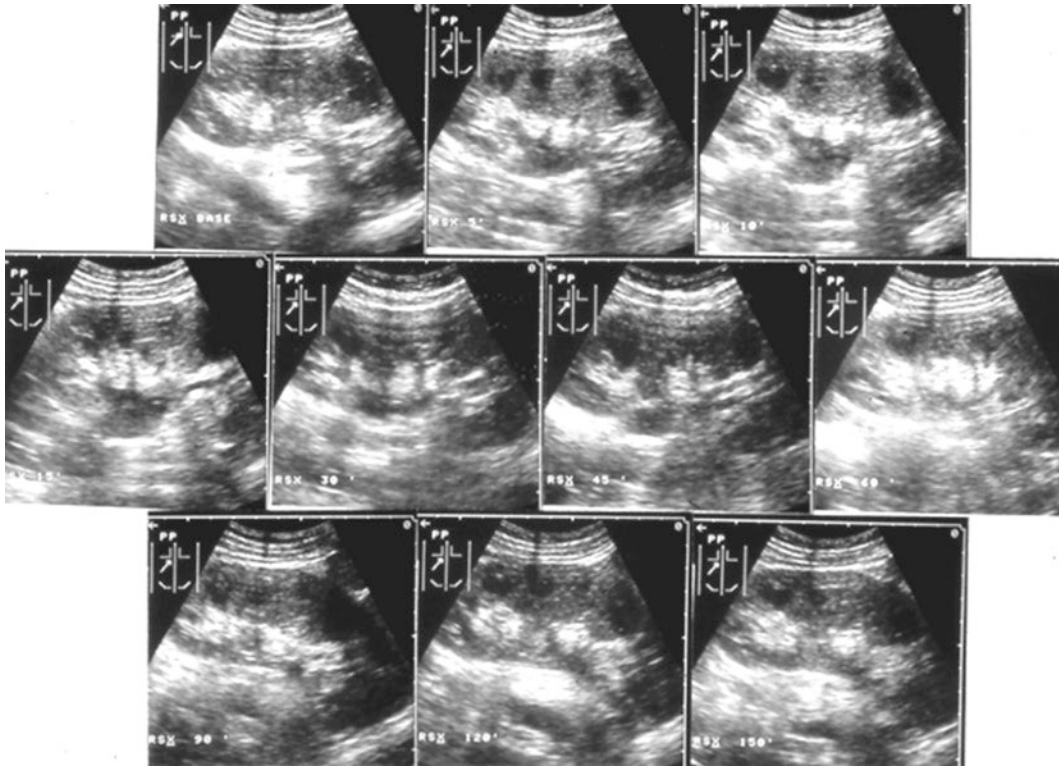

Fig. 17.2 Normal conditions, with a mild increase in pyelocalyceal diameters after USDC, and a complete return to basal conditions within 60'

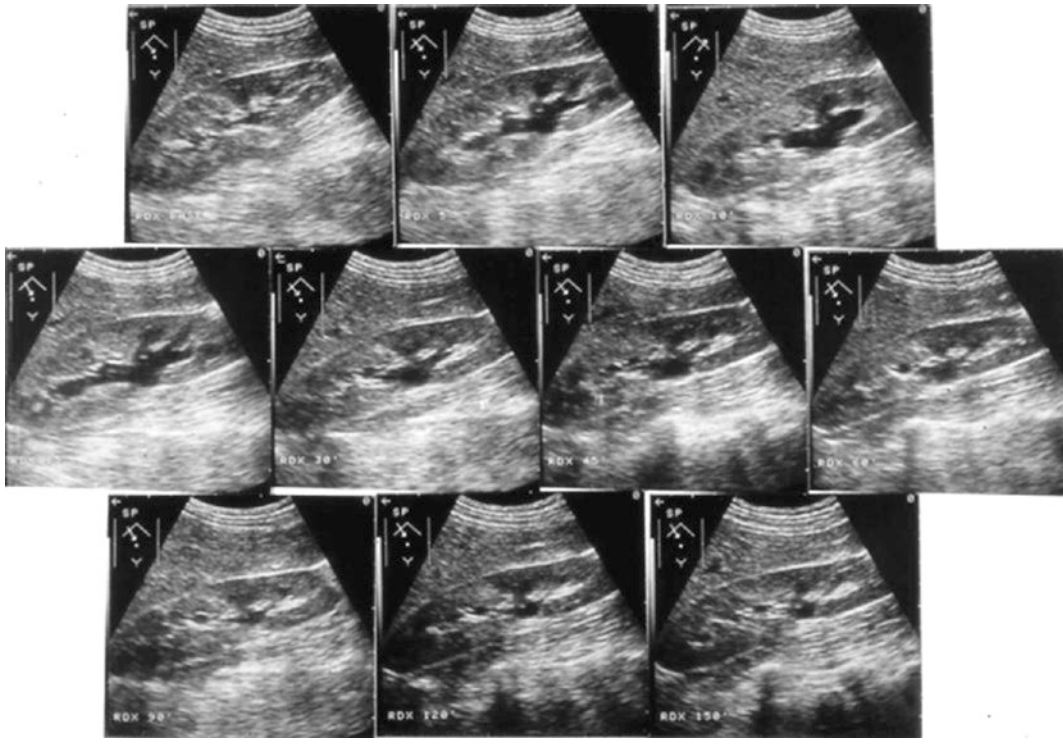

Fig. 17.3 Non-obstructive stasis conditions, with a mild increase in the pyelocalyceal diameters after USDC and return to basal conditions within 90'

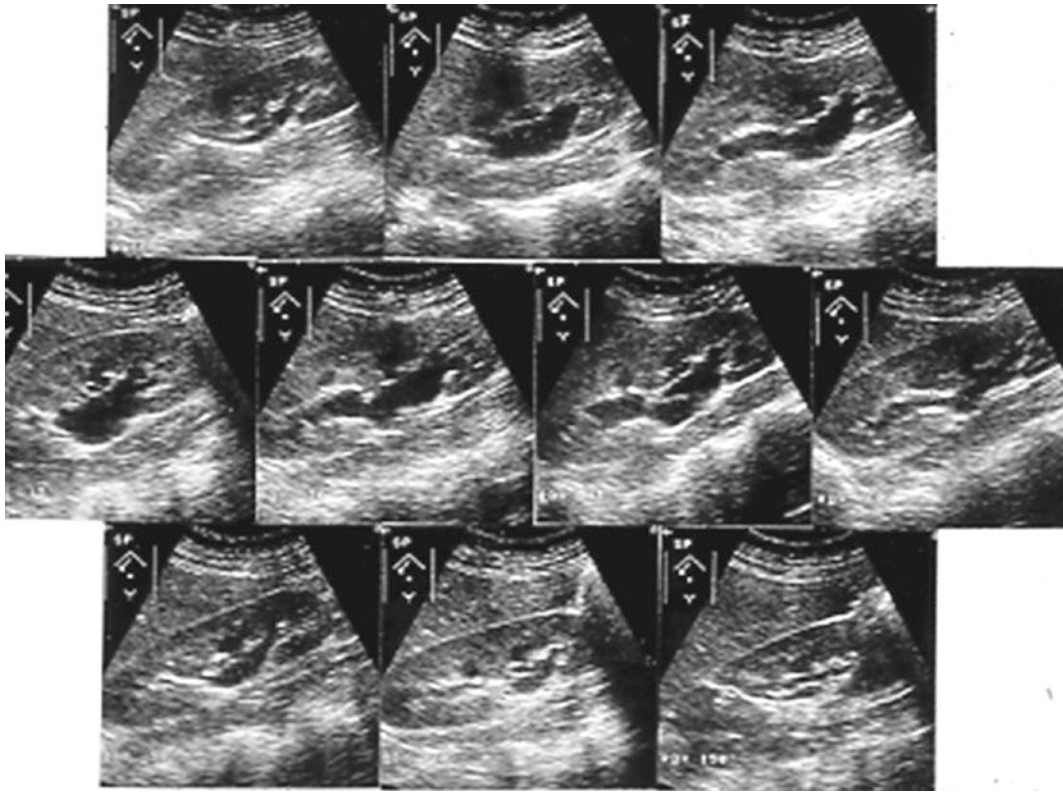

Fig. 17.4 Moderate obstruction, with very mild baseline pyelectasia that increased after USDC and returned to basal conditions by 150'

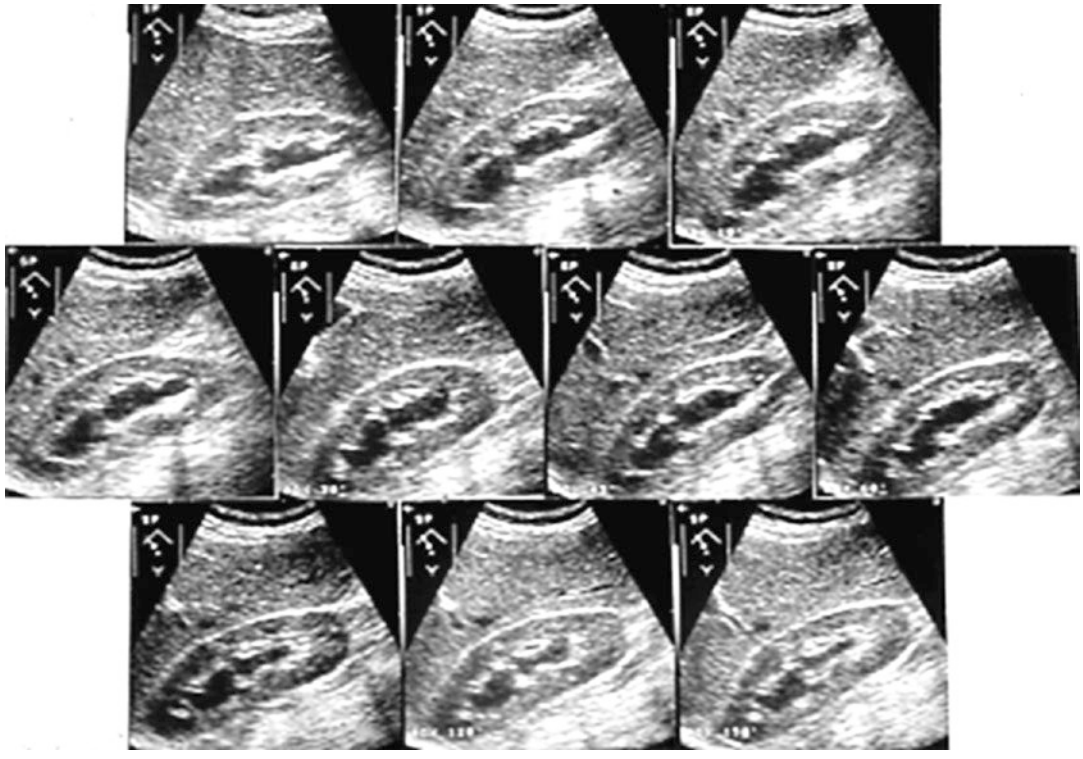

Fig. 17.5 Moderate obstruction with mild baseline pyelocalycectasia that increased after USDC and returned to baseline conditions by 150'

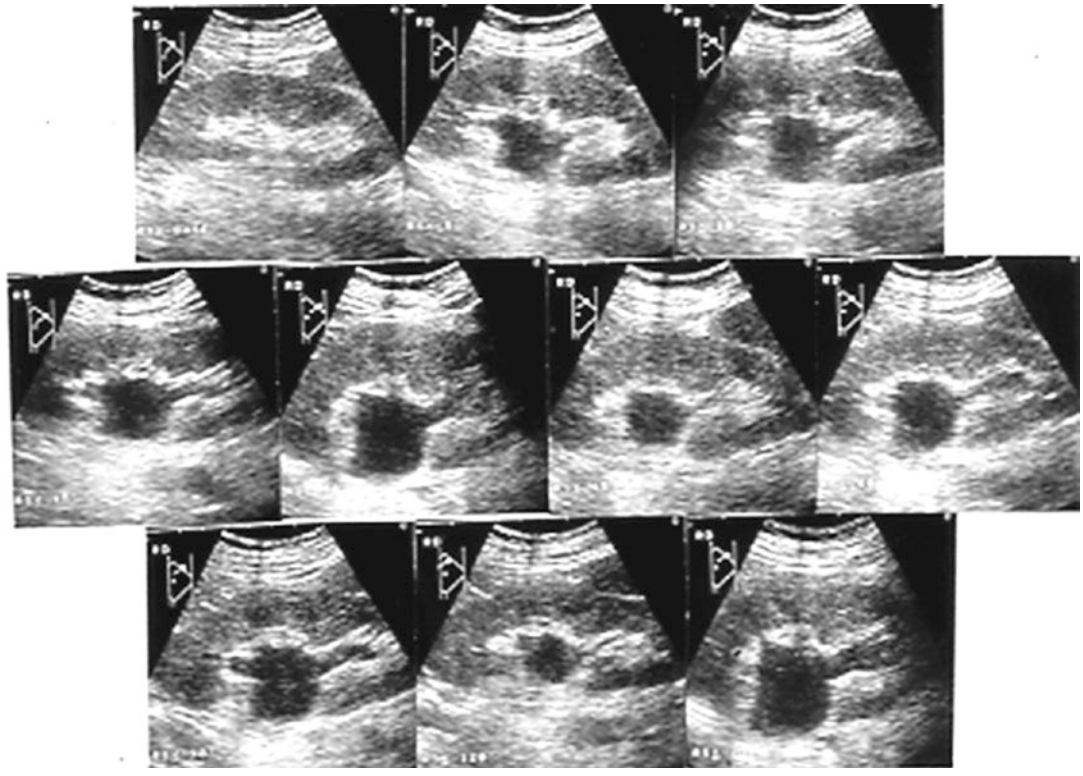

Fig. 17.6 Severe obstruction, the absence of ectasia of the intrarenal tract at baseline, increased pyelocalyceal diameters after USDC, and failure to return to basal conditions by 150' (tendance to intermittent hydronephrosis)

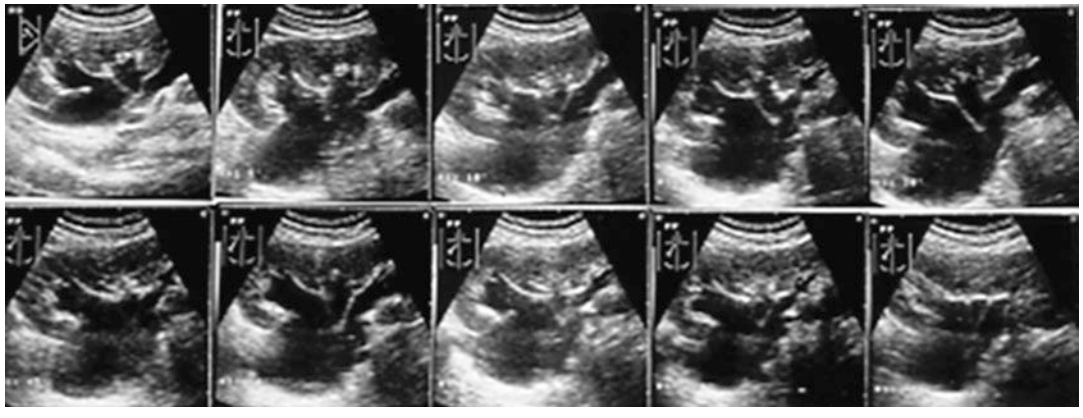

Fig. 17.7 Severe obstruction with baseline hydronephrosis (stenosis of the ureteropyelic junction) increased pyelocalyceal diameters after USDC and failure to return to basal conditions by 150'

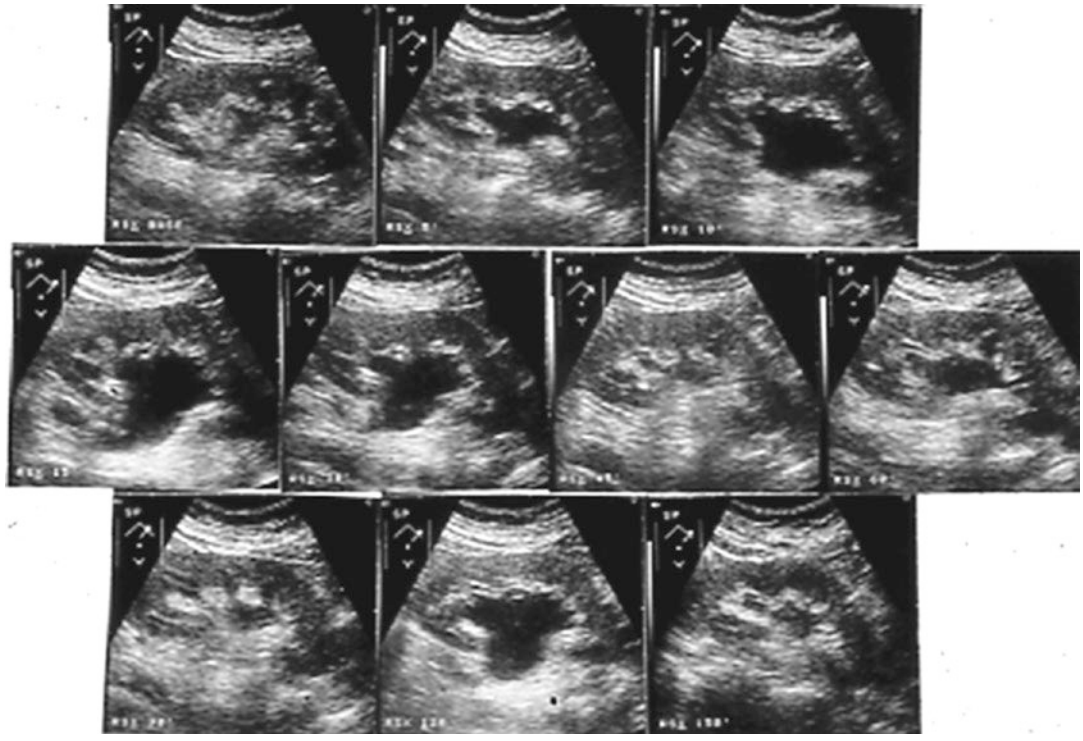

Fig. 17.8 Intermittent hydronephrosis. The patient has a neurological bladder

References

1. Rosi P et al (1990) Diuretic ultrasound. A non-invasive technique for the assessment of upper tract obstruction. Br J Urol 65(6):566–569
2. Bono AV, Bernacchi F, Fava F (1993) L'ecografia dinamica nella patologia pielo-ureterale. Urologia 53:918–921
3. Lombi R, Rosi P, Cesaroni M Una metodica ecografica di diagnosi dell'uropatia ostruttiva. In: Proceedings of the eleventh congress of the Italian Society of Urodynamics
4. Whitaker RH (1979) An evaluation of 170 diagnostic pressure flow studies of the upper urinary tract. J Urol 121:602–604

Ultrasound Study of the Urethra

18

Andrea B. Galosi and Lucio Dell'Atti

18.1 Anatomy of the Male Urethra

The male urethra is divided into two major sections: posterior and anterior separated by the urogenital diaphragm (Fig. 18.1).

The posterior urethra is composed of two anatomical segments: prostatic and membranous urethra. The prostatic urethra is almost entirely covered by the prostate gland (Fig. 18.2). The lumen of the posterior urethra is not enveloped by corpus spongiosum but covered by prostate and levator ani muscle. The membranous portion commences about 1 cm distally from the prostatic apex and lies within the urogenital diaphragm and encircled by the external urethral sphincter (levator ani muscles located laterally). Urethral stenosis is the term preferred to describe the narrowing of the urethral lumen that is not surrounded by corpus spongiosum, specifically the membranous and prostatic urethra [1].

The anterior urethra is composed of three anatomical segments: bulbar, penile urethra, and fossa navicularis/urethral meatus. The lumen of the anterior urethra is surrounded by the corpus spongiosum until the external meatus. The corpus spongiosum is covered by the deep fascia of the penis (Buck). The first segment of the anterior urethra is the bulbar urethra that is linked to membranous segment through the urogenital diaphragm. The bulbar urethra is fixed to the perineal membrane that covers the inferior part of the urogenital diaphragm. The corpus spongiosum of the bulbar segment is thick and elastic posterolaterally while rigid and thin superior-medially. During micturition, the intraluminal pressure stretches posterolaterally the expandable and elastic walls of the corpus spongiosum, and the lumen of the bulbar urethra increases significantly if compared to the penile urethra. The bulbar urethra is covered posterolaterally by the bulbospongiosus muscle and deep perineal (Gallaudet) and superficial perineal fascia (Colles) (Fig. 18.3). Ultrasound description of these fascial layers is feasible; however, it has limited clinical relevance. The penile urethra is fixed to the cavernous bodies of the penis and lies in the inferior part of the penile shaft. The penile urethra is fixed and covered by two fascial layers composed of the deep fascia of the penis (Buck) fused with deep perineal fascia and the superficial fascia of the penis. The junction between the bulbar and penile urethra is anatomically located just proximally to the penoscrotal angle. The third distal segment of the anterior urethra is the distal part of the penile urethra which enlarges into the navicular fossa completely

A.B. Galosi, MD (✉)
Institute of Urology, Marche Polytechnic University, Ancona, Italy
e-mail: galosiab@yahoo.it

L. Dell'Atti, MD
Institute of Urology, University of Ferrara, Ferrara, Italy

P. Martino, A.B. Galosi (eds.), *Atlas of Ultrasonography in Urology, Andrology, and Nephrology*,
DOI 10.1007/978-3-319-40782-1_18

covered by corpus spongiosum of the gland and then ends at the urethral meatus. Urethral stricture is the preferred term for narrowing of a segment of the urethra which is surrounded by corpus spongiosum, i.e., the urethral meatus to the bulbar urethra [1]. The severity of a urethral stricture is related to the amount of damage to the corpus spongiosum, the investing vascular layer of the urethra, resulting in a progressive process termed spongiofibrosis (Fig. 18.3b) [2, 3].

The ultrasound examination is not the up-front method to investigate the urethra, first, because distension is always required, and second, because ultrasound urethrogram is not able to study the lumen of the posterior segment which can be achieved only in few cases. Therefore, ultrasound is not a global study of the urethra, and retrograde contrast urethrography is the standard [4–6]. Nevertheless, ultrasound is the first diagnostic tool in the study of paraurethral soft tissues or perineal masses, because traditional contrast urethrography does not evaluate extraluminal lesion. Magnetic resonance is the gold standard in the imaging of the perineal soft tissues. Magnetic resonance has the potential to provide significant additional information for the staging of urethral and penile cancers [7].

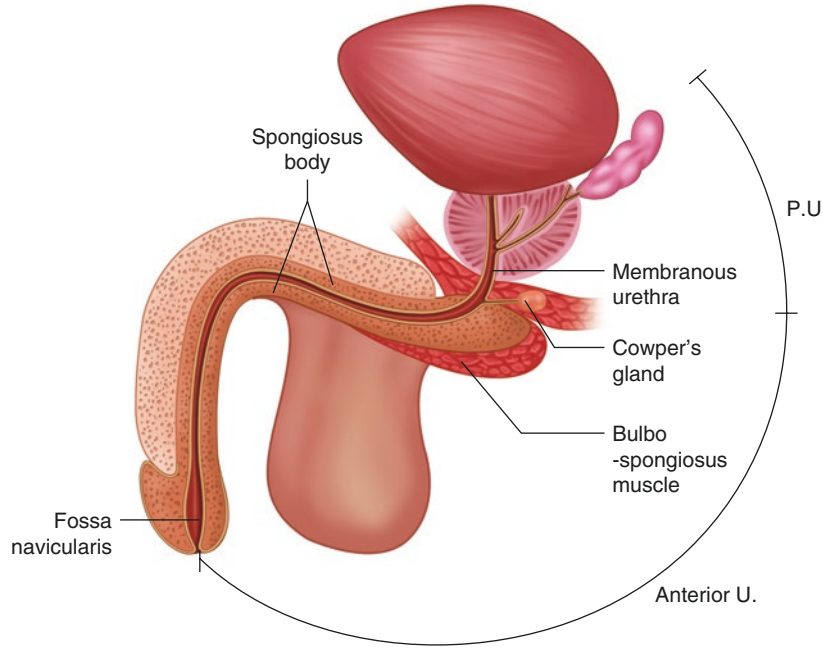

Fig. 18.1 Anatomy of the male urethra

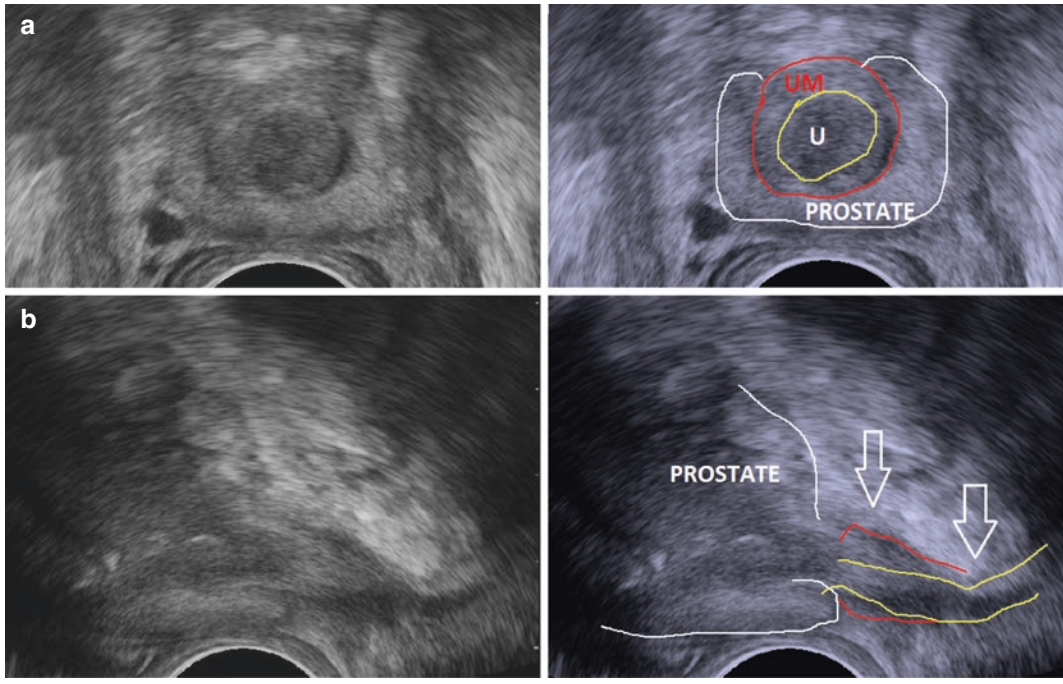

Fig. 18.2 The male posterior urethra covered by prostatic apex in axial (**a**) and longitudinal (**b**) view using end-fire transrectal probe

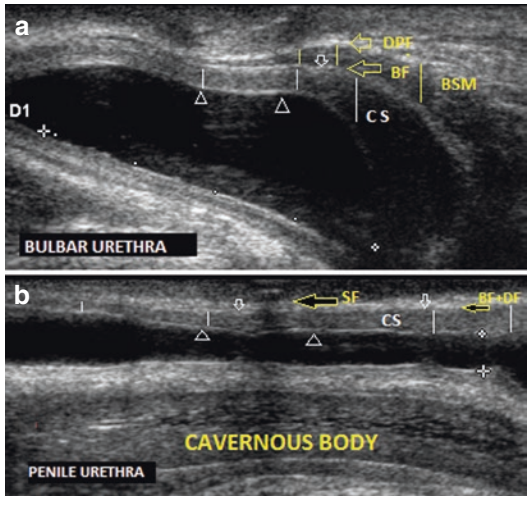

Fig. 18.3 (**a**) Normal bulbar urethra ultrasound. *White bar*, *CS* corpus spongiosum; *yellow bars*, *BSM* bulbospongiosus muscle, *DPF* deep perineal fascia, *SF* superficial fascia; *white arrows*, *BF* buck fascia, urethral epithelium (*arrowhead*). (**b**) Urethral stricture with spongiofibrosis

18.2 Ultrasound of the Male Posterior Urethra

Ultrasound of the posterior urethra, either transperineal scanning with a 3.5–5-MHz curved array probe or a transrectal probe, can be used. Distension of the posterior urethra is only well achieved by asking the man to void. However, some men may be unable to void because of inhibition. Overall posterior ultrasound urethrogram is much less reliable than micturating or descending contrast urethrography. Indications to posterior urethral ultrasound are vesicourethral anastomosis after radical prostatectomy, posterior urethra and bladder neck after surgery for benign prostatic hyperplasia, study of transurethral catheter placement or displacement, anatomy of Cowper's gland diseases, and anatomy after pelvic trauma (Tables 18.1 and 18.2).

Table 18.1 Filling defects in the urethra

Intraluminal – calculi, foreign bodies, bezoar or hair ball, blood clot
Congenital anatomical – posterior urethral valve, ureterocele
Benign lesion congenital or acquired urethral polyp
Benign inflammatory lesions – urethritis cystica
Malignant lesions – solid tissue or papillary/soft tissue

Table 18.2 Classification of posterior urethral trauma based on site of injury [16]

Grade	Clinical findings
I	Posterior urethra stretched, but integrity is maintained
II	Tear of the membranous urethra, above the urogenital diaphragm
III	Partial or complete tear of both anterior and posterior urethra, with disruption of the urogenital diaphragm
IV	Bladder injury extending into the urethra (IVa) injury of the bladder base, with periurethral extravasation

18.3 Ultrasound Urethrogram of the Male Anterior Urethra

The primary imaging modality for demonstrating the male anterior urethra is fluoroscopic contrast urethrography performed either as a retrograde study via catheter insertion into the distal urethra. The main advantages of the technique are that it has a high sensitivity for the detection of urethral strictures and that the images obtained are easy to interpret for the non-radiologist. However, there are a number of disadvantages, including the fact that it may not be possible to catheterize the distal urethra, particularly in patients with external meatus narrowing or previous surgery. Also, the technique is necessarily invasive, and interpretation may be hampered by the presence of air bubbles, which may obscure pathology or even provide a false-positive study. In addition, as the balloon of the catheter is inflated in the distal urethra, pathology in this area will not be identified.

Ultrasound urethrogram is a suitable technique for visualizing the male anterior urethra, but it cannot replace contrast urethrography. Ultrasound could be strongly considered as follow-up option in the man with known anterior urethral stricture [8, 9].

However, early studies identified not only the ability of ultrasound to demonstrate the exact length of strictures but also the added ability to define the periurethral tissues, as opposed to contrast urethrography, which only demonstrates the lumen. In particular, the presence and degree of periurethral fibrosis can be shown with a view to guiding surgery [10]. The initial experiences with ultrasound evaluation of the urethra were described separately in the late 1980s by McAninch et al. [5] and Merkle and Wagner [11].

A linear probe for superficial tissue, such as 7.5–12 MHz, with an array length of 4 cm or more, is used with direct skin contact along the ventral surface of the penis. The most used method is to distend the urethra using either a Knutson's clamp or a Foley catheter with the balloon distended in the navicular fossa. The urethra is distended using saline. We use a large syringe with saline 60 cc and manual compression on the gland to distend the urethra during ultrasound. Contrast media, unlike saline, may obscure intraurethral bodies/calculi. The anterior distended urethra is scanned in the transverse and longitudinal planes: description of smoothness of the urethral mucosal lining and narrowings of the lumen are noted; measure in length is carefully reported (Figs. 18.3 and 18.4). Strictures and subtle wall irregularities of the anterior urethra are analyzed after distension of the urethra with saline, using a flat array ultrasound probe.

The ability to visualize the stricture as well as the corresponding surrounding wall thickness change is an advantage of this technique over contrast urethrography. Whether this additional information is of clinical value in the selection of appropriate stricture therapy has been not yet supported by evidence. The length of stenosis is necessary to plan surgery urethroplasty rather than optical urethrotomy. The superiority of ultrasound over contrast urethrography is not yet proven. Moreover, some of the disadvantages associated with retrograde urethrography also apply to ascending urethral ultrasonography. The technique remains invasive, with insertion of a catheter distally, and requires two operators (one to instill fluid to distend the urethra and ensure no displacement of the catheter and the second to perform the ultrasound). Furthermore, despite trimming of the distal catheter beyond the balloon to allow visualization of the penile urethra, pathology in the fossa navicularis cannot be identified owing to the presence of the balloon. The procedure also requires a sterile technique. An alternative method is the ascending technique that has been superseded by a descending approach [12]. The patient attends with a full bladder and voids into a receptacle. Urethral distension is achieved with the urine stream, which is interrupted by the patient gently clamping the penis between thumb and forefinger during voiding, approximately 2 cm proximal to the tip after retraction of the foreskin. If needed in selected patients, views of the navicular fossa are obtained while actively voiding [7]. However, some men may be unable to void because of inhibition, and we do not suggest the self-distension.

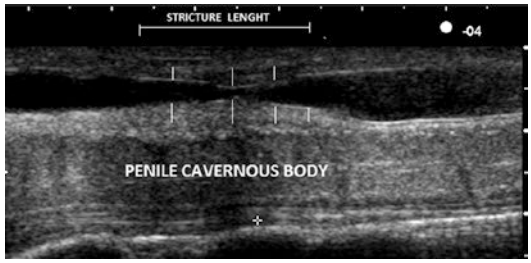

Fig. 18.4 Ultrasound urethrogram showing a stricture in the penile anterior urethra, the abnormal mucosa is more extensive than estimated by just measurement of the length of the stricture

18.4 Cowper's Gland (CG)

The CGs are two periurethral glands and are accessory sex glands that help to lubricate the semen. They are located symmetrically close to the urogenital diaphragm, and their ducts open in the bulbar urethra as separate units or singly (Fig. 18.5). The commonest anomaly is the Cowper's duct cyst or diverticulum, which is sometimes termed a syringocele. It is a retention cyst, is believed to be a congenital abnormality, and usually presents in childhood but in the occasional case may be first encountered in the adult male. It is postulated that the adult Cowper's duct cyst is the result of postinflammatory stricturing of the duct, either the result of infection or instrumentation. The underlying fault is the obstruction of the duct of the Cowper's gland, which results in cystic dilatation. It may be an incidental finding, or it may present with urinary infections, postmicturition dribbling, perineal pain, or lower urinary tract symptoms.

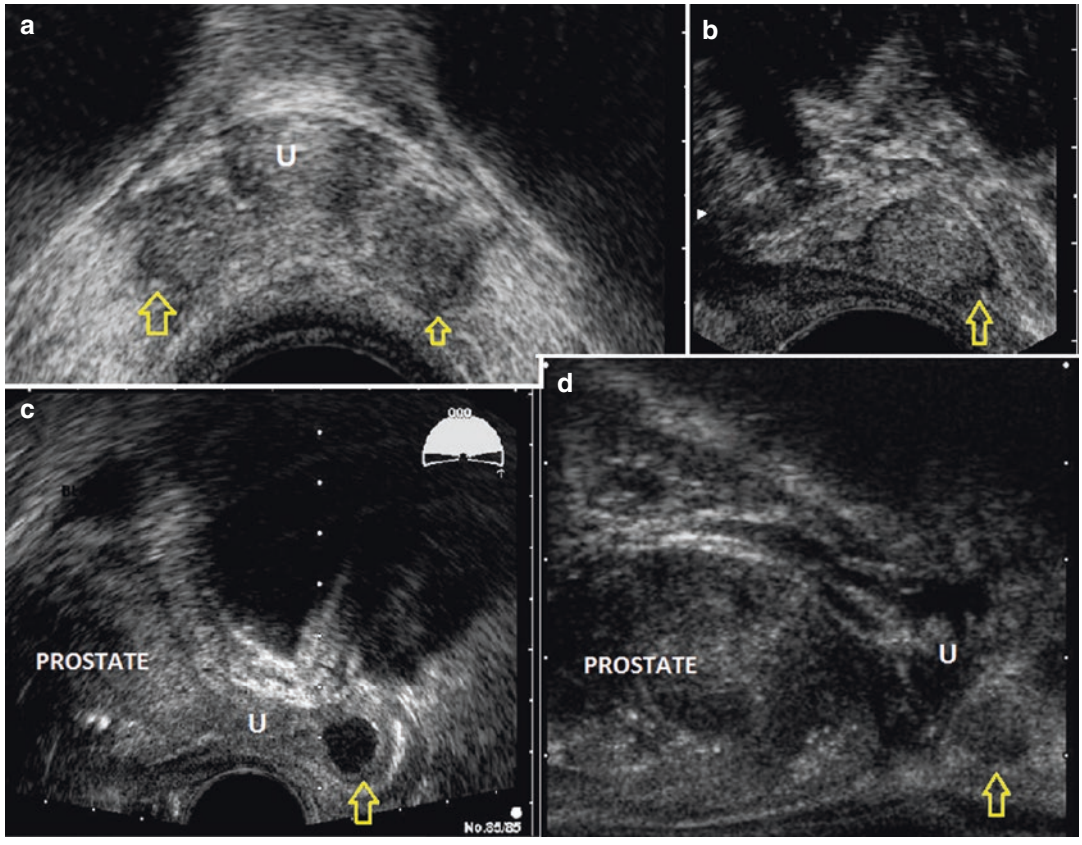

Fig. 18.5 Normal Cowper's glands (*yellow arrows*) in axial view (**a**) and longitudinal view (**b**) using end-fire transrectal probe, syringocele (*yellow arrow*, **c**) in longitudinal view, longitudinal view using linear transrectal probe (**d**)

18.5 Urethral Stenosis and Stricture

The pathologic change associated with urethral stricture disease is fibrosis of the epithelial-lined cavernous tissue [1, 9]. The urethral lumen narrows as the corpus spongiosum contracts with scar formation. The damaged urethral stratified epithelium changes to stratified squamous epithelium. The fibrotic tissue is further damaged from the hydrostatic pressure of avoiding causing worsening fibrosis. Spongiofibrosis is exacerbated by tears and fissures of the metaplastic epithelium allowing urine to leak into the underlying corpus spongiosum [2]. The process progresses either longitudinally along the urethra or circumferentially into the surrounding structures.

Urethral stricture is a common condition which results in narrowing or obliteration of the anterior urethral lumen, surrounded by corpus spongiosum, and may involve any segment of the urethra from the meatus to the bulbar urethra.

Male stenosis of the posterior urethra is a rare condition which results in the narrowing or obliteration of the posterior urethral lumen. Urethral stenosis is the term for narrowing of the membranous and prostatic urethral lumen that is not surrounded by corpus spongiosum. Posterior urethral stenosis is typically an obliterative process related to the traumatic injury and subsequent fibrosis secondary to urethral disruption [13–16].

Stricture of the female urethra is uncommon and more usually the result of mobility and kinking of the urethra rather than as a result of fibrosis. The severity of a urethral stricture is related to the amount of damage to the corpus spongiosum, the investing vascular layer of the urethra, resulting in a progressive process termed spongiofibrosis [2].

The most important information for guiding treatment is to accurately locate the site of the stricture, the length of the stricture, and the proximity of the stricture to the external urethral sphincter (Table 18.3). Bladder ultrasound may show a thickened trabeculated bladder wall that is an indirect indication of high-pressure voiding, and ureteral reflux with hydronephrosis may be seen. Finally, any incomplete bladder emptying with a postvoid residue is seen on micturition studies.

Longer strictures and failed cases are primarily treated by urethroplasty and are treated using buccal mucosa onlay graft, and the treatment of diffuse stricture disease of the penile urethra remains problematic and is managed by either repeated dilatation or total urethroplasty [15].

Table 18.3 Urethral injury classification

Urethral injuries	
Anterior urethra – *producing stricture*	Posterior urethra – *producing stenosis*
Blunt trauma	Penetrating injuries gunshot/knife wounds
Falls astride/perineal kicks	Penile surgery
Penetrating trauma	Pelvic fractures
Gunshot/knife wounds	Road traffic accidents
Sexual excess penile fractures	Endoscopic surgery, TURP
Iatrogenic injuries urethral catheters, urethroscopy	Iatrogenic injuries

18.6 Ultrasound of the Female Urethra

This is 3–4 cm in length and lies between the bladder neck and the external urethral meatus. It is less well supported by the pubourethral ligaments, which attach the urethra to the posterior part of the pubis symphysis, and the striated muscle of the external urethral sphincter [17]. The ultrasound examination is not the up-front method to investigate the female urethra, because distension is not achieved in the female. However, in our experience, the transrectal or transvaginal route is the first diagnostic tool in the study of paraurethral lesions and may be of particular value in the evaluation for a urethral diverticulum. Ultrasound can be considered the first diagnostic step to detect or rule out urethral diverticula or investigate filling defect (Table 18.1), because traditional imaging (micturating cystourethrography, double-balloon contrast urethrography, and MR) implies radiation or high costs.

18.6.1 Female Urethral Diverticulum (FUD)

FUD has incidence from 0.6 to 3 %, but it is characterized by late diagnosis. It is typically within the distal half of the urethra and located posteriorly [18]. Some cases are asymptomatic, but others are associated with infection, dyspareunia, bladder outlet obstruction, incontinence, calculi, and rarely malignancy. The cancer is usually adenocarcinoma.

FUD results from chronic infection of the periurethral glands. A micturating cystourethrogram is said to be positive in up to 95 %, while urethrography with a double-balloon catheter will identify around 90 % of diverticula. Sensitivities of transvaginal or transrectal ultrasonography (Figs. 18.6 and 18.7) is 66–100 %, and more recently, MRI has been introduced in the clinical practice. The typical appearance on MRI is of a posteriorly placed horseshoe-shaped high T2 signal structure around the mid-urethra. Important ultrasound features are summarized in Table 18.4 [19].

The following should be considered in the differential diagnosis: cyst of the vaginal mucosa, pseudodiverticulum, ureteral ectopia mimicking a urethral diverticulum, and abscess or complications after urethral surgery for incontinence (Fig. 18.8). A pseudodiverticulum represents a mucosal extrusion through a periurethral fascial defect and occurs in cases of prior urethral surgery, is relatively asymptomatic, has a broad-based ostium resulting from the fascial defect which is readily apparent on cystoscopy, and is frequently associated with urinary incontinence [20]. However differentiation by ultrasound may be not easy and it was not yet described.

Male urethral diverticulum is acquired after injury, infection, or long-term urethral catheterization and is typically in the ventral surface at the penoscrotal junction or in the bulbar urethra. Male urethral diverticulum has been described as complication of surgery after ventral patch of buccal mucosa.

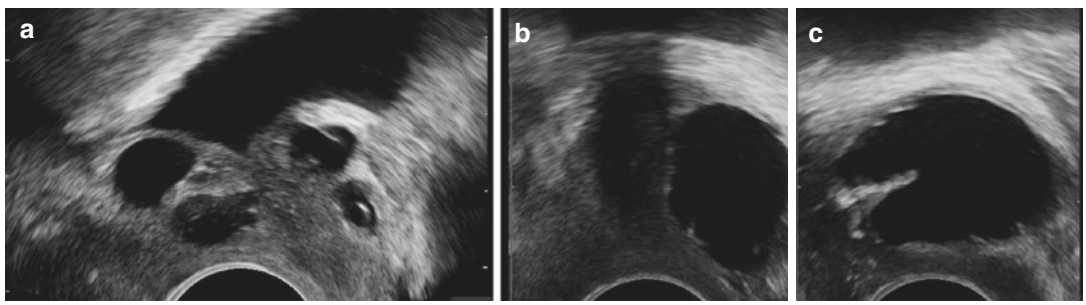

Fig. 18.6 FUD using transvaginal in ultrasound, multiple (**a**) and single FUD (**b, c**)

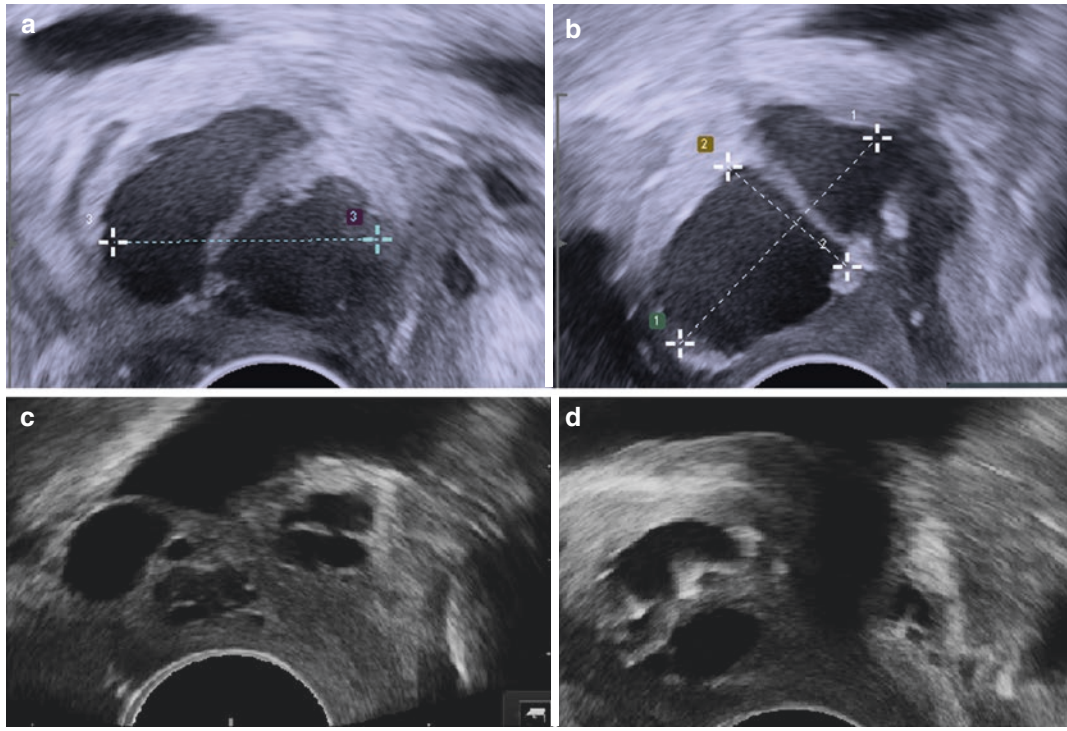

Fig. 18.7 Complicated FUD using transvaginal in ultrasound. Large single diverticular with septun and dense content (qxil view) (**a**). Located in the proximal urethra with extension beneath the bladder neck (longitudinal view) (**b**). Multiple small diverticula (oxil view) (**c**) with liquidi content and regular walls in the proximal and mid urethra (longitudinal view) (**d**)

Table 18.4 Important ultrasound features of female urethral diverticula (FUD) modified according to Leach's classification [18]

Ultrasound features of FUD	Characteristics of FUD
Location (the site) of the diverticulum	Distal, mid-, or proximal urethra, with or without extension beneath the bladder neck
Number	Single or multiple diverticula
Size	Expressed in centimeters (cm)
Configuration	Describes whether the diverticulum is single, multiloculated, or saddle shaped
Communication	Indicates the site of communication with the urethral lumen, i.e., distal, mid, or proximal urethra
Content and walls of the diverticulum	Anechoic (liquid), irregular walls, solid, dense content (infected), stones

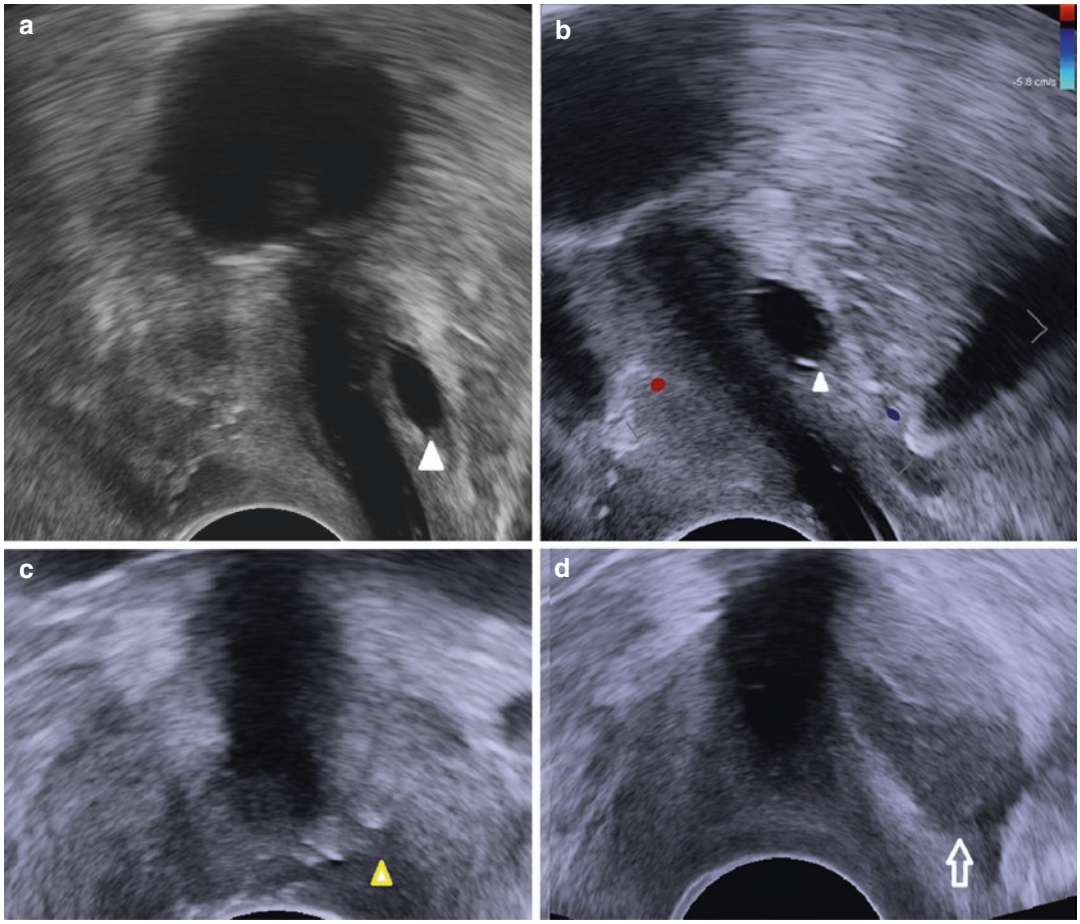

Fig. 18.8 Postoperative appearance after surgical treatment, residual anterior anechoic lacuna (*arrowhead*) (**a**, **b**) and hematoma (*white arrow*) (**d**) and hyperechoic tissue with complete disappearance of diverticula (*yellow arrowhead*) (**c**)

18.7 Cancer of the Urethra

Much less than 1 % of all urinary tract cancers occur within the urethra, but they are more common in males (by a ratio of 7:3), with a peak age of onset in the seventh decade. Primary urethral cancers, nearly 80 %, are squamous cell carcinoma, some 15 % are of transitional cell origin, and the rest are adenocarcinoma. In the male, the commonest site is the anterior urethra, and, of these, most occur in the bulbar urethra (60 % in bulbomembranous urethra, 30 % in penile urethra, 10 % within prostatic urethra). In Fig. 18.9, primary urothelial cancer of the prostatic and bulbar urethra (stage T4) is characterized by the solid hypoechoic tissue presenting with acute urinary retention. US and MR are used for staging urethral cancer the urethra (Table 18.5) [21]. Primary penile cancer of the gland or recurring cancer is the most common secondary malignancy that involves the urethra [22].

In females, primary urethral carcinomas are very rare neoplasms (less than 0.02 %): risk factors include infection with the human papilloma virus and urethral diverticula. Bladder cancer invading the whole urethra is infrequently observed (Fig. 18.10). Urethral carcinomas affect postmenopausal patients, whose symptoms may include dyspareunia, recurrent hematuria, or urinary symptoms and urinary infection. Half (two-fourths) of female urethral carcinomas arose in urethral diverticulum [23]. We report a woman (Fig. 18.11) with clear cell carcinoma raised in the mucosa of diverticulum. Her symptoms were recurrent cystitis and sporadic hematuria. Diagnosis was done by urethroscopy since transvaginal ultrasound and cystoscopy were negative. Soft/papillary cancer tissue filled completely all the diverticular cavity, and any abnormality was noted at initial transvaginal and abdominal ultrasound. Magnetic resonance showed diverticular cavity partially filled with cancer after transurethral resection (Fig. 18.11).

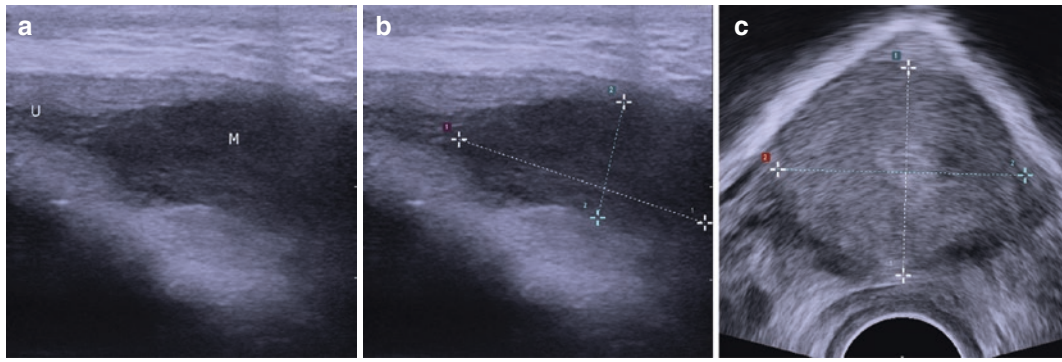

Fig. 18.9 (**a**) and (**b**) show longitudinal view using perineal linear probe: High-grade urothelial urethral cancer in the bulbar urethra (*U*) as sold hypoechoic lesion (*M*). (**c**) shows axil view using transrectal probe: tumor invading the membranous urethra and prostate

Table 18.5 Neoplasms of the urethra and TNM classification [21]

Urethral tumor classification	
Benign	Prostatic epithelial polyp, urethra fibro-epithelial polyp, hemangioma, leiomyoma
Malignant primary tumors	Squamous cell carcinoma, transitional cell carcinoma, adenocarcinoma, sarcoma, melanoma
Malignant secondary tumors	Penile cancer, metastatic prostate, bladder, testis cancer
Urethral tumor staging	
Ta – noninvasive papillary, polypoid, or verrucous carcinoma	
Tis – carcinoma in situ	
T1 – tumor invades subepithelial connective tissue	
T2 – tumor invades corpus spongiosum, prostate, periurethral muscle	
T3 – tumor invades corpus cavernosum, anterior vagina, bladder neck	
T4 – tumor invades other adjacent organs	

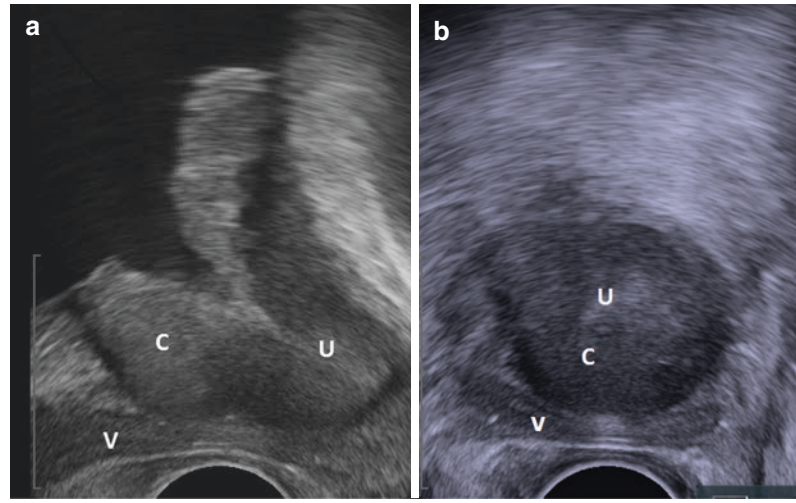

Fig. 18.10 Female urethral cancer (*C*) compressing the vaginal wall (*V*): (**a**) Longitudinal and (**b**) Axial view using transrectal endfire ultrasound probe

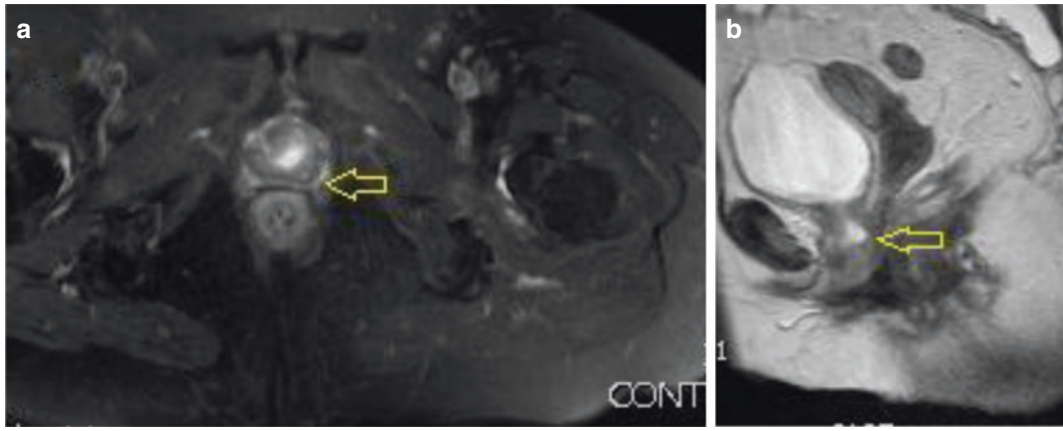

Fig. 18.11 Magnetic resonance – cancer in urethral diverticula, thick vascularized wall (*arrow*): T_2 Axial view (**a**) and Longitudinal view (**b**)

References

1. Latini JM, McAninch JW, Brandes SB, Chung JY, Rosenstein D (2014) SIU/ICUD consultation on urethral strictures: epidemiology, etiology, anatomy, and nomenclature of urethral stenoses, strictures, and pelvic fracture urethral disruption injuries. Urology 83(3 Suppl):S1–S7
2. Pavlica P, Barozzi L, Menchi I (2003) Imaging of male urethra. Eur Radiol 13(7):1583–1596
3. Buckley JC, Heyns C, Gilling P, Carney J (2014) SIU/ICUD consultation on urethral strictures: dilation, internal urethrotomy, and stenting of male anterior urethral strictures. Urology 83(3 Suppl): S18–S22
4. Patel U (2010) Imaging and urodynamics of the lower urinary tract. Springer-Verlag London Limited, New York/London. doi:10.1007/978-1-84882-836-0_10
5. McAnich JW, Laing FC, Jeffrey RB Jr (1988) Sonourethrography in the evaluation of urethral strictures: a preliminary report. J Urol 139:294–297
6. McCallum RW (1979) The adult male urethra: normal anatomy, pathology and method of urethrography. Radiol Clin North Am 17:227
7. Patel U, Lees WR (1995) Penile sonography. In: Solbiatti L, Rizzatto G (eds) Ultrasound of superficial structures. Churchill Livingstone, London; Ryu JA, Kim B (2001) MR imaging of the male and female urethra. Radiographics 21:1169–1185
8. Gallentine ML, Morey AF (2002) Imaging of the male urethra for stricture disease. Urol Clin North Am 29:361–372
9. Morey AF, McAninch JW (2000) Sonographic staging of anterior urethral strictures. J Urol 163(4): 1070–1075
10. Choudhary S, Singh P, Sundar E, Kumar S, Sahai A (2004) A comparison of sonourethrography and retrograde urethrography in evaluation of anterior urethral strictures. Clin Radiol 59:736–742
11. Merkle W, Wagner W (1988) Sonography of the distal male urethra—a new diagnostic procedure for urethral strictures: results of a retrospective study. J Urol 140:1409–1411
12. Berman LH, Bearcroft PW, Spector S (2002) Ultrasound of the male anterior urethra. Ultrasound Q 18:123–133
13. Smith TG (2016) Current management of urethral stricture disease Indian. J Urol 32(1):27–33
14. Jordan G, Schlossberg S (2012) Surgery of the penis and urethra. In: Wein AJ, Kavoussi LR, Novick AC, Partin AW, Peters CA (eds) Campbell-Walsh urology. Elsevier Saunders, Philadelphia, pp 956–1000
15. Angermeier KW, Rourke KF, Dubey D, Forsyth RJ, Gonzalez CM (2014) SIU/ICUD consultation on urethral strictures: evaluation and follow-up. Urology 83(3 Suppl):S8–S17
16. Mitterberger M, Christian G, Pinggera GM, Bartsch G, Strasser H, Pallwein L, Frauscher F (2007) Gray scale and color Doppler sonography with extended field of view technique for the diagnostic evaluation of anterior urethral strictures. J Urol 177(3):992–996
17. Song L, Xie M, Zhang Y, Xu Y (2013) Imaging techniques for the diagnosis of male traumatic urethral strictures. J Xray Sci Technol 21(1):111–123. doi:10.3233/XST-130358
18. Montironi R, Mazzucchelli R, Galosi AB (2007) Chapter 10.4. The female urethra. In: Mariuzzi G (ed) Anatomic pathology and clinical correlations, vol II. Piccin Nuova Libraria s.p.a, Padua, pp 1717–1719
19. Leach GE, Sirls LT, Ganabathi K, Zimmern PE (1993) L N S C3: a proposed classification system for female urethral diverticula. Neurourol Urodyn 12(6):523–531
20. Leng WW, McGuire EJ (1998) Management of female urethral diverticula: a new classification. J Urol 160:1297–1300
21. Sobin LH Gospodariwicz M, Wittekind C (eds) (2009). TNM classification of malignant tumors. UICC International Union Against Cancer, 7th edn. Wiley-Blackwell, Oxford, pp 266–269
22. Galosi AB, Parri G, Lacetera V, Muzzonigro G (2010) Management of large prostatic abscess associated with urethral stenosis and penile cancer recurrence. Arch Ital Urol Androl 82(3):181–185
23. Caplan J, Hartman R, Rooker G (2011) Adenocarcinoma of the female urethra: clear cell variant. Radiol Case Rep 6:1–3

19 Interventional Ultrasound-Guided Treatment of Urinary Incontinence: Insertion of ProACT

Andrea Gregori, Virginia Varca, and Andrea Benelli

19.1 Introduction

The male adjustable continence therapy (ProACT) system is an adjustable device for the treatment of stress urinary incontinence (SUI) in patients who underwent prostate surgery [1]. The SUI prevalence following open or endoscopic surgery for benign prostatic hyperplasia is about 1–2 % and certainly represents just a small segment of patients treated [2]. Despite the incessant development of new surgical techniques, the prevalence of SUI after radical prostatectomy still ranges in literature between 5 and 50 % and represents a constant challenge for the urologist [3–5]. It is important to standardize the concept of SUI; it has been defined by the International Continence Society as the involuntary leakage of urine on effort or exertion, sneezing or coughing [6]. This condition can strongly affect the patient's quality of life after prostate surgery, especially in those young patients who could still have an active life after a radical prostatectomy. The ProACT system represents a valuable and safe solution for patients with postsurgical mild SUI, thanks to the transrectal ultrasound-guided implantation; this technique allows to avoid radiation exposure under fluoroscopic guidance and achieve a more accurate placement by the use of multiplanar ultrasound imaging [1, 7].

19.2 The ProACT System

The ProACT system is an adjustable permanent implant designed to achieve continence through increased outlet resistance. It is composed of an expandable silicone balloon connected with a 2-lm conduit to a reinjectable titanium port; 1 lm contains a 15-cm × 0.8-mm wire, while the other is used for balloon inflation in order to increase the resistance. The device is available in two sizes: 12 and 14 cm. The shorter one is usually implanted in patients presenting a residual prostate after surgery for benign prostatic hyperplasia. The longer one is more useful in patients' post-RP. In these patients, two balloons are placed on each side of the vesicourethral anastomosis just above the pelvic diaphragm. The balloons are inserted transperineally using a specially designed, sharp-tipped, removable trocar contained in a 4.6-mm diameter U-shaped sheath. The two titanium ports are placed into a subcutaneous parascrotal position to allow easy access in order to adjust the balloons after the placement (maximum, 8 ml) using a 23-gauge

Electronic supplementary material The online version of this chapter (doi:10.1007/978-3-319-40782-1_19) contains supplementary material, which is available to authorized users.

A. Gregori (✉) • V. Varca • A. Benelli
Department of Urology, ASST Rhodense – Garbagnate Hospital, Milan, Italy
e-mail: AGregori@asst-rhodense.it

P. Martino, A.B. Galosi (eds.), *Atlas of Ultrasonography in Urology, Andrology, and Nephrology*,
DOI 10.1007/978-3-319-40782-1_19

noncoring needle. This allows the device to be adjusted by modifying the level of coaptation needed to achieve continence (Video 19.1).

19.3 Patients Selection and Preparation

Incontinence evaluation must be standardized as the number of pads per day (PPD) needed by the patient, ranked as mild (1 or 2 PPD), moderate (3–5 PPD) and severe (>5 PPD or use of urinary condom). We evaluate all the patients with a 24-h pad test and pad count. The preoperative evaluation should moreover include a complete medical history, a voiding diary when possible, an incontinence quality of life questionnaire [8], a flexible cystoscopy and TRUS to exclude local recurrences and urethral/anastomosis strictures. In our opinion, urodynamic investigations are also suggested in order to exclude detrusor overactivity or compliance abnormalities even if some authors describe it as optional investigations together with cystoscopy [9]. The patient must have undergone prostate surgery at least 12 months before the implantation and be free from distant metastasis. We suggest an antibiotic prophylaxis with 2 g of ceftriaxone intravenous about 30 min before surgery. An antibiotic solution is also used to immerse the system elements before surgery and to irrigate the field during the procedure.

19.4 Operative Technique

The patient is placed in the lithotomy position, and after the disinfection, a 14- or 16-Ch Foley bladder catheter is placed; it is filled with 40–50 ml of saline solution and helps a clear visualization of the urethra and the bladder neck during TRUS. The scrotum is held above the perineum with tape. The anal ring is isolated from the perineum with a drape, and TRUS is performed using a 7.5-MHz linear probe and a small convex probe. When we perform just a local anaesthesia, we use ropivacaine injected in the subcutaneous tissue around the perineal incision. Two horizontal 0.5–1-cm skin incisions are made in the perineum about 1 cm lateral to the median line and about 1.5 cm above the rectum, and then the deep local anaesthesia with 20 ml of ropivacaine 7.5 mg/ml is administered. A 20-gauge spinal needle is inserted through the skin incisions and directed bilaterally to the vesicourethral anastomosis under multiplanar TRUS guidance. With the linear probe, we monitor the advancement of the 20-gauge spinal needle towards the bladder neck, while thanks to the convex probe we monitor the distance from the urethra. The space for the balloon is created on each side of the vesicourethral anastomosis and in the pelvic diaphragm with a hydrodissection mechanism during the releasing of the anaesthetic. When no local anaesthesia is used, the dissection is performed with saline solution on a 20-gauge spinal needle.

A sharp-tipped removable trocar contained within a U-shaped sheath is now inserted through the skin incision and placed, thru the hydrodissected tissue, on one side of the bladder neck checking his position with TRUS; the trocar is then removed and the sheath left in situ. During this manoeuvre the sheath is gently advanced about 0.5 mm to occupy the space created by the trocar tip. The internal channel of the sheath is then lubrificated using sterile gel. With the help of the push wire, the ProACT device is passed along the sheath into position at the bladder neck. The sheath is withdrawn approximately 2 cm to permit balloon expansion as it is inflated with 1-ml 0.9 % saline solution via the titanium port. It should create a coaptation of the urethra with a triangular mechanism of compression between the two balloons (placed at 9 and 3 o'clock and the symphysis). The push wire is removed (Video 19.2). On both sides are placed the conduit tube and the titanium port thanks to a scissor-fashioned subcutaneous parascrotal tunnel. The incisions are closed in two layers with 4–0 resorbable sutures.

19.5 Results and Discussion

The implantation of an artificial urinary sphincter remains nowadays the gold standard treatment for patients presenting SUI after radical prostatectomy, offering continence and satisfaction rate around 90 %. However, these devices require a complex surgical procedure and are

relatively expensive; 40 % of cases require a surgical revision [10].

Since the first group of 117 patients was reported by Hubner and Sharp in 2005, the fluoroscopic-guided technique is well described in literature; just a few series regarding the transrectal ultrasound-guided positioning of the device are present. The TRUS guidance allows a three-dimensional vision of pelvic anatomical landmarks offering the surgeon a more precise and secure positioning of the balloon. Our most significant experience, published in 2010 [1], included data of 79 patients with a relative long follow-up of more than 2 years. The results were absolutely comparable in terms of success rate (66.1 % of patients) and failure rate with those reported in literature under a fluoroscopic guidance [11] (Video 19.3). We evaluated 79 patients with continence data regarding 62 of them and a mean follow-up of 25 months. Our mean operative time was 23 min which is nowadays further improved. The mean number of postoperative adjustments to obtain continence recovery was 3.6 with a mean final fill volume of 4.2 ml. The final success rate (dry patients at the 24-h pad test) was 66 % with an overall dry rate in nonirradiated patients of 75 %. The adjuvant radiotherapy seems to be a relative contraindication to the implantation of the device, being associated with a higher incidence of perioperative complications and a lower success rate. Our intra- and perioperative complication rate in nonirradiated patients is low and favourable if compared with recently published studies, probably as a result of a more precise positioning of the balloon and a more accurate introduction of the trocar during the procedure [11, 12].

Crivellaro et al. published in 2012 a work about a geometrical stepper-guided navigation system for ProACT implantation with good results in 42 patients, comparable in terms of success rate with those present in literature. They showed a slightly lower complication rate with a technique however hard to introduce in the everyday clinical practice [13].

Conclusions

We believe that ProACT system implantation under TRUS guidance is a safe and feasible procedure for patients with postsurgical SUI. It guarantees good success of complication rates avoiding radiation exposure. Adjuvant radiotherapy and severe incontinence remain relative contraindications to the device implantation. The local anaesthesia gives also the opportunity to treat those old patients who are not eligible for a general anaesthesia but could still achieve a good quality of life without dealing everyday with urinary incontinence.

References

1. Gregori A, Romano AL, Scieri F, Pietrantuono F, Incarbone P, Salvaggio A, Granata A, Gaboardi F (2010) Transrectal ultrasound–guided implantation of adjustable continence therapy (ProACT): surgical technique and clinical results after a mean follow-up of 2 years. Eur Urol 57:430–436
2. Rassweiler J, Teber D, Kuntz R, Hofmann R (2006) Complications of transurethral resection of the prostate (TURP)-incidence, management, and prevention. Eur Urol 50:969–979
3. Ostrowski I, Śledź E, Ciechan J, Golabek T, Bukowczan J, Przydacz M, Wiatr T, Stangel-Wojcikiewicz K, Chłosta PL (2015) Current interventional management of male stress urinary incontinence following urological procedures. Cent Eur J Uro 68:340–347
4. Bauer RM, Bastian PJ, Gozzi C, Stief CG (2009) Postprostatectomy incontinence: all about diagnosis and management. Eur Urol 55:322–333
5. Herschorn S, Bruschini H, Comiter C et al (2010) Surgical treatment of stress incontinence in men. Neurourol Urodyn 29:179–190
6. Abrams P, Cardozo L, Fall M et al (2002) The standardisation of terminology of lower urinary tract function: report from the Standardisation Subcommittee of the International Continence Society. Neurourol Urodyn 21:167–178
7. Gregori A, Simonato A, Lissiani A, Scieri F, Rossi R, Gaboardi F (2006) Transrectal ultrasound guided implantation of the ProACT adjustable continence therapy system in patients with post-radical prostatectomy stress urinary incontinence: a pilot study. J Urol 176:2109–2113
8. Wagner TH, Patrick DL, Bavendam TG, Martin ML, Buesching DP (1996) Quality of life of persons with urinary incontinence: development of a new measure. Urology 47:67–71
9. Venturino L, Dalpiaz O, Pummer K, Primus G (2015) Adjustable continence balloons in men: adjustments do not translate into long-term continence. Urology 85(6):1448–52
10. Carlson KV, Nitti VW (2001) Prevention and management of incontinence following radical prostatectomy. Urol Clin North Am 28:595–612

11. Rouprêt M, Misraï V, Gosseine PN, Bart S, Cour F, Chartier-Kastler E (2011) Management of stress urinary incontinence following prostate surgery with minimally invasive adjustable continence balloon implants: functional results from a single center prospective study. J Urol 186:198–203. doi:10.1016/j.juro.2011.03.016
12. Gilling PJ, Bell DF, Wilson LC, Westenberg AM, Reuther R, Fraundorfer MR (2008) An adjustable continence therapy device for treating incontinence after prostatectomy: a minimum 2-year follow-up. BJU Int 102:1426–1430
13. Crivellaro S, Tosco L, Palazzetti A, Abbinante M, Martinez G, Kocjancic E, Frea B (2012) Geometrical stepper-guided navigation system for Pro-Act implant under transrectal ultrasound control: preliminary data. Urol Int 89:473–479

Part III

Prostate and Seminal Vesicles

Prostate and Seminal Vesicles: Ultrasound Anatomy and Scanning Methods

20

Vincenzo Scattoni and Carmen Maccagnano

20.1 Introduction

The ultrasound (US) of prostate and seminal vesicles (SVs) plays a fundamental role during urological evaluation, providing several morphological and functional information in noninvasive and fast way.

20.2 Study Technique

20.2.1 Probes

The probes can be convex or transrectal (TR).

The multifrequency convex probes, whose frequency is about 2–5 MHz, are routinely used with both transabdominal (TA) and transperineal (TP) approach (Fig. 20.1).

The quality of the images is related to the number, dimensions, and structure of the crystals and to the scan converter.

The TR probes show high frequencies which range from 4 MHz up to 12 MHz. The arrangement of the transducers defines the probe: monoplanar, biplanar, and end fire [1].

1. The *monoplanar* probes are linear and slim; they show high spatial resolution, but the exam of the prostate is possible only in a single plan and, consequently, with several diagnostic limitations. Currently, the most common use is in case of anal stenosis (Fig. 20.2).
2. The *biplanar* probes have two groups of transducers, which form a 90° corner; the most important disadvantage is the big dimension of the probe itself, due to two groups of electric connections. Moreover, the employment of the biplanar probes is more difficult because the scan in the two orthogonal plans is not often simultaneous; additionally, the transducers are

V. Scattoni (✉)
Department of Urology, University Vita-Salute,
Scientific Institute H San Raffaele,
Via Olgettina 60, Milan 20132, Italy
e-mail: scattoni.vincenzo@hsr.it

C. Maccagnano
Azienda Ospedaliera S.Anna,
Via Ravona, 60 San Fermo della Battaglia (Co),
Como, Italy

P. Martino, A.B. Galosi (eds.), *Atlas of Ultrasonography in Urology, Andrology, and Nephrology*,
DOI 10.1007/978-3-319-40782-1_20

located in two different points of the probe; thus, there is no spatial correspondence between the anatomical entities observed in the sagittal and transversal plan (Fig. 20.3a–c).

3. The *end-fire* probes show a fanlike arrangement of the transducers on the distal convexity of the probe itself (Fig. 20.4). The radial disposition of the transducers is the cause of the most important limit of this kind of probe: it offers a trapezoidal vision, with imaging distortion and a reduced spatial resolution in the zones which are distant from the field of view. Additionally, the areas which are located proximally to the apex of the probe show evident reverberation phenomena, with a reduced spatial resolution. In routine practice, the spatial resolution is good if proximal to the probe, whereas it progressively reduces distally, with a final consistent reduction of the resolution power. The exam of the prostate and SV is obtained manually rotating the probe; the employment of different adaptors allows different interventional procedures, including the biopsy with TR approach.

The images from different probes are not correspondent to each other: the sagittal scans from linear probe are different from those from end-fire probe because of both the different fields of view and the compression of the probe on the posterior part of the prostate.

The images in transversal scan with biplanar probe have to be considered as axial, whereas the images from end-fire probe are coronal oblique. According to these considerations, the US anatomy of the apex is better defined with linear probes, whereas the base is well documented with the end-fire ones.

Fig. 20.1 Traditional convex probe with 3.5 MHz frequency

Fig. 20.2 The shape of monoplanar probes is linear and slim; even if the exam of the prostate is possible only in a single plan, this kind of probe shows high spatial resolution

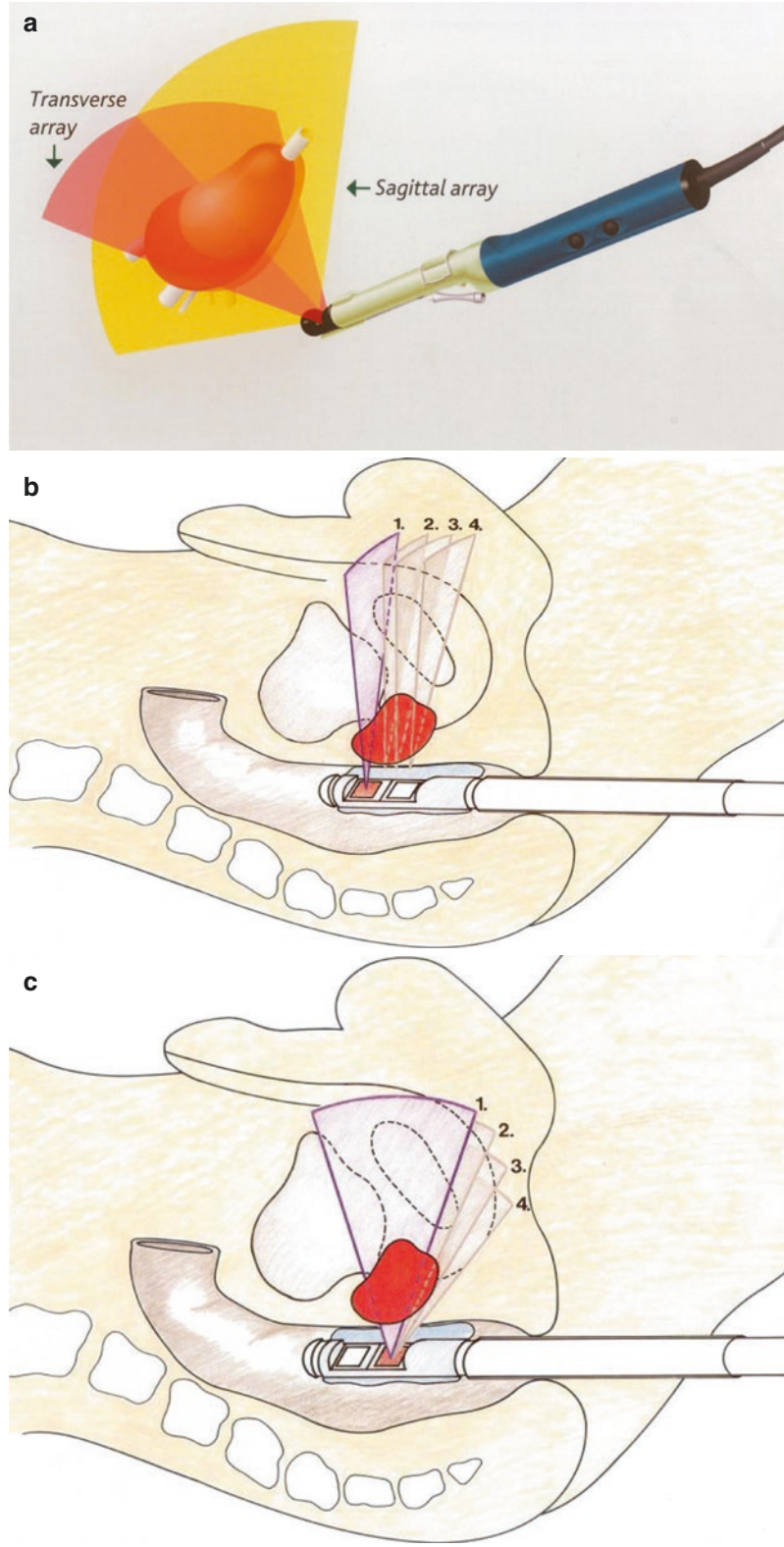

Fig. 20.3 (**a**) The biplanar probes have two groups of transducers, located in two different points of the probe, which form a 90° corner and allow almost simultaneously transverse and sagittal visualization; the presence of two distinct groups of transducers implicates the big dimension of the probe itself. It is important to note that there is no spatial correspondence between the anatomical entities observed in the sagittal and transversal plan. (**b**) Patient in semi-lithotomy position: prostate visualized according to sagittal plan. (**c**) Patient in semi-lithotomy position: prostate visualized according to transversal plan

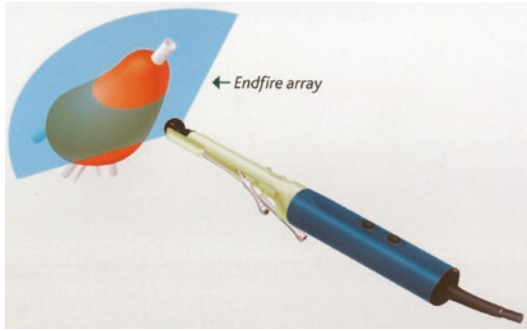

Fig. 20.4 Fanlike arrangement of the transducers on the distal convexity of the end-fire probe. This kind of probe offers a trapezoidal vision, with imaging distortion and a reduced spatial resolution in the zones which are distant from the field of view, i.e., prostate apex

20.2.2 Transabdominal Approach

The TA approach uses the acoustic window of the bladder, which has to be mildly filled; in case of empty bladder, the margins of the glands and seminal vesicles are hidden by the echoes from the adjacent bowel loops (Fig. 20.5). The multifrequency convex probe has to be inclined in cranio-caudal direction, in order to avoid the acoustic shadow of the pubis (Figs. 20.6 and 20.7).

The actual machines allow to choose the most appropriate frequency according to:

- The physical characteristics of the patient;
- The level of fatty tissue in the anterior abdominal wall;
- The thickness of abdominal muscles.

The TA approach evaluates the volume of the prostate and its relationships with the adjacent organs; nevertheless, the exam of the internal anatomy of the prostate is not possible. The third lobe, the intraprostatic cysts, or calcifications are easily recognizable. The SV are not always well defined, and they usually appear like two pear-shaped anechoic entities, with transversal orientation, cranially located respecting to the gland in the transversal plan and up to the prostate and behind the bladder in the longitudinal scans.

The TP approach is rarely used and it allows images similar to those of TA approach. This technique is applied to obese patients or those submitted to radical cystectomy or with small bladder due to chronic inflammation or radiotherapy. This approach is also useful in performing prostate biopsy in men submitted to operations because of rectal cancer or those with anal stenosis.

The patient is supine with open legs, the probe is positioned on the perineum, and it is rotated in two orthogonal plans [2, 3].

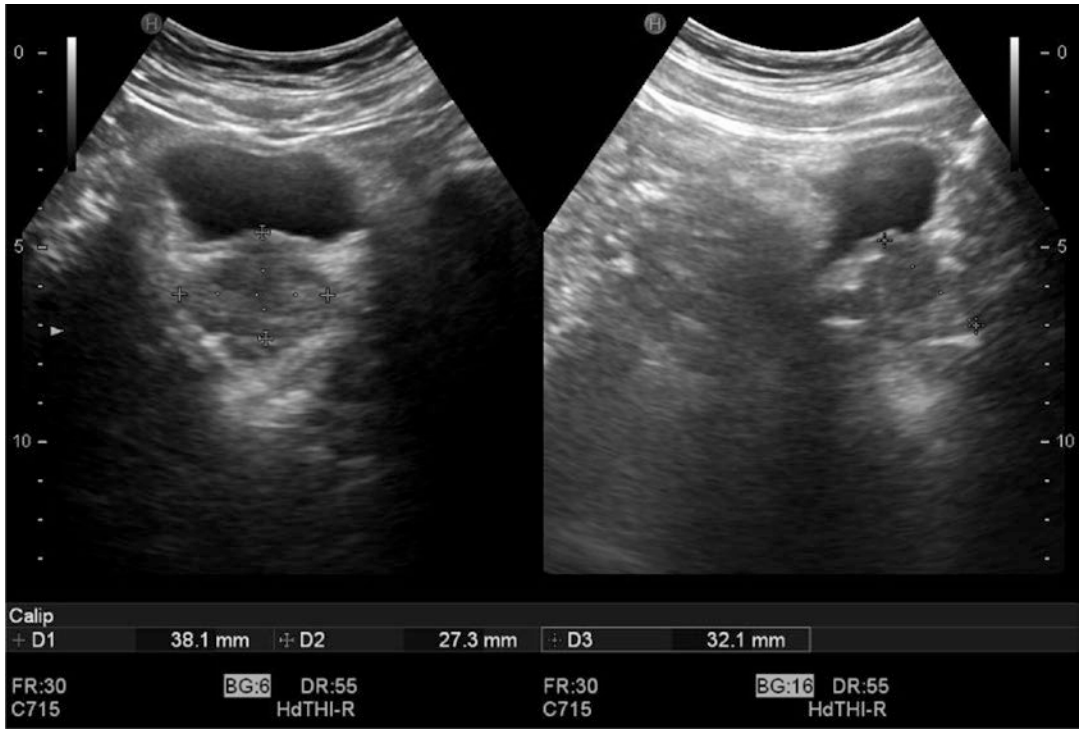

Fig. 20.5 Transabdominal approach with mildly filled bladder. The measurement of the three diameters of the prostate is easily feasible

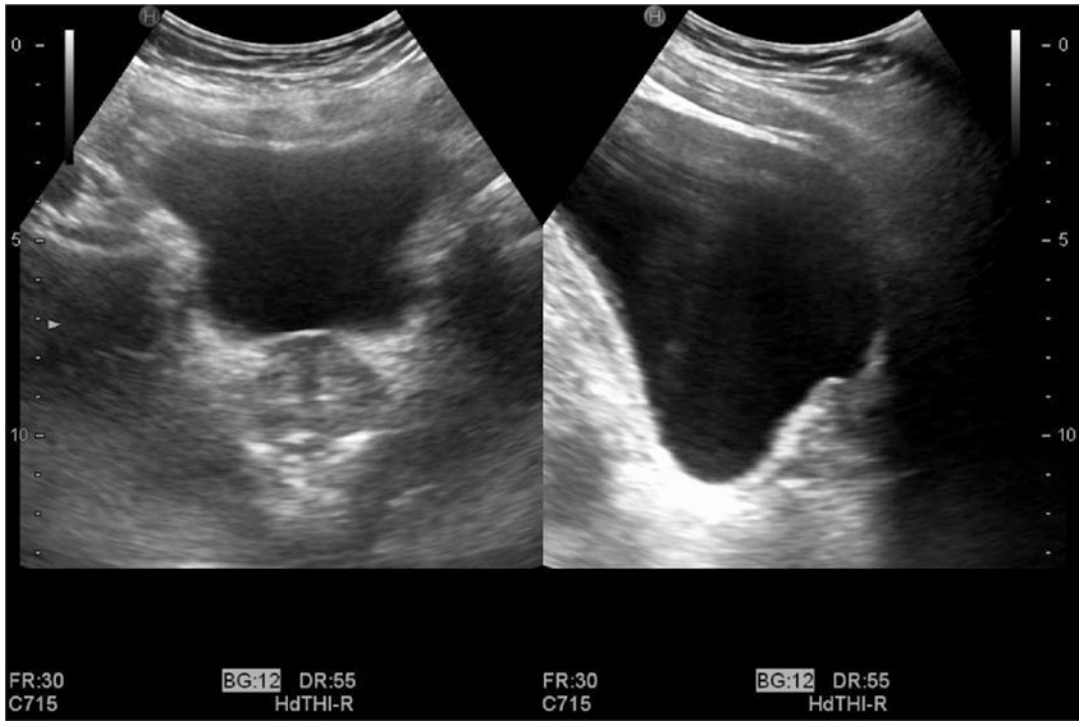

Fig. 20.6 Difficulties of visualization of the prostate with transabdominal approach caused by the acoustic shadow of the pubis and the excessively filled bladder

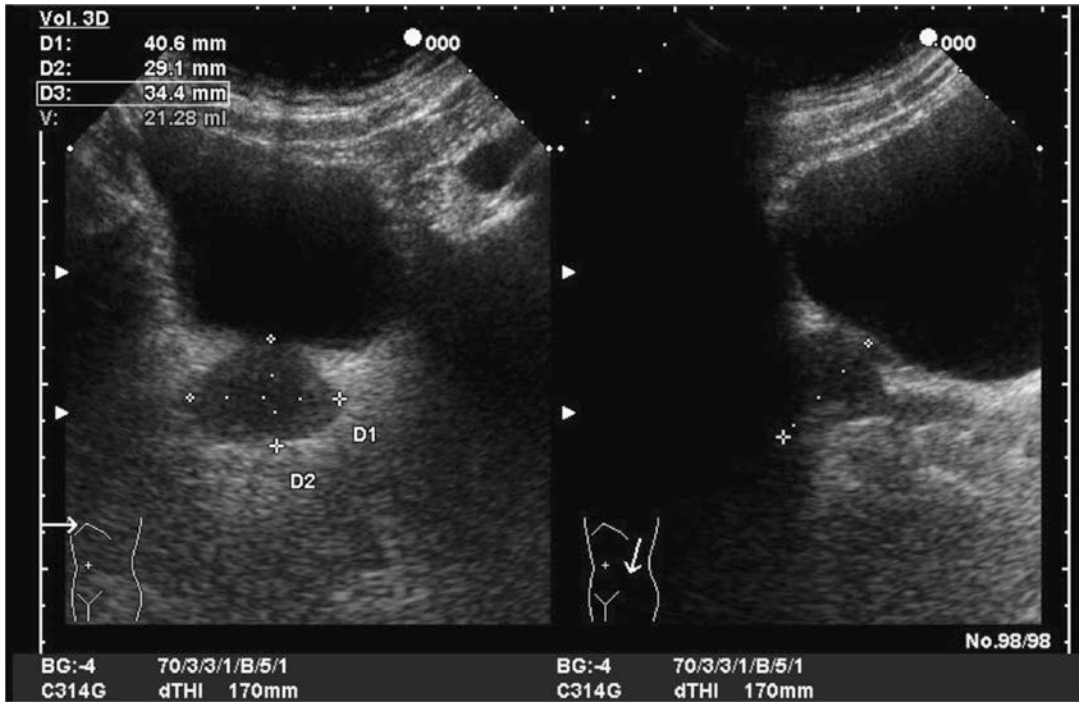

Fig. 20.7 Incorrect inclination of the convex probe in craniocaudal direction: the acoustic shadow of the pubis does not allow the visualization of the whole gland in longitudinal scan

20.2.3 Transrectal Approach

An enema 2 h before the exam is advisable. It is not necessary to have a full bladder, even if moving the bowel loops, especially the sigma-rectum, facilitates the definition of the prostatic base and SV.

The TR approach was firstly used by Watanabe and coll. in 1967, but the method diffused only after the production of manual probes with the initial frequency of 5 MHz and successively higher.

The patient is positioned on his/her left side, with the flexed knees on the hip, in order to easily introduce the probe. In the routine practice, the lithotomic position is employed only during TP approach with both free hand and template.

The probe has to be rotated and to be moved slowly in order to examine the whole gland with the focal zone of the probe. Above all, the enlarged prostates need manual regulation of position and number of focus.

The zone which has to be studied has to be positioned in the center of the scan in order to avoid loss of resolution, especially regarding the margins of the prostate; as a matter of fact, the dispersion of the US is more significant, and the spatial and contrast resolution is lower in these regions.

Currently, the simultaneous biplanar scan allows a better spatial localization of a lesion; they are particularly useful in guided prostate biopsies [2, 3].

20.3 US Anatomy

20.3.1 Prostate

The shape and the dimensions of the prostate vary according to the age of patient.

In young patients (until 40 years), it shows an ovoidal shape, whereas after 50 years of age, the shape is roundish or pear-like. It is deeply located in the pelvis, distally to the abdominal anterior wall, but closely related with the anterior wall of the rectum.

Actually, the old division into two lobes is no more used.

Following the anatomic-embryological studies in 1991, the prostate has been divided into two zones: the peripheral one, which represents the 70 % of the whole volume in patients with age inferior to 40 years, and the central zone which can be further divided into central and transitional zone.

In transrectal ultrasound (TRUS), the peripheral zone is easily recognizable because it is more homogeneous and mildly hyperechoic compared to the central one. It constitutes the posterior part and the lateral margin of the gland. The US appearance changes in the transversal scans from base to apex: half-moon shaped in the base, ovoidal proximally to the verumontanum, and roundish in the apex (Fig. 20.8). The central area, represented by the central and the transitional zone, is rarely developed in young patient, it surrounds the prostatic urethra, and the US distinction among these two zones is not possible. It localizes from the bladder neck to the veru montanum; the appearance is relatively hypoechoic, with gross and nonhomogeneous echoes. The central zone is significantly less developed than peripheral zone, and it represents the 25 % of the volume of the prostate.

After 40 years of age, the volume and the morphology of the prostate change, according to the benign prostatic hyperplasia (BPH) (the US appearance of BPH will be discussed in a specific chapter) (Fig. 20.9) [2, 3].

Additionally, the exam of other anatomical structures is possible with the help of linear probes.

In the sagittal scan, the identification of prostatic urethra is possible on the median line. It appears as a thin hypoechoic line, extended from the bladder neck until the apex. The course is arched with anterior concavity, and it is surrounded by two hyperechoic lines, corresponding to the smooth and striated muscular structures of the prostatic urethra (Fig. 20.10). This appearance is particularly evident in the prostate with normal dimensions and in young patients, but it attenuates and progressively vanishes with BPH. The veru montanum is the region where the ejaculatory ducts end; they are well recognizable in young men. The apex is not well examined with the end-fire probe; conversely its examination is better with the linear ones. The pubic

symphysis is identified as an arched hyperechoic line which blocks the US bundle.

The dense fibrous tissue constituted by the artery and veins for the penis, located under the symphysis, appears as a hyperechoic zone.

The membranous urethra and the Cowper glands can be recognized in the context of the muscles of urogenital plan.

The identification of neurovascular bundle is important; it is visible in the transversal scan in posterolateral region of the prostate. The shape can be roundish or triangular, and it is constituted by both hypo- and hyperechoic entities, corresponding to veins and arteries, and nerves, respectively (Fig. 20.11).

The periprostatic venous plexus is located on the lateral and anterior aspects of the prostate; it appears as group of anechoic areas. It is well represented in young patients, and it can be compressed in case of BPH (Fig. 20.11a, b).

The study of intraprostatic vascularization, particularly the arteries, is possible only with TRUS. The arteries derive from the bladder ones, and they are better recognizable when the incident Doppler corner is inferior to 50°. The central zone is highly vascularized compared to the peripheral one; consequently the individuation of hypervascularized area in this context is suspicious for neoplastic lesions (Fig. 20.11b). In the routine practice, the color Doppler study of the prostate has progressively lost importance during the last decades.

Denonvilliers' fascia appears as a thin hyperechoic line located in the posterior zone of the prostate. This structure is better studied with linear probes; conversely, it is too compressed by the end-fire probes, and it is too near to the probe, generating reverberation artifacts.

The embryonic residues of Müllerian ducts are frequently recognized with TRUS; they appear as small cysts on the median line in the base of the prostate. The Müllerian cysts have variable dimensions, but they range from 5 up to 10 mm; the morphology is pear shaped, and they develop between the deferential ampulla and the ejaculatory ducts, behind the urethra up to the veru montanum (Fig. 20.12).

The volume of the prostate can be calculated with both TR and TA approaches. The precise measurement of the three diameters is fundamental. The transversal diameter is the best to measure, whereas the longitudinal and the anteroposterior diameters have to be calculated in the sagittal scan with cranio-caudal inclination of US bundle. Both the anterior and the posterior margins of the prostate are definable with many difficulties. Similarly, the longitudinal diameter is often not well defined because of the blinding of the apex caused by the pubis. The volume of the prostate shows significant intra- and interobserver variability, which is around 20%. The definition of the volume is more precise with TRUS, because of the easier identification of reference points for principal diameters.

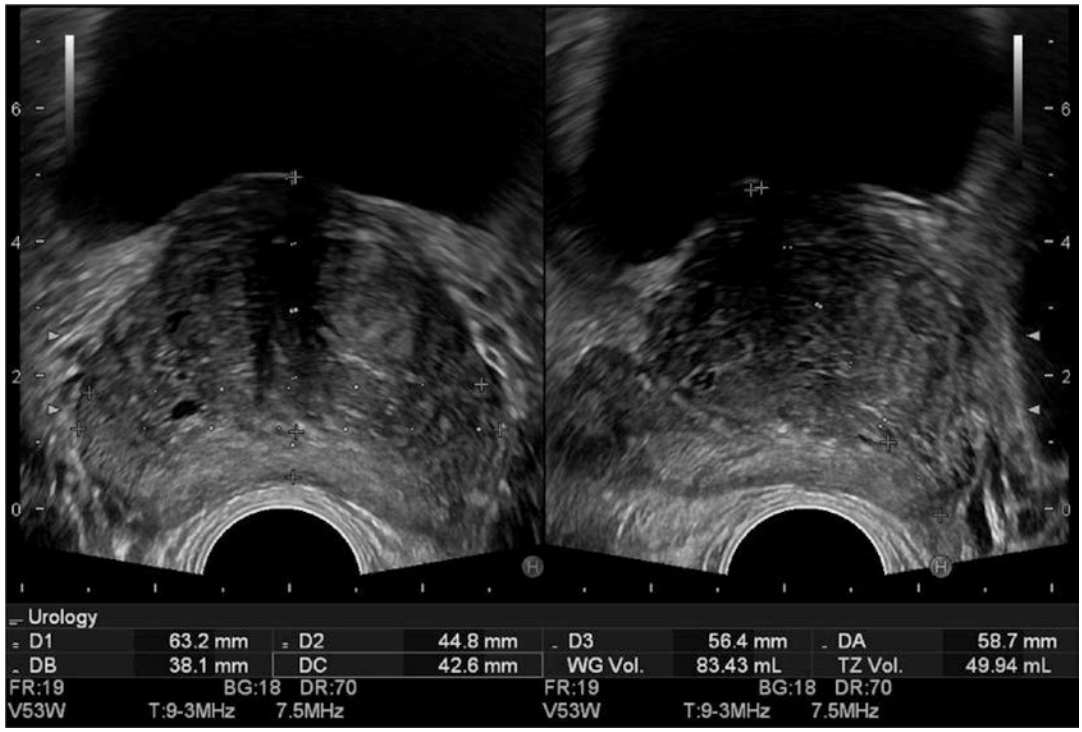

Fig. 20.8 TRUS of the prostate using an end-fire probe. The peripheral zone, which constitutes the posterior part and the lateral margin of the gland, is easily recognizable because it is more homogeneous and mildly hyperechoic compared to the central one. The US appearance changes in the transversal scans from base to apex: half-moon shaped in the base, ovoidal proximally to the verumontanum, and roundish in the apex. The simultaneous measurement of the diameters and the volume of both the whole gland and the transition zone are easily and rapidly feasible

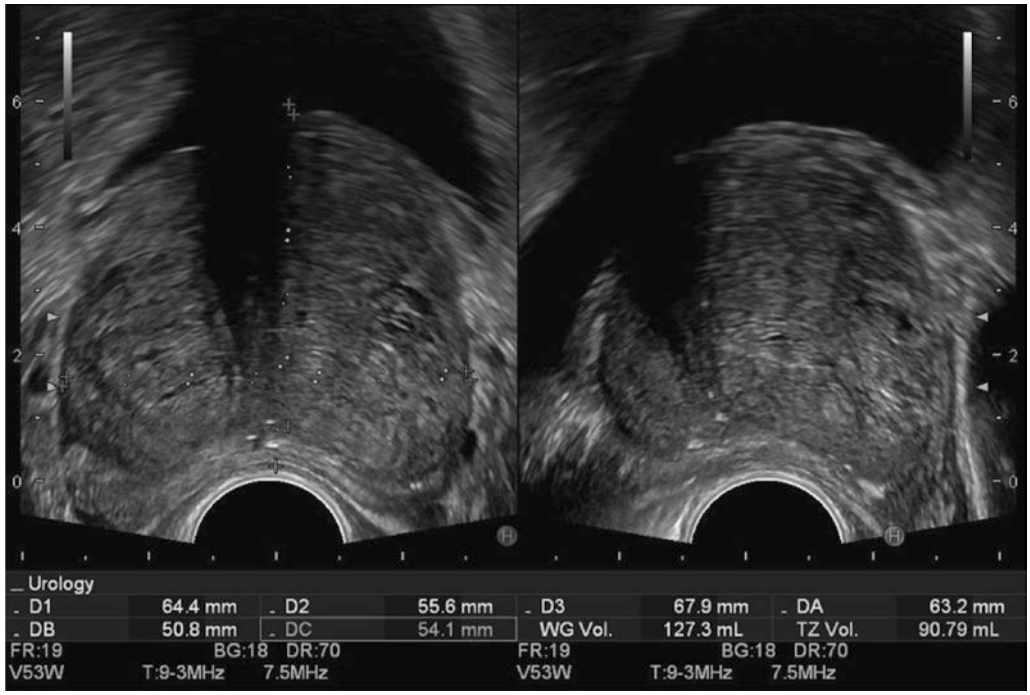

Fig. 20.9 TRUS of the prostate using an end-fire probe. The peripheral zone is compressed by transitional zone, in case of BPH. The two regions are easily distinguishable because of the difference of US appearance: mildly hypoechoic, the central zone; hyperechoic, the peripheral one

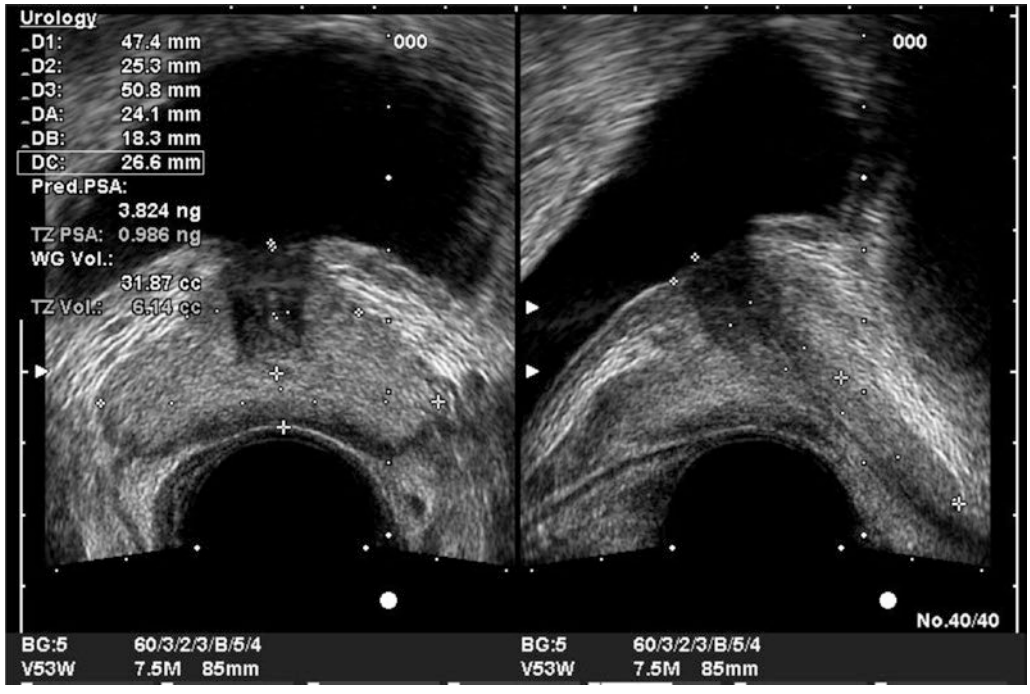

Fig. 20.10 Identification of prostatic urethra in sagittal scan, on the median line. It appears as a thin hypoechoic lines, extended from the bladder neck until the apex. The two hyperechoic lines surrounding the urethra correspond to the smooth and striated muscular structures of the prostatic urethra itself

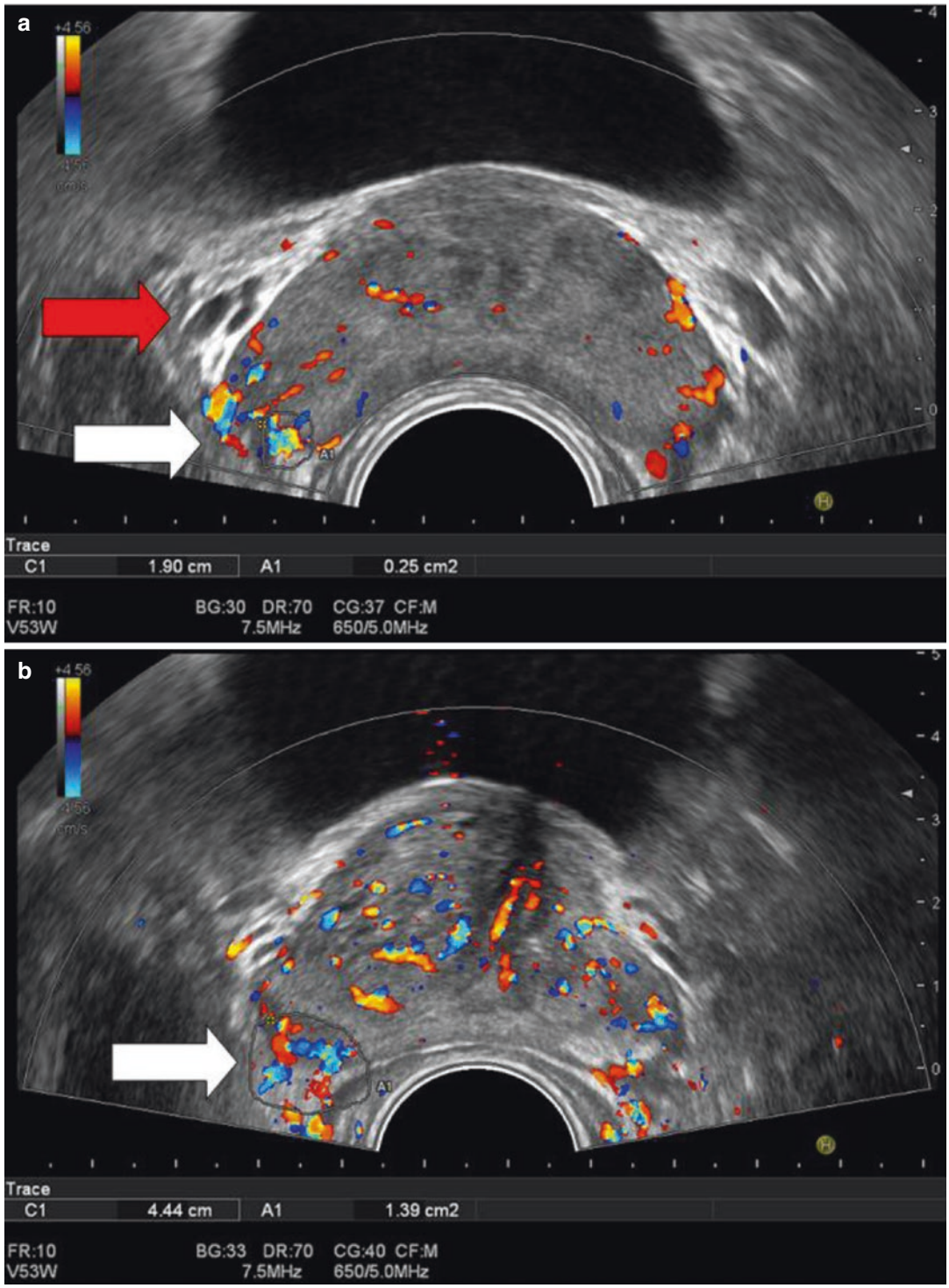

Fig. 20.11 (**a**) The neurovascular bundle is visible in the transversal scan in posterolateral region of the prostate, also with the help of color Doppler (*white arrow*). The shape can be roundish or triangular, and it is constituted by both hypo- and hyperechoic entities, corresponding to veins and arteries, and nerves, respectively. The periprostatic venous plexus is located on the lateral and anterior aspects of the prostate; it appears as group of anechoic areas (*red arrow*). (**b**) Color Doppler study of the neurovascular bundle (*white arrow*)

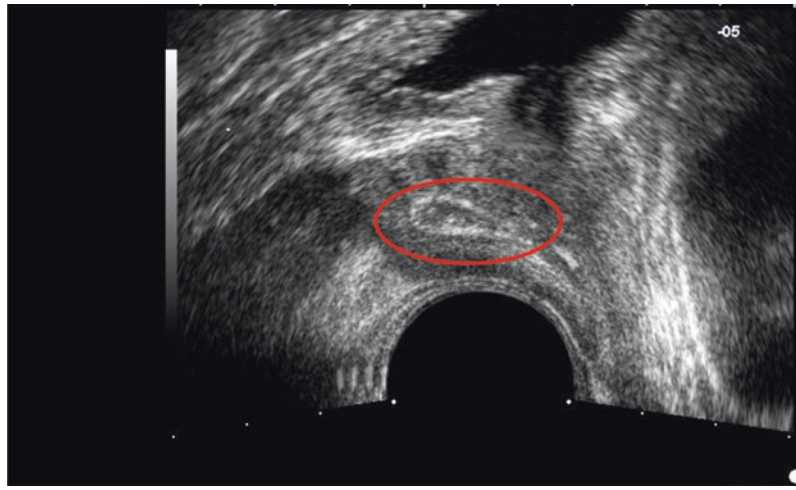

Fig. 20.12 The embryonic residues of Müllerian ducts are frequently recognized with TRUS; they appear as small cysts on the median line in the base of the prostate. The morphology is pear shaped, and they develop between the deferential ampulla and the ejaculatory ducts, behind the urethra up to the verumontanum. In this case, the wall of the cyst appears as hyperechoic because of the calcifications (*red circle*)

20.3.2 Seminal Vesicles

The SVs localize up to the prostate; for this reason, they are not always evaluable with digital rectal examination. The lateral margins are closely related with the periprostatic venous plexus, whereas the posterior wall is in contact with the anterior wall of the rectum, from which is separated by the Denonvilliers' fascia. The morphology of SVs is highly variable; they can show a simple, lengthened morphology or voluminous and convoluted one. These features have to be taken into consideration during imaging interpretation [4, 5].

In the adults, the length ranges from 3.6 up to 7.6 cm and the width from 1.2 up to 2.4 cm, according to anatomical studies. The external surface is irregular, especially in the posterior face. The evaluation of the dimensions is difficult also with TRUS; this is due to the spatial orientation of the SVs and the employment of different scans.

Terasaki and coll. evaluated the dimensions of 76 healthy patients with different age; they concluded that the major volume in TRUS progressively reduces after 50 years, with statistically significant variations [6]. The average dimensions of the SVs, vas deferens, and ejaculatory ducts with TRUS in healthy men are measurable; these parameters are all related to the age.

The SVs are small until puberty; they reach the final dimensions about 11–13 years, because of the effect of male sexual hormones. The maximal diameters are identified about 50–60 years of age; this is also due to BPH which compresses the ejaculatory ducts, promoting the stasis of seminal liquid. After 70 years, the volume reduces also because of the atrophy of the prostate, due to the reduced hormonal stimulation.

The TA approach is not useful because the images are approximate.

Instead, the TRUS with probe with a frequency which ranges from 7.5 up to 13 MHz allows a detailed study of the morphology, dimensions, and US structure of SVs in different plans, with the definition of the anatomical relationship with other pelvic organs.

The recent US machine allows also a 3D reconstruction. In the axial scan, the SV is ovoidal, with hypoechoic and irregular surface. The internal structure is characterized by multiple sepimenta which lead to a convolute honeycomb appearance, with an echogenicity which is inferior to that of the prostate (Fig. 20.13).

The dimensions reduce and the deferential ampulla, which is more centrally located, becomes visible approaching the median line (Fig. 20.14). The two entities meet between them in order to form the extraprostatic tract of the ejaculatory duct. In the sagittal scan, the SVs are not easily examinable because of their oblique development from the external to the internal aspect. Nevertheless, they are observable according to their major diameters with oblique scan (Fig. 20.15 a, b). This type of scan is easier in order to examine the distal tract of the deferential ampulla and the ejaculatory ducts, whose diameter progressively reduces in the context of the prostate (1 mm) [5].

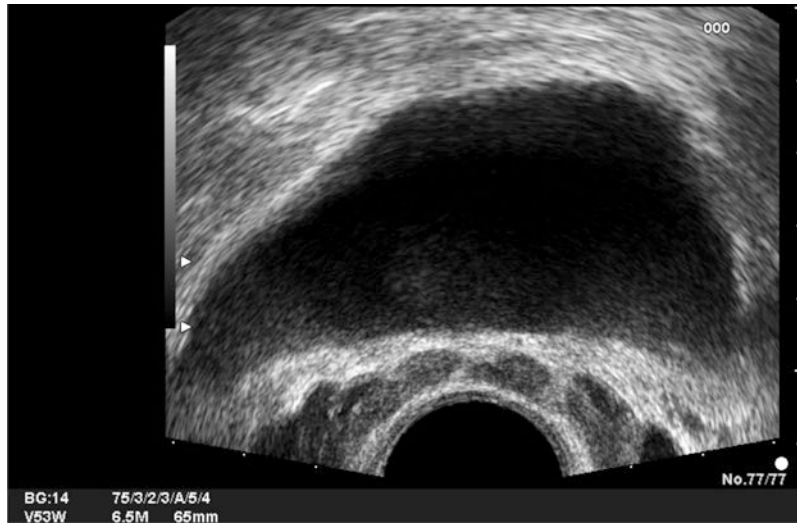

Fig. 20.13 In the axial scan, the SV are ovoidal, with hypoechoic and irregular surface. The appearance of the internal structure is honeycomb-like because of the presence of multiple sepimenta

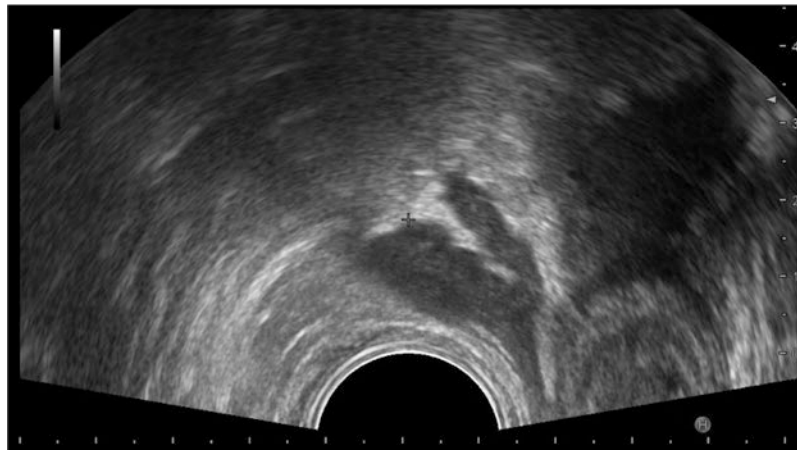

Fig. 20.14 The deferential ampulla is more centrally located, and it becomes visible approaching the median line

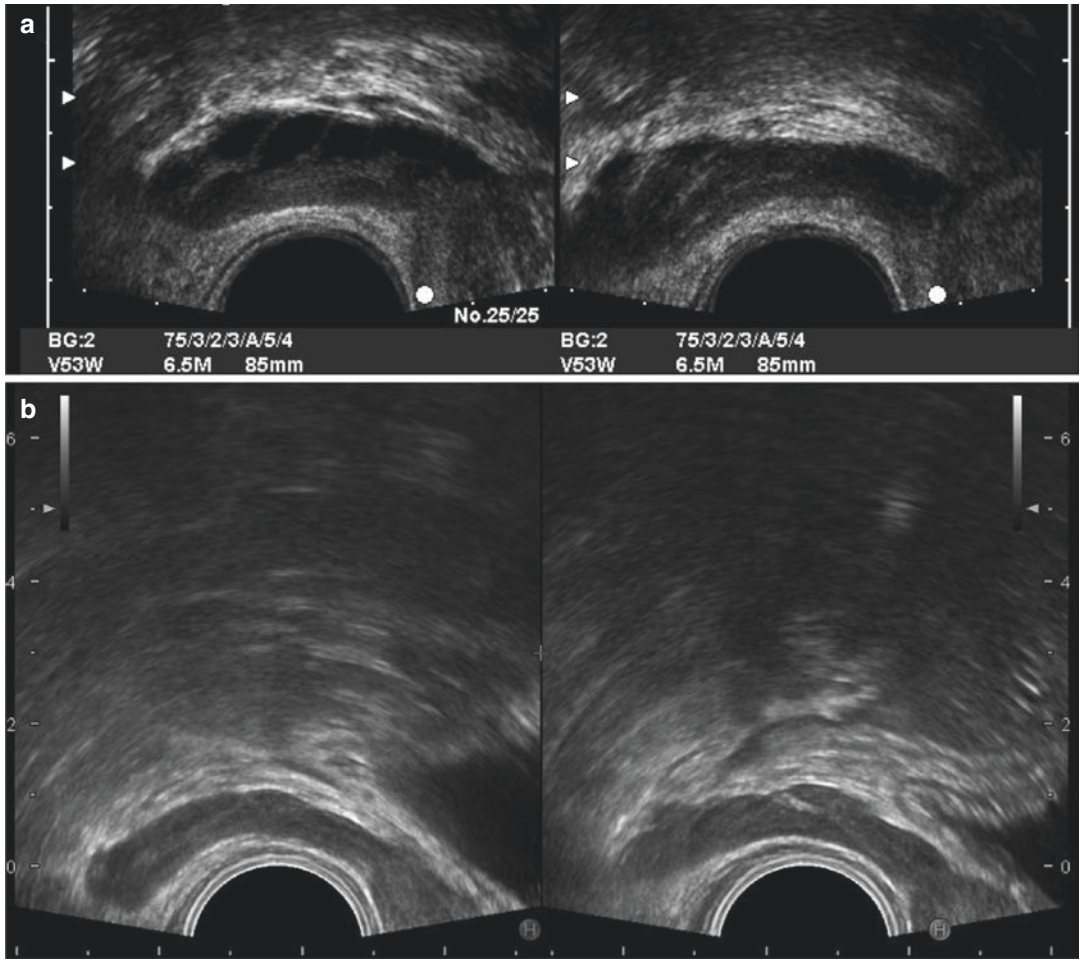

Fig. 20.15 (**a**, **b**) The oblique scan allows to examine the distal tract of the deferential ampulla and the ejaculatory ducts, together with the SV, according to their major diameters

Bibliography

1. Martino P, Galosi AB, Bitelli M, Consonni P, Fiorini F, Granata A, Gunelli R, Liguori G, Palazzo S, Pavan N, Scattoni V, Virgili G, Imaging Working Group-Societa Italiana Urologia (SIU); Societa Italiana Ecografia Urologica Andrologica Nefrologica (SIEUN) (2014) Practical recommendations for performing ultrasound scanning in the urological and andrological fields. Arch Ital Urol Androl 86(1):56–78
2. Lotti F, Maggi M (2015) Ultrasound of the male genital tract in relation to male reproductive health. Hum Reprod Update 21(1):56–83
3. Jungwirth A, Diemer T, Dohle GR, Giwercman A, Kopa Z, Tournaye H, Krausz C (2013) Guidelines on male infertility, european association of urology guidelines. EAU Guidelines Office, Arnhem
4. Montironi R, Cheng L, Galosi AB, Montorsi F, Scarpelli M (2014) Seminal vesicle intraepithelial neoplasia vs. basal cell hyperplasia in a seminal vesicle. Eur Urol 66:623–627
5. Fisch H, Kang YM, Johnson CW, Goluboff ET (2002) Ejaculatory duct obstruction. Curr Opin Urol 12: 509–515
6. Terasaki T, Watanabe H, Kamoi K, Naya Y (1993) Seminal vesicle parameters at 10-year intervals measured by transrectal ultrasonography. J Urol 150(3):914–916

Prostatic Inflammation

21

Andrea B. Galosi, Luigi Quaresima,
and Rodolfo Montironi

Prostatic inflammation implies the presence of pathological infiltration of the prostate by inflammatory cells. However, the relationship of these findings with the clinical prostatitis due to infection, prostatitis-like symptoms, and imaging is not correlated. Prostatitis is defined as "a combination of acute and chronic infectious diseases (bacterial prostatitis), chronic pelvic pain syndrome (CPPS) and asymptomatic inflammations" [1]. Prevalence in population is estimated to be 12 % [2]. However, prostatitis is a heterogeneous clinical entity, and current clinical and pathological classification is reported in Tables 21.1 and 21.2, respectively.

Diagnosis of prostatitis is sometimes difficult to make and imaging is currently underutilized [4]. Imaging can aid in the diagnosis of prostatitis and its complications: transrectal ultrasound is the first imaging available worldwide, then CT and MRI may be used in particular cases. Only in selected cases, (such as prostatic abscess) color Doppler ultrasound may be required. Abdominal-pelvis CT and MRI may be indicated in severe infections to evaluate pelvic organs, associated pathologies, and/or upper urinary tract. Contrast-enhanced multiparametric magnetic resonance is indicated to study the prostate gland in men who have infection and harbor the high risk of associated malignancy [5]. Needle biopsy may be required mostly to rule out cancer only in selected cases with persistent PSA elevation and/or in cases with granulomatous prostatitis.

A.B. Galosi, MD, PhD (✉) • L. Quaresima, MD
Institute of Urology, Polytechnic University
of Marche Region, Ancona, Italy
e-mail: galosiab@yahoo.it

R. Montironi, MD
Pathologic Anatomy, Polytechnic University
of Marche Region, Ancona, Italy
e-mail: r.montironi@univpm.it

P. Martino, A.B. Galosi (eds.), *Atlas of Ultrasonography in Urology, Andrology, and Nephrology*,
DOI 10.1007/978-3-319-40782-1_21

Table 21.1 Clinical classification of prostatitis National Institutes of Health - National Institute of Diabetes and Digestive and Kidney Diseases (NIH-NIDDK) [1]

Type	Etiology
I. Acute prostatitis	Bacterial
II. Chronic prostatitis	Bacterial
III. Chronic nonbacterial/Chronic pelvic pain syndrome	Not known
IV. Asymptomatic prostatitis	Several causes

Table 21.2 Pathological classification of prostatitis [3]

Acute inflammation (observed in type I of clinical classification)
Chronic inflammation (observed in types II and IV of clinical classification)
Chronic inflammatory cells
Granulomatous inflammatory infiltrate (observed in type II of clinical classification and type IV if asymptomatic)
Specific granulomatous disease (or infective granuloma, *Mycobacterium*)
Nonspecific granulomatous
Granuloma secondary to prostatic surgery/resection
Granulomatous prostatitis secondary to systemic disease (e.g., Wegener)

21.1 Acute Prostatitis

Acute prostatitis (AP) is often diagnosed on the basis of positive infectious culture, and it is usually associated with urinary tract bacterial infection. AP is diagnosed clinically and treated without specific imaging; anyway abdominal ultrasound is usually done to evaluate the kidney and upper urinary tract. The most frequently isolated pathogens are the following, *E. coli*, *Proteus*, *Enterobacter*, *Klebsiella*, and *Pseudomonas*, but sometimes it is not possible to identify any bacteria in urine or blood culture. Acute bacterial prostatitis appears in US as a hypoechoic rim around the prostate, and color Doppler shows an increased flow (Figs. 21.1 and 21.2).

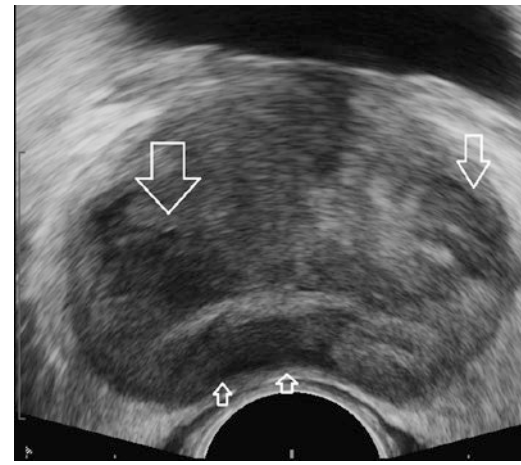

Fig. 21.1 Acute prostatitis in the peripheral zone (*small arrows*) and anterior zone (*big arrows*)

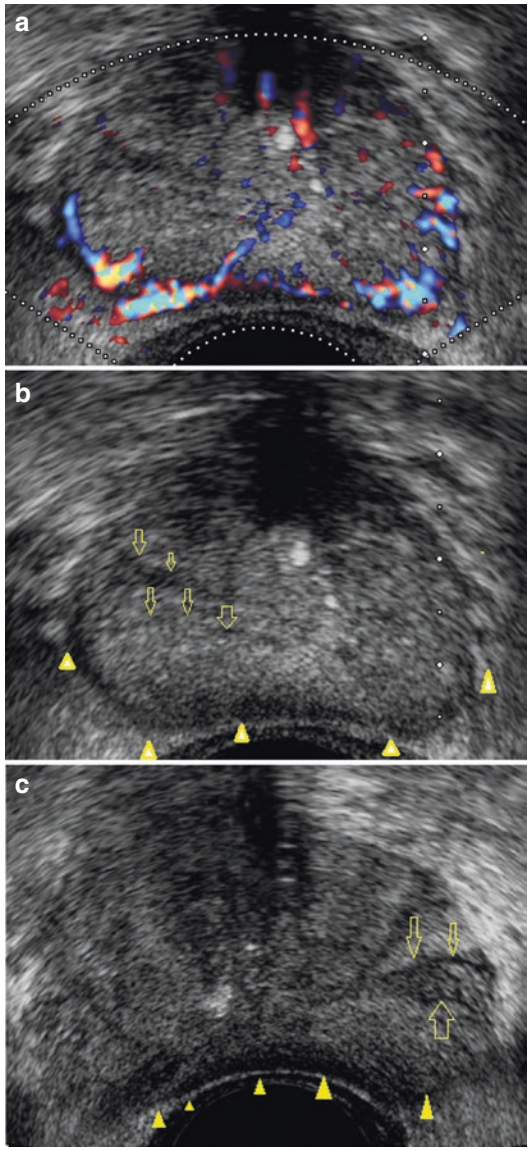

Fig. 21.2 (**b**, **c**) Acute prostatitis: subcapsular hypoechoic rim (*arrowheads*) and fine hypoechoic linear septum (*arrows*) due to edema and ducts dilatation. (**a**) Color power Doppler shows an increased flow

21.1.1 Prostatic Abscess

Prostatic abscess is a complication of acute bacterial prostatitis frequently observed in patient with diabetes and immune weakness (Fig. 21.3). Prostatic abscess appears hypoechoic with well-defined or irregular wall that is typically associated with prostatitis and located in the anterior zone with well-defined borders. Color Doppler ultrasound reveals perilesional vascularity (Fig. 21.4). In contrast prostatic cancer is hypoechoic and typically located in the peripheral zone or heterogeneous ill-defined borders, and color Doppler reveals vascularity within the lesion. In large prostatic abscess, the fluid collection may extend over the prostatic capsule in the perirectal and retrovesical spaces. In these cases, abdominal contrast CT and MRI may be indicated to evaluate pelvic organs (Fig. 21.5). Also in severe infections or upper urinary tract infection, the CT is recommended.

Ultrasound-guided drainage is very useful to further characterize the mass, may be useful to relieve symptoms and obtain bacterial culture, and therefore guides antibiotic therapy (Video). Transperineal echo-guided approach is preferred versus the transrectal approach since the rectal contamination is avoided. Furthermore, placement of drain is possible using the transperineal approach in patients with large cavity. Usually a small nephrostomy tube is left in place in the abscess cavity to flush saline solution and antibiotics [6]. Ultrasound monitoring is very useful to monitor abscess after treatment, to demonstrate residual or new fluid pockets after drainage, and to show location, size, and fluid content of the abscess during antibiotic treatment (Figs. 21.5 and 21.6).

Differential diagnosis between infected midline cyst and prostatic abscess is shown in (Fig. 21.7): well-defined borders of the cyst facilitate the diagnosis and differentiation from abscess, that is, irregular in shape and lobulated in borders.

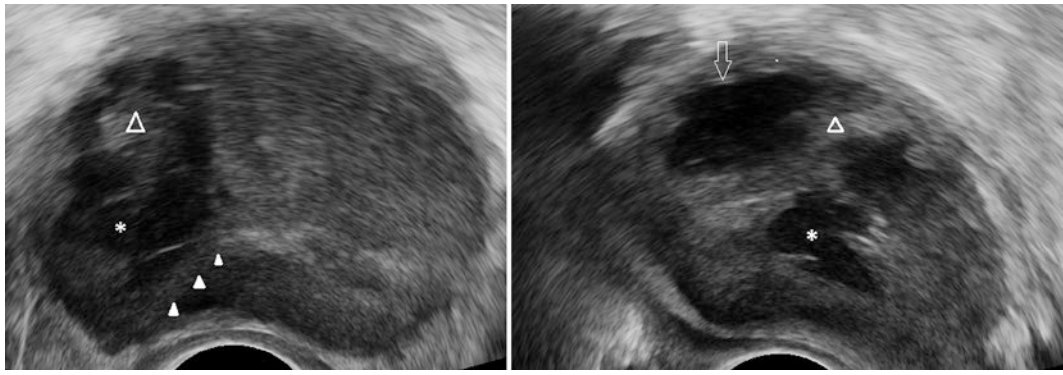

Fig. 21.3 Prostatic abscess appears hypoechoic with irregular content (*arrowheads*), anechoic (*arrow*), and irregular wall (*) that are typically associated with acute prostatitis (*arrowheads*), located in the anterior and peripheral zone

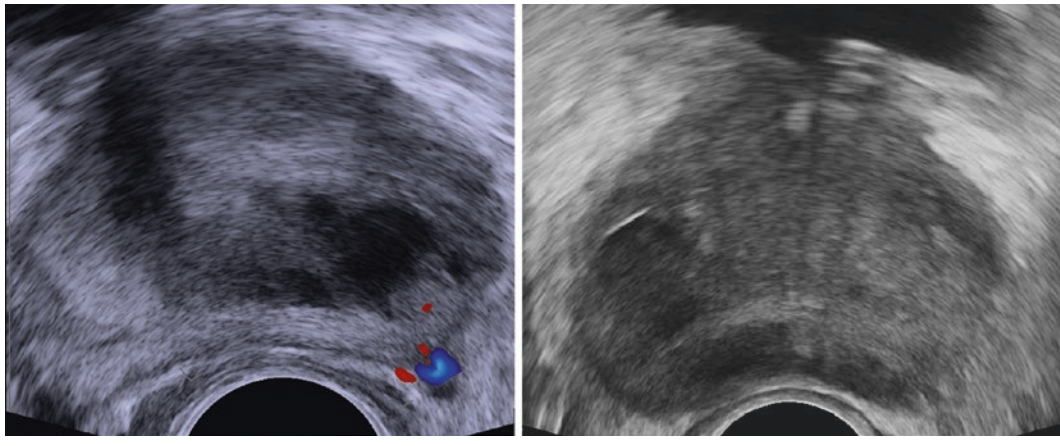

Fig. 21.4 Prostatic abscess: color Doppler ultrasound reveals perilesional vascularity

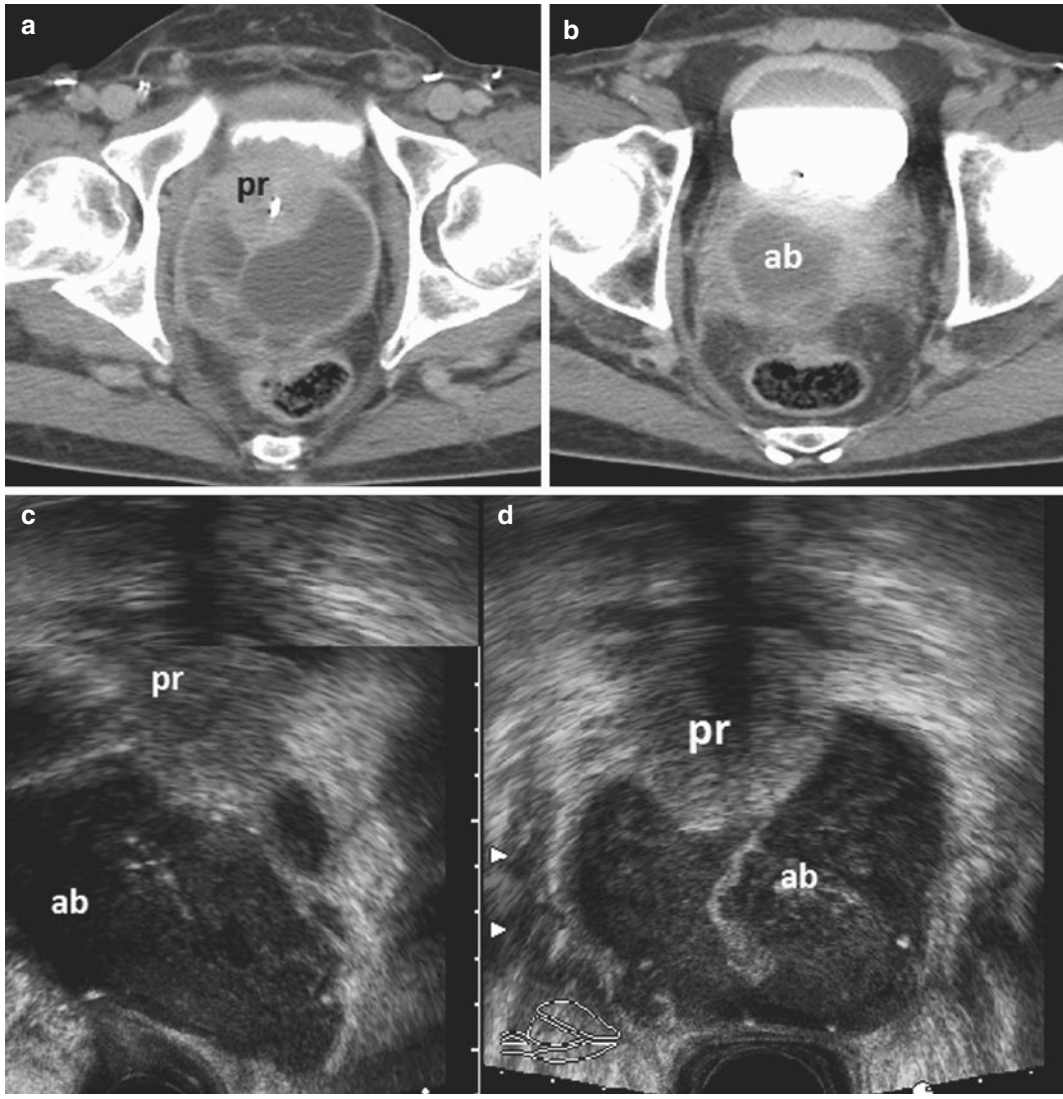

Fig. 21.5 Prostatic abscess (*ab*) extending beyond prostatic capsule (*pr*) in the perirectal tissue at CT (**a**, **b**), TRUS (**c**, **d**), and the same case after 3 months follow-up after transperineal drainage (**e**, **f** longitudinal and axial view)

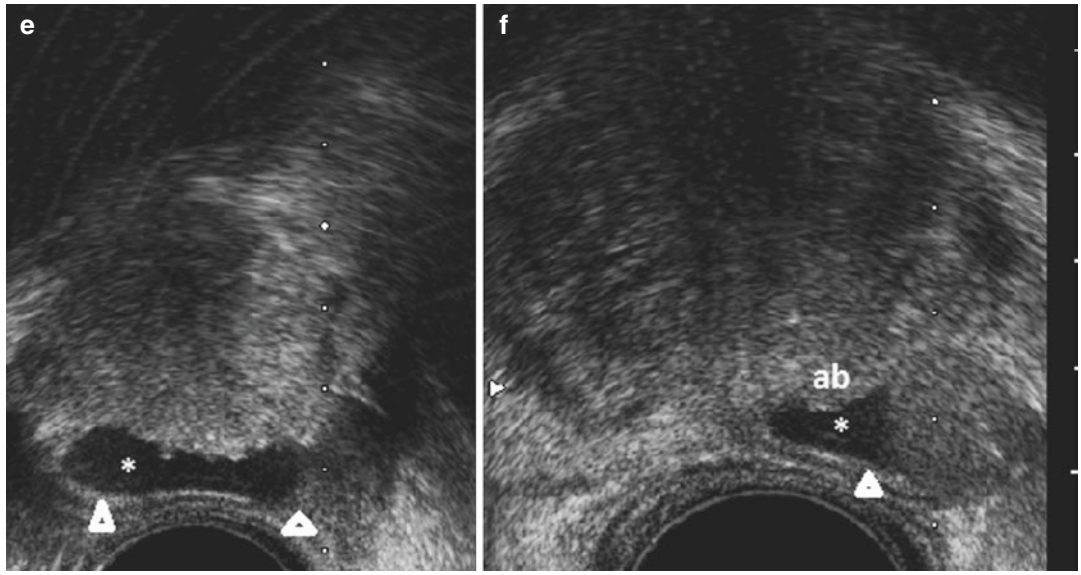

Fig. 21.5 (continued)

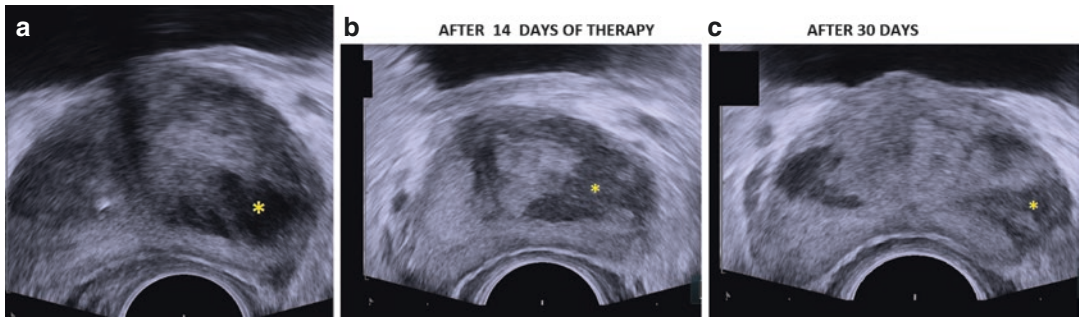

Fig. 21.6 (**a**) Ultrasound monitoring of small prostatic abscess (*) after 14 days of antibiotic treatment (**b**) and 30 days (**c**)

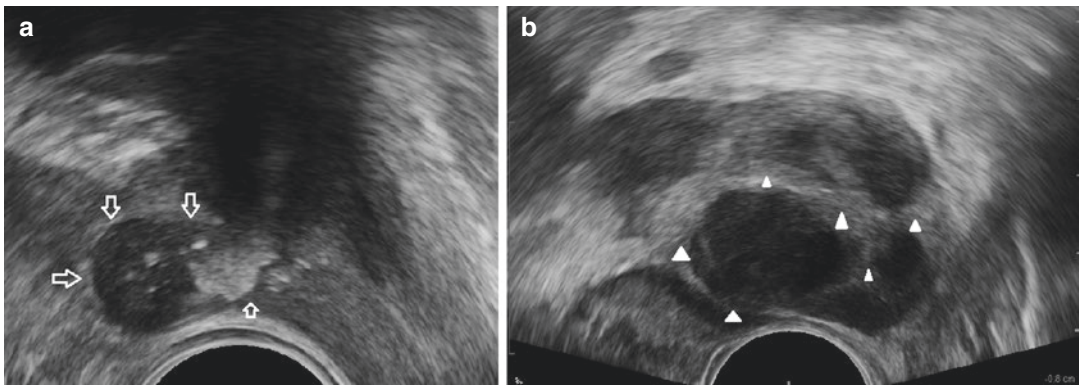

Fig. 21.7 Differential diagnosis between infected midline cyst (**a**) with regular shape (*arrows*) and prostatic abscess (**b**) with irregular shape and lobulated borders (*arrowheads*)

21.2 Chronic Bacterial Prostatitis

The diagnosis of chronic forms relies on the presentation of pelvic or perineal pain, typically lasting for longer than 3 months after acute bacterial infection. The prevalence of prostatitis ranges between 5 and 11 % [2]. Prostatitis occurs at any age and its incidence increases with age. Chronic bacterial prostatitis is associated to BPH complication and urinary tract obstruction, urethral catheter, and urinary retention. Bacteria (most commonly *Escherichia coli*) invade the prostate by an ascending urethral infection, by reflux of infected urine into prostatic ducts, or by lymphatic/hematogenous spread. In chronic bacterial prostatitis, any characteristic ultrasound pattern can be detected. Color Doppler may detect diffuse increased enhancement of contrast; however, TRUS and contrast-enhanced color Doppler are not used in routine clinical practice since no studies regarding this issue have been performed. Prostatic calculi and hyperechoic areas should be described in the ultrasound report. Hyperechoic area that may be interpreted as post-inflammatory signature does not have posterior acoustic shadow compared to hyperechoic image linked to calculi (Fig. 21.8). The relationship between chronic prostatic inflammation, prostatic calculi, and infection was suspected in the past. Kim et al. [7] studied the relationship between inflammation and prostatic calculus and clinical parameters of benign prostatic hyperplasia in 225 patients. They showed that prostatic calculi had no significant association with chronic inflammation. Chronic inflammation was associated with the volume of the prostate and storage symptoms; thus, it is not only presumed to be related to the progression of BPH, but may also be one of the causes of lower urinary tract symptoms. This hypothesis was supported by Ficarra [8] that proposed the prostatic calculi as "marker" of chronic inflammation linked to BPH.

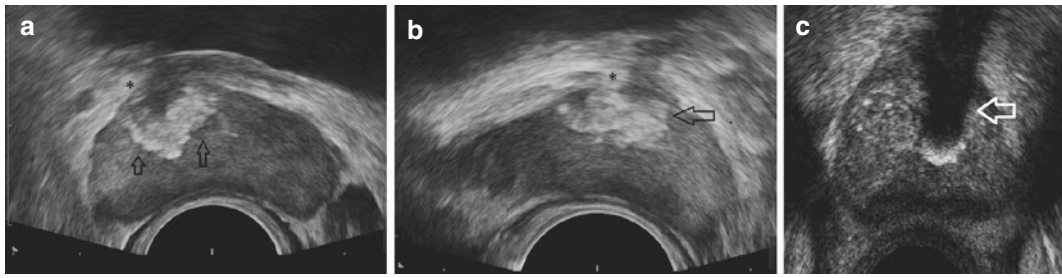

Fig. 21.8 Hyperechoic (*arrows*) without posterior acoustic shadow (*) in axial (**a**) and longitudinal view (**b**) compared to hyperechoic calculi (**c**) with posterior shadow (*white arrow*)

21.2.1 Granulomatous Prostatitis

Granulomatous prostatitis (GP) is an unusual benign inflammatory condition of the prostate that rarely presents clinically in urologic practice. Clinically, GP presents as a focal or diffuse area of induration at the digital rectal examination and is often mistaken for carcinoma (Figs. 21.9 and 21.10). PSA levels have also been shown not to be of value in differentiating carcinoma from granulomatous prostatitis. However, a clinical history of urinary tract infections or recent acute prostatitis is noticed frequently in patient's history. GP and carcinoma can produce similar findings on transrectal ultrasound: hypoechoic lesion with ill-defined borders, even anatomical location, may be in the peripheral zone. GP in any characteristic of ultrasound pattern is possible to differentiate them from carcinoma. Therefore, definitive diagnosis is combined with TRUS-guided biopsy. In these cases target biopsies are recommended in addition to random biopsy. The diagnosis of granulomatous prostatitis can only be made via histopathologic examination [9, 10].

Based on its histopathology and probable etiology, granulomatous prostatitis has been classified into the following types: idiopathic (nonspecific), infective (specific), iatrogenic (post-surgery), malakoplakia, and cases associated with systemic granulomatous disease and allergy. Nonspecific granulomatous prostatitis is the most common type, accounting for 60–80 % cases of granulomatous prostatitis. Infective granulomatous prostatitis can be caused by *Mycobacterium tuberculosis*, attenuated *Mycobacterium bovis* (Bacillus Calmette-Guerin) as endovesical immunotherapy for bladder cancer, *Treponema pallidum*, viruses, and fungal organisms.

Prostatic involvement in Wegener granulomatosis is unusual. A Mayo Clinic series found prostatic involvement in 4/174 patients (2.3 %) [11], whereas Walton [12] found prostatic involvement in 4/54 patients (7.4 %). A literature review found only 18 case reports of prostatic symptoms due to Wegener granulomatosis (five hematuria, eight chronic obstruction, five acute retention) and only 7/18 reported prostatic symptoms as initial complaint [13].

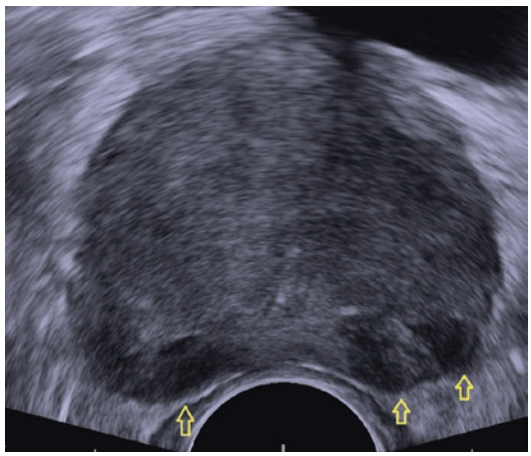

Fig. 21.9 Granulomatous nodules in the peripheral zone (*arrows*)

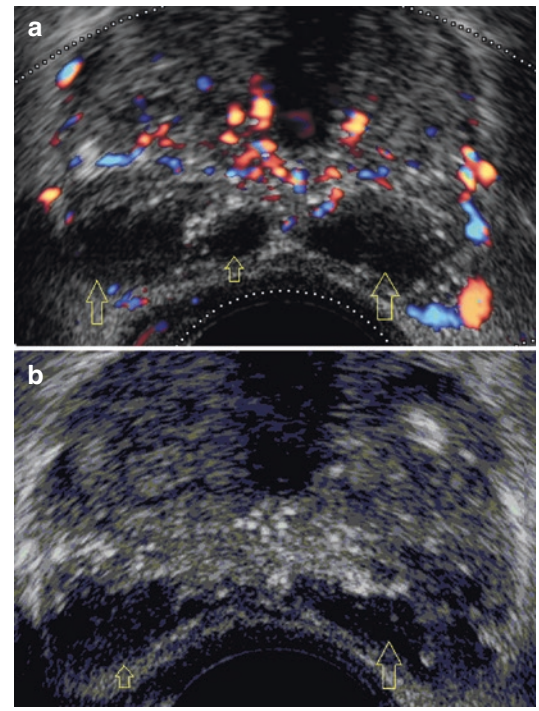

Fig. 21.10 (**b**) Granulomatous nodules in the peripheral zone (*arrows*), power Doppler (**a**) shows perilesional vascularity

21.3 Chronic Nonbacterial Prostatitis/Chronic Pelvic Pain Syndrome

The chronic nonbacterial prostatitis is the most common form (up to seven to eight times more common than other forms). The pathophysiology of nonbacterial prostatitis is not well understood. Prostatitis-like symptoms, for example, the presence of perineal/pelvic pain and/or ejaculatory pain or discomfort, can be associated with prostatitis, but they should not be confused with prostatitis [14]. Prostatitis-like symptoms are a cluster of bothersome complaints which impair the patient's quality of life. Currently gray-scale transrectal and color Doppler ultrasound signs are neither recognized as hallmarks of prostate inflammation, nor do they have clear cutoffs [15]. Imaging of the prostate-vesicular region is considered as an "optional" tool in evaluating CP/CPPS.

21.4 Asymptomatic Prostatitis

The asymptomatic inflammation is usually detected by histology in patients who underwent prostate biopsy since elevated serum prostate-specific antigen levels. This is not a disease, but can be defined as a pathological detection of prostatic inflammation. This inflammation is the most common form of pathologically detected prostatic inflammation, whereas in real-life clinical practice chronic prostatitis is the most frequent form. Etiology is unknown: bacterial, vascular, immune, and other hypotheses have been supposed. Asymptomatic inflammation is usually associated with large prostate glands with benign hyperplasia and lower urinary tract symptoms related to urinary obstruction. Pathological classification including grading, extension, and location of acute and chronic inflammatory infiltrates of the prostate based on surgical specimen or needle biopsy is reported in Table 21.3.

Moreira et al. [16] analyzed 886 men with benign prostatic enlargement and PSA elevation using prostate biopsy in the Reduction by Dutasteride of Prostate Cancer Events (REDUCE) study. Chronic, acute inflammation, and both were detected in 531 (60%), 12 (1%), and 84 (9%) baseline biopsies, respectively. Acute and chronic inflammation were significantly associated with each other ($P<0.001$). Chronic inflammation was associated with larger prostate ($P<0.001$).

A chronic asymptomatic prostatic inflammation seems to play a crucial role in benign prostatic hyperplasia (BPH) pathogenesis and progression. Ficarra et al. [8] analyzed the evidence supporting the role of inflammation in the onset and progression of BPH. Indeed, several data favor the role of infiltrating lymphocytes in the development and progression of prostate adenoma as an effect of a self-maintaining remodeling process.

Table 21.3 Pathological grading, extension, and location of acute and chronic inflammatory infiltrates of the prostate based on surgical specimen or needle biopsy

Feature	Histology details of inflammatory cells (ICs)
Location	Histologic pattern (acute and chronic infiltrates)
1. Luminal	1. ICs lie within glandular lumens
2. Intraepithelial	2. ICs lie within the glandular epithelium
3. Stromal, periglandular	3. ICs within stroma, centered around glands, approach <50 μm
4. Stromal, nonperiglandular	4. ICs within stroma, not centered on glands and lie ≥50 μm
Extent	Tissue area involved by inflammatory cells
1. Focal	<10 %
2. Multifocal	10–50 %
3. Diffuse	>50 %
Grade (luminal)	Morphological description
1/mild	1. Scattered individual ICs (≤5 cells/lm)
2/moderate	2. Loose collection of ICs without nodule formation
3/severe	3. Dense cluster of inflammatory cells with nodule formation
Grade (intraepithelial)	Morphological description
1/mild	1. Rare ICs (≤1/10 epithelial cells)
2/moderate	2. Few ICs with no cluster formation (1–5/10 epithelial cells)
3/severe	3. Cluster of ICs (>5/10 epithelial cells)
Grade (stromal)	Morphological description
1/mild	1. Scattered ICs
2/moderate	2. Clusters of ICs with no nodule/follicle formation
3/severe	3. Confluent sheets of ICs with nodule/follicle formation

Modified from Nickel et al. [3]
The modification is the addition of intraepithelial inflammation according to Magi-Galluzzi et al.

References

1. Krieger JN, Nyberg L Jr, Nickel JC (1999) NIH consensus definition and classification of prostatitis. JAMA 282:236
2. Krieger JN, Lee SW, Jeon J, Cheah PY, Liong ML, Riley DE (2008) Epidemiology of prostatitis. Int J Antimicrob Agents 31 Suppl 1:S85–S90
3. Nickel JC, True LD, Krieger JN et al (2001) Consensus development of a histopathological classification system for chronic prostatic inflammation. BJU Int 87:797–805
4. Nickel JC (2003) Recommendations for the evaluation of patients with prostatitis. World J Urol 21: 75–81
5. Naik KS, Carey BM (1999) The transrectal ultrasound and MRI appearances of granulomatous prostatitis and its differentiation from carcinoma. Clin Radiol 54:173
6. Galosi AB, Parri G, Lacetera V, Muzzonigro G (2010) Management of large prostatic abscess associated with urethral stenosis and penile cancer recurrence. Arch Ital Urol Androl 82(3):181–185
7. Kim SH, Jung KI, Koh JS, Min KO, Cho SY, Kim HW (2013) Lower urinary tract symptoms in benign prostatic hyperplasia patients: orchestrated by chronic prostatic inflammation and prostatic calculi? Urol Int 90(2):144–149
8. Ficarra V, Rossanese M, Zazzara M, Giannarini G, Abbinante M, Bartoletti R, Mirone V, Scaglione F (2014) The role of inflammation in lower urinary tract symptoms (LUTS) due to benign prostatic hyperplasia (BPH) and its potential impact on medical therapy. Curr Urol Rep 15:463–469
9. Tamsel S, Killi R, Ertan Y, Demirpolat G (2007) A rare case of granulomatous prostatitis caused by Mycobacterium tuberculosis. J Clin Ultrasound 35:58–61
10. Mohan H, Bal A, Punia RPS et al (2005) Granulomatous prostatitis: an infrequent diagnosis. Int J Urol 12:474
11. Stillwell TJ, DeRemee RA, McDonald TJ, Weiland LH, Engen DE (1987) Prostatic involvement in Wegener's granulomatosis. J Urol 138:1251–1253
12. Walton EW (1958) Giant-cell granuloma of the respiratory tract (Wegener's granulomatosis). Br Med J 2:265–270
13. Middleton G, Karp D, Lee E, Cush J (1994) Wegener's granulomatosis presenting as lower back pain with prostatitis and ureteral obstruction. J Rheumatol 21: 566–569
14. Schaeffer AJ (2006) Clinical practice: chronic prostatitis and the chronic pelvic pain syndrome. N Engl J Med 355:1690–1698
15. Lotti F, Corona G, Mondaini N, Maseroli E, Rossi M, Filimberti E, Noci I, Forti G, Maggi M (2014) Seminal, clinical and colour-doppler ultrasound correlations of prostatitis-like symptoms in males of infertile couples. Andrology 2:30–41
16. Moreira DM, Nickel JC, Andriole GL, Castro-Santamaria R, Freedland SJ (2015) Chronic baseline prostate inflammation is associated with lower tumor volume in men with prostate cancer on repeat biopsy: results from the REDUCE study. Prostate 75(13):1492–1498

Prostatic Cysts

22

Andrea Benedetto Galosi, Luigi Quaresima,
Roberta Mazzucchelli, and Rodolfo Montironi

22.1 Introduction

Thanks to the widespread use of prostatic transrectal ultrasound (TRUS) scanning in uro-andrological practice today, there has been an increase in the incidental diagnosis of cystic lesions of the prostate; the mean rate is now 5 % (range 0.5–7.9 %) in patients with lower urinary tract symptoms (LUTS) [1]. The clinical relevance of this finding is still under debate, but cysts have been associated with inflammation, obstruction of the seminal or urinary tract, as well as cancer. Making a correct differential diagnosis is therefore extremely important. During scanning, and also in the final ultrasound (US) report, prostatic cysts often tend to be largely ignored, neglecting to state both their identification and any characterization [2]. In fact, there are no uniform, shared criteria for the final US report classification and description of their characteristics.

A.B. Galosi (✉) • L. Quaresima
Institute of Urology, Polytechnic University of Marche Region, Azienda Ospedaliero-Universitaria United Hospitals, Ancona, Italy
e-mail: galosiab@yahoo.it

R. Mazzucchelli • R. Montironi
Polytechnic University of Marche Region, Ancona, Italy
e-mail: r.mazzucchelli@univpm.it; r.montironi@univpm.it

TRUS has a central role in promoting a correct clinical examination of prostatic cysts, because abdominal US shows a very limited diagnostic accuracy. Different types of cysts can be present in the same individual, and only a proper description can help to orient the therapeutic choices of the clinical urologist or andrologist.

The classification presented in this chapter is based exclusively on transrectal ultrasound that provides an excellent image quality even of small lesions owing to the use of high-resolution devices and transducers with a frequency ranging from 5 to 9 Mhz. TRUS is considered the first-line examination for the diagnosis and classification of cysts. In particular cases, it may also be necessary to resort to magnetic resonance imaging (MRI) that relies on a multiparametric technique for the diagnosis of prostate cancer.

The pathophysiogenesis of prostatic cysts is not yet entirely understood, and it is equally difficult to estimate their clinical repercussions that will manifest only at a late stage when a voluminous lesion obstructs the urethra or seminal ducts [3]. It is now thought that the clinical impact of small lesions may be underestimated because of their having been ignored in the initial diagnostic phase. The origin of cystic lesions has been attributed to various pathogenic causes, namely, inflammation, benign prostatic hyperplasia, calculi, and in rare cases cancer, or parasites.

P. Martino, A.B. Galosi (eds.), *Atlas of Ultrasonography in Urology, Andrology, and Nephrology*,
DOI 10.1007/978-3-319-40782-1_22

Epithelial atrophy has also been recently linked to the formation of cysts. In 2006, a new classification of focal atrophy of the prostate epithelium was published that included four different patterns, one of which was simple atrophy with cyst formation [4]. Thus, on the basis of current histopathological knowledge, some cystic lesions of the prostate, even small ones, can be correlated to focal epithelial atrophy and may be a clinical marker of this condition.

Various different classifications of prostatic cysts have been published up to now [5, 6] that differ as regards the clinical presentation criteria (e.g., correlated to urinary symptoms, infertility, infections, or cancer) and the diagnostic method employed (e.g., MRI, TRUS, histology). In this chapter, we present the classification of prostatic cysts (Table 22.1) previously published by Galosi et al. [7]. The classification features a subdivision of cysts into six groups according to their pathogenesis, US findings, and pathological characteristics. It is based on an ample case series and integrates clinical and pathology findings, US features and findings after biopsy, simple and radical prostatectomy, and cystoprostatectomy. Table 22.2 shows a comparative illustration of the essential elements of diagnosis and therapy.

Table 22.1 Prostatic cyst classification [7]

1. Midline cyst
(a) Prostatic utricle cyst (PUC)
(b) Cystic utricle (*or cystic dilation of the prostatic utricle*)
(c) Enlarged prostatic utricle
2. Cysts of the ejaculatory ducts
3. Parenchyma cyst
(a) Simple parenchymal cysts
(b) Multiple parenchymal cysts (*ductal ectasia or microcysts*)
(c) Small cystic parenchymal nodules
(d) Large cystic parenchymal nodules
4. Cyst complicated
(a) Cysts complicated by infection
(b) Hemorrhagic cysts
5. Cystic tumors
(a) Cystadenoma
(b) Cystadenocarcinoma or high-grade tumor
(c) Dermoid cyst
6. Parasitic cysts

Table 22.2 Prostatic cysts classification with subclassification, essential characteristics and treatment

Cyst	Anatomical location/US features	Content	Pathogenesis	Differential diagnosis	Treatment
1. Midline (a) Utricular (b) Cystic dilatation (c) Enlarged prostatic utricle	Round shape and anechoic Absent communication with urethra Presence of communication with urethra Wide opening in the prostatic urethra	Clear liquid without sperm	Congenital or acquired	Bladder diverticula Ejaculatory duct cyst Cystadenoma Simple cyst	Transperineal aspiration and alcohol injection in noncommunicating cyst, TURED if symptoms or communicating cyst
2. Cysts of the ejaculatory ducts	Paramedian or lateral, above the verumontanum, could touch the seminal vesicle	Sperm	Congenital or acquired Mono-/bilateral	Midline cyst Duct dilatation	Aspiration, resection, retrograde endoscopic dilatation if infertility, or hemospermia
3. Parenchyma (a) Simple (b) Multiple/microcysts (c) Small cystic nodules (d) Large cystic nodules	(a) Single or multiple, sizing 0.5–9 cm, subcapsular or paraurethral (b) Oval, small anechoic space of 1 mm (c) and (d) Cysts <1 cm grape shape, with pseudocapsule containing several cysts (1–20 mm)	Clear liquid without sperm	Congenital or acquired BPH retention of prostatic fluid, inflammation, atrophy, and cystic degeneration of BPH	Midline cyst Ejaculatory duct cyst Cystadenoma Abscess	Observation BPH medical therapy TURP (or deroofing) if urinary symptoms
4. Complicated cyst (a) Infection (b) Hemorrhagic	Irregular iso-/hyperechoic liquid collection (a) Not well-defined border (b) Well-defined borders	Purulent or hemorrhagic secretions	Abscess (es.TBC) Hemorrhagic infarction and hematoma after biopsy	Parasitic cyst Pararectal abscess Fistule	If symptoms not responsive to antibiotics: Percutaneous drain placement TURP
5. Cystic tumors (a) Cystadenoma (b) Cystadenocarcinoma (c) Dermoid cyst	(a) Large and complex cyst with iso-/hypoechoic content, invading (the bladder, rectum, and seminal vesicles) without infiltration, pseudocapsule is present (b) Absence of pseudocapsule, infiltrating pelvic organs (c) Hyperechoic content (squamous diff.)	Biopsy or TURP Cytology is not useful	Cancer transformation of the cuboidal epithelium of the cyst	*Grandi noduli cistici* Ductal cancer with cystic pattern Others neoplasms (colon, metastasis) Computerized tomography or magnetic resonance	(a) Prostatectomy (b) Cystoprostatectomy ± radiation/hormonal therapy (c) Observation or surgery
6. Parasitic cyst	Single or multiple large cysts with compressing pattern of growth without infiltrating	Parasitic tests Biopsy	Bilharziasis, Hydatidosis infection	Large cystic nodules Ductal cancer	Medical treatment Transperineal drain with cytology analysis

TURED transurethral resection of the ejaculatory ducts, *BPH* benign prostatic hyperplasia, *TURP* transurethral prostatic resection

22.2 Classification of Cystic Prostatic Lesions

22.2.1 Midline Cysts

Three distinct categories come under this heading: (a) *prostatic utricle cyst* (*PUC*), (b) *cystic utricle* (or cystic dilation of the prostatic utricle), and (c) *enlarged prostatic utricle*. This is in agreement with Kato et al. [8, 9], who proposed a subclassification of these cysts according to whether they have an outlet to the urethra: a *utricular cyst* has no outlet, while a *cystic utricle* has an obliterated and an *enlarged prostatic utricle* an open urethral outlet. US identification of an outlet from the cyst to the urethra is not always possible or easy to document, especially in cases with an obstructed outlet, where it will appear as a hyperechogenic stripe surrounded by a narrow hypoechogenic rim. Histologically, it is always possible to demonstrate the outlet [8, 9].

Another classification in the literature was published by Ritchey et al. [10], in whose subdivision, utricular cysts were denominated Ritchey Type 1. However, this classification has the limit that it defines cysts according to the site, whereas not all midline cysts are *utricular cysts*. In fact, a differential diagnosis must be made among midline cysts, parenchymal cysts, and cystadenomas.

22.2.1.1 Utricular Cysts

These are denominated cysts of the M*üllerian ducts* by some authors. At US, they appear as rounded or oval formations that can also be palpable and as large as several centimeters in diameter. They are localized on the midline, proximally to the seminal colliculus, and extend inside the prostatic base toward the insertion of the seminal vesicles (Fig. 22.1).

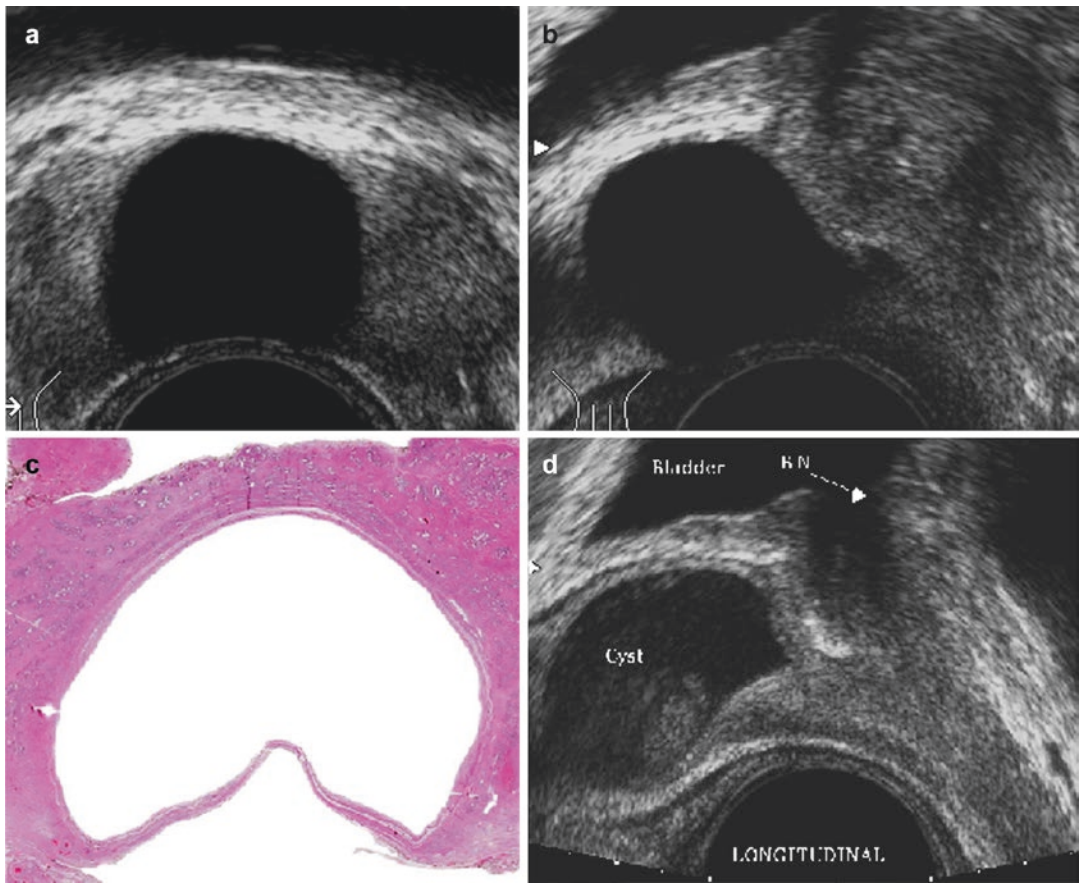

Fig. 22.1 Midline cyst (**a**, **b**). Macrosection of a radical prostatectomy surgical sample with a voluminous *utricular cyst* (**c**). US appearance of the prostatic utricular cyst (*bn* bladder neck, *sv* seminal vesicle) (**d**)

Histologically, there is no communication with the urethra, and the utricle has a normal morphology with a cuboid or columnar epithelium [8, 9]. Infectious complications of these cysts are less frequent because of the lack of communication with the urethra. Yasumoto et al. reported the characteristics of the fluid aspirate obtained by transperineal puncture of midline cysts, referring that the fluid did not contain spermatozoa and the prostate-specific antigen (PSA) concentration in the fluid was 90,000 ng/ml [11].

22.2.1.2 Cystic Utricle

Unlike *utricular cysts*, in a cystic utricle, there is an outlet from the cyst to the urethra, which is why it can also be called a *cystic dilation of the utricle*. It is drop shaped (owing to the communication with the urethra) or ovoid and localized on the midline. It is sometimes indistinguishable from a utricular cyst as regards the site and US features, although in other cases, it is possible to identify a virtual (obliterated) or a real (pervious) outlet. The former picture is visible as a hyperechogenic line at the level of the seminal colliculus surrounded by a narrow hypoechogenic rim (Fig. 22.2). On the basis of embryological studies, it seems that these cysts develop during the last stages of maturation of the utricle as a consequence of an obstruction of the physiological communication with the urethra. Histologically, the communication between the urethra and the cystic utricle is recognizable [8]. Infectious complications of these cysts are frequent because of the urethral outlet, and so they may have a homogeneous content (see *infected cyst*).

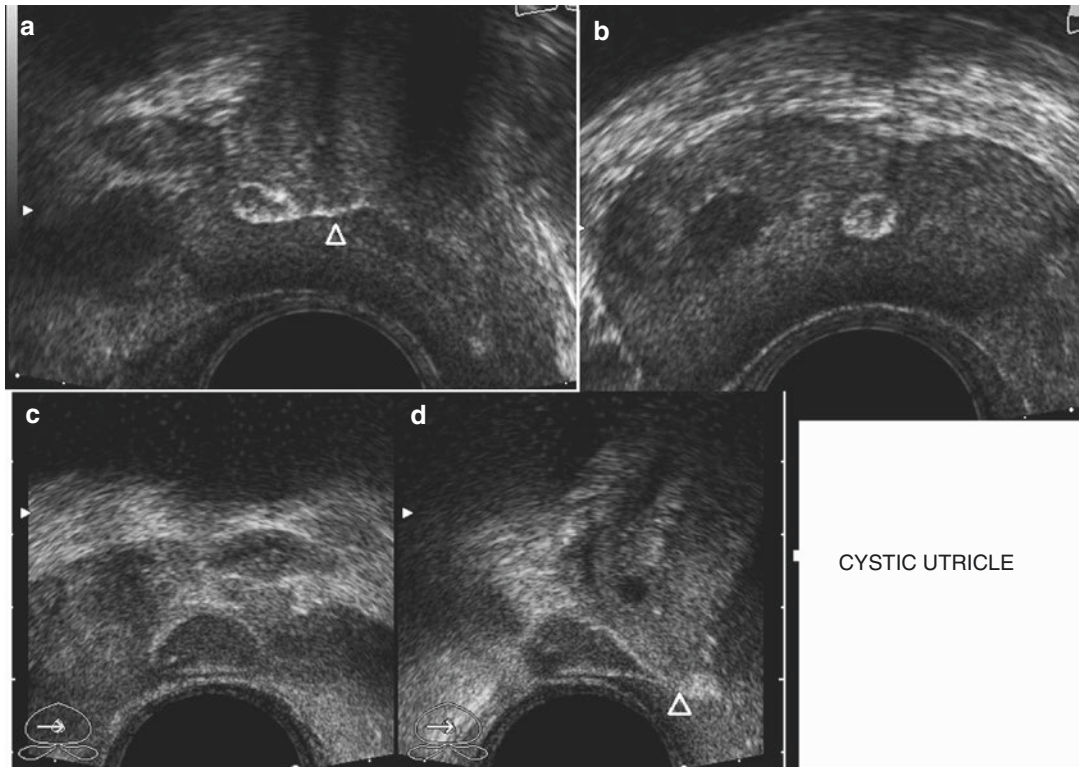

Fig. 22.2 Midline cyst Journal of Urology. Cystic utricle: (**a**, **b**) cyst wall showing microcalcifications (**c**, **d**) *complicated cyst* with a dyshomogeneous content due to infection. The cystic utricle outlet to the urethra (that is functionally obstructed) appears as a narrow hypoechoic line (at longitudinal scanning) connecting it to the seminal colliculus

22.2.1.3 Enlarged Prostatic Utricle

This shows a characteristic, wide outlet from the utricle to the urethra. It is a congenital malformation that is also known as a remnant of the *Müllerian* duct or a *male vagina* and is generally diagnosed in youths or boys with other malformations like hypospadias or virilization defects. It is not a true cystic formation, because a wide defect is present that causes an ample passage between the utricular cavity and the urethra. The seminal colliculus is sometimes absent, while a dilated tubular structure with a squamous epithelium is evident at histology [9]. Both at US and at retrograde cystourethrography, a cyst with an anechoic content is evident on the posterior midline, showing an ample outlet to the prostatic urethra (Fig. 22.3). The *enlarged utricle* corresponds to a Ritchey Type 2 cyst [10]. Symptoms include urinary infections, recurrent epididymitis, pain, and post-micturition dribbling. The cyst cavity may be palpable during rectal exploration. Rarely, complications such as calculi in the cystic cavity or neoplastic degeneration can be observed (reported by Sondergaard et al. in 6.3% of autopsies) [12]). The tumors that can originate from these structures have a distinct histology, prognosis, and clinical behavior: those that originate from the multistratified epithelium of the cyst wall give rise to squamous carcinoma, whereas those that originate from the ductal epithelium of the seminal colliculus develop into ductal (or endometrioid) adenocarcinoma [13].

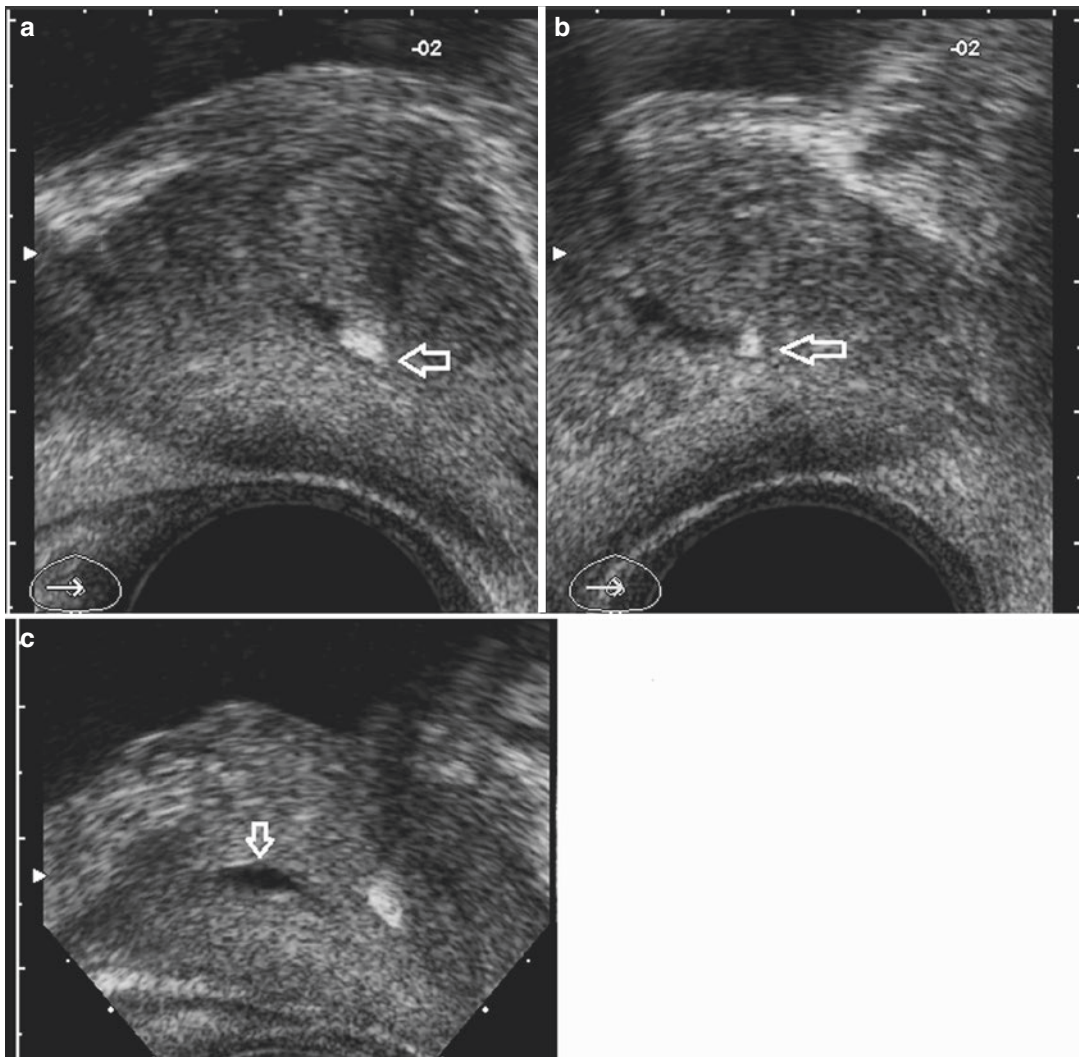

Fig. 22.3 Acquired cystic enlargement of the ejaculatory ducts (**c**, *arrow*) due to the presence of calculi at the level of the outlet to the prostatic urethra. Calculi appear as hyperechoic with black shadow (*arrow*) (**a**, **b**)

22.2.2 Cysts of the Ejaculatory Ducts

Cysts of the ejaculatory ducts are rare and may be congenital or acquired. Cyst can be unilateral or bilateral, rounded or oval, localized in the paramedian site lying between the verumontanum and the bladder neck, and extended from the paraurethral site to the base of the prostate (Fig. 22.4). Cysts of the ejaculatory ducts are linked to obstruction or compression and can contain spermatozoa, but some of these cysts have no outlet. Microscopic examination of the fluid is essential to identify spermatozoa, aspirated transperineally to reduce the risk of infection. In addition, puncture of these cysts combined with chromatography using iodinated contrast medium makes it possible to check for any outlet to the urethra or seminal tracts.

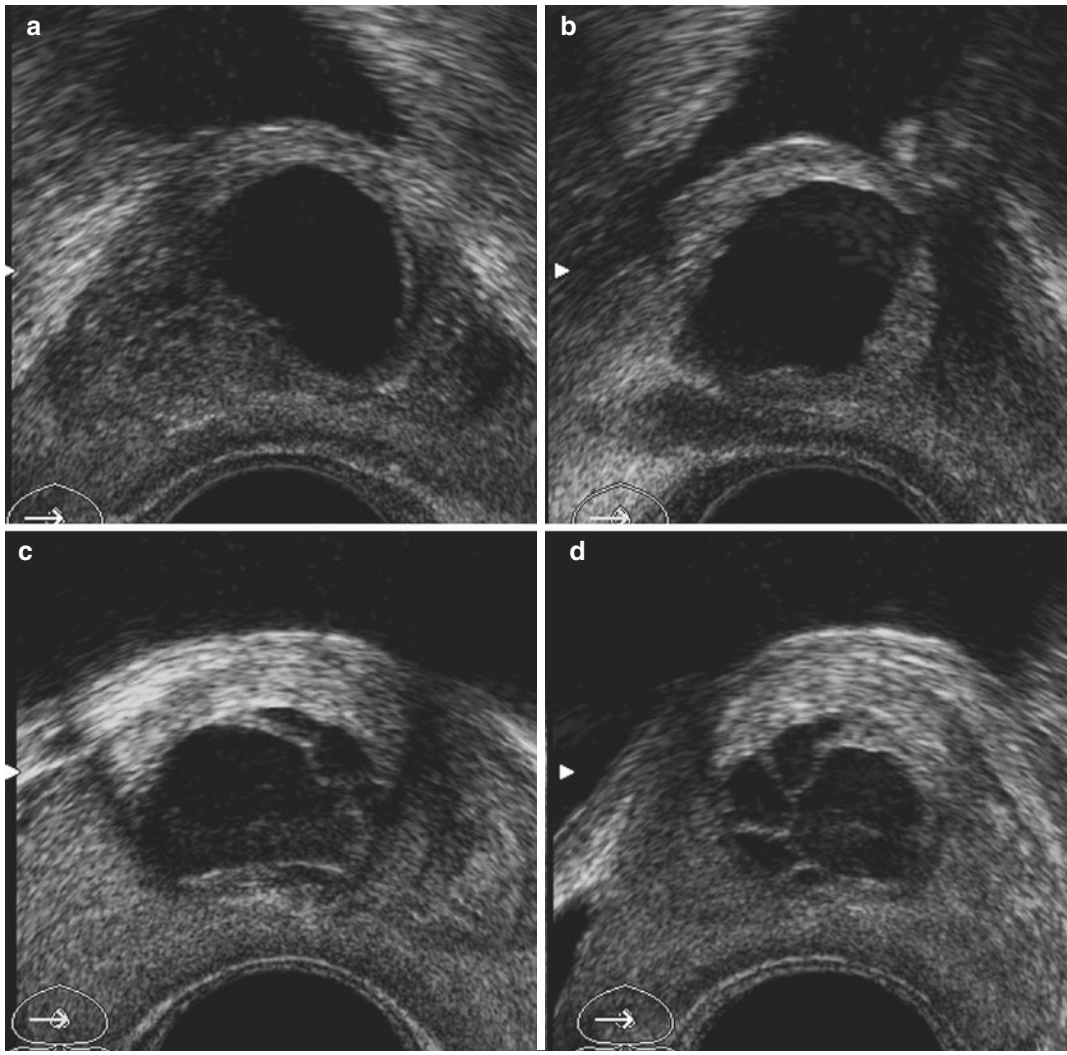

Fig. 22.4 Simple parenchyma cysts located close to the bladder neck and prostatic urethra that cause obstructive urinary symptoms. Ultrasound axial view of simple (**a**) and loculated (**c**) cyst; longitudinal view (**b**) of simple and loculated (**d**) cyst

22.2.3 Parenchymal Cysts

These cysts are the lesions most commonly observed. *Parenchymal cysts* are classified in four distinct subgroups. Symptoms depend largely on the volume of such cysts: if they are larger than 3 cm or if they subvert the gland parenchyma, they can cause obstructive symptoms. *Large cystic parenchymal nodules* have a clinical significance and require differential diagnosis with cystic tumors.

22.2.3.1 Simple Parenchymal Cysts

These acquired forms, also known as prostatic retention cysts, are seen as isolated masses inside a normal gland parenchyma. At US, they are oval or irregularly shaped and small or medium sized (mean diameter < 8 mm) but may also be larger (>3 cm). The content is anechoic, with thin uniform walls, and sometimes thin internal septa are visible. They are localized in a lateral subcapsular site or periurethrally or medially at the level of the bladder neck. These cysts can develop asymmetrically (Figs. 22.5, 22.6, and 22.7). The pathogenesis is attributable to difficulties in the drainage of secretions, secondary to obstruction caused by compression due to benign hyperplasia or inflammation. Obstructive symptoms are rare but possible in cases of voluminous cysts >3 cm localized at the level of the bladder neck.

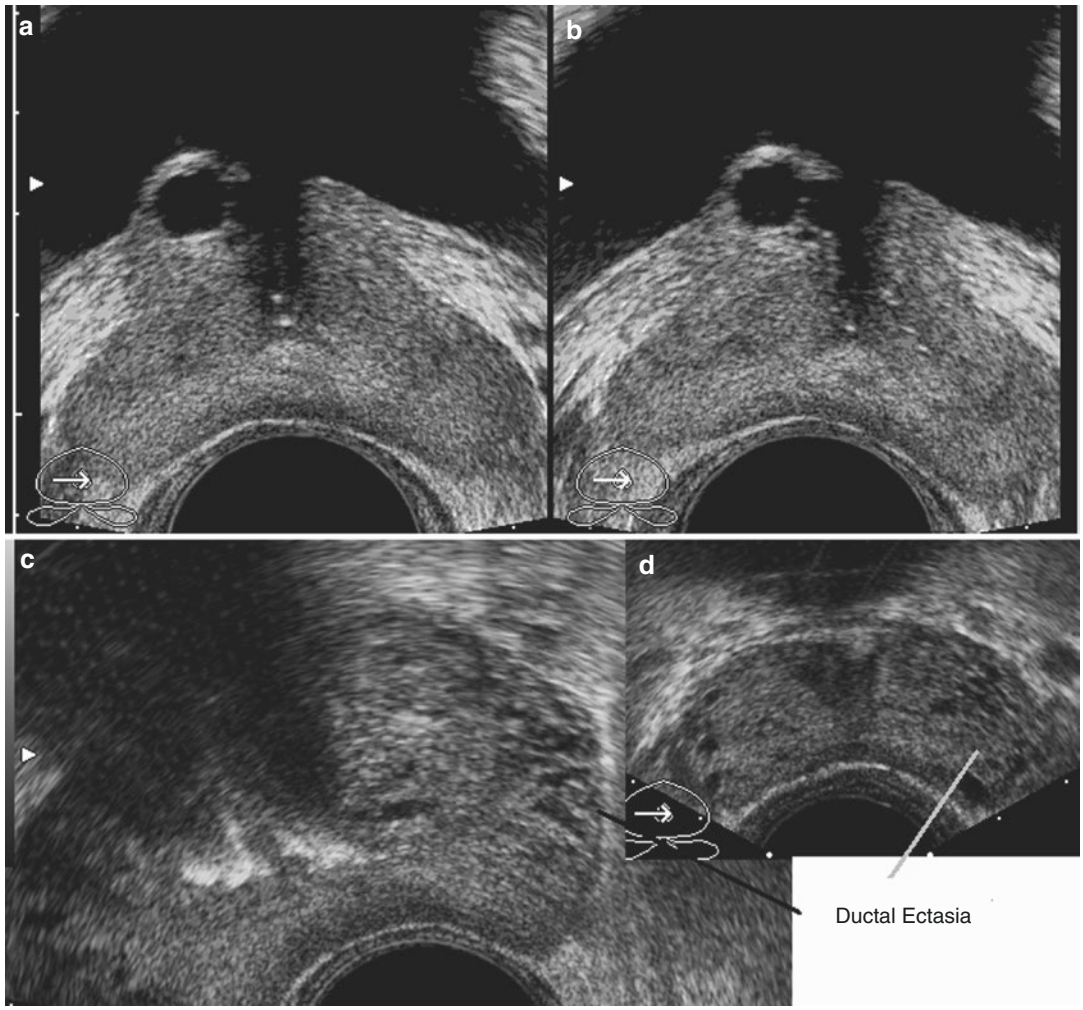

Fig. 22.5 *Simple cysts* of the bladder neck (**a**, **b**) and *multiple parenchyma cyst* (**b**, **c**) also related to ductal ectasia (**c**, **d**)

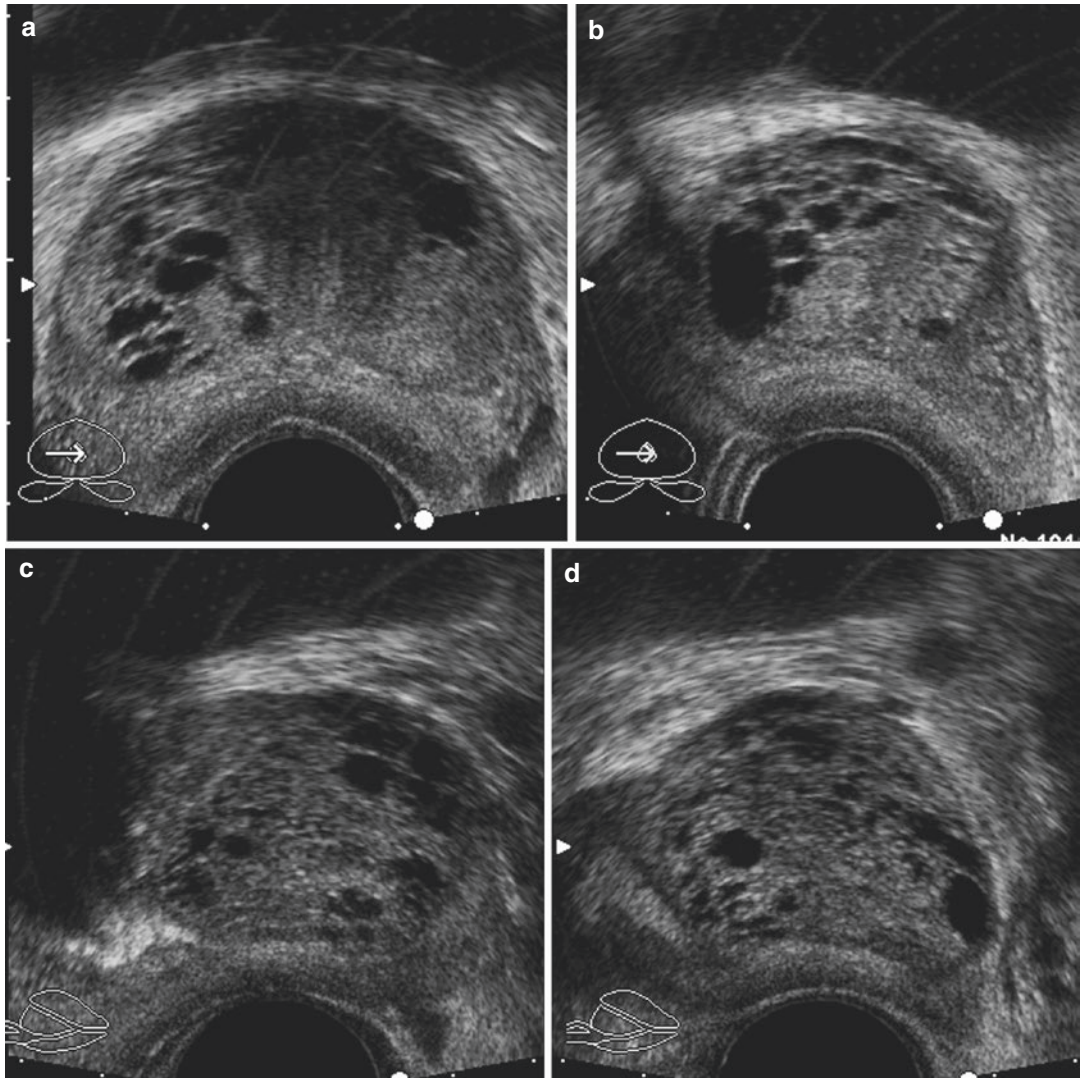

Fig. 22.6 (**a**, **b**) TRUS appearance of multiple *simple parenchymal cysts* (**a**, **b**) differentiated from large parenchymal nodule due to absence of the pseudocapsule (**c**, **d**)

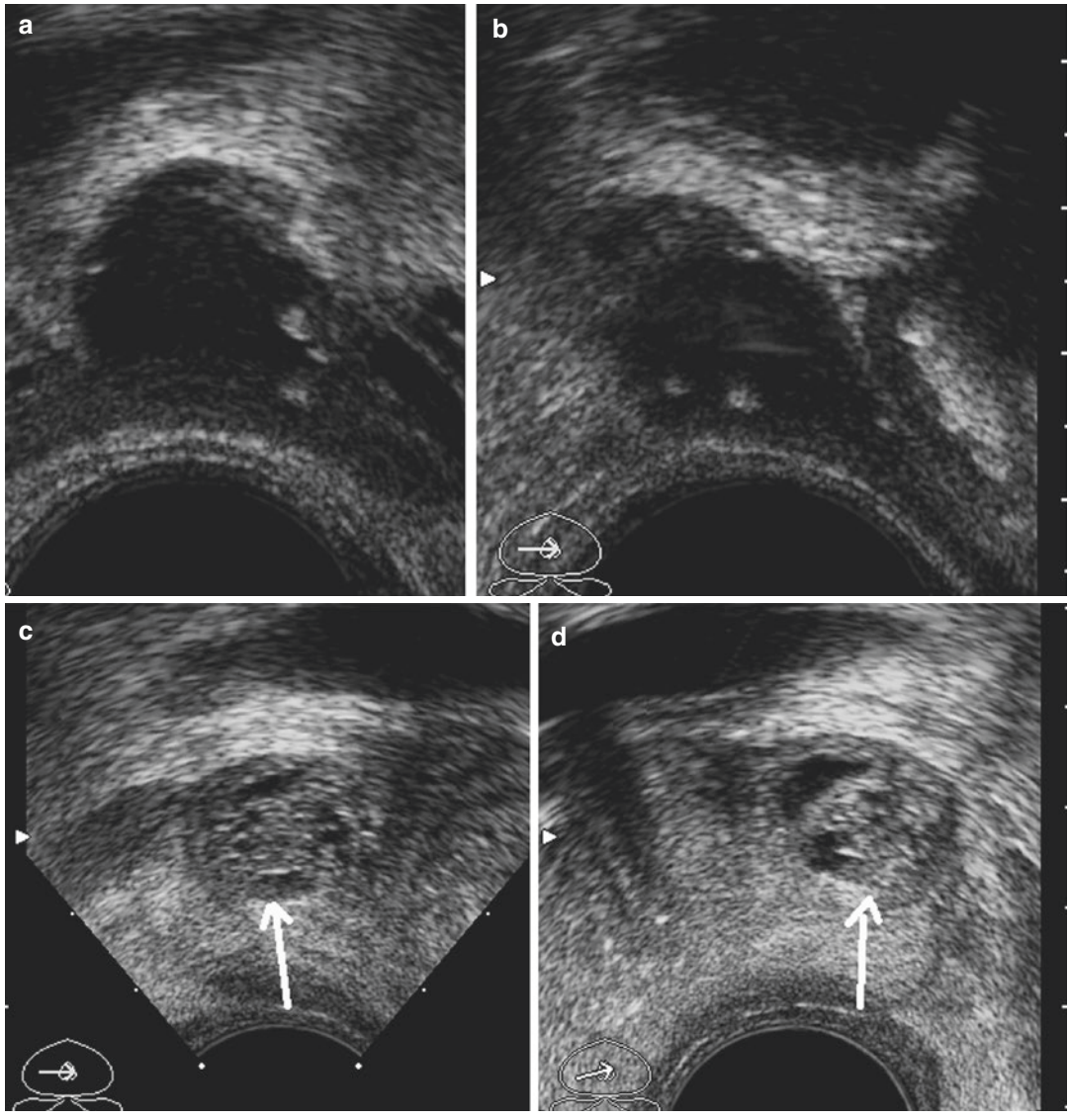

Fig. 22.7 Complicated midline cysts (**a**, **b**). Small parenchymal nodule delimitated by pseudocapsule (*arrows*) (benign prostatic hyperplasia with cystic differentiation) (**c**, **d**)

22.2.3.2 Multiple Parenchymal Cysts

Also known as *ductal ectasia* or *microcysts*, at transrectal US, they are seen as homogeneous tissue consisting of cystic lacunae measuring about 0.5–1 mm in diameter (Figs. 22.6 and 22.7) [1]. They can also be attributed to the retention of prostatic secretions or to simple atrophy with cyst formation (SACF) and will involve large parts of the gland, showing small cystic acini. In our experience, they are mainly found in men with an infrequent or irregular sexual activity.

Differential diagnosis must be made with subcapsular fluid collection resulting from intraprostatic urine reflux and acute prostatic inflammation.

22.2.3.3 Small Cystic Parenchymal Nodules

These consist of small cysts bunched together inside a small nodule (mean Ø 5–8 mm), easily distinguishable from the surrounding parenchyma, that at TRUS look like a bunch of grapes outlined by a thin pseudo-capsule. Histologically, these small cystic nodules are correlated to simple atrophy with cyst formation or else they can mark the initial phase of prostatic hyperplasia with cystic degeneration (Fig. 22.8).

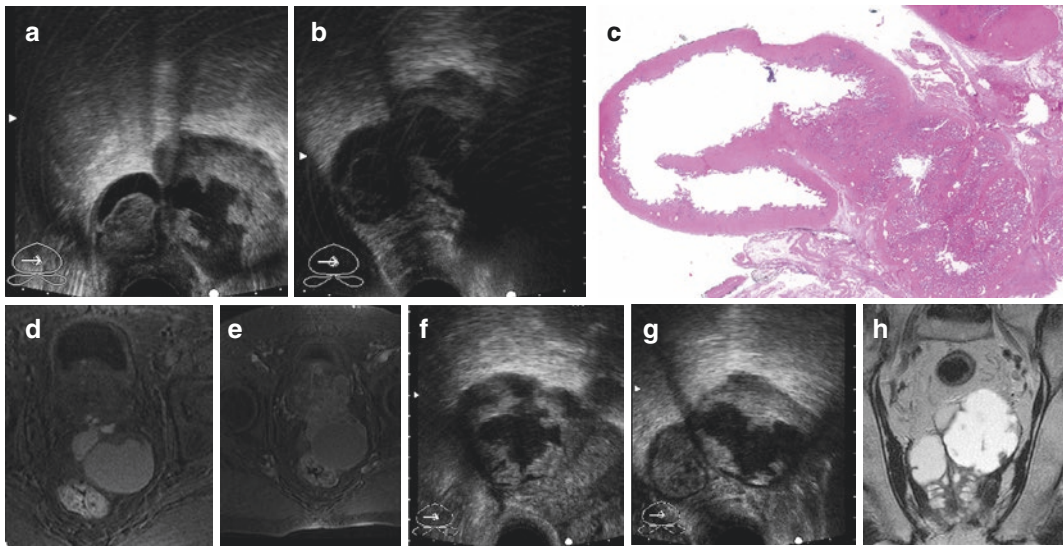

Fig. 22.8 *Cystic tumor*: (**a**, **b**, **f**, **g**) (TRUS); (**c**) (histology); (**d**–**f**, **h**) (magnetic resonance imaging). High-grade prostatic neoplasia with invasive pattern of growth toward the bladder and rectum, the cystic wall, and content and is mostly irregular

22.2.3.4 Large Cystic Parenchymal Nodules (LCPN)

These nodules have completely replaced the parenchyma and are surrounded by a pseudocapsula. LCPN consist of an agglomeration or bunch of many simple cysts with different diameters. The denomination large multicystic nodule is the preferred terminology because it better describes the US appearance that resembles polycystic kidney. Cystic nodules can be localized practically anywhere but are most commonly observed in the transition zone and central zone. LCPN are generally unilateral and develop asymmetrically. They compress the surrounding parenchyma and the urethra, deforming the prostatic capsule (Fig. 22.8). These cysts contain anechoic fluid attributable to prostatic secretions. At histology, large cystic nodules are an expression of prostatic hyperplasia with cystic degeneration. Prostatic hyperplasia nodules with cystic degeneration, or SACF, or atypical polypoid prostatic hyperplasia can be histopathologically correlated to LCPN. Differential diagnosis must be made with cystadenoma and cystadenocarcinoma. MRI may be useful to ascertain the diagnosis in cases of multiseptal cysts with irregular walls and an iso-/hyperechoic content.

22.2.4 Complicated Cysts

22.2.4.1 Cysts Complicated by Infection

A preexisting cyst can be complicated by an acute or chronic bacterial infection (generally Gram negative). Sometimes the presence of a cyst will foster evolution to an abscess. A prostatic abscess can then form a pseudocystic cavity. The content of complicated cysts is generally dyshomogeneous with an iso-/hyperechoic, dyshomogeneous component. The cystic content, fluid, corpusculated, or solid, will depend on any associated granulomatous inflammation in the surrounding parenchyma. At US, an infected cyst appears as a mass with irregular margins as compared to the rest of the parenchyma and a mixed tenuously hypo-/anechoic echostructure. Internal echoes depict the inflammatory tissue containing necrotic matter. At color Doppler, there is generally an increased vascular signal around the lesion, while the center usually lacks any visible vascularization at echo power Doppler (Fig. 22.9). Treatment of infected cysts may be medical, but sometimes transperineal percutaneous drainage is indicated or surgical treatment consisting of transurethral endoscopic resection.

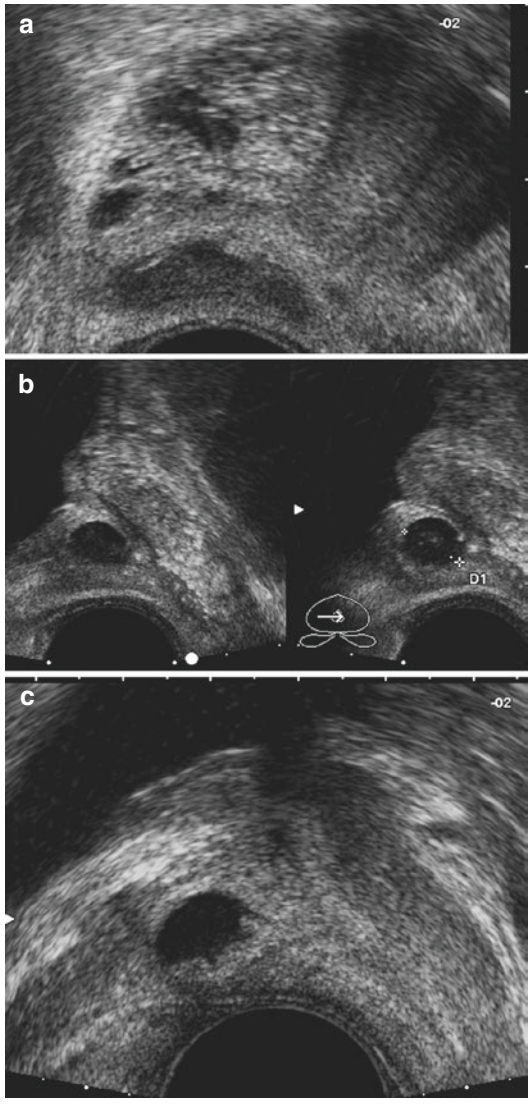

Fig. 22.9 *Complicated cysts*: (**a**) infected cyst with abscess formation; (**b**, **c**) infection of preexisting cysts

22.2.4.2 Hemorrhagic Cysts

The content of hemorrhagic cysts appears as mixed hypoechoic/slightly hyperechoic depending on whether the fluid is liquid or blood filled. Color Doppler shows a diminished or absent blood flow both in the cysts and the surrounding tissue (Fig. 22.9). Hemorrhagic cysts are a rare observation but have an incidence of 1.3 % after prostate biopsy [14]. They are not associated with clinical signs of a urinary or systemic infection. Hemorrhagic cysts have clear-cut margins and are surrounded by normal parenchyma. At US, they are differentiated from infected cysts by their regular margins (infected cysts and abscesses have irregular margins), and the cyst walls are clearly distinct from the surrounding parenchyma, unlike the picture observed in the case of infected cysts.

22.2.5 Cystic Tumors

These neoplasms are extremely rare and sometimes curable. Isolated cases have been reported in the literature. A proper knowledge of these formations, of differential diagnosis aspects and of the diagnostic-therapeutic workup, is essential during the ultrasound examination.

22.2.5.1 Cystadenoma

At US, these appear as multiseptate masses, with a mixed anechoic/isoechoic (liquid/solid) content, irregular shape, and thick surrounding pseudocapsula. They show an expansive growth and can extend from the prostate to the pelvis and extraprostatic tissues. These tumors are extremely voluminous, with a mean diameter at diagnosis of 16 cm (range 9–45 cm) [15]. Computed tomography (CT) scan or MRI depicts a multilocular cystic mass originating in the prostate and extending into the extraprostatic pelvic tissues and to the suprapubic level (Fig. 22.10). Histologically, cystadenoma has peculiar features: the epithelium is single-layer cuboidal, and there are parabasal cells in the cystic walls, while the nuclei do not show atypia or prominent nucleoli. The growth of cystadenoma is expansile but not infiltrating. This justifies both the prognosis and the symptoms that are attributable to compression of the nearby structures and include urinary retention, perineal pain, urinary discomfort during bladder filling, and voiding. PSA can be normal or high. Surgical treatment is necessary.

22.2.5.2 Cystadenocarcinoma

This tumor is very rare; it consists of irregularly sized cystic masses with a variable content depending on the distribution of neoplastic or intracystic hemorrhagic areas. Cystadenocarcinoma has a large diameter ranging from 12 to 20 cm at diagnosis and is distinguished from cystadenoma by its infiltrating and compressive growth pattern [16]. It has no capsule and can infiltrate the surrounding pelvic tissues and even invade the rectum and bladder. Ultrasound examination shows an irregular infiltrating mass without a pseudocapsula, extending into the periprostatic tissues. The walls show irregular thicknesses and vascularized septa that are better visualized at MRI. Symptoms arise due to compression/infiltration of the pelvic structures (urinary retention, LUTS, pelvic pain). PSA may be normal or increased. CT scanning or MRI is necessary for a correct diagnosis and staging (Fig. 22.10), as well as histology. The histological diagnosis is generally made on transurethral resection tissue or prostatic biopsy, although in cystic tumors, it is not easy to perform biopsy because of the prevalently liquid component. The histological picture of cystadenocarcinoma features nuclear stratification, papillary proliferation, and Roman archlike structures. It has a highly invasive growth pattern, showing marked destruction of the prostatic parenchyma and aggressive invasion of the periprostatic and rectal fat [16]. In rare cases, high-grade ductal carcinoma has a similar morphological cystic pattern to cystadenocarcinoma. In short, the diagnostic suspicion of cystic tumors is based on US examination. Treatment will be surgery if this is technically feasible and/or radiotherapy.

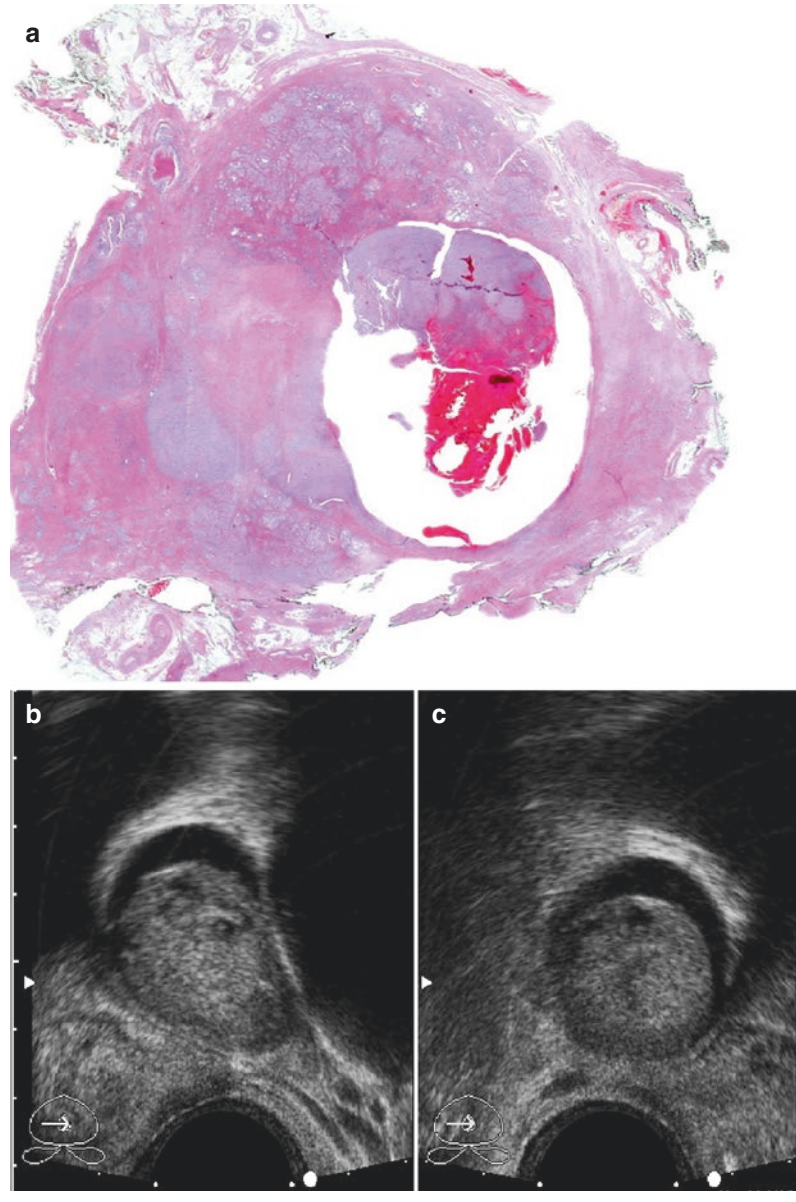

Fig. 22.10 *Hemorrhagic cystic*: (**a**) (histology) and (**b**) (ultrasound) longitudinal and (**c**) axial view

22.2.5.3 Dermoid Cysts

These are extremely rare and are also benign. Such cysts are well demarcated from the surrounding parenchyma. The epithelium of dermoid cysts consists of pluristratified squamous cells with keratinized areas. The keratin accumulation makes the US hyperechoic, and it may be associated with a posterior cone shadow due to calcification deposits.

Dermoid cysts are thus unlike cystic tumors that have cuboid monostratified cells, as do congenital cysts. Only the dilated cystic utricle has a pluristratified epithelium without keratin differentiation pattern [17]. A correct diagnosis of dermoid cysts depends on CT scan or MRI.

22.2.6 Parasitic Cysts

Parasitic infections are rare in western nations; these cysts arise due to bilharziasis or hydatidosis (*Echinococcus* cysts) [18].

22.3 Symptoms and Clinical Significance of Prostatic Cysts

The most frequent clinical scenario is a diagnosis of prostatic cysts made during the performance of TRUS for lower urinary tract symptoms. The connection between the symptoms and the cysts has still to be clarified. Scientific evidence published in the literature has attempted to correlate cysts with their clinical impact. Dik et al. [2] reported the incidence of symptoms in patients with midline cysts: 77% had prostatitis-like symptoms, 62% scrotal pain, 35% hypospermia or ejaculatory pain, and 12% infertility.

In the study by Jarow et al. [19], prostatic cysts were found in 17 cases among 150 infertile men, accounting for 11%, but were also present in 30% (9/30) of fertile volunteers. Yagci et al. [20] observed the presence of cysts in the ejaculatory ducts in 6/54 (11%) patients with hemospermia. Hemospermia is often studied by transrectal US, but it is difficult to demonstrate a causal relationship with prostatic cysts [21], so any clinical considerations should be interpreted with some caution.

Various case reports of symptomatic prostatic cysts have been reported in literature. In the Tambo et al.'s report of 34 cases of symptomatic cysts, 40% of the cases suffered from dysuric symptoms, 33% from urinary retention, 9% stranguria, and 6% infertility [22]. Nayyar et al. described a case of a symptomatic medial cyst treated by incision and transurethral marsupialization [23]. Chang et al. described a case of a simple cyst causing urinary obstruction, treated with transurethral resection that completely resolved the symptoms [24]. Dell' Atti [25] reported a 28-year-old with severe urinary symptoms of obstructive and irritant type due to a simple cyst of the bladder neck that resolved after incision and transurethral marsupialization. Other very similar cases have been reported by other authors [26, 27]. By contrast, Diaz et al. [28] described a case in which the obstructive symptoms persisted after laser vaporization of the prostate; they were found to be secondary to a voluminous prostatic cyst at the 12 o'clock position on the bladder neck that contributed to a cervico-urethral obstruction; this had been missed in the earlier assessment. The symptoms resolved after treatment of the cyst. This clinical case highlights the importance of the differential diagnosis of urinary symptoms. Prostatic cysts, even if they contain very high concentrations of PSA, do not alter the blood levels of PSA.

22.4 Possible Developments in Scientific Research

Recent studies have advanced the hypothesis that inflammatory atrophy may have a role in cystic transformation to carcinoma, since the tissue shows a high level of proliferation as compared to normal epithelium [29]. According to biopsy findings, epithelial atrophy is greater in subjects with a high PSA [30]. The possibility of identifying cystic atrophy by means of US marker lesions could be a promising clinical research direction. Another interesting field for research development is the influence of prostatic cysts on the volume of the gland and on the stroma/epithelium ratio. Voluminous or multiple cysts can artificially increase the prostate volume, but in actual fact, the glandular epithelium is reduced not increased. Due to this observation, cysts could cause a false reduction in the PSA density (PSA/prostate volume), having the effect of delaying the diagnosis of a tumor (Figs. 22.11 and 22.12).

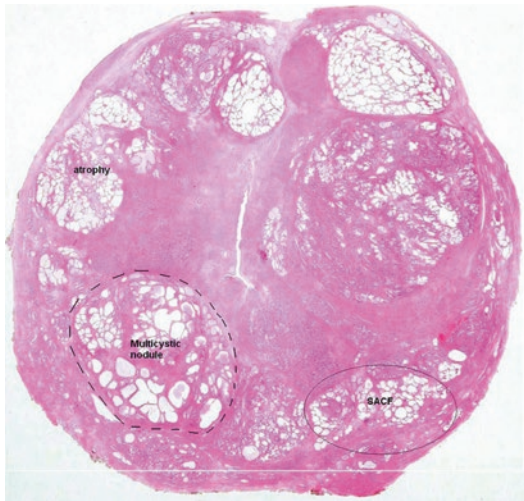

Fig. 22.11 Multicystic nodule associated with focal atrophy (microcysts observed at US)

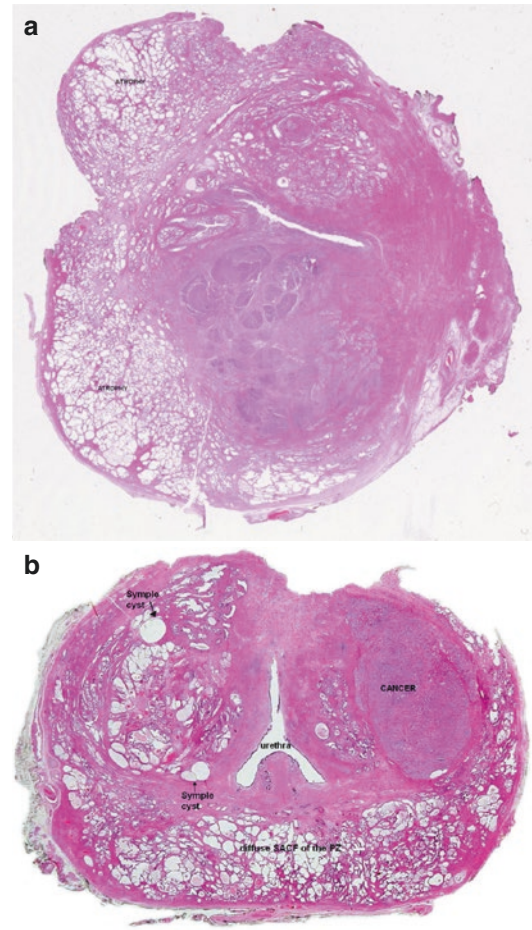

Fig. 22.12 (**a**, **b**) Focal atrophy (microcysts observed at US)

Conclusions

TRUS plays a central, first-line role in the diagnosis and classification of prostatic cysts. The etiopathogenesis of such cysts is correlated to disorders such as prostatic hyperplasia, inflammation, anatomical variants of the prostatic utricle, and focal atrophy. They very rarely degenerate to cystadenocarcinoma.

Treatment is reserved only to symptomatic patients, those with LUTS or obstruction of the seminal pathways and hence infertility, or those with evolution of the cysts to abscesses.

References

1. Patel U, Rickards D (2002) Transrectal ultrasound of the abnormal prostate: less common prostate abnormalities. In: Handbook of transrectal ultrasound and biopsy of the prostate. Dunitz, London, pp 85–90
2. Hamper UM, Epstein JI, Sheth S, Walsh PC, Sanders RC (1990) Cystic lesions of the prostate gland. A sonographic-pathologic correlation. J Ultrasound Med 9(7):395–402
3. Dik P, Lock TM, Schrier BP, Zeijlemaker BY, Boon TA (1996) Transurethral marsupialization of a medial prostatic cyst in patients with prostatitis-like symptoms. J Urol 155:1301–1304
4. De Marzo AM, Platz EA, Epstein JI et al (2006) A working group classification of focal prostate atrophy lesions. Am J Surg Pathol 30:1281–1291
5. Curran S, Akin O, Agildere AM, Zhang J, Hricak H, Rademaker J (2007) Endorectal MRI of prostatic and periprostatic cystic lesions and their mimics. Am J Roentgenol 188(8):1373–1379
6. McDermott VG, Meakem TJ, Stolpen AH, Schnall MD (1995) Prostatic and periprostatic cysts: findings on MR imaging. Am J Roentgenol 164:123–127
7. Galosi AB, Montironi R, Fabiani A, Lacetera V, Gallé G, Muzzonigro G (2009) Cystic lesions of the prostate gland: an ultrasound classification with pathological correlation. J Urol 181:647–657
8. Kato H, Komiyama I, Maejima T, Nishizawa O (2002) Histopathological study of the mullerian duct remnant: clarification of disease categories and terminology. J Urol 167:133–136
9. Kato H, Hayama M, Furuya S, Kobayashi S, Islam AM, Nishizawa O (2005) Anatomical and histological studies of so-called müllerian duct cyst. Int J Urol 12:465–468
10. Ritchey ML, Benson RC, Kramer SA, Kelalis PP (1988) Management of mullerian duct remnants in the male patient. J Urol 140:795–799
11. Yasumoto R, Kawano M, Tsujino T, Shindow K, Nishisaka N, Kishimoto T (1997) Is a cystic lesion located at the midline of the prostate a mullerian duct cyst ? Analysis of aspirated fluid and histopathological study of the cyst wall. Eur Urol 31:187–189
12. Sondergaard G, Vetner M, Christensen PO (1987) Peripheral cystic hyperplasia of the prostate gland. Acta Pathol Microbiol Immunol Scand 95(3):137–139
13. Nogueira March JL, Figueiredo L, Mata J, Jamardo D, Ojea A et al (1982) Coexisting cyst of the utricle and carcinoma of the endometrial type in the prostate. Eur Urol 8(1):42–44
14. Herranz Amo F, Verdu Tartajo F, Diez Cordero JM et al (1999) Hemorrhagic prostatic cyst following ultrasound guided biopsy: a case report. Arch Esp Urol 52:379–380
15. Maluf HM, King ME, DeLuca FR, Navarro J, Talerman A, Young RH (1991) Giant multilocular prostatic cystadenoma: a distinctive lesion of the retroperitoneum in men. A report of two cases. Am J Surg Pathol 15:131–135
16. Tuziak T, Spiess PE, Abrahams NA, Wrona A, Czerniak B (2007) Multilocular cystadenoma and cystadenocarcinoma of the prostate. Urol Oncol 25:19–25
17. Uthmann U, Terhorts B (1981) Dermoid cyst of the prostate with contralateral renal agenesis. Br J Urol 53(5):479
18. Nouira Y, Binous MY, Nouira K, Mekni A, Kallel Y, Fitouri Z (2006) Intraprostatic hydatid cyst: an unusual presentation. Scientific World Journal 231:15–18
19. Jarow JP (1993) Transrectal ultrasonography of infertile men. Fertil Steril 60:1035–1039
20. Yagci C, Kupeli S, Tok C, Fitoz S, Baltaci S, Gogus O (2004) Efficacy of transrectal ultrasonography in the evaluation of hematospermia. Clini Imag 28:286–290
21. Galosi AB (2012) Editorial comment on: the value of transrectal ultrasound in the diagnosis of hematospermia in a large cohort of patients. J Androl 33(5):904–905
22. Tambo M, Okegawa T, Nutahara K, Higashihara E (2007) Prostatic cyst arising around the bladder neck cause of bladder outlet obstruction: two case reports. Acta Urol Jpn 53:401–404
23. Nayyar R, Dogra PN (2009) Anteriorly placed midline intraprostatic cyst. J Endourol 23:595–597
24. Chang SG, Hwang IC, Lee JH, Park YK, Lim JW (2003) Infravesical obstruction due to benign intraurethral prostatic cyst. J Korean Med Sci 18:125–126
25. Dell'Atti L (2012) Disorders of bladder depletion in a young man because of a prostatic cyst: a case report. Arch Ital Urol Androl 84(1):44–46
26. Dogan B, Canda AE, Akbulut Z, Atmaca AF, Balbay DE (2011) Prostatic cyst causing severe infravesical obstruction in a young patient. Urol J 8(4):330–332
27. Lee JY, Kang DH, Park HY, Park JS, Son YW, Moon HS, Choi HY (2010) An anteriorly positioned midline prostatic cyst resulting in lower urinary tract symptoms. Int Neurourol J 14(2):125–129

28. Diaz RR, Lee JY, Choi YD, Cho KS (2013) Unroofed midline prostate cyst misled into a stricture with obliterative bladder neck contracture following a laser prostatectomy. Int Neurourol J 17(1):34–37
29. Sfanos KS, De Marzo AM (2012) Prostate cancer and inflammation: the evidence. Histopathology 60(1): 199–215
30. Billis A, Meirelles LR, Magna LA, Baracat J, Prando A, Ferreira U (2007) Extent of prostatic atrophy in needle biopsy and serum PSA levels: is there an association ? Urology 69:927

Benign Prostatic Hypertrophy

23

Vincenzo Scattoni and Carmen Maccagnano

23.1 Introduction

Benign prostatic hyperplasia (BPH) can be considered a benign but progressive disease that can determine the insurgence of voiding symptoms. The identification of men with this disease could have a significant impact on the decision among the different therapeutic options. Numerous pieces of evidence demonstrate the impact of the prostate volume on the disease progression and on the decision-making for a therapeutic approach.

It has been accepted that digital rectal examination, serum prostatic-specific antigen (PSA), and transrectal prostate ultrasound are the available tools for the prostate volume estimation. Nevertheless, symptom assessment followed by transrectal ultrasound (TRUS) of the prostate is considered as the most important diagnostic examinations affecting the decision about individual treatment options.

BPH may be studied with ultrasound (US) with both transabdominal and transrectal approach.

V. Scattoni (✉)
Department of Urology, University Vita-Salute,
Scientific Institute H San Raffaele,
Via Olgettina 60, Milan 20132, Italy
e-mail: scattoni.vincenzo@hsr.it

C. Maccagnano
Azienda Ospedaliera S.Anna,
Via Ravona, 60 San Fermo della Battaglia (Co),
Como 22020, Italy

P. Martino, A.B. Galosi (eds.), *Atlas of Ultrasonography in Urology, Andrology, and Nephrology*,
DOI 10.1007/978-3-319-40782-1_23

23.2 Transabdominal Approach

The patient is in supine position, and the bladder has to be filled with about 250–300 cc of urine. In some case, it is necessary to move the patient on the left or right side, in order to verify the mobility of some lesions (i.e., stones, neoplasms, prostatic lobes).

The probes are convex, with a frequency of 3.5 MHz or with multiple frequencies. The choice depends on the body of the patient and, consequently, on the depth of the prostate in the pelvis. The PSA is an important parameter to be considered.

The actual indications of the exam are:

1. Measurement of the dimensions and of the volume of the prostate before medical, surgical, or radiation therapy [1, 2]. The volume is obtained with the multiplication of the three diameters (latero-lateral × anteroposterior × craniocaudal) × 0.52 (according to ellipsoid formula) (Fig. 23.1). This formula might overestimate the volume, with a range from 20 up to 50% [2, 3]. Nevertheless, these reports are fundamental in order to plan the surgical approach (transabdominal vs transurethral). The intravesical prostatic protrusion (IPP) is another important parameter; it is calculated with the measurement of the height (protrusion) of the prostate starting from the bladder circumference passing through the base of the prostate (Fig. 23.2); IPP has shown a significant correlation with the severity of symptoms, especially those of emptying phase.
2. Indirect signs of detrusor failure, i.e., diverticula, pseudo-diverticula, and bladder stones. The measurement of the post-voiding urinary volume, preferably together with the urination diary, is highly suggestive of the severity of BPH (Table 23.1).
3. Definition of the third lobe in the prostate and its relationship with the bladder floor (Fig. 23.3) [1].

The resolution limit of the method is 5 mm. Additionally, this approach is not able to define the morphology of the peripheral zone. Finally, the diagnostic power is low; consequently, this approach is not suggested by the official guidelines.

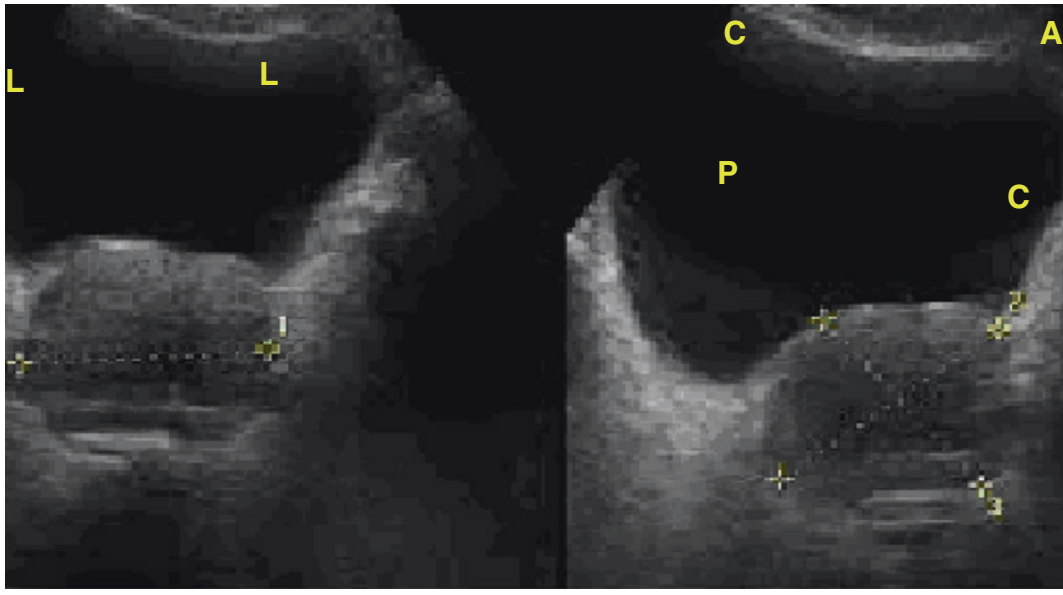

Fig. 23.1 The prostate volume is obtained with the multiplication of the three diameters (latero-lateral × anteroposterior × craniocaudal) × 0.52 (according to ellipsoid formula), in transabdominal approach

Table 23.1 American Continence Society has evaluated the appropriateness criteria on obstructive voiding symptoms secondary to prostatic disease

Radiologic procedure	Rating	Comments
Ultrasound pelvis (bladder and prostate) transabdominal	7	Post-void to measure residual urine. If there is significant residual urine, evaluation of the upper urinary tract is indicated. Gives estimate of prostate size and bladder wall thickness
Ultrasound pelvis (prostate) transrectal	2	The resistive index has been shown to be elevated after transurethral vaporization of the prostate, suggesting that it can be used to evaluate the severity of BPH and monitor therapy

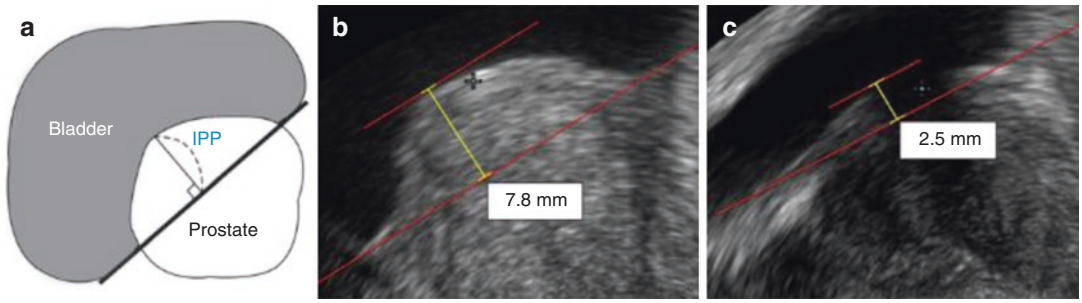

Fig. 23.2 Intravesical prostatic protrusion (IPP) with transabdominal approach. (**a**) IPP measurement. The prostate in longitudinal scan. The oblique line indicates the margin of separation between the prostate and bladder. The measurement of the height of the prostate protruding in the bladder represents IPP (**b**, **c**) US example of IPP measurements

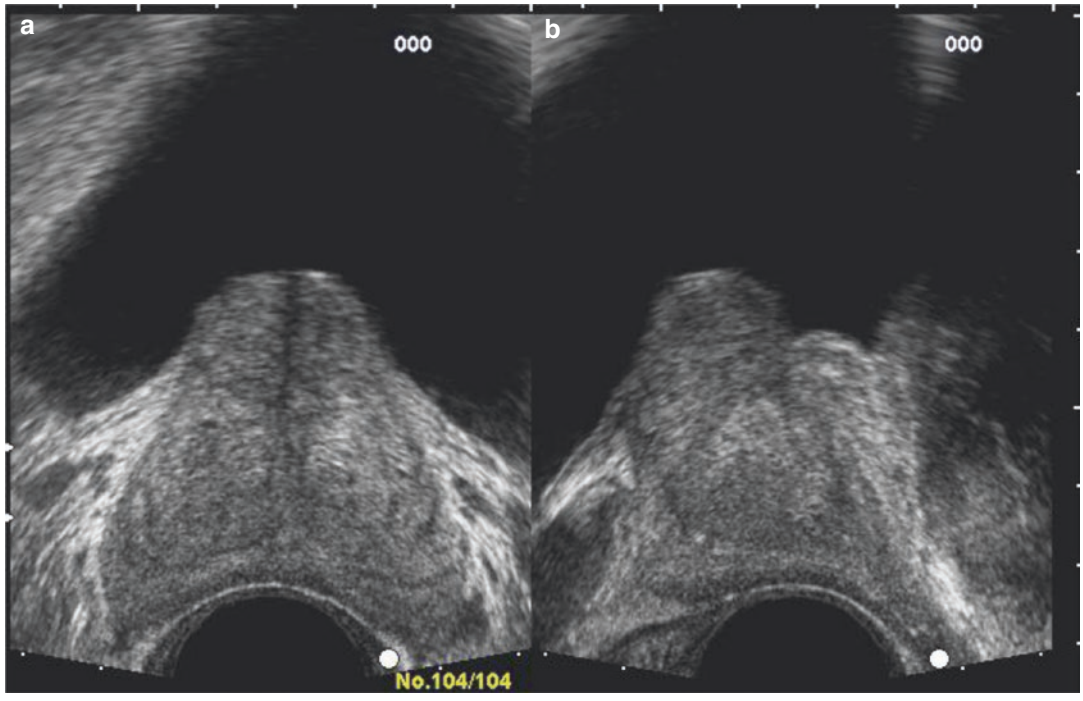

Fig. 23.3 Example of highly protruding medium lobe in the bladder. (**a**) Longitudinal scan. (**b**) Transversal scan

23.3 Transrectal Approach

The TRUS of the prostate is usually executed with the patient on the left side. The administration of an enema two hours before the exam is mandatory in order to avoid artifacts due to the presence of feces. The fasting is not necessary. The bladder has to be filled with 250–300 cc in order to better define the base of the prostate and the seminal vesicles.

The probes are transrectal, with high frequencies (≥7.5 MHz); this is due to the superficial position of the prostate respecting to the plan of the probe (internal wall of the rectum). Currently, the commercially available probes are:

- Mono-planar linear: it analyzes the prostate with longitudinal scan.
- Biplanar convex linear or biconvex: it analyzes the prostate with longitudinal scan together with transversal scan, through two orthogonal plans.
- End fire (with variable frequency): it allows all possible scans.

The prostate has to be studied with two orthogonal scans, transversal and longitudinal, together with the evaluation of the volume of the whole prostate and the adenoma.

This clinical data plays a fundamental role in a therapeutic and surgical context [1–8] (Fig. 23.4).

Like in suprapubic sonography, BPH can usually be visualized as a low-echo area in transrectal sonography and can easily be distinguished from the peripheral gland with higher echo density. But it is also true that many adenomas are echo equal to the rest of the gland. It is still possible to detect an echo-equal adenoma, if a so-called tangential artifact occurs on the periphery of the adenoma.

This physical phenomenon occurs if the sound wave hits the peripheral surface at an angle. The ultrasound cone is thus split and an acoustic shadow generated. In the adenoma, there are frequently hyperechoic echos that occur more rarely in the peripheral gland. These can be residues of chronically recurrent focal prostatitis. They can be found in many cases where anamnestically no prostatitis has been diagnosed, so it must be assumed that many of these infections proceed subclinically. This would match the frequent histological findings after transurethral resection in patients, the majority of which had shown neither clinical nor anamnestic indications of prostatitis. In autopsies such pathological changes are found in over 50 %. In addition, corpora amylacea may show up as soundproof echos with a consecutive acoustic shadow. They are most likely to be found at the borderline between an adenoma and the peripheral gland. As their position is ventral to the peripheral gland, they do not detriment its feasibility in transrectal sonography (in contrast to suprapubic sonography). Small cystic alterations in adenomas are also not rare although still fairly infrequent, like the soundproof echos in the peripheral gland. Usually, these alterations are distended glandular vessels and in some cases also residues after minor tissutal necrosis. Utriculus cysts are found in the middle line dorsal from the urethra and can sometimes grow up to several cubic centimeters in volume.

It is not normally possible to differentiate anatomically between the central and peripheral zone sonographically, despite its crude and irregular vessel structures. The normal peripheral and central zone presents a homogeneous area in the central zone of the dorsal gland. In contrast to these latter zones, the ventrally located transition zone seems rather low in echo density.

TRUS is a very reliable instrument for the evaluation of BPH and to calculate the BPH. The diagnostic accuracy of the TRUS is very high, with a risk of overestimating the real volume and weight of the gland which ranges only 4–10 % [9–15]. Roehrborn et al. have shown that there was a distinct underestimation of prostate size by DRE when compared with TRUS measurement. The underestimation of prostate volume increased with increasing TRUS volume, particularly if the volume was greater than 30 mL. The average underestimation was between 9 and 12 % for prostate volumes 30–39 mL and between 17 and 27 % for prostate volumes 40–49 mL.

Ahmad et al. have shown that DRE had positive predictive value of 94 % in identifying the prostate

above 30 cc. Hence, when considering treatment with 5-ARIs, DRE may be sufficient to identify suitable patients for 5-ARI therapy. However, for prostate volumes between 25 and 30 cc and above 80 cc, TRUS may be required [16].

Additionally, TRUS allows the identification of the medium lobe, its dimensions, and its relationship with the bladder floor [1].

Moreover, the measurement of the transition zone is a fundamental moment during TRUS examination. Different authors have shown that the transition zone volume represents an important parameter predictive of the severity of these symptoms [17, 18] (Fig. 23.5).

The TZ volume strongly correlates with the urodynamic parameters, especially when the transition zone index (TZI) is >0.5 [20]. The TZI is the result of ratio between the volume of the transition zone and the volume of the whole prostate. Additionally, the TZI correlates with the severity of the emptying symptoms [18, 19], and it is very accurate in predicting the risk of acute urinary retention [20] (Figs. 23.6 and 23.7).

The intravesical prostatic protrusion has a good correlation with the severity of the emptying symptoms which is classified in three grades, referring to IPP values (Table 23.2). Several authors have reported that a high-grade IPP is strongly associated with both the severity of the emptying symptoms and a post-voiding volume >100 cc [21–23]. Mariappan and coll. have reported that IPP is a stronger predictive factor than prostate volume regarding the risk of acute urinary retention [24]. Intravesical prostatic protrusion (IPP) is dependent on the bladder filling. When the bladder volume exceeds 100 mL, IPP may be overestimated, and at bladder volumes above 400 mL, the prostate recedes below the pubic symphysis, resulting in underestimation of IPP.

Inflammatory outcomes with a diameter ≥3 mm may be represented by hypo- or hyperechoic areas with or without posterior cone of shadow (Figs. 23.8 and 23.9). Conversely, the abscessual zones present a prevalent liquid component and, consequently, the appearance is anechoic.

The American College of Radiology suggests to perform a TRUS examination [25] in the following situation:

1. Measurement of the dimensions and of the volume of the prostate before medical and surgical treatments
2. Diagnosis of inflammatory or abscessual zone
3. Functional and morphologic study of the bladder neck
4. Surgical follow-up (Fig. 23.10)

The American College of Radiology suggests also a TRUS to diagnose a bladder cancer or stones located in the distal ureter [25]. The ACS has evaluated the appropriateness criteria on obstructive voiding symptoms secondary to prostatic disease (Table 23.1). TRUS has been evaluated with a rate of 2 with ultrasound of the prostate and bladder with a rate of 7.

The color Doppler and the power Doppler are usually used for the identification of neovascularized foci, which may be the possible expression of abscessual or tumoral diseases. Particularly, the vascularization is absent in the center of the abscessual areas [26–29].

The color Doppler allows another parameter, the resistive index (RI): it evaluates the grade of the tension in the venous system of the prostate. If it is >0.7, it indicates a severe obstruction in >70 % of patients (Fig. 23.11).

Finally, the main role of the TRUS for BPH is the surgical planning and follow-up. It has to be integrated with other parameters such as DRE and PSA [30, 31].

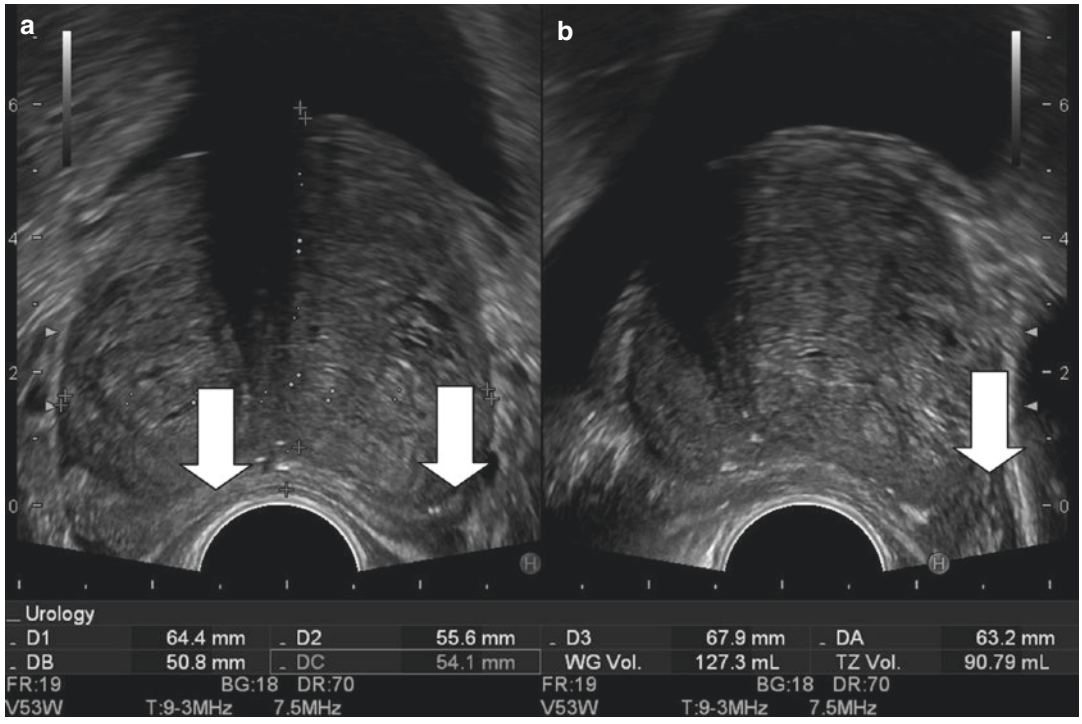

Fig. 23.4 Measurement of the volume of the whole prostate and of the adenoma. Usually the appearance of the adenoma is hypoechoic comparing to the peripheral region of the gland [3, 4]. The net difference of echogenicity between the two regions allows the identification of a definite margin corresponding to the surgical enucleation plan. (**a**) Transversal scan. (**b**) Longitudinal scan

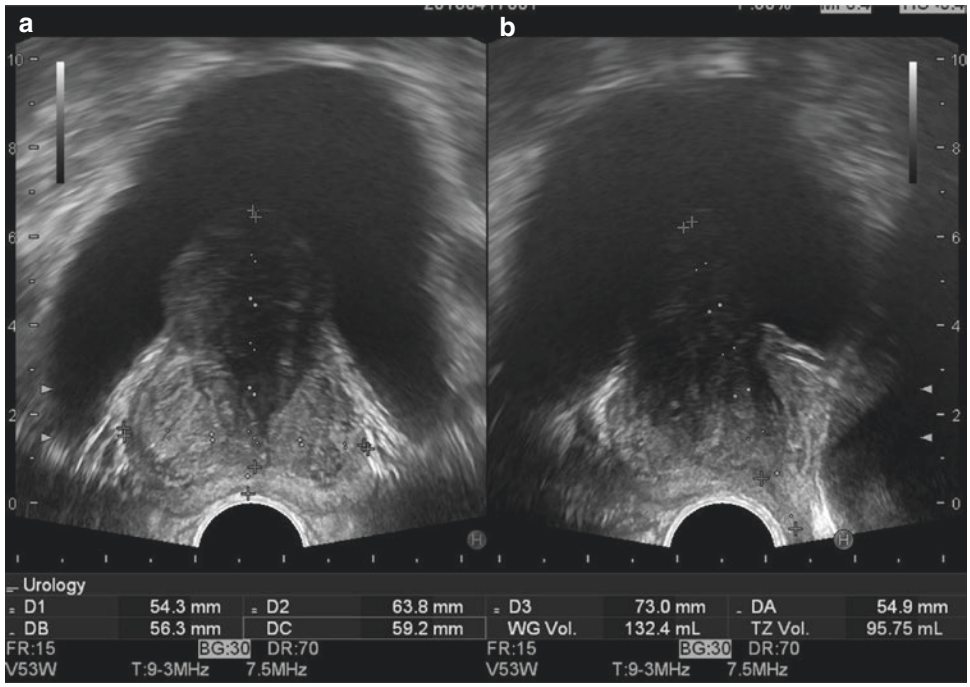

Fig. 23.5 TRUS may evidence a median lobe, whose dimension may correlate with the severity of urinary symptoms. The echogenicity of the lesion protruding into the bladder lumen is the same of the prostate, without a definite margin. All these features indicate a medium prostatic lobe. The differential diagnosis with bladder cancer is essential. (**a**) Transversal scan. (**b**) Longitudinal scan

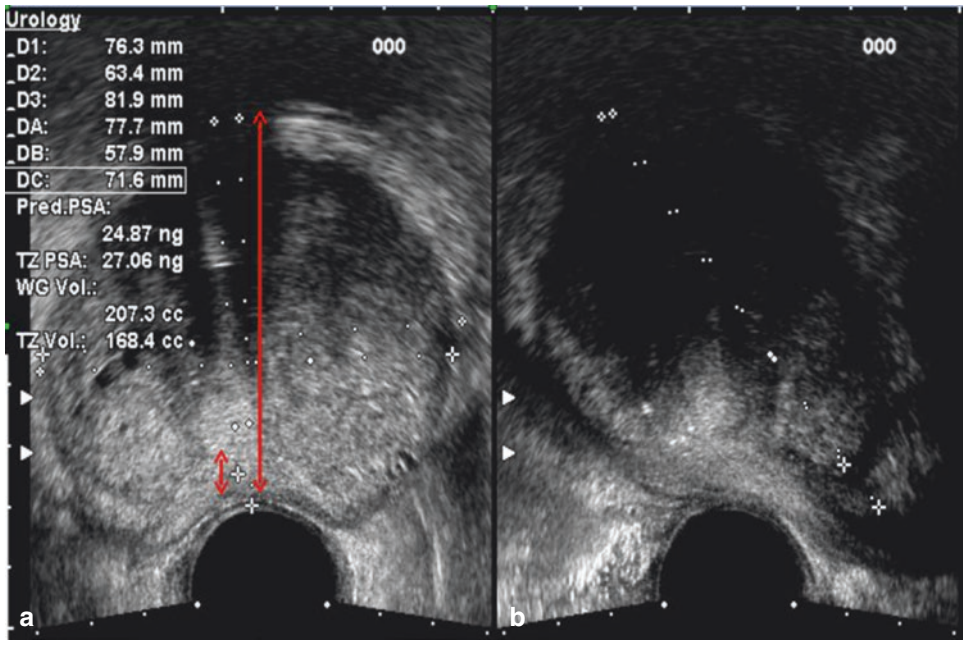

Fig. 23.6 TZI measurement: transition zone volume (TZV)/total prostate volume (TPV) ratio. In this case, the value is 0.8 (168/207); thus the correlation with the severity of the obstruction is significant. (**a**) Transversal scan. (**b**) Longitudinal scan

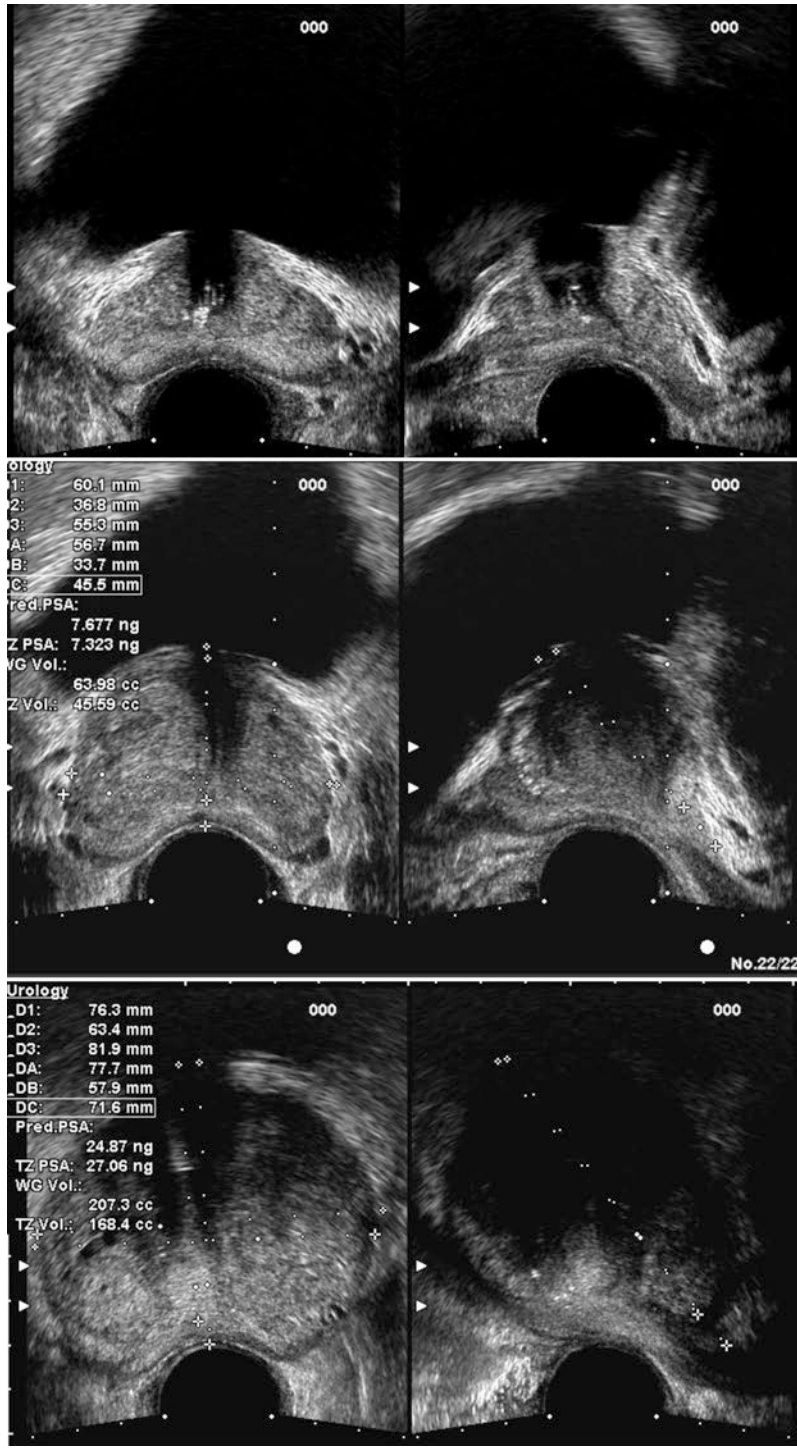

Fig. 23.7 Three examples of a small, medium, and large TZ volume and BPH

Table 23.2 Correlation between the severity of the emptying symptoms and IPP measurement

Grade	IPP measurement (mm)
1	<5
2	05/10/15
3	>10

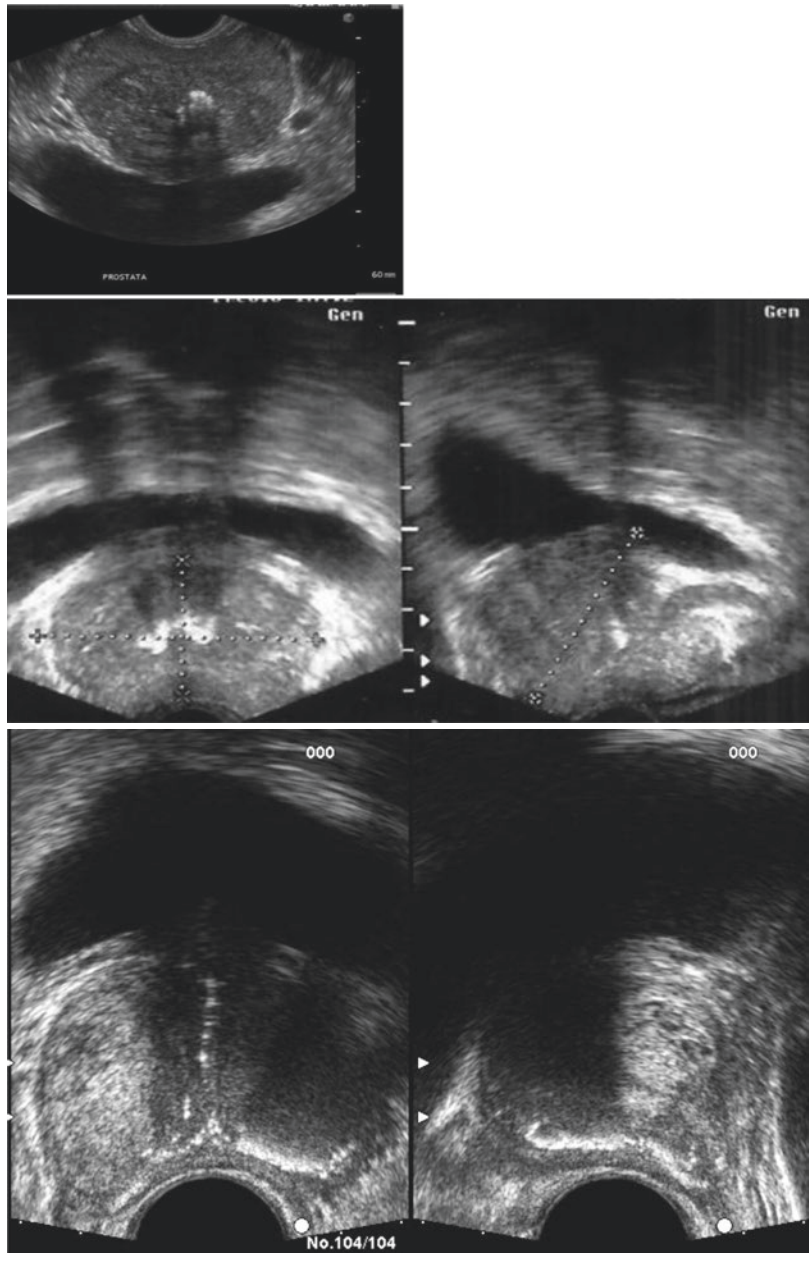

Figs. 23.8 and 23.9 Hyperechoic areas with posterior cone of shadow (intraprostatic calcifications) localized on the margin between adenomatous and peripheral region of the prostate (surgical plane)

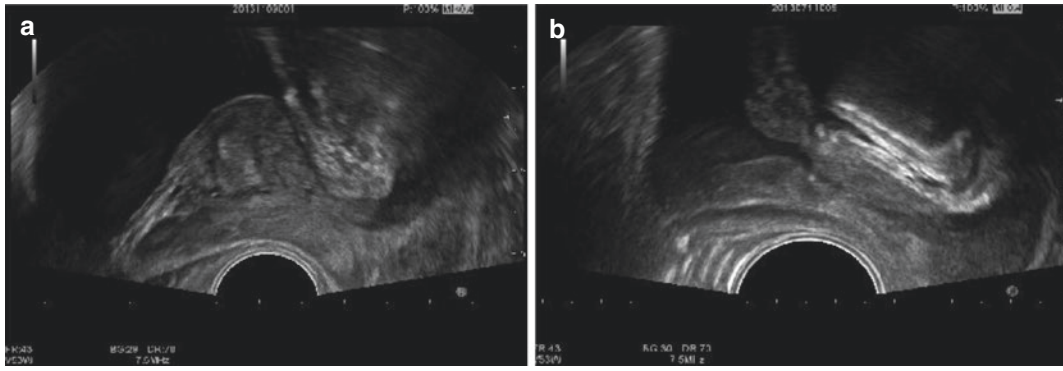

Fig. 23.10 TRUS may be useful in the surgical follow-up. (**a**) A regrowth of the adenoma after the surgery is evident. There are no calcifications, which are typical surgical outcomes. (**b**) Large bladder neck after the surgery, which may correlate with a significant improvement of the urinary symptoms

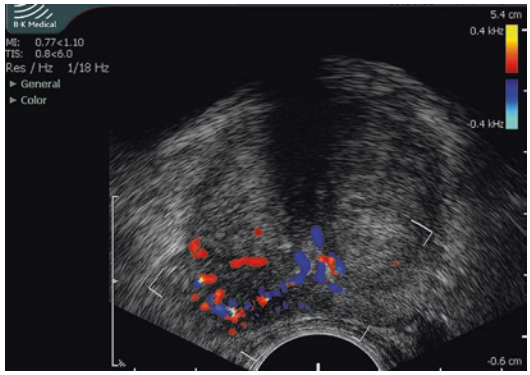

Fig. 23.11 The use of echo-color Doppler during TRUS with the evaluation of the resistive index – RI – plays a fundamental role in the consideration of the severity of symptoms

References

1. Stravodimos KG, Petrolekas A, Kapetanakis T, Vourekas S, Koritsiadis G, Adamakis I, Mitropoulos D, Constantinides C (2009) TRUS versus transabdominal ultrasound as a predictor of enucleated adenoma weight in patients with BPH: a tool for standard preoperative work-up? Int Urol Nephrol 41(4): 767–771
2. Ash D, Flynn A, Battermann J, de Reijke T, Lavagnini P, Blank L, ESTRA/EAU Urological Brachytherapy Group, EORTC Radiotherapy Group; ESTRO/EAU/EORTC (2000) Recommendations on permanent seed implantation for localized prostate cancer. Radiother Oncol 57:315–321
3. Meraj S, Nagler HM, Homel P, Shasha D, Wagner JR (2003) Radical prostatectomy: size of the prostate gland and its relationship with acute perioperative complications. Can J Urol 10:1743–1748
4. Giubilei G, Ponchietti R, Biscioni S, Fanfani A, Ciatto S, DI Loro F, Gavazzi A, Mondaini N (2005) Accuracy of prostate volume measurements using transrectal multiplanar three dimensional sonography. Int J Urol 12(10):936–938
5. Pierangeli T, Muraro GB (2002) Role of 3D-ultrasonography in the assessment of transitional zone PSA. Arch Ital Urol Androl 74:282–284
6. Strasser H, Janetschek G, Reissigl A, Bartsch G (1996) Prostrate zones in three dimensional transrectal ultrasound. Urology 47:485–490
7. Aarnick RG, Huynen AL, Giesen RJ, De la Rosette JJ, Debruyne FM, Wijkstra H (1995) Automated prostate volume determination with double ultrasonographic imaging. J Urol 153:1549–1554
8. Alkan I, Turkeri L, Biren T, Cevik I, Akdas A (1996) Volume determinations by transrectal ultrasonography in patients with benign prostatic hyperplasia: correlation with removed prostate weight. Int Urol Nephrol 28:517–523
9. Loeb S, Han M, Roehl KA, Antenor JA, Catalona WJ, Loeb S, Han M, Roehl KA, Antenor JA, Catalona WJ (2005) Accuracy of prostate weight estimation by digital rectal examination versus transrectal ultrasonography. J Urol 173:63–65
10. Lee JS, Chung BH (2007) Transrectal ultrasound versus magnetic resonance imaging in the estimation of prostate volume as compared with radical prostatectomy specimens. Urol Int 78:323–327
11. Rahmouni A, Yang A, Tempany CM, Frenkel T, Epstein J, Walsh P, Leichner PK, Ricci C, Zerhouni E (1992) Accuracy of in vivo assessment of prostatic volume by MRI and transrectal ultrasonography. J Comput Assist Tomogr 16:935–940
12. Cabello Benavente R, Jara Rascon J, Monzo JI, Lopez Diez I, Subira Rios D, Lledo Garcia E, Herranz Amo F, Hernandez Fernandez C (2006) Volume determinations of the whole prostate and of the adenoma by transrectal ultrasound: correlation with surgical specimen. Actas Urol Esp 30:175–180

13. Bland JM, Altman DG (1986) Statistical methods for assessing agreement between two methods of clinical measurement. Lancet 1:307–310
14. Nathan MS, Seenivasagam K, Mei Q, Wickham JE, Miller RA (1996) Transrectal ultrasonography: why are estimates of prostate volume and dimension so inaccurate? Br J Urol 77:401–407
15. Ahmad S, Manecksha RP, Cullen IM, Flynn RJ, McDermott TE, Grainger R, Thornhill JA (2011) Estimation of clinically significant prostate volumes by digital rectal examination: a comparative prospective study. Can J Urol 18(6):6025–6030
16. Terris MK, Hammerer PG, Nickas ME (1998) Comparison of ultrasound imaging in patients undergoing transperineal and transrectal prostate ultrasound. Urology 52(6):1070–1072
17. Kaplan SA, Te AE, Pressler LB, Olsson CA (1995) Transition zone index as a method of assessing benign prostatic hyperplasia: correlation with symptoms, urine flow and detrusor pressure. J Urol 154(5):1764–1769
18. Greene DR, Egawa S, Hellerstein DK, Scardino PT (1990) Sonographic measurements of transition zone of prostate in men with and without benign prostatic hyperplasia. Urology 36(4):293–299
19. Kurita Y, Masuda H, Terada H, Suzuki K, Fujita K (1998) Transition zone index as a risk factor for acute urinary retention in benign prostatic hyperplasia. Urology 51(4):595–600
20. Lim KB, Ho H, Foo KT, Wong MY, Fook-Chong S (2006) Comparison of intravesical prostatic protrusion, prostate volume and serum prostatic-specific antigen in the evaluation of bladder outlet obstruction. Int J Urol 13(12):1509–1513
21. Tan YH, Foo KT (2003) Intravesical prostatic protrusion predicts the outcome of a trial without catheter following acute urine retention. J Urol 170(6 Pt 1): 2339–2341
22. Chia SJ, Heng CT, Chan SP, Foo KT (2003) Correlation of intravesical prostatic protrusion with bladder outlet obstruction. BJU Int 91(4):371–374
23. Mariappan P, Brown DJ, McNeill AS (2007) Intravesical prostatic protrusion is better than prostate volume in predicting the outcome of trial without catheter in white men presenting with acute urinary retention: a prospective clinical study. J Urol 178(2): 573–577; discussion 577
24. American College of Radiology –Ultrasound Guidelines. http://www.acr.org/Quality-Safety/Standards-Guidelines/Practice-Guidelines-byModality/Ultrasound
25. Novis MI, Baroni RH, Cerri LM, Mattedi RL, Buchpiguel CA (2011) Clinically low-risk prostate cancer: evaluation with transrectal doppler ultrasound and functional magnetic resonance imaging. Clinics (Sao Paulo) 66(1):27–34
26. Morelli G, Pagni R, Mariani C, Minervini R, Morelli A, Gori F, Ferdeghini EM, Paterni M, Mauro E, Guidi E, Armillotta N, Canale D, Vitti P, Caramella D, Minervini A (2011) Results of vardenafil mediated power Doppler ultrasound, contrast enhanced ultrasound and systematic random biopsies to detect prostate cancer. J Urol 185(6): 2126–2131
27. Inahara M, Suzuki H, Nakamachi H, Kamiya N, Shimbo M, Komiya A, Ueda T, Ichikawa T, Akakura K, Ito H (2004) Clinical evaluation of transrectal power doppler imaging in the detection of prostate cancer. Int Urol Nephrol 36(2):175–180
28. Shinbo H, Kurita Y (2011) Application of ultrasonography and the resistive index for evaluating bladder outlet obstruction in patients with benign prostatic hyperplasia. Curr Urol Rep 12(4):255–260
29. Società Italiana di Radiologia Medica –Linee guida della diagnostica per immagini 2009. http://www.sirm.org/it/documenti/cat_view/66-linee-guida.html
30. European Association of Urology –2012 Guidelines. http://www.uroweb.org/guidelines/online-guidelines
31. Kijvikai K (2009) Digital rectal examination, serum prostatic specific antigen or transrectal ultrasonography: the best tool to guide the treatment of men with benign prostatic hyperplasia. Curr Opin Urol 19(1): 44–48

Prostatic Carcinoma

24

Vincenzo Scattoni, Carmen Maccagnano, and Marco Roscigno

24.1 Introduction

In Western countries prostatic carcinoma (PC) is the most frequent neoplasm and the second cause of death due to tumor in males. The PC epidemiology has radically changed during the last decades, with a tendency to an increasing number of diagnosis and a concomitant reduction of mortality. This evident modification is surely due to the improving of urological diagnostic instruments that allow a more precocious diagnosis of the PC. The introduction and the diffusion of PSA as a screening test, the improving of imaging, and the standardization of prostate biopsy (PB) techniques have been crucial in fostering this important change.

Since its first description and introduction by the end of the 1960s [1], the transrectal ultrasound (TRUS) of the prostate has played a fundamental but controversial role in PC diagnosis. Nevertheless, it has been considered the gold standard for its employment as a guide for PB during the last decades [2].

The anatomical and morphological TRUS parameters are:

- Prostate volume
- Volume of the transitional prostatic zone (and possible prostatic adenoma)
- Glandular echogenicity (peripheral area differentiated from transitional area)
- Relationship with adjacent organs:
  - Individuation of altered echogenicity (hypo- or hyperechoic)
  - Integrity of the prostate capsule

The prostate can be divided into two distinct areas, ascertained by TRUS [3, 4]: a peripheral zone with a relatively homogenous echogenicity; a central zone with reduced echogenicity in comparison with the peripheral zone, with an irregular echogenicity of the periurethral transitional area. The central zone is often hardly identifiable in the transitional zone, particularly in young patients, in whom the peripheral zone represents up to 75 % of the total prostate volume. The ratio between the central and peripheral zone tends to invert with increasing age, depending on the amount of hyperplastic prostatic tissue in the transitional zone. Whereas a consistent prostatic capsule is not often clearly identifiable, a boundary line can be noted between the peripheral prostatic parenchyma and the periprostatic fat tissue.

V. Scattoni (✉)
Ospedale San Raffaele, Via Olgettina, 60,
Milan 20132, Italy
e-mail: vincenzo.scattoni@hsr.it

C. Maccagnano
Azienda Ospedaliera S.Anna –Como, Via Ravona, 60,
San Fermo della Battaglia (Co) 22020, Italy

M. Roscigno
Azienda Ospedaliera Papa Giovanni XXIII,
Piazza OMS, 1, Bergamo 24127, Italy

P. Martino, A.B. Galosi (eds.), *Atlas of Ultrasonography in Urology, Andrology, and Nephrology*,
DOI 10.1007/978-3-319-40782-1_24

The US inspection of the prostate, aiming at recognizing a PC, has to focus on asymmetries, on areas with increased vascularization, on areas with different echogenicity in comparison with surrounding tissue (hyperechoic or hypoechoic), and on eventual irregularities of the prostatic capsule.

Effectively, all these variants are indicative of focal alterations whose significance has to be duly investigated.

Currently, TRUS represents the gold standard radiological exam for prostate imaging. This is due to the best costs/benefits ratio (absence of ionizing radiations, low invasiveness, reduced costs). Nevertheless, in literature it has been reported a diagnostic accuracy ranging from 50 up to 60 %, with a low positive predictive value (about 6 %) also using probes with high frequencies. Moreover, the reliability of local staging is still under discussion.

24.2 Topography

Classically, PCs originate from the peripheral zone in 70 % of cases (Fig. 24.1), from the central zone in 10 % of cases, and from the transitional zone (the place where benign prostate hyperplasia develops) in 20 % of cases [5]. Similar percentages can also be found both in the autopsic series and in the bioptic clinical data. It is worth considering the exam of the anterolateral horn, which is part of the transitional zone, and which is often possible to investigate with DRE (Fig. 24.2). The nodules in the transitional zone are, on the contrary, hyperplastic in most cases, with a variable echogenicity. For this reason, a PC diagnosis is rare and difficult to perform with a biopsy of the transitional zone nodules, even in case of hypoechoic nodules (Fig. 24.3). A PC of important diameter might be suspected only in case of significant asymmetry of the transitional zone, with the presence of hypervascularized and homogeneous tissue during Doppler examination (Fig. 24.4).

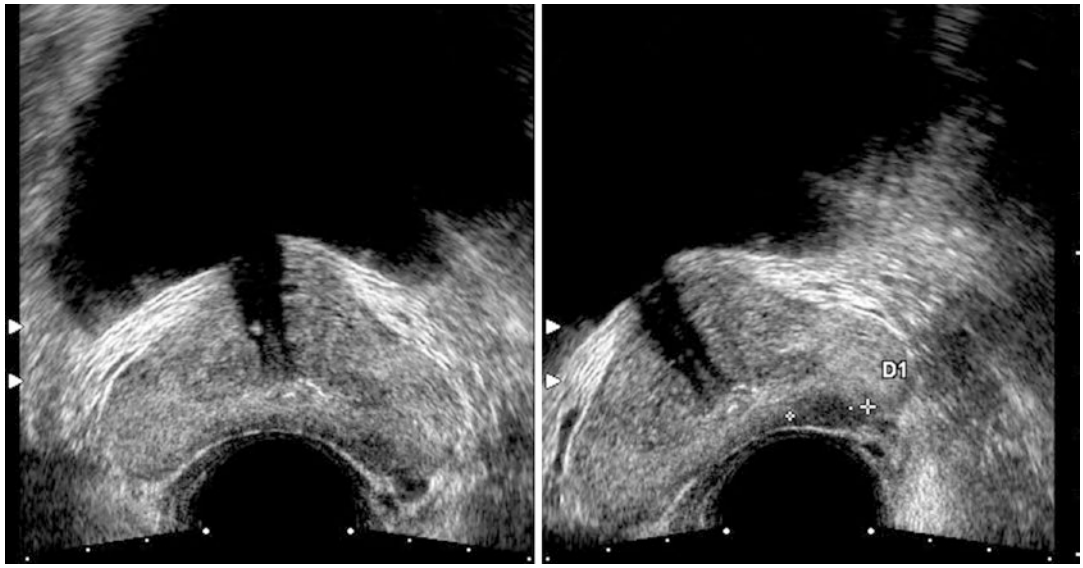

Fig. 24.1 Hypoechoic area localized in the peripheral portion of the left prostatic lobe

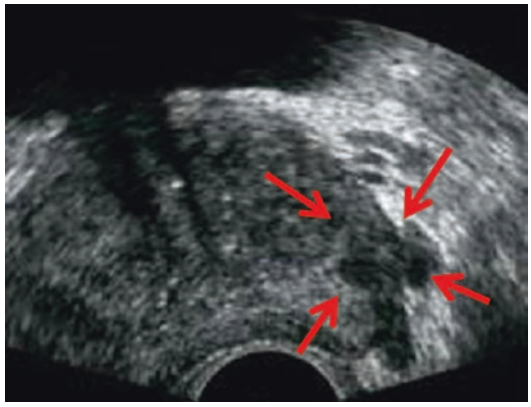

Fig. 24.2 Neoplasm localized in the anterior horn in the left prostatic lobe (*Red arrows*)

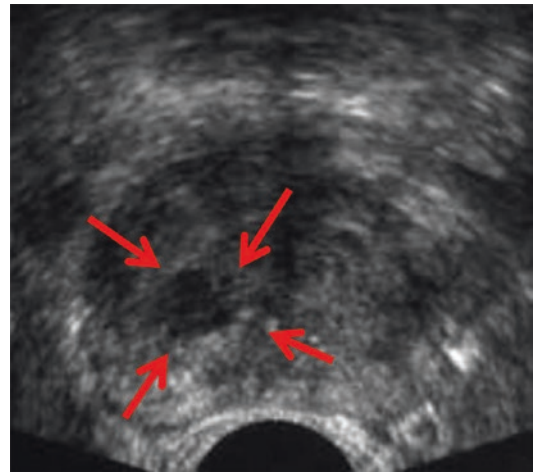

Fig. 24.3 Hypoechoic focus of nodular hyperplasia. This area is not suspicious for PC, because of its localization in the TZ (*Red arrows*)

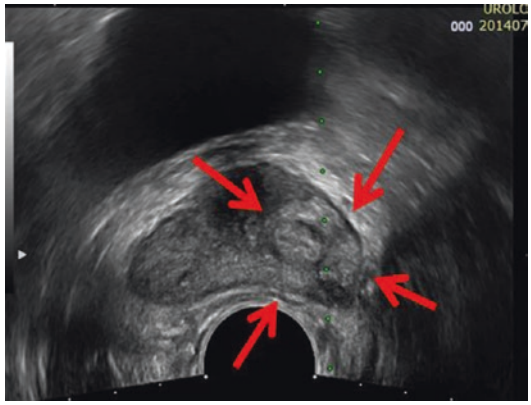

Fig. 24.4 Large PC, involving also the TZ, which is hyperechoic, with asymmetrical left prostatic lobe (*Red arrows*)

24.3 Echogenicity

24.3.1 Hypoechoic Lesions

Hypo-echogenicity is the most frequent presentation of neoplastic lesions (Fig. 24.5). About 60 % of involved areas with PC are hypoechoic, but only 17–57 % of hypoechoic areas are PC at final histology. The difference of the echogenicity of the different tissues is not always so clear (Fig. 24.6), and diagnosis of a PC requires an optimization of the gray scale and of the set of US machine. The color Doppler might be helpful in the identification of structural anomalies in some cases.

The intraprostatic hypoechoic images, particularly those located in the peripheral zone, are considered suspicious for neoplasia [6], and several studies revealed the correlation between this finding and PC [7, 8]. Recent publications [9] highlight the presence of hypoechoic areas as significantly related to the diagnosis of high-grade PC (Gleason score >7) and that they might be considered predictive of a clinically significant disease.

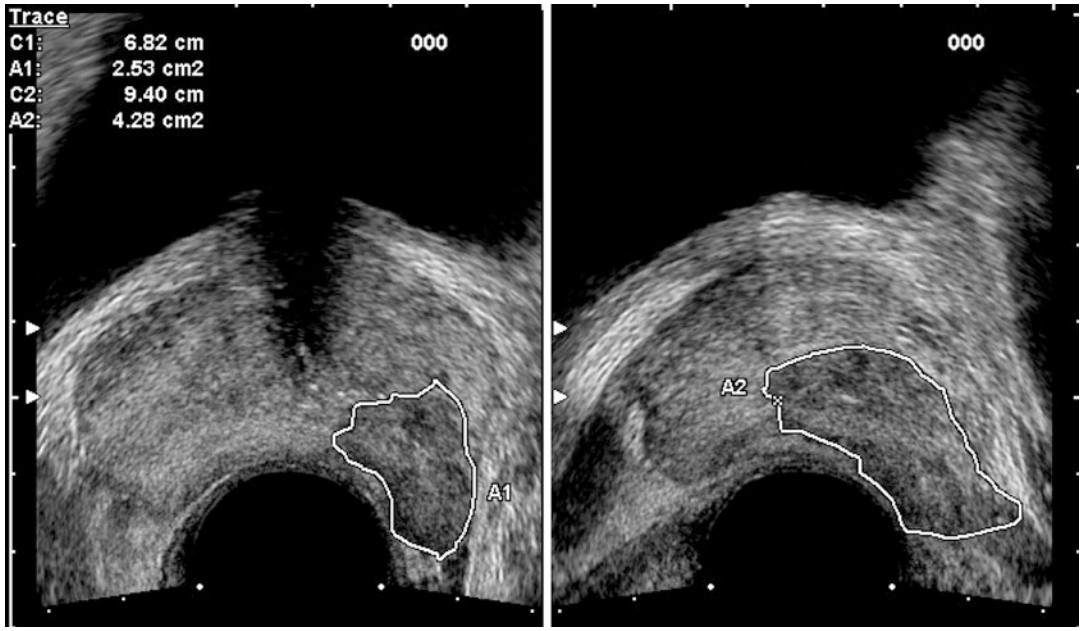

Fig. 24.5 Large hypoechoic focus in the left prostatic lobe

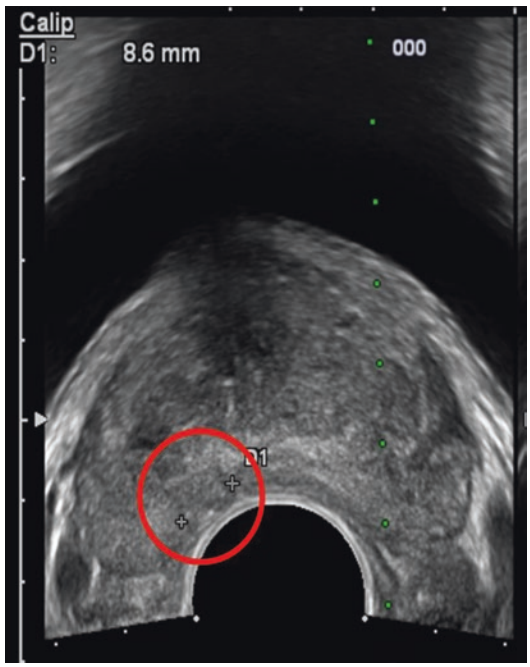

Fig. 24.6 Mildly hypoechoic nodule located in the peripheral zone, in the right paramedian part. This nodule corresponds to an area with increased consistence during palpation (*Red circle*)

24.3.2 Isoechoic Lesions

Thirty to forty percent of PC shows an isoechoic appearance. The isoechoic lesions may be very different: small lesions, usually with low histological grade, only identified by random PB (T1c stage), classical lesions, whose echogenicity is similar to the adjacent prostatic parenchyma that is not highlighted only with US. In these cases, color Doppler might be helpful in pinpointing lesions and in suggesting bioptic sampling (Fig. 24.7). Eventually, sometimes, even voluminous and infiltrating lesions might be difficult to be diagnosed in US, if no attention is paid in evaluating the anomalies of the margins or of the lack of differentiation between the peripheral and the transitional zone.

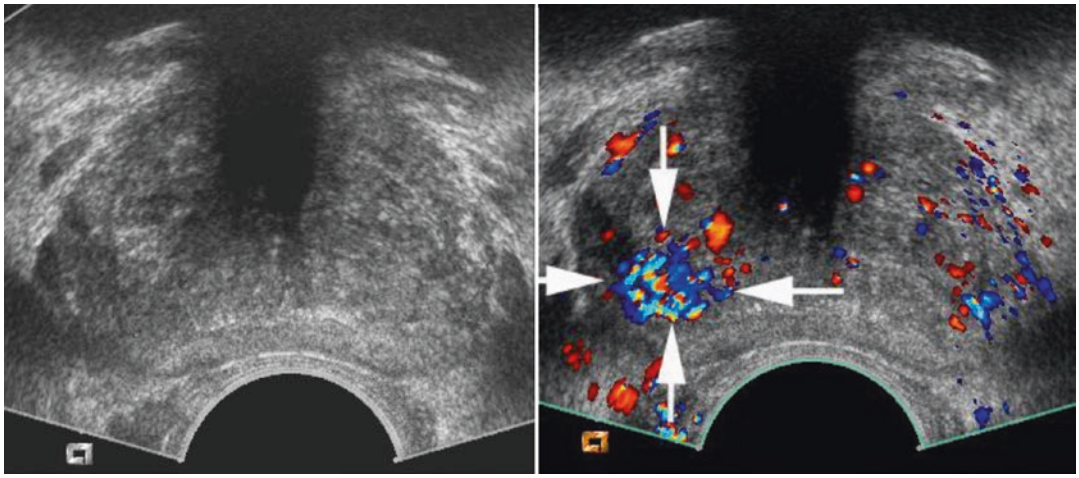

Fig. 24.7 Prostatic neoplasm with isoechoic structure, evidenced with ecocolordoppler help, with contrast medium (*white arrows*)

24.3.3 Hyperechoic Lesions

The hyperechoic lesions are the most rare (5–10 %), and the observation of microcalcifications inside the neoplasia ("black and white") occurs in about 2 % of diagnoses (Fig. 24.8). These US features are generally associated with cancer with poorly differentiated histology (Gleason score 9–10) (Fig. 24.9).

The pseudo-cystic lesions are very rare. They show a significant cystic component, an extra prostatic evolvement, and a compressed and often hypervascularized tissue margin (Fig. 24.10).

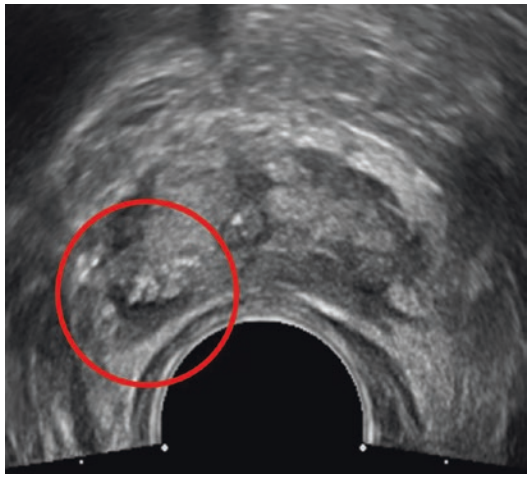

Fig. 24.8 Apical right lesion with microcalcifications inside (*Red circle*)

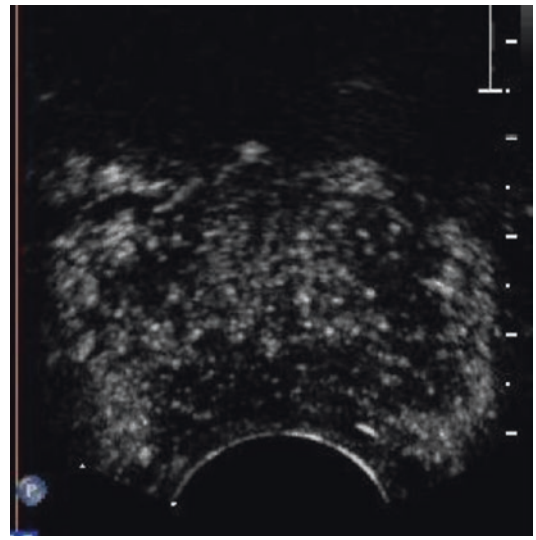

Fig. 24.9 Prostatic neoplasm approximately extended to all the prostate, with "black and white" appearance. The pathological exam showed a poorly differentiated neoplasm (5 + 4 Gleason score)

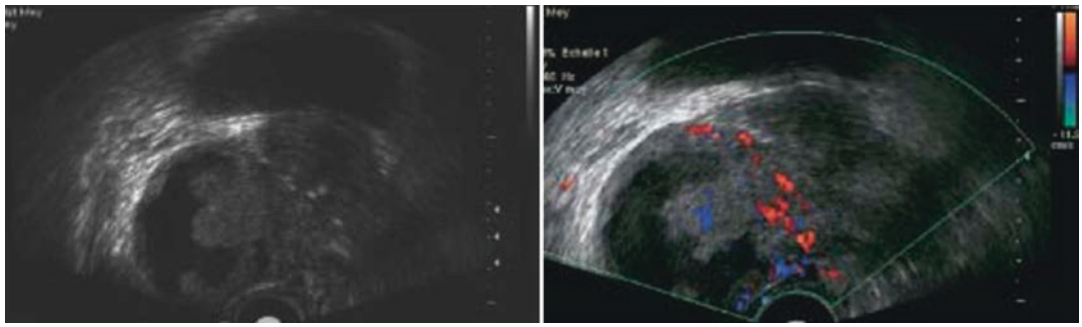

Fig. 24.10 Unusual pseudo-cystic neoplasm with extraprostatic extension and a hypervascularized solid component

24.4 Role of TRUS in Prostatic Cancer Diagnosis

About 30 % of US detectable PCs shows a nodular and engaged appearance, whereas in more than 50 %, the images show irregular margins with infiltrating appearance. It has been demonstrated that the presence of US-suspected lesions is closely related to the cancer-detection rate and, above all, to high-grade neoplasms [10, 11].

Nevertheless, the TRUS has many limits in PC diagnosis, and these limits reduce the sensitivity and the specificity of this method [12, 13].

There are many factors that could be considered:

- About one third of neoplasms might be isoechoic or with an echogenicity similar to "normal" peripheral zone (in particular well-differentiated lesions with a glandular morphology very similar to the normal structure).
- Hypoechoic area may be observed during acute flogosis (Fig. 24.11), with the presence of post-ischemia necrotic areas, of small nodular hyperplastic areas either of vascular structures or of fibro-muscular tissue.
- Up to 20 % of the PCs may originate from transitional zone, and their differentiation from the normal tissue with altered echogenicity is very difficult.

The TRUS accuracy in staging PC is low [13] with a sensitivity that has been reported to be 50–85 % and a specificity 46–90 % in detecting an extracapsular extension (cT3) (Figs. 24.12, 24.13, and 24.14). These parameters are even lower when considering the seminal vesicle invasion (accuracy <70 %).

The future of US is to offer, in conjunction with MRI, a guide for prostate biopsy, in order to reduce the side effects of multiple random biopsies, to focus the diagnosis only to clinically significant neoplasm, and to reduce the diagnosis of incidental microfoci which are clinically irrelevant.

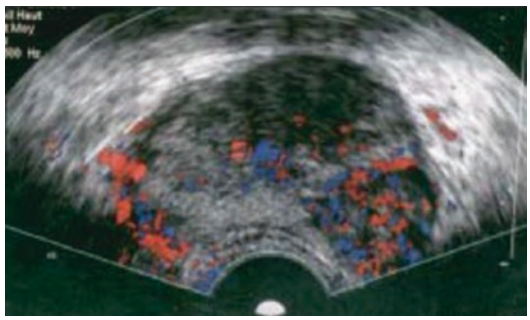

Fig. 24.11 Hypervascularized and hypoechoic lesions in granulomatous prostatitis (post-BCG) might simulate neoplastic lesions

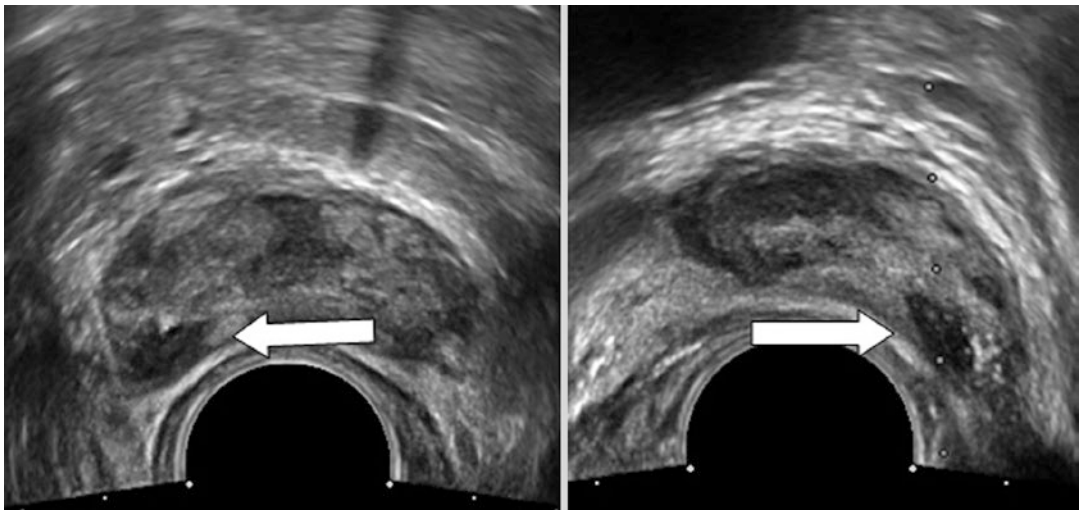

Fig. 24.12 Hypoechoic lesions with poorly defined margins, in recent acute prostatitis (*white arrows*)

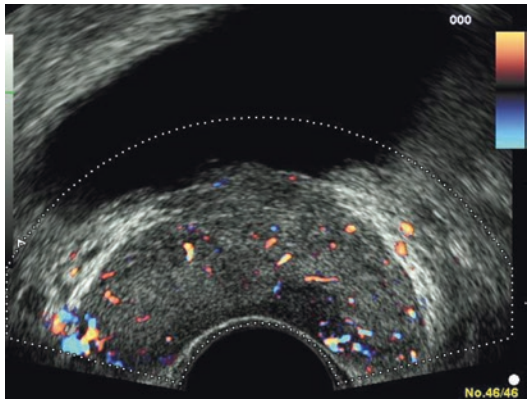

Fig. 24.13 Hypoechoic lesion located in the left lobe; in the sagittal plane, the irregularity of capsule is evident

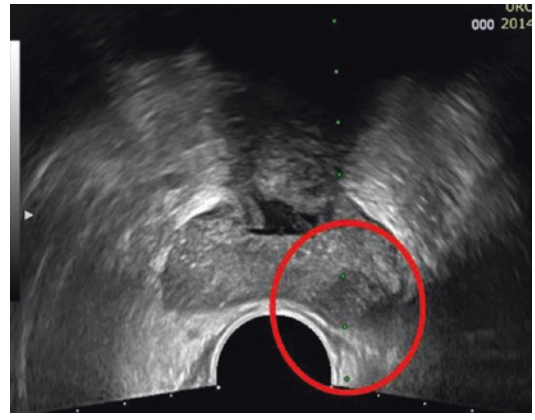

Fig. 24.14 Hypoechoic area in the left lobe. In this case the extracapsular extension is not so evident (*Red circle*)

24.5 Color Doppler Role in Prostate TRUS

In physiological conditions the prostate shows very low, but generally recognizable, parenchymal flows, with a symmetrical representation. More intense Doppler signals are visible proximally to the neurovascular bundles and in the peri-capsular and periprostatic zones (Fig. 24.15). At first, the color/power Doppler was accepted with enthusiasm, because of the improvement of sensitivity; nevertheless, later on, the published data evidenced a low specificity: even if several neoplasms show a hypo-vascular pattern and a high number of benign inflammatory lesions show a hyper-vascularization during Doppler exam [14], similar results have been reported with the power Doppler [15]. Turgut et al. described some vascularization patterns (peri-lesional hyper-vascularization, asymmetrical vascular organization, especially in terms of dimensions and number) which demonstrated an important correlation with PC foci and reported an improved specificity of about 5–10% [16]. Despite these techniques did not show a substantial improvement in the accuracy of the method, their use may result effective both for focused PB and standard PB.

24.5.1 Contrast Ultrasound (Microbubbles)

The neoangiogenesis is recognized as an essential mechanism in the oncogenesis. The microvasa are inside the neoplastic tissue, and their density is higher than in the normal tissue, as shown in specimens [17]. Imaging techniques, which are potentially able to evidence the presence of micro-network of neoformed vasa, may offer very accurate information in order to diagnose the neoplastic foci (Fig. 24.16). The diameter of these microvasa ranges from 10 up to 50 nm, which is lower than the resolution of conventional Doppler (limit: 1 mm). The use of micrububble contrast medium allows the individuation of vasa with diameter lower than 50–100 nm [18, 19]. Moreover, it is possible that the realization of trials is focused on the contrast medium distribution, in order to evidence the "functionally" more active lesions (this is similar to the iodine contrast medium in CT) [20]. Some groups have shown that the use of this method as guidance during the performance of focused PB improves the diagnostic accuracy [21, 22].

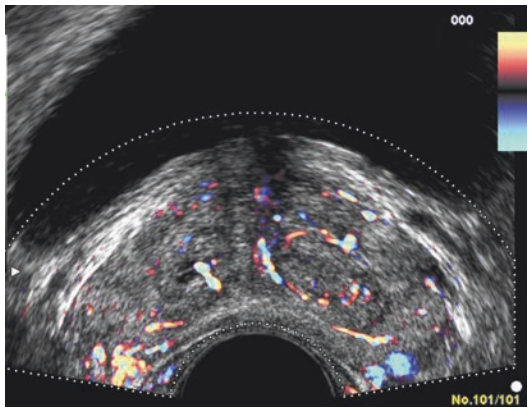

Fig. 24.15 More intense Doppler signals are observable proximally to neurovascular bundles and in the peri-capsular and periprostatic zone

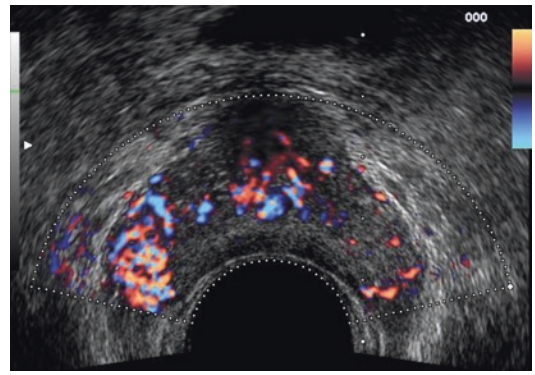

Fig. 24.16 PC with isoechoic structure, evidenced with the help of contrast-enhanced US

24.6 TRUS Lesion-Guided Prostatic Biopsies

One of the controversial issues is whether it is necessary to take samples from a TRUS visible lesion area in addition to systematic biopsies or simply to add more biopsies to the standardized sextant biopsy scheme in order to increase the detection rate of prostate cancer. Indubitably, hypoechoic prostatic lesions are more than twice as likely to have cancer on biopsy than isoechoic prostatic tissue, and the average biopsy yield of a peripheral zone hypoechoic lesion is 30–50% [23]. On the contrary, hypoechoic lesions in the transition zone are less specific in terms of prostatic cancer owing to the fact that benign prostatic hyperplasia nodules may normally appear hypoechoic.

Since only 60% of clinically diagnosed prostate cancer is hypoechoic and owing to the fact that transition zone cancers are generally concentrated in the farthest anterior areas of the prostate near the midline (a zone in which it is virtually impossible to detect prostate cancer based on TRUS alone), TRUS lesion-guided biopsies would detect only about 50% of all prostate cancers. Moreover, the identification of hypoechoic lesions in the peripheral zone is subjective [23].

For these reasons, in all cases, most urologists perform the standard sextant biopsy protocol and do not take additional biopsy samples from visible lesions located outside the predetermined location for standardized biopsies. They maintain that TRUS findings are clinically irrelevant because the sensitivity and specificity of a TRUS visible lesion is too low. Many authors have reported that the exclusive use of TRUS lesion-guided biopsies has such a low sensitivity that up to 60% of the cancer would be missed if systematic biopsies were not used. In a large series of 2,231 consecutive patients who underwent six sextant biopsies, Melchior and Brawer reported that cancer was found in 31% of patients with a hypoechoic sector [24]. Even if the positive predictive value of hypoechoic lesion was 90% in patients with a suspicious DRE, performing directed biopsies of hypoechoic lesions would only have resulted in misdiagnosing 25% of patients. Their results strongly suggested the need to obtain biopsy samples of the normal-appearing peripheral zone as opposed to directed biopsies which only sample areas showing abnormality with ultrasound.

Nowadays, lesion-guided biopsies only play a role in the combination of systematic biopsies in prostates with visible lesions. There is some convincing data that the cancer yield is higher in those patients with some hypoechoic lesions seen at TRUS compared to those with no pathological ultrasound findings.

Fleshner et al. have also demonstrated the advantages of biopsying small hypoechoic lesions in patients with negative results following digital rectal examination and a PSA of less than 10 ng/ml [25]. Although they detected cancer in 17% of the patients with a small visible lesion at TRUS, the overall yield of a separate hypoechoic area biopsy was less than 4%. The authors recommended the identification and biopsying of small hypoechoic lesions in patients with suspected clinical stage T1c prostate cancer with minimal PSA elevations owing to the fact that a significant proportion of small hypoechoic lesions are positive for malignancy.

It is surprising to note that the detection rate of suspect findings for cancer by TRUS may vary from one institution to another. Melchior et al. reported that 72% out of 2,231 patients had a hypoechoic lesion. On the contrary, Scattoni et al. recently reported a positive TRUS in only 6% out of 396 patients who underwent extended multisite biopsies [23]. In fact, an accurate imaging study showed that only 12% of men with nonpalpable carcinoma of the prostate have no TRUS or endorectal coil magnetic resonance imaging abnormalities. Different cancer yields of the various studies may depend on the amount of the prostate following a positive TRUS or digital rectal examination [23].

In conclusion, in the absence of any proof that an extensive biopsy protocol may eliminate the need for directed biopsy, it seems wise to add one single biopsy targeted at the peripheral hypoechoic lesions located outside the standard biopsy location. Moreover, the ultimate biopsy scheme (12 or more cores) in patients with TRUS visible lesions is yet to be determined.

Conclusions

Currently, TRUS is the standard choice in order to evaluate a prostate, despite the known limits of accuracy in the identification of

neoplastic lesions and in the PC staging. The use of Doppler, especially if associated with medium contrast, demonstrates encouraging results, opening the way to the development of techniques which allow a more precise individuation of the "suspicious areas."

References

1. Watanabe H, Kato H, Kato T, Morita M, Tanaka M (1968) Diagnostic application of ultrasonography to the prostrate. Nihon Hinyokika Gakkai Zasshi 59:273–279
2. Holm HH, Gammelgard J (1981) Ultrasonically guided precise needle placement in prostate and seminal vesicles. J Urol 125:385–387
3. Onur R, Littrup PJ, Pontes JE, Bianco FJ Jr (2004) Contemporary impact of transrectal ultrasound lesions for prostate cancer detection. J Urol 172:512–514
4. Patel U, Rickards D (2002) Handbook of transrectal ultrasound and biopsy of the prostate. Martin Dunitz, London
5. Loch T (2007) Urologic imaging for localised prostate cancer in 2007. World J Urol 25:121–129
6. Lihrup PJ, Bailey SE (2000) Prostate cancer: the role of transrectal ultrasound and its impact on cancer detection and management. Radiol Clin North Am 38:87–113
7. Shinohara K, Wheeler TM, Scardino PT (1989) The appearance of prostate cancer on transrectal ultrasonography: correlation of imaging and pathological examinations. J Urol 142:76–78
8. Hou AH, Swanson D, Barqawi AB (2009) Modalities for imaging of prostate cancer. Adv Urol 81. Article ID 818065
9. Noh TI, Shin YS, Shim JS, Yoon JH, Kim JH, Bae JH, du Moon G, Park JY (2013) Are hypoechoic lesions on transrectal ultrasonography a marker for clinically significant prostate cancer? Korean J Urol 54(10):666–670
10. Toi A, Neill M, Lockwood G, Sweet J, Tammsalu L, Fleshner N (2007) The continuing importance of transrectal ultrasound identification of prostatic lesions. J Urol 177:516–520
11. Raja J, Ramachandran N, Munneke G, Patel U (2006) Current status of transrectal ultrasound-guided prostate biopsy in the diagnosis of prostate cancer. Clin Radiol 61:142–153
12. Harvey CJ, Pilcher J, Richenberg J, Patel U, Frauscher F (2012) Applications of transrectal ultrasound in prostate cancer. Br J Radiol 85:S3–S17
13. Patel U (2011) The prostate and seminal vesicles. In: Allan P, Baxter G, Weston M (eds) Clinical ultrasound, 3rd edn. Churchill-Livingstone, Edinburgh, pp 572–592
14. Turgut A, Dogra V (2008) Prostatic cancer: evaluation using transrectal sonography. In: Hayat M (ed) Methods of cancer diagnosis, therapy and prognosis. Elvesier, New York, pp 499–520
15. Halpern E, Strup S (2000) Using gray scale and color and power Doppler sonography to detect prostatic cancer. AJR Am J Roentgenol 174:623–627
16. Turgut A, Olcucuoglu E, Kosar P, Geyik PO, Kosar U, Dogra V (2007) Power Doppler ultrasonography of the feeding arteries of the prostate gland: a novel approach to the diagnosis of prostate cancer? J Ultrasound Med 26:875–883
17. Bigler SA, Deering RE, Brawer MK (1993) Comparison of microscopic vascularity in benign and malignant prostate tissue. Hum Pathol 24: 220–226
18. Leen E, Averkiou M, Arditi M, Burns P, Bokor D, Gauthier T et al (2012) Dynamic contrast enhanced ultrasound assessment of the vascular effects of novel therapeutics in early stage trials. Eur Radiol 22: 1442–1450
19. Harvey CJ, Pilcher J, Eckersley R, Blomley MJK, Cosgrove DO (2002) Advances in ultrasound. Clin Radiol 57:157–177
20. Goossen TE, de la Rosette JJ, Hulsbergen-van de Kaa CA, van Leenders GJ, Wijkstra H (2003) The value of dynamic contrast enhanced power Doppler ultrasound imaging in the localization of prostate cancer. Eur Urol 43:124–131
21. Frauscher F, Klauser A, Volgger H, Halpern EJ, Pallwein L, Steiner H et al (2002) Comparison of contrast-enhanced color Doppler targeted biopsy with conventional systematic biopsy: impact on prostate cancer. J Urol 167:1648–1652
22. Harvey CJ, Sidhu P (2010) Ultrasound contrast agents in genitourinary imaging. Ultrasound Clin 5: 489–506
23. Scattoni V, Zlotta AR, Nava L, Roscigno M, Montorsi F, Rigatti P (2002) Prostatic transrectal ultrasound (TRUS) guided biopsy schemes and TRUS prostatic lesion-guided biopsies. Eur Urol Suppl 1(6):28–34
24. Melchior SW, Brawer MK (1996) Role of transrectal ultrasound and prostate biopsy. J Clin Ultrasound 24:463–471
25. Fleshner NE, O'Sullivan M, Premdass C, Fair WR (1999) Clinical significance of small (less than 0.2 cm3) hypoechoic lesions in men with normal digital rectal examinations and prostate-specific antigen levels of less than 10 ng/ml. Urology 53:356–358

The Seminal Vesicles: Normal and Pathological Pictures

25

Carmen Maccagnano, Andrea Benedetto Galosi, and Vincenzo Scattoni

25.1 Introduction

The seminal vesicles (SVs) are part of the male reproductive system. They are located proximally to the posterior aspect of the prostate; they secrete a viscous fluid which constitutes the 70 % of the ejaculate [1, 2].

These two SVs are tubular structures which, if stretched, show a length of about 15 cm. In the fold, orthotopic conformation, the length is about 5–7 cm and the diameter is about 2–3 cm. The capacity range is 3–6 ml. Their shape is cone-like and they join to the deferential ampoules through their apex, originating the ejaculatory duct. The ejaculatory duct is 2 cm long and the lumen is 1 mm width. The ejaculatory duct joins the urethra with orifice located on the veru montanum. The SVs are located between the posterior wall of the bladder neck and the prostate, and they join the ampoules of the deferens duct, situated above the prostate. They are posteriorly related with the rectal anterior wall. The peritoneum covers only the posterior aspect of the SV bottom. The SVs are palpable during digital rectal examination, because of their close relation with the rectum. The two SVs, which connect each other with dense fibrous tissue, are laterally related to the venous periprostatic plexus.

Every SV is made up of a duct with irregular diameter, provided with several ampullar or tubular diverticula, of variable length. One extremity of the duct shows a blind end, whereas the other is linked to the deferential ampulla. The curvy coils and diverticula are placed one against the other, with the interposition of connective sepimenta which thicken on the surface of SV, forming the adventitial tonaca.

The wall of SV is made of three layers: mucosal, muscularis, and adventitial. The mucosal layer is represented by covering simple cylindrical epithelium, with interposed basal cells, and by the lamina propria. The cylindrical cells, defined as principle or secretory, contain the secretory vesicles which are more represented in the apex, where they open on the cell surface and transfer their fluid into the lumen. The basal cells are deeply located among the cylindrical cells. The role of the basal cells is substituting and/or sustaining the main cylindrical cells. The thin lamina propria contains several elastic fibers and some isolated fibrous muscular cells.

C. Maccagnano
Department of Surgery, Division of Urology,
Azienda Ospedaliera S.Anna –Como,
Via Ravona, 20, San Fermo della Battaglia (Co), Italy
e-mail: carmen.maccagnano@gmail.com

A.B. Galosi (✉)
Institute of Urology, Marche Polytechnic University,
Ancona, Italy
e-mail: galosiab@yahoo.it

V. Scattoni
Department of Urology, Scientific Institute H San Raffaele, University Vita-Salute, Via Olgettina 60,
Milan 20132, Italy

P. Martino, A.B. Galosi (eds.), *Atlas of Ultrasonography in Urology, Andrology, and Nephrology*,
DOI 10.1007/978-3-319-40782-1_25

The mildly thick muscular layer contains small bundles made of fibrous muscular cells, organized in a circular internal layer and in an external longitudinal one. It is equipped with a rich nervous plexus (which derived from the hypogastric plexus), with small groups of interposed ganglion cells.

The adventitial layer is represented by the more peripheral layers made of connective tissue, with several elastic fibers which send thin sepimenta to the inner part of the organ.

In the past, the SVs were considered as the storage for spermatozoa, which are observable indeed inside the SVs.

Currently, the established role of SVs is the production of a fluid enriched with fructose, which constitutes the 70% of the seminal fluid. This fluid also contains aminoacids, prostaglandins, citrate, and proteins. Nevertheless, the fructose is the most important element, also because it is the energetic source for the spermatozoa. The ejaculation mechanism in the SV comprehends also a contraction of SV, with secretion pushed along the ejaculatory duct. Then, the spermatozoa, accumulated in the deferential ducts and in the caudal part of the epididymis, are given off along the deferential ampoules. During the third phase, a new SV contraction pushes the liquid through the deferential ducts, enriched with spermatozoa [3].

25.2 Ultrasound Study

The SV morphology is evaluable with transabdominal approach with a convex probe or, more in detail, with a transrectal probe (transrectal ultrasound – TRUS). In TRUS the SV appearance is club-like, with finely irregular margins and mildly irregular echogenicity, slightly lower intense than the prostate. The range length is 40–60 mm and is extremely variable among the individuals; the width (15–20 mm) and the thickness (7–12 mm) show, instead, an inferior range of variability. Body width, whose range is 7–12 mm, is the most unvarying parameter among the individuals. When this parameter is over 14 mm, a dilation of the vesicle is observed [4].

Using an end-fire probe, it is possible to note and assess both SVs, which look like two down-directed big whiskers, on an axial plan. In this way a precise evaluation of the effective symmetry and dilation is possible. With an oblique scan, the exam of the entire SV is also feasible. It is also possible to calculate the longitudinal (length) and axial (thickness) diameters and to examine the ejaculatory duct and its end in the urethra in detail. The ultrasound look is slightly irregular and hypoechoic in comparison with the prostate (Figs. 25.1 and 25.2).

Standard criteria, divided into conventional and unconventional, are used to evaluate the modifications of ultrasound imaging of SV.

The conventional criteria are:

1. Increased thickness (anterior-posterior diameter – APD), mono- or bilateral (>14 mm);
2. Asymmetry (>2.5 mm) between the two SVs, even with normal APD (7–14 mm);
3. Reduced APD, mono- or bilateral (<7 mm)
4. Thickened glandular epithelium or with calcification/s;
5. The presence of polycyclic areas separated by hyperechoic septa (honeycomb shaped) in one or both SVs (Fig. 25.3) [3, 4].

The unconventional criteria are:

1. Glandular bottom-body ratio inferior to 1 or superior to 2.5;

2. APD of the body unmodified after ejaculation. Currently there are no literature data about the description of the SV dilation with a volumetric cut-off. Nevertheless, an elevated volume after ejaculation is highly associated with SV anomalies, with large prostate or with the presence of median cysts which might cause obstruction of the ejaculatory ducts. A reduced volume of the SV is defined as hypoplasia, and it principally refers to congenital forms with small SV. Nevertheless, acquired forms, associated with testosterone deficiency, exist. Hypoplasia is defined such by some authors when the APD VS is <5 or <7 mm, whereas other authors suggest to refer to the longitudinal diameter (normal if >25 mm, hypoplastic if 16–25 mm, and atrophic if <16 mm).

TRUS allows the individuation of possible alterations with malformed reasons:

1. Bilateral agenesis;
2. Monolateral agenesis (Fig. 25.4);
3. Mono- or bilateral hypoplasia (Fig. 25.4);
4. Vesicular cyst.

In these cases, the evaluation of the renal loggia and of the urinary tract on the same side of the anomaly is fundamental, in order to verify the presence of congenital defects of the urinary tract (mesonephric/metanephric defects). The monolateral agenesis generally arises before the seventh gestational week, consequently to a disturbance of the process, when the ureteral chip is generated by the mesonephric duct. It is often associated with ipsilateral agenesis (79 %) or with other kidney anomalies (12 %).

The bilateral SV agenesis is associated with mutations of CFTR gene in 64–73 % of cases, with CBAVD in the half of the cases and with normal kidneys. SV anomalies are observable in 50 % of children and in 90 % of adults with cystic fibrosis, in whom the agenesis is bilateral in half of the cases [3–5].

The congenital SV hypoplasia might be isolated or associated with other genitourinary anomalies.

The SV cysts are rare and might be congenital or acquired. The congenital forms may be isolated or associated with other genitourinary anomalies in most of the cases. The congenital cysts are mainly due to ejaculatory duct obstruction (EDO), caused by malformation of the distal part of mesonephric duct. They are associated with homolateral renal agenesis or dysgenesis in two thirds of cases.

Bilateral cysts have been diagnosed in 44–60 % of patients with autosomal dominant polycystic renal disease. Thus, the TRUS diagnosis of the cysts is clinically relevant, because it can induce to a precise evaluation of the urinary tract.

The acquired cysts are usually unilateral and associated with EDO, as a result of inflammation. Increased SV dimensions, together with an echogenicity reduction and with the diagnosis of multiple liquid micro-areas, are highly suspicious for inflammatory disease. Enlarged SVs, with liquid area of residual secretion, which do not modify after ejaculation are suggestive of vesicle-ampullar emptying defect.

This might be due to ejaculatory duct obstruction caused by inflammatory events, stones, or prostate neoplasms involving the ducts.

The US accurately evaluates these clinical situations associated with infertility (in case of hypoposia), hemospermia, or prostate cancer in elderly patients (Figs. 25.5 and 25.6) [6].

A reduced SV length and thickness of the SV, sometimes with pseudo-cystic appearance at the bottom, is evocative of vesicular sclero-atrophy, and is typical of a specific inflammatory disease [6].

The vesicular stones, as the ampullar ones, are very rare, and they are part of a chronic prostatitis-vesiculitis (Figs. 25.7 and 25.8).

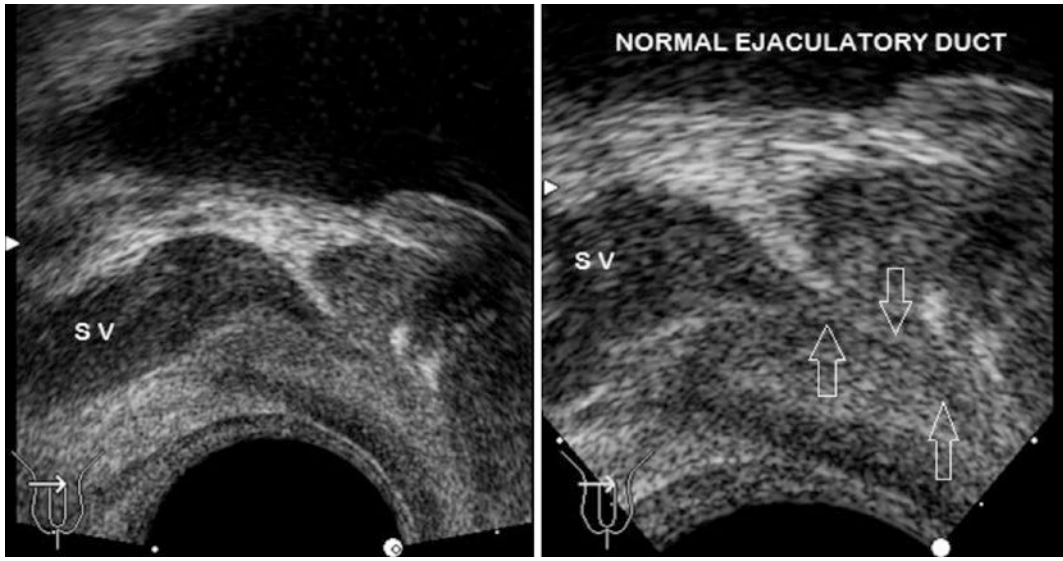

Fig. 25.1 TRUS: normal seminal vesicle (*SV*) (*right image*) and ejaculatory duct (*arrows, left image*)

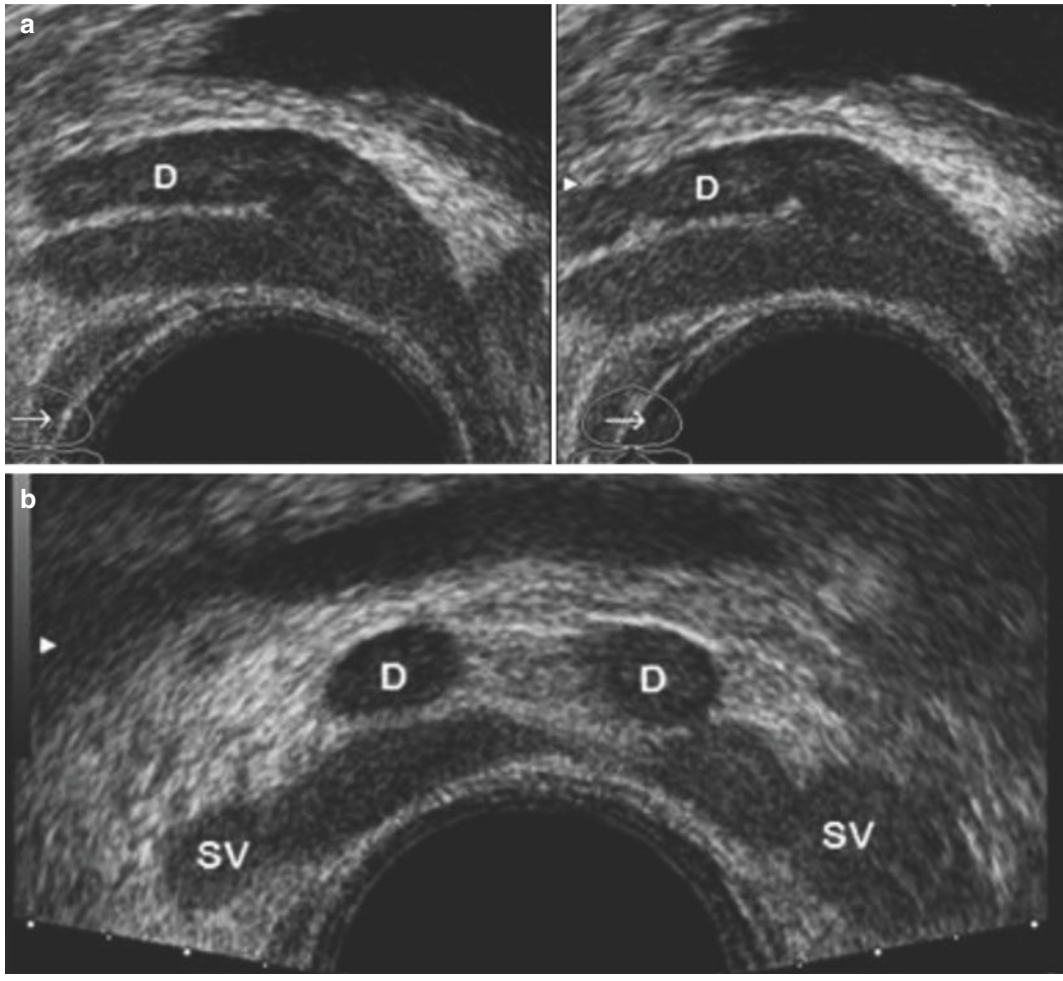

Fig. 25.2 Axial plan (**a**) and oblique longitudinal plan (**b**) of normal seminal vesicles (*SVs*) (*D* = deferential duct)

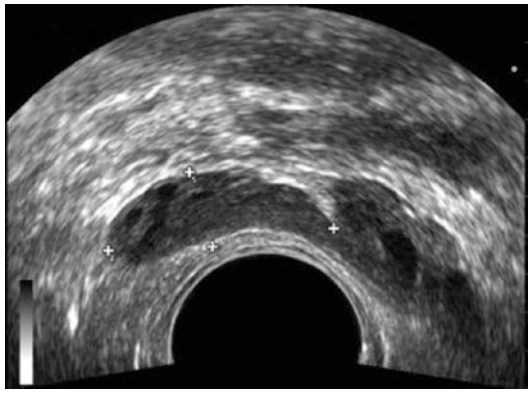

Fig. 25.3 Dilated seminal vesicles with thick wall

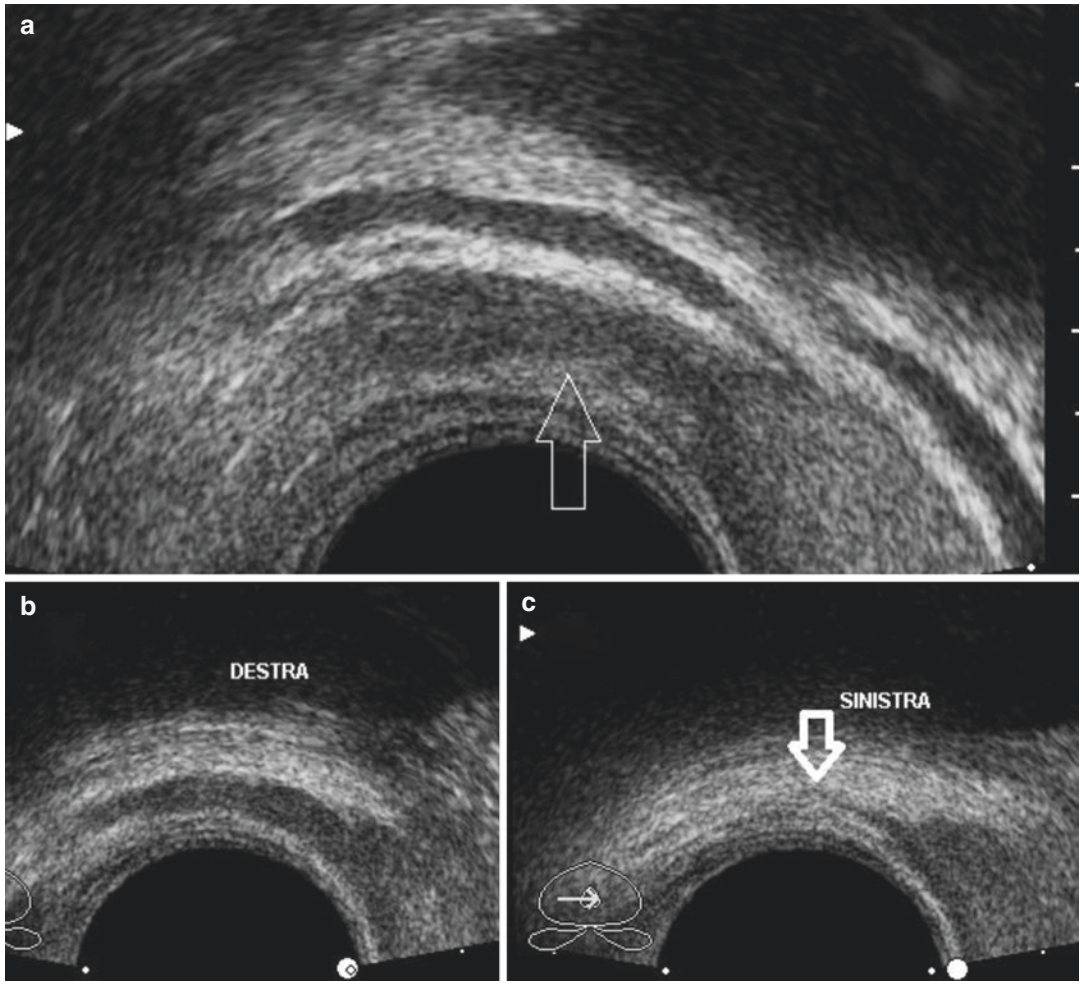

Fig. 25.4 Longitudinal view: hypoplastic-hypotrophic SV (*thon arrow* **a**, **b**) and absent left SV (**c**, *large arrow*)

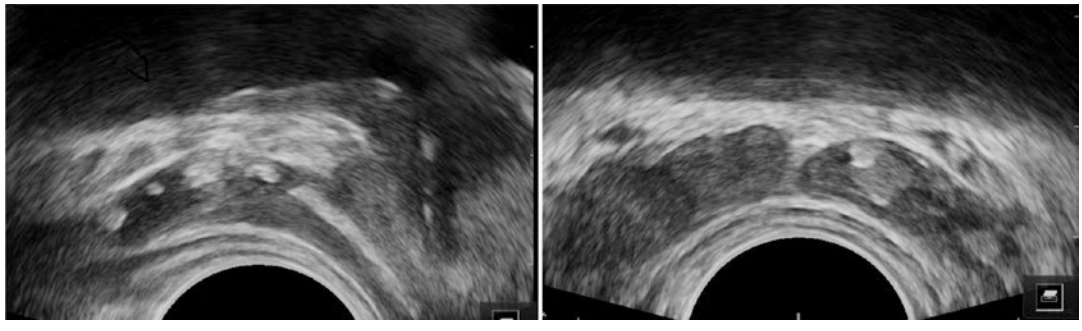

Fig. 25.5 Hyperechoic content in the left SV with hyperechoic material in the ejaculatory duct in the patient with hematospermia and infection

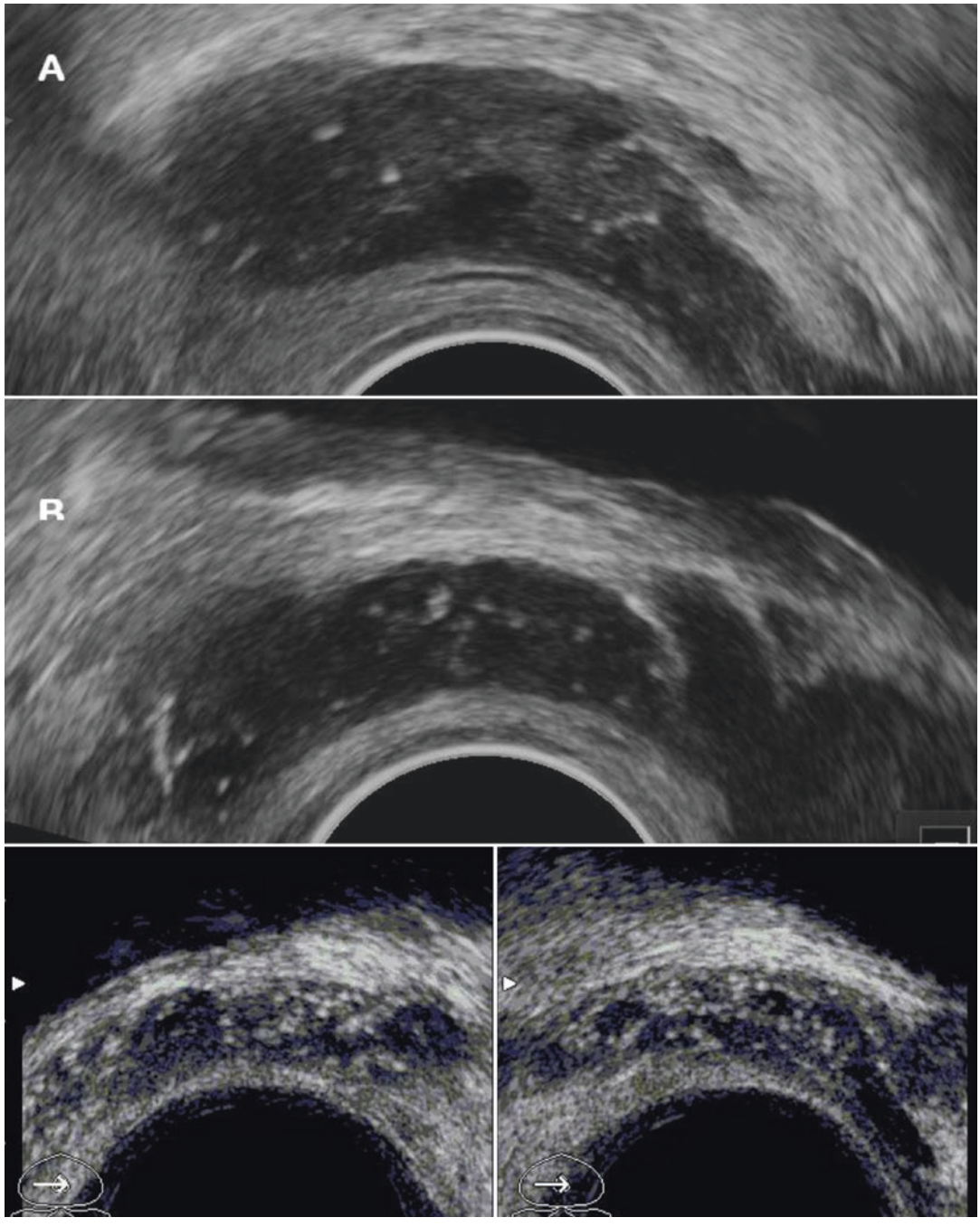

Fig. 25.6 Chronic inflammatory features of the SV, with the presence of calcifications and hypo- and hyperechoic appearance

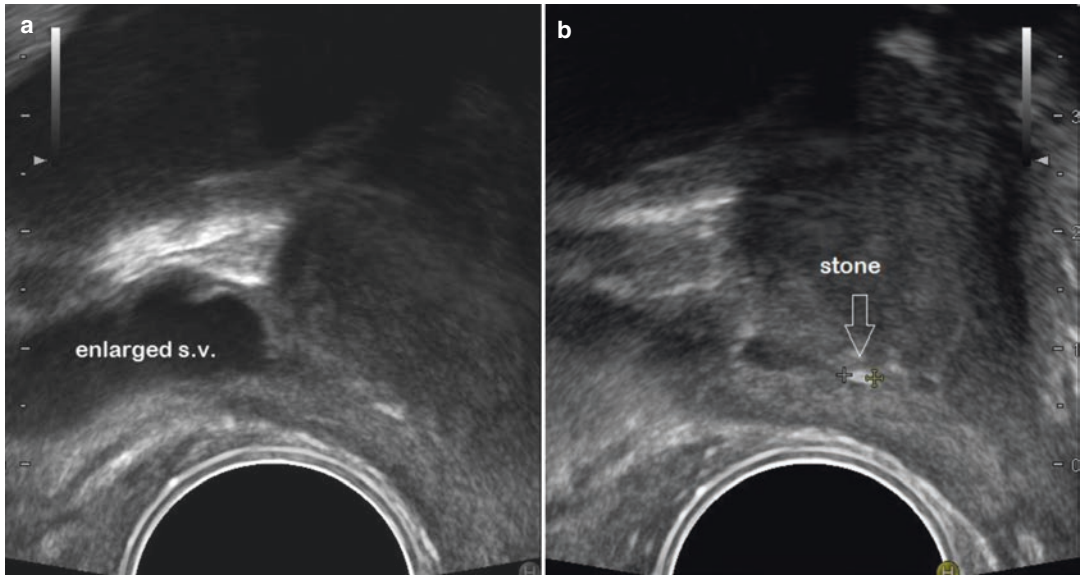

Fig. 25.7 (**a**) Stone in the ejaculatory duct. (**b**) Stone in the ejaculatory duct with dilated SV

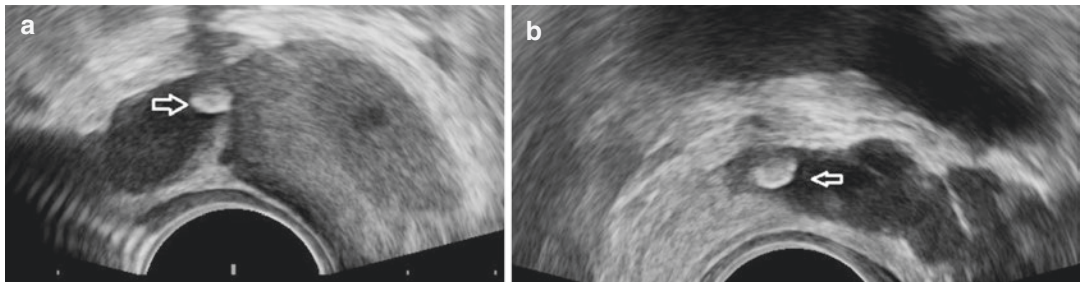

Fig. 25.8 Calcification in the SV (**a**) with acoustic posterior shadow, hyperechoic granule non-calcific without posterior acoustic shadow (**b**)

References

1. Lotti F, Maggi M (2015) Ultrasound of the male genital tract in relation to male reproductive health. Hum Reprod Update 21(1):56–83
2. Vicari E (1999) Seminal leukocyte concentration and related specific reactive oxygen species production in patients with male accessory gland infections. Hum Reprod 14:2025–2030
3. Martino P, Galosi AB, Bitelli M, Consonni P, Fiorini F, Granata A, Gunelli R, Liguori G, Palazzo S, Pavan N, Scattoni V, Virgili G, Imaging Working Group-Societa Italiana Urologia (SIU), Societa Italiana Ecografia Urologica Andrologica Nefrologica (SIEUN) (2014) Practical recommendations for performing ultrasound scanning in the urological and andrological fields. Arch Ital Urol Androl 86(1): 56–78
4. Jungwirth A, Diemer T, Dohle GR, Giwercman A, Kopa Z, Tournaye H, Krausz C (2013) Guidelines on male infertility, European Association of Urology guidelines. EAU Guidelines Office, Arnhem
5. Montironi R, Cheng L, Galosi AB, Montorsi F, Scarpelli M (2014) Seminal vesicle intraepithelial neoplasia vs. basal cell hyperplasia in a seminal vesicle. Eur Urol 66:623–627
6. Fisch H, Kang YM, Johnson CW, Goluboff ET (2002) Ejaculatory duct obstruction. Curr Opin Urol 12: 509–515

26 Interventional Ultrasound: Transperineal and Transrectal Prostatic Biopsy

Andrea Fandella and Pietro Pepe

26.1 Indications for Baseline Biopsy

PSA and/or rectal examination suspects remain the main indications for biopsy [1–4]. A prostate biopsy may be indicated for PSA values that exceed the thresholds of common use and almost always for values above 10 ng/ml; in this regard it is suggested to always repeat the PSA before making a decision. PSA level should be verified after a few weeks using the same assay under standardized conditions (i.e., no ejaculation, manipulations, urinary tract infections, prostate inflammation, and trauma) in the same laboratory [2, 3]. Empiric use of antibiotics in an asymptomatic patient in order to lower the PSA should not be undertaken [4].

Age, comorbidity of the patient, and therapeutic consequences are variables to consider when prescribing this procedure. Risk stratification is a potential tool for reducing unnecessary biopsies [1].

The transrectal ultrasound is considered the standard method to guide prostate biopsy and the removal of frustules done with transperineal or transrectal technique.

In rare cases, such as rectal amputation, it may require a transperineal guide.

It suggests a careful informed consent that explains to the patient the consequences of a possible clinical diagnosis of cancer before the biopsy [5].

26.2 Preparation for Prostate Biopsy

Sampling of the frustules of the prostate can result in bleeding inside the lodge and bladder. This occurrence is more frequent and severe in patients taking medications that interfere with clotting. For this reason it is wise to suspend, whenever possible, these drugs before the biopsy (aspirin, ticlopidine). In particular, the Coumadin and the Sintrom must be replaced by low molecular weight heparins [5].

To minimize the risk of infections, it is appropriate to take an antibiotic before the examination; oral or intravenous antibiotics are state of the art. Quinolones are the drugs of choice, with ciprofloxacin being superior to ofloxacin [6]; prophylaxis should be made taking into account the proportion of bacterial resistance in the region where biopsy is performed, and then the patient

Electronic supplementary material The online version of this chapter (doi:10.1007/978-3-319-40782-1_26) contains supplementary material, which is available to authorized users.

A. Fandella (✉)
Unit of Urology, Casa di Cura Giovanni XXIII, Monastier di Treviso, TV, Italy
e-mail: afandella@alice.it

P. Pepe
Unit of Urology, "Cannizzaro" Emergency Hospital, Catania, Italy

P. Martino, A.B. Galosi (eds.), *Atlas of Ultrasonography in Urology, Andrology, and Nephrology*,
DOI 10.1007/978-3-319-40782-1_26

choose the antibiotic accordingly. In addition, the patient should be questioned about previous urinary infections and if he/she has taken antibiotics for 3 months prior to biopsy. If this occurs, he/she should choose an antibiotic different from the previous.

Increased quinolone resistance [7] is associated with a rise in severe post-biopsy infection [8].

In cases of doubt, and if there has already been a prostatitis, the resistance of the intestinal germs by culture obtained by rectal swab should be tested [9–12]. Furthermore, to reduce the risk of infections, the preparation involves running the morning of an enema to clear the rectum [5].

26.3 How Do the Biopsy?

Biopsy without complications does not require hospitalization. The overall duration of the procedure is less than 30 min.

Based on the operator's preferences, the patient is encouraged to take the following positions: the side (Fig. 26.1), gynecological, and knee-chest positions. The first two positions are the most frequently used.

In Fig. 26.2, the instruments needed are biopsy gun, syringe with anesthetic, 18 cm needle, and sterile container for the samples.

The next stage involves the introduction of an ultrasound probe in the rectum. This tool will allow the operator to view the loggia, the prostate, and the bladder. In particular, the operator will proceed to the measurement of the volume of the prostate. The most important function of the ultrasound probe is to provide an image of the area and to drive accurately the operator in the selection of the different areas in which to execute withdrawal prostate.

A biopsy gun with a hook cutting edge (crypt) is able to take small frustules of suspicious tissue. The quick-snap mechanism with which the needle is pushed and withdrawn from the prostate minimizes the feeling of discomfort.

The biopsy needle may reach the prostate through the rectum (transrectal approach) or the skin of the area located between the testicles and anus (transperineal approach). Both of these methods have proved particularly effective and safe. The choice essentially depends on the operator's preference.

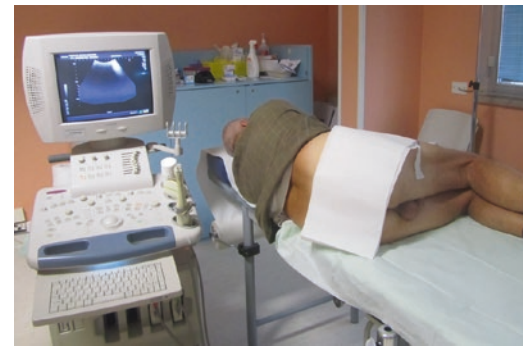

Fig. 26.1 Patient in positions on the side ready for transrectal biopsy

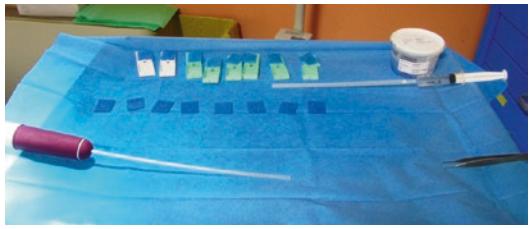

Fig. 26.2 Instruments: biopsy gun 25 cm 18 gauge needle, syringe with anesthetic with a 25 cm 22 gauge echogenic needle tip, and the sterile cassettes for the samples

26.3.1 Transrectal Approach

The procedure can be performed both in the lateral decubitus position (lying on your side and with your legs bent) (Fig. 26.1) and in gynecological position.

Before any operation is practiced, rectal examination to rule out the presence of concomitant abnormalities of the rectal wall should be performed.

Transrectal biopsy is performed under local anesthesia. The ultrasound probe introduced into the rectum is provided with a channel for the passage of fine needles. So with an 18 gauge 25 cm needle, it is possible to reach every part of the prostate (Figs. 26.3, 26.4, and 26.5).

Only patients with high comorbidity may require the procedure in the operating room under sedation or anesthesia.

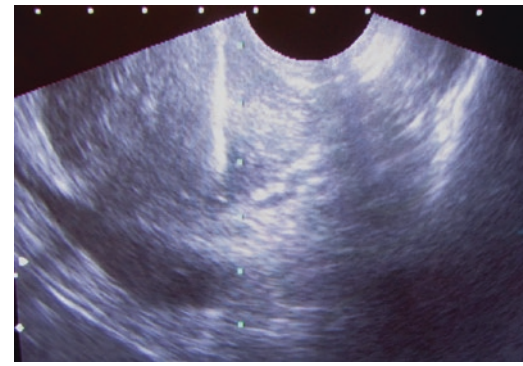

Fig. 26.3 Transrectal biopsy in the peripheral rear area

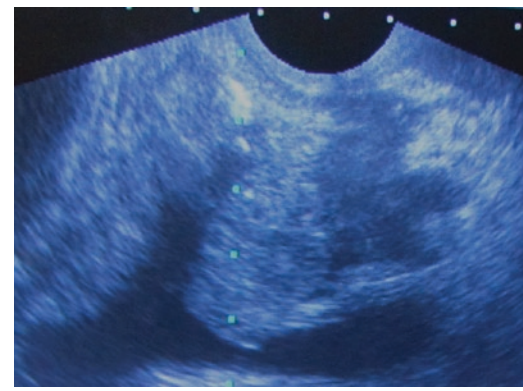

Fig. 26.4 Transrectal biopsy in the apex

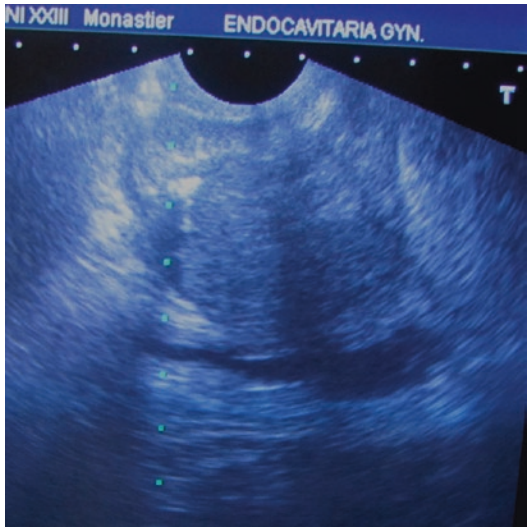

Fig. 26.5 Transrectal biopsy in the peripheral right area

26.3.1.1 Local Anesthesia Prior to Biopsy

Ultrasound-guided periprostatic block is state of the art [13] (Video 26.1). It is not important whether the depot is apical or basal. Intrarectal instillation of local anesthesia is inferior to periprostatic infiltration [14].

26.3.2 Transperineal Approach

The procedure is performed in gynecological position. The doctor performs a rectal examination to rule out the presence of concomitant abnormalities of the rectal wall. The patient is asked to raise a hand with the testicles, or claims are with gauze fixed with patches to "hammock" groin. The skin located between the testicles and the anus is shaved and disinfected. The entry point of the needle is located 1.5 cm above the anus. At this level, it injects a few ml of local anesthetic with a needle thin and short. In point prior anesthesia, a thin needle of greater length that allows the injection of the local anesthetic around the prostate is then introduced.

A thin metal channel cable is introduced along the path anesthetized until reaching the suspected area. This system will make it easy and not annoying for the patient because of the repeated passage of the needle biopsy. The ultrasound probe allows the patient to see at any time the areas that are reached by the needle biopsy. When the procedure is performed, a mild compression dressing is performed with the entry of the needle.

Transperineal prostate biopsy has come to the foreground as a result of lower incidence of sepsis, better detection rate for anterior prostate cancer (PCa), and the opportunity to perform the template-guided prostate biopsy [15, 16]. Transrectal and transperineal prostate biopsy procedures require different techniques and are recommended with the same level of evidence [17]. Candidates for transperineal biopsy should be studied with coagulation blood tests and receive antibiotic prophylaxis; if sedation is required (saturation or template-guided biopsy), both blood tests and cardiologic evaluation are recommended. Transperineal biopsy needs multifrequency linear or biplanar probes to show perineal passage of the needle; this approach is recommended for patients that have been previously subjected to abdominoperineal amputation or that are affected by severe disease of the rectum (Figs. 26.6 and 26.7).

Transperineal and transrectal prostate biopsy provides similar detection rates for prostate cancer (PCa) both for first procedure (34–40 %) and for repeat procedure (22–43 %) performing at least 12 (extended biopsy) vs. >20 (saturation biopsy) cores, respectively [18–31]. Transperineal route allows for easier access to the anterior zone of the gland, where incidence of PCa is from 10 to 20 % at repeat biopsy [32–36]. Transperineal template-guided biopsy, utilizing 30–60 cores, is suggested for men with previously negative biopsies and persistent suspicious of cancer, in local PCa staging and in the re-evaluation of patients enrolled in active surveillance (AS) protocols [37–40].

Despite ultrasound sensitivity improvement through combined use of color power Doppler (CDU) and a contrast medium agent [41–43] or elasto-sonography [44], the accuracy of transperineal and transrectal approach in the diagnosis of PCa performing targeted biopsies has not improved. On the contrary, combined use of multiparametric MRI (magnetic resonance imaging) and MRI/TRUS transperineal fusion targeted biopsy has high accuracy in detecting significant PCa [44–51]. In fact, multiparametric MRI/TRUS targeted biopsy produces a higher detection rate of PCa for each single core compared to extended biopsy schemes (15–20 % vs. 5–10 %) [50, 51] (Video 26.7) (Figs. 26.8, 26.9, 26.10, and 26.11); multiparametric MRI/TRUS transperineal targeted biopsy improves diagnosis of significant PCa most notably in AS protocols [44, 48–52].

Prostate biopsy is the gold standard in re-evaluation of men enrolled in AS protocols, and the highest percentage of patients being reclassified at confirmatory prostate biopsy repeat biopsy (25–30 % of the cases) [48] following unfavourable histology results (i.e., Gleason score >6, number of positive cores >2, greatest percentage of cancer "GPC" >50 %). Despite the fact that both the appropriate number of biopsy cores (extended vs. saturation vs. template-guided schemes) and the approach (transrectal vs. transperineal) [43–55] have not been established, transperineal biopsy seems more accurate in the identification of patients at risk of PCa in AS protocols [48], resulting in a lower incidence of adverse definitive histology

specimens compared to transrectal approach [53–56]. Multiparametric MRI/TRUS fusion targeted biopsy has improved staging in AS giving 10 % reassignment [57] in patients undergoing standard biopsy [58, 59]; moreover, MRI/TRUS fusion transperineal targeted biopsy has good accuracy in the diagnosis of anterior PCa [59–63] and in the re-evaluation of micro-focal cancer (a single positive core of Gleason score equal to 6 and GPC <5 %) [64] at risk for clinically insignificant PCa. Highest diagnostic accuracy of clinically significant PCa in the re-evaluation of men in AS [65] is still, at present, obtained through extended or saturation prostate biopsy schemes combined with MRI/TRUS targeted biopsy.

Finally, the transperineal approach reduces the incidence of sepsis (at most 0.07 %) compared with 1–2 % for the transrectal approach [11, 61, 66–74].

In conclusion, the transperineal approach could be recommended in persistent suspicion of PCa following one or more negative transrectal biopsies as this approach increases the detection of anterior PCa; furthermore, the transperineal route significantly reduces the incidence of sepsis in patients with previous prostatitis and/or recurrent urinary tract infection [75–77].

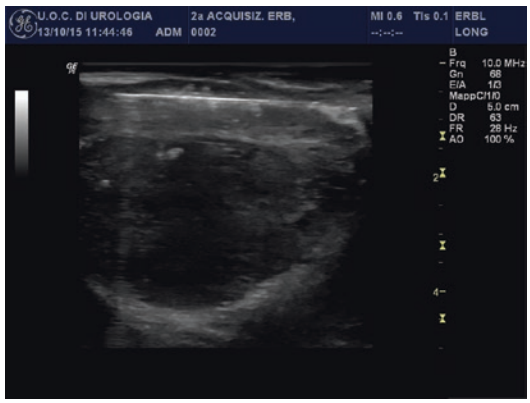

Fig. 26.6 Transperineal prostate biopsy (longitudinal scan): the needle (18 gauge tru-cut) is used to perform the biopsy in the periphery of the gland

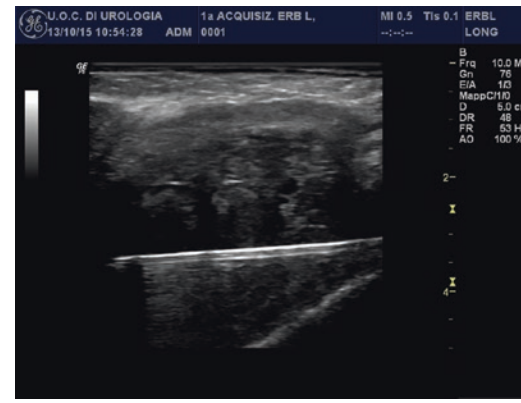

Fig. 26.7 Transperineal prostate biopsy (longitudinal scan): the needle (18 gauge tru-cut) is used to perform the biopsy in the anterior zone of the gland

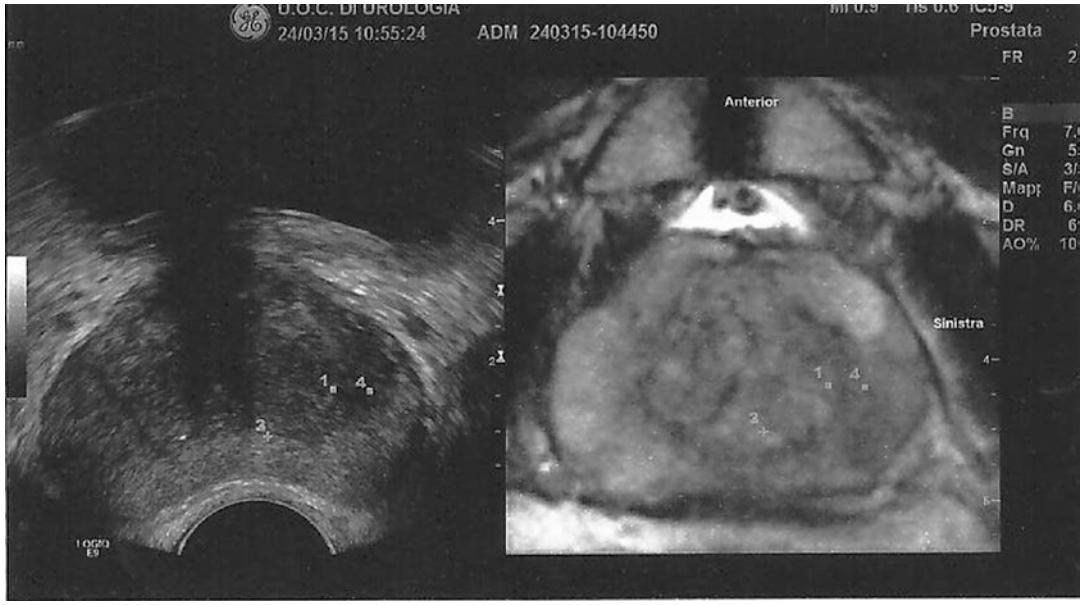

Fig. 26.8 3.0 Tesla pelvic multiparametric MRI/TRUS fusion imaging (axial scan) (ACHIEVA 3.0 Tesla; Philips Healthcare Best, the Netherlands – Logiq E9 General Electric; Milwaukee, WI): multiparametric MRI/TRUS fusion procedure and the application of markers

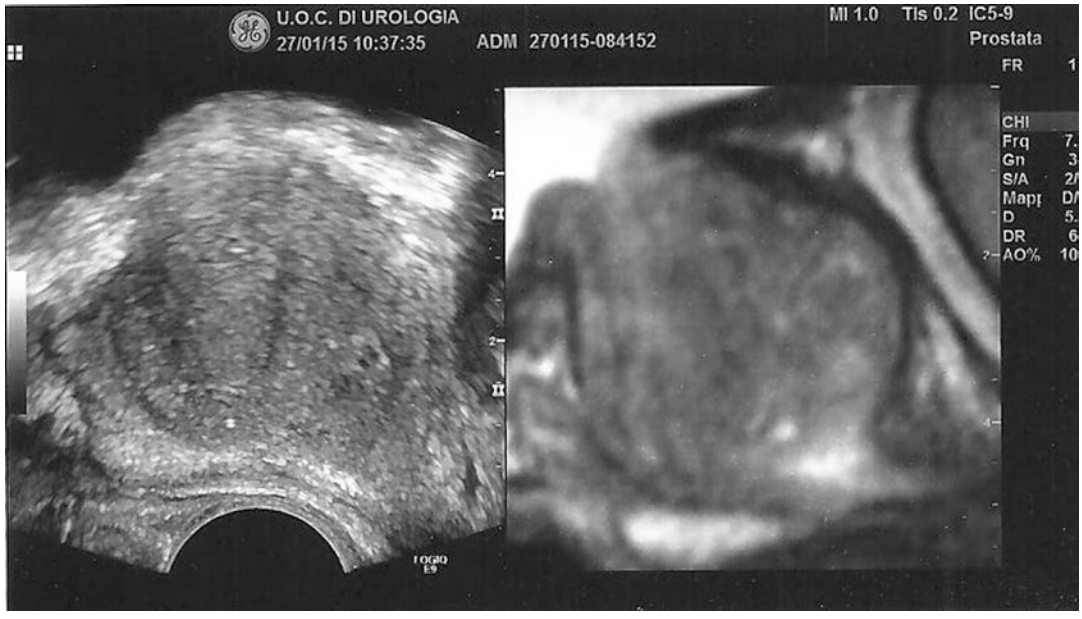

Fig. 26.9 3.0 Tesla pelvic multiparametric MRI/TRUS fusion imaging (longitudinal scan) (ACHIEVA 3.0 Tesla; Philips Healthcare Best, the Netherlands – Logiq E9 General Electric; Milwaukee, WI)

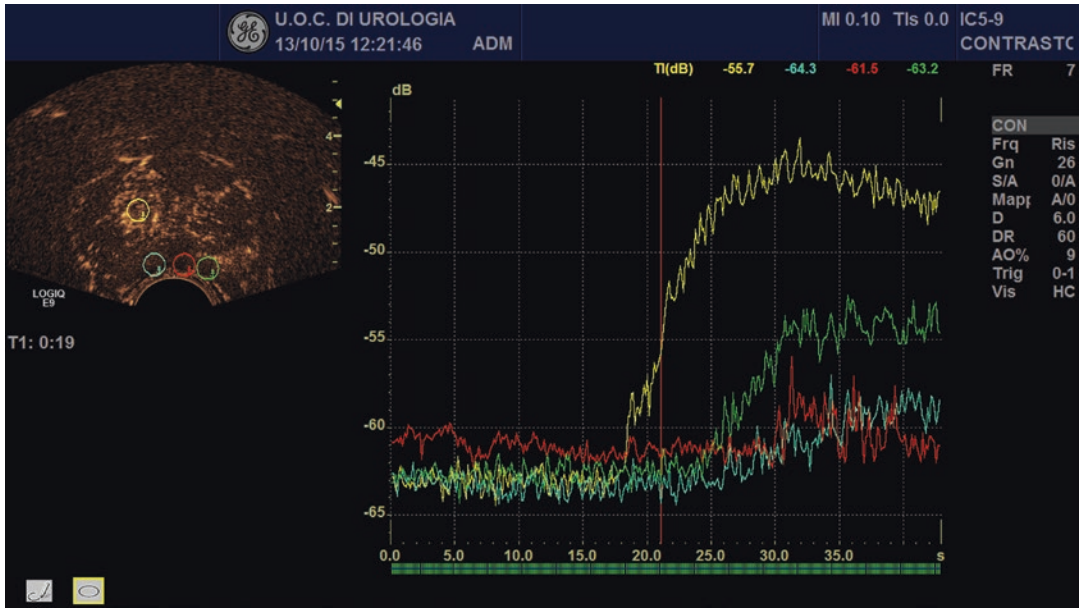

Fig. 26.10 Visual and quantitative analysis of SonoVue® concentration in the prostate after intravenous administration of ultrasound contrast medium: the markers evaluate the concentration of SonoVue® in different areas of the gland

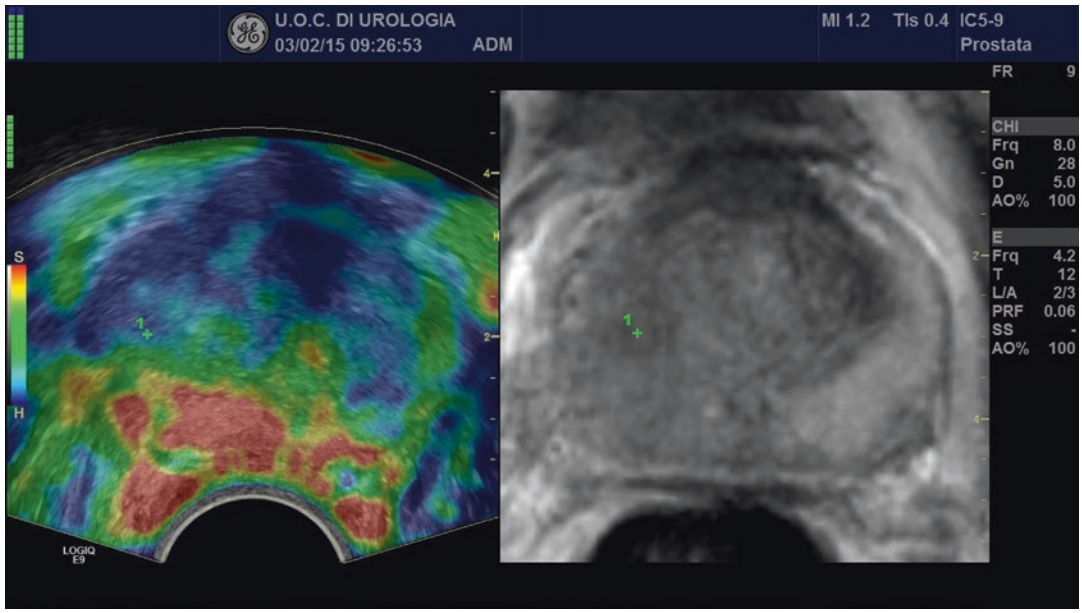

Fig. 26.11 3.0 Tesla pelvic multiparametric MRI/TRUS/elasto-sonography fusion imaging (ACHIEVA 3.0 Tesla; Philips Healthcare Best, the Netherlands – Logiq E9 General Electric; Milwaukee, WI): ultrasound evaluation of multiparametric MRI suspicious lesion (marker) is also conducted using elasto-sonography

26.4 Sampling Sites and Number of Cores

On baseline biopsies, the sample sites should be bilateral from apex to base as far as posteriorly and laterally as possible in the peripheral gland (Videos 26.2, 26.3, 26.4, 26.5, and 26.6). Additional cores should be obtained from suspect areas by DRE/TRUS and MRI (Video). Sextant biopsy is no longer considered adequate. Ten to 12 core biopsies are recommended [78], with >12 cores not being significantly more conclusive [79, 80].

26.4.1 Transition Zone Biopsy

Transition zone sampling during baseline biopsies has a low detection rate and should be confined to repeat biopsies [81].

26.5 Indications for Re-biopsy

26.5.1 After a Previous Negative Biopsy

Indications include (a) persistent increase in PSA, (b) suspicious DRE, (c) ASAP (atypical small acinar proliferation), and (d) extended PIN (prostatic intraepithelial neoplasia). The number of frustules taken must be higher than the first biopsy; you should also perform the transitional zone biopsy.

Alternatively, the re-biopsy can be done by technical saturation (20–24 samples). Approximately, 20 % re-biopsies are positive.

26.5.2 Repeat Biopsy After Previously Negative Biopsy

Isolated high-grade PIN in one or two biopsy sites is no longer an indication for repeat biopsy [82–85].

26.5.3 After a Previous Positive Biopsy

The re-biopsy is provided in most of the protocol for the patient in the active surveillance.

26.6 Possible Complications of Biopsy

The prostate biopsy is a safe procedure and generally associated with few complications.

During the execution of the biopsy, with both transperineal and transrectal approaches, the patient may experience pain even after executing anesthesia. Rarely, the patient may experience a general malaise characterized by increased sweating and feeling of loss of consciousness. Exceptional is the appearance of allergic reactions to the local anesthetic.

After the procedure, a rare complication (less than 2 % of cases) can be represented by the inability to empty the bladder spontaneously. In such a case, the placement of a urinary catheter which may be held in place for a few days or removed immediately is necessary.

For a few weeks after the biopsy with transrectal approach, you can assist in the loss of blood from the rectum (rectal). Such event is observed in 10–40 % of cases. The presence of blood in urine (hematuria) and/or urethrorrhagia is common in both the transrectal and the transperineal biopsies. Both are observed in approximately 30–60 % of cases; they persist for some days and generally disappear spontaneously.

Prostate biopsy is considered a safe technique, with incidence of severe complications <1 %; among these are the most dangerous infections of antibiotic-resistant germs. Severe postprocedural infections were initially reported in 1 % of cases, but have increased as a consequence of antibiotic resistance [8–11].

Low-dose aspirin is no longer an absolute contraindication [86]. Percentage of complications per biopsy session, irrespective of the number of cores, are as follows: hematospermia 37.4 %, hematuria >1 day 14.5 %, rectal bleeding <2 days 2.2 %, prostatitis 1 %, fever >38.5 °C 0.8 %, epididymitis 0.7, rectal bleeding >2 days +/− surgical intervention 0.7 %, urinary retention 0.2 %, and other complications requiring hospitalization 0.3 % [11].

After transperineal biopsy, seldom is the formation of a hematoma at the site of entry of the needle (less than 0.5 % of cases). The clinical

complications following transperineal prostate biopsy in men submitted to extended vs. saturation biopsy are listed in Table 26.1 [68].

In less than 1 % of cases, it is possible to observe the onset of high fever with shivering that may require hospitalization.

After the "execution of the procedure is an appropriate observation period of about a" time to highlight the appearance of any immediate complications. After transperineal biopsy, a mild compression level with the entry of the needle could be instituted.

Table 26.1 Complications following transperineal prostate biopsy in 3,000 patients submitted to 12 vs. 18 vs. >24 needle cores

Complications	12 cores* 915 pts	vs.	18 cores*° 1330 pts	vs.	>24 cores° 630 pts
Hematuria	92 (8.1 %)		130 (9.7 %)		66 (10.4 %)
Urethrorrhagia	20 (2 %)		30 (1.5 %)		19 (3 %)
Hematospermia	98 (10.7 %)		280 (21 %)		192 (30.4 %)
Acute urinary retention	38 (4.1 %)		95 (7.1 %)		70 (11.1 %)
Prostatitis	6 (0.6 %)		10 (0.7 %)		6 (0.9 %)
Sepsis	–		–		–
Orchiepididymitis	4 (0.4 %)		7 (0.5 %)		4 (0.6 %)
Urinary tract infection	27 (3 %)		30 (2.2 %)		16 (2 %)
Perineal hematoma	3 (0.3 %)		4 (0.3 %)		5 (0.8 %)
Vagal syndrome	9 (0.9 %)		–		–
Fever	4 (0.4 %)		8 (0.6 %)		5 (0.8 %)
Systemic adverse events[a,b]	1 (0.1 %)		–		–
Hospital admission (within 20 days)	9 (1 %)		18 (1.3 %)		10 (1.6 %)
Emergency department visit (within 20 days)	55 (6 %)		128 (9.6 %)		91 (14.4 %)

[a]Prostate biopsy performed under local anesthesia (*) or sedation (°) [72]
[b]Acute cardiac ischemia

References

1. Roobol MJ, Steyerberg EW, Kranse R et al (2010) A risk-based strategy improves prostate-specific antigen driven detection of prostate cancer. Eur Urol 57(1): 79–85
2. Richie JP, Catalona WJ, Ahmann FR et al (1993) Effect of patient age on early detection of prostate cancer with serum prostate-specific antigen and digital rectal examination. Urology 42(4):365–374
3. Carvalhal GF, Smith DS, Mager DE et al (1999) Digital rectal examination for detecting prostate cancer at prostate specific antigen levels of 4 ng/mL or less. J Urol 161:835–839
4. Okotie OT, Roehl KA, Han M et al (2007) Characteristics of prostate cancer detected by digital rectal examination only. Urology 70(6):1117–1120
5. Eastham JA, Riedel E, Scardino PT, Polyp Prevention Trial Study Group et al (2003) Variation of serum prostate-specific antigen levels: an evaluation of year-to-year fluctuations. JAMA 289(20):2695–2700
6. Stephan C, Klaas M, Muller C et al (2006) Interchangeability of measurements of total and free prostate specific antigen in serum with 5 frequently used assay combinations: an update. Clin Chem 52(1):59–64
7. Fandella A, Benvenuto S, Guidoni E, Giampaoli M, Bertaccini A (2014) Empiric antibiotics therapy for mildly elevated prostate-specific antigen: helpful to avoid unnecessary biopsies. Arch Ital Urol Androl 86(3):202–204
8. Bertaccini A, Fandella A, Prayer-Galetti T, Scattoni V, Galosi AB, Ficarra V, Trombetta C, Gion M, Martorana G, Italian Group for Developing Clinical Practice Guidelines on Performing Prostate Biopsy (2007) Systematic development of clinical practice guidelines for prostate biopsies: a 3-year Italian project. Anticancer Res 27(1B):659–666
9. Liss MA, Peeples AN, Peterson EM (2011) Detection of fluoroquinolone resistant organisms from rectal swabs by use of selective media prior to a transrectal prostate biopsy. J Clin Microbiol 49:1116
10. Cuevas O, Oteo J, Lázaro E, Spanish EARS-Net Study Group et al (2011) Significant ecological impact on the progression of fluoroquinolone resistance in Escherichia coli with increased community use of moxifloxacin, levofloxacin and amoxicillin/clavulanic acid. J Antimicrob Chemother 66(3):664–669
11. Loeb S, Carter HB, Berndt SI et al (2011) Complications after prostate biopsy: data from SEER-medicare. J Urol 186(5):1830–1834
12. Duplessis CA, Bavaro M, Simons MP et al (2012) Rectal cultures before transrectal ultrasound-guided prostate biopsy reduce postprostatic biopsy infection rates. Urology 79:556–563
13. von Knobloch R, Weber J, Varga Z et al (2002) Bilateral fine-needle administered local anaesthetic nerve block for pain control during TRUS-guided multi-core prostate biopsy: a prospective randomised trial. Eur Urol 41(5):508–514; discussion 514
14. Adamakis I, Mitropoulos D, Haritopoulos K et al (2004) Pain during transrectal ultrasonography guided prostate of lidocaine-prilocaine cream. World J Urol 22(4):281–284
15. Acher P, Dooldeniya M (2013) Prostate biopsy: will transperineal replace transrectal? BJU Int 112:533–534
16. Pepe P, Aragona F (2014) Prostate biopsy: results and advantages of the transperineal approach – twenty-year experience of a single center. World J Urol 32:373–377
17. Mottet N, Bellmunt J, Briers E, van den Bergh RCN, Bolla M, van Casteren NJ, Cornford P, Culine S, Joniau S, Lam T, Mason MD, Matveev V, van der Poel H, van der Kwast TH, Rouvière O, Wiegel T (2015) Prostate cancer guidelines. European Association of Urology
18. Ravery V, Goldblatt L, Royer B, Blanc E, Toublanc M, Boccon-Gibod L (2000) Extensive biopsy protocol improves the detection rate of prostate cancer. J Urol 164:393–396
19. Eskew LA, Bare RL, McCullough DL (1997) Systematic 5 region prostate biopsy is superior to sextant method for diagnosing carcinoma of the prostate. J Urol 157:199–202
20. Beurton D, Izadifar V, Barthelemy Y, Desgrippes A, Fontaine E (2000) 12 systematic prostate biopsies are superior to sextant biopsies for diagnosing carcinoma: a prospective randomised study. Eur Urol 37:296–299
21. Scattoni V, Raber M, Abdollah F, Roscigno M, Dehò F, Angiolilli D, Maccagnano C, Gallina A, Capitanio U, Freschi M, Doglioni C, Rigatti P, Montorsi F (2010) Biopsy schemes with the fewest cores for detecting 95% of the prostate cancers detected by a 24-core biopsy. Eur Urol 57:1–8
22. Pepe P, Aragona F (2005) Prostate needle biopsy: 12 vs. 18 cores – is it necessary? Urol Int 74:19–22
23. Cormio L, Scattoni V, Lorusso F, Perrone A, Di Fino G, Selvaggio O, Sanguedolce F, Bufo P, Montorsi F, Carrieri G (2014) Prostate cancer detection rates in different biopsy schemes. Which cores for which patients? World J Urol 32:341–346
24. Abdollah F, Novara G, Briganti A, Scattoni V, Raber M, Roscigno M, Suardi N, Gallina A, Artibani W, Ficarra V, Cestari A, Guazzoni G, Rigatti P, Montorsi F (2011) Trans-rectal versus trans-perineal saturation rebiopsy of the prostate: is there a difference in cancer detection rate? Urology 77:921–925
25. Remzi M, Fong YK, Dobrovits M, Anagnostou T, Seitz C, Waldert M, Harik M, Marihart S, Marberger M, Djavan B (2005) The Vienna nomogram: validation of a novel biopsy strategy defining the optimal number of cores based on patient age and total prostate volume. J Urol 174:1256–1260
26. Shen PF, Zhu YC, Wei WR, Li YZ, Yang J, Li YT, Li DM, Jia Wang J, Zeng H (2012) The results of transperineal versus transrectal prostate biopsy: a systematic review and meta-analysis. Asian J Androl 14: 310–315
27. Stewart CS, Leibovich BC, Weaver AL, Lieber MM (2001) Prostate cancer diagnosis using a saturation

needle biopsy technique after previous negative sextant biopsies. J Urol 166:86–91
28. Rabets JC, Jones JS, Patel A, Zippe CD (2004) Prostate cancer detection with office based saturation biopsy in a repeat biopsy population. J Urol 172:94–97
29. Fandella A, Bertaccini A, Consonni P, Introini C, Gunelli R, Gruppo Italiano Biopsia Prostatica (2005) Prostate biopsy: re-biopsy after first negative biopsy. Arch Ital Urol Androl 77:39–49
30. Pepe P, Aragona F (2007) Saturation prostate needle biopsy and prostate cancer detection at initial and repeat evaluation. Urology 70:1131–1135
31. Pepe P, Dibenedetto G, Pennisi M, Fraggetta F, Colecchia M, Aragona F (2014) Detection rate of anterior prostate cancer in 226 patients submitted to initial and repeat transperineal biopsy. Urol Int 93:189–192
32. Mabjeesh NJ, Lidawi G, Chen J, German L, Matzkin H (2012) High detection rate of significant prostate tumours in anterior zones using transperineal ultrasound-guided template saturation biopsy. BJU Int 110:993–997
33. Seles M, Gutschi T, Mayrhofer K, Fischereder K, Ehrlich G, Gallé G, Gutschi S, Pachernegg O, Pummer K, Augustin H (2015) Sampling of the anterior apical region results in increased cancer detection and upgrading in transrectal repeat saturation biopsy of the prostate. BJU Int 117(4):592–597. doi:10.1111/bju.13108
34. Orikasa K, Ito A, Ishidoya S, Saito S, Endo M, Arai Y (2008) Anterior apical biopsy: is it useful for prostate cancer detection? Int J Urol 15:900–904
35. Galosi AB, Tiroli M, Cantoro D, Conti A, Muzzonigro G (2010) Biopsy of the anterior prostate gland: technique with end-fire transrectal ultrasound. Arch Ital Urol Androl 82:248–252
36. Hossack T, Patel MI, Huo A, Brenner P, Yuen C, Spernat D, Mathews J, Haynes AM, Sutherland R, del Prado W, Stricker P (2012) Location and pathological characteristics of cancers in radical prostatectomy specimens identified by transperineal biopsy compared to transrectal biopsy. J Urol 188:781–785
37. Fernandez Gomez JM, Garcia Rodriguez J (2014) Optimization of prostate biopsy in patients considered for active surveillance. The role of the confirmatory biopsy and transperineal techniques. Arch Esp Urol 67:409–418
38. Symons JL, Huo A, Yuen CL, Haynes AM, Matthews J, Sutherland RL, Brenner P, Stricker PD (2013) Outcomes of transperineal template-guided prostate biopsy in 409 patients. BJU Int 112:585–593
39. Bittner N, Merrick GS, Butler WM, Bennett A, Galbreath RW (2013) Incidence and pathological features of prostate cancer detected on transperineal template guided mapping biopsy after negative transrectal ultrasound guided biopsy. J Urol 190:509–514
40. Taira AV, Merrick GS, Bennett A, Andreini H, Taubenslag W, Galbreath RW, Butler WM, Bittner N, Adamovich E (2013) Transperineal template-guided mapping biopsy as a staging procedure to select patients best suited for active surveillance. Am J Clin Oncol 36:116–120
41. Pepe P, Patanè D, Panella P, Aragona F (2003) Does the adjunct of ecographic contrast medium Levovist improve the detection rate of prostate cancer? Prostate Cancer Prostatic Dis 6:159–162
42. Pepe P, Candiano G, Pennisi M, Aragona F (2010) Can Sonovue targeted biopsy replace extended or saturation biopsy in prostate cancer diagnosis? Our experience at primary and repeat biopsy. Arch Ital Urol Androl 82:155–159
43. Taverna G, Morandi G, Seveso M, Giusti G, Benetti A, Colombo P, Minuti F, Grizzi F, Graziotti P (2011) Colour Doppler and microbubble contrast agent ultrasonography do not improve cancer detection rate in transrectal systematic prostate biopsy sampling. BJU Int 108:1723–1727
44. Pinto PA, Chung PH, Rastinehad AR, Caccala AA Jr, Kruecker J, Bejamin CJ (2011) Magnetic resonance imaging/ultrasound fusion guided prostate biopsy improves cancer detection following transrectal ultrasound biopsy and correlates with multiparametric magnetic resonance imaging. J Urol 186:1281–1285
45. Aboumarzouk OM, Ogston S, Huang Z, Evans A, Melzer A, Stolzenberg JU, Nabi G (2012) Diagnostic accuracy of transrectal elastosonography (TRES) imaging for the diagnosis of prostate cancer: a systematic review and meta-analysis. BJU Int 110: 1414–1423
46. Hara R, Jo Y, Fujii T, Kondo N, Yokoyoma T, Miyaji Y, Nagai A (2008) Optimal approach for prostate cancer detection as initial biopsy: prospective randomized study comparing transperineal versus transrectal systematic 12-core biopsy. Urology 71:191–195
47. Kuru TH, Saeb-Parsy K, Cantiani A, Frey J, Lombardo R, Serrao E, Gaziev G, Koo B, Roethke M, Gnanapragasam V, Warren A, Doble A, Hadaschik B, Kastner C (2014) Evolution of repeat prostate biopsy strategies incorporating transperineal and MRI-TRUS fusion techniques. World J Urol 32:945–950
48. Komai Y, Numao N, Yoshida S, Matsuoka Y, Nakanishi Y, Ishii C, Koga F, Saito K, Masuda H, Fujii Y, Kawakami S, Kihara K (2013) High diagnostic ability of multiparametric magnetic resonance imaging to detect anterior prostate cancer missed by transrectal 12-core biopsy. J Urol 190:867–873
49. Mozer P, Rouprêt M, Le Cossec C, Granger B, Comperat E, de Gorski A, Cussenot O, Renard-Penna R (2015) First round of targeted biopsies with magnetic resonance imaging/ultrasound-fusion images compared to conventional ultrasound-guided transrectal biopsies for the diagnosis of localised prostate cancer. BJU Int 115:50–57
50. Pepe P, Garufi A, Priolo G, Candiano G, Pietropaolo F, Pennisi M, Aragona F (2013) Prostate cancer detection at repeat biopsy: can pelvic phased-array multiparametric MRI replace saturation biopsy? Anticancer Res 33:1195–1199
51. Quentin M, Biondin D, Klasen J, Schek J, Buchbender C, Miese FR, Antoch G, Barski D, Albers P, Arsov C (2012) Evaluation of a structured report of functional prostate magnetic resonance imaging in patients with

suspicion for prostate cancer or under active surveillance. Urol Int 89:25–29
52. Hoeks CM, Somford DM, van Oort IM, Vergunst H, Oddens JR, Smits GA, Roobol MJ, Bul M, Hambrock T, Witjes JA, Fütterer JJ, Hulsbergen-van de Kaa CA, Barentsz JO (2014) Value of 3-T multiparametric magnetic resonance imaging and magnetic resonance-guided biopsy for early risk restratification in active surveillance of low-risk prostate cancer: a prospective multicenter cohort study. Invest Radiol 49:165–172
53. Scott S, Samaratunga H, Chabert C, Breckenridge M, Gianduzzo T (2015) Is transperineal prostate biopsy more accurate than transrectal biopsy in determining final Gleason score and clinical risk category? A comparative analysis. BJU Int 116(Suppl 3):26–30. doi:10.1111/bju.13165
54. Bul M, Zhu X, Valdagni R, Pickles T, Kakehi Y, Rannikko A, Bjartell A, van der Schoot DK, Cornel EB, Conti GN, Boevé ER, Staerman F, Vis-Maters JJ, Vergunst H, Jaspars JJ, Strölin P, van Muilekom E, Schröder FH, Bangma CH, Roobol MJ (2013) Active surveillance for low-risk prostate cancer worldwide: the PRIAS study. Eur Urol 63:597–603
55. Chung PH, Darwish OM, Roehrborn CG, Kapur P, Lotan Y (2015) Histologic upgrading in patients eligible for active surveillance on saturation biopsy. Can J Urol 22:7656–7660
56. Thompson JE, Hayen A, Landau A, Haynes AM, Kalapara A, Ischia J, Matthews J, Frydenberg M, Stricker PD (2015) Medium-term oncological outcomes for extended vs. saturation biopsy and transrectal vs. transperineal biopsy in active surveillance for prostate cancer. BJU Int 115:884–891
57. Phan KN, Porter CR, Odem-Davis K, Wolff EM, Jeldres C, Wei JT, Morgan TM (2015) Transperineal template guided prostate biopsy selects candidates for active surveillance: how many cores are enough? J Urol 194:674–679
58. Katz DJ, Pinochet R, Richards KA, Godoy G, Udo K, Nogueira L, Cronin AM, Fine SW, Scardino PT, Coleman JA (2014) Comparison of transperineal mapping biopsy results with whole-mount radical prostatectomy pathology in patients with localized prostate cancer. Prostate Cancer 2014:781438. doi:10.1155/2014/781438, Epub 2014 May 11
59. Ouzzane A, Renard Penna R, Marliere F, Mozer P, Olivier J, Barkatz J, Puech P, Villers A (2015) Magnetic resonance imaging targeted biopsy improves selection of patients considered for active surveillance for clinically low risk prostate cancer based on systematic biopsies. J Urol 194:350–356
60. Kamrava M, Kishan AU, Margolis DJ, Huang J, Dorey F, Lieu P, Kupelian PA, Marks LS (2015) Multiparametric magnetic resonance imaging for prostate cancer improves Gleason score assessment in favorable risk prostate cancer. Pract Radiat Oncol. pii: S18798500(15)00154X. doi: 10.1016/j.prro.2015.04.006. [Epub ahead of print]
61. Radtke JP, Kuru TH, Boxler S, Alt CD, Popeneciu IV, Huettenbrink C, Klein T, Steinemann S, Bergstraesser C, Roethke M, Roth W, Schlemmer HP, Hohenfellner M, Hadaschik BA (2015) Comparative analysis of transperineal template saturation prostate biopsy versus magnetic resonance imaging targeted biopsy with magnetic resonance imaging-ultrasound fusion guidance. J Urol 193:87–94
62. Kuru TH, Roethke MC, Seidenader J, Simpfendörfer T, Boxler S, Alammar K, Rieker P, Popeneciu VI, Roth W, Pahernik S, Schlemmer HP, Hohenfellner M, Hadaschik BA (2013) Critical evaluation of magnetic resonance imaging targeted, transrectal ultrasound guided transperineal fusion biopsy for detection of prostate cancer. J Urol 190:1380–1386
63. Fascelli M, George AK, Frye T, Turkbey B, Choyke PL, Pinto PA (2015) The role of MRI in active surveillance for prostate cancer. Curr Urol Rep 16:42
64. Kim TH, Jeong JY, Lee SW, Kim CK, Park BK, Sung HH, Jeon HG, Jeong BC, Seo SI, Lee HM, Choi HY, Jeon SS (2015) Diffusion weighted magnetic resonance imaging for prediction of insignificant prostate cancer in potential candidates for active surveillance. Eur Radiol 25:1786–1792
65. Guo R, Cai L, Fan Y, Jin J, Zhou L, Zhang K (2015) Magnetic resonance imaging on disease reclassification among active surveillance candidates with low-risk prostate cancer; a diagnostic meta-analysis. Prostate Cancer Prostatic Dis 18:221–228
66. Pepe P, Dibenedetto G, Garufi A, Priolo G, Pennisi M (2015) Multiparametric pelvic MRI accuracy in diagnosing clinically significant prostate cancer in the re-evaluation of biopsy microfocal tumor. Anticancer Res 35:395–399
67. Volkin D, Turkbey B, Hoang AN, Rais-Bahrami S, Yerram N, Walton-Diaz A, Nix JW, Wood BJ, Choyke PL, Pinto PA (2014) Multiparametric MRI and subsequent MR/ultrasound fusion-guided biopsy increase the detection of anteriorly located prostate cancers. BJU Int 114(6b):E43–E49. doi:10.1111/bju.12670
68. Pepe P, Aragona F (2013) Morbidity following transperineal prostate biopsy in 3,000 patients submitted to 12 VS 18 VS more than 24 needle cores. Urology 81:1142–1146
69. Grummet JP, Weerakoon M, Huang S, Lawrentschuk N, Frydenberg M, Moon DA, O'Reilly M, Murphy D (2014) Sepsis and 'superbugs': should we favour the transperineal over the transrectal approach for prostate biopsy? BJU Int 114:384–388
70. Minamida S, Satoh T, Tabata K, Kimura M, Tsumura H, Kurosaka S, Matsumoto K, Fujita T, Iwamura M, Baba S (2011) Prevalence of fluoroquinolone-resistant Escherichia coli before and incidence of acute bacterial prostatitis after prostate biopsy. Urology 78:1235–1239
71. Pinkhasov GI, Lin YK, Palmerola R, Smith P, Mahon F, Kaag MG, Dagen JE, Harpster LE, Reese CT, Raman JD et al (2012) Complications following prostate needle biopsy requiring hospital admission or emergency department visits – experience from 1000 consecutive cases. BJU Int 110:369–374
72. Ehdaie B, Vertosick E, Spaliviero M, Giallo-Uvino A, Taur Y, O'Sullivan M, Livingston J, Sogani P, Eastham

J, Scardino P, Touijer K (2014) The impact of repeat biopsies on infectious complications in men with prostate cancer on active surveillance. J Urol 191:660–664
73. Chang DT, Challacombe B, Lawrentschuk N (2013) Transperineal biopsy of the prostate – is this the future? Nat Rev Urol 10:690–702
74. Rosario DJ, Lane JA, Metcalfe C, Donovan JL, Doble A, Goodwin L, Davis M, Catto JW, Avery K, Neal DE, Hamdy FC (2012) Short term outcomes of prostate biopsy in men tested for cancer by prostate specific antigen: prospective evaluation within ProtecT study. BMJ 344:d7894. doi:10.1136/bmj.d7894
75. Yuan LR, Zhang CG, Lu LX, Ruan L, Lan JH, Feng SQ, Luo JD (2014) Comparison of ultrasound-guided transrectal and transperineal prostate biopsies in clinical application. Zhonghua Nan Ke Xue 20:1004–1007
76. Merrick GS, Taubenslag W, Andreini H, Brammer S, Butler WM, Adamovich E, Allen Z, Anderson R, Wallner KE (2008) The morbidity of transperineal template-guided prostate mapping biopsy. BJU Int 101:1524–1529
77. Nam RK, Saskin R, Lee Y, Liu Y, Law C, Klotz LH, Loblaw DA, Trachtenberg J, Stanimirovic A, Simor AE, Seth A, Urbach DR, Narod SA (2010) Increasing hospital admission rates for urological complications after transrectal ultrasound guided prostate biopsy. J Urol 183:963–968
78. Donovan J, Hamdy F, Neal D, ProtecT Study Group et al (2003) Prostate Testing for Cancer and Treatment (ProtecT) feasibility study. Health Technol Assess 7(14):1–88
79. Eichler K, Hempel S, Wilby J et al (2006) Diagnostic value of systematic biopsy methods in the investigation of prostate cancer: a systematic review. J Urol 175(5):1605–1612
80. Shariat SF, Roehrborn CG (2008) Using biopsy to detect prostate cancer. Rev Urol 10(4):262–280
81. Pelzer AE, Bektic J, Berger AP et al (2005) Are transition zone biopsies still necessary to improve prostate cancer detection? Results from the Tyrol screening project. Eur Urol 48(6):916–921; discussion 921
82. Epstein JI, Herawi M (2006) Prostate needle biopsies containing prostatic intraepithelial neoplasia or atypical foci suspicious for carcinoma: implications for patient care. J Urol 175(3 Pt 1):820–834
83. Merrimen JL, Jones G, Walker D, Leung CS, Kapusta LR, Srigley JR (2009) Multifocal high grade prostatic intraepithelial neoplasia is a significant risk factor for prostatic adenocarcinoma. J Urol 182(2):485–490; discussion 490
84. Kronz JD, Shaikh AA, Epstein JI (2001) High-grade prostatic intraepithelial neoplasia with adjacent small atypical glands on prostate biopsy. Hum Pathol 32(4):389–395
85. Moore CK, Karikehalli S, Nazeer T et al (2005) Prognostic significance of high grade prostatic intraepithelial neoplasia and atypical small acinar proliferation in the contemporary era. J Urol 173(1): 70–72
86. Giannarini G, Mogorovich A, Valent F et al (2007) Continuing or discontinuing low-dose aspirin before transrectal prostate biopsy: results of a prospective randomized trial. Urology 70(3):501–505

27 Role of Imaging and Biopsy to Assess Local Recurrence After Definitive Treatment for Prostate Carcinoma

Pasquale Martino, Vincenzo Scattoni [$], Andrea B. Galosi [$], Paolo Consonni, Carlo Trombetta, Silvano Palazzo, Carmen Maccagnano, Giovanni Liguori, Massimo Valentino, Michele Battaglia, and Libero Barozzi

27.1 Introduction

Recurrence after a definitive treatment for prostate cancer (PCa) (i.e., radical prostatectomy [RP], radiotherapy [RT], high-intensity focused ultrasound [HIFU], and cryotherapy [CT]) is defined by an increase in the serum value of PSA after reaching the nadir. Generally, the definition of recurrence after RP has relied on a single elevated PSA level, but the reported level of PSA which indicates failure after RP varies. Various PSA thresholds have been used, including >0.1, >0.2, >0.4, and >0.5 ng/ml [1–4]. After radiotherapy, the RTOG-ASTRO Phoenix consensus has assessed that a rise by 2 ng/ml or more above the nadir as standard definition of biochemical failure after RT (or 3 ng/ml after brachytherapy).

The PCa recurrences may be classified into four main categories: (1) PSA-only relapse, (2) local recurrence, (3) distant metastases (most commonly nodal or osseous), and (4) combination of local and distant recurrences. Detecting the site of recurrence is difficult, since an increasing PSA level is rarely associated with symptoms or findings at physical examination [5–10]. Thus, PSA doubling time (in months), PSA velocity (in ng/ml/year), and nomograms have been advo-

[$] Author contributed equally with all other contributors.

P. Martino, MD (✉) • S. Palazzo, MD • M. Battaglia, MD
Department of Emergency and Organ Transplantation – Urology, Andrology and Kidney Transplantation Unit, University of Bari, Bari, Italy
e-mail: martino@urologia.uniba.it

V. Scattoni, MD • C. Maccagnano, MD
Department of Urology, Vita Salute San Raffaele-University, Milan, Italy

A.B. Galosi, MD, PhD
Institute of Urology, Ospedali Riuniti, Azienda Ospedaliero-Universitaria, Ancona, Italy

P. Consonni, MD
Multimedica Hospital, Castellanza, VA, Italy

C. Trombetta, MD • G. Liguori, MD
Department of Urology, University of Trieste-Cattinara Hospital, Trieste, Italy

M. Valentino, MD • L. Barozzi, MD
Department of Emergency, Surgery and Trasplantation, Radiology Unit, University Hospital Policlinico S. Orsola-Malpighi, Bologna, Italy

P. Martino, A.B. Galosi (eds.), *Atlas of Ultrasonography in Urology, Andrology, and Nephrology*,
DOI 10.1007/978-3-319-40782-1_27

cated in order to improve the discrimination between local or distant recurrence [11–13].

From a practical point of view, detecting the site of recurrence (local vs distant) is critical for defining the optimum treatment [14, 15]. For instance, patients submitted to RRP with a local recurrence with no detectable distant metastases may benefit from salvage radiotherapy with or without androgen deprivation (according to the Consensus Statement on Radiation Therapy of Prostate Cancer and to the Society of Therapeutic Radiation Oncologist guidelines), whereas those with distant disease may be treated with systemic treatments [16].

Currently, different imaging methods are suggested, together with the biopsy of prostatic fossa or prostate biopsy after treatment which may help the urologists and the oncologists to assess local recurrence in patient with PSA relapse after definitive treatments for PCa.

We have reviewed the available literature on this topic and analyzed all the advantages and disadvantages of all the available imaging techniques.

27.2 Material and Methods

A systematic review of the literature was performed by searching Medline from January 1995 up to January 2011. Electronic searches were limited to the English language, and the keywords prostate cancer, RT, HIFU, CT, transrectal ultrasound [TRUS], magnetic resonance imaging [MRI], PET/TC, and prostate biopsy were used.

27.2.1 Local Recurrence After Radical Prostatectomy

After surgery, it is possible to perform different imaging modalities to detect a local recurrence [17, 18]. Traditionally, transrectal ultrasound (TRUS) is easily performed, but it has shown to have many limitations when differentiating between recurrent or residual tumor and postsurgical scarring. Nevertheless, the biopsies of the prostatic fossa after RP are still executed under TRUS-guidance.

27.2.1.1 TRUS

Although several trials have shown that TRUS is better than digital rectal examination (DRE) for detecting local recurrence, it lacks specificity.

TRUS appearance of local recurrence of PCa in the prostatic fossa in patients with no clinical or biochemical evidence of recurrence after RP includes asymmetric thickening or fullness of the anastomosis, loss of the integrity of the retro-anastomotic fat plane, and/or the presence of hypoechoic lesion in the peri-anastomotic area, surrounded by a variable amount of tissue that is more prominent anteriorly and that is hypoechoic relative to the surrounding fat [19–21].

The most common TRUS-detectable lesion site is the vesico-urethral anastomosis (VUA) area. The other sites include the anterior and the posterior bladder neck and, less frequently, the retrovesical space (posterior to the bladder neck). Particularly, TRUS provides a substantial advantage compared with DRE in the PCa recurrence localized at the bladder neck, since these lesions may be more difficult to be palpable because of the anterior location or because of merging of the lesion with the bladder wall.

Thus, lesions that occupied more than one site within the prostatic fossa had a greater likelihood of having positive biopsy findings, and the lesions are more likely to be palpable compared with those that occupied one site, as reported by Leventis et al. [19].

In the last decade, several studies have addressed the clinical utility of TRUS in detecting local recurrence and described a statistically significant correlation between TRUS-suspected areas in the prostatic fossa and positive biopsies [20]. As indicated by Leventis et al. and Scattoni et al., local recurrences are more often hypoechoic (65 % of cases), whereas about 30 % of local recurrences are isoechoic with VUA appearance, with about 20 % of patients with a final positive biopsy [19, 22]. Unfortunately, the ability of TRUS to detect a local recurrence depends on the PSA levels. Scattoni et al. have demonstrated that TRUS was able to detect every biopsy-proven local recurrence lesion only with a PSA >2.0 ng/ml [22]; therefore, the use of TRUS is questionable.

27.2.1.2 TRUS-Guided Biopsies

Due to the low accuracy of TRUS in the detection of recurrent prostate cancer especially at low PSA levels, it may be useful to perform a prostatic fossa biopsy. The optimal biopsy strategy regarding location and number of cores has not been proved. Scattoni et al. [22] have suggested that a sampling with 6 cores in the VUA region is an efficient tool in the detection of local recurrence after RP, even with PSA <0.5 ng/ml. However, the likelihood of biopsy-proven local recurrence after RP has been reported to vary between 35 and 54 % with nearly a third of patients requiring two or more TRUS-guided biopsy sessions to obtain a final diagnosis [23, 24]. Different authors agree that increasing the core number do not markedly improve the detection rate of recurrence [19–21]. It has been suggested that a more easy sampling may be performed using an end-fire probe to guide the biopsy, with the final aim to direct the needle into the prostatic fossa at a more orthogonal angle. Conversely, side-fire or biplanar probes sample a longer segment of the retrotrigonal space and prostatic fossa, where local recurrence is less frequent but more often visible.

Several authors have tried to find further factors that may predict PCa recurrence detection in the prostatic fossa, but the results are still controversial. Shekarriz et al. [25] have demonstrated that the pathological stage or status of the margins following RP (including seminal vesicle involvement) or recurrence time may predict the results of VUA biopsy. Saleem et al. [26] have reported that the pathological stage, Gleason score, and PSA velocity are unhelpful in predicting biopsy results. Conversely, Scattoni et al. [22] have found that only an abnormal TRUS and DRE may be considered as significant predictors of PCa recurrence detection, while PSA, pathological stage, the Gleason score, margins' status following RP, or the PSA elevation time have no correlation with a positive biopsy. Zietman et al. [27] reported that the likelihood of a positive rebiopsy is dependent on original tumor size and current PSA levels.

Unfortunately, the clinical utility of TRUS biopsy of the prostatic fossa is controversial and highly dependent to PSA levels. Shekarriz et al. [25] have reported that the higher the serum PSA level, the higher the positive biopsy rate, with a PSA cutoff of 1.0 ng/ml. TRUS biopsy of the VUA shows a low incidence of detection with a PSA level <0.5 ng/ml, as reported by both Saleem [26] and Connolly [28]. Similarly, Naya et al. [29] have, more recently, reported that none of the men with a serum PSA concentration of less than 0.5 ng/ml at biopsy who had normal results for both TRUS and DRE had a biopsy-proven local recurrence. On the contrary, Scattoni et al. [30] have documented that the sensitivity of a TRUS extends even to those patients with very low serum PSA levels since more than 70 % of the patients having a positive TRUS and PSA <0.5 ng/ml had a biopsy-proven local recurrence (Table 27.1).

While some studies have supported the need for histologic or radiographic confirmation of the recurrence before salvage radiotherapy, more recently, others demonstrated no differences in survival rates after RT between patients with PSA recurrence only and those with a documented local recurrence. A recent study has demonstrated that a biopsy of VUA before RT seems unnecessary for PSA ≤0.9 ng/ml. For higher values, a positive biopsy of VUA seems to always justify a salvage RT, which may not be recommendable, given the non-negligible risk of an already micrometastatic disease, if the biopsy results are negative [31].

In conclusion, TRUS biopsy of the prostatic fossa seems to be more accurate than TRUS in the detection of prostate cancer recurrence, even if its accuracy is highly correlated to PSA levels. Moreover, the clinical value of TRUS biopsy of the VAU remains in question.

Table 27.1 Accuracy (PPV and NPV) of TRUS as a function of VUA biopsy results according to PSA values in positive cases and different authors

Authors	No. of patients	TRUS	Mean PSA values (ng/ml) with positive biopsy
Connolly et al. [28]	114	Positive: 66.9 PPV Negative: 69.6 NPV	5.7 (range 0.2–35)
Saleem et al. [26]	91	Positive: 52 % Negative: 25 %	7.8 ± 13
Shekarriz et al. [25]	45	Positive: 65 % Negative: 18 %	5.2 ± 5.4
Leventis et al. [19]	99	Positive: 62 % Negative: 20 %	2.4
Scattoni et al. [22]	119	Positive: 69 % Negative: 34 %	1.6 ± 3.1
Naya et al. [29]	100	Positive: 45 % Negative: 12 %	1.6

PPV positive predictive value, *NPV* negative predictive value

27.2.1.3 MR Imaging

MR has a better diagnostic yield than TRUS and allows an evaluation of pelvic lymph node and bone status, with the detection of all sites of pelvic relapse in a single examination.

The administration of MR contrast medium, i.e., gadolinium, seems to improve further the overall accuracy. It theoretically allows detection of cancerous tissue in cases where morphological anomalies are not evidenced on unenhanced MR images and differentiation between tumor relapse and postoperative fibrosis or scar tissue.

MRI and dynamic contrast-enhanced MRI (DCE-MRI) can identify different site of local recurrence: VUA (52 %), retrovesical space (20 %), bladder neck (16 %), and circumferential areas (12 %).

Recurrences were, in most cases, slightly hyperintense to internal obturator muscle on T2-weighted sequences as found by Sella et al. [32] and in fewer cases markedly hyperintense on T2-weighted sequences.

Nodules that appear slightly hyperintense or markedly hyperintense on T2-weighted sequences may represent not only recurrences but also prostatic or seminal vesicle residues with different amounts of fibrosis.

The peri-anastomotic fibrosis appears hypointense on T2w images, with absent enhancement on DCE-MRI images (Fig. 27.1). After DCE-MRI, all benign nodules showed signal enhancement of less than 50 % in the early phase, whereas all recurrences showed fast signal enhancement in the early phase followed by plateau or washout. Recurrences appear as lobulated masses with intermediate signal intensity on T2w images, enhancing after intravenous injection of contrast medium (Fig. 27.1).

Silverman et al. [33] have achieved a high sensitivity and specificity (100 %) evaluating a group of patients with T1- and T2-weighted sequences and T1-weighted images with fat-suppression technique after gadolinium administration. All nodules showed signal enhancement after gadolinium administration, strengthening the suspicion that they were recurrences.

Also Sella et al. [32] have achieved a high sensitivity (95 %) and specificity (100 %) using

T1- and T2-weighted sequences. All the local recurrences seen on MR images were isointense on T1-weighted sequences and slightly hyperintense to muscle on T2-weighted sequences. However, in the Sella study, the mean PSA level was 2.1 ng/ml, and in the Silverman study, 74 % had palpable recurrence and 88 % had a PSA >0.4 ng/ml; there would not have been any need of MRI to detect these recurrences. Therefore, the clinical benefit of current imaging is very low.

Casciani et al. [34] reported that MRI alone showed a poorer accuracy in detecting recurrences, probably due to the smaller size (between 0.4 and 3.0 cm) of the recurrences compared with those in the study of Silverman and the study of Sella et al. (0.7–3.8 cm and 0.8–4.5 cm, respectively). This comparison showed a statistically significant lower diagnostic accuracy of unenhanced eMR in comparison to CE-eMR (70 vs. 86 %), a statistically significant lower sensitivity (60 vs. 84 %) and no significant specificity differences (82 % vs. 89 %). Cosciani et al. [34] have supported the accuracy of eMR after RP providing high sensitivity of 84 % and specificity of 89.3 %, in patients with high PSA levels.

Recently, great interest has been shown to anatomic T2w imaging with functional MRI techniques such as DCE-MRI, DWI, and MR with spectroscopic imaging. In particular, DCE-MRI is useful for differentiating fibrosis in the prostatectomy fossa, remnants of normal prostatic tissue, and hyperplastic nodules from prostate cancer recurrence. DWI increases the accuracy of DCE-MRI well correlating with tissue cellularity of malignant tumors of the prostate.

In conclusion, MRI has proved to be useful at PSA values (generally higher than 1 ng/ml) for which the identified recurrence after RP cannot be treated with success.

Furthermore, MRI showed a limited clinical benefit in early diagnosis of recurrence after surgery since the lower detection limit is above 0.5 cm.

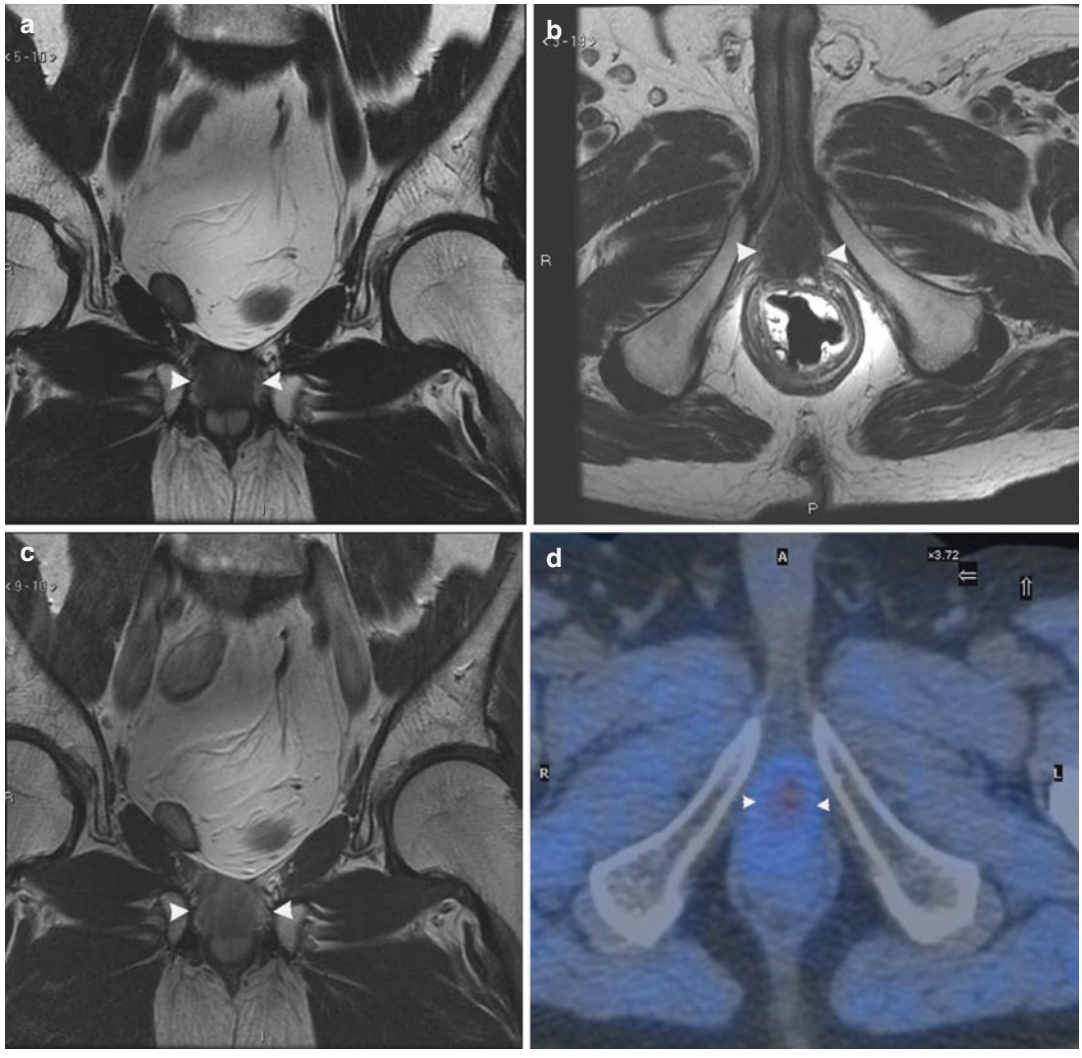

Fig. 27.1 A 56-year-old man with rising PSA after radical prostatectomy. (**a**, **b**) MR T2-weighted coronal and axial images with endorectal coil show a soft-tissue mass (*arrowheads*) anterior to the rectum. (**c**) Post-contrast dynamic image shows clear enhancement of the tissue. (**d**) PET/CT using 11C-choline image shows the uptake of the mass (*arrowheads*). The mass was proved to be a local recurrence by using transrectal US-guided biopsy

27.2.1.4 PET

Improvement about the detection of local recurrence may be reached by employing an imaging technique based on metabolism rather than an anatomic imaging technique. In this respect, PET may play a role, with the use of different tracers [35].

Few studies [36–51] have reported on the detection of local recurrence after RP with ^{18}F-fluoro-2-deoxy-D-glucose (^{18}FDG). Its use in PCa is limited by a low sensitivity. There is a modest glucose consumption by PCa cells, and the uptake of this medium in the recurrent tumor has been shown to be similar to the uptake in postoperative scar or benign prostate tissue. Moreover, ^{18}FDG is highly excreted into urine. Thus, results have been particularly disappointing for the diagnosis of recurrences.

Promising results in the detection of recurrent PCa have been obtained with the newer PET tracers: ^{11}C-acetate, ^{11}C-choline (Ch-PET), and ^{18}F-fluorocholine. Since Ch-PET is not rapidly excreted in urine, Ch-PET show clear images of the pelvic region and of the PCa and pelvic lymph node metastases in the absence of urinary radioactivity.

Generally, Ch-PET provides good sensitivity and specificity values in detecting distant and local recurrences after RP and RT, but only in patients with high PSA levels.

Only few studies have assessed the accuracy of PET in RP patients with low PSA values; most of them report a low sensitivity of PET in detecting local recurrence. In a recent study, also Vees et al. [52] did not recommended Ch-PET as a standard diagnostic tool if early relapse is suspected because the high levels of PSA (<1 ng/ml) needed to detect local residual or recurrent disease after RP in about half the patients.

Recently, Heinisch et al. [53] have recommended using a ^{18}F-fluorocholine PET/CT at PSA levels of >5 ng/ml. By contrast, de Jong et al. have reported that Ch-PET cannot be used to visualize prostate cancer on restaging at a PSA level of <4.5 ng/ml. Rinnab et al. [54] recommend using PET, even at PSA levels of <2.5 ng/ml, because early detection of recurrence can be an advantage for patients with increasing PSA levels.

In integrated PET/CT (computed tomography), the focal uptake of choline can be more easily assigned to anatomical structures, with a better differentiation of physiological (rectum and bladder) uptake from residual/recurrent PCa, resulting in a higher accuracy.

Moreover, with respect to conventional imaging techniques, the most important advantage is the staging of the disease in one step. Rinnab et al. have reported an overall sensitivity and positive predictive value of 95 and 86 %. The overall specificity was 40 % with a negative predictive value of 67 %.

In conclusion, Ch-PET detection rate of recurrences increases together with the increase of PSA serum value, and, according to the current available data, the use of choline PET/CT cannot be recommended for PSA values lower than 1 ng/ml.

27.2.2 Local Recurrences After Radiotherapy

Diagnosing local recurrence after radiotherapy (RT) is challenging because of radiation-induced fibrosis and shrinkage of the prostate. The sensitivity and specificity of TRUS are reported to be 49 % and 57 %, respectively [55]. Prostate cancer visualization by MRI is also critical, because the tissue contrast between recurrent cancer and benign irradiated tissue is decreased as the recurrent cancer after radiation therapy demonstrates low signal intensity on T2w imaging [56].

Results for T2w imaging at 3 T using a phased-array coil showed a poor diagnostic performance in predicting recurrent cancer in patients with biochemical failure after radiation therapy [57].

DCE-MRI can predict locally recurrent cancer more accurately than T2w imaging showing a hypervascular area within the slow/low enhancement of postradiation fibrosis. DWI added to MRI examination protocol increases the accuracy of the technique showing focal low signal intensity relative to the surrounding prostate tissue on ADC maps [57].

After RT, MR spectroscopy imaging demonstrates intraprostatic voxels with no detectable peaks for choline, polyamines, creatine, and citrate (so-called metabolic atrophy). However, residual prostate cancer can still be identified by a relative increase in the (choline + creatine)/citrate ratio or by an increase in the choline peak with no detectable citrate.

Using these criteria, good correlations between spectroscopic data and biopsy findings have been reported [58]. However, for unclear reasons, some benign glands can exhibit high levels of choline after RT and cause false-positive findings [59].

The use of choline PET/CT can be recommended since local recurrence after RT is associated with PSA values greater than 2 ng/ml (Fig. 27.2).

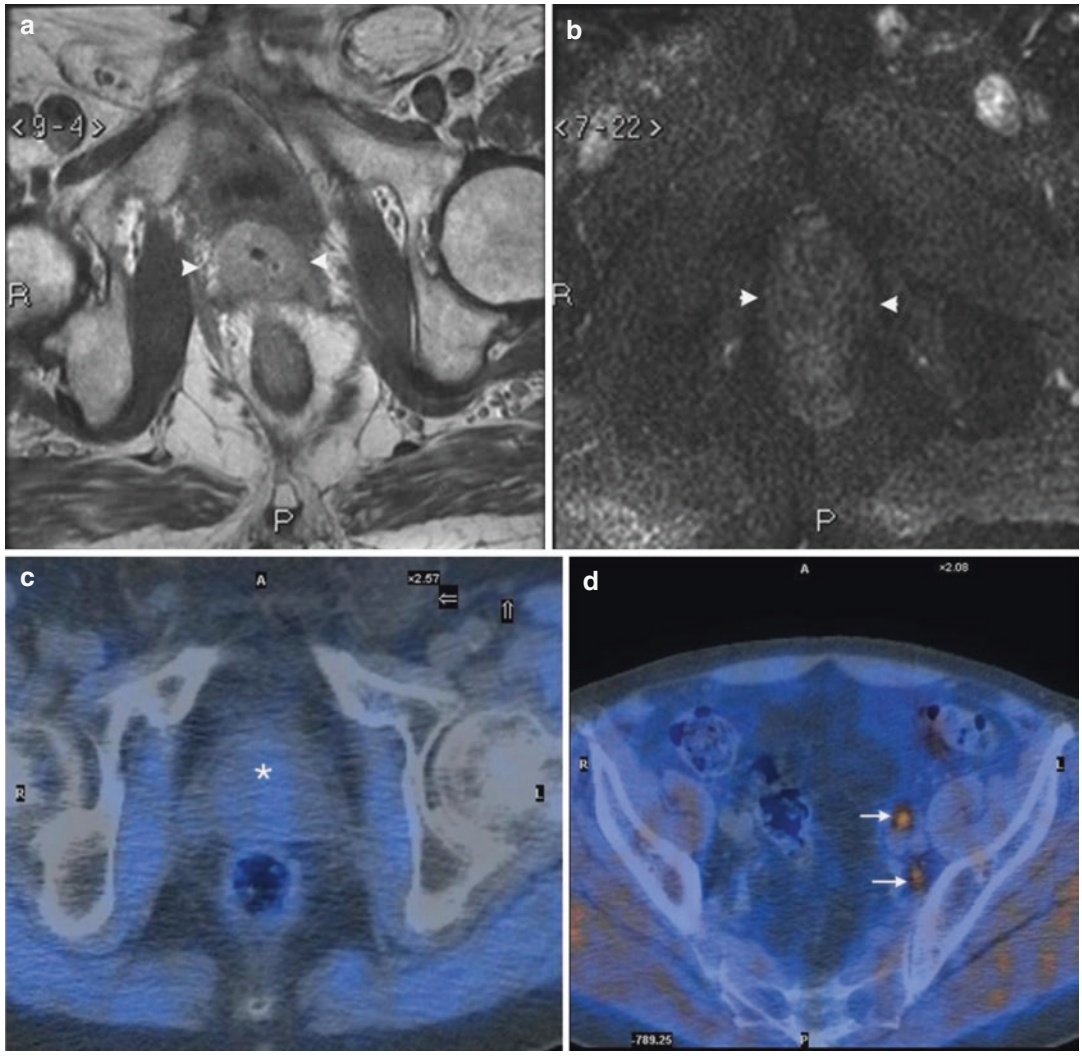

Fig. 27.2 A 78-year-old man with rising PSA after radiotherapy. (**a**) MR T2-weighted axial image shows low signal intensity of the irradiated tissue (*arrowheads*). (**b**) DWI image shows normal low signal intensity of prostate (*arrowheads*). (**c**, **d**) PET/CT using 11C-choline images confirm (c) low uptake of the prostate (*asterisk*) and (**d**) focal site of pathologic increase of 11C-choline uptake in the left internal iliac lymph node (*arrows*)

27.2.2.1 Biopsy After Radiotherapy

Biopsy is performed to identify a persistence or recurrence following RT, when PSA failure occurs according to Phoenix or ASTRO criteria. Biopsy is not a considered a gold standard of treatment efficacy, but is an independent predictor of outcome [60].

The role of biopsy after RT are (1) to provide pathological analysis and diagnosis of local recurrence, (2) to rule out local recurrence, and (3) to describe grade and tumor spread in the gland.

Biopsy mapping is indicated after not less than 24 months from the end of RT cycle. Crook et al. [60] recommended that biopsies should be performed at least 30–36 months following RT since false-negative results were observed in 19 % and false positive in 30 % when early biopsies at 12 months were performed.

The transrectal approach is usually performed; however, the transperineal route is preferred in patients with proctitis or previous events of post-RT rectorrhagia. Biopsy should be performed as random mapping (8–12 cores) to the whole prostatic gland and to the base of seminal vesicles. Target biopsy directed to visible nodules by TRUS or MRI should be performed due to the high probability of recurrence.

The information provided in the surgical pathology report of a prostate needle biopsy with carcinoma has become critical in the subsequent salvage therapy. Map distribution of cancer based on biopsy is important to assess tumor spread, and it is essential for planning the salvage therapy [61].

In conclusion, histologically proved local relapse is mandatory only if salvage treatment (cryosurgery or prostatectomy) is planned.

27.2.3 Local Recurrence After Cryotherapy

Cryotherapy (CT) of the whole prostate is widely used as primary treatment or salvage treatment for local recurrence after radiation therapy. Focal CT has been considered an investigational procedure in well-selected patient cases as alternative to achieve surveillance or total treatments (surgery or radiation or total CT). Role of imaging to detect local recurrence after total cryoablation is very limited. Absolute PSA levels (>0.5 ng/ml) or PSA kinetic (ASTRO or Phoenix definitions) is widely used and may predict recurrence [62]. B-mode transrectal ultrasound (TRUS) has a low diagnostic accuracy of local recurrence for several pitfalls: (1) isoechoic cancer, (2) posttreatment modifications, and (3) small-volume recurrent cancer. All these pitfalls explain also the limited value of TRUS. The goal of prostate CT is to produce complete necrosis of the prostate glands. Difficulty arises in the evaluation after total CT, because of the large damage zone, created by the treatment. In particular areas located at the margins of the ice ball (anterior zone, far basal zone close to seminal vesicles, distal apical tissue, periprostatic urethra, or subcapsular tissue) may persist a thin rim of untreated tissue (Fig. 27.3) or cancer [61]. These small areas may remain undetected by imaging techniques because of their irregular shape and volume (less than 5 mm) that also could be under the detection limits of MR.

New ultrasound (US) functions and magnetic resonance (MR) applications have the potential to enhance visualization of the residual prostate tissue and local recurrence. Contrast-enhanced US is a useful tool to detect untreated areas but no studies have been reported so far. Elastosonography [63] is not useful after CT since scar tissue and dense fibrosis are seen as hard tissue mimicking tumor. Color Doppler ultrasound may help in the detection of areas with residual vasculature.

There is a strong correlation between magnetic resonance imaging with gadolinium defects and amount of coagulation and necrosis caused by CT. However, gadolinium defects were not seen in areas of viable tissue as determined by histopathologic evaluation [64]. Some investigators reported that findings of postoperative gadolinium enhancement MR were not predictive of six-moth biopsy results or following PSA levels [65].

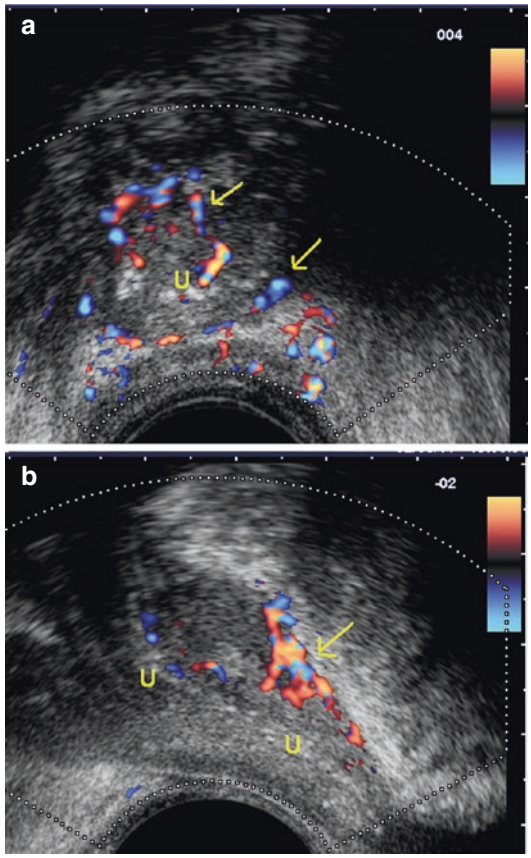

Fig. 27.3 Viable benign tissue after cryoablation: (**a**) Axial view, located at the distal apex (*arrows*); (**b**) Longitudinal view, viable tissue in the anterior fibromuscular stroma in front of urethra (*U*)

27.2.3.1 Biopsy After Cryotherapy

Diagnosis of local recurrence after CT is done by pathological analysis of core-biopsy specimens using end-fire TRUS probe. To date, few studies have assessed long-term pathological findings. After primary CT, biopsy may detect residual carcinoma in 7–23 % of cases and viable benign glands in 45–70 % of patients [66]. After salvage CT, Chin JL et al. reported residual cancer, viable benign prostate glands, and viable stroma in 14 %, 42 %, and 27 %, respectively [67].

Biopsy scheduled per protocol after 6, 12, or 24 months after total cryoablation is rarely performed [68]. Biopsy "for cause" is usually performed in most of the case series reported in literature.

Indication to for-cause biopsy is based on serum PSA level (>0.5 ng/ml) and kinetic (according to ASTRO or Phoenix definition) and digital rectal findings (nodule). In the COLD registry after primary total cryoablation, only 16 % of patients underwent biopsy.

Galosi et al. reported on 80/95 patients who underwent >2 biopsy sessions per protocol after a median follow-up of 70 months: overall disease-free survival was 61.1 %. Cancer in follow-up biopsy was detected in 21.1 % and normal prostatic tissue in 55 % [69].

Biopsy results should be obtained with eight or more core samplings in order to reduce the risk of under detection of residual cancer (Fig. 27.4). Target plus extended random biopsy schemes should be used to evaluate patients with PSA failure after CT in particular in the areas located at the margins of the ice ball.

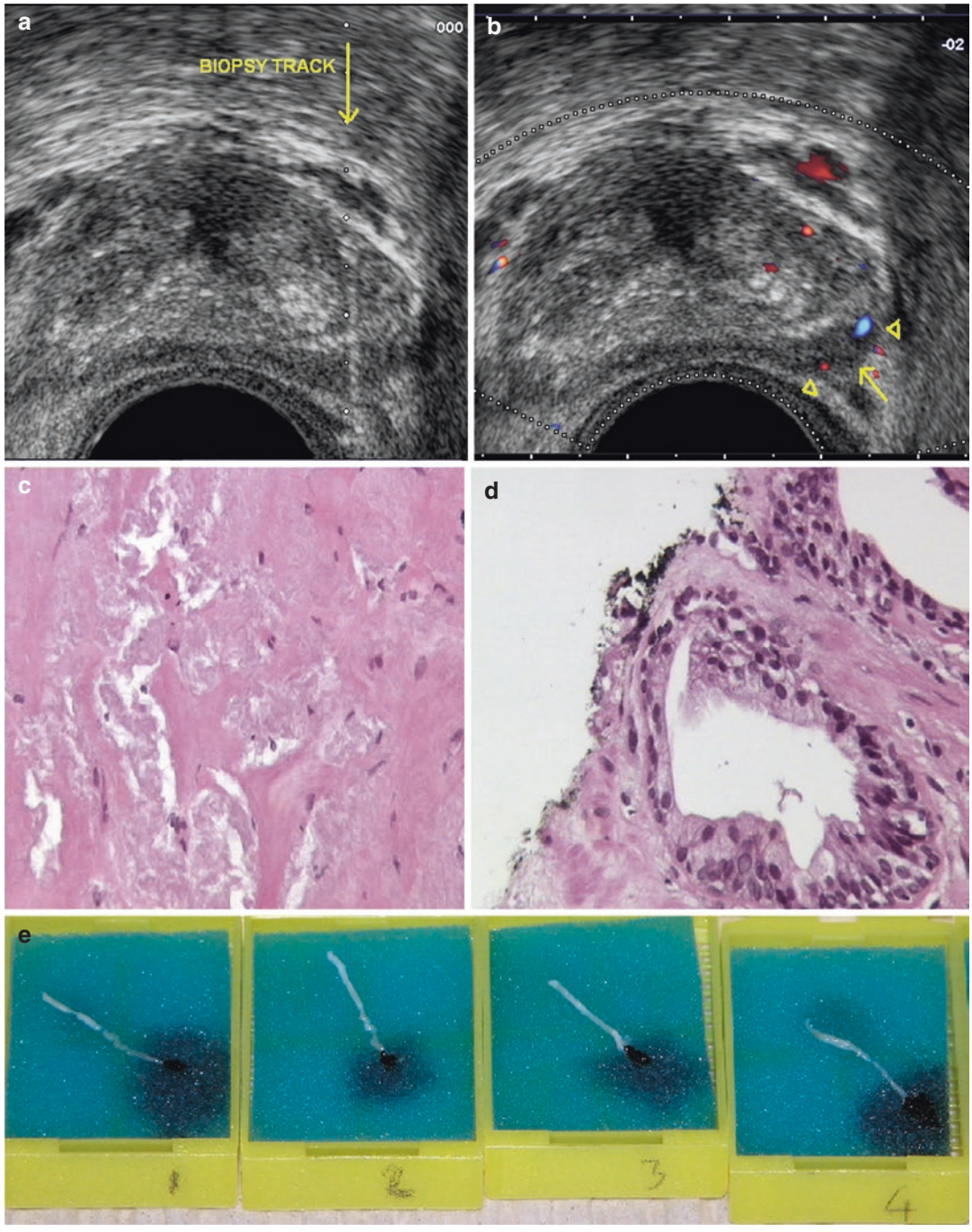

Fig. 27.4 (**a**, **b**) TRUS-guided biopsy in B-mode (axial view), (**c**) fibrosis after cryoablation, (**d**) viable glands located at the inked end of the biopsy (rectal or pericapsular), (**e**) biopsy fragments pre-embedded and inked in the rectal end

27.2.4 Local Recurrences After HIFU Ablation

High-intensity focused ultrasound (HIFU) is a minimally invasive treatment for prostate cancer. Recommendations concerning HIFU in international guidelines are still conflicting [70, 71].

The overall quality of references about local recurrence is generally low because of small series, absence of pre-HIFU study, different timing in the scheduled posttreatment evaluation (1, 3, or 6 months), and generally retrospective evaluation of the results.

TRUS has a limited utility in patients treated with HIFU, since the gland appears diffusely heterogeneous after treatment. Conventional transrectal ultrasound (TRUS) is useless in identifying areas suspected for local recurrence, and even elastography was unable to precisely correlate with biopsy results. Color Doppler can improve recurrent cancer detection by guiding the biopsies towards hypervascular foci, but only 38 % of the sites with recurrent cancer show positive Doppler findings [72]. False-positive results are mostly due to residual benign tissue [73].

MRT2w imaging is difficult to interpret after HIFU ablation, because the gland is heterogeneous and diffusely hypointense. However, recurrent cancer can be visible in some patients as a nodular hypointense lesion [74]. Recurrent cancers are easier to distinguish from post-HIFU fibrosis using DCE imaging [75]. MRSI has been evaluated in few cases of patients, and it has shown to add no additional information than T2w imaging [74]; furthermore, when MRI is used as an indicator or residual viable tissue, it is very difficult to precisely match suspected areas at MRI with ultrasound-guided biopsy [76]. Again, the diagnosis of a local recurrence in this setting is based on the PSA values and PSA kinetics as well as the biopsy of the residual prostate after 12–18 months from treatment.

Conclusions

The diagnosis of local recurrence is highly dependent on the primary treatment used.

After surgery (RP), the role of imaging and biopsy is limited since PSA define very early recurrence as biochemical failure ≥0.2 ng/ml. TRUS and novel imaging have shown limited accuracy at least at early stages and very low PSA values. Choline PET/CT and MR can be recommended for PSA values higher than 1 ng/ml.

After conservative treatments (RT, CT, HIFU), a combined approach using specific imaging, PSA cutoff (>1 ng/ml), and PSA kinetics with image-guided biopsy is necessary to assess the presence of a local recurrence or benign residual tissue. Anatomic (T2w) and functional MR (DCE-MRI, DWI, and MRS) seems particularly promising for differentiating fibrosis from cancer.

Final diagnosis of local recurrence is based on pathological analysis of image-guided core biopsy, and TRUS end-fire remains the most used imaging method to guide biopsy.

Even if different imaging techniques will be extensively used in the future, their accuracy in the detection and localization of prostate cancer local recurrences before salvage treatment remains low, and their clinical utility remains in question.

Conflict of Interest The authors report no conflict interest.

References

1. Lightner DJ, Lange PH, Reddy PK, Moore L (1990) Prostate specific antigen and local recurrence after radical prostatectomy. J Urol 144(4):921–926
2. Abi-Aad AS, Macfarlane MT, Stein A, deKernion JB (1992) Detection of local recurrence after radical prostatectomy by prostate specific antigen and transrectal ultrasound. J Urol 147(3 Pt 2):952–955
3. Wasserman NF, Kapoor DA, Hildebrandt WC, Zhang G, Born KM, Eppel SM, Reddy PK (1992) Transrectal US in evaluation of patients after radical prostatectomy. Part II. Transrectal US and biopsy findings in the presence of residual and early recurrent prostatic cancer. Radiology 185(2):367–372
4. Wasserman NF, Kapoor DA, Hildebrandt WC, Zhang G, Born KM, Eppel SM, Reddy PK (1992) Transrectal US in evaluation of patients after radical prostatectomy. Part I. Normal postoperative anatomy. Radiology 185(2):361–366

5. Salomon CG, Flisak ME, Olson MC, Dudiak CM, Flanigan RC, Waters WB (1993) Radical prostatectomy: transrectal sonographic evaluation to assess for local recurrence. Radiology 189(3):713–719
6. Foster LS, Jajodia P, Fournier G Jr, Shinohara K, Carroll P, Narayan P (1993) The value of prostate specific antigen and transrectal ultrasound guided biopsy in detecting prostatic fossa recurrences following radical prostatectomy. J Urol 149(5):1024–1028
7. Koppie TM, Grossfeld GD, Nudell DM, Weinberg VK, Carroll PR (2001) Is anastomotic biopsy necessary before radiotherapy after radical prostatectomy? J Urol 166(1):111–115
8. Fowler JE Jr, Brooks J, Pandey P, Seaver LE (1995) Variable histology of anastomotic biopsies with detectable prostate specific antigen after radical prostatectomy. J Urol 153(3 Pt 2):1011–1014
9. Wood DP Jr, Peretsman SJ, Seay TM (1995) Incidence of benign and malignant prostate tissue in biopsies of the bladder neck after a radical prostatectomy. J Urol 154(4):1443–1446
10. Lepor H, Chan S, Melamed J (1998) The role of bladder neck biopsy in men undergoing radical retropubic prostatectomy with preservation of the bladder neck. J Urol 160(6 Pt 2):2435–2439
11. Laufer M, Pound CR, Carducci MA, Eisenberger MA (2000) Management of patients with rising prostate-specific antigen after radical prostatectomy. Urology 55(3):309–315
12. Pound CR, Christens-Barry OW, Gurganus RT, Partin AW, Walsh PC (1999) Digital rectal examination and imaging studies are unnecessary in men with undetectable prostate specific antigen following radical prostatectomy. J Urol 162(4):1337–1340
13. Ferguson JK, Oesterling JE (1994) Patient evaluation if prostate-specific antigen becomes elevated following radical prostatectomy or radiation therapy. Urol Clin North Am 21(4):677–685
14. Lange PH, Ercole CJ, Lightner DJ, Fraley EE, Vessella R (1989) The value of serum prostate specific antigen determinations before and after radical prostatectomy. J Urol 141(4):873–879
15. Partin AW, Pearson JD, Landis PK, Carter HB, Pound CR, Clemens JQ, Epstein JI, Walsh PC (1994) Evaluation of serum prostate-specific antigen velocity after radical prostatectomy to distinguish local recurrence from distant metastases. Urology 43(5):649–659
16. Cox JD, Gallagher MJ, Hammond EH, Kaplan RS, Schellhammer PF (1999) Consensus statements on radiation therapy of prostate cancer: guidelines for prostate re-biopsy after radiation and for radiation therapy with rising prostate-specific antigen levels after radical prostatectomy. American Society for Therapeutic Radiology and Oncology Consensus Panel. J Clin Oncol 17(4):1155
17. Kane CJ, Amling CL, Johnstone PA, Pak N, Lance RS, Thrasher JB, Foley JP, Riffenburgh RH, Moul JW (2003) Limited value of bone scintigraphy and computed tomography in assessing biochemical failure after radical prostatectomy. Urology 61(3):607–611
18. Krämer S, Görich J, Gottfried HW, Riska P, Aschoff AJ, Rilinger N, Brambs HJ, Sokiranski R (1997) Sensitivity of computed tomography in detecting local recurrence of prostatic carcinoma following radical prostatectomy. Br J Radiol 70(838):995–999
19. Leventis AK, Shariat SF, Slawin KM (2001) Local recurrence after radical prostatectomy: correlation of US features with prostatic fossa biopsy findings. Radiology 219(2):432–439
20. Parra RO, Wolf RM, Huben RP (1990) The use of transrectal ultrasound in the detection and evaluation of local pelvic recurrences after a radical urological pelvic operation. J Urol 144(3):707–709
21. Kapoor DA, Wasserman NF, Zhang G, Reddy PK (1993) Value of transrectal ultrasound in identifying local disease after radical prostatectomy. Urology 41(6):594–597
22. Scattoni V, Roscigno M, Raber M, Montorsi F, Da Pozzo L, Guazzoni G, Freschi M, Rigatti P (2003) Multiple vesico-urethral biopsies following radical prostatectomy: the predictive roles of TRUS, DRE, PSA and the pathological stage. Eur Urol 44(4):407–414
23. Ornstein DK, Colberg JW, Virgo KS, Chan D, Johnson ET, Oh J, Johnson FE (1998) Evaluation and management of men whose radical prostatectomies failed: results of an international survey. Urology 52(6):1047–1054
24. Bott SR (2004) Management of recurrent disease after radical prostatectomy. Prostate Cancer Prostatic Dis 7(3):211–216
25. Shekarriz B, Upadhyay J, Wood DP Jr, Hinman J, Raasch J, Cummings GD, Grignon D, Littrup PJ (1999) Vesicourethral anastomosis biopsy after radical prostatectomy: predictive value of prostate-specific antigen and pathologic stage. Urology 54(6): 1044–1048
26. Saleem MD, Sanders H, Abu El Naser M, El-Galley R (1998) Factors predicting cancer detection in biopsy of the prostatic fossa after radical prostatectomy. Urology 51(2):283–286
27. Zietman AL, Shipley WU, Willett CG (1993) Residual disease after radical surgery or radiation therapy for prostate cancer. Clinical significance and therapeutic implications. Cancer 71(3 Suppl):959–969
28. Connolly JA, Shinohara K, Presti JC Jr, Carroll PR (1996) Local recurrence after radical prostatectomy: characteristics in size, location, and relationship to prostate-specific antigen and surgical margins. Urology 47(2):225–231
29. Naya Y, Okihara K, Evans RB, Babaian RJ (2005) Efficacy of prostatic fossa biopsy in detecting local recurrence after radical prostatectomy. Urology 66(2): 350–355
30. Scattoni V, Roscigno M, Raber M, Montorsi F, Bertini R, Bua L, Da Pozzo L, Rigatti P (2002) Diagnostic value of ultrasound-guided anastomotic biopsies in patients with high PSA (> or = 0,4 ng/ml) after radical prostatectomy. Arch Ital Urol Androl 74(3):129–131
31. Roscigno M, Cozzarini C, Scattoni V, Bertini R, Da Pozzo L, Pasta A, Montorsi F, Bolognesi A, Fiorino C, Colombo R, Fazio F, Rigatti P (2007) A reappraisal of

the role of vesicourethral anastomosis biopsy in patient candidates for salvage radiation therapy after radical prostatectomy. Radiother Oncol 82(1):30–37
32. Sella T, Schwartz LH, Swindle PW, Onyebuchi CN, Scardino PT, Scher HI, Hricak H (2004) Suspected local recurrence after radical prostatectomy: endorectal coil MR imaging. Radiology 231(2):379–385
33. Silverman JM, Krebs TL (1997) MR imaging evaluation with a transrectal surface coil of local recurrence of prostatic cancer in men who have undergone radical prostatectomy. AJR Am J Roentgenol 168(2):379–385
34. Cosciani E, Polettini E, Carmenini E, Floriani I, Masselli G, Bertini L, Gualdi GF (2008) Endorectal and dynamic contrast-enhanced MRI for detection of local recurrence after radical prostatectomy. AJR Am J Roentgenol 190(5):1187–1192
35. Cirillo S, Petracchini M, Scotti L, Gallo T, Macera A, Bona MC, Ortega C, Gabriele P, Regge D (2009) Endorectal magnetic resonance imaging at 1.5 Tesla to assess local recurrence following radical prostatectomy using T2-weighted and contrast-enhanced imaging. Eur Radiol 19(3):761–769
36. Yeh SD, Imbriaco M, Larson SM, Garza D, Zhang JJ, Kalaigian H, Finn RD, Reddy D, Horowitz SM, Goldsmith SJ, Scher HI (1996) Detection of bony metastases of androgen-independent prostate cancer by PET-FDG. Nucl Med Biol 23(6):693–697
37. Schöder H, Herrmann K, Gönen M, Hricak H, Eberhard S, Scardino P, Scher HI, Larson SM (2005) 2-[18F]fluoro-2-deoxyglucose positron emission tomography for the detection of disease in patients with prostate-specific antigen relapse after radical prostatectomy. Clin Cancer Res 11(13):4761–4769
38. Liu IJ, Zafar MB, Lai YH, Segall GM, Terris MK (2001) Fluorodeoxyglucose positron emission tomography studies in diagnosis and staging of clinically organ-confined prostate cancer. Urology 57(1): 108–111
39. Effert PJ, Bares R, Handt S, Wolff JM, Büll U, Jakse G (1996) Metabolic imaging of untreated prostate cancer by positron emission tomography with 18fluorine-labeled deoxyglucose. J Urol 155(3): 994–998
40. Hofer C, Laubenbacher C, Block T, Breul J, Hartung R, Schwaiger M (1999) Fluorine-18-fluorodeoxyglucose positron emission tomography is useless for the detection of local recurrence after radical prostatectomy. Eur Urol 36(1):31–35
41. Haseman MK, Reed NL, Rosenthal SA (1996) Monoclonal antibody imaging of occult prostate cancer in patients with elevated prostate-specific antigen. Positron emission tomography and biopsy correlation. Clin Nucl Med 21(9):704–713
42. Sanz G, Robles JE, Giménez M, Arocena J, Sánchez D, Rodriguez-Rubio F, Rosell D, Richter JA, Berián JM (1999) Positron emission tomography with 18fluorine-labelled deoxyglucose: utility in localized and advanced prostate cancer. BJU Int 84(9):1028–1031
43. Morris MJ, Akhurst T, Osman I, Nunez R, Macapinlac H, Siedlecki K, Verbel D, Schwartz L, Larson SM, Scher HI (2002) Fluorinated deoxyglucose positron emission tomography imaging in progressive metastatic prostate cancer. Urology 59(6):913–918
44. de Jong IJ, Pruim J, Elsinga PH, Vaalburg W, Mensink HJ (2003) 11C-choline positron emission tomography for the evaluation after treatment of localized prostate cancer. Eur Urol 44(1):32–38; discussion 38–9
45. Price DT, Coleman RE, Liao RP, Robertson CN, Polascik TJ, DeGrado TR (2002) Comparison of [18 F]fluorocholine and [18 F]fluorodeoxyglucose for positron emission tomography of androgen dependent and androgen independent prostate cancer. J Urol 168(1):273–280
46. Oyama N, Miller TR, Dehdashti F, Siegel BA, Fischer KC, Michalski JM, Kibel AS, Andriole GL, Picus J, Welch MJ (2003) 11C-acetate PET imaging of prostate cancer: detection of recurrent disease at PSA relapse. J Nucl Med 44(4):549–555
47. Kotzerke J, Volkmer BG, Glatting G, van den Hoff J, Gschwend JE, Messer P, Reske SN, Neumaier B (2003) Intraindividual comparison of [11C]acetate and [11C]choline PET for detection of metastases of prostate cancer. Nuklearmedizin 42(1):25–30
48. Fricke E, Machtens S, Hofmann M, van den Hoff J, Bergh S, Brunkhorst T, Meyer GJ, Karstens JH, Knapp WH, Boerner AR (2003) Positron emission tomography with 11C-acetate and 18F-FDG in prostate cancer patients. Eur J Nucl Med Mol Imaging 30(4):607–611
49. Reske SN, Blumstein NM, Glatting G (2006) PET and PET/CT in relapsing prostate carcinoma. Urologe A 45(10):1240, 1242–4, 1246–8, 1250
50. Kotzerke J, Volkmer BG, Neumaier B, Gschwend JE, Hautmann RE, Reske SN (2002) Carbon-11 acetate positron emission tomography can detect local recurrence of prostate cancer. Eur J Nucl Med Mol Imaging 29(10):1380–1384
51. Picchio M, Briganti A, Fanti S, Heidenreich A, Krause BJ, Messa C, Montorsi F, Reske SN, Thalmann GN (2011) The role of choline positron emission tomography/computed tomography in the management of patients with prostate-specific antigen progression after radical treatment of prostate cancer. Eur Urol 59(1):51–60
52. Vees H, Buchegger F, Albrecht S, Khan H, Husarik D, Zaidi H, Soloviev D, Hany TF, Miralbell R (2007) 18F-choline and/or 11C-acetate positron emission tomography: detection of residual or progressive subclinical disease at very low prostate-specific antigen values (<1 ng/mL) after radical prostatectomy. BJU Int 99(6):1415–1420. Epub 2007 Apr 8
53. Heinisch M, Dirisamer A, Loidl W, Stoiber F, Gruy B, Haim S, Langsteger W (2006) Positron emission tomography/computed tomography with F-18-fluorocholine for restaging of prostate cancer patients: meaningful at PSA < 5 ng/ml? Mol Imaging Biol 8(1):43–48
54. Rinnab L, Mottaghy FM, Blumstein NM, Reske SN, Hautmann RE, Hohl K, Möller P, Wiegel T, Kuefer R, Gschwend JE (2007) Evaluation of [11C]-choline

positron-emission/computed tomography in patients with increasing prostate-specific antigen levels after primary treatment for prostate cancer. BJU Int 100(4):786–793
55. Crook J, Robertson S, Collin G et al (1993) Clinical relevance of trans-rectal ultrasound, biopsy, and serum prostate-specific antigen following external beam radiotherapy for carcinoma of the prostate. Int J Radiat Oncol Biol Phys 27:31–37
56. Yakar D, Hambrock T, Huisman H, Hulsbergen-van de Kaa CA, van Lin E, Vergunst H, Hoeks CM, van Oort IM, Witjes JA, Barentsz JO, Fütterer JJ (2010) Feasibility of 3T dynamic contrast-enhanced magnetic resonance-guided biopsy in localizing local recurrence of prostate cancer after external beam radiation therapy. Invest Radiol 45(3):121–125
57. Kim CK, Park BK, Park W, Kim SS (2010) Prostate MR imaging at 3T using a phased-arrayed coil in predicting locally recurrent prostate cancer after radiation therapy: preliminary experience. Abdom Imaging 35(2):246–252
58. Pickett B, Kurhanewicz J, Coakley F, Shinohara K, Fein B, Roach M 3rd (2004) Use of MRI and spectroscopy in evaluation of external beam radiotherapy for prostate cancer. Int J Radiat Oncol Biol Phys 60:1047–1055
59. Pucar D, Shukla-Dave A, Hricak H, Moskowitz CS, Kuroiwa K, Olgac S, Ebora LE, Scardino PT, Koutcher JA, Zakian KL (2005) Prostate cancer: correlation of MR imaging and MR spectroscopy with pathologic findings after radiation therapy – initial experience. Radiology 236:545–553
60. Crook J, et al (2000) Postradiotherapy prostate biopsies: what do they really mean? Results for 498 patients. Int J Radiat Oncol Biol Phys 48(2):355–367
61. Galosi AB, Lugnani F, Muzzonigro G (2007) Salvage cryosurgery for recurrent prostate carcinoma after radiotherapy. J Endourol 21(1):1–7
62. Rukstalis DB, Katz A (eds) (2007) Handbook of urologic cryoablation. Informa UK Ldt, London, pp 31–38
63. Loch T (2007) Urologic imaging for localized prostate cancer in 2007. World J Urol 25(2):121–129
64. Larson BT, Collins JM, Huidobro C, Corica A, Vallejo S, Bostwick DG (2003) Gadolinium enhanced MRI in the evaluation of the minimally invasive treatment of the prostate: correlation with histopatologic findings. Urology 62:900–904
65. Donnely SE, Donnely BJ (2004) Prostate cancer: gadolinium enhanced MR imaging at three weeks compared with needle biopsy at six months after cryoablation. Radiology 232:830–833
66. Shinohara K (2003) Prostate cancer. Cryotherapy. Urol Clin North Am 30:725–736
67. Chin JL, Touma N, Pautler SE, Guram KS, Bella AJ, Downey DB, Moussa M (2003) Serial histopathology results of salvage cryoablation for prostate cancer after radiation failure. J Urol 170(4 Pt 1):1199–1202
68. Galosi AB, Muzzonigro G, Polito M Jr, Minardi D, Dellabella M, Lugnani F, Polito M (2000) Role of transrectal ultrasonography in the follow-up of patients treated with prostatic cryosurgery. Arch Ital Urol Androl 72(4):276–281
69. Galosi AB, Parri G, Montironi R et al (2009) Prostate cryoablation as primary treatment of prostate cancer: oncological results with follow-up biopsy. Poster at the 2nd international workshop focal therapy and imaging in prostate & kidney cancer. Amsterdam, 10–13 June 2009
70. Heidenreich A, Bolla M, Joniau S et al Guidelines on prostate cancer. European Association of Urology Web site. http://www.uroweb.org/gls/pdf/prostate%20Cancer%202010%20June%2017th.pdf. Retrieved 19 July 2010
71. Guideline for the management of clinically localized prostate cancer: 2007 update. American Urological Association Web site. http://www.auanet.org/content/guidelines-and-quality-care/clinical-guidelines.cfm?sub=pc. Retrieved 10 Feb 2010
72. Rouviere O, Mege-Lechevallier F, Chapelon JY, Gelet A, Bouvier R, Boutitie F, Lyonnet D (2006) Evaluation of color doppler in guiding prostate biopsy after HIFU ablation. Eur Urol 50:490–497
73. Rouvière O, Curiel L, Chapelon JY et al (2004) Can color doppler predict the uniformity of HIFU-induced prostate tissue destruction? Prostate 60:289–297
74. Cirillo S, Petracchini M, D'Urso L, Dellamonica P, Illing R, Regge D, Muto G (2008) Endorectal magnetic resonance imaging and magnetic resonance spectroscopy to monitor the prostate for residual disease or local cancer recurrence after transrectal high-intensity focused ultrasound. BJU Int 102:452–458
75. Kim CK, Park BK, Lee HM, Kim SS, Kim E (2008) MRI techniques for prediction of local tumor progression after high-intensity focused ultrasonic ablation of prostate cancer. AJR Am J Roentgenol 190: 1180–1186
76. Warmuth M, Johansson T, Mad P (2010) Systematic review of the efficacy and safety of high-intensity focused ultrasound for the primary and salvage treatment of prostate cancer. Eur Urol 58:803–815

28 Interventional Ultrasound: Prostatic Biopsy with Special Techniques (Saturation, Template)

Vincenzo Scattoni and Carmen Maccagnano

28.1 Introduction

Prostate cancer (PC) is the most common neoplasm in the Western hemisphere, and its incidence is still increasing mostly due to the introduction of prostate-specific antigen (PSA) blood tests and the widespread use of ultrasound-guided prostate biopsy (PB) that have increased correspondingly, with up to a million procedures performed annually in the USA [1].

PB has evolved from the standard sextant biopsy method, described by Hodge and colleagues in 1989, which provides a PC detection rate (DR) between 20 and 35 %, to more accurate PB schemes, with the final aim to increase this DR [1, 2]. Intuitively, this aim could be achieved by adding more biopsies to prostatic areas not sampled by standard sextant schemes. Thus, the concepts of "extended biopsy" (EPBx) (10–12 cores) and "saturation biopsy" (SPBx) (≥20 cores) have rapidly evolved in the last 10 years, radically changing the general idea of PB [1, 2]. Nowadays, a random PB is still the most important diagnostic tool to detect PC, but it also allows an accurate morphological characterization of the disease, leading to both new therapeutic and follow-up perspectives (Fig. 28.1).

V. Scattoni (✉)
Department of Urology, Scientific Institute
H San Raffaele, University Vita-Salute,
Via Olgettina 60, 20132 Milan, Italy
e-mail: scattoni.vincenzo@hsr.it

C. Maccagnano
Azienda Ospedaliera S.Anna –Como,
Via Ravona, 60, San Fermo della Battaglia (Co), Italy

P. Martino, A.B. Galosi (eds.), *Atlas of Ultrasonography in Urology, Andrology, and Nephrology*,
DOI 10.1007/978-3-319-40782-1_28

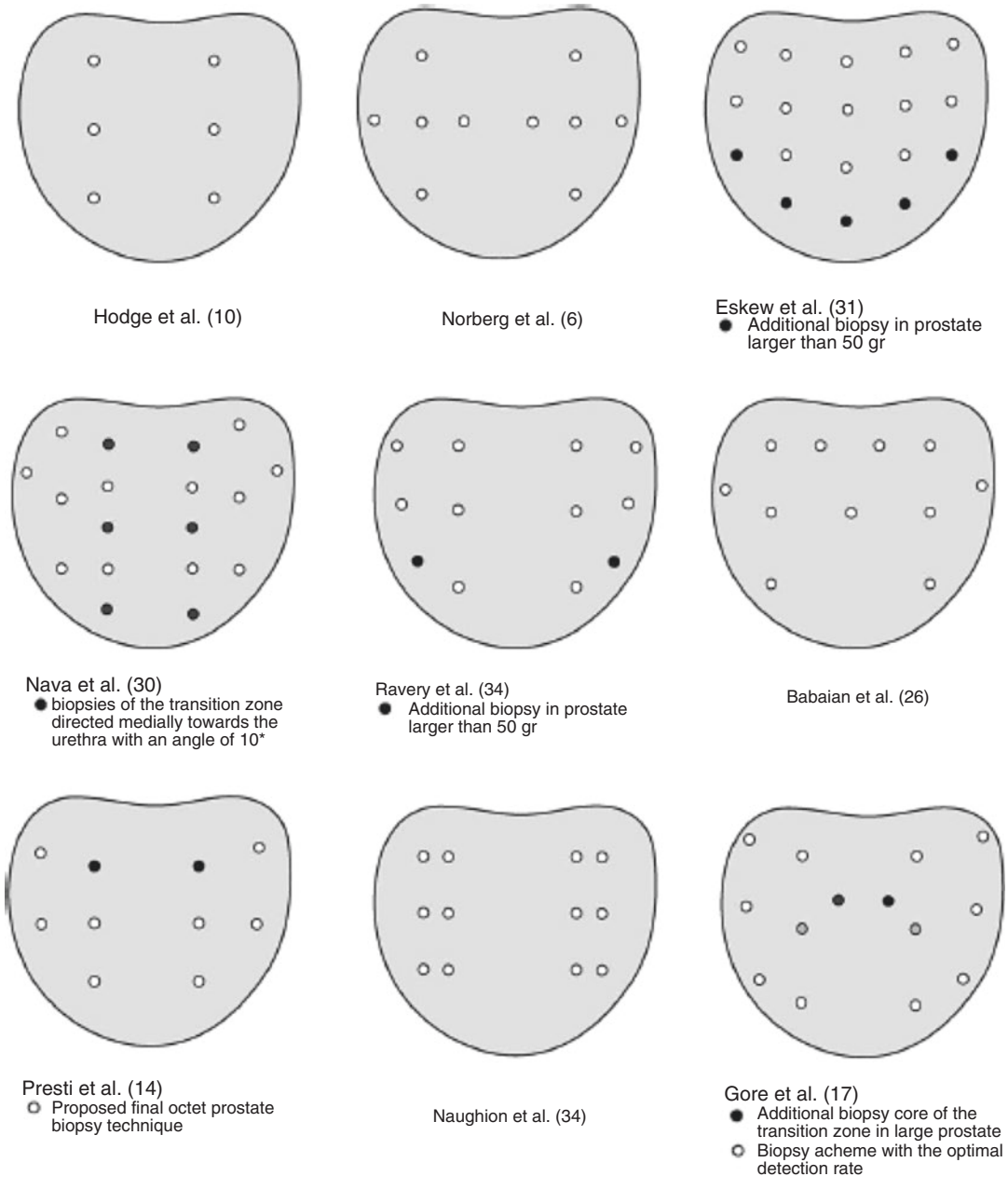

Fig. 28.1 Bioptic schemes. It is important to lateralize the cores in order to improve the cancer detection rate

28.2 Timing of Prostate Biopsy

Since PC is generally iso-echoic and not visible during trans-rectal ultrasound (TRUS), the most frequent indication to perform a PB is given by the PSA. Several trials have demonstrated that the probability of diagnosing a PC increases proportionally to PSA levels: the overall probability of finding a PC is about 15%, 30% and 60% with a PSA <4 ng/mL, 4.0–10.0 ng/mL and >10 ng/mL, respectively [3–5]. Thompson and colleagues have demonstrated that a PSA cut-off which might undoubtedly exclude a PC does not exist [5]. In the last few years, literature has totally focused on early PC diagnosis with low PSA values. Several studies have suggested to consider no more valid the 4.0 ng/mL cut-off to reduce it to a level of 2.5 ng/mL, especially in patients with a positive familiar anamnesis for PC (one relative at least with PC, with an age inferior to 60 years). The 2014 NCCN (National Comprehensive Cancer Network) guidelines suggest to perform PB with PSA >3 ng/mL and consider also PSA velocity or PSA density in order to better discriminate the candidates to PB. The 2014 European Association of Urology (EAU) guidelines recommend to consider PSA as a risk index without a precise cut-off.

In cases of PSA range between 4 and 10 ng/mL ("grey zone"), the free PSA/total PSA ratio may improve the selection of candidates to a PB. In a meta-analysis the free PSA/total PSA ratio has been demonstrated to be the most informative parameter which provides a reduction of the number of useless biopsies [6]. The data about the utility of the PSA density and of the PSA density of the transition zone (TZ) are still very controversial, even though Stephan and colleagues have recently confirmed their utility when PSA ranges between 4 and 10 ng/mL but also when PSA is <4 ng/mL [7]. The PSA kinetics (PSA velocity and PSA doubling time) has progressively lost its importance because there are not so strong evidences to support its routine use in PC diagnosis. Moreover, PSA kinetics is strongly influenced by PSA variations related to other variables not associated with neoplasms. Nevertheless, a significant increase of PSA in the long time may suggest to perform a PB independently of total PSA [8].

The indication to perform a PB has to be considered when the diagnosis drives to a treatment which may improve the quantity or the quality of life and when one or more of the following clinical conditions are present:

- Total PSA >10 ng/mL: indication to perform a PB is very strong.
- Total PSA range between 4 and 10 ng/mL ("grey zone"): the free PSA/total PSA ratio may improve the patients' selection for PB. The data about the utility of PSA density and about PSA density in the TZ are still very controversial. Thus, their systematic use is still not advisable.
- Total PSA range between 2.5 and 4 ng/mL: the indication is weak but suggested in case of relatives affected by PC (at least one relative with PC, with age inferior to 60 years), suspicious DRE and very low PSA ratio (<10%).
- Abnormal DRE: actually a single hypo-echoic lesion (not supported by an abnormal DRE or by a high PSA) does not represent a recommendation to a targeted biopsy [1].

The data about pro-PSA and PHI (prostate health index) are still preliminary, and these parameters are not advisable in the routine use, also because of their difficult dosage methods [9].

In this scenario, some predictive models, such as nomograms, have been developed, with the aim to increase the predictive capacity of the PB results. These instruments are often based on familial history, age, DRE, TRUS results, PSA values and emptying symptoms. The use of nomograms and risk calculators does not eliminate the uncertain features typical of oncologic patients, but they allow an evidence-based guide and facilitate the discussion with patients themselves.

28.3 Patient Preparation and Anaesthesia

It is possible not to assume the antibiotic prophylaxis in case of trans-perineal (TP) approach, because the risk of infectious complications is low (inferior to 1%) [10]. The antibiotic prophylaxis is necessary with the trans-rectal (TR) approach because it allows the reduction of infectious complications. It has to be started 12 h before the procedure and it has to be continued

for 2–3 days. The most used drugs are quinolones and sulfamethoxazole that show similar results.

It has been demonstrated that the enema does not prevent the infections after TR PB.

Anaesthesia is mandatory while performing a PB with TP approach.

Many trials have been published about anaesthesia during PB with TR approach, and they have shown that all forms of anaesthesia (compared to placebo) provide the same efficacy in reducing pain both during and after the PB. Moreover, they are safe and easily reproducible, without significant complications. The use of anaesthesia is beneficial for patients, regardless of the number of cores. Using anaesthesia is beneficial in cases of saturation protocols (>20 cores) or repeated biopsies (HGPIN, persistently elevated PSA, etc.), especially in younger patients, who demonstrate anxiety and sensitivity levels higher than elderly patients [11]. The TR administration of an anaesthetic gel (lidocaine 2%, 10 cc) is considered less efficacious than the peri-prostatic administration of lidocaine (2%, 10 cc per side). Different anaesthesia techniques, both local and systemic, have been experimented, and despite the fact that the most effective method has not been established yet, the peri-prostatic administration of lidocaine actually represents the most advantageous technique in order to control pain.

28.4 How and How Many Cores in the Initial Setting

TRUS represents the standard-of-care technique when a decision is taken to perform PB. Two different types of probes are available: end-fire and side-fire probe configurations; the choice of probe remains operator-dependent. TRUS should be performed in both transverse and sagittal planes, with the best visualization of the biopsy needle path in the last one. Moreover, the TP approach, which is less popular, and the TR one have shown to be equivalent in PC DR when the same number of cores was used, as demonstrated by different authors and according to international guidelines.

The TP approach has an advantage in terms of sampling the apex, because of the direction of the biopsy needle.

28.4.1 Extended Biopsy

Since the diffusion of sextant scheme, several authors had shown limitations in PC detection of six-core biopsy and had reported high rates of false-negative biopsies. Therefore, over the last years, there has been increasing interest in defining more accurate PB schemes in order to increase PC DR, the so-called EPBx. As defined by the National Comprehensive Cancer Network, EPBx is essentially a sextant template with at least four additional cores from the lateral peripheral zone, as well as biopsies directed to lesions found on palpation or imaging. To date, little controversy exists regarding the usefulness of the EPBx scheme compared with the sextant scheme in increasing the PC DR.

Nevertheless, the optimal number and location of biopsies needed to identify all patients with PC at the earliest stage possible for optimal treatment, outcome and survival are still controversial. In a systematic review, Eichler et al. showed that there is no significant benefit in taking more than 12 cores and methods requiring more than 18 cores have a poor side-effect profile [3]; other investigators have advocated for additional biopsies. Particularly, Ploussard et al. found that a 21-biopsy scheme improved the rate by 6.7% overall ($p < 0.001$) with the six far lateral cores with the highest efficiency in terms of DR. The authors also identified a cut-off PSAD (0.20 ng/mL per gram) below which an extended 21-core scheme might be systematically proposed to significantly improve the overall DR, without increasing the rate of detected insignificant PC [12].

The search for and targeting hypo-echoic lesion on TRUS remains controversial. Some authors demonstrated that the cores directed to the hypo-echoic areas are not considered necessary because their probabilities of being positive are equal to cores directed to the next adjacent area [13]. Conversely, Toi et al. found that biopsies taken when a prostate lesion is identified by TRUS are almost twice as likely to show cancer than when no lesion is visible. The cancers were found to be of higher volume and grade [13].

Even if the extended random PB scheme remains standard in the initial setting, many

patients demand advances beyond the "old-fashioned" random biopsy, which is not considered the "future" (Figs. 28.2 and 28.3).

This is due to the fact that standard greyscale TRUS technology has limited specificity and sensitivity to detect PC. This situation has led to the development of new imaging techniques suitable for TRUS, such as the contrast-enhancement US. Newly developed US contrast agents enable to delineate the neo-vascular anatomy of PC foci by enhancing the signal strength form of neovessels. Nevertheless, the technique alone is not sufficient to predict which patient has benign or malignant disease.

Additionally, real-time elastography (RTE) is a relatively new imaging modality of PC detection. The differences in tissue stiffness, produced by compression and relaxation of the tissue, can be visualized under real-time conditions, with a mean sensitivity of about 80 % [14]. The major limitation of this technique consists of dependence on user's experience and on the pressure applied on the probe. The published trials have shown promising results of RTE in PC imaging and detection, especially in conjunction with TRUS, in order to reduce the cores' number. Nevertheless further clinical studies are mandatory.

Nowadays, multi-parametric magnetic resonance imaging (mpMRI) has demonstrated to have a high degree of accuracy for the detection of clinically significant PC and can be used to define a target area before PB [14–16] (Fig. 28.4). In the last 5 years, the role of image-guided targeted biopsy has grown. The likelihood of detecting cancer in such a visible lesion is definitely higher than with a random biopsy if the DR per core is considered [16]. mpMRI-targeted biopsies have demonstrated superiority over systematic random biopsies for the detection of clinically significant disease and representation of disease burden, while deploying fewer cores [16]. There is evidence that the Gleason score obtained in a targeted biopsy reflects the true Gleason score better than the Gleason score obtained by a random PB [16]. In a recent review about mpMRI-targeted biopsies, men with a clinical suspicion of PC, a PB that used MRI to inform the sampling was associated with a DR of clinically significant PC of 42 %. This approach might permit a reduction in the number of men who need to undergo biopsy if they are deemed to have a normal MRI [15]. The efficiency of the targeted sampling appeared superior to the standard approach (70 % vs. 40 %). Since the random PB was associated with a diagnosis of insignificant PC in 10 % of men biopsied, this cancer diagnosis might have been avoided if men had undergone targeted biopsy alone. The authors also concluded that adopting mpMRI-targeted biopsies rather than random PB, fewer men are biopsied overall, a greater proportion of men with clinically significant PC are biopsied, and fewer men are attributed a diagnosis of clinically insignificant PC.

Conversely, other authors have shown that in cases of combining targeted and random biopsies during one PB session, a substantial number of cancers were detected in only the random cores [15, 16]. Relying on the targeted biopsy alone would have led to a significant rate of underdetection in these studies. There is no doubt that EPBx might better characterize PC volume and cancer extent than just a targeted biopsy: the positive cores give us information on not only the cancer extent but also the number of negative cores. Targeted biopsies seem to reflect the true Gleason score, yet they might underestimate the extent of the cancer.

Probably the combination of both targeted and extended biopsies will show the most appropriate information about the correct characteristics of cancer.

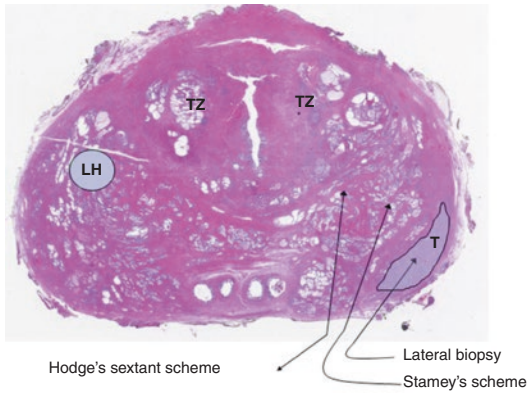

Fig. 28.2 Moving the cores to the lateral aspect of the gland allows to detect more PC and to improve cancer definition

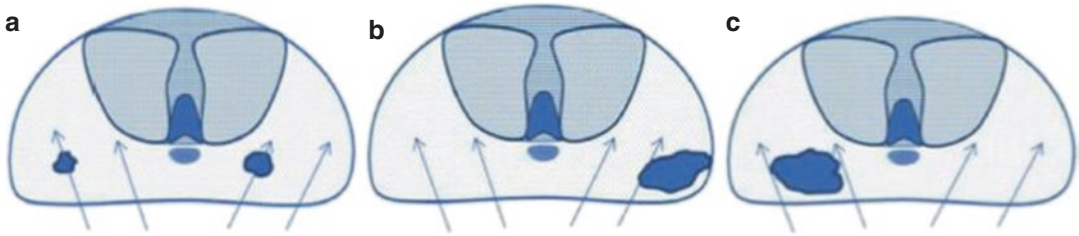

Fig. 28.3 Limits of the random bioptic schemes. (**a**) Oversampling. (**b**) Undersampling. (**c**) Undersampling – missing

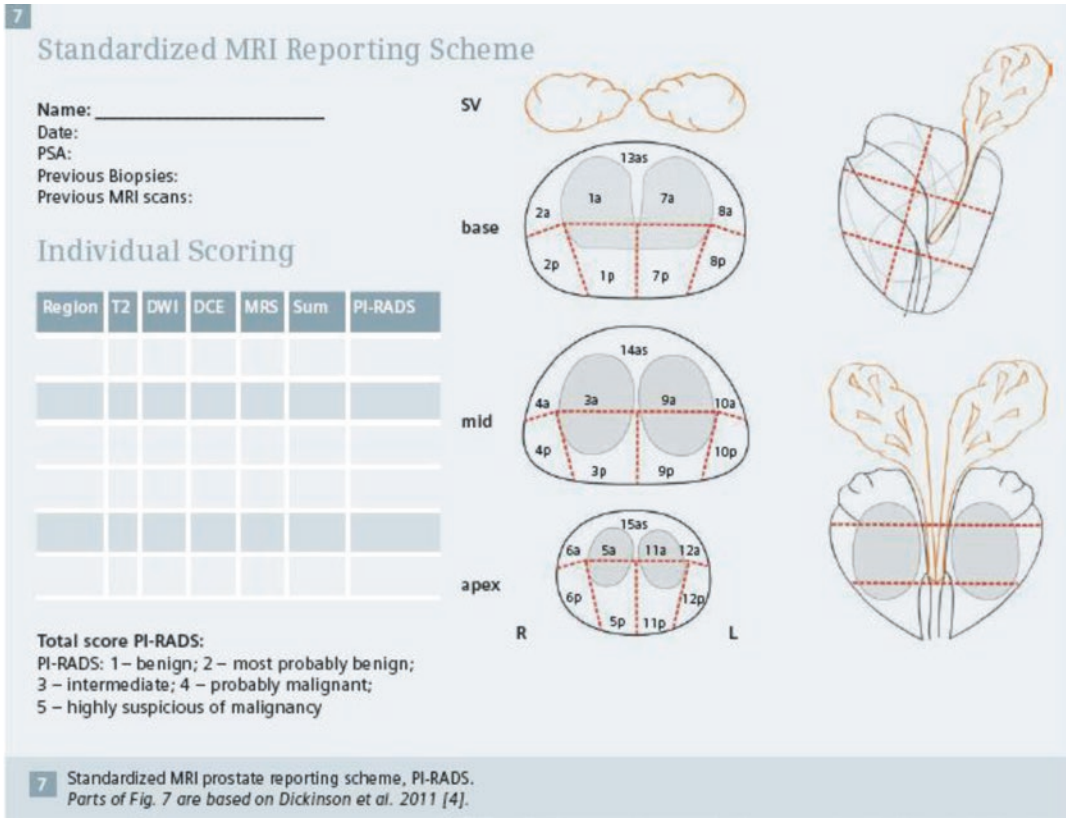

Fig. 28.4 Drawing of a report of a mpMRI

28.4.2 Saturation Biopsy

The concept of increasing the number of cores has led to the idea SPBx. In physics and chemistry, saturation refers to a condition or state in which a substance has reached its plateau concentration. Then, the rate of reaction tends to maximum and does not increase by additional substrate (Figs. 28.5 and 28.6). When applied to the field of PB, saturation should theoretically define a sampling technique that detects all PC. In this context, the curve shows that the rate of reaction tends to maximum and does not increase by additional substrate in which 20 or more cores are taken in a systematic fashion, in order to detect all PC [17].

Despite the fact that, in the last decade, several investigators have tried to optimize the number of cores in the single patient, most of the authors reported no significant benefit accrues by taking ≥12 cores in the initial setting [3].

However, even if SPBx, as an initial strategy, remains unsupported by the literature, there is a recent evidence that the cancer DR considerably increases with an increasing number of cores. The Cleveland Clinic's experience has previously reported that SPBx did not increase the cancer DR in a 2006 pilot study comparing 139 men who underwent SPBx with 87 men undergoing EPBx [4]. More recently, the same authors have reported that SPBx in the initial setting significantly improved cancer detection compared with EPBx in men with PSA <10 ng/mL, without increasing the detection of clinically insignificant cancer. They have shown that men who underwent SPBx had significantly higher DR than EPBx only when the PSA was <10 ng/mL, especially with a PSA <4 ng/mL (47.1 % vs. 32.8 %; $p = 0.008$) and when PSAD was <0.25 ng/mL per gram. The authors concluded that, if SPBx is to be considered for initial biopsy, it should be reserved for men with PSA <10 ng/mL [4].

Jiang et al. [18] performed a systematic review and meta-analysis. They concluded that SPBx scheme showed a significant advantage in PC detection. Their meta-analysis has demonstrated that an initial SPBx scheme is more efficient than an EPBx scheme in PC detection, especially for those men with lower PSA, higher PV or lower PSAD. They concluded that the exact number and location of biopsy cores required for optimal PC detection should depend on the clinical characteristics of individual patients. However, some of the studies selected were not directly related to the current clinical question.

In the initial setting, it is not clear whether it is always necessary to rely on the same scheme or to modify the number and location of the cores according to the different clinical parameters, such as PSA value, DRE findings or prostate volume. Scattoni et al. have performed SPBx in the initial setting in order to identify the most advantageous PB scheme, defined as the combination of sampling sites that detected the 95 % of all cancers with the minimal number of biopsy cores. They have confirmed that the larger the number of cores taken, the higher the PC DR found, with a difference of about 10 % between the cancers detected with 24- and 14-core schemes. The analysis revealed that the most advantageous schemes for patients with DRE negative, PV ≤60 and age ≤65 were a combination of a 16-core biopsy, for patients with DRE negative and PV ≤60 and age >65 or DRE negative and volume >60 two different combinations of a 14-core biopsy (Figs. 28.7 and 28.8). Finally, the sampling that allows to detect 95 % of cancers in patients with DRE positive was a combination of a ten-core biopsy [17]. Thus they have shown that, in the initial setting, the scheme that performed the best is a specific combination with a variable number and location of cores (10–16 cores), according to the clinical characteristics of the patients.

In conclusion, the recommended approach in initial setting is still the extended scheme. However, there is now a growing evidence in the literature that:

(a) SPBx might be indicated in patients with PSA <10 ng/mL or low PSA density or large prostate.
(b) An individualized approach with more than 12 cores according to the clinical characteristics of the patients may optimize cancer detection in the single patient.

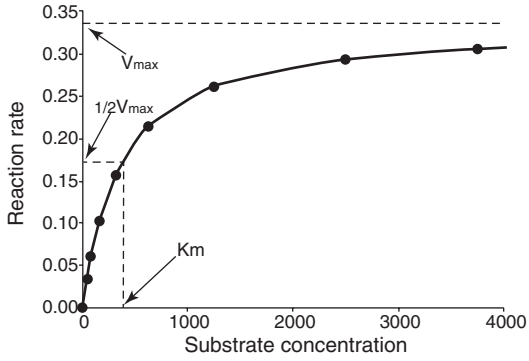

Fig. 28.5 The curve shows that the rate of reaction tends to maximum and does not increase by additional substrate

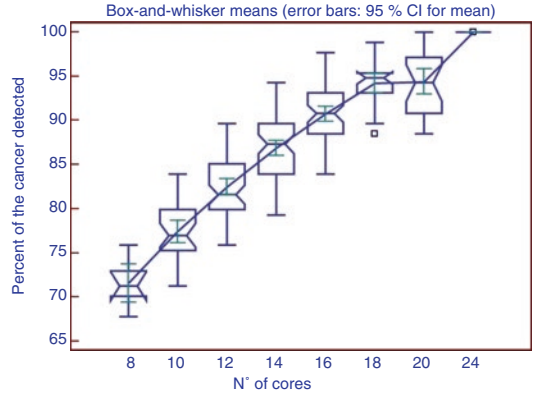

Fig. 28.6 The bars show the cross-validated mean percentages of cancer detected according to the number of cores at initial biopsy. Box and whisker report the range and mean values. Error bars report the 95 % CI

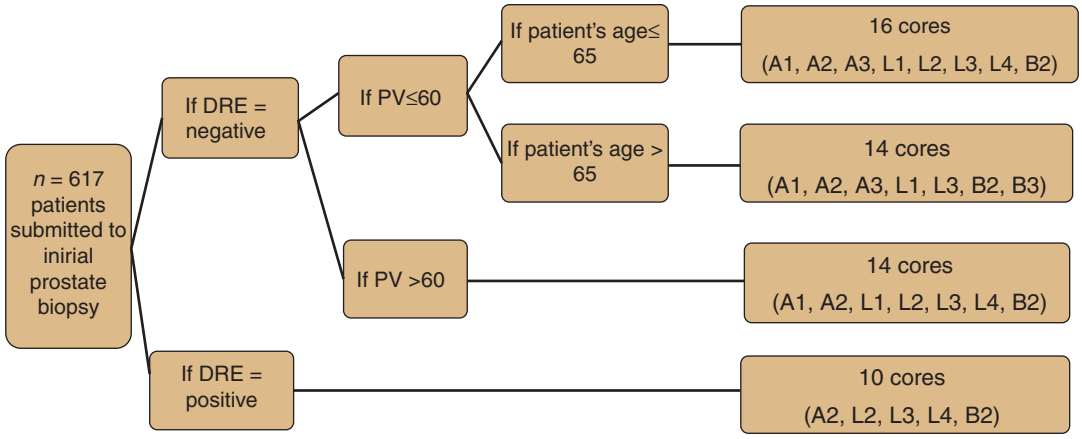

Fig. 28.7 Baseline saturation biopsy: flow chart

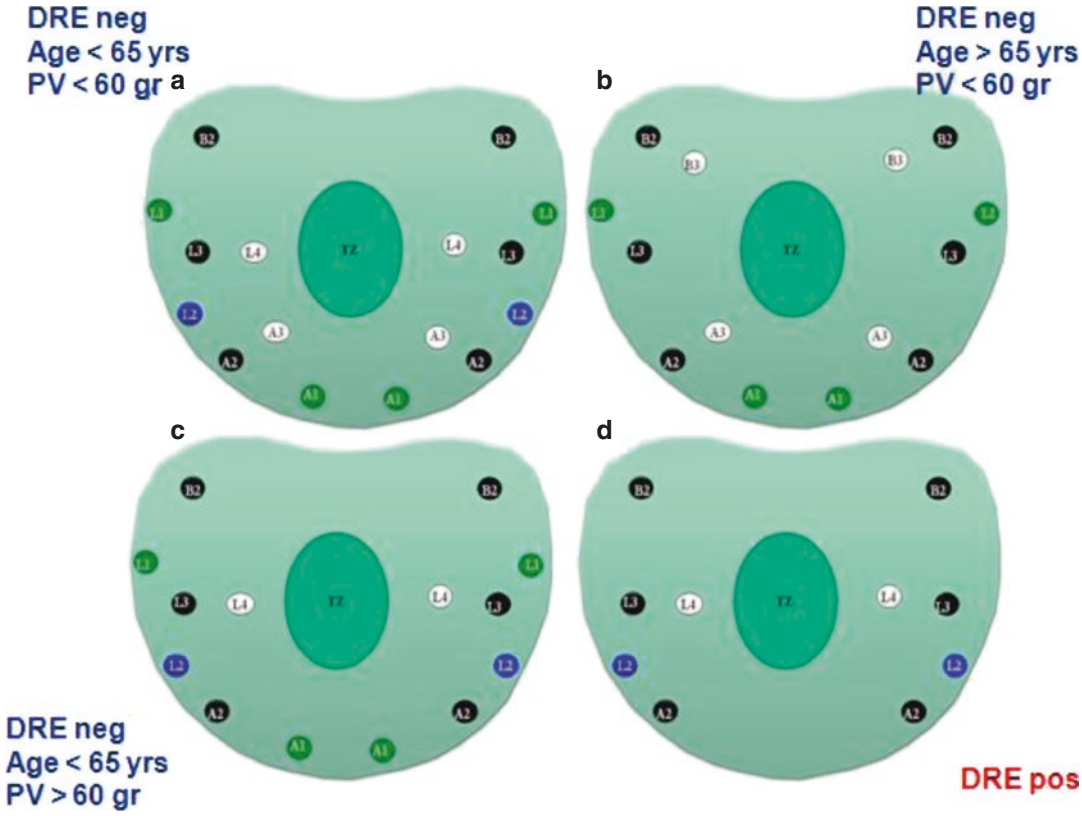

Fig. 28.8 Bioptic schemes to improve prostate cancer detection. *A* Apex, *B* Base, *L* Lateral, *T2* Transition Zone

28.5 Prostate Biopsy Strategy in Repeated Setting

Candidates to repeat PB include patients with a prior negative PB but with a persistent suspicion of PC on the basis of repeated PSA values and/or DRE findings (and other markers such us %FPSA, complexed PSA, PSAD, PSA velocity and urinary PCA3 score), previous peculiar histological diagnosis (such as atypical small acinar proliferation of prostate (ASAP) or high-grade prostatic intraepithelial neoplasia (HGPIN)) and candidates to active surveillance or to focal therapy. How and how many cores should be taken in these different scenarios is still unclear and schemes may significantly change in the different patients.

Based on the findings that even initial EPBx schemes miss almost a third of cancers, SPBx has been adopted to improve PC DR in patients with suspicious clinical findings following previous negative standard PB.

There is now a good evidence in the literature that SPBx are superior than EPBx in this setting. Zaytoun et al. reported their experience at the Cleveland Clinic where they compared EPBx with SPBx in a clearly defined, heterogeneous population of patients undergoing repeat biopsy after a single prior biopsy that failed to diagnose PC [19]. They showed that office-based SPBx significantly increases DR in repeat biopsy compared to EPBx. SPBx detected almost one-third more cancers. For patients with benign initial biopsy, SPBx demonstrated significantly greater PC detection. For previous ASAP and/or HGPIN, a trend for higher PC DR was demonstrated in the saturation group but did not reach statistical significance.

Similarly, Scattoni et al. recently tried to identify the optimal combination of sampling sites (number and location) to detect PC in patients previously submitted to an initial negative prostatic biopsy [20]. They prospectively performed a TRUS-guided systematic 24-core PB in 340 consecutive patients after a first negative biopsy (at least 12 cores). Subsequently, they set the cancer-positive rate of the 24-core PB at 100% and calculated PC DR for 255 possible combinations of sampling sites. They reported that the more cores taken, the higher the cancer DR. They showed a continuum of improvement of the cancer DR when increasing the number of cores, even if the cancer DR of the 24 cores was significantly higher than only the mean DR rates of 14-core schemes. Moreover, at a given number of cores, the DR rates varied significantly according to the different combination of sites considered [12].

All of these studies demonstrate that SPBx provides a higher cancer DR than the extended approach in the repeat setting and that the higher the number of cores, the higher the number of cancers detected (Figs. 28.9, 28.10, 28.11 and 28.12).

Nevertheless, the regular use of SPBx in clinical practice is not approved. The NCCN suggests performing a second extended protocol after an initial negative extended scheme and suggests considering SPBx only in patients with a high risk of cancer after multiple negative biopsies. The 2015 European Association of Urology (EAU) guidelines on PC do not indicate the template that should be used. Consequently, the ideal strategy for a second PB procedure has yet to be fully elucidated [21].

Recently, interest has increased in defining more efficient biopsy schemes for PC detection with the minimum number of cores. Different variables, both clinical and not clinical, may have an impact on the cancer DR. Apart from the clinical characteristics of the patients, some procedural characteristics may have an even greater impact on the cancer DR. Intuitively, adding more biopsies to prostatic areas not sampled by common extended schemes should increase the DR. It should be noted, however, that increasing the number of biopsy cores is not the solution to the problem and that the relationship between the number of biopsy cores and the resulting cancer DR does not correlate linearly. As a matter of fact, the curve tends to plateau, and the increase of cores taken in the template is not equivalent to the increase of cancer detected.

All of these data demonstrate that cancer detection is influenced not only by the number of cores, but also by the exact location of the cores. The

report by Delongchamps et al. is a reminder that the urologist needs to do a better job of biopsying the prostate. A fairly extensive 36-core biopsy performed in 48 autopsied prostates (median volume, 35 mL) missed 5 of 12 (42%) cancers found on whole-mount pathologic analysis. In fact, the 36-core biopsy offered no benefit over an 18-core protocol in terms of PC detection [22].

Adopting a scheme that is able to maximize the DR with the fewest number of cores represents a possible new modality of performing PB. This approach is clinically preferable to adopting a saturation scheme that is unable to increase the cancer DR with the same proportion of increasing numbers of cores. Scattoni et al. recently demonstrated that both the number and the location of biopsy cores taken affect cancer DR in a repeated biopsy setting [20]. They also showed that the "optimal" repeat biopsy scheme varies according to the clinical characteristics of the patients.

Analysis revealed that, for patients with previous ASAP diagnosis, the most advantageous scheme was a combination of a 14-core biopsy (without TZ biopsies). For patients with no previous ASAP diagnosis and percentage of free prostate-specific antigen (%fPSA) of 10% or less, the most advantageous scheme was a 14-core biopsy (including four TZ biopsies). The most advantageous sampling scheme for patients with no previous ASAP and %fPSA greater than 10% was a combination of a 20-core biopsy (including four TZ biopsies).

Moreover, the number of repeated biopsy is controversial, also because the DR is inversely related to the subsequent procedure.

Djavan and colleagues reported in 2001 an original work on the risk of PC on repeat biopsies performed 6 weeks after an initial negative set. These investigators found that cancer detection rates on biopsies 1, 2, 3 and 4 were 22%, 10%, 5% and 4%, respectively, and that 58, 60.9, 86.3 and 100% of patients who had RP had organ-confined disease on biopsies 1, 2, 3 and 4. The investigators concluded that biopsy 2 in all cases of a negative finding on biopsy 1 seems justified [23]. Similarly, Campos-Fernandes and colleagues, in a cohort with extended biopsies found that 18%, 17% and 14% of patients had PC in the second, third and fourth biopsies, respectively. PC detected at these sets of biopsies was significant in 85% of cases [24]. Similarly, Tan and colleagues found significant PC detected on third or greater PB [25].

Detection of clinically insignificant PC (according to Epstein's criteria) is an inevitable risk of repeat biopsy, and its association with the number of biopsy cores is an issue of considerable debate. Moreover, SPBx has been evaluated as a staging tool to improve the characterization of low-volume and well-differentiated PC, but whether SPBx improves prediction of tumour insignificance remains open to debate. It should be also noted that, in general, cancer missed on initial PB is likely to be smaller or more insignificant than those cancers identified on the first attempt.

In this context, the real issue with PC detection is not overdiagnosis, since only diagnosis or misdiagnosis exists, but rather potential overtreatment. Detection and treatment of PC should always be considered independent processes, and concern about over-detection must be weighed against the risk of missing clinically significant cancers.

Finally, in patients with a diagnosis of PC, candidates to active surveillance, SPBx is preferable even if not mandatory, while in cases of focal therapy, SPBx may not be sufficient and considered a surrogate to TP grid template biopsy. However, the optimal number and location of PB in patients in active surveillance with a low-grade and low-volume PC and patients who are candidate to focal therapy have not been established.

In conclusions, SPBx clearly improves cancer detection if clinical suspicion persists after previous biopsy with negative findings and is able to provide an accurate prediction of prostate tumour volume and grade. Nevertheless, international guidelines do not strongly recommended SPBx in all situations of repeated setting.

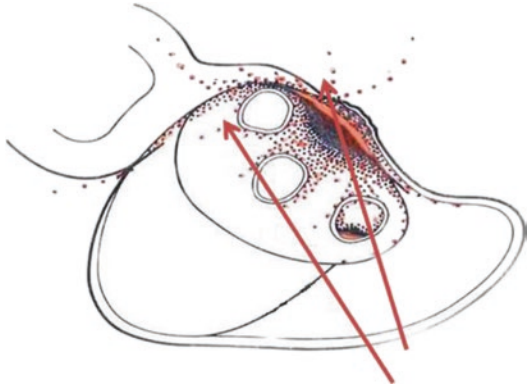

Fig. 28.9 The figure shows the correct direction of the two cores for the biopsy of the TZ zone of each lobe of the prostate (reprinted by Galosi AB personal comunication)

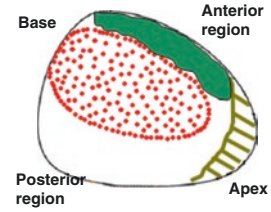

Fig. 28.12 Site of the prostate where the tumours may be located

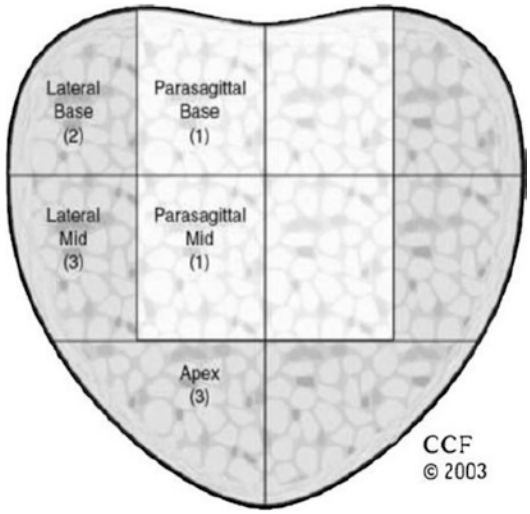

Fig. 28.10 The Cleveland Clinic experience

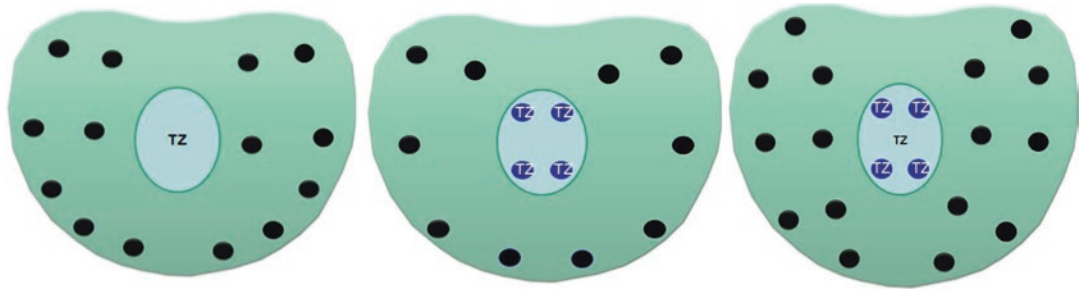

Fig. 28.11 Different schemes in the repeated setting

Conclusions

The issue about the number and location of the cores is still a matter of debate both in initial and in repeat setting also because the scenarios in which PB is required are changing. At present, EPBx is sufficient, in most of the cases, to provide adequate diagnosis and PC characterization in the initial setting. SPBx seems to be necessary in some cases in the initial setting (mostly when PSA <10 ng/mL) and in the repeat setting. However, random PB does not represent the future, while imaging target biopsy is becoming more popular.

References

1. Scattoni V, Zlotta S, Montironi R, Schulman C, Rigatti P, Montorsi F (2007) Extended and saturation prostatic biopsy in the diagnosis and characterisation of prostate cancer: a critical analysis of the literature. Eur Urol 52:1309–1322
2. Scattoni V, Roscigno M, Raber M, Dehò F, Maga T, Zanoni M, Riva M, Sangalli M, Nava L, Mazzoccoli B, Freschi M, Guazzoni G, Rigatti P, Montorsi F (2008) Initial extended transrectal prostate biopsy – are more prostate cancers detected with 18 cores than with 12 cores? J Urol 179(4):1327–1331
3. Eichler K, Hempel S, Wilby J et al (2006) Diagnostic value of systematic biopsy methods in the investigation of prostate cancer: a systematic review. J Urol 175:1605–1612
4. Li YH, Elshafei A, Li J, Gong M, Susan L, Fareed K, Jones JS (2013) Transrectal saturation technique may improve cancer detection as an initial prostate biopsy strategy in men with prostate-specific antigen <10 ng/ml. Eur Urol 65(6):1178–1183
5. Thompson IM, Pauler DK, Goodman PJ, Tangen CM, Lucia MS, Parnes HL, Minasian LM, Ford LG, Lippman SM, Crawford ED, Crowley JJ, Coltman CA Jr (2004) Prevalence of prostate cancer among men with a prostate-specific antigen level <=4.0 ng per milliliter. N Engl J Med 350(22):2239–2246
6. Gilbert SM, Cavallo CB, Kahane H, Lowe FC (2005) Evidence suggesting PSA cutpoint of 2.5 ng/mL for prompting prostate biopsy: review of 36,316 biopsies. Urology 65(3):549–553
7. Stephan C, Stroebel G, Heinau M, Lenz A, Roemer A, Lein M, Schnorr D, Loening SA, Jung K (2005) The ratio of prostate-specific antigen (PSA) to prostate volume (PSA density) as a parameter to improve the detection of prostate carcinoma in PSA values in the range of <4 ng/mL. Cancer 104(5):993–1003
8. Perrin P (2006) PSA velocity and prostate cancer detection: the absence of evidence is not the evidence of absence. Eur Urol 49(3):418–419
9. Lazzeri M, Haese A, de la Taille A, Palou Redorta J, McNicholas T, Lughezzani G, Scattoni V, Bini V, Freschi M, Sussman A, Ghaleh B, Le Corvoisier P, Alberola Bou J, Esquena Fernández S, Graefen M, Guazzoni G (2013) Serum isoform [−2]proPSA derivatives significantly improve prediction of prostate cancer at initial biopsy in a total PSA range of 2–10 ng/ml: a multicentric European study. Eur Urol 63(6): 986–994
10. Ukimura O, Coleman JA, de la Taille A, Emberton M, Epstein JI, Freedland SJ, Giannarini G, Kibel AS, Montironi R, Ploussard G, Roobol MJ, Scattoni V, Jones JS (2013) Contemporary role of systematic prostate biopsies: indications, techniques, and implications for patient care. Eur Urol 63(2):214–230
11. Maccagnano C, Scattoni V, Roscigno M, Raber M, Angiolilli D, Montorsi F, Rigatti P (2011) Anaesthesia in transrectal prostate biopsy: which is the most effective technique? Urol Int 87(1):1–13
12. Ploussard G, Nicolaiew N, Marchand C, Terry S, Vacherot F, Vordos D, Allory Y, Abbou CC, Salomon L, de la Taille A (2014) Prospective evaluation of an extended 21-core biopsy scheme as initial prostate cancer diagnostic strategy. Eur Urol 65(1):154–161
13. Toi A, Neill M, Gina A et al (2007) The continuing importance of transrectal ultrasound identification of prostatic lesions. J Urol 177:516–520
14. Pummer K, Rieken M, Augustin H, Gutschi T, Shariat SF (2014) Innovations in diagnostic imaging of localized prostate cancer. World J Urol 32(4):881–890
15. Moore CM, Robertson NL, Arsanious N, Middleton T, Villers A, Klotz L, Taneja SS, Emberton M (2013) Image-guided prostate biopsy using magnetic resonance imaging-derived targets: a systematic review. Eur Urol 63(1):125–140
16. Siddiqui MM, Rais-Bahrami S, Truong H, Stamatakis L, Vourganti S, Nix J, Hoang AN, Walton-Diaz A, Shuch B, Weintraub M, Kruecker J, Amalou H, Turkbey B, Merino MJ, Choyke PL, Wood BJ, Pinto PA (2013) Magnetic resonance imaging/ultrasound-fusion biopsy significantly upgrades prostate cancer versus systematic 12-core transrectal ultrasound biopsy. Eur Urol 64(5):713–719
17. Scattoni V, Raber M, Abdollah F et al (2010) Biopsy schemes with the fewest cores for detecting 95% of the prostate cancers detected by a 24-core biopsy. Eur Urol 57(1):1–8
18. Jiang X, Zhu S, Feng G, Zhang Z, Li C, Li H, Wang C, Xu Y (2013) Is an initial saturation prostate biopsy scheme better than an extended scheme for detection of prostate cancer? A systematic review and meta-analysis. Eur Urol 63(6):1031–1039
19. Zaytoun OM, Moussa AS, Gao T, Fareed K, Jones JS (2011) Office based transrectal saturation biopsy improves prostate cancer detection compared to extended biopsy in the repeat biopsy population. J Urol 186(3):850–854

20. Scattoni V, Raber M, Capitanio U, Abdollah F, Roscigno M, Angiolilli D, Maccagnano C, Gallina A, Saccà A, Freschi M, Doglioni C, Rigatti P, Montorsi F (2011) The optimal rebiopsy prostatic scheme depends on patient clinical characteristics: results of a recursive partitioning analysis based on a 24-core systematic scheme. Eur Urol 60(4):834–841
21. Scattoni V, Maccagnano C, Capitanio U, Gallina A, Briganti A, Montorsi F (2014) Random biopsy: when, how many and where to take the cores? World J Urol 32(4):859–869
22. Delongchamps NB, de la Roza G, Jones R, Jumbelic M, Haas GP (2009) Saturation biopsies on autopsied prostates for detecting and characterizing prostate cancer. BJU Int 103(1):49–54
23. Djavan B, Ravery V, Zlotta A et al (2001) Prospective evaluation of prostate cancer detected on biopsies 1, 2, 3 and 4: when should we stop? J Urol 166:1679–1683
24. Campos-Fernandes JL, Bastien L, Nicolaiew N et al (2009) Prostate cancer detection rate in patients with repeat extended 21-sample needle biopsy. Eur Urol 55:600–609
25. Tan N, Lane B, Li J et al (2008) Prostate cancers diagnosed at repeat biopsy are smaller and less likely to be high grade. J Urol 180:1325–1329

Interventional Ultrasound: US-Guided Puncture of the Bladder

29

Pasquale Martino, Saverio Forte, Domenico Martino, and Carlos Miacola

29.1 Indications

There are various different indications for positioning suprapubic drainage (Cystofix) [1–4]. It is nearly always the first choice in cases when ureteral catheterization is difficult or could be dangerous [5, 6], typically after ureteral trauma. Another indication is acute or chronic urine retention, in cases when ureteral catheterization is not advised. In acute forms, catheter insertion may be needed as an emergency procedure, while in chronic forms the choice may be elective or due to particular patient conditions (in elderly or poorly compliant patients). In neurological conditions (spinal cord lesions, multiple sclerosis), this procedure is preferable to transurethral catheterization because it guarantees long-term urine drainage, is simpler to manage [7–10], and has a lower incidence of complications due to infection.

Suprapubic cystostomy can also be useful for long-term drainage in cases of urinary incontinence, and in some anatomical alterations such as hypospadias, and in ventral division of the male gland. It is also useful in women if they are prone to frequent expulsion of the ureteral catheter balloon or else continual leakage around the catheter. Cystofix positioning is also indicated in some surgical and/or diagnostic maneuvers that require nonureteral bladder drainage (like in urological and colorectal surgery and urodynamic tests) [11–15].

29.2 Contraindications

In various medical conditions, there are absolute or relative contraindications to positioning an epicystostomy. These include patients taking anticoagulant or antiaggregant therapy; patients with a pelvic fracture, in which case the catheter could inadvertently be positioned in the hematoma, posing a risk of infection and sepsis; patients with vascular grafts such as femorofemoral anastomosis; patients with bladder carcinoma; and patients who have undergone abdominal surgery due to the risk of abdominal perforation.

Electronic supplementary material The online version of this chapter (doi:10.1007/978-3-319-40782-1_29) contains supplementary material, which is available to authorized users.

P. Martino (✉) • S. Forte • C. Miacola
Department of Emergency and Organ Transplantation – Urology, Andrology and Kidney Transplantation Unit, University of Bari, Bari, Italy
e-mail: pasqualeluciomartino@libero.it; luciomartino@tin.it; pasquale.martino@uniba.it

D. Martino
ASL BA – Day Surgery Service – "Fallacara" Hospital, Triggiano, Bari, Italy

P. Martino, A.B. Galosi (eds.), *Atlas of Ultrasonography in Urology, Andrology, and Nephrology*,
DOI 10.1007/978-3-319-40782-1_29

29.3 Ultrasound Assessment

The catheter must be inserted by a surgeon with adequate experience and familiar with the US device. In general, 3.5/5.0/7.5 MHz probes are employed [B], associated with a guiding device (Fig. 29.1).

The bladder must be well distended to ensure an optimal view (more than 300 ml), so that the bladder dome is palpable at least 5 cm above the pubic symphysis [16] (Fig. 29.2).

In patients who do not suffer from urinary retention, the distension can be achieved by filling the bladder with saline solution through a ureteral catheter or in particular cases during cystoscopy.

Transabdominal US allows the bladder to be examined on the longitudinal and transverse planes, showing the margins, the degree of filling, the viscera, and the catheterization region. In transverse scanning the probe is positioned parallel to the pubic symphysis and the needle in medial position to the probe: it will appear as a luminous dot. Moving the probe from side to side can make it easier to see the needle, even if in this scan the needle may often be pushed beyond the correct location because of the difficulty in visualizing the point due to echo artifacts. In longitudinal scanning the probe is placed sagittally. The needle is pushed forward through the end of the probe, and so the needle point, needle, and course are visible at all times (Fig. 29.3).

In most cases, the bladder content is anechogenic; in patients already fitted with a catheter, there may sometimes be air inside the bladder that will appear as a hyperechogenic area in the bladder dome. The small intestine, unless it contains gas, will appear as a circular or linear compressible image. However, it should be borne in mind that only some authors have claimed that the ultrasound device is reliable in excluding the presence of a bowel loop in the suprapubic region [4, 17, 18].

Once the reference points have been identified (the peritoneal reflection, the pubic symphysis, and the best point for bladder puncture), after preparing the skin, a sterile drape is placed through which an opening will be created at the level of the incision zone.

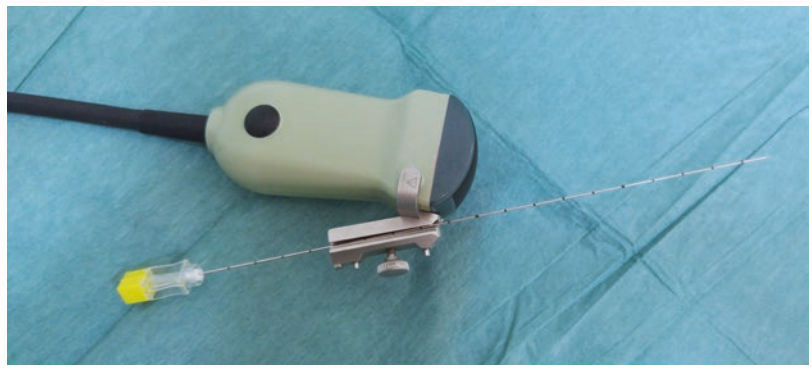

Fig. 29.1 Ultrasound probe with puncture adaptor

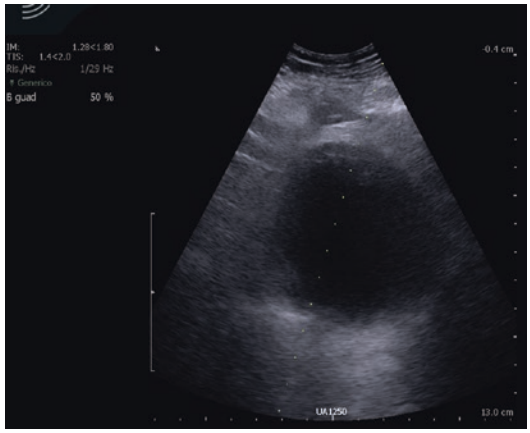

Fig. 29.2 Suprapubic bladder ultrasound

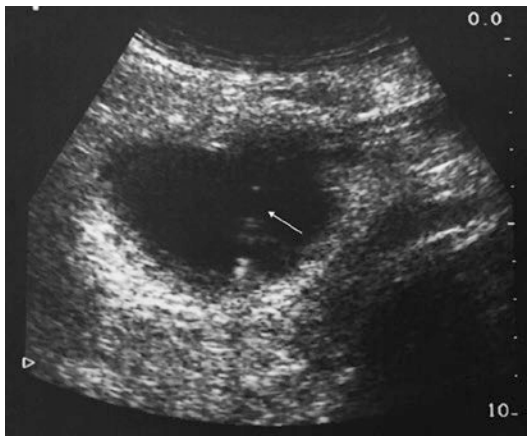

Fig. 29.3 Placing the needle during the maneuver (shadow)

29.4 Positioning Technique

The puncture site is generally 2–4 cm above the pubic symphysis. In obese patients it is advisable to position the Cystofix above the skinfold in the suprapubic region, to reduce the risk of local infections and dermatitis.

The needle must be angled at 60–90° to the abdominal wall, to make sure that the catheter balloon does not rest on the trigone.

The procedure must be performed under local anesthesia infiltrating sufficient anesthetic (typically between 5 and 20 ml of 1 % lidocaine) to cover the calculated course of the catheter; more rarely, intravenous sedation may be administered (midazolam 2.5–5 mg) or regional or general anesthesia. In the specific case of a patient with a spinal cord injury at level T6 or above, local anesthesia is not enough to prevent a possible dysreflexia.

Antibiotic prophylaxis is always advisable to reduce the risk of infection [19], also bearing in mind that in long-term bearers of a catheter, colonization of the urine with antibiotic-multiresistant bacteria is very probable. Moreover, interruption or modification of the anticoagulant or antiaggregant therapy is recommended, to reduce the risk of bleeding.

On the market, various kits are available that can be used for the catheterization procedure: those for direct puncture (Fig. 29.4) or those for drainage with the Seldinger technique [20].

Direct puncture involves piercing the bladder at the suprapubic level, under US guidance, with a metal stylet of a suitable caliber, to be positioned in the bladder lumen. When urine is seen to flow, the drainage tube is inserted in the stiletto caliber, which is easily visible at US scanning (Fig. 29.5). The drainage is anchored with silk stitches to the skin and connected to a urine collection bag (Fig. 29.6).

The Seldinger technique is the safest for inserting a suprapubic catheter. Once the needle has been positioned (mean caliber 1.2 mm) in the bladder under US guidance, the rigid Lunderquist-type guidewire with a soft point is introduced (mean caliber 0.7 mm) and the needle is withdrawn. At this point urine flow should be

observed, confirming the correct position, and the skin incision area can be widened with a triangular scalpel blade.

On the guidewire, progressive dilators up to a maximum of 12 F are fitted. The dilation must be achieved by sliding the dilators along the guidewire with a gentle "screwing" type maneuver. Excessive tension will increase the risk of twisting the guidewire and damaging the bladder. During the maneuver, it is necessary to ensure that the dilator sheath follows the line of the guidewire at all times and the thread remains free.

Subsequently, a silicone balloon catheter is positioned, generally 8–10 F, proceeding along the guidewire. The Foley balloon is inflated with 5–10 cc of physiological solution and then the guidewire is removed. The correct positioning of the catheter inside the bladder is demonstrated by a visible urine flow. Finally, the catheter can be fixed to the skin with a stapling device or silk stitches.

Alternative measures to US guidance include CT and MRI guidance that offer the maximum certainty as to the true positions of any bowel loops.

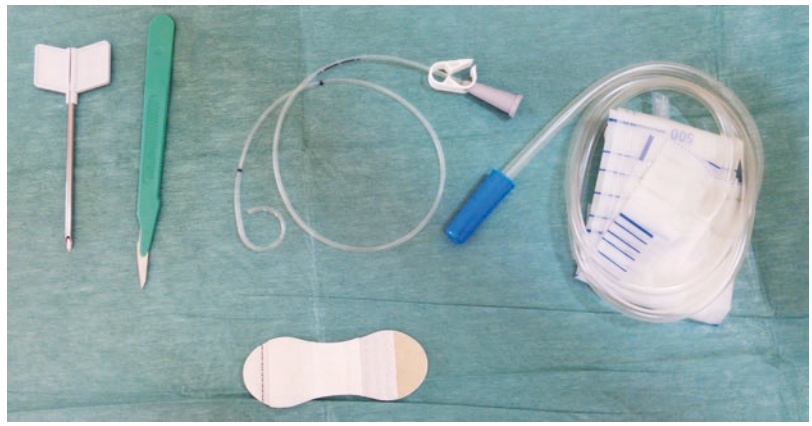

Fig. 29.4 Suprapubic catheter placement kit

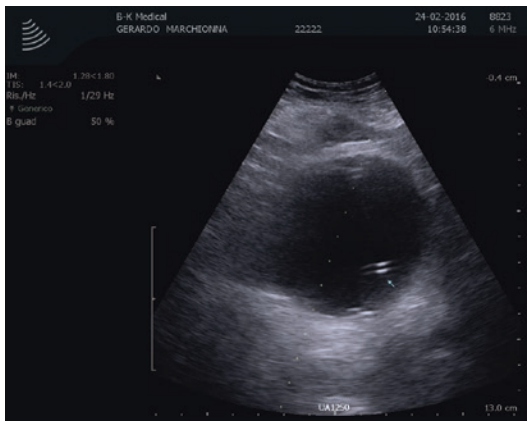

Fig. 29.5 Drainage tube in the bladder (shadow)

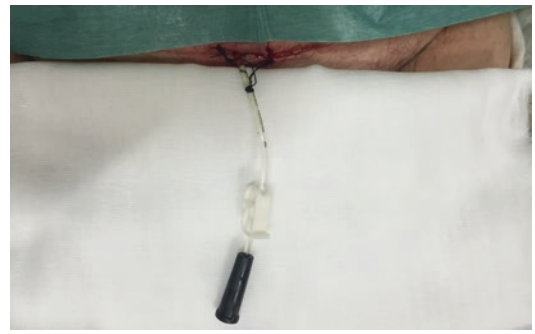

Fig. 29.6 Suprapubic catheter in place after the procedure

29.5 Management of Complications

Being an invasive procedure, the described suprapubic cystostomy entails various risks such as intra-abdominal bleeding and hematuria. If any of these should occur, immediate hemostasis must be applied.

Of the reported complications, lesions of abdominal organs are among the most severe. In some studies [7, 19, 21] the percentage of bowel lesions is 1–2 %, associated with a mortality rate at 30 days of 1.8 %. Other complications include infections of both the urinary tract and the access route.

References

1. Røhl L, Rasmussen OS (1997) Ultrasound-guided percutaneous suprapubic cystostomy. Eur J Ultrasound 6:57–61
2. Aguilera PA, Choi T, Durham BA (2004) Ultrasound-guided suprapubic cystostomy catheter placement in the emergency department. J Emerg Med 26(3): 319–321
3. Harrison SCW, Lawrence WT, Morley R, Pearce I, Taylor J (2011) British Association of Urological Surgeons' suprapubic catheter practice guidelines. BJU Int 107:77–85
4. Khan A, Abrams P (2009) Suprapubic catheter insertion is an outpatient procedure: cost savings resultant on closing an audit loop. BJU Int 103:640–644
5. Ichsan J, Hunt DR (1987) Suprapubic catheters: a comparison of suprapubic versus urethral catheters in the treatment of acute urinary retention. Aust N Z J Surg 57:33–36
6. Horgan AF, Prasad B, Waldron DJ, O'Sullivan DC (1992) Acute urinary retention. Comparison of suprapubic and urethral catheterisation. Br J Urol 70:149–151
7. Sheriff MK, Foley S, McFarlane J, Nauth-Misir R, Craggs M, Shah PJ (1998) Long-term suprapubic catheterization: clinical outcome and satisfaction survey. Spinal Cord 36:171–176
8. Fowler CJ, Panicker JN, Drake M et al (2009) A UK consensus on the management of the bladder in multiple sclerosis. J Neurol Neurosurg Psychiatry 80: 470–477
9. Mitsui T, Minami K, Furuno T, Morita H, Koyanagi T (2000) Is suprapubic cystostomy an optimal urinary management in high quadriplegics? A comparative study of suprapubic cystostomy and clean intermittent catheterization. Eur Urol 38:434–489
10. Feifer A, Corcos J (2008) Contemporary role of suprapubic cystostomy in treatment of neuropathic bladder dysfunction in spinal cord injured patients. Neurourol Urodyn 27:475–479
11. Klaaborg KE, Kronborg O (1986) Suprapubic bladder drainage in elective colorectal surgery. Dis Colon Rectum 29:260–262
12. Perrin LC, Penfold C, McLeish A (1997) A prospective randomized controlled trial comparing suprapubic with urethral catheterization in rectal surgery. Aust N Z J Surg 67:554–556
13. Ratnaval CD, Renwick P, Farouk R, Monson JR, Lee PW (1996) Suprapubic versus transurethral catheterisation of males undergoing pelvic colorectal surgery. Int J Colorectal Dis 11(4):177–9
14. Andersen JT, Heisterberg L, Hebjørn S et al (1985) Suprapubic versus transurethral bladder drainage after colposuspension/vaginal repair. Acta Obstet Gynecol Scand 64:139–143
15. Branagan GW, Moran BJ (2002) Published evidence favors the use of suprapubic catheters in pelvic colorectal surgery. Dis Colon Rectum 45:1104–1108
16. Albrecht K, Oelke M, Schultheiss D, Tröger HD (2004) The relevance of urinary bladder filling in suprapubic bladder catheterization. Urologe A 43: 178–184
17. Irby PB 3rd, Stoller ML (1993) Percutaneous suprapubic cystostomy. J Endourol 7:125–130
18. Lee MJ, Papanicolaou N, Nocks BN, Valdez JA, Yoder IC (1993) Fluoroscopically guided percutaneous suprapubic cystostomy for long-term bladder drainage: an alternative to surgical cystostomy. Radiology 188:787–789
19. Ahluwalia RS, Johal N, Kouriefs C, Kooiman G, Montgomery BS, Plail RO (2006) The surgical risk of suprapubic catheter insertion and long-term sequelae. Ann R Coll Surg Engl 88:210–213
20. NHS Technology Adoption Centre. The Seldinger suprapubic catheter kit. Available at: http://webarchive.nationalarchives.gov.uk/20130701143131/http://www.ntac.nhs.uk/HowToWhyToGuides/SuprapubicFoleyCatheterKit/Catheter-Executive-Summary.aspx. Accessed 26 Sept 2015
21. National Patient Safety Agency. Rapid Response Report NPSA/2009/RRR005: minimising risks of suprapubic catheter 16 insertion (adults only). Available at: http://www.npsa.nhs.uk/EasySiteWeb/GatewayLink.aspx?alId=59454. Accessed 29 Sept 2015

Fiducial Marker Implantation in Prostate Radiation Therapy

30

Andrea Benedetto Galosi, Vito Lacetera, Giovanna Mantello, and Massimo Cardinali

30.1 Introduction

Over the last decade, the simultaneous application of intensity-modulated radiotherapy (IMRT) and image-guided radiotherapy (IGRT) conformal techniques to the treatment of prostate cancer has made it possible to deliver extremely high doses of radiation to the cancer while to a large extent sparing critical organs like the rectum and bladder. This approach is yielding a more successful local control of the disease, with limited side effects.

The positioning of fiducial markers in the prostate is an essential part of the IGRT technique that allows maximal doses of radiation to be delivered to the tumor while reducing side effects to a minimum. Thus, their use increases the accuracy, efficacy, and safety of radiotherapy treatment [1, 2].

IMRT is an extreme form of three-dimensional conformal radiotherapy (3DCRT) that combines conformal geometric delivery with targeted conformal beam dosage. However, to perform this technique correctly, it is essential to make a highly accurate check at each session both of the patient's position and of the tumor target area for IGRT.

Being a mobile organ, the prostate gland inevitably undergoes changes of position both between one session and another and even during the same session. Such changes, largely attributable to the degree of filling of the bladder and rectum, can be by more than 10 mm on each orthogonal axis. Clearly, this poses a risk not only of underdelivery of the planned volume to the target but also of exceeding the tolerance dose to healthy tissue. To overcome this difficulty of alignment of the patient and the target organ, when planning the treatment schedule, around the planned treatment area (planning target volume, PTV), the radiotherapist will add a safety margin to the clinical target volume (CTV), in short, the CTV-PTV margin, of a mean size of 10 mm [2].

Fiducial markers confine patient setup and organ movement errors to a minimum, as well as limit the expansion margins (CTV vs. PTV). The reduction in the irradiated volume scatter will provide significant clinical benefit for the patient [3].

Should the volume of rectal wall included in the PTV still be too wide, posing a risk of delayed rectal toxicity, it is possible to resort to the insertion of a tissue equivalent spacer between the rectum and the prostate so as to protect the rectum from higher isodoses.

A.B. Galosi, MD, PhD (✉)
Institute of Urology, Marche Polytechnic University, Ancona, Italy
e-mail: galosiab@yahoo.it

V. Lacetera, MD
Urology Unit, Area Vasta 1, ASUR Marche, Urbino, Italy
e-mail: vlacetera@gmail.com

G. Mantello, MD • M. Cardinali, MD
Radiation Therapy Unit, Azienda Ospedaliero-Universitaria Ospedali Riuniti, Ancona, Italy
e-mail: gio@mobilia.it; massimo.cardinali@ospedaliriuniti.marche.it

P. Martino, A.B. Galosi (eds.), *Atlas of Ultrasonography in Urology, Andrology, and Nephrology*,
DOI 10.1007/978-3-319-40782-1_30

30.2 US Technique

30.2.1 Patient Selection

In our practice, we reserve the insertion of fiducial markers to patients with very-low-, low-, and intermediate-risk category of prostate cancer (according to the NCCN 2015 classification). In these cases, the target is generally only the prostate gland or at most the gland and the base of the seminal vesicles [4]. In high- and very high-risk disease, instead, it is necessary to include within the target area also the seminal vesicles and/or pelvic lymph nodes, so there is clearly far less benefit gained from localizing just the prostate gland via these markers.

Another patient category that may benefit from the implantation of these markers (or even just one marker) is those who, after radical prostatectomy, present macroscopic recurrence of the disease. These patients are candidates for salvage radiotherapy, and the role of the markers is to make an extremely precise identification of the disease localization (the most frequent site is the vesicourethral anastomosis) where boost radiotherapy needs to be delivered. The marker will be positioned only if a nodule is present at US and the recurrence is confirmed by histology (Fig. 30.1).

There is another small patient category eligible for marker implantation, namely, those with a hip replacement with prosthesis, especially if this has been done bilaterally. In such cases, the prostate tissue is practically indistinguishable at the CT centering scan, due to the lack/distortion of the image caused by the metal prosthesis parts. In these cases, our protocol stipulates the positioning of intraprostatic markers, followed by radiotherapy centering with MVCT using the TomoTherapy System. The expected advantage, fully confirmed by our own experience [5], is that of being able to make a precise localization of the prostate via the markers on an artifact-free image.

However, fiducial markers are contraindicated in the presence of bilateral prostatic calcifications (>7 mm) that are recognizable at centering CT. The markers are not considered indicated in this case because they are jumbled in with the calcifications and so only go to increase the CT "noise." It should be remembered that prostatic calcifications that have a clear-cut posterior acoustic shadow are easily visible at US, while hyperechogenic areas do not have a posterior shadow and so appear isointense at CT.

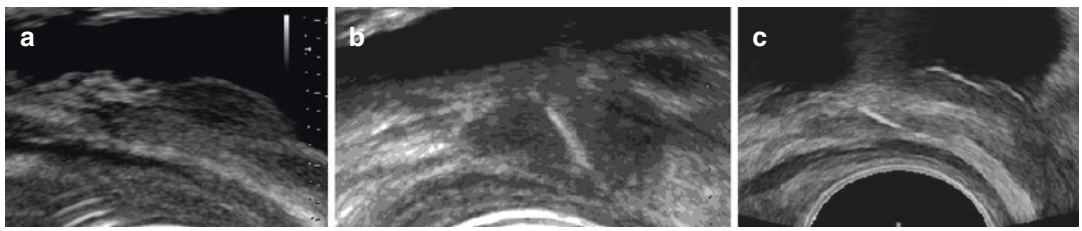

Fig. 30.1 Local recurrence (10 mm) after radical prostatectomy, confirmed by histology (**a**). After single fiducial marker implantation (gold, 12 mm) (**b**). The same case, after 5 years (**c**) with tissue athropy

30.2.2 Patient Preparation and Materials Needed

Patient preparation is just the same as for transrectal prostate biopsy: the patient will use a microenema in the morning of the procedure. Antibiotic prophylaxis is indicated, as it is for biopsy, to be started the day of the examination and continued for 3–4 days after the implantation. A few days before, the radiotherapist will have provided the patient with the specific informed consent form, illustrating the relative risks and benefits that must be signed prior to commencing the procedure.

Unless contraindicated, there will be suspension of any antiaggregant/anticoagulant therapy 7 days before; if necessary, this can be replaced by low molecular weight heparin. The hemorrhagic risk during the implant is less than during biopsy. The procedure can be performed without suspending low-dose aspirin therapy.

US-guided implantation of markers can be done by either the transrectal or the transperineal approach. In the latter, a US device with an endocavitary end-fire probe (6–8 MHz) is used, with disposable biopsy forceps. In patients with a history of infections or immune depression, instead, transperineal access using a linear/biplanar probe is advisable.

Transrectal access is the technique most commonly employed nowadays, and no particular complications have been reported. However, it is important to implement all possible precautions to prevent infection; from that standpoint, the transperineal approach is more advantageous. Nevertheless, in our experience, based on more than 100 cases performed using the transrectal technique and adopting proper precautions to prevent infection, no clinically relevant infections were recorded [4].

The materials needed include a local anesthesia needle (21 gauge, 25 cm length for the transrectal approach, spinal needle for the transperineal approach) and three needles containing the gold or carbon fiducial markers, mounted on an 18 gauge cannula that will release the markers, measuring 0.35/0.9 mm in diameter x 3/4 mm in length, as well as an enema with povidone-iodine (2.5 cc in a 2.5 ml syringe), to be administered rectally before the procedure. Carbon markers are preferable if a CBCT is available, because they produce less artifacts than gold markers (Fig. 30.2a), whereas gold is preferable for MVCT TomoTherapy (Fig. 30.2b).

Neither gold nor carbon markers preclude later magnetic resonance imaging.

The examination findings (two copies, one for the patient and one for the radiotherapy unit) will include images and a description of the procedure: sites where the markers were positioned and the technique employed, any complications, and the antibiotic prophylaxis adopted. The marker labels must be attached to the patient's radiotherapy record and archived with the signed informed consent form. The procedure is performed in an outpatient regimen.

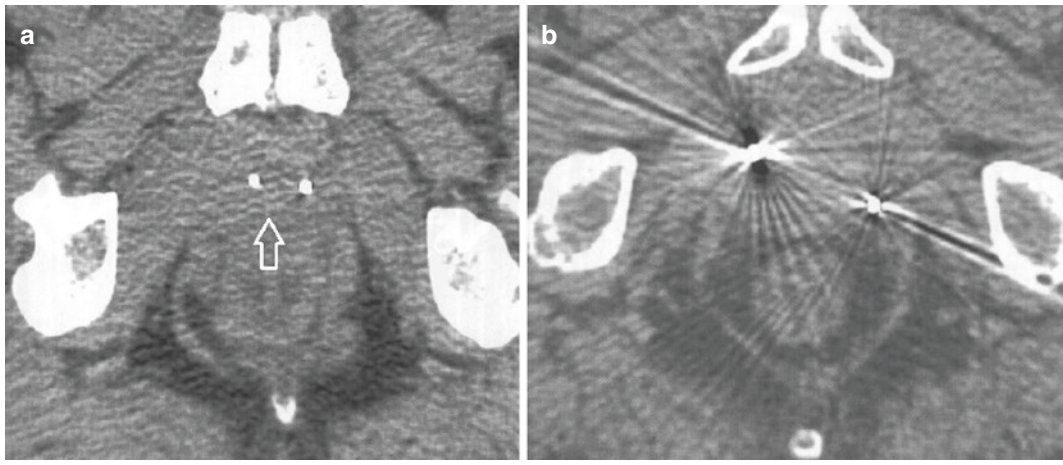

Fig. 30.2 (**a**) Gold marker (*arrow*) image with TomoTherapy (IMRT), the same marker image with IGRT (**b**)

30.2.3 US-Guided Marker Positioning Technique

With the patient in left lateral decubitus, an antiseptic enema with 2.5 ml povidone-iodine is administered immediately prior to the procedure. This can be combined, before starting the procedure, with a local application of anesthetic cream (lidocaine-prilocaine) or lidocaine spray to the rectum and anus as painkiller before probe insertion to ensure patient comfort. Nowadays, hydrophilic gels containing lidocaine and antiseptic (lidocaine and chlorhexidine gel (Farcosedan ®)) are available on the market in prefilled syringes, fitted with a plastic cannula for endorectal insertion of the gel.

The endocavitary probe is introduced, and a periprostatic nerve block is then induced with 10 ml of lidocaine 1 % bilaterally at the vesicle-prostate angle under longitudinal US scanning.

The next steps are to prepare a sterile field, open the preloaded disposable needles (each contains just one marker), and push the needle down through the cannula to release the marker in the prostatic tissue.

The three radiopaque markers (we employ 0.9×3 mm) are positioned under US guidance; by convention, they are placed in the base and apex of the left lobe and mid gland in the right lobe. This arrangement may vary, but it is important in all cases to specify the final positioning in the record and to avoid overlap of the markers (Fig. 30.3).

The markers should lie on different planes, avoiding overlap on the spatial lines uniting them (Figs. 30.4, 30.5, and 30.6).

This spatial distribution is ideal in order to monitor the prostate position and movements. Once the ideal position has been identified with the aid of biopsy tracer on the US screen (Fig. 30.6c), the needle is inserted inside the gland parenchyma, at a depth of about 10 mm from the capsule margin to prevent one end of the marker from remaining in the rectum. The plunger is pushed to release the gold seed through the needle point and the barrel is retracted with the plunger fully inserted. The fiducial marker is left in position. Two scanning plane images are printed to document its position (Figs. 30.4 and 30.5). Once the needle is withdrawn, checked to see that it is empty, it is thrown out, while the product label is attached to the record. If the marker is seen partially inserted in the rectum not the prostate, this suggests a partial spontaneous expulsion. If it is seen to be inserted in the rectum and only partially in the prostate, a US/radiological control is necessary, and endoscopic removal of the marker is advisable with gastroenterologist. The positioning scheme of the markers is decided in concordance with the radiotherapist.

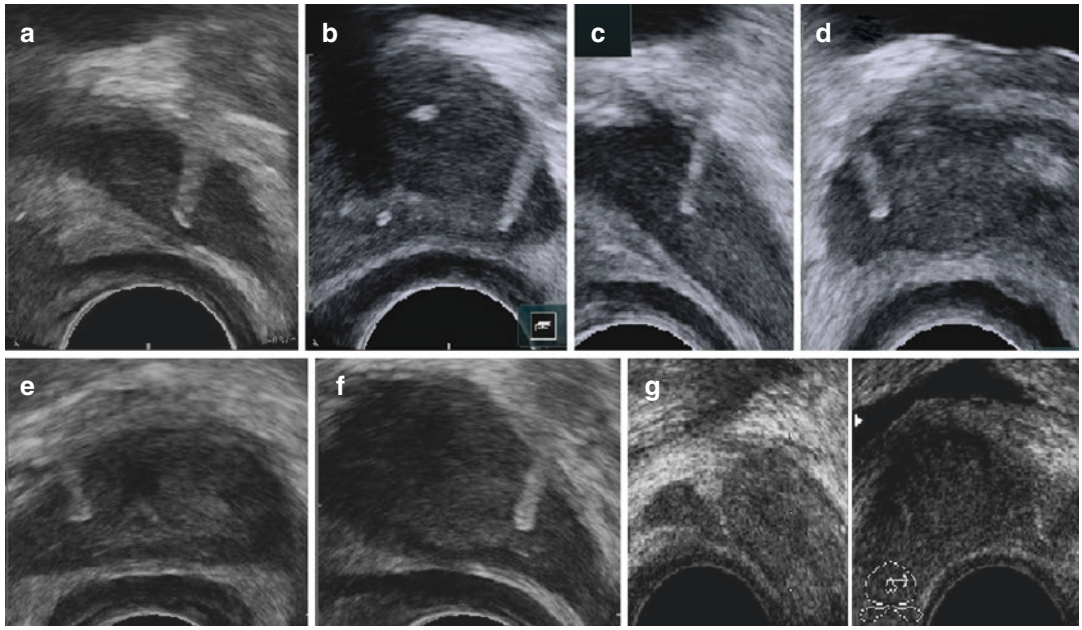

Fig. 30.3 Marker in the left lobe (**a** longitudinal, **b** axial), marker in the right base (**c**, **d**), marker in the right apex (**e** axial, **f** longitudinal). Marker in the left base between the capsule and seminal vesicle (**g**)

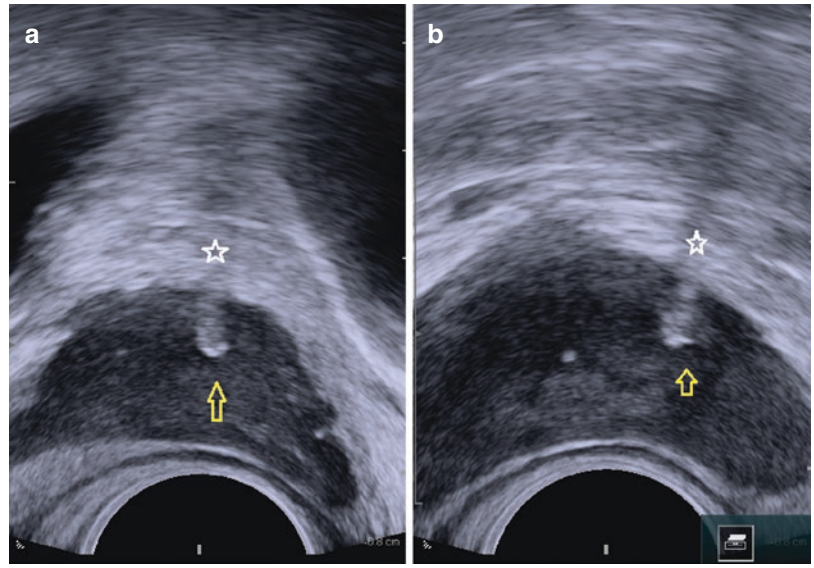

Fig. 30.4 Marker (*arrow*) in the mid left prostate lobe in longitudinal view (**a**) and axial view (**b**) using end-fire probe. Posterior acoustic shadow cone is shown (*star*)

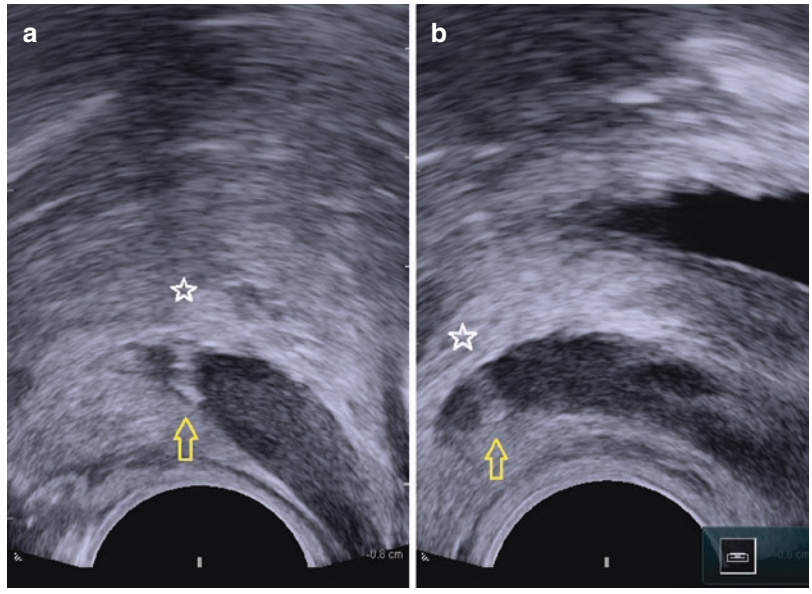

Fig. 30.5 Marker (*arrow*) in the far lateral right base in subcapsular space, longitudinal view (**a**) and axial (**b**), end-fire probe; posterior acoustic shadow cone is shown (*star*)

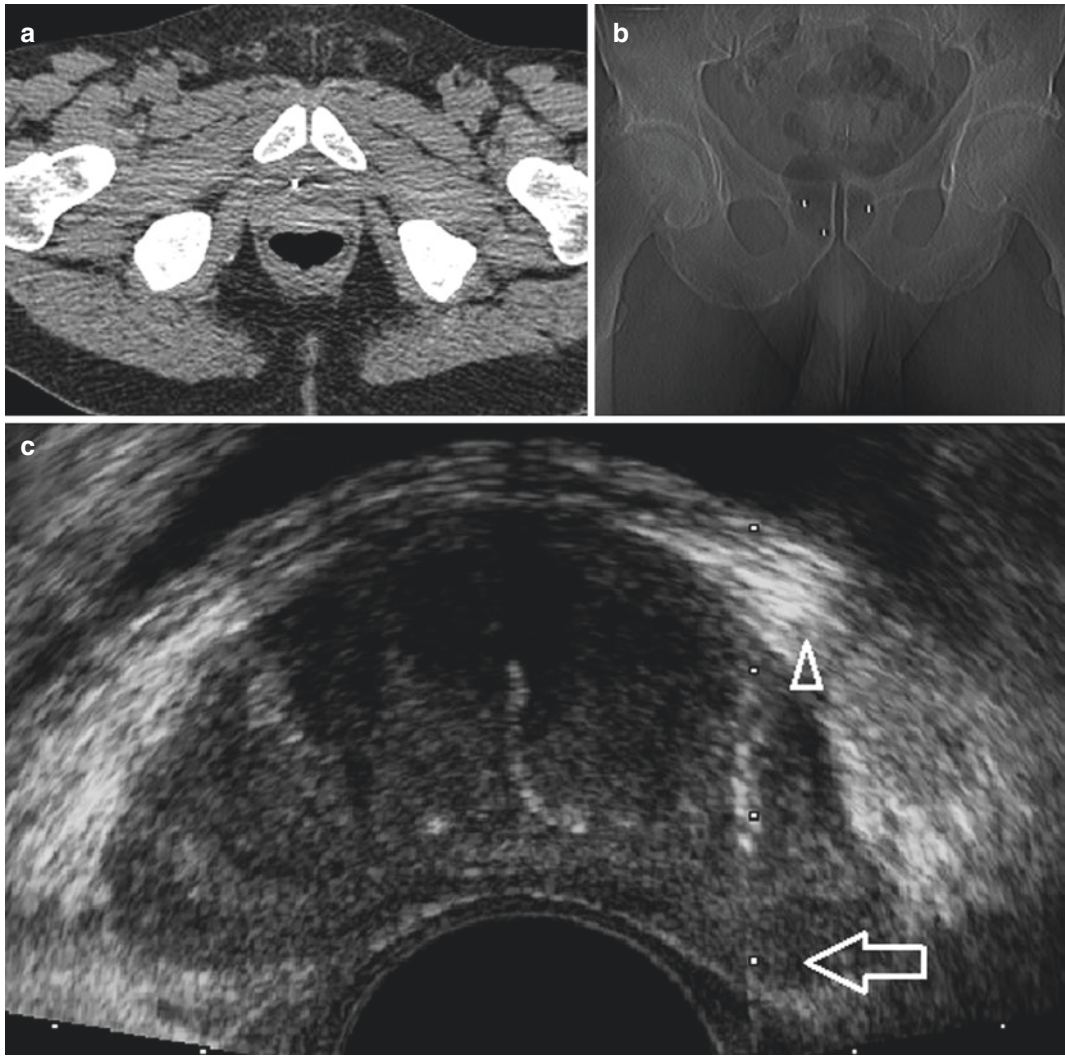

Fig. 30.6 Marker implantation at CT (**a**) and X-ray (**b**). Ultrasound view (**c**) during marker release from the tip of the needle (*arrow*) with posterior shadow cone (*arrowhead*)

30.2.4 Spatial Triangulation of the Markers

The best scheme is termed the "triangulation scheme" that avoids overlap of the markers on the three orthogonal visualization planes. This scheme is successful when only one marker is visualized on each US scanning plane, not two simultaneously. Especially during the learning curve period, it is useful to make fluoroscopic X-ray controls after the procedure to correlate the US and radiographic geometries (Fig. 30.7a, b). In our experience, we did this in the first 50 cases, thereby progressively improving our awareness of when the markers were correctly positioned.

The implantation sequence we adopt is paraurethral right apex, pericapsular/lateral right base, and medial left (halfway between the other two). To improve marker positioning and interoperator reproducibility, it is advisable to follow the biopsy pathway on the US screen. It is also wise to keep some distance away from cysts (that can dislodge the marker) and intraparenchymal small calcifications or hyperechoic areas that could mask it, as well as from the urethral lumen (especially in cases with vesicourethral anastomosis) and anterolaterally from Santorini's anterior venous plexus (that could offer a migration route).

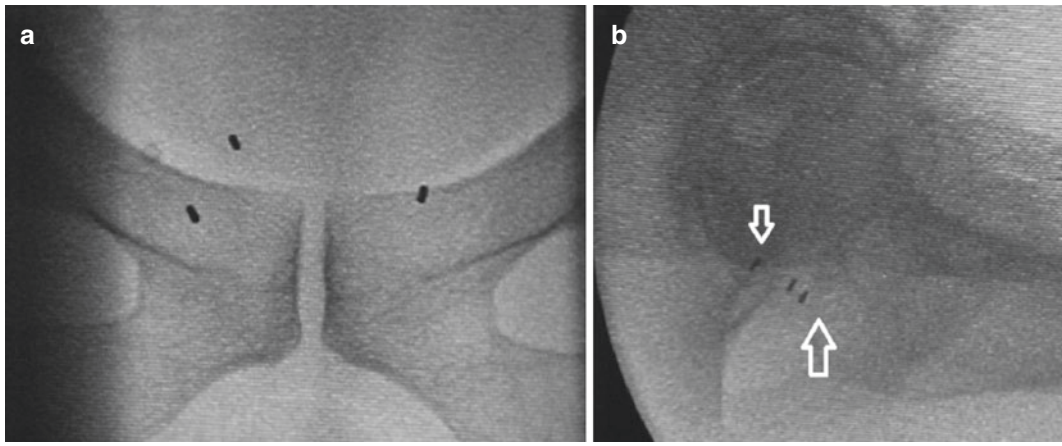

Fig. 30.7 X-ray control (**a** anteroposterior; **b** latero-lateral): exact placement according to spatial triangulation rule – any marker is located on the same spatial plane

30.2.5 Marker Inversion

It can be particularly difficult to achieve the desired triangulation in small glands (<25 cc) or glands with a short latero-lateral diameter (<4 cm). In such cases, it is difficult to insert two markers on the right while keeping the right basal marker higher than the medial left marker, because the space between the two may be so small as to cause overlap. We therefore advise inversion of the basal markers in such cases, positioning the medial marker in the right lobe rather than the left, as far laterally as possible to avoid overlap with the apex (mid) marker, and then inserting the basal marker on the left, as far cranially as possible because if it is not in medial position, being contralateral, it cannot overlap with the apex (mid) marker (Fig. 30.8).

30.2.6 Our Experience and Considerations on the Literature

Both a transrectal and a transperineal technique under US guidance have been described for positioning gold seeds as prostate markers, although the transrectal technique is the most common. Only few authors have reported an endoscopic transurethral technique. The number of prostate markers implanted can vary from 3 to a maximum of 5 [6–9].

In our practice, we have established a standardized technique, positioning three radiopaque markers by transrectal access under US guidance with an end-fire probe. We adopt the "triangulation" scheme described above, releasing markers at the lateral right base, distal right apex, and mid left of the prostate [5].

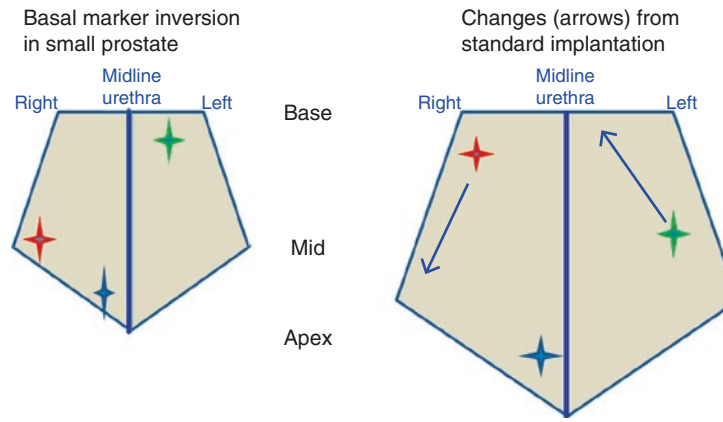

Fig. 30.8 Marker inversion scheme used in small or narrow prostate gland with less than 4 cm in the lateral greatest dimension

This positioning scheme is easily obtained in almost all prostates because the needle is very well visualized and an ample freedom of movement is guaranteed both by the transrectal technique with end-fire probe and by the transperineal technique using a biplanar linear probe, depending on the operator's experience. An exception to this rule is small glands with a reduced latero-lateral diameter, in which we implant one left basal marker, one right apex, and one right medial marker.

Our experience began in 2007; we evaluated results in 78 patients with low-risk prostate cancer and in 12 patients with local disease recurrence after surgery [4]. No major complication (bleeding, infection) has ever occurred after the insertion procedure nor any case of migration of the marker to the urethra or rectum. The optimal triangulation scheme was achieved in 95 % of cases. Minor complications (mild hematuria, hemospermia, and urinary irritant symptoms) were recorded in 10 % of patients. The procedure was well tolerated, with a mean visual analog score for pain of 2 (range 0–7).

In large glands or in cases with moderate to severe urinary obstruction symptoms, combining therapy for prostatic hyperplasia is recommended, with 5-ARIs and alpha-blockers to reduce the gland volume and prevent worsening of the symptoms after the procedure or during the radiotherapy treatment. By contrast, it is not useful to combine therapy with 5-ARIs in patients who have already undergone antiandrogen or androgen suppression therapy.

The advent of radiopaque markers for IGRT has resulted in:

1. A significant reduction in the CTV-PTV as compared to the mean standard margin of 10 mm used before them: 1 mm in the cranial and caudal direction, 3.5 mm anteriorly and 3 mm posteriorly, and 2.5 mm on the right and 2 mm on the left.
2. A mean reduction of PTV by 37 % (range 23–59 %).
3. Very low delayed toxicity, assessed in 57 patients with a minimum follow-up of 12 months (mean 36 months, range 12–89 months): grade 1 rectal toxicity in 8/57 (14 %) and grade 2 in 5/57 (8 %) and grade 1 bladder toxicity in 8/57 (14 %), grade 2 in 1/57 (1.7 %), and grade 3 in 2/57 (3.4 %) using the LENT SOMA assessment scale. Our results are comparable with those in literature [6–9].

Deipolyi et al. [10] reported a 98 % success rate with their technique using three markers in 111 patients with localized disease and a major early complication rate of 0.9 %, while Linden et al. [7] reported a 100 % success rate using 1–3 markers in 98 patients, with no early complication.

Moman et al. [11] have described the largest case series of intraprostatic marker implantation: 914 patients with the transrectal technique and end-fire probe, in which there were 2/914 cases of major early complications (severe infection) and 5/914 cases of marker migration to the urethra or rectum. Kably et al. [12] reported 75 cases, with a 99 % success rate, 1.3 % major complication rate, and 0.3 % of marker migration. Other experiences have been described by Gill et al. [13], Igdem et al. [14], and Langenhuijsen et al. [15], featuring similar results.

As compared to our experience, few studies in literature have quantified a comparable quantity of periprostatic tissue spared IGRT treatment, in terms of reductions in the CTV-PTV margin. Only Langenhuijsen et al. [16] reported a mean CTV-PTV circumference reduction by 3 mm and PTV reduction by 27 %.

It is difficult to make any comparative assessment of the studies of delayed toxicity recorded using this method, because the radiotherapy techniques were different, as were the doses and CTV-PTV margins adopted [17–19].

In any case, if the rectal volume included in the treatment field is too large or else the patient presents particular risk factors for delayed rectal toxicity, it is possible to insert a tissue equivalent between the rectum and the prostate to protect from high isodoses [20]. Prostate-rectum hydrogen spacers offer a better safety margin on the posterior plane, exposing the rectum to less radiation [21], and permit dose escalation to the target without underdosing the PTV and so making the treatment less radical.

Indeed, a combination of these treatments (markers plus spacers) is progressively gaining

ground as an additional option to IGRT/IMRT, in which small treatment volumes are usually adopted, with high dose gradients.

Conclusion

Implanting radiopaque markers in the prostate allows a highly precise localization of the gland with IGRT and hence a correct application of the treatment plan (3D-CRT or IMRT), delivering the maximum planned conformal dose to the target. This offers the clinical advantage of less side effects especially of delayed type.

Latest-generation linear particle accelerators are all fitted with IGRT technology, and this radiotherapy technique is spreading rapidly. In our view, the urologist should know about this field so as to be able to cope with the radiotherapist's needs. The technique is very similar to that of prostate biopsy, and so it has a low learning curve to attain a standardized expertise. We are convinced that it is important for the urologist to have some knowledge of these techniques so as to be able to interact efficaciously with the radiotherapist.

References

1. Dehnad H, Nederveen AJ, van der Heide UA et al (2003) Clinical feasibility study for the use of implanted gold seeds in the prostate as reliable positioning markers during megavoltage irradiation. Radiother Oncol 67:295–302
2. Cardinali M, Galosi AB, Fenu F et al (2011) Adaptative radiotherapy with gold markers to reduce radiotherapy-related toxicity in low risk prostate cancer patients. Anticancer Res 31:1889–1890
3. Susil RC, McNutt TR, DeWeese TL, Song D (2010) Effects of prostate-rectum separation on rectal dose from external beam radiotherapy. Int J Radiat Oncol Biol Phys 76:1251–1258
4. Lacetera V, Cardinali M, Mantello G, Fenu F, Sbrollini G, Tombolini F, Conti A, Maggi S, Muzzonigro G, Galosi AB (2014) Prostatic fiducial markers implantation by transrectal ultrasound for adaptive image guided radiotherapy in localized cancer: 7-years experience. Arch Ital Urol Androl 86(4):349–352
5. Cardinali M, Mantello G, Fenu F, Costantini S, Scricciolo M, Lacetera V, Muzzonigro G, Galosi AB, Valenti M, Maggi S (2015) MVCT and intraprostatic markers make feasible the treatment of patients with bilateral hip prosthesis. Anticancer Res 35:3703–3704
6. Shirato H, Harada T, Harabayashi T et al (2003) Feasibility of insertion/implantation of 2.0-mm-diameter gold internal fiducial markers for precise setup and real-time tumor tracking in radiotherapy. Int J Radiat Oncol Biol Phys 56:240–247
7. Linden RA, Weiner PR, Gomella LG et al (2009) Technique of outpatient placement of intraprostatic fiducial markers before external beam radiotherapy. Urology 73:881–886
8. Shinohara K, Roach M 3rd (2008) Technique for implantation of fiducial markers in the prostate. Urology 71:196–200
9. Henry AM, Wilkinson C, Wylie JP et al (2004) Transperineal implantation of radio-opaque treatment verification markers into the prostate: an assessment of procedure related morbidity, patient acceptability and accuracy. Radiother Oncol 73:57–59
10. Deipolyi AR, Mueller P, Efstathiou J et al (2013) Transrectal ultrasound-guided prostate fiducial marker placement for prostate localization during external beam radiotherapy: a safe and reliable procedure. J Vasc Interv Radiol 24:S98–S99
11. Moman MR, van der Heide UA, Kotte AN et al (2010) Long-term experience with transrectal and transperineal implantations of fiducial gold markers in the prostate for position verification in external beam radiotherapy; feasibility, toxicity and quality of life. Radiother Oncol 96:38–42
12. Kably I, Bordegaray M, Shah K et al (2014) Single-center experience in prostate fiducial marker placement: technique and midterm follow-up. J Vasc Interv Radiol 25:1125–1132
13. Gill S, Li J, Thomas J et al (2012) Patient-reported complications from fiducial marker implantation for prostate image-guided radiotherapy. Br J Radiol 85:1011–1017
14. Igdem S, Akpinar H, Alço G et al (2009) Implantation of fiducial markers for image guidance in prostate radiotherapy: patient reported toxicity. Br J Radiol 82:941–945
15. Langenhuijsen JF, van Lin EN, Kiemeney LA et al (2007) Ultrasound guided transrectal implantation of gold markers for prostate localization during external beam radiotherapy: complication rate and risk factors. Int J Radiat Oncol Biol Phys 69:671–676
16. Langenhuijsen JF, Smeenk RJ, Louwe RJ et al (2011) Reduction of treatment volume and radiation doses to surrounding tissues with intraprostatic gold markers in prostate cancer radiotherapy. Clin Genitourin Cancer 9:109–113
17. Al-Mamgani A, Heemsbergen WD, Peeters ST et al (2009) Role of intensity-modulated radiotherapy in reducing toxicity in dose escalation for localized prostate cancer. Int J Radiat Oncol Biol Phys 73:685–691
18. Zelefsky MJ, Levin EJ, Hunt M et al (2008) Incidence of late rectal and urinary toxicities after three-dimensional conformal radiotherapy and intensity-modulated radiotherapy for localized prostate cancer. Int J Radiat Oncol Biol Phys 70:1124–1129

19. Mantello G, Fenu F, Vagnoni B et al (2015) Intraprostatic fiducial markers' stability during radiation treatment. Anticancer Res 35:3700–3701
20. Pinkawa M, Piroth MD, Holy R et al (2013) Spacer stability and prostate position variability during radiotherapy for prostate cancer applying a hydrogel to protect the rectal wall. Radiother Oncol 106:220–224
21. Eckert F, Alloussi S, Paulsen F et al (2013) Prospective evaluation of a hydrogel spacer for rectal separation in dose-escalated intensity-modulated radiotherapy for clinically localized prostate cancer. BMC Cancer 13:27

Ultrasound Guided Treatment of Prostatic Cancer: Cryoablation

31

Andrea Benedetto Galosi and Luigi Quaresima

31.1 Introduction

Prostate cryoablation was introduced in the clinical practice in 1995. Thanks to the intraoperative ultrasound imaging control, it was among the first treatment echo-guided approach in urology. The role of ultrasound is essential both for verifying the positioning of cryoprobes and for monitoring the freezing phases. The liquid nitrogen, used by the first-generation machines, was then replaced by argon (an inert gas), which is based on the Joule-Thomson effect in the modern cryoprobes. The argon in the transition – from liquid to gaseous – allows to reach temperatures of −180 °C in a very short time.

Nowadays the prostate cryoablation is considered by the European Guidelines 2015 [1] as a possible treatment option (level of evidence 2, grade C) both as a primary treatment of localized prostate cancer and as a salvage treatment in localized prostate cancer relapsed after radiotherapy [2].

A.B. Galosi (✉)
Polytechnic University of Marche Region, Azienda Ospedaliero-Universitaria United Hospitals, Ancona, Italy
e-mail: galosiab@yahoo.it

L. Quaresima
Institute of Urology, Polytechnic University of Marche Region, Ancona, Italy
e-mail: luigiquaresima@yahoo.it

We describe the procedure and the role of ultrasound in the cryoablation treatment, patient selection, and follow-up.

31.2 Ultrasound Criteria for Patients' Selection

Cryoablation has a particular versatility and it is also applicable in large glands or unusual anatomy (median lobe, asymmetric gland, benign prostatic hyperplasia *BPH*) and is not affected by pubic bone anatomy; moreover this technique is less influenced by the restrictions that are related to brachytherapy and high-intensity focused ultrasound (HIFU). Cryoablation is indicated as a primary treatment of prostate cancer (cT1-T2 or limited T3a) and for the treatment for local recurrence after brachytherapy or radiation therapy. The critical analysis of case studies made it possible to identify clinical parameters that influence the cure rate of treatment and predict the zero setting of the PSA with minimum mobility [3, 4]:

The following criteria should be evaluated before cryoablation:

(a) Glandular volume ≤45 cc at the moment of treatment; the neoadjuvant hormonal therapy may be used to reduce the volume [5].
(b) The absence of the third lobe with intravesical prostatic protrusion more than 14 mm, as this tissue could survive to the freezing or

P. Martino, A.B. Galosi (eds.), *Atlas of Ultrasonography in Urology, Andrology, and Nephrology*,
DOI 10.1007/978-3-319-40782-1_31

request a later resection for obstructive symptoms.

(c) The absence of a large defect of the neck for outcomes of surgery for BPH [6], as this asymmetry frequently may produce freezing of the prostatic urethra with the onset of sloughing syndrome.

(d) The inability to adopt the lithotomy position is a contraindication, for example, a severe arthrosis or the coxal-femoral joint disease.

(e) The absence of widespread glandular calcifications that do not allow the ultrasound monitoring.

(f) The absence of urethral stenosis such as to enable the transit of catheter >16 ch (urethral warmer).

(g) The absence of bulky disease (cT3b/T4 or N+).

The presence or absence of these factors lays the foundation for a correct patient identification suitable to cryoablation.

From an oncologic point of view, other criteria are identified: the indication is for localized neoplasms of stage T1c, T2 up to T3a initially, excluding the bulky and seminal vesicle invasion [7–9].

Cryoablation can be performed under spinal and general anesthesia, in obese subjects with a history of colorectal surgery and/or pelvic radiotherapy, with inflammatory bowel disease or hip replacement. It does not require the use of electric scalpels nor exposes at risk for blood transfusion. It requires a complete bowel preparation, perineal, and suprapubic trichotomy.

31.3 Surgical Technique

Cryoablation requires a transperineal approach for the placement of cryoprobes and an ultrasound monitoring using a biplane probe (convex + linear). The ultrasound image orientation is identical to the CT: in the transverse scanning, the rectum is located at the bottom and at the top the pubic symphysis; the right side is located on the left side of the ultrasound monitor. In the longitudinal scanning, it easily studied the external sphincter, the prostatic apex, and the base.

The positioning of cryoprobes takes place by the transperineal tract with two possible approaches: (1) freehand (Fig. 31.1) and (2) transperineal grid (template or grid like that used for brachytherapy) (Fig. 31.2). The last one has the advantage of reducing the learning curve and reducing intra- and interoperator variability, but the times are longer and it always requires a cystoscopy to check the posterior urethra.

The current cryoablation equipment has the ultrasound probe incorporated in the cryo-equipment and system. The ultrasound probe in the standard technique is supported by the operator, but it is possible to use a stepper to keep the probe in place, letting the surgeon's hands free. The stages of cryoablation are summarized in Table 31.1.

Once diameters of the gland have been measured, the ultrasound images' setting is completed in axial and longitudinal views. Six to ten cryoprobes are inserted in the prostate gland under ultrasound control through perineal pathway (Fig. 31.3). Three to five cryoprobes are inserted in each side depending on the prostate volume, anatomy, and freezing power of cryoprobes that depends on technology and diameter (from 3 or 1.7 mm) (Fig. 31.4). The operating table is set in flat position without inclinations or Trendelenburg position. The procedure takes place with distended bladder (>250 ml) with urethral Foley catheter. The cryoprobes are positioned in order to cover uniformly the gland with temperatures at least below −20 °C and extend their effect to some mm beyond the capsule [6, 9]: whole-gland treatment therefore does not provide a nerve-sparing technique. Subsequently we proceed to the insertion of thermocouples: in the soft tissue close to the capsule at the basal level bilaterally and in the subcapsular prostatic tissue in the apex, one additional thermometer is placed in the external urethral sphincter in the median and suburethral position. From three up to six thermometers can be used. Any additional thermal sensors are positioned in order to evaluate the effect of the freezing process in a target area and to monitor the integrity of the external sphincter muscle. The thermometers are positioned in key points, at the edges of the gland to ensure homogeneous and complete ablation reaching target temperatures. Temperature control and ultrasound images provide the operator with an important feedback during the freezing procedure stages.

The urethroscopy is necessary in the learning phase or if a transperineal grid to place cryoprobes has been used. A flexible urethroscopy is useful to verify whether the cryoprobes are not penetrated into the lumen of the urethra, while insertion in the bladder is avoided using ultrasound control. At this stage, some surgeons insert a suprapubic catheter as an alternative to transurethral catheter. In our experience with the freehand technique, the ultrasound control is sufficient to exclude accidental transurethral placements [10]. We do not use routinely the suprapubic catheter.

Once the cystoscope is unthreaded, the guidewire is inserted on the warming catheter at 37° (called urethral warmer) which is useful to avoid damage of the urothelium and mucosa of the prostatic urethra. Leaving viable mucosa on the prostatic urethra prevents the urethral necrosis that is also called sloughing syndrome.

The freezing process begins with the activation of the gas Argon in the cryoprobes, starting from the anterior ones and then activation of probes located in the posterior/peripheral zone. This procedure aims to create an ice ball that gradually joins and reaches the peripheral area and incorporates the capsule. It is easy to monitor the freezing process by ultrasound, because the ice reflects the ultrasounds and appears as a thin, sharp hyperechoic edge with dark posterior acoustic shadow (Fig. 31.5). The temperature at

the level of the hyperechoic edge of the ice ball is equal to the freezing water (0°/−5 °C). The ice growing is ultrasound monitored both in axial and longitudinal planes until the posterior capsule, the apex, and the base are covered by the hyperechoic edge. Meanwhile the freezing power is modulated in order to avoid an excessive increase toward the sphincter and Denonvillier's fascia on the rectum. The Denonvillier's fascia which covers the rectal adventitia is recognizable by ultrasound and should be always free from the ice ball edges (Figs. 31.6, 31.7, and 31.8). The first freezing cycle reaches temperatures about −40°/−20 °C in target areas for at least 5 min. Once the first cycle has been completed, it starts the heating stage of cryoprobes by activating the circulation of the helium gas; this stage takes 15 min. The ultrasound monitoring shows during this phase the almost complete disappearance of the ice ball, and the glandular parenchyma comes back visible, as well as temperatures return all above zero. The second freezing cycle takes place right after and takes altogether 15 min reaching the target temperatures. In the end, the cryoprobes are heated to allow an easy removal and are unthreaded. A compressive dressing is applied on the perineum. Finally the urethral warming catheter is removed, which is then replaced by a transurethral catheter using an hydrophilic guide. The time for the bladder catheter removal is about 2 weeks. If the suprapubic catheter was inserted, spontaneous voiding is encouraged after 1 or 2 weeks, and it will be removed soon after the post-voiding residual urine will be less than 50 cc.

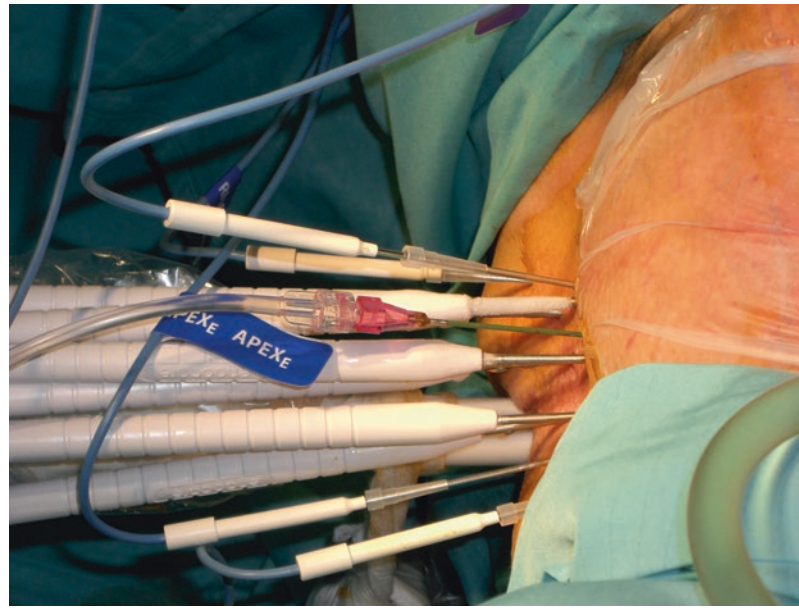

Fig. 31.1 Transperineal placement of cryoprobes using the "freehand technique": cryoprobes (large white tubes) and thermometers (small white tubes with blue wires)

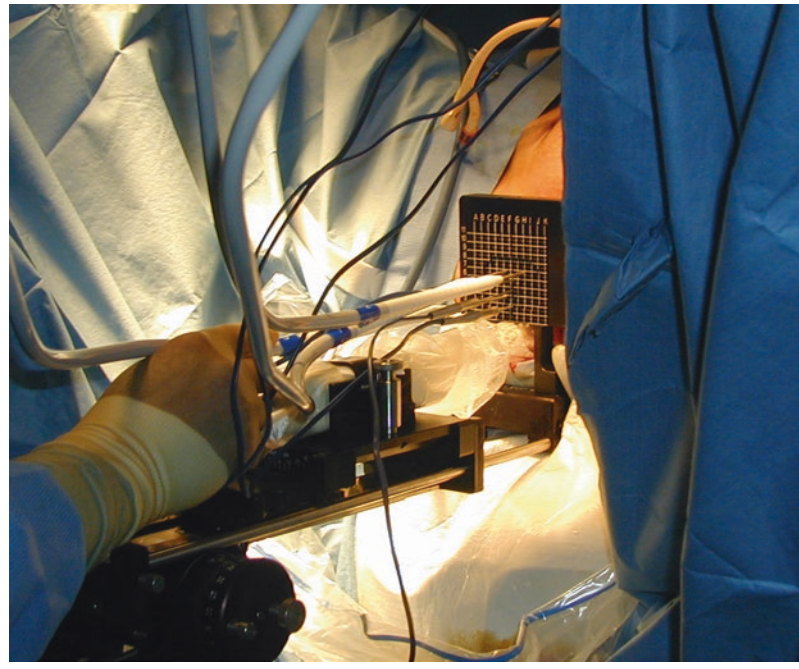

Fig. 31.2 Transperineal placement of cryoprobes using the transperineal grid (template or grid like that used for brachytherapy)

Table 31.1 Stages of cryoablation

1. Ultrasound study of the prostatic anatomy, stepper placement
2. Planning treatment strategy based on real-time transrectal ultrasound
3. Cryoprobes
4. Thermocouple placing
5. Flexible urethroscopy
6. Suprapubic catheter placement [optional]
7. Urethral warmer
8. Denonvillier's dissection (Onik's technique) [optional]
9. 1° Freezing – active heating with helium – 2° freezing
10. Perineal dressing
11. Urethral warmer removal and transurethral catheter placement

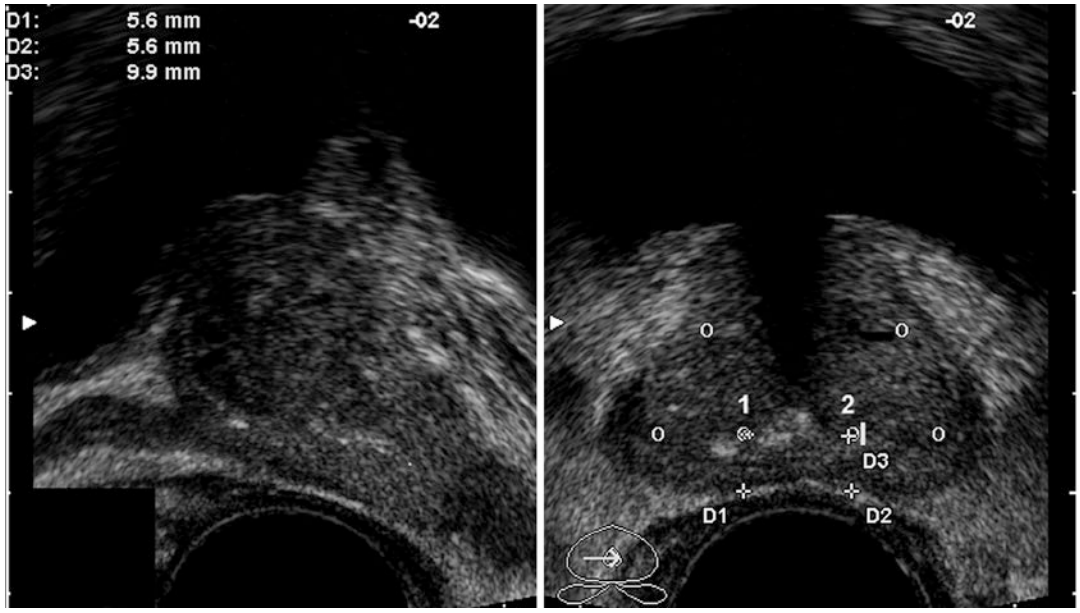

Fig. 31.3 Treatment planning: cryoprobe (*o*) placements based on spatial distribution to obtain ice ball. Distance capsule probe is 5 mm (D1, D2), distance between probes 9.9 mm (D3)

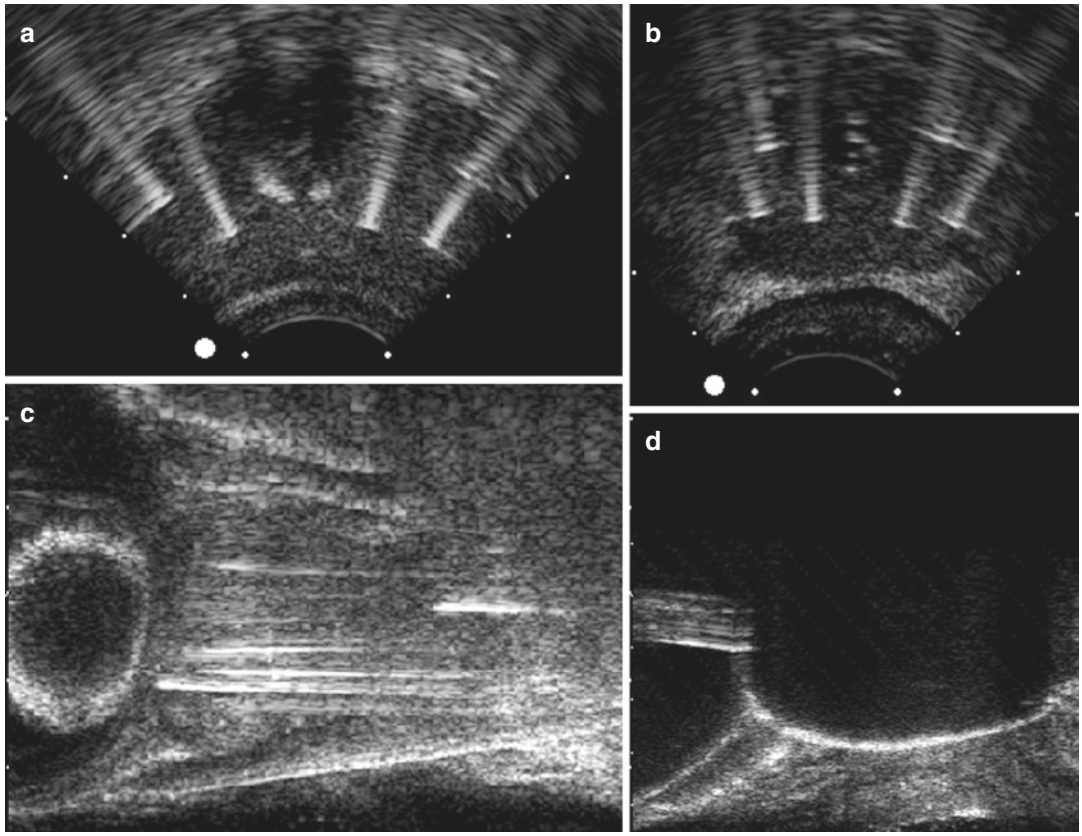

Fig. 31.4 Before cryoablation, the placement of four probes (**a**) or 6 (**b**) in axial view according the treatment planning, longitudinal view (**c**), completed prostate freezing (**d**)

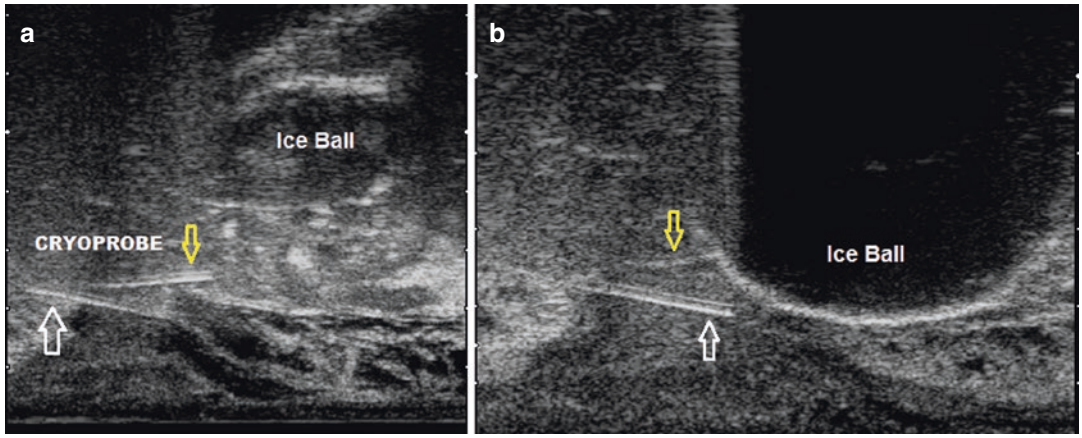

Fig. 31.5 Chiba needle (*white arrow*) to inject antibiotic solution in the space between two layers of Denonvillier's fascia, during and after complete freezing of the prostate. Ultrasound longitudinal view

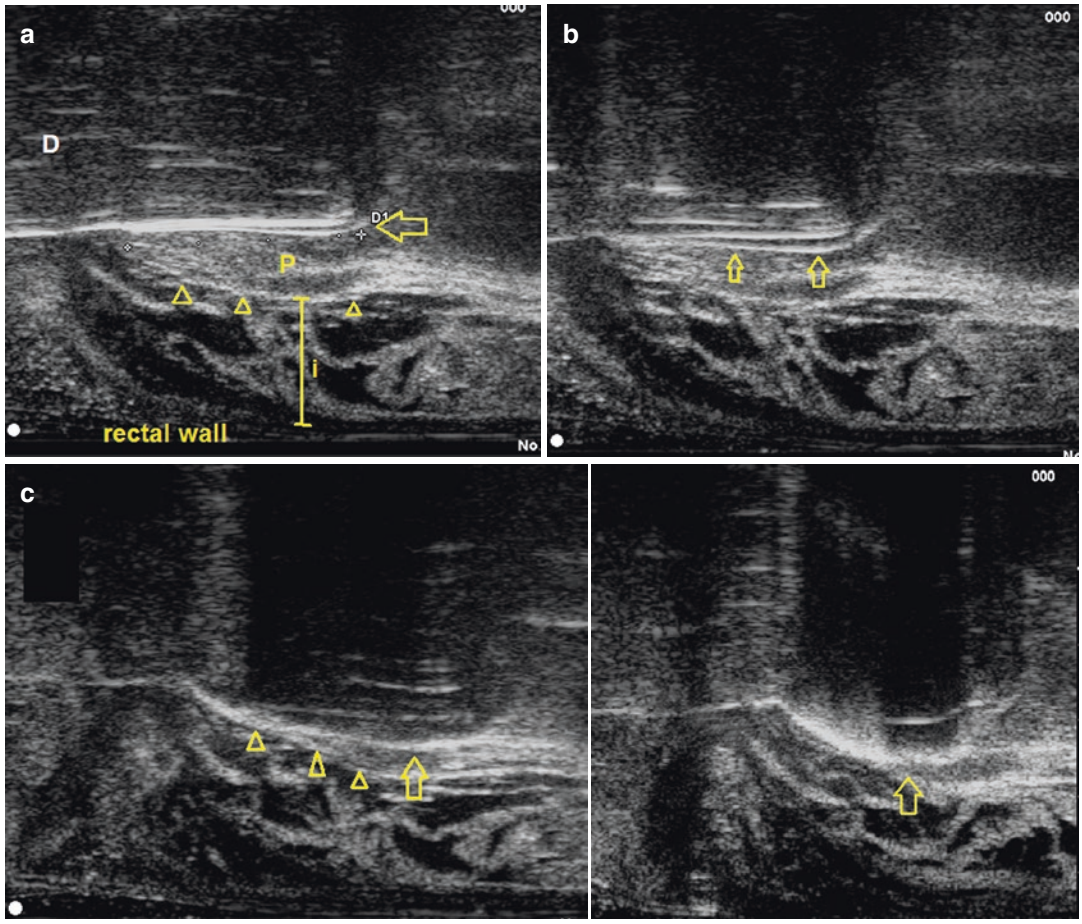

Fig. 31.6 Onik's technique during cryoablation process (longitudinal view): *yellow arrows* show cryoprobe with growing ice ball in the prostate (*P*), prostatic capsule (*arrowheads*), and space between the rectal wall and prostate (*yellow bar*)

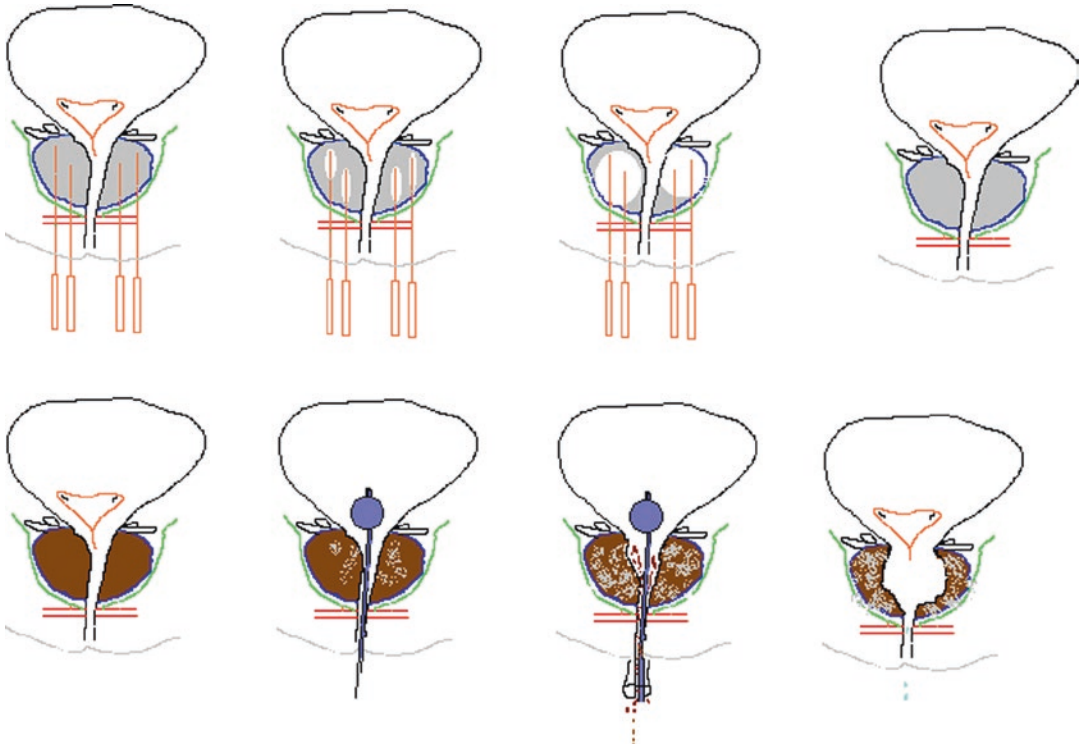

Fig. 31.7 Cryoablation process and sloughing syndrome due to necrosis of the prostatic urethra

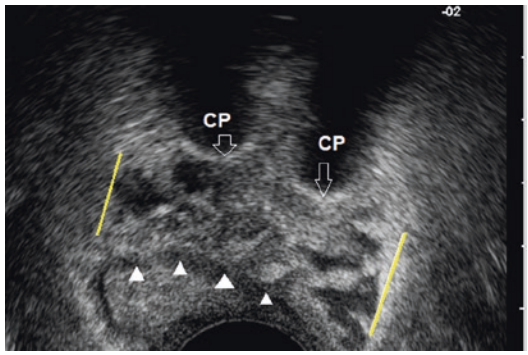

Fig. 31.8 Salvage cryoablation process in axial view: cryoprobe with ice ball (*CP*), space (*yellow bar*) between the capsule and rectal wall (*arrowheads*)

31.4 The Rectal Dissection According to Onik's Technique

The technique was defined by Onik [11] as infiltration of the solution (saline with antibiotic) into the Denonvillier's fascia space; this solution cuts away the tissue and widens the space between the rectum and prostate gland, the aim being to provide extra safety space between these structures. This procedure is performed immediately before the freezing beginning and is repeated between the first and the second freezing cycle.

The rectal wall is from the prostate to have a safety margin from 1 cm up to 3 cm (Figs. 31.5, 31.6, and 31.8). Through a thin needle long at least 12 cm and positioned in transperineal tract under ultrasound guidance, it is injected as a saline solution (60 cc) with an antibiotic (e.g., piperacillin 2 g) in order to increase also the liquid freezing temperature [10]. This space is the same that it is used for the anesthetic injection during biopsies. To facilitate the operation of rectal dissection, it is possible to apply a weight (1 kg) to the ultrasound probe to avoid the compression of the probe on the rectum. This technique is particularly useful in salvage cryoablation for local recurrence after radiation therapy. Using this technique, it is not possible to insert the thermocouple under the Denonvillier's fascia. An alternative procedure for the protection of the rectum is the placement of one to two thermometers in the prerectal fascia.

31.5 Technical Aspects

The cryoablation involves the whole-gland ablation including an oncological safety margin, which exceeds for some mm beyond the prostatic capsule including extraprostatic tissue and parts of the neurovascular bundles. The cryoablation of the prostatic apex occurs constantly in all procedures and it is verified with the presence of one or two thermometers that measure the nadir of temperature included between −20 ° and −40 °C. In cases with longitudinal length >39 mm of the prostate, it may happen that optimal temperatures are not registered in the apex. This phenomenon is linked to 40 mm functional length of the cryoprobes. Therefore it suggested to carry out the procedure of retraction of cryoprobes of 4–5 mm, also called *probe pullback*. This procedure allows to reach optimal temperatures in the apex in the case they have not been reached with the initial treatment planning. During the apex ablation, the temperature of the external urethral sphincter is lowered, but it is good that it never reaches temperatures below 0 °C. The only area, which remains at nonlethal temperatures, is the periurethral one where the warmer maintains the tissue at 37°.

31.6 Focal Ablation

The focal cryoablation of the prostate is considered a targeted treatment only in controlled clinical trials [12–14]. There are possible technical changes in order to save and spare from treatment healthy prostate tissue: true focal (target area plus mm of tissue around), regional (hemiablation, quadrant, hemiablation plus quadrant), or subtotal ablation (saving of the neurovascular bundles and subcapsular tissue). All these prostate-sparing treatments are defined as focal therapy.

Even experience with radical whole-gland treatment has shown that small amounts of glandular epithelium can survive to the freezing in particular in peripheral areas located at the edges of the ice ball; this untreated area where prostate tissue may survive to cryoablation seems to be related to several factors:

(a) Anatomical conformation that creates asymmetry or protrusions of the parenchyma at the external limits of the gland
(b) Large gland (>60 ml)
(c) Tissue located in the anterior fibromuscular area or median lobe
(d) Few millimeters of the periurethral tissue for the presence of the warming catheter

(e) Areas that can remain warm as they are related to large blood vessels
(f) Incorrect procedure due to inadequate positioning of cryoprobes or incomplete freezing because of low freezing power

Temperature monitoring using thermometers, experience, and transperineal grid application avoids operator and machine variables. Also the repeated freezing process leading to target temperatures (−40 °C) ensures the definitive ablation of neoplastic and normal cells [15]. The persistence of vital tissue in the periurethral area is not to be considered a failure: it has a low relevance from an oncologic point of view since the periurethral area is a possible site of necrosis (2–10 %) in a later stage [16]. Minimum PSA levels between 0.2 and 0.8 ng/ml may be related to the persistence of vital glandular tissue, but they are easily monitored over the time [17].

31.7 Ultrasound Follow-Up and Complications

After the prostate cryoablation, the eco-structure of the gland varies in relation with the elapsed time from the treatment with fibrotic and regressive phenomena. A final healing appears after 8 months with the disappearance of granulation tissue. The necrosis reabsorption is complete and is replaced by fibrosis. A check is scheduled each 3 months for the first 9 months and then twice a year.

The gland ultrasound volume initially increases in relation to the coagulative necrosis phenomena, edema (Fig. 31.5). The parenchyma is predominantly hypoechoic at the beginning; therefore, the appearance/disappearance of nodules is not clinically relevant soon after cryoablation. A correlation also with the PSA is indispensable. The granulation tissue has an increased consistency than the glandular parenchyma. The role of ultrasound is not relevant because it is not correlated with the oncological outcome, which is mostly monitored through the nadir PSA [17]. Biopsies in the first 6 months after the surgery are not recommended as it increases complications. The only role of ultrasonography in the short term is to exclude the post-void residual urine, to calculate the volume and the appearance of complications: rectal fistulas and sloughing. Rectal fistulas are a rare complication (0–0.9 %); in our experience on 180 cases, it has never been observed. It was observed mostly within the first 2 months with liquid stools, hematochezia, infection, and pain: subjects at highest risk are those who have received a previous radiotherapy. The rectal examination and ultrasound may raise suspicion of fistula, while the urethrocystography, urethra cystoscopy, and rectum endoscopy confirm the fistula and its extent. The healing is sometimes spontaneous with catheterization and parenteral nutrition, but often it requires an intervention based on the extension of the necrosis of the rectal wall.

The sloughing syndrome includes symptoms and signs related to the necrosis of the prostatic urethral mucosa. It occurs in the 1–8 % of cases. The necrosis caused by freezing can be focal or over its entire length. This side effect is a consequence of freezing which also extends to the urethra. Necrotic tissue determines dysuria and lengthens the healing time as necrotic tissue is expelled through the urethra and the necrosis which is in contact with the urine may cause urinary obstructive symptoms, frequency, infections, and sometimes perineal pain. In such cases, the ultrasound aspect is peculiar with the presence of iso-/hyperechoic patchy tissue with hypo-/anechoic lines with liquid and soft texture. In the short-term follow-up, it is good to report any hypo-/anechoic collections attributable to liquefaction both in intra- and in extraprostatic area. These are not abscesses but collections of necrotic tissue with variable fluid component [18]. A correlation with rectal examination should be performed. The treatment of sloughing is conservative (bladder catheter) and resolute in most cases. Only after 3 months, for a complete demarcation of necrotic tissue, in case of necessity, a resection and endoscopic toilet only of the necrotic part can be performed.

In the follow-up >1 year [10], the coagulative necrosis of the first months is progressively replaced by fibrous and connective tissue. In the follow-up, the ultrasound anatomy of the prostate is still recognizable although the parenchyma becomes hypoechoic; the capsule remains recognizable like the seminal vesicles and the bladder neck. It can be detected in some cases of anechoic liquid gaps (Figs. 31.9, 31.10, and 31.11). The glandular volume decreases and reaches average values of 10–14 cc. At the rectal examination, the gland is not palpable and the lodge appears empty as after prostatectomy.

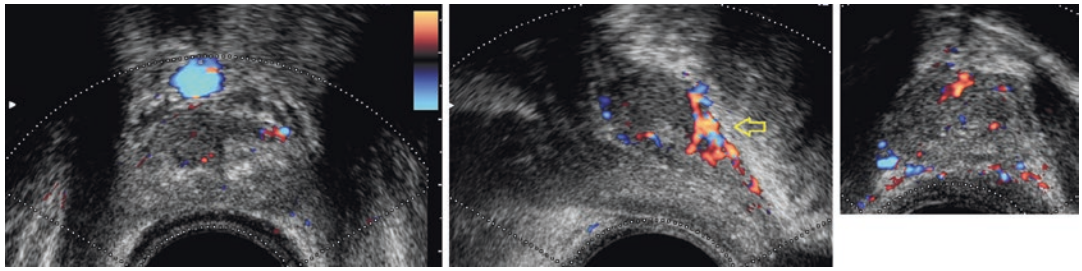

Fig. 31.9 Eco-power Doppler images 18 months after cryoablation, showing absent vascular signal and residual viable tissue in the anterior zone in fibromuscular stroma (*middle*)

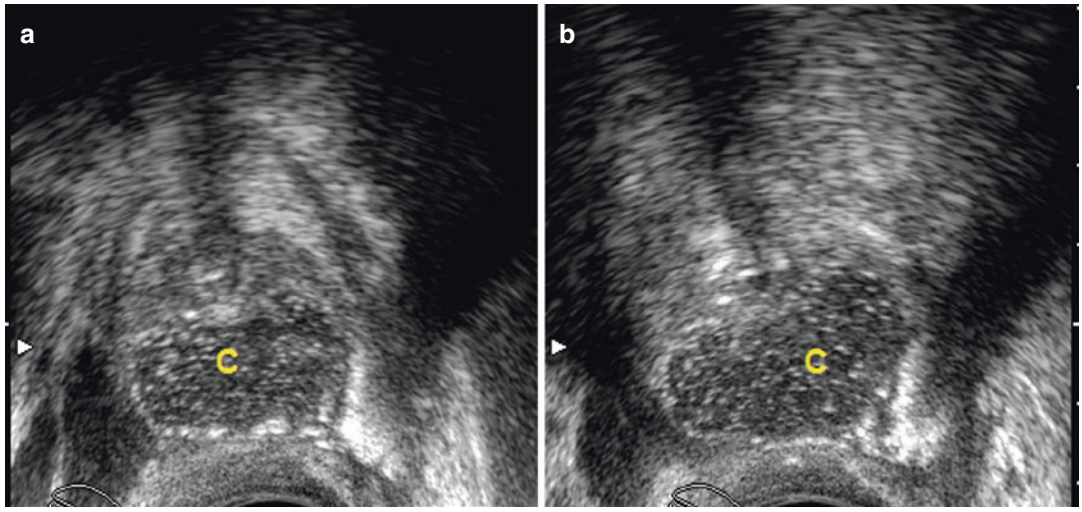

Fig. 31.10 Fluid collection (*C*) after cryoablation due to necrosis and sloughing syndrome (**a**, **b**) axial view

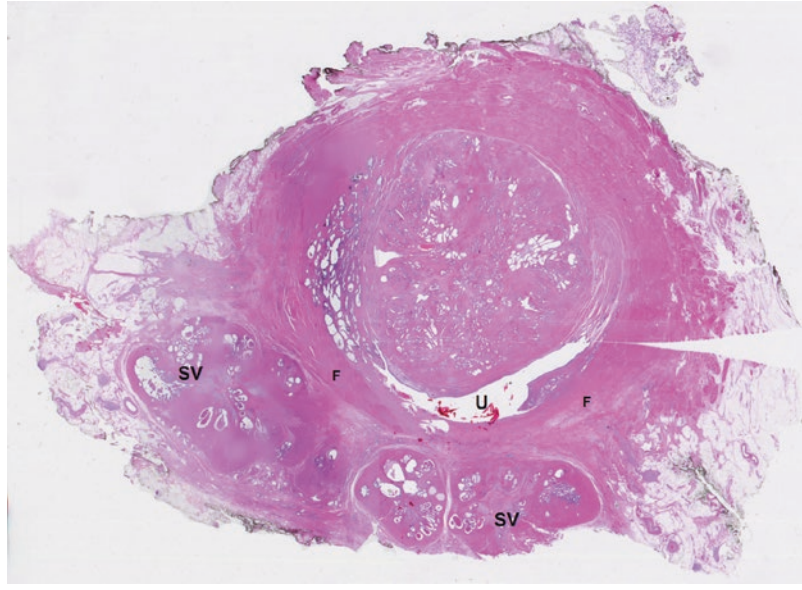

Fig. 31.11 Residual and untreated healthy prostatic tissue in the anterior zone. Histology after cystoprostatectomy performed for bladder cancer in patient who had prostatic cryoablation (*SV* seminal vesicles, *F* fibrosis, *U* urethra)

31.8 Follow-Up

We assess PSA every 3 months for 2 years and then every 6 months for 5 years. Transrectal ultrasound and DRE at 3, 6, 12, and then yearly, while prostate biopsies were performed if PSA value was >0.5 ng/ml or raised in three consecutive determinations. Multiparametric magnetic resonance was carried out before surgery and in the follow-up. Disease-free survival after prostate cryoablation is defined as absence of local or distant relapse and stable serum PSA and PSA value ≤l.0 ng/ml. Biochemical recurrence was defined as serum PSA >1.0 ng/ml or any PSA value raising in three consecutive determinations above 1.0 ng/ml. Local disease recurrence (cancer in postoperative gland biopsy), distant disease progression (metastatic disease assessed by imaging: bone scan, TC or MR, XR).

Distinction between local residual disease after ablation (persistence) from recurrence of disease has to defined. Persistence is identified in patients whose biopsies resulted positive for neoplasia at 6 months of treatment or early PSA failure (3 months PSA >1.0). Recurrent disease (>12 months) is identified in patients who resulted positive for neoplasia after complete clinical and biochemical response after cryoablation.

Viable untreated tissue may be evaluated using high-definition transrectal ultrasound with power Doppler (Figs. 31.9 and 31.11) or multiparametric magnetic resonance [19–21].

31.9 Results

The oncological results in terms of biochemical relapse at 5 years are 88 % for low risk, 80 % for the intermediate risk, and 43 % for the high risk and, at 10 years, 68 %, 74 %, and 36 %, respectively [1, 2, 16, 19]. The rate of positive posttreatment biopsies is variable according to the levels of PSA and varies from 5 to 21 % in different cases [20, 21], in which the biopsy is reserved only where occurs an elevation of PSA> 0.5–1.0 ng/ml. Urinary incontinence is less than 3 %. The erectile dysfunction rate is 60–75 %. The PSA nadir is reached after 3–6 months after treatment. For PSA values, posttreatment comprised between 0.2 and 1.0 ng/ml; it is preferred to have a close follow-up in order to observe the PSA trend, which can be also linked to the persistence of healthy vital tissue, which can also be documented by biopsy carried out not before 6 months. The relapse of disease can be suspected in case of PSA values > 1.0 ng/ml, and in these cases, it is useful to perform a biopsy and/or CT/PET with choline [21].

The relapse is likely high with PSA values ≥ 2.0 ng/ml compared to the nadir after the treatment: in such cases, the local biopsy is recommended in combination with systemic staging.

In case of local relapse documented by biopsy, the possible treatment options are (a) a new treatment of cryoablation that is executable with good chances of success (65 %); (b) external radiotherapy, which is executable without difficulty or increase in complications; (c) hormonal therapy; and (d) monitoring, if PSA values remain stable.

31.10 Palliative Cryoablation and Particular Indication

The cryoablation can be used as a palliative treatment or debulking in cases in which the urinary symptoms are associated with bleeding, pain, or local progression especially in previously irradiated subjects. The haemostatic effect of freezing is known, thanks to the induced thrombosis in the vessels. The indication for these treatments must be evaluated in a multidisciplinary approach and entrusted to expert hands as an alternative to endoscopic resection, the cystoprostatectomy, or selective arterial embolization.

The treatment of local recurrence after radical prostatectomy and adjuvant radiotherapy was performed only on few cases with clear nodules defined by imaging. Oncological results were inconclusive. In our experience, we treated only few patients with cryoablation for nodular biopsy-proven local recurrence after prostatectomy and salvage radiotherapy: both cases showed local and distant failure after 4 years of follow-up.

Conclusions

The cryoablation represents a valid option as primary treatment for prostate cancer in particular in patients unfit for surgery and radiotherapy; it is a versatile treatment that improves obstructive urinary symptoms and has a positive impact on patient quality of life by eliminating the need of hormonal therapy. It is also applicable in elderly patients in whom are precluded further treatments. The salvage cryoablation represents an option for the local relapse after radiotherapy, provided that there is an early diagnosis and that there is not an androgen-independent pathology.

Hemiablation of the prostate using cryosurgery is the most popular technology used for focal treatment of prostate cancer. Evidence is based on case series with different selection criteria and methods of evaluation and treatment protocol. Therefore, focal cryoablation is still considered as experimental and it is allowed in approved clinical trial.

References

1. Heidenreich A, Bastian PJ, Bellmunt J et al; European Association of Urology (2014) EAU guidelines on prostate cancer. part 1: screening, diagnosis, and local treatment with curative intent-update 2013. Eur Urol 65(1):124–137.
2. Wenske S, Quarrier S, Katz AE (2013) Salvage cryosurgery of the prostate for failure after primary radiotherapy or cryosurgery: long-term clinical, functional, and oncologic outcomes in a large cohort at a tertiary referral centre. Eur Urol 64(1):1–7
3. Caso JR, Tsivian M, Mouraviev V, Polascik TJ (2012) Predicting biopsy-proven prostate cancer recurrence following cryosurgery. Urol Oncol 30(4):391–395
4. Levy DA, Jones JS (2011) Impact of prostate gland volume on cryoablation prostate-specific antigen outcomes. Urology 77(4):994–998
5. Grossgold E, Given R, Ruckle H, Jones JS (2014) Does neoadjuvant androgen deprivation therapy before primary whole gland cryoablation of the prostate affect the outcome? Urology 83(2):379–383
6. Ullal AV, Korets R, Katz AE, Wenske S (2013) A report on major complications and biochemical recurrence after primary and salvage cryosurgery for prostate cancer in patients with prior resection for benign prostatic hyperplasia: a single-center experience. Urology 82(3):648–652
7. Ukimura O, de Castro Abreu AL, Hung AJ, Gill IS (2014) Cryosurgery for clinical T3 prostate cancer. BJU Int 113(5):684–685
8. Sverrisson EF, Nguyen H, Kim T, Pow-Sang JM (2014) Primary cryosurgery for clinically localized prostate cancer – do perioperative tumor characteristics correlate with post-treatment biopsy results? Urology 83(2):376–378
9. Chin JL, Al-Zahrani AA, Autran-Gomez AM, Williams AK, Bauman G (2012) Extended follow-up oncologic outcome of randomized trial between cryoablation and external beam therapy for locally advanced prostate cancer (T2c-T3b). J Urol 188(4):1170–1175
10. Minardi D, Polito M, Galosi AB et al (2000) Ultrasound-guided cryosurgery of the prostate: short- and long-term experience. Arch Ital Urol Androl 72(4):270–275
11. Onik G (2001) Image-guided prostate cryosurgery: state of the art. Cancer Control 8(6):522–531
12. Ward JF, Jones JS (2012) Focal cryoablation for localized prostate cancer: a report from the national Cryo On-Line Database (COLD) Registry. BJU Int 109(11): 1648–1654
13. Roach M 3rd (2010) Primary focal unilateral nerve-sparing cryoablation for very early prostate cancer: is it enough or too much, or do we know? Cancer J 16(5):542–543
14. de Castro Abreu AL, Bahn D, Leslie S, Shoji S, Silverman P, Desai MM, Gill IS, Ukimura O (2013) Salvage focal and salvage total cryoablation for locally recurrent prostate cancer after primary radiation therapy. BJU Int 112(3):298–307
15. Robilotto AT, Baust JM, Van Buskirk RG, Gage AA, Baust JG (2013) Temperature-dependent activation of differential apoptotic pathways during cryoablation in a human prostate cancer model. Prostate Cancer Prostatic Dis 16(1):41–49
16. Padilha MM, Stephen Jones J, Streator Smith K, Zhou M, Walker E, Magi-Galluzzi C (2013) Prediction of prostate cancer to urethra distance by a pretreatment nomogram: urethral thermoprotection implication in cryoablation. Prostate Cancer Prostatic Dis 16(4): 372–375
17. Galosi AB, Lugnani F, Muzzonigro G (2007) Salvage cryosurgery for recurrent prostate carcinoma after radiotherapy. J Endourol 21(1):1–7
18. Pitman M, Shapiro EY, Hruby GW, Truesdale MD, Cheetham PJ, Saad S, Katz AE (2012) Comparison of biochemical failure definitions for predicting local cancer recurrence following cryoablation of the prostate. Prostate 72(16):1802–1808
19. Galosi AB, Muzzonigro G, Polito M Jr, Minardi D, Dellabella M, Lugnani F, Polito M (2000) Role of transrectal ultrasonography in the follow-up of patients treated with prostatic cryosurgery. Arch Ital Urol Androl 72(4):276–281
20. Ko YH, Kang SH, Park YJ, Park HS, du Moon G, Lee JG, Yoon DK, Kim JJ, Cheon J (2010) The biochemical efficacy of primary cryoablation combined with

prolonged total androgen suppression compared with radiotherapy on high-risk prostate cancer: a 3-year pilot study. Asian J Androl 12(6):827–834
21. Martino P, Scattoni V, Galosi AB, Consonni P, Trombetta C, Palazzo S, Maccagnano C, Liguori G, Valentino M, Battaglia M, Barozzi L (2011) Role of imaging and biopsy to assess local recurrence after definitive treatment for prostate carcinoma (surgery, radiotherapy, cryoablation, HIFU) Word. J Urol 29(5):595–605

32 Ultrasound-Guided Treatment of Prostate Cancer: High-Intensity Focused Ultrasound

Giario Natale Conti, Antonello Paulesu, and Carmen Maccagnano

32.1 Introduction

Prostate cancer (PC) is the most frequent neoplasm in men over 50 years of age; it represents the second most frequent cause of death from a tumour, following lung cancer, in industrialised countries [1].

The disease shows a large prognostic spectrum, which ranges from the indolent to the lethal form. These two extremes can be cured by two extreme kinds of therapy: "doing nothing" ("active surveillance") and "destroying the prostate" ("radical surgical or radiotherapeutic treatment").

The distance between these two extremes has been covered by the concept of focal therapy (FT). As a matter of fact, the aim of this type of therapy, which is adaptable to every single patient, treats only the affected part of the prostate [2].

For more than 18 years, "prostatic transrectal thermo-ablation" (PTTA) with high-intensity focused ultrasound (HIFU) has been added to the therapeutic arsenal for treating PC [3]. This treatment, with the same aim of therapeutic efficacy as traditional therapy (consisting of surgery and radiotherapy), has different features: minimally invasive, reduced incidence of side effects (in terms of urinary incontinence and sexual impotence), adaptability to the concept of FT, and short hospitalisation. In summary, HIFU therapy requires the prostate tissue to increase in temperature to obtain coagulative necrosis.

The treatment is widespread, especially in Europe and in Japan, with about 500,000 procedures executed in the past 18 years; in the USA, however, a study protocol, approved by the US Food and Drug Administration, is still ongoing [4, 5].

The first instrument available for PTTA/HIFU was the Ablatherm (EDAP-TMS, Lyon, France), which is now in its third generation, to which the Sonablate (FOCUS Surgery, Indianapolis, IN, USA) has been added. Currently, the Ablatherm is more prevalent than the Sonablate, with regard to distribution, number of treatments, number of trials, and publications. The Focal One (EDAP-TMS) was recently specifically proposed for implementing PTTA/HIFU [4, 6].

In 1996, the first treatments with the Ablatherm were carried out in patients with both localised PC and local recurrence after radiotherapy [3]. More recently, the use of PTTA/HIFU has been proposed as FT at the initial stage of PC and as salvage therapy in the case of local recurrence after radical prostatectomy [6].

In this chapter, the principles on which focused ultrasound is based, the history and technical devel-

G.N. Conti (✉) • A. Paulesu • C. Maccagnano
Ospedale S. Anna –Como, Via Ravona, 20,
San Fermo della Battaglia 22020, Como, Italy
e-mail: giario@tin.it

P. Martino, A.B. Galosi (eds.), *Atlas of Ultrasonography in Urology, Andrology, and Nephrology*,
DOI 10.1007/978-3-319-40782-1_32

opment are introduced and the clinical results on the use of HIFU in the treatment of PC are analysed.

32.2 Historical Hints

The first report on the experimental applications of focused ultrasound on biological tissue was published in 1942 by Lynn and colleagues [7].

In the 1950s, the Fry Brothers (Francis and William) studied the possibility of treating neurological disorders, including Parkinson's disease, generating small lesions in the cerebral cortex, using an extracorporeal approach, focusing ultrasound on the area considered to be pathological (Fig. 32.1) [8].

In the 1980s, Lizzi proposed a machine that used focused ultrasound for the treatment of glaucoma and intraocular neoplasms (which was rapidly substituted by a laser; Fig. 32.2) [9].

At the end of the 1980s, the INSERM (French National Institute for Medical Research), the Hospital of Lyon, and EDAP Technomed started a research programme on the interaction of HIFU with tissues. The main aim of this study was the use of focused ultrasound in the treatment of cancers: thus, the Ablatherm prototype, dedicated to the treatment of PC, was created (Fig. 32.3).

The crucial impulse for using HIFU in the treatment of cancers started at the beginning of the 1980s because of the development of diagnostic imaging, which led to the adequate planning and monitoring of treatments, with the help of ultrasound and magnetic resonance imaging.

A first clinical trial begun in 1992 by Gelet and colleagues (Fig. 32.4). This trial reported observations on 12 patients subjected to adenomectomy following prostate therablation with HIFU. The specimen of prostate tissue revealed that the tissue lesions varied according to the ultrasound dosage with homogeneous coagulative necrosis and net margins if used with high dosages. In this study, no major complications were described, but anomalies of rectal mucosa were found in a quarter of the patients [10].

Gelet and colleagues started the first clinical study on patients with PC in 1993; the first results were published in 1996 [3].

Since that moment, the method has been widely distributed, especially in Europe, involved in 30,000 treatments (both as first-line therapy and re-treatment/salvage treatment after radiotherapy failure), using EDAP machines, excluding the Focal One (Fig. 32.5).

Fig. 32.1 Prof. W. Fry

Fig. 32.2 Prof. F.L. Lizzi

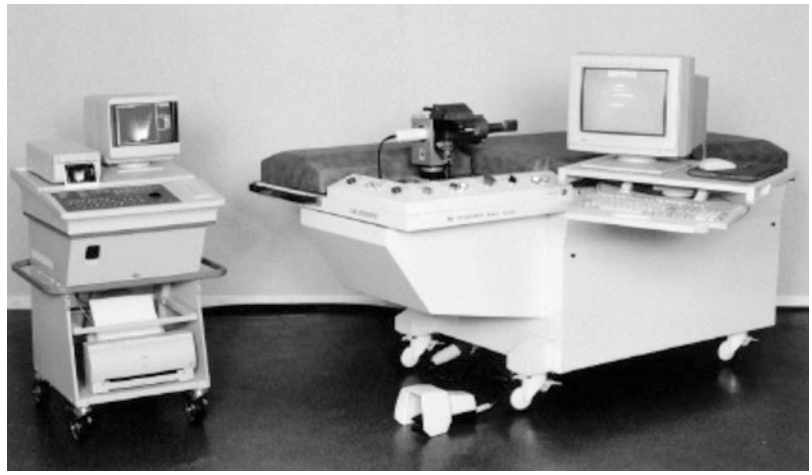

Fig. 32.3 Ablatherm prototype

Fig. 32.4 Prof. A. Gelet

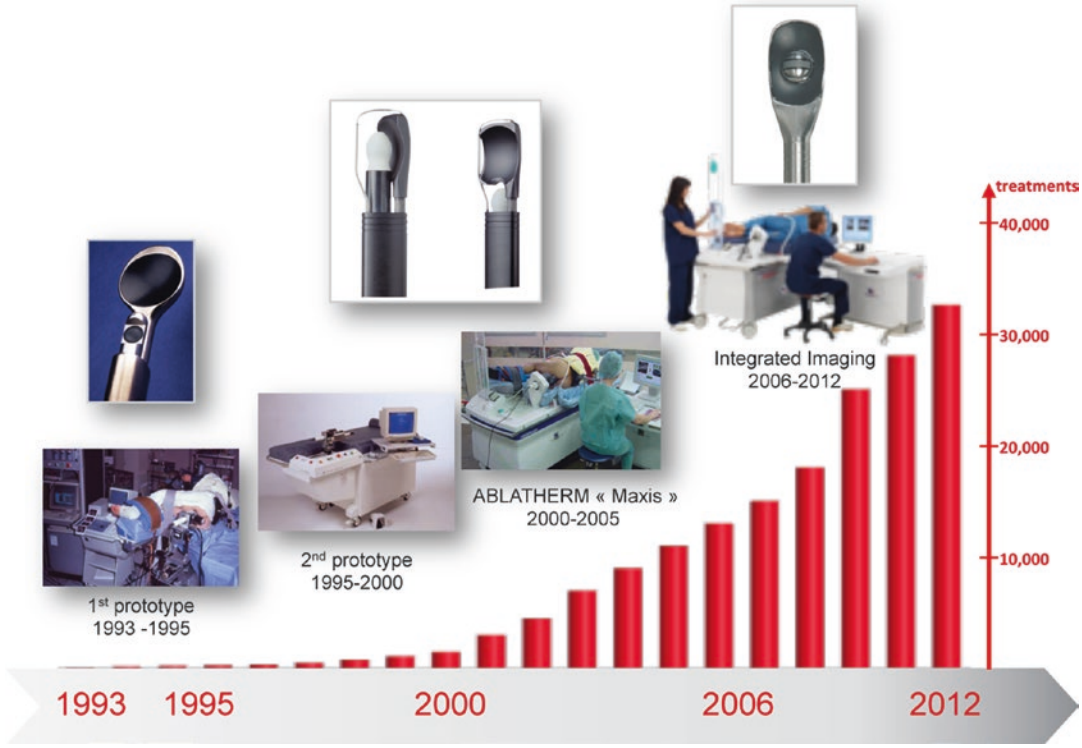

Fig. 32.5 Spread of high intensity focused ultrasound (HIFU) over the last 30 years

32.3 Physics Principles of HIFU

Focused ultrasound is based on the same principles as conventional ultrasound, which are inaudible sound waves with a frequency of > 20,000 Hz. They are generated by a piezoelectric crystal, which vibrates, with a peculiar frequency for the crystal itself, if crossed by electricity. When ultrasound propagates across the human body, the energy also propagates and the waves attenuate; their passage across the tissues determines energy release, which is absorbed by the tissues themselves. This implicates the use in diagnostic imaging of low intensity ultrasound (720 mW/cm^2) to induce minor perturbation in the tissues [11]. Conversely, in the case of HIFU, the high intensity, which ranges from 100 up to 10,000 W/cm^2, and the consequent release of energy, allow tissue damage, which may have therapeutic importance if applied to neoplastic lesions [4].

The HIFU source is represented by a piezoelectric transducer with a spherical shape, which is able to generate and focus ultrasound on a fixed point. According to the voltage used, both the ultrasound frequency (range about 3–4 MHz in the case of HIFU used for thermoablation) and the power applied to the target (values ranging from 1300 up to 2200 W/cm^3) are established [12–14].

32.4 Thermoablation and Mechanism of Action of HIFU

The thermoablation is defined as the necrosis induced in human tissues by the increasing temperature obtained by the transmission of energy and its conversion to heat. The ablation can be obtained with a temperature of 56 °C for 1 s [15, 16]. This exposure causes immediate cell death, because of the denaturation of the protein, damage to mitochondrial enzymes and cell cytosol, and of the formation of histone complexes [17, 18]. Considering the pathological aspect, the damage is typical of coagulative necrosis, followed by secondary fibrotic tissue involvement (Fig. 32.6) [3, 19].

The phenomena of evaporation and carbonisation are typical when the temperature is higher than 100 °C; these are not useful because they limit the transmission of thermal energy and the consequent extent of necrosis in the area (Table 32.1). Thus, the main aim of thermoablative treatments is to reach a temperature of about 65 °C for a few seconds.

Thermoablative procedures are largely used in oncology in the treatment of neoplasm in the liver, lung, bone, kidney, prostate, thyroid, breast and pancreas; the procedures differ from each other because of the transmitting source, which can be electromagnetic waves, lasers, radiofrequencies, microwaves and HIFU. The thermoablative effect of HIFU is caused by the controlled release of a large amount of energy inside the tissue, owing to the increasing intensity of ultrasound waves and focus on a single site. The temperature increases in this way in a well-defined tissue volume and this volume is destroyed because of coagulative necrosis [20].

Thus, HIFU is able to induce an increasing temperature inside the tissue, in the fastest way (few seconds). The intensity, which is very high in the focal area (generally very small), rapidly decreases in the adjacent tissue zones. Starting from this concept, HIFU is causes tissue damage at the focused site, sparing the proximal areas (Fig. 32.7).

There are three mechanisms involved in the generation of tissue damage: thermal effect, mechanical effect and a cavitation effect.

The energy of the ultrasound is absorbed by biological tissues and transformed into heat with the change of the intracellular water into steam (thermal effect). A bubble is then formed with a rapidly increasing temperature and pressure [15]. When the resonance dimension is reached, the bubble implodes and generates cavitation, giving back the accumulated energy to the surrounding space (Fig. 32.8).

Consequently, there are shock waves with high pressure, the release of active free radicals and the manifestation of intense mechanical forces that participate in the determination of tissue damage [18].

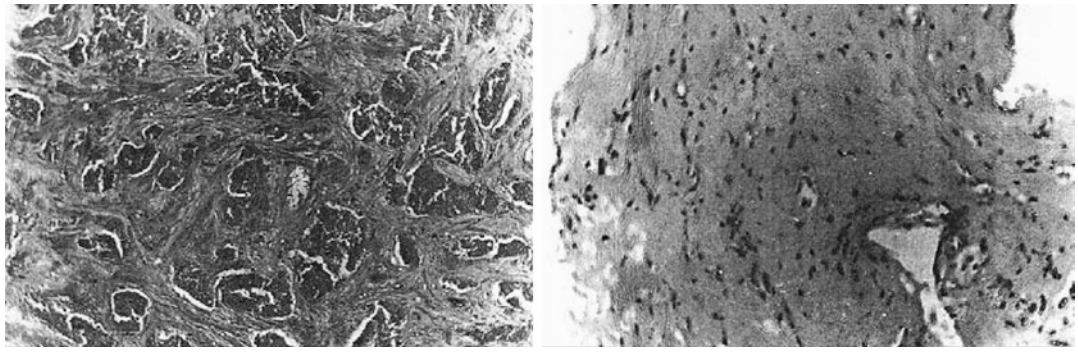

Fig. 32.6 On the *left*, a pathological examination of a prostate biopsy 2 days after HIFU: evidence of coagulative necrosis in the tissue. On the *right*, a pathological examination of a prostate biopsy 3 months after HIFU: the tissue has been completely replaced by fibrosis

Table 32.1 Effects of temperature on the tissues

Temperature (°C)	Biological effect of tissue	Exposure time
>300	Fusion	<1 s
>100	Carbonisation	<1 s
100	Formation of bubbles of vapour, mechanical ruptures	Seconds
56	Denaturation of proteins, coagulation of tissues	Seconds/minutes
>50	Reduction of enzymatic activity, inactivation of the mechanisms of cell reparation	Minutes
42–50	Hyperthermia, destruction of links	Hour/minutes

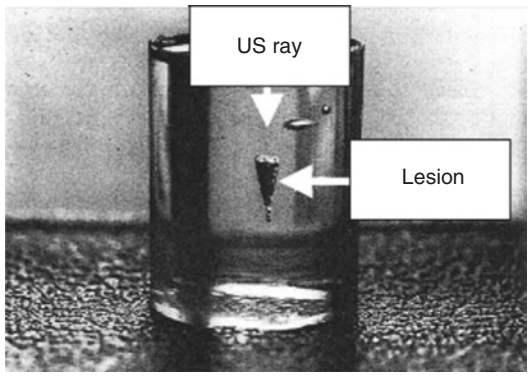

Fig. 32.7 Silicone gum block used as a target to explain the specific form of the elementary lesion. The area around the lesion is uninjured (Reproduced from Chapelon et al. [21])

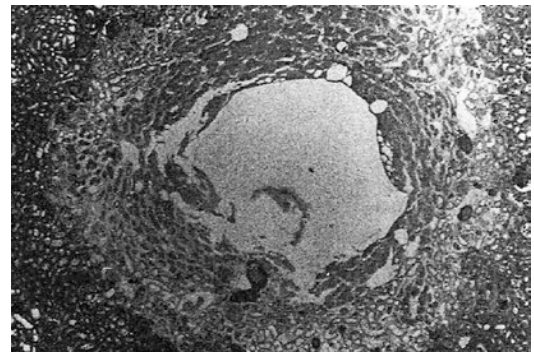

Fig. 32.8 Specimen showing a coagulative necrosis surrounding a cavitation area. The tissue slide comes from a site proximal to the focal point, in a perpendicular plane to the axis of the ultrasound (Reproduced from Chapelon et al. [21])

32.5 Transrectal Prostate Thermoablation with HIFU

One of the peculiarities of HIFU is that it can be applied through the rectum with minimal risk of rectal injury.

The prostate is an ideal target for HIFU because it is located proximal to the anus, with a depth about 1–4 mm, respecting the internal rectal wall, which is not influenced by respiratory movements (Figs. 32.9 and 32.10)

Elementary lesions caused by the HIFU machines currently available for curing PC have an elliptical shape, similar to a cigar (Fig. 32.11), with a maximum volume of about 300 mm^3 and a length that differs according to the machine used, from 5 up to 26 mm and a width of 5 mm [22]. The effects of this kind of energy are summarised in the Table 32.2.

The overlapping of the single elementary lesions allows a homogeneous thermoablation of prostate tissue that has to be treated (Fig. 32.12).

Every single lesion requires 5 s, then a pause lasting a few seconds follows, before a new lesion is generated; the aim is the formation of bubbles, which may interfere with treatment.

It is possible following the treatment, after the planning phase, to monitor the progress of the thermoablation, with regard to both the single lesions in a plane and all the programmed planes (Figs. 32.13, 32.14, and 32.15).

The treatment can be executed under both spinal and general anaesthesia and includes the introduction of a probe into the rectum, the features of which vary according to the machine used. The probe allows both the distribution of ultrasound to the prostate parenchyma and the ultrasound monitoring of the procedure. The position of the patient, on the right side or in the lithotomy position, depends on the type of machine used. The duration of the treatment, which is usually about 2 h, depends on the prostate volume that has to be treated.

When there is a cervical–urethral obstruction caused by glandular hyperplasia, a transurethral resection of prostate (TURP) may be associated with HIFU, even during same surgery. The TURP is also indicated when there are many fibrous calcifications in the prostate, because they may interfere with the diffusion of the HIFU inside the gland; the procedure is also suggested in the case of a large prostate to reduce the dimensions and consequently allow complete thermoablative treatment of the gland [23].

The action of focused ultrasound is already recognisable in the USA because of the hyperechogenicity acquired by the tissue during treatment; instead, the RM represents the best method currently available to evaluate the extent of the necrosis produced by HIFU [24].

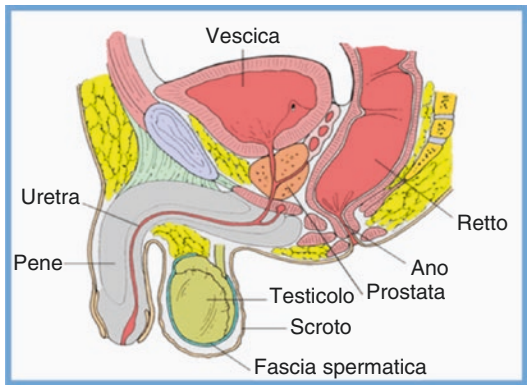

Fig. 32.9 Male anatomy

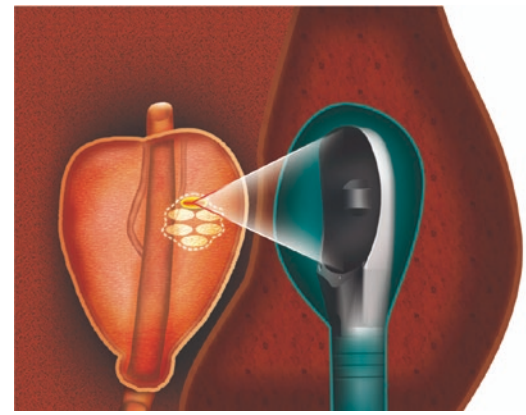

Fig. 32.10 Modality of action of HIFU probe

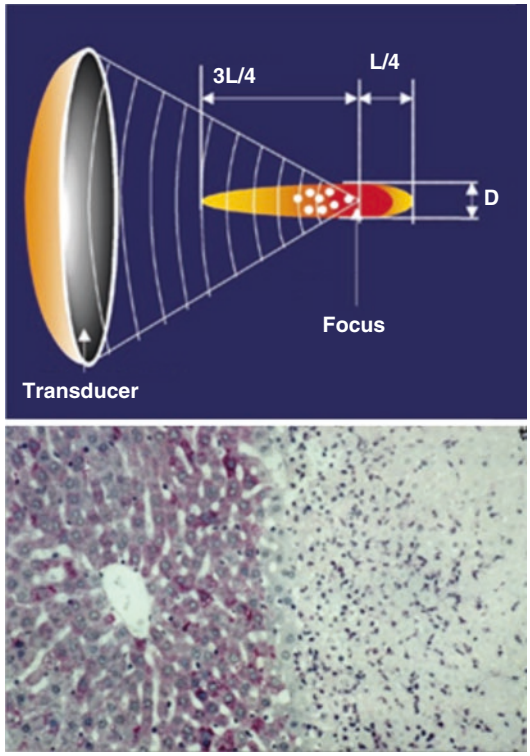

Fig. 32.11 Modality of action of HIFU probe and tissue variation

Table 32.2 Effects of high intensity focused ultrasound (HIFU) energy

Thermal	Mechanical	Tissue
Heat induction into the focus	Generation of bubbles	Immediate: coagulative necrosis
Rapidly increasing temperature (>80 °C) induction into the focus	Collapse of the cavities	After 7 days: inflammatory response
	Rupture of the cell membranes	After 14 days: induction of fibrosis

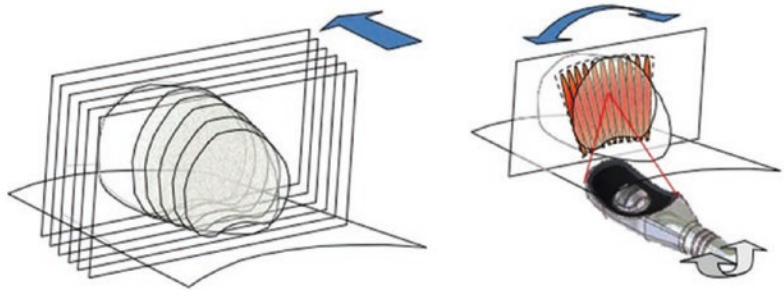

Fig. 32.12 Overlapping of the elementary lesions to cover the whole desired volume

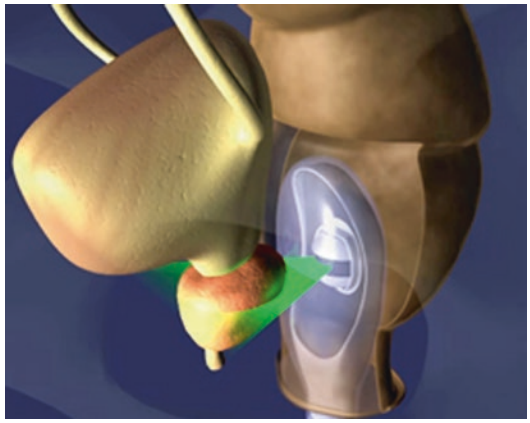

Fig. 32.13 First phase of the treatment: planning

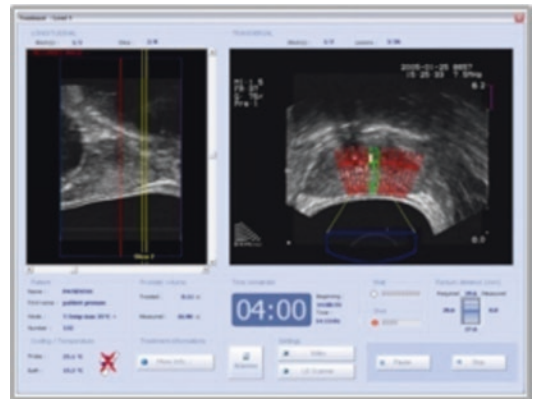

Fig. 32.15 Third phase of the treatment: treatment

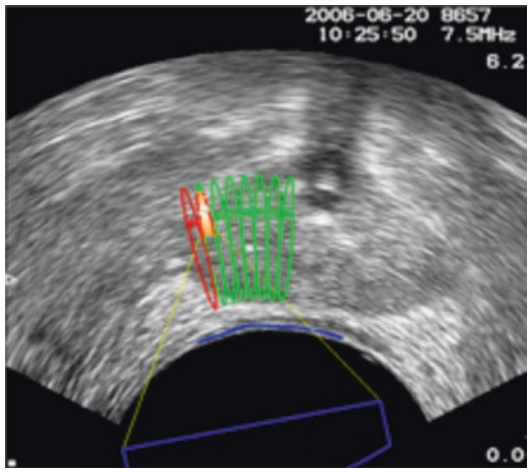

Fig. 32.14 Second phase of the treatment: imaging

32.6 Machines

The machines currently available are: the Ablatherm® (EDAP-TMS), the Sonablate® (SonaCare Medical, Charlotte, NC, USA), and the Focal One® (EDAP-TMS).

Ablatherm Starting from the prototype in 1995 [3], in 2000, the Ablatherm Maxim was launched as the first commercial machine used in clinical practice, and in 2005, Ablatherm Integrate Imaging was created. The latter, compared with previous models, is equipped with dedicated software for patients previously subjected to radiotherapy and previous thermoablative HIFU. The probe is also equipped with a transrectal probe, the end of which has both therapeutic (3 MHz), focusing at 40 mm and ultrasound (7.5 MHz), and real-time visualisation during treatment. The Ablatherm executes the treatment in a single event with elementary elliptical lesions 19 up to 26 mm long in an anterior–posterior plane and only 5 mm wide.

Sonablate The Sonablate 500 is the most recent SonaCare model and is equipped with a unique 4-MHz transducer for ultrasound visualisation and treatment. It is equipped with multiple probes with different focusing (25–45 mm), and every single probe is able to produce elementary lesions 10 mm long in the anteroposterior plane. This implies the necessity of executing more than one step to treat the entire prostate volume using more than one probe during a single treatment.

Focal One The Focal One is a new-generation machine, projected to better satisfy the needs of FT. A transducer with dynamic focusing (dynamic focused transducer) consists of 16 isocentric rings that allow eight focal points simultaneously with a transducer distance ranging from 32 to 67 mm. The elementary lesion produced at every single point is about 15 mm in length; starting from this, there is the possibility of treating prostatic anteroposterior diameters of 15–40 mm. The activation of all eight focal points, or only a few of them, allows the treatment to be modelled as desired, with lesions that may be inserted at every site of the gland. The Focal One allows the acquisition of RM imaging, which can be combined with the ultrasound images for better planning of treatment. Moreover, ultrasound study with contrast medium in the form of microbubbles administered during the procedure is possible (Sonovue®, Bracco, Switzerland): the absence of vascularisation in the treated sites may confirm the adequacy of the treatment.

A refrigeration system for the rectal wall is included in all the machines, to protect it from thermal damage; there are also safety systems that are able to identify any movements in the patients and to monitor the distance between the transducer and the rectal wall (Figs. 32.16, 32.17, and 32.18).

The Ablatherm is equipped with a bed where the patient is on the right-hand side with flexed knees; the Sonablate and Focal One use a standard operating bed with the patient in the lithotomy position in the former and on the right-hand side with flexed knees in the latter.

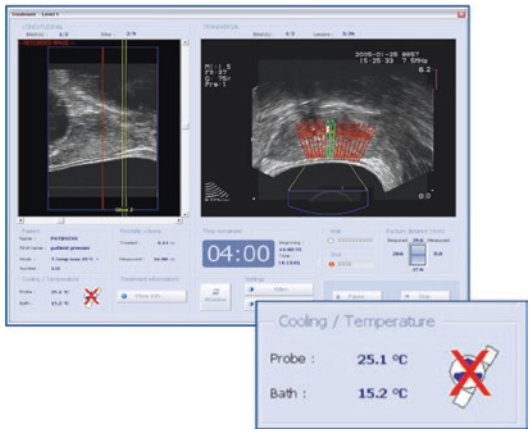

Fig. 32.16 Safety control: temperature

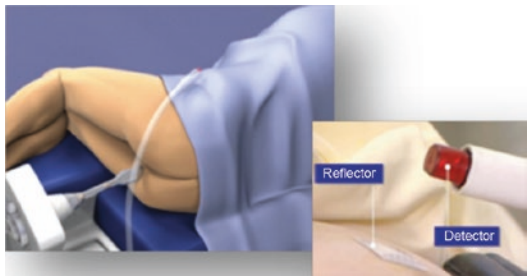

Fig. 32.17 Safety control: movements

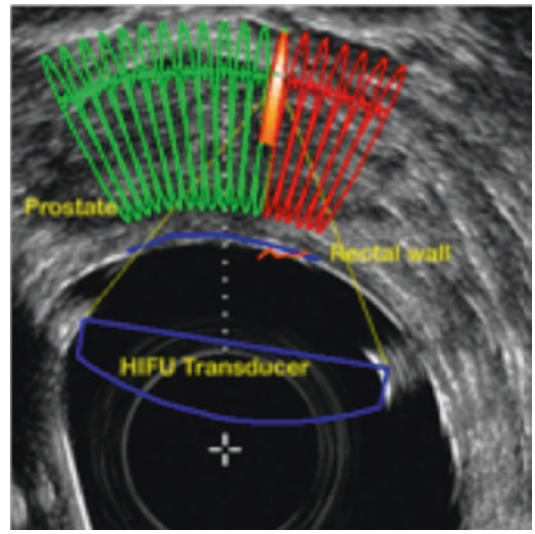

Fig. 32.18 Safety control: rectal wall

32.7 Main Indications for Treatment

Over the last few years, the indications for and the limits of HIFU have gradually been defined. In summary, it is possible to establish the indications that are currently available.

Primary Treatment This mainly addresses localised neoplasms with a low or intermediate risk: T1–T2; Gleason 3+3, 3+4, 4+3, iPSA <10 ng/mL or 10–20 ng/mL. HIFU is also possible for patients with locally advanced cancer, but with the aim of neoplastic debulking rather than oncologically radical results.

Salvage Treatment First, failure after external radiotherapy (and after brachytherapy in selected cases) is becoming the standard indication for this category of patients. A salvage treatment is possible after the failure of the first HIFU. Treatment after surgical failure is possible, although more difficult. In these cases, the decisive factor is the presence or absence of a definite and distinguishable lesion that may be the target of the treatment.

Data published by Gelet and colleagues, on 290 patients subjected to HIFU after radiotherapy failure, reported a 5-year cancer-specific survival of 80 % and a 5-year metastasis-free interval of about 79.6 % using the specific parameters for post-radiotherapy treatment (Fig. 32.19). Moreover, the side effects, in this setting of patients, have been described as limited. In particular, the incidence of urinary incontinence of first, second and third grade was about 25 %, 11 % and 8 % respectively (Fig. 32.20). Urinary obstruction showed an incidence of about 12 %. Urethral–rectal fistulas are sporadic events (0.4 %), similar to pubic osteitis (2.5 %) [25].

Focal Treatments Focal treatments constitute the most promising future development, especially with the use of the new robotic technologies or imaging fusion. Moreover, the efficacy for low-risk patients is superior compared with nerve-sparing treatment. Thus, hemiablation of the prostate is technically feasible, or even zonal ablation, focusing on pre-defined areas with the help of the imaging (Fig. 32.21).

The results in terms of preservation of the quality of life and in terms of the incidence of side effects are promising.

Currently, the published trials demonstrate a risk of severe incontinence in less than 10 % (6–8 %) of patients and the risk of erectile dysfunction ranges from 10 to 60 %, depending on the techniques used [26].

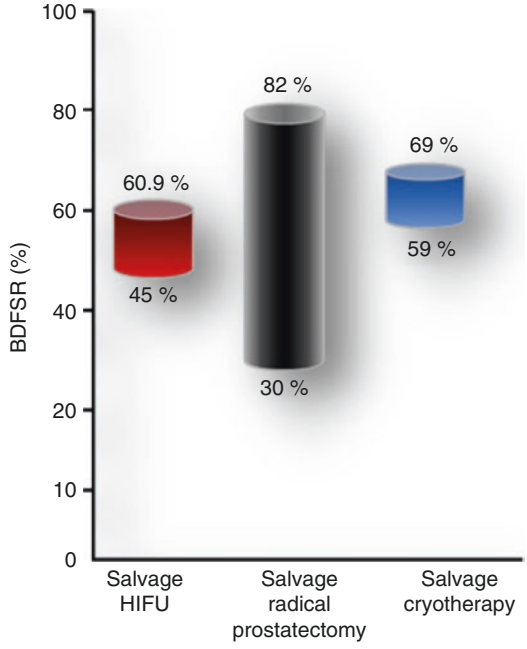

Fig. 32.19 Efficacy: biochemical disease-free survival rate

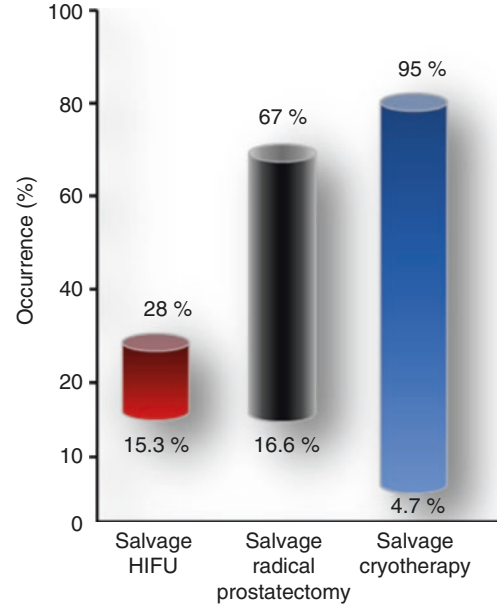

Fig. 32.20 Urinary incontinence

Fig. 32.21 Treatment modalities

Bibliography

1. American Cancer Society (2013) Cancer facts & figs. 2013. American Cancer Society, Atlanta
2. van den Bergh RCN et al (2007) Prospective validation of active surveillance in prostate cancer: the PRIAS study. Eur Urol 52(6):1560–1563
3. Gelet A, Chapelon JY, Bouvier R, Souchon R, Pangaud C, Abdelrahim AF, Cathignol D, Dubernard JM (1996) Treatment of prostate cancer with transrectal focused ultrasound: early clinical experience. Eur Urol 29(2):174–183
4. Rewcastle JC, Gill IS (2014) High-intensity focused ultrasound for the treatment of prostate cancer. In: Image guided prostate cancer treatments, vol 255. doi:10.1007/978-3-642-40429-0_22. ©Springer-Verlag Berlin Heidelberg
5. Harris GR (2009) FDA regulation of clinical high intensity focused ultrasound (HIFU) devices. Engineering in Medicine and Biology Society, 2009. EMBC 2009. Annual International Conference of the IEEE. IEEE, 2009
6. Crouzet S et al (2014) High-intensity focused ultrasound as focal therapy of prostate cancer. Curr Opin Urol 24(3):225–230
7. Lynn JG, Zwemer RL, Chick AJ (1942) The biological application of focused ultrasound waves. Science 96:119–120
8. Fry WJ, Barnard JW, Fry FJ, Krumins RF, Brennan JF (1955) Ultrasonically produced localized selective lesions in the central nervous system. Am J Phys Med 34:413–423
9. Lizzi FL, Coleman DJ, Driller J, Franzen LA, Leopold M (1981) Effects of pulsed ultrasound on ocular tissue. Ultrasound Med Biol 7(3):245–252
10. Gelet A, Chapelon JY, Margonari J, Theillère Y, Gorry F, Souchon R, Bouvier R (1993) High-intensity focused ultrasound experimentation on human benign prostatic hypertrophy. Eur Urol 23(Suppl 1):44–47
11. Woodward B, Warwick R (1970) How safe is diagnostic sonar? Br J Radiol 43(514):719–725
12. Foster RS, Bihrle R, Sanghvi NT, Fry FJ, Donohue JP (1993) High- intensity focused ultrasound in the treatment of prostatic disease. Eur Urol 23(S1):29–33
13. Ter Haar G, Coussios C (2007) High-intensity focused ultrasound: physical principles and devices. Int J Hyperthermia 23:89–104
14. Madersbacher S, Kratzik C, Marberger M (1997) Prostatic tissue ablation by transrectal high intensity focused ultrasound: histological impact and clinical application. Ultrason Sonochem 4:175–179
15. Haar GT (2012) Principles of high-intensity focused ultrasound. In: Interventional oncology. Springer, New York, pp 51–63
16. Sapareto SA, Dewey WC (1984) Thermal dose determination in cancer therapy. Int J Radiat Oncol Biol Phys 10:787–800
17. Goldberg SN, Solbiati L, Gazelle GS, Tanabe KK, Compton CC, Muller PR (1998) Treatment of intra hepatic malignancy with radio-frequency ablation: pathologic correlation in 16 patients. AJR Am J Roentgenol 170:1023–1028
18. Thompson S (1991) Pathologic analysis of photothermal and photochemical effects of laser-tissue interactions. Photochem Photobiol 53:825–835
19. Farjado LF, Egbort B, Marmor J, Hahn GM (1980) Effects of hyperthermia on a malignant tumour. Cancer 45:613–623
20. Linke CA, Carstensen EL, Frizzell LA, Elbadawi A, Fridd CW (1973) Localized tissue destruction by high-intensity focused ultrasound. Arch Surg 107(6):887–891
21. Chapelon JY, Margonari J, Theillère Y, Gorry F, Vernier F, Blanc E, Gelet A (1992) Effects of high-energy focused ultrasound on kidney tissue in the rat and the dog. Eur Urol 22:147–152
22. Coleman JA, Scardino PT (2013) Targeted prostate cancer ablation: energy options. Curr Opin Urol 23:123–128
23. Chaussy C, Thüroff S (2003) The status of high-intensity focused in the treatment of localized prostate cancer and the impact of a combined resection. Curr Urol Rep 4:248–252
24. Rouviere O, Lyonnet D, Raudrant A, Colin-Pangaud C, Chapelon JY, Bouvier R et al (2001) MRI appearance of prostate following transrectal HIFU ablation of localized cancer. Eur Urol 40:265–274
25. Crouzet S, Murat FJ, Pommier P, Poissonnier L, Pasticier G, Rouviere O, Chapelon JY, Rabilloud M, Belot A, Mège-Lechevallier F, Tonoli-Catez H, Martin X, Gelet A (2012) Locally recurrent prostate cancer after initial radiation therapy: early salvage high-intensity focused ultrasound improves oncologic outcomes. Radiother Oncol 105(2):198–202. doi:10.1016/j.radonc.2012.09.014
26. Crouzet S, Chapelon JY, Rouvière O, Mege-Lechevallier F, Colombel M, Tonoli-Catez H, Martin X, Gelet A (2014) Whole-gland ablation of localized prostate cancer with high-intensity focused ultrasound: oncologic outcomes and morbidity in 1002 patients. Eur Urol 65(5):907–914. doi:10.1016/j.eururo.2013.04.039

Ultrasound-Guided Treatment of Prostatic Cancer: Brachytherapy

33

Tommaso Cai

33.1 Introduction

Prostate cancer is, today, one of the most common causes of cancer death amongst Caucasian men [1]. With the introduction of the prostate-specific antigen (PSA) testing in the mid-1980s and the 'multicore' schemes of prostate biopsy, prostate cancer incidence rate increased drastically, at about 12 % per year [2]. Recently, in Europe, data from Surveillance, Epidemiology, and End Results Program (SEER) showed that the distribution of prostate cancer stage and grade has also dramatically changed, with localised and moderately differentiated tumours becoming predominant [3]. The incidence of small, localised, well-differentiated prostate cancer is, then, increasing, suggesting that many men with localised prostate cancer will benefit from mini-invasive treatment, and it is estimated that 45 % of men with a PSA-detected prostate cancer are candidates for conservative management [4, 5]. For these evidences, recently the interest for the use of brachytherapy in prostate cancer increased. In fact, patients with low-risk prostate cancer are the most suitable candidates for brachytherapy [4].

33.1.1 History

Brachytherapy (the term is derived from the Greek word *brachys*, which means brief or short), defined as the delivery of radiotherapy from a source placed close to the target site, is one of the oldest forms of radiation therapy [6]. From year 1901, in which Pierre Curie loaned a quantity of radium to the famed dermatologist Henri-Alexandre Danlos for the purpose of treating cutaneous conditions, brachytherapy has been involved in the treatment of nearly all sites in radiation therapy [6]. In the 1970s, several centres used brachytherapy for prostate cancer treatment. Implants were placed into the prostate under direct vision after open pelvic lymphadenectomy. Unfortunately, long-term follow-up revealed less than satisfactory results in terms of cancer control. In 1983, Holm et al. described the transperineal method with endorectal sonography, in which the patient is positioned in a dorsal decubitus gynaecological position [7] (Fig. 33.1). From this first experience, the use of brachytherapy for localised prostate cancer patients increased.

T. Cai
Department of Urology, Santa Chiara Regional Hospital, Trento, Italy
e-mail: ktommy@libero.it

P. Martino, A.B. Galosi (eds.), *Atlas of Ultrasonography in Urology, Andrology, and Nephrology*,
DOI 10.1007/978-3-319-40782-1_33

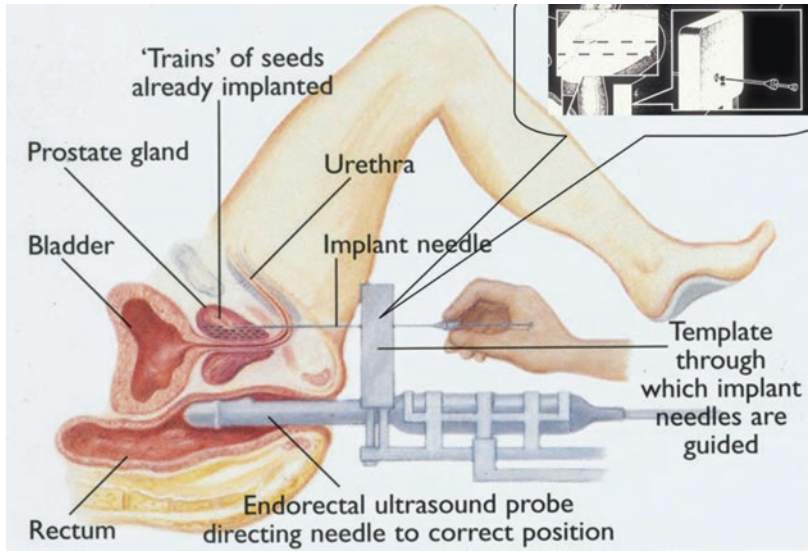

Fig. 33.1 Brachytherapy for prostate cancer treatment (Picture taken from the Internet: http://www.prostatecancertreatment.co.uk/treatment-options/brachytherapy)

33.1.2 Eligibility Criteria for Transperineal Brachytherapy

Transperineal brachytherapy has been demonstrated a safe and effective technique in all patients affected by prostate cancer if they have the following characteristics [8]:

- Stage cT1b-T2a
- No pathologic evidence of pelvic lymph node involvement
- No distant metastases
- Gleason score <7
- An initial PSA level of <10 ng/mL
- <50 % of biopsy cores involved with cancer
- A prostate volume of <50 cm^3
- An International Prostate Symptom Score (IPSS) <12

33.1.3 Procedure

The brachytherapy procedure involves two phases:

- Treatment planning
- Treatment section

The treatment planning phase can be performed prior to or at the time of brachytherapy using nomograms or treatment planning computers. Brachytherapy sources may be implanted temporarily or permanently:

1. Permanent seed implants (*low-dose-rate brachytherapy*) (*LDR*) – Low-dose brachytherapy treatments can be delivered with iodine or palladium seeds.
2. A high-dose-rate brachytherapy (HDR) (pick-up existing figure, sample HDR brachytherapy case) implant is a temporary seed containing iridium 192 (Ir-192).

33.1.3.1 Low-Dose-Rate Brachytherapy (LDR)

With the patient in gynaecological position, with urinary catheter and under general anaesthesia or spinal block, an ultrasound probe is inserted into the rectum and multiple measurements taken to assess the dimensions and configuration of the prostate and its relationship to other structures, such as the urethra (Fig. 33.2).

In brachytherapy, catheter reconstruction is one of the most important procedures in treatment planning and relates the source tracks and dwell positions to the patient's anatomy (e.g. targets and organs at risk) [6]. All information obtained from the ultrasound study of the prostate are acquired and analysed by dedicated software in order to establish a treatment plan, individualised to

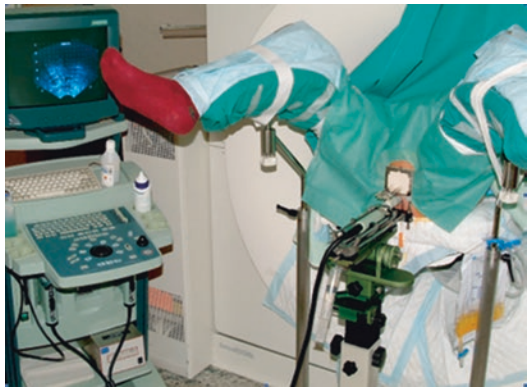

Fig. 33.2 Gynaecological patient's position under anaesthesia (Picture taken from the Internet: http://tidsskriftet.no/article/21010/en_GB)

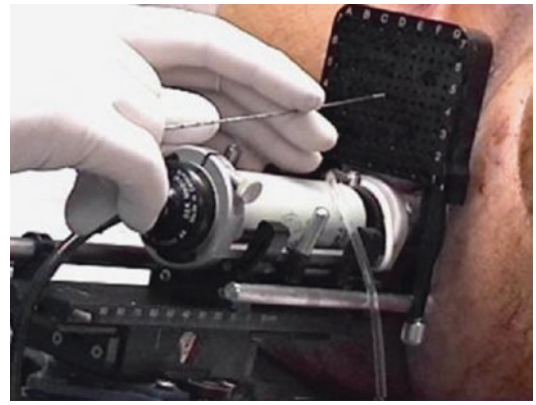

Fig. 33.4 Seed implantation (Picture taken from the Internet: http://emedicine.medscape.com/article/453349-technique)

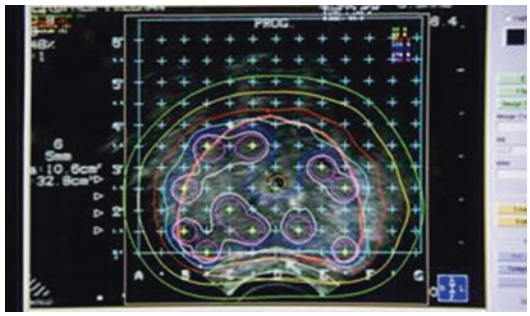

Fig. 33.3 Treatment planning and dose calculation (Picture taken from the Internet: http://www.cancertherapyadvisor.com/prostate-cancer/prostate-cancer-low-dose-brachytherapy-boost-survival-improvement/article/400686/)

produce an ideal 'bespoke' plan of therapy for that person. The analysis phase is performed by a urologist, dedicated radiotherapist and physicist.

The dosimetric planning of the implant is generally performed in all patients during seed insertion. The dose is quantified in terms of the unit of absorbed energy per weight of tissue. In brachytherapy, the sharp radiation dose falloff allows a high degree of rectal sparing and permits delivery of a higher total dose to the prostate gland itself (Fig. 33.3). The average dose rates are 10 Gy/week for IMRT, 40 Gy/week for Pd-103 brachytherapy implants and 13 Gy/week for I-125 brachytherapy.

The metal grid is set up and secured to the operating table. Through the grid, needles are inserted through the skin of the perineum into the prostate gland, under direct vision using the transrectal probe. When the positioning of the needles is satisfactory and matches the defined radiotherapy treatment plan, the seeds are deposited (Fig. 33.4). The time taken for this procedure ranges from 1 to 2 h.

33.1.3.2 High-Dose-Rate Brachytherapy

High-dose-rate (HDR) brachytherapy can be used as the only treatment for prostate cancer, or it can be used in combination with external beam radiation therapy (EBRT). In the first case, it is known as 'HDR monotherapy', and when given with external beam, it is known as 'combined HDR and EBRT':

- *HDR monotherapy*
  - Used for localised prostate cancer disease (T1c-T2b; PSA <15; GS ≤3+4).
- *Combined high-dose-rate (HDR) brachytherapy and external beam radiation therapy (EBRT)*
  - Used for patients with locally more advanced disease within or around the prostate, those with higher PSA levels or higher pathology (Gleason 8–10) grade. EBRT is generally performed 2 weeks later.

High-dose-rate prostate brachytherapy, originally used as a boost together with external

beam treatment, has been receiving more attention as monotherapy for suitable patients, due to its better-controlled dosimetry, no residual radioactivity, higher dose rate and better suitability for low α/β ratio prostate cancer [6]. Typically, in a template-guided prostate HDR implant, 15–18 catheters are inserted through the perineum into the prostate, under the guidance of transrectal ultrasound (TRUS) (Figs. 33.5 and 33.6).

The treatment plan can be based either on the TRUS images or on a computed tomography (CT) scan of the patient with all the catheters in place (Fig. 33.7) [6].

In order to improve the catheter reconstruction and the dosimetric accuracy, the electromagnetic tracking (EMT) system to automatically track catheter position has been developed and introduced into clinical practice [6]. In this system a computer communicates with the control box through a USB interface. Both transmitter and sensor are connected to the control box [6] (*see the figures below*).

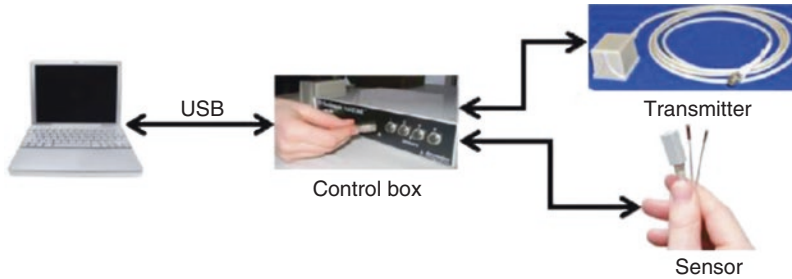

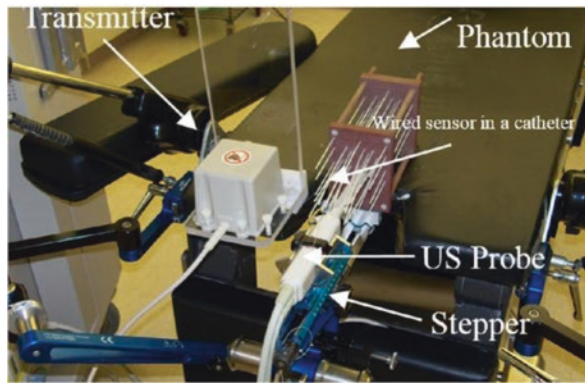

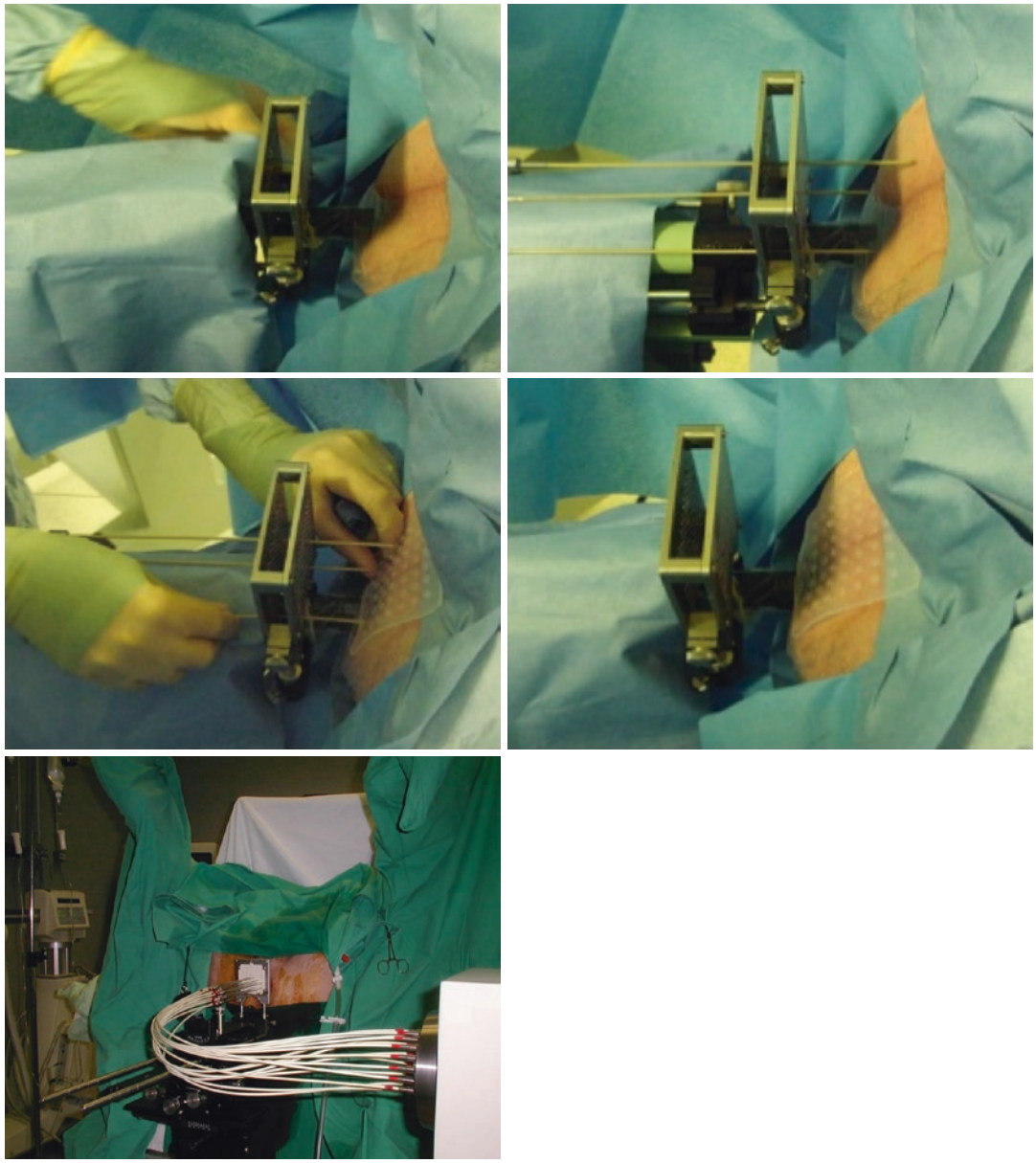

Figs. 33.5 and 33.6 The figure shows the temporary seed implant containing iridium 192 (Ir-192). Because no permanent seeds are left inside the body, there are no immediate radiation precautions. The catheters are kept in place to deliver a series of two to four radiation treatments over 1–2 days, with about 6 h between treatments (Pictures taken from the Internet: Fig. 33.5 – http://www.slideshare.net/jackinlawrence/prostate-hdr-technique - Fig. 33.6 – http://www.intechopen.com/books/advances-in-prostate-cancer/high-dose-rate-interstitial-brachytherapy-as-monotherapy-in-one-fraction-for-the-treatment-of-favora)

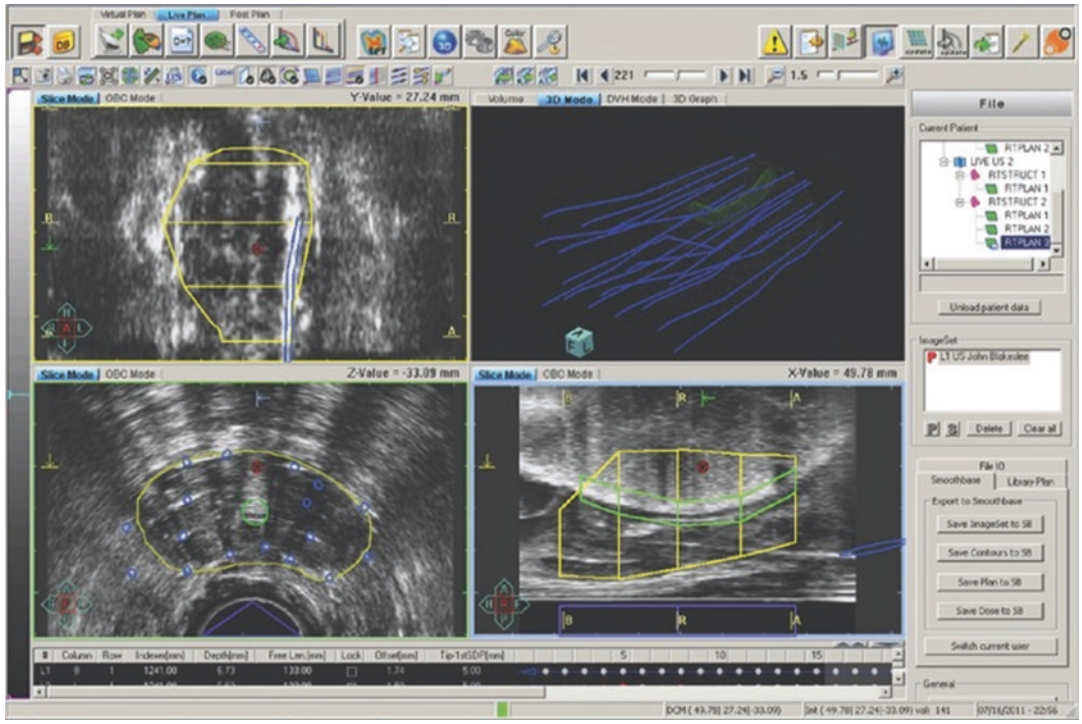

Fig. 33.7 In the figure the prostate is detailed in *yellow* contour and urethra in *green* [6]

Zhou et al., recently, reported their experience with EMT, in which they found that the performance of an EMT system can be improved by reducing the interference from surrounding equipment, decreasing the distance from the field generator to the tracking area and choosing an appropriate sampling frequency. Moreover, they found an accuracy of 0.9 ± 0.2. Furthermore, Bharat et al., by using electromagnetic tracking system for catheter reconstruction in high-dose-rate brachytherapy for prostate cancer treatment and attaching electromagnetic sensors to a robotic arm, found an accuracy of 0.26 ± 0.16 mm in the ideal environment [9].

33.2 Novel One-Stage Procedure: 4D Brachytherapy

Recently, a new technique, named 4D brachytherapy, has been developed: a one-stage real-time brachytherapy technique using stranded seeds with improved time efficiency and clinical outcome. This technique utilises a nomogram to calculate the seed requirement in advance of the implant [10]. This allows stranded seeds to be pre-ordered and loaded prior to the procedure rather than peroperatively [10]. The use of both stranded and loose seeds may reduce the risk of migration, whilst maintaining the flexibility to optimise the dose within the prostate and especially at the apex of the gland [10]. Recent data show significantly improved dosimetry: median D90 143 and 153 Gy ($P<0.005$) and median V100 88 and 93 % ($P<0.005$) for the Seattle technique and 4D brachytherapy implant technique, respectively [10]. Moreover, the use of 4D brachytherapy allows a reduced short-term urinary morbidity at 3 months and 1 year compared with the Seattle technique [10].

33.2.1 4D Brachytherapy Procedure [10]

1. The five prostate measurements required to generate the seed order for 4D brachytherapy.

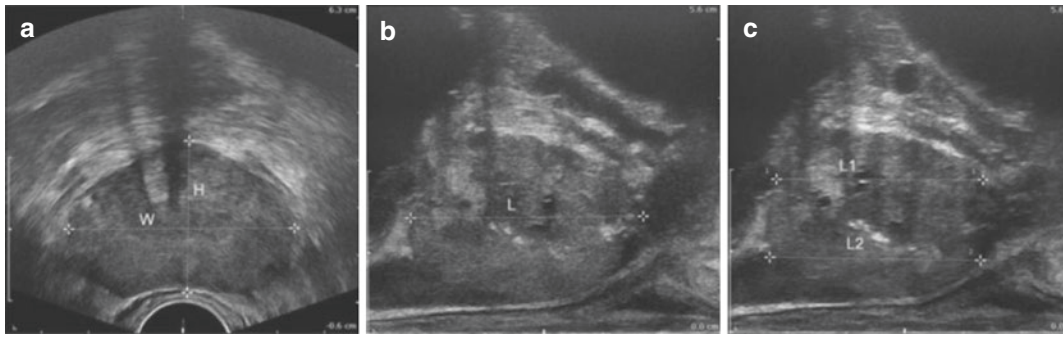

2. (a) Position of the stranded seeds around the periphery of the prostate (red); the anterior rectal wall (blue) and urethra (green) are also shown. (b) Sleeve of radiation created by these stranded seeds. (c) The completed radiation dose cloud (145 Gy) achieved by subsequently implanting the centre of the prostate with loose seeds [10].

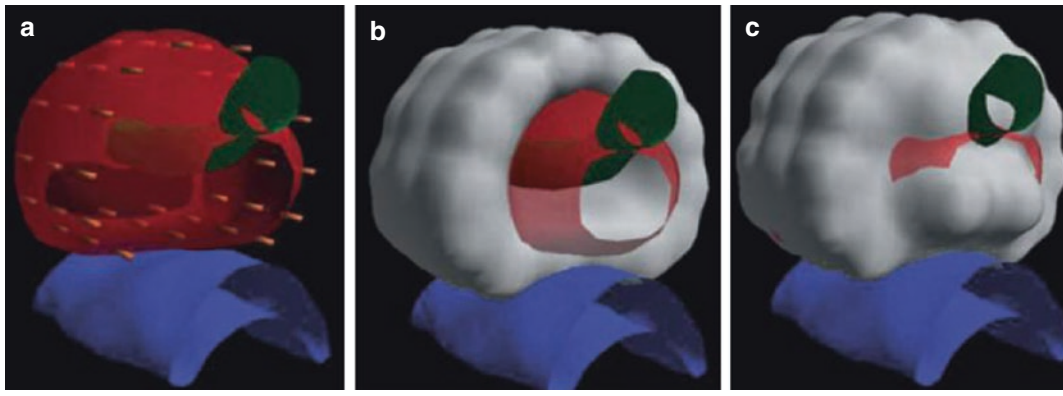

The combination of the stranded seeds with the placement of loose seeds centrally in the 4D brachytherapy procedure allows the apex of the prostate to be carefully implanted, minimising the dose to the membranous urethra and the penile bulb and thereby reducing the risk of urethral stricture rate and optimising erectile function [10].

33.2.2 Side Effects and Tolerability

All side effects reported from brachytherapy procedure are summarised into three categories:

- Immediate side effects
- Short-term side effects
- Long-term side effects

After the procedure, the patient may report discomfort and swelling in the treatment area, sometimes accompanied by bruising. Generally, all side effects in the first couple of days after the procedure are caused by the instruments used during the procedure. These include slight bleeding or burning beneath the scrotum or blood in your urine. After 2 weeks from the procedure, the patients may experience frequent, urgent or uncomfortable urination. These symptoms usually decrease in severity as time goes on, as the seeds lose their radioactive strength. The rate of significant urinary complications following implantation is as follows: urinary retention (1.5–22 %); postimplantation transurethral resection of the prostate (TURP), which is required in up to 8.7 % of cases; and incontinence (0–19 %) [4, 11]. Chronic urinary morbidity can occur in up to 20 % of patients [4]. Some authors demonstrated that previous TURP procedure increases the risk of postimplantation incontinence and urinary morbidity [4]. Erectile dysfunction develops in about 40 % of the patients after 3–5 years [4]. Recently, Chen et al. showed that the urinary, bowel and erectile morbidity rates were 33.8 %, 21 % and 16.7 %, respectively, with invasive procedure rates of 10.3 %, 0.8 % and 4 %, respectively [12]. Finally, the incidence of grade III toxicity is less than 5 % [4].

33.2.3 Oncological and Functional Results

The EAU guidelines highlight that there have been no randomised trials comparing brachytherapy with other curative treatment modalities [4] and the outcomes are based on nonrandomised case series, with a median follow-up ranging from 36 to 120 months [4, 13]. The recurrence-free survival after 5 and 10 years has been reported to range from 71 % to 93 % and from 65 % to 85 %, respectively [4, 14, 15]. Moreover, a significant correlation has been shown between the implanted dose and recurrence rates [4]. There is no benefit from adding neoadjuvant or adjuvant ADT to LDR brachytherapy [4, 11].

33.2.4 Final Remark for the Everyday Clinical Practice

The European Association of Urology suggested that the use of brachytherapy should be limited to patients with cT1-T2a, Gleason score <7 (or 3 + 4), PSA <10 ng/mL, prostate volume <50 mL, without a previous TURP and with a good IPSS.

References

1. U.S. Cancer Statistics Working Group (2010) United States Cancer Statistics: 1999–2006 incidence and mortality web-based report. U.S. Department of Health and Human Services, Centers for Disease Control and Prevention and National Cancer Institute, Atlanta, 2010
2. Welch HG, Albertsen PC (2009) Prostate cancer diagnosis and treatment after the introduction of prostate-specific antigen screening: 1986–2005. J Natl Cancer Inst 101(19):1325–1329
3. Jani AB, Johnstone PAS, Liauw SL, Master VA, Brawley OW (2008) Age and grade trends in prostate cancer (1974–2003): a surveillance, epidemiology, and end results registry analysis. Am J Clin Oncol 31(4):375–378
4. European Association of Urology (EAU) guidelines on prostate cancer – http://uroweb.org/wp-content/uploads/1607-Prostate-Cancer_LRV3.pdf
5. Godtman RA, Holmberg E, Khatami A et al (2013) Outcome following active surveillance of men with screen-detected prostate cancer. Results from the Göteborg randomised population-based prostate cancer screening trial. Eur Urol 63(1):101–107

6. Zhou J, Zamdborg L, Sebastian E (2015) Review of advanced catheter technologies in radiation oncology brachytherapy procedures. Cancer Manag Res 7: 199–211
7. Holm HH, Juul N, Pedersen JF et al (1983) Transperineal seed implantation in prostatic cancer guided by transrectal ultrasonography. J Urol 130(2): 283–286
8. Ash D, Flynn A, Batterman J et al; ESTRO/EAU Urological Brachytherapy Group; EORTC Radiotherapy Group (2000) ESTRO/EAU/EORTC recommendations on permanent seed implantation for localized prostate cancer. Radiother Oncol 57(3):315–321
9. Bharat S, Kung C, Dehghan E, Ravi A, Venugopal N, Bonillas A, Stanton D, Kruecker J (2014) Electromagnetic tracking for catheter reconstruction in ultrasound-guided high-dose-rate brachytherapy of the prostate. Brachytherapy 13(6):640–650
10. Langley SE, Laing RW (2012) 4D Brachytherapy, a novel real-time prostate brachytherapy technique using stranded and loose seeds. BJU Int 109(Suppl 1): 1–6
11. Budäus L, Bolla M, Bossi A et al (2012) Functional outcomes and complications following radiation therapy for prostate cancer: a critical analysis of the literature. Eur Urol 61(1):112–127
12. Chen AB, D'Amico AV, Neville BA et al (2006) Patient and treatment factors associated with complications after prostate brachytherapy. J Clin Oncol 24(33):5298–5304
13. Machtens S, Baumann R, Hagemann J et al (2006) Long-term results of interstitial brachytherapy (LDR brachytherapy) in the treatment of patients with prostate cancer. World J Urol 24(3):289–295
14. Grimm PD, Blasko JC, Sylvester JE et al (2001) 10-year biochemical (prostate-specific antigen) control of prostate cancer with (125)I brachytherapy. Int J Radiat Oncol Biol Phys 51(1):31–40
15. Potters L, Morgenstern C, Calugaru E et al (2008) 12-year outcomes following permanent prostate brachytherapy in patients with clinically localized prostate cancer. J Urol 179(5 Suppl):S20–S24

Part IV

The Bladder and Female Pelvic Floor

Bladder: Ultrasound Anatomy and Scanning Methods

34

Roberta Gunelli

Over the past 10 years, the study of the urinary bladder has been improved by an imaging technique that is easy to perform in an outpatient setting, reproducible, and relatively inexpensive: the ultrasound scan. The potential for using ultrasound in both diagnostic and follow-up stages of benign and malignant diseases has led to its becoming an invaluable tool for the urologist. However, as ultrasound is also highly user dependent, it has become crucial to establish accurate guidelines for the correct execution of the exam to reduce the risk of incorrectly interpreting bladder morphology which varies according to the different phases of bladder filling.

Despite the efforts of the most important international urological associations, there are still no universally accepted standards of practice for ultrasound. Thus, the impossibility of giving an unequivocal interpretation to a set of images built by the ability, or lack thereof, of the user highlights the need to define a basic set of best practice norms to avoid the biases of a poor execution of the scan. Regardless of the equipment used, it is indispensable for the physician performing the exam to have specific training in the use of the ultrasound in order to obtain the maximum information and the most accurate results.

R. Gunelli
Department of Urology,
Morgagni-Pierantoni Hospital, Forlì, Italy
e-mail: fiorifo@tin.it

The following recommendations for a correct scanning technique are based on standardisation approaches proposed in the literature.

Main uses of static ultrasound of the bladder:

- Measurement of post-void residual urine volume
- Calculation of bladder volume
- Evaluation of the anatomical changes associated with bladder outlet obstruction
- Evaluation of the hypermobility of the bladder neck in women with stress incontinence
- Evaluation of haematuria of the lower urinary tract
- Evaluation of suspected intramural calculi
- Identification of congenital malformations (ureterocele, diverticula, etc.)
- Post-operative monitoring (bladder tamponade, position of catheter, etc.)
- Follow-up of non-invasive tumours
- Follow-up of orthotopic neobladder after cystectomy

34.1 Equipment

A convex 3.5 MHz probe is used for the standard exam in adults (a transducer of higher frequency – 7.5/10 MHz – can be used in paediatric patients and for measuring bladder wall thickness). The scan lines are perpendicular to the transducer face.

P. Martino, A.B. Galosi (eds.), *Atlas of Ultrasonography in Urology, Andrology, and Nephrology*,
DOI 10.1007/978-3-319-40782-1_34

Transrectal or transvaginal probes are used for dynamic ultrasound imaging, e.g. in the assessment of cystocele.

Bladder tumours can be staged using transrectal probes.

Post-void bladder volume can be measured by an automated device.

On the technical and quality side, the ultrasound equipment need to be checked for calibration requirements at least every year.

34.2 Technique

The patient is usually examined in a supine position; standing position can be useful to evaluate bladder neck mobility.

It may be necessary to put the patient in a lateral recumbent position (right or left) when evaluating the presence of proliferating endovesical lesions to rule out prostatic involvement or to differentiate between mobile bodies such as calculi or blood clots. When an oblique image is required, the probe is turned 40° with respect to its longitudinal axis, and the bladder should not contain more than 250–300 cc to avoid the risk of poor visualisation of the ureters.

An adequate quantity of gel is indispensable for the correct transmission of the ultrasound waves.

A comfortably full bladder is needed for optimal imaging, avoiding overdistension, especially in patients with outlet obstruction [1].

Usually the scan is performed with a sagittal view followed by a transversal one, and any modifications in the ultrasound appearance of the bladder wall (detrusor trabeculation, diverticula, endophytic tumours, diverticulosis, lithiasis) and bladder neck at rest (presence of third prostatic lobe, bladder neck open at rest) should be recorded.

The site and dimension of focal lesions (especially those of neoplastic origin) and other conditions (diverticula, (Fig. 34.1) calculi, blood clots, etc.) must be accurately noted.

When indicated, distal ureters can be evaluated for dilation or the presence of other anomalies (intramural (Fig. 34.2) or juxtavesical calculi).

Echo Doppler is not generally necessary for bladder scanning but can be used to assess for the presence of ureteral jets (Fig. 34.3) and in the differential diagnosis of bladder tumours [2].

It is recommended that small adjustments in gain and focus settings be made to improve both the quality of the images and the visualisation of the anterior wall (superficial to the skin) and posterior wall (deep to the skin).

Second harmonic tissue imaging can be used to further enhance images and reduce reverberation echoes.

Bladder volume, if not obtained automatically, can be calculated using the ellipsoid formula: $v = 0.52 \times r1 \times r2 \times r3$.

Post-void residual urine should always be evaluated by scanning the bladder immediately after voiding [9].

In the event of a significant post-void residual volume, the patient is asked to empty the bladder again, and the scan is repeated to obtain a reliable indication of the emptying capacity.

Detrusor thickness (normally $\leq$3 mm) is best assessed when the bladder is partially full (250–300 cc), and it is based on the average of three measurements made on the same image. To optimise results, the measurement should be made at the anterior bladder wall, and a high-frequency (7.5 MHz) convex or linear probe should be used [1].

On ultrasound, the detrusor has a sandwich-like structure (hypoechogenic muscular wall between mucous structures that appear slightly hyperechogenic). The thickness of the bladder wall must always be measured in areas that are orthogonal to the ultrasound beam [3–10]. When measuring detrusor thickness (Fig. 34.4) or estimating bladder weight, it is necessary to calculate bladder volume capacity (reliable for values $\geq$250 cc) [11–12].

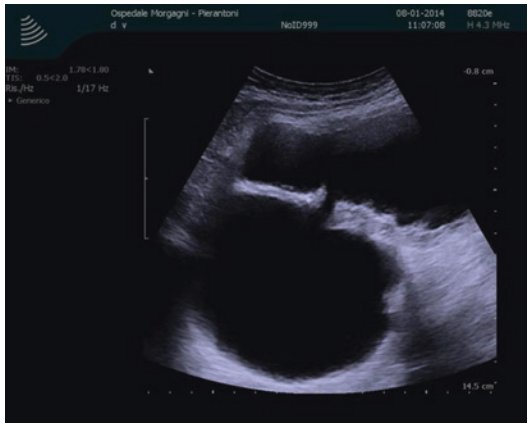

Fig. 34.1 Diverticulum

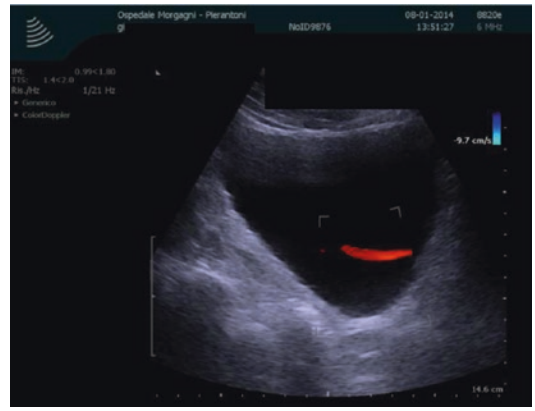

Fig. 34.3 Ureteral jet

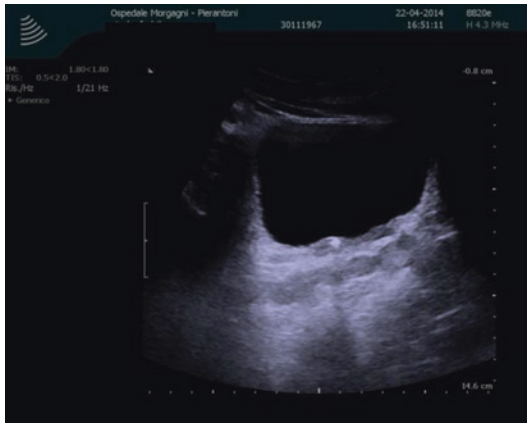

Fig. 34.2 Intramural calculi

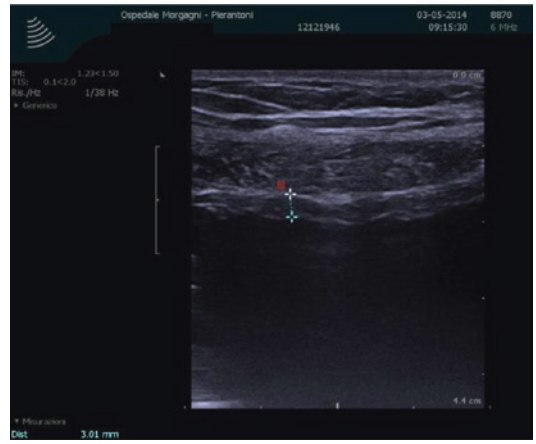

Fig. 34.4 Evaluation of detrusor thickness

34.3 Patient Preparation

1. Fasting is not necessary.
2. The bladder must be comfortably full (≥300 cc). Patients are asked to drink 500 cc of water 3 h before the exam and not to empty their bladder 2 h before the scan.

34.3.1 Example of Information Contained in Final Referral

1. Presence or absence of urinary bladder
2. Orthotopic site and symmetry
3. Shape
4. Degree of distension of the organ (indispensable for the reliability of the exam)
5. Presence of alterations in the bladder wall (evaluation of lesions >3 mm)
6. Presence of third prostatic lobe (if present, the volume and/or measurements of the protrusion into the bladder should be indicated); intravesical prostatic protrusion
7. Presence and dimension of fixed or movable calcifications (diameter >3 mm)
8. Characteristics of the bladder neck
9. Presence of ureters with details on any dilatation, abnormal outlet or endoluminal calculi
10. Presence of pelvic masses or extrinsic compression of the bladder
11. Quantification of post-void residual urine [9]

The *referral* should include:

- The patient's name and other demographic information.
- The name of the unit/department providing the service and contact details.
- Date on which the exam was performed.
- Name of requesting physician.
- Relevant clinical information, including the indications for the exam.
- Type of ultrasound scan performed and type of transducer used. If endocavity techniques are used, the method should be specified.
- Orientation of the ultrasound image (if necessary).
- Appropriate anatomical and ultrasound terminology. In the event of variations in normal dimensions, exact measurements should be given (e.g. increase in detrusor thickness, diverticula, endoluminal neoformations, etc.).
- Comparison between previous imaging studies and latest exam; recommendations for further tests needed; hypothesis of differential diagnosis.
- It is important to describe any clinical conditions preventing adequate filling of the bladder (urgency, incontinence, pain on full bladder).
- The final referral must be signed and dated.

If the results of the ultrasound exam are considered to require urgent follow-up action, it is recommended that the physician who performed the exam contacts the patient's GP directly to ensure that the referral has been received. A description of the other pelvic organs should only be given when there is medical competence to do so. The degree of bladder distension must be specified as it could influence the visualisation of both the seminal vesicles and the ureters in the juxtavesical and intramural tract. Any difficulties encountered during the scan (collaboration and physical make-up of the patient, presence of meteorism) should be indicated, as should any limits of the exam which could influence its diagnostic value.

Images to attach to the referral (to be evaluated on the basis of the overall clinical picture):

1. Transverse image of the bladder.
2. Longitudinal image of the bladder.
3. Transverse/longitudinal image of the bladder with visualisation of the bladder neck.
4. One or more images representative of any anomalies detected.
5. If an obstruction of the juxtavesical ureter is detected (calculus or vegetative lesion), an oblique image is required.

A Web-based search was performed for guidelines and review articles published over the last 10 years on the use of ultrasound for the evaluation of the urinary bladder:

- *AIUM Practice guidelines for the performance of an ultrasound examination in the practice of urology*. American Institute of Ultrasound in Medicine (2011)
- *AIUM Standards and guidelines for the accreditation of ultrasound practices*. American Institute of Ultrasound in Medicine (2014)
- *Standard per una corretta esecuzion dell'esame ecografico*. Journal of Ultrasound 2009 (SIUMB monograph)
- *EAU Guidelines on urinary incontinence*. European Association of Urology (2014)
- *Guidelines on non-muscle-invasive bladder cancer* (*TaT1 and CIS*). European Association of Urology (2014)
- *Guidelines on pain management*. European Association of Urology (2014)

References

1. Kanu GB (2010) Ultrasonography of the urinary bladder. J Med Ultrasound 18:105–114
2. Seung HK (2007) Ultrasound of the urinary bladder, revisited. J Med Ultrasound 15:77–90
3. Aganovich D, Hasanbegovich M, Prcic A, Kulovac B, Hadziosmanovic O (2012) Which is a better indicator of bladder outlet obstruction in patients with benign prostatic enlargement – intravesical protrusion of prostate or bladder wall thickness? Med Arch 66:324–328
4. Athanasiou S (1999) Imaging the urethral sphincter with three-dimensional ultrasound. Obstet Gynecol 94:295–301
5. Blatt A, Chan L (2009) The Importance of bladder wall thickness in the assessment of overactive bladder. Curr Bladder Dysfunct Rep 4:220–224
6. Franco G, De Nunzio C, Leonardo C, Tubaro A, Ciccariello M, De Dominicis C, Milano L, Laurenti C (2010) Ultrasound assessment of intravesical prostatic protrusion and detrusor wall thickness – new standard for non-invasive bladder outlet obstruction diagnosis? J Urol 186:2270–2274
7. Galosi AB, Mazzaferro D, Lacetera V, Muzzoniglro G, Martino P, Tucci G (2012) Modifications of the bladder wall (organ damage) in patients with bladder outlet obstruction: ultrasound parameters. Arch Ital Urologia Androl 84:263–267
8. Oelke M (2010) International Consultation on incontinence – Research Society (ICI-RS) report on non-invasive urodynamics: the need of standardisation of ultrasound bladder and detrusor wall thickness measurements to quantify bladder wall hypertrophy. Neurourol Urodynam 29:634–639
9. Asimakopoulos AD, De Nunzio C, Kocjancic E, Tubaro A, Rosier PF, Finazzi Agrò E (2016) Measurement of post-void residual urine. Neurourol Urodyn 35(1):55–7
10. Bright E, Oelke M, Tubaro A, Abrams P (2010) Ultrasound estimated bladder weight and measurement of bladder wall thickness - useful noninvasive methods for assessing the lower urinary tract? J Urol 184:1847–1854
11. Rukstalis DB (2014) Pelvic ultrasound evaluation for benign prostatic hyperplasia: prediction of obstruction. Curr Urol Rep 15:403
12. Robinson D, Cardozo L (2002) Can ultrasound replace ambulatory urodynamics when investigating women with irritative urinary symptoms? BJOG 109:145–148

Neoplastic and Nonneoplastic Disease of the Bladder

35

Luigi Mearini, Elisabetta Nunzi, and Michele Del Zingaro

35.1 Introduction

The presence of blood in the urine as macroscopic (visible on gross examination) or microscopic (invisible, more than 3–5 red blood cells per high-power field on microscopic urine analysis) hematuria is a very common problem that can represent many different common benign or malignant underlying diseases. The causes of hematuria can be broadly categorized into renal (glomerular and non-glomerular) and/or extrarenal.

Apart from a detailed history, which is essential in driving the diagnostic process in cases of hematuria and baseline laboratory evaluations, further investigation with noninvasive imaging studies [1] is imperative to confirm or exclude the presence of malignant disease.

The most common conditions of the bladder that cause hematuria include infection, inflammation, stones, and malignancy.

Although hematuria's characteristics and symptoms are suggestive of underlying disease (e.g., symptomatic hematuria with frequency suggests an infectious or irritative disease), most bladder cancers are asymptomatic.

Ultrasound scanning (US) is a useful, relatively simple noninvasive imaging modality for the evaluation of the urinary bladder [2, 3]. The bladder is an abdominal organ ideally suited to US [4] for many reasons, including its superficial location and the acoustic properties of the fluid (urine) inside. The functions of the bladder include urine storage and removal, and when the bladder is filled with urine, its content should be anechoic upon US evaluation, thus permitting the ideal examination of its content and walls.

Before proceeding with bladder US, it is crucial to remember that upon normal filling, the bladder wall appears as a typical three-layer structure with a detrusor muscle of medium homogeneous echogenicity, while the outer serosa layer and the inner mucosa (urothelial) layer are usually hyperechoic compared with the middle detrusor smooth muscle (muscularis propria) layer.

L. Mearini, MD (✉) • E. Nunzi • M.D. Zingaro
Urology Department, University Hospital, Perugia, Italy

Urology Department, Perugia Hospital University of Perugia, Perugia, Italy
e-mail: luigi.mearini@tin.it

P. Martino, A.B. Galosi (eds.), *Atlas of Ultrasonography in Urology, Andrology, and Nephrology*,
DOI 10.1007/978-3-319-40782-1_35

35.2 Technology

The most common method used to scan the urinary bladder is an external, suprapubic, abdominal approach using a convex 2.5–5-MHz probe. Linear probes with higher frequencies (7.5–16 MHz) can be used in specific cases. The bladder floor, including the distal and intramural part of the ureter, can be visualized more accurately with a higher frequency transrectal ultrasound scan (TRUS) in men or with a vaginal probe in women. A transurethral approach into the bladder with high-frequency miniprobes is an antiquated procedure and is not currently a standard approach due to its invasiveness and limits [5–7], although still promising with less invasive probe in tumor staging [8] (Figs. 35.1, 35.2, and 35.3).

The patient is usually examined in the supine position with a sufficiently full bladder (200–300 ml). Bladder US requires careful and complete scanning with transverse and longitudinal sections.

The fine regulation of light is essential to obtain a significantly improved image quality and to correctly visualize the anterior wall (superficial compared to the skin) and posterior wall (deep). The use of high-frequency probing or the use of a second tissue harmonic imaging tool improves the quality of the imaging by reducing some reverberation artifacts. Effectively, abdominal ultrasound is limited in the evaluation of the anterior bladder wall due to reverberation artifacts, such as the rain effect.

Echo-Doppler may be useful to assess the ureteral jet and make a differential diagnosis of a bladder lesion.

Table 35.1 briefly resumes the quality of images obtained by different approaches and probes.

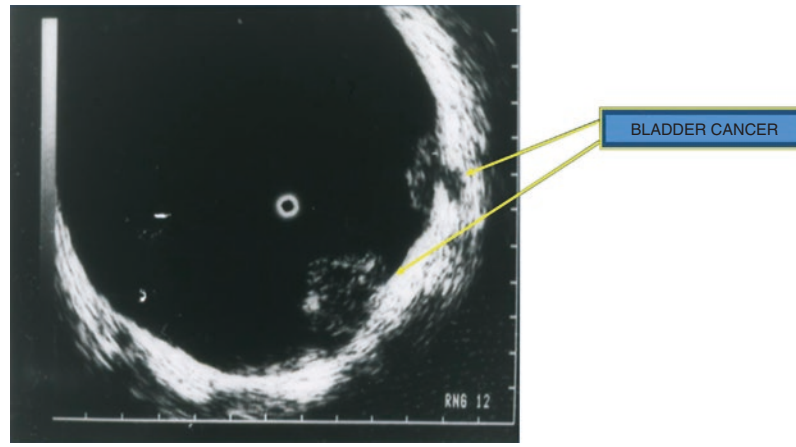

Fig. 35.1 Historical image of transurethral US of the bladder. The picture demonstrates two small intraluminal bladder masses. Bladder wall is easily identified, showing that one of the bladder mass involves a small diverticulum

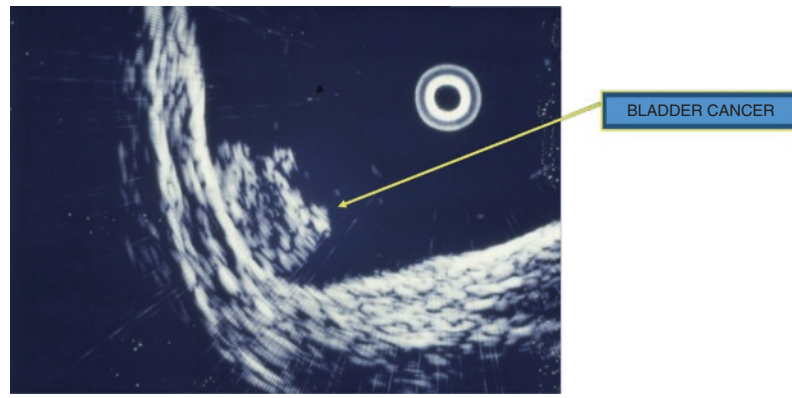

Fig. 35.2 Another "antique" image of transurethral US. Note the integrity of the echostructural pattern of bladder wall at tumor's base

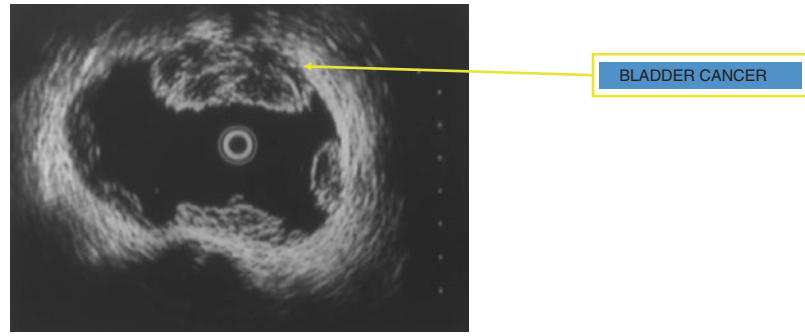

Fig. 35.3 A deep infiltrating bladder mass seen at transurethral US. The echostructural pattern of anterior bladder wall is easily seen, and it demonstrates a diffuse interruption

Table 35.1 Synthetic overview of imaging quality according to different probes and approaches to the bladder

	Abdominal	Transrectal or transvaginal	Transurethral
Instrument	Convex 3.5–5-MHz probe	Linear biplanar 7.5-MHz probe	Endoscopic probe 5–7.5 MHz
Overall view	+++	+	++
Bladder wall appearance	+	+	+++
Trigone	++	+++	–
Anterior wall	+–	–	+
Lateral wall	++	–	+
Bladder dome	+	–	+
Surrounding organ	++	++	–

35.3 Report

The findings report should [9]:

- Include the name of the physician examiner, place, and date.
- Include the patient's name, surname, and date of birth.
- Briefly include all clinical information and the indications for the specific investigation.
- Describe type of current ultrasound examination and the probe.
- Use standard anatomical and ultrasound terminology.
- Describe all abnormal findings, including number, side, shape, dimension, and characteristics.
- Try to obviate to any difficulties or limits encountered while performing the investigation; underline the diagnostic accuracy of current test.
- Suggest types of studies for further investigation; in case of serious findings, inform the patient and contact the patient's doctor.

Example: Bladder Ultrasound Examination

Dr. Samuel Smith; Urology Department, NY City Hospital; June 26th, 2015

Patient: Richard Doyle; October 23th, 1947

Queries: asymptomatic hematuria

Abdominal bladder ultrasound by convex 5-MHz probe

Ultrasound findings:

Bladder filling volume is sufficient for exhaustive examination. The bladder wall thickness is normal. The right and left ureteral jets are present. Presence of a polypoid hypoechoic mass in the right bladder wall, 1.5×5 mm; the hyperechoic line of inner mucosa is not interrupted. Power Doppler images show considerable vascularity of the mass. The post-micturition volume is 20 ml.

Urologist consultation and cystoscopy are strongly suggested since these ultrasound and power Doppler images are suggestive of carcinoma of the urinary bladder.

The exams included:

1. Two pictures of the bladder in transverse and longitudinal scan
2. Two pictures of the mass in transverse and longitudinal scan (Fig. 35.4)

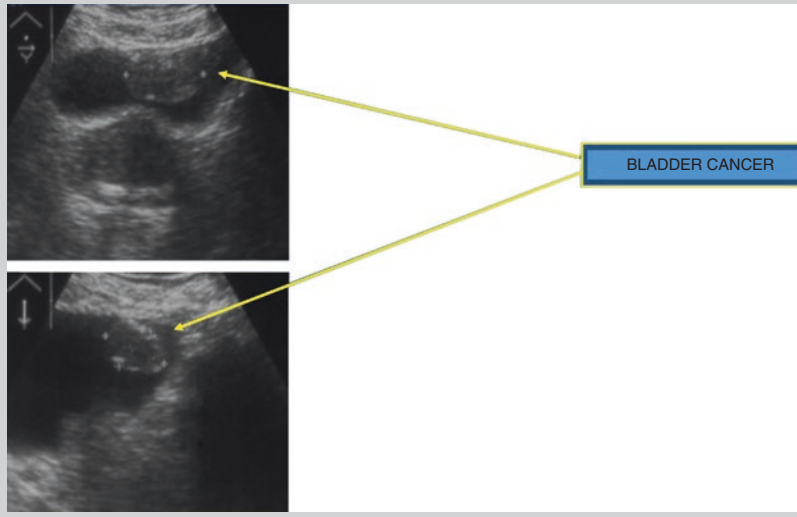

Fig. 35.4 An example of exhaustive US report in case of bladder cancer. The two images describe in detail the bladder mass with a transverse and longitudinal scan

35.4 Diagnosis

In the diagnosis of luminal defects of the bladder, it is of paramount importance to remember the normal bladder wall anatomy, which consists of mucosa, detrusor smooth muscle, and adventitia. This anatomical distinction is easily visualized by US, as the ultrasound appearance of the bladder wall is as a sandwich structure with a hypoechogenic muscular wall between the mucosa and adventitial layers, which are slightly hyperechogenic.

The possibility of distinguishing each component of the bladder wall depends upon bladder wall thickness, which varies with the state of urine filling; the upper limits are 3 and 5 mm for a full bladder and empty bladder, respectively. The trigone represents an important landmark: it is the triangular area which lies between the two ureteral orifices and the internal urethral orifice; in this region, the musculature of the bladder floor is dense and usually hypertrophied, forming the interureteric ridge.

All these concepts explain why a bladder ultrasound scan requires adequate bladder filling and the limits of US evaluation in cases of detrusor hypertrophy or small lesions.

35.4.1 Neoplastic Bladder Disease

Most bladder tumors are transitional cell carcinomas, accounting for approximately 90% of all primary malignant lesions. They are usually found in the region of the trigone or bladder base or on the lateral walls as unique or multiple lesions. According to their intrinsic characteristics, they show different patterns in growth, with papillary, sessile (or infiltrative), and mixed papillary and sessile shape.

On ultrasound [10], they appear as a papillary (polypoid) or sessile (plaque with large base) lesions projecting into the lumen, usually quite echogenic and fixed with changes in the patient's position. Ultrasound must describe the presence of wall alterations (assessment of lesions >3 mm), number, size, shape, and tumor staging.

In cases of superficial lesions, the bladder wall shows no echostructural alterations with a normal ultrasound appearance of the sandwich pattern (Figs. 35.5, 35.6, 35.7, and 35.8). Endophytic tumors appear as hypoechogenic, fixed proliferative lesions; however, they are sometimes hyperechogenic due to the presence of superficial calcifications.

In cases of infiltrating lesions, the bladder wall shows an interruption [11] or deformation, and sometimes the bladder tumor extends beyond the bladder wall. The hyperechoic layer of bladder mucosa is interrupted (Figs. 35.9, 35.10, and 35.11).

The diagnostic accuracy of US for bladder tumor diagnosis and staging [12] is generally considered to be poor (with a sensitivity ranging 50–94% [13]) in comparison with other diagnostic modalities such as CT scan or MRI. This wide discrepancy in sensitivity is related to some tumor factors (e.g., size, location, macroscopic aspects), patient factors (gender, body mass index, bladder filling), and operator-dependent factors (different levels of experience [14]; moreover, the type of US device and the technical modality of performing the ultrasound examination may explain such a wide variation in results for the diagnosis and staging of bladder cancer.

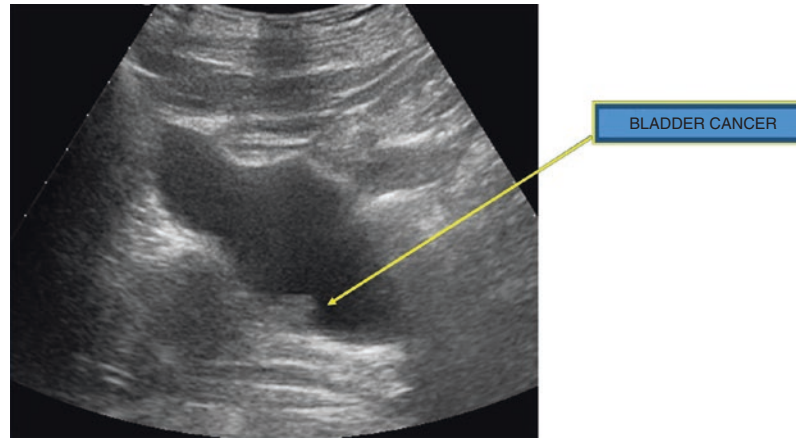

Fig. 35.5 A small exophytic tumor at bladder neck

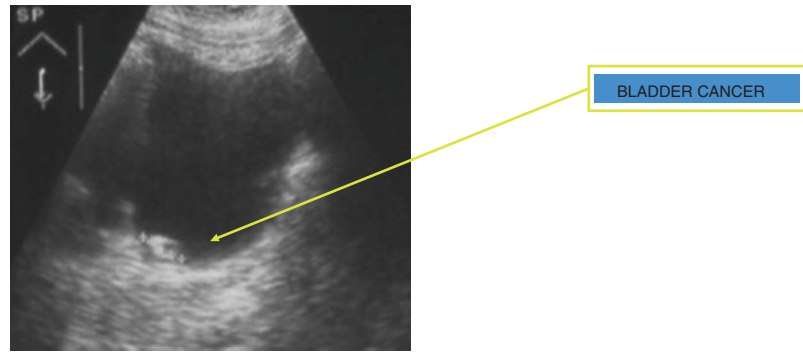

Fig. 35.6 A small, diffuse hyperechoic exophytic tumor at bladder wall. The normal hyperechoic internal layer is continued at tumor's base. This is a typical pattern of superficial bladder cancer

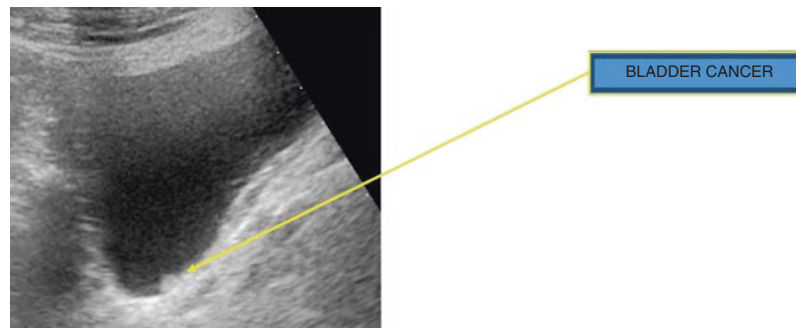

Fig. 35.7 Another small exophytic bladder mass at bladder base

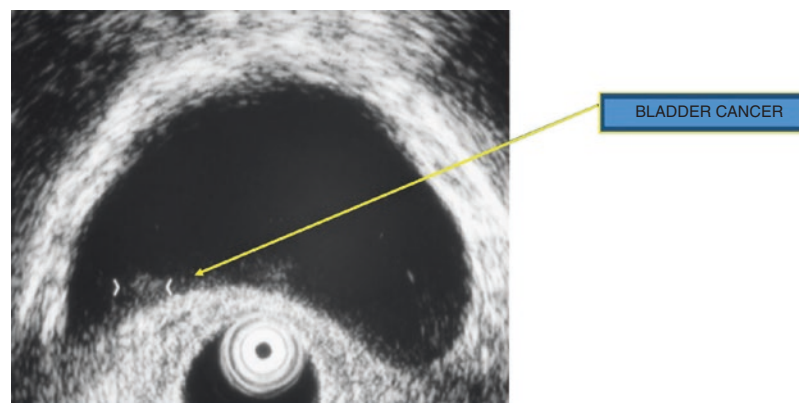

Fig. 35.8 Bladder scan by means of transrectal US. Abdominal US is negative

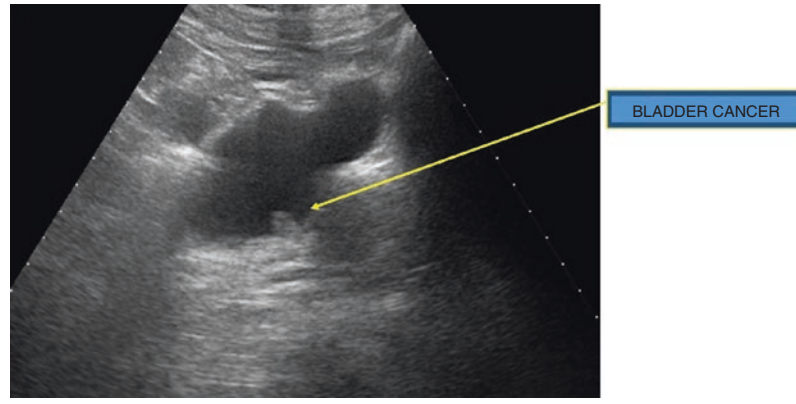

Fig. 35.9 Small bladder tumor at bladder neck. Despite small size, US shows partial interruption of the hyperechoic mucosa layer. This is a histologically confirmed case of infiltrating bladder cancer

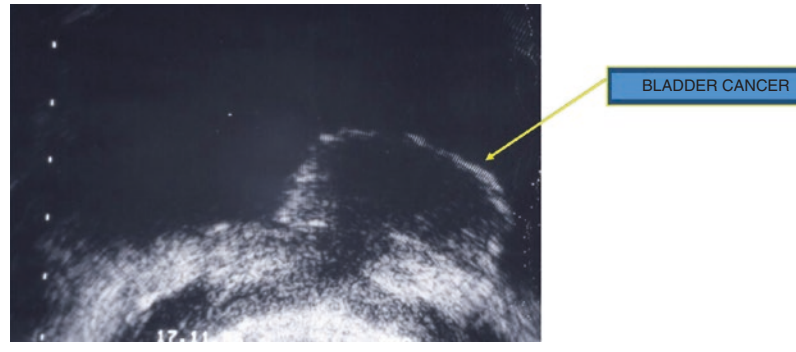

Fig. 35.10 A transrectal US showing an infiltrating bladder cancer. The entire bladder wall is diffusely interrupted, and the mass seems to reach the plane of seminal vesicle

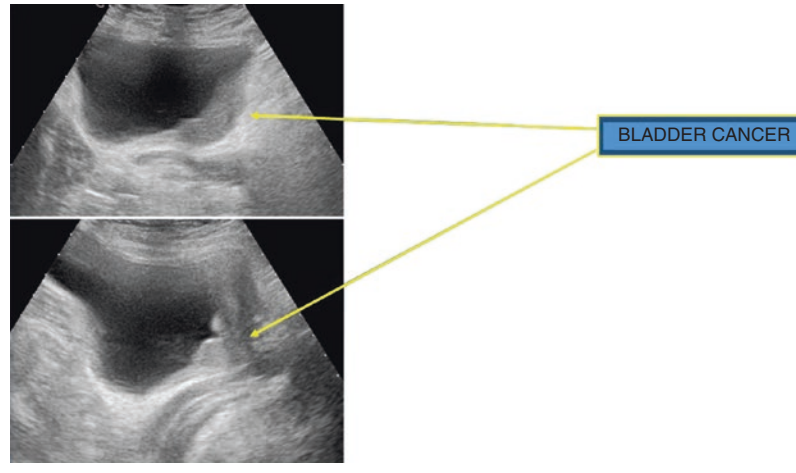

Fig. 35.11 A transverse and longitudinal picture of an infiltrating bladder cancer. The mass is partially exophytic with a large base, and the echostructural pattern of bladder wall is diffusely interrupted

35.4.1.1 Sensitivity and False-Negative Findings

The main limits of bladder ultrasound scanning depend upon spatial resolution and thus on the size, shape, and side of the bladder tumor.

Moreover, apart from the characteristics of bladder tumors, the ultrasound scan is limited by:

Bladder filling, which should be suboptimal in cases of acute or chronic cystitis

Bladder content, which is altered in cases of bladder catheterization by the balloon itself or by the presence of an air bubble or the contemporary presence of lithiasis

Bladder wall characteristics, such as in cases of progressive changes in the bladder wall observed in patients with lower urinary tract obstruction (bladder wall hypertrophy, diverticulosis, trabeculations)

Size: bladder lesions smaller than 5 mm may not be identified on ultrasound, especially on the bladder dome. On the other hand, the ability to diagnose vegetating/papillary lesions >5 mm is high.

Shape: flat or slow-growing non-vegetative tumors, such as carcinoma in situ, are not diagnosed by imaging.

Side: during abdominal US, the rain effect at the anterior bladder wall reduces spatial resolution [15] (Fig. 35.12), even for tumors >5 mm. Some small wall defects at the bladder neck or trigone could be confused with a median lobe (Fig. 35.13).

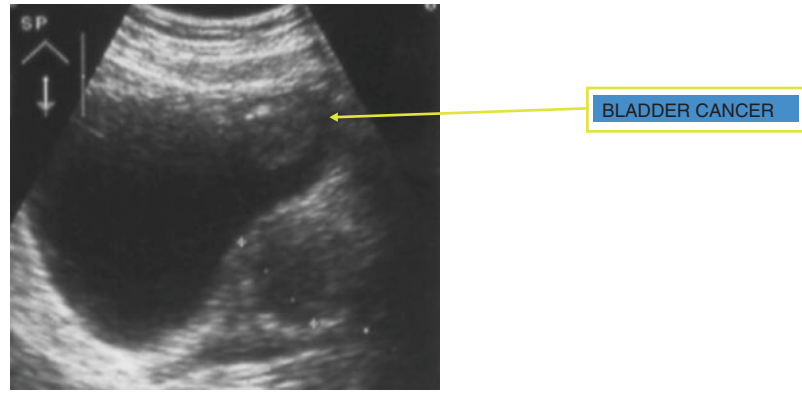

Fig. 35.12 A large, exophytic mass at anterior bladder wall. Note the difficulties in the correct identification of tumor's base, mainly due to the side of the tumor

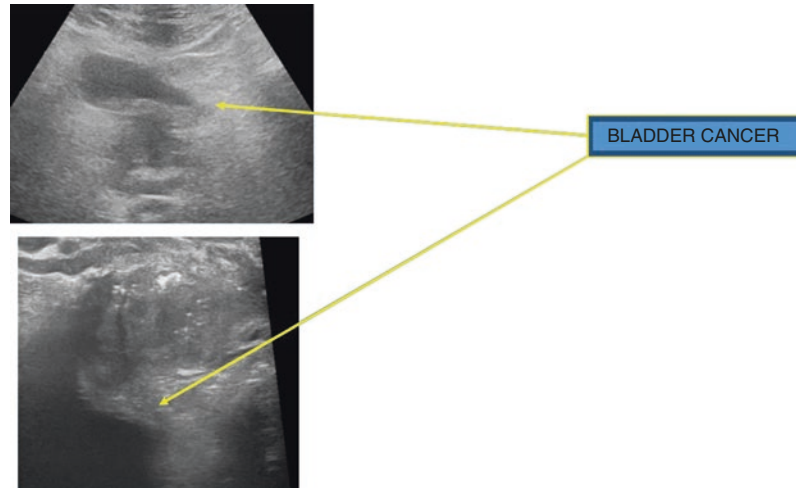

Fig. 35.13 An infiltrating bladder tumor at the bladder neck. At transverse abdominal US, due to tumor's side and reduced bladder filling, the ultrasound appearance of tumor is confusing. At linear transrectal US, bladder tumor is easily identified and distinctive from the normal prostate

35.4.1.2 Specificity and False-Positive Findings

A false-positive finding on an ultrasound scan is particularly frequent in cases of macroscopic hematuria or in cases of reduced bladder filling.

The most frequent cause of false-positive findings is represented by bladder wall hypertrophy caused by lower urinary tract obstruction. Bladder wall hypertrophy or diverticulosis or trabeculations could be confused with wall defects.

Other false-positive findings are represented by endovesical clots, which are frequent in cases of macroscopic hematuria independent from the primary cause. Clots appear as variably sized hyperechoic masses, usually on the bladder floor; they are mobile, depending on decubitus movements. In cases of clot adhesion to the bladder wall, the use of color Doppler will show the absence of a color signal.

Other common conditions associated with false-positive findings include acute or chronic cystitis. In acute conditions (Fig. 35.14), there is diffuse increased hypoechogenicity and an increased thickness of the bladder wall at the mucosa layer, especially at the level of the bladder floor and at the trigone. Anechoic bladder content is substituted by fine, mobile echoic pattern.

In chronic conditions, increased hyperechogenicity and thickness of the bladder wall at the mucosa level is more nonspecific, except in cases of tuberculosis or bilharziasis.

Another common cause of false positives is the presence of small or irregular prostatic median lobes.

Another rare condition associated with false-positive findings is the presence of urachal remnants.

Table 35.2 shows false-negative and false-positive findings related to bladder and tumor ultrasound scan.

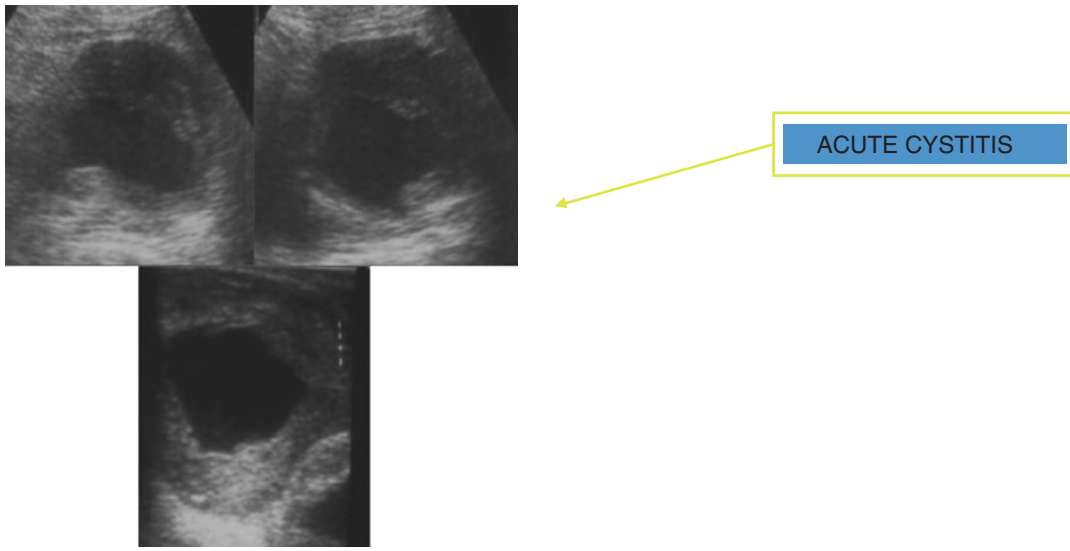

Fig. 35.14 A typical abdominal US in case of acute cystitis. The bladder filling is markedly reduced, and the irregular increased thickness of bladder wall is diffused

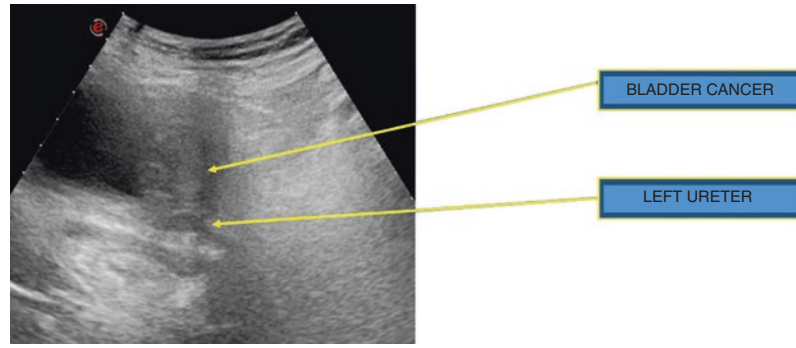

Fig. 35.15 Another picture showing an infiltrating bladder cancer causing distal ureteral dilation. Note the reduced bladder filling caused by the tumor

Table 35.2 Main reasons for false-negative and false-positive findings at bladder ultrasound scan

	False negative	False positive
Bladder	Filling (low or excessive)	Filling (low)
	Content (catheter, air, clots, stone)	Content (clots, stone)
	Detrusor hypertrophy	Detrusor hypertrophy
		Acute or chronic cystitis
Tumor	Size (<5 mm)	
	Side (anterior bladder wall, bladder neck, or trigone)	Side (median lobe)
	Shape (flat lesion)	

35.4.2 Nonneoplastic Bladder Disease

There are a number of nonneoplastic and inflammatory disorders that can manifest as a focal or diffuse bladder wall and alterations of bladder content and can sometimes mimic malignancy; therefore, ultrasound examination represents one helpful diagnostic tool.

Diffuse bladder wall thickening can develop secondary to many nonneoplastic conditions, including acute or chronic infection or inflammation and detrusor hypertrophy, while focal bladder wall alterations are derived from extrinsic causes, creating bladder filling defects, such as ureteral disease, urachal remnants, the median lobe of an enlarged prostate gland, and endometriosis. Alterations of content include bladder stones or clots.

35.4.2.1 Acute Cystitis

Acute cystitis symptoms often include a strong, persistent urge to urinate with pelvic discomfort and the presence of hematuria or strong-smelling urine.

While all these symptoms strongly suggest the diagnosis, they influence the ultrasound examination of the bladder with a reduction in bladder filling and/or the presence of abnormal bladder content (clots). Despite this, US is helpful in excluding secondary causes of cystitis, such as bladder outlet obstruction and bladder calculi.

A typical ultrasound picture of acute cystitis is characterized by diffuse and increased hypoechogenicity and increased thickness of the bladder wall accompanied by reduced bladder filling. The trigone area is frequently altered.

35.4.2.2 Chronic Cystitis

Chronic cystitis symptoms often include a chronic and persistent urge to urinate with pelvic pain and discomfort. It is derived from recurrent infection or other conditions, such as interstitial cystitis, cystitis cystica, cystitis glandularis, tuberculosis, schistosomiasis, and radiation and chemotherapy cystitis. Apart from the underlying cause, the most typical ultrasound feature of chronic bladder inflammation is the reduction of bladder filling.

Other aspects of US are mostly nonspecific. In chronic disease, the bladder wall presents irregular increased hyperechogenicity and increased thickness of the bladder wall. These US pictures should be diffuse or focal, the latter mimicking bladder tumors. This is typical of cystitis cystica or cystitis glandularis.

35.4.2.3 Detrusor Hypertrophy

Patients with lower urinary tract obstruction secondary to benign prostatic enlargement develop progressive changes in the bladder wall and in detrusor muscle. The high-pressure discharge causes an increase in the proportion of smooth muscle (hyperplasia/hypertrophy of the detrusor) to changes in the advanced stages of bladder decompensation (fibrosis), hyperactivity, and decreased functional capacity.

US easily depicts detrusor hypertrophy by a diffuse increase of bladder wall thickness or detrusor wall thickness by measuring the thickness of the hypoechoic detrusor muscle between the two layers of hyperechoic serosa and mucosa at a bladder filling of at least 250 ml. In the context of lower urinary tract obstruction and detrusor hypertrophy, conventional US detects established indirect signs of bladder damage, such as the presence of diverticula, stones, and post-void residual urine.

35.4.2.4 Ureteral Disease

Under normal conditions, US is relatively useless in studying the ureter. The lower end of the ureter, i.e., the vesicoureteric junction, is observed through the full bladder at the trigone level as a thin hypoechoic line within two hyperechoic lines.

In some circumstances, the ureteral orifices appear as protruding images, easily depicted on color Doppler examination when the urine reaches the bladder (ureteric jet).

The ureterocele is a particular thin-walled dilatation affecting the distal portion of the ureter which bulges into the bladder. The picture of US is that of a cystic structure projecting into the bladder, often near the normal location of the vesicoureteric junction. The associated ureter is usually noticeably dilated.

35.4.2.5 Urachal Remnants

The urachus is an important fetal structure connecting the dome of the bladder to the umbilical cord during fetal life, in the Retzius space. At birth, the urachus is obliterated becoming a vestigial structure anatomically known as the median umbilical ligament.

In the absence of normal involution process through complete obliteration, the urachus persists in a number of different abnormalities, which depends on the location and degree of obliteration: patent urachus, urachal cyst, and urachal diverticulum.

In cases of patent urachus, US shows an hypoechoic tubular structure between the bladder and the umbilicus; in cases of urachal cysts, US shows a midline lesion just above the anterosuperior aspect of the bladder; it is a protruding, hypoechoic lesion, which communicates within the bladder in cases of urachal diverticulum.

35.4.2.6 Prostate Median Lobe

Benign prostatic hyperplasia depicts a benign prostatic enlargement that causes progressive obstruction of the bladder outlet. This prostatic enlargement, however, does not occur homogeneously; this is the case for prostatic protrusion into the bladder, creating the so-called prostate median lobe. As a consequence, the hypertrophied median lobe of the prostate projects into the bladder lumen, simulating a bladder mass.

At US, a median lobe appears as a solid echogenic mass, which continues within the prostate and protrudes into the urinary bladder lumen.

Table 35.3 briefly illustrates most common ultrasound appearances of neoplastic and nonneoplastic disease of the bladder.

35.5 New Technology in Ultrasound

Conventional US is an easily repeatable, safe, cost-effective, and a noninvasive technique which furthermore does not require a special

Table 35.3 Most common ultrasound pattern of different bladder disease

		Ultrasound appearance
Neoplastic disease	Superficial	In small tumor (<5 mm), generally no echostructural alterations of the entire wall. Endophytic tumors appear as hypoechogenic, fixed proliferative lesions, but sometimes they are hyperechogenic due to the presence of superficial calcifications. Hypervascularization is observed on color Doppler
	Infiltrating	Interruption or deformation of the wall, which appears thickened; some extension beyond the bladder wall. Hypervascularization is observed on color Doppler
Nonneoplastic disease	Acute cystitis	Increased hypoechogenicity, diffuse increased thickness of bladder wall between the serosa and mucosa. Reduced bladder filling
	Chronic cystitis	Irregular increased hyperechogenicity, increased thickness of bladder wall. No characteristic pattern except for reduced bladder filling
	Detrusor hypertrophy	Increased detrusor thickness (>3 mm) with irregularities (trabeculations or even pseudo diverticula). Increased hypoechogenic tissue included between the two lines of hyperechogenic tissue representing mucosa and bladder serosa. Presence of diverticula with the formation of anechogenic paravesical areas with the presence of a sonic funneling to the bladder (diverticular neck)
	Stone	Hyperechoic lesion with acoustic shadow, mobile depending on decubitus movements
	Clot	Hypo-/hyperechoic lesion usually without acoustic shadow, mobile depending on decubitus movements. No vascularization is observed on color Doppler
	Ureteral disease	Hyperechogenic image with posterior shadow included in the thickness of the ureteral wall in cases of ureteral stones. Anechogenic formation (cyst) at the level of the ureteral meatus with evidence on color Doppler of ureteral jet in cases of ureterocele. Hypo- or hyperechogenic image with ureteral dilation in case of infiltrative bladder cancer (Figs. 35.15) involving ureteral meatus
	Urachal remnant	Hypoechoic structure between the bladder and the umbilicus in the Retzius space as a tubular structure, a hypoechoic cystic lesion just above the anterosuperior aspect of the bladder, or as a protruding, hypoechoic lesion. Different aspects of US depend upon the existence of complications, such as infection, stones, and carcinoma after puberty
	Prostatic median lobe	Hypoechogenic area at the bladder neck, which continues within the prostate on transrectal ultrasound scan

preparation; in the same session, it provides images of both the upper and lower renal tract. However, US is still considered to be an imaging tool with low accuracy. The progressive evolution of ultrasound devices and dedicated software has increased the diagnostic accuracy of this examination through the combination of different transducers and the use of color Doppler imaging [16, 17] (Fig. 35.16), which increases the accuracy in the detection of intraluminal filling defects of the bladder, reducing the limits introduced by patients or tumor characteristics.

35.5.1 Contrast-Enhanced Ultrasound

In the diagnosis of bladder disease and bladder cancer, conventional ultrasound relies on the detection of isolate bladder wall thickening or by the detection of a >5-mm mass protruding into the bladder lumen. These concepts easily explain the overall accuracy of US in the detection of bladder lesions which variably depends on several factors, including the US equipment, distension of the bladder, size, morphology, and location of the lesions. Consequently, conventional US has some

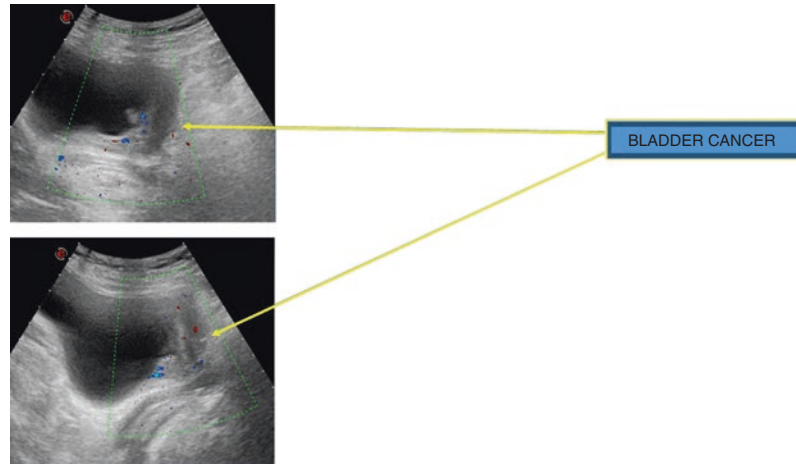

Fig. 35.16 Infiltrating bladder mass at color Doppler transverse and longitudinal scans

limits in detecting tumors that are small, or flat, or located on the anterior bladder wall or bladder floor in presence of BPH.

A common tumor characteristic is the presence of a proliferative pattern with an increase in vascularity, and this pattern is the basis for the use of contrast-enhanced US (CEUS) [18]. The contrast agents used in ultrasound equipment are characterized by a microbubble structure composed of gas bubbles stabilized by a shell. This US contrast agent is exclusively intravascular and together with the aid of a specific contrast software is very helpful in the detection of tissue or tumor microvascularization.

The most commonly used contrast agent is SonoVue (SonoVue, Bracco, Italy) at a standard intravenous dose of 2.4 ml using a 21-gauge peripheral intravenous cannula, followed by a 5-ml saline flush.

After a complete baseline US evaluation of the bladder, dynamic CEUS was performed using the specific contrast software currently available. CEUS was performed using a low mechanical index [19] to avoid microbubble disruption (the power of the ultrasound beam must be set to a mechanical index of 0.06–0.09), and in these conditions, the dynamic real-time evaluation of bladder wall enhancement, including the arterial and venous phases, is achieved.

Under normal conditions and upon adequate bladder filling, the bladder wall appears as a thin 2–3-mm wall demonstrating a progressive, diffuse enhancement starting 15–20″” after the intravenous administration of contrast agent; this contrast enhancement usually lasts more than 2 min. In case of a neovascularization such as in case of bladder cancer, the contrast-enhanced ultrasound scan depicts an early enhancement in a protruding papillary or sessile lesion or in a flat focal wall thickening, which is earlier than the rest of normal surrounding bladder wall. This typical enhancement is generally intense and homogeneous, while in some large invasive tumors, the enhancement may be more heterogeneous since large bladder tumors sometimes contain avascular necrotic areas. After the early arterial phase, a steady state with a signal plateau may be observed, followed by a slow washout pattern. In case of infiltrating bladder cancers, this typical contrast slow washout becomes faster.

The use of a US contrast agent improves the detection rate of bladder cancer, which is particularly helpful in the differential diagnosis between tumors and clots and in cases of reduced bladder distension, stones, intravesical catheters, cystitis, and the prostatic median lobe. It is also beneficial as an adjunctive tool for the differential diagnosis

of bladder cancer from other benign bladder entities that mimic bladder cancer [20].

In bladder cancer staging, CEUS is helpful to determine wall invasion [21] by evaluating the early enhancement and a faster washout in invasive bladder cancers and in differentiating low- and high-grade disease [22].

35.5.2 Three-Dimensional US (Virtual Cystoscopy) and Three-Dimensional Contrast-Enhanced Ultrasound

The use of conventional two-dimensional US is limited by many factors, including the expertise of the examiner, while the 3D images generated from software similar to CT or MR imaging overcome many technical and examiner limits [23].

Three-dimensional US and three-dimensional contrast-enhanced ultrasound (3D CEUS) imaging [24–26] are new imaging techniques that allow the examiner to review all the images that are spatially reconstructed using different visual angles.

Three-dimensional sonography with virtual sonographic cystoscopy [27, 28] has some advantages over other virtual techniques because catheterization is not necessary [29]. The 3D images, however, depend upon the quality of image acquisition since 3D reconstruction represents all of the original artifacts. The most common cause of inadequate pictures is patient motion or transducer movement during acquisition, following the rule that the faster the data can be acquired, the less likely it is that artifacts will occur. Other common artifacts related to US itself (shadowing, reverberations) are amplified by post-image processing.

35.6 Follow-Up of Bladder Cancer

At the time of presentation, approximately 75 % of patients with bladder cancer have superficial tumors confined to the mucosa (Ta) or the lamina propria, and despite the efficacy of transurethral resection and adjuvant therapy, most tumors will recur at follow-up. Despite the evidence that most recurrent tumors are of low stage and grade, 10–25 % may progress to a higher grade and stage. This explains the need for stringent, long-term follow-up to detect recurrence and/or the progression of bladder tumors.

After conservative treatment, the current guidelines recommend a cystoscopic surveillance protocol at 3 months initially, continuing at increasing intervals. The follow-up protocol usually includes a cystoscopy, which is effective but invasive; therefore, many investigators have sought noninvasive tests to replace it [30, 31]. Because bladder US may be able to detect small bladder tumors, many studies [32–35] have analyzed the sensitivity and specificity of US in the detection of recurrent tumors, resulting in a sensitivity ranging from 50 to 74 % [36] and a specificity ranging from 83 to 90 % [37]. However, as for the primary diagnosis of bladder tumors, US is limited as an accurate tool for the detection of small or flat tumors, such as CIS.

Bibliography

1. Totaro A, Pinto F, Brescia A, Racioppi M, Cappa E, D'Agostino D, Volpe A, Sacco E, Palermo G, Valentini A, Bassi P (2010) Imaging in bladder cancer: present role and future perspectives. Urol Int 85:373–380
2. Datta SN, Allen GM, Evans R, Vaughton KC, Lucas MG (2002) Urinary tract ultrasonography in the evaluation of haematuria a report of over 1000 cases. Ann R Coll Surg Engl 84:203e5
3. Francica G, Bellini SA, Scarano F, Miragliuolo A, De Marino FA, Maniscalco M (2008) Correlation of transabdominal sonographic and cystoscopic findings in the diagnosis of focal abnormalities of the urinary bladder wall: a prospective study. J Ultrasound Med 27:887–889
4. Pavlica P, Gaudiano C, Barozzi L (2004) Sonography of the bladder. World J Urol 22:328–334
5. Koraitim M, Kamal B, Metwalli N, Zaky Y (1995) Transurethral ultrasonographic assessment of bladder carcinoma: its value and limitation. J Urol 154:375–378
6. Horiuchi K, Tsuboi N, Shimizu H, Matsuzawa I, Kimura G et al (2000) High-frequency endoluminal ultrasonography for staging transitional cell carcinoma of the bladder. Urology 56:404–407

7. Saga Y, Numata A, Tokumitsu M, Yamaguchi S, Fujii H et al (2004) Comparative study of novel endoluminal ultrasonography and conventional transurethral ultrasonography in staging of bladder cancer. Int J Urol 11:597–601
8. Xu C, Zhang Z, Wang H, Song Q, Wei R, Yu Y, Li J, Sun Y (2014) A new tool for distinguishing muscle invasive and non-muscle invasive bladder cancer: the initial application of flexible ultrasound bronchoscope in bladder tumor staging. PLoS One 9(4):e92385. doi:10.1371/journal.pone.0092385
9. Martino P, Galosi AB, Bitelli M, Consonni P, Fiorini F, Granata A, Gunelli R, Liguori G, Palazzo S, Pavan N, Scattoni V (2014) Virgili G; Imaging Working Group-Societa Italiana Urologia (SIU); Società Italiana Ecografia Urologica Andrologica Nefrologica (SIEUN). Practical recommendations for performing ultrasound scanning in the urological and andrological fields. Arch Ital Urol Androl 86:56–78
10. Dibb MJ, Noble DJ, Peh WC et al (2001) Ultrasonographic analysis of bladder tumors. Clin Imaging 25(6):416–420
11. Singer D, Itzchak Y, Fischelovitch Y (1981) Ultrasonographic assessment of bladder tumors. Part II. Clinical staging. J Urol 126:34–36
12. McLaughlin IS, Morley P, Deane RF, Barnett E, Graham AG, Kyle KF (1975) Ultrasound in the staging of bladder tumours. Br J Urol 47:51–56
13. Knox MK, Cowan NC, Rivers-Bowerman MD, Turney BW (2008) Evaluation of multidetector computed tomography urography and ultrasonography for diagnosing bladder cancer. Clin Radiol 63:1317–1325
14. Francica G, Scarano F, Bellini SA, Miragliuolo A (2011) Prospective evaluation of interobserver diagnostic agreement for focal urinary bladder wall abnormalities detected by ultrasound. J Ultrasound 14:1–6
15. Ozden E, Turgut AT, Turkolmez K, Resorlu B, Safak M (2007) Effect of bladder carcinoma location on detection rates by ultrasonography and computed tomography. Urology 69:889–892
16. Horstman WG, McFarland RM, Gorman JD (1995) Color Doppler sonographic findings in patients with transitional cell carcinoma of the bladder and renal pelvis. J Ultrasound Med 14:129e33
17. Karahan OI, Yikilmaz A, Ekmekcioglu O, Ozturk F, Sevinc H (2004) Color Doppler ultrasonography findings of bladder tumors: correlation with stage and histopathologic grade. Acta Radiol 45:481e6
18. Nicolau C, Bunesch L, Sebastia C, Salvador R (2010) Diagnosis of bladder cancer: contrast-enhanced ultrasound. Abdom Imaging 35:494–503
19. Drudi FM, Cantisani V, Liberatore M et al (2010) Role of low-mechanical index CEUS in the differentiation between low and high grade bladder carcinoma: a pilot study. Ultraschall Med 31:589–595
20. Nicolau C, Bunesch L, Peri L et al (2010) Accuracy of contrast-enhanced ultrasound in the detection of bladder cancer. Br J Radiol 84:1091–1099
21. Caruso G, Salvaggio G, Campisi A, Melloni D, Midiri M, Bertolotto M, Lagalla R (2010) Bladder tumor staging: comparison of contrast-enhanced and gray-scale ultrasound. AJR Am J Roentgenol 194:151–156
22. Li QY, Tang J, He EH, Zhou Y, Li YM, Fei X, Zhang Y (2012) Role of contrast-enhanced ultrasound in the differentiation of high- and low-grade urothelial carcinoma. Zhongguo Yi Xue Ke Xue Yuan Xue Bao 34(4):364–368
23. Mitterberger M, Pinggera GM, Neuwirt H et al (2007) Three-dimensional ultrasonography of the urinary bladder: preliminary experience of assessment in patients with haematuria. BJU Int 99:111–116
24. Wagner B, Nesslauer T, Bartsch G Jr, Hautmann RE, Gottfried HW (2005) Staging bladder carcinoma by three-dimensional ultrasound rendering. Ultrasound Med Biol 31:301–305
25. Li QY, Tang J, He EH, Li YM, Zhou Y, Zhang X, Chen G (2012) Clinical utility of three-dimensional contrast-enhanced ultrasound in the differentiation between noninvasive and invasive neoplasms of urinary bladder. Eur J Radiol 81:2936–2942
26. Park HJ, Hong SS, Kim JH et al (2010) Tumor detection and serosal invasion of bladder cancer: role of three-dimensional volumetric reconstructed US. Abdom Imaging 35:265–270
27. Lopes RI, Nogueira L, Albertotti CJ, Takahashi DY, Lopes RN (2008) Comparison of virtual cystoscopy and transabdominal ultrasonography with conventional cystoscopy for bladder tumor detection. J Endourol 22:1725–1729
28. Kocakoc E, Kiris A, Orhan I, Poyraz AK, Artas H, Firdolas F (2008) Detection of bladder tumors with 3-dimensional sonography and virtual sonographic cystoscopy. J Ultrasound Med 27(1):45–53
29. Song JH, Francis IR, Platt JF et al (2001) Bladder tumor detection at virtual cystoscopy. Radiology 218:95–100
30. Vera-Donoso CD, Llopis B, Oliver F, Server G, Alonso M, Jimenez-Cruz JF (1990) Follow-up of superficial bladder cancer: how to spare cystoscopies? Eur Urol 17:17e9
31. Pegoraro C, Bondavalli C, Molani L et al (1997) Suprapubic bladder ultrasonography and urinary cytology: indications and limits in the follow-up of superficial bladder tumors. Arch Ital Urol Nefrol Androl 63:127–129
32. Vallancien G, Veillon B, Charton M, Brisset JM (1986) Can transabdominal ultrasonography of the bladder replace cystoscopy in the follow up of superficial bladder tumors? J Urol 136(1):32–34
33. Berlac PA, Holm HH (1992) Bladder tumor control by abdominal ultrasound and urine cytology. J Urol 147(6):1510–1512
34. Nisman B, Yutkin V, Peretz T, Shapiro A, Barak V, Pode D (2009) The follow-up of patients with non-muscle-invasive bladder cancer by urine cytology,

abdominal ultrasound and urine CYFRA 21–1: a pilot study. Anticancer Res 29(10):4281–4285
35. Stamatiou K, Moschouris H, Papadaki M, Perlepes G, Skolarikos A (2011) Accuracy of modern ultrasonographic techniques in the follow up of patients with superficial bladder carcinoma. Med Ultrason 13:114–119
36. Cariou G, Maaraoui N, Cortesse A (1997) Can the combination of bladder ultrasonography and urinary cytodiagnosis replace cystoscopy in the diagnosis and follow-up of tumors of the bladder? Prog Urol 7:51e5
37. Davies AH, Cranston D, Meagher T, Fellows GJ (1989) Detection of recurrent bladder tumours by transrectal and abdominal ultrasound compared with cystoscopy. Br J Urol 64:409.e11

Functional Ultrasound: Assessment of the Weight and Thickness of the Detrusor

36

Cosimo De Nunzio, Fabrizio Presicce, and Andrea Tubaro

36.1 Introduction

Lower urinary tract symptoms (LUTS) are a clinical condition commonly found in men over 50 years and also tend to rise progressively with age. Because of increased life expectancy, the number of patients with LUTS and the relative costs of diagnosis and treatment are still growing in Western countries [1]. LUTS may include voiding and storage urinary symptoms or a combination of both, and they may be considered a consequence of benign prostatic obstruction (BPO) with its related effect on detrusor function [2, 3].

Urodynamic investigation with pressure-flow studies (PFS) is the gold standard for the evaluation and grading of BPO and detrusor contractility. However, it represents an invasive procedure with possible side effects, which make its routine clinical application controversial and not universally used. Moreover, costs and invasiveness of PFS might not be justified by the actual clinical benefit for the patient [2, 4, 5].

PFS is also an expensive, invasive, time-consuming procedure, associated with several complications in up to 19 % of investigated men, including macroscopic haematuria, urinary tract infections, sepsis, or urinary retention [6]. Therefore, over the last few years, several alternative methods to pressure-flow study have been proposed to predict BOO, as the ultrasound assessment of the bladder/detrusor wall thickness (BWT/DWT).

36.2 Background

The modification of bladder wall secondary to an obstruction has been evaluated in several studies mainly using animal models of BOO. All studies agree that a significant increase in the thickness and weight of the bladder is recorded, after partially induced BOO.

Ghoniem et al. reported that mean bladder wall thickness in control, partially obstructed and severely obstructed rabbits was 1.57, 2.04 and 2.77 mm, respectively, with most thickening in the detrusor layer [7]. Histological analysis revealed smooth muscle cell hypertrophy and hyperplasia, raised collagen deposition collagen and increased expression of muscarinic

Electronic supplementary material The online version of this chapter (doi:10.1007/978-3-319-40782-1_36) contains supplementary material, which is available to authorized users.

C. De Nunzio, MD, PhD (✉)
Department of Urology, Sant'Andrea Hospital, "Sapienza" University of Rome, Rome, Italy
e-mail: cosimodenunzio@virgilio.it

F. Presicce • A. Tubaro
Department of Urology, Sant'Andrea Hospital, "Sapienza" University of Rome, Rome, Italy

P. Martino, A.B. Galosi (eds.), *Atlas of Ultrasonography in Urology, Andrology, and Nephrology*,
DOI 10.1007/978-3-319-40782-1_36

cholinergic receptors [7]. Analogous histological patterns were observed in patients with BOO and detrusor overactivity (DO) and in those undergoing augmentation surgery for high intravesical pressure [8]. Furthermore, smooth muscle cell hypertrophy, collagen accumulation and increased bladder weight have been shown to partially regress after BOO relief in pig models [9]. Therefore, all this evidence suggested a close correlation between the thickness of the bladder wall and BOO.

Tubaro and Miano firstly proposed the similarity between the effects of an increased workload in the myocardium and in the bladder detrusor. Notwithstanding the evident differences between the detrusor and the heart muscle fibres, at both levels increased outlet resistance may arise up in case of BOO and hypertension, respectively, leading to an early hypertrophic compensatory reaction, eventually followed by decompensation leading to acute urinary retention and congestive heart failure, respectively [10].

With this knowledge in mind, Kojima in 1996 suggested the ultrasound-estimated bladder wall (UEBW) as a proxy to predict BOO [11]. Two years later, Manieri et al. first proposed the evaluation of the bladder thickness as a predictor of BOO [12]. After these initial experiences, several papers on the same topics were published, suggesting that the evaluation of bladder weight and thickness as further area of application of ultrasound technology in the field of urology.

36.3 Bladder Wall Thickness (BWT)/Detrusor Wall Thickness (DWT)/ Ultrasound-Estimated Bladder Weight (UEBW): Measurement Techniques

In 2010 an International Consensus of the Incontinence Research Society (IRS) supported the standardization of measurement techniques to increase the reproducibility and comparability of the assessments [13]. The bladder wall can be measured either with an external approach (suprapubic and perineal) that intracavitary (transrectal in male patients and transvaginal in female). There is little evidence comparing the different methods, but the available data show a good deal of overlap between the transrectal and suprapubic techniques; for this reason and because of less invasiveness, the latter was the method mostly adopted [13].

The resolution of the ultrasound image is frequency dependent: a higher ultrasound frequency is associated to a better resolution. High-frequency probes (i.e. 7.5 MHz) have a resolution of less than 0.13 mm, while ultrasonic probes with a frequency of 3.5 MHz have a resolution of about 0.3 mm. DWT ranges between 1.1 and 1.8 mm in filled bladder of healthy male volunteers or non-obstructed patients and reaches about 2 mm or more in obstructed patients. Therefore, high-frequency probes are needed to capture small differences.

Furthermore, it is necessary to adequately enlarge the ultrasound images to allocate precise markers and place an accurate bladder assessment. Digital ultrasound machines for clinical use are able to enlarge the image from 5 to 15 times. If the image has not been properly enlarged, inaccurate placement of the markers would result in large differences in measurement and could lead to miscalculations.

During the ultrasound assessment, the inner and outer layers of the bladder wall appear hyperechoic (white) and represent the mucosa with submucosa and adventitia, respectively. The detrusor seems hypoechoic (black) and is "sandwiched" between the hyperechoic lines of the adventitia and mucosa. BWT assessment consists in the measurement of all three bladder layers; DWT includes only detrusor (Fig. 36.1). Therefore, the values of BWT are always higher than the values of DWT in the same patient, and the direct comparison of the two values is not possible [13]. Oelke et al. supported the need to exclusively evaluate DWT instead of BWT in order to minimize possible interferences considering that the detrusor is the only layer of the bladder involved in the process of thickening, whose muscle cells experience hyperplasia and hypertrophy due to the increased workload of the bladder [13]. Moreover, the adventitious and/or

mucosa may be affected by other diseases (e.g. inflammation or tumour), and the measurement of these layers may cause an increase in false-positive BWT. However, in clinical practice, it is sometimes difficult to distinguish the adventitious hyperechoic from fat perivesical causing erroneous placement of the markers [13].

The optimal solution for the correct measurement is placing the probe's beam perpendicular to the bladder wall, so that both the adventitia and the mucosa appear as straight and parallel lines. Video 36.1 shows the measurement technique of DWT proposed by Oelke et al.

A critical element to consider when making a measurement is that the BWT and the DWT depend on bladder filling in the range between 50 and 250 ml. Khullar et al. firstly showed no significant differences of BWT in almost empty bladder and those filled up to 50 ml [14]. Additionally, Oelke found that in healthy adult volunteers of both sexes, the DWT decreases rapidly between 50 and 250 ml of bladder filling (or up to 50% of the capacity of the bladder), but then reaches a plateau with only small and insignificant differences between 250 ml and the maximum bladder capacity [15] (Fig. 36.2).

Therefore, to avoid possible bias related to bladder filling, it is important to follow some recommendations: perform the assessment at the same volume, by inserting a catheter and filling the bladder until a preset value of 150 ml in the technique proposed by an Italian group coordinated by Prof. Tubaro [12] (Video 36.2), or use an empty bladder as proposed in female patients by Khullar V or use at least 250 ml of bladder volume (Oelke technique). The latter option could be the more advantageous because it is less invasive than that proposed by Tubaro et al. and easier to perform. Notwithstanding all these techniques, bladder volume is still a controversial issue in BWT/DWT assessment as detrusor thickness changes according to a different bladder volume (Video 36.3).

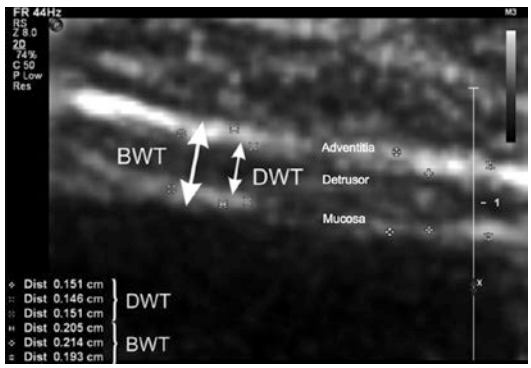

Fig. 36.1 The inner and outer layers of the bladder wall appear hyperechoic (*white*) and represent the mucosa with submucosa and adventitia, respectively. The detrusor seems hypoechoic (*black*) and is "sandwiched" between the hyperechoic lines of the adventitia and mucosa. BWT assessment consists in the measurement of all three bladder layers; DWT includes only detrusor

Kojima proposed an alternative approach to definitively overcome the influence of bladder filling [11]. The Japanese group adopted the UEBW as a parameter to evaluate detrusor thickness instead of BWT/DWT. They considered the bladder as a ball, and the volume of the bladder wall was calculated by subtracting the volume of intravesical bladder to total volume. The UEBW was obtained by multiplying this parameter with the specific weight (Fig. 36.3). However, the technique presents the disadvantage that small errors of the volume evaluation (since based on measurements in the third potency) have a great impact on UEBW.

Another important issue in BWT/DWT assessment is in which bladder site to perform the measurements. Several evidences showed that all parts of the bladder (dome, anterior, posterior or lateral walls) presented the same thickness in the same patient at the same degree of bladder filling; therefore, any portion of the bladder can be used for the assessment of the thickness [13]. However, some authors recommend performing the measurement at the level of the anterior wall. In fact, using ultrasound probes with high frequency and with high magnification, the anterior wall is the portion of the bladder better accessible. Finally, it is recommended not to be limited to a single measurement but performing at least three and calculating the BWT or DWT as the average of three measurements [13].

Applying all these recommendations, in selected centres, achieved excellent results in terms of reproducibility, since intraexaminer

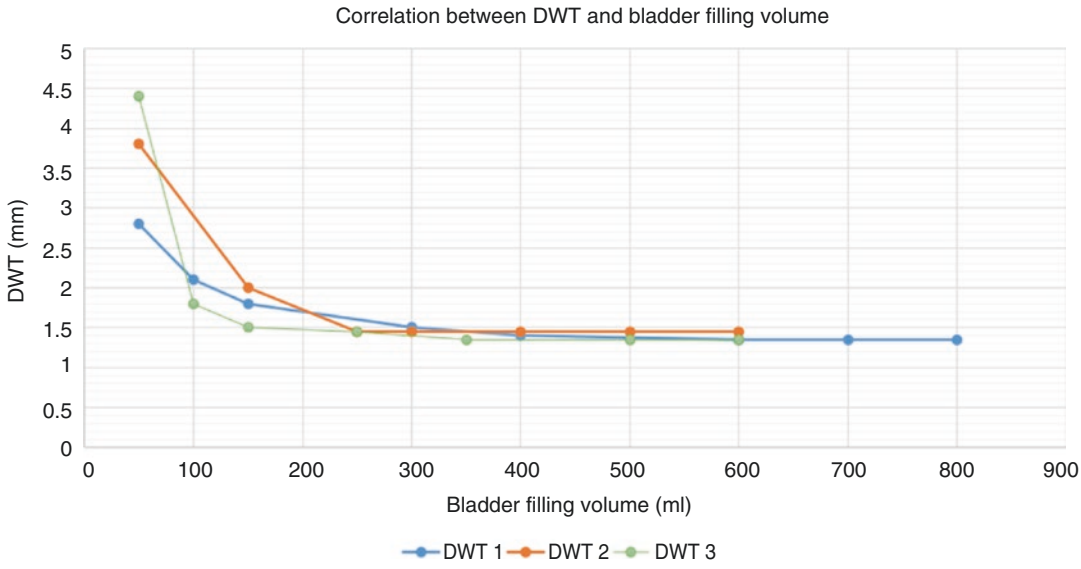

Fig. 36.2 Correlation between DWT and bladder filling volume in three unobstructed male volunteers. The DWT decreases rapidly up to a bladder filling of 250 ml and then reaches a plateau (Adapted from Oelke et al. [15])

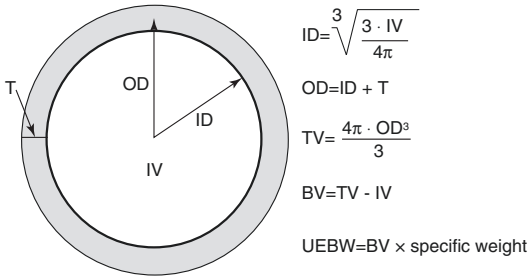

Fig. 36.3 Formula and schematic design for UEBW measurement (Adapted from Kojima et al. [11])

variability was less than 5 % and interexaminer ranged between 4 and 12 % [16, 17].

36.4 Bladder Wall Thickness (BWT)/Detrusor Wall Thickness (DWT) and Bladder Outlet Obstruction (BOO)

First in 1996, the Japanese group led by Kojima proposed a relationship between UEBW and BOO [7] assessed by pressure/flow study (PFS). They found that the mean UEBW was significantly higher in obstructed patients (mean UEBW 46.2 g) than in healthy ones (mean UEBW 29.3 g). Choosing a threshold of more than 35 g for UEBW to predict BOO, ROC analysis showed 87.9 % of diagnostic accuracy [11]. However, the study was conducted only on Asian patients; therefore, it is questionable that a threshold value of 35 g is applicable in other populations. Furthermore, all subsequent studies about UEBW were always conducted in Asian populations.

The first experience regarding the BWT assessment as tool to predict BOO in patients with prostatic hypertrophy dates back to 1998. Manieri et al. showed that obstructed patients presented a significantly higher BWT than those without BOO (mean BWT 5.0 versus 3.6 mm) and the degree of obstruction was directly correlated with the BWT [12]. A threshold value of 5 mm for BWT seemed the most accurate cut-off to distinguish between patients with or without BOO: patients with BWT less than 5 mm were not obstructed (Schaefer class < 2 at PFS) in 63 % of cases, while 88 % of those with BWT of 5 mm or more presented BOO (Schaefer class ≥ 3 at PFS). The BWT showed a diagnostic accuracy of 0.8608 at ROC analysis [12].

Afterwards, Oelke et al. successfully evaluated the correlation between BOO and DWT, assessed according to their technique. Using a threshold value of 2 mm, they correctly classified 95 % of men with BOO [18]. The same technique was adopted by Kessler et al., who measured the DWT in 102 patients with clinical benign prostatic hyperplasia (BPH). Using the threshold values of 2.0, 2.5 or 2.9 mm, they correctly identified 81, 89 and 100 % of patients with BOO, respectively [17]. In a further experience, Oelke et al. evaluated the DWT in 70 patients with lower urinary tract symptoms. The values of DWT in non-obstructed, equivocal, and obstructed patients, thus classified according to PFS results, were 1.33 mm (95 % CI, 1.17–1.48), 1.62 mm (95 % CI, 1.48–1.76) and 2.4 mm (95 % CI, 2.12–2.68), respectively. Moreover, they found a statistically significant difference of DWT ($p < 0.001$) between obstructed and non-obstructed patients and between patients with equivocal PFS for obstruction and obstructed patients. No significant differences were observed between non-obstructed and equivocal patients ($p = 0.349$) [19]. As described in their previous study, a threshold of 2 mm was the best cut-off for discriminating patients with or without BOO with the highest specificity (97.3 %) and positive predictive value (95.5 %). Despite these experiences seem to confirm a positive correlation between BWT and BOO, there are some controversial studies showing no associations. Blatt et al. found no significant differences of BWT in patients with BOO ($n = 39$) compared to those with normal PFS ($n = 69$) [20]. However, inexperience with the measurement technique, the inclusion in the study of patients of both sexes and with mainly low-grade BOO, inappropriate placement of markers and assessing the concomitant treatment with α-blockers may have led to these controversial results. Nevertheless, recently Franco et al. confirmed the effectiveness of BWT in predicting a condition of BOO. They included in the study one hundred male patients with LUTS. BWT was assessed according to Tubaro technique, and a threshold value of 6 mm was chosen to predict BOO. BWT demonstrated a diagnostic accuracy evaluated by ROC analysis of 0.845 (95 % CI 0.78–0.91), even better than other non-invasive methods of evaluation of BOO: maximum flow rate (Qmax) 0.779, the post-void residual (0.699) and prostate volume (0.626) [21]. Moreover, in the same study, Franco et al. evaluated the intravesical prostatic protrusion (IPP), another ultrasound parameter recently proposed as non-invasive technique for the assessment of BOO. The addition of IPP to BWT has determined the best diagnostic accuracy, reaching 87 % [21].

Table 36.1 lists the results obtained in terms of diagnostic accuracy in the various experiences mentioned above.

BWT/DWT evaluation has been also proposed as a possible parameter to evaluate patients' response to medical and surgical treatment in patients with LUTS/BPH. Tubaro et al. measured BWT in 32 LUTS/BPH patients undergoing transvesical adenomectomy (ATV) [22]. BWT values have been significantly reduced even after 1 week from the operation, reaching a nadir at 6 weeks, and remaining stable up to 12 months (mean BWT before surgery versus BWT 1-year after surgery: 5.2 ± 0.7 mm compared to 2.9 ± 0.9 mm, $p < 0.01$) [22]. Moreover, Egilmez et al. evaluated the modification of BWT in LUTS/BPH patients treated with α-blockers. After 3 months of treatment, the reduction of the BWT was directly correlated with the reduction of symptoms assessed by IPSS; they also showed that in these patients α-blockers can reduce the BWT of 23 % already after 1 month of treatment and this reduction seems to correlate with the improvement of Qmax [23].

36.5 Bladder Wall Thickness (BWT)/Detrusor Wall Thickness (DWT) and Detrusor Overactivity (DO)

The hypothesis that an increased bladder thickness is related to an increased workload, Khullar V firstly proposed the use of BWT for

Table 36.1 Measurement techniques of BWT/DWT and outcomes

Studies	Bladder filling at measurement	Ultrasound approach (MHz)	Evaluated parameter	Threshold value	Outcome (AUC)
Male patients with BOO					
Manieri et al. [12]	150 ml	TAUS (3.5)	BWT	BOO if BWT >5 mm	0.860 (95 % CI not available)
Oelke et al. [18]	Maximum bladder capacity	TAUS (7.5)	DWT	BOO if DWT >2 mm	0.955 (95 % CI not available)
Kessler et al. [17]	Maximum bladder capacity	TAUS (7.5)	DWT	BOO if DWT >2.9 mm	0.88 (95 % CI 0.81–0.94)
Oelke et al. [19]	≥250 ml	TAUS (7.5)	DWT	BOO if DWT >2 mm	0.930 (95 % CI 0.88–0.98)
Kojima et al. [11]	100–300 ml	TAUS (7.5)	UEBW	BOO if UEBW >35 g	0.862 (95 % CI not available)
Blatt et al. [20]	200 ml	TAUS (10–5)	BWT	Not calculable	Not significant
Franco et al. [21]	150 ml	TAUS (3.5)	BWT	BOO if BWT >6 mm	0.78 (95 % CI 078–0.91)
Female patients with DO					
Khullar et al. [25]	<50 ml	TVUS (5)	BWT	DO if BWT >5 mm	0.940 (95 % CI not available)
Lekskulchai et al. [27]	<50 ml	TLUS (8–4)	BWT	DO if BWT >5 mm	0.606 (95 % CI not available)
Chung et al. [27]	≥250 ml	TAUS (8)	DWT	Not calculable	Not significant

TAUS transabdominal ultrasound, *TVUS* transvaginal ultrasound, *TLUS* translabial ultrasound

the diagnosis of Detrusor overactivity (DO) [14]. DO is a common condition in women and the incidence ranges between 9 and 43 %. DO is defined as a urodynamic observation characterized by involuntary detrusor contractions during the filling phase that may be spontaneous or provoked [24]. According to Khullar, the increase of bladder contractions can determine the thickening and hypertrophy of the bladder wall over time. Therefore, the BWT/DWT evaluation may discriminate women with and without DO. Khullar et al. assessed the BWT using a transvaginal approach, a bladder filling of less than 50 ml; BWT value was obtained from the average of 3 measurements acquired at the level of the dome, trigone and anterior wall, respectively [14]. They found a significant difference in the mean BWT value between women with DO (6.7 mm) and without DO (3.5 mm). Khullar et al. also confirmed this result in a larger series of 180 patients [25]. Moreover, the mean BWT value was 6.3 mm in women with DO vs. 3.9 mm in those with normal PFS or with stress/mixed incontinence. Adopting a threshold of 5 mm, the positive predictive value for diagnosis of DO was 94 %. Interestingly, in 42 women with PFS normal, but with BWT greater than 5 mm, an additional assessment by urodynamic confirmed the presence of DO in 36 women (85.7 %) [25]. Despite the encouraging results obtained from Khullar et al., we have to consider that the transvaginal approach can be as invasive as PFS; consequently, some authors proposed less invasive approaches to evaluate the BWT in female patients. Unfortunately the results were less satisfactory. Lekskulchai et al. showed statistically significant association between BWT and DO ($p < 0.001$) even by translabial approach [26]. However, in the ROC analysis, BWT measured by translabial approach reached only 0.606 as accuracy to predict DO [26]. While by suprapubic approach proposed by Chung et al., BWT even failed to show a significant correlation with DO [27]. Consequently, considering this evidence, though more invasive, the transvaginal approach appears the most effective. Table 36.1 lists the results obtained in terms of

diagnostic accuracy in the various experiences mentioned above.

Finally, similarly to LUTS/BPH male patients treated with surgical/pharmacological therapy, in female patients with overactive bladder, antimuscarinic treatments may determine BWT reduction associated with a significant improvement of the clinical symptoms. In fact, Panayi et al. assessed BWT according to the Khullar technique in a group of 58 female patients affected by DO. They evaluated BWT at baseline and during/after treatment with antimuscarinic drugs. At baseline mean BWT value was 5.7 mm (5.6–5.9); after 6 weeks of treatment, a 20% reduction of BWT was recorded [4.6 mm (4.4–4.8)], then keeping a plateau [4.6 mm (4.4–4.8)] until the 12th week of treatment [28].

36.6 Latest Innovations in BWT/DWT Assessment

As previously mentioned, BWT/DWT assessment could be a promising, non-invasive proxy to monitor the effects of medical therapy in male patients with BPH and female patients with DO. In BPH patients, previous experiences only focused on the effects of alpha-adrenergic antagonists.

We have recently investigated the effect of dutasteride add-on therapy to alpha-adrenergic antagonist on DWT/BWT. In this preliminary experience, combination treatment was associated with a significant reduction of DWT from 2.5 mm (IQR, 1.8/4) to 1.6 mm (IQR, 1/2.4), $p=0.001$, and BWT from 4.9 mm (IQR, 3.5/7) to 2.9 mm (IQR, 2.4/3.7), $p=0.001$. These preliminary results confirm the efficacy of dutasteride in reducing bladder outlet obstruction and the ability of BWT/DWT assessment to monitor the effects of LUTS/BPE medical treatment. Conversely, a recent study has cast doubt on the accuracy of BWT assessment in monitoring the efficacy of antimuscarinics in female patients with DO. After 12 weeks of follow-up, solifenacin treatment has been associated with improvements in efficacy and patient satisfaction endpoints, but there has been no significant reduction found in BWT from baseline to 12 weeks when compared with placebo (−0.24 mm vs. −0.16 mm, $p=0.095$) [29].

Moreover, no previous study has investigated a possible correlation between increased BWT/DWT and the presence of DO in male patients with LUTS; we recently have explored this association in a study presented at the 30th EAU congress (Madrid 2015).

We enrolled 600 male patients with LUTS secondary to benign prostatic enlargement (BPE) in two tertiary hospitals. Patients underwent a standard diagnostic assessment of LUTS that included family history, physical examination, prostate-specific antigen measurement, uroflowmetry, prostate volume and the evaluation of post-voiding residual volume. Furthermore, for each patient, they performed the assessment of BWT according to Manieri's technique and a PFS. To avoid the possible effect of BOO on BWT, we excluded patients with Schaëfer class ≥2. Overall data from 196 patients (98 with DO and 98 without DO) were analysed. No significant differences in the evaluated parameters between the two groups, except the BWT were observed. A significantly thicker bladder wall was recorded in patients with DO when compared to patients without DO (4.3 mm versus 3.6 mm, $p=0.001$). Moreover, the accuracy of BWT to predict DO by ROC analysis was 0.705, CI: 0.59–0.75. According to these results, BWT could be an effective non-invasive predictor of DO in male patients with LUTS and with no evidence of BOO.

Our findings suggested for the first time that BWT in male patients is related not only to BOO but it can also reflect the presence of DO. If this hypothesis is confirmed in further studies, it can reduce the significant value of a BWT evaluation to predict the presence of BOO in male patients with LUTS and with possible DO. In fact, these results showed that DO and BOO could equally contribute to the increase in BWT, observed in male patients with LUTS and BPH, and therefore the role of BWT as a proxy of BOO could be arguable and further investigated in patients with DO.

Despite this possible emerging limitation, recently Güzel et al. have explored the correla-

tion between BWT, uroflowmetric parameters and IPSS in male patients with LUTS. The authors have reported a positive association between BWT and IPSS, PVR and duration of LUTS, whereas a negative relationship was found between BWT and Qmax ($p<.001$). Furthermore, the authors identified several BPO risk factors as IPSS >19, Qmax <15 ml/min and PVR >100 ml. A greater BWT was also observed in patients with more than one risk factor. BWT was 2.9 mm in patients without risk factors, whereas BWT was 3.5, 4.1 and 4.5 mm in patients with one, two or three risk factors [30].

Another possible innovation in BWT evaluation is the development and implementation of automated systems. In particular, the BladderScanTM BVM 6500 (Diagnostic Ultrasound, Bothell, WA) has recently been developed. The instrument adopts a modern technology for measuring bladder volume. It achieves 24 isocentric bladder scans, and a special algorithm allows the identification of the remaining parts and the inner edges of the bladder wall. In a validation study of the instrument, the variability between measurements was less than 5 % for bladder fillings between 200 and 400 ml [31]. On-going studies should confirm the accuracy and the short learning curve of the instrument, allowing to overcome the limitations associated with the manual BWT/DWT assessment [32].

Conclusion

Ultrasound assessment of the BWT/DWT seems to be an innovative non-invasive technique to evaluate the presence of BPO in patients with LUTS/BPE. However, the lack of standardization due to the different techniques and the influence of bladder volume represent an important limitation, and the EAU guidelines still consider BWT/DWT evaluation as an experimental procedure [33, 34]. However, if future clinical studies will overcome all these limitations, the ultrasound evaluation of bladder thickness could be used routinely in the evaluation and follow-up of patients with LUTS/BPE as an alternatively to pressure-flow study.

References

1. Abrams P, Chapple C, Khoury S et al (2009) Evaluation and treatment of lower urinary tract symptoms in older men. J Urol 181:1779
2. De Nunzio C, Autorino R, Bachmann A et al (2014) The diagnosis of benign prostatic obstruction: development of a clinical nomogram. Neurourol Urodyn. doi:10.1002/nau.22705
3. Abrams P, Chapple C, Khoury S, Roehrborn C, de la Rosette J, Committee IS (2009) Evaluation and treatment of lower urinary tract symptoms in older men. J Urol 181:1779–1787
4. McConnell JD (1994) Why pressure-flow studies should be optional and not mandatory for evaluating men with benign prostatic hyperplasia. Urology 44:156–158
5. AUA Practice Guidelines Committee (2003) AUA guideline on management of benign prostatic hyperplasia (2003). Chapter 1: Diagnosis and treatment recommendations. J Urol 170(2 Pt 1):530–547
6. Oelke M, Kirschner-Hermanns R, Thiruchelvam N, Heesakkers J (2012) Can we identify men who will have complications from benign prostatic obstruction (BPO)? ICI-RS 2011. Neurourol Urodyn 31:322–326
7. Ghoniem GM, Regnier CH, Biancani P et al (1986) Effect of vesical outlet obstruction on detrusor contractility and passive properties in rabbits. J Urol 135:1284
8. Landau EH, Jayanthi VR, Churchill BM et al (1994) Loss of elasticity in dysfunctional bladders: urodynamic and histochemical correlation. J Urol 152:702
9. Nielsen KK, Andersen CB, Petersen LK et al (1995) Morphological, stereological, and biochemical analysis of the mini-pig urinary bladder after chronic outflow obstruction and after recovery from obstruction. Neurourol Urodyn 14:269
10. Tubaro A, Miano L (2002) Managing the consequence of obstruction. Eur Urol 1(Suppl):21–27
11. Kojima M, Inui E, Ochiai A, Naya Y, Ukimura O, Watanabe H (1996) Ultrasonic estimation of bladder weight as a measure of bladder hypertrophy in men with infravesical obstruction: a preliminary report. Urology 47:942–947
12. Manieri C, Carter SS, Romano G, Trucchi A, Valenti M, Tubaro A (1998) The diagnosis of bladder outlet obstruction in men by ultrasound measurement of bladder wall thickness. J Urol 159:761–765
13. Oelke M (2010) International Consultation on Incontinence-Research Society (ICI-RS) report on non-invasive urodynamics: the need of standardization of ultrasound bladder and detrusor wall thickness measurements to quantify bladder wall hypertrophy. Neurourol Urodyn 29:634–639

14. Khullar V, Salvatore S, Cardozo L et al (1994) A novel technique for measuring bladder wall thickness in women using transvaginal ultrasound. Ultrasound Obstet Gynecol 4:220
15. Oelke M, Hofner K, Jonas U et al (2006) Ultrasound measurement of detrusor wall thickness in healthy adults. Neurourol Urodyn 25:308
16. Naya Y, Kojima M, Honjyo H, Ochiai A, Ukimura O, Watanabe H (1998) Intraobserver and interobserver variance in the measurement of ultrasound-estimated bladder weight. Ultrasound Med Biol 24:771–773
17. Kessler TM, Gerber R, Burkhard FC, Studer UE, Danuser H (2006) Ultrasound assessment of detrusor thickness in men—can it predict bladder outlet obstruction and replace pressure flow study? J Urol 175:2170–2173
18. Oelke M, Höfner K, Wiese B et al (2002) Increase in detrusor wall thickness indicates bladder outlet obstruction (BOO) in men. World J Urol 19:443–452
19. Oelke M, Hofner K, Jonas U et al (2007) Diagnostic accuracy of noninvasive tests to evaluate bladder outlet obstruction in men: detrusor wall thickness, uroflowmetry, postvoid residual urine, and prostate volume. Eur Urol 52:827
20. Blatt AH, Titus J, Chan L (2008) Ultrasound measurement of bladder wall thickness in the assessment of voiding dysfunction. J Urol 179:2275
21. Franco G, De Nunzio C, Leonardo C et al (2010) Ultrasound assessment of intravesical prostatic protrusion and detrusor wall thickness–new standards for noninvasive bladder outlet obstruction diagnosis? J Urol 183:2270–2274
22. Tubaro A, Carter S, Hind A, Vicentini C, Miano L (2001) A prospective study of the safety and efficacy of suprapubic transvesical prostatectomy in patients with benign prostatic hyperplasia. J Urol 166(1):172–176
23. Egilmez T, Pourbagher MA, Guvel S et al (2006) Effects of selective alpha-1-adrenergic receptor blockers on bladder weight. Urol Int 76:42–50
24. Abrams P, Cardozo L, Fall M, Griffiths D, Rosier P et al (2002) The standardisation of terminology of lower urinary tract function: report from the Standardisation Sub-committee of the International Continence Society. Neurourol Urodyn 21:167–178
25. Khullar V, Cardozo LD, Salvatore S et al (1996) Ultra- sound: a noninvasive screening test for detrusor instability. Br J Obstet Gynaecol 103:904
26. Lekskulchai O, Dietz HP (2008) Detrusor wall thickness as a test for detrusor overactivity in women. Ultrasound Obstet Gynecol 32:535
27. Chung SD, Chiu B, Kuo HC, Chuang YC, Wang CC et al (2010) Transabdominal ultrasonography of detrusor wall thickness in women with overactive bladder. BJU Int 105:668–672
28. Panayi DC, Tekkis P, Fernando R, Khullar V (2010) Is the beneficial effect of antimuscarinics related to motor or sensory changes in the bladder? Int Urogynecol J 21(7):841–845
29. Robinson D, Oelke M, Khullar V, Wijkstra H, Tretter R, Stow B, Compion G, Tubaro A (2016) Bladder wall thickness in women with symptoms of overactive bladder and detrusor overactivity: Results from the randomised, placebo-controlled shrink study. Neurourol Urodyn 35(7):819–825
30. Güzel Ö, Aslan Y, Balcı M, Tuncel A, Keten T, Erkan A, Atan A (2015) Can bladder wall thickness measurement be used for detecting bladder outlet obstruction? Urology 86(3):439–444
31. Oelke M, Mamoulakis C, Ubbink DT et al (2009) Manual versus automatic bladder wall thickness measurements: a method comparison study. World J Urol 27:747–753
32. Tubaro A, Mariani S, De Nunzio C, Miano R (2010) Bladder weight and detrusor thickness as parameters of progression of benign prostatic hyperplasia. Curr Opin Urol 20(1):37–42
33. EAU Guidelines on the Management of Male Lower Urinary Tract Symptoms (LUTS), including Benign Prostatic Obstruction (BPO) 2014. https://uroweb.org/wp-content/uploads/Non-Neurogenic-Male-LUTS_2705.pdf
34. EAU Guidelines on the Management of Urinary Incontinence 2014. https://uroweb.org/wp-content/uploads/20-Urinary-Incontinence_LR.pdf

Functional Ultrasound: Functional Female Echo-Dynamic Study

37

Del Zingaro Michele, Rosi Paolo, Luigi Mearini, Elisabetta Nunzi, Rosi Giovanni, and Guiggi Paolo

Ultrasound is a valid diagnostic tool for the study of female cervico-urethral dynamics especially during preoperative workup for women with a prolapse. The method is also very important for postoperative control. For these purposes, surface (*transperineal or translabial*) or endocavitary (*transrectal*, *transvaginal*, *introital*) probes can be used. Transperineal access is low cost and easy to perform; it allows sufficient study of urethrocele but tends to underestimate cystocele in some cases. Transvaginal US offers an excellent definition of anatomical details and a precise view of anterior defects (urethrocele) but again tends to underestimate a bladder prolapse (cystocele) owing to the fact that the probe inside the vagina impedes the view of the bladder base [1].

Transrectal US offers a less precise imaging of anatomical details than the transvaginal method because the bowel content interferes with the imaging; it also causes considerable patient discomfort. However, it does provide a good definition of both urethrocele and cystocele since the probe does not hinder the view of the descent of the bladder base. In any case, regardless of the US technique employed, some qualitative and quantitative parameters have been established for the purposes of standardizing the study of female cervico-urethral dynamics.

Among the most important are:

- *The distance of the neck of the puborectal line that in normal subjects should be >2 cm*; *this is important in the assessment of urethrocele*.
- *The angle of mobility of the bladder base must be >30° in normal conditions*; *this is important in the assessment of cystocele*.
- *The posterior urethrovesical angle must be >110°*.

A very important anatomical element is the pubic arcuate ligament because it is a fixed point of reference for the evaluation of hypermobility of the urethrovesical junction. This cartilage structure binds the two pubic bones, seen as a hyperintense signal with a conic shadow, whereas the ligament point is weakly hyperintense and shadow-free.

US is a valid alternative to radiological examinations (MRI, perineography, etc.) in the study of the dynamics of the female pelvic floor, because it provides highly reliable imaging. Owing to the multiplicity of US approaches now adopted, awareness has been raised that universal standards need to be established for these examinations.

The techniques most commonly adopted are the suprapubic, transperineal, transvaginal, and transrectal approaches. In any case, regardless of the type of access employed, some anatomical elements and assessment parameters are constant (Fig. 37.1a–c).

D.Z. Michele (✉) • R. Paolo • L. Mearini • E. Nunzi
R. Giovanni • G. Paolo
Urological and Andrological Clinic, University of Perugia, Square Menghini 1, Perugia 16100, Italy
e-mail: micheledelzingaro@tin.it

P. Martino, A.B. Galosi (eds.), *Atlas of Ultrasonography in Urology, Andrology, and Nephrology*,
DOI 10.1007/978-3-319-40782-1_37

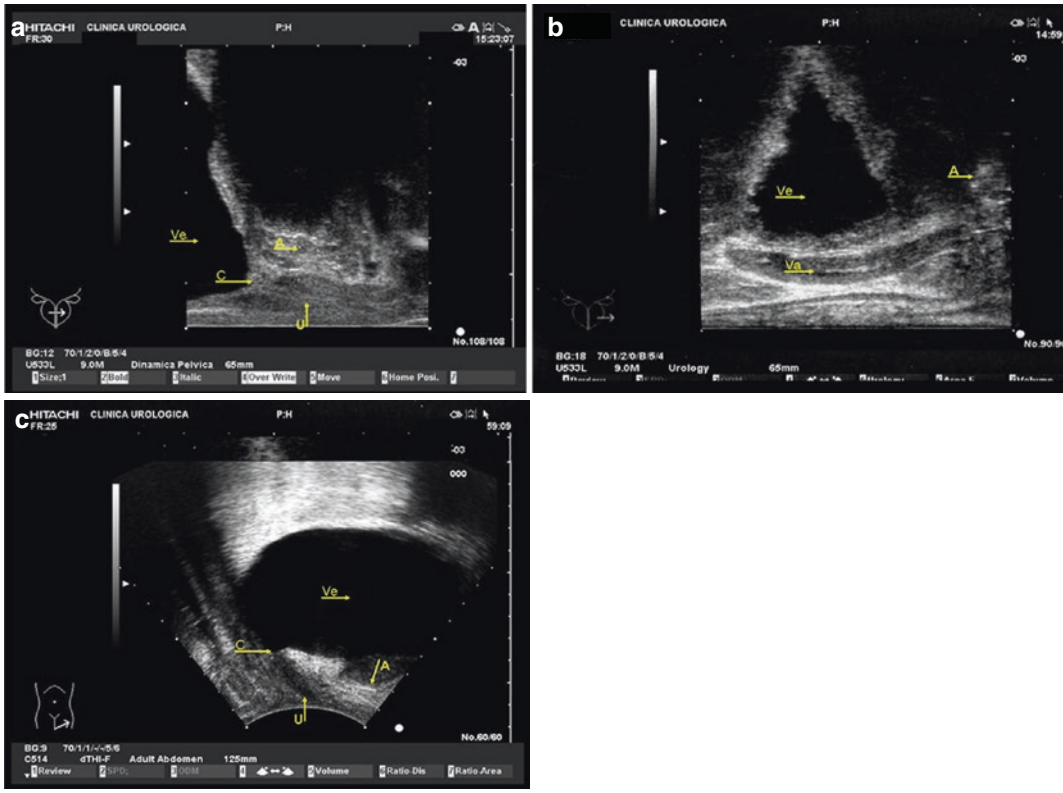

Fig. 37.1 (**a**) T*ransvaginal US. Anatomical elements*: *a* pubic arcuate ligament, *C* bladder neck, *U* urethra, and *Ve* bladder. (**b**) Transrectal US. *Anatomical elements*: *A* pubic arcuate ligament, *Ve* bladder, and *Va* vagina. (**c**) Perineal US. *Anatomical elements*: *A* pubic arcuate ligament, *C* bladder neck, *U* urethra, and *Ve* bladder

37.1 Anatomical Elements

37.1.1 Urethra

In basal conditions the urethra has a virtual lumen and is seen at US as a thin echogenic line surrounded by a hypointense; the course of the urethra basically runs parallel to the vagina and is slightly downward arched.

37.1.2 Bladder Neck

The bladder neck is an important element in both static and dynamic measurements; it presents as a small groove at the level of the bladder base, continuing up from the urethra. Generally, whatever the US technique used, the urethra and the bladder neck can easily be seen. Only rarely is it necessary to apply a catheter to show up the course of the urethra and the position of the bladder neck.

37.1.3 Bladder Base

The bladder base is rounded and situated, in normal conditions, above the inferior margin of the pubic symphysis. The bladder neck and urethra-trigonal junction are closed in basal conditions and located about 2 cm above the pubic symphysis.

37.1.4 Pubic Symphysis

At US the pubic symphysis appears as an intensely echo-reflecting meniscus-like image, located vertically underneath the median third of the urethra. An important reference point when making an assessment of dynamic modifications of the bladder base is the pubic arcuate ligament. This appears as a weakly echogenic zone above the inferior margin of the pubic symphysis, on the median line. Anatomically, it consists of a cartilage that binds the two pubic bones.

When making quantitative assessments of cervico-urethral static conditions, the measurement of some angles is extremely important:

- *The angle of mobility of the bladder neck is included between the line perpendicular to the puborectal line, at the level of the arcuate ligament, and the slightly downward arched bladder neck line.*
- *The angle of the urethral axis lies between the urethral axis and the puborectal line.*
- *The angle of mobility of the bladder base lies between the puborectal line and the line that joins the arcuate ligament to the lowest point of the bladder base.*

In normal subjects the bladder base and neck lie near to, and slightly below, the line running perpendicular to the puborectal line (distance <2 cm).

The distance between the bladder neck and the puborectal line must be >2 cm, the mobility angle of the bladder base >30°, the mobility angle of the bladder neck <45°, the urethral axis angle about 50°, and the posterior urethrovesical angle >110°.

An important point when assessing any prolapse of the bladder neck and base is to carry out a stress test in the dynamic phase and during micturition.

The patient is asked to cough repeatedly and undergo a prolonged Valsalva maneuver (not less than 5 s), repeated several times, at least three, in order to obtain a more pronounced descensus. This will make it possible to obtain an objective evaluation of an abnormal mobility of the bladder base, the urethra, and the bladder neck. It is extremely important to note any abnormal opening of the bladder neck under stress, and any urine leakage is a sign of a probable rhabdosphincter deficit that should be confirmed by a urodynamics test. In normal subjects, the position and shape of the urethra and bladder neck under stress are not much different from those in basal conditions [2].

It is essential to keep the same orientation of the images in all the examinations. As regards qualitative parameters, it is important to note

any funneling of the bladder neck, the position (high or low) and mobility (fixed or hypermobile) of the urethra, and the mobility of the bladder base (vertical, rotational shift, *descensus*).

Among the quantitative measurements mentioned above, the most important are undoubtedly the distance between the bladder neck and the puborectal line that indicates the degree of an anterior defect (urethrocele) (Fig. 37.2) and the hypermobility angle of the bladder base that defines the degree of a posterior defect (cystocele) (Fig. 37.3).

Optimal bladder filling for the examination is about 200 ml. If the bladder is too distended, the prolapse will be underestimated because the organs have no room to descend. As regards challenge tests, it should be remembered that the Valsalva maneuver provokes relaxation of the pelvic floor, whereas coughing causes contraction, so the Valsalva maneuver is better suited to testing to reveal *descensus* [3].

The longitudinal axis of the symphysis forms an angle of about 90° with the vagina and the rectum; the ideal position of the probe is therefore in alignment with the vaginal and rectal axes, which will show, on the echogram, an image of the pubic symphysis lying at 90° to the probe plane [4].

As previously pointed out, the female pelvic floor in static conditions can be studied by ultrasound using both surface and endocavitary transducers (Table 37.1).

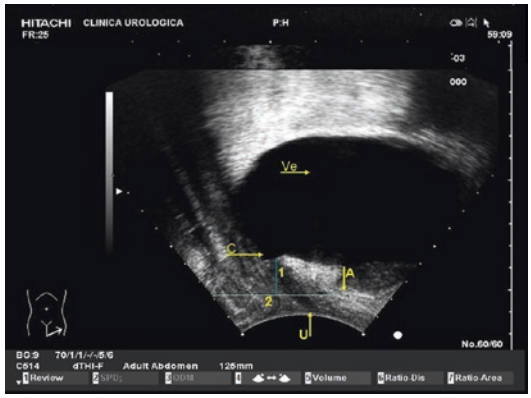

Fig. 37.2 Perineal scanning to assess urethrocele: *a* pubic arcuate ligament, *C* bladder neck, *U* urethra, *Ve* bladder, *1* distance of the neck to puborectal line, and *2* puborectal line

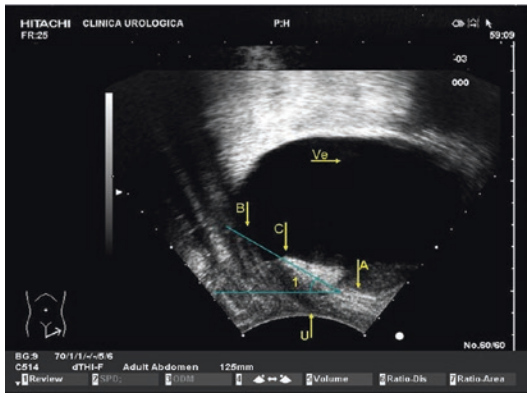

Fig. 37.3 Perineal scanning to assess cystocele: *a* pubic arcuate ligament, *C* bladder neck, *U* urethra, *Ve* bladder, and *1* angle of the bladder base

Table 37.1 Classification of urethrocele and cystocele

Classification of urethrocele	
Normal condition	The bladder neck is more than 20 mm above the longitudinal axis of the pubic symphysis
Grade I urethrocele	The bladder neck lies between 20 and 7 mm above the longitudinal axis of the pubic symphysis
Grade II urethrocele	The bladder neck lies between 7 mm above and 7 mm below the longitudinal axis of the pubic symphysis
Grade III–IV urethrocele	The bladder neck lies more than 7 mm below the longitudinal axis of the pubic symphysis
Classification of cystocele	
Normal condition	Mobility angle of the bladder base > −50
Grade I cystocele	Hypermobility angle of the bladder base between −50° and −20°
Grade II cystocele	Hypermobility angle of the bladder base between −20° and +30°
Grade III–IV cystocele	Hypermobility angle of the bladder base > +30°

37.2 Suprapubic Scanning

Surface ultrasound in suprapubic scanning is not practical for this type of investigation, because the bladder base is poorly imaged due to interference of the pubic bone, especially during stress tests and in obese women.

37.3 Transperineal Scanning

Surface US with *transperineal* (*translabial*) access is low cost and easy to perform: linear or convex 5/7.5 MHz probes are used and applied in the perineal zone. This offers a reasonably good study of urethrocele, but the image resolution, especially during the dynamic phase, is low. Moreover, if present, a urethrocele may be partly compressed by the external probe, resulting in underestimation of the lesion.

37.4 Transvaginal Scanning

In endocavitary transvaginal scanning, linear 5–7.5 MHz probes are employed; to reduce patient discomfort, the examination is done in gynecological position. It allows a detailed morphological study of the anatomical structures that are of better quality, especially of the urethra, than with other US techniques because they are not affected by interference of the bowel content. A drawback of the method is that the presence of the probe in the vagina interferes with the descent of the pelvic structures under stress and hence can result in underestimation of a cystocele. Nevertheless, in the example shown, it can be seen that when using the right technique and with some experience, even a grade III cystocele can be assessed with this scanning approach. The issue of probe positioning can interfere with the visualization of grade III prolapse but does not create particular problems with grade I or II prolapse (Fig. 37.4).

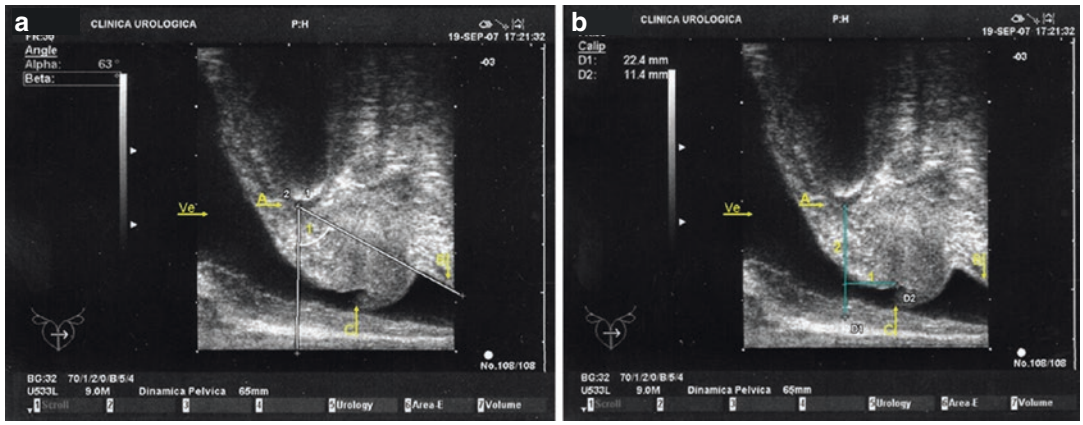

Fig. 37.4 (**a**) Transvaginal scanning: *a* pubic arcuate ligament, *C* bladder neck, *Ve* bladder, *and 1* angle of the bladder base. (**b**) Transvaginal scanning: *A* pubic arcuate ligament, *C* bladder neck, *U* urethra, *Ve* bladder, and *1* distance of the neck to puborectal line

37.5 Transrectal Scanning

In endocavitary transrectal scanning, linear 5–7.5 MHz probes are used. The patient is placed in gynecological or orthostatic position. This examination offers a good morphological resolution of the anatomical structures. The study of the urethra may be less detailed than in transvaginal scanning because of the interference of the bowel content. However, with transrectal access there is no obstacle to the descent of the pelvic structures under stress, and so even high-grade cystocele can be correctly evaluated. Nevertheless, transrectal scanning is quite uncomfortable for the patient [5].

37.6 Enterocele

During all these scanning approaches, in the dynamic phase, it is possible to assess the presence of an enterocele that will progressively descend during the Valsalva maneuver, whereas it will rise toward the pelvis when the perineal plane contracts (Fig 37.5).

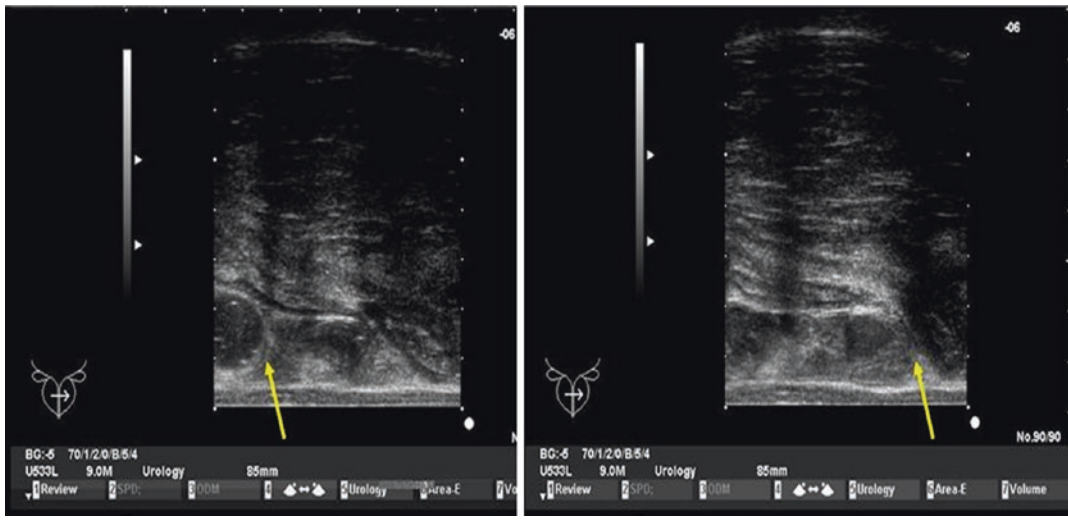

Fig. 37.5 Transvaginal scanning: the *arrow* shows an enterocele in basal conditions on the left and after Valsalva on the right; note the descent of the bowel loop

References

1. Beco J (1995) Reducing uncertainty for vesico-urethral sonography in women. Acta Urol Belg 63(2):13–29
2. Sanders R (1993) A comparison of beaking urethra symphysis and bladder angle measurement, cystocele presence and urethral rotation as sonographic signs of stress incontinence. 23" Annual Meeting of lCS
3. Schaer G et al (1996) Recommendations of the German Association of Urogynecology on functional sonography of the lower female urinary tract. Int Urogynecol J Pelvìc Floor Dysfunction 7:105–108
4. Lone F et al (2014) The value of pre-operative multi-compartment pelvic floor ultrasonography: a 1-year prospective study. Br J Radiol 87(1040):20140145
5. Lapray JF (2013) Imaging of pelvic organ prolapse. J Med Liban 61(1):13–22, French

Part V

The Scrotum

Scrotum: Ultrasound Anatomy and Scanning Methods

38

Libero Barozzi, Diana Capannelli,
Massimo Valentino, and Michele Bertolotto

38.1 Introduction

Scrotum is a superficial anatomical structure and it can be easily assessed with clinical examination. Ultrasonography (US) is the initial imaging modality for evaluating pathologic conditions of the scrotum. However, magnetic resonance (MR) imaging is useful in case of equivocal sonographic findings.

Indications of US examination include [1]:

- Testicular pain (torsion or inflammation)
- Testicular swelling/mass (inflammation or cystic vs solid mass)
- Trauma
- Causes of infertility (varicocele)
- Detection of absent or undescended testicle

38.2 US Anatomy

The scrotal sac includes many layers that are not easily visible at US in the absence of pathological processes. In detail, the scrotal wall consists of the following layers from superficial to deep: scrotal skin, superficial fascia, dartos muscle, external spermatic fascia, cremasteric fascia, and internal spermatic fascia [2, 3]. The normal scrotal wall thickness is approximately 2–8 mm and depends on the state of contraction of the cremasteric muscle. In pathological conditions, the thickness of the scrotal wall can increase, for example, in case of inflammation (associated with abscess or scrotal cellulitis), edema, or trauma (hematoma).

The testes are separated from the scrotum by the tunica vaginalis, a pouch of serous membrane derived from the processus vaginalis of the peritoneum. Tunica vaginalis is usually oblitered after the descent of the testis from the abdomen into the scrotum. It is reflected into the internal surface of the scrotum, consisting of a visceral and a parietal lamina. In normal condition, it contains a small amount of serous fluid (1–2 ml), while in case of incomplete obliteration of the processus vaginalis, a variable amount of fluid

L. Barozzi (✉)
Radiology Unit, Casa di Cura Madre Fortunata Toniolo, Via Toscana 34, Bologna 40141, Italy
e-mail: libero.barozzi@alice.it

D. Capannelli
Cardio Thoracic Vascular Department, Radiology Unit, University of Bologna, Policlinico Sant'Orsola-Malpighi, Via Massarenti 9, Bologna 40138, Italy
e-mail: diana.capannelli@yahoo.it

M. Valentino
Radiology Department, Tolmezzo Hospital, Via Morgagni 18, Tolmezzo, UD 33028, Italy
e-mail: mvm.valentino@gmail.com

M. Bertolotto
Radiology Department, University of Trieste, Ospedale di Cattinara, Strada di Fiume 447, Trieste 34149, Italy
e-mail: bertolot@units.it

P. Martino, A.B. Galosi (eds.), *Atlas of Ultrasonography in Urology, Andrology, and Nephrology*,
DOI 10.1007/978-3-319-40782-1_38

can collect within the visceral and parietal layers. This condition is called hydrocele and is the main cause of painless enlargement of the scrotum. It can also be secondary to other pathological conditions, such as inflammation (orchitis) or testicular torsion.

The tunica vaginalis surrounds the tunica albuginea, a dense fibrous layer that binds each testis and helps to maintain its shape and integrity [4]. It typically appears on US as a thin hyperechoic line that envelops each testis, not easily visualized in the absence of intrascrotal fluid.

Testicle is an ovoid shape structure (round shaped in the newborn) with smooth surface. The size, shape, and echotexture depend on testosterone effects and change from newborns to adults.

The normal adult testis is 40–50 mm in length (L), 30–35 mm in width (W), and 20–25 mm in height (H). The volume is calculated as an ellipsoid: $V = L \times W \times H \times 0.52$.

The normal testicle appears slightly echogenic with a homogeneous echotexture, similar to the liver, while prepuberal testes typically show a lower echogenicity [5].

Mediastinum testis is a connective tissue continuous with the fibrous capsule of the testis (the tunica albuginea). It appears as a central echogenic band within the testis, extended in caudocranial direction and easily visible in young patients.

Numerous fibrous thin septa extend from the mediastinum into the testis, dividing it into 250–400 lobules, each of which contains from one to three seminiferous tubules that converge into a network of tubular spaces called rete testis. In normal conditions, the rete testis can be identified at US as a hypoechoic striated area adjacent to the mediastinum testis, while in case of ectasia, it appears as multiple small cystic or tubular anechoic dilated structures that replace and enlarge the testicular mediastinum [3]. The lack of mass effect and of internal flow helps to differentiate this benign condition from a partially cystic tumor or an intratesticular varicocele.

The rete testis drains into 10–15 efferent ductules and then into the epididymis. Epididymis is an extratesticular tubular structure situated on the upper and posterior lateral aspect of the testis. The maximal size is less than 10–12 mm (mean 6–7 mm), and it can be divided into three main regions: the head, body, and tail. The head is a triangular structure that overlies the upper pole of the testis and is isoechoic to the testicular parenchyma; it is the only part that can be easily assessed in normal conditions, while the body or tail can be detected only in pathological conditions (inflammation or hydrocele).

Four types of testicular appendages have been described: the appendix testis, the appendix epididymis, the vas aberrans, and the paradidymis [3]. Only the appendix testis and the appendix epididymis can be recognized at scrotal US, especially when the amount of fluid into the tunical vaginalis is increased (hydrocele). The appendix of the testis is a developmental remnant of the Müllerian duct; it appears as an ovoidal echogenic structure of a few millimeters situated at the angle between the epididymal head and the upper pole of the testis.

The appendix of epididymis is an embryonal remnant of the Wolffian duct; it may appear as a cystic structure on the top of epididymal head. Appendiceal torsion can occur: it is a cause of painful scrotal swelling and can mimic testicular torsion. Sometimes a long-standing torsion of the epididymal appendix can evolve into a calcific scrotal phlebolith that appears as a mobile calcified structure with acoustic shadowing inside the amount of fluid between the layers of tunica vaginalis.

Spermatic cord is composed of testicular artery, pampiniform venous plexus, vas deferens (the continuation of epididymis), nerves, and lymphatics. On longitudinal scans, spermatic cord appears as a linear structure surrounded by a highly echogenic band, while on transverse scans it appears ovoid [5].

Testicular artery represents the main blood supply to the testis; it is a branch of the spermatic artery that originates from the abdominal aorta at the level of the renal hilum. Testicular artery follows the testis and penetrates the tunica albuginea at the mediastinum testis. Transmediastinal artery can mimic a focal testicular lesion at B-mode examination and appear as a hypoechoic area: in these cases color Doppler and spectral analysis

demonstrate an arterial flow signal through the vessel.

Pampiniform venous plexus is formed by the union of multiple spermatic veins from the testis and epididymis. The veins of the plexus ascend along the cord through the inguinal canal and converge on the right side into the inferior vena cava and on the left side into the left renal vein. In normal conditions, pampiniform plexus appears at color Doppler exam as a venous network along the spermatic cord. Abnormal dilatation of the pampiniform venous plexus is called varicocele. It appears as multiple tortuous anechoic tubular structures adjacent to the testis. Color Doppler imaging can be helpful in differentiating venous tubular structures from epidermoid cysts or spermatoceles. Sometimes intratesticular varicocele may mimic testicular cysts: color Doppler exam is required to differentiate these findings.

Bidirectional Doppler ultrasonography performed with the patient in the upright position helps in grading the varicocele, by demonstrating spontaneous or Valsalva-associated reflux [5, 6].

38.3 Technique

The study should be performed in a comfortable and warm room to avoid the cremasteric reflex that may cause the testicles to ascend in the scrotal sac making imaging more difficult. In particular in early childhood, a fingertip should be placed over the inguinal canal to prevent movement of the testicle [1, 5].

US examination is performed with patient in supine position with a towel draped between his thighs to support the scrotum and to help comparative views. Penis is displaced superolaterally against the abdomen.

In case of suspect varicocele, additional scanning in the upright position is helpful to assess the retrograde flow from the internal spermatic vein into the cremasteric vein and the vein of the vas deferens.

The scrotum is examined with a linear high-resolution and high-frequency (7.5–13 MHz) small-part transducer with appropriate placement of the focal zone (near focused for superficial structures). However, in case of marked scrotal enlargement or scrotal trauma, a lower-frequency curvilinear transducer may be employed, in order to have a larger field of view to assess the anatomy, the site of injury, and associated abnormalities [1, 5, 7].

Transverse and longitudinal gray-scale scans of the scrotum and inguinal regions bilaterally are performed. Color Doppler examination should be then performed and optimized to be

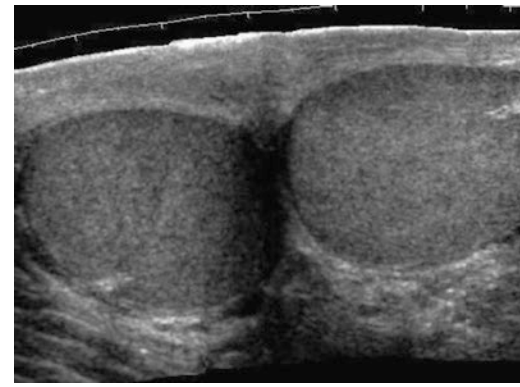

Fig. 38.1 B-mode transverse comparative scan is mandatory to compare size and echogenicity of both testes

sensitive to low-velocity flow: low pulse repetition frequency (PRF) and the highest color gain (generally over 80%) with acceptable signal-to-noise ratio.

Basic scans include:

- Longitudinal scan of each testicle by starting from the asymptomatic hemiscrotum
- Transverse comparative scan: an image including both testicles in the field of view to allow side-to-side comparison of size, echogenicity, and vascularity (Fig. 38.1)
- Transverse and longitudinal scans of epididymis (short and long axis)
- Longitudinal scan of inguinal region including spermatic cord from external inguinal foramen to the head of epididymis
- Scrotal sac wall and layers

In case of a palpable abnormality on physical examination, it is useful to perform additional targeted scanning during palpation to correlate it with US findings.

38.4 Color Doppler and Power Doppler

Testicular vascularity should be assessed both with color Doppler and power Doppler study.

Doppler settings should be optimized to detect slow flow (low PRF and maximized color gain without artifacts). In case of acute scrotum, the examination should start from the asymptomatic hemiscrotum to adjust Doppler settings and then to assess symmetrical vascularity by comparing flow findings with the pathological side [8]. Comparative evaluation acquires crucial importance in case of testicular torsion or acute inflammation.

Power Doppler has higher (5×) sensitivity than color Doppler to detect low-flow velocities because its direction is insensitive [6]; however, it is very susceptible to movement, and it is difficult to apply in case of acute scrotum of children (Fig. 38.2).

Testicular vascularity should also be assessed both with power Doppler and spectral Doppler: power Doppler confirms the presence of intratesticular flow, and spectral Doppler allows distinguishing an arterial waveform from a venous flow. Intratesticular arterial waveform typically shows a high diastolic flow with low resistance index (RI = 0.62; range 0.48–0.70), while the deferential or cremasteric artery shows a typical high resistive waveform without diastolic component and with high resistance index (RI > 0.70).

In case of acute scrotal, the important distinction between an inflammatory and ischemic cause is on spectral Doppler, by assessing a low or high resistive flow.

In case of acute orchitis, the inflammatory process causes vasodilatation with a reduction of RI mean value (Fig. 38.3) [3].

In case of testicular torsion, color Doppler and power Doppler demonstrate reduced or absent intratesticular flow compared with the unaffected side, respectively, depending on incomplete or complete torsion (Fig. 38.4). If the torsion is partial, the spectral Doppler can demonstrate a preserved arterial flow with increased RI. In case of complete torsion, no flow in the intratesticular vessels is demonstrated, and increased perfusion can be assessed in the extratesticular vessels near the scrotal wall with higher RI (Fig. 38.5) [9, 10].

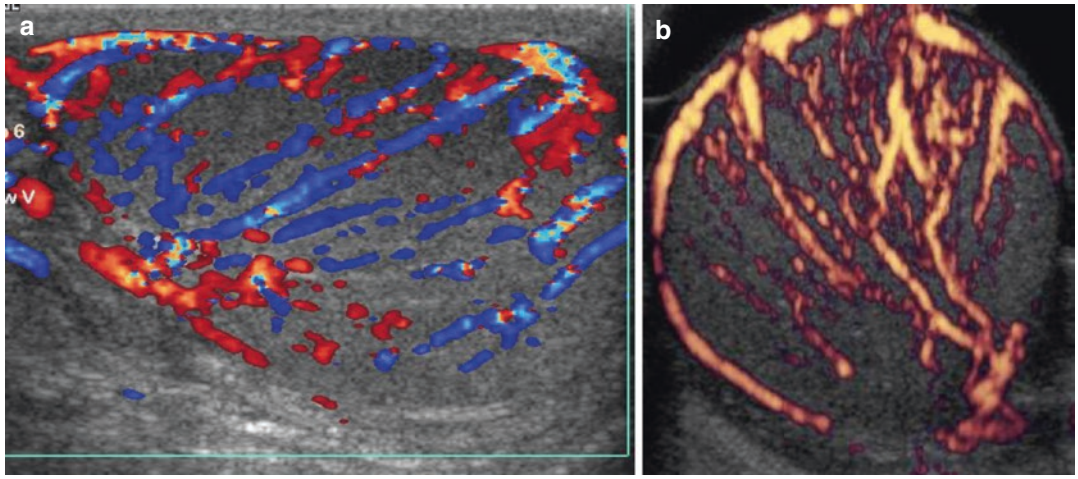

Fig. 38.2 Color Doppler (**a**) and power Doppler (**b**) allow the assessment of the vascularity of the testis

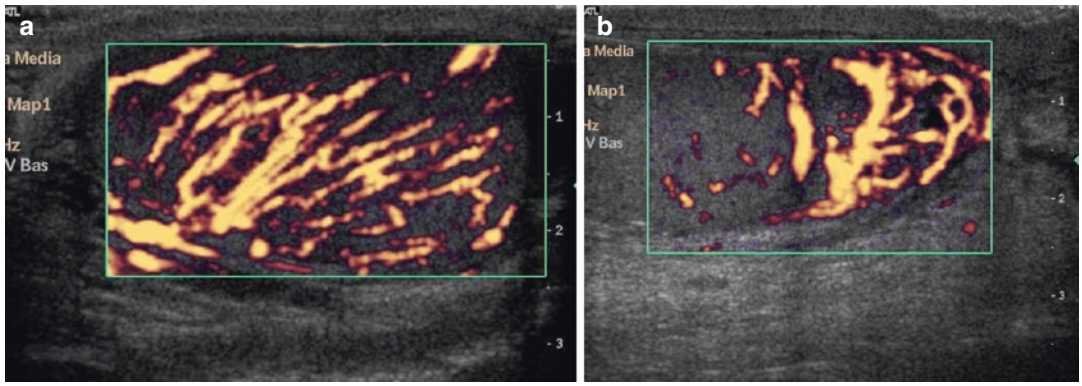

Fig. 38.3 Orchitis and epididymitis: power Doppler demonstrates a highly increased vascular signal of the inflammated testis (**a**) or epididymis (**b**) because of vasodilatation. Longitudinal power Doppler image of both epididymis and testis demonstrates no increased Doppler signal within the testis, but hyperemia and thickening of the epididymis (**b**)

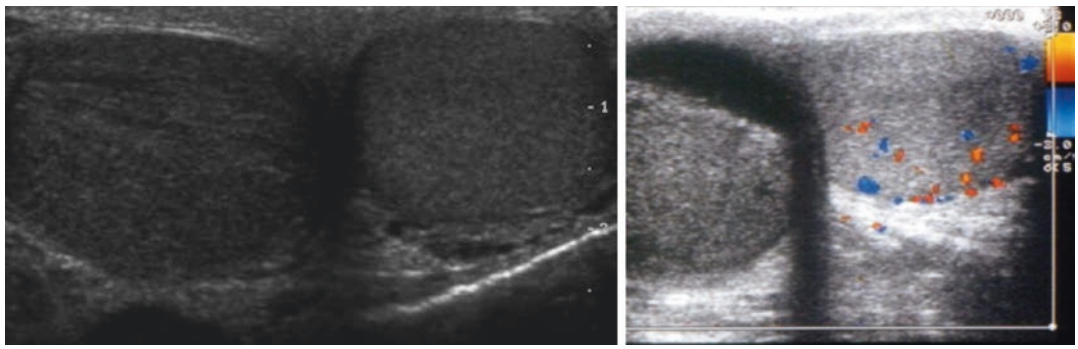

Fig. 38.4 Testicular torsion: B-mode comparative evaluation allows to detect enlargement and diffuse hypoechogenicity of the pathological testis (*right side*), compared to the normal one. Color Doppler demonstrates the complete absence of intratesticular flow into the right testis

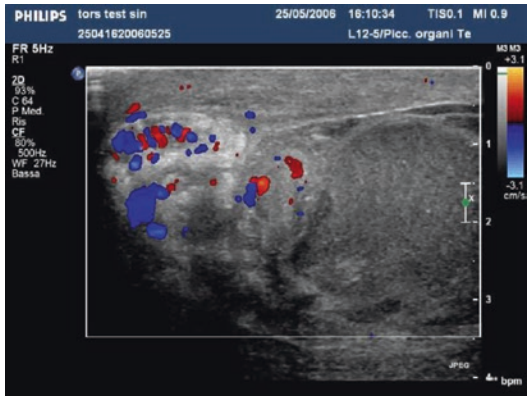

Fig. 38.5 Testicular torsion: color Doppler demonstrates complete absence of intratesticular perfusion and increased para-testicular flow from collateralization of extratesticular vessels (epididymal and funicular vessels). At the upper aspect of the testis, the torted spermatic cord appears as a thickened, edematous, and ill-defined mass

38.5 CEUS

Ultrasonography with Doppler imaging is very effective at visualizing and measuring blood flow only in large vessels with rapidly moving blood, but is unable to accurately detect flow in smaller vessels and capillaries. The development of endovascular contrast agents (as microbubbles) has subsequently allowed to obtain useful information about vascularity, perfusion rates, and potential tumor detection.

CEUS demonstrated an accuracy similar to contrast-enhanced multi-detector computed tomography (CE-MDCT) in detecting focal lesions, with the advantage of the real-time assessment of microvascular perfusion by using time-intensity curves, without the use of ionizing radiation.

Second-generation microbubble contrast agents consist of gas microbubbles (air or perfluorocarbon) stabilized by a biodegradable shell of protein, lipid, or polymer.

The small size of microbubbles (from 1 to 10 μm, as the size of a red blood cell) allows their passage unfiltered through the lungs, but the relative big size prevents entry into the interstitium allowing them to remain entirely intravascular ("pure blood pool" agents). Under US exposition, microbubbles oscillatory contract and expand themselves with the same resonance frequency of US waves, by amplifying the US signal. After circulating for several minutes, microbubbles dissolve: the gas is exhaled by the lungs, whereas the biodegradable shell is metabolized by the liver [11]. Microbubble contrast agents are not excreted by the kidney and do not affect renal function: they can be safely administrated to patients with renal insufficiency. Other advantages of CEUS include its safety, simplicity, patient tolerance, and lack of irradiation (conversely to CE-MDCT scans).

CEUS allows the visualization of testicle microvasculature and improves the detection of non-palpable focal lesions, in which color Doppler study shows several limitations [12]. In particular CEUS allows an accurate differentiation between hypervascular lesions (highly suspect for malignancy) and hypovascular ones (demonstrating the absence of flow signal in

benign lesions as epidermoid cysts, infarctions, abscess, and traumatic lesions). However, testicular neoplasms have a wide range of US presentation and sometimes can also appear as poor vascularized hypoechoic lesions on color Doppler. CEUS has a higher sensitivity in detecting vessels within the lesion, and time-intensity curves can demonstrate contrast enhancement wash-in and washout (Fig. 38.6).

CEUS is acquiring an increasing role in the assessment of acute scrotum, by differentiating avascular necrotic areas from residual parenchyma in case of testicular torsion, infarction, abscess, and trauma (Fig. 38.7) [13].

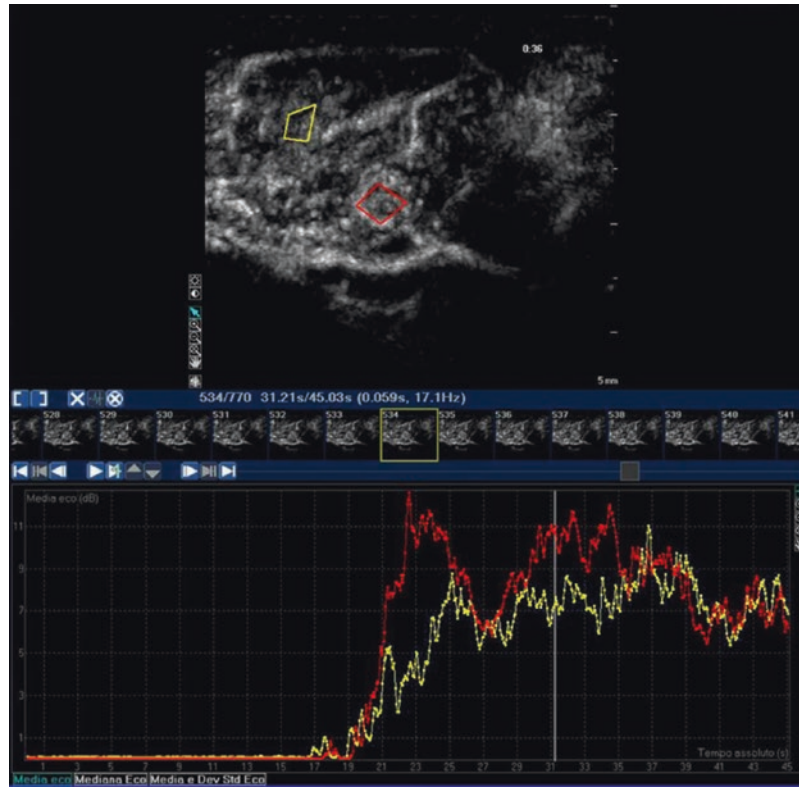

Fig. 38.6 Hypoechoic lesion on conventional US assessed with CEUS. The red ROI is drawn in a suspicious area, whereas the yellow ROI was drawn in an area representing the normal testicular parenchyma. The red time-intensity curve shows a higher fast filling hyperenhancement with reference to the normal testicular parenchyma and a rapid washout in the later phase, suggestive of testicular tumor

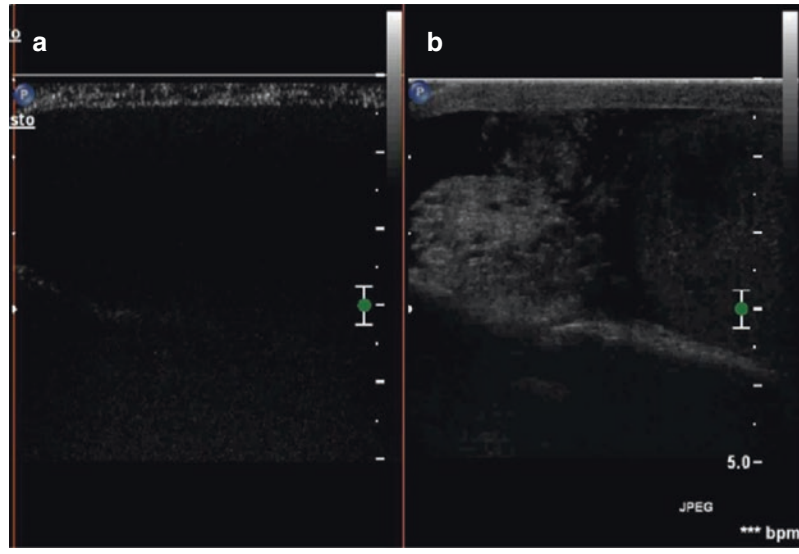

Fig. 38.7 CEUS and acute testicular torsion. Conventional US (**b**) shows a normal-sized testicle. CEUS demonstrates the complete lack of contrast enhancement within the testis due to the absolute absence of testicular blood flow (**a**)

38.6 Elastosonography

Ultrasound elastosonography is a promising technique with a wide range of potential clinical applications: it noninvasively measures mechanical properties of tissue and assesses the stiffness of a targeted lesion, a parameter in most cases associated with malignancy.

This technique is based on two methods: strain imaging, which represents how readily tissue deforms in response to an applied compression, and shear wave elastography, which represents the differences in speed of sound through tissues of varying stiffness. The fundamental principle is that stiffer tissues deform less (low strain) and propagate sound faster than softer tissues [14].

US imaging combinated with elastosonography creates the real-time sonoelastography (RTE): an elastogram superimposed to the B-mode ultrasound image of the tissue is created and updated in real time.

A targeted area of interest is focused on B-mode, and the selected portion of tissue is compressed by an external force: the degree to which it displaces is assessed and the strain ratio is calculated. The elastogram displays a color-coded map of the relative elasticity: from the softest tissue (red) to the hardest (blue) [15].

The testicle is a superficial structure, easily accessible by clinical examination. The main application of elastosonography is to assess nonpalpable small testicular nodules and pseudonodules, which is relevant in clinical practice for disease management [16].

Normal testicle shows a medium level of elasticity (displayed in green; Fig. 38.8); sometimes the parenchyma below the tunica albuginea presents less relative strain (displayed in light blue) probably due to the limited tissue displacement determined by the fibrous covering [15].

Sometimes elastosonography shows limits in differentiating benign testicular lesions from potentially malignant ones: elastosonography pattern of epidermoid cysts is similar to malignant lesions (they appear as "blue," hard lesions) because they have high cellularity and higher density compared with the surrounding normal tissue (Fig. 38.8) [16].

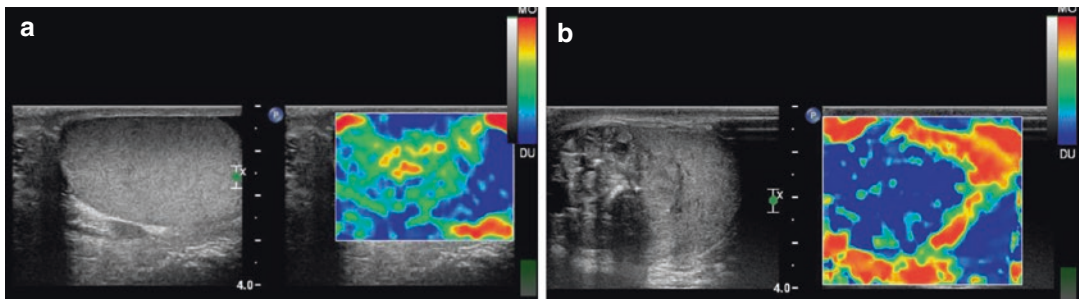

Fig. 38.8 Elastosonography. (**a**) A normal testicle has a medium level of elasticity (displayed in *green*), while malignant lesions (or epidermoid cysts as in **b**) appear as "hard" lesions (*blue*) because of the higher density compared with the surrounding normal tissue

References

1. American Institute of Ultrasound in Medicine; American College of Radiology; Society of Radiologists in Ultrasound (2011) AIUM practice guideline for the performance of scrotal ultrasound examinations. J Ultrasound Med 30(1):151U5
2. Akin EA, Khati NJ, Hill MC (2004) Ultrasound of the scrotum. Ultrasound Q 20:181–200
3. Dogra VS, Gottlieb RH, Oka M, Rubens DJ (2003) Sonography of the scrotum. Radiology 227:18–36
4. Nicola R, Carson N, Dogra VS (2014) Imaging of traumatic injuries to the scrotum and penis. AJR Am J Roentgenol 202(6):W512–W520
5. Delaney LR, Karmazyn B (2013) Ultrasound of the pediatric scrotum. Semin Ultrasound CT MR 34(3):248–256
6. Blaivas M, Brannam L (2004) Testicular ultrasound. Emerg Med Clin North Am 22(3):723–748
7. Pearl MS, Hill MC (2007) Ultrasound of the scrotum. Semin Ultrasound CT MR 28(4):225–248
8. American Institute of Ultrasound in Medicine (2011) AIUM practice guideline for the performance of an ultrasound examination in the practice of urology. J Ultrasound Med 30(1):146U5
9. Ragheb D, Higgins JL Jr (2002) Ultrasonography of the scrotum: technique, anatomy, and pathologic entities. J Ultrasound Med 21(2):171–185
10. Hamm B, Beyersdorff D, Asbach P et al (2008) Urogenital imaging. George Thieme Verlag
11. Correas JM, Bridal L, Lesavre A, Méjean A, Claudon M, Hélénon O (2001) Ultrasound contrast agents: properties, principles of action, tolerance, and artifacts. Eur Radiol 11:1316
12. Lock G, Schmidt C, Helmich F, Stolle E, Dieckmann KP (2011) Early experience with contrast-enhanced ultrasound in the diagnosis of testicular masses: a feasibility study. Urology 77(5):1049–1053
13. Valentino M, Bertolotto M, Derchi L, Bertaccini A, Pavlica P, Martorana G, Barozzi L (2011) Role of contrast enhanced ultrasound in acute scrotal diseases. Eur Radiol 21(9):1831–1840
14. Kamaya A, Machtaler S, Sanjani SS et al (2013) New technologies in clinical ultrasound. Semin Roentgenol 48(3):214–23
15. Goddi A, Sacchi A, Magistretti G et al (2012) Real-time tissue elastography for testicular lesion assessment. Eur Radiol 22:721–730
16. Correas JM, Drakonakisb E, Isidori AM et al (2013) Update on ultrasound elastography: miscellanea. Prostate, testicle, musculo-skeletal. Eur J Radiol 82:1904–1912

The Testicles: Cystic Lesions

39

Michele Bertolotto, Massimo Valentino, Mariano Iannelli, Francesca Neri, Gladiola Kaso, Libero Barozzi, and Pietro Pavlica

39.1 Introduction

Ultrasonography is the modality of choice for locating and characterizing palpable testicular lesions. Extratesticular palpable lumps are more common than intratesticular ones, and most of them are cystic. In the testis, cystic lesions represent a subset of intratesticular lesions, of which the majority are benign. It is important for the practicing sonologist to recognize this benign subset of lesions and prevent unnecessary surgical exploration.

39.2 Epididymal Cysts

Epididymal cysts are the most common scrotal masses, being reported in 20–40 % of asymptomatic individuals, 29 % of whom showing more than one cyst. They are either true cysts, likely of lymphatic origin, containing clear serous fluid and lined with epithelium, or spermatoceles filled with thicker, milky fluid containing spermatozoa, lymphocytes, and cellular debris, resulting from obstruction and dilatation of the efferent ductal system.

Both true epididymal cysts and spermatoceles appear either as anechoic, well-defined masses with increased through transmission (Fig. 39.1) or with corpuscolated fluid because of the presence of sperm, protein, white blood cells, and cell exfoliation. In practice, they are indistinguishable on ultrasound [1, 2]. Both lesions are benign; however, differential diagnosis is not necessary in the clinical practice.

Very large epididymal cysts may occasionally be difficult to differentiate from hydroceles. However, cysts displace the testis, whereas hydrocele envelops it.

M. Bertolotto, MD (✉) • M. Iannelli • F. Neri
G. Kaso
Department of Radiology, University of Trieste,
Ospedale di Cattinara,
Strada di Fiume 447, Trieste 34124, Italy
e-mail: bertolot@units.it

M. Valentino
S.O.C. Radiologia ASS 3 FVG, Ospedale
Sant'Antonio Abate, Via Morgagni 18,
Tolmezzo, UD 33028, Italy

L. Barozzi
Radiology Unit, Casa di Cura Madre Fortunata
Toniolo, Via Toscana 34, Bologna 40141, Italy

P. Pavlica
Servizio di Diagnostica per Immagini, Villalba
Hospital, Via di Rocrio 25, Bologna 40136, Italy

P. Martino, A.B. Galosi (eds.), *Atlas of Ultrasonography in Urology, Andrology, and Nephrology*,
DOI 10.1007/978-3-319-40782-1_39

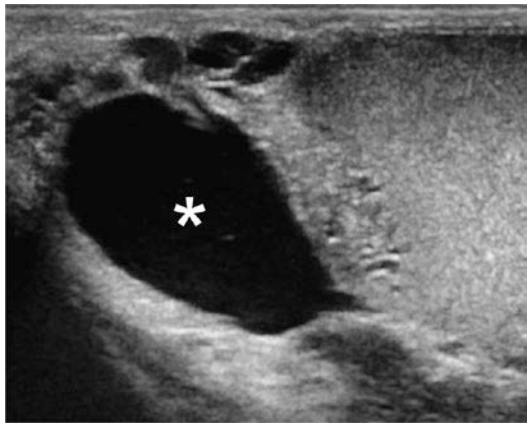

Fig. 39.1 Epididymal cyst/spermatocele. Longitudinal ultrasonographic image showing an anechoic lesion with well-defined margins in the head of the epididymis (*asterisk*)

39.3 Cysts of the Tunica Albuginea

Tunica albuginea cysts typically manifest as small palpable masses, single or multiple, mimicking clinically a testicular neoplasm. Most commonly, they are along the upper anterior or lateral aspect of the testicle. The diagnosis is usually straightforward at ultrasound (Fig. 39.2) which shows a small, peripherally located, anechoic lesion within the layers of the tunica meeting all the criteria of a simple cyst [2–4]. The presentation with internal echoes or complex appearance raising concern for a neoplasm is very rare.

Occasionally, very small cysts may be difficult to identify. Combined ultrasound and palpation allow their identification in virtually all cases (Fig. 39.3). On the other hand, large cysts of the tunica albuginea may grow compressing the testicular parenchyma and simulating an intratesticular cyst (Fig. 39.4).

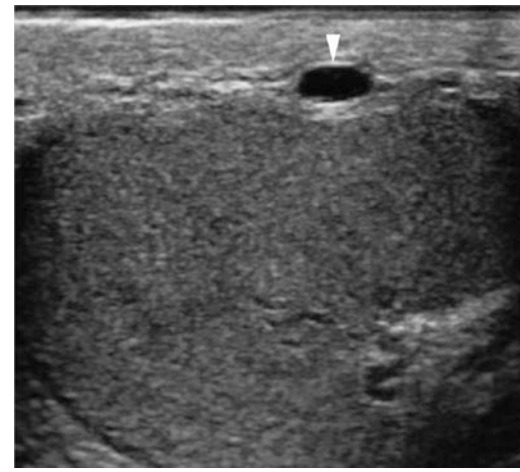

Fig. 39.2 Tunica albuginea cyst. Small, anechoic, palpable mass along the anterior aspect of the testis within the layers of the tunica albuginea (*arrowhead*)

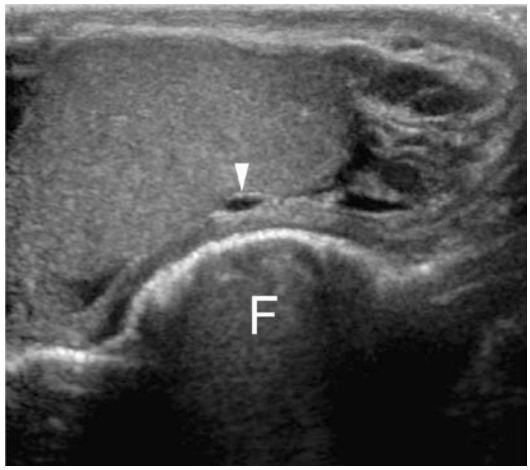

Fig. 39.3 Very small cyst of the tunica albuginea. Patient presented with a small palpable testicular lesion which was not initially identified on ultrasonography. Repeated investigation combined with palpation allows immediate identification of the palpable lesion which is characterized as a small cyst of the tunica albuginea (*arrowhead*). *F* finger of the sonologist

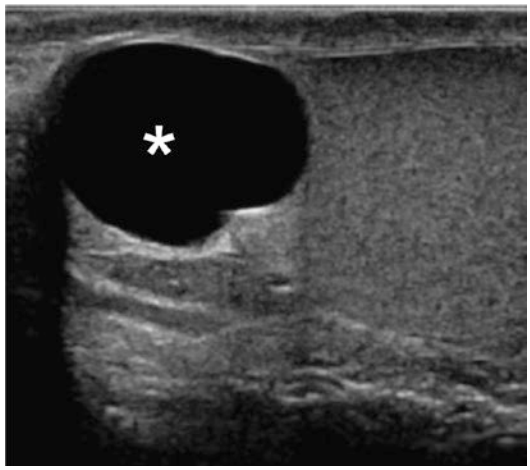

Fig. 39.4 Large cyst of the tunica albuginea (*asterisk*) compressing the testicular parenchyma and simulating an intratesticular cyst

39.4 Simple Testicular Cysts

Intratesticular cysts are usually non-palpable and thus detected incidentally. Similar to cysts elsewhere in the body, they are usually well defined and anechoic with an imperceptible wall (Fig. 39.5) [1–4]. Testicular cysts are usually solitary, but can be multiple, often associated with extratesticular spermatoceles. Simple testicular cysts can be categorized as benign. No treatment is required [5]. They can occur anywhere in the testis but are often near the mediastinum.

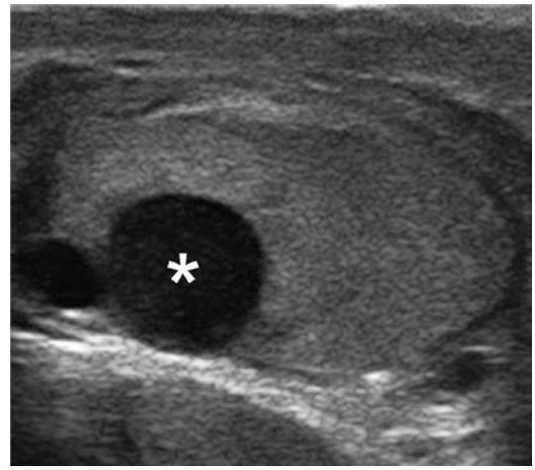

Fig. 39.5 Simple testicular cyst. Small non-palpable incidentally detected anechoic lesion within the testis (*asterisk*)

39.5 Complex Testicular Cysts

When a cyst does not fulfill the typical criteria of a simple cyst because of intracystic content, septa, or vegetations, a cystic neoplasm must be ruled out [1, 6]. Content mobilization allows diagnosis of debris, and the presence of color signal is diagnostic for vegetation. Intracystic amorphous content, however, is often not mobile, and the absence of flows at color Doppler interrogation is not sensitive enough to rule out vegetations. Complex testicular cysts often reduce in complexity and size or disappear during the follow-up, revealing their benign nature (Fig. 39.6). CEUS is of help showing avascular cystic content in complex benign cysts, while virtually all tumors with cystic components, enclosed mature teratomas, display intralesional vascularization after microbubble contrast injection [7].

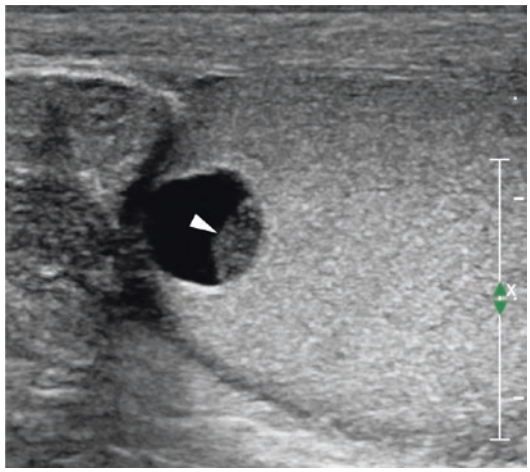

Fig. 39.6 Complex testicular cyst containing echogenic debris (*arrowhead*). The cyst disappeared during the follow-up (not shown)

39.6 Epidermoid Cysts

Epidermoid cysts are benign germ cell lesions that often present with a characteristic ultrasonographic pattern and can be correctly diagnosed preoperatively. They are true cysts with a well-defined fibrous wall containing a variable quantity of keratinizing, stratified epithelium. Their pathogenesis is uncertain: epidermoid cysts may result from monodermal development of a teratoma or due to squamous metaplasia of surface mesothelium. When an epidermoid cyst is suspected at imaging, testicular-sparing surgery and intraoperative pathological analysis are suggested. The ultrasonographic appearance of epidermoid cysts varies with the maturation, compactness, and quantity of keratin present [2, 3, 8]. Four ultrasonographic appearances have been described: type 1, classic "onion-ring" appearance with alternating hyperechoic and hypoechoic layers; type 2, densely calcified mass with an echogenic rim; type 3, cyst with a rim and either peripheral or central calcification; and type 4, mixed pattern, heterogeneous and poorly defined (Fig. 39.7). Occasionally, epidermoid cyst may resemble a simple cyst or a minimally complicated cyst with slightly inhomogeneous content and echogenic rim. Regardless of their appearance, they are hard at elastography, and intralesional vascularization is lacking both on color Doppler and CEUS modes [6, 9].

The appearance of epidermoid cysts on gray-scale ultrasonography is often characteristic, but not pathognomonic. Teratoma and other tumors must be ruled out. Care must be taken for possible signs of malignancy such as any intralesional flow, irregular borders, or irregularities within the surrounding testicular parenchyma. Negative tumor markers increase diagnostic confidence.

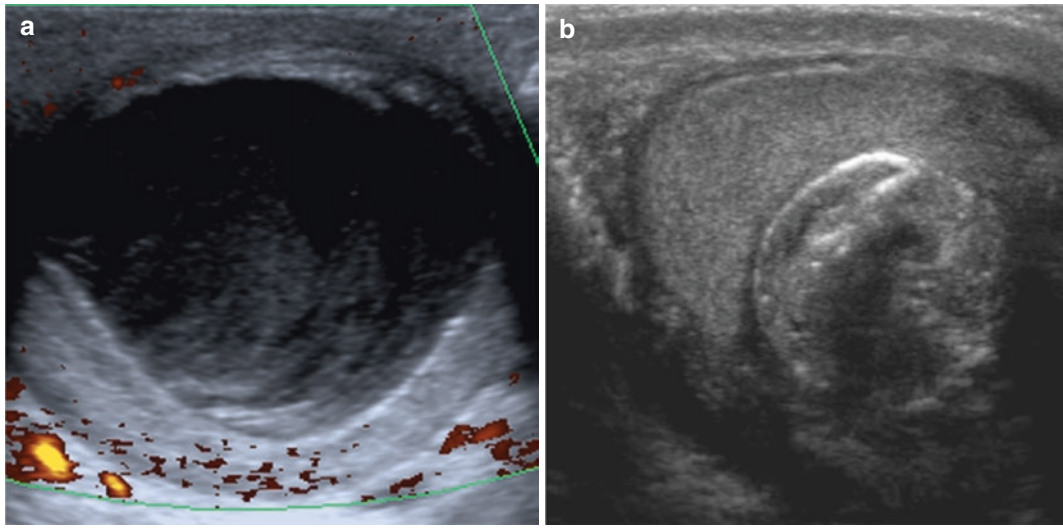

Fig. 39.7 Epidermoid cysts. (**a**) The lesion is avascular at color Doppler interrogation. It shows thin wall and relatively echogenic content with onion-ring appearance. (**b**) Another patient with epidermoid testicular cyst showing parietal and internal calcifications

39.7 Cystic Tumors

The presence of cystic components in testicular tumors is common. Tumors with prevailing cystic component, however, are rare [2, 8]. If a cystic lesion has any internal complexity, it must be considered a tumor, until its benign nature is demonstrated. Differential diagnosis between cystic tumors and benign complex cysts may be occasionally difficult based on conventional ultrasonographic modes only, as solid components often lack vascularization on color Doppler interrogation. CEUS eases the differential diagnosis, showing in virtually all tumors the vascularization of the solid components.

39.8 Tubular Ectasia of the Rete Testis

Dilatation of the rete testis is very common, often bilateral, and mostly seen in patients over 50 years of age. It can be associated with either postinfectious, post-traumatic, or post-prostatectomy epididymal obstruction. Possible contributing factors include epididymitis, testicular biopsy, and vasectomy. Epididymal abnormalities such as spermatoceles or dilated efferent ducts are frequently associated.

At ultrasonography the dilated rete testis presents with multiple, low-reflective, oval, or rounded structures within the mediastinum testis (Fig. 39.8) lacking vascularization on Doppler and contrast-specific modes [1, 3, 10].

Tubular ectasia of the rete testis is non-palpable, easily differentiated from testicular tumors due to its unique localization in the region of the mediastinum testis, characteristic ultrasonographic features, and frequent coexistence of spermatoceles.

Papillary adenocarcinoma of the rete testis is an extremely rare extratesticular neoplasm with only a few sporadic reports in the literature presenting with multilocular cystic appearance. The mass, however, is usually palpable and solid elements are associated.

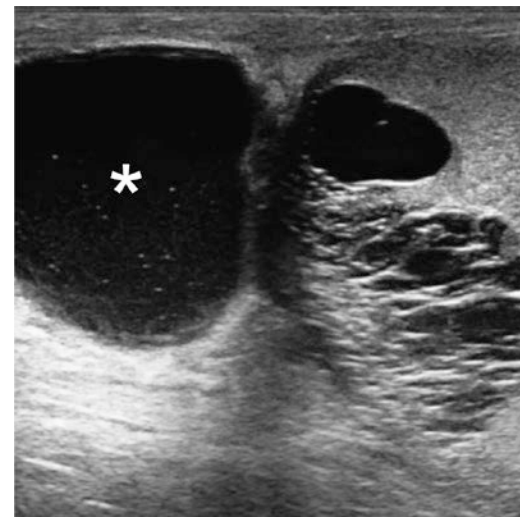

Fig. 39.8 Tubular ectasia of the rete testis. Longitudinal ultrasonographic view showing multiple cystic or tubular anechoic structures localized in the testicular mediastinum. An extratesticular spermatocele is associated (*asterisk*)

39.9 Cystic Dysplasia of the Rete Testis

Tubular ectasia of the rete testis must be differentiated from cystic dysplasia of the rete testis, a malformation arising during the testicular development due to malunion between the gonadal blastema and mesonephric ducts. The latter is usually detected in childhood, associated with ipsilateral urogenital lesions such as renal agenesis or multicystic dysplasia of the kidney. Clinically cystic dysplasia presents as an asymptomatic scrotal swelling. The age of the patient at presentation, clinical features, associated lesions, and multilocular cystic appearance on ultrasonography allow preoperative diagnosis [11].

39.10 Intratesticular Varicocele

Varicocele may be intratesticular as well, associated or not with extratesticular varicocele. The involved testis is often hypotrophic. Intratesticular varicocele is usually idiopathic but can also be secondary to conditions producing renal vein obstruction. It is bilateral in approximately 25 % of published cases. Most of series report a prevalence in the left side.

The ultrasonographic findings are similar to those of extratesticular varicocele [3, 12]. Multiple anechoic, serpiginous, tubular structures of varying sizes are identified, showing venous flows at color Doppler interrogation and spectral analysis (Fig. 39.9) with flow velocities during the Valsalva maneuver. Differential diagnosis between intratesticular varicocele and other hypo-/anechoic lesions in the testis is straightforward, since these lesions do not show flow at color Doppler interrogation. Differentiation with other intratesticular vascular pathologies is possible. Arterial pseudoaneurysms, intratesticular arteriovenous malformation, or hemangiomas characteristically show high-velocity arterial waveforms.

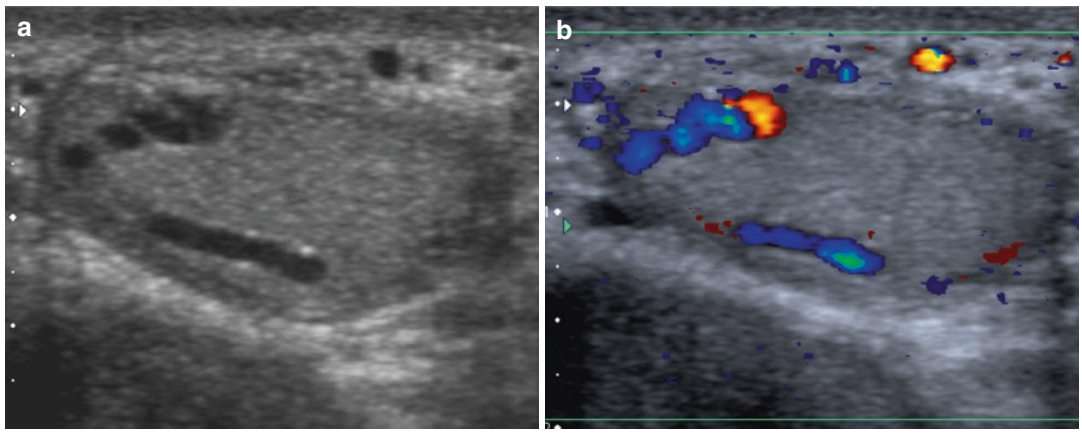

Fig. 39.9 Intratesticular varicocele. (**a**) Gray-scale ultrasonography shows intratesticular anechoic tubular structures within the testis. (**b**) Color Doppler interrogation obtained while standing during the Valsalva maneuver shows venous flows

39.11 Testicular Abscess

A testicular abscess may develop secondary to severe epididymo-orchitis or may be secondary to mumps, trauma, or infarction. Ultrasonography shows a testicular lesion with mixed echotexture (Fig. 39.10), or a corpusculated fluid collection, or a markedly hypoechoic lesion with ill-defined margins, surrounded by a hypoechoic halo. Abscess lacks vascularity at color Doppler interrogation in all cases. Hypervascularity of the surrounding parenchyma can be observed [2, 3]. In rare situations, gas bubbles are observed in the abscess cavity appearing as focal hyperechoic spots with posterior shadowing. On CEUS the lesion does not enhance, but the surrounding parenchyma may show avid enhancement [6].

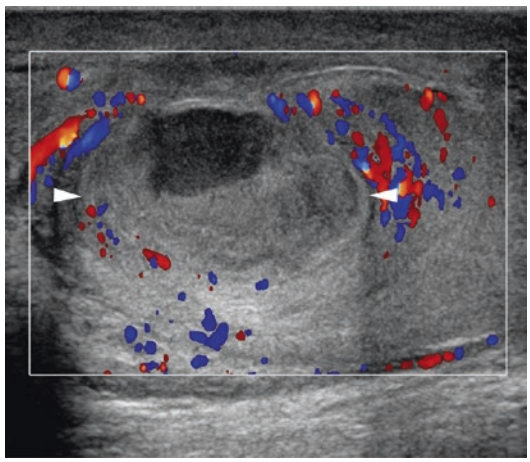

Fig. 39.10 Testicular abscess. Longitudinal scan showing a testicular lesion with mixed echotexture (*arrowheads*) lacking vascularization at color Doppler interrogation

39.12 Intratesticular Hematoma

Single or multiple intratesticular hematomas are commonly encountered in patients with scrotal traumas. Hyperacute and acute hematomas may appear hyperechoic or isoechoic to the surrounding testicular parenchyma or have a diffusely heterogeneous echotexture. Chronic hematomas are usually hypoechoic. Intralesional flow is lacking at color Doppler interrogation.

Ultrasonography is the imaging modality of choice for the detection and the follow-up of intratesticular lesions discovered in trauma patients. A tumor must be ruled out. Tumors and intratesticular hematomas may have similar appearance at gray-scale ultrasonography, but the former are vascularized, while the latter are not [13, 14]. Besides lack of vascularity, ultrasonographic appearance of hematomas changes during the follow-up with progressive reduction in size till resolution (Fig. 39.11), while tumors do not change or increase in size.

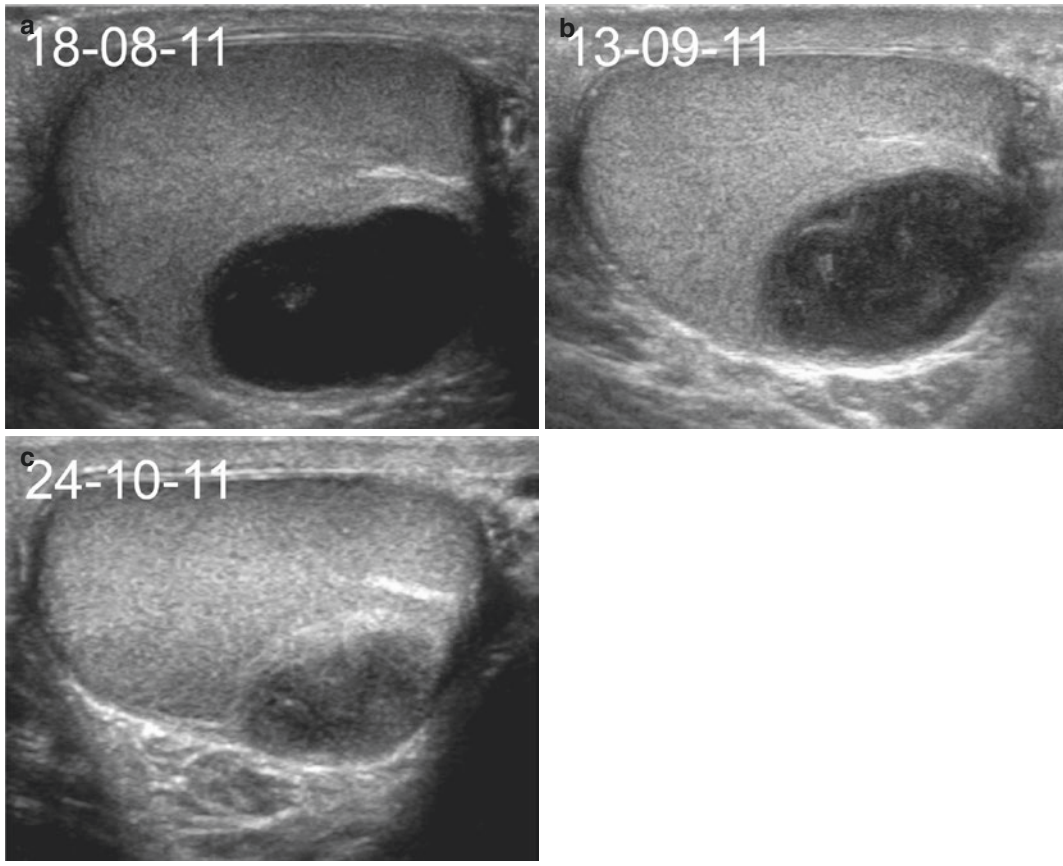

Fig. 39.11 Time changes of intratesticular hematoma. (**a**) Scan performed 2 h after the trauma shows a nearly anechoic lesion. (**b**) Repeated scan obtained 1 month later shows a smaller, inhomogeneously hypoechoic lesion. (**c**) Two months after the trauma, the size of the lesion reduced further, and echogenicity increased

39.13 Spermatic Cord Cysts

Spermatic cord cysts are revealed as palpable lesions along the course of the spermatic cord. They are usually slowly growing and asymptomatic. At ultrasonography the diagnosis is usually straightforward (Fig. 39.12) as the mass presents with the typical appearance of a simple or minimally complicated cyst [15]. Differential diagnosis with a neoplasia is more difficult for epidermoid cysts, rarely occurring in this location [16], which however lack vascularization at color Doppler and CEUS.

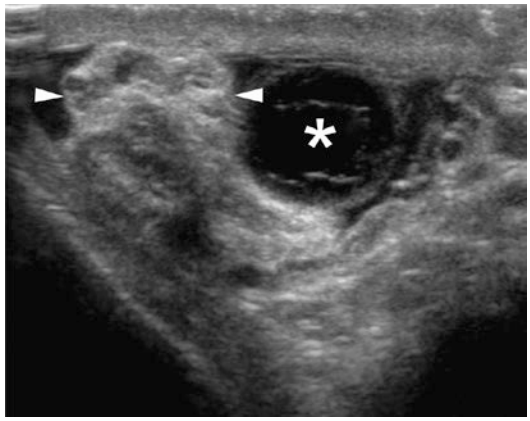

Fig. 39.12 Cyst of the spermatic cord. Axial ultrasound view of the inguinal canal showing a cyst (*asterisk*) adjacent to the spermatic cord (*arrowheads*)

39.14 Cystic Appendages

Testicular and epididymal appendages are commonly identified at ultrasonography, more often in the presence of hydrocele or other scrotal fluid collections (Fig. 39.13). The appendix testis is a remnant of the Müllerian duct. It is usually sessile and echogenic but may be pedunculated and with cystic appearance. The appendix epididymis is a remnant of the Wolffian duct. On histopathological examination it is almost invariably cystic, composed of multiple converging ducts. At ultrasound, however, it presents with cystic appearance in only about 36 % of cases [17].

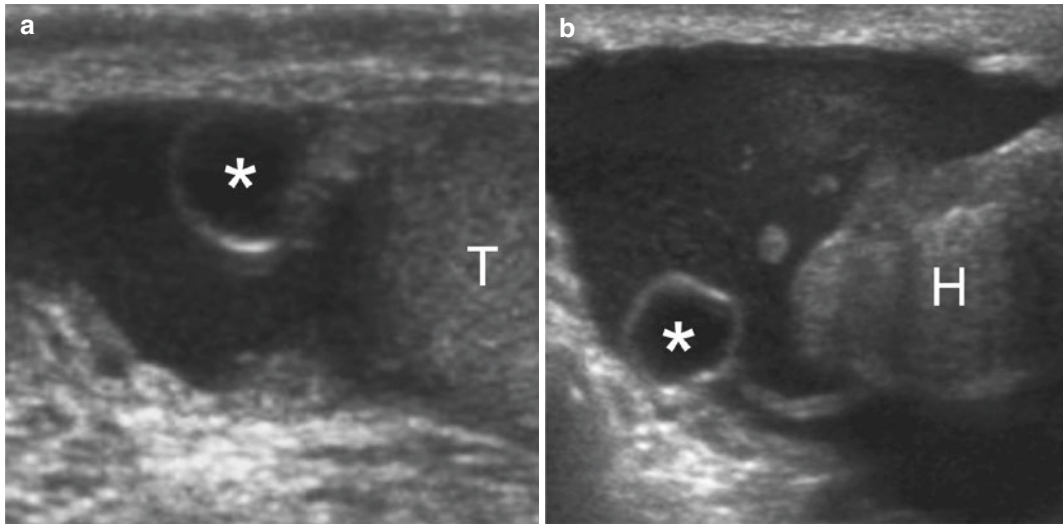

Fig. 39.13 Cystic appendices (*asterisk*) of the testis (**a**) and of the epididymis (**b**) appearing as pedunculated cystic masses arising from the upper pole of the testis (**a**) and from the head of the epididymis (**b**), respectively. *T* testis, *H* head of the epididymis

Conclusions

Most of benign scrotal cysts are characterized at gray-scale ultrasonography, and an adequate diagnosis of virtually all scrotal cystic lesions is obtained combining different ultrasonographic modes. Other imaging modalities are rarely required. The sonologist should be familiar with normal and pathological ultrasonographic anatomy in order to make a correct diagnosis of these lesions.

References

1. Valentino M, Bertolotto M, Ruggirello M, Pavlica P, Barozzi L, Rossi C (2011) Cystic lesions and scrotal fluid collections in adults: ultrasound findings. J Ultrasound 14(4):208–215. doi:10.1016/j.jus.2011.10.008
2. Bhatt S, Rubens DJ, Dogra VS (2006) Sonography of benign intrascrotal lesions. Ultrasound Q 22(2):121–136
3. Dogra VS, Gottlieb RH, Rubens DJ, Liao L (2001) Benign intratesticular cystic lesions: US features. Radiograph Rev Publ Radiol Soc N Am. Inc 21 Spec No:S273-281. doi:10.1148/radiographics.21.suppl_1.g01oc15s273
4. Bhatt S, Jafri SZ, Wasserman N, Dogra VS (2011) Imaging of non-neoplastic intratesticular masses. Diagn Interv Radiol 17(1):52–63. doi:10.4261/1305-3825.DIR.3116-09.0
5. Al-Jabri T, Misra S, Maan ZN, Khan K, Coker C, Thompson P (2011) Ultrasonography of simple intratesticular cysts: a 13 year experience in a single centre. Diagn Pathol 6:24. doi:10.1186/1746-1596-6-24
6. Huang DY, Sidhu PS (2012) Focal testicular lesions: colour Doppler ultrasound, contrast-enhanced ultrasound and tissue elastography as adjuvants to the diagnosis. Br J Radiol. 85 Spec No 1:S41–53. doi:10.1259/bjr/30029741
7. Cantisani V, Bertolotto M, Weskott HP, Romanini L, Grazhdani H, Passamonti M, Drudi FM, Malpassini F, Isidori A, Meloni FM, Calliada F, D'Ambrosio F (2015) Growing indications for CEUS: the kidney, testis, lymph nodes, thyroid, prostate, and small bowel. Eur J Radiol 84(9):1675–1684. doi:10.1016/j.ejrad.2015.05.008
8. Maizlin ZV, Belenky A, Baniel J, Gottlieb P, Sandbank J, Strauss S (2005) Epidermoid cyst and teratoma of the testis: sonographic and histologic similarities. J Ultrasound Med Off J Am Instit Ultrasound Med 24(10):1403–1409; quiz 1410–1401
9. Patel K, Sellars ME, Clarke JL, Sidhu PS (2012) Features of testicular epidermoid cysts on contrast-enhanced sonography and real-time tissue elastography. J Ultrasound Med Off J Am Instit Ultrasound Med 31(1):115–122
10. Rouviere O, Bouvier R, Pangaud C, Jeune C, Dawahra M, Lyonnet D (1999) Tubular ectasia of the rete testis: a potential pitfall in scrotal imaging. Eur Radiol 9(9):1862–1868. doi:10.1007/s003300050936
11. Emam AT, Awad FM, Elsayed EA, Alghashi M (2012) Cystic dysplasia of the rete testis: ultrasound and magnetic resonance imaging findings. Saudi J kidney Dis Transplant Off Publ Saudi Center Organ Transplant Saudi Arabia 23(3):559–561
12. Bucci S, Liguori G, Amodeo A, Salame L, Trombetta C, Belgrano E (2008) Intratesticular varicocele: evaluation using grey scale and color Doppler ultrasound. World J Urol 26(1):87–89. doi:10.1007/s00345-007-0216-1
13. Gaur S, Bhatt S, Derchi L, Dogra V (2011) Spontaneous intratesticular hemorrhage: two case descriptions and brief review of the literature. J Ultrasound Med Off J Am Instit Ultrasound Med 30(1):101–104
14. Purushothaman H, Sellars ME, Clarke JL, Sidhu PS (2007) Intratesticular haematoma: differentiation from tumour on clinical history and ultrasound appearances in two cases. Br J Radiol 80(956):e184–e187. doi:10.1259/bjr/19678081
15. Algaba F, Mikuz G, Boccon-Gibod L, Trias I, Arce Y, Montironi R, Egevad L, Scarpelli M, Lopez-Beltran A (2007) Pseudoneoplastic lesions of the testis and paratesticular structures. Virchows Archiv Int J Pathol 451(6):987–997. doi:10.1007/s00428-007-0502-8
16. Katergiannakis V, Lagoudianakis EE, Markogiannakis H, Manouras A (2006) Huge epidermoid cyst of the spermatic cord in an adult patient. Int J Urol Off J Jpn Urol Assoc 13(1):95–97. doi:10.1111/j.1442-2042.2006.01228.x
17. Kantarci F, Ozer H, Adaletli I, Mihmanli I (2005) Cystic appendix epididymis: a sonomorphologic study. Surg Radiol Anat SRA 27(6):557–561. doi:10.1007/s00276-005-0034-3

The Testicles: Solid Lesions

40

Michele Bertolotto, Massimo Valentino, Francesca Currò, Francesca Neri, Libero Barozzi, and Lorenzo E. Derchi

40.1 Introduction

Testicular neoplasms are the most common tumors in the second and third decades of life. Seminoma is the most common single cell type in adult and yolk sac tumor and mature teratoma in prepuberal boys. Lymphoma and metastases are prevalent in elderly. Non-seminomatous germ cell tumors may present with a single cell type or have multiple histologic patterns in 40–60 % of cases. More than 10 % of testicular germ cell tumors are seen in patients with cryptorchidism. Sex cord and stromal tumors are typically small, usually discovered incidentally, and benign in about 90 % of cases. Mesenchymal tumors of the testis, both benign and malignant, are rare.

M. Bertolotto, MD (✉) • F. Currò • F. Neri
Department of Radiology,
University of Trieste, Ospedale di Cattinara,
Strada di Fiume 447, Trieste 34124, Italy
e-mail: bertolot@units.it

M. Valentino
S.O.C. Radiologia ASS 3 FVG, Ospedale
Sant'Antonio Abate, Via Morgagni 18,
Tolmezzo, UD 33028, Italy

L. Barozzi
Radiology Unit, Casa di Cura Madre Fortunata
Toniolo, Via Toscana 34, Bologna 40141, Italy

L.E. Derchi
Department of Radiology, DICMI University of
Genova, Ospedale S. Martino,
Largo Rosanna Benzi 8, Genova 16132, Italy

40.2 Role of Imaging

In patients with a scrotal mass, imaging is performed to confirm the presence of a lesion and to assess whether it is intra- or extratesticular and what is its nature [1].

Ultrasonography is nearly 100 % sensitive in detecting the lesion and 98–100 % sensitive in differentiating intra- vs. extratesticular position. Simultaneous evaluation with palpation and ultrasonography is of help for identification and location.

Unfortunately, many solid lesions have no special ultrasonographic character to help in the identification of their nature, though some features are more common in some histotypes.

Assessment of vascularity is of limited help. In general, it is not correlated with histology and varies with size. In an early study of 28 patients with surgically proven testicular tumors, 95 % of lesions greater than 1.5 cm demonstrated increased vascularity, while 86 % of lesions less than 1.5 cm were hypovascular [2]. The increased sensitivity of modern ultrasonographic equipment allows nowadays detecting vessels within both benign and malignant nodules of very small size. Some truly avascular lesions do exist, however, and this finding can be useful to lower the probability of malignancy.

P. Martino, A.B. Galosi (eds.), *Atlas of Ultrasonography in Urology, Andrology, and Nephrology*,
DOI 10.1007/978-3-319-40782-1_40

40.3 Germ Cell Tumors

Germ cell tumors present as single or multiple masses, usually hypoechoic relative to normal testis. Seminoma is often homogeneous, lobulated, or multinodular. It may be multifocal (Fig. 40.1). Embryonal cell carcinoma is usually hypoechoic with poorly defined margins and inhomogeneous echotexture. Cystic components are present in 20 % of cases. Yolk sac tumor is usually inhomogeneous with echogenic hemorrhagic foci. Choriocarcinoma is markedly vascularized, usually with cystic components and hemorrhagic areas appearing as echogenic foci; in many patients widespread metastasis is present at time of diagnosis. Teratoma often presents as an inhomogeneous mass with cystic components and echogenic foci because of calcifications, cartilage, immature bone, and fibrosis. Mixed tumors have variable appearance. They usually have heterogeneous echotexture, irregular or ill-defined margins, echogenic foci, and cystic components (Fig. 40.2).

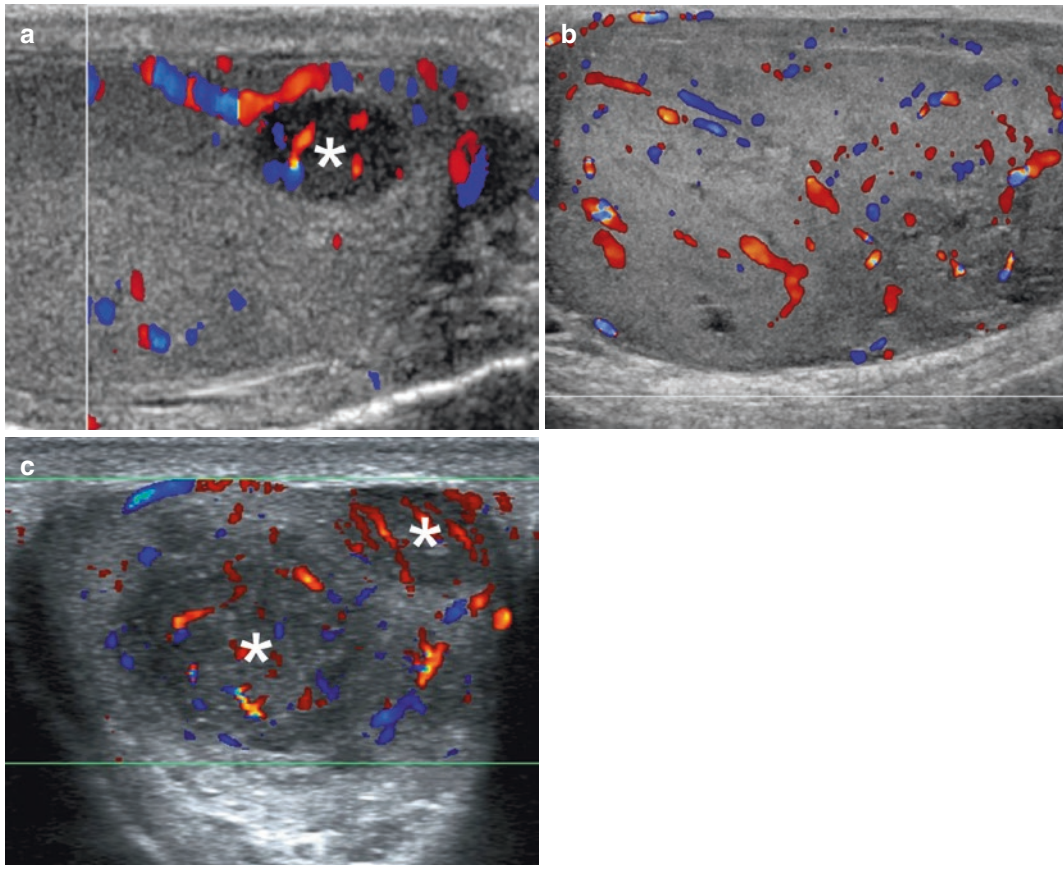

Fig. 40.1 Seminomas with different ultrasonographic appearance. (**a**) Small hypervascular, hypoechoic lesion (*asterisk*). (**b**) Large tumor involving most of the testis. (**c**) Two hypoechoic, hypervascular nodules in the same testis (*asterisks*)

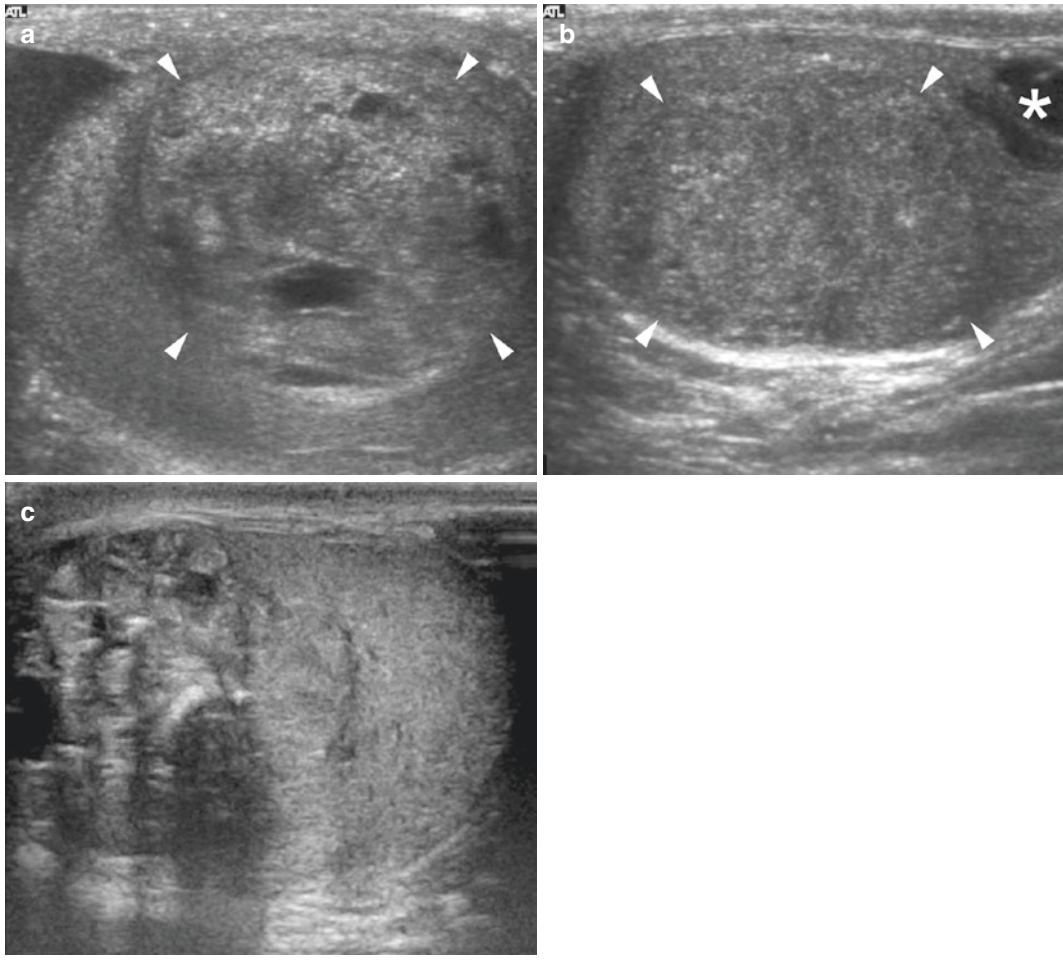

Fig. 40.2 Mixed germ cell tumors (*arrowheads*). (**a**) Lesion with solid and cystic regions containing seminoma, teratocarcinoma, and embryonal carcinoma. (**b**) Mostly solid lesion with a cystic area (*asterisk*) with components of seminoma, choriocarcinoma, and embryonal carcinoma. (**c**) Lesion with calcifications containing teratoma tissue

40.4 Sex Cord and Stromal Tumors

Small Leydig cell tumors usually present as well-defined homogeneously hypoechoic lesions, often located peripherally in the testis, with prominent vascularization at color Doppler interrogation. They are often more echogenic compared to seminoma (Fig. 40.3). Large-cell calcifying Sertoli cell tumors are usually echogenic masses with large areas of calcifications, or extensively calcified lesions. Non-calcifying Sertoli cell tumors are typically hypoechoic, well-circumscribed, round to lobulated masses. The ultrasonographic appearance of the other histotypes is not specific.

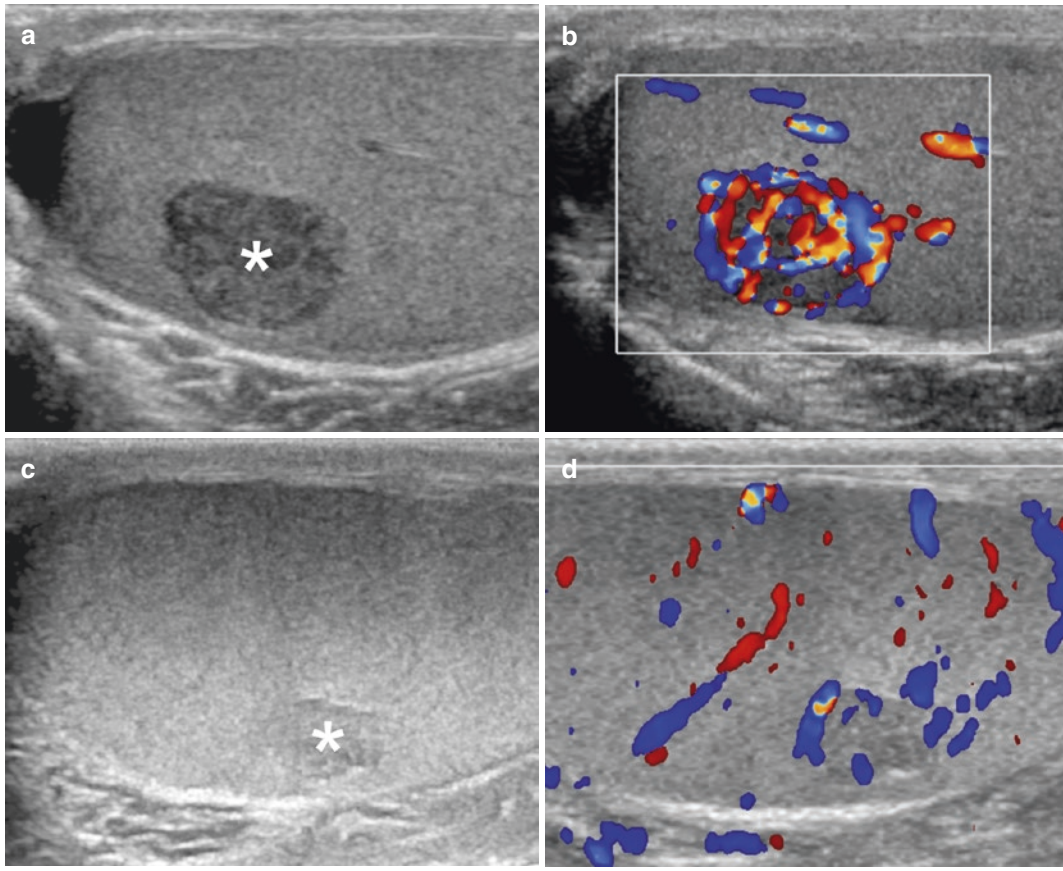

Fig. 40.3 Two different patients with Leydig cell tumors. (**a**, **b**) Hypoechoic nodule displaying marked vascularization at color Doppler interrogation. (**c**, **d**) Nearly isoechoic nodule with moderate vascularization at color Doppler interrogation

40.5 Testicular Lymphoma

While primary testicular tumors usually present as a mass-forming lump that enlarges destroying and replacing the normal parenchyma, the hallmark of lymphoma and other infiltrating neoplasms, such as plasmacytoma, is an infiltrative growth pattern in which tumor cells surround and compress the seminiferous tubules and the normal testicular vessels. Focal lymphomatous involvement presents on ultrasonography as single or multiple hypervascular lesions of decreased echogenicity. In diffuse lymphomatous infiltration, the testis is globally enlarged, with decreased echogenicity and marked hypervascularization, mimicking inflammation (Fig. 40.4). Identification of normal testicular vessels with a regular course crossing the lesion is a relatively specific feature characterizing lymphomas and other infiltrative tumors from mass-forming lesions. In a recent series of 43 pathologically proven testicular lymphomas, color Doppler ultrasonography demonstrated normal testicular vessels within the tumor in 72 % of cases [3]. Although color Doppler ultrasonography is able to differentiate between infiltrative and mass-forming tumors, nonneoplastic diseases such as chronic granulomatous orchitis and other inflammatory conditions may have similar appearance. Therefore, differential diagnosis may be difficult in the absence of clinical signs and symptoms of inflammation.

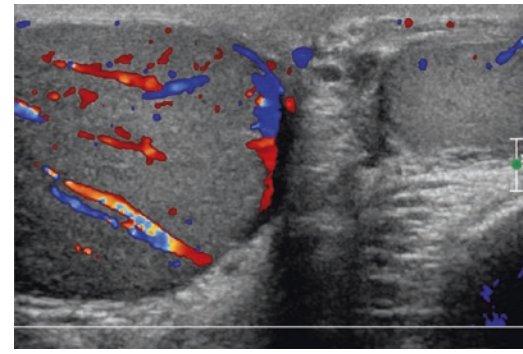

Fig. 40.4 Primary diffuse large B-cell lymphoma of the right testis. The patient presented with progressively enlarging, painless right scrotal lump. The right testis was markedly enlarged and hard at palpation. Color Doppler interrogation shows diffuse involvement of the right testis by hypervascular lymphoma tissue with no circumscribed nodules. Normal testicular vessels are shown with normal course running into the tumor tissue. The left testis is normal

40.6 Secondary Tumors

The ultrasonographic appearance of leukemic and lymphomatous infiltration is similar to primary lymphoma. Mass-forming metastatic deposits are very rare, often indistinguishable from primary neoplasms (Fig. 40.5). They present with variable echogenicity and echotexture depending on the characteristic of the primary tumor.

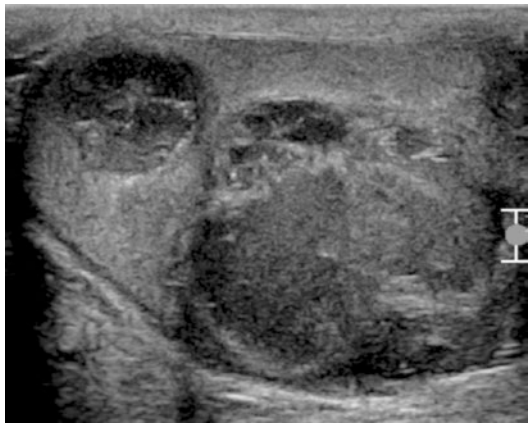

Fig. 40.5 Testicular metastatic deposits from melanoma involving the right testis in a 58-year-old patient with history of melanoma presenting with painless enlarging scrotal lump

40.7 Differential Diagnosis

Not all solid intratesticular lesions are neoplastic [4–7]. Granuloma, focal orchitis, abscess, infarction, fibrous pseudotumor, and hematoma can present as hypoechoic masses at ultrasonographic examination. The patient's age at presentation is important. Germ cell tumors are prevalent in young, while lymphoma in elderly patients, and some histotypes are much more prevalent in prepuberal boys.

Clinical correlation is vital: many nonneoplastic conditions likely manifest with acute scrotum. One needs to be cautious, however, because also tumors can occasionally manifest with pain. Also history of fever or trauma may suggest a nonneoplastic origin, permitting conservative management. In any case, the ultrasound findings of traumatic and inflammatory changes evolve rapidly; if a nonneoplastic intratesticular pathology is suspected, a short-term follow-up ultrasonographic examination allows differential diagnosis with tumor.

Tumor markers can help in the differential diagnosis between testicular tumors and nonneoplastic lesions. Human chorionic gonadotropin (hCG) is elevated in virtually all patients with choriocarcinoma and with seminomas containing syncytiotrophoblasts. Increased α-fetoprotein is found in yolk sac tumors and in mixed germ cell tumors with yolk sac elements. Sertoli cell tumors may produce excessive estrogen or testosterone, resulting in precocious virilization or feminization. Normal serum tumor markers, however, do not rule out testicular neoplasms.

40.8 Contrast-Enhanced Ultrasonography (CEUS)

Although the sensitivity of the newest equipment allows identification of vascular signals in an increasing number of small testicular masses, several lesions less than 1.5 cm may still appear avascular at color Doppler interrogation and cannot be distinguished effectively from nonneoplastic lesions. In our experience virtually, all testicular and extratesticular tumors display vascularization at CEUS [8, 9]. Cystic components in mixed tumors and areas of necrosis or hemorrhage lack contrast enhancement.

In patients with scrotal tumors, CEUS does not allow a reliable differentiation among different histotypes. The rate of the wash-in and the wash-out of contrast may help to differentiate malignant from benign tumors [10, 11], but data are not consistent enough to guide clinical management.

40.9 Elastography

The role of elastography in differentiating between malignant and benign nodules in the testes is currently still unclear. Increased tissue stiffness has been reported in testicular malignant tumors, but there is an increasing evidence of significant overlapping between benign and malignant lesions [12].

40.10 The Small and Non-palpable Testicular Lesion

Non-palpable solid testicular lesions may be incidentally discovered in patients undergoing scrotal ultrasonography for non-related purposes. Intratesticular lesions <5 mm, in particular, are frequently detected and are benign in up to 80 % of cases, rendering orchiectomy an inappropriately aggressive treatment. The practice of urologists has evolved to using serial ultrasound monitoring to follow small, incidental testicular lesions in patients with normal surrounding parenchyma and normal tumor markers (Fig. 40.6). Surgery is indicated for a lesion that shows increasing volume at follow-up [13, 14].

Although the significance of testicular microlithiasis is debated, in the general population, hypoechoic nodules associated with microlithiasis rise concern for seminoma [15]. In Klinefelter's syndrome, however, these nodules represent Leydig cell hyperplasia or Leydig cell tumors in most of cases. When infertile men first present for evaluation, Klinefelter's syndrome is often undiagnosed. The very small testes volume and the symmetric appearance should raise the possibility of this diagnosis and help prevent inappropriate orchiectomies.

40.10.1 Burned-Out Germ Cell Tumor

Patients with regressed or "burned-out" germ cell tumors present with widespread metastasis even though the primary tumor has involuted [13]. Histologic examination of the testis may reveal minute amounts of residual tumor or only fibrosis and scar tissue. Ultrasonography plays a vital role in the search for the primary regressed neoplasm. When visible, its appearance ranges from small echogenic foci to a relatively hypoechoic lesion.

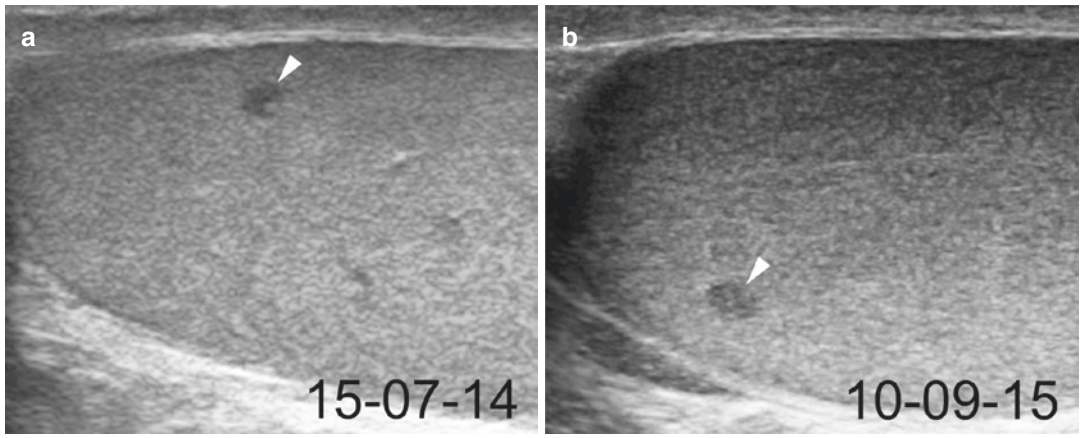

Fig. 40.6 Incidentally detected small, non-palpable testicular lesion in a 18-year-old patient. (**a**) First examination. (**b**) Follow-up examination. The lesion (*arrowhead*) remained stable after a follow-up of more than 1 year and was considered likely benign

40.11 Other Pathological Conditions

Granulomatous orchitis from tuberculosis, syphilis, fungi, and parasites can be difficult to differentiate from tumors. These processes, however, tend to involve the epididymis first and to a much greater extent than the testis.

Conclusion

Ultrasonography identifies scrotal lesions in virtually all cases and is highly sensitive to differentiate between testicular and extratesticular masses. Other imaging modalities are indicated in selected cases only. However, ultrasonographic features of solid scrotal tumors are often nonspecific, and most of them have no special character to help identification of their nature.

References

1. Dogra VS, Gottlieb RH, Oka M, Rubens DJ (2003) Sonography of the scrotum. Radiology 227(1):18–36. doi:10.1148/radiol.2271001744
2. Horstman WG, Middleton WD, Melson GL, Siegel BA (1991) Color Doppler US of the scrotum. Radiograph Rev Publ Radiol Soc N Am Inc 11(6):941–957. doi:10.1148/radiographics.11.6.1749858; discussion 958
3. Bertolotto M, Derchi LE, Secil M, Dogra V, Sidhu PS, Clements R, Freeman S, Grenier N, Mannelli L, Ramchandani P, Cicero C, Abete L, Bussani R, Rocher L, Spencer J, Tsili A, Valentino M, Pavlica P, European Society of Urogenital Radiology Scrotal Imaging S (2015) Grayscale and color Doppler features of testicular lymphoma. J Ultrasound Med Off J Am Instit Ultrasound Med 34(6):1139–1145. doi:10.7863/ultra.34.6.1139
4. Woodward PJ, Sohaey R, O'Donoghue MJ, Green DE (2002) From the archives of the AFIP: tumors and tumorlike lesions of the testis: radiologic-pathologic correlation. Radiograph Rev Publ Radiol Soc N Am Inc 22(1):189–216. doi:10.1148/radiographics.22.1.g02ja14189
5. Bertolotto M, Derchi LE, Sidhu PS, Serafini G, Valentino M, Grenier N, Cova MA (2011) Acute segmental testicular infarction at contrast-enhanced ultrasound: early features and changes during follow-up. AJR Am J Roentgenol 196(4):834–841. doi:10.2214/AJR.10.4821
6. Park SB, Lee WC, Kim JK, Choi SH, Kang BS, Moon KH, Kim YM, Jeong YK (2011) Imaging features of benign solid testicular and paratesticular lesions. Eur Radiol 21(10):2226–2234. doi:10.1007/s00330-011-2155-x
7. Bhatt S, Jafri SZ, Wasserman N, Dogra VS (2011) Imaging of non-neoplastic intratesticular masses. Diagn Interv Radiol 17(1):52–63. doi:10.4261/1305-3825.DIR.3116-09.0
8. Valentino M, Bertolotto M, Derchi L, Bertaccini A, Pavlica P, Martorana G, Barozzi L (2011) Role of contrast enhanced ultrasound in acute scrotal diseases. Eur Radiol 21(9):1831–1840. doi:10.1007/s00330-010-2039-5
9. Piscaglia F, Nolsoe C, Dietrich CF, Cosgrove DO, Gilja OH, Bachmann Nielsen M, Albrecht T, Barozzi L, Bertolotto M, Catalano O, Claudon M, Clevert DA, Correas JM, D'Onofrio M, Drudi FM, Eyding J, Giovannini M, Hocke M, Ignee A, Jung EM, Klauser AS, Lassau N, Leen E, Mathis G, Saftoiu A, Seidel G, Sidhu PS, ter Haar G, Timmerman D, Weskott HP (2012) The EFSUMB Guidelines and Recommendations on the Clinical Practice of Contrast Enhanced Ultrasound (CEUS): update 2011 on non-hepatic applications. Ultraschall in der Medizin 33(1):33–59. doi:10.1055/s-0031-1281676
10. Cantisani V, Bertolotto M, Weskott HP, Romanini L, Grazhdani H, Passamonti M, Drudi FM, Malpassini F, Isidori A, Meloni FM, Calliada F, D'Ambrosio F (2015) Growing indications for CEUS: the kidney, testis, lymph nodes, thyroid, prostate, and small bowel. Eur J Radiol 84(9):1675–1684. doi:10.1016/j.ejrad.2015.05.008
11. Drudi FM, Valentino M, Bertolotto M, Malpassini F, Maghella F, Cantisani V, Liberatore M, De Felice C, D'Ambrosio F (2015) CEUS time intensity curves in the differentiation between leydig cell carcinoma and seminoma: a Multicenter Study. Ultraschall in der Medizin. doi:10.1055/s-0034-1398841
12. Huang DY, Sidhu PS (2012) Focal testicular lesions: colour Doppler ultrasound, contrast-enhanced ultrasound and tissue elastography as adjuvants to the diagnosis. Br J Radiol. 85 Spec No 1:S41-53. doi:10.1259/bjr/30029741
13. Rocher L, Ramchandani P, Belfield J, Bertolotto M, Derchi LE, Correas JM, Oyen R, Tsili AC, Turgut AT, Dogra V, Fizazi K, Freeman S, Richenberg J (2015) Incidentally detected non-palpable testicular tumours in adults at scrotal ultrasound: impact of radiological findings on management radiologic review and recommendations of the ESUR scrotal imaging subcommittee. Eur Radiol. doi:10.1007/s00330-015-4059-7

14. Valentino M, Bertolotto M, Martino P, Barozzi L, Pavlica P (2014) Incidentally detection of non-palpable testicular nodules at scrotal ultrasound: what is new? Archivio italiano di urologia, andrologia: organo ufficiale [di] Societa italiana di ecografia urologica e nefrologica/Associazione ricerche in urologia 86(4):378–382. doi:10.4081/aiua.2014.4.378

15. Richenberg J, Belfield J, Ramchandani P, Rocher L, Freeman S, Tsili AC, Cuthbert F, Studniarek M, Bertolotto M, Turgut AT, Dogra V, Derchi LE (2015) Testicular microlithiasis imaging and follow-up: guidelines of the ESUR scrotal imaging subcommittee. Eur Radiol 25(2):323–330. doi:10.1007/s00330-014-3437-x

41 The Testicles: Trauma, Inflammation and Testicular Torsion

Stefano Bucci, Michele Rizzo, Giovanni Liguori, Paolo Umari, Giovanni Chiriacò, and Michele Bertolotto

41.1 Introduction

The majority of cases of acute scrotum are due to one of these three causes: trauma, torsion and inflammation.

Acute scrotum syndrome of any origin always merits immediate evaluation to prevent testicular function and chronic irreversible complication [1].

Correct differential diagnoses between these conditions are mandatory because uncorrected diagnosis could lead to catastrophic consequence.

Often physical examination is not sufficient to avoid suspicious conditions that require surgical correction and then imaging.

High-resolution ultrasound is the imaging modality of choice for the examination of superficially located scrotal sac and its contents. Greyscale ultrasonography in combination with colour or power Doppler imaging is a well-accepted technique for assessing scrotal lesions and testicular perfusion.

In this chapter, clinical features, greyscale and colour Doppler US appearance of testicular torsion, trauma and inflammation are described.

S. Bucci (✉) • M. Rizzo • G. Liguori • P. Umari
Department of Urology, University of Trieste, Trieste, Italy
e-mail: urostef@yahoo.it

G. Chiriacò • M. Bertolotto
Department of Radiology, University of Trieste, Trieste, Italy

41.2 Practical Considerations in the Colour Doppler and Ultrasonography Evaluation of the Scrotum

At the beginning of this discussion, we should remember that colour Doppler ultrasound is a highly operator-dependent examination.

In the clinical dilemma of the acute scrotal pain setting, the colour Doppler ultrasound is the primary imaging modality used.

The examination should be preferably done with a broadband high-frequency linear transducer (ideally up to 10 MHz).

It is a best practice, to begin the exam, analysing the asymptomatic side first in order to familiarise the patient with the procedure and to obtain an impression of the normal appearances of the testis.

The comparison of the symptomatic side with the contralateral asymptomatic side is essential to exclude technical reasons as the cause of absent flow and to allow the diagnosis of unilateral increased flow to be made [2].

Increased flow diagnosis is achieved by including both testes on the screen at the same time, with the Doppler box covering part of each of the testis in cross section.

To optimise detection of low velocity flow, the pulse repetition frequency (PRF) and filtration must be set low and a small colour sampling box should be used.

P. Martino, A.B. Galosi (eds.), *Atlas of Ultrasonography in Urology, Andrology, and Nephrology*,
DOI 10.1007/978-3-319-40782-1_41

We suggest to increase the gain until noise is seen and then slightly reduce it [3].

According to Lin, to optimise focal zone analysis, the sample volume of box flow should be inferior of the vessel lumen [4].

41.3 Testicular Torsion

Testicular torsion is the rotation of the testis along its longitudinal axis. During testicular torsion, the twist of spermatic cord elements results in initial blockage of venous drainage and a subsequent reduction in the arterial testis supply. Complete torsion (>360°) leads to ischaemic irreversible testicular damage and testicular loss if not treated timely.

The torsion of the spermatic cord may be intra- or extravaginal.

Extravaginal torsion is a rare phenomenon that occurs in the newborns when the scrotum is not securely attached to the tunica vaginalis.

Intravaginal testicular torsion, accounting for 65–80 % of the cases, is the most common type, and it may occur at any age although it is more common in the prepubertal age groups [5].

Male with intravaginal testicular torsion often presents an anatomical anomaly called 'bell clapper deformity' [6].

In this condition, the testicular mobility is increased because the tunica vaginalis is completely encircling the epididymis, distal spermatic cord and testis rather than attaching to the posterolateral aspect of the testis. Bell clapper deformity is more common in patients with a history of cryptorchidism.

In the clinical setting, symptoms can mimic other nonsurgical aetiologies such us epididymo-orchitis, testicular tumours, haematocele and strangulated hernia.

The ability to differentiate torsion from other common causes of acute scrotal pain is crucial because if surgery is performed within 5–6 hours of pain onset, the salvage rate is 80–100 % and this value falls to 20 % if surgery is delayed for more than 12 hours [7].

As said before, physicians should also be aware that torsion is more frequent in patients with history of cryptorchidism. Furthermore, any patients with undescended testes who presents with sudden abdominal pain should always be evaluated for possible torsion.

On palpation the affected testis generally tends to be higher in the scrotum and is usually in horizontal position. Clinical examination is often difficult and non-specific as the scrotum may appear swollen and reddened. In patient with testicular torsion, the cremasteric reflex is difficult to elicit. Differently from orchitis, the patient does not feel any pain relief with the testicular elevation (Prehn's sign). The epididymis in anterior position is another frequent clinical sign [8].

Body temperature, urinary sediment, leucocyte, number and markers of inflammation are usually normal in the torsion and are important criteria for epididymo-orchitis [2, 9].

If the patient presents within an early time window, ultrasound examination is critical in establishing whether the patients need surgical repair.

Because clinical presentation could be similar to the differential diagnosis in patient with acute scrotum, simultaneous assessment of clinical examination, ultrasound and laboratory findings are necessary.

41.3.1 Ultrasonographic appearances

Over the past few years, when testicular torsion is high on the differential diagnosis, ultrasound combined with colour and pulse Doppler, with the ability to reveal anatomical details and characterise testicular perfusion, has become the diagnostic imaging of choice.

It should be noted that colour Doppler ultrasonography is a procedure that largely depends on the operator experience [10].

US appearance of testicular torsion is variable depending on its duration and the degree of twisting of the spermatic cord.

In the early period immediately after the onset of the torsion, greyscale US evaluation of the testis reveals no abnormality, though a progressive hypoechogenicity develops secondary to oedema.

Initially colour Doppler US evaluation should start from the asymptomatic side so that the greyscale and colour Doppler gain settings can be set optimally allowing a baseline for comparison with the structures on the affected side [7].

Despite the fact that an asymmetry in the findings of the aforementioned evaluation may be a clue for the diagnosis of torsion, it should be kept in mind that bilateral involvement may occur in about 2 % of the cases.

US evaluation of the testis reveals no abnormality in the early period after the onset of the torsion; importantly in this patient, a second retarded evaluation is required to improve the diagnostic accuracy.

Progressive hypoechogenicity develops secondary to oedema (Fig. 41.1).

After 4 h, the testis is enlarged with a more spherical morphology and diffuse hypoechogenicity.

It should be kept in mind that a partial infarct may result in a focal or partially hypoechoic pattern (Fig. 41.2a, b).

As time passes, heterogeneous testis is seen due to focal haemorrhage and necrosis. In the late phases of torsion, the number of hyperechoic areas increases, a sign of intraparenchymal bleeding (Fig. 41.3a, b).

As the testicular arteries supply the epididymis, also this structure could be involved in the ischaemic process. If the epididymis is involved, it also became enlarged with heterogeneous and with hyperechoic areas due to haemorrhage.

Reactive hydrocele and thickening of scrotal skin are also seen (Fig. 41.4). Scrotal hyperaemia also known as the ‘rim sign’ is the cause of pitfalls of the major Doppler ultrasound. The collateral blood supply to paratesticular tissues, which is reactively increased, should not be erroneous.

On greyscale US, the testis appears more horizontal that than the contralateral testis, and the mediastinum could be in abnormal position (Fig. 41.5a, b).

In chronic torsion, the testis appears small, hard and markedly hypoechoic to anechoic, and colour Doppler shows no flow in the testis and increases the flow in the paratesticular tissue, including the epididymis complex and dartos fascia.

At the accurate US scrotal analysis in patient with testicular torsion, as a consequence, the sonographic ‘whirlpool sign’ could be detected and appear as a mass with concentric layers formed by coiling of the cord vessels secondary to the twisting of the spermatic cord (Fig. 41.6a, b) [11].

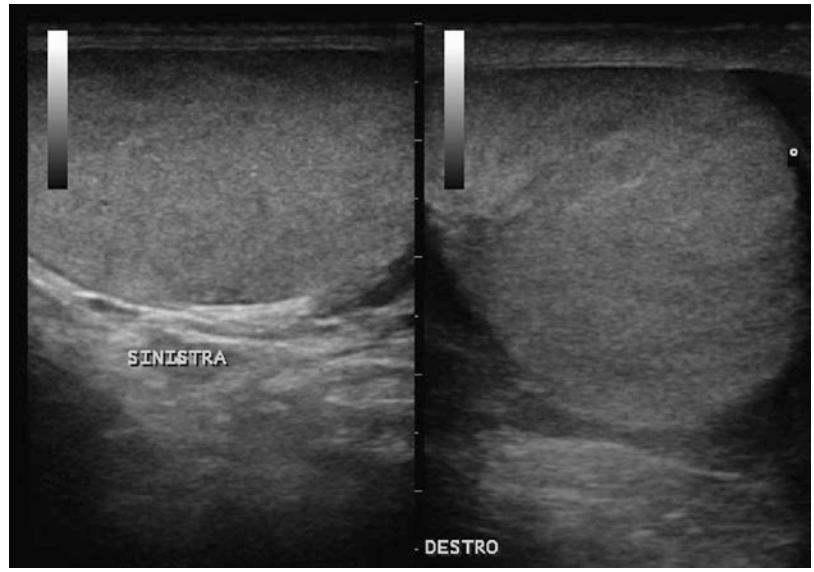

Fig. 41.1 At longitudinal greyscale ultrasound evaluation, the right twisted testis appears enlarged and oedematous with initial diffuse hypoechogenicity compared to the left healthy testis

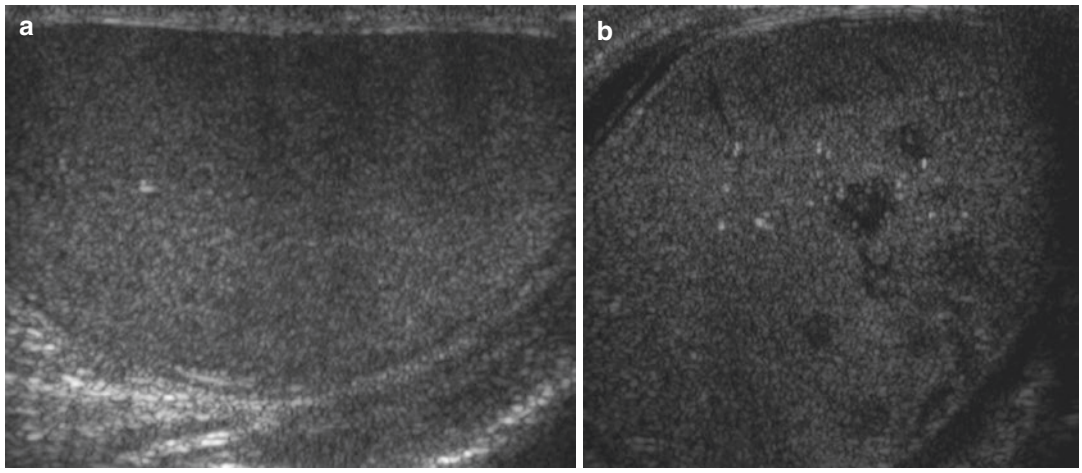

Fig. 41.2 (**a**, **b**) US appearance of partial infarct. Longitudinal greyscale US examination shows focal hypoechoic areas interspersed with normal testicular parenchyma and hyperechoic scar

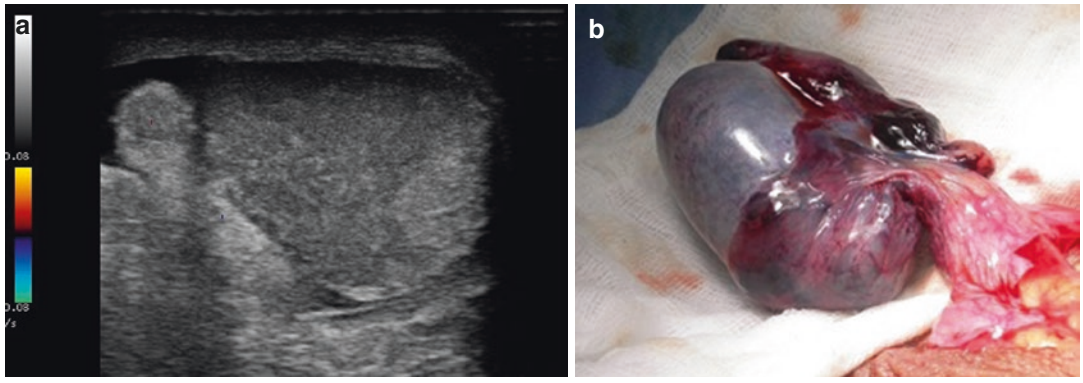

Fig. 41.3 (**a**) Testicular torsion. In transverse greyscale US, imaging shows heterogeneous testis due to focal haemorrhage and necrosis. Colour Doppler shows absence of flow. (**b**) Intraoperative image shows ischaemic testis with haemorrhage and necrosis. Usually also the epididymis could be involved in the ischaemic process

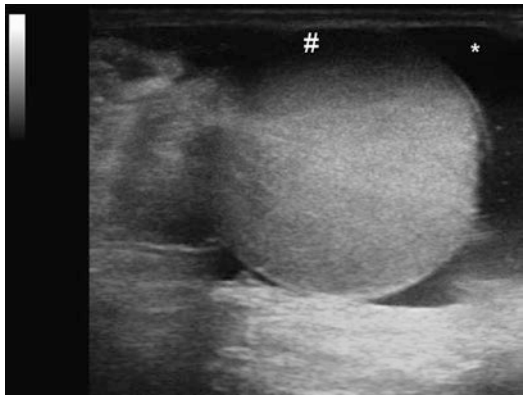

Fig. 41.4 In testicular torsion, the transverse greyscale US shows reactive hydrocele (*) and thickening of the scrotal skin (#)

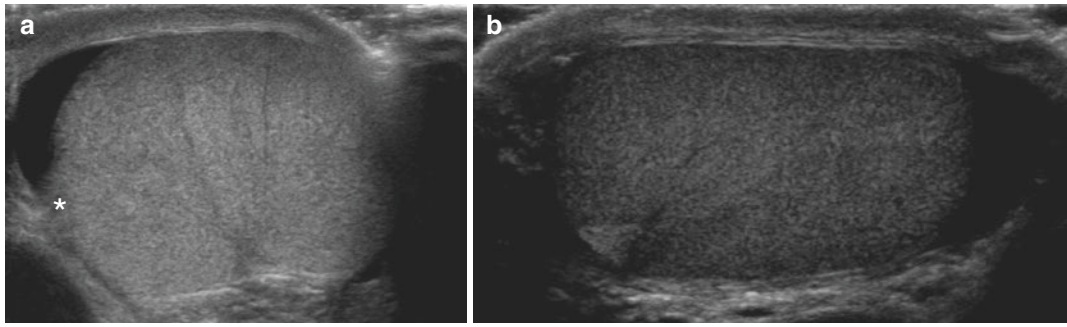

Fig. 41.5 In testicular torsion, the mediastinum (*) of the twisted testis (**a**) is in different position compared to the contralateral healthy testis (**b**)

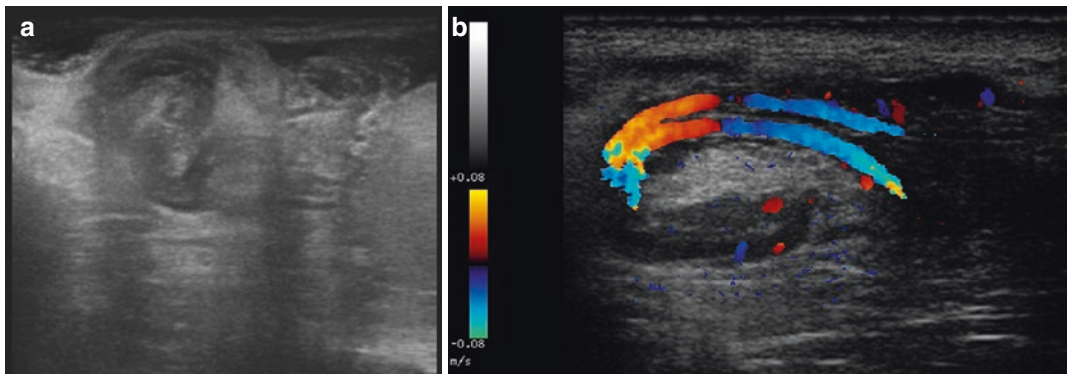

Fig. 41.6 (**a**) At the US scrotal analysis of the twisted testis, the spermatic cord presents a spiral aspect also known as 'whirlpool sign'. (**b**) At colour Doppler ultrasound, flow can be detected in the vessels of the 'whirlpool mass'

41.3.2 Colour Doppler Ultrasonographic appearances

Colour and power Doppler are the modality of choice to assess the testicular perfusion.

The impossibility to detect any blood flow in the interested testis is the most important criteria for the diagnosis of testicular torsion; furthermore, the flow can easily be detected in the normal contralateral testis (Fig. 41.7a, b) [11].

As said before, the presence of blood flow into the testis does not exclude the possibility of torsion. Again the contralateral same testis should be used as control and the examination should be repeated in a second time (Fig. 41.8a, b).

In suspected cases, where the blood flow is present, the blood flow resistance should be evaluated.

High-resistance blood flow pattern characterised by a decrease or reversal of diastolic flow in the spermatic cord suggests an impending testicular infarction.

In general the presence of testicular blood flow should always been studied using quantitative spectral Doppler evaluation.

In normal testis, the spectral waveform of the intratesticular arteries shows low-resistance pattern with high level of diastolic flow.

The mean resistive index (RI) value obtained in normal intratesticular arteries is 0.62 (range, 0.48–0.75) [12].

The possibility of the diagnosis of prenatal torsion with colour Doppler ultrasonography was described [13].

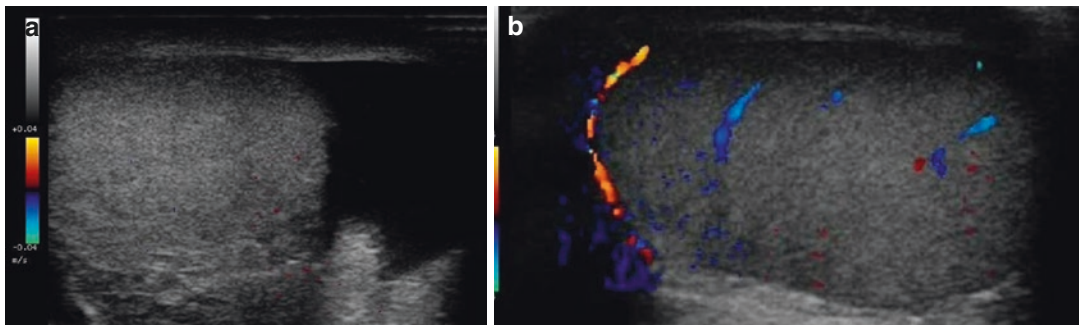

Fig. 41.7 (**a**) In testicular torsion, the longitudinal US shows the absence of blood flow in the right twisted testis. (**b**) Flow can easily be detected in the normal contralateral testis

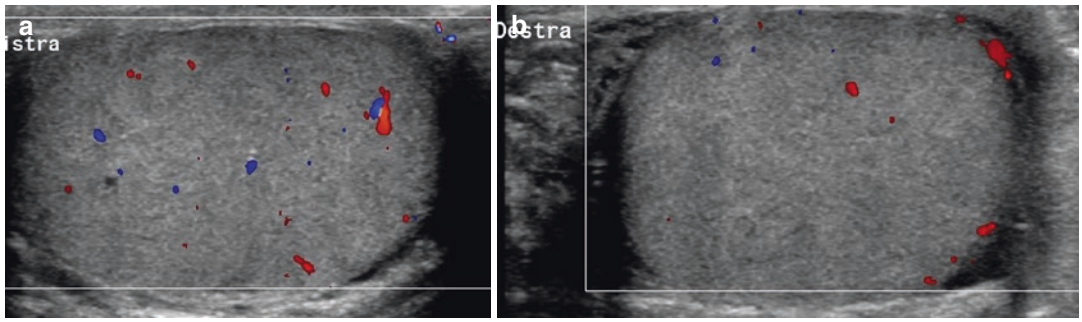

Fig. 41.8 (**a**) The US evaluation shows the presence of blood in the normal testis; (**b**) flow can also be detected in the contralateral testis with incomplete torsion

41.3.3 Incomplete or Partial Torsion

Incomplete torsion or partial torsion is a very challenging diagnosis because the blood flow appears normal; therefore, this condition is very difficult to discriminate with orchitis which can also cause partial ischaemia of the testicular parenchyma (Fig. 41.9).

Frequently it resolves spontaneously and the detorsion is characterised by increased reactive perfusion of the testis. Again clinical history and laboratory finding help to interpret this problematic condition [2].

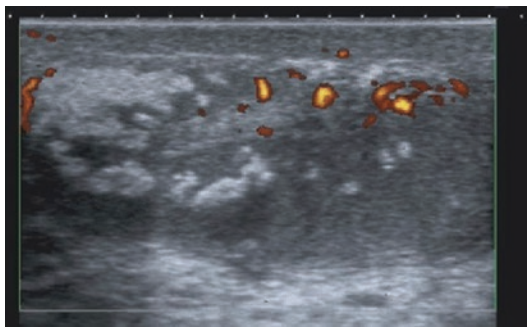

Fig. 41.9 US obtained in postoperative follow-up shows focal area of survived testicular parenchyma and hyperechoic foci of fibrosis. Power Doppler shows presence of vascular flow only in small part of tissue

41.3.4 Torsion of the Appendices

Torsion of the appendix testis and appendix epididymis can also cause acute scrotal pain, and the clinical presentation may be similar to that of testicular torsion. More than 90 % of twisted appendices involve the appendix testis. During childhood appendiceal torsion is nearly frequent as the testicular torsion. Appendiceal torsion can be asymptomatic. The so-called blue dot sign may be found in appendiceal torsion and consists of small (5 mm) tender mass on the upper pole of the testis with a visible chrematistic blue dot through the scrotal skin. The twisted appendage has been described on US as a small mass onto the upper pole of the testis with no internal blood flow and increased periappendiceal vascular signals. Colour Doppler US aspect of the testis and epididymis is normal, and the only accompanying sign is reactive hydrocele [2].

41.4 Trauma

Scrotal injuries most commonly occur in young men between 15 and 40 years and may result from either penetrating or blunt traumas.

Penetrating injuries include wounds from sharp objects and missiles as well as animal bites and self-mutilation [14].

Penetrating injuries to the scrotum require surgical exploration with conservative debridement of non-viable tissue and reconstruction of the testis and scrotum.

In blunt trauma management, the assessment of the tunica albuginea integrity is essential because if it is intact the lesion can be usually managed conservatively, while immediate operation is necessary if albugineal disruption is suspected [15].

In the assessment of patient that present with scrotal trauma, ultrasound is the first-line imaging modality to evaluate testis integrity. US examinations would be considered also in polytraumatic patient that present with scrotal swelling because often in these patients the examinations of the external genitalia are underestimated and often excessively delayed.

Today's approach of early operative exploration and repair in case of albugineal disruption is based on evidence that early diagnosis and intervention result in salvage of the testis in a high percent of cases [16].

Imaging helps urologists because clinical examination is difficult because scrotal swelling and pain could prevent evaluation of the scrotal content.

Colour Doppler examination allows direct evaluation of testicular perfusion and detection of ischaemic changes following contusion or post-traumatic torsion.

Assessment of the tunica albuginea integrity is particularly important because if it is intact the lesion can be usually managed conservatively, while immediate surgery is necessary if albugineal disruption is suspected [15].

41.4.1 Testicular Rupture

This severe condition is characterised by traumatic disruption of the tunica albuginea and extrusion of the testicular parenchyma into the scrotal sac (Fig. 41.10a, b).

Differently from the past, recent series, in which high-frequency probe is used, show that ultrasound is the imaging modality of choice in identification of testicular rupture for the diagnostic high sensitivity and specificity [17].

Irregularity of the testis is the most significant predictor for diagnosis of testicular rupture, with sensitivity, specificity and accuracy of 90% [18].

In patients with testicular rupture, as well as those 136 with other testicular parenchymal injuries in which the tunica albuginea is not interrupted, testicular echotexture may appear heterogeneous, with focal hyperechoic or hypoechoic regions corresponding to haemorrhagic or ischaemic areas.

On ultrasound, the normal tunica albuginea appears as a hyperechoic line outlining the testis. Colour Doppler interrogation is useful to determine viability of the injured testis. Tunica albuginea rupture is almost always associated with a disruption of the tunica vasculosa. As a result, testicular rupture results in ischaemia at a portion of the parenchyma of variable extension, which must be removed during surgical repair. CEUS may be performed in equivocal cases to confirm partial or complete testicular ischaemia [19] (Fig. 41.11). Limitations have been described for ultrasound in assessing patients with testicular rupture. False-negative assessment may result from lack of contour irregularity in patients with small albugineal disruption. Conversely, intratesticular and extratesticular haematomas may be isoechoic to the testis and mimic contour irregularity, leading to a false-positive diagnosis of rupture.

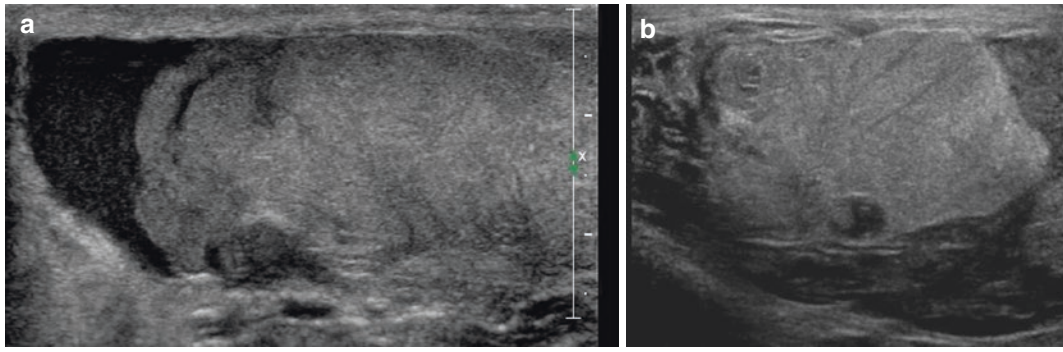

Fig. 41.10 Testicular rupture. (**a**) US shows irregularity in the contour of the upper testis pole with extrusion of the parenchyma. (**b**) Surrending haematocele is present

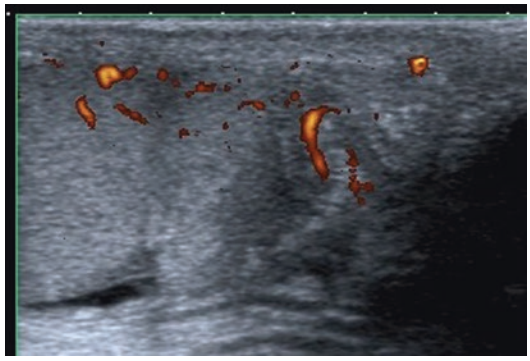

Fig. 41.11 In testicular rupture, the power Doppler shows a portion of ischaemic parenchyma

41.4.2 Testicular Fracture

In this injury, the tunica albuginea is intact but one or more fracture lines break the testicular parenchyma. Similar to injuries of other parenchymas, such as liver, kidney and spleen fracture, lines in the testis are often difficult to identify at greyscale ultrasound. Only about 17% of cases are seen. When visible, fractures appear as linear hypoechoic avascular bands extending across the testis (Fig. 41.12) [20]. Testicular shape and ultrasound appearance of the tunica albuginea are normal. Colour Doppler examination of the injured testis has achieved a very important role in the assessment and the management of this patient.

Testicular fractures are treated conservatively if normal flow is identified, while emergent surgery is recommended if flow is absent [20].

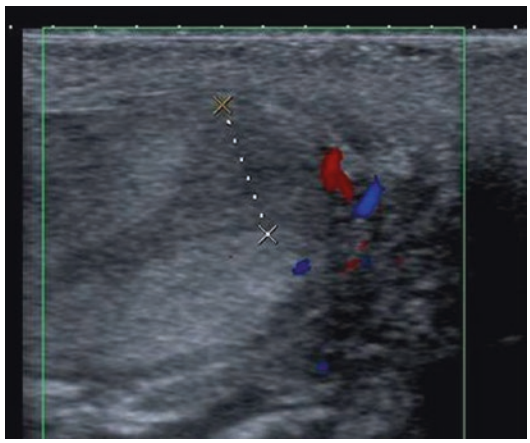

Fig. 41.12 Testicular fracture. The linear hypoechoic avascular band extending across the testis represents an intraparenchymal fracture

41.4.3 Posttraumatic Testicular Torsion

Testicular torsion is a rare manifestation of scrotal trauma which requires immediate operation. It especially occurs if predisposing factors, such as a 'bell 210 clapper deformity', are present. Clinical manifestations and ultrasound appearance are similar to those of non-trauma-related torsion [21]. Findings vary according to the duration and degree of rotation of the spermatic cord.

41.4.4 Intratesticular Haematoma

Single or multiple intratesticular haematomas are commonly encountered in patients with scrotal traumas. Ultrasound is the imaging modality of choice for evaluation and follow-up of intratesticular haematomas. The sonographic appearance of intratesticular haematomas varies with time [21]. Hyperacute and acute haematoma may appear hyperechoic or isoechoic to the surrounding testicular parenchyma or have a diffusely heterogeneous echotexture. Chronic haematoma is usually hypoechoic. Intralesional flows are lacking at colour Doppler interrogation. Differential diagnosis between haematomas and testicular tumours is important [22] because both have similar appearance at greyscale ultrasound, but most tumours display vascularisation at colour Doppler interrogation, while haematomas do not [22]. Tumour can be excluded if the lesion shows progressive resolution during follow-up. In polytraumatic patients, because the perineum is not routinely enclosed into the scan volume, or is often overlooked, the testicular dislocation is often missed (Fig. 41.13a, b).

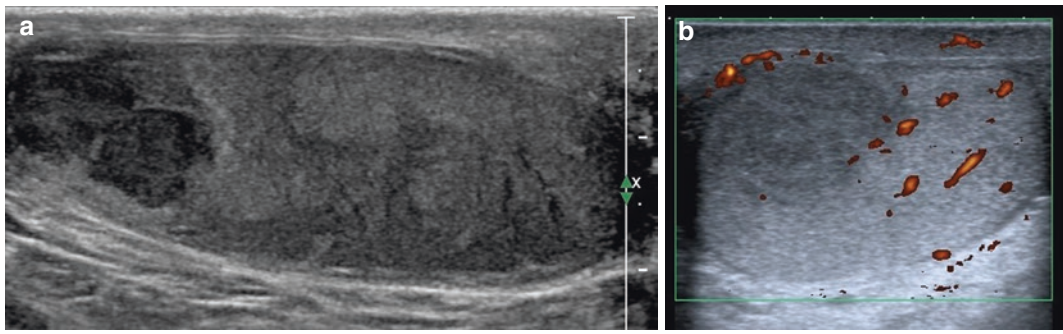

Fig. 41.13 (**a**) US evaluation shows an intact albuginea and the presence of a subalbugineal haematomas. (**b**) Power Doppler investigation reveals a large portion of ischaemic parenchyma

41.5 Inflammation

Epididymitis due to bacterial infection is the most common cause of acute scrotal pain in adolescent boys and adult patient.

In sexually active men, epididymitis is mostly caused by sexually transmitted organisms (*Chlamydia* and *Neisseria*); in prepubertal patient, urogenital anomaly could be suspected, whereas in elderly patients, it is usually due to common urinary pathogens.

Usually epididymitis is secondary to ascending infection from the prostatic urethra and seminal vesicles, but can also occur from haematogenous spread. In 20–40% of patients with epididymitis, the testis is involved; therefore, the term 'epididymo-orchitis' is more appropriate to describe this pathology; furthermore, the clinical management of these entities is the same.

Primary orchitis without involvement of the epididymis is rare but can be seen in HIV infection and in mumps.

The causative organism in epididymitis is usually bacterial and as has been said before varies according to the age of the patient.

According to the clinical course, epididymitis and orchitis are classified as acute or chronic processes.

Autoimmune phenomena are assumed to be the aetiological cause of non-specific granulomatous orchitis.

Paediatric orchitis and mumps orchitis are of haematogenous origin.

Epididymo-orchitis is also seen in systemic infections such as tuberculosis, lues, brucellosis and cryptococcal disease [23].

41.5.1 Clinical Presentation

Patients with epididymo-orchitis classically present with scrotal pain that is usually relatively acute in onset, fever, dysuria and a tender, sometimes enlarged, scrotum. As mentioned before, often the testis is involved in the inflammatory process, and we call the inflammation of these two entities epididymo-orchitis.

In the first assessment of patient presenting with scrotal pain, surgical cause must be excluded; in particular differentiation between torsion and epididymo-orchitis is mandatory.

The gradual onset associated with fever and leukocytosis is a distinctive feature in the differential diagnosis from torsion.

On clinical examination, scrotal elevation can relieve the pain caused by acute epididymo-orchitis but not pain caused by testicular torsion, a finding called Prehn's sign.

Ultrasonography is the primary imaging modality used to exclude the surgical causes of acute scrotal pain.

The US examination should start from the asymptomatic side to familiarise the patient with the procedure and to obtain an impression of the normal appearances of the testis and then proceed to the

In acute epididymitis, initial imaging will indicate that the testis on the affected side lies in its normal position in distinction with acute spermatic cord torsion, where the testis may be high riding with a more transverse orientation.

41.5.2 Greyscale and Colour Doppler Sonographic Appearances

In acute epididymitis, ultrasonography shows an enlarged epididymis with the tail usually affected first (Fig. 41.14a, b).

The scrotal oedema could cause a separation of the various layers of the scrotal wall.

A reactive hydrocele with the thickening of the overlying skin may be initially present (Fig. 41.15).

The greyscale US appearance of acute epididymo-orchitis may be normal and often does not present specific sign.

The presence of blood flow within the testis at Doppler examination is the most useful sign in distinguishing the inflammation from the testicular torsion.

The testicular hilum is the predominant site of infective change with focal hypoechoic areas which may mimic a testicular tumour. Follow-up is important in these patients with focal orchitis to ensure resolution [24].

There are several Doppler parameters that an operator must bear in mind to achieve high-quality Doppler examinations.

The inflammatory process is characterised by the increased blood flow to the area of inflammation in particular when compared with the contralateral normal side.

In acute phase of orchitis, Doppler examination could show the so-called septal accentuation that is due to an increased flow in the tunica vasculosa that appears as lines of colour flow radiating from the mediastinum testis out to the periphery. The 'septal accentuation' is supposed to be secondary to the fibrosis created by the inflammatory process. The physician must keep in mind that this pattern could be seen also in infiltrative process such as lymphoma or leukaemia [25]; therefore, in patient with this echographic pattern, the history of inflammatory process should be investigated (Fig. 41.16a, b).

Epididymo-orchitis can become abscesses; in this case, the colour Doppler examination shows the absence of flow into the lesions with increased flows in the outer margins (Figs. 41.17a, b and 41.18a, b).

In these cases, the administration of intravenous contrast agents containing microbubbles allows to check the presence or not of blood flow into the hypoechoic area. After the administration of microbubbles, the ischaemic area has no contrast enhancement.

This technique is particularly useful in the evaluation of the segmental ischaemia of the testis (Fig. 41.19a, b).

In most severe forms of epididymo-orchitis, there may be an obstruction of blood flow, and this condition can lead to ischaemia of the testis.

In the acute phase, the testis appears hypoechoic with no blood flow in the parenchyma and after will become hyperechoic with reduced size.

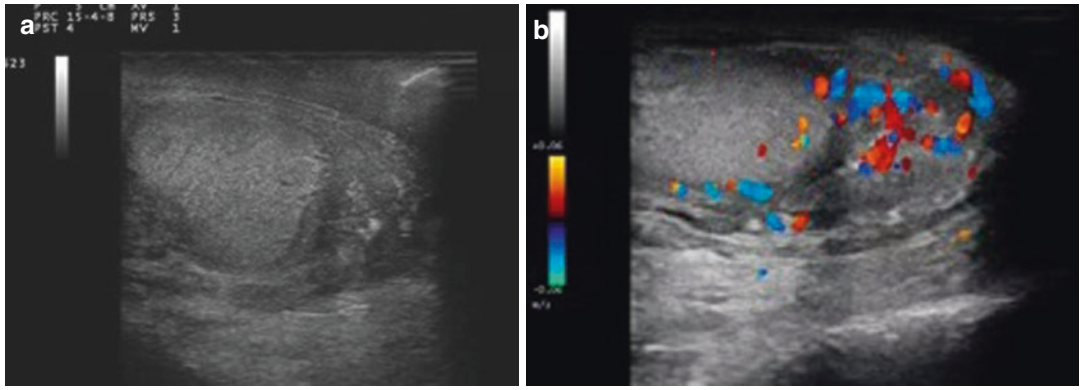

Fig. 41.14 Acute epididymitis. (**a**) The greyscale US shows an enlarged tail with heterogeneous appearance. (**b**) Colour Doppler investigation reveals an increase of vascular flow

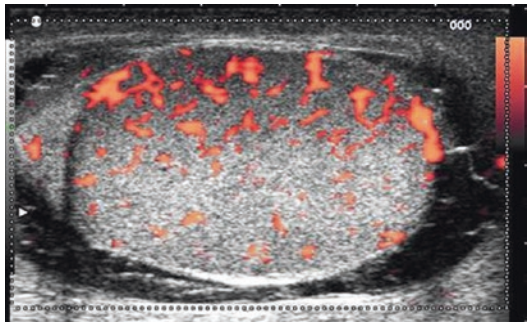

Fig. 41.15 In severe epididymo-orchitis, reactive hydrocele with the thickening of the overlying skin may be initially present

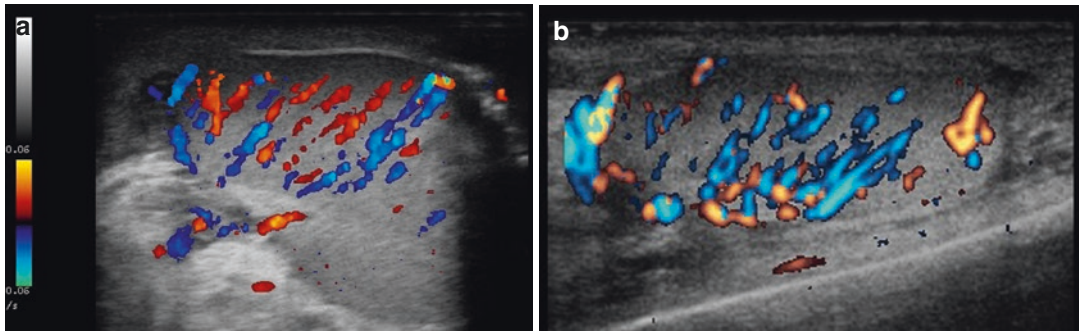

Fig. 41.16 (**a**, **b**) Colour-power Doppler image of patient with epididymo-orchitis demonstrating increased flow. The tunica vasculosa is seen as lines of colour flow radiating from the mediastinum testis out to the periphery

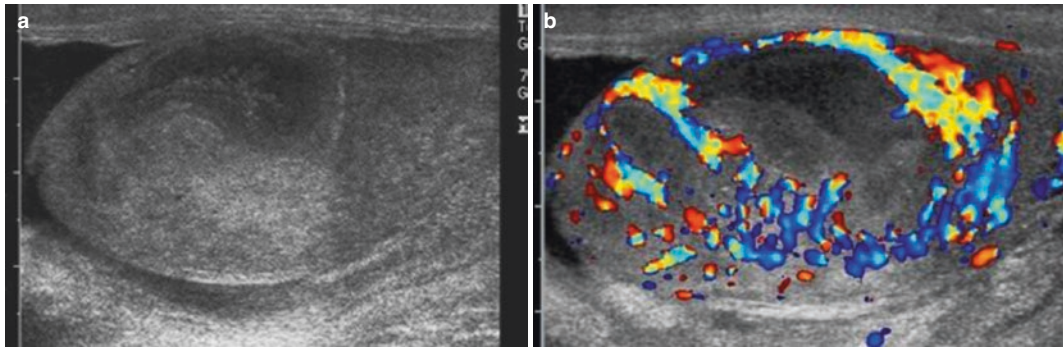

Fig. 41.17 (**a**, **b**) Epididymo-orchitis can become abscesses; in this case, the colour Doppler examination shows the absence of flow into the lesions with increased flows in the outer margins

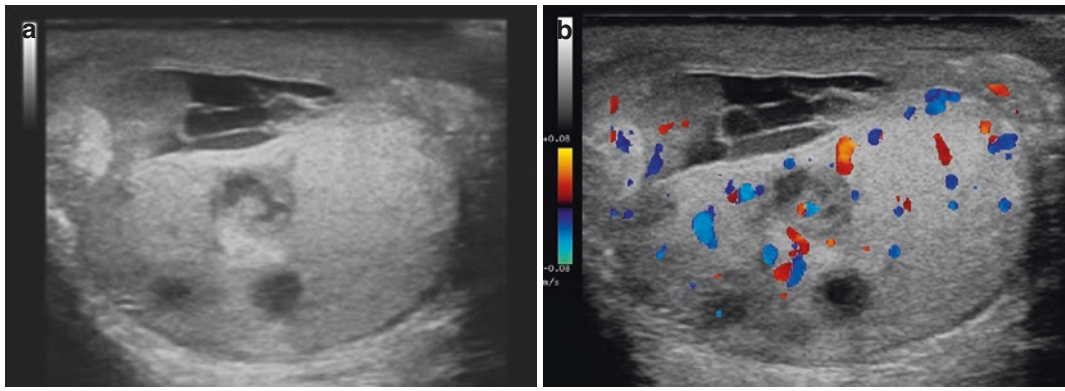

Fig. 41.18 (**a**, **b**) Patient with epididymo-orchitis after BCG not responding to therapy. (**a**) Transverse US image shows focal heterogeneous parenchymal echotexture areas in the testis. (**b**) The colour Doppler image demonstrates absence of flow within the lesion and surrounding increased flow

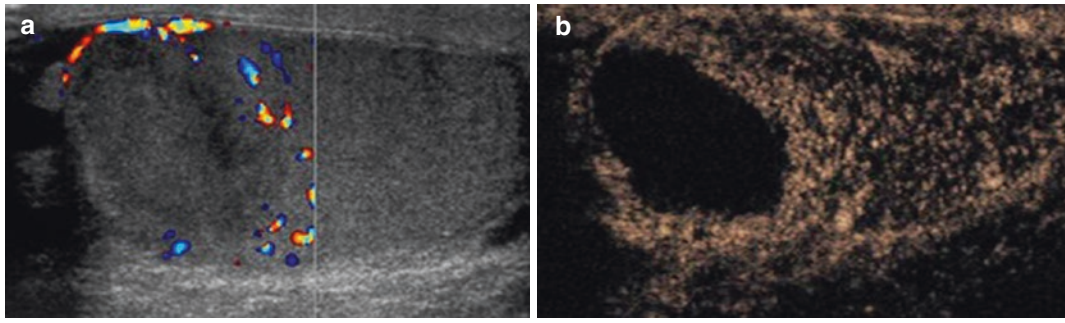

Fig. 41.19 (**a**, **b**) In segmental ischaemic testis, (**a**) the administration of intravenous contrast agents containing microbubbles allows to check the presence or not of blood flow into the hypoechoic area. After the administration of microbubbles, the ischaemic area has no contrast enhancement (**b**)

41.5.3 Testicular Infarction

Complete testicular infarction and segmental testicular infarction are clinical conditions with many aetiological causes.

Complete testicular infarction could be due to untreated torsion of the spermatic cord, severe epididymo-orchitis or trauma [26]. The greyscale appearance varies over time. In the acute stage, the testis appears enlarged and hypoechoic. Over time, as results in ischaemic lesions, there is a decrease in size and an increase in reflectivity, and the colour Doppler ultrasound reveals poor or absent flow.

Segmental testicular infarction is an uncommon cause of acute scrotal pain in adult men. Often it is diagnosed following testicular surgery [27].

The aetiology of segmental testicular infarction in most cases is idiopathic; however, the association with all this condition is described: epididymo-orchitis [28], trauma, haematological disorders such as polycythaemia and sickle cell disease [29], vasculitides such as hypersensitivity angiitis [30] and polyarteritis nodosa [31] as well as previous scrotal or inguinal surgery.

At colour Doppler examination, the most significant and frequent finding is absent vascularity within the lesion.

The greyscale ultrasound appearances of segmental infarction are variable, a focal hypoechogenic area is the usual finding, but hyperechogenic areas have also been documented [32] (Fig. 41.20a, b).

These differences may reflect whether the infarction is ischaemic (low reflectivity) or haemorrhagic (high reflectivity) in nature.

Infarcted lesions could be wedge shaped or rounded shaped.

It is suggested that the shape of the infarcted lesion depends on the type of ischaemic insult. Round lesions are secondary to an impairment of venous drainage system, and wedge-shaped lesions are due to arterial flow alteration [32, 33].

Segmental testicular infarction challenges clinicians because the difficult differential diagnosis with tumour and sometimes additional imaging or surgical exploration is required.

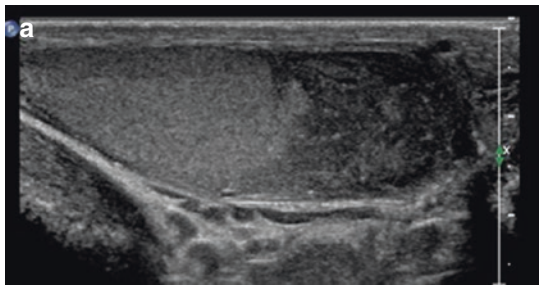

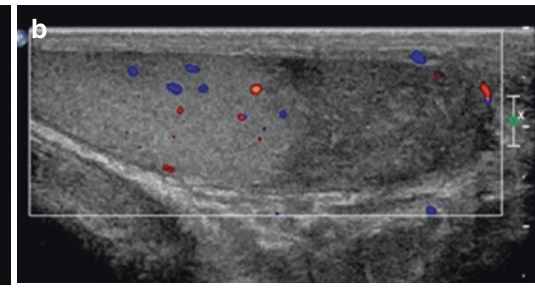

Fig. 41.20 (**a**, **b**) Segmental infarction. (**a**) The greyscale US image demonstrates a low reflective area at the lower half of the testis representing a segmental infarction. (**b**) The colour Doppler investigation image reveals the absence of vascularity

References

1. Burgher SW (1998) Acute scrotal pain. Emerg Med Clin North Am 16:781–809
2. Dogra VS, Bhatt S, Rubens DJ (2006) Sonographic evaluation of testicular torsion. Ultrasound Clin 1:55–66
3. Wilbert DM, Schaerfe CW, Stern WD et al (1993) Evaluation of the acute scrotum by color-coded Doppler ultrasonography. J Urol 149:1475–1477
4. Lin EP, Bhatt S, Rubens DJ et al (2007) Testicular torsion: twists and turns. Semin Ultrasound CT MRI 28:317–328
5. Favorito LA, Cavalcante AG, Costa WS (2004) Anatomic aspects of epididymis and tunica vaginalis in patients with testicular torsion. Int Braz J Urol 30:420–424
6. Dogra V (2003) Bell-clapper deformity. Am J Roentgenol 180:1176–1177
7. Hricak H, Lue T, Filly RA, Alpers CE, Zeineh SJ, Tanagho EA (1983) Experimental study of the sonographic diagnosis of testicular torsion. J Ultrasound Med 2(8):349–56
8. Kadish HA, Bolfe RG (1998) A retrospective review of pediatric patients with epididymitis, testicular torsion, and torsion of testicular appendages. Pediatrics 102:73–76
9. Kass EJ, Lundak B (1997) The acute scrotum. Pediatr Clin North Am 44:1251–1266
10. Middleton WD, Middleton MA, Dierks M et al (1997) Sonographic prediction of viability in testicular torsion: preliminary observations. J Ultrasound Med 16:23–27
11. Vijayaraghavan SB (2006) Sonographic differential diagnosis of acute scrotum: real-time whirlpool sign, a key sign of torsion. J Ultrasound Med 25:563–574
12. Siegel MJ (1997) The acute scrotum. Radiol Clin North Am 674(35):959–976
13. Snyder HM, Diamond DA (2010) In utero/neonatal torsion: observation versus prompt exploration. J Urol 183:1675–1677
14. Haas CA, Brown SL, Spirnak JP (1999) Penile fracture and testicular rupture. World J Urol 17:101–106
15. Buckley JC, McAninch JW (2006) Diagnosis and management of testicular ruptures. Urol Clin North Am 33:111–116, vii
16. Gross M (1969) Rupture of the testicle: the importance of early surgical treatment. J Urol 101:196–197
17. Guichard G, El Ammari J, Del Coro C et al (2008) Accuracy of ultrasonography in diagnosis of testicular rupture after blunt scrotal trauma. Urology 71:52–56
18. Kim SH, Park S, Choi SH et al (2007) Significant predictors for determination of testicular rupture on sonography: a prospective study. J Ultrasound Med 26:1649–1655
19. Moschouris H, Stamatiou K, Lampropoulou E et al (2009) Imaging of the acute scrotum: is there a place for contrast- enhanced ultrasonography? Int Braz J Urol 35:692–702; discussion 702–695
20. Deurdulian C, Mittelstaedt CA, Chong WK et al (2007) US of acute scrotal trauma: optimal technique, imaging findings, and management. Radiographics 27:357–369
21. Bhatt S, Dogra VS (2008) Role of US in testicular and scrotal trauma. Radiographics 28:1617–1629
22. Yagil Y, Naroditsky I, Milhem J et al (2010) Role of Doppler ultrasonography in the triage of acute scrotum in the emergency department. J Ultrasound Med 29:11–21
23. Naber KG, Weidner W (1999) Prostatitis, epididymitis, orchitis. In: Armstrong D, Cohen J (eds) Infectious diseases. Mosby. Harcourt Publishers Ltd, London, pp 1–58
24. Cook JL, Dewbury K (2000) The changes seen on high-resolution ultrasound in orchitis. Clin Radiol 55:13–18
25. Casalino DD, Kim R (2002) Clinical importance of a unilateral striated pattern seen on sonography of the testicle. AJR Am J Roentgenol 178:927–930
26. Sidhu PS (1999) Clinical and imaging features of testicular torsion: role of ultrasound. Clin Radiol 54: 343–352
27. Ruibal M, Quintana JL, Fernandez G et al (2003) Segmental testicular infarction. J Urol 170:187–188
28. Bird K, Rosenfield AT (1984) Testicular infarction secondary to acute inflammatory disease: demonstration by B-scan ultrasound. Radiology 152:785–788
29. Gofrit ON, Rund D, Shapiro A et al (1998) Segmental testicular infarction due to sickle cell disease. J Urol 160:835–836
30. Baer HM, Gerber WL, Kendall AR et al (1989) Segmental infarct of the testis due to hypersensitivity angiitis. J Urol 142:125–127
31. Braeckman P, Joniau S, Oyen R et al (2002) Polyarteritis nodosa mimicking a testis tumour: a case report and review of the literature. Cancer Imaging 2:96–98
32. Bilagi P, Sriprasad S, Clarke JL et al (2007) Clinical and ultrasound features of segmental testicular infarction: six-year experience from a single centre. Eur Radiol 17:2810–2818
33. Sriprasad S, Kooiman GG, Muir GH et al (2001) Acute segmental testicular infarction: differentiation from tumour using high frequency colour Doppler ultrasound. Br J Radiol 74:965–967

Varicocele

42

Giovanni Liguori, Gaetano Chiapparrone, Stefano Bucci, Francesca Vedovo, Nicola Pavan, Carlo Trombetta, and Michele Bertolotto

42.1 Introduction

Varicocele is clinically defined as an abnormal dilatation of the veins of the pampiniform plexus with continuous or intermittent reflux of the venous blood. It is actually considered the most common correctable cause of male infertility, even though the mechanisms responsible for infertility are still unclear. The prevalence of this disorder in the general population is approximately 15–20 % [1], and it is involved in up to 40 % of cases of men infertility [2–4].

Electronic supplementary material: The online version of this chapter (doi:10.1007/978-3-319-40782-1_42) contains supplementary material, which is available to authorized users.

G. Liguori, MD, PhD (✉) • G. Chiapparrone, MD • S. Bucci, MD • F. Vedovo, MD • C. Trombetta, MD
Department Urology, University of Trieste, Ospedale di Cattinara, Strada di Fiume 447, Trieste 34124, Italy
e-mail: gioliguori33@gmail.com

N. Pavan
Department of Medical, Surgical and Health Science, Urology Clinic, University of Trieste, Strada di Fiume, 447, Trieste 34149, Italy
e-mail: nicpavan@gmail.com

M. Bertolotto, MD
Department of Radiology, University of Trieste, Ospedale di Cattinara, Strada di Fiume 447, Trieste 34124, Italy

42.2 Classification of Varicocele

Varicocele is assessed and graded clinically using the criteria introduced by Dubin and Amelar [5] (Table 42.1), but this evaluation is highly subjective and strongly depends on the expertise of the physician [6] since dartos hyperactivity and contraction of the cremaster muscle induced by palpation or Valsalva maneuver may mimic or mask testicular venous distension [7]. The subjectivity of the clinical grading for varicocele is confirmed by Hargreave and Liakatas [8], who found disagreement in 26 % of patients examined by two experienced clinicians, and by a multicenter study on 141 subfertile men sponsored by the World Health Organization [9], which showed that compared with venography clinical assessment of varicocele was approximately 50 % sensitive, with a false-positive rate of 23 %. Using color Doppler ultrasound, Niedzielski et al. found reflux in only 39 % of patients in whom varicocele was suspected on clinical evaluation [10].

Since clinical diagnosis and grading of varicocele is limited, several imaging methods have been introduced to evaluate this disease, including gray-scale and color Doppler ultrasound. Color Doppler ultrasound is currently the imaging modality of choice.

The only gold standard in varicocele's diagnosis is retrograde phlebography of the spermatic veins, but it is not adequate as a routine screening test.

The most applied US classification in daily practice is the one proposed by Sarteschi et al.

P. Martino, A.B. Galosi (eds.), *Atlas of Ultrasonography in Urology, Andrology, and Nephrology*,
DOI 10.1007/978-3-319-40782-1_42

Table 42.1 Dubin and Amelar's classification

Grade 1	Varicocele is detectable by palpation only during Valsalva maneuver
Grade 2	Varicocele is detectable by simple palpation
Grade 3	Varicocele is visible on inspection and palpation

Table 42.2 Sarteschi's classification

Grade 1	Venous reflux at the emergence of the scrotal vein only during the Valsalva maneuver, hypertrophy of the venous wall without stasis
Grade 2	Supratesticular reflux only during the Valsalva maneuver, venous stasis without varicosities
Grade 3	Peritesticular reflux during the Valsalva maneuver, overt varicocele with early-stage varices of the cremasteric vein
Grade 4	Spontaneous basal reflux that increases during the Valsalva maneuver, possible testicular hypotrophy, overt varicocele, varicosities in the pampiniform plexus
Grade 5	Spontaneous basal reflux that does not increase during the Valsalva maneuver, testicular hypotrophy, overt varicocele, varicosities in the pampiniform plexus

Table 42.3 Iosa and Lazzarini's classification

Grade 1	Venous reflux lasting >1 s only during Valsalva maneuver
Grade 2	Spontaneous, discontinuous venous reflux that is not increased by the Valsalva maneuver
Grade 3	Spontaneous, discontinuous venous reflux that is increased by the Valsalva maneuver
Grade 4:	
Level A	Spontaneous, continuous venous reflux that is not increased by the Valsalva maneuver
Level B	Spontaneous, continuous venous reflux that is increased by the Valsalva maneuver

[11] (Table 42.2). Other classifications are the one proposed by Chiou et al. [12] and the most recent proposed by Iosa and Lazzarini based on an hemodynamic classification for qualitatively evaluating of venous reflux (Table 42.3).

42.3 Gray-Scale Ultrasound

The ultrasound appearance of varicocele consists of multiple, hypoechoic, serpiginous, tubular structures of varying size larger than 2–3 mm in diameter that are usually best visualized superior and/or lateral to the testis. When large, a varicocele can extend posteriorly and inferiorly to the testis [6, 13]. The size of dilated veins usually increases in the upright position and with a Valsalva maneuver. Low-level internal echoes are often detected in the dilated veins (Fig. 42.1), consistent with slow flow [13, 14]. Echoes are mobile during respiratory movements, during manual compression, and with a Valsalva maneuver.

Different threshold values of venous size are used for the diagnosis of varicocele. Most authors consider a cutoff value of 3 mm, but Gonda et al. reported a 95 % sensitivity with a cutoff of 2 mm [15]. Therefore, a diagnosis based only on the diameter of the vessels is characterized by a high number of false positives and negatives. Moreover, variability makes it difficult to compare the results of diagnostic modalities and treatments.

Besides evaluation of varices, gray-scale ultrasound allows assessment of the testis as well. Accurate and objective measurement of testicular volume can be obtained more accurately than with physical examination or using an orchidometer.

A strong association between clinical varicoceles and testicular damage was found, as reflected by testicular size [16–18]. According to Sigman et al., testicular hypotrophy is associated with a significantly decreased total motile sperm count and higher-grade varicoceles [19]. Zini et al. showed that also left subclinical varicocele may be associated with decreased left testicular volume [20]. Finally, Marks et al. showed that in patients with varicocele, a lack of testicular hypotrophy results in a higher postoperative pregnancy rate [18].

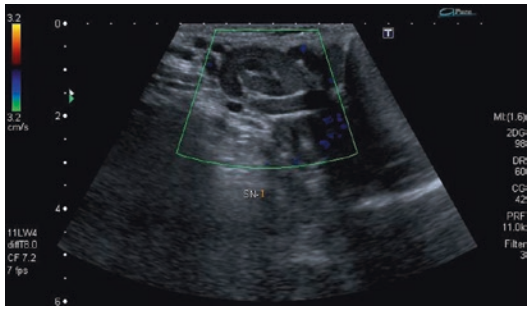

Fig. 42.1 Gray-scale appearance of varicocele. Multiple, hypoechoic, serpiginous dilated veins (*arrowheads*) larger than 2–3 mm are visible superior to the testis. Veins contain low-level internal echoes

Other studies, however, did not found a close relationship between testicular volume and subclinical varicocele [17], nor a correlation between testicular hypotrophy and clinical grading [21].

42.4 Color Doppler Ultrasound

At present, color Doppler ultrasound is the imaging modality of choice for detection and grading varicocele [11, 12, 22–27]; it is more sensitive than clinical examination and can detect up to 93 % of the reflux subsequently confirmed by spermatic venography [28].

In order to obtain a suitable evaluation of flow changes in the spermatic veins, ultrasound should be performed in the supine and then the upright positions, with and without a Valsalva maneuver.

Diagnosis is reached in case of prolonged venous flow augmentation or reflux. This must be differentiated from the mild and transient flow augmentation that can be seen with a Valsalva maneuver in normal men, lasting less than 1 s. According to Sarteschi and to the majority of investigators, we believe that in order to make a correct diagnosis of varicocele, it is necessary to detect a prolonged reflux that must be longer than 2 s. Other authors, however, use a threshold value of 1 s to distinguish between physiological reflux and varicocele [17].

Several classifications have been used for grading varicocele. We use the score system introduced by Sarteschi in 1993 [11] which divides varicocele into five grades according to the characteristics of the reflux, to its length, and to changes during Valsalva maneuver.

According to Sarteschi, grade 1 varicocele is characterized by the detection of a prolonged reflux in vessels in the inguinal channel only during Valsalva maneuver, while scrotal varicosity is not evident in the previous gray-scale study. Grade 2 is characterized by a small varicosity that reaches the superior pole of the testis and whose diameter increases during Valsalva maneuver. Color Doppler interrogation clearly demonstrates the presence of a venous reflux in the suprateticular region only during Valsalva (Fig. 42.2). Grade 3 is characterized by vessels that appear enlarged to the inferior pole of the testis when the patient is evaluated in a standing position. Color Doppler ultrasound demonstrates a clear reflux only during Valsalva maneuver (Fig. 42.3, Video 42.1). Grade 4 is diagnosed if vessels appear enlarged, even if the patient is studied in a supine position; dilatation increases in an upright position and during Valsalva maneuver (Fig. 42.4). Enhancement

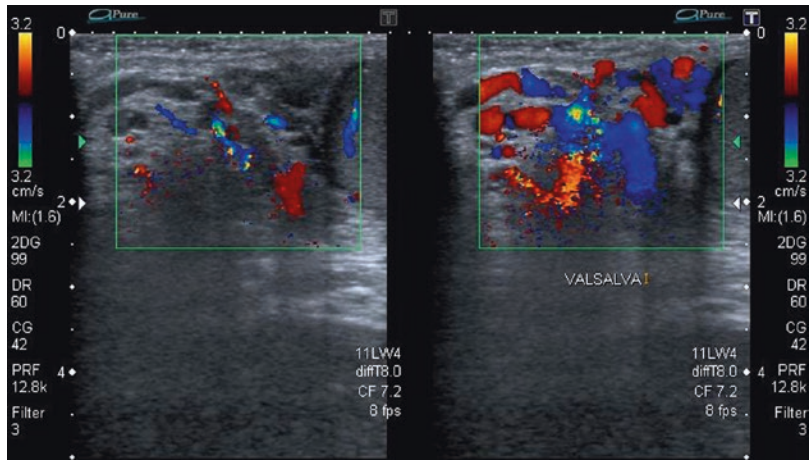

Fig. 42.2 Sarteschi's grade 2 varicocele. Color Doppler images obtained at rest and during Valsalva maneuver showing dilated veins in the supratesticular region with reflux during Valsalva

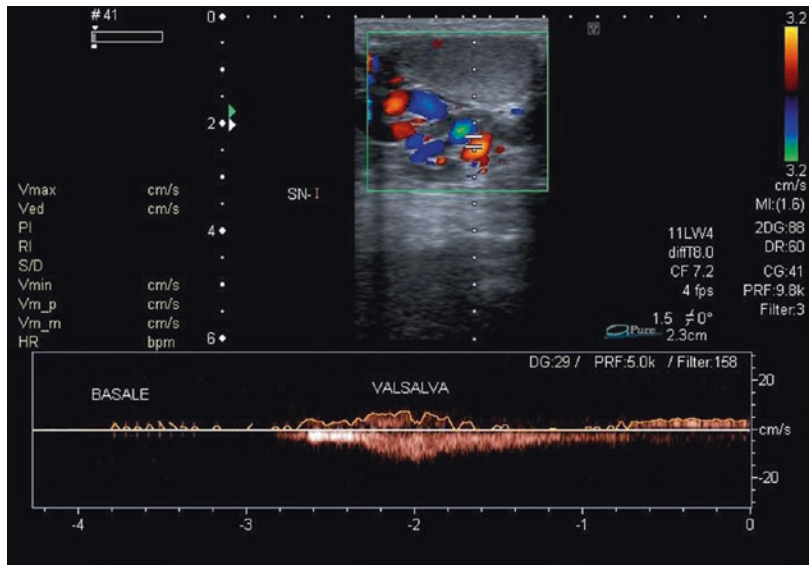

Fig. 42.3 Sarteschi's grade 3 varicocele. Color Doppler images with spectral analysis obtained at rest and during Valsalva maneuver showing dilated veins to the inferior pole of the testis with reflux during Valsalva

of the venous reflux during Valsalva maneuver is the criterion that allows the distinction between this grade from the previous and the next one. Hypotrophy of the testis is common at this stage. Grade 5 is characterized by an evident venous ectasia even in the supine position. Color Doppler interrogation demonstrates basal venous reflux that does not change substantially while standing and during Valsalva maneuver (Fig. 42.5).

The Sarteschi's classification for varicocele is the most commonly used in Europe. Other authors, however, suggested different score systems. Hoekstra [29] and Hirsh [30], for instance, suggested two similar classifications, which score varicocele in 4 and 3°, respectively (Tables 42.4 and 42.5). Oyen [31] scores 3° for varicocele mainly based on the length of reflux at pulsed Doppler interrogation (Table 42.6).

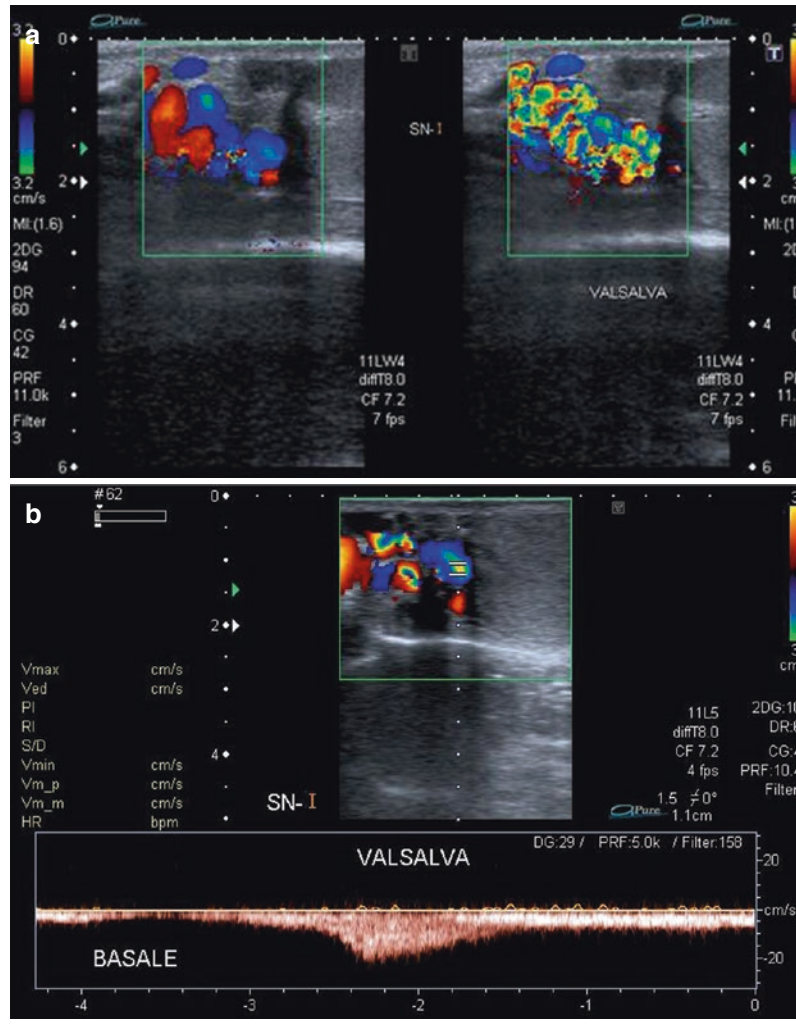

Fig. 42.4 Sarteschi's grade 4 varicocele. Color Doppler images (**a**) and spectral Doppler analysis (**b**) obtained in supine position at rest and while standing during Valsalva maneuver. Dilated veins with reflux are visible also at rest. Reflux increases while standing during Valsalva

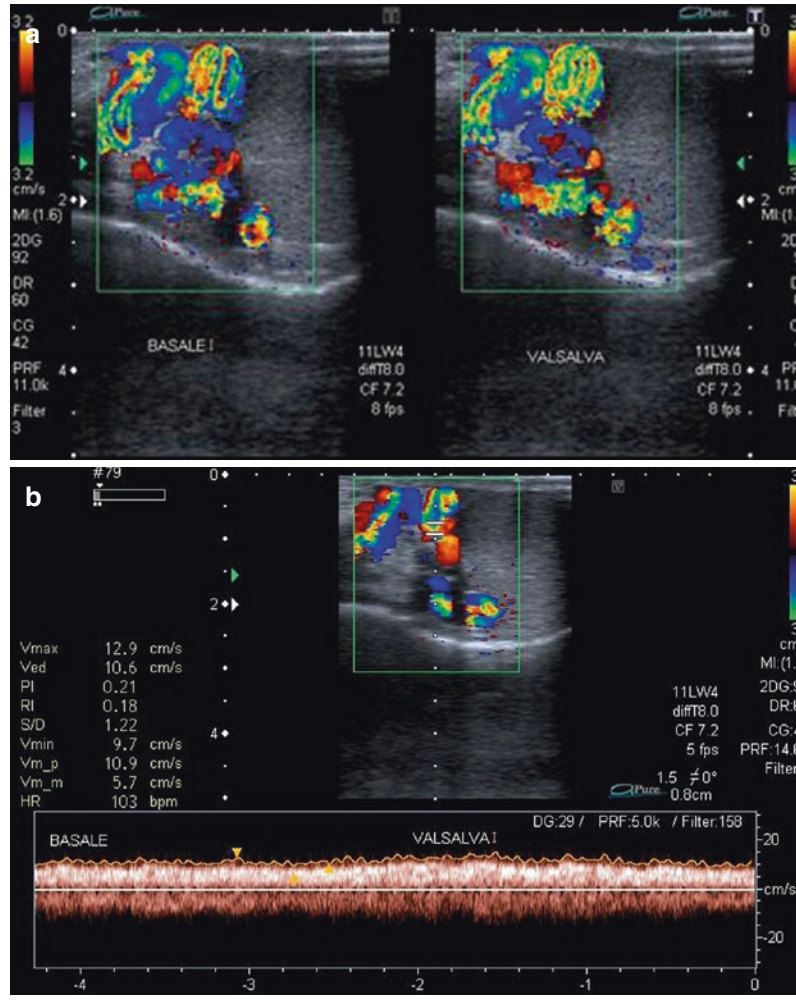

Fig. 42.5 Sarteschi's grade 5 varicocele: ecocolor Doppler (**a**) and spectral Doppler analysis (**b**)

Table 42.4 Hoekstra's classification for varicocele at color Doppler ultrasound

Grade 0	No dilated vein
Grade 1	Dilated veins <2.5 mm in diameter without flow reversal after Valsalva maneuver
Grade 2	Dilated and tortuous veins 2.5–3.5 mm in diameter and flow reversal after Valsalva maneuver
Grade 3	Dilated and tortuous veins >3.5 mm in diameter and flow reversal after Valsalva maneuver

Table 42.5 Hirsh's classification for varicocele at color Doppler ultrasound

Grade 1	No spontaneous venous reflux, but inducible reflux with Valsalva maneuver
Grade 2	Intermittent spontaneous venous reflux
Grade 3	Continuous spontaneous venous reflux

Table 42.6 Oyen's classification for varicocele at color Doppler and PW Doppler ultrasound

Grade 1	Slight reflux (<2 s) during Valsalva
Grade 2	Reflux (>2 s) during Valsalva, but no continuous reflux during the Valsalva maneuver
Grade 3	Reflux at rest during normal respiration or continuously during the entire Valsalva maneuver

42.5 Spectral Doppler Analysis

Precise duration of the reflux can be only measured at pulsed Doppler interrogation [7, 32]. Brief reflux lasting less than a second is physiological. Permanent reflux is not palpable in only 20% of cases, lasts more than 2 s, and has a plateau aspect throughout the abdominal strain (Fig. 42.6). It does not correlate with the diameter of the spermatic vein [32]. Intermediate reflux is never palpable and lasts 1–2 s in most cases. It keeps decreasing during the Valsalva maneuver and stops before the end of the maneuver. It has been suggested that, in the absence of palpable varicocele, only permanent reflux should be termed subclinical varicoceles, because the Doppler features and changes after treatment are identical to those of palpable varicocele [32]. Iosa and Lazzarini focused their attention on venous reflux and they proposed a new hemodynamic classification. In this classification, continuous venous reflux indicates complete valvular incompetence at the level of the spermatic cord; intermittent reflux indicates early-stage valve failure; and reflux lasting more than 1 s that occurs only during the Valsalva maneuver indicates that the valve is incontinent only when abdominal pressure is increased [33].

42.6 Patient Reporting

A correct ultrasound evaluation of patients with varicocele must integrate findings at gray-scale, color Doppler, and pulsed Doppler analysis. Regardless of the classification used, a series of gray-scale, color Doppler, and spectral Doppler parameters should be included in the medical report:

1. Size and position of the varices at gray-scale ultrasound while supine; the size changes while standing and during Valsalva maneuver.
2. Presence of flow at color Doppler interrogation while supine and during spontaneous breathing at the level of the inguinal channel, in the supratesticular region, and around the testis; the flow changes in the same positions while standing and during Valsalva maneuver.
3. Length and waveform characteristics of reflux at duplex Doppler interrogation while the patient is supine, while standing and during Valsalva maneuver.
4. Size and echotexture of both testes.
5. Incidental findings.

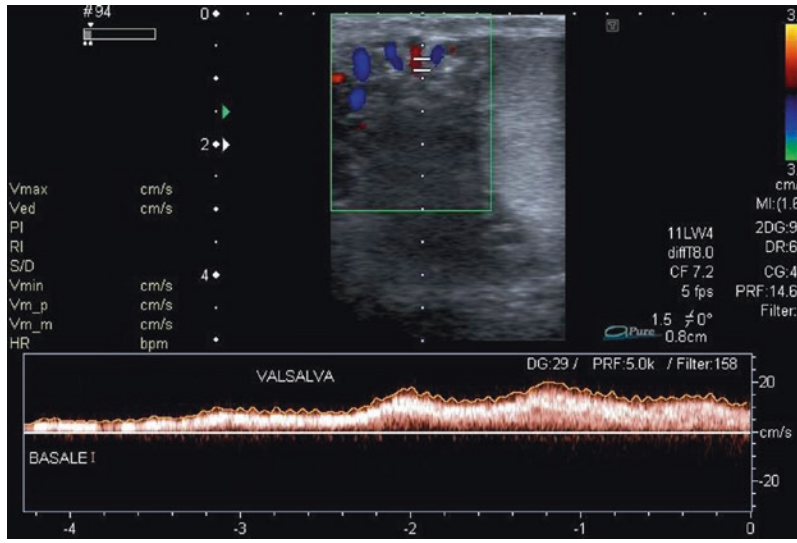

Fig. 42.6 Spectral Doppler analysis in varicocele showing a reflux during Valsalva lasting approximately 5 s

42.7 Bilateral Varicocele

Based on several methods of examination, including venography, Gat et al. showed that the prevalence of bilateral varicocele is probably much higher than originally thought [34]. In fact, many communicating vessels exist between the left and right testicular venous systems, either in the abdomen, in the pelvis, and in the scrotum. After the detection of left varicocele, it is therefore necessary to study the contralateral side in order to detect any coexistence of contralateral venous ectasia and blood reflux.

In case of bilateral scrotal venous ectasia, it is mandatory to distinguish, by the use of color Doppler interrogation of the right inguinal channel, between the so-called "false" and "real" bilateral varicocele, because these two situations require two different types of treatment [7, 35]. False bilateral varicocele is characterized by the absence of reflux in the right inguinal channel. Scrotal venous ectasia is fed by the contralateral varicosity through communicant transrectal vessels. In case of false bilateral varicocele correction on the left side usually leads to the regression of the right ectasia as well. Bilateral treatment is not recommended. Conversely, in real bilateral varicocele, venous ectasia is due to right gonadic vein reflux which is identified at color Doppler ultrasound. In these cases bilateral treatment must be performed. The limitation of this approach is that multiple communications between the right and the left testicular veins exist also in the abdomen and pelvis, which may be responsible to a "false" bilateral varicocele which cannot be diagnosed at color Doppler ultrasound.

42.8 Outcome After Varicocele Correction

There is increasing evidence that preoperative color Doppler ultrasound may be a useful tool for predicting the outcome of varicocele correction [36–39]. Liguori et al. evaluated 113 patients with left unilateral varicocele before and after correction using retrograde or anterograde sclerotization. During a postoperative control performed at least 3 months after the procedure, seminal quality improved among the entire population, regardless of patient age, and a better improvement in sperm density was found in patients with varicocele of grade 3–5, following the Sarteschi's classification, compared with patients varicocele of grade 1–2. They concluded that evidence of venous basal renospermatic reflow at preoperative color Doppler ultrasound is the main predictive factor of a better seminal response to varicocele correction [39].

42.9 Intratesticular Varicocele

Varicocele may rarely be intratesticular as well, within the mediastinum testis or in a subcapsular location. Less than 100 cases have been reported till now [40–51]. Some authors report a prevalent dilatation of the mediastinal veins [43, 47], while others do not [40]. Intratesticular varicocele is bilateral in approximately 25 % of published cases [47]. It is usually idiopathic, but can be also secondary to conditions producing renal vein obstruction, such as tumors, or renal vein thrombosis [44]. Association with cryptorchidism and previous orchiopexy has been reported [47, 52, 53].

With the exception of Das et al. [43], the different series report a high prevalence of left-sided intratesticular and associated extratesticular varicocele, usually of high degree, and of testicular hypotrophy.

Incidence of intratesticular varicocele varies in the different studies between 0.4 and 2 % of patients with proved of clinically suspected extratesticular varicocele [43, 47–51]. Preoperative recognition is important because spermatic cord compression during sclerotherapy is recommended in order to prevent gonadal damage [46, 50].

The appearance of intratesticular varicocele at gray-scale and color Doppler interrogation is similar to that already described for the extratesticular form (Fig. 42.7). Many authors report intratesticular veins of 2 mm or greater in diameter that show increased flow velocities during the Valsalva maneuver. Others, however, consider any intratesticular venous structure showing reflux during the Valsalva maneuver, regardless of the diameter. In fact, obviously dilated intratesticular veins that show conspicuous reflux may be identified whose diameter is smaller than 2 mm.

Differential diagnosis between intratesticular varicocele and other hypo-/anechoic lesions in the testes, such as cysts, tubular ectasia of the rete testis, hematoma, focal infection, and cystic intratesticular neoplasm, is straightforward, since these lesions do not show flow at color Doppler interrogation. Differentiation with other intratesticular vascular pathologies is possible. Arterial pseudoaneurysms are usually posttraumatic and display a characteristic yin-and-yang flow pattern, distinct from the venous flow of a varicocele [54], while intratesticular arteriovenous malformation or hemangiomas characteristically show high-velocity arterial waveforms [55, 56].

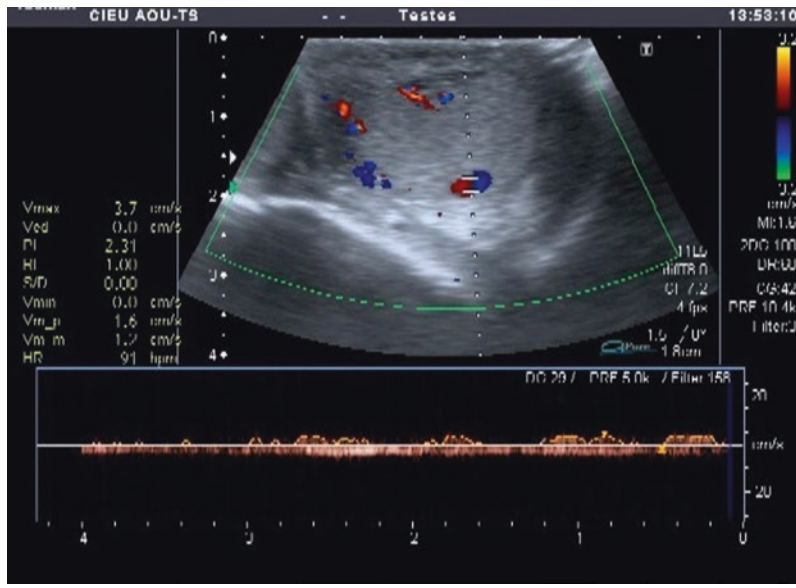

Fig. 42.7 Intratesticular varicocele. Dilated veins are appreciable within the testis showing flows at rest in the supine position

42.10 Secondary Varicocele

Increased pressure on the spermatic vein caused by various disease processes such as hydronephrosis, cirrhosis, or an abdominal mass may cause secondary varicocele. Flow characteristics are different from most idiopathic forms, because secondary varicocele is constantly evident while supine and presents basal reflux that does not change substantially during Valsalva maneuver (Sarteschi's grade 5). Neoplasm is the most likely cause of grade 5 varicocele in men over 40 years of age [13, 57]. Detection of a newly developing grade 5 varicocele on either the right or left side in older men should therefore prompt the investigation for a mass.

References

1. Meacham RB, Townsend RR, Rademacher D et al (1994) The incidence of varicoceles in the general population when evaluated by physical examination, gray scale sonography and color Doppler sonography. J Urol 151:1535–1538
2. Carlsen E, Andersen AG, Buchreitz L et al (2000) Inter-observer variation in the results of the clinical andrological examination including estimation of testicular size. Int J Androl 23:248–253
3. Naughton CK, Nangia AK, Agarwal A (2001) Pathophysiology of varicoceles in male infertility. Hum Reprod Update 7:473–481
4. Shafik A, Moftah A, Olfat S et al (1990) Testicular veins: anatomy and role in varicocelogenesis and other pathologic conditions. Urology 35:175–182
5. Dubin L, Amelar RD (1970) Varicocele size and results of varicocelectomy in selected subfertile men with varicocele. Fertil Steril 21:606–609
6. Beddy P, Geoghegan T, Browne RF et al (2005) Testicular varicoceles. Clin Radiol 60:1248–1255
7. Liguori G, Trombetta C, Garaffa G et al (2004) Color Doppler ultrasound investigation of varicocele. World J Urol 22:378–381
8. Hargreave TB, Liakatas J (1991) Physical examination for varicocele. Br J Urol 67:328
9. Comparison among different methods for the diagnosis of varicocele (1985) World health organization task force on the diagnosis and treatment of infertility. Fertil Steril 43:575–582
10. Niedzielski J, Paduch D, Raczynski P (1997) Assessment of adolescent varicocele. Pediatr Surg Int 12:410–413
11. Sarteschi LM, Paoli R, Bianchini M et al (1993) Lo studio del varicocele con eco-color Doppler. G Ital Ultrasonologia 4:43–49
12. Chiou RK, Anderson JC, Wobig RK et al (1997) Color Doppler ultrasound criteria to diagnose varicoceles: correlation of a new scoring system with physical examination. Urology 50:953–956
13. Dogra VS, Gottlieb RH, Oka M et al (2003) Sonography of the scrotum. Radiology 227:18–36
14. Pearl MS, Hill MC (2007) Ultrasound of the scrotum. Semin Ultrasound CT MR 28:225–248
15. Gonda RL Jr, Karo JJ, Forte RA et al (1987) Diagnosis of subclinical varicocele in infertility. AJR Am J Roentgenol 148:71–75
16. Jarow JP (2001) Effects of varicocele on male fertility. Hum Reprod Update 7:59–64
17. Sakamoto H, Ogawa Y, Yoshida H (2008) Relationship between testicular volume and varicocele in patients with infertility. Urology 71:104–109
18. Marks JL, McMahon R, Lipshultz LI (1986) Predictive parameters of successful varicocele repair. J Urol 136:609–612
19. Sigman M, Jarow JP (1997) Ipsilateral testicular hypotrophy is associated with decreased sperm counts in infertile men with varicoceles. J Urol 158:605–607
20. Zini A, Buckspan M, Berardinucci D et al (1997) The influence of clinical and subclinical varicocele on testicular volume. Fertil Steril 68:671–674
21. Alukal JP, Zurakowski D, Atala A et al (2005) Testicular hypotrophy does not correlate with grade of adolescent varicocele. J Urol 174:2367–2370; discussion 2370
22. Callea A, Berardi B, Dilorenzo V et al (1997) Echocolor doppler in the topographic study of varicocele. Arch Ital Urol Androl 69:189–192
23. Aydos K, Baltaci S, Salih M et al (1993) Use of color Doppler sonography in the evaluation of varicoceles. Eur Urol 24:221–225
24. Eskew LA, Watson NE, Wolfman N et al (1993) Ultrasonographic diagnosis of varicoceles. Fertil Steril 60:693–697
25. Lund L, Nielsen AH (1994) Color Doppler sonography in the assessment of varicocele testis. Scand J Urol Nephrol 28:281–285
26. Tasci AI, Resim S, Caskurlu T et al (2001) Color doppler ultrasonography and spectral analysis of venous flow in diagnosis of varicocele. Eur Urol 39:316–321
27. Winkelbauer FW, Ammann ME, Karnel F et al (1994) Doppler sonography of varicocele: long-term follow-up after venography and transcatheter sclerotherapy. J Ultrasound Med 13:953–958
28. Petros JA, Andriole GL, Middleton WD et al (1991) Correlation of testicular color Doppler ultrasonography, physical examination and venography in the detection of left varicoceles in men with infertility. J Urol 145:785–788
29. Hoekstra T, Witt MA (1995) The correlation of internal spermatic vein palpability with ultrasonographic diameter and reversal of venous flow. J Urol 153:82–84
30. Hirsh AV, Cameron KM, Tyler JP et al (1980) The Doppler assessment of varicoceles and internal

spermatic vein reflux in infertile men. Br J Urol 52:50–56
31. Oyen RH (2002) Scrotal ultrasound. Eur Radiol 12:19–34
32. Cornud F, Belin X, Amar E et al (1999) Varicocele: strategies in diagnosis and treatment. Eur Radiol 9:536–545
33. Iosa G, Lazzarini D (2013) Hemodynamic classification of varicoceles in men: our experience. J Ultrasound 16(2):57–63
34. Gat Y, Bachar GN, Zukerman Z et al (2004) Varicocele: a bilateral disease. Fertil Steril 81:424–429
35. Sarteschi LM, Liguori G, Trombetta C (2003) Varicocele. In: Sarteschi LM, Menchini-Fabris GF (eds) Ecografia andrologica, 1st edn. Athena Srl, Modena, pp 139–155
36. Shlansky-Goldberg R et al (1997) Percutaneous varicocele embolization versus surgical ligation for the treatment of infertility: changes in seminal parameters and pregnancy outcomes. J Vasc Interv Radiol 8:759–767
37. Shiraishi K, Naito K, Takihara H (2003) Indication of varicocelectomy in the era of assisted reproductive technology: prediction of treatment outcome by noninvasive diagnostic methods. Arch Androl 49:475–478
38. Hussein AF (2006) The role of color Doppler ultrasound in prediction of the outcome of microsurgical subinguinal varicocelectomy. J Urol 176:2141–2145
39. Liguori G, Ollandini G, Pomara G et al (2010) Role of renospermatic basal reflow and age on semen quality improvement after sclerotization of varicocele. Urology 75:1074–1078
40. Atasoy C, Fitoz S (2001) Gray-scale and color Doppler sonographic findings in intratesticular varicocele. J Clin Ultrasound 29:369–373
41. Weiss AJ, Kellman GM, Middleton WD et al (1992) Intratesticular varicocele: sonographic findings in two patients. AJR Am J Roentgenol 158:1061–1063
42. Ozcan H, Aytac S, Yagci C et al (1997) Color Doppler ultrasonographic findings in intratesticular varicocele. J Clin Ultrasound 25:325–329
43. Das KM, Prasad K, Szmigielski W et al (1999) Intratesticular varicocele: evaluation using conventional and Doppler sonography. AJR Am J Roentgenol 173:1079–1083
44. Abduljaleel PM, Al-Mulhim F, Nouman A et al (2006) Intratesticular varicocele and extratesticular varicocele in a patient with nephrotic syndrome complicated by left renal vein thrombosis. Ann Saudi Med 26:228–230
45. Mehta AL, Dogra VS (1998) Intratesticular varicocele. J Clin Ultrasound 26:49–51
46. DemIrbas M, Ellergezen A, CY BI et al (2001) Intratesticular varicocele treated with percutaneous embolization. Urology 58:1058
47. Tetreau R, Julian P, Lyonnet D et al (2007) Intratesticular varicocele: an easy diagnosis but unclear physiopathologic characteristics. J Ultrasound Med 26:1767–1773
48. Morvay Z, Nagy E (1998) The diagnosis and treatment of intratesticular varicocele. Cardiovasc Intervent Radiol 21:76–78
49. Diamond DA, Roth JA, Cilento BG et al (2004) Intratesticular varicocele in adolescents: a reversible anechoic lesion of the testis. J Urol 171:381–383
50. Bucci S, Liguori G, Amodeo A et al (2008) Intratesticular varicocele: evaluation using grey scale and color Doppler ultrasound. World J Urol 26:87–89
51. Conti E, Fasolo PP, Sebastiani G et al (2005) Color Doppler sonography in the intratesticular varicocele. Arch Ital Urol Androl 77:63–65
52. O'Donnell PG, Dewbury KC (1998) The ultrasound appearances of intratesticular varicocele. Br J Radiol 71:324–325
53. Erdogan N, Ekmekcioglu O, Baykara M (2003) Bilateral intratesticular varicocele in a patient with a history of bilateral cryptorchidism. Turk J Med Sci 33:117–119
54. Dee KE, Deck AJ, Waitches GM (2000) Intratesticular pseudoaneurysm after blunt trauma. AJR Am J Roentgenol 174:1136
55. Yilmaz C, Arslan M (2009) Intrascrotal arteriovenous malformation simulating varicocele. AJR Am J Roentgenol 192:W351
56. Bhatt S, Rubens DJ, Dogra VS (2006) Sonography of benign intrascrotal lesions. Ultrasound Q 22:121–136
57. Graif M, Hauser R, Hirshebein A et al (2000) Varicocele and the testicular-renal venous route: hemodynamic Doppler sonographic investigation. J Ultrasound Med 19:627–631

Scrotal Masses

43

Giovanni Chiriacò, Michele Bertolotto, Mariano Iannelli, Stefano Bucci, Nicola Pavan, Carlo Trombetta, and Giovanni Liguori

43.1 Introduction

A scrotal mass is often identified by the patient as an abnormal lump during self-palpation. Scrotal lumps can be caused by cystic lesions or solid tumours of the testis or paratesticular structures, trauma, inflammations or testicular torsion, varicocele, fluid collections, inguinoscrotal hernia or tumours of the scrotal wall. When a patient presents with a scrotal mass, it is extremely important to collect a detailed history which includes duration of symptoms, whether the mass is painful or painless, change in size of mass, sexual history, concomitant lower urinary tract symptoms, previous history of surgery, infertility or mumps and family history of testicular cancer.

Ultrasound plays a prevailing role in the evaluation of patients with scrotal masses by providing highly effective informations about presence, location and extension of the disease process and by trying to identify its nature [1–6].

G. Chiriacò, MD • S. Bucci, MD • N. Pavan, MD
C. Trombetta, MD • G. Liguori, MD, PhD (✉)
Department Urology, University of Trieste,
Ospedale di Cattinara, Strada di Fiume 447,
Trieste 34124, Italy
e-mail: gioliguori33@gmail.com

M. Bertolotto, MD • M. Iannelli, MD
Department of Radiology, University of Trieste,
Ospedale di Cattinara, Strada di Fiume 447,
Trieste 34124, Italy

P. Martino, A.B. Galosi (eds.), *Atlas of Ultrasonography in Urology, Andrology, and Nephrology*,
DOI 10.1007/978-3-319-40782-1_43

43.2 Fluid Collections

Fluid collections are common findings at ultrasonography performed in symptomatic and asymptomatic men. Most fluid collections are located in the vaginal sac and can be idiopathic or secondary to trauma, inflammation or tumour. Ultrasound findings in combination with clinical assessment are generally sufficient for the final diagnosis. Among them, hydrocele, inflammatory collections and haematocele must be differentiated [7].

43.2.1 Hydrocele

Hydrocele is described as an abnormal fluid-filled collection between the visceral and parietal layers of the tunica vaginalis of the scrotum [8]. Hydroceles can be differentiated from other testicular masses by transillumination of the fluid with a penlight. Patients with hydroceles also have a palpably normal spermatic cord and inguinal ring above the swollen area. Scrotal ultrasonography may be helpful in making the diagnosis [9, 10].

Idiopathic hydrocele, resulting from excessive fluid production or failure of the mesothelial lining to reabsorb the fluid, is frequently observed as the most common cause of scrotal enlargement. In adults acute hydrocele may occur in conjunction with an inflammatory process (epididymitis or orchitis), as a sequel of trauma or torsion, or in the presence of a testicular tumour. Hydrocele is usually painless, although palpation of the underlying testis is frequently inhibited. At ultrasonography idiopathic hydrocele appearance is an extratesticular anechoic fluid collection with smooth borders (Fig. 43.1a).

A chronic hydrocele, which may occur secondary to recurrent inflammation or protracted epididymitis, additionally shows thickening of the wall and is frequently septated (Fig. 43.1b).

Scattered reflections may be seen corresponding to fibrin, debris and inflammatory aggregations [11].

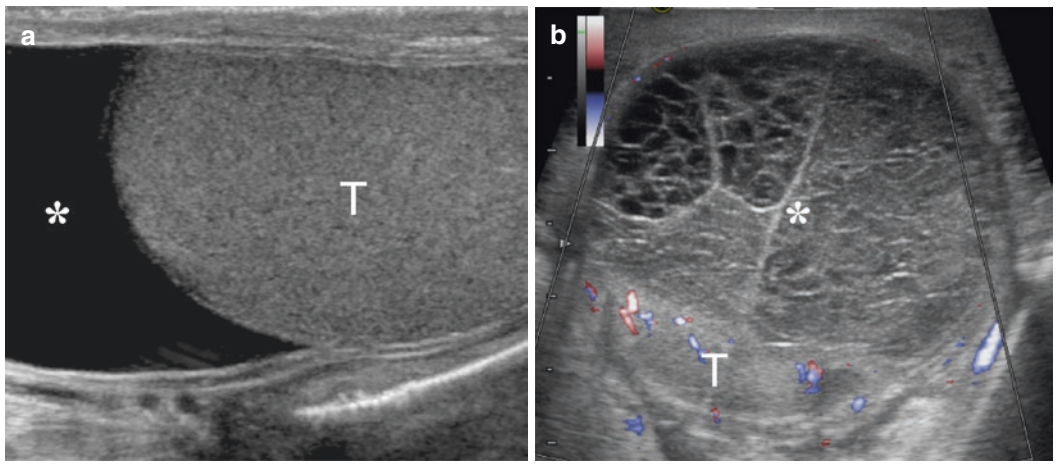

Fig. 43.1 (**a**) Scrotal hydrocele. Extratesticular fluid collection with anechogenic appearance (*asterisk*). The testis (*T*) has normal size and echogenicity. (**b**) Long-standing hydrocele (*asterisk*) presenting with multiple thin avascular septa. The testis (*T*) is normal in size, but compressed and displaced posteriorly

43.2.2 Pyocele and Extratesticular Scrotal Abscess

A pyocele or extratesticular scrotal abscess may occur as a complication of trauma, surgery or epididymo-orchitis when the mesothelial lining of the tunica vaginalis is breached and infection ensues. Clinical history and physical examination of a painful scrotum help in making the diagnosis [7].

At ultrasound, a pyocele often appears as a complex heterogeneous extratesticular fluid collection (Fig. 43.2).

In most cases, conservative treatment with antibiotics is sufficient. However, a scrotal abscess complicated by necrotizing infection of the perineum requires prompt surgery [12].

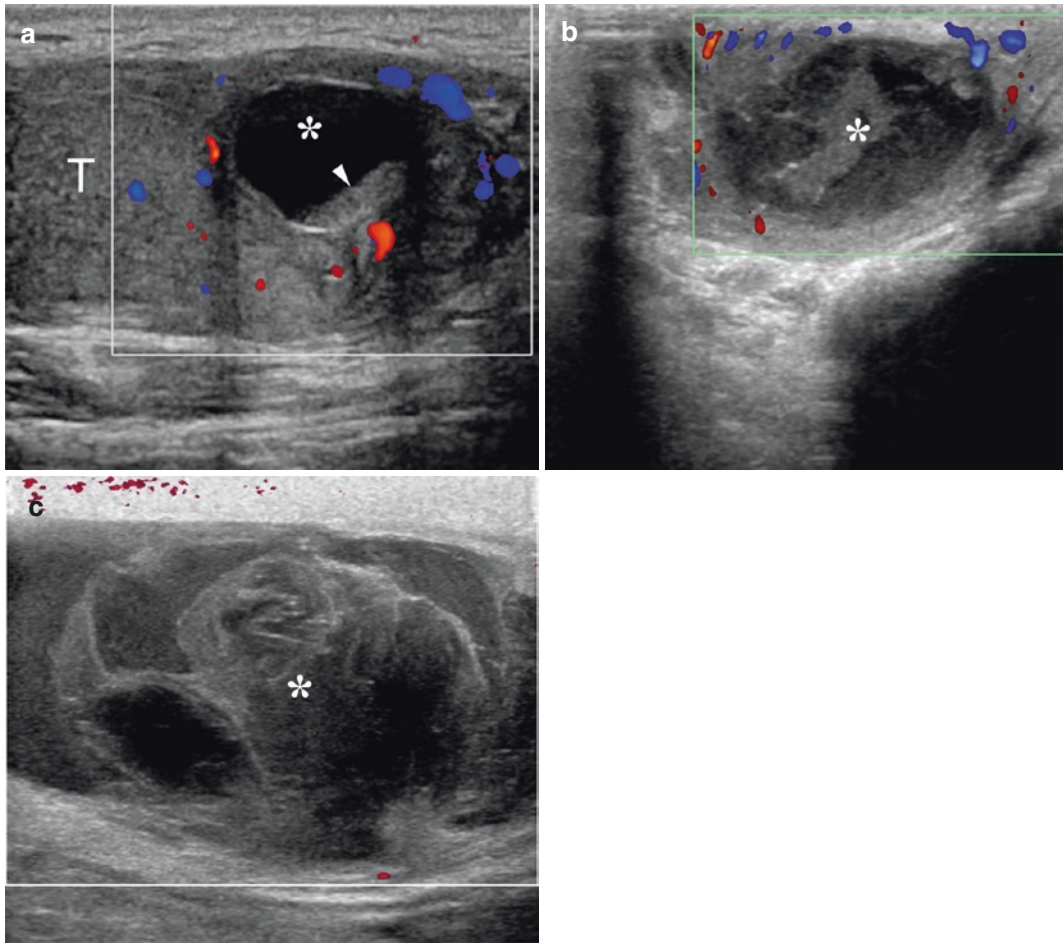

Fig. 43.2 (**a–c**) Extratesticular inflammatory fluid collections. (**a**) Epididymal abscess. Patient with severe epididymitis presenting with a complex cystic lesion (*asterisk*) in the tail of the epididymis displaying a fluid level (*arrowhead*). The testis (*T*) is normal. (**b**) Abscess of the scrotal wall (*asterisk*) presenting with an avascular fluid collection with mixed echogenicity. (**c**) Ultrasound scan in patients with inflammatory changes, acute scrotal pain and swelling showing a fluid collection of mixed echogenicity (*asterisk*) between the layers of the tunica vaginalis, consistent with pyocele

43.2.3 Haematocele

Haematocele is a collection of blood within the tunica vaginalis layers. It appears after a scrotal trauma or surgery but may also occur spontaneously or, more rarely, in association with clotting disorders, vasculitis or other inflammatory conditions. Haematocele has rarely been described as the presenting feature of malignancy [13].

In the absence of a clear history of trauma, however, the exclusion of tumour is difficult and surgical exploration may be required.

Haematocele has a variable appearance on ultrasound, with a temporal change in characteristics on repeat ultrasound. Acutely it is echogenic and becomes more complex and more hypoechoic with age (Fig. 43.3).

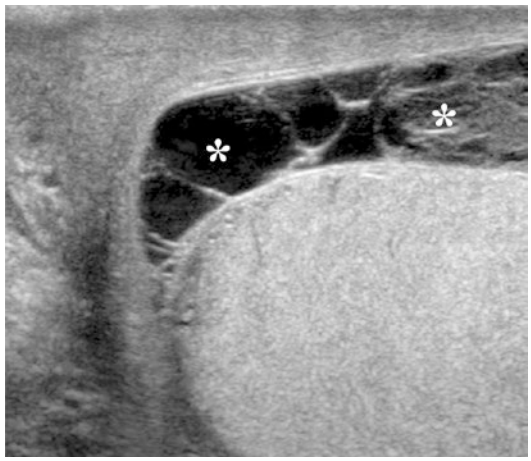

Fig. 43.3 Haematocele. Patient with blunt scrotal trauma presenting with a fluid collection of mixed echogenicity (*asterisks*) between the layers of the tunica vaginalis

43.3 Inguinoscrotal Hernia

An inguinoscrotal hernia occurs when an intestinal loop or part of the omentum passes into the scrotal cavity through an incompletely obliterated processus vaginalis. Inguinoscrotal hernias are most common in preterm neonates, but they may also develop in adults. The diagnosis can be difficult at physical examination. Ultrasound may be indicated to differentiate an inguinoscrotal hernia from other conditions and to investigate contralateral involvement [12].

At ultrasound, intestinal loops within the scrotum appear as a non-homogeneous mass, most commonly hypoechoic due to the fluid content of the bowel. The most useful finding is generally the presence of air bubbles within the cystic-appearing mass (Fig. 43.4a). Peristalsis of bowel loops is possible to detect but the herniated loops are usually filled and without movement. Colour Doppler interrogation may demonstrate vascularity of the intestinal wall. Hernias can also be diagnosed with CT, MR imaging and even plain radiography if the bowel loops contain gas [7] (Fig. 43.4b).

Occasionally, the bladder may herniate into the inguinal and femoral canals, the latter being more frequent in women. A predilection for the right side has been reported. Preoperative recognition is important to avoid complications such as urinary leakage and sepsis [14].

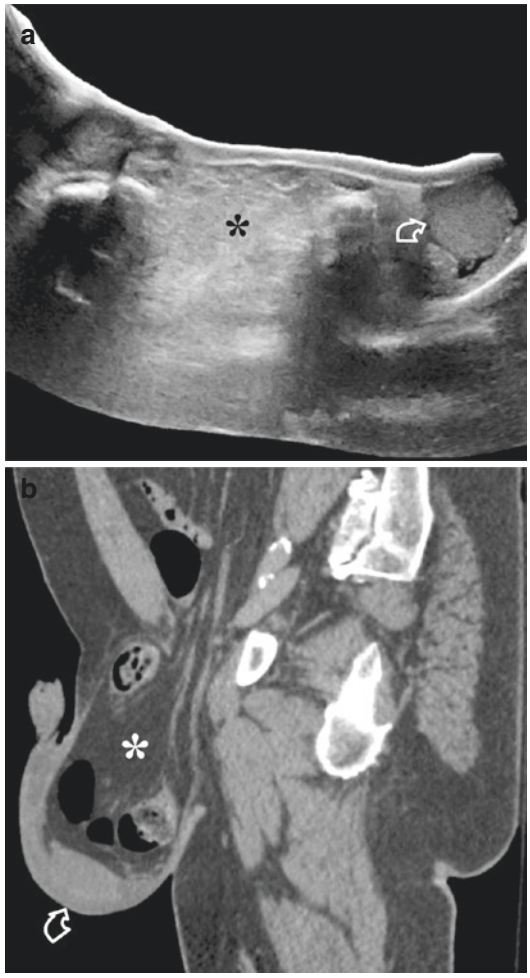

Fig. 43.4 (**a**) Inguinoscrotal hernia. Panoramic ultrasonographic view showing a bowel loop containing air (*asterisk*) within the scrotum. The testis (*curved arrow*) is normal. (**b**) Sagittal CT scan confirms scrotal herniation of a bowel loop (*asterisk*). The testis is normal (*curved arrow*)

43.4 Extratesticular Tumours

Extratesticular solid masses are malignant in about 3 % of cases [2, 3, 15, 16]. These tumours arise from paratesticular tissue. The paratesticular region is a complex anatomical area which includes the contents of the spermatic cord, testicular tunics, epididymis and vestigial remnants, e.g. the appendices epididymis and testis [17]. Histogenetically, this area is composed of a variety of epithelial, mesothelial and mesenchymal elements. Neoplasms arising from this region therefore form a heterogeneous group of tumours with different behavioural patterns. On rare occasions, tumours from distant sites may metastasize to the paratesticular region [17]. Tumours occurring in the paratesticular region may be clinically indistinguishable from testicular tumours, thus resulting in initial misdiagnosis. Most tumours of this region present as a scrotal mass or swelling, which may or may not be painful and is occasionally accompanied by a hydrocele. The preoperative distinction between the benign and malignant paratesticular tumour is rarely made, as there may be no specific finding, which results in difficulty in diagnosis and management.

The criteria which can help in the differential diagnosis are localization of the lesion and correlation with clinical history and laboratory tests. Most of inflammatory masses, in fact, are associated with acute symptoms and positive laboratory results. Imaging findings are often non-specific and not helpful to differentiate among the different types of lesions.

43.4.1 Tumours of the Epididymis

Adenomatoid tumours are the most common neoplasms of the epididymis. They are the second in frequency of all extratesticular neoplasms, following the spermatic cord lipomas. Such lesions are benign [2, 3, 15, 16, 18] and usually seen at US as solid, slightly hyperechoic nodules (Fig. 43.5).

Leiomyomas are the second most common tumour of the epididymis. They have been described at US as solid, heterogeneous nodules with cystic areas and possible calcifications [19].

Papillary cystadenoma of the epididymis is a slow-growing tumour encountered in about 60 % of patients with von Hippel-Lindau disease. Sporadic papillary cystadenoma can be rarely found. They are nodules surrounded by a fibrous capsule and made of multiple cysts lined by papillary fronds. At ultrasound it can present as predominantly solid lesions, with small internal cystic spaces, or may be primarily cystic, with internal vegetations [20, 21].

Up to 40 % of such lesions are bilateral, and this finding is virtually diagnostic of von Hippel-Lindau disease.

Other more unusual lesions such as extratesticular Leydig cell tumours may be found at the epididymis. They are usually with non-specific ultrasound pattern.

Malignant tumours of the epididymis include sarcoma, metastases and adenocarcinoma and are rare. It must be remembered that testicular lymphoma can involve the epididymis and the spermatic cord and can be difficult to differentiate from an epididymal inflammatory disease with secondary infiltration of the testis. In lymphomas, however, the testis is more extensively involved than the epididymis.

43.4.2 Tumours of the Tunica Vaginalis

The tunica vaginalis is lined by mesothelial cells, and mesotheliomas have been reported. They are less common than those arising from the pleura and peritoneum; however, lesions of both the chest or abdomen and tunica vaginalis can be encountered, and about 50 % of patients have a history of asbestos exposure. They are almost invariably associated with hydrocele and can be suspected by the presence of irregular thickening of the tunica, with vegetating parietal nodules. Cystic mesotheliomas have been reported [2, 22].

Fibromas of the tunica vaginalis are benign fibroinflammatory reaction resulting in nodules (either single or multiple) at the tunica vaginalis or tunica albuginea. At ultrasound, they are seen as solid, hypoechogenic, non-specific lesions (Fig. 43.6).

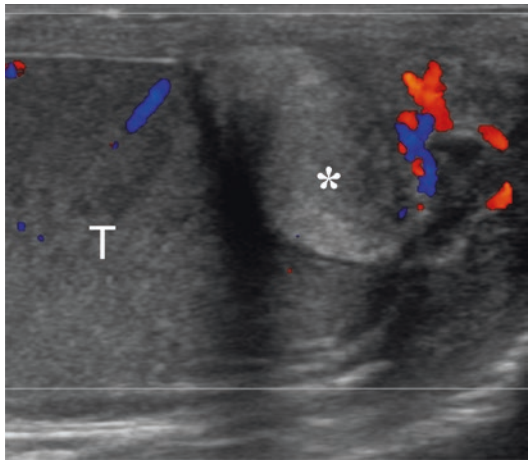

Fig. 43.5 Surgically proved adenomatoid tumour of the tail of the epididymis presenting as a small, echogenic mass (*asterisk*) hypovascular at colour Doppler interrogation. The testis (*T*) is normal

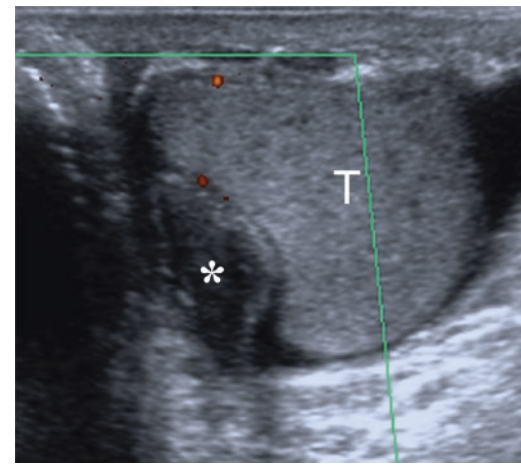

Fig. 43.6 Surgically proved fibroma of the tunica vaginalis testis presenting as a hypovascular, hypoechoic extratesticular mass (*asterisk*). *T* testis

43.4.3 Tumours of the Spermatic Cord

Most neoplasms of extratesticular structures are benign lipomas originating from the spermatic cord. Most of these lesions have a hyperechogenic structure at ultrasound. However, this is not the case in many patients, and a specific diagnosis may be not possible with this technique. Furthermore, differentiating a hyperechoic lipoma from adjacent fat can be difficult with ultrasound alone, and MR imaging is needed to evaluate the full extent of the disease process. A liposarcoma can be suspected by a more heterogeneous internal structure, however, and excision is needed to establish the diagnosis [23].

Spermatic cord may be involved in 40% of testicular lymphoma that is the most common testicular neoplasm in man over 60 years (Fig. 43.7).

Although rare, other malignant extratesticular masses, such as rhabdomyosarcomas, leiomyosarcomas, malignant fibrous histiocytomas and undifferentiated sarcomas, can be encountered.

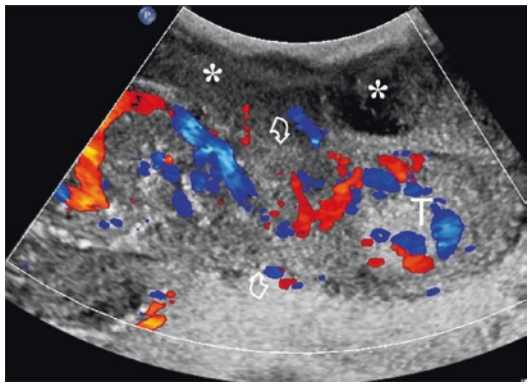

Fig. 43.7 Diffuse large B-cell lymphoma involving the testis and the surrounding tissues. Longitudinal colour Doppler image showing a large infiltrating lesion involving the testis (*T*), the spermatic cord (*curved arrows*) and the scrotal wall (*asterisk*). Note the normal vessels of the spermatic cord running within the tumour mass (*arrowheads*)

43.5 Scrotal Wall Masses

Occasionally, a scrotal wall lesion presents as a scrotal mass [24]. Scrotal skin cancer is more common in persons with a history of psoralen plus ultraviolet A therapy or human papillomavirus infection. Scrotal skin lesions that are erosive, vascular, hyperkeratotic or nonhealing or that change colour or have irregular borders should be biopsied to rule out cancer [25, 26]. Fournier gangrene is a necrotizing soft tissue infection that can present as a scrotal mass and is a surgical emergency [27].

Benign scrotal masses include scrotal edema (Fig. 43.8), genital warts, benign nevus, epidermoid cysts (Fig. 43.9a–c), seborrhoeic keratosis and angiokeratomas.

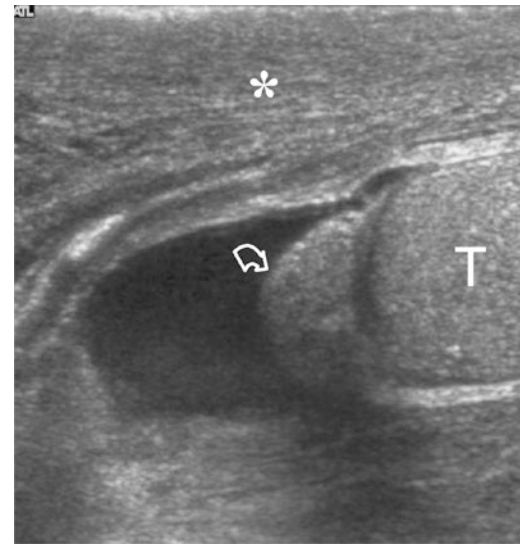

Fig. 43.8 Scrotal edema in a cirrhotic patient presenting at greyscale ultrasonography with thickened scrotal wall (*asterisk*). The testis (*T*) and epididymis (*curved arrow*) are normal. A mild amount of hydrocele is associated

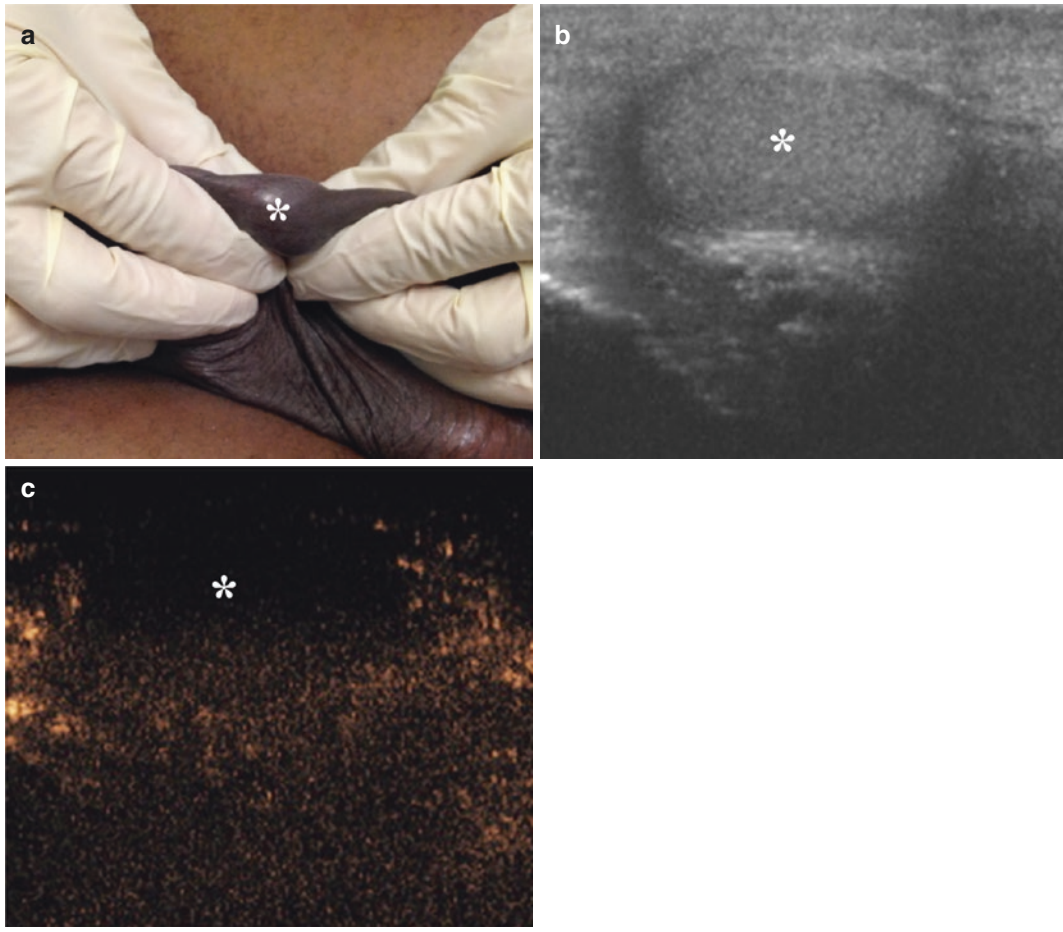

Fig. 43.9 (**a**–**c**) Epidermoid cyst of the scrotal wall. The patient reported on a small painless lump within the scrotum since several months which did not increase in size. (**a**) Physical investigation shows the lesion (*asterisk*) in the context of the scrotal wall. (**b**) Greyscale ultrasonography shows a well-circumscribed, oval mass within the scrotal wall (*asterisk*) lacking vascularity at colour Doppler interrogation (not shown). (**c**) CEUS confirms that the lesion (*asterisk*) is completely avascular

References

1. Woodward PJ, Sohaey R, O'Donoghue MJ et al (2002) From the archives of the AFIP: tumors and tumorlike lesions of the testis: radiologic-pathologic correlation. Radiographics 22:189–216
2. Woodward PJ, Schwab CM, Sesterhenn IA (2003) From the archives of the AFIP: extratesticular scrotal masses: radiologic-pathologic correlation. Radiographics 23:215–240
3. Akbar SA, Sayyed TA, Jafri SZ et al (2003) Multimodality imaging of paratesticular neoplasms and their rare mimics. Radiographics 23:1461–1476
4. Dogra VS, Gottlieb RH, Oka M et al (2003) Sonography of the scrotum. Radiology 227:18–36
5. Hamm B (1997) Differential diagnosis of scrotal masses by ultrasound. Eur Radiol 7:668–679
6. Oyen RH (2002) Scrotal ultrasound. Eur Radiol 12:19–34
7. Valentino M, Barozzi L, Pavlica P (2012) Scrotal pathology. Imaging scrotal lumps in adults. Cysts and fluid Collections. Springer-Verlag Berlin, Heidelberg
8. Shakiba B, Heidari K, Jamali A, Afshar K (2014) Aspiration and sclerotherapy versus hydrocoelectomy for treating hydrocoeles. Cochrane Database Syst Rev. 2014;(11):CD009735
9. Montgomery JS, Bloom DA (2011) The diagnosis and management of scrotal masses. Med Clin North Am 95(1):235–244
10. Winter TC (2009) There is a mass in the scrotum—what does it mean?: Evaluation of the scrotal mass. Ultrasound Q 25(4):195–205
11. Gooding GA, Leonhardt WC, Marshall G et al (1997) Cholesterol crystals in hydroceles: sonographic detection and possible significance. AJR Am J Roentgenol 169:527–529
12. Garriga V, Serrano A, Marin A et al (2009) US of the tunica vaginalis testis: anatomic relationships and pathologic conditions. Radiographics 29: 2017–2032
13. Mehra BR, Thawait AP, Narang RR et al (2007) Adenocarcinoma of the rete testis with uncommon presentation as haematocele. Singapore Med J 48:e311–e313
14. Bacigalupo LE, Bertolotto M, Barbiera F et al (2005) Imaging of urinary bladder hernias. AJR Am J Roentgenol 184:546–551
15. Frates MC, Benson CB, DiSalvo DN et al (1997) Solid extratesticular masses evaluated with sonography: pathologic correlation. Radiology 204:43–46
16. Lee JC, Bhatt S, Dogra VS (2008) Imaging of the epididymis. Ultrasound Q 24:3–16
17. Khoubehi B, Mishra V, Ali M, Motiwala H, Karim O (2002) Adult paratesticular tumours. BJU Int 90(7):707–715
18. Leonhardt WC, Gooding GA (1992) Sonography of intrascrotal adenomatoid tumor. Urology 39:90–92
19. Leonhardt WC, Gooding GA (1993) Sonography of epididymal leiomyoma. Urology 41:262–264
20. Alexander JA, Lichtman JB, Varma VA (1991) Ultrasound demonstration of a papillary cystadenoma of the epididymis. J Clin Ultrasound 19:442–445
21. Choyke PL, Glenn GM, Wagner JP et al (1997) Epididymal cystadenomas in von Hippel-Lindau disease. Urology 49:926–931
22. Chien AJ, Strouse PJ, Koo HP (2000) Cystic mesothelioma of the testis in an adolescent patient. J Ultrasound Med 19:423–425
23. Derchi L.E, Simonato A (2012) Scrotal pathology. Imaging scrotal lumps in adults. Tumors. Springer-Verlag Berlin, Heidelberg
24. Crawford P, Crop JA (2014) Evaluation of scrotal masses. Am Fam Physician 89(9):723–727
25. de la Brassinne M, Richert B (1992) Genital squamous-cell carcinoma after PUVA therapy. Dermatology 185(4):316–318
26. Eliezri YD, Silverstein SJ, Nuovo GJ (1990) Occurrence of human papillomavirus type 16 DNA in cutaneous squamous and basal cell neoplasms. J Am Acad Dermatol 23(5 pt 1):836–842
27. Anaya DA, Dellinger EP (2007) Necrotizing soft-tissue infection: diagnosis and management. Clin Infect Dis 44(5):705–710

The Role of Intraoperative Ultrasound for Testicular Masses

44

Michele Bertolotto, Nicola Pavan, Massimo Valentino, Giovanni Liguori, Stefano Bucci, Libero Barozzi, and Lorenzo E. Derchi

44.1 Clinical Evaluation

Since ultrasonography is increasingly used complementary to the clinical urological practice, incidental detection of non-palpable testicular nodules is also increased. This is not surprising, as the same phenomenon was observed in the past for the detection rate in the liver and kidney of incidental masses like haemangiomas and simple cysts, which were considered uncommon before the widespread introduction of the ultrasonographic modes. Indeed, ultrasonography discloses the actual prevalence of the testicular nodules.

Ultrasonography is sensitive for testicular lesion detection, but its specificity is low. It is quite common to find testicular lesions without a clear interpretation, whose management may be problematic.

According to the literature, the prevalence of small (<1–1.5 cm), impalpable testicular lesions identified incidentally is between 0.21 and 1 %, especially in the infertile patients. Overall, 207 cases have been described in the literature [1–7]. Among them, only 136/207 (66 %) were tumours with a prevalence of benign histotypes (96/136, 70 %). In these series, up to 34 % of lesions were non-neoplastic, including cysts, haematomas, segmental ischaemia, focal orchitis, abscesses and fibrotic areas. Recently, a prospective study described 115 non-palpable testicular lesions [7]. Forty-four were malignant tumours, 42 benign tumours and 29 non-neoplastic lesions, respectively. According to these data, orchiectomy as a first approach cannot be recommended in these patients, and a variety of possible solution have been suggested [8, 9]. Active surveillance is an option. Another choice is targeted surgical biopsy under ultrasonographic guidance followed by simple enucleation if histology shows a benign lesion.

Electronic supplementary material The online version of this chapter (doi:10.1007/978-3-319-40782-1_44) contains supplementary material, which is available to authorized users.

M. Bertolotto, MD (✉) • N. Pavan • G. Liguori
S. Bucci
Department of Radiology, University of Trieste, Ospedale di Cattinara, Strada di Fiume 447, Trieste 34124, Italy
e-mail: bertolot@units.it

M. Valentino
S.O.C. Radiologia ASS 3 FVG, Ospedale Sant'Antonio Abate, Via Morgagni 18, Tolmezzo (UD) 33028, Italy

L. Barozzi
Radiology Unit, Casa di Cura Madre Fortunata Toniolo, Via Toscana 34, Bologna 40141, Italy

L.E. Derchi
Department of Radiology, DICMI University of Genova, Ospedale S. Martino, Largo Rosanna Benzi 8, Genoa 16132, Italy

P. Martino, A.B. Galosi (eds.), *Atlas of Ultrasonography in Urology, Andrology, and Nephrology*,
DOI 10.1007/978-3-319-40782-1_44

44.2 Preoperative Features

Since many incidentally detected non-palpable testicular lesions are non-neoplastic, the first step is to attempt a better characterisation. In some cases, repeated ultrasonography performed with a high-end equipment by a dedicated sonologist is enough. Simple and minimally complicated cysts, epidermoid cysts and segmental testicular infarction can be characterised in the majority of cases combining different ultrasonographic modes: greyscale and colour Doppler appearance, elasticity features and enhancement after microbubble injection. Fat-, blood- and fibrous tissue-containing lesions, such as haematomas, spontaneous haemorrhage, fibromas and lipomas, can be characterised with MR imaging [7, 10–13].

44.3 Therapeutic Approach

Whenever the characterisation of the lesion is not possible before the operation with imaging methods, it is mandatory to choose the therapeutic approach. A strategy is to schedule a strict follow-up and operate only growing lesions [14]. The most commonly accepted strategy is testis-sparing surgery, which allows removal of the lesion with maximal preservation of testicular parenchyma and its vasculature, frozen section examination of the surgical specimen and radical orchiectomy performed in case of malignancy only [15–17]. Intraoperative ultrasonography is an important step of this procedure [18].

44.4 Intraoperative Ultrasonography in Testis-Sparing Surgery

After a preliminary clinical and ultrasonographic examination to confirm the presence, the side and the features of the lesion (Fig. 44.1), the role of the sonologist in the operating room is to find the lesion after the surgical exposure of the testis, to describe the best approach for the surgical excision (Fig. 44.2), to mark the position of the nodule on the tunica albuginea and to determine the depth of the lesion in the testicular parenchyma. In case of deeply located lesions, a 30G needle is inserted into or near the nodule to guide identification and dissection with minimum damage to the surrounding testicular tissue (Video 44.1).

Usually, the testis is exposed by an inguinal approach. In our clinical practice, ultrasound is performed before the funicular clamping to minimise the time of ischaemia and evaluate the testicular vasculature. At this point, the spermatic cord is clamped, the tunica albuginea is incised above the lesion, the lesion is enucleated with a small edge of the adjacent testicular parenchyma and sent immediately to the pathologist for frozen section analysis and the albuginea is closed (Fig. 44.3). Ultrasonography is then repeated to confirm the complete removal of the nodule. Tumour enucleation procedures should be performed under cold ischaemia with the testicle being placed in crushed ice while the frozen sections are analysed. Before removing the funicular clamp, the lesion is analysed to determine the type of tumour. If the analysis shows a malignant neoplasm, radical orchiectomy will be performed. Ideally, frozen ischaemia should last no more than 30 min, to minimise damage of the testicular parenchyma. This is the most critical step of the operation, because assessing the type of lesion on frozen sections may be difficult and time-consuming; the most important differential diagnosis between seminoma and Leydig cell tumour, in particular, may be problematic. In some centres, the surgeon prefers to remove the clamp before the results of the pathological analysis. Macroscopic findings during surgery may help the surgeon determine the possible nature of a testicular lesion. A golden-brown appearance and very well-defined margins are suggestive of a Leydig cell tumour, while whitish lesions are more suggestive of seminoma. It is important to repeat ultrasonographic investigation after the removal of the clamp and before placing again the testis inside the scrotum to rule out complications and to assess the testicular vascularisation (Fig. 44.4).

A definite benefit of testis-sparing surgery is that a significant proportion of patients do not have malignant tumours and are definitively treated with an organ-sparing approach. Despite excellent results reported in the literature, results are variable in the clinical practice. The procedure is potentially associated with recurrence, and clamping of the spermatic cord should be kept to minimum in order to grant viability of the operated testis. A trained multidisciplinary team is necessary.

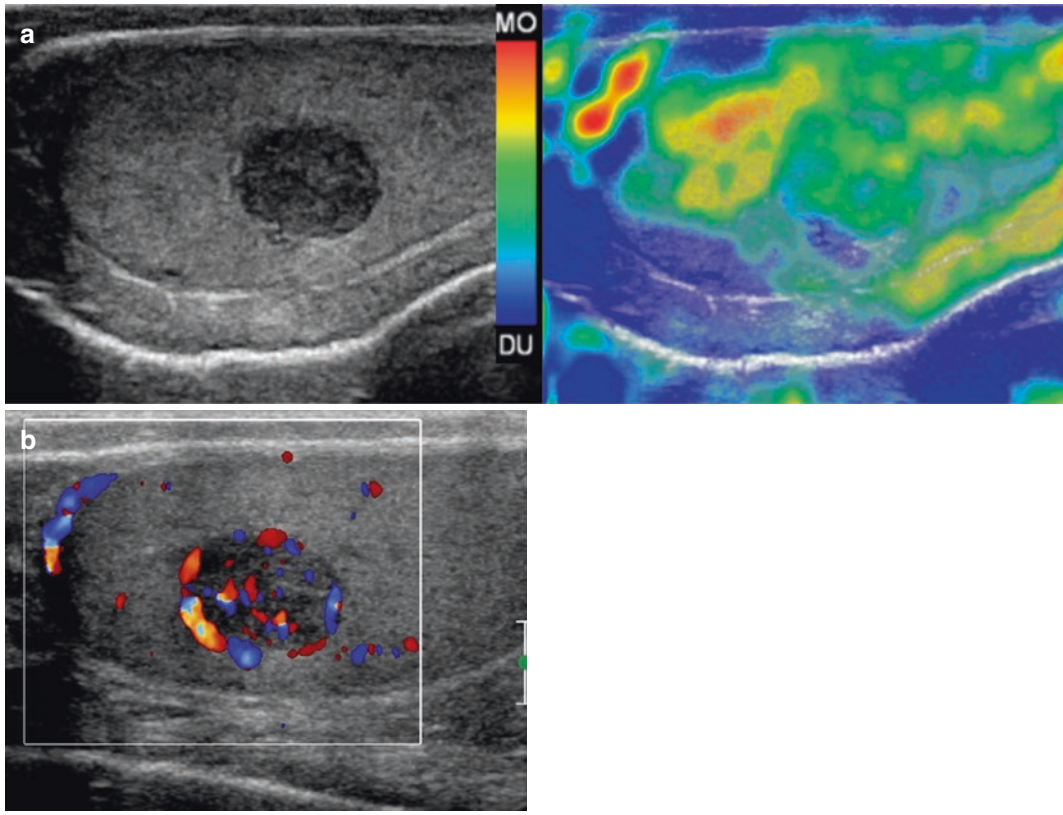

Fig. 44.1 (**a**, **b**) A 32-year-old infertile patient with a hypoechoic, non-palpable lesion of 1 cm, soft at elastography (**a**). The lesion is markedly vascularised at colour Doppler interrogation (**b**)

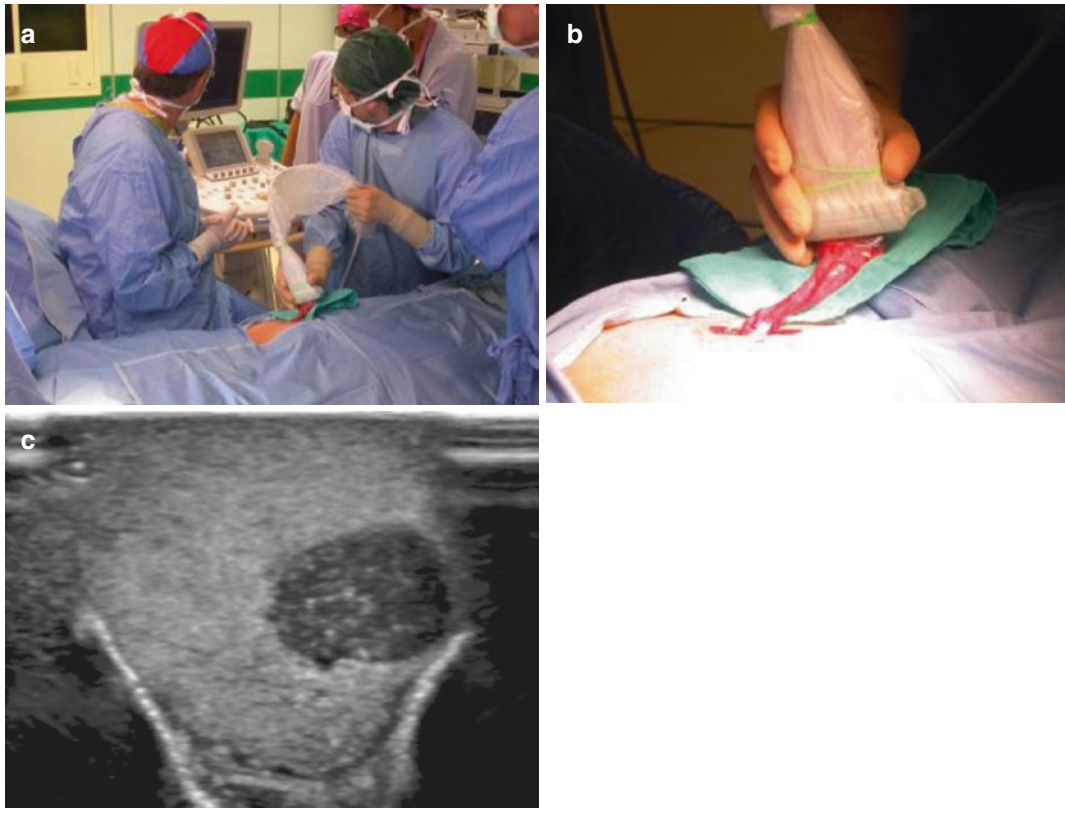

Fig. 44.2 (**a**–**c**) Intraoperative ultrasonography during testis-sparing surgery. Panoramic view of the procedure (**a**) and detail of the ultrasonographic investigation of the exposed testis (**b**). Intraoperative identification of the lesion (**c**)

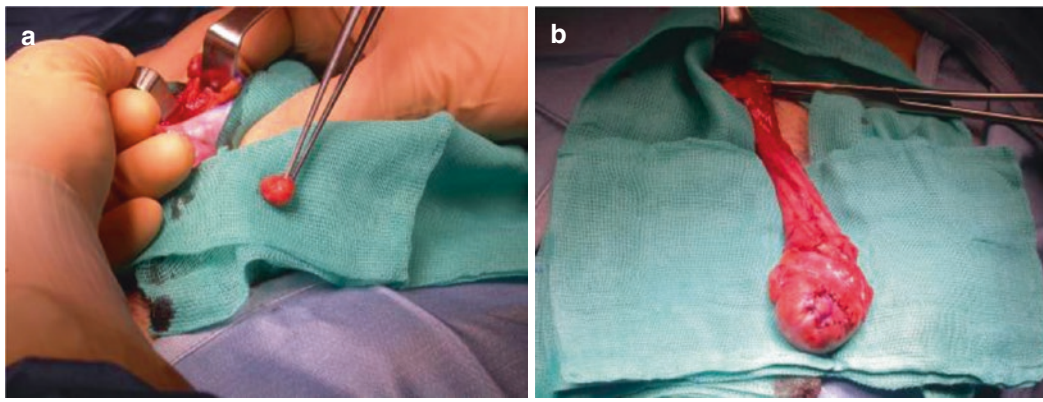

Fig. 44.3 Lesion enucleation (**a**) and appearance of the operated testis after the suture of the tunica albuginea (**b**)

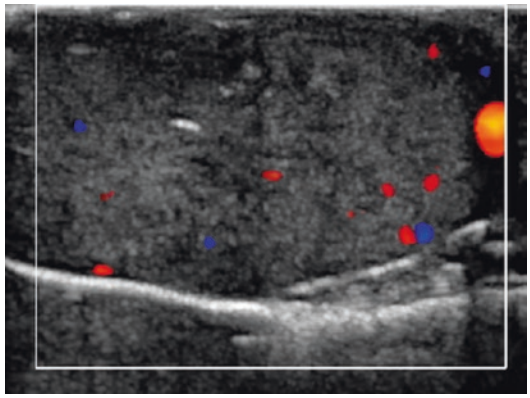

Fig. 44.4 Ultrasonographic evaluation of the operated testis after clamp removal and before moving the testis back inside the scrotum. No residual lesion nor testicular haematomas are identified. Colour Doppler interrogation shows good vascularisation of the parenchyma. Final histological diagnosis: Leydig cell tumour

44.5 Postoperative Evaluation

After testis-sparing surgery, frequent follow-up examinations are necessary, particularly when the lesion was malignant, with assessment of the serum hormonal levels and tumour markers, as well as ultrasonographic examination. According to our clinical practice, we perform an ultrasound evaluation 48 h after the surgical procedure, to report the presence of early postoperative complications such as large haematomas and ischaemic changes, reported in less than 1 % of the operated patients. We repeat ultrasound 4–6 weeks later, after disappearance of postoperative oedema and formation of the fibrotic scar (Fig. 44.5). When testis-sparing surgery is performed for a malignant neoplasm, scrotal ultrasonography is repeated every two months in the first year and every 6 months thereafter to assess the presence of recurrences. Other investigations involving abdominal CT/MR, chest x-ray or other imaging modalities are performed, with the same timing and indications as for radical orchiectomy.

Little has been written on the ultrasonographic appearance of the operated testis, and appearance of recurrent tumour has not been reported, an occurrence which, however, is extremely rare, with only two anecdotal cases reported. A recent study describes the ultrasonographic findings observed in testis of patients who have undergone testis-sparing surgery and

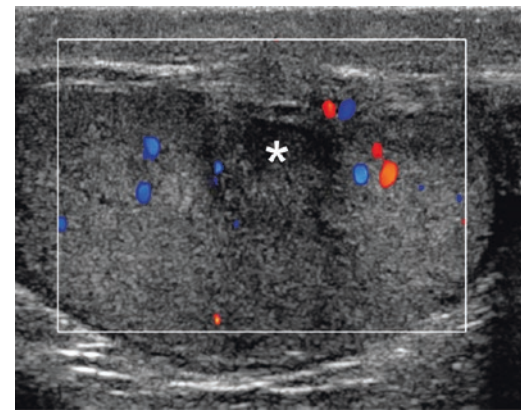

Fig. 44.5 Colour Doppler investigation obtained 6 weeks after the operation shows the postoperative scar (*)

surgical biopsies [19]. Hypoechoic and hypovascular lesions at the site of surgery were seen in the majority of patients with either linear or irregularly triangular shape, interpreted as scars. Retraction of testicular surface was detected in two cases. A peritesticular haematoma was observed in one patient early after the operation. No recurrent tumour was reported. However, only one malignant tumour was present in this series. Conclusions were that hypoechoic and hypovascular scars are "normal" postoperative pattern following testis-sparing surgery. Such findings have to be correctly interpreted and not misinterpreted as recurrences.

Conclusions

Intraoperative ultrasonography is an important tool to detect non-palpable testicular masses and guide surgical removal during testis-sparing surgery with minimum damage of the surrounding parenchyma. The use of a needle inserted into the lesion is helpful to guide the surgical procedure in deeply located nodules, reducing the operative time. The most challenging aspect is the timing to obtain an intraoperative histopathological diagnosis. This conservative approach is justified when imaging features suggest a benign tumour and in patients with a single testis or bilateral small multiple lesions.

Accurate selection of patients is the key to success: it is important to perform this procedure only to patients that accept a strict clinical and ultrasonographic follow-up.

References

1. Carmignani L, Gadda F, Gazzano G, Nerva F, Mancini M, Ferruti M, Bulfamante G, Bosari S, Coggi G, Rocco F, Colpi GM (2003) High incidence of benign testicular neoplasms diagnosed by ultrasound. J Urol 170(5):1783–1786. doi:10.1097/01.ju.0000092066.01699.90
2. Avci A, Erol B, Eken C, Ozgok Y (2008) Nine cases of nonpalpable testicular mass: an incidental finding in a large scale ultrasonography survey. Int J Urol Off J Jpn Urol Assoc 15(9):833–836. doi:10.1111/j.1442-2042.2008.02120.x
3. Powell TM, Tarter TH (2006) Management of nonpalpable incidental testicular masses. J Urol 176(1):96–98. doi:10.1016/S0022-5347(06)00496-4; discussion 99
4. Toren PJ, Roberts M, Lecker I, Grober ED, Jarvi K, Lo KC (2010) Small incidentally discovered testicular masses in infertile men – is active surveillance the new standard of care? J Urol 183(4):1373–1377. doi:10.1016/j.juro.2009.12.012
5. Carmignani L, Gadda F, Mancini M, Gazzano G, Nerva F, Rocco F, Colpi GM (2004) Detection of testicular ultrasonographic lesions in severe male infertility. J Urol 172(3):1045–1047. doi:10.1097/01.ju.0000134892.10525.39
6. Eifler JB Jr, King P, Schlegel PN (2008) Incidental testicular lesions found during infertility evaluation are usually benign and may be managed conservatively. J Urol 180(1):261–264. doi:10.1016/j.juro.2008.03.021; discussion 265
7. Isidori AM, Pozza C, Gianfrilli D, Giannetta E, Lemma A, Pofi R, Barbagallo F, Manganaro L, Martino G, Lombardo F, Cantisani V, Franco G, Lenzi A (2014) Differential diagnosis of nonpalpable testicular lesions: qualitative and quantitative contrast-enhanced US of benign and malignant testicular tumors. Radiology 273(2):606–618. doi:10.1148/radiol.14132718
8. Rocher L, Ramchandani P, Belfield J, Bertolotto M, Derchi LE, Correas JM, Oyen R, Tsili AC, Turgut AT, Dogra V, Fizazi K, Freeman S, Richenberg J (2015) Incidentally detected non-palpable testicular tumours in adults at scrotal ultrasound: impact of radiological findings on management Radiologic review and recommendations of the ESUR scrotal imaging subcommittee. Eur Radiol 26:2268–78. doi:10.1007/s00330-015-4059-7
9. Valentino M, Bertolotto M, Martino P, Barozzi L, Pavlica P (2014) Incidentally detection of non-palpable testicular nodules at scrotal ultrasound: what is new? Archivio Ialiano Di Urologia Andrologia Organo Ufficiale [di] Societa Italiana Di Ecografia Urologica e Nefrologica/Associazione Ricerche Urologia 86(4):378–382. doi:10.4081/aiua.2014.4.378
10. Patel K, Sellars ME, Clarke JL, Sidhu PS (2012) Features of testicular epidermoid cysts on contrast-enhanced sonography and real-time tissue elastography. J Ultrasound Med Off J Am Inst Ultrasound Med 31(1):115–122
11. Valentino M, Bertolotto M, Derchi L, Bertaccini A, Pavlica P, Martorana G, Barozzi L (2011) Role of contrast enhanced ultrasound in acute scrotal diseases. Eur Radiol 21(9):1831–1840. doi:10.1007/s00330-010-2039-5
12. Bertolotto M, Derchi LE, Sidhu PS, Serafini G, Valentino M, Grenier N, Cova MA (2011) Acute segmental testicular infarction at contrast-enhanced ultrasound: early features and changes during follow-up. AJR Am J Roentgenol 196(4):834–841. doi:10.2214/AJR.10.4821
13. Huang DY, Sidhu PS (2012) Focal testicular lesions: colour Doppler ultrasound, contrast-enhanced ultrasound and tissue elastography as adjuvants to the

diagnosis. Br J Radiol 85 Spec No 1:S41–S53. doi:10.1259/bjr/30029741
14. Connolly SS, D'Arcy FT, Gough N, McCarthy P, Bredin HC, Corcoran MO (2006) Carefully selected intratesticular lesions can be safely managed with serial ultrasonography. BJU Int 98(5):1005–1007. doi:10.1111/j.1464-410X.2006.06451.x; discussion 1007
15. Kirkham AP, Kumar P, Minhas S, Freeman AA, Ralph DJ, Muneer A, Allen C (2009) Targeted testicular excision biopsy: when and how should we try to avoid radical orchidectomy? Clin Radiol 64(12):1158–1165. doi:10.1016/j.crad.2009.06.008
16. Hopps CV, Goldstein M (2002) Ultrasound guided needle localization and microsurgical exploration for incidental nonpalpable testicular tumors. J Urol 168(3):1084–1087. doi:10.1097/01.ju.0000025141.88860.0d
17. Browne RF, Jeffers M, McDermott T, Grainger R, Mulvin D, Gibney RG, Torreggiani WC (2003) Technical report. Intra-operative ultrasound-guided needle localization for impalpable testicular lesions. Clin Radiol 58(7):566–569
18. Kravets FG, Cohen HL, Sheynkin Y, Sukkarieh T (2006) Intraoperative sonographically guided needle localization of nonpalpable testicular tumors. AJR Am J Roentgenol 186(1):141–143. doi:10.2214/AJR.04.1687
19. Attieh A, Benelli A, Bertolotto M, Simonato A, Carmignani G, Derchi LE (2015) Sonographic appearances of the postoperative testis. J Clin Ultrasound 44:12–16. doi:10.1002/jcu.22304

Part VI

The Penis

Penis: Ultrasound Anatomy and Scanning Methods

45

Ferdinando Fusco, Massimiliano Creta, and Vincenzo Mirone

45.1 Penile Anatomy

The human penis is made up of three cylindrical bodies consisting of endothelium-lined cavernous spaces: a pair of connected corpora cavernosa along its dorsolateral aspect and a midline corpus spongiosum along its ventral surface which anteriorly forms the glans penis [1, 2]. The corpora are covered by three different fascial layers: the tunica albuginea, the deep Buck's fascia, and the superficial Colles fascia. The tunica albuginea surrounds each corpus individually [1, 2]. The tunica albuginea is a strong structure of heterogenous thickness and anatomy. The tunica albuginea of the corpora cavernosa is a bilayered structure with multiple sublayers [3]. Inner layer bundles support and contain the cavernous tissue and are oriented circularly [3]. Radiating from this layer are intracavernous pillars acting as struts, which augment the septum and provide essential support to the erectile tissue [3]. Outer layer bundles are oriented longitudinally [3]. These fibers extend from the glans penis to the proximal crura, where they insert into the inferior pubic ramus [3]. There are no outer layer fibers between the 5 and 7 o'clock positions [3]. Elastic fibers normally form an irregularly latticed network on which collagen fibers rest [3]. The corpus spongiosum lacks both the outer layer and the struts. There is variability in albugineal thickness and strength in various locations. Thickness ranges from approximately 0.8 mm at the 5 and 7 o'clock positions (just lateral to the corpus spongiosum) to 2.2 mm at the 1 and 11 o'clock positions [4]. The two corpora cavernosa are separated by the septum penis, an extension of the tunica albuginea [1]. The septum between them is incomplete in humans, although complete in some other species. The distal penile ligament is an aggregation of the outer longitudinal layer of the tunica albuginea and acts as a buttress for the glans penis [5]. The Buck's fascia and the Colles fascia represent outer layers that cover all the three corpora [2]. Buck's fascia surrounds both cavernosal bodies dorsally and splits to surround the spongiosum ventrally. The blood flow to the penis is supplied by the cavernosal, dorsal, and urethral arteries, which are branches of the internal pudendal artery [2].

F. Fusco (✉) • V. Mirone
Department of Neurosciences, Science of Reproduction and Odontostomatology, Urology Unit, University of Naples Federico II, Naples, Italy
e-mail: ferdinando-fusco@libero.it

M. Creta
Urology Unit, Buon Consiglio Fatebenefratelli Hospital, Naples, Italy

P. Martino, A.B. Galosi (eds.), *Atlas of Ultrasonography in Urology, Andrology, and Nephrology*,
DOI 10.1007/978-3-319-40782-1_45

45.2 Technical Requirements

The penis is an organ ideally suited to ultrasound imaging because of its superficial location [6]. Penile ultrasound should be done in real-time B-mode scanning, using a linear probe [7, 8]. High-frequency (7.5 MHz or more) transducers are used to obtain high-resolution images of the penis [7, 8]. The use of real-time spatial compounding and adaptive image-processing technique is useful to reduce artifacts. Additionally, dynamic enhancement of the margins improves the visualization of tissue conspicuity and increases the diagnostic confidence [9].

45.3 Scanning Protocol

Penile ultrasound can be performed in the flaccid and erectile states. Tumescence and erection allow a better evaluation of the different anatomical features of the penis [10]. It is recommended to perform the examination in a quiet, private setting with the room warm and darkened, so that the patient is comfortable and relaxed. The patient should lie on the examination table in a supine position with legs together providing support for external genitalia, and the penis should be in the anatomical position, i.e., lying superiorly against the anterior abdominal wall [11, 12].

An alternative position is dorsal lithotomy with the penis lying on the anterior abdominal wall [11, 12]. During the examination, the patient may be asked to gently hold the corona just under the glans penis and stretch the shaft along the anterior abdominal wall in order to help keep the penis immobilized [13]. A sufficient amount of sonographic acoustic gel should be used on the surface of the penis to obtain good-quality images, and excessive compression by the transducer should be avoided, especially in patients with trauma [12]. The urethra is easily compressible, so minimal pressure should be maintained while scanning [11].

The external portion of the penis is examined starting at the level of the glans and moving down to the base of the penis [12]. The transducer can be placed on the ventral and/or dorsal aspect of the penis (Figs. 45.1 and 45.2). The dorsal approach is easier for the flaccid phallus, while the ventral approach is often performed with placement of legs in the lithotomy position and is often better with a fully erect phallus [11]. A lateral approach has been also described (Fig. 45.3) [14]. The external portion of the penis is scanned in at least two planes: longitudinal and transverse. Transverse images should be obtained in the proximal, mid, and distal portions. Longitudinal images should be obtained of both the right and left corpora cavernosa including the cavernosal artery. The anterior urethra is best examined after distention of the lumen achieved by either a retrograde or an antegrade approach [12]. The retrograde technique is generally preferred [12]. This technique requires the introduction of normal saline solution, a lubricant or an anesthetic jelly via either a Foley catheter or a syringe placed directly in the urethral meatus until the urethra appears fully distended on sonography [12]. After distension, a flexible penile clamp is applied to the glans to maintain urethral distension [12]. The antegrade technique requires the patient's voiding, and, if a full stream is achieved, a clamp is placed at the distal end of the penis to preserve distention [12]. The urethra is examined from the dorsal surface of the penis and, if needed, additional scanning from the ventral surface can be performed [12]. The distal bulbar urethra can be examined through the scrotum [12]. Longitudinal scans are more useful than transverse scans because of their wide field of view, and transverse scans are used to further examine detected focal lesions [12]. The non-external portions of the corpora cavernosa and the proximal bulbous urethra are best examined through a transperineal approach (Fig. 45.4) [12].

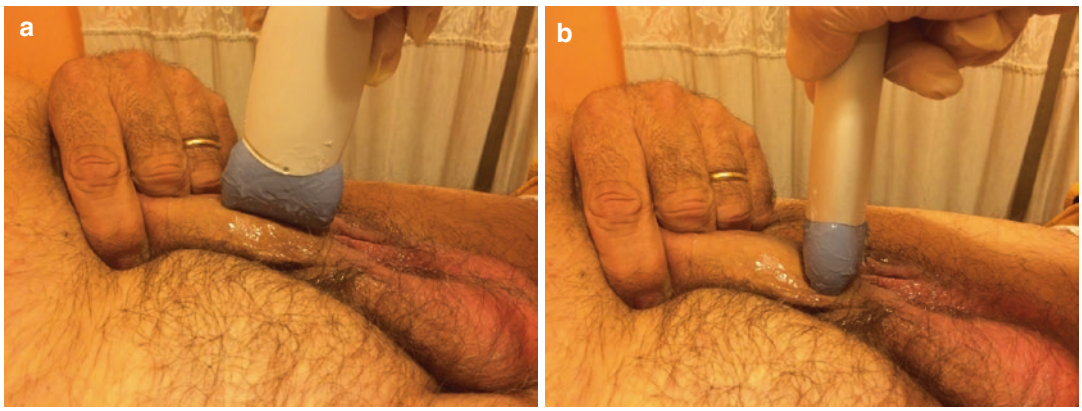

Fig. 45.1 Penile sonographic technique, ventral access. The penis is in the anatomic position, lying on the anterior abdominal wall. The patient keeps the penis immobilized by holding the corona just under the glans penis and stretching the shaft along the anterior abdominal wall. The probe is placed longitudinally (**a**) and transversally (**b**) on the ventral surface of the penis

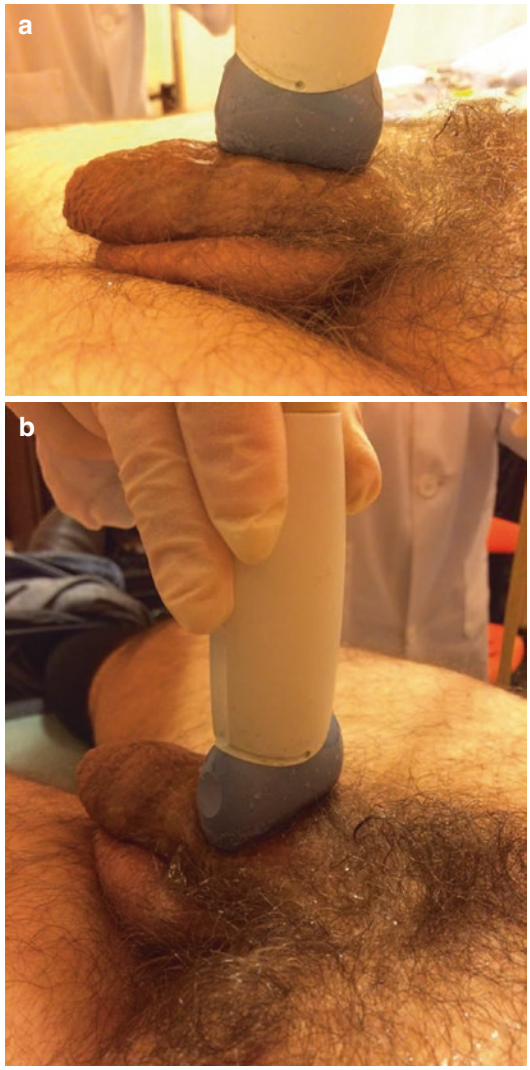

Fig. 45.2 Penile sonographic technique, dorsal access. The probe is placed longitudinally (**a**) and transversally (**b**) on the dorsal surface of the penis

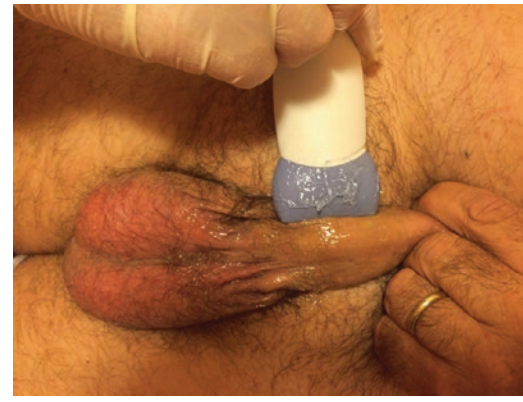

Fig. 45.3 Penile sonographic technique, lateral access to the penile shaft longitudinally from the right side of the penis

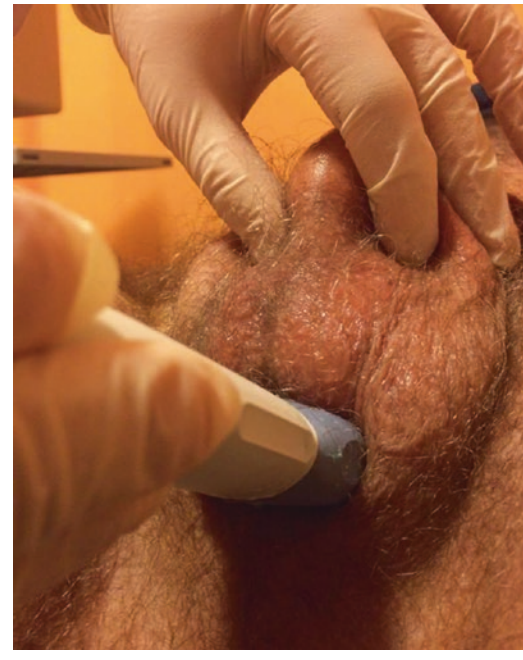

Fig. 45.4 Penile sonographic technique, transperineal approach

45.4 Normal Ultrasound Anatomy of the Penis

The sonographic appearance of the penis varies according to the degree of rigidity. In the flaccid state, the corpora cavernosa appear as two, dorsally located, circular structures with homogeneous mixed echotexture and intermediate echogenicity as a result of the innumerable interfaces created by their complex system of vascular sinusoids. The corpus spongiosum appears as a ventrally located circular structure with homogeneous echotexture and higher echogenicity with respect to the corpora cavernosa (Figs. 45.5, 45.6, 45.7, and 45.8) [11]. The glans is more echogenic than the corpora cavernosa [5]. The normal urethra is visualized as a tubular anechoic structure with a thin, smooth echogenic wall, and the lumen distends to at least 4 mm in diameter [12]. When collapsed, the urethra appears as a transverse line. The tissue layers surrounding the corpora are only partially identifiable in the flaccid state [15]. Skin, subcutaneous tissue, and dartos cannot always be readily separated [15]. An extremely thin hyperechoic line identifies the interface formed by the deep fascia of the penis [15]. The Colles fascia is barely visible [5, 16]. The tunica albuginea and the Buck's fascia are usually stuck together and appear as a thin (usually less than 2 mm) echogenic layer surrounding the corpora [5, 16]. The two distinct layers become appreciable only when fluid extravasation accumulates between them or very high-frequency transducers are used [5]. In some cases, vascular structures may provide a suitable interface to separate small portions of the Buck's fascia from the underlying tunica albuginea in normal conditions as well. In particular, the Buck's fascia becomes visible at ultrasound near dilated circumflex veins, and a subtle echogenic line representing the Buck's fascia is usually recognized in the dorsal aspect of the penis dividing the plane of the deep vessels from that of the superficial vessels [5]. The thickness of the tunica albuginea in the flaccid state is about 1–3 mm [16]. The echoes from the tunica albuginea are specular reflections and thus are demonstrated with efficiency only when the ultrasound beam is perpendicular to them. Perpendicular insonation, in particular, is of paramount importance to evaluate the echogenicity of the plaques [9]. The penile septum appears as an echogenic structure with back attenuation dividing the corpora cavernosa that can hamper visualization of the tunica albuginea in the dorsal aspect of the penis [5]. The distal penile ligament is recognized at ultrasound as a linear structure more echogenic than the surrounding glanular tissue located centrally within the glans dorsal to the distal urethra [5]. Several penile vessels can be identified at gray-scale ultrasound. The cavernosal arteries appear as a pair of dots located slightly medially in each corpus cavernosum. On longitudinal scans, they present as narrow tubular structures with echogenic wall (Fig. 45.9) [15, 17]. The diameter of the normal cavernosal arteries ranges from 0.3 to 05 mm in the flaccid state. The dorsal arteries are visible in the dorsal aspect of the shaft as anechoic structures with a similar diameter to the cavernosal arteries [5]. Dorsal veins present with less echogenic wall compared to the arteries [5]. When the penis becomes erect, the two corpora cavernosa enlarge and the sinusoids dilate [1, 15]. The echogenicity of the corpora cavernosa progressively decreases during tumescence starting from the region surrounding the cavernosal arteries because of sinusoids dilatation [5]. During maximal penile rigidity, a fine echogenic network is appreciable in the corpora cavernosa due to sinusoidal interfaces (Fig. 45.10) [5]. Sinusoidal spaces at the base of the penis are normally larger with respect to the remaining portions of the shaft. Blood entrapped within the sinusoids often appears slightly corpusculated [5]. During erection, the fibrous layers that envelop the corpora can be best visualized. The tunica albuginea thins and its thickness is about 0.5 mm [16]. The intracavernous pillars are recognizable on transverse scans as straight echogenic lines thicker than the sinusoidal walls, which run from one side to the other of the tunica albuginea [5]. The diameter of the normal cavernosal arteries increases to 0.6–1.0 mm after an intracavernosal injection of vasoactive agents. Moreover, during the onset of erection, cavernosal artery pulsation is evident in normal subjects [5, 18]. As occurs for the cavernosal arteries, also the diameter of the dorsal arteries increases during erection but to a lesser extent compared with the cavernosal arteries [5].

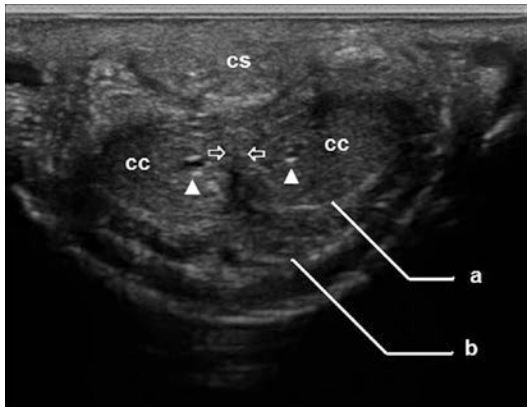

Fig. 45.5 Normal gray-scale ultrasound anatomy. Axial scan on the ventral aspect of the penis showing the paired corpora cavernosa (*cc*), the corpus spongiosum (*cs*), the penile septum (*open arrows*), the tunica albuginea (**a**), the Buck's fascia. And the cavernosal arteries (*arrowheads*)

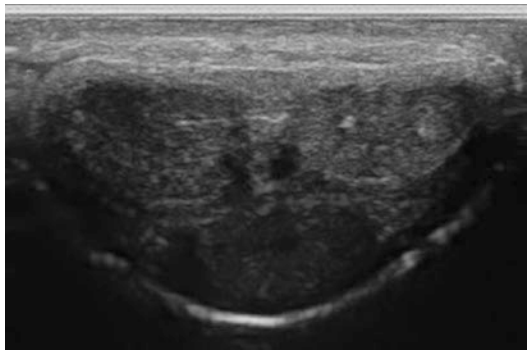

Fig. 45.6 Normal gray-scale ultrasound anatomy. Axial scan on the dorsal aspect of the penis

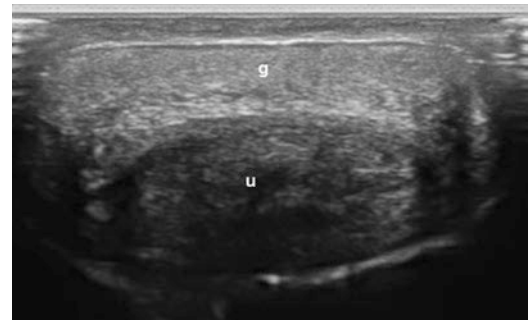

Fig. 45.7 Transverse scan obtained on the dorsal aspect of the penis at the level of the glans (*g*) and the urethra (*u*)

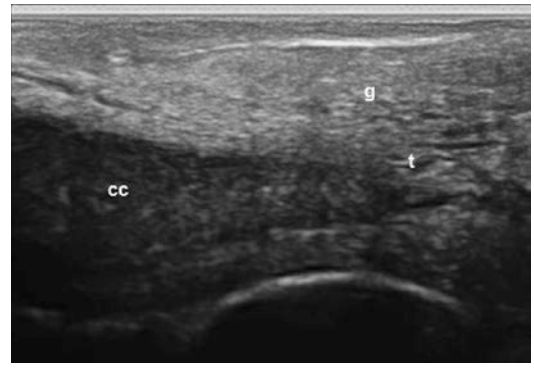

Fig. 45.8 Longitudinal scan obtained on the dorsal aspect of the penis at the level of the glans showing the glans (*g*), the corpus cavernosum (*cc*), and the tip of the corpus cavernosum (*t*)

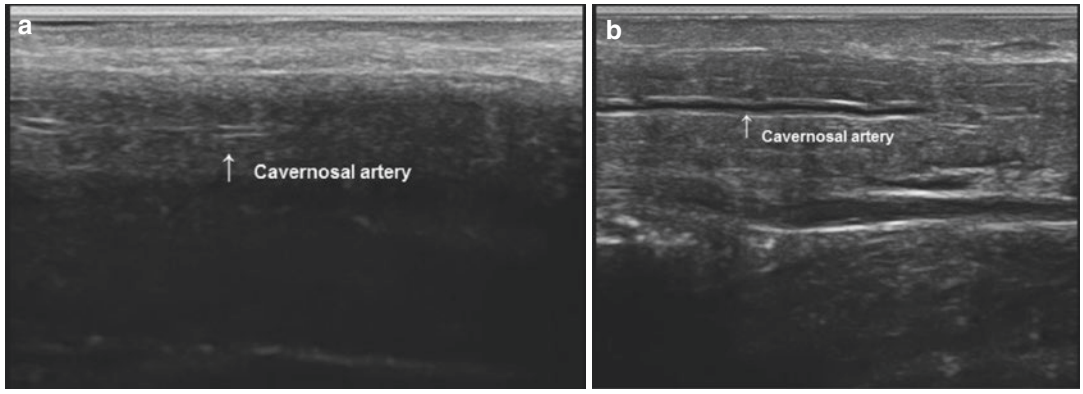

Fig. 45.9 Longitudinal scans obtained on the ventral aspect of the penis showing the cavernosal artery while flaccid (**a**) and during the onset or erection (**b**). The diameter of the artery increases during erection

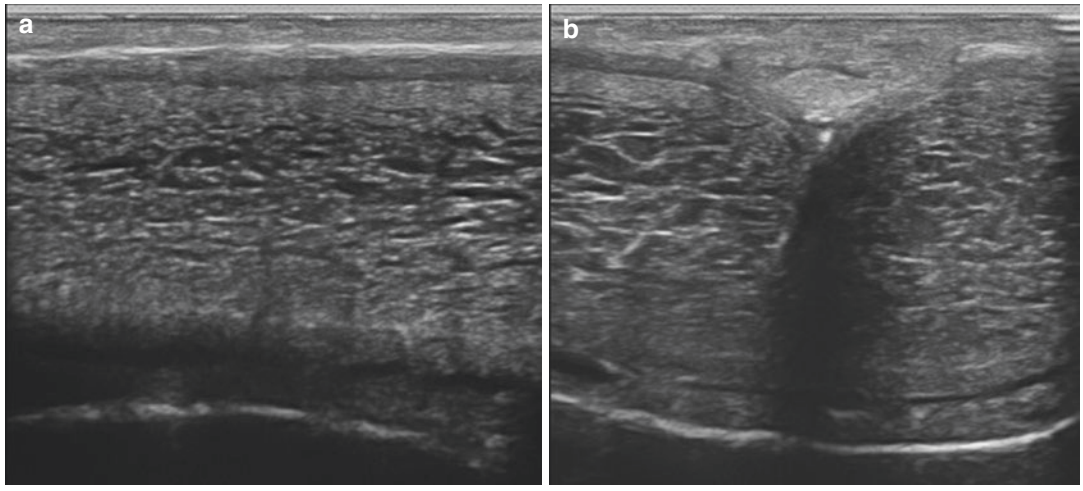

Fig. 45.10 Longitudinal (**a**) and axial (**b**) scans obtained on the ventral aspect of the penis during the onset or erection showing the sinusoids dilated

45.5 Reporting

The following details must be described and documented with appropriate images: size, echogenicity (hyper, hypo, iso), and symmetry of the corpora cavernosa [7]. The size and echogenicity of each corpus cavernosum should be compared to the contralateral side [8]. Moreover, any alterations of the layers and of the septum, either echogenic or structural, must be documented by accurate measurements both on longitudinal and transverse scans [7]. Any palpable alteration or penile anomaly must be closely studied directly on the involved zone, and documented by appropriate images [7].

Bibliography

1. Nicola R, Carson N, Dogra VS (2014) Imaging of traumatic injuries to the scrotum and penis. AJR Am J Roentgenol 202:W512–W520
2. Bertolotto M, Serafini G, Savoca G, Liguori G, Calderan L, Gasparini C, Mucelli RP (2005) Color Doppler US of the postoperative penis: anatomy and surgical complications. Radiographics 25:731–748
3. Brock G, Hsu GL, Nunes L, von Heyden B, Lue TF (1997) The anatomy of the tunica albuginea in the normal penis and Peyronie's disease. J Urol 157:276–281
4. Hsu GL, Brock G, Martínez-Piñeiro L, von Heyden B, Lue TF, Tanagho EA (1994) Anatomy and strength of the tunica albuginea: its relevance to penile prosthesis extrusion. J Urol 151:1205–1208
5. Bertolotto M, Lissiani A, Pizzolato R, Djouguela Fut M (2008) US anatomy of the penis: common findings and anatomical variations. In: Bertolotto M (ed) Color Doppler US of the penis. Springer, Berlin/New York, pp 25–38
6. Wilkins CJ, Sriprasad S, Sidhu PS (2003) Colour Doppler ultrasound of the penis. Clin Radiol 58:514–523
7. Martino P, Galosi AB, Bitelli M, Consonni P, Fiorini F, Granata A, Gunelli R, Liguori G, Palazzo S, Pavan N, Scattoni V, Virgili G, Imaging Working Group-Societa Italiana Urologia (SIU), Società Italiana Ecografia Urologica Andrologica Nefrologica (SIEUN) (2014) Practical recommendations for performing ultrasound scanning in the urological and andrological fields. Arch Ital Urol Androl 28(86): 56–78
8. AIUM practice guideline for the performance of an ultrasound examination in the practice of urology guideline developed in collaboration with the American urological association, American Institute of Ultrasound in Medicine, 2011
9. Kalokairinou K, Konstantinidis C, Domazou M, Kalogeropoulos T, Kosmidis P, Gekas A (2012) US imaging in peyronie's disease. J Clin Imaging Sci 2:63
10. Lue TF, Hricak H, Marich KW, Tanagho EA (1985) Vasculogenic impotence evaluated by high-resolution ultrasonography and pulsed Doppler spectrum analysis. Radiology 155:777–781
11. Rais-Bahrami S, Gilbert BR (2015) Penile ultrasound. In: Gilbert BR (ed) Ultrasound of the male genitalia. Springer, New York, pp 125–156
12. Bhatt S, Kocakoc E, Rubens DJ, Seftel AD, Dogra VS (2005) Sonographic evaluation of penile trauma sonographic technique for evaluation of the penis. J Ultrasound Med 24:993–1000
13. Pozniak A, Paul L (2013) Doppler ultrasound of the penis in Myron. In: Clinical Doppler ultrasound, 3rd edn. Churchill Livingstone, London/New York
14. Prando D (2009) New sonographic aspects of peyronie disease. J Ultrasound Med 28:217–232
15. Grazioli L, Olivetti L, Zappa N, Apostolopoulos E (2008) Male reproductive system: normal radiologic anatomy. In: Olivetti L, Grazioli L (eds) Imaging of urogenital diseases. A color atlas. Springer, Milan/New York, pp 47–64
16. Bertolotto M, Gasparini C, Calderan L, Lissiani A, Cova MA (2005) L'eco-color Doppler penieno: stato dell'arte. Giornale Italiano di Ecografia 8:113–127
17. Quam JP, King BF, James EM, Lewis RW, Brakke DM, Ilstrup DM, Parulkar BG, Hattery RR (1989) Duplex and color Doppler sonographic evaluation of vasculogenic impotence. AJR Am J Roentgenol 153:1141–1147
18. Lee B, Sikka SC, Randrup ER, Villemarette P, Baum N, Hower JF, Hellstrom WJJ (1993) Standardization of penile blood flow parameters in normal men using intracavernous prostaglandin E1 and visual sexual stimulation. J Urol 149:49–52

Penile Color Doppler Ultrasound in the Diagnosis of Erectile Dysfunction

46

Carlo Bettocchi, Carlos Miacola, Matteo Matera, Giuseppe Lucarelli, and Fabrizio Palumbo

46.1 Introduction

Ultrasound penile examination is an indispensable tool in clinical urology, included among the diagnostic tests available to the clinician for the study of problems of erectile dysfunction (ED), both as baseline examination and integrated by a color Doppler imaging study.

Penile echo-color Doppler is widely used in the diagnosis of ED, thanks to its ability to study the vascular system of the penis and penile blood flow, analyzing and highlighting any major changes. This study is important because erection is a complex hemodynamic event regulated by the smooth muscle tone of arterioles and venous sinusoids of the corpora cavernosa [1]. Alternative imaging modalities in the investigation of ED such as MRI and angiography, as well as the penile anatomy and the physiology of erection, will not be addressed. Erectile dysfunction is, along with premature ejaculation, the primary male disorder in sexual medicine. The advent of new oral therapies has completely changed the diagnostic and therapeutic approach [2]. Etiologically, erectile dysfunction is subdivided into psychogenic and organic forms; in 1959 Wershub reported that 90 % of cases of erectile dysfunction were psychogenic in origin; nowadays this percentage distribution has changed considerably, and organic forms have been seen to be more frequent than psychogenic, thanks to the use of new and more sophisticated equipment and diagnostic techniques.

46.2 Physiology of Erection

The maintenance of penile flaccidity and the erectile response are controlled via intercommunicating supraspinal and spinal reflex pathways. During the *flaccid state*, antierectile neural input acts, primarily via sympathetic efferents, to limit blood flow to the penis to a quantity sufficient to meet physiologic needs but insufficient for erection. In the flaccid unstimulated penis, the resting smooth muscle tonicity of the cavernosal arterioles and sinusoids is elevated, resulting in a high-resistance vascular bed with a resultant low volume inflow and outflow.

Following either physical or psychological sexual stimulation, proerectile neural signals are sent to the penis primarily via parasympathetic tracts. Nitric oxide (NO) is the main proerectile neurotransmitter. The resultant molecular cascade leads to a decrease in intracellular Ca2+ and arteriolar smooth muscle relaxation. This relaxation allows for an increased blood flow and

C. Bettocchi (✉) • C. Miacola • M. Matera
G. Lucarelli • F. Palumbo
Department of Emergency and Organ Transplantation – Urology, Andrology and Kidney Transplantation Unit, University of Bari, Bari, Italy
e-mail: carlo.bettocchi@uniba.it

P. Martino, A.B. Galosi (eds.), *Atlas of Ultrasonography in Urology, Andrology, and Nephrology*,
DOI 10.1007/978-3-319-40782-1_46

subsequent corporal engorgement with increasing *penile rigidity*. As the corpora become engorged, the emissary veins are compressed within the tunica albuginea, limiting venous outflow. The increased arterial inflow and limited venous outflow increase intracorporeal pressure and lead to erection, and when this pressure nears systolic pressure, a reduction in inflow will also normally occur. As the proerectile input ceases, the secondary molecular messenger cGMP is hydrolyzed, allowing for a rise in intracellular Ca2+, a subsequent smooth muscle contraction, a decreased penile blood flow, and a return to the flaccid state physiology.

46.3 Indications

Currently this examination provides the most secure information for a diagnosis of arteriogenic erectile dysfunction, but even this tool is unable to discriminate between organic and psychogenic forms [3]. The examination is performed at baseline (penile ultrasound), albeit this is of little diagnostic significance, and in dynamic (PDS) conditions, after intracavernous injection of a pharmacostimulant agent (ICI).

PDS aims to examine the cavernosal arteries and the response of their spectral Doppler waveforms after intracavernosal injection of a pharmacostimulant agent, commonly a prostaglandin E1 (PGE-1) derivative such as alprostadil. The fundamental principle is repeated sampling of these waveforms in a stepwise manner until maximal peak systolic and minimal diastolic velocities have been reached.

The positive aspects of this exam are low invasiveness, simplicity of execution, and the capacity to diagnose a deficient arterial flow and evaluate the dynamics of vascular erectile function. The major negative aspect is the presence of false positives for a frequent incompetence of the cavernous vein (ICV), due to the need to achieve a good relaxation of the trabecular smooth muscle.

Indications for Ultrasound Penile Examination [3]

1. Erectile dysfunction
2. Priapism
3. Penile fibrosis and Peyronie's disease
4. Penile or urethral abnormalities (found at physical examination)
5. Neoplasms of the penis
6. Trauma
7. Dorsal vein thrombosis
8. Disorders of the urethra (cysts, diverticula, stenosis)
9. Presence of foreign bodies or calculus in the urethra

Indications for PDS [3]

1. Erectile dysfunction (nonresponders to oral medication)
2. Post-traumatic ED
3. Candidates for a penile implant
4. Peyronie's disease patients considered candidates for surgery
5. Post-priapism ED
6. Lifelong (primary) ED
7. Medicolegal situations
8. If requested by the patient

46.3.1 Technical Execution

Informed consent should be obtained, especially with regard to the low risk of priapism following intracavernosal injection.

Pharmacological stimulation in the echo-color Doppler penile examination is obtained by intracavernous injection of vasoactive substances in standardized or individualized dosage to evaluate the erectile response of the patient. In recent years, a number of substances with different pharmacodynamics, such as papaverine, the α-blockers (phentolamine, phenoxybenzamine, etc.), the prostaglandin (PGE-1), and ultimately nitrates [4], have been adopted. The currently most commonly used and standardized drug for this examination is PGE-1 that has a dual action on the mechanism of erection: (a) blocking the release of norepinephrine from adrenergic terminals and (b) stimulation of adenylate cyclase resulting in an increase of cAMP [5]. In order to improve the efficacy and tolerability of this diagnostic procedure, different schemes of administration and different doses of PGE-1 (10, 20, or even 40 micrograms) have been employed. Currently, the dosage most frequently used is 20 micrograms (about 90% of PGE-1 is metabolized locally in the penis and the remaining 10% in the liver at the first pass). Prepared at the time of the test, the PGE-1 is administered in the corpora cavernosa, laterally and perpendicular to the tangent of the cavernous body, after disinfection of the skin, holding the penis with the thumb dorsally, at 12 o'clock, and with the index finger ventral to 6 o'clock, stretching the penis and blocking the skin veins.

The comprehensive review provides three measurements performed bilaterally at 3, 10, and 20 min from the drug injection. The third measurement, at 20 min, is performed after inviting the patient to achieve an optimal erection on his own. Owing to the nature of the problem under investigation, a quiet, private, and comfortable environment is essential for satisfactory PDS results. Many patients will be anxious, and a detailed explanation of the procedure is required prior to commencing: a significant percentage of patients has high values of diastolic flow arising from a minor compliance of the corpora cavernosa due to a hypertonic sympathetic response linked to anxiety. It is also useful to ask the patient to make a comparison between the erection achieved in the clinic and the one he normally reaches under normal sexual stimulation. For the execution of the color Doppler, a 7 MHz convex probe is used; the probe is grasped between the thumb and fingers, placing it between the cavernous body and the spongy body of the urethra, directing it in a latero-medial and lateral tilted direction, at a penoscrotal angle. Measurements at 3 and 10 min are performed on the dorsal aspect of the penis, proximal to the pubis. The third measurement is performed on the ventral side of the penis at the penoscrotal level. The Doppler angle used during this examination is important: for the ultrasound examination to be deemed valid, it is important to maintain a Doppler angle of <60 °. The determination of specific hemodynamic parameters substantially allows a condition of inadequate arterial flow to be diagnosed and possibly an inadequate veno-occlusive function (Figs. 46.1 and 46.2). Three flow parameters are usually evaluated during the execution of PDS:

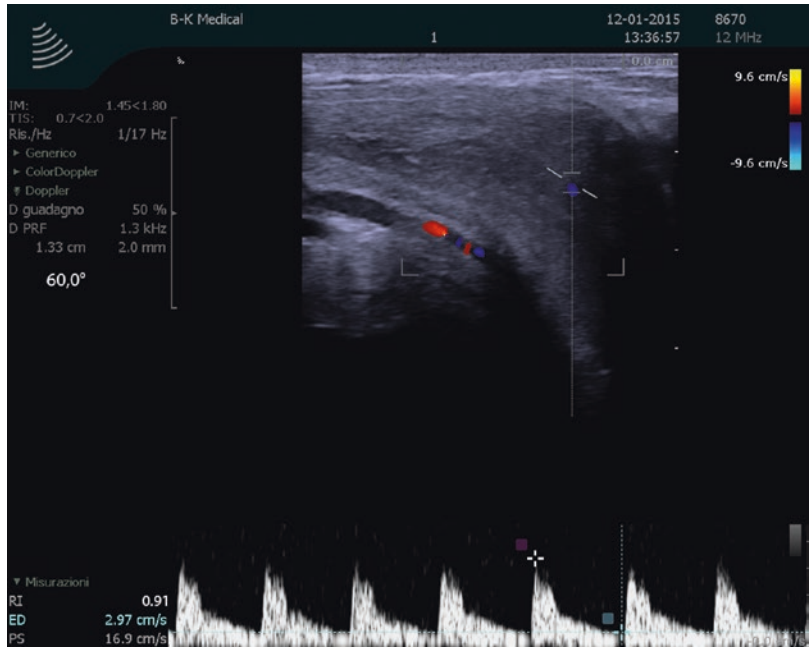

Fig 46.1 Longitudinal scans on the left corpus cavernosum showing the cavernous artery

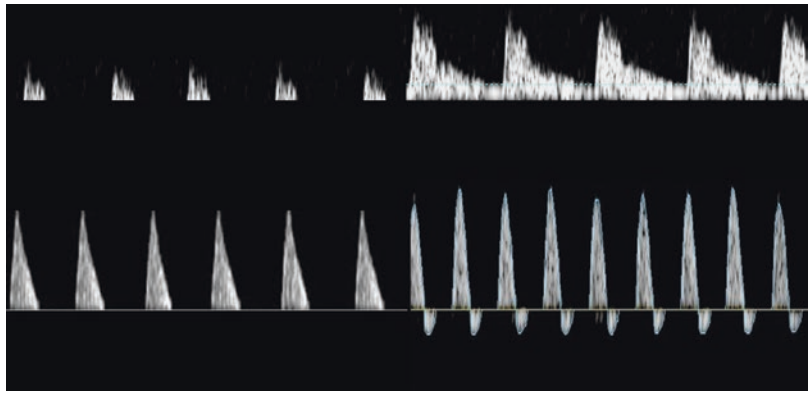

Fig 46.2 Physiological changes of cavernous arteries' Doppler. (1) In the flaccid state, they are observed at low flow speed and high strength. (2) After administration of PGE appear flows at high speed and low resistance and then (Step 2) appear at early diastole incision. With the increase of rigidity, (3) the diastolic flow disappears (Step 3), and when it reaches the erection, (4) it is observed on the reverse diastolic flow (Step 4)

1. Maximal peak systolic velocity (PSV)
2. End-diastolic velocity (EDV)
3. The resistance index (RI)

The maximal peak systolic velocity is expressed in centimeters per second (cm/s) and corresponds to the maximum flow rate during systole. For a proper evaluation, the accurate positioning of the angle of correction has a fundamental importance; it must be less than 60 ° and corrected for the direction of flow, also using a narrow sampling port, aligned along a straight portion of the cavernous artery. The evaluation of arterial flow must be performed in the artery origin segment. The end-diastolic velocity is expressed in centimeters per second (cm/s) and defines the residual flow in a vessel at the end of the diastolic phase. In physiological conditions, the blood flow increases during the phase of tumescence, determining filling of the sinusoids that press against the tunica albuginea, which is a relatively inextensible fibroelastic membrane. This determines compression of the subalbugineous venules until interruption of the venous outflow occurs, and the achievement of a higher intracavernous pressure than diastolic pressure. The resistance index is the equivalent of the semiquantitative end-diastole speed, the resulting formula being:

RI = PSV-EDV/PSV. RI is expressing peripheral resistance to blood flow.

	Pathological values	Borderline values	Normal values
PSV	<30 cm/s	25–30 cm/s	>35 cm/s
EDV	> 5 cm/s	4.5–5 cm/s	< 5 cm/s
RI	< 0.90	0.85–0.90	> 0.90

Objective evaluation of the erection is always associated with hemodynamic parameters and is expressed in fifths (x/5), based on the five basic stages of erection:

1. Lack of response (1/5)
2. Mild tumescence (2/5)
3. Tumescence insufficient for penetration (3/5)
4. Rigidity sufficient for penetration (4/5)
5. Complete rigidity (5/5)

46.4 Diagnostic Values

Threshold values for the diagnosis of ED, distinguishing organic/vascular and psychological causes, are expressed in the table below according to the interpretation of hemodynamic parameters accompanied by the objective evaluation of the erection (Figs. 46.3 and 46.4).

PSV	RI	Etiologic diagnosis
> 35 cm/s	> 0.90	Psychogenic
> 35 cm/s	< 0.85	Venogenic (veno-occlusive dysfunction)
< 25 cm/s	> 0.90	Arteriogenic (arterial insufficiency)
< 25 cm/s	< 0.85	Mixed (arteriogenic + venogenic)

According to many authors' experience and according to the American Urological Association (AUA) guidelines, when erection exceeds 2–3 h duration, along with an inversion of telediastolic velocity, a pharmacological "reverse" is indicated in order to prevent the possible need for surgical detumescence. We usually inject an alpha-selective adrenergic agonist (1 mg ethylephrine or phenylephrine) solution with a 1:10 dilution ratio. One milliliter injections are made every 5 min into the corpora with a 21G butterfly as needed, up to 1 h; the alpha-adrenergic action antagonizes the vasodilator effects of injection with PGE-1 [6]. Blood pressure and pulse frequency must be controlled.

In particular, it has been shown that the administration of varying amounts (0.3, 0.5, or 1 ml) of ethylephrine 10 mg/1 ml in patients with an IR >90 and optimal clinical response at the end of PSD with FIC determine complete detumescence in all cases with no local or systemic side effects, including iatrogenic priapism [7, 8].

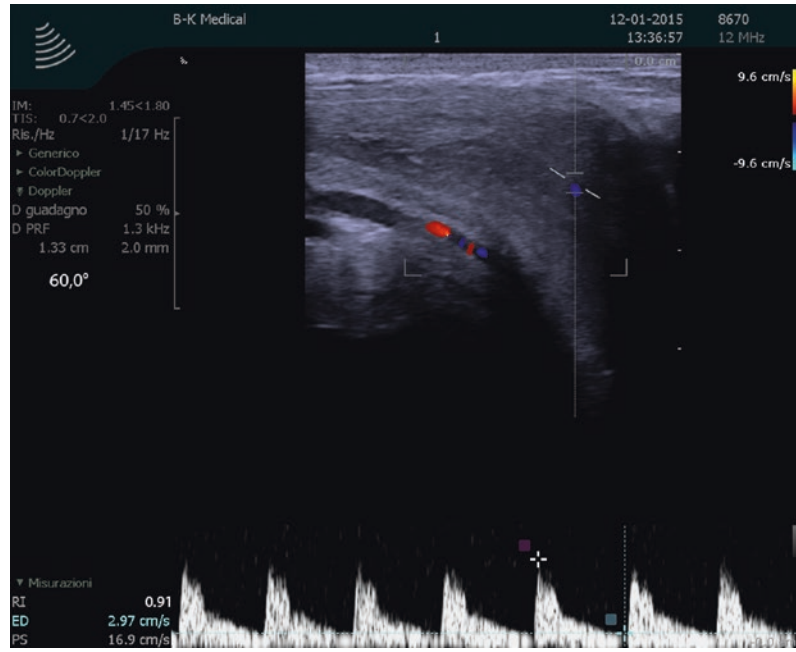

Fig. 46.3 Arteriogenic erectile dysfunction. Longitudinal scan. When fully turgid after intracavernosal administration of 20 micrograms prostaglandin E1 shows flows with low speed

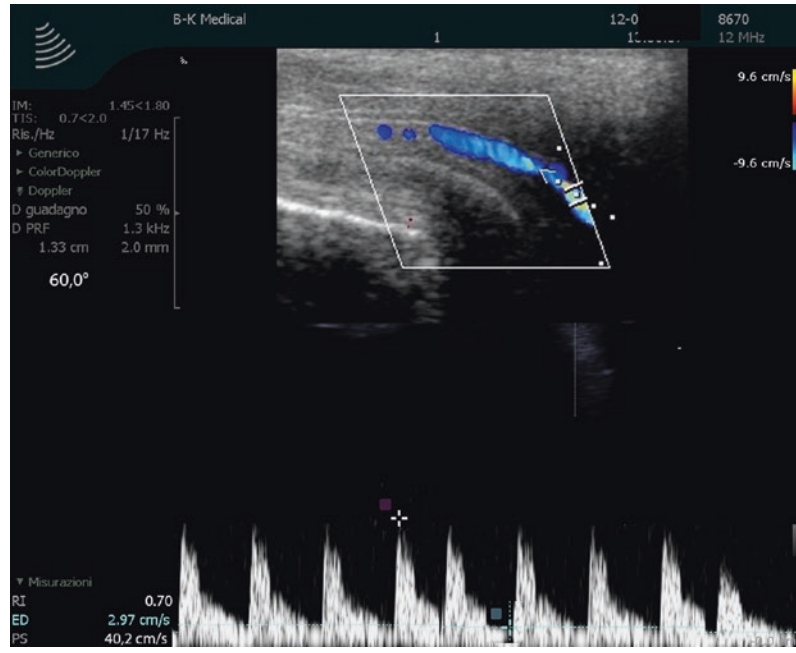

Fig. 46.4 Arteriogenic erectile dysfunction. Longitudinal scan. When fully turgid after intracavernous administration of 20 micrograms of prostaglandin E1 shows flows with high-speed peak that do not progress beyond the beginning stage of diastole

Conclusions

Nowadays, PDS with FIC is the ultrasound examination that can provide the most reliable and complete information for the study of the vascular system of the penis, especially when investigating the pathophysiology of erectile dysfunction. It is the most effective diagnostic tool available to the clinician to establish or rule out a vascular etiology of the disease, although we cannot disregard the importance of a careful sexual history and physical examination of the patient suffering from erectile dysfunction.

References

1. Lue TF. The mechanism of penile erection in the monkey. Semin Urol. 1986;4(4):217–24.
2. Lindau ST, Schumm LP, Laumann EO, et al. A study of sexuality and health among older adults in the United States. N Engl J Med. 2007;357(8):762–74.
3. Linee guida SIU (Società Italiana di Urologia) 2012 – Ecografia Urologica Ed Andrologica
4. Bettocchi C, Lucarelli G, Battaglia M, Selvaggi FP. Malattie dei Reni e delle Vie Urinarie: MacGraw-Hill- Cap. 25 pag. 613: Disfunzione erettile e disturbo dell'identità di genere
5. Cormio L, Bettocchi C, Zizzi V, Ricapito V, Pace G, Battaglia Atti del IX Congresso SIEUN 1996 Italia Ecocolor doppler penieno dinamico nella diagnostica dei disturbi dell'erezione
6. Aversa A, Sarteschi LM. The role of penile color-duplex ultrasound for the evaluation of erectile dysfunction. J Sex Med. 2007;4:1437–47.
7. Bratus D, Hlebic G, Hajdinjak T. Relation between intracavernosal dose of prostaglandin Pge 1 and mean duration of erection in men with different underlying causes of erectile dysfunction. Croat Med J. 2007;48(1):76–80.
8. Cormio L, Bettocchi C, Ricapito V, Zizzi V, Traficante A, Selvaggi FP. Resistance index as a prognostic factor for prolonged erection after penile dynamic colour doppler ultrasonography. Eur Urol. 1998;33(1):94–7.

Penile Ultrasound in Induratio Penis Plastica (IPP)

47

Marco Bitelli

Diagnostic imaging, especially ultrasound (US) scanning, is a mainstay in the evaluation and follow-up of Peyronie's disease (PD), or induratio penis plastica.

Diagnostic imaging for PD is substantially based on US – mainly penile ultrasound and colour Doppler sonography – and examination with soft x-rays. Magnetic resonance imaging (MRI) and computed tomography (CT) have a minor role. A further recently introduced imaging modality, sonoelastography (SEL), is based on the different elasticity of healthy and pathological tissue.

US imaging is not considered as a first-line examination by EAU 2010 guidelines (level of evidence 3, grade of recommendation C) [1], which in fact mention only home (self) photograph of a natural erection as a means to evaluate PD. However, in clinical practice the vast majority of urologists, andrologists and radiologists assess PD plaques by ultrasound due to its high diagnostic accuracy, reproducibility and cost-effectiveness.

US imaging is also a key approach to evaluate disease progression through the various stages [2].

Colour/power Doppler imaging provides objective data to assess vascular erectile function as well as the possible influence of tunica albuginea fibrosis on the veno-occlusive mechanism – a common problem in subjects with PD. It also provides valuable information to assess the scope for surgical management [3, 4], since the arising of vascular impairment concomitant with or subsequent to PD onset may respond to a combined surgical approach including penile curvature correction with a dermal patch and implantation of a penile prosthesis [3].

The accuracy, hence the diagnostic performance, of US is substantially affected by two factors, operator skill and equipment. As in other US diagnostic modalities, the procedure is heavily operator dependent with quite a steep learning curve. The scanner should be a last-generation machine endowed with the most recent image processing algorithms and a 5–12 MHz linear array transducer.

M. Bitelli
Servizio di Andrologia e Chirurgia Ricostruttiva UOC Urologia Ospedale S. Sebastiano Martire, Frascati, Rome, Italy
e-mail: marcobitelli@yahoo.com

P. Martino, A.B. Galosi (eds.), *Atlas of Ultrasonography in Urology, Andrology, and Nephrology*,
DOI 10.1007/978-3-319-40782-1_47

47.1 Baseline Ultrasound Scanning (B Mode)

It involves examination of all the anatomical structures of the penis (corpora cavernosa, tunica albuginea, Buck's fascia, intercavernous septum, corpus spongiosum and dorsal neurovascular bundle) with reporting of any abnormalities, particularly fibrous plaques.

Plaques may affect the dorsal, ventral and lateral tunica albuginea or the septum, with or without involvement of adjacent cavernous tissue.

The most frequent PD findings on B-mode ultrasound include:

- *Hyperechoic lesion without posterior acoustic shadowing*
  The intact tunica albuginea is depicted as a thin, predominantly hyperechoic line with variable echogenicity enveloping the corpora cavernosa bilaterally. Lesions appear as thickened and/or abnormal hyperechoic areas of the tunica or septum without posterior shadowing. Such findings account for 40–60 % of patients with early disease (inflammatory stage) [5, 6].
- *Hyperechoic lesion(s) with posterior acoustic shadowing*
  This is the most common US presentation.
  The lesion is depicted as a hyperechoic thickening of the tunica or septum with variable attenuation (posterior acoustic shadowing) due to plaque calcification [7] and is typical of stable disease (Figs. 47.1 and 47.2).
  These two presentations account for the majority of PD cases. Some patients however demonstrate less common findings that are often difficult to interpret.
  US examination approaches 100 % sensitivity in detecting and measuring calcified plaques.
- *Hypoechoic/isoechoic lesions*
  Plaques occasionally present as hypo-/isoechoic lesions with focal thickening around the corpora cavernosa [8]. Such lesions are typical of early disease, which is characterized by mild fibrosis, strong interstitial oedema [5] and retraction of the tunica albuginea at the level of the lesion, all of which result in penile curvature. In patients receiving stimulation with prostaglandin E_1 (PGE_1), US imaging depicts the actual extent of the lesion, which is often difficult to assess in the flaccid penis, and can sometimes document hyperechoic lesions that are detectable only under pharmacostimulation.
- *Focal defects of the tunica albuginea*
  Focal defects of the tunica associated with a thickened posterior area are found infrequently, except in large series. The surrounding tunica may not be thickened, but it may have an abnormal undulating appearance (Fig. 47.3).
- "*Hourglass*" *deformity*
  It is a hypoechoic or hyperechoic lesion of the tunica that involves its whole circumference, especially its proximal portion. Pharmacostimulation results in an hourglass shape of the shaft portion affected by fibrosis. It is not necessarily associated with a calcified plaque and may merely be the result of a circular lesion of the tunica [8].
  Negative US findings in presence of a clinically palpable plaque are frequently reported, but have not been specifically investigated.

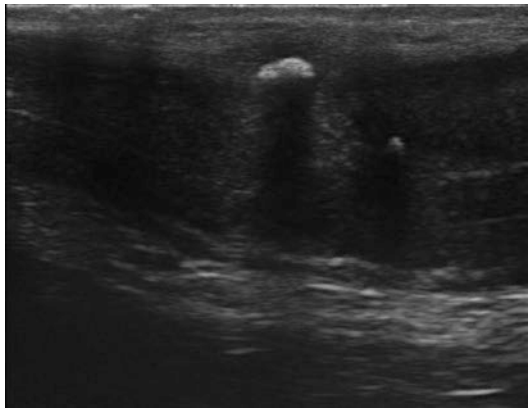

Fig. 47.1 Hyperechoic lesion(s) with posterior acoustic shadowing

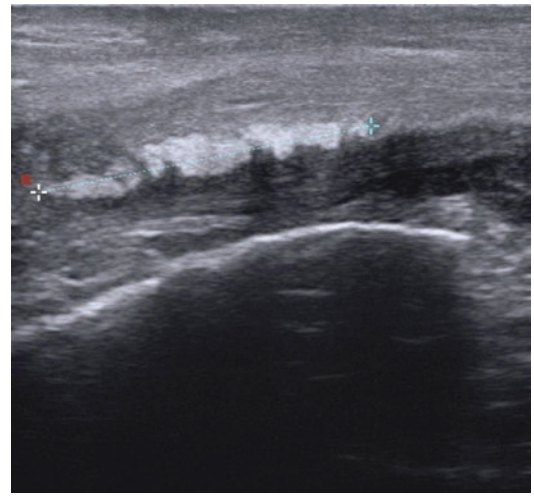

Fig. 47.2 Hyperechoic lesion of septum

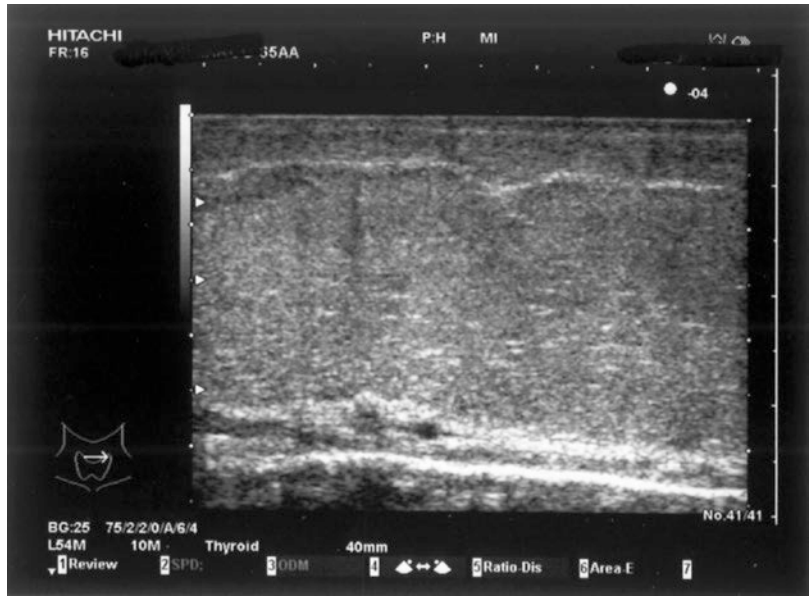

Fig. 47.3 Focal defect of the tunica albuginea

47.1.1 Colour Doppler Penile Ultrasonography

Colour Doppler penile ultrasonography is another useful US modality in the workup of suspected PD. It provides information on lesion morphology, structure and size as well as on vascular erectile function. The accuracy of US imaging, hence its diagnostic performance, depends on operator skill and equipment type. As in other US diagnostic modalities, there is a fairly steep learning curve. The scanner should be a last-generation machine endowed with the most recent image processing algorithms and a 5–12 MHz linear array transducer.

Before beginning the examination with the patient in supine position, accurate palpation is important since it allows to locate the plaque (or plaques in multifocal disease), assess its consistency and make a rough evaluation of its size, to form an idea of what will be depicted on the screen. Longitudinal and transverse scans need to be obtained along the ventral and dorsal aspects of the penis, including the urethral bulb and the crura by passing the transducer under the scrotum and along the perineum. All penile structures need to be assessed, including the tunica albuginea, corpora cavernosa, corpus spongiosum and glans, before evaluating the plaque(s). The examination consists of two phases, baseline and dynamic. The *baseline phase* involves investigation of tunica thickening (diffuse or localized); identification of plaque number, site and size; and assessment of any septum involvement. Longitudinal and transverse diameter and thickness are then measured, and plaque volume is calculated, usually automatically by the scanner. Any calcifications need to be identified, counted and individually measured for size. Plaque size and calcification are the main parameters to assess response to therapy.

The *dynamic phase* begins with intracavernosal injection of PGE_1 (usual dose 2.5/10 μcg). Spectral Doppler is essential to measure flow velocity at the level of the cavernous arteries and is commonly evaluated from the penile base, where the Doppler angle ensures more accurate measurement. Colour Doppler examination allows measuring peak systolic velocity (PSV) and end-diastolic velocity (EDV), which enable calculation of the resistance index (RI) and detection of normal helicine arteries and any cavernosum-spongiosum or cavernosum superficial shunting. Such measurements are performed at precise intervals, usually 5, 15 and 30 min from PGE_1 injection.

The erection induced in the dynamic phase also enables a photograph to be taken and calculation of the so-called angle of curvature, another useful measure for follow-up evaluation.

The subsequent morphological colour/power Doppler study of the microcirculation provides information on any associated vascular deficits, especially in patients with vasculopathy, diabetes or cardiovascular risk factors, where the three branches of the helicine arteries are difficult to depict if their angle is <90°, a finding that in turn is responsible for erectile dysfunction due to predominantly distal arterial disease.

The dynamic phase also depicts any site-specific venous leakage around the plaques – i.e. venous outflow on the edges of the hyperechoic lesion – which develops about 12 months from disease onset in patients with erectile dysfunction and a veno-occlusive defect documented by Doppler ultrasonography. These findings are seen in 12–20 % of patients and are responsible for secondary venous outflow [9] (Fig. 47.4).

In some patients with severe PD, persistent cavernosum-spongiosum shunts seen close to the plaques are associated with a higher PSV and a lower RI compared with the other cavernosum-spongiosum shunts, supporting the hypothesis that blood loss may also occur through these vessels [10].

According to some studies, Doppler examination can detect hyperperfusion around the plaques as a sign of inflammation in the active disease stage, whereas the absence of colour signal around them should be considered as a sign of disease stabilization [11, 12].

The most common vascular abnormality seen in PD patients is impaired veno-occlusive function [13]. In particular, they present an increased incidence of venous leakage than their peers [14]. Whereas in normal erection the venules draining the

corpora cavernosa are passively compressed by the expanded cavernosal tissue and the tunica albuginea, in PD patients the reduced elasticity of the tunica albuginea limits such stretching, preventing vein compression. As a consequence, Doppler flowmetry shows high diastolic velocity throughout the examination, with lower than normal RI values [15]. The severity of the veno-occlusive impairment is proportional to plaque extension and disease stage.

In patients with diseased deep cavernosal tissue due to plaque extension and severity or where the severe retraction involves its compression, the course of the cavernosal artery is affected, resulting in upstream perfusion deficit and signs of secondary arteriogenic deficiency. In such patients the reduced systolic values are accompanied by arterial entrapment on morphological colour/power Doppler (Fig. 47.5).

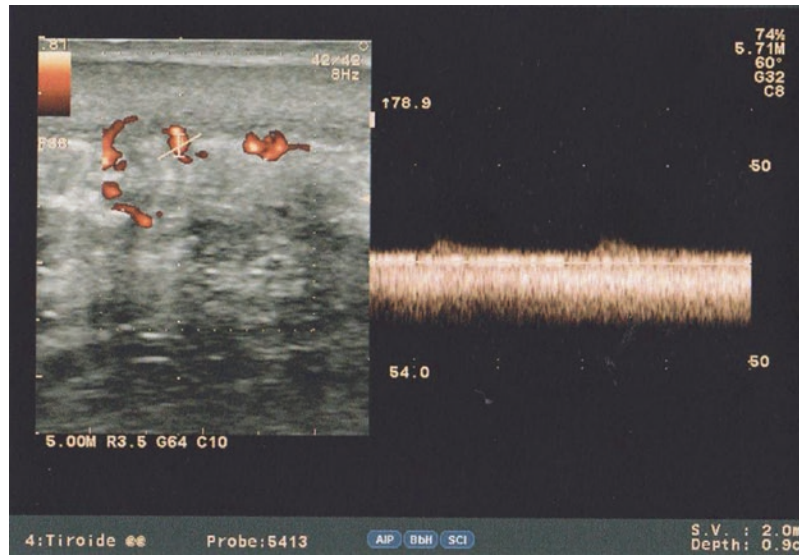

Fig. 47.4 Site-specific leak

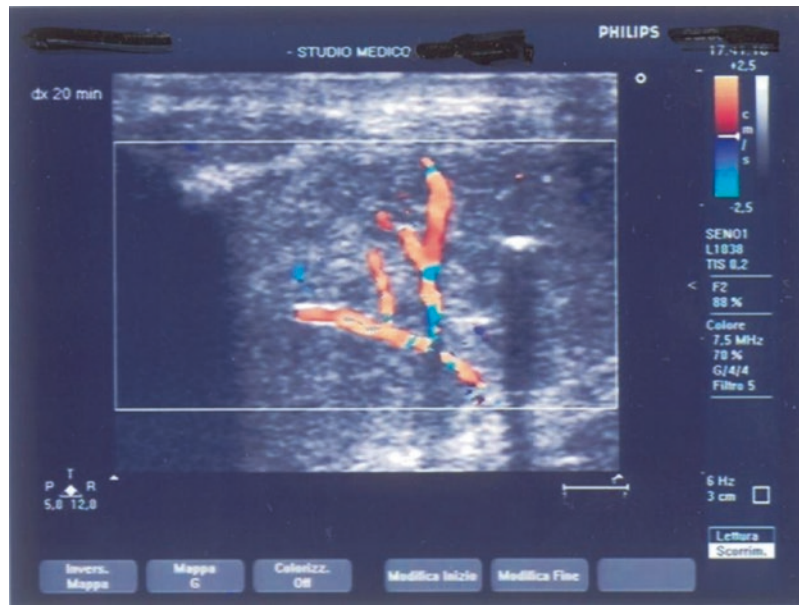

Fig. 47.5 Arterial entrapment secondary to plaque extension

47.1.2 Penile Radiography with Soft X-Rays

This technique exploits mammography units and applies x-rays with a wavelength >0.1 nm, which are especially suited to the examination of tissues like those of the penis. The approach is useful especially because of its ability to differentiate calcifications from surrounding fibrotic tissue, which, on US, share a similar echogenicity, affording more accurate measurement.

47.1.3 Penile Sonoelastography

Healthy and diseased human tissues are characterized by appreciable differences in their elastic properties. Indeed some conditions affecting tissues, such as tumours, induce changes that reduce soft tissue elasticity and mobility. This finding has inspired the notion that tissue elasticity may be assessed in vivo using US waves, i.e., US imaging, at least to examine the organs or glands lying close to the surface.

The method evaluates the change in radiofrequency pulses in a primary structure before and after manual compression (freehand SEL). The elastogram thus obtained is superimposed on the B-mode image as an overlay. The different elasticity of scanned tissues is shown in the form of a colour scale that ranges from red (elastic) to green (intermediate) and blue (stiff).

The examination lasts a few minutes and is usually the final scan after conventional US imaging has depicted suspicious nodules. Very few studies have used SEL to study penile conditions, and most of them have examined PD plaques.

In PD patients the fibrotic areas are blue. SEL is valuable in that it documents plaques in the septum, especially plaques that cannot be detected by B-mode US [16, 17]. In addition SEL can provide useful data, especially in early disease, by depicting changes in tissue inflammation around plaques [18].

47.1.3.1 Penile CT

CT examination can detect calcified PD plaques and determine their degree of calcification. However, it does not accurately depict non-calcified plaques. The information that is obtained from CT scanning does not justify its cost; therefore, the technique is seldom used to study PD plaques.

47.1.3.2 Penile MRI

MRI is the main diagnostic imaging approach used to evaluate penile trauma and fracture, penile carcinoma and selected PD patients.

In the latter subjects, MRI has proved less sensitive than US in depicting plaque extension and their relationship with adjacent structures, especially in the case of stable calcified plaques. Gadolinium-enhanced MRI has proved effective in detecting enhancement around plaques as a sign of active inflammation [19] and is more sensitive than grey-scale US scanning in assessing non-calcified plaques at the base of the penis [20]. It may also offer valuable information as an objective measure of response to therapy in patients receiving conservative drug treatment.

MRI is considered as a second-line diagnostic approach, but not due to poor diagnostic accuracy or sensitivity but rather because it cannot be used in routine clinical practice, also due to its poor cost-benefit ratio compared with US, which has become the mainstay of urological and andrological clinical practice.

MRI enables optimal visualization of penile anatomy, but does not provide significant advantages over standard diagnostic imaging techniques.

References

1. EAU Guidelines on Penile Curvature 2016; 1–21
2. Bekos A et al (2008) The natural history of Peyronie's disease: an ultrasonography-based study. Eur Urol 53:644–650
3. Ralph D, Gonzalez-Cadavid N, Mirone V et al (2010) The management of Peyronie's disease: evidence based 2010 guidelines. J Sex Med 7(7):2359–2374
4. Kadioglu A, Tefekli A, Erol H, Cayan S, Kandirali E (2000) Color Doppler ultrasound assessment of penile vascular system in men with Peyronie's disease. Int J Impot Res 12:263–267
5. Prando D (2009) J Ultrasound Med 28:217–232
6. Smith JF, Brant WO, Fradet V, Shindel AW, Vittinghoff E, Chi T, Huang YC, Davis CB, Conti S, Lue TF (2009) Penile sonographic and clinical characteristics

in men with Peyronie's disease. J Sex Med 6:2858–2867
7. Balconi G, Angeli E, Nessi R, de Flaviis L (1998) Ultrasonographic evaluation of Peyronie's disease. Urol Radiol 10:85–88
8. Kalokairinou K et al (2012) US imaging in Peyronie's Disease. J Clin Imaging Sci 2:63
9. Deveci S, Palese M, Parker M, Guhring P, Mulhall JP (2006) Erectile function profiles in men with Peyronie's disease. J Urol 175:1807–1811
10. Bertolotto M, Coss M, Neumaier C (2008) U/S evaluation of patients with Peyronie disease. In: Bertolotto M (ed) Color Doppler US of the penis. Springer-Verlag, Berlin, pp 61–69
11. Fornara P, Gerbershagen HP (2004) Ultrasound in patients affected with Peyronie's disease. World J Urol 22:365–367
12. Chen TY, Zahran AR, Carrier S (2001) Penile curvature associated with scleroderma. Urology 58:282
13. Montorsi F, Guazzoni G, Bergamaschi F, Consonni P, Rigatti P, Pizzini G et al (1994) Vascular abnormalities in Peyronie's disease: the role of color Doppler sonography. J Urol 151:373–375
14. Kadioglu A, Tefekli A, Erol B, Oktar T, Tunc M, Tellaloglu S (2002) A retrospective review of 307 men with Peyronie's disease. J Urol 168:1075–1079
15. Wilkins CJ, Sriprasad S, Sidhu PS (2003) Colour Doppler ultrasound of the penis. Clin Radiol 58:514–523
16. Pinggera G.M, Assessment of Peyronie disease by sonoelastography: preliminary results American urological association annual meeting, 19–24 May 2007, Anaheim, USA
17. Richards G, Goldenberg E, Pek H, Gilbert BR (2014) Penile Sonoelastography for the localization of a non-palpable, non-sonographically visualized lesion in a patient with penile curvature from Peyronie's disease. J Sex Med 11:516–520
18. Gazhonova V. Real-time sonoelastography in peyronie`s disease: preliminary results in diagnosis and staging European congress of radiology, 6–9 Mar, 2009, Vienna, Austria
19. Bertolotto M, Pavlica P, Serafini G, Quaia E, Zappetti R (2009) Painful penile induration: imaging findings and management. Radiographics 29:477–93
20. Vossough A, Pretorius ES, Siegelman ES, Ramchandani P, Banner MP (2002) Magnetic resonance imaging of the penis. Abdom Imaging 27:640–659

Penile Trauma and Priapism

48

Michele Bertolotto, Massimo Valentino, Francesca Currò, Mariano Iannelli, Gladiola Kaso, and Libero Barozzi

48.1 Introduction

Since the penis is mobile and largely protected by its position, it is much less frequently injured than other parts of the body. However, it can be wounded as a result of various injuries, including road or work accidents, gunshot wounds, burns, sexual activity and, in the case of mental disturbance, self-mutilation.

When a person sustains a penile injury, imaging can be required to better assess the damage and lead to appropriate therapy, either surgical or conservative. From the clinical point of view, the first important distinction is between penetrating and non-penetrating traumas. Moreover, it is important to assess whether a non-penetrating penile trauma occurred when the penis was flaccid or erect, since the resulting injuries are essentially different.

Because of its panoramicity, multiplanar capability and excellent tissue contrast, magnetic resonance imaging is the best diagnostic tool for the evaluation of the integrity of the tunica albuginea even in patients with severe pain and swelling of the penis. Ultrasonography, however, is often the only available method in emergency. In expert hands, when performed with high-end equipment using high-resolution and high-frequency probes, colour Doppler ultrasonography can provide enough clinically useful information to guide the management of the patient.

Electronic supplementary material The online version of this chapter (doi:10.1007/978-3-319-40782-1_48) contains supplementary material, which is available to authorized users.

M. Bertolotto, MD (✉) • F. Currò • M. Iannelli
G. Kaso
Department Radiology, University of Trieste,
Ospedale di Cattinara, Strada di Fiume 447,
Trieste 34124, Italy
e-mail: bertolot@units.it

M. Valentino
S.O.C. Radiologia ASS 3 FVG, Ospedale
Sant'Antonio Abate, Via Morgagni 18,
Tolmezzo (UD) 33028, Italy

L. Barozzi
Radiology Unit, Casa di Cura Madre Fortunata
Toniolo, Via Toscana 34, Bologna 40141, Italy

P. Martino, A.B. Galosi (eds.), *Atlas of Ultrasonography in Urology, Andrology, and Nephrology*,
DOI 10.1007/978-3-319-40782-1_48

48.2 Penetrating Injuries to the Penis

Diagnosis of penetrating traumas to the penis is usually straightforward. Imaging is rarely required but in complex situations which need careful preoperative assessment and in complex traumas involving the pelvis [1]. In patients with genital gunshot wounds, ultrasonography can have a role to identify haematomas, localized bullets and other foreign bodies retained within the penis and guide retrieval. Exact location of these bodies is important to ease extraction and to avoid unnecessary manipulation of the cavernous tissue, which can further affect the erectile condition of the patient. Colour Doppler interrogation of cavernosal arteries allows evaluation of associated vascular injuries. During the follow-up, cavernositis and abscess formation can be evaluated.

Rarely high-flow priapism may follow iatrogenic penetrating traumas. Shunting procedures performed in patients with low-flow priapism or needle insertion in the shaft can result in injury of a cavernous artery or of its branches [2, 3].

48.3 Non-penetrating Injuries to the Erect Penis

Most of the traumas to the erect penis result from sudden bending of the shaft during sexual foreplay, intercourse or masturbation. Penile fracture consists in rupture of the tunica albuginea of one or both corpora cavernosa associated with urethral injury in 10–20 % of cases.

Diagnosis of albugineal disruption is based on characteristic history of severe pain with a cracking or popping sound during acute bending of the erect penis, followed by immediate detumescence, penile swelling and deformity. However, imaging may be required, particularly in patients with atypical clinical presentation, limited penile haematoma and minor penile deformity or, on the contrary, with severe local pain or swelling that prohibits a thorough physical examination of the penis [4].

When available, MR imaging is the best modality in the evaluation of patients with penile fracture. Because of its multiplanar capability and excellent tissue contrast, MR imaging provides superb soft-tissue definition, depicting interruption of the cavernosal low-signal-intensity tunica albuginea even in patients with severe pain and swelling of the penis [5–7]. This capability makes MR imaging particularly helpful in determining the need for surgical intervention, which is largely based on the integrity of the tunica albuginea. However, MR imaging often is not performed in the acute setting. In expert hands, ultrasonography is able to detect the interruption of the echogenic line of the tunica albuginea [1, 8]. It can evaluate the length of the albugineal defect, determine whether cavernosal tissue is severely injured or not and examine for associated vascular injuries and haematomas (Fig. 48.1). This evaluation requires a skilled sonologist and use of high-end equipment. Identification of associated urethral injury can be difficult on ultrasound.

In traumas with intact tunica albuginea, extra-albugineal haematomas may result from rupture of the dorsal vessels or their branches [1]. Venous injuries are relatively more frequent than arterial injuries, and rupture of small venous collaterals is more common than injury to the main branches. Torn veins collapse and are not visible directly with ultrasonography, but occasionally they may undergo posttraumatic thrombosis and present at ultrasonography as noncompressible enlarged vessels with echogenic content (Fig. 48.2). If an arterial injury is associated, a posttraumatic arteriovenous fistula may develop [8]. Doppler interrogation shows dilatation of the injured vein; high-velocity, low-resistance arterial flows; and high-velocity turbulent venous flows. Isolated rupture of the deep dorsal vessels usually produce haematomas confined to the space beneath the Buck's fascia, involving only the penile shaft. When the Buck's fascia is disrupted, or superficial penile vessels are injured, the haematoma spreads through the subcutaneous tissue and in the space between the Colles' and the Buck's fascia involving the pubis, the scrotum and the perineum with characteristic "butterfly" configuration (Fig. 48.3). If an arterial lesion is associated, a posttraumatic arteriovenous fistula may result and be identified at colour Doppler interrogation.

Injury to the erect penis may produce isolated disruption of the penile septum [9]. Ultrasonographic evaluation allows identification of the resulting haematoma as a well-defined cystic-like area in the septal region (Fig. 48.4). Aspiration under ultrasound guidance is recommended to prevent circumscribed septal fibrosis and its associated symptoms, such as penile shortening or focal lack of rigidity.

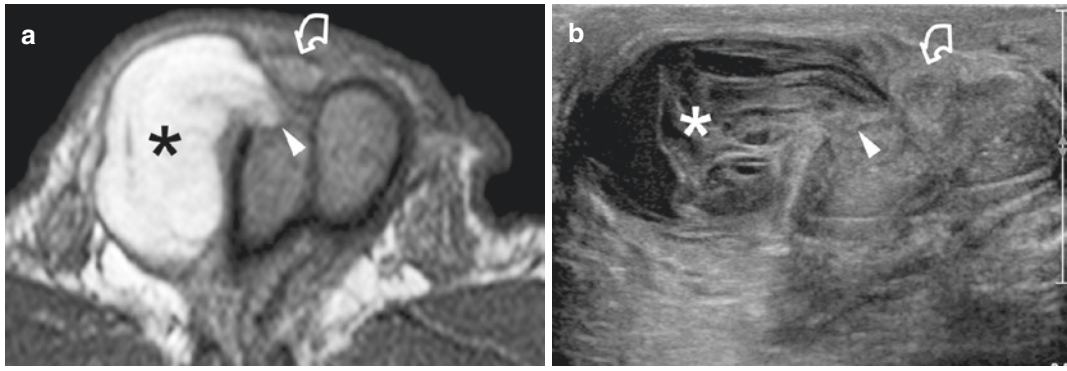

Fig. 48.1 Penile fracture of the right corpus cavernosum. (**a**) Axial T2-weighted scan shows the lesion as a ventral interruption (*arrowhead*) of the low-signal-intensity tunica albuginea. There is an associated extraalbugineal haematoma (*asterisk*). The left corpus cavernosum is intact. (**b**) Corresponding ultrasonographic scan showing the same features. The injury is identified as a ventral interruption of the echogenic line of the tunica albuginea (*arrowhead*) with associated extraalbugineal haematoma (*asterisk*). *Curved arrows* indicate the corpus spongiosum, which is intact in this patient

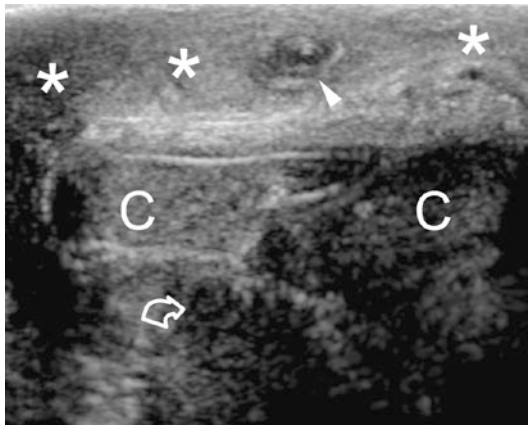

Fig. 48.2 Posttraumatic thrombosis of a superficial penile vein. Axial ultrasonographic view obtained with the transducer on the dorsal aspect of the penile shows blood extravasation in the superficial tissues (*asterisks*). A noncompressible enlarged vessel with echogenic content is seen (*arrowhead*) lacking vascularization at colour Doppler interrogation. The tunica albuginea is intact. *C* corpora cavernosa. *Curved arrow* indicates the corpus spongiosum

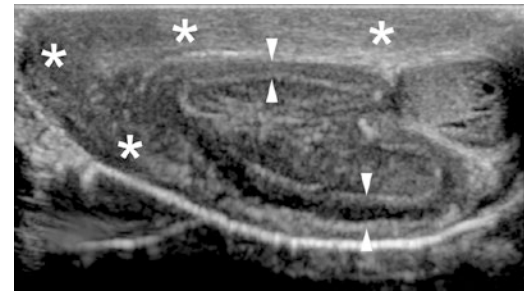

Fig. 48.3 Extracavernosal haematomas. *Arrowheads* indicate haematoma between the tunica albuginea and the Buck's fascia. *Asterisks* indicate haematoma spreading outside the Buck's fascia

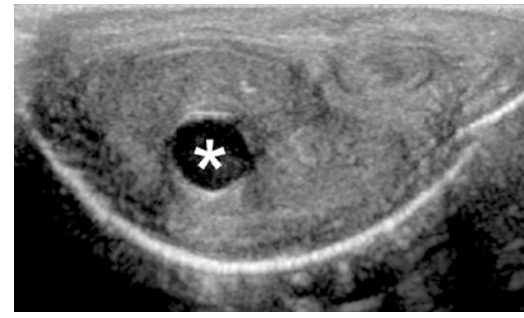

Fig. 48.4 Isolated septal haematoma. The patient presented with a lump in the mid-shaft 10 days after severe bending of the erect penis during intercourse associated with pain. Axial ultrasonographic scan shows a well-defined cystic-like lesion within the septum (*asterisk*), consistent with posttraumatic haematoma

48.4 Non-penetrating Injuries to the Flaccid Penis

Non-penetrating traumas to the flaccid penis usually follow blunt perineal injuries. The cavernosal crura are crushed against the pelvic bones. Ultrasonography allows evaluation of extratunical and cavernosal haematomas (Fig. 48.5) and of the tunica albuginea which is usually intact in these patients [1, 8]. Cavernosal artery disruption with formation of an arterial-lacunar fistula presents clinically with high-flow priapism. Colour Doppler ultrasonography is currently considered the imaging modality of choice in patients with high-flow priapism since it is sensitive, non-invasive and widely available [10]. Greyscale ultrasonography demonstrates the area of laceration of the cavernosal tissue as a hypoechoic region within the echogenic corpus cavernosum. In this area, colour Doppler interrogation demonstrates a characteristic arterial colour blush, consistent with extravasation of blood from the torn artery. Doppler interrogation of the fistula results in high-velocity, turbulent flows (Fig. 48.6, Video 48.1). Besides the arterial-lacunar fistula, the penile vasculature can be evaluated to identify the feeding vessels [10].

A careful Doppler technique allows a better evaluation of all vascular structures involved. Optimization of the colour Doppler parameters to detect low-velocity flows allows evaluation of the penile vessels and eases identification of the colour blush from the torn artery. However, visualization of high-velocity flows is not correct, and aliasing hampers visualization of the exact site of the cavernosal tear. When colour Doppler velocity scale is increased, depiction of lower-velocity flows is reduced, and the cavernosal tear is immediately recognized as a circumscribed colour spot displaying aliasing [10].

Besides identification of the arterial-lacunar fistula, colour Doppler ultrasonography allows evaluation of the penile vasculature to identify haemodynamically significant feeding vessels, providing useful information in patients undergoing embolization [11]. Usually the main feeding vessel is a cavernosal artery; a variety of collaterals can be associated, however. In particular, dorsal to cavernosal artery communications represent large vascular pathways that are able to feed the fistula and may be responsible to treatment failure after embolization of the torn cavernosal artery. Also intracavernosal arterial communications can connect the proximal portion of the torn artery with the contralateral cavernosal artery and be responsible of treatment failure. Cavernosal-spongiosal communications and other small collaterals can feed the fistula as well [11].

In patients with high-flow priapism, high-velocity systolic flows are observed at Doppler interrogation in both cavernosal arteries also when only one vessel is torn. Large communications exist between the corpora, and nitric oxide released at the level of the fistula diffuses freely in the contralateral side. Diastolic flow is variable, depending on blood pressure within the partially erected bodies. The firmer the erection, the lower the diastolic pressure.

Superselective embolization of the torn artery is currently the treatment of choice for high-flow priapism [12]. After the procedure, colour Doppler ultrasonography is performed to assess the results. Complete closure of the arterial-sinusoidal fistula can be found, or the fistula may be still patent despite arteriographic evidence of occlusion fed by non-obliterated collaterals [10, 11]. In our experience, if the fistula is smaller and penile turgidity is reduced after embolization, spontaneous closure will likely occur within few days due to reduced hyperoxygenation and endothelial shear stress. When a more significant blood supply is demonstrated at colour Doppler interrogation and penile turgidity remains unchanged in the following days, repeat angiography should be considered.

During the follow-up of patients with high-flow priapism, we recommend colour Doppler ultrasound 1–2 months after embolization to rule out the appearance of a recurrent fistula. Recanalization of the embolized cavernosal artery can be observed also when non-reabsorbable embolization material has been used [10, 13]. In patients with erectile dysfunction, the study should be performed after intracavernosal prostaglandin injection to determine whether the functional impairment is caused or not by insufficient penile blood flow [10].

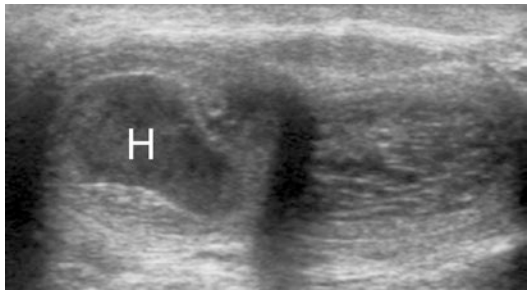

Fig. 48.5 Intracavernosal haematoma (*H*) in the right corpus of a patient who crushed the base of the penis against the petrol tank of his motorbike

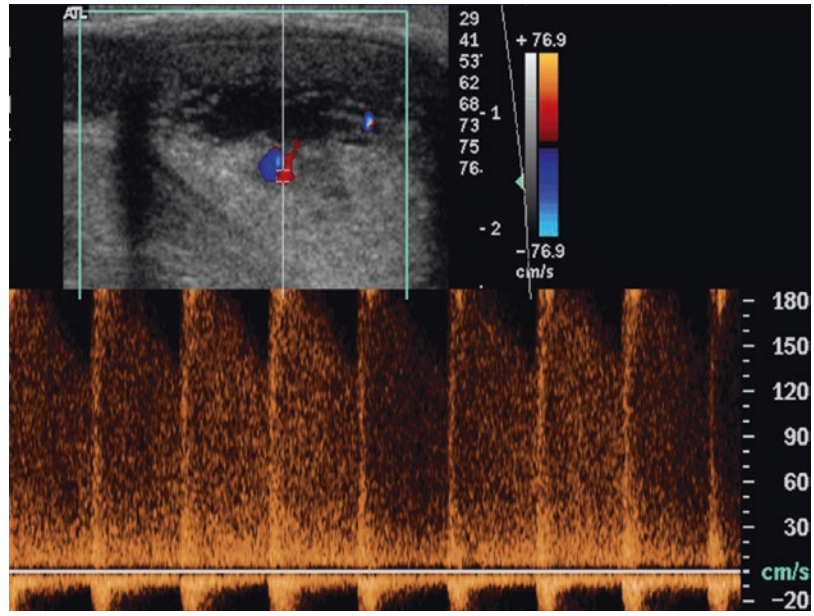

Fig. 48.6 Posttraumatic high-flow priapism. Duplex Doppler interrogation of the cavernosal artery tear showing high-velocity, turbulent flows

48.5 Ischaemic Priapism

Imaging is usually not required in patients with ischaemic priapism because this condition is considered a urological emergency, and diagnosis is based on clinics and corporeal aspiration of non-oxygenated blood. However, there is increasing evidence that the degree of venous outflow obstruction and ischaemia varies from person to person. Some patients regain potency even after days of priapism. On the contrary, other patients lose potency in a much shorter period of time. In patients with low-flow priapism, greyscale and colour Doppler ultrasonography provide information of prognostic value. The corpora cavernosa initially present with normal echogenicity and echotexture, and the corpuscolate component of blood tends to sediment downwards forming a fluid-fluid level. In more advanced situations, the corpora present with increased echogenicity, probably associated with tissue oedema. Occasionally echogenic material obliterates the cavernosal arteries [14]. In long-standing ischaemic priapism, wide echotexture alterations are recognized, consistent with fibrotic changes. Colour Doppler interrogation of cavernosal arteries may show different flow characteristics. High-peak systolic velocity and holodiastolic flow reversal can be appreciable. In other cases, progressive reduction of the peak systolic velocity is observed, till termination.

In our clinical experience, if the cavernosal arteries are patent with high-velocity flows, the patient will likely recover erectile function after the treatment within few weeks (Fig. 48.7), while patients with obliterated arteries usually develop irreversible erectile dysfunction (Fig. 48.8) [14].

The treatment of low-flow priapism typically follows a pattern of least invasive to more invasive procedures starting from penile aspiration, irrigation with saline and cavernosal injections of alpha-adrenergic receptor agonists. If these relatively simple measures fail, a variety of surgical shunts can be created between the glans and corpora cavernosa. When transglandular shunts are manufactured, they can be identified on greyscale ultrasonography as anechoic tubular ways with irregular margins extending from the glans deep into the corpora cavernosa. Interruption of the tunica albuginea at the tip of the corporeal bodies is identified [15]. Colour Doppler interrogation is not able to investigate the patency of the shunt because of very low-velocity flows. When this information is needed, microbubbles can be injected into the corpora and followed along the course of the shunts towards the glans.

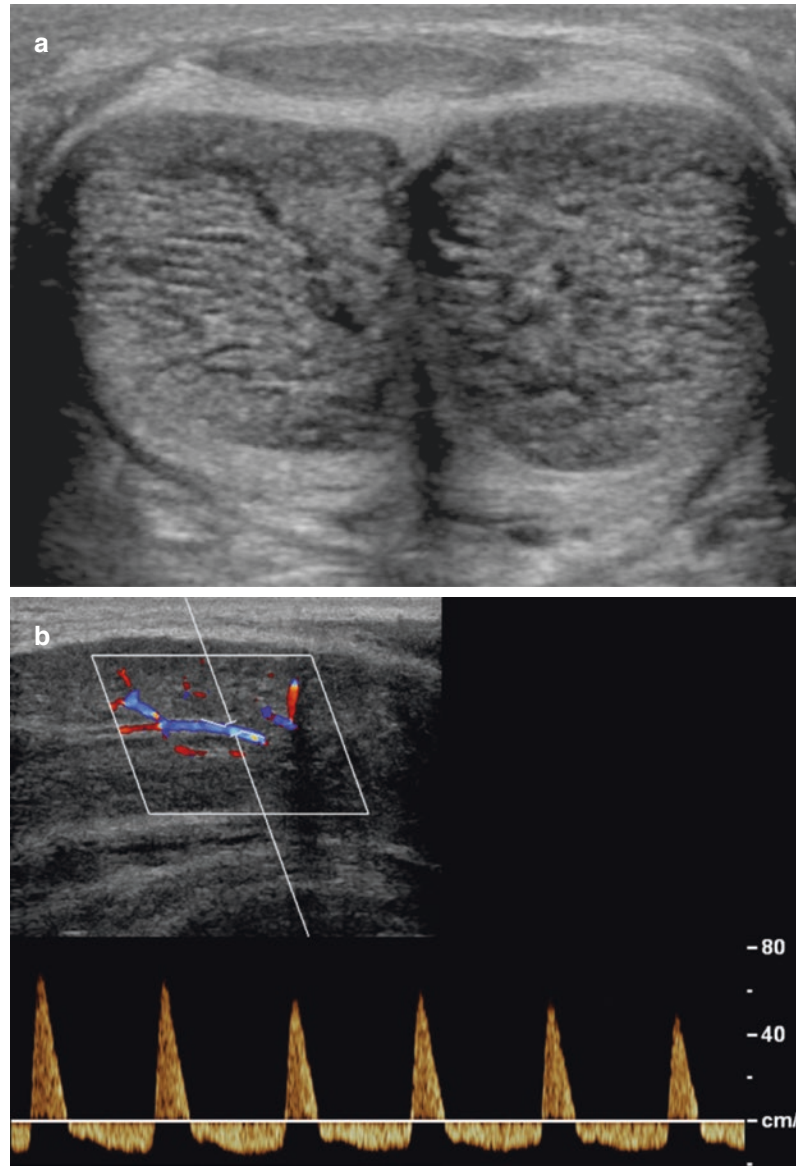

Fig. 48.7 Low-flow priapism lasting since 12 h. (**a**) Greyscale ultrasonography shows normal echotexture of the corpora cavernosa. (**b**) Spectral Doppler interrogation of the cavernosal arteries shows high-velocity flows (50 cm/s) with diastolic flow reversal. Priapism relieved with blood aspiration and injecting alpha-adrenoreceptor drugs

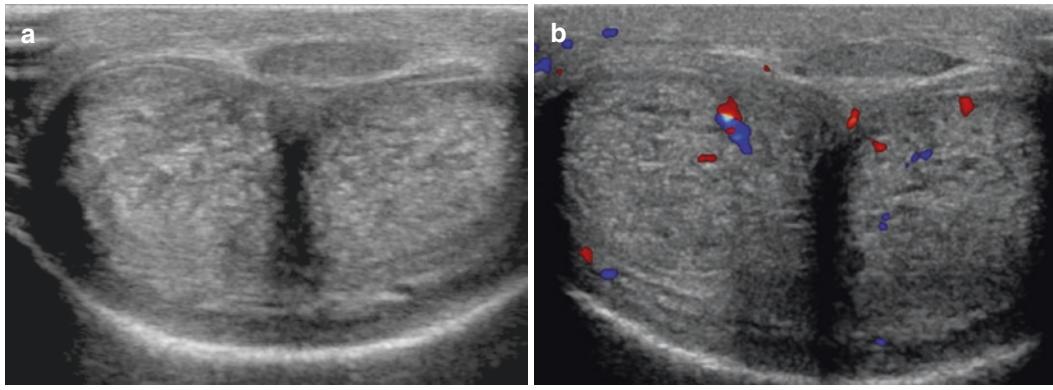

Fig. 48.8 Low-flow priapism lasting since 3 days. (**a**) Greyscale ultrasonography shows increased echogenicity of the cavernosal tissue, consistent with oedema. (**b**) Colour Doppler interrogation shows obliteration of the cavernosal arteries. Small vessels feed the periphery of the cavernosal bodies. The patient underwent surgical shunting but developed irreversible erectile dysfunction

48.6 Stuttering Priapism

Stuttering priapism, also known as recurrent ischaemic priapism, is a variant of the ischaemic type characterized by repetitive, transient, painful and self-limiting episodes of priapism. Pathophysiology is poorly understood and treatment is not yet clearly defined. It is often idiopathic or associated with various haematological disorders. If left untreated, stuttering priapism may evolve into the classic form of acute ischaemic priapism and lead to erectile dysfunction due to fibrosis of corpora cavernosa. Imaging appearance of stuttering priapism is poorly investigated. In our series of five patients investigated during the priapic episodes, colour Doppler interrogation showed high-velocity, high-resistance flow in the cavernosal arteries with diastolic flow disappearance or reversal, similar to cavernosal waveform changes observed in normal erection. When turgidity faded, relatively high-velocity, low-resistance flows are recorded, consistent with hyperafflux. The greyscale appearance of the cavernosal tissue is normal.

48.7 "Malignant" Priapism

Invasion of the corpora cavernosa by tumour tissue, either primary or secondary malignancies, can present with penile stiffness and pain simulating low-flow priapism. In these patients, greyscale ultrasonography can show circumscribed tumour nodules within the corpora cavernosa (Fig. 48.9) or diffuse infiltration of the shaft [14, 16]. When metastases spread from adjacent organs, disruption of the tunica albuginea can be identified along the pathway of tumour invasion. Doppler interrogation usually shows hypervascular cavernosal bodies due to tumour lesion vascularity; cavernosal artery flows are variable. Venous stasis can be associated, resulting from infiltrations of the normal venous leakage pathways. Contrast-enhanced ultrasound (CEUS) often eases differentiation between normal cavernosal tissue and tumour infiltration, which usually displays different enhancement kinetics.

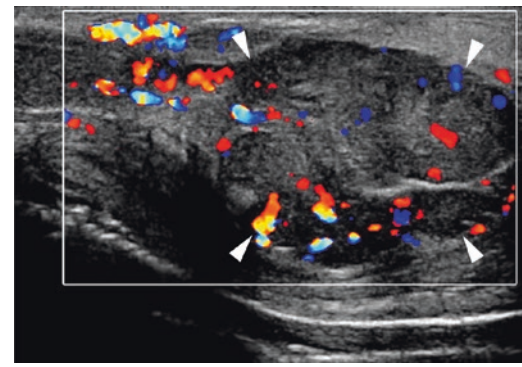

Fig. 48.9 Metastatic involvement from prostate cancer. A 79-year-old patient with already known prostate cancer presented with painful induration of the penis. Colour Doppler ultrasonography shows tumour tissue growing within the corpora cavernosa, most prominent in the crura (*arrowheads*), consistent with metastatic deposits of the prostatic cancer

48.8 Scarring and Fibrosis

Untreated albugineal disruption can result in segmental fibrosis characterized at ultrasonography by echogenic foci within the corpus cavernosum showing reduced expansion during erection. The lesions are already visible on ultrasonography when the penis is flaccid, but they are more prominent with erection when the surrounding sinusoids are distended with blood. During the erection, the fibrotic scars may cause penile bending. Cavernosal-spongiosal communications can remain patent near the scar also when the penis is erect with high-velocity, low-resistance flows, causing venous leakage and venous-occlusive erectile dysfunction.

Low-flow priapism is a well-known cause of diffuse cavernosal tissue fibrosis. Cavernosal tissue damage leading to fibrotic changes can occur also in patients with stuttering priapism and, occasionally, with long-standing high-flow priapism. Other situations associated with diffuse cavernosal tissue fibrosis are penile irradiation or denervation and cavernositis. At ultrasonography diffuse cavernosal fibrosis is recognized as hyperechogenic tissue prevailing around the cavernosal arteries and replacing the sinusoids of the corpora cavernosa. Little or no changes are appreciable after prostaglandin intracavernosal injection. Doppler interrogation usually shows pathological waveform changes in the cavernosal arteries consistent with veno-occlusive dysfunction. Peak systolic velocity is variable. When impairment of the cavernosal artery inflow is present, small peripheral vessels can be demonstrated feeding the outer portions of the corpora through collaterals from extra-albugineal vessels. After microbubble contrast agent injection, the corpora characteristically display reduced enhancement around the cavernosal arteries and prominent vascularization of the sub-albugineal space.

Conclusions

In patients with penile traumas, an excellent depiction of the tunica albuginea is obtained at greyscale ultrasonography with identification of tears and other pathological changes. Side, site and anatomical relationships of fluid collections can be readily identified, and colour Doppler interrogation allows full evaluation of the penile vasculature and of its changes. Colour Doppler ultrasonography is the imaging modality of choice for the diagnosis of high-flow priapism and to evaluate penile blood flow changes after angiographic embolization of the injured vessel. In low-flow priapism, greyscale and colour Doppler modes can have a prognostic value. If the sonologist is confident with ultrasonographic penile anatomy and its changes, other imaging techniques such as cavernosography and magnetic resonance imaging are rarely needed to evaluate patients with penile traumas and priapism.

References

1. Bertolotto M, Calderan L, Cova MA (2005) Imaging of penile traumas – therapeutic implications. Eur Radiol 15(12):2475–2482. doi:10.1007/s00330-005-2900-0
2. Bertolotto M, Ciampalini S, Martingano P, Mucelli FP (2009) High-flow priapism complicating ischemic priapism following iatrogenic laceration of the dorsal artery during a winter procedure. J Clin Ultrasound JCU 37(1):61–64. doi:10.1002/jcu.20479
3. Liguori G, Garaffa G, Trombetta C, Capone M, Bertolotto M, Pozzi-Mucelli F, Belgrano E (2005) High-flow priapism (HFP) secondary to Nesbit operation: management by percutaneous embolization and colour Doppler-guided compression. Int J Impot Res 17(3):304–306. doi:10.1038/sj.ijir.3901251
4. Pavan N, Tezzot G, Liguori G, Napoli R, Umari P, Rizzo M, Chiriaco G, Chiapparrone G, Vedovo F, Bertolotto M, Trombetta C (2014) Penile fracture: retrospective analysis of our case history with long-term assessment of the erectile and sexological outcome. Archivio Italiano Di Urologia, Andrologia Organo Ufficiale [Di] Societa Italiana Di Ecografia Urologica e Nefrologica/Associazione Ricerche In Urologia 86(4):359–370. doi:10.4081/aiua.2014.4.359
5. Pretorius ES, Siegelman ES, Ramchandani P, Banner MP (2001) MR imaging of the penis. Radiographics: a review publication of the Radiological Society of North America, Inc 21 Spec No:S283–298; discussion S298–289. doi:10.1148/radiographics.21.suppl_1.g01oc24s283
6. Choi MH, Kim B, Ryu JA, Lee SW, Lee KS (2000) MR imaging of acute penile fracture. Radiographics Rev Publ Radiol Soc N Am Inc 20(5):1397–1405. doi:10.1148/radiographics.20.5.g00se051397
7. Avery LL, Scheinfeld MH (2013) Imaging of penile and scrotal emergencies. Radiographics Rev Publ

Radiol Soc N Am Inc 33(3):721–740. doi:10.1148/rg.333125158
8. Bertolotto M, Mucelli RP (2004) Nonpenetrating penile traumas: sonographic and Doppler features. AJR Am J Roentgenol 183(4):1085–1089. doi:10.2214/ajr.183.4.1831085
9. Brant WO, Bella AJ, Garcia MM, Tantiwongse K, Dean RC, Lue TF (2007) Isolated septal fibrosis or hematoma – atypical Peyronie's disease? J Urol 177(1):179–182. doi:10.1016/j.juro.2006.08.065; discussion 183
10. Bertolotto M, Quaia E, Mucelli FP, Ciampalini S, Forgacs B, Gattuccio I (2003) Color Doppler imaging of posttraumatic priapism before and after selective embolization. Radiographics Rev Publ Radiol Soc N Am Inc 23(2):495–503. doi:10.1148/rg.232025077
11. Bertolotto M, Zappetti R, Pizzolato R, Liguori G (2008) Color Doppler appearance of penile cavernosal-spongiosal communications in patients with high-flow priapism. Acta Radiol 49(6):710–714. doi:10.1080/02841850802027026
12. Ciampalini S, Savoca G, Buttazzi L, Gattuccio I, Mucelli FP, Bertolotto M, De Stefani S, Belgrano E (2002) High-flow priapism: treatment and long-term follow-up. Urology 59(1):110–113
13. Savoca G, Pietropaolo F, Scieri F, Bertolotto M, Mucelli FP, Belgrano E (2004) Sexual function after highly selective embolization of cavernous artery in patients with high flow priapism: long-term followup. J Urol 172(2):644–647. doi:10.1097/01.ju.0000132494.44596.33
14. Bertolotto M, Pavlica P, Serafini G, Quaia E, Zappetti R (2009) Painful penile induration: imaging findings and management. Radiographics Rev Publ Radiol Soc N Am Inc 29(2):477–493. doi:10.1148/rg.292085117
15. Bertolotto M, Serafini G, Savoca G, Liguori G, Calderan L, Gasparini C, Mucelli RP (2005) Color Doppler US of the postoperative penis: anatomy and surgical complications. Radiographics Rev Publ Radiol Soc N Am Inc 25(3):731–748. doi:10.1148/rg.253045100
16. Bertolotto M, Serafini G, Dogliotti L, Gandolfo N, Gandolfo NG, Belgrano M, Prefumo F (2005) Primary and secondary malignancies of the penis: ultrasound features. Abdom Imaging 30(1):108–112

Part VII

New Technologies

3D US

49

Pasquale Martino and Silvano Palazzo

49.1 Introduction

The use of 3D ultrasonography in urology is a recent acquisition that has been developed in the last few years. The versatility of the 3D US device, as well as the huge potential offered by image acquisition on a third scanning plane, makes this a highly promising tool in the urologist's hands for use in diagnostic workup and to make a close study of the diseases more commonly observed in clinical practice. The multiplane images and pictures of the surfaces that can be obtained in 3D optimize the knowledge of the anatomical structures, guaranteeing more detailed images and, in practice, better measurements and diagnostic insights than traditional ultrasound.

The history of three-dimensional ultrasound is very recent. The first 3D device was presented to the public during the International Congress of Radiology held in Paris in 1989. The 3D method in current use is the fruit of technological evolutions and, in particular, of computer processing of the ultrasound images obtained.

These 3D devices are designed to acquire a large number of images in a very short time. The images are memorized and can be inspected by the operator and selected according to the information they offer. Three images are displayed simultaneously on the monitor, representing the sagittal, transverse, and coronal images of the organ under study. The latter plane is an artificial section obtained by computer processing of the images obtained on the other two scanning planes (Fig. 49.1). While immobilizing the image on one of the three planes, it is possible to move the cursor over the other two planes to follow the anatomical structures, delineate pathological areas, and define margins and relationships.

The US device also makes it possible to perform Doppler studies of the arterial and venous vessels and, thanks to the software applied, subtraction studies can be made, thereby visualizing the entire vascular tree of the organ under study, "cleared" of US images taken simultaneously that are extraneous to the specific investigation (Fig. 49.2).

Due to its peculiar characteristics, very precise technical requisites are needed for the 3D US device. First of all, the probe must be suitable for pyramidal scanning of the organ along a single linear direction. Various probes are currently available for both surface and endocavitary scanning.

Electronic supplementary material The online version of this chapter (doi:10.1007/978-3-319-40782-1_49) contains supplementary material, which is available to authorized users.

P. Martino (✉) • S. Palazzo
Department of Emergency and Organ Transplantation – Urology, Andrology and Kidney Transplantation Unit, University of Bari, Bari, Italy
e-mail: pasqualeluciomartino@libero.it; luciomartino@tin.it; pasquale.martino@uniba.it

P. Martino, A.B. Galosi (eds.), *Atlas of Ultrasonography in Urology, Andrology, and Nephrology*,
DOI 10.1007/978-3-319-40782-1_49

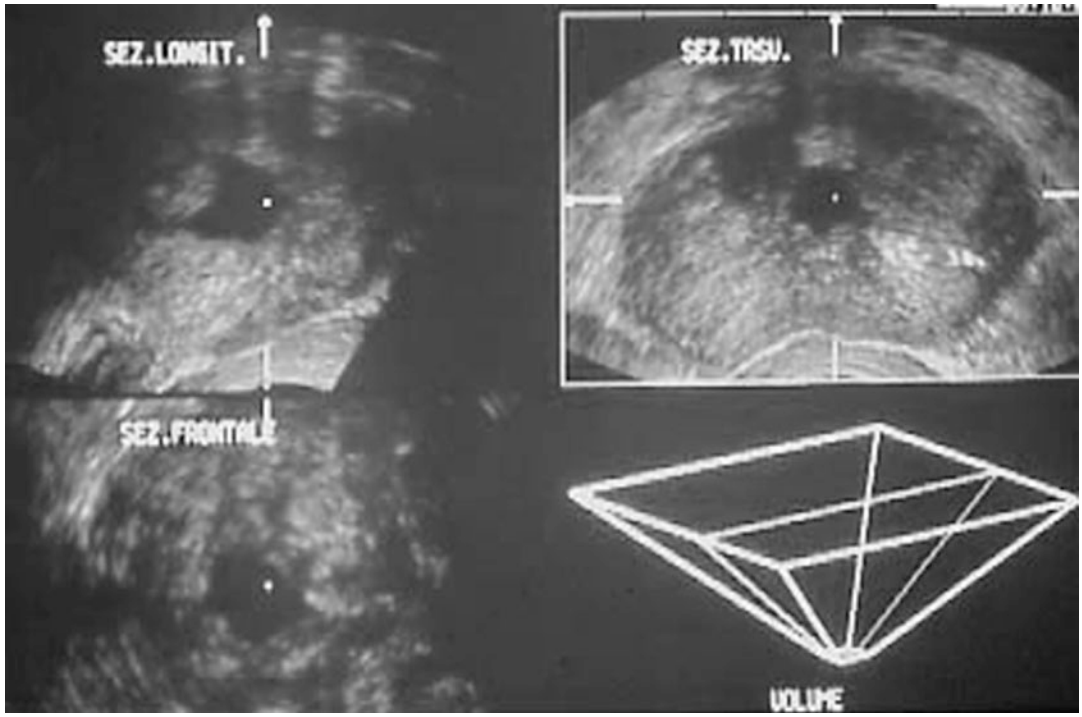

Fig. 49.1 3D reconstruction scheme (computer processing of the images obtained from sagittal, transverse, and coronal plane scans of the organ)

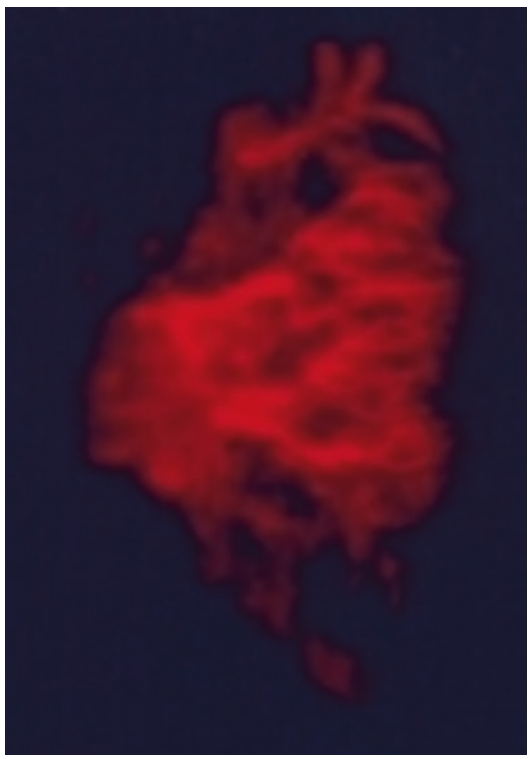

Fig. 49.2 Doppler 3D image of the arterial vessels of the kidney

49.2 Uses

The organ that has been most closely studied in urology with the 3D US device is surely the prostate. Owing to its particular anatomical position, the prostate gland is ideally suited to US studies of normal or pathological characteristics. Although the ultrasound devices in most common use can provide considerable information on the organ under study, their 2D view and impossibility of scanning the coronal plane pose limitations. These were not recognized as limits until magnetic resonance imaging with an endorectal bobbin demonstrated the far greater diagnostic and staging potential of three-dimensional study of the prostate gland.

The fact that 3D US is a novelty, and so its use in clinical practice is still limited, means that its full potential has not yet been entirely realized. Most research has been focused on understanding this novelty in terms of the images obtained with 3D US.

Scanning the coronal plane makes it possible to reveal some anatomical details that cannot otherwise be assessed. In fact, the central zone of the gland is only visible on the frontal plane. It appears as a cuneiform hypoechogenic area, surrounded by the isoechogenic peripheral gland. The transition zone is a tenuous, symmetrical hypoechogenic area lying to the sides of the proximal urethra. Moreover, it is possible to follow the complete course of the ejaculatory ducts up to their outlet in the verumontanum region (Fig. 49.3).

With increasing biological aging of the organ, the transition zone tends to become much more voluminous. This modifies the appearance of the prostate on the coronal plane; it has been shown, in fact, that the increased tissue volume in BPH occurs exclusively in this prostatic zone.

The remarkable reliability of volumetric calculations of the prostate done with the 3D US device fitted with a multiplanar transrectal probe is due to the highly precise definition of the images. The practical advantage of correct volumetric measurements of the prostate is that it allows assessment of the true efficacy of surgical treatment, as well as its feasibility in benign prostatic hyperplasia and in prostatic carcinoma. Naturally, a more accurate estimate of the disease extent allows a better assessment of the diagnostic and prognostic factors [1]. In fact, 3D US can overcome the difficulties encountered using conventional TRUS for local staging of cancer. The visualization of an additional scanning plane can clarify the anatomical relationships between the tumor and surrounding healthy prostate tissue, including the capsule. A precise view of the whole length of the ejaculatory ducts can demonstrate any invasion by the tumor, that is, the first step toward involvement of the seminal vesicles, a well-known unfavorable prognostic factor. In addition, the bladder-prostate angle is more easily visualized and investigated [2] Video 49.1.

Thus, 3D US can play a major role in the diagnostic workup of prostatic carcinoma. As is well known, the disease mostly originates in the peripheral zone of the gland, but in 20% of tumors it arises in the transition zone. Some important studies have demonstrated a greater incidence of tumors in the transition zone if the biopsy is done under 3D rather than the usual 2D ultrasound guidance. This higher percentage of tumors identified in the TZ does not seem to be due so much to being able to visualize anomalous areas as to a better visualization of the transition zone thanks to the coronal plane scans. In short, a precise visualization of the transition zone on the coronal plane allows targeted biopsies to be performed, resulting in a demonstrated increase in the number of diagnoses of carcinoma in this prostate area. In short, 3D US allows a greater diagnostic accuracy of prostatic biopsies, reducing the number of false-negative cases [3]. In addition, the biopsy course followed can be recorded, which can be an extremely useful point if any further biopsy needs to be done.

The 3D ultrasound method is also indicated in cases where a dynamic assessment of prostatic lesions is required, when planning ablative treatments as an alternative to traditional surgery. Its use has been proposed to determine BPH areas to be treated with interstitial laser therapy, for example. This method demands a highly precise positioning of the laser fibers, and this can be guaranteed, thanks to the clear differentiation of the different prostatic zones

that can be obtained with 3D US. In particular, a much better precision of ultrasound-guided puncture in the prostate apex and base regions has been shown using the 3D device. Furthermore, this technique allows a perfect insertion of cryoprobes in the prostate in patients undergoing cryoablation of the gland.

Some studies have also been focused on its promising role for the assessment of bladder tumors. A higher diagnostic sensitivity of 3D than traditional US has been demonstrated, above all in patients with hematuria, with small lesions and with bladder infections. Although the gold standard for tumoral forms is cystoscopy, the greater accuracy of 3D US can reduce the need to perform this invasive diagnostic procedure [4]. The method has also been used in the follow-up of kidney transplant patients to exclude rejection. 3D echocolordoppler enables a precise definition of the volumetrics, as well as identifying and visualizing arterial and venous anastomoses, following the course of the vessels along their main axis. It can also show the vascular tree up to the arcuate vessels, allowing a more accurate measurement of the resistance index, an essential parameter in the study of rejection [5] (Fig. 49.4).

Moreover, the 3D US device offers considerable aid in the diagnosis of vascular diseases in the andrology field. The possibility of displaying the arterial and venous vascularization of the penis, "isolating" it from the parenchyma, allows a precise assessment to be made, both anatomical and functional, of the vascular flow and correlated diseases (Fig. 49.5).

This type of ultrasound has also been tested for the assessment of micturition anomalies in young boys with suspected vesicoureteral reflux. A promising role in diagnosis and patient follow-up has been illustrated, demonstrating the better definition of the degree of reflux [6, 7]. Finally, thanks to its greater accuracy, it can be useful to define the morphology and function of the pelvic floor in women (e.g., in patients with bladder exstrophy epispadias complex) [8].

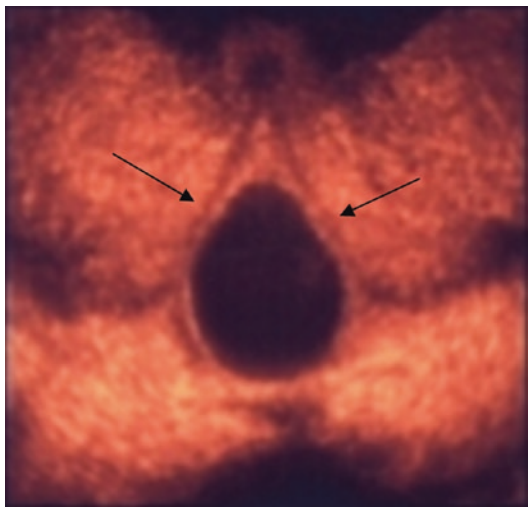

Fig. 49.3 Course of the ejaculatory ducts (*arrow*) and their outlet in the verumontanum region

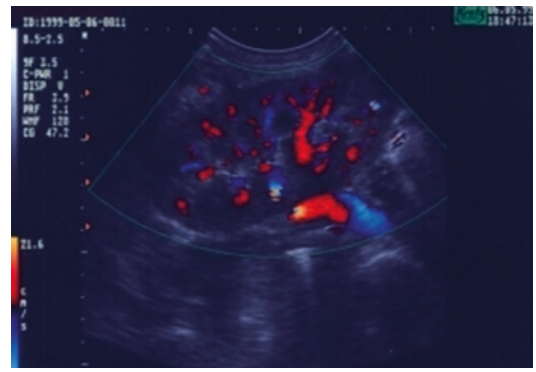

Fig. 49.4 Echocolordoppler of a transplanted kidney

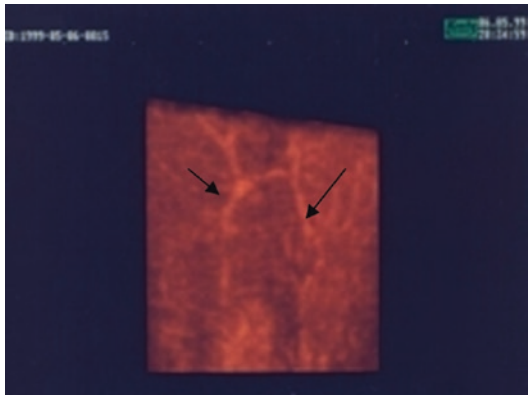

Fig. 49.5 Echocolordoppler of the penis, showing the arterial vessels: corpus cavernosus arteries in 3D (*arrow*)

Conclusion

At the current state of the art, the 3D US method offers the clinician many different advantages, namely [5]:

- *Standardization of the procedures, reducing the operator-dependent variables*
- *A very high definition of the images*
- *An optimal visualization of the volumes and vascularization*
- *The depiction of anatomical structures and pathological lesions on the coronal plane, offering a large amount of extra information as compared to conventional ultrasound*
- *Improved diagnosis and staging procedures of space-occupying urological masses*
- *The possibility of use also for interventional and intraoperative purposes*

Nowadays, although 3D US is still relatively underused, it is a safe, rapid, replicable, and relatively inexpensive method that can improve the clinical approach to patients affected by urological diseases. It will likely play an ever more important role in the diagnosis, therapy, and follow-up of urological diseases.

References

1. Gianluca G, Roberto P, Stefano B, Andrea F, Stefano C, Filippo Di L, Andrea G, Nicola M (2005) Accuracy of prostate volume measurements using transrectal multiplanar three-dimensional sonography. Int J Urol 12:936–938
2. Martino P, Palazzo S, Bufo L, Garofalo L, Selvaggi FP (2000) Three dimensional (3D) digital ultrasound in early staging of prostatic Adenocarcinoma. J Urol 164:456, (Bibliografia *aggiungere)*
3. Walter WJ IIIa, Nyea JA, Schustera DM, Niehb PT, Masterb VA, Votawa JR, Feia B (2013) Accuracy evaluation of a 3D ultrasound-guided biopsy system. NIH 8671. doi:10.1117/12.2007695
4. Silva-Ramos M, Louro N, Versos R, Cavadas V, Marcelo F (2012) Does 3D ultrasound enhance the diagnosis of bladder tumours in patients with haematuria? ISRN Urol 2012:158437, 5 pages. doi:10.5402/2012/158437
5. Martino P, Palazzo S, Selvaggi FP (2000) Ecografia tridimensionale digitale in urologia. Arch Ital Urol Androl LXXII(4):163–167
6. Pichler R, Buttazzoni A, Bektic J, Schlenck B, Radmayr C, Rehder P, Oswald J (2011) Endoscopic treatment of vesicoureteral reflux using dextranomer/hyaluronic acid copolymer in children: results of postoperative follow-up with real-time 3D sonography. Urol Int 87(2):192–198. doi:10.1159/000327609, Epub 2011 Aug 24
7. Wozniak MM, Pawelec A, Wieczorek AP, Zajczkowska MM, Nachulewicz P, Borzcka H, Lublin/PL (2014) The usefulness of 3D/4D techniques during voiding urosonography (VUS) in the diagnostics and monitoring of treatment of vesicoureteral reflux in children. European Society of Radiology. ECR 2014 poster C0344. doi:10.1594/ecr2014/C-0344
8. Ebert AK, Falkert A, Germer U, Rösch WH (2009) Biometry of the pubovisceral muscle and levator hiatus assessed by three-dimensional ultrasound in females with bladder exstrophy–epispadias complex after functional reconstruction. Ultrasound Obstet Gynecol 34:98–103

Elastosonography

50

Massimo Valentino, Michele Bertolotto, Pezzetta Valdi, Libero Barozzi, Pietro Pavlica, and Lorenzo Derchi

50.1 Introduction

The mechanical properties of the living tissue can be evaluated with an imaging method defined as ultrasound elastography. This technique gives a visual representation of the tactile information usually provided by physical palpation of the tissue. It has opened new clinical applications of US providing complementary information to gray-scale and color Doppler ultrasound.

Diseases of kidney, prostate, testis, and penis directly affect the biomechanical properties that can be studied with sonoelastography which has been shown to aid in the characterization of focal and diffuse disease. It has been also applied in the guidance of tissue biopsies and in the monitoring of therapeutic applications.

There are several elastography methods available for clinical users, depending on the way in which the stress is applied.

Electronic supplementary material The online version of this chapter (doi:10.1007/978-3-319-40782-1_50) contains supplementary material, which is available to authorized users.

M. Valentino, MD (✉) • P. Valdi, MD
Tolmezzo hospital, via Morgagni 18,
Tolmezzo (UD) 33028, Italy
e-mail: mvm.valentino@gmail.com

M. Bertolotto, MD
Department of Radiology, University of Trieste,
Ospedale di Cattinara, Strada di Fiume 447,
Trieste 34149, Italy

L. Barozzi, MD
Radiology Unit, Casa di Cura Madre Fortunata
Toniolo, Via Toscana 34, Bologna 40141, Italy

P. Pavlica, MD
GVM Care and Research, Villalba Hospital,
Bologna, Italy

L. Derchi, MD
Dicmi-Radiologia, University of Genova,
Largo R. Benzi 8, Genoa 16132, Italy

P. Martino, A.B. Galosi (eds.), *Atlas of Ultrasonography in Urology, Andrology, and Nephrology*,
DOI 10.1007/978-3-319-40782-1_50

50.2 Principles of Elastography

The elasticity of biological tissue differs depending on the direction and rate of deformation. Differences in the elasticity of soft tissues can be evaluated after externally applying a stress force and measuring strain or after applying a radiation force impulse and measuring the propagation speed. The former is referred to as *strain imaging* and the last as *ARFI imaging and shear wave imaging*. Both strain and ARFI/shear wave imaging require mechanical excitation that can be divided into a manual compression (by hand) and an acoustic radiation force impulse (ARFI) or external mechanical vibration. The main differences between these technologies are the following:

1. In strain elastography, strain induced by quasi-static methods such as manual compression or cardiovascular/respiratory pulsation is estimated, and the distributions of strain or normalized strain values within a region of interest (ROI) are displayed.
2. In ARFI, focused acoustic radiation force "pushing" pulses are used to deform the tissue. The resulting tissue displacement is measured within the focal region of each push within a specified ROI, and the distribution of displacement or its normalized values within the ROI is displayed.
3. In shear wave, speed measurement and imaging using acoustic radiation force impulse excitation, focused acoustic radiation force pushing pulses of short duration are used to generate shear waves, and the speed of the shear waves propagating away from the pushing location is measured. The information can be reported as either an average value within a ROI or as a color-coded image.

Strain imaging was first developed in the 1970s and named elastography by J. Ophir [1]. Through various investigations of approaches for measurement of strain and its imaging [2–4], the method of strain elastography has been commercialized, with the pressure applied manually, similar to palpation or by cardiovascular pulsation and is currently being used in various fields of clinical medicine. Strain is a relative indicator of stiffness, which changes depending on the degree of compression. An example is shown in Fig. 50.1. For clinical use, the display method of the elastogram is superimposed as a colored image on the B-mode image. The color scale was firstly proposed by Ueno [5], but at present, in most equipment, users can select the color scale as desired. Because strain imaging is qualitative, it is difficult to perform quantitative comparisons between cases. Therefore, pseudo-quantitative methods such as the strain ratio [6] can be used. Recently, elasticity score has been proposed for suggesting a possible cancer.

ARFI imaging has been introduced in 2001 [7]. Similar to FibroScan®, focused acoustic radiation force pulses are used to monitor the tissue displacement (as a measure of deformation) within the ROI. The tissue displacement response is inversely related to the tissue stiffness. ARFI imaging does not rely on transducer compression, and thus it has the advantage of being able to be compared between cases.

Shear wave imaging is are the most recent elastographic method. In shear waves imaging, the waves propagate in a direction orthogonal to the direction of the tissue displacement, and the system estimates the speed of shear wave propagation through tissues, which is (almost) related to the underlying material stiffness. This technique is displayed in a color-coded image similar to strain imaging but without the disadvantages of the handheld deformation and a better resolution and deepness penetration.

Strain imaging and shear wave imaging have the advantages of being easy to use and provide elasticity images with a high spatial resolution in a manner similar to palpation (i.e., tissue deformation). Currently, many manufacturers produce ultrasonographic equipment with a strain elastography function. ARFI can be used to obtain a quantitative assessment of a focal lesion detected by the B-mode US.

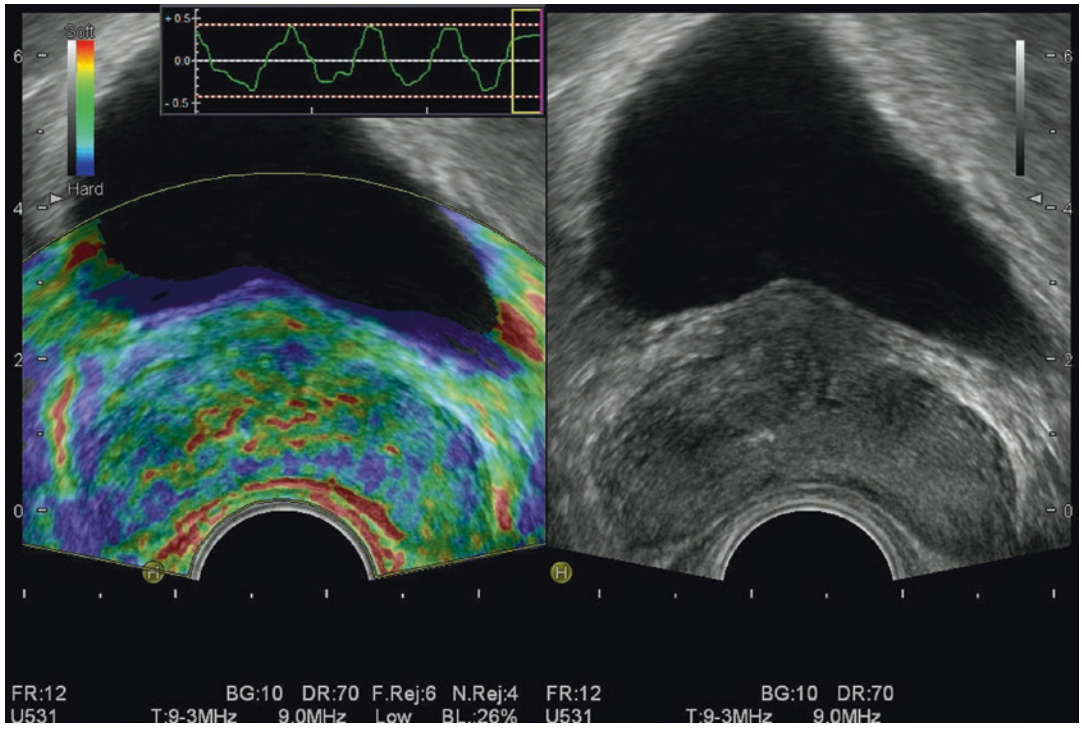

Fig. 50.1 Strain elastography of the prostate. The movie shows the normal pattern of the prostate. Using manual compression it is possible to estimate the strain of the prostate. The information are reported on the display as a colored image on the B-mode image

50.3 Kidney

Few studies have attempted to apply elastography in the imaging of renal masses. Fahey and colleagues investigated the use of acoustic radiation force impulse (ARFI) imaging for real-time visualization of abdominal malignancies, including renal masses [8]. Clevert and colleagues reported shear wave velocity values in a small series of 12 solid renal cell carcinomas, using ARFI [9]. Tan and colleagues demonstrated the feasibility of real-time elastography in differentiating angiomyolipomas from renal cell carcinomas, by the use of both elasticity patterns and strain ratios [10]. In our opinion more experience is necessary to evaluate the potential role of elastography in separating benign and malignant tumors.

Sonoelastography has been also proposed as noninvasive method to detect fibrosis in chronic kidney diseases. Several studies have been performed on renal transplants because the superficial location allow a more accurate measurements. Most of them were performed with high-frequency probes (Fig. 50.2). The results reported in the literature are quite controversial, and the number of enrolled patients for biopsy is quite limited [11].

In pediatric patients with VU reflux, ARFI values decrease in the kidneys with secondary reflux compared to the normal kidney [12].

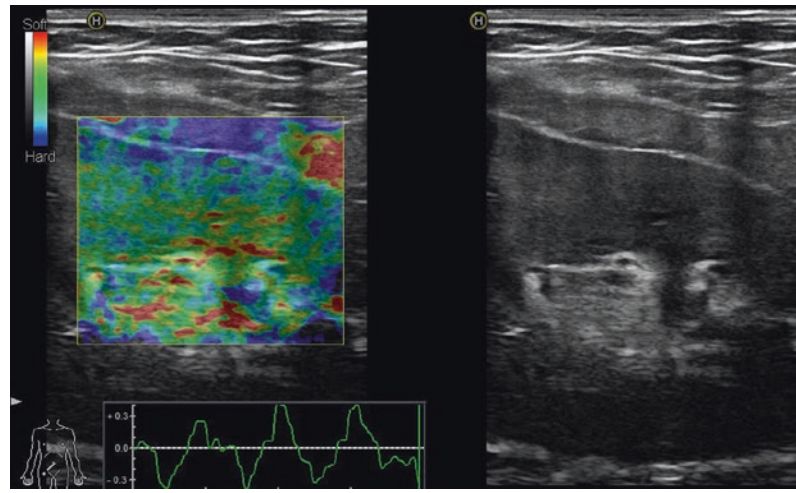

Fig. 50.2 Strain elastography of transplanted kidney. Elasticity map of the kidney transplant acquired with a 5–12 MHz linear probe, showing higher values in the cortex than in the medulla

50.4 Prostate

It is well known that B-mode US has a limited sensitivity and specificity (40–50 %) for prostate cancer detection. The use of US-based elasticity imaging for the detection of prostate cancer relies on the fact that these tumors can be detected because they are firmer than the surrounding normal parenchyma. Usually, the normal gland has a green-coded strain with blue parts near the capsule (Fig. 50.3). In the prostate having a benign prostate hyperplasia, the map is less homogeneous and the blue areas are more present. Normally periurethral zone appears firmer due to its sphinterial component. Prostate carcinoma (Pca) appears as a firmer area with respect to the surrounding parenchyma (Fig. 50.4). For Pca detection, strain elastography and shear wave imaging are used. In the case of strain elastography, the tissue to be examined is compressed by the examiner using the ultrasound probe. The comparison of ultrasound images before and after compression makes it possible to make conclusions about the stiffness of the tissue based on the degree of deformation. Adequate application of compression and the interpretation of the color-coded images in real time are difficult to standardize and yield heterogeneous, examiner-dependent results. In shear wave elastography, the forces are applied directly by the ultrasound probe, and the stiffness of the tissue is calculated based on the propagation speed of the shear waves in the tissue. The main advantage of this method is the high intraindividual and interindividual reproducibility [13]. In general, the firmer areas are suspicious of cancer, but prostatitis, fibrosis, atrophy, or nodule of benign prostate hyperplasia can also be associated with increased stiffness. False-negative findings can be also present in Pca with a Gleason score ≤7 in which normal tissue and prostate cancer cells can relay next to one another [14].

Several recent studies demonstrated that this technique is promising. These studies are of two types. The first type of studies evaluated the technique as a diagnostic tool for Pca detection [15]. Most of these studies showed that elastography improved the detection rate of Pca and the detection increased with higher Gleason scores [16]. The second type of studies is based on elastography-targeted biopsy results and evaluated the method as a tool to support TRUS-guided systematic random biopsy [15].

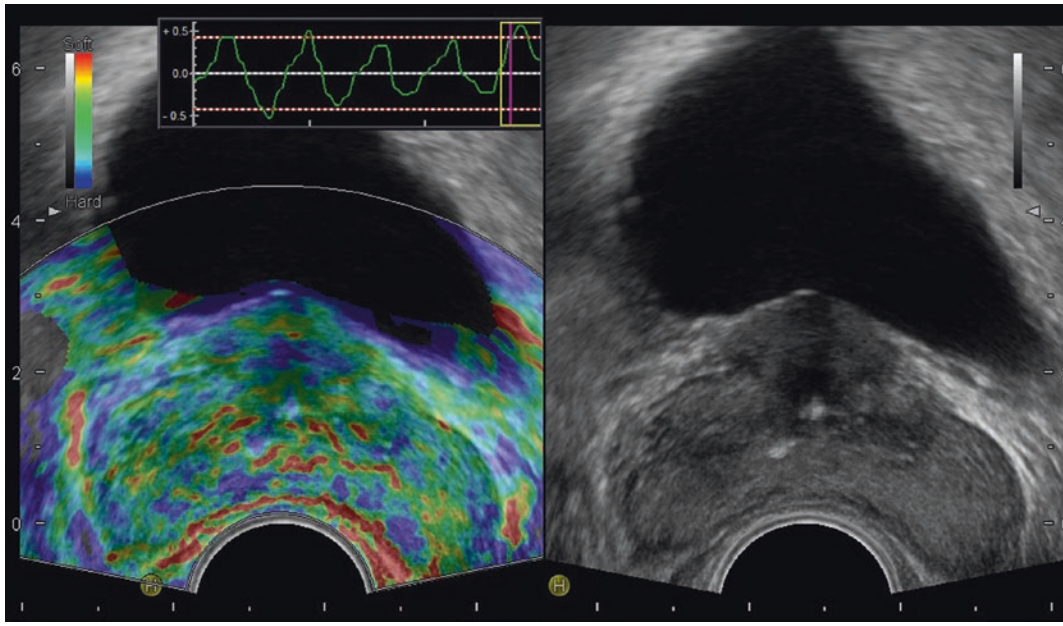

Fig. 50.3 TRUS image with strain elastography of a 70-year-old patient: Homogeneous prostate tissue of medium hardness (*green*) is visible. The region of the capsule or the neurovascular bundle and the urethra typically appear soft (*red*). Periurethral zone appears as harder areas (*blue*)

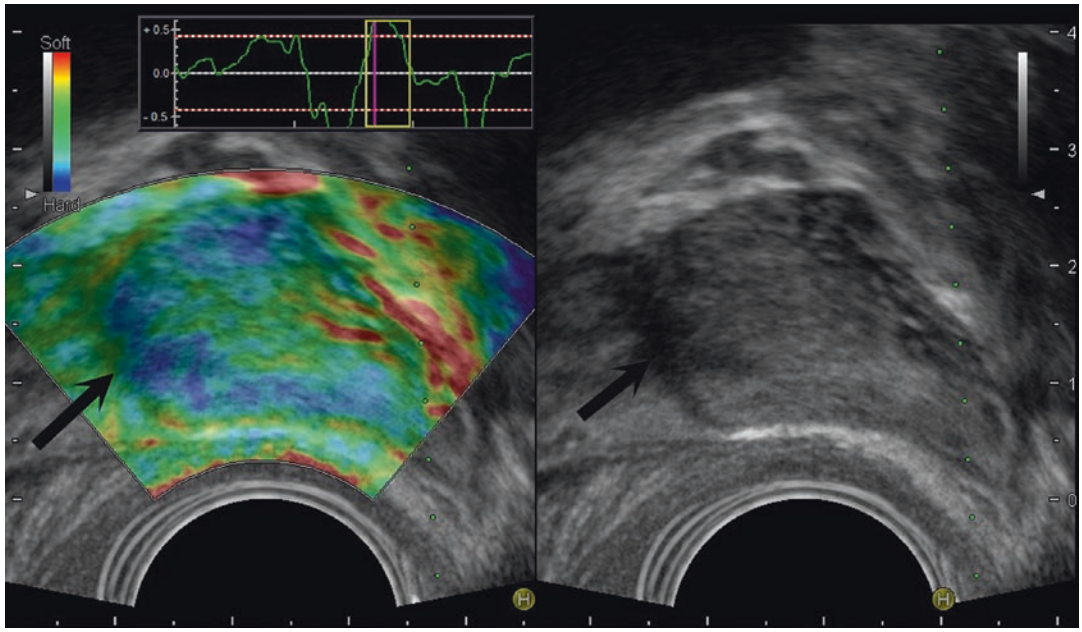

Fig. 50.4 TRUS image with strain elastography of the prostate of an 84-year-old patient. A *blue area* is clearly visible in the *right* base (*arrow*). Prostate biopsy confirmed a prostate cancer (Gleason score 3 + 4)

50.5 Testis

Elastosonography can be used also to discriminate malignant from benign testicular lesions. At elastosonography the normal testicles show mainly a medium level of elasticity (displayed in green); some linear "red" structures within the testes are related to fluid component, such as vessels and cysts (not ever). After some anecdotal reports, in 2012 Goddi et al. have published an interesting paper about 88 patients having 144 focal lesions [17]. They proposed a 5-point scale based on Itoh classification for breast lesions [5], finding a strong correlation with the biological characteristics of the tissues. In their research, the results of the elastograms gave 28 TP, 110 TN, 2 FP, and 4 FN cases, accounting for 87.5 % sensitivity, 98.2 % specificity, 93.3 % PPV, 96.4 % NPV, and 95.8 % accuracy in differentiating malignant from benign lesions in the 144 nodules/pseudo-nodules. Similar results were found by Aigner et al. [18] in 50 patients, reaching a sensitivity of 100 %, a specificity of 81 %, a negative predictive value of 100 %, a positive predictive value of 92 %, and an accuracy of 94 % in the diagnosis of testicular tumors. In our experience, elastosonography is useful in the differentiation of malignant lesions from most of benign lesions (Fig. 50.5) [19].

According to Huang DY [20], this new ultrasound technique, together with color Doppler ultrasound and contrast-enhanced ultrasound, should aid in the characterization of both benign and malignant intratesticular lesions.

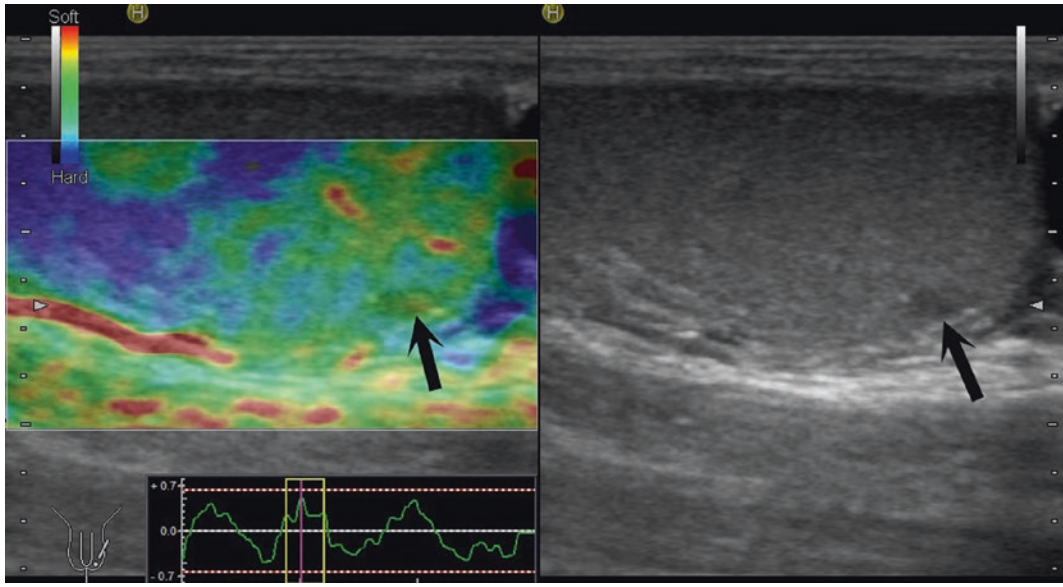

Fig. 50.5 Strain elastography of the testis. In the *lower* part of the testis, a hypoechoic nodule is visible. The strain image shows a soft lesion (*arrow*) corresponding to a benign lesion. The final diagnosis was a Leydig cell tumor

50.6 Penis

Recently some authors have proposed elastosonography for studying the penis. Shear wave elastography has been used for evaluating Peyronie's disease. Riversi et al. proposed the technique complementary to B-mode US in the cases in which US and clinical examination were discordant, improving the accuracy of B-mode US in detecting penile lesions [21]. Richards et al. found that elastosonography was an additional way to characterize, localize, and deliver therapy to a lesion in patients with Peyronie's disease in which palpation and B-mode US have failed to demonstrate a plaque [22]. Elastosonography can identify the firmer areas nonvisible at B-mode US (Fig. 50.6). Since stiffness of corpus cavernosum penis tissue is closely associated with age and sex hormone levels, Zhang JJ et al. [23] proposed to use elastosonography for evaluating the tissue structure of the penis. Because the change of tissue structure of the penis has important effects on penis erection and evaluating the tissue structure of corpus cavernosum penis is of great significance in the cases of impotence, they proposed to use elastosonography instead of penis biopsy.

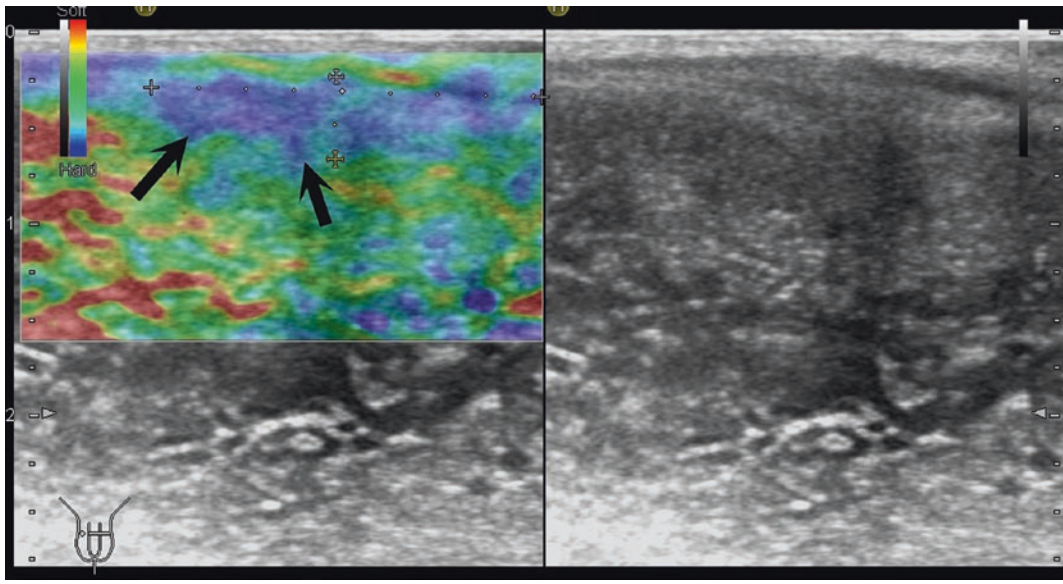

Fig. 50.6 Strain elastography of the penis. The plaque (*arrows*) is clearly displayed as hard (*blue*) tissue in comparison to the surrounding softer (*red and green*) tissue

Conclusions

In conclusion, based on the available results, it seems that elastosonography allows for better diagnosis in urological diseases, especially in distinguishing benign from malignant lesions of the prostate and testis and in identifying the invisible plaque in the Peyronie's disease. In kidney diseases, quantification of tissue stiffness using ultrasound is more complex, due to high tissue heterogeneities.

Therefore, more experience is needed in preclinical models and in patient cohorts with pathological correlation to better understand which are the physical factors of variation and the histopathological causes of elasticity changes.

References

1. Ophir J, Cespedes I, Ponnekanti H, Yazdi Y, Li X (1991) Elastography: a quantitative method for imaging the elasticity of biological tissues. Ultrason Imaging 13:111–134
2. Varghese T, Ophir J (1997) A theoretical framework for performance characterization of elastography: the strain filter. IEEE Trans Ultrason Ferroelectr Freq Control 44:164–172
3. Bamber JC, Barbone PE, Bush NL, Cosgrove DO, Doyely MM, Fueschsel FG, Meaney PM, Miller NR, Shiina T, Tranquart F (2002) Progress in freehand elastography of the breast. m E85D:5–14
4. Hall TJ, Zhu YN, Spalding CS (2003) In vivo real-time freehand palpation imaging. Ultrasound Med Biol 29:427–435
5. Itoh A, Ueno E, Tohno E, Kamma H, Takahashi H, Shiina T, Yamakawa M, Matsumura T (2006) Breast disease: clinical application of US elastography for diagnosis. Radiology 239:341–350
6. Farrokh A, Wojcinski S, Degenhardt F (2011) Diagnostic value of strain ratio measurement in the differentiation of malignant and benign breast lesions. Ultraschall Med 32:400–405
7. Nightingale K, Palmeri M, Nightingale R, Trahey G (2001) On the feasibility of remote palpation using acoustic radiation force. J Acoust Soc Am 110:625
8. Fahey BJ, Nelson RC, Bradway DP et al (2008) In vivo visualization of abdominal malignancies with acoustic radiation force elastography. Phys Med Biol 53: 279–293
9. Clevert DA, Stock K, Klein B, Slotta-Huspenina J, Prantl L, Heemann U et al (2009) Evaluation of Acoustic Radiation Force Impulse (ARFI) imaging and contrast-enhanced ultrasound in renal tumors of unknown etiology in comparison to histological findings. Clin Hemorheol Microcirc 43:95–107
10. Tan S, Ozcan MF, Tezcan F, Balci S, Karaoğlanoğlul M, Huddam B, Arslan H (2013) Real-time elastography for distinguishing angiomyolipoma from renal cell carcinoma: preliminary observations. AJR 200:W369–W375
11. Ozycan F, Yavuz YC, Inci MF, Bulent A, Ozkan N, Yuksel M, Sayarlioglu H, Dogan E (2013) Interobserver variability of ultrasound elastography in transplant kidneys: correlation with clinical-Doppler parameters. Ultrasound Med Biol 39:4–9
12. Bruno C, Caliari G, Zaffanello M, Brugnara M, Zuffante M, Cecchetto M, Minniti S, Pedot A, Talamini G, Pozzi-Mucelli R (2013) Acoustic radiation force impulse (ARFI) in the evaluation of renal parenchymal stiffness in paediatric patients with vescicoureteral reflux: preliminary results. Eur Radiol 23:3477–3484
13. Wells PN, Liang HD (2011) Medical ultrasound: imaging of soft tissue strain and elasticity. J R Soc Interface/the Royal Soc 8:1521–1549
14. Junker D, Schafer G, Aigner F et al (2012) Potentials and limitations of real-time elastography for prostate cancer detection: a whole-mount step section analysis. Scientific World Journal 2012:193213
15. Boehm K, Salomon G, Beyer B, Schiffmann J, Simonis K, Graefen M, Budaeus L (2015) Shear wave elastography for localization of prostate cancer lesions and assessment of elasticity thresholds: implications for targeted biopsies and active surveillance protocols. J Urol 193:794–800
16. Nygard Y, Haukaas SA, Halvorsen OJ et al (2014) A positive real-time elastography is an independent marker for detection of high-risk prostate cancers in the primary biopsy setting. BJU Int 113:E90–E97
17. Goddi A, Sacchi A, Magistretti G et al (2012) Real-time tissue elastography for testicular lesion assessment. Eur Radiol 22(4):721–730
18. Aigner F, De Zordo T, Pallwein-Prettner L, Junker D, Schäfer G, Pichler R, Leonhartsberger N, Pinggera G, Dogra VS, Frauscher F (2012) Real-time sonoelastography for the evaluation of testicular lesions. Radiology 263:584–589
19. Valentino M, Bertolotto M, Martino P, Barozzi L, Pavlica P (2014) Incidentally detection of non-palpable testicular nodules at scrotal ultrasound: what is new? Arch Ital Urol Androl 86:378–382
20. Huang DY, Sidhu PS (2012) Focal testicular lesions: colour Doppler ultrasound, contrast-enhanced ultrasound and tissue elastography as adjuvants to the diagnosis. Br J Radiol 85(Spec No 1):S41–S53
21. Riversi V, Tallis V, Trovatelli S et al (2012) Realtime-elastosonography of the penis in patients with Peyronies' disease. Arch Ital Urol Androl 84:174–177
22. Richards G, Goldenberg E, Pek H, Gilbert BR (2014) Penile sonoelastography for the localization of a non-palpable, non-sonographically visualized lesion in a patient with penile curvature from Peyronie's disease. J Sex Med 1:516–520
23. Zhang JJ, Qiao XH, Gao F, Li F, Bai M, Zhang HP, Liu Y, Du LF, Xing JF (2015) A new method of measuring the stiffness of corpus cavernosum penis with ShearWave™ Elastography. Br J Radiol 88(1048):20140671

HistoScanning

51

Carmen Maccagnano and Vincenzo Scattoni

51.1 Introduction

HistoScanning (HS) is an ultrasound (US) method used since 2006. The first area of interest concerned the ovarian neoplasms, and the HS sensitivity and specificity were 98 and 77 %, respectively, in this clinical scenario [1, 2]. Thus, HS was used for prostate in 2006 for the first time.

The prostate HistoScanning (PHS) is able to individuate the variations in the morphology of the prostate tissue, caused by elasticity, vascularization, lymphatic drainage and patterns of cellular growth.

PHS detects specific changes in the tissue morphology by extracting and quantifying statistical features from backscattered ultrasound data. The core of HS consists of 'characterization algorithms' applied on these data (i.e. the 'radiofrequency, RF, data' or the 'raw data') before they are transformed by the built-in software of US machines necessary for forming the grey-scale video image. HS works on a personal computer and can be embedded in computers installed in US machines. The characterization algorithms exploit the physical changes to sound waves that result from the interaction of the ultrasound beam and the cancer tissue. These can be summarized as energy loss, erratic spatial distribution of energy and increased entropy. One important attribute of these characterization algorithms is that they can be applied in discrete regions of interest (ROIs) throughout the prostate. Thus, the presence or absence of prostate cancer (PC) can be ascertained within small and discrete volumes of tissue. The identification of cancer within ROIs means that once identified, PHS can spatially orientate the cancer within the gland. This enables both the location of the cancer to be determined and its volume [3–6] (Table 51.1) (Fig. 51.1).

C. Maccagnano (✉)
Department of Surgery, Division of Urology,
Azienda Ospedaliera S. Anna –Como-,
Via Ravona, 60, San Fermo della Battaglia (Co), Italy
e-mail: carmen.maccagnano@gmail.com

V. Scattoni
Department of Urology, University Vita-Salute,
Scientific Institute H San Raffaele,
Via Olgettina 60, Milan 20132, Italy
e-mail: scattoni.vincenzo@hsr.it

P. Martino, A.B. Galosi (eds.), *Atlas of Ultrasonography in Urology, Andrology, and Nephrology*,
DOI 10.1007/978-3-319-40782-1_51

Table 51.1 Cell and tissue features that influence the interaction between the ultrasound beam and the cancer tissue

Cell features	Tissue features
Cell density	Vascularization
Cell irregularities	Elasticity
Water content	

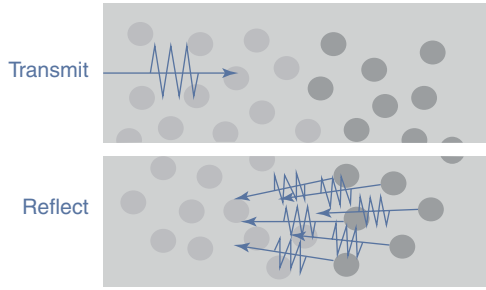

Fig. 51.1 Principle of 'backscattered ultrasound' in a heterogeneous medium

51.2 Method of Examination and Imaging Processing

The patient urinates and takes an enema 3 h before the exam, in order to reduce the possible artifacts. The bed position is on the right side, with flexed knees. Thus, a preliminary prostate trans-rectal ultrasound (TRUS) is executed using a 9 MHz probe with the aim of defining the glandular volume, which can be visualized.

During the imaging acquisition time (whose duration is about 45 s), the silence and no movement by the patient are necessary. The probe automatically rotates on a sagittal plan with 180° from the right to the left lobe and vice versa. This leads the acquisition of 895 frames (a frame every 1/5 of grade). In this context, the operator has to manually define the margins of the prostate.

Thus, the total volume of the prostate is divided in single volumes of about 0.04 ml, with the help of a specific algorithm. These volumes are defined as 'tagged units'; the number of the units is related to the dimensions of the gland. The suspicious adjacent 'tagged units' are considered all together, and the total volume is shown to the operator (Fig. 51.2) with red colour and in the three plans: axial, sagittal and coronal (Fig. 51.3, 51.4, 51.5 and 51.6).

In this context, the artifacts play a fundamental role in interpreting the images (Table 51.2).

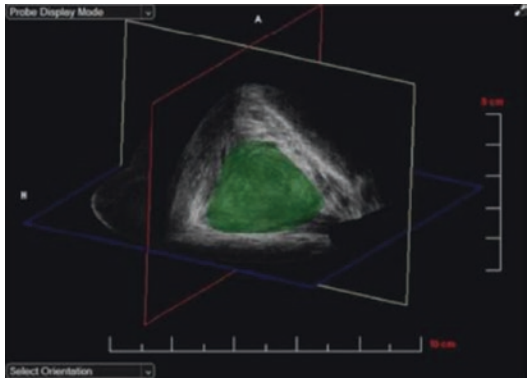

Fig. 51.2 3D reconstruction of the prostate with the help of PHS algorithm, with a resolution of about 0.2 mm. The visualization and the study of the images are interactive

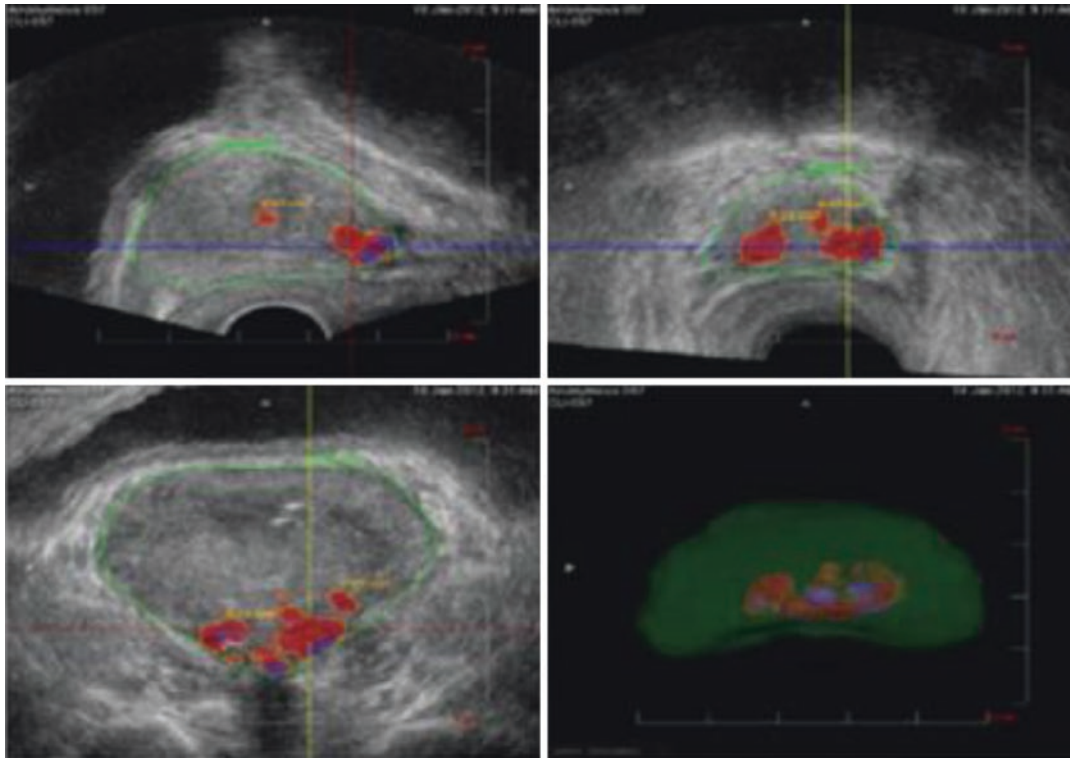

Fig. 51.3 Suspicious lesions are *red marked*. The margin of the prostate is evidenced with a continuous green line and it has to be traced by the operator

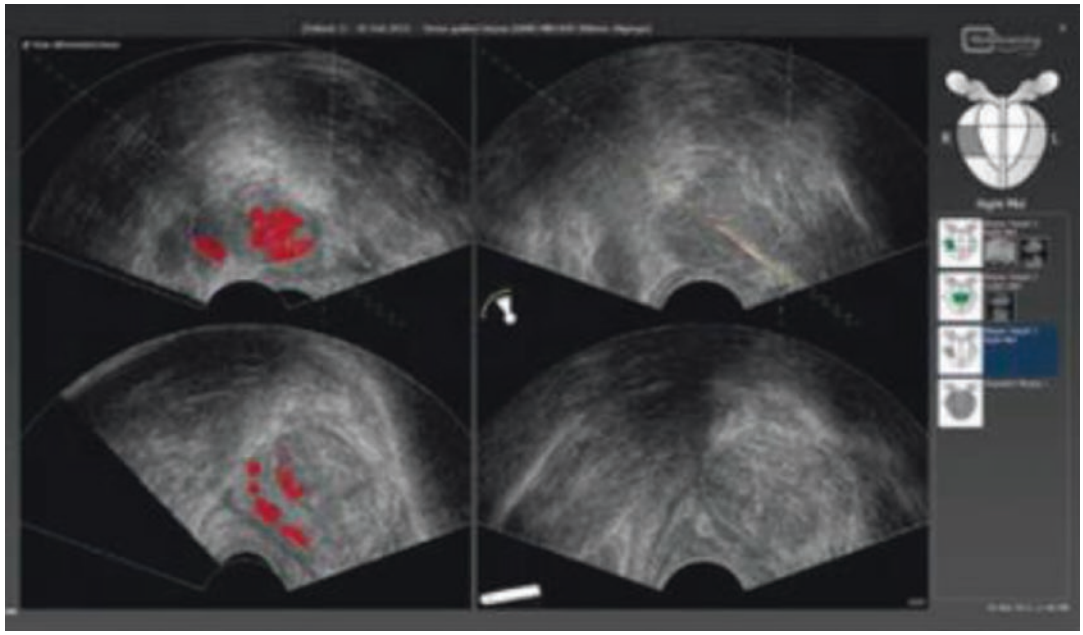

Fig. 51.4 The 2D images in the different plans are real-time visualized, in order to modify the position of the probe, according to the preference of the operator

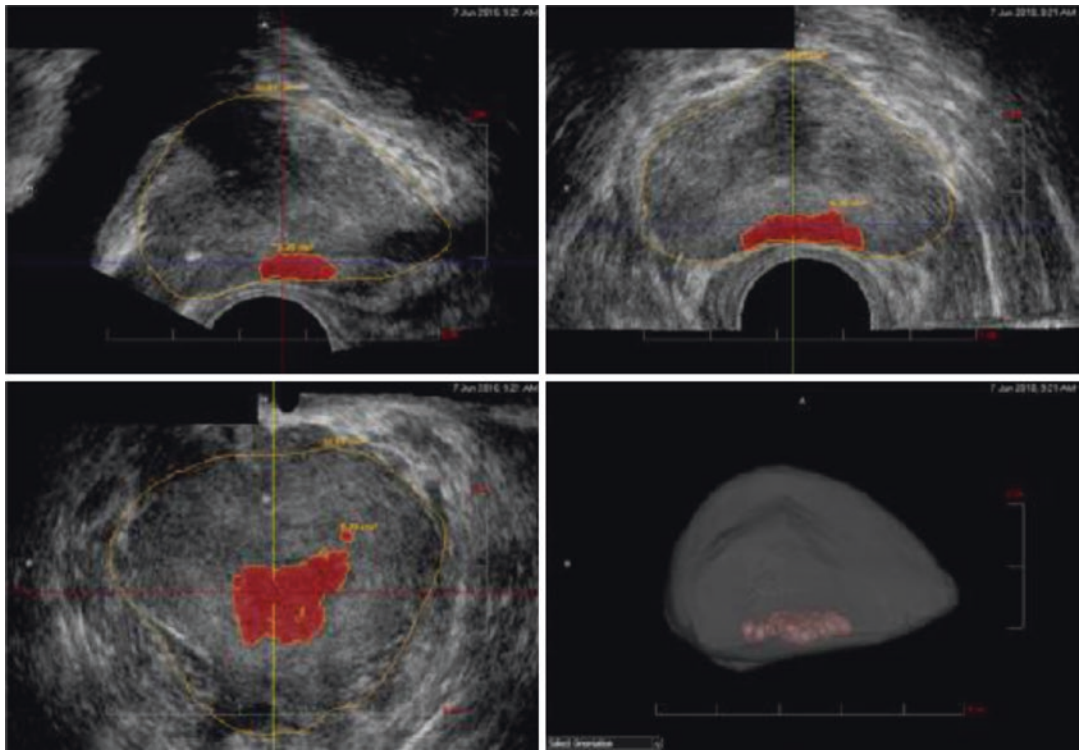

Fig. 51.5 Single-focus lesion with a volume of 0.78 ml. The total volume of the prostate is about 32 ml

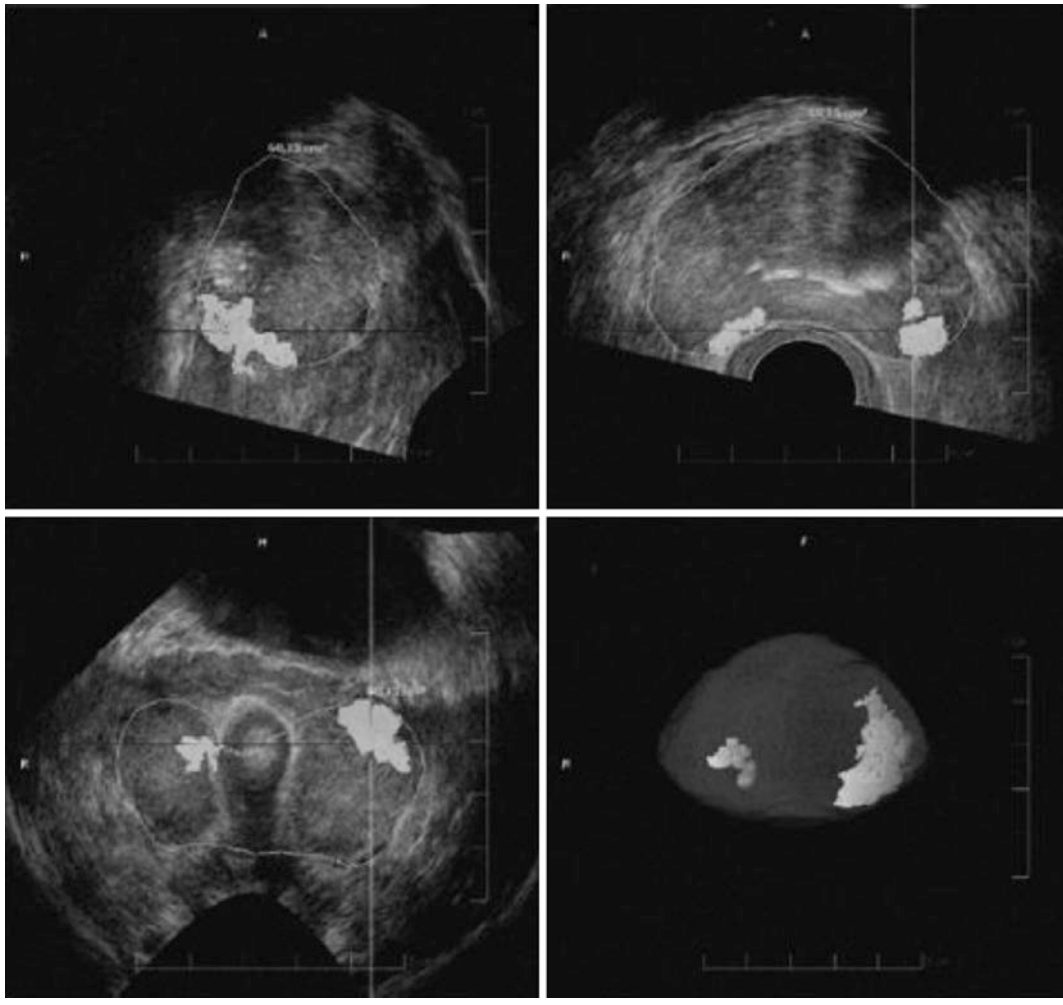

Fig. 51.6 Basal bilateral lesion

Table 51.2 Features causing artefacts in PHS images

Operator related	Patient related	Anatomical
Excessive compression on the rectum (the compression in the medium part of the prostate is higher than the rest of the gland. The use of rotating piezoelectric crystals inside the probe may solve this problem)	Movements during the execution of the exam	Sphinteric muscular structures [1]
Operator's experience about US The interpretation of HS images is made by the same urologist who will execute PBx, accordingly also to HS results	Number of past PBx (first vs repeated) [3]	Calcifications
Learning curve of about 80 procedures [3]		Seminal vesicles
		Urethra
		Large prostates (reduction of evaluable tissue) [4]

51.3 Possible Indications of Prostate HistoScanning

51.3.1 Prostate Biopsy

As it was shown that it can accurately visualize and locate lesions as small as 0.50 mL inside the prostate, PHS has the potential to assist in addressing many of the issues facing current biopsy procedure techniques [7–12].

Nevertheless, the role of PHS as guidance for prostate biopsy (PB) is still a matter of debate, also because most of the published trials are retrospective and involve a small number of patients (Table 51.3).

The first studies reported a sensitivity of about 90 % and a detection rate (DR) of about 100 % for neoplastic lesions, especially for multifocal neoplasms or for establishing the side where cancer is located [3, 7–12].

De Coninck and Coll. have reported an increase of the DR of about five times comparing to random PB; this is due to the reduction of both the error sampling and the percentage of false positives [1].

Salomon and Coll. have demonstrated that there is accuracy of about 91 % for lesion of not being cancer if PHS does not individuate a neoplastic focus with a diameter < 0,2 mm. This implicates a reduction of about 40 % of extemporaneous specimens of the margins.

On the contrary, Hamann and Coll. have reported a DR of about 35 % if PHS is used as guidance for PB, especially with trans-perineal approach [3].

Moreover, in a retrospective study of 2014, Schiffmann and Coll. have reported high percentage of false-positive cases (77 %) in the general population. Similarly, the sensitivity and specificity are low, even when increasing the volumetric cut-off from 0.2 to 0.5 ml.

In conclusion, the sensitivity, the specificity and the predictive positive value are lower comparing with the DR of standard PB [14, 15].

Recently Javed and Coll. have evaluated the ability of prostate PHS to detect, characterize and locally stage PC, by comparing it with TRUS-guided PBx, trans-perineal template prostate biopsies (TTBs) and whole-mount radical prostatectomy specimens. The PHS-targeted biopsies had an overall cancer DR of 38.1%, compared with 62.5% with standard TRUS-guided biopsies. The sensitivity and specificity of PHS for localizing tumour to the correct prostate sextant, compared with standard TRUS-guided biopsies, were 100 and 5.9 %, respectively. The PHS-targeted biopsies had an overall cancer DR of 13.4 %, compared with 54.4 % for standard TTB. PHS had a sensitivity and specificity for cancer detection in the posterior gland of 100 and 13 %, respectively, and for the anterior gland, 6 and 82 %, respectively. No correlation between total tumour volume estimates from PHS and radical prostatectomy pathology was found (Pearson correlation coefficient −0.096). Sensitivity and specificity of PHS for detecting tumour foci ≥0.2 mL in volume were 63 % and 53 % respectively. The authors concluded that in these three independent studies in 105 patients, PHS did not reliably identify and characterize PC in the routine clinical setting [4].

51.3.2 Active Surveillance

The use of PHS in active surveillance is based on both the ability of diagnosing small neoplastic foci and on reduction of necessity of executing reclassification PB (which is actually about 28 %).

Table 51.3 Trials about PHS and PBx

Author	Sensitivity	Specificity	Positive predictive value	Negative predictive value
Schiffmann [13]	84.1	27.7	29.5	89.2
Javed [4]	100	19.2	–	–
Nunez-Mora [11]	93.5	79.5	67.5	96.5
Simmons [7]	100	82	–	–
Braeckman [8]	100	83	80	100

51.3.3 Surgical Planning

This argument is one of the most controversial. In this context, Javed and Coll. have demonstrated that that a significant statistical correlation between the total amount of the cancer individuated by PHS and the final pathologic exam does not exist. Moreover, a correlation between the volume analysed according to sextants and the final pathologic exam has not been proved. The same absence of correlation has been reported also for the identification of the 'index lesion'. The eventual definition of lesions proximally located to the neurovascular bundles has to be considered more useful in the context of surgical planning, especially for 'nerve sparing' techniques [4, 10].

51.3.4 Focal Therapy

The possibility of planning focal therapy may depend on the individuation of the side affected by neoplasm [4]. This indication is still a matter of debate. Particularly, Javed and Coll. have reported no correlation between the side of the lesion in the gland identified by HS and the final pathologic specimen after radical prostatectomy [4].

Conclusions

PHS is a promising method, but lack of strong scientific data does not support its routine use in the clinical setting. The small number of patients in the trials, the law quality of the trials and the several biases of the selection of the patients are the major limits of the studies that have been published at the present.

References

1. De Coninck V, Braeckman J, Michielsen D (2013) Prostate HistoScanning: a screening tool for prostate cancer? Int J Urol 20(12):1184–1190
2. Lucidarme O, Akakpo JP, Laurate B (2006) HistoScanning: a new computer aided diagnostic tool for distinguishing benign from malignant ovarian masses; a multicentric study report. Scientific Assembly and Annual Meeting
3. Hamann MF, Hamann C, Schenk E, Al-Najar A, Naumann CM, Jünemann KP (2013) Computer-aided (HistoScanning) biopsies versus conventional transrectal ultrasound-guided prostate biopsies: do targeted biopsy schemes improve the cancer detection rate? Urology 81(2):370–375
4. Javed S, Chadwick E, Edwards AA, Beveridge S, Laing R, Bott S, Eden C, Langley S (2014) Does prostate HistoScanning™ play a role in detecting prostate cancer in routine clinical practice? Results from three independent studies. BJU Int 114(4):541–548
5. Aigner F, Frauscher F (2009) RE: Computer-aided ultrasonography (HistoScanning): a novel technology for locating and characterizing prostate cancer. BJU Int 103(1):115; author reply 115–6
6. Simmons LAM, Autier P, Moore CM, Emberton M (2011) Ultrasound spectral interrogation of histological grade in prostate cancer using prostate HistoScanning. Eur Urol Suppl 10:302; abstract nr. 967
7. Simmons LA, Autier P, Zat'ura F, Braeckman J, Peltier A, Romic I, Stenzl A, Treurnicht K, Walker T, Nir D, Moore CM, Emberton M (2012) Detection, localisation and characterisation of prostate cancer by prostate HistoScanning. BJU Int 110(1):28–35
8. Braeckman J, Autier P, Garbar C, Marichal MP, Soviany C, Nir R, Nir D, Michielsen D, Bleiberg H, Egevad L, Emberton M (2008) Computer-aided ultrasonography (HistoScanning): a novel technology for locating and characterizing prostate cancer. BJU Int 101(3):293–298
9. Braeckman J, Autier P, Soviany C, Nir R, Nir D, Michielsen D, Treurnicht K, Jarmulowicz M, Bleiberg H, Govindaraju S, Emberton M (2008) The accuracy of transrectal ultrasonography supplemented with computer-aided ultrasonography for detecting small prostate cancers. BJU Int 102(11):1560–1565
10. Salomon G, Spethmann J, Beckmann A, Autier P, Moore C, Durner L, Sandmann M, Haese A, Schlomm T, Michl U, Heinzer H, Graefen M, Steuber T (2013) Accuracy of HistoScanning for the prediction of a negative surgical margin in patients undergoing radical prostatectomy. BJU Int 111(1):60–66
11. Nunez-Mora C, Garcia-Mediero JM, Patino P, Orellana C, Garrido A, Rojo A, Rendon D (2013) Utility of Histoscanning prior to prostate biopsy for the diagnosis of prostate adenocarcinoma. Actas Urol Esp 37(6):342–346
12. Macek P, Barret E, Sanchez-Salas R, Galiano M, Rozet F, Ahallal Y, Gaya JM, Durant M, Mascle L, Giedelman C, Lunelli L, Validire P, Nesvadba M, Cathelineau X (2014) Prostate Histoscanning in clinically localized biopsy proven prostate cancer: an accuracy study. J Endourol 28(3):371–376
13. Schiffmann J, Tennstedt P, Fischer J, Tian Z, Beyer B, Boehm K, Sun M, Gandaglia G, Michl U, Graefen M, Salomon G (2014) Does HistoScanning™ predict positive results in prostate biopsy? A retrospective analysis of 1,188 sextants of the prostate. World J Urol 28(3):371–376
14. Schiffmann J, Fischer J, Tennstedt P, Beyer B, Böhm K, Michl U, Graefen M, Salomon G (2014) Comparison of prostate cancer volume measured by HistoScanning™ and final histopathological results. World J Urol 32(4):939–944

15. Bul M, Zhu X, Valdagni R, Pickles T, Kakehi Y, Rannikko A, Bjartell A, van der Schoot DK, Cornel EB, Conti GN, Boeve ER, Staerman F, Vis-Maters JJ, Vergunst H, Jaspars JJ, Strolin P, van Muilekom E, Schroder FH, Bangma CH, Roobol MJ (2013) Active surveillance for low-risk prostate cancer worldwide: the PRIAS study. Eur Urol 63(4): 597–603

US Contrast Media in Renal Disease

52

Libero Barozzi, Diana Capannelli,
Massimo Valentino, and Michele Bertolotto

Contrast-enhanced ultrasound (CEUS) is a new technique that employs microbubble contrast agents and complementary harmonic pulse sequences to demonstrate parenchymal perfusion.

CEUS is widely employed in several fields of clinical practice. The 2011 updated European Federation of Societies for Ultrasound in Medicine and Biology (EFSUMB) Guidelines and Recommendations on the Clinical Practice of CEUS have identified the current indications for the administration of US contrast agents for the study of different parts of the body, including the kidneys [1].

CEUS is useful in the detection and characterisation of lesions, by differentiating solid neoplastic masses from pseudotumours, graduating complex cystic lesions according to the Bosniak system [2, 3] and detecting renal ischaemia, infections and trauma. CEUS demonstrated an accuracy similar to contrast-enhanced multidetector computed tomography (CE-MDCT) in detecting focal lesions, with the advantage of the real-time assessment of microvascular perfusion by using time-intensity curves. Other advantages of CEUS include its safety, simplicity, patient tolerance and lack of irradiation (conversely to CE-MDCT scans) [4–6].

Microbubble contrast agents are not excreted by the kidney and do not affect renal function: they can be safely administrated to patients with renal insufficiency. Current contraindications are known hypersensitivity to any of the contrast agent components (even if US contrast agents have low rate of anaphylactic reactions) and recent acute cardiopulmonary diseases.

The main limit of this technique is that contrast agents are not concentrated in the collecting system, and CEUS cannot give information about urinary excretory system.

CEUS has the same limitations of conventional US: poor sonic window due to bowel gas, ribs or patients with large body habitus (obesity) prevents good quality images. In these cases, CE-MDCT can give more information.

L. Barozzi (✉)
Radiology Unit, Casa di Cura Madre Fortunata Toniolo, Via Toscana 34, Bologna 40141, Italy
e-mail: libero.barozzi@alice.it

D. Capannelli
Radiology Unit. Cardio Thoracic Vascular Department, University of Bologna, Policlinico Sant'Orsola-Malpighi,
Via Massarenti 9, Bologna 40138, Italy
e-mail: diana.capannelli@yahoo.it

M. Valentino
Radiology Department, Tolmezzo Hospital,
Via Morgagni 18, Tolmezzo (UD) 33028, Italy
e-mail: mvm.valentino@gmail.com

M. Bertolotto
Radiology Department, University of Trieste,
Ospedale di Cattinara,
Strada di Fiume 447, Trieste 34149, Italy
e-mail: bertolot@units.it

P. Martino, A.B. Galosi (eds.), *Atlas of Ultrasonography in Urology, Andrology, and Nephrology*,
DOI 10.1007/978-3-319-40782-1_52

52.1 Microbubble Contrast Agents

Microbubble contrast agents consist of gas microbubbles (air or perfluorocarbon) stabilised by a biodegradable shell of protein, lipid or polymer. The small size of microbubbles (from 1 to 10 μm, as the size of a red blood cell) allows their passage unfiltered through the pulmonary capillary bed but prevents entry into the interstitium allowing them to remain entirely intravascular ("pure blood pool" agents) [4, 5, 7]. Under US exposition, microbubbles oscillatory contract and expand themselves with the same resonance frequency of US waves, by amplifying the US signal.

After circulating for several minutes, microbubbles dissolve: the gas is exhaled by the lungs, whereas the biodegradable shell is metabolised by the liver.

52.2 Technique

The kidney has a single arterial blood supply, conversely to the liver. After endovascular bolus injection of the contrast agent, microbubbles diffuse to the blood pool. The renal cortex rapidly enhances from 15 to 20 s after microbubble injection, while the vessels of the renal medulla are progressively filled from 30 to 35 s and completely filled after 40 to 50 s. Corticomedullary differentiation is evident only in the early phase and lasts for 20–40 s. This is because the renal medulla presents a lower global perfusion than the renal cortex. During the later phase (45–120 s), the enhancement is homogeneous and the differentiation between cortex and medulla is lost (Fig. 52.1). The lesion contrast enhancement is evaluated in comparison with the surrounding parenchyma [4]. Kidneys are highly vascularised and the contrast enhancement is faster than other abdominal organs: this allows the characterisation of renal parenchyma but also the evaluation of liver (in the remaining 3 min after kidneys) and spleen (that retrains the contrast agent for as long as 7 min).

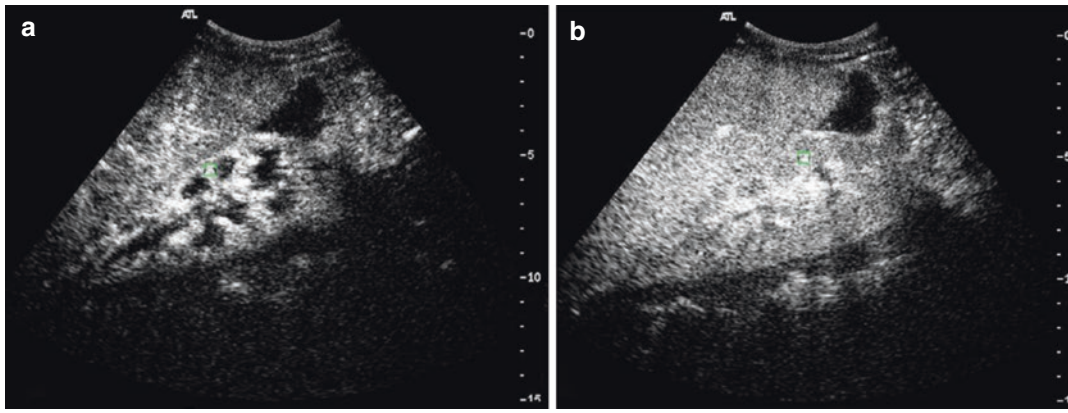

Fig 52.1 (**a**) Early phase (20 s after microbubbles injection) corticomedullary differentiation is evident due to the rapid and intense enhancement of the renal cortex. (**b**) Late phase (45 s after microbubbles injection) corticomedullary differentiation is lost because of progressive and later enhancement of medulla

52.3 Renal Infections

The diagnosis of acute pyelonephritis is based on clinical evaluation and laboratory findings [1]. Conventional baseline US can demonstrate increased size of the kidney and cortical scarring, suggestive of previous episodes of infections. CEUS plays an important role when the patient is still febrile after 72 h despite of antibiotic treatment and a complicated pyelonephritis is suspected. As CE-MDCT, CEUS can show focal parenchymal areas of pyelonephritis that appear as wedge-shaped areas of reduced enhancement because of the parenchymal oedema (Fig. 52.2).

Sometimes pyelonephritis can complicate with parenchymal abscessualization: a focal inhomogeneous nonenhancing area with intense peripheral uptake (Fig. 52.3).

Purulent material in pelvicalyceal system can be easily detected as echogenic material with no contrast uptake, since contrast agents are not concentrated in the collecting system. This finding is useful to differentiate pus from uro-endothelial tumours [5].

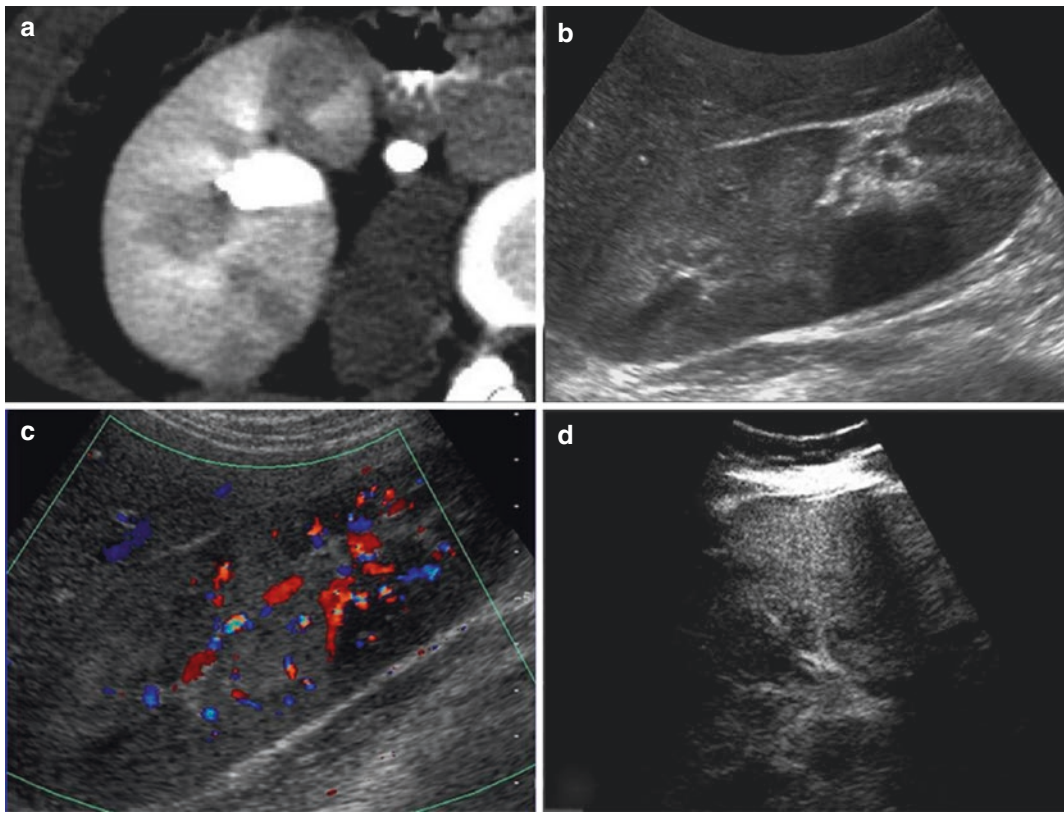

Fig 52.2 Contrast-enhancement CT shows an inhomogeneous parenchymal enhancement (**a**). Baseline US (**b**) demonstrates a wedge-shaped ipoechogenic area with poor vascularisation on colour Doppler evaluation (**c**). CEUS confirms the lack of contrast enhancement in this area (**d**)

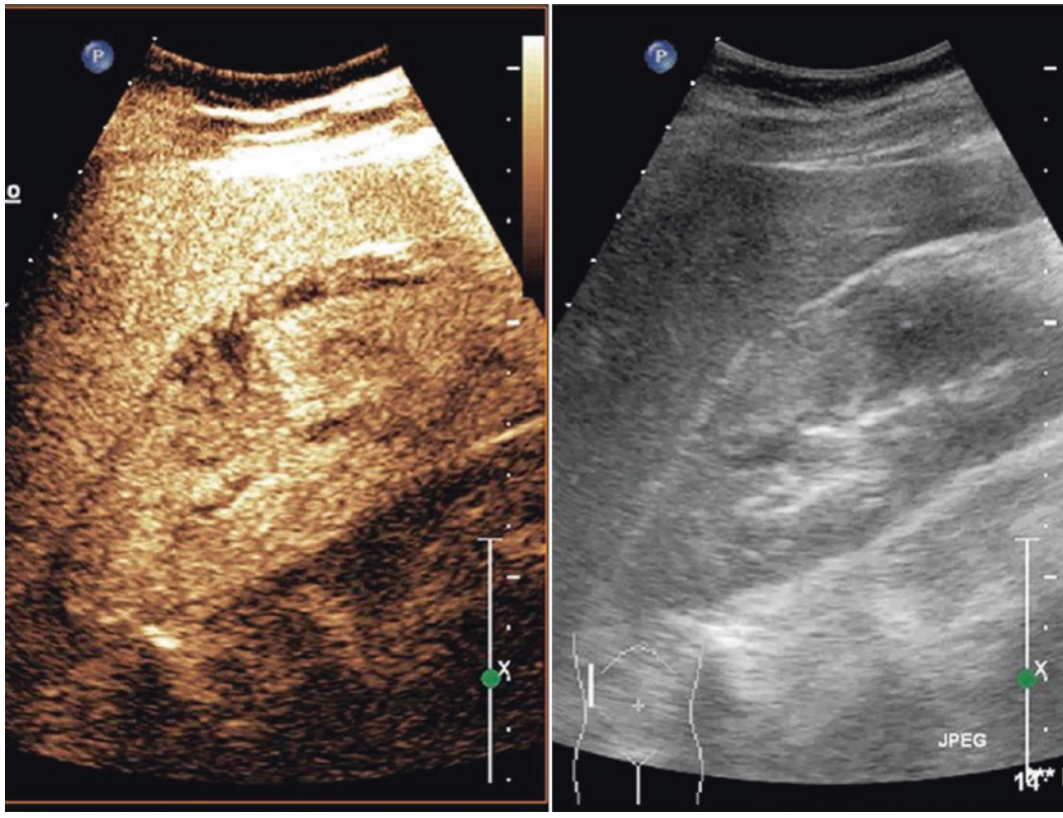

Fig 52.3 Renal abscess. CEUS shows a poor-defined area of lack of contrast with intense peripheral enhancement

52.4 Renal Ischaemia

The kidney has a rich blood flow but can undergo a variety of vascular injuries.

CEUS demonstrates high accuracy in detecting kidney parenchymal ischaemia, comparable to CE-MDCT. CEUS shows a higher sensibility in comparison to colour of power Doppler by detecting smaller blood vessels with slower blood flow. Microbubbles reach the microvasculature and amplify the US signal, allowing a direct evaluation of parenchymal perfusion.

Renal ischaemia appears as single or multiple focal triangular or wedge-shaped area of absent, diminished or delayed contrast enhancement, easily detectable in comparison with the surrounding normal parenchyma (Fig. 52.4).

CEUS may also provide more precise information about tissue vitality: it can differentiate infarcts from areas of diminished perfusion. Even if both injuries appear at colour Doppler as non-vascularised areas, only infarcts show complete lack of contrast enhancement after injection of microbubbles.

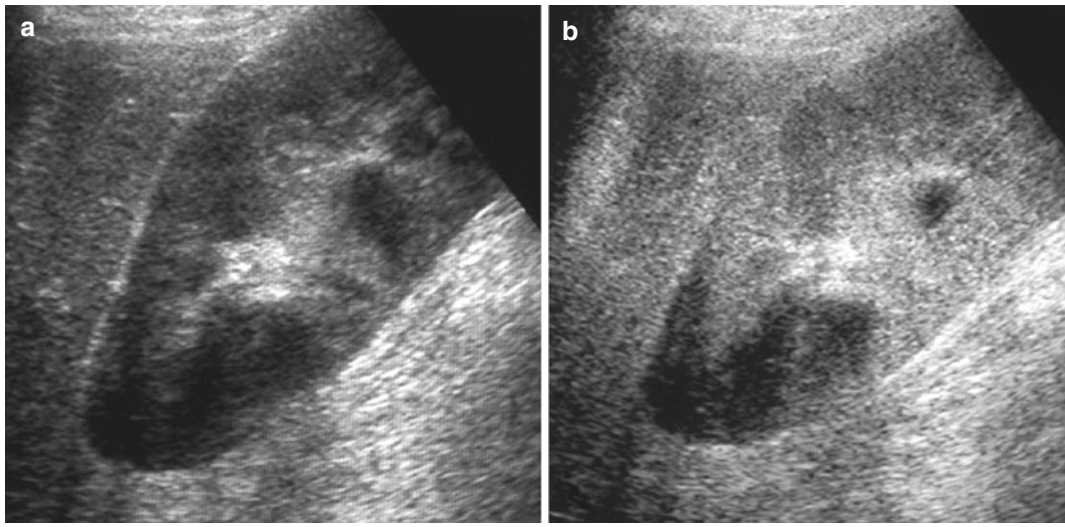

Fig 52.4 Baseline US examination shows an ipoechogenic area involving the upper pole of the right kidney (**a**). CEUS demonstrates a well-defined, triangular-shaped area of enhancement defect, suggestive of renal ischaemia (**b**)

52.5 Kidney Transplant

The renal transplant represents the ideal application of CEUS because the organ is superficial and well vascularised. An important advantage is that microbubbles are not nephrotoxic and do not compromise the renal function, conversely to CT contrast agents. Renal transplant can undergo a wide range of possible complications in the early postoperative period. The main important is the acute rejection. The first-line evaluation is typically performed with spectral Doppler measurements in order to assess abnormal values in resistance index (RI).

Spectral Doppler assessment only provides indirect information about the parenchymal perfusion, whereas microbubble contrast agents allow a direct visualisation of microcirculation. CEUS findings are also earlier than abnormal RI [8–10].

In acute rejection, the parenchymal perfusion is delayed. The time-intensity curves can demonstrate a diffuse delayed and slow contrast enhancement of the renal parenchyma. In a later phase, CEUS can also show perfusional defects (Fig. 52.5). CEUS is also useful in monitoring the antirejection therapy, by assessing an improved parenchymal perfusion [11].

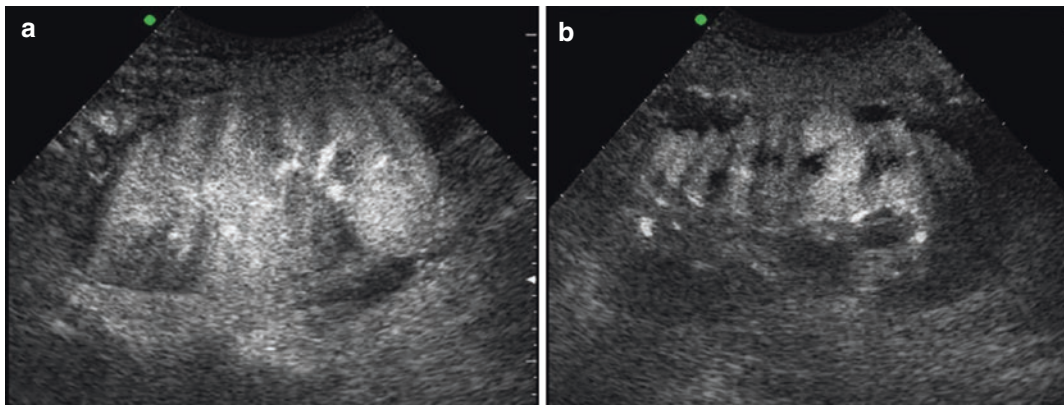

Fig 52.5 Normal kidney transplant: regular and homogeneous perfusion (**a**). Acute rejection in kidney transplant: CEUS demonstrates a wide lack of parenchymal perfusion at the upper pole of the kidney transplant, due to insufficient blood supply through the superior polar arteriosus anastomosis (**b**)

52.6 Cystic Lesions

Renal cysts are a common finding, but any cyst that does not show the typical features of a benign cyst is by definition "complicated" and requires further assessment.

CEUS can be useful in differentiating benign cysts from cystic tumours. Even if the Bosniak classification system was developed on the basis of contrast-enhancement findings of cystic renal masses on CE-MDCT [2, 3], CEUS can provide useful information for the management of these lesions: surgical treatment or observation.

CEUS is acquiring an increasing role in the assessment of indeterminate cystic lesions (Bosniak IIF and III) by detecting the presence and the enhancement of solid components. Recent comparative studies [12, 13] between CEUS and CT revealed that CEUS imaging was superior to CT in terms of detecting additional septa, thickness of the wall or septa and solid components. Microbubble contrast agents circulate in the microvessels of septa and walls, and CEUS provides the evaluation of sophisticated internal structures of cystic renal masses with a higher resolution than CE-MDCT. In particular, the demonstration of solid components is the key factor in differential with the categories III and IV that are considered malignant and must be surgically removed (Figs. 52.6 and 52.7).

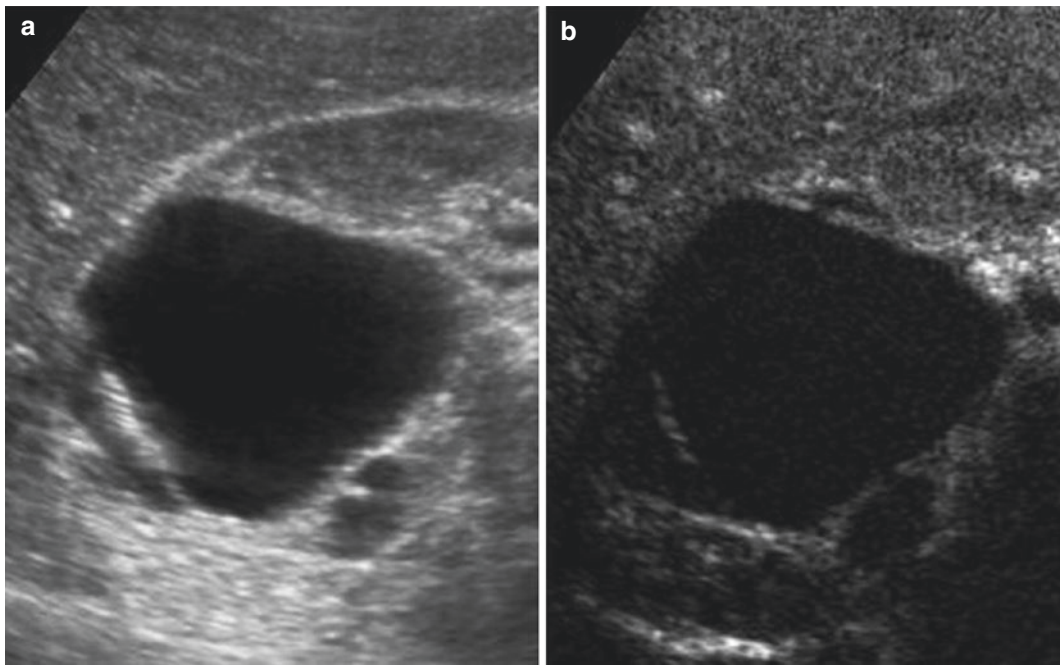

Fig 52.6 Baseline US examination shows a cyst with thin septa (**a**). CEUS demonstrates an enhancement of these septa, suggestive of Bosniak II category (**b**)

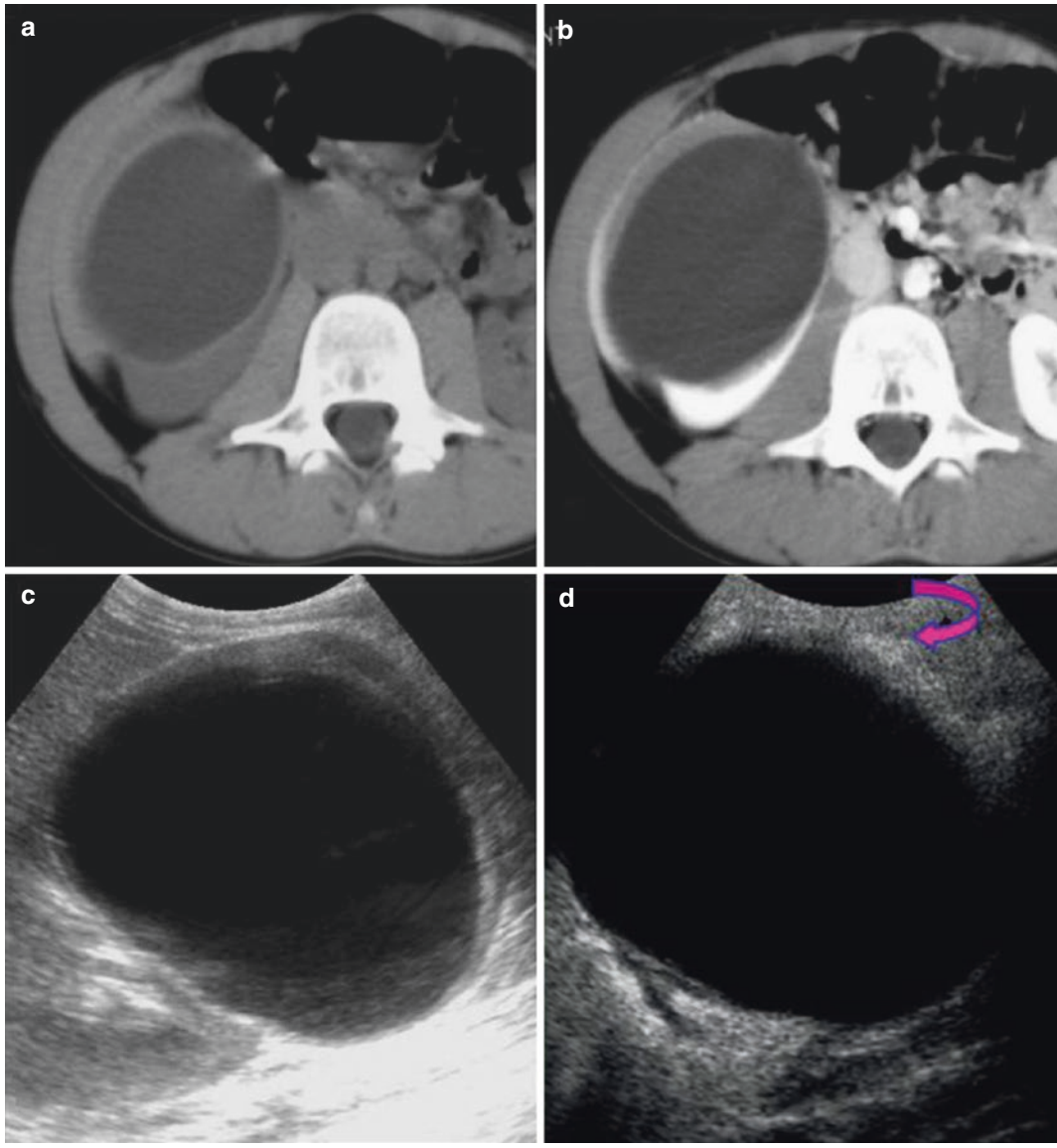

Fig 52.7 Contrast-enhancement CT scan shows a complicated cystic lesion with grossly thickened walls (**a**), well marginated, without significant CE of the walls (**b**), suggestive of Bosniak category III. Baseline US examination shows echoic content (solid/haemorrhagic echo in the liquid content of the cyst) and confirms the CT finding of thickened walls (**c**). CEUS demonstrates a well-enhancing mural nodule (arrow) within the lesion, suggestive of Bosniak IV category (**d**)

52.7 Solid Masses

The majority of renal tumours are renal cell carcinomas, whereas oncocytomas and angiomyolipomas represent a small part of renal solid lesions.

Renal malignancies have a rich blood supply, and CEUS can show an increased and heterogeneous enhancement (Fig. 52.8), fast filling and rapid washout (Fig. 52.9). However, the kidney itself has abundant blood supply, and the lesion may appear isoechoic to the surrounding renal cortex [5, 14].

CEUS is not currently used for differentiating between benign and malignant solid lesions. Even if several studies propose new methods for qualitative and quantitative assessment of contrast enhancement, solid malignancies do not show a specific perfusion pattern [5, 15]. In particular, specific analysis with time-intensity enhancement curves can help in differentiating a hyperenhancing from a hypoenhancing lesion (Fig. 52.9).

CEUS may also provide useful information in case of haemorrhage by detecting an underlined lesion into the haematoma that appears on conventional US evaluation as a large heterogeneous mass.

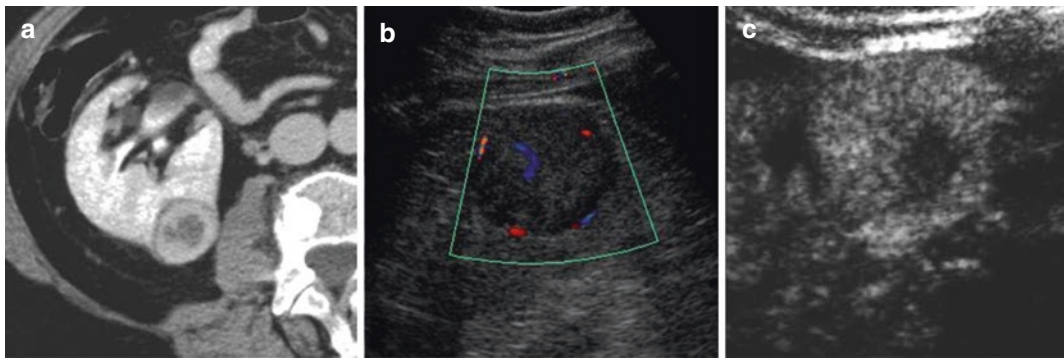

Fig 52.8 Contrast-enhancement CT scan shows a heterogeneous solid lesion, with intense peripheric enhancement (**a**). Colour Doppler examination shows an increased vascularisation, both intralesional and peripherical (**b**). CEUS demonstrates an intense peripherical hyperenhancement, suggestive of renal clear cell carcinoma (**c**)

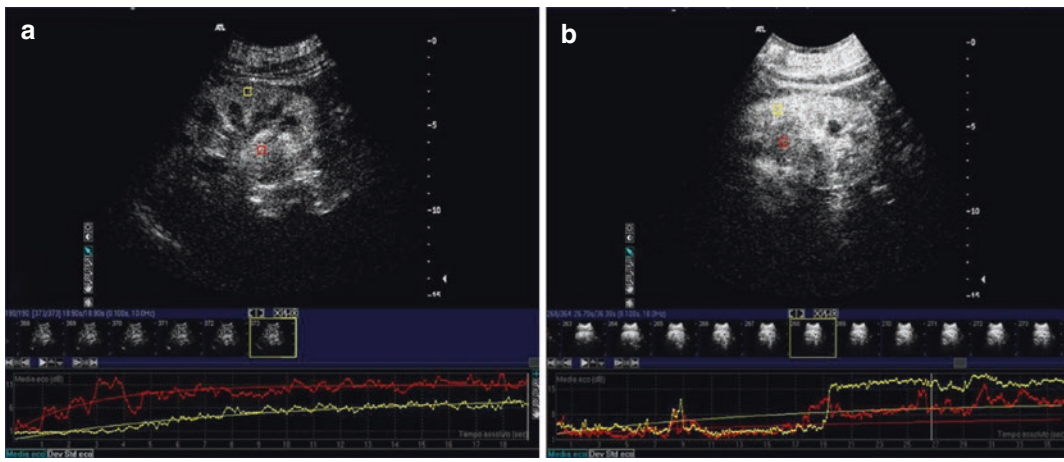

Fig 52.9 Time-intensity curves display two different patterns of solid lesion contrast enhancement. In the first case (**a**), the lesion time-intensity curve (*red*) shows a higher fast filling hyperenhancement with reference to the normal renal parenchyma, suggestive of renal clear cell carcinoma, whereas in the second case (**b**), the lesion time-intensity curve (*red*) shows a later and lower enhancement with reference to the normal cortex, suggestive of ipovascularizated solid malignant lesion

52.8 Trauma

CEUS with second-generation contrast agents shows a high sensitivity both in lesion detection and grading, but CEUS should be reserved for the assessment of stable, low-energy isolated trauma patients with unilateral pain. These patients have low risk for multiorgan and severe traumatic involvement, are haemodynamically stable and can be conservatively treated and evaluated during the follow-up [16, 17].

Instead, the modality of choice for the first-line evaluation in emergency room of severe traumatic patients is the conventional focused assessment with sonography for trauma ultrasound (FAST-US). FAST-US allows to exclude free abdominal, pleural and pericardial fluids, but it has low sensitivity in detection of parenchymal traumatic lesions, which may be isoechoic and can be missed [18].

CE-MDCT remains the reference examination in high-energy multitrauma because of high spatial resolution, very fast execution and higher sensibility. CE-MDCT also allows to exclude active bleeding, multitraumatic involvement of deep organs (pancreatic trauma) and gut perforations.

The main indication of CEUS is in the second-line evaluation of patients with low-energy isolated abdominal trauma. CEUS demonstrates an accuracy similar to CE-MDCT in detecting and grading renal traumatic lesions. Parenchymal lacerations and haematomas appear as nonenhancing areas after contrast injection.

The main limit of CEUS in kidney traumatic lesions is the impossibility to visualise pelvicalyceal and ureter injuries, since contrast agents are not concentrated in the collecting system. In these cases, CE-MDCT should be always performed in CEUS-positive patients to exclude active bleeding and urinomas.

52.9 Urinary Excretory System

The main limit of CEUS in the study of urinary excretory system is that contrast agents are not concentrated in the collecting system, and only voluminous pelvicalyceal neoplastic masses can be detected.

CEUS is also acquiring an increasing role in the assessment of vesicoureteral reflux in children, because of the safety of the technique and the lack of irradiation (conversely to retrograde cystourethrography). After intrabladder administration of microbubble, CEUS is able to assess and quantify the grade of vesicoureteral reflux.

References

1. Piscaglia F, Nolsøe C, Dietrich CF, Cosgrove DO, Gilja OH, Bachmann Nielsen M, Albrecht T, Barozzi L, Bertolotto M, Catalano O, Claudon M, Clevert DA, Correas JM, D'Onofrio M, Drudi FM, Eyding J, Giovannini M, Hocke M, Ignee A, Jung EM, Klauser AS, Lassau N, Leen E, Mathis G, Saftoiu A, Seidel G, Sidhu PS, ter Haar G, Timmerman D, Weskott HP (2012) The EFSUMB Guidelines and Recommendations on the Clinical Practice of Contrast Enhanced Ultrasound (CEUS): update 2011 on non-hepatic applications. Ultraschall Med 33:33
2. Bosniak MA (1997) Diagnosis and management of patients with complicated cystic lesions of the kidney. AJR Am J Roentgenol 169:819
3. Bosniak MA (1997) The use of the Bosniak classification system for renal cysts and cystic tumors. J Urol 157:1852
4. McArthur C, Baxter GM (2012) Current and potential renal applications of contrast-enhanced ultrasound. Clin Radiol 67:909
5. Cokkinos DD, Antypa EG, Skilakaki M, Kriketou D, Tavernaraki E, Piperopoulos PN (2013) Contrast enhanced ultrasound of the kidneys: what is it capable of? Biomed Res Int 59:5873
6. Jakobsen JA, Oyen R, Thomsen HS, Morcos SK (2005) Members of Contrast Media Safety Committee of European Society of Urogenital Radiology (ESUR). Safety of ultrasound contrast agents. Eur Radiol 15:941
7. Correas JM, Bridal L, Lesavre A, Méjean A, Claudon M, Hélénon O (2001) Ultrasound contrast agents: properties, principles of action, tolerance, and artifacts. Eur Radiol 11:1316
8. Lebkowska U, Janica J, Lebkowski W et al (2009) Renal parenchyma perfusion spectrum and resistive index (RI) in ultrasound examinations with contrast medium in the early period after kidney transplantation. Transplant Proc 41:3024
9. Fischer T, Filimonow S, Dieckhöfer J et al (2006) Improved diagnosis of early kidney allograft dysfunction by ultrasound with echo enhancer-a new method for the diagnosis of renal perfusion. Nephrol Dial Transplant 21:2921

10. Granata A, Andrulli S, Fiorini F et al (2011) Diagnosis of acute pyelonephritis by contrast-enhanced ultrasonography in kidney transplant patients. Nephrol Dial Transplant 26:715
11. Fischer T, Mühler M, Kröncke TJ et al (2004) Early postoperative ultrasound of kidney transplants: evaluation of contrast medium dynamics using time-intensity curves. Rofo 176:472
12. Park BK, Kim B, Kim SH, Ko K, Lee HM, Choi HY (2007) Assessment of cystic renal masses based on Bosniak classification: comparison of CT and contrast-enhanced US. Eur J Radiol 61:310
13. Ascenti G, Mazziotti S, Zimbaro G et al (2007) Complex cystic renal masses: characterization with contrast-enhanced US. Radiology 24(1):158–165
14. Ignee A, Straub B, Schuessler G, Dietrich CF (2010) Contrast enhanced ultrasound of renal masses. World J Radiol 2:15
15. Wang XH, Wang YJ, Lei CG (2011) Evaluating the perfusion of occupying lesions of kidney and bladder with contrast-enhanced ultrasound. Clin Imaging 35:447
16. Valentino M, De Luca C, Barozzi L et al (2010) Contrast-enhanced US evaluation in patients with blunt abdominal trauma. J Ultrasound 13:22
17. Cokkinos DD, Antypa E, Kalogeropoulos I et al (2013) Contrast-enhanced ultrasound performed under urgent conditions. Indications, review of the technique, clinical examples and limitations. Insights Imaging 4:185

US Contrast Media in Prostatic Disease

53

Vincenzo Scattoni and Carmen Maccagnano

53.1 Introduction

Contrast-enhanced ultrasound (CEUS) is a recent developing technology with high diagnostic accuracy.

The contrast ultrasound media are constituted by microbubbles with a diameter which ranges from 1 up to 7 μm, similar to that of red cells [1]. They are able to persist in the vascular bed for a long time and to design the microvascularization [2, 3, 4]. This may be particularly useful in case of neoangiogenesis (i.e., cancer foci) (Video 53.1) (Figs. 53.1 and 53.2).

The wall of the bubble is made of denatured albumin or phospholipids, and its thickness is about 10–200 nm [2]. The microbubbles contain a gas with high molecular weight of low solubility, i.e., perfluorocarbon or sulfur esafluorate.

The SonoVue® is a 2nd-generation contrast medium made by stabilized microbubbles of sulfur esafluorate (Table 53.1). Currently, it is the most used contrast medium for the diagnosis of prostate cancer, with transrectal approach.

The ultrasound technology needed to image microbubble contrast agents is available with most of the modern ultrasound devices. As tumor is usually associated with a higher blood flow, targeted prostate biopsies may be performed. However, the method is limited by the hypervascularity of benign prostatic hyperplasia (BPH) and prostatitis, which can lead to false-positive results.

Electronic supplementary material The online version of this chapter (doi:10.1007/978-3-319-40782-1_53) contains supplementary material, which is available to authorized users.

V. Scattoni (✉)
Department of Urology, University Vita-Salute,
Scientific Institute H San Raffaele,
Via Olgettina 60, Milan 20132, Italy
e-mail: scattoni.vincenzo@hsr.it

C. Maccagnano
Azienda Ospedaliera S. Anna –Como-,
Via Ravona, 60, San Fermo della Battaglia (Co)
22020, Italy

P. Martino, A.B. Galosi (eds.), *Atlas of Ultrasonography in Urology, Andrology, and Nephrology*,
DOI 10.1007/978-3-319-40782-1_53

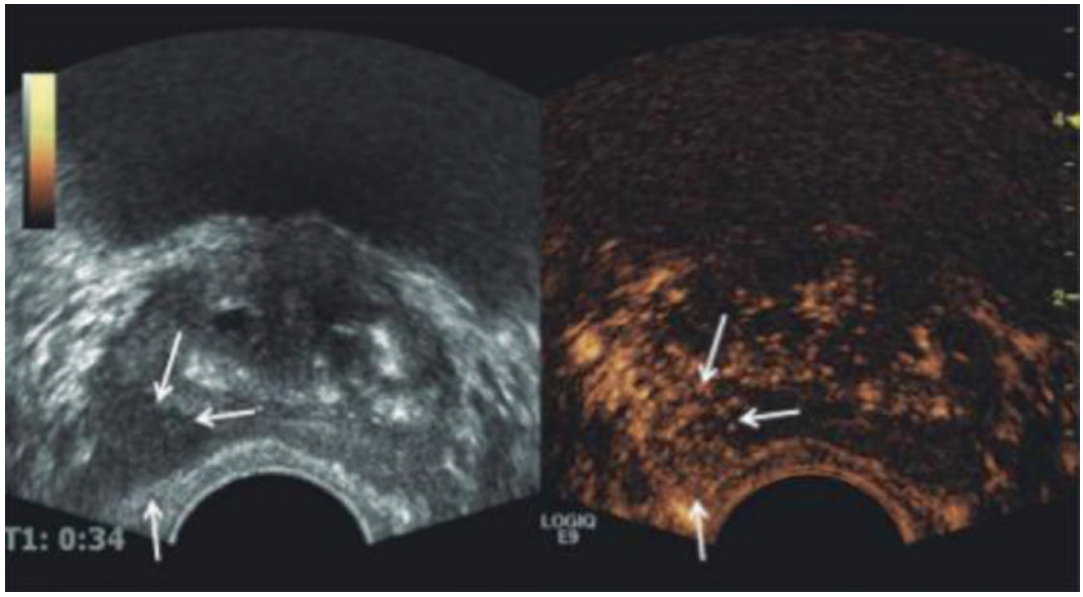

Fig. 53.1 The CEUS image shows an increasing vascularization in the *left* peripheral zone, which is hypoechoic in the US with gray scale (*white arrows*). The pathologic exam confirmed a cancer in the identified lesion

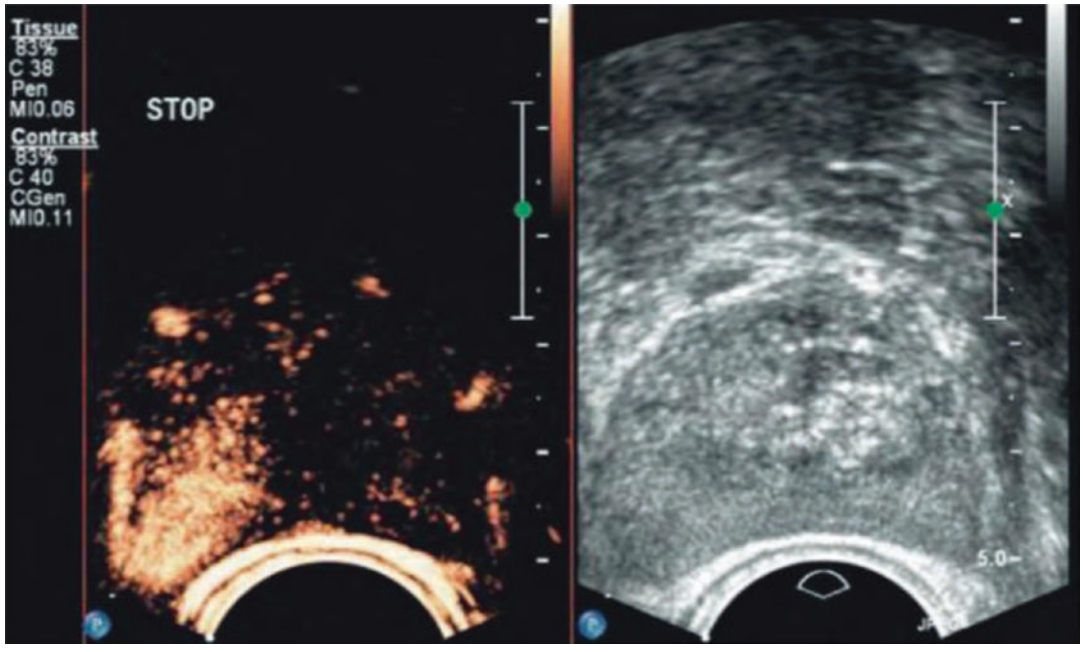

Fig. 53.2 Image with gray scale on the *right*, which shows a hypoechoic area in the *left* apical region; on the left, the enhancement caused by the contrast medium is evident, 28 s after the administration. The lesion is highly suspicious for cancer

Table 53.1 Ultrasound 2nd-generation contrast media currently in use

Commercial name	Company	Content of the microbubbles
SonoVue	BR1, Bracco, SpA	Stabilized microbubbles of sulfur esafluorate
OPTISON	FS069, Mallinckrodt Inc.	Microbubbles of perfluoropropane covered by albumin
Imavist	AF0150, Alliance Pharmac. Corp. and Schering AG	Microbubbles of perfluorohexane
DEFINITY	MRX115, DuPont-Merck, Inc.	Liposomes full with perfluoropropane
Sonazoid	NC100100, Nycomed Imaging as/ Amersham ltd	Microbubbles of perfluorocarbon

53.2 Contrast-Enhanced Ultrasound as Guidance for Prostate Biopsy

In 2012, Halpern and colleagues have demonstrated a significant benefit of CEUS comparing to systematic biopsy (PBx) in individuating aggressive neoplasms (Gleason score > 7) and with large volume (>50 % of the core affected by cancer) [5]. Moreover, Frauscher et al. have reported an important increase of detection rate (DR) of prostate cancer (PCa) with CEUS, with a probability 2.6 times higher than PBx in individuating PCa [6].

Mitterberger and colleagues have reported a higher PCa DR with the help of CEUS used together with Doppler during PBx (26 % vs 20 %). Additionally, the Gleason score was higher in the first group [7] (Fig. 53.3, 53.4, 53.5, and 53.6). This approach has the potential to perform targeted biopsies and to reduce the number of cores that can be taken.

In a meta-analysis about the performance of CEUS in patients affected by PCa, Li et al. have concluded that CEUS represents a promising instrument in the identification of PCa, even if it actually cannot substitute PBx [8].

In a recent review, Walz and colleagues have identified six studies about the use of CEUS as guidance for PBx. The authors have reported a higher DR using CEUS compared with standard PBx. The improvement of cancer DR has ranged from 2 up to 18 % [9].

False positives may be due to benign prostatic hyperplasia (BPH) and prostatitis, both acute and chronic [10–12] (Fig. 53.7). Nevertheless, Zhao and colleagues have reported that the percentage of false positives with CEUS is significantly inferior compared with standard US with gray scale [12]. Currently, there are no precise parameters of reference. The study of the intensity curves of wash-in and washout may potentially improve the DR and reduce the percentage of false positives.

False-negative cases may be due to low neoplastic volume or well-differentiated and not aggressive cancers (low Gleason score) or a localization in the transition zone where the cancer is visible with more difficulty [12].

Initially the neoplastic lesions usually show small dimensions and low malignancy. Consequently, they may show a vascular microdensity that is too small to be detected because they are not able to generate signals for CEUS [13–16]. Moreover, the lesions localized inside the transition zone may have a vascularization similar to normal prostatic tissue [17, 18].

Particularly, SonoVue® is the most used contrast media and is able to define the microvascularization of both the lesion and the adjacent tissue, especially due to the real-time observation of its behavior. The recommended dosage is ≥2.4 ml [23, 24]. There are other contrast media and the list is provided in Table 53.1. The main clinical indications for the use of CE-TRUS are resumed in Table 53.2.

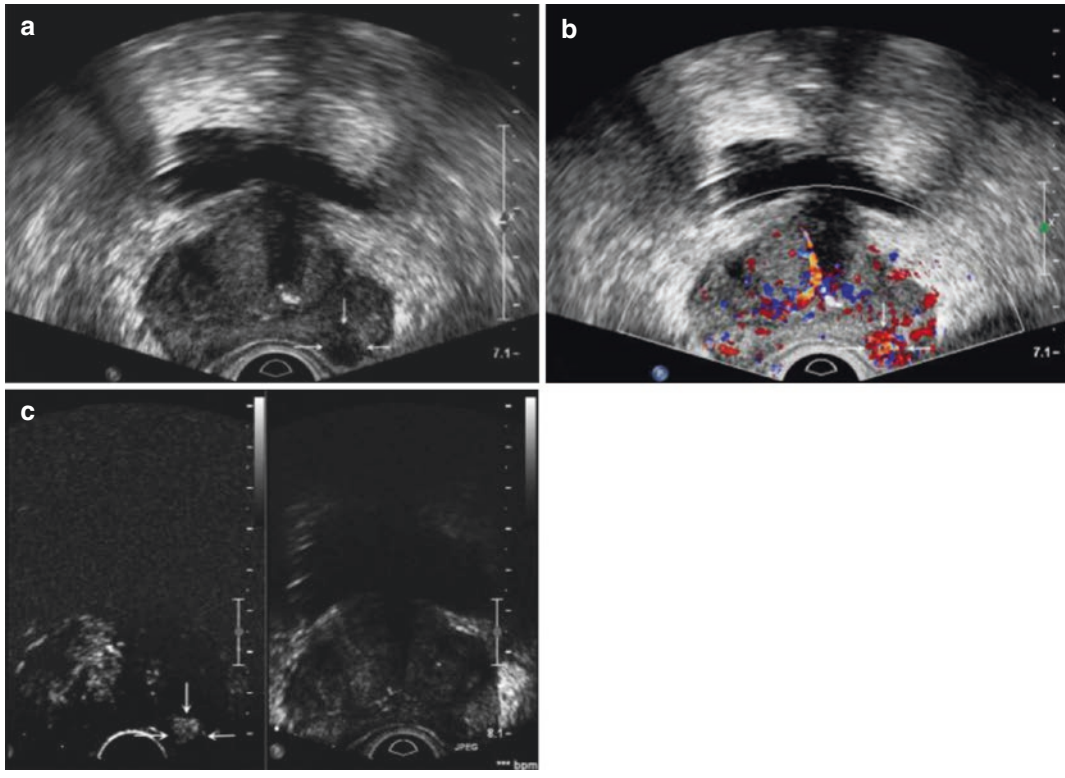

Fig. 53.3 An 84-year-old patient with prostate-specific antigen (PSA) of 8.8 ng/mL. (**a**) The image with gray scale demonstrates a round hypoechoic area in the left median region (*arrows*). (**b**) The color Doppler image demonstrates an increasing vascular flow in the region (*arrows*). (**c**) The CEUS image evidences a significant enhancement in the lesion, 20 s after the administration of the contrast medium. The pathologic exam evidenced BPH. The guided biopsy documented PCa Gleason score 3 + 3

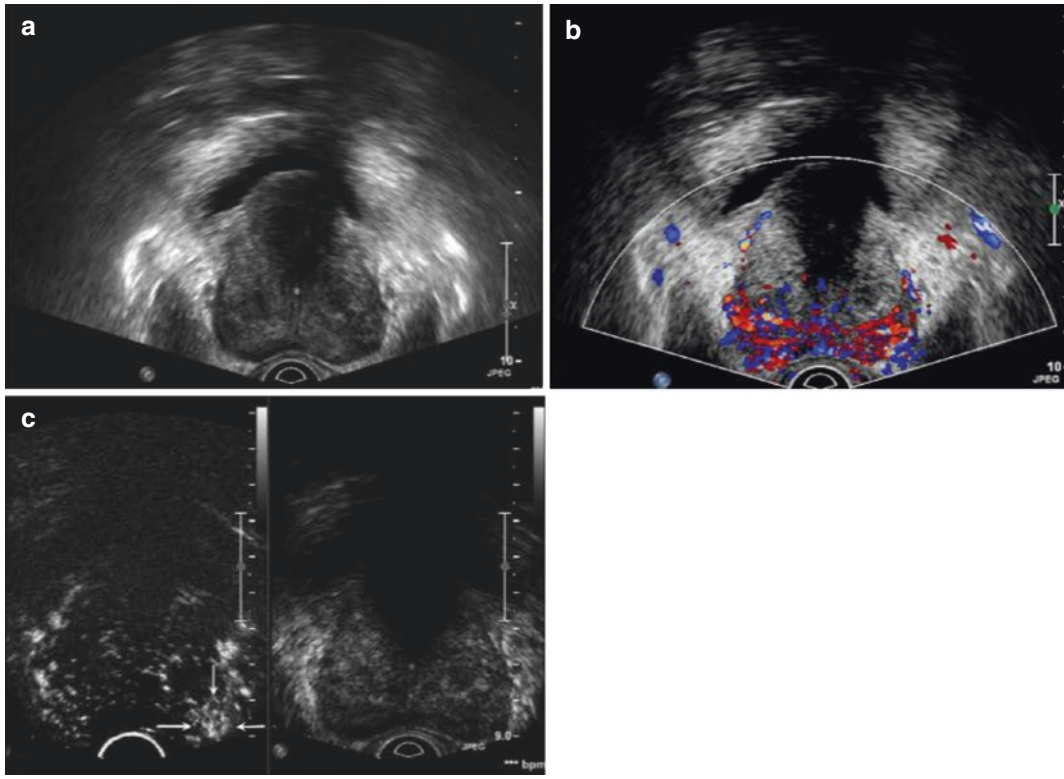

Fig. 53.4 A 70-year-old patient with PSA of 3.3 ng/mL. (**a**) The image with gray scale does not demonstrate alterations in the basal region of the prostate. (**b**) The color Doppler image demonstrates a symmetric, significant increasing vascular flow in the basal region of the prostate. (**c**) The CEUS image evidences a mild enhancement in the lesion in the left basal zone (*arrows*), 19 s after the administration of the contrast medium. The guided biopsy documented PCa Gleason score 3+2

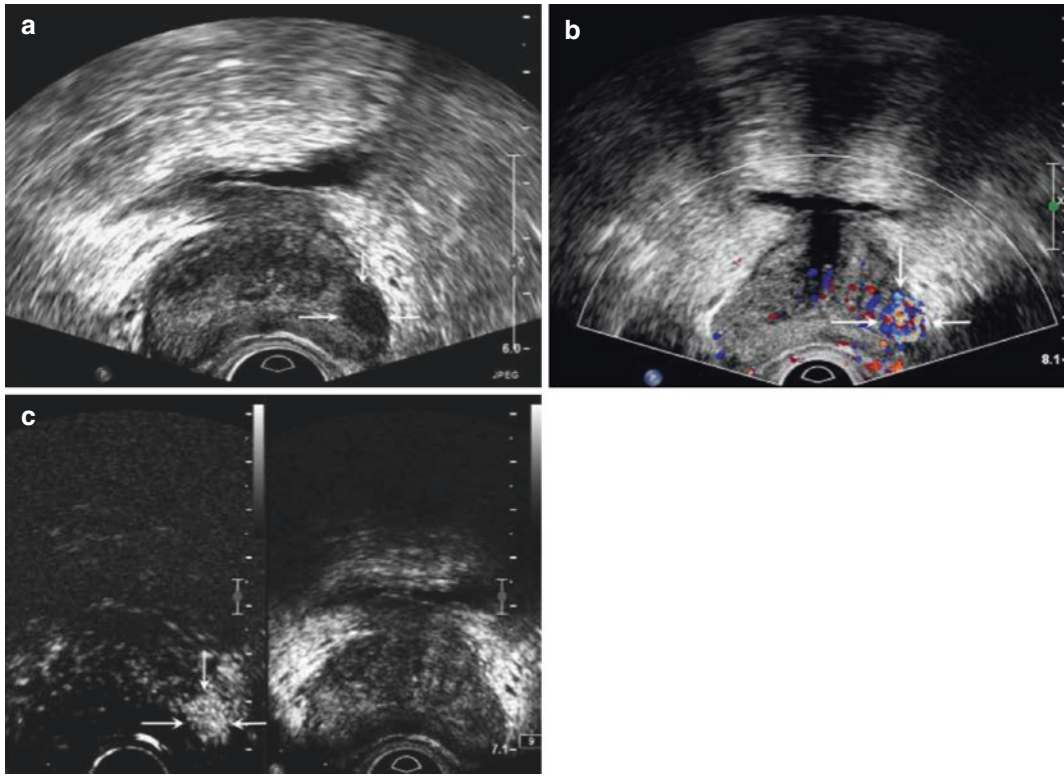

Fig. 53.5 A 76-year-old patient with PSA of 4.1 ng/mL. (**a**) The image with gray scale demonstrates a hypoechoic area in the left median region (*arrows*). (**b**) The color Doppler image demonstrates an increasing vascular flow in the region (*arrows*). (**c**) The CEUS image evidences a significant enhancement in the lesion, which shows irregular morphology, 17 s after the administration of the contrast medium. The final pathologic exam evidenced BPH

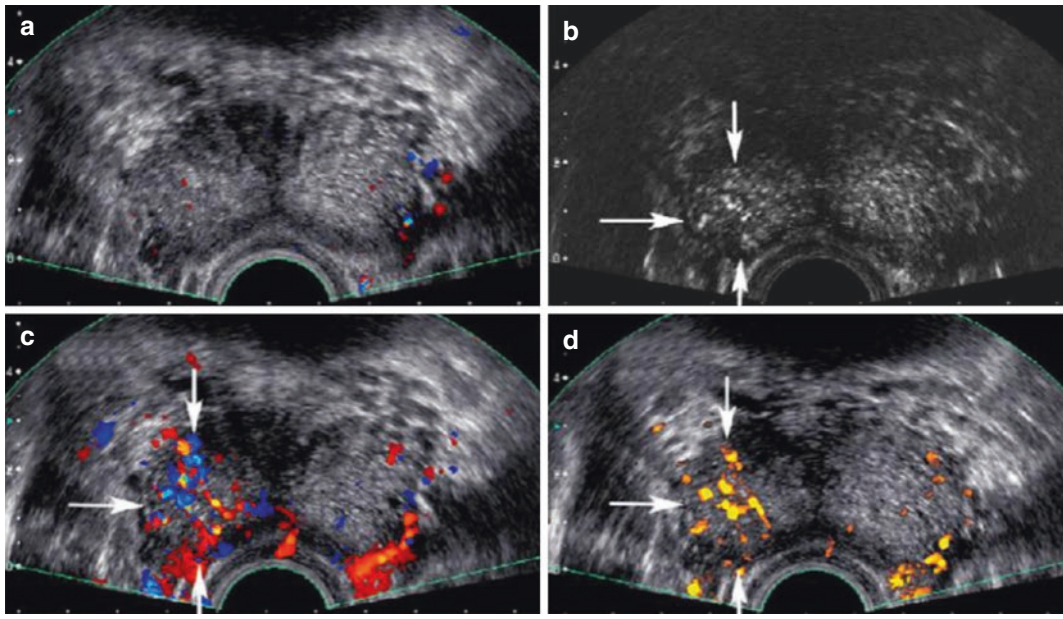

Fig. 53.6 A 62-year-old. (**a**) The image with gray scale does not identify neoplasms. (**b**) Power Doppler image after administration of contrast medium. (**c**) Power color Doppler after administration of contrast medium. (**d**) The CEUS image evidences a significant increase of vascularization (*arrows*)

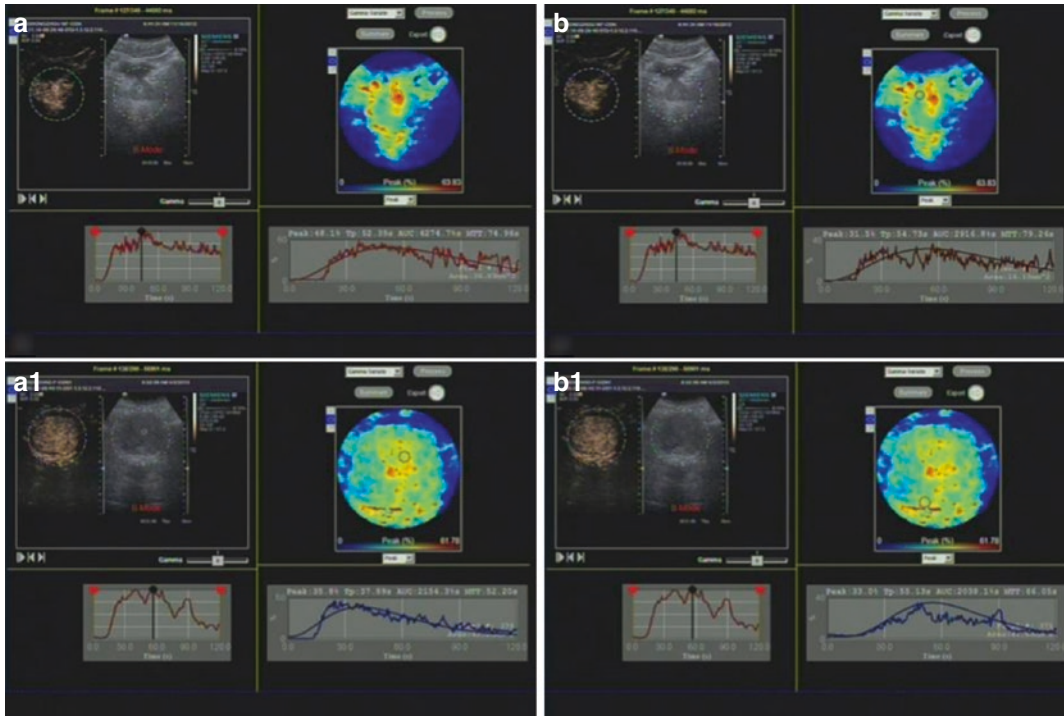

Fig. 53.7 BPH appearance with contrast medium. (**a**) Central region of the prostate, normal. (**b**) Peripheral zone of the prostate, normal. (**A1**) Central region of the prostate, BPH. (**B1**) Peripheral region of the prostate, BPH

Table 53.2 Main clinical fields of use of ultrasound 2nd-generation contrast media

Diagnosis	Follow-up	Experimental
Guidance for prostate biopsy	Active surveillance	Planning and follow-up of brachytherapy
Identification of index lesion and surgical planning	Post high-intensity focused ultrasound	

53.3 Specific Contrast Media for Prostate Cancer

The contrast media for a specific disease are very recent; they are constituted by microbubbles with additional ligands directed to specific sites. The possible target receptors for PCa are molecules upregulated during the angiogenesis, especially the vascular endothelial growth factor (VEGF) receptors [19, 20].

Particularly, the prostate-specific membrane antigen (PMSA) is a type II transmembrane glycoprotein exposed on the membrane of the prostatic cells, with different levels of expression among normal prostatic tissue, BPH, first diagnosis-PCa, hormone-refractory PCa, and metastasis, respectively.

Loading nanoscale microbubbles with PCa-targeted specific ligands or antibodies is critical for specific ultrasound imaging in PCa. It has been shown that targeted nanoscale microbubbles can significantly increase peak intensity and duration of contrast enhancement than blank nanoscale microbubbles in transplanted prostate tumors. Increased peak intensity and prolonged duration of enhanced contrast are the main characteristics of targeted nanoscale microbubbles enhanced imaging.

Actually, it represents the most important target of both imaging and immune-mediated therapies [21, 22].

53.4 Role of Contrast-Enhanced Ultrasound in Benign Prostatic Hyperplasia

The BPH localizes in the central zone of the gland, and its pathogenesis is complex. Some trials have demonstrated higher levels of the angiogenetic growth factors in the urine of patients affected by BPH compared with the levels in normal tissue. It suggests that an increased angiogenesis may play a fundamental role in the pathogenesis of the BPH itself [25, 26].

Some trials have shown that an increase in the vascularization proximally to BPH nodules and a reduction of the microvascularization in the peripheral can be easily identified. This effect is due to the compression of the adenoma on the peripheral gland.

Shi and colleagues have recently demonstrated that the enhancement induced by the contrast medium is visible in an initial time in the central portion and later in the peripheral one during the wash-in dynamic phase. Moreover, the peak intensity, the medium time of passage, and the extinction time in the central zone have been longer compared to the peripheral zone. The diagnostic accuracy, the sensitivity, and the specificity were about 95.6 %, 95 %, and 96.7 %, respectively [27].

53.5 Role of Index Lesion

In the context of the definition of PCa, often multifocal, the "index lesion" (IL) is identified as the largest focus, and, consequently, it is directed related to the whole volume of the neoplasm and the risk of neoplastic recurrence, the Gleason score, and the prognosis of the patient [28–31].

Particularly, the dimensions of the IL represent one of the most important criteria in order to evaluate an eventual focal therapeutic approach with sparing of the neurovascular bundles or of the urinary sphincter, with the final aim of minimizing the side effects.

In this context, despite the fact that focal therapy should be considered as an experimental therapy, the most recent trials have demonstrated that the treatment of the IL is sufficient to control the cancer, even in patient affected by multifocal neoplasms.

Currently, there are no imaging methods able to precisely identify the IL. According to a pathologic point of view, the microvascular density of the prostatic neoplastic tissue is significantly higher than that of the adjacent tissue. This feature is well delineated by the contrast medium [32].

Moreover, the contrast medium has revealed as particularly efficient in the identification of the more aggressive lesions, i.e., in pT3 or Gleason ≥7 or with larger dimensions (cut off of 15 mm) (Fig. 53.8 and 53.9) [33, 34].

The more frequent site of the IL is the peripheral zone, whereas the identification is resulted more difficult in the transition zone, probably due to a heterogeneous enhancement, related to BPH [35].

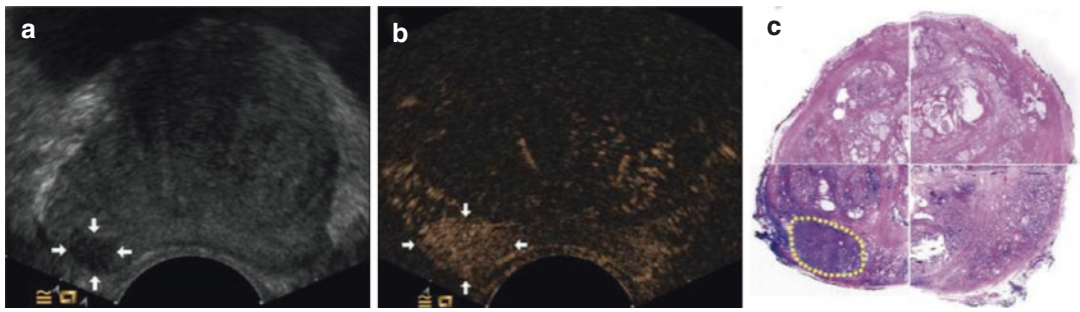

Fig. 53.8 Patient with PSA 9.91 ng/mL and clinical stage pT2c. (**a**) The basal image with gray scale demonstrates a hypoechoic area in the right peripheral zone (*white arrows*). (**b**) The CEUS image demonstrates fast and significant increasing vascular flow in the region (*white arrows*). (**c**) The final pathologic exam evidenced adenocarcinoma Gleason 4+4 without infiltration of the capsule (*dashed line*)

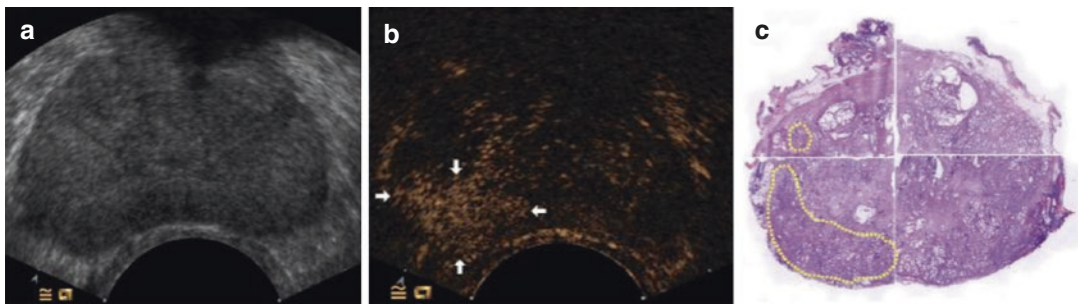

Fig. 53.9 Patient with PSA 9.91 ng/mL and clinical stage pT2c. (**a**) The basal image with gray scale does no evidence lesions. (**b**) The CEUS image demonstrates fast and significant increasing vascular flow in the right peripheral zone (*white arrows*). (**c**) The final pathologic exam evidenced an index lesion with adenocarcinoma Gleason 3+4 with infiltration of the capsule (*dashed line*) and adenocarcinoma Gleason 3+3 in the adjacent region (*dashed line*)

53.6 Role of Contrast-Enhanced Ultrasound in the Follow-Up of Focal Therapies

The role of CEUS may result particularly intriguing in the patients submitted to ablative therapies, where the efficacy of the therapy itself may involve a vascular response [36]. In 2011, Rouvier and colleagues have demonstrated that the CEUS may be used for differentiating the treated tissue from the untreated one in patients submitted to high-intensity focused ultrasound (HIFU). The enhancement has been judged as low, mild, and high in 6, 34, and 60% of the sites, respectively [37]. Even if this method is not able to differentiate the benign from the malignant tissue, the CEUS constitutes a promising technique.

Conclusions

The CEUS may be executed in day off clinic context and is an easily repeatable, technically feasible, and safe method. Despite these considerations, actually, its main limit is the absence of a standard definition of enhancement, also because the images per se may be influenced by several local anatomical factors and by the interpretation of the single operator.

References

1. Cosgrove D (2006) Ultrasound contrast agents: an overview. Eur J Radiol 60(3):324–330
2. Quaia E, D'Onofrio M, Cabassa P, Vecchiato F, Caffarri S, Pittiani F, Wittkowski KM, Cova MA (2007) Diagnostic value of hepatocellular nodule vascularity after microbubble injection for characterizing malignancy in patients with cirrhosis. AJR Am J Roentgenol 189(6):1474–1483
3. Burns PN, Wilson SR (2006) Microbubble contrast for radiological imaging: 1 principles. Ultrasound Q 22(1):5–13
4. Ma F, Cang Y, Zhao B, Liu Y, Wang C, Liu B, Wu T, Song Y, Peng A (2012) Contrast-enhanced ultrasound with SonoVue could accurately assess the renal microvascular perfusion in diabetic kidney damage. Nephrol Dial Transplant 27(7):2891–2898
5. Halpern EJ, Gomella LG, Forsberg F, McCue PA, Trabulsi EJ (2012) Contrast enhanced transrectal ultrasound for the detection of prostate cancer: a randomized, double-blind trial of dutasteride pretreatment. J Urol 188(5):1739–1745
6. Frauscher F, Klauser A, Halpern EJ, Horninger W, Bartsch G (2001) Detection of prostate cancer with a microbubble ultrasound contrast agent. Lancet 357(9271):1849–1850
7. Mitterberger M, Aigner F, Pinggera GM, Steiner E, Rehder P, Ulmer H, Halpern EJ, Horninger W, Frauscher F (2010) Contrast-enhanced colour Doppler-targeted prostate biopsy: correlation of a subjective blood-flow rating scale with the histopathological outcome of the biopsy. BJU Int 106(9):1315–1318
8. Li Y, Tang J, Fei X, Gao Y (2013) Diagnostic performance of contrast enhanced ultrasound in patients with prostate cancer: a meta-analysis. Acad Radiol 20(2):156–164
9. van Hove A, Savoie PH, Maurin C, Brunelle S, Gravis G, Salem N, Walz J (2014) Comparison of image-guided targeted biopsies versus systematic randomized biopsies in the detection of prostate cancer: a systematic literature review of well-designed studies. World J Urol 32(4):847–858
10. Roy C, Buy X, Lang H, Saussine C, Jacqmin D (2003) Contrast enhanced color Doppler endorectal sonography of prostate: efficiency for detecting peripheral zone tumors and role for biopsy procedure. J Urol 170(1):69–72
11. Newman JS, Bree RL, Rubin JM (1995) Prostate cancer: diagnosis with color Doppler sonography with histologic correlation of each biopsy site. Radiology 195(1):86–90
12. Zhao HX, Xia CX, Yin HX, Guo N, Zhu Q (2013) The value and limitations of contrast-enhanced transrectal ultrasonography for the detection of prostate cancer. Eur J Radiol 82(11):e641–e647
13. Jack GS, Cookson MS, Coffey CS, Vader V, Roberts RL, Chang SS, Smith JA Jr, Shappell SB (2002) Pathological parameters of radical prostatectomy for clinical stages T1c versus T2 prostate adenocarcinoma: decreased pathological stage and increased detection of transition zone tumors. J Urol 168(2):519–524
14. Bono AV, Celato N, Cova V, Salvadore M, Chinetti S, Novario R (2002) Microvessel density in prostate carcinoma. Prostate Cancer Prostatic Dis 5(2):123–126
15. Yi A, Kim JK, Park SH, Kim KW, Kim HS, Kim JH, Eun HW, Cho KS (2006) Contrast-enhanced sonography for prostate cancer detection in patients with indeterminate clinical findings. AJR Am J Roentgenol 186(5):1431–1435
16. van Niekerk CG, Witjes JA, Barentsz JO, van der Laak JA, Hulsbergen-van de Kaa CA (2013) Microvascularity in transition zone prostate tumors resembles normal prostatic tissue. Prostate 73(5):467–475
17. Sano F, Terao H, Kawahara T, Miyoshi Y, Sasaki T, Noguchi K, Kubota Y, Uemura H (2011) Contrast-enhanced ultrasonography of the prostate: various

imaging findings that indicate prostate cancer. BJU Int 107(9):1404–1410
18. Uemura H, Sano F, Nomiya A, Yamamoto T, Nakamura M, Miyoshi Y, Miki K, Noguchi K, Egawa S, Homma Y, Kubota Y (2013) Usefulness of perflubutane microbubble-enhanced ultrasound in imaging and detection ofprostate cancer: phase II multicenter clinical trial. World J Urol 31(5): 1123–1128
19. Sedelaar JP, van Leenders GJ, Hulsbergen-van de Kaa CA, van der Poel HG, van der Laak JA, Debruyne FM, Wijkstra H, de la Rosette JJ (2001) Microvessel density: correlation between contrast ultrasonography and histology of prostatecancer. Eur Urol 40(3):285–293
20. Fischer T, Thomas A, Tardy I, Schneider M, Hünigen H, Custodis P, Beyersdorff D, Plendl J, Schnorr J, Diekmann F, Gemeinhardt O (2010) Vascular endothelial growth factor receptor 2-specific microbubbles for molecular ultrasound detection ofprostate cancer in a rat model. Invest Radiol 45(10):675–684
21. Perner S, Hofer MD, Kim R, Shah RB, Li H, Möller P, Hautmann RE, Gschwend JE, Kuefer R, Rubin MA (2007) Prostate-specific membrane antigen expression as a predictor of prostate cancer progression. Hum Pathol 38(5):696–701
22. Wang L, Li L, Guo Y, Tong H, Fan X, Ding J, Huang H (2013) Construction and in vitro/in vivo targeting of PSMA-targeted nanoscale microbubbles in prostate cancer. Prostate 73(11):1147–1158
23. Jiang J, Chen YQ, Zhu YK, Yao XH, Qi J (2012) Factors influencing the degree of enhancement of prostate cancer on contrast-enhanced transrectal ultrasonography: correlation with biopsy and radical prostatectomy specimens. Br J Radiol 85(1019): e979–e986
24. Bertolotto M, Trincia E, Zappetti R, Bernich R, Savoca G, Cova MA (2009) Effect of Tadalafil on prostate haemodynamics: preliminary evaluation with contrast-enhanced US. Radiol Med 114(7):1106–1114
25. Strohmeyer D, Rössing C, Bauerfeind A, Kaufmann O, Schlechte H, Bartsch G, Loening S (2000) Vascular endothelial growth factor and its correlation with angiogenesis and p53 expression in prostate cancer. Prostate 45(3):216–224
26. Weingärtner K, Ben-Sasson SA, Stewart R, Richie JP, Riedmiller H, Folkman J (1998) Endothelial cell proliferation activity in benign prostatic hyperplasia and prostate cancer: an in vitro model for assessment. J Urol 159(2):465–470
27. Shi J, Yin X, Xu R, Wang Y, Jin L, Gao W (2014) Clinical application of contrast enhanced ultrasound to diagnose benign prostatic hyperplasia. Diagn Pathol 9:133
28. Qi T, Chen Y, Zhu Y, Jiang J, Wang L, Qi J (2014) Contrast-enhanced transrectal ultrasonography for detection and localization of prostate index tumor: correlation with radical prostatectomy findings. Urology 84(1):138–143
29. Ahmed HU (2009) The index lesion and the origin of prostate cancer. N Engl J Med 361(17): 1704–1706
30. Bott SR, Ahmed HU, Hindley RG, Abdul-Rahman A, Freeman A, Emberton M (2010) The index lesion and focal therapy: an analysis of the pathological characteristics of prostate cancer. BJU Int 106(11): 1607–1611
31. Karavitakis M, Winkler M, Abel P, Livni N, Beckley I, Ahmed HU (2011) Histological characteristics of the index lesion in whole-mount radical prostatectomy specimens: implications for focal therapy. Prostate Cancer Prostatic Dis 14(1):46–52
32. Russo G, Mischi M, Scheepens W, De la Rosette JJ, Wijkstra H (2012) Angiogenesis in prostate cancer: onset, progression and imaging. BJU Int 110(11 Pt C):E794–E808
33. Xie SW, Li HL, Du J, Xia JG, Guo YF, Xin M, Li FH (2013) Influence of serum prostate-specific antigen (PSA) level, prostate volume, and PSA density on prostate cancer detection with contrast-enhanced sonography using contrast-tuned imaging technology. J Ultrasound Med 32(5):741–748
34. Xie SW, Li HL, Du J, Xia JG, Guo YF, Xin M, Li FH (2012) Contrast-enhanced ultrasonography with contrast-tuned imaging technology for the detection of prostate cancer: comparison with conventional ultrasonography. BJU Int 109(11):1620–1626
35. Strazdina A, Krumina G, Sperga M (2011) The value and limitations of contrast-enhanced ultrasound in detection of prostate cancer. Anticancer Res 31(4):1421–1426
36. Rosoff JS, Prasad SM, Savage SJ (2013) Ultrasound in prostate cancer: current roles and potential applications in radiorecurrent disease. World J Urol 31(6):1353–1359
37. Rouvière O, Glas L, Girouin N, Mège-Lechevallier F, Gelet A, Dantony E, Rabilloud M, Chapelon JY, Lyonnet D (2011) Prostate cancer ablation with transrectal high-intensity focused ultrasound: assessment of tissue destruction with contrast-enhanced US. Radiology 259(2):583–591

US Contrast Media in Andrology

54

Massimo Valentino, Michele Bertolotto,
Libero Barozzi, Pietro Pavlica, and Lorenzo Derchi

54.1 Introduction and Technique

Ultrasound (US) is recognized as a useful first-line imaging modality, being esteemed its characteristics such as real-time scanning, no radiation, easy performance, and cost-effectiveness. However, it is regarded inferior to computed tomography and magnetic resonance because of its low ability to depict organ vascularization especially for tumor characterization.

Recently a new generation of contrast media specific for ultrasound has been developed. This new technique, named "contrast-enhanced ultrasound" (CEUS), improved the diagnostic performance of US in numerous pathological conditions changing the status of US. In fact, CEUS provides unique information on the vascularization of the pathologic lesions obtaining fundamental diagnostic advantages without the need of more complex diagnostic procedures.

Ultrasound contrast agents (UCAs) are elements able to interact with the US beam, increasing the echoes and producing an intense signal. The first generation of UCAs was able to improve the Doppler signal from vessels of large to intermediate diameter, allowing increased detection of arteries and veins and improved demonstration of their luminal abnormalities. These UCAs used a stationary imaging, were affected by signal artifacts which interfere with lesion assessment, and were substantially unable to demonstrate signal from small vessels located within tumors [1]. Subsequently, a second generation of UCAs was produced. It consists of microbubbles stabilized with different substances, having a diameter less than 8μm which guarantees that the UCA can pass the pulmonary circulation and reach various organs [2]. These new UCAs have long activity (about 8–10 min) and strong harmonic response. The UCAs interact with the US beam, developing nonlinear resonance with the generation of harmonic imaging. At low mechanical index (<0,2),

Electronic supplementary material The online version of this chapter (doi:10.1007/978-3-319-40782-1_54) contains supplementary material, which is available to authorized users.

M. Valentino, MD (✉)
Tolmezzo Hospital, via Morgagni 18,
Tolmezzo (UD) 33028, Italy
e-mail: mvm.valentino@gmail.com

M. Bertolotto, MD
Department of Radiology, University of Trieste,
Ospedale di Cattinara, Strada di Fiume 447,
Trieste 34149, Italy

L. Barozzi, MD
Radiology Unit, Casa di Cura Madre Fortunata
Toniolo, Via Toscana 34, Bologna 40141, Italy

P. Pavlica, MD
GVM Care and Research, Villalba Hospital,
Bologna, Italy

L. Derchi, MD
Dicmi-Radiologia, University of Genova,
Largo R. Benzi 8, Genoa 16132, Italy

P. Martino, A.B. Galosi (eds.), *Atlas of Ultrasonography in Urology, Andrology, and Nephrology*,
DOI 10.1007/978-3-319-40782-1_54

they are not destroyed and permit a real-time imaging. The UCA is introduced in the circulation following intravenous injection at a dose of 1.2–2.4 ml followed by a rapid flush of 5–10 ml of saline solution (Video 54.1). In the examination of the superficial structures, like testis, it is advisable to use a higher dose (4.8 ml), as the harmonic response to the high-intensity probes is lower due to the greater rupture of the microbubbles.

Numerous clinical experiences of its use are reported in the literature, although these substances obtained the clearance to be only used in echocardiography, liver pathology, breast disease, and micro- and macrovessel examination. The official registration does not include the authorization to study other organs as the kidney and the urogenital tract. The product has not been registered to be used in pediatric patients, in pregnancy, and in breastfeeding women. To obtain more extensive information for the clinical use of SonoVue, the technical leaflet can be downloaded from the Agenzia Italiana del Farmaco (AIFA) website [www.farmaci.agenziafarmaco.gov.it/aifa]. Moreover, the microbubbles actually used have showed an excellent safety profile with no signs of toxicity on different organs as the kidney, liver, and brain. Adverse reactions are very rare, and when they appear, they are short lasting and mild [3].

The use of US contrast media in urology and andrology has been proposed in many clinical studies regarding the kidney, prostate, bladder, and scrotal pathology. The European Federation of Societies for Ultrasound in Medicine and Biology (EFSUMB) has recently published guidelines and recommendation on the nonhepatic applications of contrast media, and the document can be downloaded from the EFSUMB website [www.efsumb.org].

54.2 Kidney

54.2.1 Renal Masses

CEUS is frequently employed in the characterization of cystic lesion of the kidney. Numerous comparative studies have shown that its diagnostic accuracy is equivalent to computed tomography (CT) with iodinated contrast injection [4]. The contrast-enhanced imaging techniques used have a very high sensitivity in the detection of the signals coming from the resonating bubbles and identification of the enhancement at the level of cystic wall, intracystic septa, focal wall thickening, or small nodules. The cystic wall thickness is measured after contrast injection, because this measurement is frequently difficult with traditional gray-scale imaging, due to echoes coming from debris usually present in the cyst (Fig. 54.1). CEUS has been also proposed to investigate solid renal lesions [5], but the information obtained are usually inferior to those acquired with CT or MR imaging with contrast media.

Renal clear cell carcinoma is the most common renal malignancy, and it is the lesion most usually studied with CEUS. Solid renal tumors < 3 cm in size appear usually as hypoechoic masses at gray-scale sonography; in 30% of cases, they can be slightly hyperechoic. When the lesion reaches a diameter superior to 3 cm, it shows frequently an inhomogeneous internal structure. At color Doppler imaging, these masses have a mild increased peripheral arterial vascularization, and seldom internal vessels are identified. When the neoplastic lesion is over 4 cm in size, the echostructure is that of an inhomogeneous mass due to intratumoral necrotic or hemorrhagic areas and calcifications. At CEUS, renal carcinoma has a homogeneous or inhomogeneous enhancement in comparison to normal renal parenchyma in the arterial phase, with progressive enhancement reduction in the late phase (Fig. 54.2). The detection of a hypervascular peripheral rim, sometimes observed, is due to the tumoral pseudocapsule [6]. Angiomyolipoma (AML) is a benign tumor and usually appears as a hyperechoic well-defined solid mass at gray-scale sonography. After microbubbles injection, it is homogeneously enhanced and hypoenhanced in the arterial and late phase [7]. Renal oncocytoma, another benign tumor, usually is detected as a homogeneous hypoechoic mass with a central stellate scar. At color power Doppler imaging, they can show a wheel aspect. After contrast injection, the enhancement is diffuse and homogeneous in the arterial phase, with the depiction of the central scar as a hypoechoic area (Fig. 54.3).

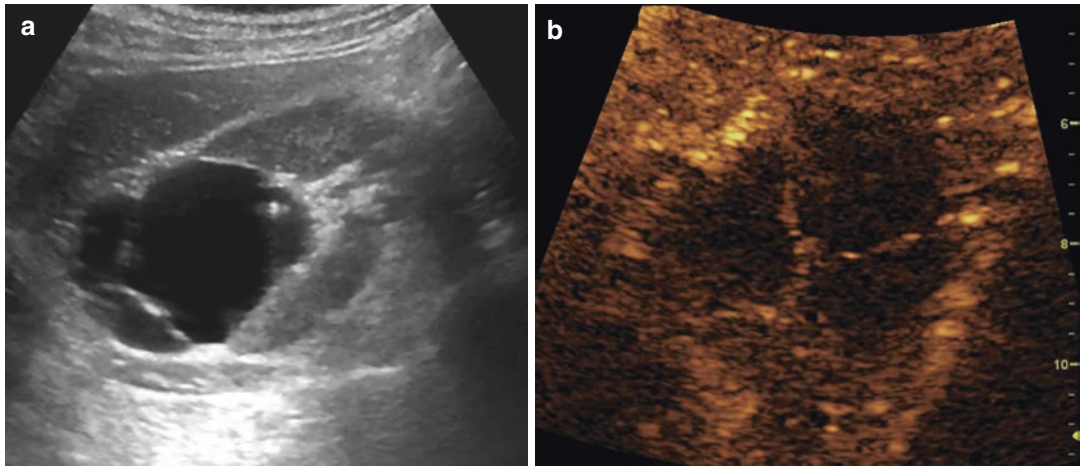

Fig. 54.1 Complex cyst type 3 (**a**). CEUS demonstrates thick septa of the cyst (**b**)

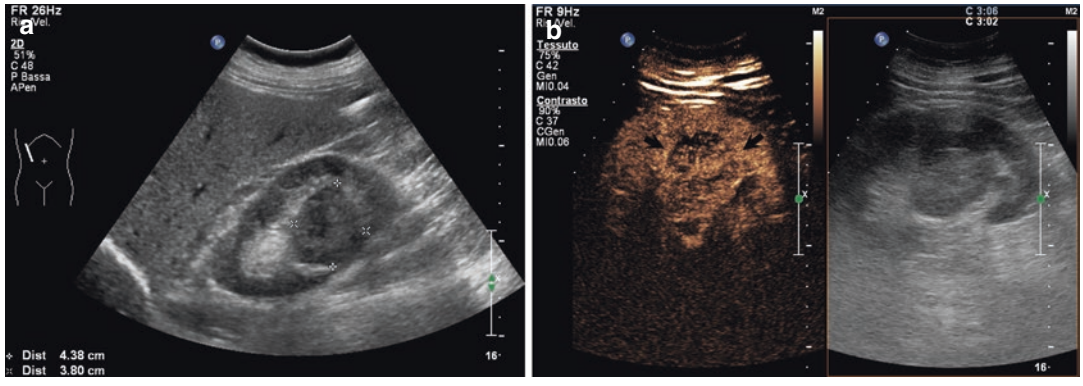

Fig. 54.2 Hypoechoic mass of the right kidney (**a**). CEUS (**b**) shows enhancement of this tumor (*black arrows*). It was an adenocarcinoma

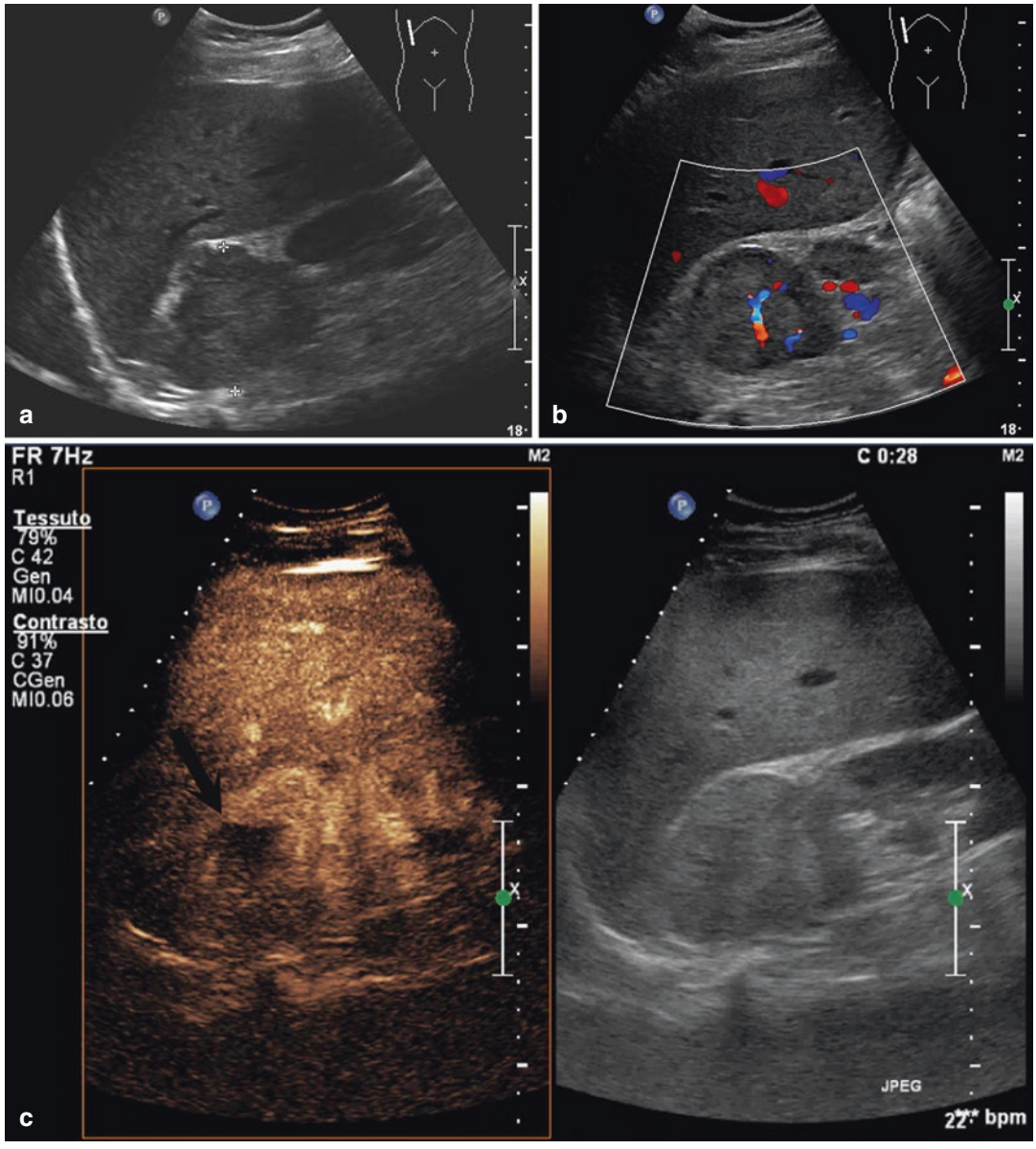

Fig. 54.3 Large mass of the right kidney (**a**) with central vessel at color Doppler (**b**). After contrast injection, there is a strong enhancement with depiction of a central scar (*black arrow*), suggestive of oncocytoma (surgery confirmed) (**c**)

54.2.2 Segmental Renal Ischemia

Thromboembolic disease is the most common cause of renal infarction and is observed in patients with cardiovascular diseases. Gray-scale sonography is not able to detect ischemic areas, and even color power Doppler, commonly used to detect great vessels' pathology, usually is not useful in old patients with reduced kidney perfusion. The CEUS is particularly useful in the diagnosis of this disease and has the advantages compared to CT and MR which require the use of nephrotoxic contrast agents [8]. The ischemic areas appear as nonperfused areas or show a late enhancement compared to the normally perfused adjacent renal tissue. The ischemic parenchyma shows sometimes a triangular shape, with the base at the renal capsule (Fig. 54.4).

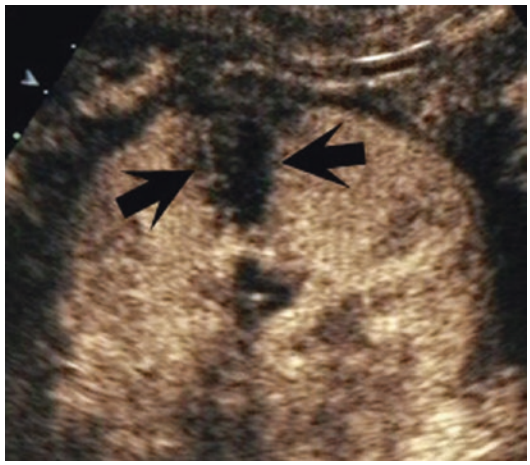

Fig. 54.4 Renal ischemia visible as a hypoechoic area of triangular shape (*black arrows*)

54.2.3 Acute Cortical Necrosis

Acute cortical necrosis is a rare cause of acute renal failure, and it is the consequence of a diffuse and rapid renal cortical ischemic necrosis, without medullary parenchyma involvement. The process can be multifocal or diffuse and is commonly bilateral. CEUS is proposed as a diagnostic procedure in patients with rapidly evolving renal failure and when an acute tubular necrosis can be excluded. Acute cortical necrosis diagnosis at CEUS is characterized by a markedly hypoperfused cortex (Fig. 54.5) [8].

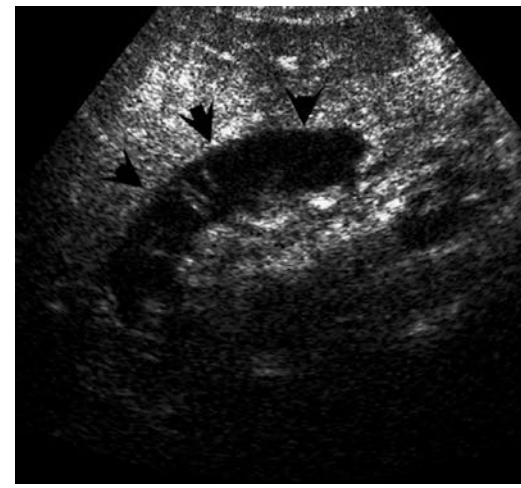

Fig. 54.5 Renal cortical necrosis (*black arrows*)

54.2.4 Acute Pyelonephritis and Renal Abscess

The diagnosis of acute pyelonephritis is based on clinical data, and imaging is usually not necessary. This can be employed when clinical improvement is not observed during therapeutic observation or when a renal abscess is suspected. Gray-scale sonography is not diagnostic or shows nonspecific signs. At CEUS, the involved parenchyma appears as a hypoperfused area of triangular shape (Fig. 54.6) [9]. The renal abscess is characterized as a hypoechoic area with peripheral contrast enhancement (Fig. 54.7).

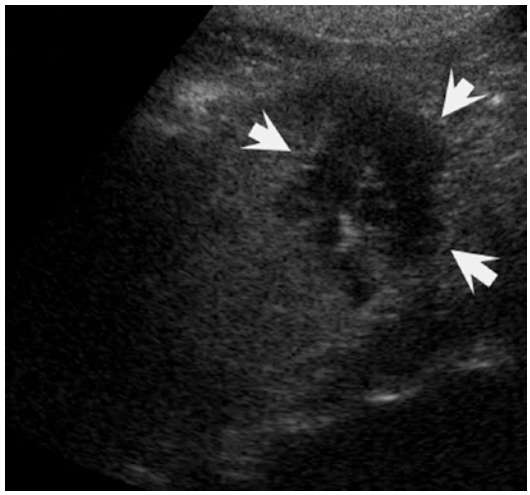

Fig. 54.6 Acute pyelonephritis visible as hypoechoic area (*arrowheads*)

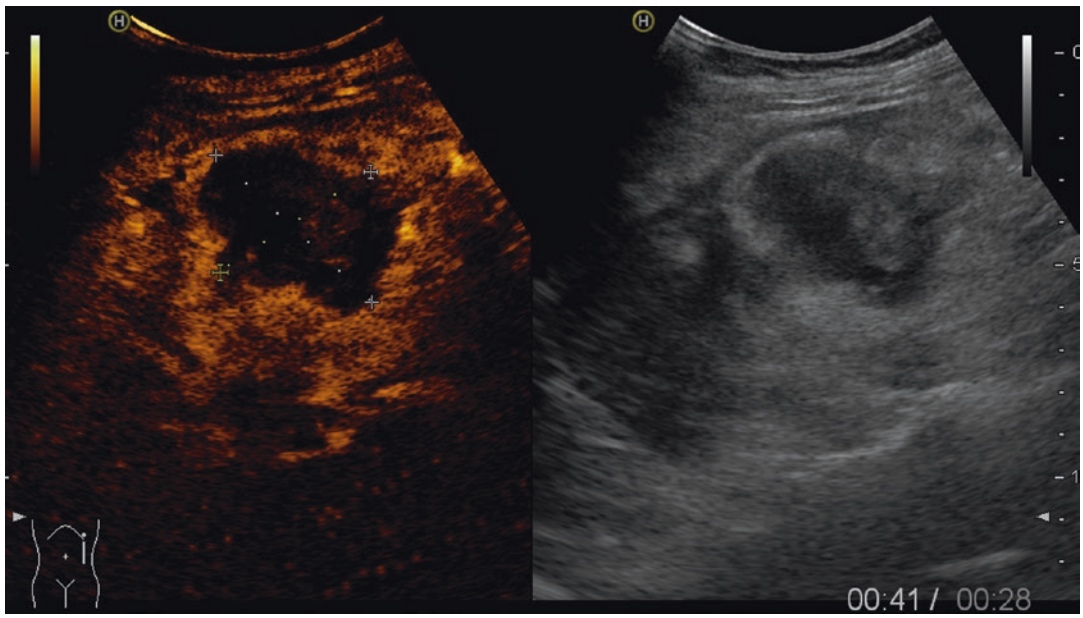

Fig. 54.7 Renal abscess

54.2.5 Renal Trauma

UCAs can be used in trauma with the aim to detect posttraumatic lesions of abdominal organs not visible on gray-scale sonography [10]. Kidney traumatic lesions show a reduced or absent contrast enhancement, appearing as hypo- or anechoic lesions. Parenchymal changes are more evident in the venous phase, even if they can be detected in all the phases of contrast flow. Parenchymal lacerations appear as hypo-anechoic areas with well-defined margins, while contusions appear as hypo-anechoic areas with shading margins (Fig. 54.8). In subcapsular renal hematomas, an anechoic fluid collection can be seen around the kidney's profile. In hematuria with persistent bleeding, CEUS is able to detect bubbles flowing into the hematoma, easily identified in the arterial phase of the examination. Traumatic lesions of the main arterial vessels are characterized by absence of typical contrast enhancement of the renal parenchyma. The lesions of the excretory tract cannot be detected with CEUS, because the bubbles are not filtered by the glomeruli and do not pass in the urinary tract. Other imaging techniques are necessary to identify lesions when they are clinically suspected.

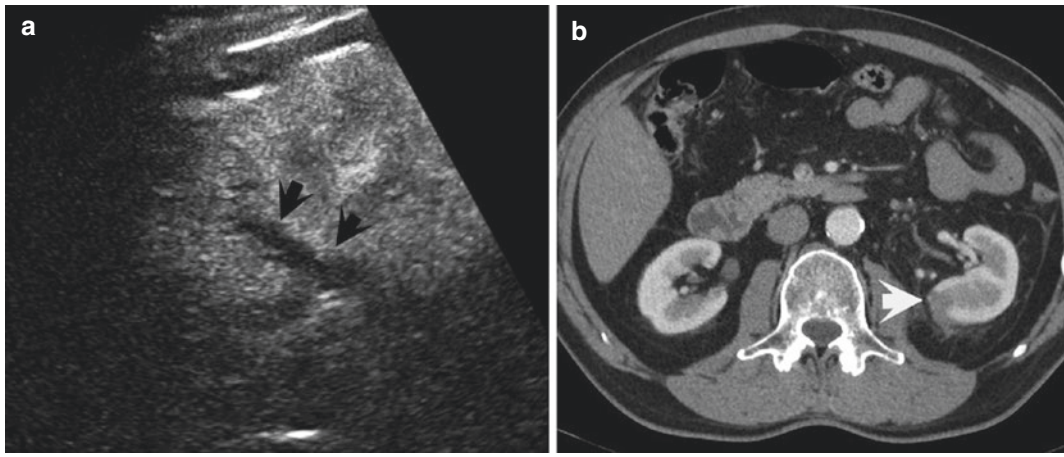

Fig. 54.8 Renal trauma with fracture of the posterior labrum (*black arrows*) (**a**) confirmed at CT (*white arrow*) (**b**)

54.3 Vesicoureteral Reflux

The urine reflux from bladder into the upper urinary tract can be unilateral or bilateral and is secondary to congenital or acquired anatomical or functional anomaly of the ureterovesical junction. The vesicoureteral reflux (VUR) is the most common urologic pathology in children, and it is observed in 1–2% of all pediatric population and in 30–40% of children with urinary tract infections. VUR is the main cause of chronic renal damage in infancy. The cystosonography (bladder sonography with retrograde contrast introduction), named also voiding urosonography (VUS), is performed after bladder catheterization and subsequent transcatheter introduction of the US contrast [11]. Preliminary baseline urinary tract (kidney and bladder) sonography is mandatory to detect possible pathology, followed by endovesical infusion of saline solution and the contrast medium. For this type of investigation, a concentration of 0.5/100 ml of UCA is used. Real-time observation and video registration are mandatory to document the bladder distension and the bubbles' flow into the ureters and renal pelvis. This observation must be performed during the filling phase and during voiding (Fig. 54.9). With CEUS, it can be applied the International Reflux System for the radiology voiding cystourethrography. Based on the grade of distension of the upper urinary tract, five grades of VUR are recognized.

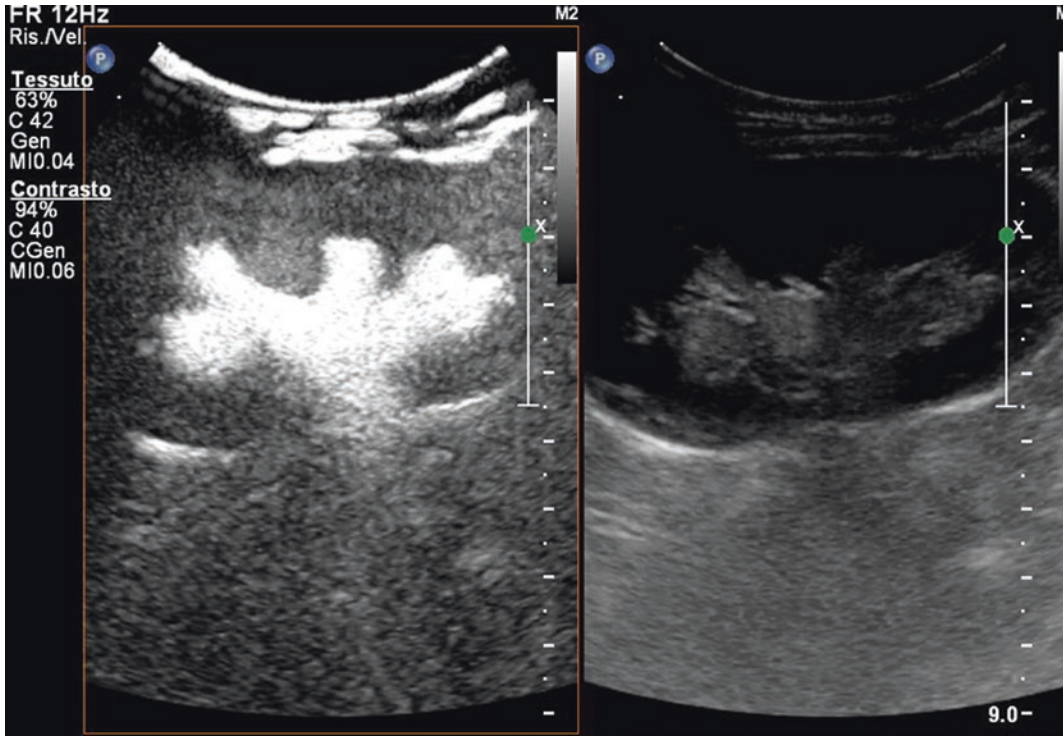

Fig. 54.9 Vesicoureteral reflux with UCA in the pelvis

54.4 Prostate

CEUS has been employed to detect prostate carcinoma non-visible on gray-scale sonography or to guide biopsy in selected cases. Some preliminary studies showed very suggestive results, which have not been confirmed in other research. The method is still considered as a procedure subject to clinical investigation.

Some studies have shown focal areas of disturbed enhancement in the arterial phase, sometimes with increased vascularization and sometimes with reduced vascularization compared to adjacent glandular tissue. In the late venous phase, a focal hypoechoic area can be detected (Fig. 54.10). Selected use of contrast medium has been proposed in patients in active surveillance, after hormonal therapy and radiotherapy, or in patients proposed for high-intensity focused ultrasound (HIFU) [12].

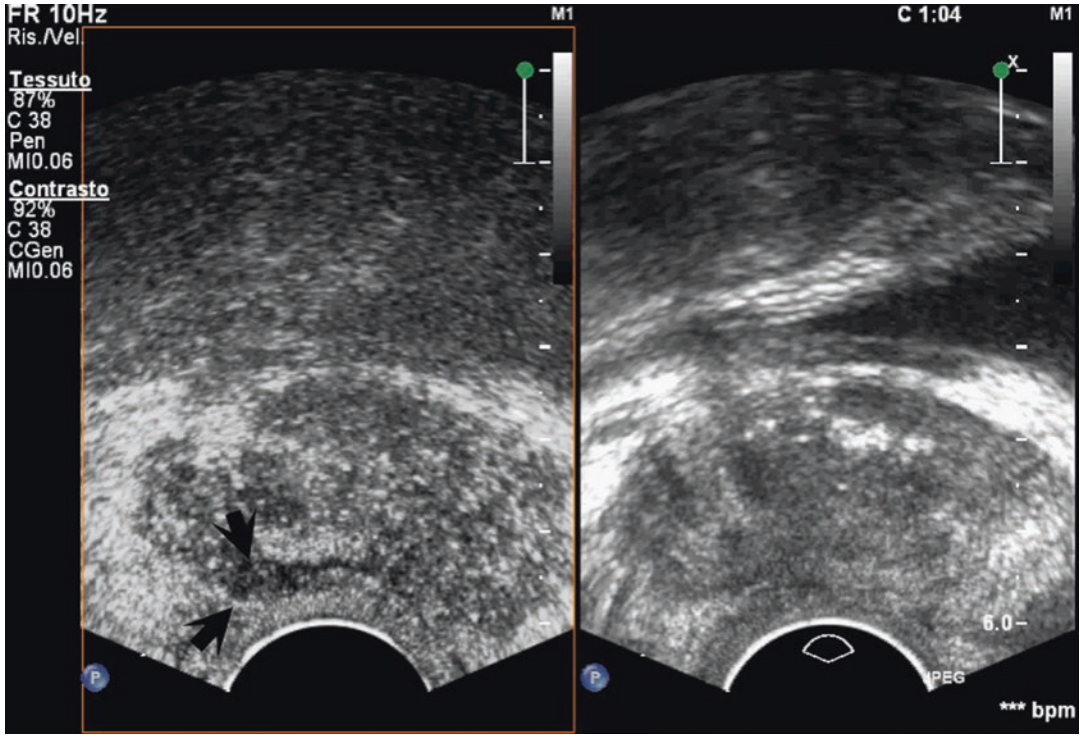

Fig. 54.10 Prostate cancer CEUS shows hypoechoic area (*black arrow*) in the late peripheral gland

54.5 Scrotum

54.5.1 Testicular Anatomy

The testis and epididymis show an intense and early enhancement after contrast injection, with visualization of the feeding artery, followed few seconds later by the visualization of venous and homogeneous parenchymal enhancement (Video 54.2). This intense enhancement disappears completely after 3 min of observations.

54.5.2 Testicular Tumors

The majority of testicular masses are easily detected in gray-scale imaging employing up-to-date machines and the vascularization identified with color power Doppler. In clinical practice, nonvascularized hypoechoic testicular lesions are observed, and the distinction between tumoral and nontumoral lesions is difficult or nonattending. CEUS allows to identify tiny areas of vascularization in all neoplastic lesions [13], detecting cystic or fibrotic areas from cellular proliferating nodules. The method is particularly useful in the detection of vascularization of very small hypoechoic nodules (Fig. 54.11). The procedure is not able to distinguish between different testicular tumors, but this problem is clinically less relevant because all solid and vascularized testicular lesions must be removed.

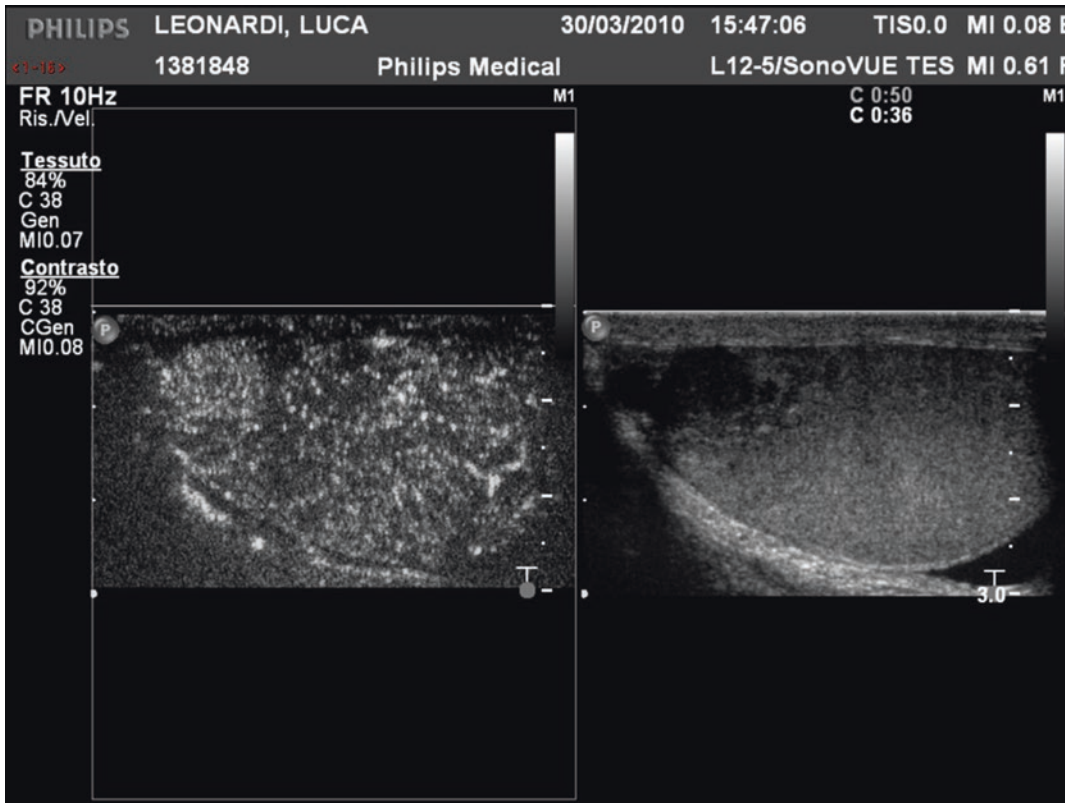

Fig. 54.11 Small seminoma of the upper pole of the testis. CEUS demonstrates strong enhancement of the nodule

54.5.3 Complex Cystic Lesions

Simple intratesticular cystic lesions without internal echogenic signal are easily characterized by gray-scale sonography. More difficult is to define the nature of so-called complex cysts that show some internal echoes. Most frequently these aspects are due to solid parenchymal material. CEUS allows with great certainty to separate easily the solid abnormality from nonviable material present in the cyst.

The most typical complex cyst observed in the clinical practice is the epidermoidal cyst which appears as a solid mass at gray-scale sonography, with an onion-like internal structure. CEUS allows to demonstrate the completely avascular nature of the lesion (Fig. 54.12) and confirms the benign nature, without the need of other imaging tests [14].

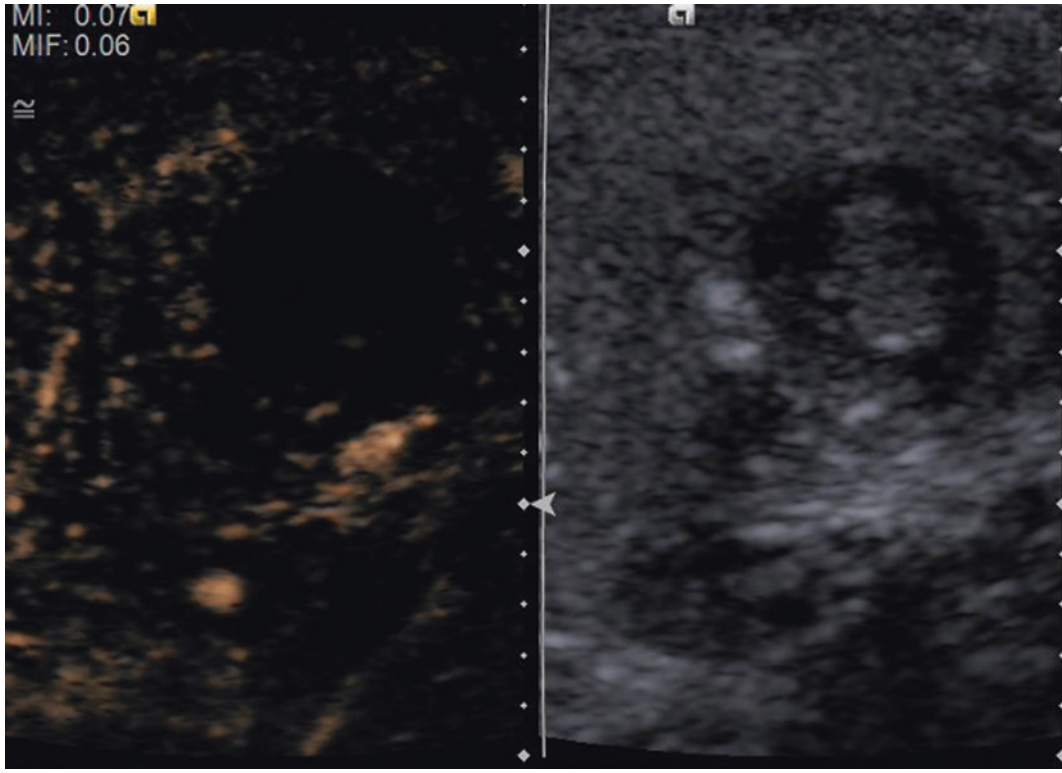

Fig. 54.12 Epidermoid cyst of the testis. CEUS demonstrates the absence of enhancement

54.5.4 Segmental Testicular Infarction

It is a rare pathology, commonly idiopathic, but can be observed in patients with coagulation abnormalities, vasculitis, testicular torsion, infection, or trauma. Gray-scale sonography associated with color Doppler is usually diagnostic for their typical morphology. Sometimes the lesion can mimic a hypovascular tumor, and in these cases, CEUS is more accurate showing the avascular nature of the lesion. Subacute segmental infarction characteristically shows a perilesional rim of enhancement (Fig. 54.13), while appearance of chronic infarction is not characteristic as the lesion presents as a hypovascular nodule [15].

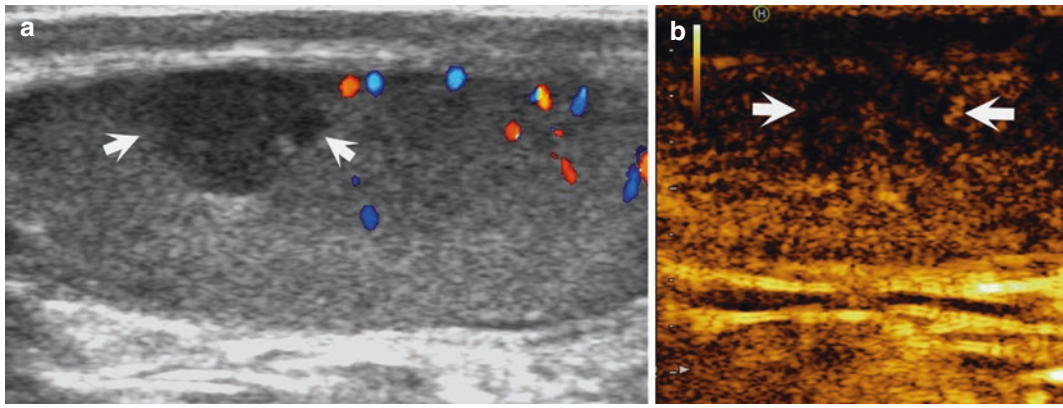

Fig. 54.13 Segmental testicular infarction. Color Doppler image shows a hypoechoic nonvascular lesion (*white arrows*) (**a**). After contrast injection, the lesion (*white arrows*) shows no enhancement confirming its avascular nature (**b**)

54.5.5 Scrotal Trauma

In scrotal trauma, gray-scale sonography and associated color Doppler are the main diagnostic procedures for a correct diagnosis. The extent of the traumatic lesion is sometimes difficult to quantify because it is difficult to separate a simple contusion, hematoma, or complete rupture of the testis. CEUS is very useful because it allows to detect the fracture extension and the hematoma and separate it from viable residual parenchyma which is enhanced by contrast medium (Fig. 54.14). The use of the contrast medium allows to identify the albuginea rupture, to quantify the residual testicular tissue, and to guide therapeutic solutions [13].

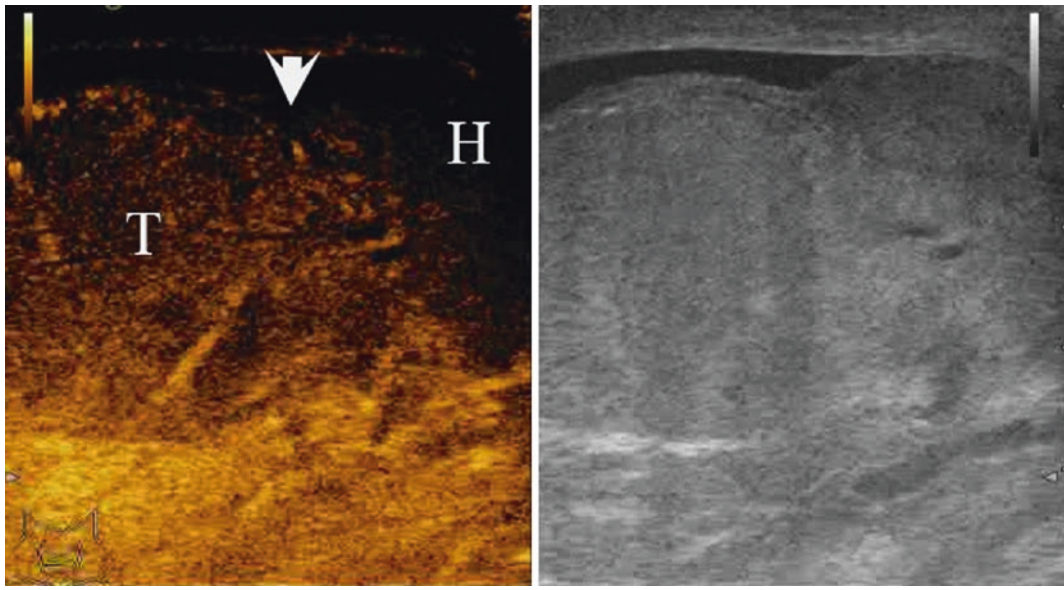

Fig. 54.14 Scrotal trauma. CEUS depicts the interruption of the tunica vaginalis (*white arrow*) and the large hematoma (H)

54.6 Penis

CEUS of the penis can be performed by introducing the contrast intravenously or directly into the corpora cavernosa, without or after vasoactive drugs injection to obtain erection [16]. At CEUS, the maximum enhancement is obtained during the initial phase of erection when the blood inflow is high and the intracorporeal pressure low. The cavernosal and the helicine arteries show an intense enhancement, with refilling of the sinusoids. When the contrast injection is performed during rigid erection, the arterial and sinusoid enhancement is reduced and delayed. Direct intracavernosal contrast injection shows a bilateral spread of microbubbles with homogeneous enhancement of both corpora cavernosa. CEUS of the penis has been employed in the investigation of penile malformations instead of radiologic cavernosography in congenital penile curvature or hypoplasia. The use of CEUS in erectile dysfunction and in Peyronie's disease has not shown clinical value, as reported in rare clinical reports. In penile traumas, contrast injection can be useful to confirm or detect the site of the albuginea tear, with bubble extravasation from the corpora cavernosa (Fig. 54.15). It is conceivable that it can allow the detection of smaller tears and of urethral tears. Primary and metastatic tumors of the corpora cavernosa display early inhomogeneous enhancement, less intense than the normal corporal bodies, followed by rapid washout. Tumor spreading within corpora cavernosa can be better evaluated as areas of reduced enhancement after 1–2 min after the injection. In diffuse metastatic involvement of the erectile tissue, the lesion can be barely visible at gray-scale ultrasound, while CEUS shows an extensive alteration of the normal penile vasculature and inhomogeneous enhancement of the penis. There are few experiences reported on the use of CEUS in penile scars and fibrosis and in cases of acute penile ischemia.

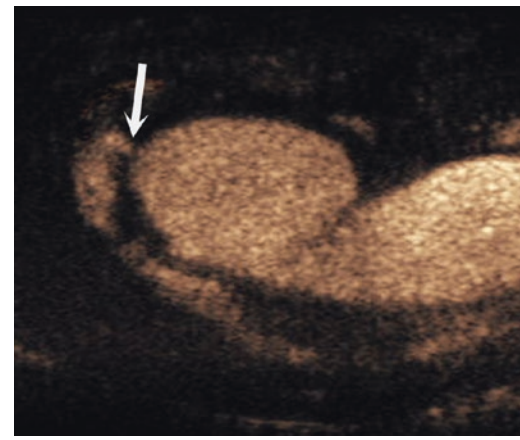

Fig. 54.15 Penis trauma. CEUS detects the site of the albuginea tear, with bubble extravasation from the corpora cavernosa (*arrow*)

Conclusion

The use of CEUS in the clinical practice improves significantly the diagnostic role of ultrasonography. Intravenous injection of gas containing bubbles increases the sensitivity and specificity of sonography, and the diagnostic performance is very similar to that of CT and MR imaging, without the need of radiation and iodinated or gadolinium-based contrast media.

To be useful, CEUS needs technical skill of the physician and adequate technology. Its more extensive use in uro-andrologic pathology can improve the diagnostic possibilities offered by gray-scale sonography, reducing time and cost of assistance.

References

1. Derchi LE, Rizzatto G, Solbiati L (1992) Contrast media in echography. Radiol Med 84(3):208–215
2. Harvey CJ, Blomley MJ, Eckersley RJ et al (2001) Developments in ultrasound contrast media. Eur Radiol 11(4):675–689
3. Piscaglia F, Bolondi L (2006) The safety of Sonovue in abdominal applications: retrospective analysis of 23188 investigations. Ultrasound Med Biol 32(9):1369–1375
4. Quaia E, Bertolotto M, Cioffi V et al (2008) Comparison of contrast-enhanced sonography with unenhanced sonography and contrast-enhanced CT in the diagnosis of malignancy in complex cystic renal masses. AJR Am J Roentgenol 191(4):1239–1249
5. Tamai H, Takiguchi Y, Oka M et al (2005) Contrast enhanced ultrasonography in the diagnosis of solid renal tumors. J Ultrasound Med 24(12):1635–1640
6. Jiang J, Chen Y, Zhou Y, Zhang H (2010) Clear cell renal cell carcinoma: contrast-enhanced ultrasound features relation to tumor size. Eur J Radiol 73: 162–167
7. Fan L, Lianfang D, Jinfang X, Yijin S, Ying W (2008) Diagnostic efficacy of contrast-enhanced ultrasonography in solid renal parenchymal lesions with maximum diameters of 5 cm. J Ultrasound Med 27:875–885
8. Siracusano S, Bertolotto CS et al (2011) The current role of contrast-enhanced ultrasound (CEUS) imaging in the evaluation of renal pathology. World J Urol 29:633–638
9. Mitterberger M, Pinggera GM, Colleselli D et al (2008) Acute pyelonephritis: comparison of diagnosis with computed tomography and contrast-enhanced ultrasonography. BJU Int 101(3):341–344
10. Valentino M, Serra C, Zironi G, De Luca C, Pavlica P, Barozzi L (2006) Blunt abdominal trauma: emergency contrast-enhanced sonography for detection of solid organ injuries. AJR Am J Roentgenol 186(5): 1361–1367
11. Zimbaro G, Ascenti G, Visalli C (2007) Contrast-enhanced ultrasonography (voiding urosonography) of vesicoureteral reflux: state of the art. Radiol Med 112:1211–1224
12. Eckersley RJ, Sedelaar JP, Blomley MJ et al (2002) Quantitative microbubble enhanced transrectal ultrasound as a tool for monitoring hormonal treatment of prostate carcinoma. Prostate 51(4):256–267
13. Valentino M, Bertolotto M, Derchi L, Bertaccini A, Pavlica P, Martorana G, Barozzi L (2011) Role of contrast enhanced ultrasound in acute scrotal diseases. Eur Radiol 21(9):1831–1840
14. Patel K, Sellars ME, Clarke JL, Sidhu PS (2012) Features of testicular epidermoid cysts on contrast-enhanced sonography and real-time tissue elastography. J Ultrasound Med 31:115–122
15. Bertolotto M, Derchi LE, Sidhu PS, Serafini G, Valentino M, Grenier N, Cova MA (2011) Acute segmental testicular infarction at contrast-enhanced ultrasound: early features and changes during follow-up. AJR Am J Roentgenol 196(4):834–841
16. Bertolotto M, Bucci S, Zappetti R (2008) Contrast-enhanced US of the penis. In: Bertolotto M (ed) Color-Doppler US of the penis. Medical imaging. Springer, Berlin/Heildelberg/New York, pp 183–192

Ultrasound MRI Fusion Biopsy in Prostate Gland

55

Francesco Porpiglia and Matteo Manfredi

55.1 Introduction

Until recently, the diagnosis of prostate cancer (PCa) has been based on blinded, systematic, template-based sampling strategy under transrectal ultrasound (TRUS) guidance. This test has undergone considerable modification in order to improve the sampling efficiency: from the original six cores [1] to the standardized 12 cores [2, 3]. Nevertheless, 12-core TRUS biopsy conferred an incremental benefit in terms of detection; there is a wide consensus that it remains prone to errors. These principally comprise undersampling of significant and oversampling of insignificant PCa [4–6].

The introduction of multiparametric magnetic resonance imaging (mp-MRI) has made it possible to change the way in which prostate biopsy is done, allowing to direct biopsies to suspicious lesions rather than randomly. The subject of this chapter relates to the use of a software to assist in targeting an MRI-derived suspicious lesion.

55.2 Interpretation of Multiparametric MRI

The MRI acquisition and reporting by the radiologist is the initial step of all MRI targeted biopsy strategies. mp-MRI includes three components: high-resolution T2-weighted MR images (T2WI) and at least two functional MRI techniques including diffusion-weighted imaging (DWI) and dynamic contrast-enhanced MRI (DCE-MRI) [7–9] (Fig. 55.1). MR spectroscopic imaging (MRSI) remains an optional technique in most centers. The use of an endorectal coil (ERC) to increase the spatial resolution of the technique is still under debate, especially with the recent improvement in signal-to-noise ratios achieved by the use of the 3-T scanner [10].

To describe suspected lesions diagnosed by MRI in a standardized manner, radiologists use standardized suspicion scores and graphical templates to show locations. The most used scores are the 1–5-point Likert scale (based on radiologist's subjective score) or the prostate imaging reporting and data system (PI-RADS) score (based on determined criteria) [11–13]. In particular, concerning PI-RADS score, the inter-reader agreement performs well, and the inter-reader reproducibility improves with increasing experience.

Electronic supplementary material The online version of this chapter (doi:10.1007/978-3-319-40782-1_55) contains supplementary material, which is available to authorized users.

F. Porpiglia (✉) • M. Manfredi
Division of Urology, Department of Oncology,
University of Turin, "San Luigi" Hospital,
Regione Gonzole 10, Orbassano (Turin) 10043, Italy
e-mail: porpiglia@libero.it

P. Martino, A.B. Galosi (eds.), *Atlas of Ultrasonography in Urology, Andrology, and Nephrology*,
DOI 10.1007/978-3-319-40782-1_55

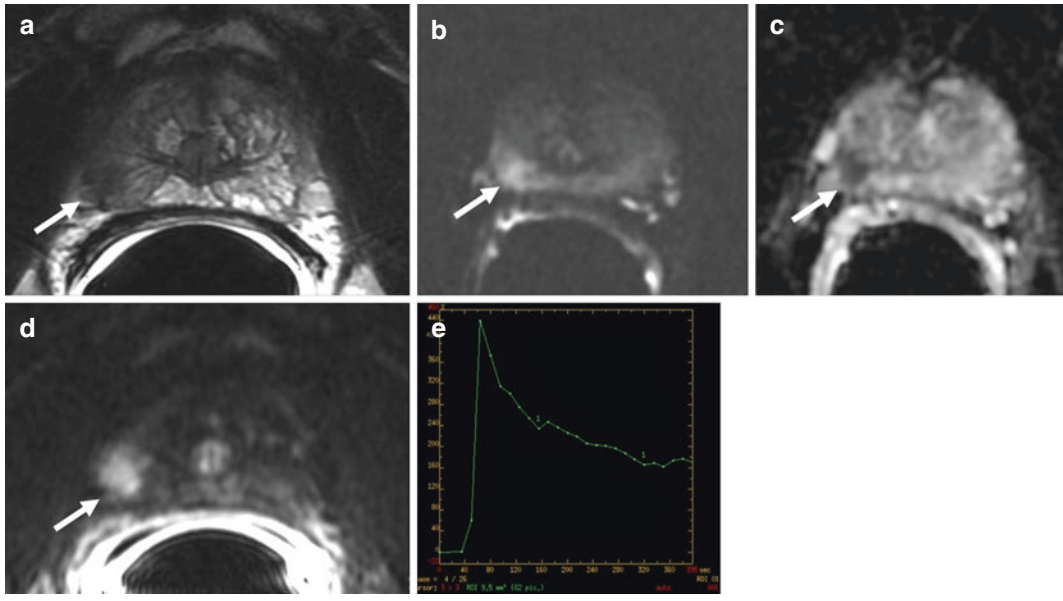

Fig. 55.1 Images from a 59-year-old male with serum PSA 7.92 ng/mL, and one previous biopsy underwent an mp-MRI. The MRI demonstrated a PI-RADS 5 right posterior apex to mid-peripheral zone lesion (white arrow) on axial T2W (**a**), DWI (**b**), ADC (**c**), and DCE (**d**, **e**). MRI/US fusion software-based targeted biopsy demonstrated Gleason score 7 (3+4) prostate cancer (67% in three cores)

55.3 MRI-Guided Targeted Biopsy

An MRI targeted biopsy can be performed in three ways: in-bore MRI targeted biopsy, MRI/US fusion visual targeted biopsy, and MRI/US fusion software-based targeted biopsy. These three approaches are all informed by tumor location diagnosed by the MRI. It is just the manner in which the target volume is "represented" to the operator that differentiates them.

Concerning in-bore MRI targeted biopsies, needles are introduced only into the areas of interest by performing a transrectal or transperineal biopsy. Serial MRI scans are performed to confirm biopsy needle placement (Fig. 55.2). Multiple studies demonstrated that in-bore MRI targeted biopsies are feasible with a median detection rate significantly higher than random biopsies. Moreover, this approach reduces the number of sampled cores with a real-time feedback of its placement, allowing a high likelihood of hit target [14, 15]. Nevertheless, in-bore MRI targeted biopsy is time-consuming and costly, not commonly available, and performed in prone position under general anesthesia.

The simplest targeted strategy concerns the use of MRI/US fusion visual targeted biopsies directed to the suspicious areas highlighted on the MRI. The first step, as in the other strategies, is represented by the detection of suspicious lesions on MRI. Then the urologist performs a standard US-guided biopsy, either by a transrectal or a transperineal approach, trying to direct the needles toward the areas suspicious on mp-MRI. Many authors suggest better efficiency and accuracy compared to standard biopsy [16, 17]. The most important disadvantage relates to the learning curve and reproducibility of this strategy. This approach requires an experienced urologist to translate the information of the mp-MRI onto real-time US, which can be challenging according to the deformation and the anatomical characteristics of the prostate.

Finally, MRI/US fusion software-based targeted biopsies represent a novel approach developed to improve the accuracy of prostate biopsy, allow dissemination of the technique, and permit the storage of images for future resampling. MRI/US fusion software-based targeted biopsy devices allow to align the pre-biopsy MR images with intraoperative TRUS in order to enable the urologist to perform targeted biopsy directed toward MR-visible lesions. This approach combines the high diagnostic accuracy of MRI for detecting PCa with TRUS, which represents a procedure well mastered by urologists. The process of coregistration of MRI and US images is automatized by the use of a fusion device, and therefore the results are likely to be more consistent across different centers.

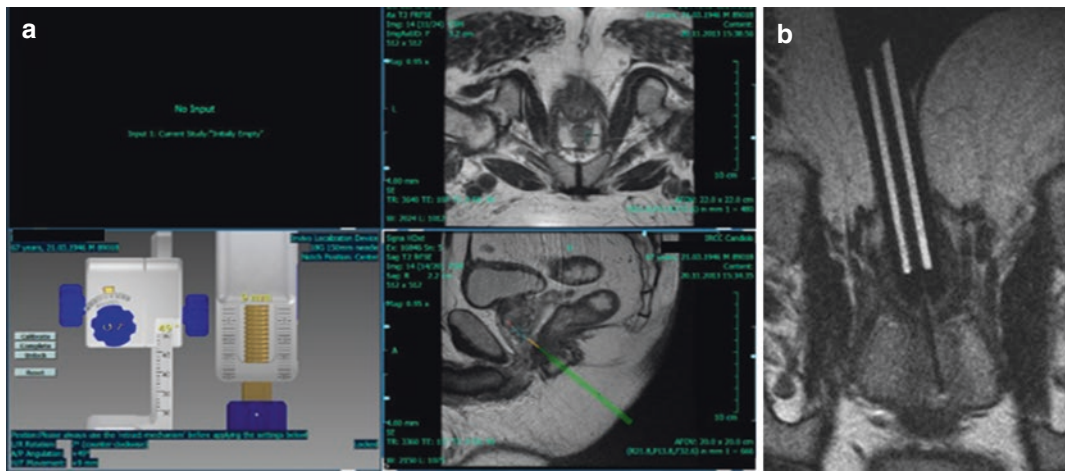

Fig. 55.2 In-bore biopsy. (**a**) Needle-in control scans are performed in two different planes (axial and coronal); (**b**) targeted cores are taken from each lesion using an MRI-compatible, 18G, fully automatic biopsy gun

55.3.1 Coregistration of MRI and US Images

MRI to US cognitive fusion is complicated by the significant deformation of the prostate shape that occurs between TRUS and MRI (with or without an endorectal coil). The software-based registration method corrects this effect to achieve better diagnostic accuracy [18].

There are two different methods to register MR images to live TRUS: rigid and elastic registration. Both of them aim to align the MR and US images through the identification of landmarks present on both corresponding images. The outer shape of the prostate is used to match the MRI contour to the live US image.

Elastic registration allows deformation, warping, and dimensional changes between images, based on mathematical algorithms. As every prostate is different in density and elasticity, these calculations are estimations. Rigid registration permits only rotational and translational variations between images, without changing the images themselves. The urologist needs to make some adjustments in case of error due to the rigid registration, using manual correction of the alignment and targeting or using different degrees of pressure/insertion depth of the US probe (Fig. 55.3) [19].

While overlapped images obtained from rigid registration usually have discontinuous borders looking less pleasant to the eye than elastic registration, it is difficult to define which method is able to achieve better accuracy. Elastic registration should guarantee better matching, but some experts think the cognitive adjustment might overcome the issues encountered with rigid registration and allow better spatial precision, especially in patients having unusual gland dimensions.

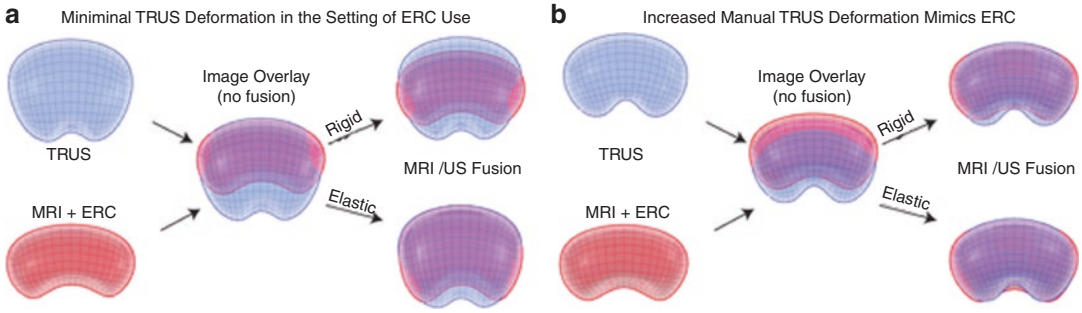

Fig. 55.3 Elastic and rigid methods to register MR images to live TRUS. (**a**) MRI/US registration with minimal US-probe deformation and use of an endorectal coil (ERC) for MRI; (**b**) MRI/US registration with increased manual US-probe deformation that can mimic ERC deformation. In middle images in (a) and (**b**) is shown the simple overlap of US and MR images, resulting in reduced correlation between imaging modalities. Rigid registration permits only rotational and translational variations between images. Elastic registration allows local deformation, e.g., caused by an endorectal coil or TRUS probe. *ERC* endorectal coil (Reproduced from Logan et al. [19])

55.3.2 Fusion Platforms

MRI/US fusion software-based targeted biopsy first of all requires a diagnostic mp-MRI with a report scheduling all the suspicious lesions edited by an expert uro-radiologist (Fig. 55.4). mp-MRI images are loaded in the specific software and regions of interest are then outlined. The patient is positioned, and a TRUS is performed, with MR images superimposed on real-time US images (Fig. 55.5). Targeted biopsies directed to mp-MRI-suspicious lesions are then performed (Figs. 55.6 and 55.7).

A standardized report of the biopsy session should be provided, including a detailed notification of MRI/US fusion software-based targeted biopsies, and eventually standard biopsies, that were performed. It can be done in the same manner as for mp-MRI, using a standardized diagram of the prostate, including drawings of the sampled lesions. The report must underline how good the MRI/US fusion software-based targeted biopsy matched the mp-MRI one (e.g., visibility of the lesion). All this information will be useful for analyzing the final histopathology results (Fig. 55.8).

The different devices currently in use to allow MRI/US fusion software-based targeted biopsy are reported in Table 55.1. To date, there are no available studies directly comparing the different platforms in terms of accuracy, nor detection rate.

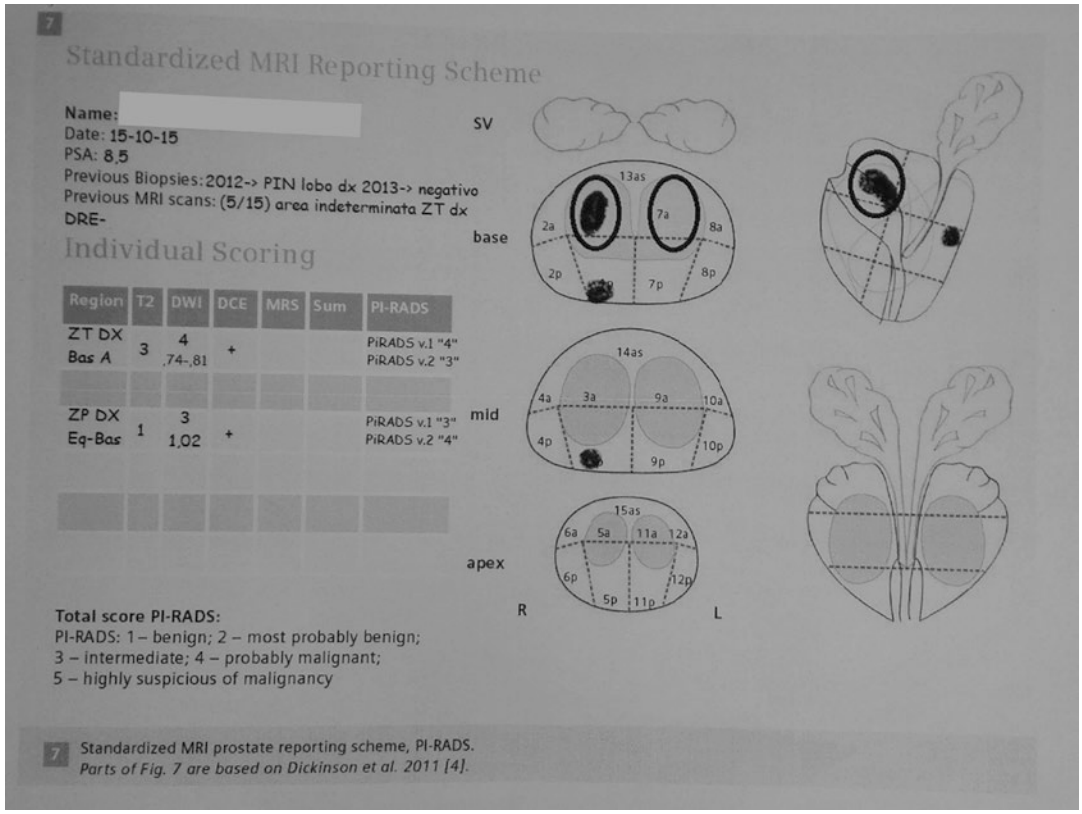

Fig. 55.4 mp-MRI report scheduling all the suspicious lesions classified by PI-RADS score

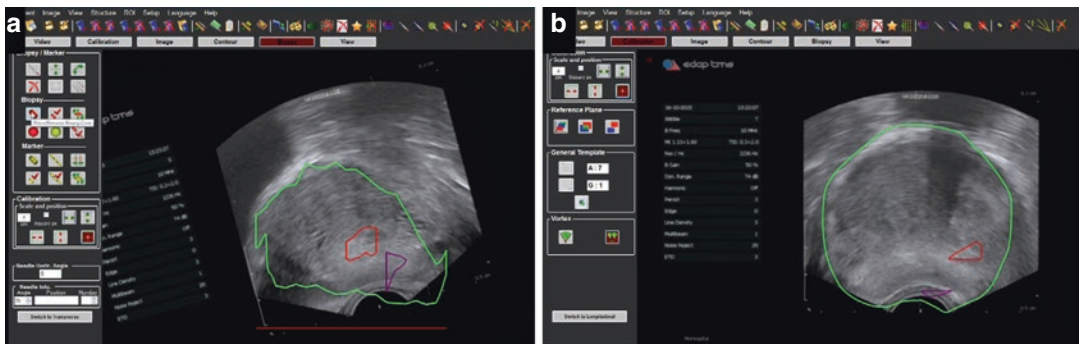

Fig. 55.5 Superimposition of MR and US images: the outer shape of the prostate is used to match the MRI contour to the real-time US image. (**a**) Longitudinal view; (**b**) transversal view

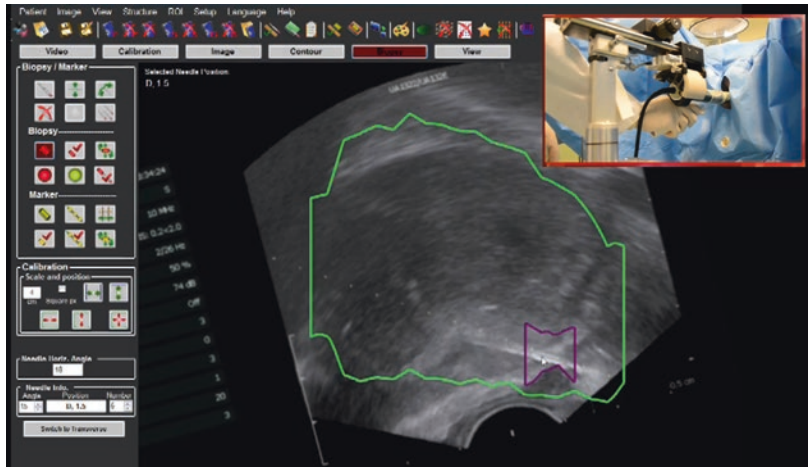

Fig. 55.6 Targeted biopsies directed to mp-MRI-suspicious lesions: transrectal approach

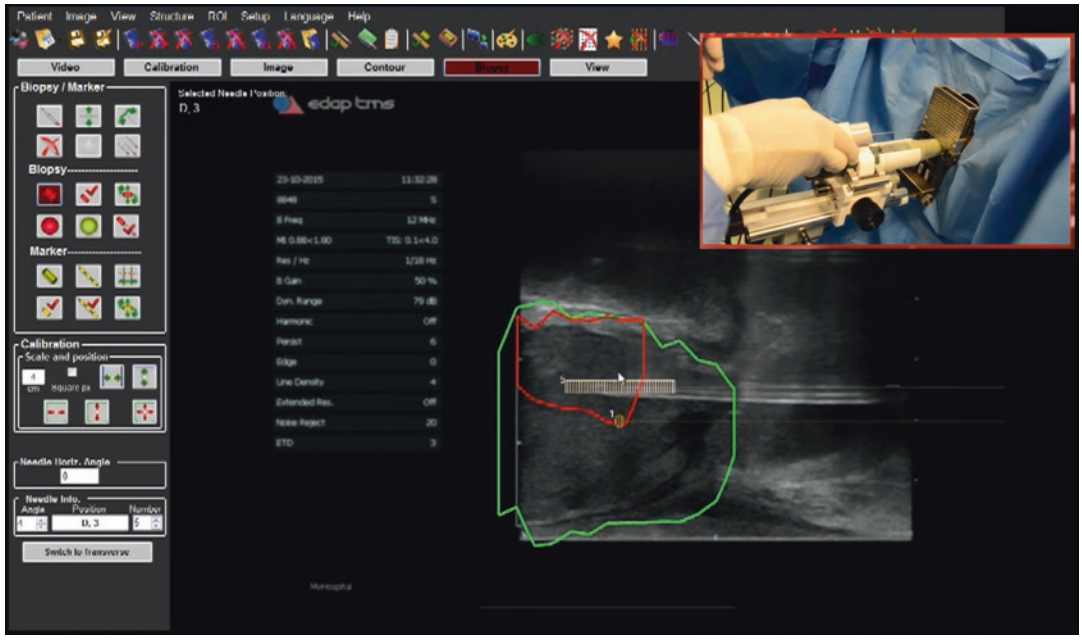

Fig. 55.7 Targeted biopsies directed to mp-MRI-suspicious lesions: transperineal approach

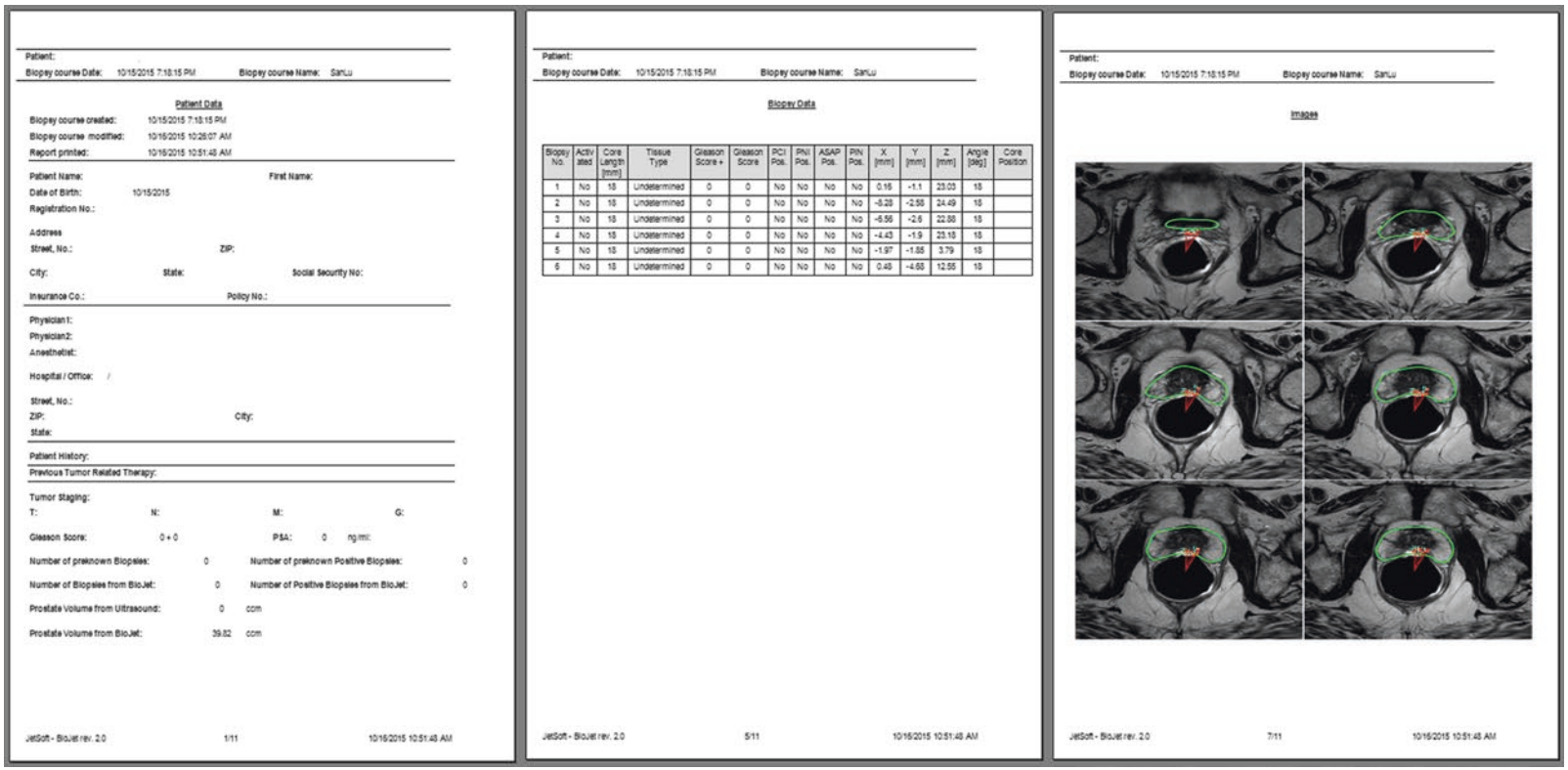

Fig. 55.8 Example of a report of the biopsy session

Table 55.1 Summary of MR/TRUS fusion software-based targeted biopsy platform specifications

MRI/US fusion software (manufacturer)	US image acquisition	Method of registration	Tracking system	Manipulation	Sampling route	Year of FDA approval
Artemis (Eigen)	Manual	Elastic	Mechanical arm with encoders	Via mechanical arm	Transrectal or transperineal	2008
BioJet (D&K Technologies)	Manual	Rigid (elastic for minor deformations)	Stepper with digital encoders	Via stepper	Transrectal or transperineal	2012
BiopSee (MedCom)	Manual	Rigid (elastic for minor deformations)	Stepper with digital encoders	Via stepper	Transrectal or transperineal	NR
Real-time virtual sonography (Hitachi)	Manual	Rigid	Electromagnetic	Freehand	Transrectal or transperineal	2010
UroNav (Invivo/Philips)	Manual	Rigid	Electromagnetic	Freehand	Transrectal or transperineal	2005
Urostation (Koelis)	Automatic	Elastic	3D ultrasound	Freehand	Transrectal	2010
Virtual Navigator (Esaote)	Manual	Rigid	Electromagnetic	Freehand	Transrectal	2014

MRI/TRUS magnetic resonance imaging/transrectal ultrasound, *FDA* Food and Drug Administration, *NR* not reported

55.4 Indications of MRI/US Fusion Software-Based Targeted Biopsy

55.4.1 Main Indications

- Re-biopsy in men with persistent suspicion of PCa after first negative prostate biopsy: persistently increased PSA and/or positive digital rectal examination (DRE) [20–25] and/or diagnosis of extensive high-grade prostatic intraepithelial neoplasia (HG-PIN) or atypical small acinar proliferation (ASAP) of the prostate [26]. As expected, a number of studies have shown that in this subgroup of men, MRI/US fusion software-based targeted biopsy allowed the detection of more clinically significant PCa than standard biopsy [27].
- Follow-up of patients under active surveillance (AS). Many authors evaluated fusion systems to perform confirmatory targeted biopsy in patients under AS. Hu et al. recently proved in a series of 113 patients that confirmatory MRI/US fusion software-based targeted biopsy resulted in reclassification in 36% of men, ranging from 24 to 100% according to the MRI score, from low to high grade, respectively [28]. Sonn et al. demonstrated that in a series of 171 patients, MRI/US fusion software-based targeted biopsy was three times more likely to identify cancer than standard biopsy (21% versus 7% ,respectively), and of the men with clinically significant PCa initially enrolled for AS, 38% had disease detected only on targeted biopsies [29]. Moreover, MRI/US fusion software-based targeted biopsy permits to track the location of all biopsy cores, allowing the urologist to perform a re-biopsy in the same suspicious areas, which is mandatory in the correct follow-up of patients under AS.

55.4.2 Other Indications

Other indications, as recommended by many authors but to be confirmed by further studies, could be:

- The follow-up of men suspicious for local recurrence after local treatment [30]
- The guidance of focal therapy [31]
- The characterization of suspicious lesions even at the first biopsy [32, 33]

55.5 Results of MRI/US Fusion Software-Based Targeted Biopsy

55.5.1 Standard Biopsy Versus MRI/US Fusion Software-Based Targeted Biopsy

The two approaches did not differ significantly in overall detection of PCa. When considering a core-by-core analysis, Rastinehad et al. reported an increased detection rate of MRI/US fusion software-based targeted biopsy with respect to standard biopsy (37.9% vs 12.5%, respectively, $p<0.001$) [34]. The detection rate of clinically significant PCa seems higher performing a MRI/US fusion software-based targeted biopsy than performing a standard biopsy. In the study of Siddiqui et al., MRI/US fusion software-based targeted biopsy diagnosed 30% more high-risk cancers versus standard biopsy ($p<0.001$) and 17% fewer low-risk cancers ($p=0.002$) [35]. On the other hand, two recently published randomized controlled trial (RCT) concluded that detection rates for any cancer and clinically significant PCa did not significantly differ between the two approaches, as reported later (see Sect. 55.6) [36, 37].

Concerning the length of biopsy positive cores, Puech et al. reported a statistically significant longest core cancer length in MRI/US fusion software-based targeted biopsy compared to standard biopsy (mean: 7.3 mm ± 3.8 vs 4.6 mm ± 3.1, respectively; $p=0.0001$) [38].

In all studies reporting the data, MRI/US fusion software-based targeted biopsy necessitates fewer cores to diagnose PCa compared to standard biopsies. In the systematic revision of Valerio et al., MRI/US fusion software-based targeted biopsies detected more clinically significant cancers using fewer cores compared with standard biopsy (median, 9.2 vs 37.1, respectively) [27].

Finally, in terms of more accurate grading of PCa, Lanz et al. published a study including 125 men undergoing radical prostatectomy for PCa diagnosed both by MRI/US fusion software-based targeted and standard biopsy. Targeted biopsy detected 126 lesions in 115 patients. The primary Gleason grade, secondary Gleason grade, and Gleason score of the 126 individual tumors were determined accurately in 114 (90 %), 75 (59 %), and 85 (67 %) cases, respectively [39].

55.5.2 Template Systematic Biopsy vs MRI/US Fusion Software-Based Targeted Biopsy

Radtke et al. reported a comparative analysis of 294 consecutive patients undergoing systematic transperineal biopsy and MRI/US fusion software-based targeted biopsy. The authors reported that sampling efficiency was in favor of the second method, with 46.0 % of MRI/US fusion software-based targeted biopsy versus 7.5 % of systematic biopsy cores detecting PCa with a Gleason score ≥7. However, as 12.8 % Gleason score ≥7 was missed by the targeted approach, the authors concluded that the gold standard for cancer detection is a combination of systematic and targeted cores [40].

55.5.3 MRI/US Fusion Visual Targeted Biopsy vs MRI/US Fusion Software-Based Targeted Biopsy

Only two studies directly compared MRI/US fusion software-based targeted biopsy with MRI/US fusion visual targeted biopsy [37, 40], thus indicating the need for further studies. In details, Puech et al. reported that in 79 MR imaging targets among 95 patients, positivity for cancer was 47 % with cognitive and 53 % with MRI/US fusion software-based targeted biopsy ($p=0.16$) [38]. The same results were reported in a prospective study in 125 consecutive men by Wysock et al. concluding that MRI/US fusion software-based targeted biopsy was more often histologically informative than visual targeting but did not increase cancer detection [41]. Moreover, Cool et al. reported the results of 225 simulated targeted biopsies on suspected lesions on MRI, with MRI/US fusion visual targeted biopsy sampling the 45–48 % of clinically significant lesions compared with 100 % obtained with MRI/US fusion software-based targeted biopsy [42]. Delongchamps et al. indirectly compared various targeted biopsy approaches in a consecutive series of patients. They reported that rigid and elastic MRI/US fusion software-based targeted biopsies performed significantly better than standard biopsies ($p=0.0065$ and 0.0016, respectively), while MRI/US fusion visual targeted biopsy did not perform better ($p=0.66$) [32]. Finally, in a preliminary study including 32 consecutive patients, Mouraviev et al. divided 32 consecutive patients into three groups based on the method used to target the suspected lesion. They concluded that MRI/US fusion software-based targeted biopsy (using two different platforms) increases diagnostic accuracy compared with MRI/US fusion visual targeted biopsy [43].

55.5.4 In-Bore MRI Biopsy vs MRI/US Fusion Software-Based Targeted Biopsy

Recently, Arsov et al. compared in a prospective randomized trial the PCa detection between in-bore MRI biopsy and MRI/US fusion software-based targeted biopsy + 12-core standard biopsy in 210 patients with at least one negative standard biopsy. They reported that PCa detection ($p=0.7$), detection rates for significant PCa ($p=0.7$), and the highest percentage tumor involvement per biopsy core ($p=0.4$) were similar between the arms [44].

55.6 Future Perspectives

The most important issue that will have to be addressed with the current use of MRI/US fusion software-based targeted biopsy concerns its role in the diagnostic pathway. The actual scenario is

represented by an existing test, the standard 12-core biopsy. The new test, the MRI/US fusion software-based targeted biopsy, could add on or replace the existing test. In most studies, patients underwent standard prostate biopsy in combination with MRI/US fusion software-based targeted biopsies in the same session. The first high-quality study with a very large sample size that examined the utility of MRI/US fusion software-based targeted biopsy against standard biopsy combined was published by Siddiqui et al. In this paper, there was little utility to include standard biopsy in the protocol as 200 men would be needed to be additionally sampled in order to diagnose one additional high-risk PCa, missed by MRI/US fusion software-based targeted biopsy. Further, the two combined approaches lead to a change in Gleason score risk stratification in 15 % of cases, of which 2 % increased to high-risk PCa [35]. Two RCT were recently published comparing MRI/US fusion software-based targeted biopsy and standard biopsy. In the study by Baco et al. [36], including 175 patients, the 2-core MRI/US fusion software-based targeted biopsy was comparable to 12-core standard biopsy in terms of clinically significant PCa detection (38 % vs 49 %, respectively, $p=0.2$) and was more effective for MRI-detected PCa with a PI-RADS score of 4–5 [36]. They concluded that the traditional biopsy may be replaced by two-core MRI/TRUS targeted biopsy. Tonttila et al. reported similar results for one-/two-core MRI/US fusion software-based targeted biopsy and 12-core standard biopsy in terms of any cancer (64 % vs 57 %, respectively, $p=0.5$) and clinically significant (55 % vs 45 %, respectively, $p=0.8$) PCa [37]. Further evidence about the role of MR/US fusion software-based targeted biopsy in the pathway of PCa diagnosis will be acquired in the near future when the results of ongoing trials will be available [45–47].

The next aspect to evaluate before adopting the new procedure as a new standard of care will be cost-effectiveness. Certainly, the time spent to coregister MRI and US images and to perform the biopsy is longer for MRI/US fusion software-based targeted prostate biopsies compared to the standard approach. Recently, Shoji et al. reported that the number of cases to perform a MRI/US fusion software-based targeted prostate biopsy within 20 min was five [48]. With regard to cost, while the fusion biopsy itself has some intrinsic expenses, the greatest increase in cost is due to the necessity to perform MRI on each patient. Nevertheless, some initial studies have shown that the overall cost-effectiveness might be still in favor of a software-based approach [49].

Conclusions

In men at risk with mp-MRI-suspicious lesion, the MRI/US fusion software-based targeted approach seems to have valuable features to be added in the standard diagnostic pathway of PCa for achieving accurate risk stratification. Although it seems to detect more clinically significant PCa as compared to standard biopsy, whether this approach should replace or support the TRUS-guided random biopsy will be determined by ongoing trials.

References

1. Singh H, Canto EI, Shariat SF et al (2004) Improved detection of clinically significant, curable prostate cancer with systematic 12-core biopsy. J Urol 171(3):1089–1092
2. Irani J, Blanchet P, Salomon L et al (2013) Is an extended 20-core prostate biopsy protocol more efficient than the standard 12-core? A randomized multicenter trial. J Urol 190(1):77–83
3. Ukimura O, Coleman JA, de la Taille A et al (2013) Contemporary role of systematic prostate biopsies: indications, techniques, and implications for patient care. Eur Urol 63(2):214–230
4. Washington SL, Bonham M, Whitson JM et al (2012) Transrectal ultrasonography-guided biopsy does not reliably identify dominant cancer location in men with low-risk prostate cancer. BJU Int 110(1):50–55
5. Belas O, Hupertan V, Comperat E et al (2012) Low accuracy of routine ultrasound-guided systematic 12-core biopsies in prostate tumor mapping. Can J Urol 19(4):6366–6372
6. Loeb S, Carter HB, Berndt SI et al (2011) Complications after prostate biopsy: data from SEER-Medicare. J Urol 186(5):1830–1834
7. Fütterer JJ, Briganti A, De Visschere P et al (2015) Can clinically significant prostate cancer be detected with multiparametric magnetic resonance imaging? a

systematic review of the literature. Eur Urol 68(4):738. [Epub ahead of print]
8. Rud E, Klotz D, Rennesund K et al (2014) Detection of the index tumour and tumour volume in prostate cancer using T2-weighted and diffusion-weighted magnetic resonance imaging (MRI) alone. BJU Int 114(6b):E32–42
9. Tan CH, Paul Hobbs B, Wei W et al (2015) Dynamic contrast-enhanced MRI for the detection of prostate cancer: meta-analysis. AJR Am J Roentgenol 204(4):W439–W448
10. Turkbey B, Merino MJ, Gallardo EC et al (2014) Comparison of endorectal coil and nonendorectal coil T2W and diffusion-weighted MRI at 3 Tesla for localizing prostate cancer: correlation with whole-mount histopathology. J Magn Reson Imaging 39(6):1443–1448
11. Jung JA, Coakley FV, Vigneron DB et al (2004) Prostate depiction at endorectal MR spectroscopic imaging: investigation of a standardized evaluation system. Radiology 233(3):701–708
12. Barentsz JO, Richenberg J, Clements R et al (2012) ESUR prostate MR guidelines 2012. Eur Radiol 22(4):746–757
13. Vargas HA, Hötker AM, Goldman DA et al (2015) Updated prostate imaging reporting and data system (PIRADS v2) recommendations for the detection of clinically significant prostate cancer using multiparametric MRI: critical evaluation using whole-mount pathology as standard of reference. Eur Radiol 26(6):1606–12. [Epub ahead of print]
14. Pokorny MR, de Rooij M, Duncan E et al (2014) Prospective study of diagnostic accuracy comparing prostate cancer detection by transrectal ultrasound-guided biopsy versus magnetic resonance (MR) imaging with subsequent MR-guided biopsy in men without previous prostate biopsies. Eur Urol 66(1):22–29
15. Quentin M, Blondin D, Arsov C et al (2014) Prospective evaluation of magnetic resonance imaging guided in-bore prostate biopsy versus systematic transrectal ultrasound guided prostate biopsy in biopsy naïve men with elevated prostate specific antigen. J Urol 192(5):1374–1379
16. Kasivisvanathan V, Dufour R, Moore CM et al (2013) Transperineal magnetic resonance image targeted prostate biopsy versus transperineal template prostate biopsy in the detection of clinically significant prostate cancer. J Urol 189(3):860–866
17. Haffner J, Lemaitre L, Puech P et al (2011) Role of magnetic resonance imaging before initial biopsy: comparison of magnetic resonance imaging-targeted and systematic biopsy for significant prostate cancer detection. BJU Int 108(8 Pt 2):E171–178
18. Byrne TE (2005) A review of prostate motion with considerations for the treatment of prostate cancer. Med Dosim 30(3):155–161
19. Logan JK, Rais-Bahrami S, Turkbey B et al (2014) Current status of magnetic resonance imaging (MRI) and ultrasonography fusion software platforms for guidance of prostate biopsies. BJU Int 114(5):641–652
20. Sonn GA, Chang E, Natarajan S et al (2014) Value of targeted prostate biopsy using magnetic resonance-ultrasound fusion in men with prior negative biopsy and elevated prostate-specific antigen. Eur Urol 65(4):809–815
21. Lawrence EM, Tang SY, Barrett T et al (2014) Prostate cancer: performance characteristics of combined T_2W and DW-MRI scoring in the setting of template transperineal re-biopsy using MR-TRUS fusion. Eur Radiol 24(7):1497–1505
22. Vourganti S, Rastinehad A, Yerram NK et al (2012) Multiparametric magnetic resonance imaging and ultrasound fusion biopsy detect prostate cancer in patients with prior negative transrectal ultrasound biopsies. J Urol 188(6):2152–2157
23. Abdi H, Zargar H, Goldenberg SL et al (2015) Multiparametric magnetic resonance imaging-targeted biopsy for the detection of prostate cancer in patients with prior negative biopsy results. Urol Oncol 33(4):165.e1–7
24. Portalez D, Mozer P, Cornud F et al (2012) Validation of the European Society of Urogenital Radiology scoring system for prostate cancer diagnosis on multiparametric magnetic resonance imaging in a cohort of repeat biopsy patients. Eur Urol 62(6):986–996
25. Salami SS, Ben-Levi E, Yaskiv O et al (2015) In patients with a previous negative prostate biopsy and a suspicious lesion on magnetic resonance imaging, is a 12-core biopsy still necessary in addition to a targeted biopsy? BJU Int 115(4):562–570
26. Raskolnikov D, Rais-Bahrami S, George AK et al (2015) The role of image guided biopsy targeting in patients with atypical small acinar proliferation. J Urol 193(2):473–478
27. Valerio M, Donaldson I, Emberton M et al (2015) Detection of clinically significant prostate cancer using magnetic resonance imaging-ultrasound fusion targeted biopsy: a systematic review. Eur Urol 68(1):8–19
28. Hu JC, Chang E, Natarajan S et al (2014) Targeted prostate biopsy in select men for active surveillance: do the Epstein criteria still apply? J Urol 192(2):385–390
29. Sonn GA, Natarajan S, Margolis DJ et al (2013) Targeted biopsy in the detection of prostate cancer using an office based magnetic resonance ultrasound fusion device. J Urol 189(1):86–91
30. Muller BG, Kaushal A, Sankineni S et al (2015) Multiparametric magnetic resonance imaging-transrectal ultrasound fusion-assisted biopsy for the diagnosis of local recurrence after radical prostatectomy. Urol Oncol 33(10):425.e1–6
31. van den Bos W, Muller BG, Ahmed H et al (2014) Focal therapy in prostate cancer: international multidisciplinary consensus on trial design. Eur Urol 65(6):1078–1083
32. Delongchamps NB, Peyromaure M, Schull A et al (2013) Prebiopsy magnetic resonance imaging and prostate cancer detection: comparison of random and targeted biopsies. J Urol 189(2):493–499

33. Mozer P, Rouprêt M, Le Cossec C et al (2015) First round of targeted biopsies using magnetic resonance imaging/ultrasonography fusion compared with conventional transrectal ultrasonography-guided biopsies for the diagnosis of localised prostate cancer. BJU Int 115(1):50–57
34. Rastinehad AR, Turkbey B, Salami SS et al (2014) Improving detection of clinically significant prostate cancer: magnetic resonance imaging/transrectal ultrasound fusion guided prostate biopsy. J Urol 191(6):1749–1754
35. Siddiqui MM, Rais-Bahrami S, Turkbey B et al (2015) Comparison of MR/ultrasound fusion-guided biopsy with ultrasound-guided biopsy for the diagnosis of prostate cancer. JAMA 313(4):390–397
36. Baco E, Rud E, Eri LM et al (2015) A randomized controlled trial to assess and compare the outcomes of two-core prostate biopsy guided by fused magnetic resonance and transrectal ultrasound images and traditional 12-core systematic biopsy. Eur Urol 69(1):149–56. [Epub ahead of print]
37. Tonttila PP, Lantto J, Pääkkö E et al (2015) Prebiopsy multiparametric magnetic resonance imaging for prostate cancer diagnosis in biopsy-naive men with suspected prostate cancer based on elevated prostate-specific antigen values: results from a randomized prospective blinded controlled trial. Eur Urol 69(3):419–25. [Epub ahead of print]
38. Puech P, Rouvière O, Renard-Penna R et al (2013) Prostate cancer diagnosis: multiparametric MR-targeted biopsy with cognitive and transrectal US-MR fusion guidance versus systematic biopsy--prospective multicenter study. Radiology 268(2):461–469
39. Lanz C, Cornud F, Beuvon F et al (2016) Gleason score determination with TRUS-MRI fusion guided prostate biopsies: are we gaining in accuracy? J Urol 195(1):88–93. [Epub ahead of print]
40. Radtke JP, Kuru TH, Boxler S et al (2015) Comparative analysis of transperineal template saturation prostate biopsy versus magnetic resonance imaging targeted biopsy with magnetic resonance imaging-ultrasound fusion guidance. J Urol 193(1):87–94
41. Wysock JS, Rosenkrantz AB, Huang WC et al (2014) A prospective, blinded comparison of magnetic resonance (MR) imaging-ultrasound fusion and visual estimation in the performance of MR-targeted prostate biopsy: the PROFUS trial. Eur Urol 66(2):343–351
42. Cool DW, Zhang X, Romagnoli C et al (2015) Evaluation of MRI-TRUS fusion versus cognitive registration accuracy for MRI-targeted, TRUS-guided prostate biopsy. AJR Am J Roentgenol 204(1):83–91
43. Mouraviev V, Verma S, Kalyanaraman B et al (2013) The feasibility of multiparametric magnetic resonance imaging for targeted biopsy using novel navigation systems to detect early stage prostate cancer: the preliminary experience. J Endourol 27(7):820–825
44. Arsov C, Rabenalt R, Blondin D et al (2015) Prospective randomized trial comparing magnetic resonance imaging (MRI)-guided in-bore biopsy to MRI-ultrasound fusion and transrectal ultrasound-guided prostate biopsy in patients with prior negative biopsies. Eur Urol 68(4):713–720
45. Simmons LA, Ahmed HU, Moore CM et al (2014) The PICTURE study -- prostate imaging (multiparametric MRI and Prostate HistoScanning™) compared to transperineal ultrasound guided biopsy for significant prostate cancer risk evaluation. Contemp Clin Trials 37(1):69–83
46. El-Shater Bosaily A, Parker C, Brown LC, et al (2015) PROMIS Group. PROMIS - Prostate MR imaging study: A paired validating cohort study evaluating the role of multi-parametric MRI in men with clinical suspicion of prostate cancer. Contemp Clin Trials 42:26–40
47. Kasivisvanathan V (2015) https://clinicaltrials.gov/ct2/show/NCT02380027. Accessed 02 Oct 2015
48. Shoji S, Hiraiwa S, Endo J et al (2015) Manually controlled targeted prostate biopsy with real-time fusion imaging of multiparametric magnetic resonance imaging and transrectal ultrasound: an early experience. Int J Urol 22(2):173–178
49. de Rooij M, Crienen S, Witjes JA et al (2014) Cost-effectiveness of magnetic resonance (MR) imaging and MR-guided targeted biopsy versus systematic transrectal ultrasound-guided biopsy in diagnosing prostate cancer: a modelling study from a health care perspective. Eur Urol 66(3):430–436

US and Arteriovenous Fistulas for Hemodialysis

56

Antonio Granata, Pasquale Zamboli, Pasquale Fatuzzo, and Fulvio Fiorini

56.1 Introduction

Arteriovenous fistula (AVF) created with native vessels is the vascular access of choice for hemodialysis: the AVF is associated with a lower incidence of complications and longer survival than prosthetic grafts or central venous catheters [1, 2]. Nephrologists and vascular surgeons find it increasingly difficult to locate native vessels suitable for creation of a well-functioning, persistently patent AVF because of increasing prevalence among requiring dialysis patients of advanced age and comorbidities, such as diabetes mellitus and vascular disease [3].

Preoperative mapping and identification of suitable vessels by Doppler ultrasound (DUS) has a central role in increasing the number of AVFs created with native vessels. Indeed DUS also improves AVF survival by facilitating postoperative monitoring and surveillance with early diagnosis and rapid correction of complications [4–8].

A. Granata (✉)
Nephrology and Dialysis Unit, "S. Giovanni di Dio" Hospital, Agrigento, Italy
e-mail: antonio.granata4@tin.it

P. Zamboli
School of Nephrology, University of Naples, Naples, Italy

P. Fatuzzo
School of Nephrology, University of Catania, A.O.U. "Policlinico- Vittorio Emanuele", Catania, Italy

F. Fiorini
Nephrology and Dialysis Unit, "S. Maria della Misericordia" Hospital, Rovigo, Italy

P. Martino, A.B. Galosi (eds.), *Atlas of Ultrasonography in Urology, Andrology, and Nephrology*,
DOI 10.1007/978-3-319-40782-1_56

56.2 Preoperative Vascular Mapping

Selection of vessels for constructing an AVF was based for decades exclusively on physical examination of the upper limbs. Although this approach provides acceptable information on the superficial venous circulation (vessel palpability, caliber, patency, and course), it furnishes much more limited data on the arterial vessels (pulse palpability and patency of the arterial circulation of the hand based on the results of the Allen test) [9–11]. In addition, physical examination alone is insufficient in a considerable percentage of patients (~25–50%) [10]. DUS is more time-consuming than physical examination and requires both experienced examiner and special equipment. However, it provides more information on the superficial and deep veins of the arm and a wealth of additional data on the arterial circulation. It is completely noninvasive, safe, and repeatable [9]. DUS allows simultaneous visualization of the anatomy (B-mode imaging) and blood supply (color and Doppler imaging) of the upper arm. It can be performed directly by the physician who will be creating the vascular access. International guidelines recommend its use in all patients who are candidates for an AVF, as a natural complement to the physical examination [12].

56.2.1 Technical Requirements and Examination Technique

The ultrasound scanner used to map the upper extremity vasculature must be equipped with a linear probe with minimum frequencies of 7 MHz for the B-mode examination and 5 MHz for the Doppler study [13]. The patient should be examined in the supine position with the trunk moderately elevated or, alternatively, may be seated in front of the operator with the forearm resting on a stand. Most examiners prefer the supine position because it simplifies the assessment of the vascular structures of the arm and is more comfortable for the patient [13, 14]. The examination should be carried out in a comfortably warm room, and the gel should also be warmed to avoid triggering vasoconstriction of the structures being examined [13, 14]. Ideally, the arterial district should be evaluated with transverse and/or longitudinal scans from the root of the arm toward the hand while the venous district from the periphery toward the thorax. A thorough examination of the circulation of the arm must include B-mode assessment of morphological aspects as well as color and Doppler evaluation of arterial and venous blood flow.

56.2.2 Preoperative Arterial Mapping

Preoperative arterial DUS should include evaluation of subclavian, axillary, brachial, radial, and ulnar arteries [15]. DUS allows thorough assessment of the arterial circulation of the arm based on a series of morphological and functional parameters [10] including vessel diameter, wall thickness, wall alterations, vessel course, steno-obstructive lesions blood flow, and artery's ability to dilate. The internal diameter of an artery can be measured on either longitudinal or transverse scans [14], but the former allows better visualization of the intimal layers of vessel walls, thereby facilitating more precise measurement of the internal diameter of the vessel [9] (Fig. 56.1).

AVF failures were found to be quite frequent when small-caliber (<1.5–1.6 mm) arteries were used to create the fistula. Malovrh et al. reported immediate and early failure rates of 55 and 64%, respectively, when the arteries used had diameters of ≤1.5 mm, whereas much lower rates (8 and 17%, respectively) were observed when the arterial diameters were >1.5 mm [17] Silva et al. proposed a minimal diameter of 2 mm, which was associated with an early failure rate of 8% and a 1-year primary patency rate of 83% [5]. However, AVF success rates of approximately

50 % have been reported even when the arterial diameter is <1.5 mm [18]. Definitively, the likelihood of AVF patency and survival increases with the diameter of the artery used to create the fistula [5, 10, 11, 17, 19].

Indeed, diameter is only one of the factors that affect the probability of successful AVF creation, and it has to be evaluated in conjunction with the functional status of artery and with the optimal site for AVF construction [9]. Arterial wall changes are common in patients with chronic renal insufficiency, diabetes, and atherosclerosis [10]. An increased thickness seems to be closely correlated with fistula failure [20]. Calcifications are easy to identify as areas of hyperechogenicity (with or without posterior shadowing) within the arterial wall and irregularities of the intimal lamina. They do not represent contraindications to the creation of a fistula although they can influence its outcome and/or render surgery more difficult [14].

DUS is also a very accurate method for identifying stenotic arterial lesions, obstructive arterial lesions [21], and vascular abnormalities such as brachial artery bifurcation in the most proximal portion of the arm.

Functional study involves the assessment of blood flow and the artery's ability to dilate. Blood flow can be evaluated by measuring the vessel diameter and mean flow velocity (cm/s) on longitudinal scans. Malovrh et al. [10] found that successful radial-cephalic AVF construction was associated with radial artery flow exceeding 50 ml/min, and in the study by Sato et al. [22], a preoperative radial artery flow of 20 ml/min was associated with an increased risk of "primary AVF failure" within 8 months of surgery. After surgery, adequate fistula maturation is associated with dilation of the artery that feeds the AVF. As a result, blood flow within the vascular access increases, and the previously triphasic (high resistance) arterial spectrum becomes biphasic (low resistance).

The artery's ability to increase its caliber (distensibility) can be estimated preoperatively on the basis of variations in the radial artery Doppler spectrum during the reactive hyperemia test [10]. Ischemia is induced by having the patient make a fist for 2 min, and the increase in arterial flow (reactive hyperemia) is observed immediately after the hand is reopened [10]. During the phase of ischemia, the Doppler spectrum of the artery is normally triphasic, reflecting high resistance. If the vessel is capable of dilatation, the arterial spectrum becomes biphasic during the phase of reactive hyperemia [10] (Fig. 56.2). Spectral variation can be quantified by calculating the resistance index (RI) [RI = (peak systolic velocity – end diastolic velocity)/peak systolic velocity]: the greater the intensity of the reactive hyperemia, the lower the RI will be [10]. Malovrh et al. [10] demonstrated that the absence of reactive hyperemia (reflected by an RI > 0.7 after the fist is opened) indicates insufficient increase in arterial flow during the test, which is predictive of immediate postoperative AVF failure.

The reactive hyperemia test provides an excellent index of artery's functional status and is particularly useful for selecting the surgical site (wrist, forearm, and elbow) for AVF construction.

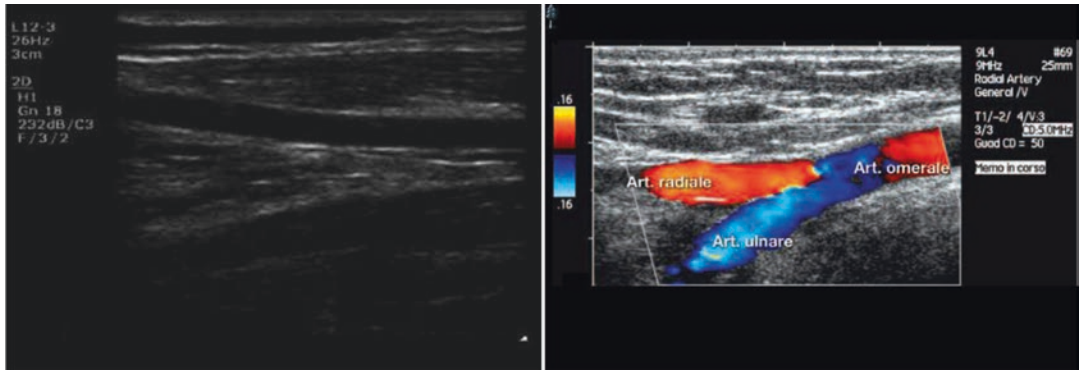

Fig. 56.1 Preoperative arterial mapping. DUS allows thorough assessment of the arterial circulation of the arm based on morphological and functional parameters. *Left*: B-mode evaluates vessel diameter, wall thickness, wall alterations, vessel course, and possible steno-obstructive lesions. *Right*: ECD allows blood flow direction assessment by codifying red flow moving toward the probe and blue flow moving away

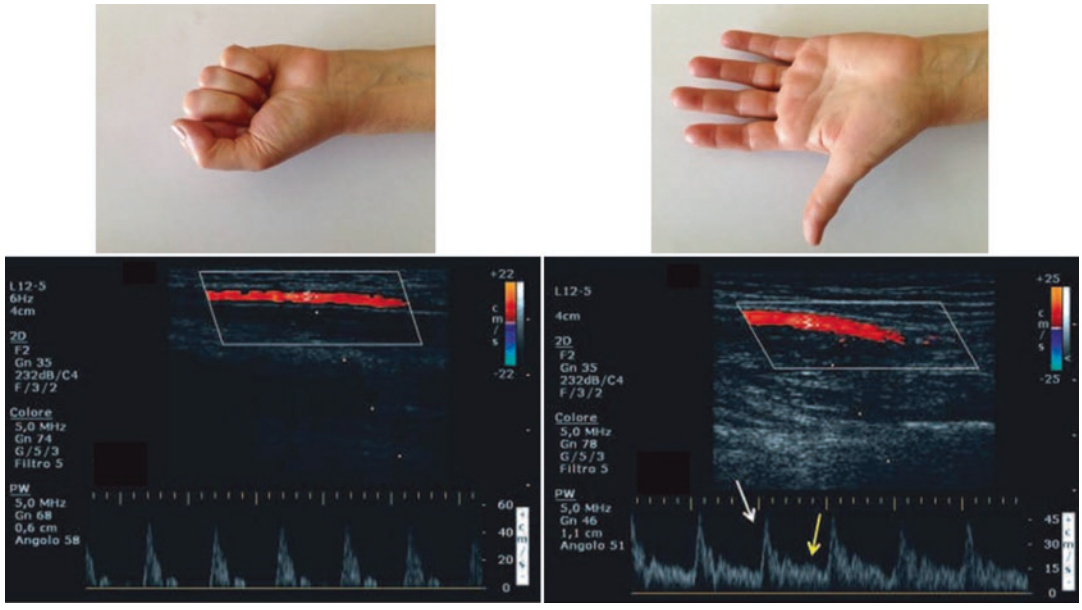

Fig. 56.2 Reactive hyperemia test. *Left*: ischemic phase (*closed fist*) with high-resistance triphasic Doppler spectrum. *Right*: reactive hyperemia (*opened hand*) with low-resistance biphasic Doppler spectrum (*arrows*)

56.2.3 Preoperative Venous Mapping

Preoperative venous DUS involves evaluation of the superficial and deep venous systems of the upper limb from the wrist up to the central veins. With ultrasound, direct visualization of the proximal portions of the subclavian vein and the innominate vein is not always possible [13]. A tourniquet is placed around the root of the arm, and the superficial venous circulation is examined with transverse scans, beginning with the cephalic vein, from the wrist to the point where it drains into the deep venous system [9]. The full course of the basilic vein should also be examined, but this is often done only if the cephalic vein is not suitable for AVF creation [9]. A map of the whole superficial venous circulation can be drawn (Fig. 56.3).

Several ultrasound parameters can be helpful in deciding whether a superficial vein can be used to create an AVF. They include the appearance of the vein wall, the course of the vessel, its patency, caliber and distensibility, and the presence of collateral circuits [9, 13].

A normal vein is characterized by thin, regular walls, and a completely anechoic lumen [23]. The course of the vein must be sufficiently linear (for a distance of at least 8–10 cm), and it should lie less than 6 mm below the skin surface to facilitate venipuncture [24]. Vein patency is assessed by exerting intermittent pressure with the transducer which causes complete collapse of the vessel walls [9]. Noncompressibility of the vein under the transducer's pressure is a sign of obstruction and is often associated with the presence of echogenic material in the lumen [23]. Patency can be confirmed using the color Doppler module with a low pulse repetition frequency or verifying the presence of the Doppler trace in a longitudinal scan [23]. A normal venous Doppler spectrum is characterized by continuous, low velocity flow, which becomes increasingly phasic as the examination proceeds toward the central veins; the absence of such flow confirms the presence of an obstruction. The presence at the level of the subclavian and internal jugular veins of flow that varies in velocity with the respiratory and cardiac activity is an indirect index of the patency of the ipsilateral innominate vein and the superior vena cava, whereas a monophasic curve is indicative of steno-occlusion [10, 13, 14].

Fistulas created with small-caliber veins (<1.6 mm) are at high risk for early failure [11], but there is no consensus on the minimum cephalic vein diameter that will ensure good maturation of a radial-cephalic AVF. Silva et al. [5] suggest a minimum diameter of ≥2.5 mm when a tourniquet has been applied; in the absence of a tourniquet, Mendes et al. [25] propose a diameter of >2 mm. Well-documented indications on the minimum diameter for the veins of the arm are also lacking, but a value of at least 3 mm is recommended [14]. After the AVF has been created, the vein tends to dilate as a result of the increased blood flow. The vein's ability to dilate (venous distensibility) can be evaluated during preoperative mapping. The diameter of the vessel is measured before and at least 2 min after placement of a tourniquet (or a sphygmomanometer cuff inflated to a pressure of 50–60 mmHg), and the percentage of increase is evaluated [14, 26]. Malovrh et al. [10] concluded that venous distensibility is a predictor of outcome since the mean percentage of vein dilatation observed in veins used for successfully constructed AVFs was 48 versus 11 % in those used for fistulas that ended in immediate failure. Lockhart et al. [27, 28] reported that cephalic veins with a pretourniquet diameter of ≥2.5 mm and smaller veins with a post-tourniquet diameter ≥2.5 mm were equally useful for creating dialysis fistulas. They concluded that distensibility testing should be used mainly to identify the actual maximum diameter of apparently small-caliber arm veins.

The presence of accessory veins less than 5 cm from the site chosen for the anastomosis can alter the functionality of the fistula [11], while higher frequencies of non-maturation are reported when the AVF is near large collateral veins [29].

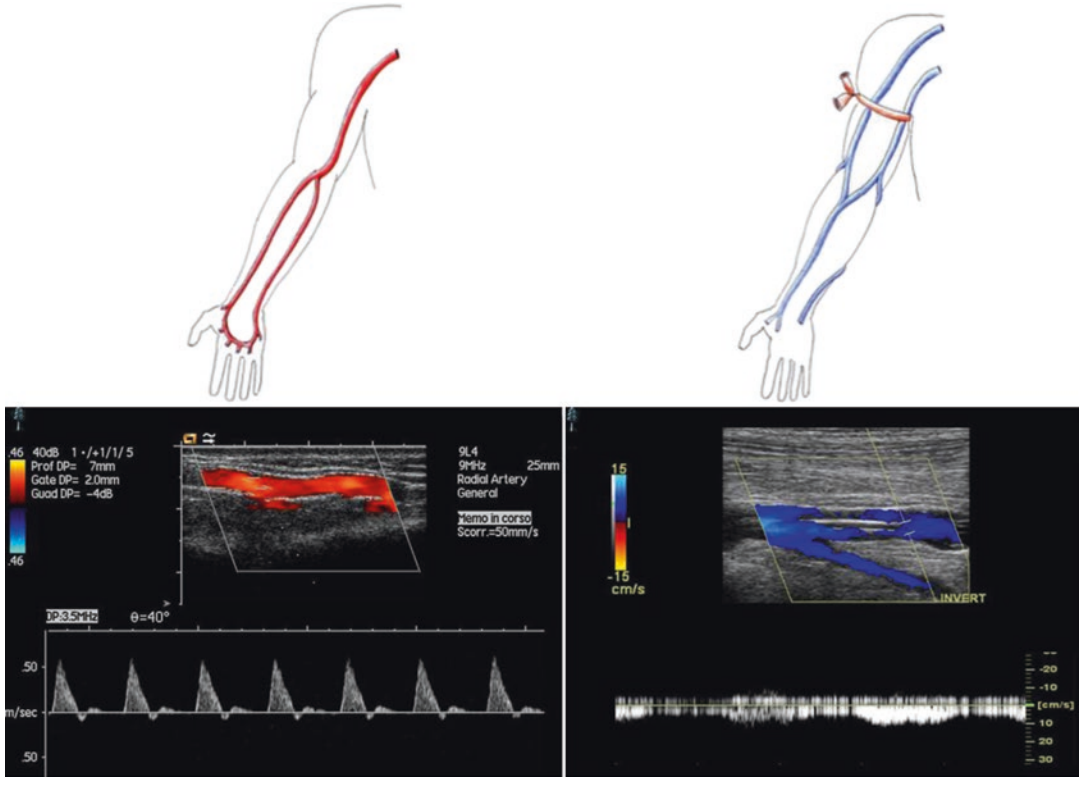

Fig. 56.3 Examples of preoperative vascular mapping. *Left*: arterial mapping with radial artery Doppler analysis showing a normal high-resistance flow. *Right*: superficial vein mapping is enabled by a tourniquet placed around the root of the arm; cephalic vein is characterized by continuous, low velocity flow

56.3 AVF Maturation and Calculation of Blood Flow

Arteriovenous anastomoses with native vessels have been associated with a high incidence of early occlusion and failure to mature (FTM) during the postoperative period. The incidence of FTM for radiocephalic AVFs ranges from 30 to 60 % [15, 30]. When AVF does not appear clearly mature on inspection, ultrasound examination and assessment of hemodynamic parameters (AVF blood flow, RI) can help to determine whether the AVF is suitable for cannulation or whether it has instead failed to mature. In obese subjects, even well-developed veins can be difficult to visualize or palpate; in these cases, DUS can reveal whether the fistula is mature, and US mapping of the outflow veins can facilitate the first cannulation and simplify subsequent punctures [15]. "The Rule of Six," incorporated by the K-DOQI guidelines [24], identifies ultrasound features that confirm fistula maturation: flow volume of >600 ml/min, outflow vein diameter of ≥6 mm, and outflow vein depth of ≤6 mm below the skin surface.

For slowly maturing AVFs, it is important to assess maturation with periodic calculation of flow volume at the brachial artery level. Serial measurement of AVF flow volumes during the first month after surgery can help distinguish fistulas that will mature correctly from those destined to fail. Maturation is likely if blood flow through the fistula is 250–500 ml/min on postoperative day 1 and 500–900 ml/min 1 month after construction of the anastomosis [33]. If lower flow rates are encountered, proper maturation is unlikely, and the fistula will probably become unsuitable for use in dialysis wing to problems of thrombosis or low flow.

56.3.1 Calculation of AVF Flow Volume

Calculation of the AVF flow volume by DUS is a simple procedure that can be completed in a few minutes with high reproducibility. The following formula is used to calculate flow volumes: area x mean velocity x 60, where area is the cross-sectional area of the vessel in square centimeters (since the vessel is cylindrical, its section is a circle whose area is calculated as the square of the radius × 3.14). Mean velocity (in cm/s) is that of the red blood cells measured from the Doppler trace recorded at the site used to measure area, and 60 is the number of seconds in a minute (since flow volumes are expressed in milliliters per minute) [13, 32]. Vessel diameter and mean flow velocity can be measured on a single longitudinal scan of the vessel. The vessel diameter is measured on the appropriately enlarged B-mode image. The pulsed Doppler module is then activated and the PRF adjusted to eliminate artifacts, and the mean flow velocity is calculated from the time/velocity curve (using the time-averaged velocity option available on most scanners) (Fig. 56.4).

Measuring the flow volume at the level of the inflow artery improves accuracy and reproducibility. In clinical practice, brachial artery is the preferred site for the flow volume measurement of distal and proximal/proximalized AVFs [13, 24, 32, 33]. It is easy to sample and does not collapse under normal transducer pressures. Just above the elbow crease, there is an oblique segment of the brachial artery, where the sample volume can be easily positioned at an appropriate insonation angle. Finally, its laminar flow allows one to record suitable tracings for precise calculation of the mean velocity. In prosthetic grafts, the flow volume can be measured directly in the prosthetic conduit, which is more regular in caliber than a native outflow vein and more resistant to pressure exerted with the transducer.

Sample volume should be oriented parallel to the direction of blood flow and the angle of insonation maintained at <60°. The sample volume must always be positioned at the center of the vessel, but the amplitude should be adjusted to allow sampling of 50–70 % of the vessel lumen. Acquisition of velocity data must be as precise as possible; this can be achieved by careful regulation of the PRF to eliminate all types of artifacts.

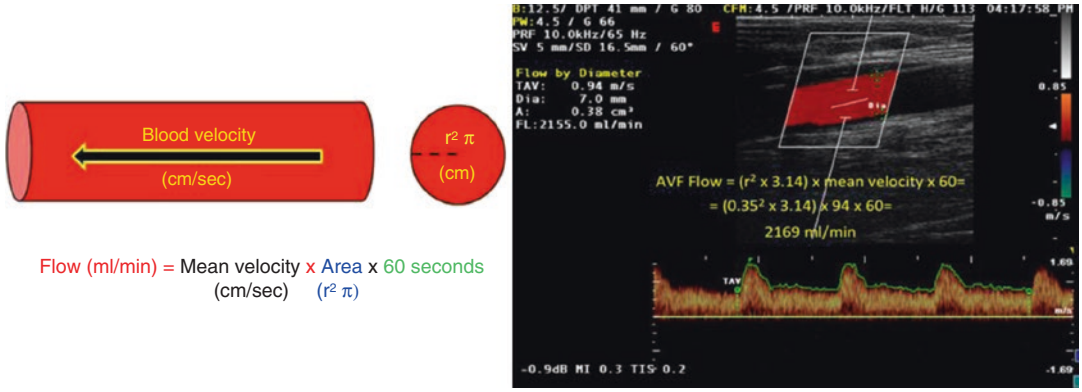

Fig. 56.4 Calculation of the AVF flow volume. *Left*: theoretical basis of the formula used to calculate blood flow volume of a blood vessel. *Right*: example of AVF flow volume calculated at the level of the brachial artery, manually with the proposed formula (*AVF flow volume*) and with scanner software (*Flow by diameter*)

56.4 AVF Monitoring/Surveillance (Follow-Up and Early Detection of Complications)

Measurement of blood flow is considered the best means of surveillance for a vascular access [24]: reduced flow volumes or values that decrease over time are predictive of thrombosis for both native and prosthetic AVFs [32, 34, 35]. DUS can document a low AVF flow volume and simultaneously explore possible causes [13, 15, 32]. Anyway, AVF examination through DUS should be used when monitoring/surveillance methods have revealed anomalies or when problems arise that prevent regular dialysis (difficult venipuncture, insufficient blood flow, high venous pressure, and prolonged bleeding after removal of fistula needles) (Fig. 56.5).

To minimize the risk of underestimates caused by hemodynamic factors (e.g., hypotension), DUS should not be used to calculate AVF flow volumes during the immediate post-dialysis period: measurements made between one session and the next or immediately before a dialysis session are preferable.

The examination should include the following steps: study of arterial inflow side of the fistula (including AVF flow volume), study of anastomotic chamber, and study of venous outflow side of the fistula. A thorough evaluation of the AVF includes exploration of each of these three areas with both transverse and longitudinal scans and assessment of morphological (B-mode) as well as hemodynamic aspects (with color Doppler and Doppler analysis) (Fig. 56.6).

A well-functioning AVF will be characterized by a flow rate of 700–1,300 ml/min [32, 33]. Values of <500 ml/min [13, 24] and <300 ml/min [13, 32] are considered predictive of access dysfunction and imminent thrombosis, respectively (Fig. 56.7). In a vascular access that has previously been stable with flow volumes of >1,000 ml/min, further investigation is warranted when consecutive monthly measurements reveal a decrease in flow volume of >25 % over a relatively short period of time (1–4 months) [15, 16, 24, 31, 34].

DUS calculation of AVF flow volume can also be useful for assessing the effectiveness of a therapeutic intervention carried out to resolve a complication. The absence of an increase in flow of at least 20 % after such an intervention (e.g., percutaneous transluminal angioplasty to eliminate stenosis) indicates that the treatment has failed and an alternative solution is needed [24].

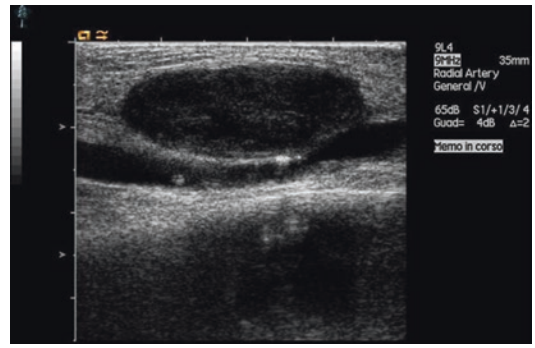

Fig. 56.5 Early detection of hematoma secondary to incorrect venipuncture. AVF provides vascular access for hemodialysis allowing repeated needle insertions. Bleeding from the AVF with development of hematoma is a frequent complication which can be easily detected by ultrasound. Echo guide can also help in the correct cannulation in case of hematoma surrounding the vessel

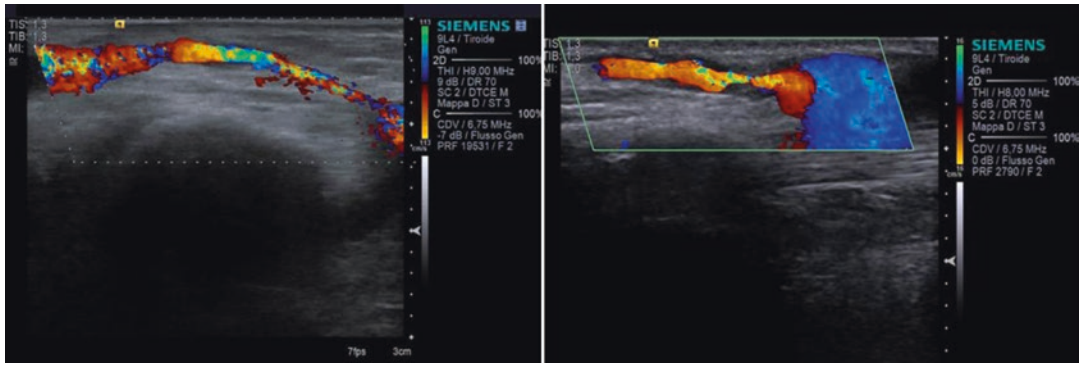

Fig. 56.6 Stenotic complication of AVF venous outflow. Doppler examination should always be performed with a beam-steering transducer to maintain the correct angle of incidence (30°–60°) relative to the direction of flow. Right PRF regulation is essential to avoid false positive: high PRF is required to sample faster fluxes in AVF. Stenosis is revealed by the dramatic blood flow acceleration which is codified with aliasing in color map

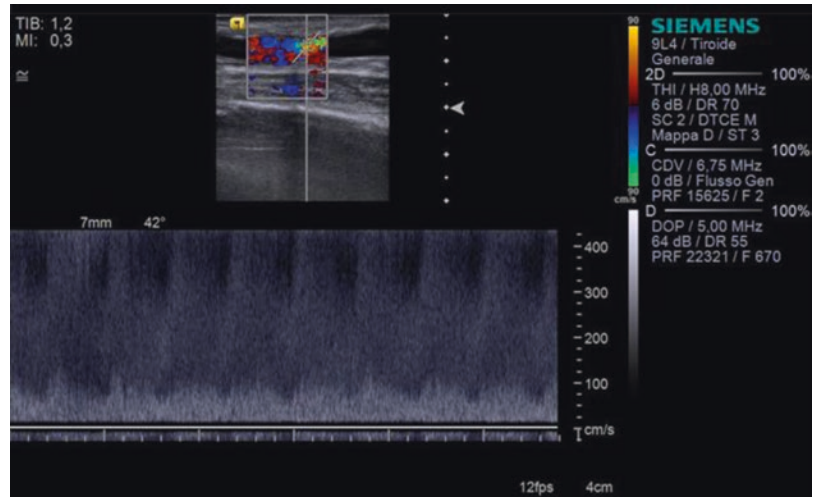

Fig. 56.7 Spectral analysis identifying AVF stenosis. In case of stenosis, when angle of incidence, PRF, gain, and focus are correctly set, the sample volume located in the color-aliasing area identifies a marked spectral broadening due to stenotic blood flow acceleration. Post-stenotic turbulence may promote aneurismal enlargement of the outflow vein

56.4.1 Morphological Assessment (B-Mode)

The study typically begins with an examination of the brachial artery. On a longitudinal view, a normal artery appears as a completely anechoic band delimitated by two three-layered walls. The brachial artery is followed down to the antecubital crease, where it divides into radial and ulnar arteries, which run along the lateral and medial side of the forearm, respectively. The AVF inflow artery, generally the radial artery, is characterized by a constant, regular increase in caliber and modest tortuosity, which are more marked in high-flow AVFs.

Exploration of the arterial side of the fistula proceeds distally to the surgical anastomosis, which frequently has a winding course. Vessel pulsatility at the anastomotic region is so marked that it produces a "thrill" caused by the turbulence of the flow. It is characterized by fine, rapid, palpable, and sonographically documented vibrations involving the tissues surrounding the vessel [23, 32]. The sonographic image of the anastomotic region can help us to define the AVF type: end-to-end (E-E), side-to-end (S-E), or side-to-side (S-S) (Fig. 56.8). The outflow vein is characterized by tortuosity, ectasia, and segmental variations in caliber that are generally due to wall damage caused by repeated venipuncture. The vessel walls generally appear to be mildly thickened as a result of intimal hyperplasia, a phenomenon that renders the vessel capable of withstanding repeated venipuncture with large caliber needles [23, 32].

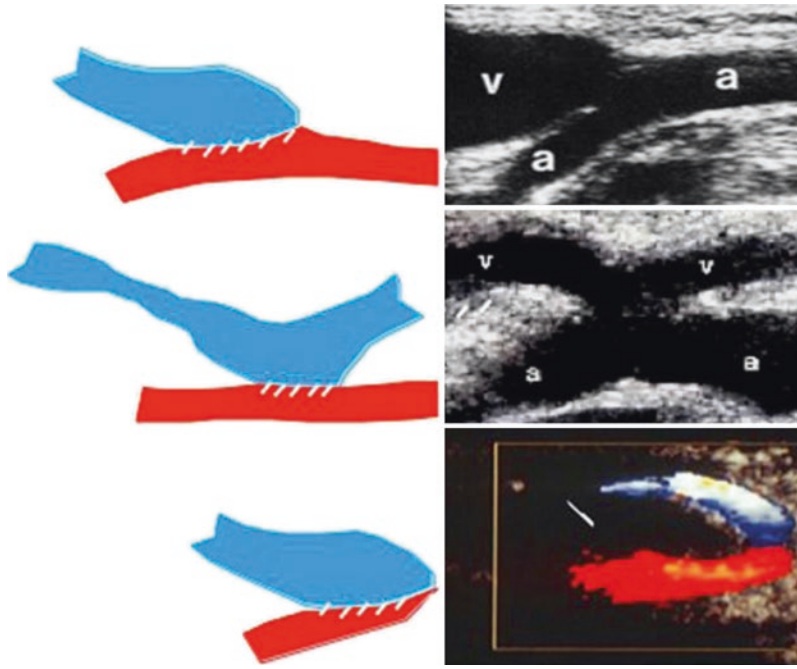

Fig. 56.8 Ultrasound scans of the anastomotic region of various AVF types. Longitudinal sonographic image of the anastomotic region can help to define the AVF type. *Top*: side-to-end AVF (S-E). *Centrum*: side-to-side AVF (S-S). *Bottom*: end-to-end AVF (E-E). If nonlinearity of the anastomotic chamber precludes acquisition of such images, the presence or absence of arterial and distal venous segment with respect to the anastomosis site can be used to identify AVF type

56.4.2 Color Doppler Examination

The appearance of color confirms the patency of the vessels being examined. As a general rule, the scanner is usually set to "map" arterial flow in red (flow moving toward the transducer) and venous flow in blue (moving away from the transducer) (Fig. 56.9). Pulse repetition frequency (PRF) is one of the most important settings that need to be adjusted for a proper flow metric analysis. The PRF selected for AVFs is usually higher (1,000–6,000 Hz) than those commonly used to study the upper limbs, because of the higher flow velocities in AVFs [23, 32].

This is a "dynamic" setting, which has to be readjusted several times during the examination to eliminate aliasing (especially near the anastomosis, where the flow is faster) and to avoid noncoding of the venous flow, which can occur, for example, during exploration of the outflow vein after assessment of the AVF with a high PRF [23, 32]. Lower PRFs (<1,000 Hz) can be used when a vessel seems to be patent on the basis of morphological findings and responses to compression maneuvers, but intraluminal flow signals are lacking. This can occur, for example, at the level of large venous aneurysms, where flow slows considerably as a result of the large caliber of the lumen. Low PRFs are also recommended during exploration of collateral vessels near a thrombosed or complex AVF [23, 32]. On color Doppler imaging, the inflow artery of the AVF is characterized by relatively homogeneous, laminar flow (with maximum velocity at the center of the lumen and the lowest values near the vessel walls). Near the anastomosis, there is an increase in flow velocity (reflected by lighter colors, even white) and turbulence (reflected by a disorderly alternation of reds and blues within the same luminal segment). Areas of vortex flow are often observed at this level, especially near the anastomosis. They are reflected by alternating intraluminal color signals with a typical spiroidal configuration [23, 32]. Moving away from the AVF, the caliber of the vessel tends to decrease, vortexing diminishes, and the venous flow gradually becomes more homogeneous and regular [23, 32].

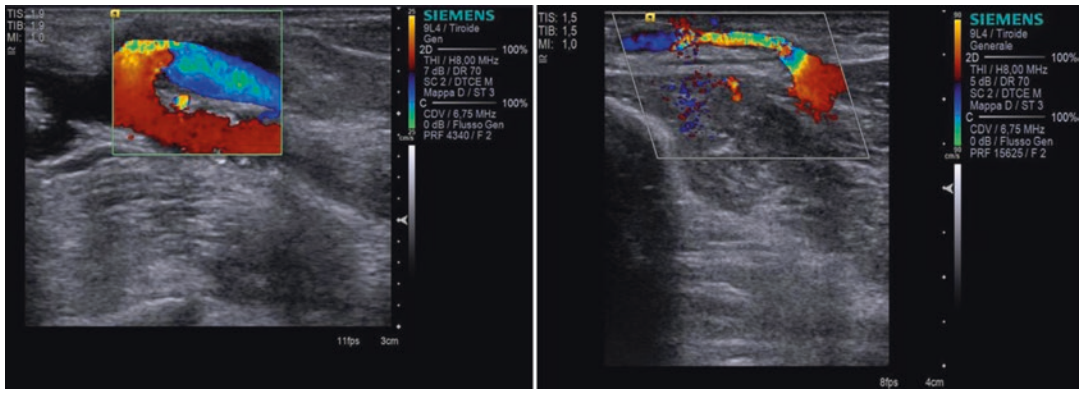

Fig. 56.9 Echo color Doppler of the anastomotic chamber. *Left*: color map with intermediate PRF identify radial artery, cephalic vein, and their anastomotic chamber in unique scan. Arterial flow moving toward the transducer is shown in red, while venous flow moving away from the transducer is shown in blue. Color aliasing at anastomosis level points out the presence of turbulent flow. *Right*: radial artery anastomosis with cephalic vein can be affected by significant stenosis that prevent to set the appropriate blood pump flow

56.4.3 Doppler Ultrasound Assessment

On Doppler ultrasound imaging, the inflow side of a normal AVF is characterized by an appreciable reduction in peripheral resistance relative to the contralateral limb, with copious anterograde flow during the entire diastolic phase [23]. As the transducer moves closer to the anastomosis, flow through the afferent artery undergoes a progressive and constant increase in velocity that involves both the systolic and diastolic phases, and spectral broadening is observed, which is maximal in vicinity of the anastomosis, where it reaches the baseline with the disappearance of the acoustic window [23]. At the level of the anastomosis, purely turbulent flow profiles are observed, with loss of arterial phasicity, a broad spectrum extending above and below the baseline, and high peak systolic velocities that are extremely variable in subsequent moments [23]. On the venous side, near the anastomosis, flow is "arterialized" with obvious systolic–diastolic phasicity and a particularly broad spectrum. As the distance from the AVF increases, arterial phasicity is progressively lost, the mean flow velocity diminishes, and the spectrum takes on the characteristics of regular venous flow [23].

Conclusions

The native AVF is the vascular access of choice for patients who require hemodialysis: it lasts longer and is associated with fewer complications than other types of vascular access; for hemodialysis patients, these benefits translate into better quality of life and longer survival.

DUS is fundamental for identifying vessels that are suitable for creating an AVF (preoperative mapping) and for early detection of complications (surveillance). Indeed, DUS is the only surveillance method that allows one to monitor AVF blood flow and simultaneously explore possible causes of vascular access malfunction.

References

1. NKF-K/DOQI III (2001) NKF-K/DOQI Clinical practice guidelines for vascular access: update 2000. Am J Kidney Dis 37(Suppl 1):S137–S181
2. Gibson KD, Gillen DL, Caps MT, Kohler TR, Sherrard DJ, Stehman-Breen CO (2001) Vascular access survival and incidence of revisions: a comparison of prosthetic grafts, simple autogenous fistulas, and venous transposition fistulas from the United States Renal Data System Dialysis Morbidity and Mortality Study. J Vasc Surg 34:694–700
3. Konner K, Hulbert-Shearon TE, Roys EC, Port FK (2002) Tailoring the initial vascular access for dialysis patients. Kidney Int 62:329–338
4. Allon M, Lockhart ME, Lilly RZ, Gallichio MH, Young CJ, Barker J et al (2001) Effect of preoperative sonographic mapping on vascular access outcomes in hemodialysis patients. Kidney Int 60:2013–2020
5. Silva MB Jr, Hobson RW 2nd, Pappas PJ, Jamil Z, Araki CT, Goldberg MC et al (1998) A strategy for increasing use of autogenous hemodialysis access procedures: impact of preoperative non invasive evaluation. J Vasc Surg 27:302–307
6. Shenoy S, Darcy M (2013) Ultrasound as a tool for preoperative planning, monitoring and interventions in dialysis arteriovenous access. AJR 201(4):W539–W543
7. Wong CS, McNicholas N, Healy D, Clarke-Moloney M, Coffey JC, Grace PA et al (2013) A systematic review of preoperative duplex ultrasonography and arteriovenous fistula formation. J Vasc Surg 57:1129–1133
8. Ilhan G, Esi E, Bozok S, Yu¨rekli I, Ozpak B, Ozelci A et al (2013) The clinical utility of vascular mapping with Doppler ultrasound prior to arteriovenous fistula construction for hemodialysis access. J Vasc Access 14(1):83–88
9. Ferring M, Henderson J, Wilmink A, Smith S (2008) Vascular ultrasound for the pre-operative evaluation prior to arteriovenous fistula formation for haemodialysis: review of the evidence. Nephrol Dial Transplant 23:1809–1815
10. Malovrh M (2002) Native arteriovenous fistula: preoperative evaluation. Am J Kidney Dis 39:1218–1225
11. Wong V, Ward R, Taylor J, Selvakumar S, How TV, Bakran A (1996) Factors associated with early failure of arteriovenous fistulae for haemodialysis accesses. Eur J Vasc Endovasc Surg 12:207–213
12. Tordoir J, Canaud B, Haage P, Konner K, Basci A, Fouque D et al (2007) EBPG on vascular access. Nephrol Dial Transplant 22(Suppl 2):ii88–ii117
13. Wiese P, Nonnast-Daniel B (2004) Colour Doppler ultrasound in dialysis access. Nephrol Dial Transplant 19:1956–1963
14. Malovrh M (2003) The role of sonography in the planning of arteriovenous fistulas for hemodialysis. Semin Dial 16:299–303

15. Davidson I, Chan D, Dolmatch B, Hasan M, Nichols D, Saxena R et al (2008) Duplex ultrasound evaluation for dialysis access selection and maintenance: a practical guide. J Vasc Access 9:1–9
16. Ferring M, Claridge M, Smith SA, Wilmink T (2010) Routine preoperative vascular ultrasound improves patency and use of arteriovenous fistulas for hemodialysis: a randomized trial. Clin J Am Soc Nephrol 5(12):2236–2244
17. Malovrh M (1998) Non-invasive evaluation of vessels by duplex sonography prior to construction of arteriovenous fistulas for haemodialysis. Nephrol Dial Transplant 13:125–129
18. Parmar J, Aslam M, Standfield N (2007) Pre-operative radial arterial diameter predicts early failure of arteriovenous fistula (AVF) for haemodialysis. Eur J Vasc Endovasc Surg 33:113–115
19. Lemson MS, Leunissen KM, Tordoir JH (1998) Does pre-operative duplex examination improve patency rates of Brescia-Cimino fistulas? Nephrol Dial Transplant 13:1360–1361
20. Ku YM, Kim YO, Kim JI, Choi YJ, Yoon SA, Kim YS et al (2006) Ultrasonographic measurement of intima-media thickness of radial artery in pre-dialysis uremic patients: comparison with histological examination. Nephrol Dial Transplant 21:715–720
21. Wittenberg G, Schindler T, Tschammler A, Kenn W, Hahn D (1998) Value of color coded duplex ultrasound in evaluating arm blood vessels-arteries and haemodialysis shunts. Ultraschall Med 19:22–27
22. Sato M, Io H, Tanimoto M, Shimizu Y, Fukui M, Hamada C et al (2012) Relationship between preoperative radial artery and postoperative arteriovenous fistula blood flow in hemodialysis patients. J Nephrol 25(5):726–731
23. Zamboli P, Fiorini F, D'Amelio A, Fatuzzo P, Granata A (2014) Color Doppler ultrasound and arteriovenous fistulas for hemodialysis. J Ultrasound 17(4):253–263
24. NKF-K/DOQI (2006) Clinical practice guidelines for vascular access update 2006. Am J Kidney Dis 48(Suppl 1):s176–s322
25. Mendes RR, Farber MA, Marston WA, Dinwiddie LC, Keagy BA, Burnham SJ (2002) Prediction of wrist arteriovenous fistula maturation with preoperative vein mapping with ultrasonography. J Vasc Surg 36:460–463
26. Planken RN, Keuter XH, Hoeks AP, Kooman JP, van der Sande FM, Kessels AG et al (2006) Diameter measurement of the forearm cephalic vein prior to vascular access creation in end-stage renal disease patients: graduated pressure cuff versus tourniquet vessel dilatation. Nephrol Dial Transplant 21: 802–806
27. Lockhart ME, Robbin ML, Fineberg NS, Wells CG, Allon M (2006) Cephalic vein measurement before forearm fistula creation: does use of a tourniquet to meet the venous diameter threshold increase the number of usable fistula? J Ultrasound Med 25: 1541–1545
28. Planken RN, Tordoir JH, Duijm LE, de Haan MW, Leiner T (2007) Current techniques for assessment of upper extremity vasculature prior to hemodialysis vascular access creation. Eur Radiol 17:3001–3011
29. Beathard GA, Arnold P, Jackson J, Litchfield T, Physician Operators Forum of RMS Lifeline (2003) Aggressive treatment of early fistula failure. Kidney Int 64:1487–1494
30. Dember LM, Beck GJ, Allon M, Delmez JA, Dixon BS, Greenberg A et al (2008) Effect of clopidogrel on early failure of arteriovenous fistula for hemodialysis: a randomized controlled trial. JAMA 299(18): 2164–2171
31. Rayner HC, Pisoni RL, Gillespie BW, Goodkin DA, Akiba T, Akizawa T et al (2003) Creation, cannulation and survival of arteriovenous fistulae: data from the dialysis outcomes and practice patterns study. Kidney Int 63:323–330
32. Zamboli P, Calabria M, Camocardi A, Fiorini F, D'Amelio A, Lo Dico C et al (2012) Color-Doppler imaging and arteriovenous fistula: preoperative evaluation and surveillance. G Ital Nefrol 29(Suppl 57): S36–S46
33. Lomonte C, Casucci F, Antonelli M, Giammaria B, Losurdo N, Marchio G et al (2005) Is there a place for duplex screening of the brachial artery in the maturation of arteriovenous fistulas? Semin Dial 18(3): 243–246
34. Smits JH, van der Linden J, Hagen EC, Modderkolk-Cammeraat EC, Feith GW, Koomans HA et al (2001) Graft surveillance: venous pressure, access flow or the combination? Kidney Int 59:1551–1558
35. Kim YO, Yang CW, Yoon SA, Chun KA, Kim NI, Park JS et al (2001) Access blood flow as a predictor of early failures of native arteriovenous fistulas in hemodialysis patients. Am J Nephrol 21:221–225

US-Assisted Positioning of Central Venous Catheter

57

Anna Clementi, Pasquale Zamboli, Viviana Rosalia Scarfia, Fulvio Fiorini, and Antonio Granata

57.1 Introduction

Central venous catheter placement is a common procedure which has been introduced in the clinical setting over the past 50 years. It is performed in 8 % of hospitalized patients, and more than 5 million central venous catheters are placed every year in the United States [1, 2]. A central venous access is usually necessary for specific intravenous therapies, such as chemotherapy, parenteral nutrition, central venous and arterial pressure monitoring, heart pacemaker positioning, and extracorporeal therapies, such as plasma exchange and hemodialysis.

Since the introduction of Seldinger technique in 1953, central venous catheter insertion has become an easier and safer procedure [3, 4]. The addition of ultrasound (US) has been shown to decrease complications even further. Ultrasounds, indeed, allow clinicians to visualize internal jugular vein and its anatomical features, as well as needle direction. Moreover, US-guided central venous catheter placement is characterized by a lower incidence of unsuccessful attempts, and it requires less time to be performed [5–8]. International guidelines recommend the use of ultrasounds in case of central venous catheter positioning [9–13].

In the following paragraphs, we will describe internal jugular vein catheterization, but this technique can be used in case of other central vein catheter placement as well.

57.2 Type of Ultrasound Scanner

Ultrasound scanner characteristics may vary widely depending on manufacturing companies and the type of monitors available on the market. Anyway, it is possible to perform US-guided central venous catheter placement with all ultrasound scanners (B-mode, color Doppler, and pulsed Doppler). In particular, B-mode (brightness mode) provides bidimensional images of tissues in a gray scale, whereas color Doppler and pulsed Doppler provide information about both direction and speed of blood flow. Ultrasound scanner should be placed in front of the operator, thus avoiding an excessive head and arm rotation, which may lead to a difficult control of the probe and the needle, with an increased risk of complications.

Electronic supplementary material The online version of this chapter (doi:10.1007/978-3-319-40782-1_57) contains supplementary material, which is available to authorized users.

A. Clementi • V.R. Scarfia • A. Granata (✉)
Nephrology and Dialysis Unit, "S. Giovanni di Dio" Hospital, Agrigento, Italy
e-mail: antonio.granata4@tin.it

P. Zamboli
School of Nephrology, University of Naples, Naples, Italy

F. Fiorini
Nephrology and Dialysis Unit, "S. Maria della Misericordia" Hospital, Rovigo, Italy

P. Martino, A.B. Galosi (eds.), *Atlas of Ultrasonography in Urology, Andrology, and Nephrology*,
DOI 10.1007/978-3-319-40782-1_57

57.3 Type and Position of Ultrasound Probe

Central veins used for venous catheter placement are situated few centimeters under skin surface; the use of linear probes (high-frequency probes of 5–12 mHz) allows to obtain high-resolution images of deep tissues. The probe should be kept between the inch and the other fingers of the hand (Fig. 57.1), which should lay on the patient's body, in order to reach a stable position of the transducer and, subsequently, a stable image of the needle and the vein to be cannulated. It is important that the probe is well oriented because the wrong position of the transducer during the catheter placement may lead to an incorrect visualization of the needle progression in respect of the anatomical structures near the vein. Probe marker (a bright led located on a side of the transducer) is usually positioned at the left of the operator and the scanner, so that the left of the patient is visualized on the left of the scanner and the needle movements through the patient's tissues correspond to those of ultrasound images.

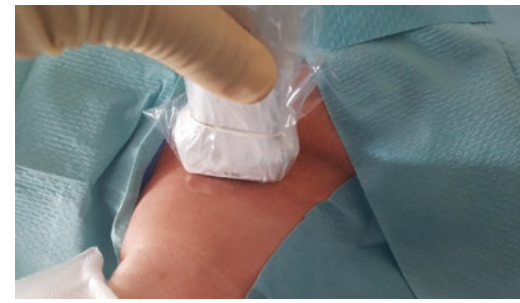

Fig. 57.1 Right probe position. The probe should be kept between the inch and the other fingers of the hand

57.4 Ultrasound Setting

Ultrasound setting is fundamental before starting to perform any US-guided procedure. Indeed, each type of setting is characterized by specific parameters, such as probe frequency, total gain, focus position, and number, which allow to obtain the best quality of ultrasonography images in respect of the anatomical region which should be studied. Usually, vascular setting is the ideal modality for central venous catheter placement [14, 15].

Once ultrasound setting is completed and the vein to be cannulated is visualized, total gain (image brightness in B-mode), depth (number of tissue centimeters under the probe), and focus position (depth corresponding to the one of the vein to be cannulated) might be modified in order to improve the quality of the ultrasonography image even further [14, 15].

57.5 Ultrasound Scan and Anatomy

Central vein to be cannulated may be visualized in a longitudinal scan (*in plane* – the long axis) where the probe is positioned in parallel to the longitudinal axis of the vein or in a transversal scan (*out of plane* – the short axis) where the probe is positioned perpendicularly to the longitudinal axis of the vein (Fig. 57.2a, b) [14–16]. In the transversal scan, both the artery and the vein appear as round anechoic images (Fig. 57.3). Usually, the vein presents thinner walls than the artery, collapses with a slight probe pressure in the absence of thrombosis, and dilates in case of increased venous blood flow (Valsalva maneuver, Trendelenburg position) [14–16]. Conversely, the artery does not collapse. In the longitudinal scan, both the vein and the artery appear as ribbon images with an anechoic lumen delimited by parallel and echogenic walls [14–16]. The use of color Doppler and pulsed Doppler may help clinicians in distinguishing the artery from the vein. It is important to remember that red and blue colors indicate only blood flow direction in respect of the probe (the red color indicates that flow is toward the probe, while the blue color indicates that the flow is leaving). Pulsed Doppler provides graphic and acoustic images of both arterial and venous flow. In particular, arterial flow is characterized by a Doppler wave with a typical systolic peak (Fig. 57.4) and an acute sound which are expressions of the cardiac systolic activity. On the contrary, venous flow is characterized by a Doppler wave which changes according to respiratory and cardiac activity and the hydration state.

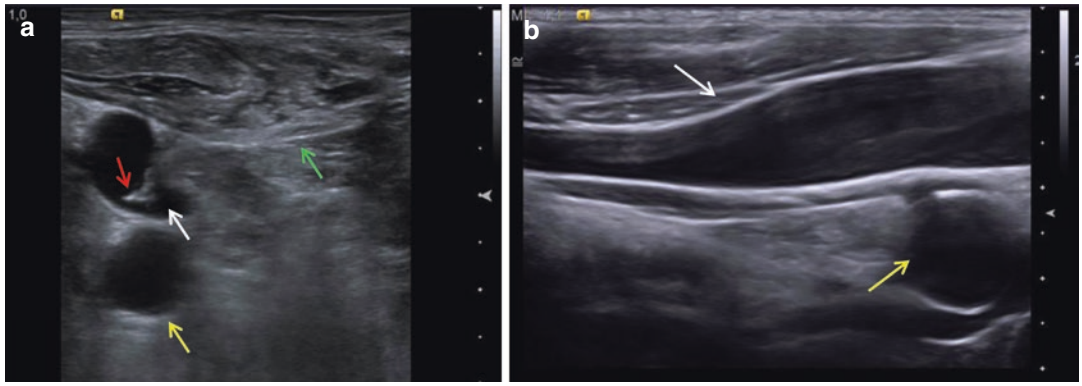

Fig. 57.2 (**a**). Longitudinal scan (*in plane*). Carotid artery (*yellow arrow*); internal jugular vein (*white arrow*); needle tip (*red arrow*); sternocleidomastoid muscle (*green arrow*) which appears edematous due to previous anesthetic administration (**b**). Transversal scan (*out of plane*). Carotid artery (*yellow arrow*); internal jugular vein (*white arrow*)

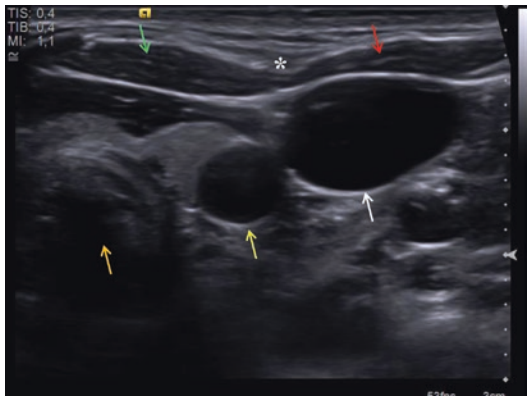

Fig. 57.3 Transversal scan. Carotid artery (*yellow arrow*); internal jugular vein (*white arrow*); sternal part of sternocleidomastoid muscle (*green arrow*); clavicle part of sternocleidomastoid muscle (*red arrow*); jugular dimple (*white star*); trachea (*orange arrow*)

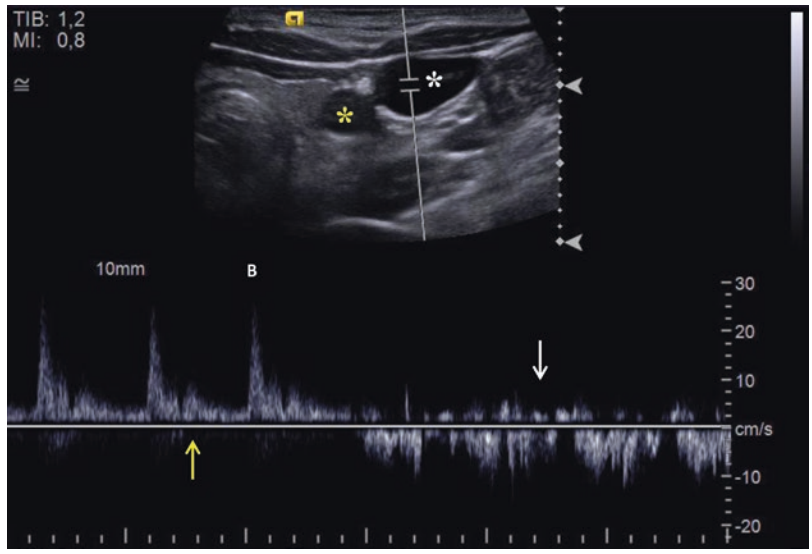

Fig. 57.4 Pulsed Doppler image. Carotid artery (*yellow star*); internal jugular vein (*white star*); arterial flow (*yellow arrow*); venous flow (*white arrow*)

57.6 Preoperative Evaluation of the Patient

Before central venous catheter placement, even if ultrasounds are not used, it is important to perform an ultrasonography evaluation of the vein which should be cannulated [14–16]. Echo color Doppler allows clinicians to rule out the presence of thrombosis (Fig. 57.5) and possible vascular injury due to previous catheter placement (Fig. 57.6), as well as to evaluate anatomical characteristics of the vein (Fig. 57.7). Before the procedure, chest evaluation should be performed as well to confirm the presence of "pleural sliding" (Fig. 57.8). Indeed, after central venous catheter placement, it will be possible to rule out the presence of pneumothorax, a possible complication of the technique which is characterized by "pleural sliding" loss in real-time ultrasonography [17].

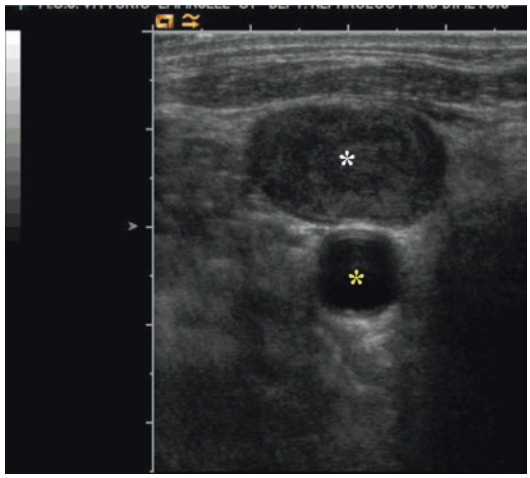

Fig. 57.5 Internal jugular vein thrombosis. Carotid artery (*yellow star*); internal jugular vein (*white star*)

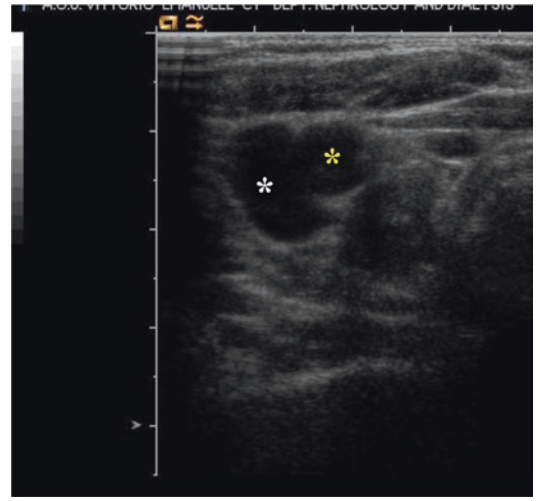

Fig. 57.7 Anatomical variation of internal jugular vein (*white star*); carotid artery (*yellow star*)

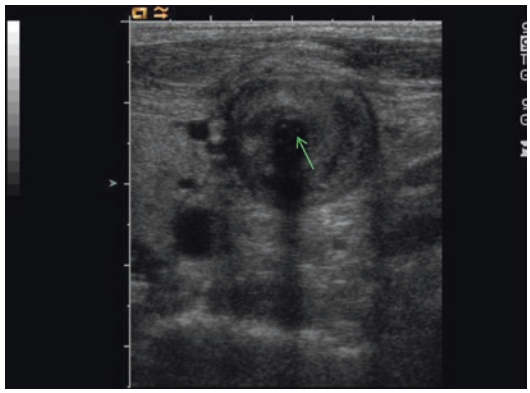

Fig. 57.6 Vein thrombosis secondary to central venous catheter placement (*green star*)

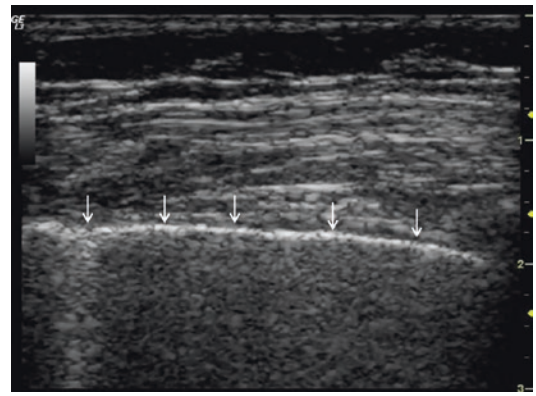

Fig. 57.8 B-mode illustrating the pleural sliding (*white arrows*). The pneumothorax US pattern is characterized by pleural sliding loss which becomes evident in real-time US

57.7 Ultrasonography Techniques

There are two different techniques of ultrasound-guided central venous catheter placement [14–16]:

1. "Static" ultrasound-guided technique
2. "Dynamic" or "real-time" ultrasound-guided technique

In the first one, ultrasonography is used only to identify the vein to be cannulated and confirm the absence of thrombosis. The exact region should be marked with an indelible pen and the procedure is performed without ultrasounds [14–16].

In the "dynamic" ultrasound-guided technique, the probe is used during all the procedure in order to follow the needle trajectory in real time (clip) [14–16]. This technique has been shown to be superior to the first one [18]. In the "dynamic" ultrasound-guided technique, it is possible to keep the needle free (ultrasound assisted procedure) or to allocate the needle in a system which does not allow to change its direction or angulation (ultrasound-guided procedure) [14–16]. According to our experience, the ultrasound assisted procedure should be preferred because it allows clinicians to correct needle direction and inclination, if necessary.

In the transversal scan of the "dynamic" ultrasound-guided technique, the needle appears as a hyperechoic image (Fig. 57.9), and its trajectory may be followed in real time with minimal hand movements. Conversely, in the longitudinal scan the needle is visualized entirely and more clearly. Nevertheless, according to our experience longitudinal scan is not the scan of choice in case of central venous catheter placement in the neck for several reasons.

First of all, when using linear probes, catheter insertion point results to be too far from the clavicle in the longitudinal scan, thus inducing kinking and malfunctioning of permanent catheters for hemodialysis (which require thoracic tunneling). Secondly, during vein cannulation the operator may have problems in distinguishing the vein from the artery in the longitudinal scan, while transversal scan allow clinicians to change the needle trajectory more easily. Dynamic technique requires more experience since a perfect coordination between eyes and hands is necessary.

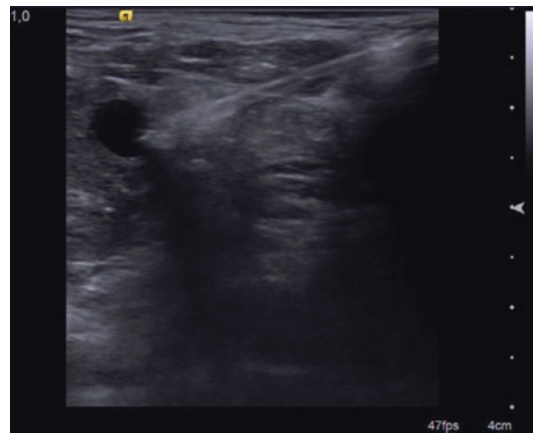

Fig. 57.9 Needle direction

57.8 Material

Ultrasound-guided central venous catheter placement requires:

1. Kit for central venous catheter placement (catheter of different dimensions and length depending on clinical characteristic of the patient, guidewire, venous dilator, 18-gauge needle, and syringe to perform venipuncture)
2. 10–20 ml syringes to administer anesthetic to aspirate blood from the catheter
3. 10–20 ml syringes with saline solution and heparin for catheter washing
4. Antiseptic towels, gloves, and albs
5. Mask, glasses, and headset
6. Disinfectant (chlorexidine is preferred)
7. Antiseptic gauzes
8. Needle holder, surgical tweezer, and sutures
9. Local anesthetic (lidocaine 1–2%)
10. Scalpel
11. Ultrasound scanner with a high-resolution linear probe
12. Antiseptic gel
13. Antiseptic probe and cover
14. Elastics to fix probe and cover
15. Monitor with ECG and oximeter

57.9 Procedure

1. The patient should lay in a supine position. Trendelenburg position should be kept if internal jugular vein has to be cannulated in order to increase venous return and to reduce air embolism risk.
2. Evaluation of the anatomical referral points of the region where the catheter should be inserted is fundamental (Fig.57.10).
3. Antiseptic towels should be positioned and the region should be disinfected.
4. Ultrasound probe with antiseptic gel and cover should be positioned in order to obtain a clear image of the vein to be cannulated and of the near anatomical structures; some gel or disinfectant solutions (chlorexidine or iodopovidone) or saline solution can be used as means of ultrasound conducting (Fig. 57.11).
5. When administering local anesthetic, use ultrasound probe in order to avoid stinging the vein or the artery and to deliver an excessive amount of the drug, thus altering the regional anatomical structure.
6. The needle should be positioned under the probe and the syringe should be kept in aspiration, until blood is drawn.
7. Once the blood is drawn into the syringe, the probe should be removed, the syringe separated from the needle, which should not be moved.
8. It is important to verify that the blood comes out from the needle continuously and not in a pulsatile way.
9. Insert the guide into the needle and push it into the vein without tissue resistance (Fig. 57.12); in case of cardiac rhythm alterations, it is important to remove the guide until cardiac rhythm becomes normal.
10. Remove the needle, leaving the guide in situ, and cut the skin near the guide with a scalpel.
11. Insert the guide into the dilator in order to reach the tissues and the vein.
12. Remove the dilator and insert the guide into the catheter into the vein.
13. Remove the guide and verify the correct functioning of the catheter.

14. Verify the correct position of the tip with an chest X-ray or a endocavitary ECG.
15. In case of long-term catheter, tunneling should be performed after local anesthetic is administered.
16. Fix the catheter with surgical sutures and perform an antiseptic medication.
17. Perform chest or abdominal X-ray (in case of internal jugular vein and subclavian vein or femoral vein, respectively) in order to confirm the right catheter placement and identify possible complication of the procedure.

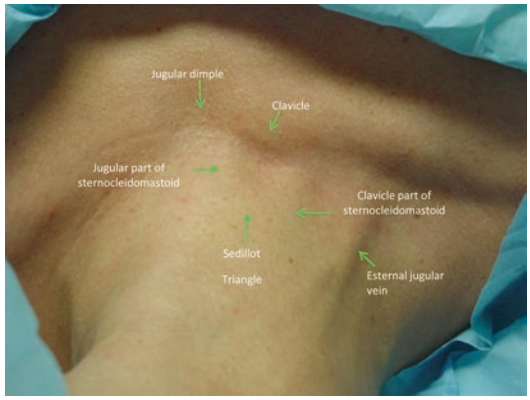

Fig. 57.10 Anatomical referral points

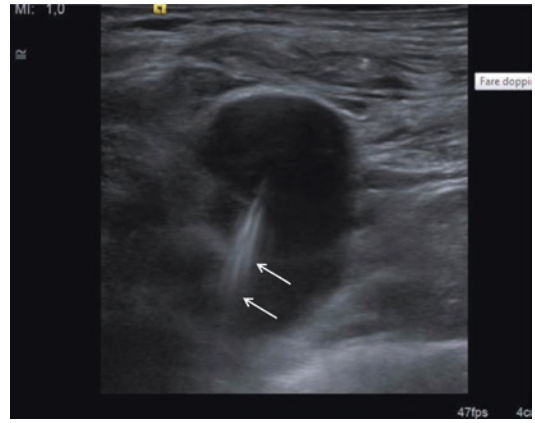

Fig. 57.12 Needle guidewire

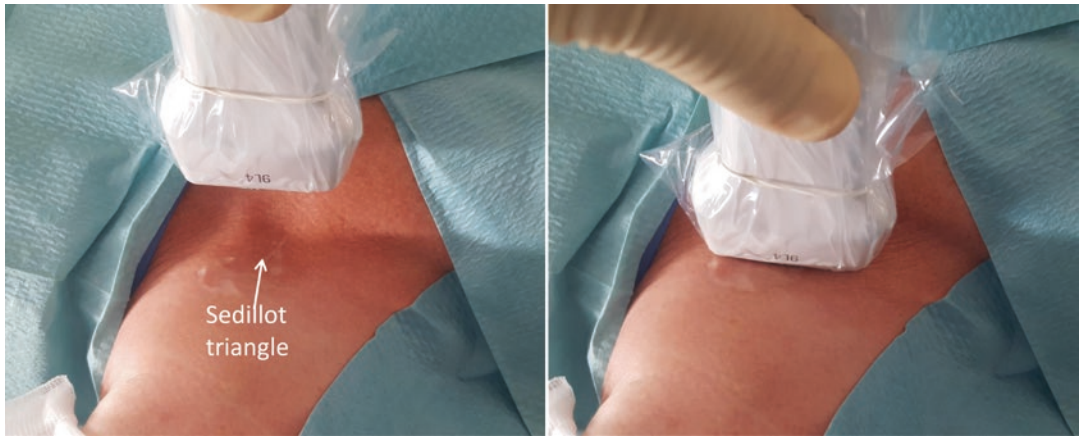

Fig. 57.11 Sterile probe and cover

Conclusion

The use of ultrasounds for central venous catheter placement reduces the incidence of complications related to the technique and allows the clinician to perform a correct procedure. Anyway, operator experience about ultrasonography anatomy and surgical technique is fundamental for a successful central venous catheter placement.

References

1. Ruesch S, Walder B, Tramar MR (2002) Complications of central venous catheters: internal jugular versus subclavian access-a systematic review. Crit Care Med 30(2):454–460
2. McGee DC, Gould MK (2003) Preventing complications of central venous catheterization. N Engl J Med 348(12):1123–1133
3. Seldinger SI (1953) Catheter replacement of the needle in percutaneous arteriography; a new technique. Acta Radiol 39:368–376
4. Higgs ZC, Macafee DA, Braithwaite BD, Maxwell-Armstrong CA (2005) The Seldinger technique: 50 years on. Lancet 366(9494):1407–1409
5. Rabindranath KS, Kumar E, Shail R et al (2011) Use of real-time ultrasound guidance for the placement of hemodialysis catheters: a systematic review and meta-analysis of randomized controlled trials. Am J Kidney Dis 58(6):964–970
6. Hind D, Calvert N, McWilliams R et al (2003) Ultrasonic locating devices for central venous cannulation: meta-analysis. BMJ 327:361
7. Rabindranath KS, Kumar E, Shail R, Vaux EC (2011) Ultrasound use for the placement of haemodialysis catheters. Cochrane Database Syst Rev (11):CD005279
8. Londrino F, Floccari F, Granata A et al (2013) Internal jugular vein cannulation: why ultrasound guidance should be expanded as much as possible. J Vasc Access 14(4):400–401
9. NKF-K/DOQI Vascular Access Work Group (2006) Clinical practice guidelines for vascular access. Am J Kidney Dis 48:S176–S273
10. Dariushnia SR, Wallace MJ, Siddiqi NH et al (2010) Society of Interventional Radiology Standards of Practice Committee. Quality improvement guidelines for central venous access. J Vasc Interv Radiol 21:976–981
11. ACS Committee on Perioperative Care (2011) Revised statement on recommendations for use of real-time ultrasound guidance for placement of central venous catheters. Bull Am Coll Surg 96:36–37
12. Lamperti M, Bodenham AR, Pittiruti M et al (2012) International evidence-based recommendations on ultrasound-guided vascular access. Intensive Care Med 38:1105–1117
13. Rupp SM, Apfelbaum JL, Bitt C et al (2012) American Society of Anesthesiologists Task Force on Central Venous Access: a report by the American Society of Anesthesiologists Task Force on Central Venous Access. Anesthesiology 116:539–573
14. Siverberg MJ, Kory P (2013) Intensive care ultrasound: II. Central vascular access and venous diagnostic ultrasound. Ann Am Thorac Soc 10(5):549–556
15. Mitchell E, Averill LW (2014) Principles of ultrasound-guided venous access. www.uptodate.com. Accessed 11 July 2014
16. Troianos CA, Hartman GS, Glas KE et al (2011) Guidelines for performing ultrasound guided vascular cannulation: recommendations of the American Society of Echocardiography and the Society of Cardiovascular Anesthesiologists. J Am Soc Echocardiogr 24:1291–1318
17. Fiorini F, Zanforlin A, D'Amelio A et al (2014) L'ecografia polmonare in nefrologia. G Ital Nefrol 31(3):1–11
18. Milling TJ, Rose J, Briggs WM et al (2005) Randomized, controlled clinical trial of point-of-care limited ultrasonography assistance of central venous cannulation: the Third Sonography Outcomes Assessment Program (SOAP-3) Trial. Crit Care Med 33:1764–1769

Applications of Ultrasound in Emergency

58

Valentino Massimo, Bertolotto Michele, Barozzi Libero, Pavlica Pietro, and Derchi Lorenzo

58.1 Introduction

Acute urinary tract disorders are a common complaint of patients who present to the emergency department. The pain is often poorly localized and it can have a variety of causes. Laboratory and clinical findings are neither sensitive nor specific for determining the cause of the pain. Accordingly, imaging is an important tool for diagnosis and management. The most common conditions for these patients are renal colic, renal infection, hematuria, acute scrotal pain, and trauma.

Electronic supplementary material The online version of this chapter (doi:10.1007/978-3-319-40782-1_58) contains supplementary material, which is available to authorized users.

V. Massimo, MD (✉)
Radiology, Tolmezzo hospital,
via Morgagni 18, Tolmezzo (UD) 33028, Italy
e-mail: mvm.valentino@gmail.com

B. Michele, MD
Department Radiology, University of Trieste,
Ospedale di Cattinara, Strada di Fiume 447,
Trieste 34149, Italy

B. Libero, MD
Radiology Unit, Casa di Cura Madre Fortunata
Toniolo, Via Toscana 34, Bologna 40141, Italy

P. Pietro, MD
GVM Care and Research, Villalba Hospital,
Bologna, Italy

D. Lorenzo, MD
Dicmi-Radiologia, University of Genova,
Largo R. Benzi 8, Genoa 16132, Italy

P. Martino, A.B. Galosi (eds.), *Atlas of Ultrasonography in Urology, Andrology, and Nephrology*,
DOI 10.1007/978-3-319-40782-1_58

58.2 Renal Colic

Renal colic is secondary to ureteral obstruction by stone. It is a common cause of visits to the emergency department and often requires imaging evaluation [1]. In most institutions, non-enhanced multidetector computed tomography (MDCT) is considered the gold standard technique to evaluate these patients because of its accuracy in the detection of stones as well as of other pathological conditions mimicking renal colic [2]. Moreover, ultrasound (US) is considered accurate to diagnose renal colic [3]. Ultrasound (US) is a safe, noninvasive and non-expensive technique able to evaluate patients with renal colic. It can be safely managed also by the emergency clinician [4]. However, its use remains controversial as it has good capability to identify dilatation of the excretory system but can have difficulties in directly demonstrating the stones, especially in the ureters. Several papers, including a recent multicenter comparative study between US and CT, have demonstrated the usefulness of US in the diagnosis and management of renal colic patients [5]. In the 2014 guidelines on urolithiasis of the European Association of Urology, it is stated that in patients with renal stone disease, US should be used as the primary procedure [6], and CT should be reserved for those patients who do not improve with conservative treatment or on suspicion of a non-urologic process. The US diagnosis of renal colic is based on the detection of stones and the consecutive obstruction of the excretory system (Fig. 58.1). The detection of dilatation of the excretory tract is considered very useful in the context of renal colic, but this sign may be absent, as calculi cannot be cause dilatation, and the degree of dilatation does not reflect the severity of obstruction. Stones are identified at US as hyperechogenic images with posterior shadowing. Small calculi (<5 mm) may be not recognized because of a hyperechogenicity of the pelvis or the absence of posterior shadowing, and their detection in the ureters can be masked by overlying intestinal loops and gas, especially in the middle part of the ureters. Renal calculi must not be confused with vascular or parenchymal calcifications, clots, or arcuate arteries; all of them can appear as hyperechoic foci. The sensitivity of US in the detection of lithiasis varies greatly depending on the studies, with a wide range of sensitivities that usually depends on the size and location of the stones. [7]. A complete study should include the kidney, ureterovesical joint (UVJ) and ureters. The presence of UVJ edema is considered a useful sign of a recent stone passage that can help to confirm the diagnosis of renal colic. Regarding the detection of ureteral stones, the visualization of the ureter can be improved by compressing the area with the transducer or changing the patient's position. Sometimes dilatation of the excretory tract may be not present because the patient is dehydrated. For this reason, the US study should be performed after patient hydration to ensure a better visualization of the pelvis and the ureter and to distend the urinary bladder allowing the visualization of the terminal ureter and to appreciate the ureteral jet (produced by the passage of urine from the ureter into the bladder). The accuracy of diagnosing renal obstruction and stones can improve with the use of Doppler US and color Doppler identifying secondary signs. An absent, asymmetric, and/or reduced ureteric jet from the ureteric orifices evaluated by color Doppler is an additional indicator of obstruction. However, the presence of a positive ureteral jet does not rule out the presence of ureteral stones [7] since ureteral stones quite often only cause partial obstruction. Increased resistive index may be a useful sign of acute obstruction, distinguishing between obstructive and nonobstructive dilatation [8]. A renal RI>0.70 and/or a 10% difference between the kidneys is considered as diagnostic of obstructive uropathy. Another useful sign for a better identification of the stones is the twinkling artifact [9]. This artifact is a mixture of red and blue pixels on color Doppler secondary to the "noise" produced from rough interfaces composed of sparse reflectors such as urinary stones (Fig. 58.2). The artifact should be useful for confirming the findings of grayscale, especially in doubtful cases due to the small size of the stone or its location in difficult-to-visualize ureteral portions. In the study of Ripolles et al., the sensitivity of US using the twinkling artifact for detecting renal calculi was 90% and the specificity 100%.

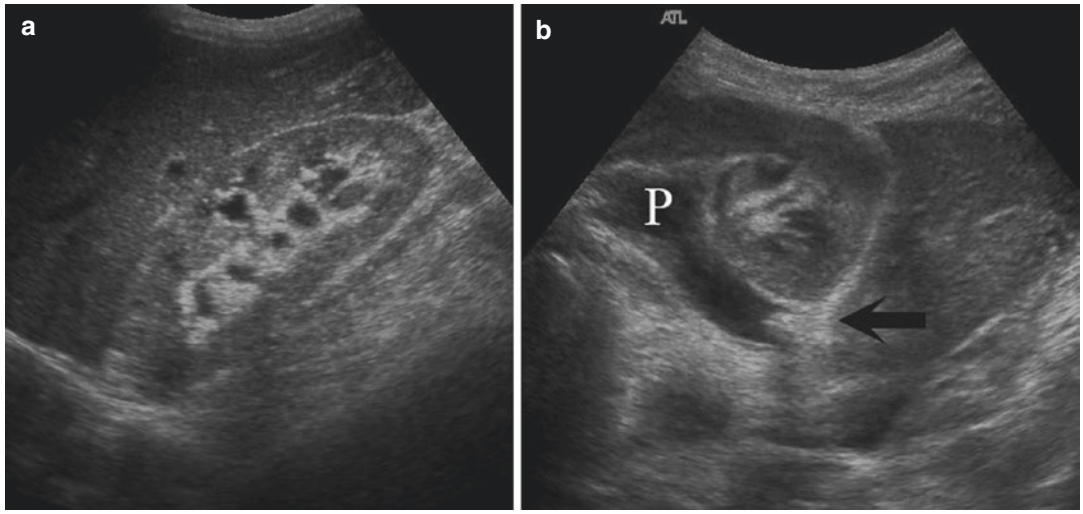

Fig. 58.1 Renal colic. The right kidney shows moderate hydronephrosis (**a**). The pelvis is enlarged (*P*) due to a stone (*arrow*) inside the proximal ureter (**b**)

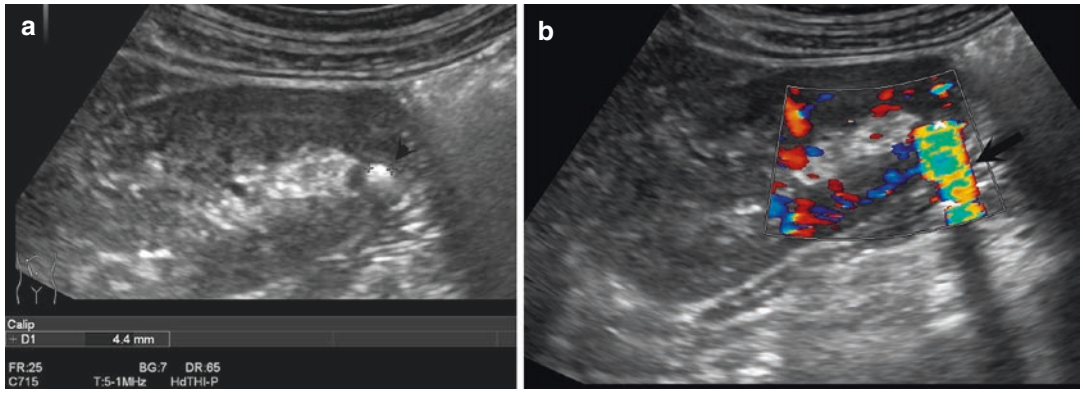

Fig. 58.2 Renal stone. In (**a**), the stone is identified as hyperechogenic foci with posterior shadowing (*arrowheads*). Using color Doppler (**b**), the stone produces the twinkling artifact, a mixture of red and blue pixels (*arrow*)

58.3 Pyelonephritis

It is a common diagnosis, mostly related to gram-negative enteric bacteria [10]. Urinalysis and urine culture are usually sufficient to confirm the diagnosis. Imaging is only necessary in the patients who do not demonstrate clinical improvement within 72 h of initiating antibiotic therapy. The purpose of imaging is to assess for an obstructing stone and rule out complications (such as abscess). US findings are usually normal in the setting of pyelonephritis; therefore, it is useful to exclude obstruction as a cause for the infection. US can be used to look for dilatation of the pelvicalyceal system, but, when present, echogenic mass is the most reliable sign of pyonephritis [11] (Fig. 58.3). In the case of renal abscess, US is able to show a hypoechoic mass that lacks internal flow on color Doppler flow images (Fig. 58.4). Less common findings are focal hypoechoic region with decreased vascular flow, renal enlargement, and loss of the sinus fat and/or corticomedullary differentiation [12]. Xanthogranulomatous pyelonephritis is a chronic destructive granulomatous process that is believed to result from an atypical, incomplete immune response to subacute bacterial infection. US typically demonstrates an enlarged kidney, with a large amorphous central echogenicity that corresponds to a renal pelvis staghorn calculus. The calculus is generally associated with acoustic shadowing. A loss of normal renal architecture is seen in most cases, but, because the disease is usually diffuse, a discrete inflammatory mass is uncommon. Although the US findings in diffuse xanthogranulomatous pyelonephritis are characteristic, US is usually followed by CT for definitive assessment [13].

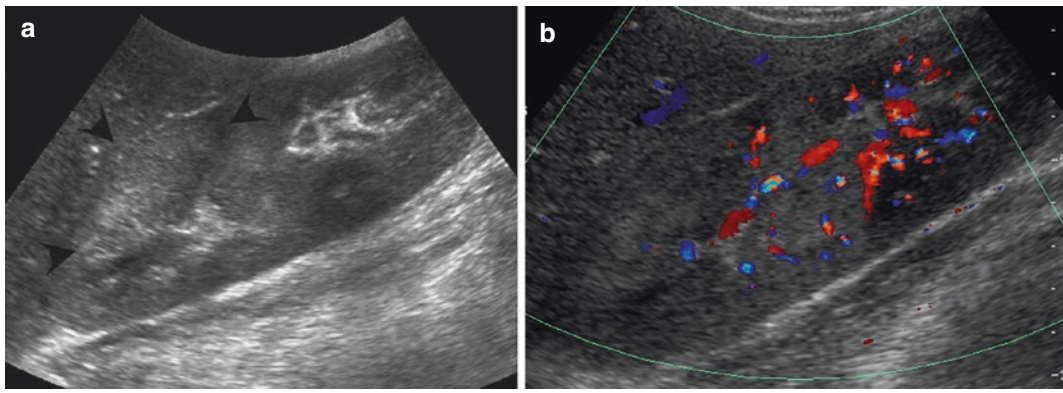

Fig. 58.3 Acute pyelonephritis. The (**a**) shows an echogenic mass in the upper part of the left kidney (*arrowheads*). At color Doppler (**b**), the mass appears without vascularization, confirming the diagnosis

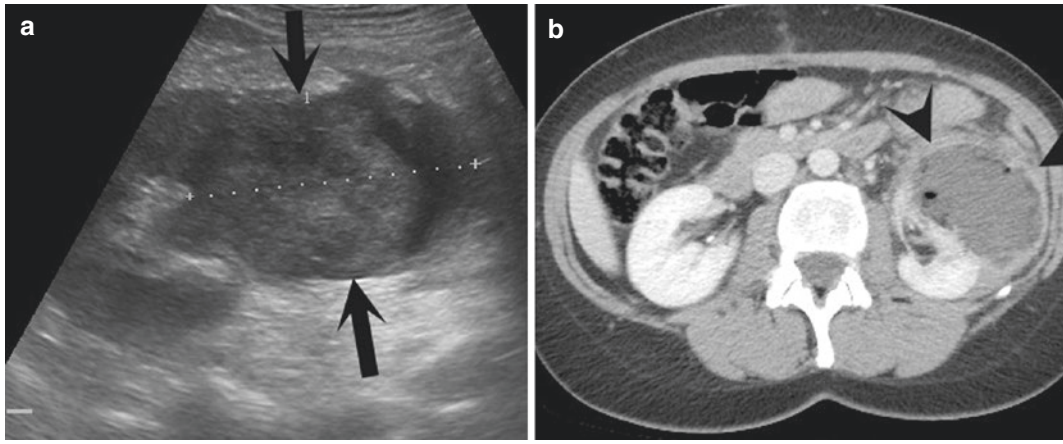

Fig. 58.4 US (58.4a) demonstrated a large mass in the middle part of the left kidney (*arrows*). Immediately, he underwent a contrast enhanced CT (58.4b) that confirmed the large abscess (*arrowhead*)

58.4 Hematuria

The major and proper concern in the investigation of hematuria is the detection of bladder cancer. Other causes are renal stones, pyelonephritis, urinary tract and prostate cancer, and prostate hyperplasia. Anticoagulants could also be a cause for hematuria, although they should never be accepted as the cause without the exclusion of a urinary tract or prostate cancer [14]. US is mandatory in the clinical evaluation of hematuria to detect eventually bladder tumors because it is easy to perform and safe for the patient. At US, most tumors appear as non-mobile, papillary, hypoechoic masses or as an area of focal wall thickening (Fig. 58.5). Doppler imaging demonstrates flow within the mass, aiding differentiation between tumor and blood clot. Also moving the patient on his flank allows the differentiation with the clots. Transabdominal ultrasound cannot, however, provide useful information regarding tumor staging and depth invasion. CEUS is not usually present in the assessment of bladder cancer. Moreover, it can be useful to identify a bladder mass when the bladder is full of clots. Recently, three-dimensional US and CEUS have been proposed for the detection of bladder cancer. The ability of three-dimensional US has been demonstrated by several studies, but nowadays it remains not applied in the clinical practice [15].

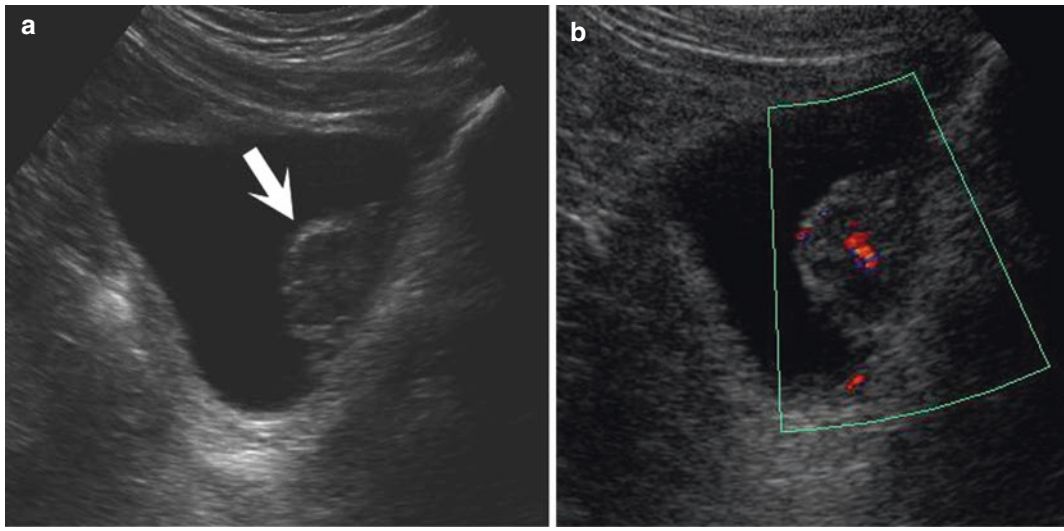

Fig. 58.5 Bladder cancer. The tumor appears as papillary hypoechoic masses (**a**). At color Doppler, the flow within the mass is appreciable, allowing the differentiation with a clot (**b**)

58.5 Acute Scrotal Pain

Grayscale US together with color Doppler is the imaging modality of choice for evaluating patients who present with acute scrotal pain. Disease processes are mainly related to testicular torsion and epididymo-orchitis and less frequently may be due to intratesticular tumors with hemorrhagic complication. All these pathologies have the same symptom of pain at presentation, and US-CD evaluation helps in differentiating patients who require surgical from patients for whom can managed conservatively.

Acute epididymo-orchitis or epididymitis is the most common cause of acute scrotum in adolescent boys and adults. Epididymitis first affects the tail of the epididymis and then spreads to involve the body and head of the epididymis. Orchitis develops in 20–40 % of cases of epididymo-orchitis by direct spread of infection. At US, the epididymis is enlarged and hypoechoic; sometimes it can appear hyperechoic if hemorrhage is present [16]. Secondary signs are reactive hydrocele or pyocele and scrotal wall thickening. In the case of testicular involvement, US shows the enlargement and inhomogeneous testicular parenchyma. At CD examination, the epididymis and testis show clearly increased colored signals: this is the most important criterion for the diagnosis of epididymo-orchitis (Videos 58.1 and 58.2) [17]. Sometimes, it may be difficult to differentiate focal areas of heterogeneity from neoplastic lesions. In this case, the use of CEUS is able to achieve the differential diagnosis [18].

Torsion of the testis is the most important urological nontraumatic emergency. The ability to differentiate torsion from other causes of acute scrotal pain like epididymo-orchitis is crucial. Apart from clinical history and physical examination, US can usually suggest the proper diagnosis addressing the correct management of the patients. US findings depend on the duration of torsion and the degree of twisting of the spermatic cord. In the period immediately following torsion, the testes may appear normal on grayscale images. After 4–6 h, the testis becomes swollen, enlarged, and diffusely hypoechoic. Necrosis, vascular congestion, and hemorrhage occur after 24 h, producing a heterogeneous echotexture within the testes [19]. In the same time, the testis appears completely avascular. The absence of testicular flow at color and power Doppler is considered diagnostic of ischemia (Videos 58.3 and 58.4). For obtaining the correct diagnosis, the scanner must be optimized for detection of slow flow, using the contralateral testis adjusting the color gain for the lowest repetition frequency and the lowest possible threshold setting. According to Baker et al., color Doppler has a sensitivity of 88.9 % and specificity of 98.8 % [20]. In the setting of testicular torsion, normal testicular echogenicity is a strong predictor of testicular viability [21]. Another sign is the twisting of the spermatic cord. In the torsion of the testis, spermatic cord is twisted, changing in size and shape, and appears as a round or oval homogeneous extratesticular mass with or without blood flow.

58.6 Trauma

58.6.1 Kidney

Renal injuries account for 8–10% of blunt abdominal trauma [22]. The sensitivity of focused assessment with sonography for trauma (FAST) is 67% for all urological injuries and 56% for isolated urological injuries [23]. The sonographic appearance of renal injuries are parenchymal abnormalities characterized by a hyperechoic, hypoechoic, or mixed echogenicity, with or without perirenal free fluid (Fig. 58.6). The major limitation of US is its poor ability to detect the lesion of the renal pelvic disruption of the proximal ureter, the major renal vascular injuries, and the renal parenchymal fragmentation accompanied by hemorrhage. A better performance of US can be obtained by using contrast agents. In our experience, contrast-enhanced sonography was found to be more sensitive than sonography and almost as sensitive as CT in the detection of traumatic abdominal solid organ injuries [24]. With CEUS, a laceration is a clear hypoechoic band, associated with a nonhomogeneous collection surrounding the kidney when a subcapsular hematoma is present. In the case of avulsion of the renal hilum, CEUS shows total absence of parenchymal enhancement. Active hemorrhage is identifiable as an extravasation of microbubbles into the hematoma and indicates a potentially life-threatening injury [24].

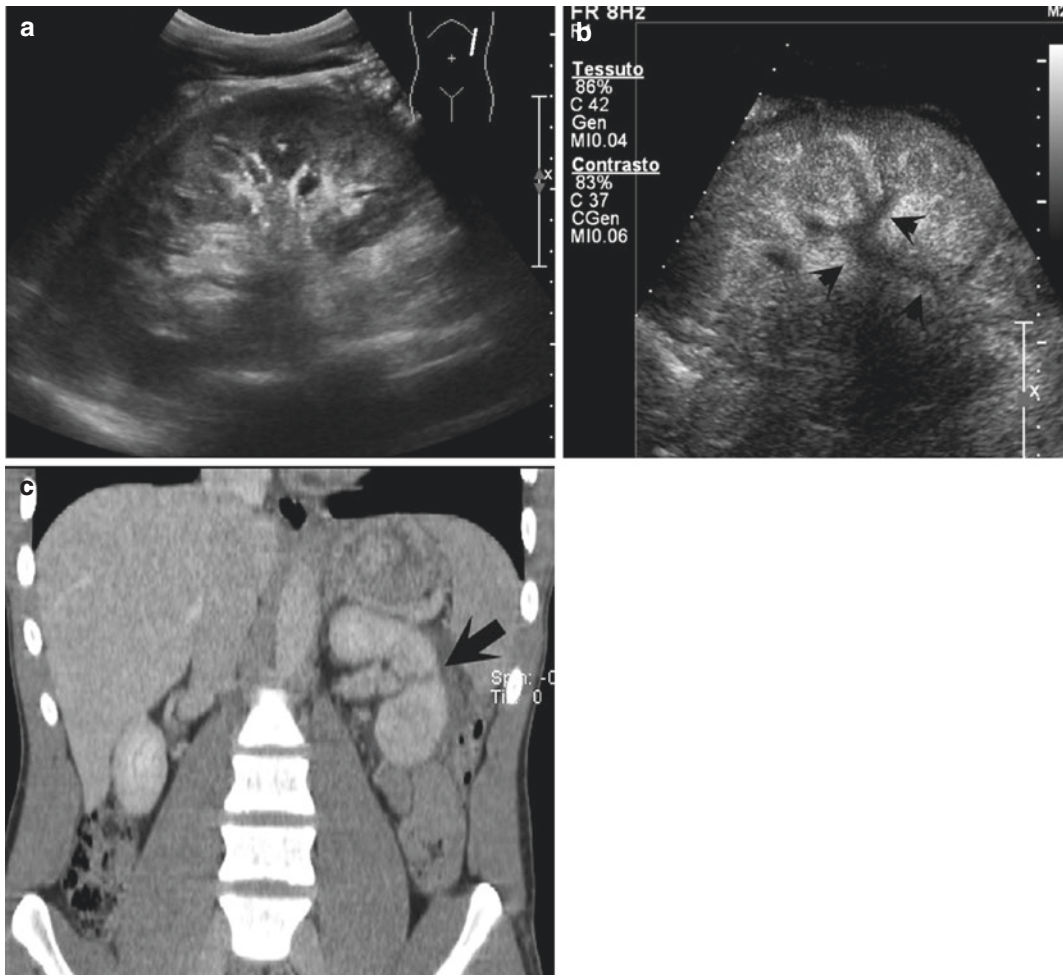

Fig. 58.6 Renal trauma. This 19-year-old man arrived in the emergency room after an abdominal blunt trauma presenting hematuria. At this B-mode image (**a**), his left kidney appears normal without any parenchymal abnormalities. After i.v. injection of ultrasound contrast medium (**b**), it was possible to visualize a fracture in the middle part of the kidney (*arrowheads*). The following contrast-enhanced CT (**c**) confirmed the diagnosis (*arrow*)

58.6.2 Scrotum

Testicular trauma usually is blunt trauma resulting from sport injury, motorcycle accident, direct blow, and straddle injury, or more rarely is penetrating trauma. Penetrating injuries often undergo immediate surgical exploration and imaging is not performed. In blunt traumas, imaging helps urologists in improving patient's management. Usually clinical examination is difficult due to scrotal swelling and pain. Ultrasonography is the first-line imaging modality, and MR imaging has a secondary role when ultrasound is inconclusive. Scrotal traumas include rupture of the testis, testicular fracture, hematoma, hematocele, and epididymal injury. The task of the imaging is to recognize the rupture of the tunica albuginea because in this case an immediate surgical exploration is required. US findings in testicular trauma include heterogeneous testis with irregular, poorly defined borders, contour abnormality, scrotal wall thickening, and hematocele (Fig. 58.7). Color and power Doppler are helpful because either can detect disruption of the normal capsular blood flow of the tunica vasculosa [25]. Direct visualization of a fracture line is rare as it is seen only in 17 % of cases [26]. Hematocele appears as an echogenic collection, different from hydrocele. The presence of hematocele-associated hyperechoic or hypoechoic changes in the testicular parenchyma suggests testicular rupture. Color Doppler sonography in posttrauma patients may reveal focal or diffuse hyperemia of epididymis, which is called traumatic epididymitis [27]. Limitations have been described for ultrasound in assessing patients with testicular rupture. False negative assessment may result from lack of contour irregularity in patients with small albugineal disruption. Conversely, intratesticular and extratesticular hematomas may be isoechoic to the testis and mimic contour irregularity, leading to a false-positive diagnosis of rupture [28]. Contrast-enhanced US has been reported as useful in scrotal trauma [18]. In our experience, all testicular fractures were correctly diagnosed with a clear depiction of the fracture, its relation with the tunica albuginea and the presence of hematoma.

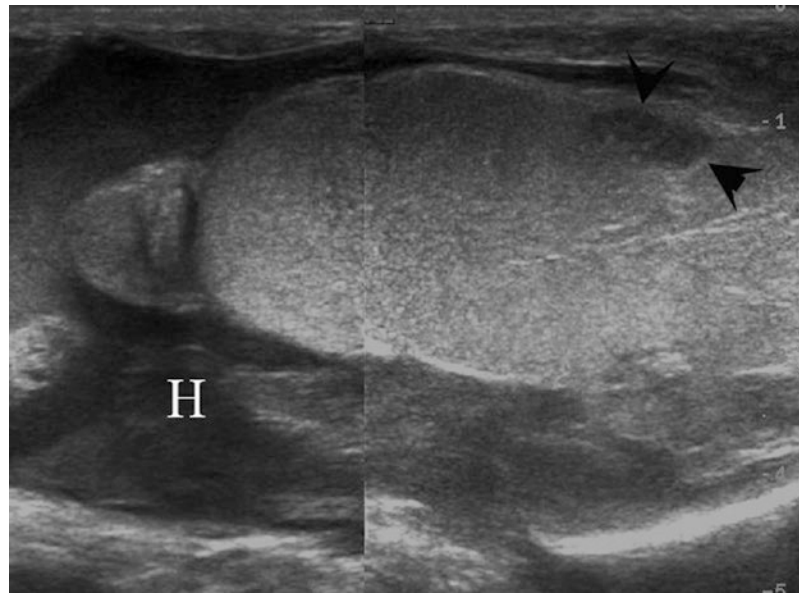

Fig. 58.7 Testicular trauma. This compounded image shows a heterogeneous testis with focal abnormality (*arrowheads*) in the lower part of the testis and large hematocele

58.6.3 Penis

Injury to the penis may result from penetrating and blunt trauma or from acute bending of the erect shaft. Ultrasonography is the preferred imaging technique for evaluating patients with penile trauma because it can accurately depict the nature and extent of injury. The main role of sonography in these patients is to exclude albugineal tears because extratunical and cavernous hematomas can be treated conservatively, but surgery is required when rupture of the tunica albuginea cannot be excluded. US can detect the tear as an interruption of the thin echogenic line of the tunica albuginea with associated hematoma (Fig. 58.8). Associated urethral injuries may be difficult to detect. Evaluation of the urethra with sonography can help identify interruption of the urethral wall, but retrograde urethrography may be needed [29]. In the absence of external penetrating traumas, an indirect sign of urethral injury is the presence of air in the cavernosal bodies [30].

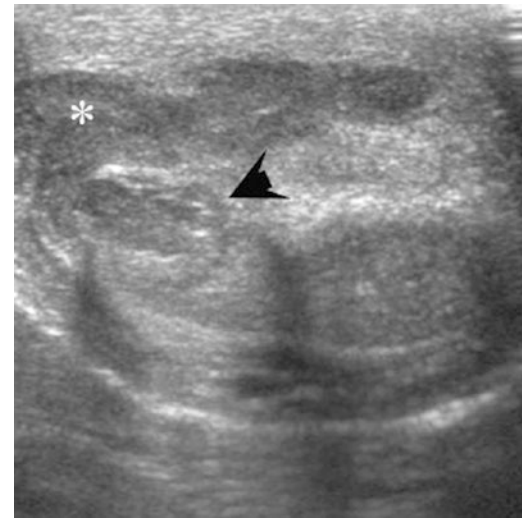

Fig. 58.8 Penis trauma. Rupture of the penis with hematoma in the cavernosal body (*arrowhead*) and hematoma (*asterisk*)

References

1. Rucker CM, Menias CO, Bhalla S (2004) Mimics of renal colic: alternative diagnoses at unenhanced helical CT. Radiographics 24:S11–S33
2. Rosen MP, Siewert B, Sands DZ, Bromberg R, Edlow J, Raptopoulos V (2003) Value of abdominal CT in the emergency department for patients with abdominal pain. Eur Radiol 13:418–424
3. Nicolau C, Claudon M, Derchi LE, Adam EJ, Nielsen MB, Mostbeck G, Owens CM, Nyhsen C, Yarmenitis S (2015) Imaging patients with renal colic-consider ultrasound first. Insights Imaging 6(4):441–447
4. Dalziel PJ, Noble VE (2013) Bedside ultrasound and the assessment of renal colic: a review. Emerg Med J 30:3–8
5. Smith-Bindman R, Aubin C, Bailitz J et al (2014) Ultrasonography versus computed tomography for suspected nephrolithiasis. N Engl J Med 371:1100–1110
6. (2014) Guidelines on urolithiasis. European Association of Urology. In: http://www.uroweb.org/gls/pdf/22%20Urolithiasis_LR.pdf. http://www.uroweb.org/gls/pockets/english/22Urolithiasis_LR.pdf.
7. Sheafor DH, Hertzberg BS, Freed KS et al (2000) Nonenhanced helical CT and US in the emergency evaluation of patients with renal colic: prospective comparison. Radiology 217:792–797
8. Piazzese EMS, Mazzeo GI, Galipò S et al (2012) The renal resistive index as a predictor of acute hydronephrosis in patients with renal colic. J Ultrasound 15:239–246
9. Ripollés T, Martínez-Pérez MJ, Vizuete J et al (2013) Sonographic diagnosis of symptomatic ureteral calculi: usefulness of the twinkling artifact. Abdom Imaging 38:863–869
10. Craig WM, Wagner BJ, Travis MD (2008) From the archives of the AFIP: pyelonephritis: radiologic-pathologic review. Radiographics 28:255–276
11. Subramanyam BR, Raghavendra BN, Bosniak MA, Lefleur RS, Rosen RJ, Horii SC (1983) Sonography of pyonephrosis: a prospective study. AJR Am J Roentgenol 140:991–993
12. Hammond NA, Nikolaidis P, Miller FH (2012) Infectious and inflammatory diseases of the kidney. Radiol Clin North Am 50:259–270
13. Craig WD, Wagner BJ, Travis MD (2008) Pyelonephritis: radiologic-pathologic review. RadioGraphics 28:255–276
14. Culclasure TF, Bray VJ, Hasbargen JA (1994) The significance of haematuria in the anticoagulated patient. Arch Intern Med 154:649–652
15. Mitterberger M, Oinggera GM, Neuwirt H (2007) Three dimensional ultrasonography of the urinary bladder: preliminary experience of assessment in patients with hematuria. BJU Int 99:111–116
16. Siegel MJ (1997) The acute scrotum. Radiol Clin North Am 35:959–976
17. Horstman WG, Middleton WD, Melson GL (1991) Scrotal inflammatory disease: color Doppler US findings. Radiology 179:55–59
18. Valentino M, Bertolotto M, Derchi L, Bertaccini A, Pavlica P, Martorana G, Barozzi L (2011) Role of contrast enhanced ultrasound in acute scrotal diseases. Eur Radiol 21(9):1831–1840
19. Dogra VS, Gottlieb RH, Oka M et al (2003) Sonography of the scrotum. Radiology 227:18–36
20. Baker LA, Sigman D, Mathews RI et al (2000) An analysis of clinical outcomes using color Doppler testicular ultrasound for testicular torsion. Pediatrics 105:604–607
21. Middleton WD, Middleton MA, Dierks M, Keetch D, Dierks S (1997) Sonographic prediction of viability in testicular torsion: preliminary observations. J Ultrasound Med 16:23–27
22. Novelline RA, Rhea JT, Bell T (1999) Helical CT of abdominal trauma. Radiol Clin North Am 37: 591–612
23. McGahan PJ, Richards JR, Bair AE, Rose JS (2005) Ultrasound detection of blunt urological trauma: a 6-year study. Injury 36:762–770
24. Valentino M, Serra C, Zironi G, De Luca C, Pavlica P, Barozzi L (2006) Blunt abdominal trauma: emergency contrast-enhanced sonography for detection of solid organ injuries. AJR Am J Roentgenol 186(5): 1361–1367
25. Dogra V, Bhatt S (2004) Acute painful scrotum. Radiol Clin N Am 42:349–363
26. Jeffrey RB, Laing FC, Hricak H, McAninch JW (1983) Sonography of testicular trauma. AJR Am J Roentgenol 141:993–995
27. Gordon LM, Stein SM, Ralls PW (1996) Traumatic epididymitis: evaluation with color Doppler sonography. AJR Am J Roentgenol 166:1323–1325
28. Kim SH, Park S, Choi SH et al (2007) Significant predictors for determination of testicular rupture on sonography: a prospective study. J Ultrasound Med 26:1649–1655
29. El-Bahnasawy MS, Gomha MA (2000) Penile fractures: the successful outcome of immediate surgical intervention. Int J Impot Res 12:273–277
30. Bertolotto M, Pozzi Mucelli R (2004) Nonpenetrating penile traumas: sonographic and Doppler features. AJR 183:1085–1089

59 Practical Recommendations for Performing Ultrasound Scanning in the Urological and Andrological Fields

Archives of Italian Urology and Andrology 2014;86,1:56–78

Pasquale Martino and Andrea Benedetto Galosi

Coordinators: Pasquale Martino and Andrea Benedetto Galosi
Imaging Group – Società Italiana Urologia (*SIU*)
In collaboration with the Società Italiana Ecografia Urologica Andrologica Nefrologica (*SIEUN*)
Reviewers:
Barozzi Libero, Radiologist, Bologna (Società Italiana Radiologia)
Bertolotto Michele, Radiologist, Trieste
Fandella Andrea, Urologist, Treviso
Galosi Andrea Benedetto, Urologist, Fermo, Asur Marche
Martino Pasquale, Urologist, Bari (President of SIEUN, Associate Member of ESUI-EAU)
Rosi Paolo, Radiologist and Urologist, Perugia
Trombetta Carlo, Urologist and Andrologist, Trieste (Member of ESUI-EAU)
Authors:
Bitelli Marco, Urologist and Andrologist, Rome
Consonni Paolo, Urologist, Castellanza (Va)
Fiorini Fulvio, Nephrologist, Rovigo
Granata Antonio, Nephrologist, Agrigento
Gunelli Roberta, Urologist, Forlì
Liguori Giovanni, Urologist and Andrologist, Trieste
Palazzo Silvano, Urologist, Bari
Pavan Nicola, Urologist, Trieste
Scattoni Vincenzo, Urologist, Milan
Virgili Guido, Urologist, Rome
Reprint with permission of Archives of Italian Urology and Andrology

P. Martino (✉)
Department of Emergency and Organ, Transplantation – Urology, Andrology and Kidney Transplantation Unit, Bari, Italy

University of Bari, Bari, Italy
e-mail: pasqualeluciomartino@libero.it; luciomartino@tin.it; pasquale.martino@uniba.it

A.B. Galosi
Institute of Urology - Polytechnic, University of Marche, Ancona, Italy

59.1 Introduction

These recommendations have been drawn up by the "Imaging" work group of the Società Italiana di Urologia (SIU) in collaboration with the Società Italiana di Ecografia Urologica Andrologica Nefrologica (SIEUN). The specialists involved in the work include urologists, andrologists, nephrologists, and radiologists.

The aim of this work is to support specialist urologists in clinical practice, supplying a series of recommendations to be followed during the phases of ultrasound diagnosis of renal, prostatic, bladder, scrotal, and penile diseases. The recommendations are based on a review of the literature, on previous recommendations, and on the opinions of the experts (5-7). This document is the first to be devoted to this sector, although the American Urological Association (AUA) and the American Institute of Ultrasound in Medicine (AIUM) recently (November 2011) published practical guidelines for the performance of ultrasound in the urological field [www.aium.org].

P. Martino, A.B. Galosi (eds.), *Atlas of Ultrasonography in Urology, Andrology, and Nephrology*,
DOI 10.1007/978-3-319-40782-1_59

The references will serve to make a constructive comparison with other clinical experiences. These recommendations were developed and drawn up with the aim of ensuring minimum standards of excellence for ultrasound imaging in urological practice, based on the assumption that ultrasound plays an essential part in this practice.

Doctors specializing in urology can gain particular skills and training in the use of ultrasound scanning during their residency years, in postgraduate dedicated courses organized by universities, and in training courses organized by urological scientific societies (SIU, SIA, EAU, AUA) and dedicated societies (ESUI, SIEUN), both nationally and internationally.

For the urologist, US scanning is an integral part of the processes of diagnosis and follow-up to manage diseases of the urinary tract and male genitals in patients of all ages, in both a hospital and an outpatient setting. The ability to perform and interpret diagnostic imaging studies has become an integral part of clinical practice in all nations, also in order to optimize resources and provide patients with efficacious, rapid care. US scanning has been defined as the urologist's stethoscope. This also applies in the andrological field.

Urologists must combine skillful use of sophisticated imaging devices with a deep knowledge of the physiological and pathological processes affecting the human body. If the diagnostic test will be performed in another department, they must be able to select the best test or series of tests to be made for the specific patient, to optimize the management of the urological patient.

These recommendations may be useful to ensure minimum shared or reference standards in the urological and andrological fields also for other medical specialists who perform urological US scanning, such as radiologists, internists, geriatricians, gynecologists, or other doctors who study the urinary tract.

The *aims* of the present recommendations are:

- To define the purpose of each specific ultrasound investigation (to clarify what each investigation aims to discover)
- To define the indications
- To establish the requisite technological standards of the devices
- To outline the method of performance of the investigation
- To establish the expected accuracy of the investigation in question
- To indicate the reporting method

Apart from their utility as a theoretical-practical tool for making a correct ultrasound examination of the genitourinary apparatus, the recommendations we propose have the aim of guiding the urologist in the assessment of the risks and benefits of diagnostic imaging so as to optimize the management of the urological patient ("patient care is optimized when urologists coordinate the use of imaging techniques and dedicated devices in the most advantageous place for their patients" – see [*AUA, AIUM develop joint guidelines for urologic ultrasound exams*]).

Below, brief recommendations regarding the equipment, documentation, reporting of the findings, training requirements, and patient safety in ultrasound studies are listed.

59.1.1 Equipment

Ultrasound scanning must be performed with devices that can provide images in real time, thanks to the use of transducers that can optimize the penetration of the ultrasound waves inside the tissues, with excellent resolution obtained by setting appropriate frequency intervals. The advised transducer frequencies are 3.0–5.0 MHz for abdominal scanning, 6.0–9 MHz for transrectal, and 7.0–12.0 MHz for genital scanning, while intraoperative renal or testicular scanning can be done with the transducer set at 6–10 MHz in linear mode. The correct setting of the device must also include the generation of good documentation of the investigations made.

59.1.2 Documentation

Each ultrasound investigation must be concluded with the production of appropriate, unequivo-

cally clear images, recorded on a durable support (digital format is preferable) and saved in the patient's clinical files. The operator must check that the images are correctly recorded on the electronic support and readable in terms of contrast and luminosity.

The ultrasound images must also be labeled with the patient's personal data and those of the health-care facility where the investigation is made (hospital department or outpatient clinic). The date and type of probe are automatically specified by the device.

59.1.3 Reporting of Findings

Apart from acquiring full documentation of the investigation, complete reporting of the findings must be made, specifying any conditions during the execution phase that could affect the reliability or accuracy of the test (e.g., anatomical causes [bowel gas, malformations], causes depending on the patient [poor compliance, pain during the test], conduction in emergency regime, etc.). The report must include the name and signature of the doctor. Ultrasound scanning is performed for specific purposes, and the simple production of images, even of good quality, can never replace a description of the clinical picture and the interpretation of the findings by the operator.

59.1.4 Training Requirements

Adequate training is an essential prerequisite for the correct performance and interpretation of ultrasound investigations. This training must be obtained both by residents at the specialist schools and by those who are already specialists in urology. They should all undergo regular updating of their ultrasound scanning skills, the former during their specialist studies and the latter at regular periodical updating courses. The main scientific societies are active in organizing such updates and issue certificates of attendance at such training and updating courses.

59.1.5 Patient Safety

Ultrasound procedures must be performed only for the specific indications of the case, like any other imaging technique. In fact, like all specialists, urologists should comply with the principles of ALARA (1), reducing to a minimum patients' exposure to acoustic energy (2).

In addition, the operator must ensure that the ultrasound probe is clean and protected, to comply with the guidelines of the CDC (Centers for Disease Control and Prevention) for the standards of disinfection and sterilization of the devices (3, 4), as well as the technical recommendations specified by the manufacturers of the various devices.

Regular periodical controls of the devices must be made, with the collaboration of the manufacturers and complying with the safety norms they list.

59.1.6 Process of Assessment of the Recommendations

An assessment of the true effectiveness of these recommendations in modifying behavior and improving the clinical outcome will be made using control procedures that are currently being defined.

59.1.7 Updating

In the expectation of upcoming technological and/or diagnostic advances, the present recommendations will be integrated by further publications, likely every 3 years.

59.2 Ultrasound Scanning of the Kidney

59.2.1 Introduction

The kidneys are a pair of organs located at the retroperitoneal level: each kidney is situated along the lateral margin of the psoas muscle that lines it posteriorly, while it is adjacent to the bowel anteriorly. The right kidney lies about 2–3 cm lower than the left. The kidneys have the function of purging

the organism of a great number of substances and also play a part in many metabolic pathways (protein, lipid, and glucides), including the metabolism of hormones and vitamins, as well as control of the blood pressure. Healthy kidneys are easily assessed by ultrasound scanning because the parenchymal component is well delineated by the capsule and has a different echostructure from the perirenal fat and the pyelic structures.

59.2.2 Measurements

Measurements of the kidney length are made by scanning along the major axis parallel to the adjacent psoas muscle. The oblique plane of this long axis is measured by scanning the superior pole more medially and the inferior plane more laterally/anteriorly. The angle between the long axis and the sagittal plane ranges between 8 and 10° (8). Variations in this angle produce the variability between ultrasound measurements of the length and measurements made with conventional radiology or urography (9). With ultrasound scanning it is easy to make reliable, repeatable real-time measurements of the kidney long axis.

It is clear that to make a precise measurement of the kidney axis, it is necessary to identify the superior and inferior poles: this may be complex in cases of a malrotated, ectopic, ptosic, or scoliotic kidney. Measurement of the interpolar renal diameter is more accurate when the patient is placed in supine decubitus, slightly turned toward the contralateral side. Oblique posterior longitudinal scanning is performed with the patient holding the homolateral arm above the head and breathing deeply, to shift the kidney under the ribs. Measurements in prone position tend to result in an underestimation of the kidney length, but may need to be done if the kidney is poorly visualized in other scans (10).

In clinical practice ultrasound measurement of the kidney volume is not performed because it is difficult to do and highly error-prone, even if it can be useful to assess renal anomalies (11). Renal volume can be assessed by measuring the three orthogonal diameters and applying the following formula:

volume $V = 0.49 \times L \times W \times \mathrm{AP}$

where L is the length of the major axis (longitudinal scan), W is the length measured at the renal hilum (transverse scan), and AP is the anteroposterior diameter again measured at the hilum (transverse scan) (12). The photos on which the measurements were based should be stored in the documentation of the investigation.

It may soon be possible to make ultrasound measurements of the renal volume using 3D probes that allow a greater precision than the common 2D probes (13).

In any case, correct measurement of the volume of the kidneys requires good operator skills and knowledge of the renal anatomy, consisting of four different components:

1. The hyperechogenic external capsule
2. The hypo-isoechogenic parenchyma as compared to the echostructure of the liver and spleen, between the capsule and pelvis, consisting of:
   (a) The external echogenic cortex, being the functional portion
   (b) The internal hypoechogenic medulla, corresponding to the medullary pyramids with a triangular structure and the base toward the outside
3. The kidney sinus, hyperechogenic due to the presence of many interfaces consisting of the intrarenal adipose tissue

59.2.3 Indications

Renal ultrasound scanning is indicated in the first approach to patients with renal disease and in the follow-up. The investigations include:

- Assessment of the kidneys, in normal or ectopic sites
- Assessment of the ultrasound morphology
- Diagnostic workup in patients with acute or chronic kidney disease
- Assessment of any dilation of the excretion pathways and differential diagnosis between obstructive and non-obstructive acute renal failure (ARF)

- Identification of space-occupying lesions (cysts and tumors)
- Searching for stones
- Echo-color Doppler assessment of the renal vascularization (both with color-power Doppler and, in selected cases, contrast-enhanced ultrasound [CEUS])
- Assessment of the intrarenal resistance indexes (RI) at the level of the interlobar and/or arcuate arteries in nephropathic, hypertense, diabetic, and nephroangiosclerotic patients
- Guidance of renal needle biopsy performed in the course of kidney disease or to exclude cancer
- Guidance of renal puncture in the course of hydronephrosis and abnormal cysts inducing symptoms
- Assessment of kidney transplant(s) (just like the native kidney) and complications
- Intraoperative guidance in conservative kidney surgery, percutaneous lithotripsy, and nonsurgical ablation of expanding lesions
- Postsurgical monitoring or endourological treatments

59.2.4 Preparation for the Investigation

Although no specific preparation is considered strictly necessary, some suggestions are made with the aim of optimizing the performance of the investigation. If the patient is asked to refrain from drinking fizzy drinks and eating fermented cheeses, vegetables, fruits, wholemeal foods, and pulses. In cases of a "sluggish" bowel, the patient should take a laxative the evening before. Since renal studies should always include a study of the bladder, this should be repleted but not distended.

59.2.5 Specifications of the Minimum Requirements for the Echograph and Probes

To study the kidney, a latest generation echograph, if necessary portable, should be used, of average range equipped with color-power Doppler module and, if possible, suitable software for contrast enhancement. Multifrequency convex probes allow the study of the native and transplanted kidney, but for facilities that receive kidney transplant patients, it is very useful to be able to employ a multifrequency linear probe. A thermal printer is indispensable, as is a magnetic image storing system. A recent generation US device offers pre-settings of the parameters to be assessed for each organ and probe, especially during echo-color Doppler investigations. These settings are defined during the installation but must be checked by the operator, updated, or modified according to the need and the characteristics of the tools available, as approved by the manufacturer.

59.2.6 Parameter Assessed

1. Position of each kidney:
   - presence/absence
   - ptosis/ectopia
   - malrotation
   - dysmorphic anatomy
2. Kidney size (14):
   - Maximum interpolar diameter (normal: right, 10.6 ± 1.3 cm; left, 10.1 ± 1.1 cm)
   - Transverse diameter (normal: right, 4.9 ± 0.6 cm; left, 5.3 ± 0.7 cm)
   - Parenchymal thickness (normal: 1.5–2.0 cm) [measurement of cortical thickness is not always possible due to poor cortico-medullary differentiation, and suffers from high inter- and intraobserver variability, so it is not commonly used] (15, 16)
3. Assessment of the kidney outline that may feature the persistence of fetal lobes in the tract between two consecutive pyramids and/or the presence of grooves (scars after pyelonephritis) at one or more calyces.
4. Check for stones (hyperechogenic image measurable by posterior shadow cast).
5. Check for distension of the kidney, ampulla, and calyces (pyelic ectasia, calico-pyelic ectasia, or hydronephrosis).

6. Check for distension of the ureter (hydroureteronephrosis).
7. Check for space-occupying lesions and differentiate between fluid (cysts) and solid lesions (neoplasia).
8. Assess renal vascularization using color and power Doppler to identify "minus" signs (16).
9. Assess renal vascularization by contrast enhancement (CEUS) that improves diagnostic confidence in the assessment of deficiency signs (18).
10. Assess the intrarenal resistance indexes (RI), vn < 0.70 (17) (optional, depending on the clinical picture).

59.2.7 Facsimile of Findings Report

59.2.7.1 Kidney Ultrasound

Kidneys in situ, maximum longitudinal/transverse size within normal limits (right cm…../……; left cm……/……..), regular outlines. Parenchyma thickness normal (……cm). Regular echogenicity of parenchyma. No direct or indirect signs of kidney stones.

Regular excretion pathways with no ectasia or calico-pyelic dilation (or distinguish ectasic/pyelic, calico-pyelic dilation, associated or not with ureteral dilation). No space-occupying lesions. Adrenal loggia, no expanding lesions.

59.2.7.2 Renal Eco-Color Doppler

Intrarenal resistance indexes (interlobar or arcuate arteries) within normal limits (RI < 0.70)

Systolic peak velocity (SPV) of the renal arteries at the ostium, initial, medial, distal, and anterior and posterior segmentary tracts within normal limits. Flowmetry normal. Pervious renal veins. At power Doppler, good vascular appearance of parenchyma

Minimum imaging documentation to be included:

1. Two images per kidney: transverse and longitudinal scans with measurements.
2. Orientation of images (liver/spleen on left).
3. Arrow on the photo, indicating organ analyzed and side.
4. Accessory images illustrating any anomalies.
5. If the bladder is described in the findings, at least one bladder scan image must be included.

59.3 Ultrasound of the Bladder

59.3.1 Indications

- To measure post-voiding residue
- To measure bladder filling volume
- To assess anatomic modifications/complications associated with obstruction (diverticuli, trabeculation/columnar thickening, stones, detrusor thickness)
- To assess hypermobility of the bladder neck in women with stress incontinence
- To assess hematuria originating in the lower urinary tract
- To assess lower urinary tract symptoms – LUTS
- To check for suspected ureteral stone migrating intramurally
- To check for congenital malformations (ureterocele, diverticuli, etc.)
- Postsurgical monitoring (vesical bleeding, position of the catheter, etc.)
- Follow-up in non-infiltrating cancer
- Follow-up of bowel loop orthotopic bladder after cystectomy

59.3.2 Tools

During standard investigations in the adult, a convex 3.5 MHz probe (range 3–5.5 MHz) is used (in pediatric patients a higher-frequency transducer can be used). To measure bladder volume in post-voiding controls, automatic equipment can be used. In dynamic studies (e.g., assessment of cystocele), transrectal or trans-vaginal probes can be used. To stage bladder tumors, transrectal probes can be used.

59.3.3 Technique

Use adequate amounts of gel.

For optimal imaging of the bladder, it should be full but not overdistended, especially in cases of obstruction. The patient should be lying supine (supine or lithotomic or in orthostatic position in cases of use of a transrectal probe).

The bladder wall and lumen will be assessed during the investigation, with both transverse and sagittal scans (25).

Systematic search and documentation must be made of any changes in the echographic appearance of the bladder wall and neck at rest, trabeculature of the detrusor, endophytic neoplasia, diverticuli, stones, and the presence of a third prostatic lobe. Any focal lesions observed (in particular masses) and other diseases (diverticuli, stones, clots, etc.) must be described, specifying site and size.

When indicated, the distal ureters should be assessed to exclude dilation or other anomalies (intramural or juxtavesical stones).

Echo Doppler study may be useful to assess ureteral jet and make a differential diagnosis of bladder tumors (33).

Fine regulation of the light is essential to obtain a significantly improve image quality and correctly visualize the anterior wall (superficial as compared to the skin) and posterior wall (deep). Use the second tissue harmonic imaging tool to improve the imaging and reduce reverberation artifacts.

Calculate bladder volume (ellipsoid formula, $v = 0.52 \times r1 \times r2 \times r3$).

Always assess post-voiding residue (to measure the residue, scan the bladder immediately after voiding, using automatic measurement tools, on the basis of the ellipsoid formula, if available).

In cases of a significant post-voiding residue, the patient should be asked to make a further attempt to void and then the measurements repeated until a reliable indication of the voiding capacity is obtained.

In cases of assessment of the detrusor thickness (not normally more than 3 mm), the study will be conducted with moderate bladder filling (calculated as between 250 and 350 ml, with 250 ml as threshold value); the mean of three measurements made on the same image is calculated.

To obtain the best results, the assessment must be made at the level of the anterior wall/apex, and it is better if a high-frequency (7.5 MHz) convex or linear probe is employed.

The ultrasound appearance of the detrusor is as a sandwich structure (hypoechogenic muscular wall between the mucosa and adventitial layers that is slightly hyperechogenic).

The detrusor thickness must always be measured in areas that are orthogonal to the ultrasound focus (19–21).

The findings report should include:

- The patient's name and surname.
- The name of the service where the investigation was performed and the telephone number (in case further clarification should be required).
- The date of the ultrasound examination.
- If possible include all pertinent clinical information, including the indications for the investigation.
- The type of ultrasound examination performed, and if endocavitary techniques are employed, the method must be specified.
- Specify the orientation of the image, if different from standard (superior part on the right of the screen).
- Use appropriate anatomical and ultrasound terminology; in cases of variations from normal sizes, the measurements must be specified (e.g., increased detrusor thickness, diverticuli, endoluminal masses, etc.).
- Compare with previous imaging studies if available; suggest types of studies for further investigation, any differential diagnosis hypotheses.
- Name and signature of the examiner and date.
- If the results of the ultrasound are considered by the doctor performing the investigation to be of particular clinical importance and unexpected, such as to require urgent intervention

to guarantee proper patient care, ideally the doctor who did the investigation should contact the patient's doctor directly to check that the findings report has been received.
- Describe the state of other organs in the abdomen only if qualified to do so.
- Pay attention to the degree of distension of the bladder that can negatively affect the visualization of the ureters in the juxtavesical tract and the seminal vesicles.
- Use the tissue harmonic imaging tool to reduce reverberation artifacts and obtain better detail.
- Indicate any difficulties encountered while performing the investigation (patient's collaboration and constitution, presence of bowel gas), underlining any limits of the test and so its diagnostic value.

59.3.4 Example of Final Report

1. Presence or absence of the bladder
2. Orthotopic site and symmetry
3. Shape
4. Degree of bladder distension [essential for reliability of investigation]
5. Presence or absence of wall alterations (assessment of lesions > 3 mm)
6. Presence or absence of a third lobe (in cases where present, volume, and/or degree of extension into the bladder: intravesical prostatic protrusion)
7. Presence and size of calcifications (diameter >3 mm), fixed or mobile with patient's movements in decubitus
8. Characteristics of the bladder neck (in man, protrusion of prostate)
9. Presence of the ureters and any dilation or abnormal outlet or stones
10. Presence of pelvic masses and ab-extrinseco compression of the bladder
11. Quantification of post-voiding residue

Note

It is necessary to calculate the bladder filling volume only if needing to measure the detrusor thickness or estimate the bladder weight (reliable for values ≥ 250 ml) or if needed for clinical reasons.

Describe any clinical conditions that prevent adequate bladder filling (incontinence, pain due to reduced compliance).

Images to be included (not all are always indispensable, depending on the clinical picture)

1. One image of the bladder in transverse scan.
2. One image of the bladder in longitudinal scan.
3. One image of the bladder in transverse/longitudinal scan showing the bladder neck.
4. One or more images of any anomaly.
5. In cases of a lesion obstructing the juxtavesical ureter (stone or vegetating lesion), oblique scanning must be done.

59.3.5 Preparation for Investigation and Patient Position

1. The patient does not need to be fasting.
2. The bladder must be repleted with at least 300 cc; to ensure this it is necessary:
   (a) For the patient to drink at least 500 cc of fluids during the three hours before the investigation
   (b) For the patient to refrain from urinating within two hours before the investigation
   (c) For the patient to feel the urge to urinate (this latter parameter is extremely subjective and not always reliable)

The investigation is normally performed with the patient in supine position. Lateral right or left decubitus may rarely be necessary, in cases where a lesion, likely of prostatic origin, extends into the lumen and its mobility must be checked.

In cases requiring oblique scanning, this is done by rotating the probe by about 40° to its longitudinal axis, taking care that the bladder filling is not more than 250–300 cc (otherwise the ureters would appear crushed by the bladder volume itself).

59.3.6 US Parameters to Evaluate Bladder Modifications in Patients with Bladder Outlet Obstruction

Progressive changes in the bladder wall are observed in men with lower urinary tract obstruction secondary to benign prostatic enlargement (BPE).

The high pressure discharge cause initially an increase in the proportion of smooth muscle (hyperplasia/hypertrophy of the detrusor) to changes in the advanced stages of bladder decompensation (fibrosis), hyperactivity and decreased functional capacity. Early identification of bladder changes by noninvasive transabdominal ultrasound can move towards therapeutic choices that can prevent further organ damage in the bladder wall.

Measurement of the Bladder Wall Thickness (BWT) or Detrusor Wall Thickness (DWT) by US is reliable, at least 3 measurements of the anterior bladder wall taken at a filling volume of ≥ 250 ml. In particular, the DWT [thickness of the muscle hypoechoic between two layers hyperechoic serosa and mucosa] is considered the best diagnostic tool to measure detrusor hypertrophy using cut-off value >2.9 mm in men. US derived measurements of bladder weight (Estimated Bladder Weight, EBW) is another noninvasive tool for assessing bladder modifications in patients with Bladder Outlet Obstruction (BOO): cut-off value 35 gr. Technique for measuring the BWT and EBW relies in conventional US 7.5-4 MHz or using the automatic system of calculation (BVM 6500 3.7 MHz). The variability of measuring intra (4.6 to 5.1%) and interoperator (12.3 %) is acceptable. Also conventional US detects established signs of bladder damage: diverticulosis, trabecolations in the bladder wall (pseudodiverticula), calculi and post-void residual urine (>50 cc). Furthermore the Intravescical Prostate Protrusion (IPP), easy measured by transabdominal ultrasound, is strongly correlated to obstruction in men with BPE (cut-off 12 mm). Measure, quantify and monitor the cervico-urethral obstruction in men with symptomatic BPE is possible by non-invasively US monitoring the response of the bladder wall. Early identification has the advantage of adopting therapeutic measures sufficient to prevent progression of bladder damage measuring DWT, EBW in addition to established US parameters (20, 21, 31).

59.3.7 Diagnostic Accuracy

In the diagnosis and follow-up of bladder tumors or hematuria, it should be noted that the standard method is ureterocystoscopy. Ultrasound scanning is an alternative for noninvasive low-grade tumors and for the initial assessment of hematuria. Cystoscopy allows the operator to assess and solve any doubts about the integrity and regularity of the bladder wall raised at ultrasound scanning. Bladder lesions smaller than 5 mm may not be identified at ultrasound. Not all bladder tumors are observed at ultrasound: slow-growing non-vegetative tumors like carcinoma in situ are not diagnosed by imaging. The diagnostic capacity for vegetating/papillary lesions >5 mm is high, even if in some circumstances differential diagnosis with clots may be difficult despite echo-color Doppler.

59.3.7.1 Nonneoplastic Diseases

	Parameter	Pattern
Acute cystitis	Wall thickness and echogenicity	Increased hypoechogenicity, increased thickness of the bladder wall, between the serosa and mucosa
Chronic cystitis		No characteristic pattern, assessment of post-micturition residue, search for foreign bodies in the bladder
Bullous cystitis	Wall thickness, echogenicity	Increased bladder wall thickness, anechogenic areas Wall hypoechogenicity
Diverticuli	Presence/absence	Formation of anechogenic paravesical areas with the presence of asonic funneling to the bladder (diverticular neck) Transrectal scanning can better reveal the diverticular neck Color Doppler can enable DD between tumors and endodiverticular clots, although it is not the ultimate test In doubtful cases CEUS or other radiological or endourological imaging should be done
Detrusor hypertrophy	Thickness detrusor wall (calculated at ≥ 250 ml of filling, as mean of three measurements, the hypoechogenic tissue included between two lines of hyperechogenic tissue: mucosa and bladder serosa)	Increased (>3 mm) with irregularities (trabeculatures or even pseudodiverticuli) low-level evidence, recommendations need to be verified on vast scale, evidence levels based on opinions of experts and case series Parameter to be assessed, advised by experts. For use in clinical studies
Ureterocele		Anechogenic formation (cyst) at the level of the ureteral meatus with evidence at color Doppler of ureteral jet
Juxtavesical ureter lesion	Juxtavesical ureter obstructive lesion (stone or vegetating lesion)	Hyperechogenic image with posterior shadow included in the thickness of the ureteral wall (between hyperechogenic serosa) Eco-color Doppler: useful to identify color signals (artifacts) in the shadow area and in DD of vegetating lesions also with eco-power Doppler Evidence or not of urethral jet at color Doppler
Stones		Hyperechogenic images with shadow, mobile depending on decubitus movements
Hyperactive bladder	Bladder weight (UEBW, ultrasound-estimated bladder weight)	No consensus in literature as to standardized cutoff values to be used in clinical studies

59.3.7.2 Neoplastic Diseases

Although staging is not currently approved on the basis of the ultrasound findings, we report indications for a possible interpretation.

	Parameter	Pattern
Superficial lesions	Bladder wall structure	Generally no echostructural alterations of the wall Endophytic tumors appear as hypoechogenic, fixed proliferative lesions, but sometimes they are hyperechogenic due to the presence of superficial calcifications. At color Doppler hypervascularization is observed
Infiltrating lesions	Bladder wall structure	Interruption/deformation of the wall that appears thickened, sometimes extension beyond the bladder wall

59.3.7.3 Ultrasound of the Pelvic Floor (19, 22–24, 26–30, 32, 34–38)

	Trans-perineal	Introital	Trans-vaginal	Transrectal
Instruments	*Convex* 3.5–5 Mhz probe	Sector *end-fire* 5–7.5 Mhz probe	*Linear biplanar* 7.5 Mhz probe	*Linear biplanar* 7.5 Mhz probe
Patient position		Lithotomic	Lithotomic Orthostatic	Lithotomic Orthostatic
Quality of image	+	+	+++	+++
Measurement of mobility	++	++	+++	+++
Invasiveness	+	+	++	+++
Artifacts in 3–4 grade cystocele	++	++	+++	+

Addendum: possible use of 3D studies, especially for postsurgical assessment (sling). Clinical studies to assess the presence of funneling of the neck, hypermobility of the neck-urethra complex, cystocele, and ureteral fixity. *No standards have yet been established for mobility parameters* (among proposals see Schaer et al. Int Urogynecol J Pelvic Floor Dysfunc 1996, Pajoncini C. in Atlante di ecografia uro nefrologica ed andrologica 1996 ed.CIC, Merz et al. *Ultraschall Med* 2004, Tunn R. et al. Update recommendations on ultrasonography in urogynecology. *Int Urogynecol J* 2005 16, 236–241).

59.3.8 Reference Texts

A literature search of guidelines and reviews on the use of ultrasound in bladder studies published in the last 10 years was made:

- *AIUM Practice Guideline for Documentation of an Ultrasound Examination* – 2008 American Institute of Ultrasound in Medicine
- *AIUM Official Statements Training Guidelines for Physicians Who Evaluate and Interpret Diagnostic Ultrasound Examinations* American Institute of Ultrasound in Medicine 2011
- *Standards and Guidelines for the Accreditation of Ultrasound Practices*. 2011 American Institute of Ultrasound in Medicine
- *Documento SIUMB per le linee guida in Urologia* Giornale Italiano di ecografia I.R. al vol.8 n.4 2005
- *EAU Guidelines on Urinary Incontinence* Eur Urol 59 (2011) 387–400
- *Guidelines on Non-muscle-invasive Bladder Cancer* (*TaT1 and CIS*) EAU 2012
- *Guidelines on Pain Management* EAU 2012

59.4 Prostate and Seminal Vesicles

59.4.1 Prostatic Ultrasound Scanning with the Suprapubic Technique

59.4.1.1 Method

The prostate must be analyzed on two orthogonal planes: transverse and longitudinal. In this study it is essential to examine:

- Juxtavesical ureters
- Bladder
- Prostate
- Seminal vesicles

The prostate diameters to be assessed are latero-lateral, anteroposterior, and cranio-caudal.

In cases of an obstructive lesion of the juxtavesical ureter (stone or vegetating lesion), oblique scans must be made.

Images to be included (*not all are always indispensable, depending on the clinical picture*)

1. One image of the bladder in longitudinal/transverse scan
2. One image of the prostate in transverse scan showing the bladder
3. One image of the prostate in longitudinal scan showing the bladder
4. One image of the right juxtavesical ureter in oblique scan
5. One image of the left juxtavesical ureter in oblique scan
6. One or more images of any anomalies

Report of the findings

1. Date and place of performance of the investigation
2. Patient data (including birth date)
3. Mention of clinical history and diagnostic purpose
4. Value of the last total PSA blood test
5. Comparison with previous tests if available

Both the images and findings must be easy to read by other operators and at later dates. The findings must therefore be reported as unambiguously as possible. In cases of any diagnostic doubt, this must be pointed out, indicating possible hypotheses and suggesting any further instrumental investigations that may help to solve any doubts.

59.4.1.2 Terminology

1. Identification of the medial lobe and its size and relations with the pelvic floor
2. Any picture of cervico-ureteral obstruction due to prostatic hypertrophy causing severe detrusor impairment and any presence of bladder stones [Table 59.1].

Table 59.1 Stones and hyperechogenic prostatic images

Pathologic mechanism	Size	Macroscopic evidence	Number	Site
(*Increased intraprostatic pH and increased precipitation of calcium salts*)				
Endogenous Amyloid bodies Reaction to foreign body in intra-acinar site	Macrolithiasis (max. diameter ≥ 2 mm)	Disseminated ±posterior shadow	Single	Periureteral
Exogenous Stasis of prostatic secretion Intraprostatic Reflux Prostatitis	Microlithiasis (max. diameter ≤ 2 mm)	Thickened ± posterior shadow	Multiple	Lobar Perinodular Ejaculatory ducts

59.4.1.3 Indications

1. To assess the size and volume of the prostate gland before medical, surgical, or radiation treatment (in particular, to assess the volume displacement caused by the third lobe and correlations with detrusor hypertrophy and the presence of bladder pseudodiverticuli and diverticuli)
2. To assess the patient with lower urinary tract symptoms
3. To assess congenital anomalies

59.4.1.4 Essential Parameters to Be Specified in the Final Report

Prostate

1. Presence or absence of the prostate
2. Orthotopic or heterotopic site
3. Shape
4. Size
5. Presence or absence of a third lobe (if present, volume and/or size of protrusion into the bladder: intravesical prostatic protrusion)
6. Presence and size of any gross calcifications (diameter >5 mm)
7. Presence and size of any gross abscesses/cysts (diameter >5 mm)
8. Presence of the ureters and any dilation or anomalous outlet
9. Quantification of post-voiding residue

Note

Lesions of any nature with a diameter of ≤ 5 mm are not identifiable with suprapubic ultrasound scanning. The suprapubic technique cannot visualize the echostructure of the peripheral zone of the prostate due to technical image resolution limitations.

Seminal Vesicles

1. Presence or absence
2. Site
3. Symmetry

Bladder

An accurate description of the bladder is essential; see previous chapter.

59.4.1.5 Preparation for Investigation and Patient Position

1. The patient does not need to be fasting.
2. The bladder must be repleted with at least 300 cc; to ensure this it is necessary:
   (a) For the patient to drink at least 500 cc of fluids during the three hours before the investigation
   (b) For the patient to refrain from urinating within two hours before the investigation
   (c) For the patient to feel the urge to urinate (this latter parameter is extremely subjective and not always reliable)

The investigation is normally performed with the patient in supine position. Lateral right or left decubitus may rarely be necessary, in cases where a lesion, likely of prostatic origin, extends into the lumen, and its mobility must be checked.

In cases requiring oblique scanning, this is done by rotating the probe by about 40° to its longitudinal axis, taking care that the bladder filling is not more than 250–300 cc (otherwise the ureters would appear crushed by the bladder volume itself).

59.4.1.6 Facsimile of the Final Report

Mention of clinical history:_____

Diagnostic purpose: _____

Last total PSA value

The bladder…

Yes/no hyperechogenic bladder images depicting stones, nor dilation of the juxtavesical and intramural bilateral ureters

The prostate is shown in orthotopic/heterotopic site and is grossly triangular, size within normal limits (more/less), (LL × AP × CC), having a theoretical calculated volume of about ___ml.

Presence of third lobe protruding into the bladder by ____cm

Post-voiding residue is about cc.

Mild/fair/marked tenderness or pain on palpation of the hypogastrium at the start/throughout the duration of the investigation

59.4.1.7 Diagnostic Accuracy

It is important to note that the elective method for the study of the prostate gland includes the use of endocavitary probes (see relative chapter). In fact, suprapubic ultrasound scanning is not contemplated in the guidelines for the study of the prostate drawn up by the main scientific societies due to its limited diagnostic power (see references).

In particular, it is thought that prostate ultrasound results in an overestimation by more than 30–50 % of the true prostate volume.

According to some authors, moreover, the use of the ellipsoid formula to calculate the prostate gland volume with the aid of suprapubic ultrasound leads to an error of about 20 %.

59.4.1.8 Notes on Clinical Practice

A. Attention must be paid to the degree of distension of the bladder that can affect the visualization of the juxtavesical ureters and seminal vesicles.
B. Use the tissue harmonic imaging tool to reduce reverberation artifacts and obtain better detail.
C. Indicate any difficulties encountered while performing the investigation (patient's collaboration and constitution, presence of bowel gas), underlining any limits of the test and so its diagnostic value.
D. Remember that if the prostate is larger than normal, its morphology may vary, especially in cases of prostatic hyperplasia.

59.4.1.9 Devices and Transducers Used

Convex transducer with a frequency of 3.5 MHz or multifrequency 5–2 MHz probes depending on the patient's constitution and how deeply the gland is located

59.4.2 Transrectal Prostatic Ultrasound

59.4.2.1 Method

The investigation is dynamic, and apart from longitudinal and transverse scans, with the probe inclined more cranio-caudally than for the study of the bladder, oblique scans will also be performed to study the seminal vesicles that generally lie on the transverse/oblique plane.

The prostate must be analyzed on two orthogonal planes: transverse and longitudinal, from the apex to the base of the gland.

At the same time, it is essential to study:

- The urethra sphincter, Cowper's glands
- The seminal vesicles
- The juxtavesical tract of the ureters
- The deferens ducts
- The bladder (insofar as it is explorable)

Additionally, any gross alterations of the rectal wall should be pointed out and referred to the competent specialist colleague.

The diameters to be assessed are latero-lateral, anteroposterior, and cranio-caudal, to calculate the total volume and also the volume of the transition zone (periureteral hypertrophy).

For the seminal vesicles, the diameters assessed are anteroposterior. The apparent size of the latter may be affected by the degree of distension of the bladder, by ejaculation and by forms of obstruction.

Images to be included (*not all are always indispensable, depending on the clinical picture*)

1. One image of the prostate in transverse scan (indicating the diameters of both the entire gland and adenoma)
2. One image of the prostate in longitudinal scan (indicating the diameters of both the entire gland and adenoma)
3. One image of the prostate in transverse scan showing the bladder
4. One image of the prostate in longitudinal scan showing the bladder
5. One image of the seminal vesicles in transverse scan
6. One or more images of any anomalies
7. Any images of the juxtavesical ureter in longitudinal scan

Calculation of total prostatic volume and transition zone volume It is important to note that

all latest generation ultrasound devices automatically calculate the volume of the prostate, bladder, and seminal vesicles. If this is not possible, multiply the three diameters by 0.52 according to the ellipsoid formula. Data on the volume of the entire gland and adenoma are clinically essential for therapeutic and surgical workup purposes.

Orientation of the ultrasound images The ultrasound probe always appears at the bottom of the image. In transverse scans: the patient's right side is conventionally on the left side of the image (as also in CT and MR images). In longitudinal scans: the superior/proximal part/patient's head is conventionally on the left side (as in abdominal ultrasound imaging) and the distal part on the right side.

Documenting the findings

1. Date and place where the investigation was performed
2. Patient data (including birth date)
3. Mention of clinical history and diagnostic query
4. Value of the last total PSA blood test
5. Outcome of rectal exploration that should always be done before the investigation
6. Comparison with previous examinations, if available

Both the images and findings must be easy to read by other operators and at later dates. The findings must therefore be reported as unambiguously as possible.

In cases of any diagnostic doubt, this must be pointed out, indicating possible hypotheses and suggesting any further instrumental investigations that may help to solve any doubts.

59.4.2.2 Terminology

1. Hypoechogenic pars adenomatosa, as compared to pars peripherica of the prostate
2. Identification of medial lobe and its size and relationships with the bladder floor
3. Presence of calcifications (diameter ≥3 mm) that appear hyperechogenic with a posterior shadow (possibly showing signs of previous inflammation)
4. Presence of focal hyperechogenic areas with no posterior shadow (diameter ≥3 mm) (possibly showing signs of previous inflammation)
5. Presence of abscesses of hypo-/anechogenic areas (diameter ≥ 3 mm) that appear prevalently with a fluid anechogenic or dyshomogeneous component, possibly showing inflammation processes in active phase. Anechogenic/echogenic areas of inflamed abscesses [Table 59.2]
6. In a picture of cervico-ureteral obstruction due to prostatic hypertrophy causing severe detrusor impairment, any presence of bladder stones [Table 59.1]
7. Dilation/cysts of the ejaculatory ducts
8. Perviousness and funneling of the cervical or anastomotic region in surgical scars

Table 59.2 Definition of ultrasound characteristics of different disease pictures

Disease picture	Morphology	Echogenicity	Vascularization	Margins	Peculiarities	Differential diagnosis
Prostatic hypertrophy	Increased size due especially to enlarged pars adenomatosa	Showing pars peripherica separate from pars adenomatosa, thanks to an evident cleavage plane and different echogenicity (pars adenomatosa is hypoechogenic and dyshomogeneous as compared to pars peripherica)	No variation	Free	Shows pars peripherica separate from pars adenomatosa, thanks to a cleavage plane and different echogenicity (pars adenomatosa is more hypoechogenic than pars peripherica) There may be nodular oval or rounded areas, with distinct margins, and an isoechogenic appearance to the surrounding parenchyma, expressing prostatic hyperplasia intra-adenomatous areas or focal prostatitis areas	Abscess areas, in very hypoechogenic images Calcification areas, in very hyperechogenic images Tumoral areas (possible only with biopsy)
Acute prostatitis	Increased gland size	Less than normal	Increased Doppler signal, correlated to increased vascularization due to inflammatory processes	Normally free, sometimes blurred in cases of subcapsular abscess and direct involvement of the margins	In cases of abscess, this will show distinct margins and a highly hypo-/anechogenic content. Hyperechogenic lesions may be present within the abscess area, showing an irregular morphology demonstrating partial colliquation of such abscesses	Neoplasia, especially in cases of suspected abscess colliquation

Disease picture	Morphology	Echogenicity	Vascularization	Margins	Peculiarities	Differential diagnosis
Chronic prostatitis	Increased size or no change	Tendency to be increased, in cases with calcifications as inflammatory outcomes	Variable	Free	In cases of inveterate chronic prostatitis, there may be a dyshomogeneous appearance, with alternating hypo-isoechogenic and hyperechogenic areas	Neoplasia, especially in cases of granulomatous prostatitis observed in subjects with a history of endovesical chemo-immunoprophylaxis with BCG

59.4.2.3 Indications

1. To assess the size and volume of the gland for medical/surgical workup, regardless of the type of treatment or underlying disease
2. Prostatic biopsy guidance
3. Suspected prostatitis and/or prostatic abscess
4. To examine congenital anomalies
5. In infertility of the couple (morphological study of the seminal tracts)
6. Study of the bladder neck
   - Functional diseases of the bladder neck (sclerosis, iatrogenic stenosis, or ndd)
   - Neurological bladder
   - Outcome of surgery of the cervico-prostatic region (prostatic trans-vesical adenomectomy, endoscopic resection or enucleation of prostatic adenoma, endoscopic incision of the bladder neck)
   - Identification and examination of cysts of the bladder neck or third prostatic lobe
7. Postoperative controls (post-disobstructive surgery or radical prostatectomy)
8. Posttreatment controls for prostatic tumors (radiotherapy, HIFU, cryotherapy)

59.4.2.4 Essential Parameters That Must Be Specified in Final Report

For All Types of Report

Preliminarily, transrectal exploration must be performed, indicating the presence, size (*X*2–3), surface, consistency, margins, presence or absence of a medial groove, any nodules, their characteristics and localization, and tenderness or pain on palpation of the gland.

Prostate

1. Presence or absence of the prostate
2. Orthotopic or heterotopic site
3. Symmetry
4. Size/volume of the gland (latero-lateral, anteroposterior, and cranio-caudal, to be multiplied by 0.52, according to the ellipsoid formula, if the device does not make an automatic calculation)
5. Size/volume of the transition zone/adenoma
6. Presence or absence of a third lobe (if present, volume and/or measurements of protrusion into the bladder)
7. Presence and size of calcifications (diameter ≥3 mm) [Table 59.1]
8. Presence and size of abscesses/cysts (diameter ≥3 mm)
9. Presence and size of intraprostatic cysts or bladder neck cysts (diameter ≥3 mm)
10. Echostructure of the peripheral portion
11. Integrity of the prostatic capsule
12. Presence of the ureters and any dilation or anomalous outlet
13. Any pain elicited during the investigation [Table 59.2]

59.4.2.5 Addendum in Particular Cases

Presence of the deferens and any dilation

Urethra

Any lesions evident at ultrasound. Morphology and function of the internal urethral sphincter (only in cases of ultrasound performed for functional purposes)

Seminal Vesicles

1. Presence or absence
2. Site
3. Symmetry
4. Morphology
5. Any dilation (>12 mm in anteroposterior site)

Bladder

1. Morphology of walls
2. Morphology of content
3. Presence of vegetation and description
4. Presence of stones

Prostatic Biopsy Guidance

1. In cases of suspected tumor areas, describe:
   - Site
   - Size
   - Morphology

- Ultrasound appearance
- Margins
- Relations of lesion with the capsule, bladder neck, and seminal vesicles in cases of basal nodules with extracapsular extension

  If several nodules are present, each must be detailed as described above.

2. In cases of multiple prostatic biopsy sampling, indicate:
   - Type of patient preparation
   - Antibiotic prophylaxis administered
   - Results of preliminary rectal exploration (and any agreement between increased consistency areas at palpation and suspicious ultrasound images)
   - Type of anesthesia (site, drug, and dosage)
   - Number of samples, specifying the scheme adopted
   - Course of procedure
   - Indications for patient care in days after the maneuver
   - Any home antibiotic therapy

Assessment of Congenital Anomalies

In particular, apart from studying alterations of the course of the juxtavesical ureters, transrectal prostatic ultrasound is able to demonstrate intraprostatic cysts. Cystic lesions appear as round or oval, with distinct margins and asonic content. The definition of the site is particularly important, namely:

1. Vesical
2. Medial posterior: mullerian/prostatic utricle
3. Paramedial/lateral: ductal dilatation/cysts of the ejaculatory duct
4. Due to retention

Morphologic Study of the Seminal Tract

Ejaculatory ducts:

1. Presence or absence
2. Presence or absence of calcifications and any obstruction caused
3. Any dilation

Deferens ducts:

1. Presence or absence
2. Presence or absence of calcifications or lesions and any obstruction caused
3. Any dilation

Seminal vesicles:

1. Diameters (latero-lateral, anteroposterior, and cranio-caudal)
2. Any dilation
3. Any congestion
4. Anomalies with the deferens

Study of the Bladder Neck

1. Morphology
2. Symmetry
3. Any calcifications
4. Any cysts

Study of the Prostatic Loggia After Radical Prostatectomy or Other Treatments

Presence of areas suggesting disease recurrence in the perianastomotic region:

- Site
- Size
- Localization with respect to the anastomotic region and rectal wall
- Ultrasound appearance
- Margins
- Vascularization
- Presence/absence of seminal vesicle residues

The ultrasound data must necessarily be correlated with the total PSA values and clinical history, because subsequent treatments for postoperative urinary incontinence may modify the echostructure and mimic lesions (macroplastique, collagen, Bulkamid).

If biopsy samples are taken from the perianastomotic region, all suspicious areas should be sampled; this can be done under ultrasound guidance.

59.4.2.6 Preparation for the Investigation and Patient Position

The patient must undergo at least one enema two hours before the investigation, to avoid artifacts caused by fecal matter in the rectum.

Fasting is not necessary.

The patient must not urinate for at least two hours before the investigation (the bladder must be repleted).

The investigation is normally performed with the patient in lateral left decubitus. If this is impossible, it can be done in lateral right decubitus or semilithotomic position.

Facsimile of Final Report

Standard Transrectal Prostatic Ultrasound

Mention of clinical history:_____

Last total PSA value:_____

Preliminary rectal exploration shows the prostate in situ, enlarged (X), with a smooth surface, parenchymatous consistency, distinct margins, and flattened medial groove. No tenderness or pain on palpation.

The prostate, investigated with a transrectal "end-fire" ultrasound probe with variable frequency, is visible in situ and roughly triangular in shape; the size is X X mm (LL X AP X CC), for a theoretical calculated volume of about cc. A central nodular area of hyperplasia is present, with a dyshomogeneous echostructure and theoretical calculated volume of about cc.

Along the cleavage plane of the nodular hyperplasia, and in the periureteral site, calcifications are evident, likely the outcome of previous inflammatory processes.

Within the nodular hyperplasia area, there are gross calcifications as well as some anechogenic images compatible with cysts due to retention/microabscesses.

The peripheral gland shows a substantially homogeneous structure, with no signs of disease foci in course.

The seminal vesicles are orthotopic and normal in shape.

The bladder is in situ, moderately distended. No ultrasound alterations of the posterior bladder wall are apparent, insofar as the area is visible through the transrectal acoustic window. Post-voiding urinary residue is ….

Transrectal Prostatic Ultrasound to Study the Seminal Vesicles

The prostate is described as above.

No evidence of obstructive lesions of the ejaculatory ducts and deferens ducts bilaterally.

The seminal vesicles are orthotopic and normal in shape. The maximum diameters of the right seminal vesicles are X X X mm (CC × AP × LL), for a theoretical calculated volume of about cc. The maximum diameters of the left seminal vesicle are X X X mm (CC × AP × LL), for a theoretical calculated volume of about cc. Post-voiding urinary residue is cc.

Deferens present, symmetrical and not dilated.

Prostatic Ultrasound of the Perianastomotic Region After Prostatectomy

The perianastomotic region appears homogeneous/dyshomogeneous, showing areas of… in size, localized at the level of…, with… margins, vascularized, suspicious for growth processes.

59.4.2.7 Diagnostic Accuracy

The diagnostic accuracy of transrectal prostatic ultrasound varies according to the diagnostic query.

In particular, as regards assessing the size of the prostatic adenoma, the diagnostic accuracy of transrectal prostatic ultrasound is extremely high, while the risk of overestimation of the true prostatic volume and weight (later measured in the various studies on the anatomic piece) ranges between 4 and 10 %.

As regards the identification of prostatic nodules suspected of growth processes, it should be noted that 60 % of them appear hypoechogenic, 30 % isoechogenic, and 10 % hyperechogenic. Therefore, the overall diagnostic accuracy of this method alone is about 30 % (this is why in most cases prostatic biopsy sampling is done randomly, in the absence of ultrasound areas raising suspicion).

The presence of a hypoechogenic image alone is not the only criterion indicating the need for

prostatic biopsy. The criteria for mapping prostatic biopsies are clinical and based on the PSA values and trend, on rectal exploration, on the presence of risk factors, and also on the prostatic volume and ultrasound findings.

Granulomatous prostatitis (acute or chronic) can induce hypoechogenic modulations that are indistinguishable from those of neoplasia.

Finally, as regards the use of transrectal ultrasound to assess the perianastomotic region, the diagnostic accuracy of this investigation is strictly linked to the total PSA value. The positive predictive value is about 65 %, and the negative predictive value about 20 %.

For all lesions suspected to be cancerous, ultrasound alone can never replace biopsy.

59.4.2.8 Notes on Clinical Practice

- Use tissue harmonic imaging to reduce reverberation artifacts and obtain better detail.
- Indicate any difficulties encountered while performing the investigation (patient's collaboration and constitution, presence of bowel gas, presence of artifacts due to insufficient bowel cleansing), underlining any limits of the test and so its diagnostic value.
- If the prostate is larger than normal, its morphology may vary, especially in cases of prostatic hyperplasia.
- When performing ultrasound guidance for prostatic biopsy sampling, it is useful to ask the patient to void the bladder after the diagnostic phase
- The longitudinal diameter of the seminal vesicles varies according to the size of the gland and also the degree of bladder repletion.
- In cases with many gross calcifications along the cleavage plane between the pars adenomatosa and pars peripherica, in the periureteral intra-adenomatous site, the shadow created by the calcifications may make ultrasound exploration of the bladder or pars peripherica difficult.

59.4.2.9 The Role of Eco-Color Doppler

Color Doppler and power Doppler are generally used to identify neovascularization foci, possibly expressing abscesses (vascularization absent in the center) or tumors.

59.4.2.10 New Technologies

The limited sensitivity and specificity of gray scale ultrasound in transrectal prostatic ultrasound have led to the adoption of new technologies based on the different vascular pattern identifiable in neoplastic foci and hence on Doppler techniques. The use of 3D ultrasound and histoscanning seems to be able to reduce the overall number of cores necessary, contributing to a better definition of the target, but such investigations should only be considered in clinical studies.

The Use of Contrast Medium

Recent studies have not reported any increased sensitivity in the detection rate of prostatic tumors by contrast-enhanced ultrasound (CEUS), as compared to extensive mapping.

Elastosonography

The use of elastosonography increases the detection rate by about 20 % as compared to traditional ultrasound, ultimately leading to a reduction in the number of necessary cores.

However, operator experience and the degree of pressure exerted on the tissues strongly limit large-scale use of this technique.

3D Ultrasound

Thanks to the inclusion of the coronal plane, 3D ultrasound provides information helping to assess the seminal vesicles and ejaculatory ducts, as well as offering a better detection rate of prostatic tumors, according to some studies.

59.4.2.11 Devices and Transducers Used

Real-time endocavitary transducer (transrectal) with a frequency ≥ 6 MHz (or anyway high)

High frequency is used because the prostate is superficial as compared to the probe plane (internal rectal wall):

- A linear monoplanar probe: for prostate sections along the longitudinal plane

- A convex-linear or biconvex biplanar probe: associates transverse and longitudinal scanning, through two orthogonal convex probes
- A variable frequency probe (end-fire): allows transverse, longitudinal, and oblique scanning

59.5 Ultrasound of the Scrotum

59.5.1 Indications

1. To evaluate the acute scrotum: testicular trauma, ischemia, suspected torsion, and infectious or inflammatory diseases
2. To assess palpable masses in the inguinal or scrotal site
3. To assess any asymmetry and increased volume of the scrotum
4. To assess a possible scrotal hernia
5. For diagnosis and staging of varicocele
6. To evaluate male infertility
7. In follow-up of previous lesions shown at ultrasound
8. To assess cryptorchidism
9. To search for an occult primitive tumor in a patient with germinal tumor metastases
10. In follow-up of patients with a primitive testicular tumor, lymphoma, or leukemia
11. In follow-up after testicular surgery
12. In diagnostic workup for anomalies observed at other imaging studies like CT, MRI, or PET
13. To assess intersexual conditions

59.5.2 Essential Parameters in the Study of the Scrotum

1. The scrotal wall
2. The testicular volume
3. The testicular echostructure
4. The epididymis (volume and echostructure)
5. Vascularization
6. The pampiniform plexus

59.5.3 Preparation for the Investigation and Patient Position

The investigation must be performed in a darkened room, to protect the patient's privacy, and the room temperature must not be cold because this could elicit the cremasteric reflex, in a more accentuated form in children that could cause the testicle to rise up.

Initially, the patient should lie supine with a scrotal support to facilitate exposure. The penis will be positioned superiorly or supero-laterally.

After examining the content of the scrotal sac in clinostatic position, the investigation should be continued with the patient in orthostatic position, making a careful evaluation of the venous flow of the spermatic cords. B-mode study will already reveal the presence of varicose veins, but it is convenient to go on immediately to color Doppler study to examine the characteristic patterns of varicocele.

59.5.4 Notes on Clinical Practice and Indications for Echo-Color Doppler

The first task in scrotal ultrasound is to make a *correct calculation of the testicular volume*. The formula most commonly used today is the ellipsoid (*volume in ml = product of the three diameters* (*in cm*) × *0.52*).

The testicles must be assessed on two planes: longitudinal and transverse. The transverse plane is focused on the superior medial and inferior testicular portions, and the longitudinal plane on the central portion, as also medial and lateral. Once the whole testicle has been measured, the investigation continues with the epididymis (head, body, and tail). The testicular measurements and echogenicity should then be compared with those of the contralateral testicle.

Color Doppler can be helpful, especially in cases of acute pain. In this case, too, both

longitudinal and transverse scanning are useful, as well as comparison of the two testicles. The Doppler parameters must be set to analyze slow flow. Should it be impossible to visualize the flow, power Doppler can be employed to highlight the images.

Color Doppler is essential in the diagnosis and staging of varicocele.

59.5.5 Devices and Transducers

The investigation is conducted using a real-time scanner, preferably with a linear transducer. The transducer is set to scanning mode at the highest frequency of the device. In the latest ultrasound devices, the frequency may range from 8 to 15 MHz or more. The transducer length may range between 4 and 8 cm. Resolution must be sufficient to discriminate different ultrasound characteristics in any lesions observed. If there is a markedly increased volume of the scrotum, the use of lower frequencies is indicated to make a correct study of the gonads; alternatively, it is possible to rely on the trapezoid assessment available in more modern ultrasound devices.

The Doppler frequencies must be as high as possible to optimize the resolution and show the blood flow. Modern devices offer a frequency range of 5–10 MHz.

59.5.6 Important Notes in Clinical Practice

Table 59.3 Lesions of the scrotal wall

	Cause	Ultrasound appearance	Second-level investigations
Noninflammatory	Heart failure Idiopathic lymphedema Lymphatic and venous obstruction Epidermoid cysts	Thickened scrotal wall, with alternating hyperechogenic and hypoechogenic layers (onion-like appearance)	
Inflammatory	Cellulitis	Thickening of the scrotal wall and presence of hypoechogenic areas, showing increased blood flow	
	Fournier gangrene	Thickening of the scrotal wall with signs of inflammation; gas may be visible as numerous hyperechogenic foci	CT, MRI

Table 59.4 Inguinal or scrotal swelling

	Ultrasound appearance	Second-level investigations
Inguinal hernia	Shows bowel wall, presence of peristalsis, and hyperechogenic area if omentum present. Distinguish direct or indirect if inferior epigastric art. Shown by Doppler. Presence of stricture (SS 90 %, SP 93 %)	CT
Hydrocele	Anechogenic fluid collection surrounding the testicular parenchyma	
Hematocele	Appearance similar to cysts, with septs and loculi	
Pyocele		

Table 59.5 Spermatic cord

	Ultrasound appearance	Second-level investigations
Varicocele	Multiple tortuous vascular structures, hypoechogenic with variable diameters exceeding 2 mm Color Doppler set for low flow to show a characteristic flow pattern, with phase alterations and retrograde filling during Valsalva (SS and SP 100 %)	Spermiogram
Tumors of spermatic cord	Lipoma, sarcoma, and rhabdomyosarcoma have the same nonspecific ultrasound appearance	CT, and better MRI, to enhance visualization of the tissues

Table 59.6 Epididymis

	Ultrasound appearance
Orchi-epididymitis	Epididymis enlarged and hyperechogenic or hypoechogenic. A reactive hydrocele may be present, and if there is testicular involvement, the didymis will be enlarged, with a dyshomogeneous ultrasound appearance. The Doppler will show hyperemia and increased blood flow (peak systolic rate > 15 cm/s)
Chronic epididymitis	Epididymis enlarged and increased echogenicity and possibly calcifications
Epididymis masses	Spermatocele and epididymis cysts are shown as hypoechogenic lesions that may be as much as 1–2 cm in diameter, with acoustic enhancement in the posterior wall. They may contain protein fluid or spermatozoa with a low echogenicity
Adenomatoid tumors can be hypoechogenic, isoechogenic, or hyperechogenic	

Table 59.7 Testicle

	Ultrasound appearance	Second-level investigations
Testicular torsion	Absence of intratesticular blood flow (SS 86 %, SP 100 %) Increased testicular volume and reduced echogenicity (4–6 h) After 24 h, dyshomogeneous echostructure due to vessel congestion, hemorrhage, and infarction Spiral appearance under the torsion point that appears as a homogeneous extratesticular oval or rounded mass, with or without blood flow	
Orchitis	Hyperemia and dyshomogeneous ultrasound appearance Increased or enhanced intratesticular blood flow	
Testicular microlithiasis	Multiple echogenic foci with no shadow (at least five microliths per field)	
Benign lesions	Cysts of tunica albuginea: may be uniloculated or multiloculated, with calcifications	
	Simple cysts: may be multiple or solitary, generally adjacent to the mediastinum. They appear anechogenic and with no wall	
	Epidermoid cysts: ultrasound appearance of a halo with a central area and increased echogenicity or else as a mass defined by an echogenic circle or else a classic "onion" appearance. The Doppler will not show blood flow	
	Ectasia of rete testis: visible at US as fluid-filled tubular structures. Possible presence of cysts	
	Intratesticular varicocele: multiple, anechogenic tortuous tubular structures. Blood flow shows characteristic reflux during Valsalva	
Malignant lesions	Seminomatous tumors: homogeneous hypoechogenic lesions, with uniform smooth margins. Very often the tumor occupies much of the parenchyma	Tumoral markers
	Non-seminomatous tumors: may have very variable US appearance; dyshomogeneous echostructure (71 %), irregular or with poorly defined margins (45 %), echogenic foci (35 %), and a cystic component (61 %)	Tumoral markers
	Lymphomas: testicles homogeneously hypoechogenic or with multifocal hypoechogenic lesions of various diameters. The didymis, in diffuse forms, appears hypervascularized (d.d. with orchitis)	
Testicular trauma	Rupture or interruption of the albuginea, irregular echostructure with poorly defined margins. Color-power Doppler can help to show the vascular pattern of the parenchyma, capsule	MRI

59.5.7 Facsimile of Findings Report

59.5.7.1 Scrotal Echo-Color Doppler

Toshiba Aplio: *examination performed with linear probe 11.5 MHz*

History: *Previous right orchiectomy for embryonal testicular K. Known left varicocele*

Didymi: *left didymis in situ with normal echostructure and volume*, *markedly hyopotrophic approx. 3.5 cc* (*ellipsoid formula calc. 0.52 x 3 diameters*)

Epididymi: *normal echostructure and size*; *small cyst of head of left epididymis. Small scrotolite present*

Vascularization of didymus-epididymis: *within normal limits*

Left pampiniform plexus: *severe peritesticular ectasia with vessel diameter exceeding 4 mm*

Color Doppler investigation of pampiniform plexus in orthostatic position

Left pampiniform plexus: basal reflux little modified by functional maneuvers

Diagnostic conclusion: left varicocele, grade V according to Sarteschi classification

Images to be included (not all are always indispensable, depending on the clinical picture)

1. One image of each testicle and epididymis in transverse scan
2. One image of each testicle and epididymis in longitudinal scan
3. One image of both testicles and epididymi for direct comparison
4. One image of the prostate in longitudinal scan showing the bladder
5. One or more images of the pampiniform plexus at rest and under Valsalva
6. One or more images of any palpable anomalies

59.5.8 Reference Texts

- American Institute of Ultrasound in Medicine; American College of Radiology; Society of Radiologists in Ultrasound. AIUM practice guideline for the performance of scrotal ultrasound examinations. J Ultrasound Med. 2011; 30 (1): 151–5
- Practice Guideline for the Performance of an Ultrasound Examination in the Practice of Urology http://www.auanet.org/content/education-and-meetings/aium-ultrasound-guidelines.cfm

59.6 Ultrasound of the Penis

Penile US is an essential tool in urological clinical practice both as an investigation in itself and integrated with color Doppler of the penile vascularization.

59.6.1 Indications

Indications for penile US:

1. Erectile dysfunction
2. Priapism
3. Penile fibrosis and plastic induratio penis
4. Penile or urethral anomalies observed at physical examination
5. Neoplasia of the penis
6. Penile trauma
7. Thrombosis of the dorsal vein
8. Urethral disorders (cysts, diverticuli, stenosis)
9. Stones or foreign bodies in the urethra or penis

59.6.2 Technique of Investigation

At least two scans must be performed: transverse and longitudinal. The probe is positioned dorsally or centrally to obtain a better visualization of the corpi cavernosi, the intercavernous septum, the tunica albuginea and Buck's, and the urethra.

The transverse scan must be done in the proximal, medial, and distal portions of the penis. The longitudinal scan must be done on the two corpi cavernosi, visualizing the cavernosum artery. In addition, to study the crural

portion of the corpi cavernosi, the transducer is placed perineally. Size, echogenicity (hyper, hypo, iso), and symmetry of the corpi cavernosi must be described and documented with appropriate images.

Any alterations of the tuniche, either echogenic or structural, must be documented by accurate measurements both on longitudinal and transverse scans. Any palpable alteration or penile anomaly must be closely studied directly on the involved zone and documented by appropriate images.

Assessment of the vascular integrity is done by integrating color Doppler.

To study the urethra, hydrosoluble gel is injected through a catheter positioned at the level of the navicular fossa; longitudinal scans are done to study any alterations of the urethral lumen.

59.6.3 Specific Devices

Penile US is done in real-time B-mode scanning, using a linear probe with a frequency of 7.5/10 MHz and more.

59.6.4 Penile Echo-Color Doppler

Penile echo-color Doppler is generally performed in the following cases:

- Erectile dysfunction (after intracavernous injection (FIC) of PGE1)
- La Peyronie's disease
- To assess penile morphology and vascularization after trauma
- In cases of blood collection or infection

59.6.4.1 Methodology

Assessment Pre-FIC

- The investigation must be performed in calm surroundings avoiding outside interruptions. Detailed explanation of the different phases must be given, as well as of the possible complications, obtaining written informed consent.
- The basal study must include longitudinal and transverse scans to make an accurate study of the corpora cavernosa, corpus spongiosum, and intercavernous septum and morphology of the cavernous arteries, the gland, and the urethra. The cavernous arteries are shown as parallel lines, fine and echogenic, and any anatomical variants, even lacking clinical significance (e.g., duplication of the cavernous artery must be documented).

FIC

- Single intracavernous injection of PGE1 in basal cavernous site, at variable doses (2.5 mcg in young, psychogenic men with a high risk of priapism due to correlated disease) and if necessary redosing. Remember that a state of anxiety in the patient could delay the effect of the drug.

POST FIC Assessment

- Spectral Doppler must be done at 0, 5, 10, 15, 20, 25, and 30 min after FIC at the level of the proximal third of the cavernous arteries and/or in the crural site.
- Measurement of peak systolic velocity (PSV), telediastolic velocity (TDV), and resistance index (RI) using an ideal spectral angle of 60°.
- Manual or visual stimulation is not usually necessary to obtain an adequate erection.
- If the flowmetry result is considered adequate, the investigation can be interrupted before the measurements at 25 and 30 min.
- After flowmetry it is useful to make a morphological study of the penile vascularization by power imaging, to assess the microcirculation, describing whether the helical branches are visible or not, and their angle of incidence on the cavernous artery (normally >90°). This method is also used to visualize traumatic lesions.
- The dynamic phase after FIC is also useful to study Peyronie's disease plaques, both in B-mode and color-power imaging, as well as fibrosis, structural variations, and any zones of venous leakage around the plaques.

- Describe the degree of erectile response in terms of tumescence and rigidity at 20/30 min after FIC.

Diagnostic Criteria

- B-mode: Detailed description of the anatomical symmetry of the corpi cavernosi, fibrous septum, any plaques or calcifications of the intracavernous zone or tuniche, and any hypoechogenic lesions.
- Arterial compartment: Any increased diameter post FIC, intravascular flow. Values of PSV >35 cm/s are considered normal in the literature, between 25 and 35 cm/s "borderline" that should be integrated with the degree of erectile response; values < 25 cm/s are considered pathologic.
- Venous compartment: With an increased intracavernous pressure and so increased PSV, there is a decrease in TDV that may become negative with inversion of the diastolic wave, a sign of integrity of the veno-occlusive mechanism. A persistence of TDV values > 5–7 cm/s throughout all the phases of the test indicates a deficit of the veno-occlusive mechanism.
- It is important always to integrate flowmetry data with the degree of erectile response to FIC because a poor rigidity (low dosage of PGE1, a state of anxiety) and hence a minor arterial inflow will limit the degree of response of the venous compartment and hence the sensitivity and specificity of the test.
- In the findings, note the patient's psychoemotional approach to the test.

After the Test

- Ascertain complete detumescence before the patient leaves, informing him of the possibility of a prolonged erection/priapism and the management of this complication, as well as how to obtain further assistance if necessary.
- Produce an accurate report with appropriate images both of the flowmetry and the morphology.

59.6.4.2 Tools

High-frequency 7.5 MHz or more linear transducer, US device equipped with color-power spectral Doppler, and high Doppler frequencies are advisable (higher than 10 MHz) because they provide optimal resolution and facilitate the examination of intravasal flow.

59.6.4.3 Facsimile of Final Report

Test performed with linear probe (7.5/10) MHz.

Test performed in basal conditions and after drug infusion of … mcg of prostaglandins (PGE1); patient gave written informed consent to the procedure.

Normal conformation of the corpi cavernosi that appear symmetrical and of the corpus spongiosum of the urethra; otherwise describe any alterations/irregularities of the tunica and septum, such as hyper-reflection, hyperechogenicity, and any images suggesting induratio penis plastica.

Cavernous arteries present, with a twisted course, pulsating.

After FIC, increased volume of the corpi cavernosi with dilation and straightening of the cavernous arteries that appear pulsating/non-pulsating.

Erectile response to FIC at ….minutes (poor/fair/good/excellent) for tumescence and rigidity with/without deviation of the penile axis (in cases of deviation, describe whether it is dorsal, ventral, or lateral, and the degree)

Grade of EAS (erection assessment scale): 1–5 (no erectile response/full rigidity)

Flowmetry study performed in crural site: measurement of the systo-diastolic velocities with spectral Doppler analysis at 5, 10, 15, 20, 25, and 30 min after FIC.

PSV (peak systolic velocity) equal to ….cm/s on left and …cm/s on right at …minutes after FIC showing normal/reduced arterial inflow.

TDV (telediastolic velocity) …cm/s with/without progressive reduction or with/without negativization of the diastolic wave at 20/30 min after FIC, showing integrity/deficit of the veno-occlusive mechanism.

IR </=/> 1

Phase 3 obtained at …minutes

Phase 4 obtained/not obtained at ….minutes

Morphological study performed with color-power Doppler:

Cavernous arteries morphologically normal, well distended, and straightened.

Good/fair/poor visualization of the helicine branches by 1°, 2°, and 3° presenting an angle of incidence </> 90°, demonstrating integrity/deficit of the microcirculation

(In cases of IPP) presence/absence of periplaque venous leakage

At ….. minutes after FIC, there is/is no progressive penile detumescence.

Psychoemotional attitude to test: poor/fair/good

Images to include (not all are indispensable, depending on clinical picture)

1. Two basic images
2. Six Doppler spectral images with relative flowmetry values
3. Two images showing microcirculation

References

1. Bevelacqua JJ (2010) Practical and effective ALARA. Health Phys 98 Suppl 2:S39–47
2. Eeg KR, Khoury AE, Halachmi S, Braga LH, Farhat WA, Bägli DJ, Pippi Salle JL, Lorenzo AJ (2009) Single center experience with application of the ALARA concept to serial imaging studies after blunt renal trauma in children–is ultrasound enough? J Urol 181(4):1834–1840; discussion 1840
3. Rutala WA. Disinfection and Sterilization in Healthcare: new CDC guidelines, 2008
4. Velázquez-Estades LJ, Wanger A, Kellaway J, Hardten DR, Prager TC (2005) Microbial contamination of immersion biometry ultrasound equipment. Ophthalmology 112(5):e13–e18
5. Giornale Italiano di Ecografia (SIUMB Editore) I.R. al vol.8-N4. December 2005: Documento SIUMB per le Linee Guida in Ecografia
6. AUA (2011) AIUM practice guideline for the performance of an: ultrasound examination in the practice of urology, www.aium.org
7. Linee guida SIEOG Società Italiana di Ecografia Ostetrico Ginecologica, Edition 2010

Ultrasound Scanning of the Kidney

8. Griffiths GJ, Cartwright G, McLachlan MSF (1974) Estimation of renal size from radiographs: is the effect worthwhile? Clin Radiol 26:249–256
9. Dure-Smith P, McArdle GH (1972) Tomography during excretory urography. Technical aspects. Br J Radiol 45:896–901
10. De Sanctis JT, Connoly SA, Bramson RT (1998) Effect of patient position on sonographically measured renal length in neonates, infants, and children. Am J Roentgenol 170:1381–1383
11. Jones TB, Riddick LR, Harpen J et al (1983) Ultrasonographic determination of renal mass and renal volume. J Ultrasound Med 2:151–154
12. Hricak H, Lieto RP (1983) Sonographic determination of renal volume. Radiology 148:311–312
13. Partik BL, Stadler A, Schamp S et al (2002) 3D versus 2D ultrasound: accuracy of volume measurement in human cadaver kidneys. Invest Radiol 37:489–495
14. Brandt TD, Neiman HL, Dragowski MJ et al (1982) Ultrasound assessment of normal renal dimension. J Ultrasound Med 1:49–52
15. Emamian SA, Nielsen MB, Pedersen JF (1995) Intraobserver and interobserver variations in sonographic measurements of kidney size in adult volunteers. A comparison of linear measurements and volumetric estimates. Acta Radiol 36:399–401
16. Fiorini F, Barozzi L (2007) The role of ultrasound in the study of medical nephropathy. J Ultrasound 10(4):161–167
17. Granata A, Bigi MC, Andrulli S, Logias F, Scuderi R, Fiorini F (2010) L'analisi del segnale Doppler. In: Granata A, Fiorini F, D'Amelio A, Logias F, Andrulli S. L'ecocolorDoppler nella pratica nefrologica. Forum Service, Italy, 1:49–61
18. Piscaglia F et al (2012) The EFSUMB guidelines and recommendations on the clinical practice of contrast enhanced ultrasound (CEUS): update 2011 on non-hepatic applications. Ultraschall Med 33(1):5–7

Ultrasound of the Bladder

19. Athanasiou S et al (1999) Imaging the urethral sphincter with three-dimensional ultrasound. Obstet Gynecol 94(2):295–301
20. Blatt A et al (2009) The importance of bladder wall thickness in the assessment of overactive bladder. Curr Bladder Dysfunction Rep 4:220–224
21. Bright E, Oelke M, Tubaro A, Abrams P (2010) Ultrasound estimated bladder weight and measurement of bladder wall thickness—Useful noninvasive methods for assessing the lower urinary tract? J Urol 184:1847–1854
22. Costantini S et al (2006) Ultrasound imaging of the female perineum: the effect of vaginal delivery on pelvic floor dynamics. Ultrasound Obstet Gynecol 27(2):183–187
23. Costantini S et al (2005) Perineal ultrasound evaluation of the urethrovesical junction angle and urethral mobility in nulliparous women and women following

vaginal delivery. Int Urogynecol J Pelvic Floor Dysfunct 16(6):455–459
24. Granados Loarca EA et al (1999) The usefulness of perineal ultrasound in urinary incontinence in women. Arch Esp Urol 52(7):778–782
25. Kanu GB (2010) Ultrasonography of the urinary bladder. J Med Ultrasound 18(3):105–114
26. Masata J et al (2000) Ultrasonography of the funneling of the urethra. Ceska Gynekol 65(2):87–90
27. Martan A et al (2000) The effect of bladder filling on changes in ultrasonography parameters of the lower urinary tract in women with urinary stress incontinence. Ceska Gynekol 65(1):10–13
28. Minardi D et al (2007) Correlation between urodynamics and perineal ultrasound in female patients with urinary incontinence. Neurol Urodyn 26:176–182
29. Peschers UM et al (2001) Bladder neck mobility in continent nulliparous women. BJOG 108(3):320–324
30. Reilly ETC et al (2002) Prevention of postpartum stress incontinence in primigravidae with increased bladder neck mobility: a randomised controlled trial of antenatal pelvic floor exercises. Br J Obstet Gynecol 109:68–76
31. Robinson D (2002) Cardozo L Can ultrasound replace ambulatory urodynamics when investigating women with irritative urinary symptoms? BJOG 109(2):145–148
32. Schaer GN et al (1996) Perineal ultrasound: determination of reliable examination procedures. Ultrasound Obstet Gynecol 7(5):347–352
33. Seung HK (2007) Ultrasound of the urinary bladder. Revisited J Med Ultrasound 15(2):77–90
34. Siracusano S et al (2001) Colour Doppler ultrasonography of female urethral vascularization in normal young volunteers: a preliminary report. BJU Int 88(4):378–381
35. Strasser H et al (2000) Anatomic and functional studies of the male and female urethral sphincter. World J Urol 18(5):324–329
36. Tunn R et al (2005) Update recommendations on ultrasonography in urogynecology. Int Urogynecol J 16:236–241
37. Umek WH et al (2001) Three-dimensional ultrasound of the female urethra: comparing transvaginal and transrectal scanning. Ultrasound Obstet Gynecol 17(5):425–430
38. Piscaglia F et al (2012) The EFSUMB guidelines and recommendations on the clinical practice of contrast enhanced ultrasound (CEUS): update 2011 on non-hepatic applications. Ultraschall Med 33(1):5–7

Prostate and Seminal Vesicles:Prostatic Ultrasound Scanning with the Suprapubic Technique

39. Tokgöz Ö, Tokgöz H, Ünal I, Delibaş U, Yıldız S, Voyvoda N, Erdem Z (2012) Diagnostic values of detrusor wall thickness, postvoid residual urine, and prostate volume to evaluate lower urinary tract symptoms in men. Diagn Interv Radiol 18(3):277–281
40. Società Italiana di Radiologia Medica –Linee guida della diagnostica per immagini 2009. http://www.sirm.org/it/documenti/cat_view/66-linee-guida.html
41. American College of Radiology –Ultrasound Guidelines. http://www.acr.org/Quality-Safety/Standards-Guidelines/Practice-Guidelines-byModality/Ultrasound
42. European Association of Urology – 2012 Guidelines. http://www.uroweb.org/guidelines/online-guidelines
43. American Association of Urology Guidelines. http://www.auanet.org/content/clinical-practice-guidelines/clinical-guidelines.cfm
44. Stravodimos KG, Petrolekas A, Kapetanakis T, Vourekas S, Koritsiadis G, Adamakis I, Mitropoulos D, Constantinides C (2009) TRUS versus transabdominal ultrasound as a predictor of enucleated adenoma weight in patients with BPH: a tool for standard preoperative work-up? Int Urol Nephrol 41(4):767–771
45. Strasser H, Janetschek G, Reissigl A, Bartsch G (1996) Prostate zones in three dimensional transrectal ultrasound. Urology 47:485–490
46. Aarnick RG, Huynen AL, Giesen RJ, De la Rosette JJ, Debruyne FM, Wijkstra H (1995) Automated prostate Volume determination with double ultrasonographic imaging. J Urol 153:1549–1554
47. Tong S, Downey DB, Cardinal HN, Fenster A (1996) A three dimensional ultrasound prostate imaging system. Ultrasound Med Biol 22(6):735–746

Prostate and Seminal Vesicles: Transrectal Prostatic Ultrasound

48. Società Italiana di Radiologia Medica –Linee guida della diagnostica per immagini 2009. http://www.sirm.org/it/documenti/cat_view/66-linee-guida.html
49. American College of Radiology –Ultrasound Guidelines. http://www.acr.org/Quality-Safety/Standards-Guidelines/Practice-Guidelines-byModality/Ultrasound
50. European Association of Urology – 2012 Guidelines. http://www.uroweb.org/guidelines/online-guidelines
51. American Association of Urology Guidelines. http://www.auanet.org/content/clinical-practice-guidelines/clinical-guidelines.cfm
52. Stravodimos KG, Petrolekas A, Kapetanakis T, Vourekas S, Koritsiadis G, Adamakis I, Mitropoulos D, Constantinides C (2009) TRUS versus transabdominal ultrasound as a predictor of enucleated adenoma weight in patients with BPH: a tool for standard preoperative work-up? Int Urol Nephrol 41(4):767–771
53. Giubilei G, Ponchietti R, Biscioni S, Fanfani A, Ciatto S, DI Loro F, Gavazzi A, Mondaini N (2005) Accuracy of prostate volume measurements using

transrectal multiplanar three dimensional sonography. Int J Urol 12(10):936–938
54. Pierangeli T, Muraro GB (2002) Role of 3D-ultrasonography in the assessment of transitional zone PSA. Arch Ital Urol Androl 74:282–284
55. Strasser H, Janetschek G, Reissigl A, Bartsch G (1996) Prostrate zones in three dimensional transrectal ultrasound. Urology 47:485–490
56. Aarnick RG, Huynen AL, Giesen RJ, De la Rosette JJ, Debruyne FM, Wijkstra H (1995) Automated prostate Volume determination with double ultrasonographic imaging. J Urol 153:1549–1554
57. Tong S, Downey DB, Cardinal HN, Fenster A (1996) A three-dimensional ultrasound prostate imaging system. Ultrasound Med Biol 22(6):735–746
58. Watanabe H, Igari D, Tanahashi Y, Harada K, Saitoh M (1974) Measurement of size and weight of the prostate by means of transrectal ultrasonotomography. Tohoku J Exp Med 114:277–285
59. Aarnink RG, De La Rosette JMCH, Debruyne FMJ, Wijkstra H (1996) Reproducibility of prostate volume measurements from transrectal ultrasonography by an automated and a manual technique. Br J Urol 78:219–223
60. Purohit RS, Shinohara K, Meng MV, Carroll PR (2003) Imaging clinically localized prostate cancer. Urol Clin North Am 30:279–293
61. Kijvikai K (2009) Digital rectal examination, serum prostatic specific antigen or transrectal ultrasonography: the best tool to guide the treatment of men with benign prostatic hyperplasia. Curr Opin Urol 19(1):44–48
62. Shinbo H, Kurita Y (2011) Application of ultrasonography and the resistive index for evaluating bladder outlet obstruction in patients with benign prostatic hyperplasia. Curr Urol Rep 12(4):255–260
63. de la Rosette J, Alivizatos G, Madersbacher S, Rioja Sanz C, Nordling J, Emberton M, Gravas S, Michel MC, Oelke M (2007) EAU2007 guidelines on benign prostatic hyperplasia. Eur Assoc Urol 5–59
64. Grayhack JT, McVary KT, Kozlowski JM (2002) Benign prostatic hyperplasia. In: Gillenwater JY, Grayhack JT, Howards SS, Mitchell ME (eds) Adult and pediatric urology, 4th edn. LWW, Philadelphia, pp 1401–1470
65. Kaplan SA, McConnell JD, Roehrborn CG, Meehan AG, Lee MW, Noble WR, Kusek JW, Nyberg LM Jr, Medical Therapy of Prostatic Symptoms (MTOPS) Research Group (2006) Combination therapy with doxazosin and finasteride for benign prostatic hyperplasia in patients with lower urinary tract symptoms and a baseline total prostate volume of 25 ml or greater. J Urol 175:217–220. doi:10.1016/S0022-5347(05)00041-8
66. Uchida T, Ohori M, Soh S, Sato T, Iwamura M, Ao T, Koshiba K (1999) Factors influencing morbidity in patients undergoing transurethral resection of the prostate. Urology 53:98–105. doi:10.1016/S0090-4295(98)00524-X
67. Ash D, Flynn A, Battermann J, de Reijke T, Lavagnini P, Blank L, ESTRA/EAU Urological Brachytherapy Group, EORTC Radiotherapy Group (2000) ESTRO/EAU/EORTC recommendations on permanent seed implantation for localized prostate cancer. Radiother Oncol 57:315–321. doi:10.1016/S0167-8140(00)00306-6
68. Meraj S, Nagler HM, Homel P, Shasha D, Wagner JR (2003) Radical prostatectomy: size of the prostate gland and its relationship with acute perioperative complications. Can J Urol 10:1743–1748
69. Kalish J, Cooner WH, Graham SD Jr (1994) Serum PSA adjusted for volume of transition zone (PSAT) is more accurate than PSA adjusted for total gland volume (PSAD) in detecting adenocarcinoma of the prostate. Urology 43:601–606. doi:10.1016/0090-4295(94)90170-8
70. Zlotta AR, Djavan B, Marberger M, Schulman CC (1997) Prostate specific antigen density of the transition zone: a new effective parameter for prostate cancer prediction. J Urol 157:1315–1321. doi:10.1016/S0022-5347(01)64961-9
71. Zlotta AR, Djavan B, Damoun M, Roumeguere T, Petein M, Entezari K, Marberger M, Schulman CC (1999) The importance of measuring the prostatic transition zone: an anatomical and radiological study. BJU Int 84:661–666. doi:10.1046/j.1464-410x.1999.00214.x
72. Aus G, Bergdahl S, Hugosson J, Norle'n L (1994) Volume determinations of the whole prostate and of adenomas by transrectal ultrasound in patients with clinically benign prostatic hyperplasia: correlation of resected weight, blood loss and duration of operation. Br J Urol 73:659–663. doi:10.1111/j.1464-410X.1994.tb07552.x
73. Baltaci S, Yagci C, Aksoy H, Elan AH, Go¨gu¨s O (2000) Determination of transition zone volume by transrectal ultrasound in patients with clinically benign prostatic hyperplasia: agreement with enucleated prostate adenoma weight. J Urol 164:72–75. doi:10.1016/S0022-5347(05)67452–6
74. Aarnink RG, Beerlage HP, De La Rosette JJ, Debruyne FM, Wijkstra H (1998) Transrectal ultrasound of the prostate: innovations and future applications. J Urol 159:1568–1579. doi:10.1097/00005392-199805000-00045
75. Sajadi KP, Terris MK, Hamilton RJ, Cullen J, Amling CL, Kane CJ, Presti JC Jr, Aronson WJ, Freedland SJ (2007) Body mass index, prostate weight and transrectal ultrasound prostate volume accuracy. J Urol 178:990–995. doi:10.1016/j.juro.2007.05.049
76. Matthews GJ, Motta J, Fracehia JA (1996) The accuracy of transrectal ultrasound prostate volume estimation: clinical correlations. J Clin Ultrasound 24:501–505. doi:10.1002/(SICI)1097-0096(199611/12)24:9\501::AID-JCU2[3.0.CO;2-R
77. Tewari A, Indudhara R, Shinohara K, Schalow E, Woods M, Lee R, Anderson C, Narayan P (1996) Comparison of transrectal ultrasound prostatic volume estimation with magnetic resonance imaging volume estimation and surgical specimen weight in

patients with benign prostatic hyperplasia. J Clin Ultrasound 24:169–174. doi:10.1002/(SICI)1097-0096(199605)24:4\169::AID-JCU2[3.0.CO;2-D
78. Alkan I, Turkeri L, Biren T, Cevik I, Akdas A (1996) Volume determinations by transrectal ultrasonography in patients with benign prostatic hyperplasia: correlation with removed prostate weight. Int Urol Nephrol 28:517–523. doi:10.1007/BF02550959
79. Loeb S, Han M, Roehl KA, Antenor JA, Catalona WJ, Loeb S, Han M, Roehl KA, Antenor JA, Catalona WJ (2005) Accuracy of prostate weight estimation by digital rectal examination versus transrectal ultrasonography. J Urol 173:63–65
80. Lee JS, Chung BH (2007) Transrectal ultrasound versus magnetic resonance imaging in the estimation of prostate volume as compared with radical prostatectomy specimens. Urol Int 78:323–327. doi:10.1159/000100836
81. Rahmouni A, Yang A, Tempany CM, Frenkel T, Epstein J, Walsh P, Leichner PK, Ricci C, Zerhouni E (1992) Accuracy of in vivo assessment of prostatic volume by MRI and transrectal ultrasonography. J Comput Assist Tomogr 16:935–940
82. Cabello Benavente R, Jara Rascon J, Monzo JI, Lopez Diez I, Subira Rios D, Lledo Garcia E, Herranz Amo F, Hernandez Fernandez C (2006) Volume determinations of the whole prostate and of the adenoma by transrectal ultrasound: correlation with surgical specimen. Actas Urol Esp 30:175–180
83. Bland JM, Altman DG (1986) Statistical methods for assessing agreement between two methods of clinical measurement. Lancet 1:307–310
84. Nathan MS, Seenivasagam K, Mei Q, Wickham JE, Miller RA (1996) Transrectal ultrasonography: why are estimates of prostate volume and dimension so inaccurate? Br J Urol 77:401–407
85. Galosi AB, Montironi R, Fabiani A, Lacetera V, Gallé G, Muzzonigro G (2009) Cystic lesions of the prostate gland: an ultrasound classification with pathological correlation. J Urol 181:647–657
86. Piscaglia F et al (2012) The EFSUMB guidelines and recommendations on the clinical practice of contrast enhanced ultrasound (CEUS): update 2011 on non-hepatic applications. Ultraschall Med 33(1):5–7
87. Martino P, Palazzo S, Bufo P, Garofano L, Selvaggi FP (2000) Three-dimensional digital ultrasound for early staging of prostatic adenocarcinoma. J Urol 164:456
88. Martino P, Scattoni V, Galosi AB, Consonni P, Trombetta C, Palazzo S, Maccagnano C, Liguori G, Valentino M, Battaglia M, Barozzi L (2011) Role of imaging and biopsy to assess local recurrence after definitive treatment for prostate carcinoma (surgery, radiotherapy, cryotherapy, HIFU). World J Urol 29(5):595–605

Ultrasound of the Scrotum

89. Akin EA, Khati NJ, Hill MC (2004) Ultrasound of the scrotum. Ultrasound Q 20:181–200
90. Baldisserotto M, de Souza JC, Pertence AP, Dora MD (2005) Color Doppler sonography of normal and torsed testicular appendages in children. AJR Am J Roentgenol 184:1287–1292
91. Basu S, Howlett DC (2001) High-resolution ultrasound in the evaluation of the nonacute testis. Abdom Imaging 26:425–432
92. Bhatt S, Dogra VS (2008) Role of US in testicular and scrotal trauma. Radiographics 28(6):1617–1629
93. Bertolotto M, Trombetta C (eds) (2012) Scrotal pathology, 1st edn. Springer, Berlin
94. Casalino DD, Kim R (2002) Clinical importance of a unilateral striated pattern seen on sonography of the testicle. AJR Am J Roentgenol 178:927–930
95. Dogra VS, Bhatt S (2004) Acute painful scrotum. Radiol Clin North Am 42:349–363
96. Dogra VS, Gottlieb RH, Oka M, Rubens DJ (2003) Sonography of the scrotum. Radiology 227:18–36
97. Dogra VS, Rubens DJ, Gottlieb RH, Bhatt S (2004) Torsion and beyond: new twists in spectral Doppler evaluation of the scrotum. J Ultrasound Med 23:1077–1085
98. Dogra VS, Gottlieb RH, Rubens DJ, Liao L (2001) Benign intratesticular cystic lesions: US features. Radiographics 21(1)
99. Gorman B, Carroll BA (2005) Scrotal sonography. In: Rumack CM, Wilson SR, Charboneau JW (eds) Diagnostic ultrasound, 3rd edn. CV Mosby Co, Chicago, pp 849–888
100. Hörmann M, Balassy C, Philipp MO, Pumberger W (2004) Imaging of the scrotum in children. Eur Radiol 14:974–983
101. Karmazyn B, Steinberg R, Kornreich L et al (2005) Clinical and sonographic criteria of acute scrotum in children: a retrospective study of 172 boys. Pediatr Radiol 35:302–310
102. Kim W, Rosen MA, Langer JE, Banner MP, Siegelman ES, Ramchandani P (2007) US MR imaging correlation in pathologic conditions of the scrotum. Radiographics 27(5):1239–1253
103. Mirochnik B, Bhargava P, Dighe MK, Kanth N (2012) Ultrasound evaluation of scrotal pathology. Radiol Clin North Am 50(2):317–332
104. Pavlica P, Barozzi L (2001) Imaging of the acute scrotum. Eur Radiol 11(2):220–228
105. Pearl MS, Hill MC (2007) Ultrasound of the scrotum. Semin Ultrasound CT MR 28(4):225–248
106. Philips S, Nagar A, Dighe M, Vikram R, Sunnapwar A, Prasad S (2012) Benign non-cystic scrotal tumors and pseudotumors. Acta Radiol 53(1):102–111
107. Ragheb D, Higgins JL Jr (2002) Ultrasonography of the scrotum: technique, anatomy, and pathologic entities. J Ultrasound Med 21(2):171–185

108. Sudakoff GS, Quiroz F, Karcaaltincaba M, Foley WD (2002) Scrotal ultrasonography with emphasis on the extratesticular space: anatomy, embryology, and pathology. Ultrasound Q 18:255–273
109. Woodward PJ, Sohaey R, O'Donoghue MJ, Green DE (2002) From the archives of the AFIP: tumors and tumorlike lesions of the testis—radiologic-pathologic correlation. Radiographics 22:189–216
110. Yang DM, Kim SH, Kim HN, et al (2003) Differential diagnosis of focal epididymal lesions with gray scale sonographic, color Doppler sonography, and clinical features. J Ultrasound Med 22(2):135–42
111. Galosi AB, Lacetera V, Muzzonigro G (2008) Clinica delle malattie testicolari di interesse ecografico. Urologia 75(4):S12, s59–66

Ultrasound of the Penis

112. Bassiouny HS, Levine LA (1991) Penile duplex sonography in the diagnosis of venogenic impotence. J Vasc Surg 13:75–82
113. Bearcroft PW, Berman LH (1994) Sonography in the evaluation of the male anterior urethra. Clin Radiol 49:621–626
114. Broderick GA, Lue TF (1991) The penile blood flow study: evaluation of vasculogenic impotence. In: Jonas U, Thon W, Stief CG F (eds) Erectile dysfunction. Springer, Berlin
115. Chou YH, Tiu CM, Pan HB et al (1987) High-resolution real-time ultrasound in Peyronie's disease. J Ultrasound Med 6:67–70
116. Choudhary S, Singh P, Sundar E, Kumar S, Sahai A (2004) A comparison of sonourethrography and retrograde urethrography in evaluation of anterior urethral strictures. Clin Radiol 59:736–742
117. Kadioğlu A, Tefekli A, Erol H, Cayan S, Kandirali E (2000) Color Doppler ultrasound assessment of penile vascular system in men with Peyronie's disease. Int J Impot Res 12:263–267
118. Kim B, Kawashima A, LeRoy AJ (2007) Imaging of the male urethra. Semin Ultrasound CT MR 28:258–273
119. King BF, Lewis RW, McKusick MA (1994) Evaluation of impotence. In: Bennett AH (ed) Impotence: diagnosis and management of erectile dysfunction. WB Saunders Co, Philadelphia
120. Morey AF, McAninch JW (2000) Sonographic staging of anterior urethral strictures. J Urol 163:1070–1075
121. Patel U, Lees WR (1995) Penile sonography. In: Solbiati L, Rizzatto G (eds) Ultrasound of superficial structures. Churchill Livingstone, London, pp 229–242

Ultrasound of the Penis: Penile Echo Color Doppler

122. Halls J, Bydawell G, Patel U (2009) Erectile dysfunction: the role of penile Doppler ultrasound in diagnosis. Abdom Imaging 34(6):712–725
123. Broderick GA (1998) Evidence based assessment of erectile dysfunction. Int J Impot Res 10 Suppl 2:S64–73; discussion S7–9.
124. Benson CB, Aruny JE, Vickers MA Jr (1993) Correlation of duplex sonography with arteriography in patients with erectile dysfunction. AJR Am J Roentgenol 160(1):71–73
125. Quam JP, King BF, James EM, Lewis RW, Brakke DM, Ilstrup DM et al (1989) Duplex and color Doppler sonographic evaluation of vasculogenic impotence. AJR Am J Roentgenol 153(6):1141–1147
126. Patel U, Amin Z, Friedman E, Vale J, Kirby RW, Lees WR (1993) Colour flow and spectral Doppler imaging after papaverine-induced penile erection in 220 impotent men: study of temporal patterns and the importance of repeated sampling, velocity asymmetry and vascular anomalies. Clin Radiol 48(1):18–24
127. Fitzgerald SW, Erickson SJ, Foley WD, Lipchik EO, Lawson TL (1991) Color Doppler sonography in the evaluation of erectile dysfunction: patterns of temporal response to papaverine. AJR Am J Roentgenol 157(2):331–336
128. Bertolotto M (ed) (2008) Color Doppler US of the penis. Berlin: Springer; 2008, ISBN:978-3-540-36676-8